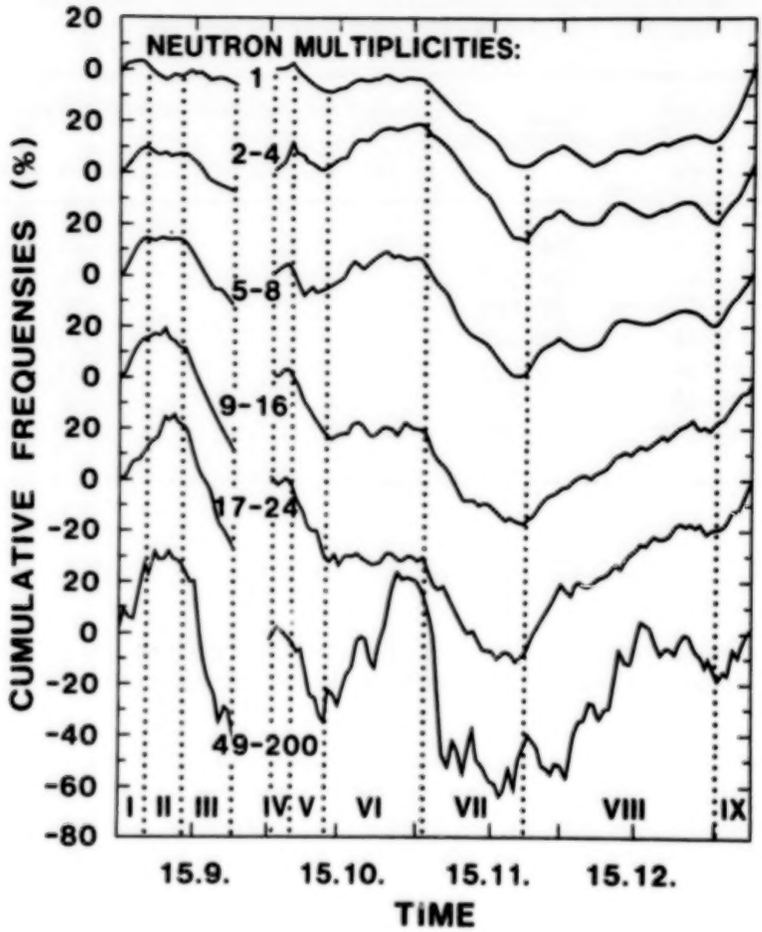


Fig. 1. Cusum curves for various multiplicity categories.

For each interval I-IX we calculated the average intensities. In fig. 2 the deviations of these averages from overall mean intensities are given as a function of the median sea-level energy corresponding to various multiplicity categories.

4. Discussion. An interesting result of this analysis is the fact that the relative intensity deviation does not approach zero as the median energy increases from 0.1 GeV to 100 GeV. It is a contradiction with the generally accepted form of modulations, $\Delta f/f = AE^{-\gamma}$ with $\gamma > 0$.

On the contrary to this general view, e.g. during period I the deviation shows quite a smooth increase up to 3 GeV above which the deviation remains clearly positive up to the highest energy. During period III the negative deviation becomes stronger as the energy increases from 0.1 GeV to 10 GeV. The deviation is -2.4 % at 21 GeV and -6.3 % at 98 GeV. A similar behaviour is seen during the period V.

The deviations from the mean intensity are more or less constant during VII and IX. They are between -1.5 % and -2.6 % and between 2.4 % and 3.1 %, during period V.

Periods II, IV, VI, and VIII represent cases where the energy spectra do not deviate to any noteworthy degree from the mean spectrum.

According to our estimation, the highest multiplicity category cor-

N85-35050

ORIGINAL PAGE IS
OF POOR QUALITY

SP 5.1-16

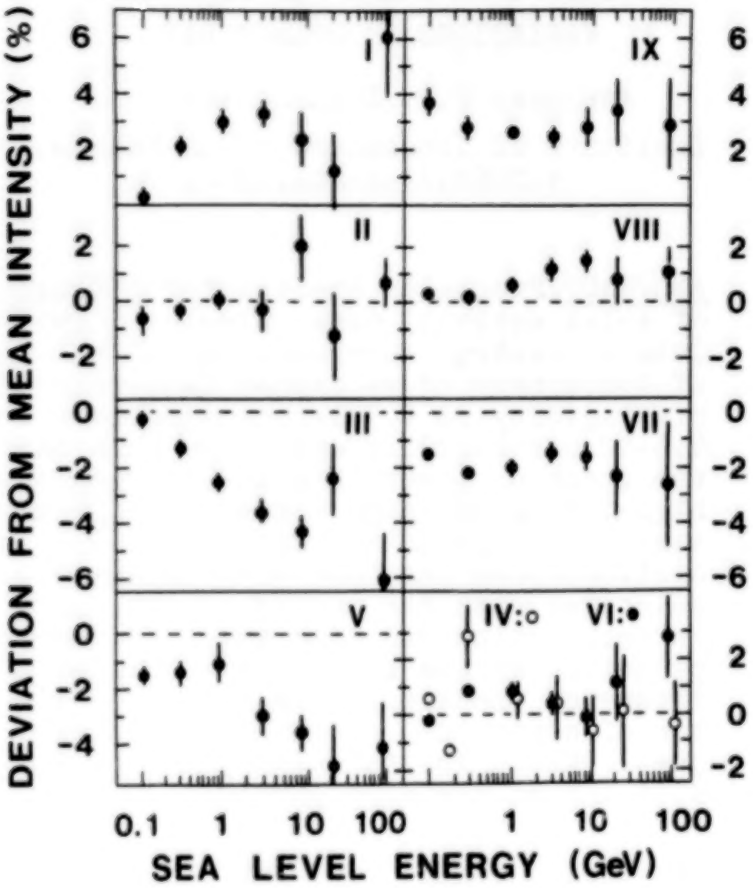


Fig. 2. Deviations of the daily counting frequencies from the mean frequencies during periods I-IX.

responds to primary radiation with median energy of 1100 GeV in free space. In all cases in which the energy spectrum deviates systematically from the mean (I, II, V, VII, and IX), the deviations in the highest category are towards the same direction as in all other categories corresponding to lower median energies. In addition, the estimated standard deviation of these points is smaller than the deviation of the points from the mean intensity. Quite unexpected is the result that in the cases where spectrum modulation is present, no clear indication is seen for decrease of the modulation amplitude in high-energy region.

5. Conclusions. According to the present results the long-term variation of cosmic radiation extends at least upto energies of several hundreds of GeV in free space. There are indications that the relative deviation, $\Delta f/f$, is of the order of a few percent in the energy range above 100 GeV. In some cases, the amplitude of the modulation shows systematic increase in the energy range 15-300 GeV in free space.

References:

/1/ Caulcutt, R., Statistics in Research and Development, Chapman and Hall, London, 1983.
/2/ Lumme, M., et al., J. Phys. G, 10, 683-694, 1984.

N85-35070

SH 5.1-17

FREQUENCY SPECTRA OF SHORT-PERIOD VARIATIONS OF COSMIC RAY

Antonova V.P., Zusmanovich A.G.

Institute of Ionosphere of AN KazSSR,
480068, Alma-Ata, USSR.

ABSTRACT. Frequency spectra for different periods of solar activity were calculated by 5-minutes data of neutron super-monitor of the Institute of Ionosphere of AN KazSSR (altitude 3340 m, cut-off rigidity is 6,7 GV, counting rate is about $4.5 \cdot 10$ per hour). It was shown that shifting of the spectrum power from low-frequency range to high-frequency range takes place from minimum to maximum of the solar activity. It was reliably distinguished the peak with 160-minutes period coincided with the period of the Sun's atmosphere oscillation and some types of geomagnetic pulsation by the method of accumulation of the frequency spectra. It was conducted the comparison of cosmic ray spectra with spectra of geomagnetic field for the same point of the registration and at the same period.

The short-period cosmic rays variations origins from different nonstationary processes in the interplanetary space, magnetosphere and atmosphere of the Earth and these variations may be used for the study of the such processes. The high-altitude neutron monitor of the Institute of Ionosphere of AN KazSSR permits to investigate the spectrum of cosmic ray fluctuations up to $1.7 \cdot 10^{-3}$ Hz. In this paper the spectral density of cosmic ray fluctuations in the range of 10^{-5}--$5 \cdot 10^{-4}$ Hz was calculated by the method of Blacman and Tukey /1/, using 15-minute data of this monitor for the time period from 1974 to 1983. The all data were corrected for the barometric pressure. The solar activity cycle was devided to the four periods: 1-1974-1976-the solar activity minimum, 2-1977-1978-solar activity increase, 3-1979-1980-activity maximum and 4-1981-1983-activity decrease. The calculation of the spectral density was carried out on the week-interval data with the filtrating of the low-frequency band. It was obtained that at solar activity minima the main power of the spectral density concentrated in the low-frequency range. When the solar activity increased, the spectral power shifts to the high-frequency range. In Fig.1 are shown the summary power spectra $G_{xx}(f)$ for the period mentioned above; a-1st period, b-2nd period, c-3rd period and

ORIGINAL PAGE IS
OF POOR QUALITY

d-4th period.The unifirm distribution of the spectral density at the all frequency interval at solar maximum and the presence of large power at low frequency range at solar minimum are observed.

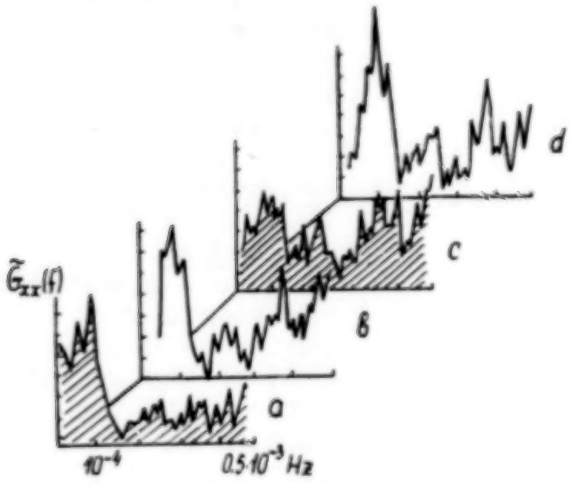


Figure 1.

It was shown earlier that the peak at frequency near 10^{-4} Hz (the period of 160 minutes) is presented in the frequency spectrum of the cosmic ray intensity,but ones was instable and observed irregular.The study of this peak is rather intresting becouse of the stable pulsations of the solar atmosphere /3,4/ and geomagnetic pulsations /5/ were observed at the same frequency.In this paper we calculated the summary power spectrum by the data for 1981-1983 (during the quiet periods) and this spectrum $\tilde{G}_{xx}(f)$ is shown in Fig.2.It is seems the peak at 160 minutes predominates in the summary spectrum.It should be noted that the period of this isolate peak equal to 160 minutes precisely in summary spectrum while it drifted around this period in separate frequency spectra.The amplitude of this peak,standing out against a background of intensity fluctuations, exceedes the 95-% significance level,which denoted the dotted line in fig.2.

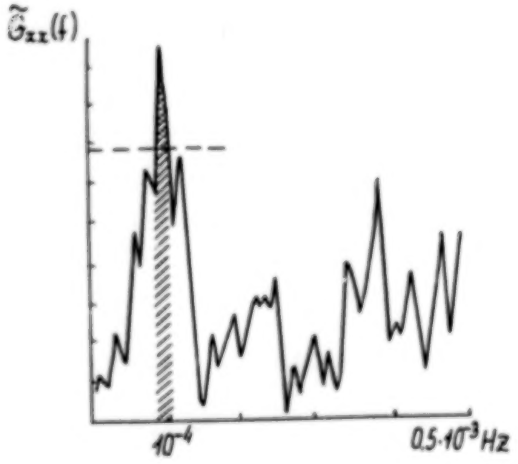


Figure 2.

It was compared the frequency spectra of cosmic ray intensity and the spectra of the geomagnetic field (H-component),registered in Alma-Ata also.The summary spectra of geomagnetic data are shown in Fig.3,for the same intervals of the solar activity cycle as in Fig.1.The main power in these spectra concetrated at low-frequency range and there no statistically significant peaks which could influenced on the cosmic ray fluctuations.There are no the statisti-

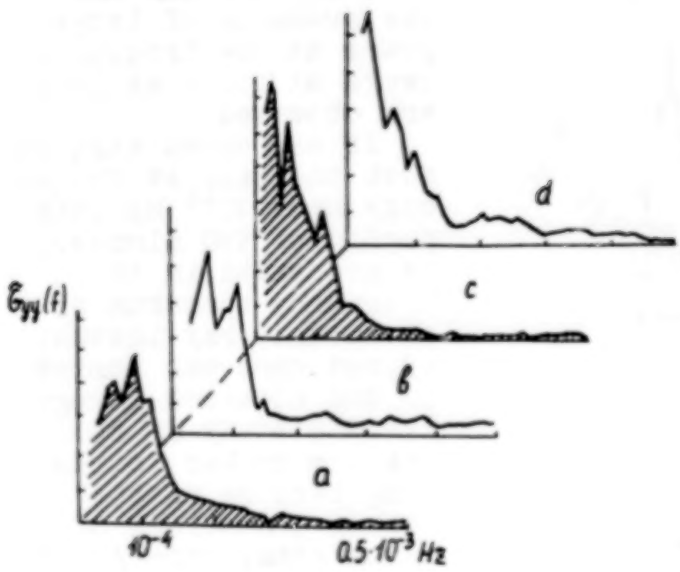


Figure 3.

cal significant values of the spectral density in the coherence spectra of cosmic ray intensity and quiet geomagnetic data for the all investigated periods from 1974 to 1983.

RESULTS. The frequency spectra of the cosmic ray intensity and H-component of the geomagnetic field were studied in the frequency range (10^{-5}-$5 \cdot 10^{-4}$)Hz for period 1974-1983.We can draw a following conclusions from obtained results:

1.The main power of the spectral density in the cosmic ray frequency spectra shifted from low-frequency range to high-frequency range when the solar activity increased.

2.The distinctive peak with the period of 160 minutes observed in the summary frequency spectrum of the cosmic ray intensity.

3.There is no relation between the cosmic ray fluctuations and fluctuations of the geomagnetic field during quiet periods.

REFERENCES.

1.Blackman R.B.,Tukey J.W. The measurement of power spectra. Dover pub.,N.Y.,1958.

2.Antonova V.P.,Zusmanovich A.G. Proc.17th ICRC,Paris,1981, 4,193.

3.Severny A.B.,Kotov V.A.,Tsap T.T. Nature,1976,256,87.

4.Kotov V.A.,Severny A.B.,Tsap T.T. Izv.Krimean Astrophys. Observ.,1983,66,3.

5.Vladimirsky B.M.,Bobova V.P.,Bondarenko N.M.,Veretennikova V.K. Izv.Krimean Astrophys.Observ.,1983,68,75.

N85-35071
SH 5.1-18

STUDY OF COSMIC RAY SCINTILLATIONS FROM 5-MINUTE DATA OF THE SCINTILLATOR TELESCOPE "IZMIRAN" AND WORLD-WIDE NEYWORK STATIONS

O.V.Gulinsky, L.I.Dorman, I.Ya.Libin, R.E.Prilutsky, K.F.Yudakhin

Institute of Terrestrial Magnetism, Ionosphere and Radio Wave propagation, USSR Academy of Sciences, I42092 Troitsk, Moscow Region, USSR

During cosmic ray propagation in interplanetary space there appear characteristic cosmic-ray intensity scientillations /I/ which are due to charged particle scattering on random inhomogeneities of the interplanetary magretic field (IMF). Particles of rather low energies which are sensitive not only to IMF inhomogeneities, but also to the fine structure of approaching shock fronts, undergo the largest scintillations. Nonetheless, the high-energy (more than several Gev) cosmic ray scintillations, which are registered in the most sensitive way be ground-based devices used for recording cosmic radiation, are similarly informative. From the physical point of view this is also connected with the fact that a particle with a large Larmor radius ($R = cp/eH \gg R_C$, R_C is the correlation radius of a random magnetic field) "sees" a wide spectrum of IMF inhomogeneities, whereas when interacting with the high-frequency part of the magnetic inhomogeneity spectrum, low-energy particles bring information about a comparatively narrow region of the IMF turbulence spectrum.

The smallness of scintillation amplitude in the high-energy range is compensated by the fact that measurements in this energy range are made by ground-based devices with a significant statistics and a high accuracy /2/.

The power spectra of cosmic ray scintillations on the Earth during some intervals from I977 to I982 (for quiet periods, for solar flares and Forbush decreases due to power shock waves, Fig. I) have been calculated from five-minute, one- and two-hour values of the cosmic-ray intensity measured by the scintillator supertelescope IZMIRAN and in stations of the world-wide network (Moscow, Utrecht, Kerguelen, Apatity, Tixie Bay, Norikura). The spectra were estimated by the methods of spectral analysis and by autoregressive methods which mutually control each other /3/ and make it possible not only to analyze scintillation powers at distinguished frequencies, but also to determine the behavior of spectrum slopes in some frequency ranges.

If the power-law spectrum of cosmic ray scintillations is described by the power function $P(f) \sim A \cdot f^{-\delta}$, then using the ratio of the spectrum values in different frequency ranges $f < 8 \cdot 10^{-5}$ Hz and $10^{-5} \leq f \leq 10^{-4}$ Hz (for neutron monitors and scintillator telescopes of the world-wide net of

stations), one can evaluate the product H_0V (in the assumption that the IMF spectrum remains unchanged in the entire frequency range):

$$300 H_0 \cdot V = \frac{2\pi}{\cos\psi}\left[\frac{n-1}{n+3}\cdot\frac{A_1}{A_2}\cdot f^{\gamma_2-\gamma_1+2}\right]^{1/2}\cdot\left[\frac{\int_{R_c} R^{-2} W(R)\,dR}{\int_{R_c} W(R)\,dR}\right]^{-1/2}$$

The IMF scintillation spectrum is determined as

$$B(f) = \left(\frac{2}{n+3}\right)^{-1}\frac{4\pi V_{\parallel}^2}{(2\pi)^4 (V_{\perp}\cdot\delta)^2}\cdot f^2\cdot P(f)$$

where H_0 is the mean IMF strength, V is the solar wind velocity, n is the index of pitch-angular distribution, W(R) are coupling coefficients of the devices.

Mean estimations of the indices of the slopes of CR scintillation power spectra for different devices in the stations Moscow, Utrecht, Kerguelen, Lomnicky Stit, Vostok, Baksan, Apatity in quiet periods give the following results: for frequencies $f < 3\cdot10^{-5}$ Hz the spectral index γ lies in the interval $1.45 \leq \gamma \leq 1.75$, for frequencies $4\cdot10^{-5} \leq f \leq 10^{-4}$ the index lies within $1.95 \leq \gamma \leq 3.35$ and, finally, for frequencies $f > 3\ 10^{-4}$ Hz $1.55 \leq \gamma \leq 2.10$ (the latter is due to the competition between the CR scintillation power and the noise power $P(f)/n_0^2 = 2/n_0$). The calculations of the power spectra ($B\cdot f^{-\nu}$) of IMF fluctuations give the values of ν of the order of 1.8 ± 0.1, which agrees well both with the results of field experiments and of ref./4/ (the relation between the spectral indices of IMF, ν and CR, γ, has the form $\gamma = \nu + 2$ in the frequency range $4\cdot10^{-5} \leq f \leq 10^{-4}$ and $\gamma = \nu$ for frequencies $f \leq 3\ 10^{-5}$Hz). Figure 2 presents the power spectra for CR scintillations averaged over the investigated stations for different periods of the maximum (curve 1) and the minimum (curves 2,3) of solar activity. For all the frequencies the power values coincide well with the theoretically calculated values /4/ (for $H_0 = 5\cdot10^{-5}$ Gs and $v = 5\cdot10^7$ cm·s^{-1}) both in the absolute values (in the high-frequency range they differ by a factor of 1.2-1.5 and in the low-frequency range by a factor of 1.5-2) and in the behaviour of the spectra: the values of the indices coincide with an accuracy to 10 %.

There exist also other possibilities for studying the CR scintillation spectrum: one can not only estimate the power spectrum of IMF fluctuations, but also establish a one-to-one correspondence with the level of perturbation in interplanetary medium of both distinguished scintillations at certain frequencies and the spectrum as a whole - the slope of the CR scintillation spectrum in the range $f < 10^{-4}$Hz increases gradually up to the maximum value several hours before the perturbation of interplanetary medium comes to the Earth. Figure 3 shows the behaviour of the index of the po-

wer spectrum of CR scintillations for the events in September 1977 from the data of the Utrecht and Kerguelen stations. It is seen from the figure that at least 18 hours before perturbation the spectral index in the range $10^{-5} \leq f \leq 10^{-4}$ Hz starts increasing whereas the quantity A (if the spectrum is given in the form $A \cdot f^{-\delta}$) decreases. That CR go ahead of perturbation can be easily explained: CR feel inhomogeneities at a distance of their free path for scattering (about $10^{12} - 10^{13}$ cm) and their velocity is a thousand times larger than the velocity of propagation of perturbation. Hence, CR bring information practically instantaneously, whereas perturbation travels to the Earth long hours. Therefore, the distances between perturbations approaching the Earth can be essentially different: recording particles of different energies, one can observe inhomogeneities at distances up to several AU.

REFERENCES

1. L.I. Dorman., I.Ya. Libin - Space Sci.Rev., 1984, 39, 91-152.
2. L.I. Dorman., I.Ya. Libin, Ya.L. Blokh - Scintillation method for cosmic ray scintillation studies - M., Nauka, 1979.
3. O.V. Gulinsky., L.I. Dorman., R.E. Prilutsky. Proc. of the Conference,
4. L.I. Dorman., M.E. Katz, M. Steglik et al. - Izv. AN SSSR ser. fiz. 1983, 47, N9, 1986.

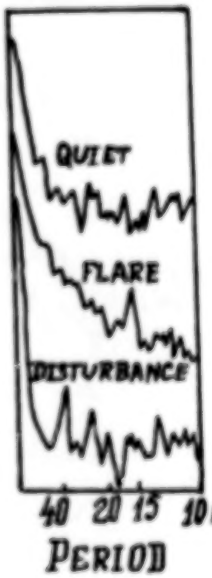


Fig. 1

ORIGINAL PAGE IS
OF POOR QUALITY

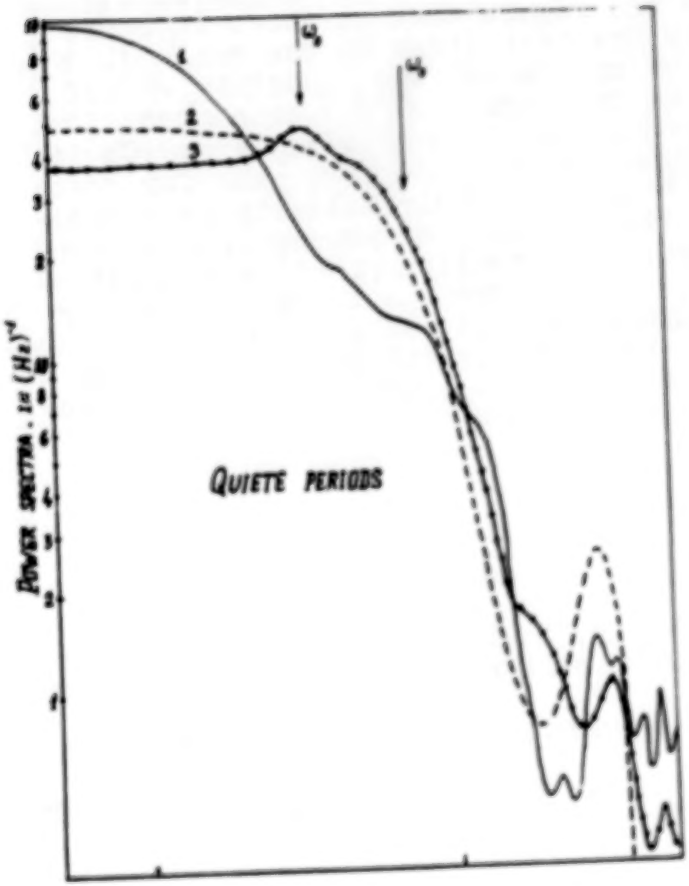
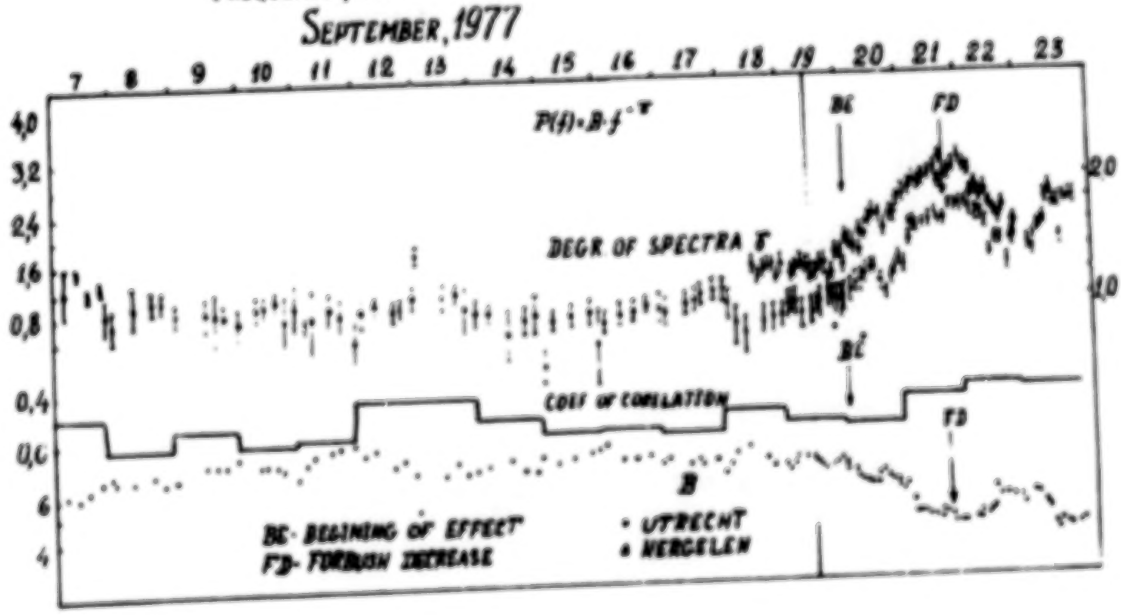


Fig. 2

Fig. 3



N85-35072

SH 5.1-20

THE THEORETICAL AND EXPERIMENTAL INVESTIGATION OF COSMIC RAY FORBUSH-EFFECTS

Alania M.V., Bakradze T.S., Bochorishvili T.V.
Bochikashvili D.P., Despoteshvili M.A., Nachkebia N.A.

The Institute of Geophysics, Georgian Academy of Science, Z.Rukhadze str. 1, 380093, Tbilisi

ABSTRACT

The theoretical results of analysis of the expected spatial distributions of density, gradients and anisotropy of cosmic rays, obtained on the basis of the numerical solution of anisotropic diffusion equation in the presence of the disturbances of shock wave type in the interplanetary space are presented. The theoretical calculations on the definition of the energy spectrum and anisotropy of galactic cosmic rays during Forbush - effect are compared with the experimental data.

The theoretical model. Cosmic ray Forbush-effects have a complex structure and nature /1,2/. They differ from each other both by power and by energy spectrum indices et al. However, there exist the indications such as the recurrence and sporadicity of Forbush-effect origin, the character of shock wave development causing Forbush-effects, the change of energy spectrum index in time et al. by with the definite classification of Forbush-effects can be carried out /3-4/.

In this paper the study of cosmic ray Forbush-effects on the basis of the processes occurring in the interplanetary space in the presence of the disturbance passage limited by the heliolongitudes, but having no boundary in the radial direction is carried out i.e. the type of recurrent Forbush--effect is considered.

The anisotropic diffusion equation/5/ is taken as modeling of the electromagnetic conditions occurring in the interplanetary space under the following assumptions: a) solar wind velocity u and the diffusion coefficient $\varkappa$ of cosmic rays in the disturbed region changes nearly twice in comparison with the environment, b) the disturbed region is given in a cone form for which the helioequator is a symmetry plane, i.e. along the trajectory of the Earth the heliolatitudinal gradient $\partial n/\partial\theta = 0$, c) it is considered that, since the disturbed region across the heliolatitude is limited in the range of several a.u., and in the radial direction the process is stationary, the stationary approximation is quite true, i.e. $\partial n/\partial t = 0$. Hence, the anisotropic diffusion equation has the following form:

$$\nabla_i(\varkappa_{ik}\nabla_k n) - \nabla_i(n \cdot u_i) + \frac{1}{3R^2}\cdot\frac{\partial}{\partial R}(R^3 n)\cdot\nabla_i u_i = 0 \qquad (1)$$

where n and R -the density and the rigidity of cosmic ray particles, and u_i the solar wind velocity. Taking into

account the above assumptions for solar wind velocity U and the diffusion coefficient $\partial\ell$: $U=U_0(1+d_1\tau)$ (see Fig. 1a) and $\partial\ell=\partial\ell_0(1-d_2\tau)$ (see Fig.1b), where $d_1=3,4$; $d_2=1,75$; and $\tau=\frac{1}{\pi^2}[arctg(2(\varphi-30))-arctg((\varphi-70)/7)]$.

The equation (1) is solved by net method under the following boundary conditions:

$$\frac{\partial n}{\partial \tau}+\alpha n+\beta\frac{\partial n}{\partial R}\Big|_{\tau=0}=0\,,\quad n\Big|_{R=430}=1\,,\quad n\Big|_{\tau=\tau_0}=1\,,\quad n\Big|_{\varphi=0}=n\Big|_{\varphi=\pi}\,,$$

where $\alpha=(3/2)d$, $\beta=d\cdot R/3$ and $d=U\cdot r_0/\partial\ell$.

The expected change depending on the heliolongitude during Forbush-effect for two rigidities $R=10$ GV and $R=20$ GV is presented in Fig. 2. It is seen , that the change of solar wind velocity U and the diffusion coefficient $\partial\ell$ (see Fig.1a,b) induce a gradual decrease and restoration of cosmic ray intensity that is characteristic of the recurrent Forbush-effects.

For the case, when the approximation is given by $\frac{\delta D}{D}(R)\sim R^{-\gamma}$, the energy spectrum index of Forbush-effect is equal $\gamma=1,06$.

The expected change of socmic ray anisotropy before, during and after the cosmic ray Forbush-effect duration for the rigidity $R=10GV$ is presented in Fig. 3. It is seen that after strong disturbances of anisotropy vectors near the minimum of Forbush-effect the monotone restoration to the initial position is observed.

The experimental data. The change of intensity of cosmic ray neutron (1) and muon component at a level 0 and 7 m.w.e. (2) and (3) in Tbilisi station for the period February 14-17, 1978 is presented in Fig.4a. The change of the energy spectrum of this Forbush-effect in time has been studied by two independent methods. The first one is a well-known spectrographic method /5/ and the second one - the method of the coupling coefficients, presented by the Japanese authors /6/. The analysis by the spectrographic method has been carried out by the intensity of cosmic ray neutron and hard μ -meson components at Tbilisi station and by method of the coupling coefficients - by the data of Tbilisi station and the world network. The changes of the energy spectrum index γ , obtained by the spectrographic method (the dashed curve) and by the coupling coefficients (the solid curve) are presented in Fig. 4b. It is seen that the results obtained by both methods show the same temporal changes, however, the values of the energy spectrum index obtained by the spectrographic method are systematically higher than the values obtained by the method of the coupling coefficients. In the Fig.4c the changes of DSt variation of the Earth's magnetic field (dashed) and the cutoff rigidity threshold ΔR_c (solid) are presented.

Discussion and Conclusion. The obtained result is explained easily. The fact is that the change of the cutoff rigidity threshold ΔR is not taken into account in the process of calculating the energy spectrum index by the me-

ORIGINAL PAGE IS
OF POOR QUALITY

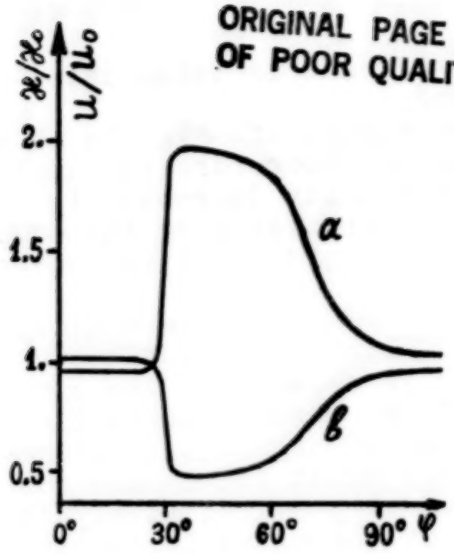


Fig. I

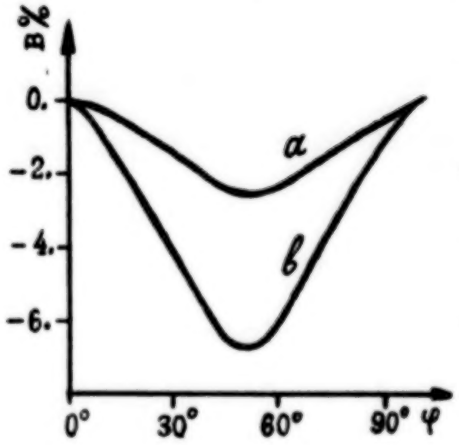


Fig. 2

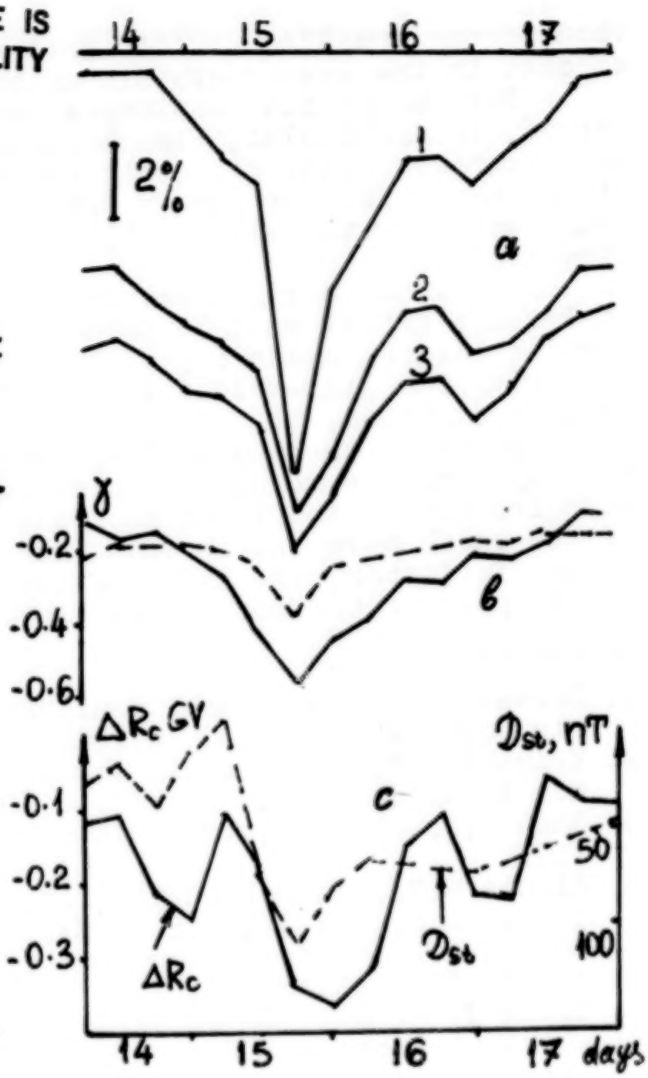


Fig. 4

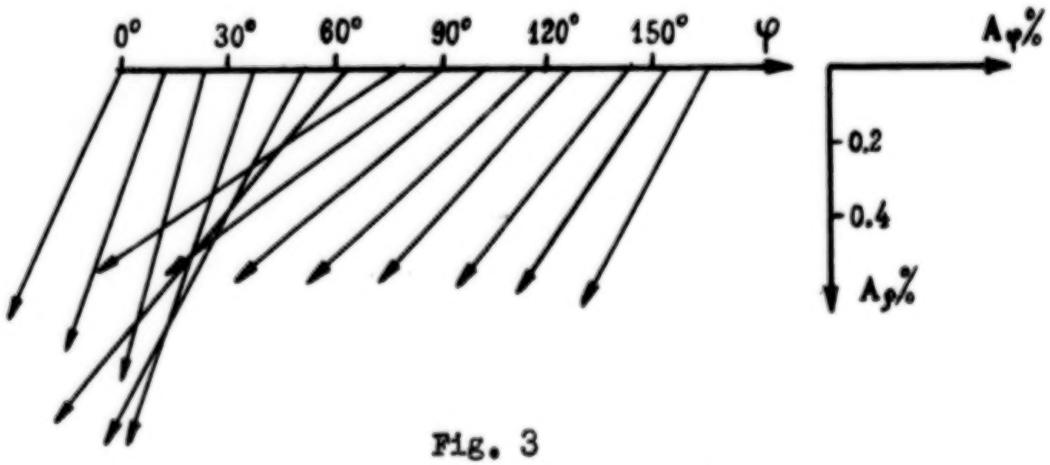


Fig. 3

thod of the coupling coefficients /6/, and is taken into account in the spectrographic method.

For the period considered the change of ΔR_c is observed, in particular, its decrease and therefore the amplitude absolute value of cosmic ray intensity decrease is diminished, i.e. the energy spectrum calculated by the coupling coefficients method will be more rigid, that is really observed.

The rigid energy spectrum before reaching the minimum of Forbush-effect must be connected with the predominant carring out of cosmic ray particles of relatively low energies with the high-velocity flux of the chromospheric flare /8/. In addition, the energy spectrum of magnetic inhomogeneity power of the medium frequencies which can induce cosmic ray particle modulation predominantly of relatively low energies can be increased in front of the magnetic cushion of the shock wave and in the cushion itself. Apparently, the geometric factor, the size of the compressed cavity in the front part of the shock wave plays an important role.

REFERNCES

I. Dorman L.I. "Variatsee Cosmicheskikh Luchei I Issledovanie Cosmosa". AN SSSR, M.I963.
2. Krimski G.F. "Modulatsia Cosmicheskikh Luchei V Mejplanetnom Prostranstve". "Nauka". M.I969.
3. Shah G.N. et al., Proc. I6th ICRC, Kyoto, Japan 3, 423, I979.
4. Alania M.V., Bochikashvili D.P. I8th ICRC, Bangalore, India, L.p. Vol.IO, I68, I983.
5. Dorman L.I. "Astrofizicheskie Aspecti Cosmicheskikh Luchei". "Nauka". M.6, I975.
6. Yasue S. et al., Coupling Coefficients of Cosmic Ray Daily Variations for Neutron Monitor Stations. Nagoya, Japan, I982.
7. Solar-Geophysical Data, Febr. I978, numb. 505, part I.
8. Alania M.V. Autoreferat of Doct. Dissertation, Kiev, I98I.

N85-35073
SH 5.1-21

PECULIARITIES OF GALACTIC COSMIC RAY (GCR) ANISOTROPY VARIATION IN CONNECTION WITH THE RECURRENT AND SPORADIC FORBUSH EFFECTS

B.D. Naskidashvili, N.A.Nachkebia, G.L.Tsereteli, L.Kh.Shatashvili

The Institute of Geophisics, Georgian Academy of Sciences, Z.Rukhadze str. I, 380093, Tbilisi, USSR

ABSTRACT

It has been establised, that the beginning of the change of vector of Solar-diurnal anisotropy of Galactic Cosmic Rays(GCR) preceeds the beginning of Forbush-decrease(FD), which is due to the disturbed region (DR) of Solar wind existing time of which is $\tau \gtrsim$ 8 days. The meridional gradient $\nabla_\theta n$ of density during the reccurent FD is valued.

I. Anisotropy of GCR due to the long lived DR ofsolar wind

As is known, the sporadic Forbush decreases (SFD) are caused by thepowerful solar flares on the day-side of the solar disc. If the flare occurs near the central meridian of the Sun, then in this case DR of the Interplanetory me - dium, at the starting point of SFD will have the spatial sizes of order of one a.u. Considerable small size of DR of Solar wind, causing SFD, attaches some definite character on the behaviour of solar-diurnal anisotropy vector of GCR.

The typical case of behaviour of the anisotropy vec - tor, according to the data of Kiel(FRG) during the SFD (06. 09.1982) is given (on fig.Ia). Before the beginning of SFD, vector of anisotropy is not changed, while after the SFD the vector turns to the direction of the Sun. The behaviour of vector of the GCR anisotropy has essentialy distinctive feature during such FD-s, which aren't necessarily connected with the flares on the Sun, arising not far from the central meridian, but are due to the high-velocity flow of Solar wind existing in the interplanetory medium in the course of time $\tau \gtrsim T/4$ (T -is the period of Solar rotation). In such cases, it is easy to notice, that at the starting point of FD the DR of the SW occupies the space area with the sizes of $L \gtrsim 4$ a.u. The corresponding model configuration lines of forces of IMF is presented (in Fig.1b). The passage of the Earth through the inhanced regions of IMF corresponds to the beginning of FD. In front of this region, as it is seen in (Fig.1b) is the nondisturbed region of the Solar wind, however access of GCR into this region is complicated due to the compressing of the lines of forces of IMF at far distances, where the GCR particles come from, mainly directed across the IMF lines of forces. The latter means, that

in this region of SW, similar to the charged particles trap, the diffusional flow of GCR must be greatly decreased. Hence, the GCR anisotropy in this non-dirturbed region of SW will be mainly due to the convectional flow of GCR, which is due to cause the turning of the anisotropy vector to the direction of the Sun. FD on 28.IX.1978 serves as a good example of this case. Before the beginning of the FD in the course of 20 days, not a single Solar powerful flare with importance ≥ 2 was observed. Consequently, FD must be due to the long-lived DR of SW. As it is seen from Fig. 1c. the anisotropy vector of GCR , for 8 days earlier before the beginning of FD, is essentialy turning to the direction of the Sun, but after the beginning of FD- tends to orientate to the direction of IMF. The latter is connected with that fact, that after the front passage through the DR, the Earth comes out of the "trap" region and the recovery of GCR intensity occurs due to the diffusional flow across the IMF lines of forces, which at far distances are spread, contributing to the free penetration of the GCR particles from the far distances of the Sun, where the GCR density is large.

2. The meridional gradient of GCR during the recurrent Forbush decreases.

In paper /I/ the classification of FDs is presented and in paper /2/ it is shown that the spectrum of the recurrent FDs is more rigid, than the one of the sporadic FDs. In the given paper the meridional gradient of CR during the recurrent FD is valued /3/.

The data of the world network of station of CR neutron component are analysed as well as the data of the SW, of the IMF, according to /4/ and of Solar activity (Solar Geophysical Data, NOAA). The considering of the FDs with the amplitude $\geq 1\%$ is mainly made according to the data of the high-latitudinal stations of CR. Superposition of effects, due to flaring and non-flaring flows complicates the view of recurrent FDs. If the recurrend FD is not preceeded by the chromosperic flare and FD is not created by interactional high-velocity flows of SW, then during the FD the IMF sign must not change. Therefore we've analysed only those FD-s, during which the IMF sign is not changed. Data for the period 1971-1978, when the polarity of the general magnetic field of the Sun was not changed, have been taken for the analysis.

After such selection 47 cases of FD were left. 22 cases out of them were arisen at a time, when IMF sign was negative (towards the Sun). In 25 cases, FDs were arisen at a time, when the IMF sign was positive (from the Sun). Each of these groups we divided into 2 subgroups, according to the IMF sign before and during FD, i.e. while dividing into subgroups, it was taken into account, whether the IMF signs coincided with each-other or not before and during the FD. Thus, we've obtained 4 groups of cases of FDs.

In DR of the SW the CR density is less than out of it, therefore the azimuthal gradient $\nabla_\varphi n$ of CR density

changes its direction near the minimum of recurrent FDs,i.e. in the minimum of recurrent FDs it can be admitted that $\nabla_\varphi n = 0$. Therefore, the meridional gradient $\nabla_\theta n$ will cause the CR additional flow of the Hall type, directed perpendicular to the IMF and $\nabla_\theta n$ /5/.

The observed CR anisotropy A near the minimum of the recurrent FDs can be presented as the sum of $A = A_0 + A_\perp$, when A_0 -is a general anisotropy connected with the convectional -diffusional transforming in the high-velocity plasma flow, $A_\perp$ - is the constituent, due to the appearance of $\nabla_\theta n$. The value of A_0 was calculated by data averaging after the minimum of FDs.

In Fig.2a,b, where effective regions of CR modulation are denoted by the circles, the orbit of the Earth-by dashes, the neutral layer of IMF - by the solid line, the origination of the anisotropy under the influence of $\nabla_\theta n$, during those recurrent FDs, when the IMF is directed from the Sun, is shown schematically. The calculated values $A_\perp$ and values of IMF are also given (in the right part of Fig.2a, b) in the minimum of FDs. It is seen, that in case of 2a (I7 cases of FDs are averaged) the vector $A_\perp$ is really directed perpendicular to the IMF. In case 2b(8 cases of FDs are averaged) the vector $A_\perp$ is turned relatively towards $A_\perp$ corresponding to the case 2a almost by I80° as it was to be expected

In Fig. 3a,b the same as in Fig.2 , is presented only for those recurrent FDs during which IMF is directed to the Sun. In case 3a-I8 cases of FDs are averaged, but in 3b- 4 ones of FDs.

For the more exact definition of $A_\perp$, we've examined those FD-s, which correspond to the cases presented in Fig. 2a,b. The anysotropy A in the minimum FD has the form: In case 2a $A_1 = A_0 + A_\perp$; In case 2b $A_2 = A_0 - A_\perp$. Hence, $A_\perp = (A_1 - A_2)/2 = (0,I2 \pm 0,06)\%$.

According to /5/ $A_\perp = \Lambda[\nabla_\theta n \times \kappa]$, where Λ is the transport path of CR; κ -unit vector along the lines of force of IMF.

In paper /5/ the following is shown

$$\Lambda = (1-F)\rho \qquad \rho = R/(45B)$$

where ρ -is the Larmor radius in a.u. F - degree of irregularity of IMF. R-rigidity (in Gv) B-value of IMF (in $n T_\lambda$). Then $\nabla_\theta n = 45 A_\perp B (1-F)^{-1} R^{-1}$,where $\nabla_\theta n$ is expressed in %/a.u. $A_\perp$ -in %, If $F = 0,I \pm 0,3$ then with R=I0 GV, from the experimental data we obtained, that during the recurrent FD-s meridional gradient of CR density on the Earth orbit is $\nabla_\theta n = (3 \div 4)\%/a.u.$

REFERENCES:

I. Shah G.N., Kaul C.L., Razdan H.Proc.I6th ICRC , v.3, Kyoto, I979, p.423.

2. Nachkebia N.A., Shatashvili L.Kh. I8th ICRC, Bangalore, Late Papers, v.I0, p.I52.

ORIGINAL PAGE IS
OF POOR QUALITY

3. Nachkebia N.A., Shatashvili L.Kh., Geomagnetism i aeronomia, t.XXV, №2, I89.
4. King J.H. IMDB, NSSDC, WDCA, I977, I979.
5. Samsonov D.S., Krimsky G.F., Samsonova Z.N., Chirkov N.P. V kn.: "Issledovania po Kosmofisike i aeronomii.Iakytsk: SOAN, SSSR, I975, I72.



Fig.I

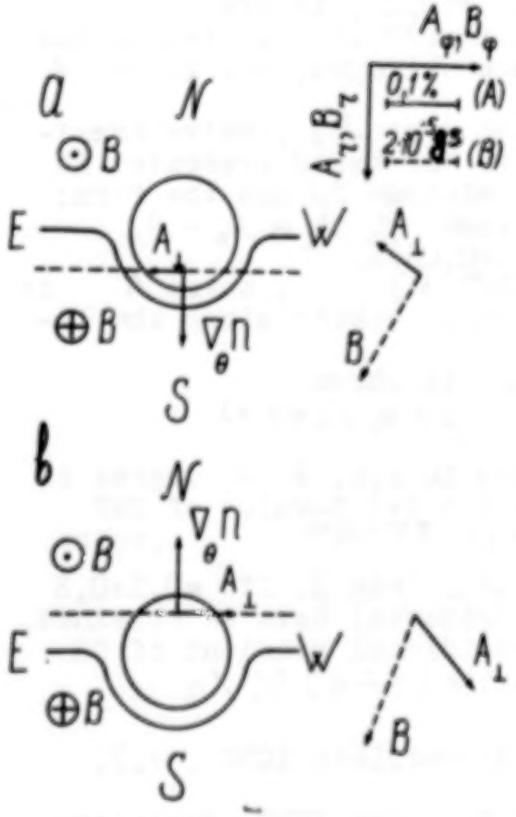


Fig.2

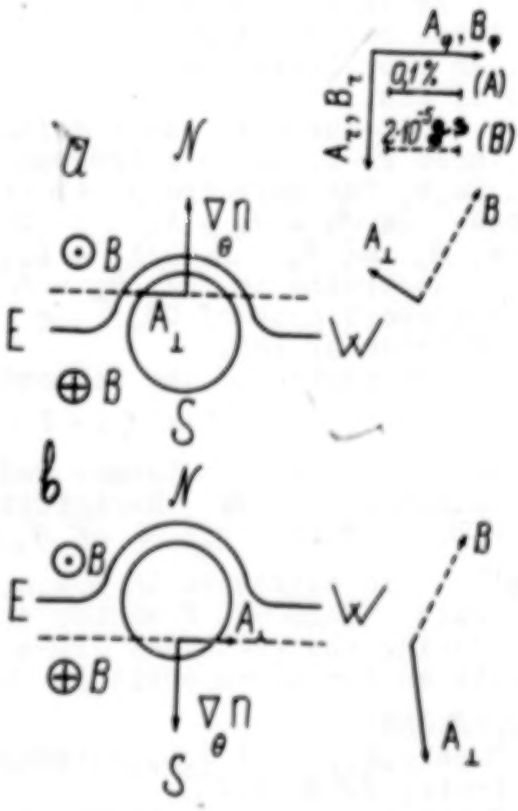


Fig.3

SH 5.1-22

COSMIC RAY MODULATION BY HIGH-SPEED SOLAR WIND FLUXES

N85-35074

Dorman L.I., Kaminer N.S.
Institute of Terrestrial Magnetism, Ionosphere and Radio Wave Propagation, USSR Academy of Sciences, I42092 Troitsk, Moscow Region, USSR

Kuz'micheva A.E., Mymrina N.V.
Uralsk Pedagogical Institute, Uralsk, USSR

Abstract. Cosmic ray intensity variations connected with recurrent high-speed fluxes (HSF) of solar wind are investigated. The increase of intensity before the Earth gets into a HSF, north-south anisotropy and diurnal variation of cosmic rays inside a HSF as well as the characteristics of Forbush decreases are considered.

I. Introduction. Recurrent high-speed fluxes of solar wind connected with coronal holes change essentially the cosmic ray density distribution in interplanetary medium. When such fluxes cross the Earth, different types of cosmic ray (CR) variations are observed. The characteristics of these CR variations may essentially differ from those observed when CR pass sporadic HSF of flare origin.

Below we consider a number of CR variations connected with recurrent HSF observed in I973-I974.

2. Intensity increase before Forbush effect. I2 fluxes of velocities $U \gtrsim 600$-800 km/s were considered, which were accompanied by Forbush effects. The data on the CR neutron component obtained on the Deep River station were used. After the low-frequency trend and the diurnal CR variation were eliminated by the method of superposition of epochs the CR variation was found before the Earth got into a HSF. It is seen from Fig.I that before Forbush effect CR intensity increases with amplitude by about 0.4 %.

3. N-S anisotropy of CR. The N-S anisotropy was investigated from the CR neutron component data obtained in the stations of Thule and Mc Murdo. I8 HSF with a positive IMF direction and I8 HSF with a negative IMF direction were picked. All of them were divided into three groups depending on their speed: I-$v \leq 600$ km/s, II - $v = 600$-700 km/s, III - $v > 700$ km/s.

The results of determining N-S anisotropy by the method of superposition of epochs are presented in Fig.2. The N-S anisotropy is seen to exist in the back part of a HSF (5%) and to be absent in the front part of a HSF. Such a peculiar behaviour of N-S anisotropy is qualitatively explained by

ORIGINAL PAGE IS
OF POOR QUALITY

a non-radial plasma outflow from the coronal hole - the flux is divergent. The sign of N-S anisotropy becomes inverse as the IMF direction changes. This means that N-S anisotropy results from the Hall effect. This conclusion is confirmed by the behaviour of the B_z-component of IMF at different IMF directions. The amplitude of N-S anisotropy does not depend on the HSF speed.

4. Diurnal CR variation. The behaviour of the diurnal CR variation was investigated from the data on the neutron component for 58 HSF. It turned out that the amplitudes of first and second harmonics are larger inside a HSF than in a quiet solar wind, that the phase of first harmonic shifts towards earlier hours, and the phase of second harmonic towards later hours (Fig.3). This difference increases with an increasing HSF speed. The characteristics of diurnal CR variation do not depend on the field direction in HSF.

5. Forbush effects of recurrent HSF. The analysis of data on the CR neutron component for 62 HSF has shown that if the HSF width $\Delta t \gtrsim 3$ days, a Forbush decrease is practically absent. Inside each HSF there exists a good correlation ($r_{\sim}7$) between plasma velocity and CR intensity decrease. The amplitude of Forbush effect A_F increases with an increase of the HSF velocity (about a 5-% increase for an increase of v by 100 km/s). The shape of Forbush decreases and their amplitude do not depend on the IMF direction. The energy spectra of Forbush decreases for HSF of different velocities have been determined. It turned out that as the HSF velocity increases, the spectral index γ monotonously decreases: from $\gamma = 0.7$ for $v \leq 600$ km/s to $\gamma = 0.5$ for $v > 700$ km/s.

All these results, as well as the results of analogous papers by other authors make it possible to conclude that the main parameter of recurrent HSF which determines the characteristics of various CR variations is their velocity.

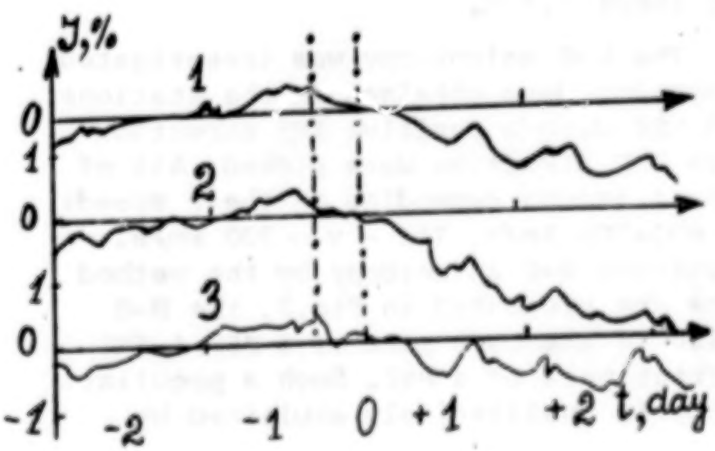


Fig.I. CR intensity increase before side-end of SHF calculated by superposition of epochs from 12 events. Curve 2-effect due to particles coming from transition region. Curve 3-effect due to particles coming from other directions. Curve I-effect averaged over all directions.

ORIGINAL PAGE IS
OF POOR QUALITY

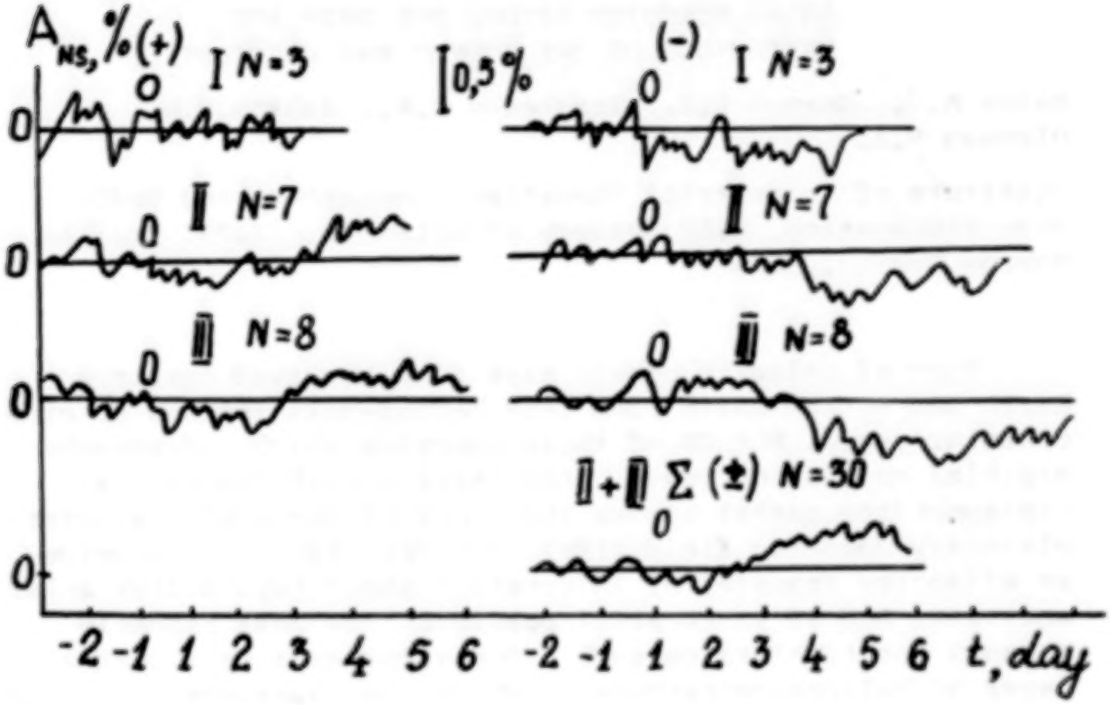


Fig.2. N-S anisotropy of CR inside a HSF. On the left - for the positive IMF direction, on the right - for the negative IMF direction. I - for HSF with v ≤ 600 km/s, II - for HSF with v = 600-700 km/s, III- for HSF with v > 700 km/s. At the bottom is the sum curve for the II-nd and III-d groups of HSF.

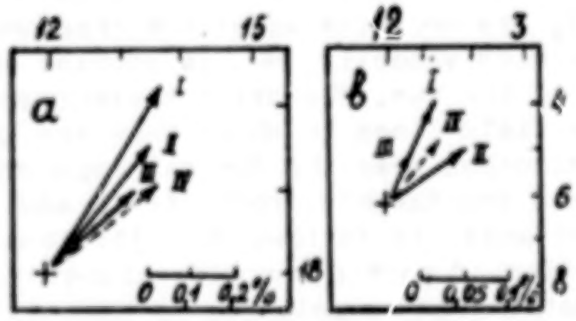


Fig.3. Vectors of a diurnal (a) and semidiurnal (b) CR variations: I - in the front part of HSF, II - in the middle part of HSF, III - in the back part of HSF, IV - in a quiet solar wind

ORIGINAL PAGE IS
OF POOR QUALITY

N85-35075

SH 5.1-23

SOLAR ACTIVITY BEYOND THE DISK AND VARIATIONS OF THE COSMIC RAY GRADIENT

Belov A.V., Dorman L.I., Eroshenko E.A., Ishkov V.N., Oleneva V.A.

Institute of Terrestrial Magnetism, Ionosphere and Radio Wave Propagation, USSR Academy of Sciences, 142092 Troitsk, Moscow Region, USSR

Part of galactic cosmic rays (CR) observed near the Earth and on the Earth come from beyond-disk regions of circumsolar space. But CR of those energies which undergo substantial modulation cover too large a path (we mean a transport free pathr) across the lines of force of the interplanetary magnetic field (IMF) in order they could provide an effective transfer of information about beyond-disk solar activity. And if it is still possible, the most probable channel for tranferring such information must be a neutral layer of heliomagnetosphere in which the transverse CR transport is facilitated by their drift in an inhomogeneous magnetic field /1,2/

For charged particles of sufficiently high energy the thickness of the neutral layer is negligibly small as compared with the gyroradius of particles, ρ . In a plane neutral layer the driving centres of such particles will shift along the line (which can be called a drift trajectory) determined by the relation

$$\Delta\varphi = \varphi - \varphi_0 = \int_{r}^{r_0} \frac{u}{\Omega} \frac{dr}{r^2} \qquad (1)$$

Here r and φ are heliocentric radius and heliolongitude, r_0 and φ_0 are coordinates of the observation point, u is solar wind velocity, Ω is angular velocity of synodic rotation of the Sun. The drift trajectories (Fig.1), contrary to the field lines to which they are perpendicular, are almost azimuthal near the Sun and approach the radial direction beyond the Earth's orbit. If u and Ω do not depend on the coordinates, it follows from (1) that $r/r_0 = \left(1+\Delta\varphi \frac{\Omega r_0}{u}\right)^{-1}$. The direction of particle motion along the drift trajectories will be determined by polarity of the total magnetic field of the Sun. So, in the seventies, in the special region of "one-way" particle motion near the neutral layer, protons and other positively charged particles had mostly to shift from the Sun to overstep the Earth's orbit. At that time the drift trajectories could bring to the Earth the information of Forbush decreases which occurred in the opposite to us side of cir-

cumsolar space and were caused by powerful beyond-disk flares.

A simple diffusion model for an expected CR variation in a neutral layer near the Earth gives /3/

$$\delta(x_s)=\int_0^{x_s}\frac{\delta(x)}{v_d\tau}\exp\left(\frac{x-x_s}{v_d\tau}\right)dx \qquad (2)$$

where x is the distance measured along the trajectory, $\delta(x)$ is variation of CR concentration at different points of the trajectory, v_d is effective drift velocity, τ is the mean time necessary for a particle to shift by one gyroradius across the field. High values of $\delta(x_s)$ (for example, >1 %) should hardly be expected even for large beyond-disk decreases. However, since the main effect must be concentrated on one gyroradius from the neutral layer, sufficiently large variations of the CR gradients are possible here. The CR gradient variations and consequent anisotropy variations are just the response to beyond-disk events which one may hope to discover by observing CR near the Earth.

The CR gradient near the Earth can be obtained by using the data on the CR concentration and anisotropy along with the data on the velocity of solar wind and IMF /4,5/.

If $\vec{A}$ is the CR anisotropy vector, $\vec{A}_c$ is its convective part, and $\vec{g}$ is the gradient of the logarithm of CR concentration, then in the convective-diffusion anisotropy model /6/ $\vec{A}-\vec{A}_c=-\Lambda\vec{g}$. In the local right-handed coordinate system in which the x-axis is directed along the solar wind velocity and the y-axis lies in the plane of IMF line, the matrix of transport free paths is

$$\Lambda=\rho\begin{pmatrix}\frac{c^2+\kappa s^2}{\sqrt{\kappa}} & cs\frac{1-\kappa}{\sqrt{\kappa}} & -s\sqrt{1-\kappa}\\ sc\frac{1-\kappa}{\sqrt{\kappa}} & \frac{s^2+\kappa c^2}{\sqrt{\kappa}} & c\sqrt{1-\kappa}\\ s\sqrt{1-\kappa} & -c\sqrt{1-\kappa} & \sqrt{\kappa}\end{pmatrix}$$

Here ρ is gyroradius of particles in the total magnetic field /4/, k is the transverse-to-longitudinal diffusion coefficients ratio, $s=\sin\Psi$, $c=\cos\Psi$, Ψ is the angle between $\vec{A}_c$ and the IMF strength vector. It can be shown that the inverse Λ matrix has the following simple form

$$\Lambda^{-1}=\frac{1}{\rho}\begin{pmatrix}\sqrt{\kappa} & 0 & s\sqrt{1-\kappa}\\ 0 & \sqrt{\kappa} & -c\sqrt{1-\kappa}\\ -s\sqrt{1-\kappa} & c\sqrt{1-\kappa} & \sqrt{\kappa}\end{pmatrix}$$

This matrix is convenient in the determination of $\vec{q}$ /5/.

The active regions whose appearance from behind the eastern disk or disappearance behind the western one was accompanied by active phenomena were distinguished with the help of (7). Thus, the periods with a high probability of powerful flares in the invisible side of the Sun were chosen. One of such periods is shown in Fig.2. We can see there substantial variations of the CR gradient and especially its heliolatitudinal component g_z. A considerable part of such variations is observed in a close vicinity of the neutral layer. It is of importance that variations of the CR gradient are not at all always accompanied by considerable variations of IMF and solar wind velocity at the point of observation. And although the observed variations of anisotropy and CR gradient should not necesserily be associated just with beyond-disk events, the experimental data, along with the above estimates and qualitative considerations give grounds for further search for the evidence in favour of beyond-disk solar activity in the behaviour of galactic CR near the Earth.

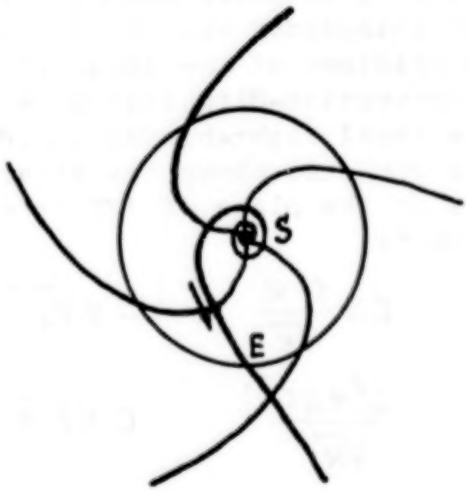


Fig.I. The drift trajectory passing near the Earth. It is calculated by formula (I). Arrow indicates the proton drift direction in the seventies.

N85-35015

ORIGINAL PAGE IS
OF POOR QUALITY

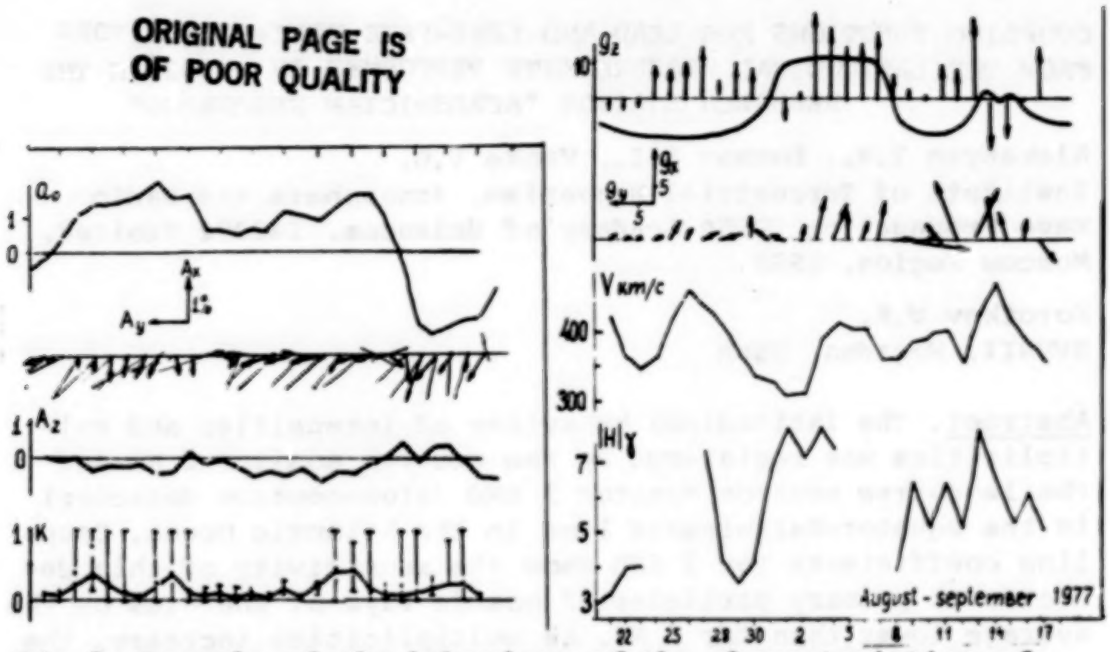


Fig.2. Example of the behaviour of the characteristics of cosmic rays and interplanetary medium in August-September, I977.
a_o - variation of concentration of CR with a rigidity of IO GV.
A_x, A_y, A_z - components of the first harmonic of CR anisotropy. The position of IMF line is shown along with A_x, A_y.
g, g_x, g_y, g_z - gradient and its components for CR with a rigidity of IO GV. The hypothetic configuration of the neutral layer of heliomagnetosphere is shown along with g_z.
K is the degree of anisotropy of CR diffusion (O ≤ K I). The directly calculated values of K are shown by points, the smoothed ones - by a solid line.
u - solar wind velocity
H - IMF strength /8/.

REFERENCES

I. Levy E.H. Proc.I6-th ICRC, v.3, p.47, I979.
2. Jokipii J.R., Levy E.H., Hubbard W.B., Astroph.J., 2I3, 86I, I977.
3. Belov A.V., Ishkov V.N. YI Symp. CAPG (Theses of the report) Sochi, November, I984.
4. Belov A.V. et al., Izv.AN SSSR, ser.fiz., 42, IOI3, I978.
5. Belov A.V. et al., Izv.AN SSSR, ser.fiz., 48, , I984.
6. Krymsky G.F. Thesis, I973, FIAN, Moscow.
7. Cataloque of solar proton events in I970-I979, M., IZMIRAN I982.
8. King J.H., Interplanetary Magnetic Field Book, NSSDC 79-08.

N85-35076

SH 6.1-1

COUPLING FUNCTIONS FOR LEAD AND LEAD-FREE NEUTRON MONITORS FROM THE LATITUDINAL MEASUREMENTS PERFORMED IN 1982 IN THE RESEARCH STATION "ACADEMICIAN KURCHATOV"

Alekanyan T.M., Dorman L.I., Yanke V.G.
Institute of Terrestrial Magnetism, Ionosphere and Radio Wave Propagation, USSR Academy of Sciences, I42092 Troitsk, Moscow Region, USSR

Korotkov V.K.
SVKNII, Magadan, USSR

Abstract. The latitudinal behaviour of intensities and multiplicities was registered by the neutron monitor 2 NM and the lead-free neutron monitor 3 SND (slow-neutron detector) in the equator-Kaliningrad line in the Atlantic Ocean. Coupling coefficients for 3 SND show the sensitivity of this detector to primary particles of cosmic rays of energies on the average lower than for 2 NM. As multiplicities increase, the coupling coefficients shift towards higher energies.

The data of latitudinal expeditions have given information on the planetary CR distribution, but mainly from the results of measurements of the summary intensity registered by the neutron monitor, e.g./I,2/. But the available results for measurements of multiplicities are contradictory /3,4/, although it is obvious that large multiplicities must be connected on the average with high energies of primary particles with the exception of a first multiplicity, where the influence of the muon component can be observed. It is also reasonable to specify the known results /5,6/ for the lead-free neutron monitor NMD (Neutron maderated detector) and to compare them with the data for the standard neutron monitor NM-64.

The approximation of the dependence of the recorded intensity I on the geomagnetic cutoff rigidity R has the form /I-6/

$$I = I_o\left[1 - exp\left(-\alpha R^{-\kappa}\right)\right] . \qquad (I)$$

It appears impossible to determine simultaneously three parameters, I_o, α, k in (I) by the method of least squares because of divergency of the iteration process. Therefore, one usually determines the parameter I_o from expedition measurements and then calculates and k by solving the system of equations $\ln\ln\left[I_o/(I_o-I)\right] = \ln\alpha - k\ln R$, where I are experimental data. But this method turns out invalid for multiplicities because a statistical accuracy of measurements rapidly decreases, as multiplicity increases, and because in many cases the data of measurements in polar zones are absent. Besides, we cannot

use part of the data, for which $I \gg I_0$ because of statistical difference.

The aim of this papaer is the development of the method of simultaneous calculation of all the parameters in (I) and practical application of this method..

The planetary distribution of CR was measured by the detectors on the research ship "Academician Kurchatov" from 6 to 22 of April, I982 in the Atlantic Ocean in the northern hemisphere. The standard two-counter neutron monitor 2 NM and the three-counter lead-free neutron monitor 3 NMD were used for measurements. Correction due to atmospheric pressure variation was made similarly to /7/. The correction due to variations of extraterrestrial origin was introduced according to the Kiel station; the dependence of the amplitude of variations on the geomagnetic cutoff rigidity was also determined by analogy with /7/. The geomagnetic cutoff rigidities were calculated according to /8/. The results of latitudinal measurements are shown in Fig.I.

The successive approximation method /9/ is proposed for finding the parameters of the approximation (I). The expansion of (I) in a Taylor series with an accuracy to first-order terms at the point of the initial approximation of paramaters has the form

$$I=\left[I_0\left(1-e^{-\alpha R^{-k}}\right)\right]_0+\left(1-e^{-\alpha R^{-k}}\right)_0\Delta I_0+\left(I_0 R^{-k} e^{-\alpha R^{-k}}\right)_0\Delta\alpha+\left(I_0\alpha R^{-k} e^{-\alpha R^{-k}}\ln R\right)_0\Delta k, \quad (2)$$

where the expressions in brackets are taken at the point of the initial approximation $I_0=I_0^{(0)}$, $\alpha=\alpha^{(0)}$, $k=k^{(0)}$. Then one minimizes the sum of the squares of the differences of the calculated values of I according to (2) and experimental values of I

$$S=\Sigma\left(q\Delta I_0+I_0\tau\Delta\alpha-I_0\alpha\tau\ln\tau\Delta k-I_0 q-I\right)=min \quad (3)$$

where $q=1-exp(-\alpha R^{-k})$, $\tau=R^{-k}exp(-\alpha R^{-k})$. The condition of the minimum (3) $\partial S/\partial I_0=0$, $\partial S/\partial\alpha=0$, $\partial S/\partial k=0$ gives the system of equations

$$\begin{cases}\Delta I_0\Sigma q^2+I_0\Delta\alpha\Sigma q\tau-I_0\alpha\Delta k\Sigma q\tau\ln R=\Sigma q(I-I_0 q)\\ \Delta I_0\Sigma q\tau+I_0\Delta\alpha\Sigma\tau^2-I_0\alpha\Delta k\Sigma\tau^2\ln R=\Sigma\tau(I-I_0 q)\\ \Delta I_0\Sigma q\tau\ln\tau+I_0\Delta\alpha\Sigma\tau^2\ln R-I_0\alpha\Delta k\Sigma(\tau\ln R)^2=\Sigma\tau(I-I_0 q)\ln R\end{cases} \quad (4)$$

the solution of which $\Delta I_0, \Delta\alpha, \Delta k$ determines the following approximation of the parameters $I_0^{(i)}=I_0^{(a)}+\Delta I_0$, $\alpha^{(i)}=\alpha^{(a)}+\Delta\alpha$, $K^{(i)}=K^{(a)}+\Delta K$. This cycle of operations is repeated for subsequent approximations until stable values of the parameters I_0, α, k are obtained. The results of the calculations are shown in Fig.I (solid curve) for all the recording channels: total intensity of the neutron monitor 2 NM, multiplicities m=I-5, ≥ 6 and a lead-free monitor. The successive approximation method proved

convergent only for multiplicities m ≥ 6, which is explained by a low statistical accuracy of measurement of higher multiplicities. For comparison the calculated curves in Fig.2 are normalized for R=0. The polar coupling coefficients calculated in line with /I-3/ as $W(R)=\alpha k R^{-k-1}\exp(-\alpha R^{-k})$ are shown in Fig.3. The table presents the parameters I_0, α, k, as well as the maximal values of the coupling coefficients W_{max} and the corresponding values of the rigidities R_{max}

	I_0	α	k	R_{max}, GV	W_{max}, %/GV
2NM	42930	8.318	0.866	4.76	4.55
3NMD	59076	6.550	0.800	3.80	4.99
m=I	28592	7.155	0.808	4.21	4.58
m=2	4481.8	I0.255	0.951	5.43	5.99
m=3	I055.5	I3.483	0.978	6.96	3.76
m=4	325.63	20.298	I.060	9.I5	3.23
m=5	63.56	42.83	I.29I	II.77	3.30

The measurements give the form of multiplicity distribution

$$I_m = C\exp(-\varkappa m^{\delta}), \qquad (5)$$

where I_m is the number of cases of recording of multiplicity m; $C, \varkappa, \delta$ are the distribution parameters. In a particular case of the use of multiplicities I,2,4 it is easy to obtain explicit expressions for determining the parameters

$$\delta = \ln[\ln(I_2/I_4)/\ln(I_1/I_2)]/\ln 2, \quad \varkappa = \ln(I_1/I_2)/(2^{\delta}-1), \quad C = I_1 e^{\varkappa}. \qquad (6)$$

From Fig.4 it follows that these parameters are functionally connected with one another, in this case $\varkappa = (1{,}87\pm0{,}01)\delta^{(2{,}26\pm0{,}03)}$, $C = (5{,}77\pm0{,}04)\cdot10^{4}\exp((0{,}81\pm0{,}01)\varkappa)$. This means that a change in the cutoff rigidity leads to an interdependent change in the multiplicity distribution parameters. The dependence of these parameters on the geomagnetic cutoff rigidity is shown in Fig. 5. If $\delta(R)$ is represented by a straigt line according to Fig. 4, $\varkappa(R)$ and C(R) are represented according to (6), then it is easily verified that the expression is not transformed into (I), i.e. $\delta(R)$ has a more complicated form. It can be obtained if (I) is substituted into (6) and then (6) into (5). The $\delta(R)$ thus obtained is illustrated in Fig.5 by a dashed line.

The main results: I. Coupling coefficients shift towards higher rigidities as multiplicity increases; 2. The lead-free monitor NMD is sensitive to lower energies than NM-64. 3. The multiplicity distribution parameters are functionally connected. 4. All the parameters of (I) are determined by the successive approximation method.

REFERENCES : I. E.A.Andreev et al. Cosmic rays, I974,NI4,p.34
2.T.M.Alekcanjan et al.,Proc.I7 ICRC,Paris,I98I,v.4,p.266.
3.T.M.Alekcanjay et al.Proc.I6 ICRC.Kioto,I979,v,4,p.3I5.

ORIGINAL PAGE IS
OF POOR QUALITY

4. T.M.Alekcanjan et al. Cosmic Rays,1978,N18,p.72.
5. T.M.Alekcanjan et al.ProcI6 ICRC,Kioto,1979,v.4,p.32I.
6. L.I.Dorman et al.Proc.I6 ICRC,Kioto,1979,v.4,p.325.
7. M.Kadama and A.Inaue.Yare Scientific Reports,Japan,I970, Ser.A,N 0.9,p.I.
8. M.A.Shea and D.T.Smart. J.Geophys.Res.I967,v.22,N 07,p.202I
9. B.P.Demidovich et al.Numerical methods of analysis. Fizmatgiz, I962.

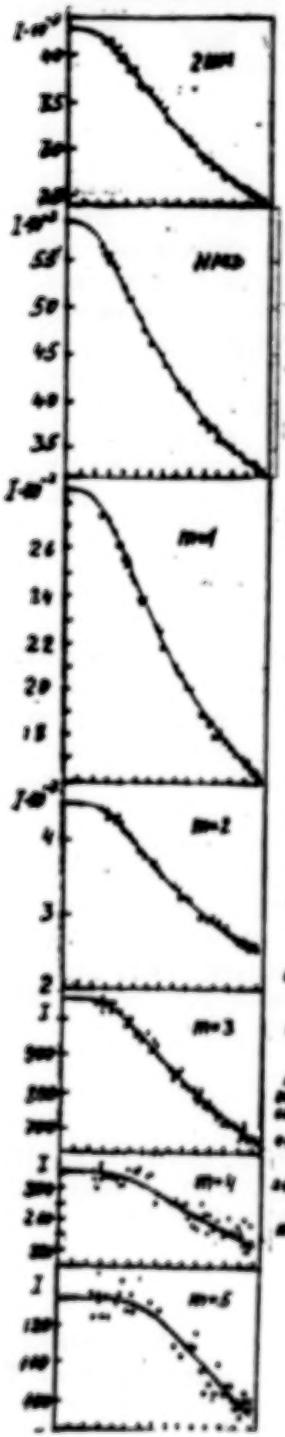


Fig.1

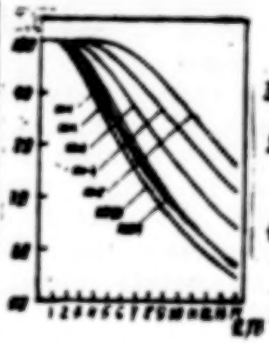


Fig.2

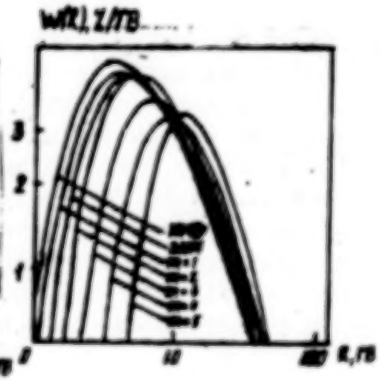


Fig.3

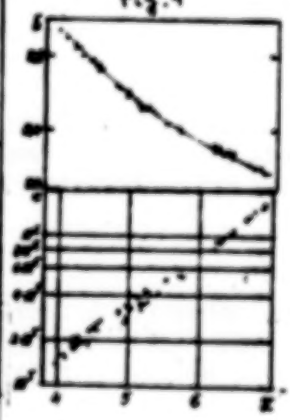


Fig.4

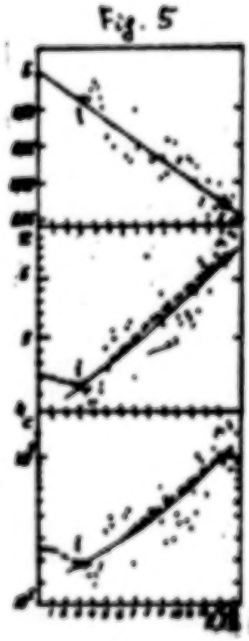


Fig.5

ORIGINAL PAGE IS
OF POOR QUALITY

N85-35077

ON THE SOLAR CYCLE VARIATION IN THE BAROMETER COEFFICIENTS OF HIGH LATITUDE NEUTRON MONITORS

M. Kusunose and N. Ogita*

Department of Physics, Kochi University,
Akebono-cho 2-chome, Kochi 780, Japan

* The Institute of Physical and Chemical Research,
Hirosawa, Wako-shi, Saitama 351-01, Japan

ABSTRACT

Evaluation of barometer coefficients of neutron monitors located at high latitudes has been performed by using the results of the spherical harmonic analysis based on the records from around twenty stations for twelve years from January 1966 to December 1977. The average of data at eight stations, where continuous records are available for twelve years, show that the absolute value of barometer coefficient is in positive correlation with the cosmic ray neutron intensity. The variation rate of the barometer coefficient to the cosmic ray neutron intensity is influenced by the changes in the cutoff rigidity and in the primary spectrum.

1. Introduction

Many authors[1] have indicated an eleven year change of the barometer coefficients of the cosmic ray neutron monitors. Since there was no unique technique for determing the coefficient, the results obtained by different authors may be different. We developed a systematic method to examine the barometer coefficient[2-4] and clarified the solar cycle variation of the barometer coefficient more precisely.

To evaluate the barometer coefficient of neutron monitor, it is necessary to separate strictly the cosmic ray intensity variation induced by the primary cosmic ray variation from the one caused by the atmospheric pressure variation. For this purpose, we used the results obtained by the spherical harmonic analysis[5] which is performed on the basis of the neutron monitor records from around twenty stations at high latitudes where the cutoff rigidities Rc's are below 2.3 GV.

2. Residual barometer coefficient

The difference ΔI_p between the pressure corrected neutron monitor data I_p (percentage value) and the estimated neutron intensity $\overline{Y}$ calculated from the spherical harmonic analysis is expressed as

$$\Delta I_p = I_p - \overline{Y}.$$

This subtraction enables to eliminate the effect of the intensity variation of the primary cosmic rays outside the magnetosphere. The

residual barometer coefficient $\Delta\beta$ is obtained as a linear regression coefficient by the statistical analysis of correlation be tween the pressure p and the diffrednce ΔI_p. Results of $\Delta\beta$ for the period, from 1966 to 1977 are presented in the reference(4). The corrected pressure coefficient β_{cor} is derived according to the equation

$$\beta_{cor} = \beta_0 + \Delta\beta,$$

where β_0 is the reported barometer coefficient from each station.

3. Solar cycle variation of the barometer coefficient

Figure 1 shows the year-to-year variation of cosmic ray intensity $\bar{I}$ and barometer coefficient $\bar{\beta}$. where $\bar{I}$ and $\bar{\beta}$ are the averages of yearly mean data of eight stations (Alert, Deep River, Goose Bay, Inuvik, Kerguelen, Kiel, Oulu and Sanae) where the continuous data are available through twelve years from 1966 to 1977. Mean intensity of neutron component $\bar{I}$ is normalized to 100 percent at the point of the year 1966. C_0 is the yearly mean value of the isotropic component of spherical harmonic coefficients and normalized to the value of 1966, but plotted 4% higher level, and Rz, the sunspot number which is an index of solar activity is plotted inversely.

In order to investigate the solar modulation of barometer coefficient, we analyzed the relation between the barometer coefficient and the cosmic ray intensity. Figure 2 shows the relation between the barometer coefficient $\bar{\beta}$ and the cosmic ray intensity $\bar{I}$. The linear regression coefficient throughout the whole period is $\alpha_\gamma = (1.83 \pm 0.24) \times 10^{-3}$ mmHg with a correlation coefficient, r=0.92.

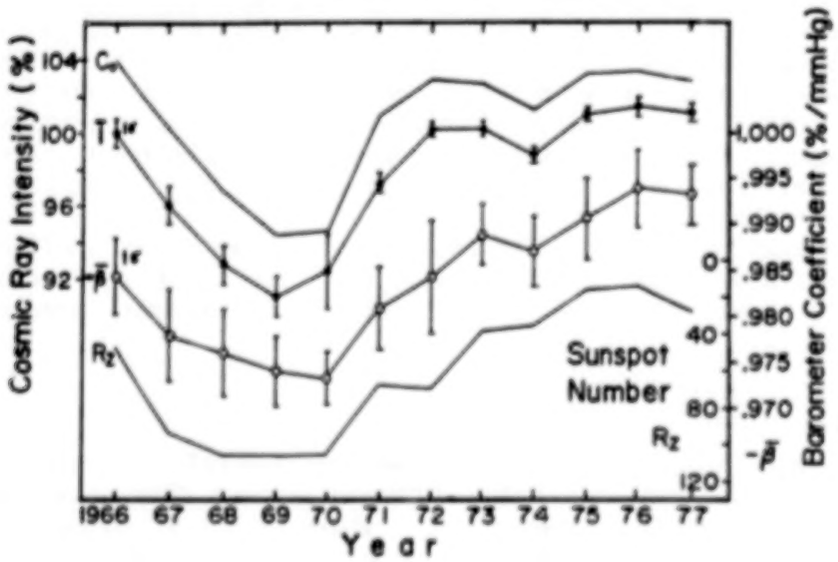


Fig.1. The yearly variation of C_0: the isotropic component of the spherical harmonic coefficients. $\bar{I}$: cosmic ray neutron intensity and $\bar{\beta}$ barometer coefficient, they all are averages of eight stations and error bars indicate the scatter of individual station, and Rz: the sunspot number.

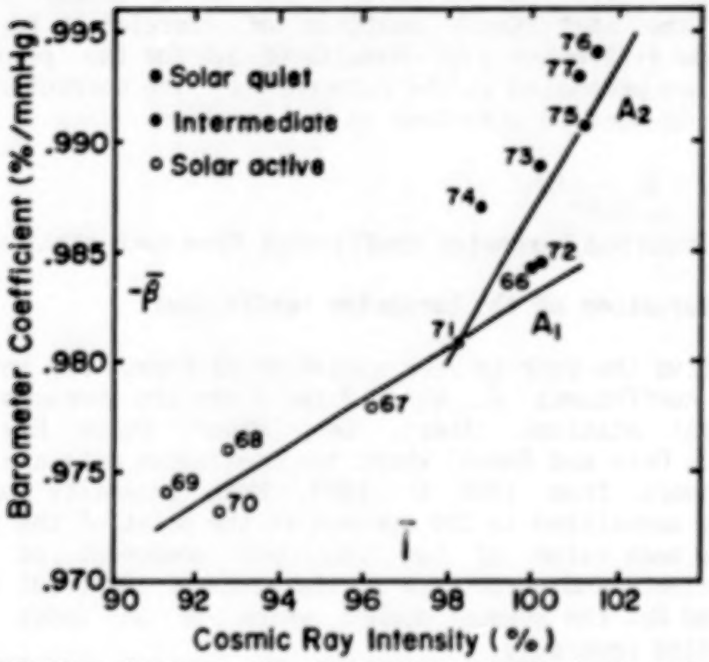


Fig.2. Relation between the barometer coefficient and cosmic ray intensity variations. Lines A_1 and A_2 represent the linear regression line between the barometer coefficient and the cosmic ray intensity in the solar active and the solar quiet period respectively.

4. Relation between the barometer coefficient and the cosmic ray primary spectrum variation

In a previous paper,[4] it was reported that the variation rate of the barometer coefficient to the cosmic ray intensity is larger in the solar quiet period than in the solar active period. About the quantitative relation between the barometer coefficient variation and primary cosmic ray rigidity spectrum, an analysis is performed. The present report is concerned with the numerical calculation to clarify the relation between the barometer coefficient and the cosmic ray primary spectrum variation.

We calculated the variation rate of the barometer coefficent α_γ which is defined as $\alpha_\gamma = \delta\beta/\delta I$. The ratio $\delta J/J_0$ represents the variation of the primary cosmic radiation. For a primary variational spectrum, we assumed as

$$\frac{\delta J(R)}{J_0(R)} = \begin{cases} AR^{-\gamma} & for \quad R \leq Ru \\ 0 & for \quad R > Ru \end{cases}$$

The calculations[6,8] were performed for several different values of pover γ, where A=constant and Ru = 40GV are assumed. The curve in Fig.3 represents the distribution of α_γ, where $\gamma = 1.7$ is assumed. It is clearly illustrated by the changes in the cutoff rigidity and in the primary spectrum. As for the computation of α_γ when the solar activity is high, it is necessary to estimate the rigidity dependence of barometer coefficient.

N83-35015

ORIGINAL PAGE IS
OF POOR QUALITY

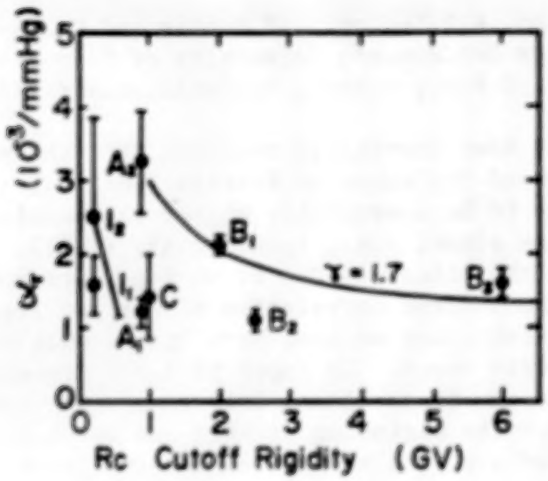


Fig.3. Distribution of α_γ is plotted in absolute value. The abscissa is the cutoff rigidity, where the neutron monitor is located, or the mean rigidity at several stations. Curve represents the distribution of α_γ, which is the result of numerical calculation[8], where γ=1.7 is assumed. A_1 and A_2 (Averages of eight high latitude stations)[4]; I_1 and I_2 (Inuvik)[7]; B_1, B_2 and B_3 (Averages of several stations)[9]; C(Deep River)[10].

6. Acknowledgments

We are indebted to the investigators of the cosmic ray stations for supplying us valuable data through the World Data Center C2 for Cosmic Rays Tokyo by the courtesy of Dr. M. Wada. We are grateful to the staffs of the Division of Electronic Computers of the Institute of Physical and Chemical Research. Numerical calculations were performed mainly on a FACOM 270-30 computer.

References

1) For instance, J. L. Kamphouse, (1968), J. Geophys. Res., **68**, 5608; W. K. Griffiths *et al.*, (1968), Canad. J. Phys., **46**, S1041; M. V. Alaniya *et al.*, (1970), Acta Phys. Acad. Scient. Hungaricae, **29**, Suppl. 2, 605; and the references therein.
2) Ogita, N. *et al.*, (1973), *Proc. 13th Int. Cosmic Ray Conf., Denver*, 2, 831.
3) Kusunose, M. *et al.*, (1981), *Proc. 17th Int. Cosmic Ray Conf., Paris*, 10, 281.
4) Kusunose, M., (1984), J. Phys. Soc. Japan, **53**, 4488.
5) Yoshida, S. *et al.*, (1971), J. Geopys. Res., **76**, 1.
6) Belov, A. V. and L. I. Dorman, (1979), *Proc. 16th Int. Cosmic Ray Conf., Kyoto*, 4, 310.
7) Kusunose, M., (1984), Mem. Fac. Sci., Kochi Univ., **6**, Ser. B, 15.
8) Kusunose, M., (1984), Mem. Fac. Sci., Kochi Univ., **6**, Ser. B, 21.
9) Bachelet *et al.*, (1971), Nuovo Cimento, **11 B**, 1.
10) Carmichael *et al.*, (1972), *Proc. 12th Int. Cosmic Ray Conf., Hobart*, 3, 887.

N85-35078

ATMOSPHERIC EFFECTS ON THE UNDERGROUND MUON INTENSITY

A.G.Fenton, K.B.Fenton, J.E.Humble and G.B.Hyland
Physics Department, University of Tasmania
Box 252C, G.P.O., Hobart, Tasmania, Australia, 7001

1. Introduction. We have previously reported that the barometric pressure coefficient observed for muons at Poatina (vertical absorber depth 357 hg cm^{-2}) appears to be appreciably higher than would be expected from atmospheric absorption alone, e.g., Lyons et al. (1981). We have explored the possibility that the effect is due to an upper atmospheric temperature effect arising from an inverse correlation of surface pressure with stratospheric temperature, but we have been unable wholly to account for the observations by this means. In paper SH 4.4-4 presented to this Conference we refer to a new proportional telescope which has been operating at Poatina since about the beginning of 1983 and which has a long term stability suitable for studying variations of atmospheric origin.

2. New Results. Data from the proportional counter telescope for February to December 1983 have been analysed to obtain the total barometric coefficient, the result being -0.042 ± 0.004 % mb^{-1}. This is in agreement with the value obtained for the years 1972-76 with the smaller GM counter telescopes, namely -0.047 ± 0.002 % mb^{-1} (Lyons et al., 1981). These values are to be compared with the coefficient to be expected on the basis of atmospheric absorption, -0.007 % mb^{-1}.

We plan to carry out a more detailed investigation using upper atmospheric data in conjunction with the muon data obtained with the new telescope, taking advantage of its long term stability to compare directly the results obtained in winter and summer, as well as from year to year.

3. Acknowledgements. We wish to thank the Hydro-Electric Commission of Tasmania and its staff for the excellent facilities provided at Poatina. This work is supported in part by the Australian Research Grants Scheme.

Reference.

Lyons,P.R.A., Fenton,A.G. and Fenton,K.B., (1981), 17th ICRC, Paris, Conference Papers 4, 300.

ORIGINAL PAGE IS
OF POOR QUALITY

N85-35079

SH 6.1-5

ALTITUDE VARIATIONS OF COSMIC-RAY SOFT AND HARD COMPONENTS OBSERVED BY AIRBORNE DETECTORS

K.Takahashi, A.Inoue, M.Wada, K.Nishi
The Institute Of Physical and Chemical Research
7-13 Kaga-1, Itabashi, Tokyo 173, Japan

K.Murakami
Cosmic Ray Reseach Laboratory, Nagoya University
Furo-cho, Chikusa-ku, Nagoya 464, Japan

ABSTRACT

The altitude variations of cosmic-ray total and hard components were measured upto 12,000 m on voard a jet liner over Japan island on December ,1981. Observed results together with soft component arepresented conparing with the model calculations through the atmosphere by applying the hardronic cascade.

1. Introduction

Since last two air-borne experiments(1979,1981), the altitude and latitude variation of various components of cosmic rays have been analyzed from various points of view (1),(2). In the analyses, we showed that our results did not contradict with Rossi's (3). And the model calculations through the atmosphere by applying the hadronic cascades were compared with the observed results (4),(5).

We used telescopes composed of two plastic scintillators of thickness of 3 cm ,of which geometric factor was 96 cm^2sr(6).

2. Altitude variation of vertical intesity of hard component

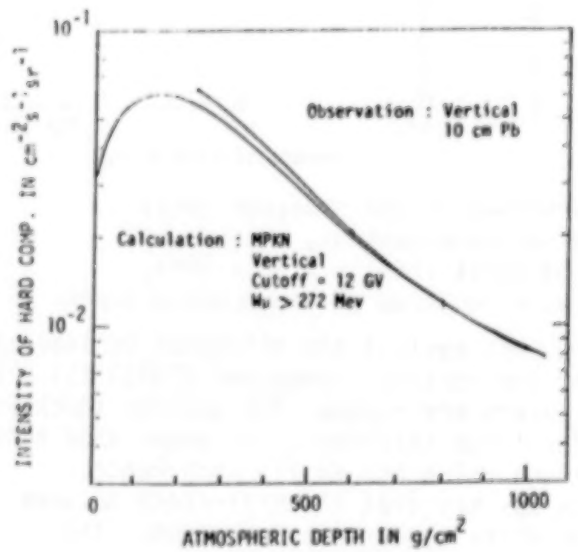


Fig. 1. The observed and calculated integral growth curves of hard components. The calculated curve shows the total of intensities of muons, pions, kaons, and protons. The observation curve is obtained by means of the weighted best fit of the data in 1981.

In Fig. 1 are included the altitude variations of hard component for vertical. The obserbation curve is obtained by means of the weighted best fit of the 41 data points with regard to 4 level flights at the depths of 221, 243, 560, and 1038 g/cm^2, including the ascending and the

descending.

The calculation curve represents the total of intensities of muons, pions, kaons, and protons with threshold energies of 273, 315, 751, and 1260 MeV respectively, at cutoff rigidity of 12 GV.

At the smaller atmospheric depth, it seems that the slight discrepancy exists between the observed and the calculated curve because the observation curve contains some components with high energy other than the calclated four components.

3. Analysis of the total, hard and soft components

In Fig. 2, curve(T) represents the total component measured without lead absorber. The observed total component contains the electronic component of electrons and photons other than the calculated total(H') of muons, pions, kaons,and protons without lead absorber. Curve(H) is the obserbed hard component capable of penetrating 10 cm lead absorber. Curve(S) represents the soft component which are stopped by 10 cm lead, that is to say (S) is the difference between (T) and (H).

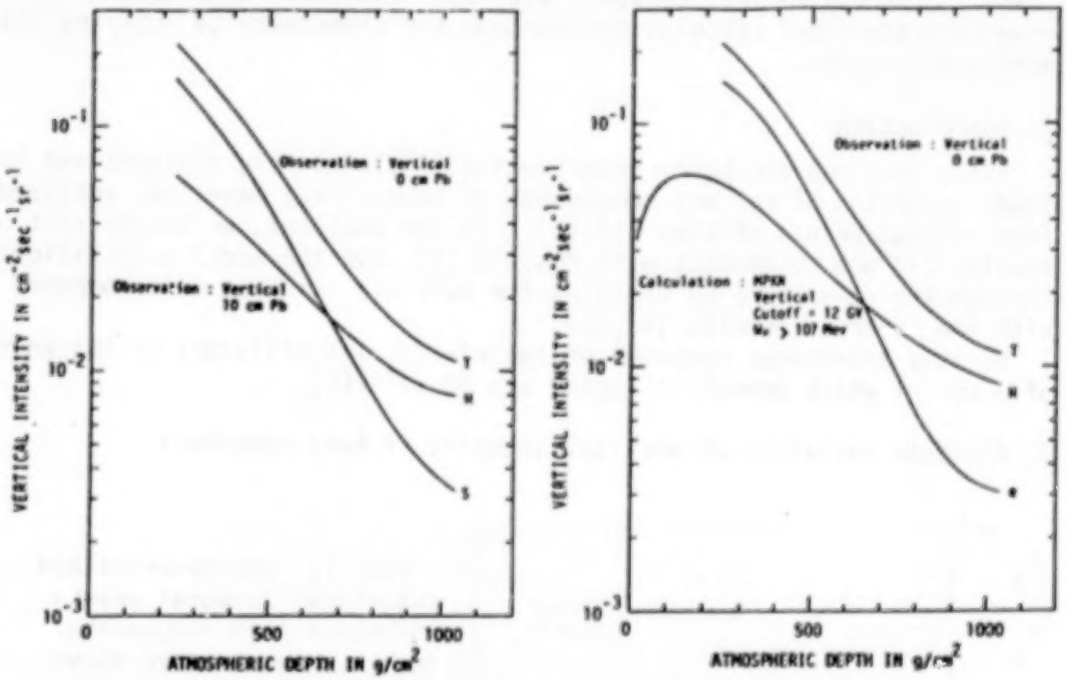


Fig. 2. The vertical intensities of the observed total component(T), of the observed hardcomponent(H), of the soft component(S), of the calculated total like in Fig. 1 (H'), of the (T)-(H') component(e) as a function of atmospheric depth.

We obtained the attenuation curves against the thickness of lead absorber at different altitudes for the vertical component (1979) (1). It is shown in the report that the curves are steeper for smaller thickness than 10 cm of lead and flatter for large thickness. It seems that this is due to the existance of electrons which are easily absorbable.

From what descrived above, we may say that the difference between (T) and (H'), namely (e) represents the electronic component. The energy of electrons are greater than nearly 10 MeV.

ORIGINAL PAGE IS
OF POOR QUALITY

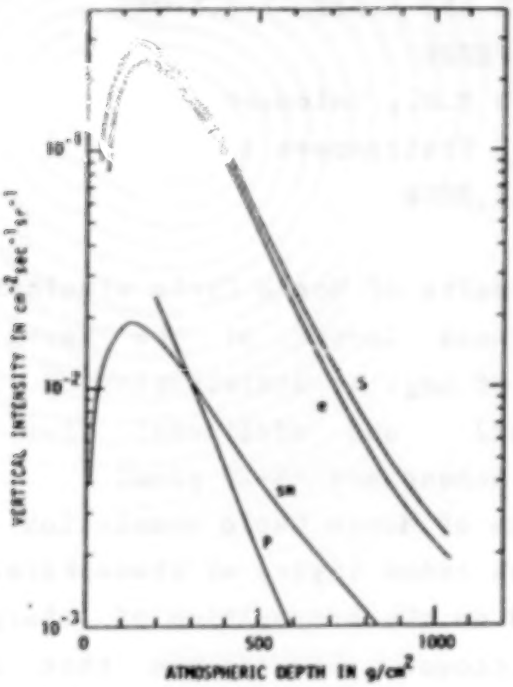


Fig. 3. Analysis of the soft component by B.Rossi. The curves represent vertical intensities as a function of atmospheric depth for slow mesons with momenta smaller than $3 \cdot 10^8$ eV/c (sm), proton (or other charged N-rays) with momenta between $4 \cdot 10^8$ eV/c and 10^9 eV/c (p), electrons of practically all energies above 10^7 eV (e).

Fig. 3 shows analysis of the soft component by B.Rossi (3). At small depth, there are enhancements of (s) and (e) by Rossi compared with ours. It may be caused by a enhancement of low energy electron at high latitude greater than 45°.

At atmospheric depth of 600 g/cm^2, the attenustion meanfree pathes for (s) and (e) by Rossi and us are nearly equal to 140 g/cm^2.

As mentioned above, it seems that the total,hard,soft,and electronic components are able to be explained by means of combining the observed result with the calculated one.

Reference

(1). Takahashi, K. (1979) Conf. Papers 16th ICPC, 4, 342.
(2). Takahashi, K. et al. (1983) Conf. Papers 18th ICRC, 10, 218.
(3). Rossi,B. (1948) Rev. Mod. Phys., 20, 537-583.
(4). Murakami, K. et al. (1979) Nuovo Cimento 2C, 635.
(5). Murakami, K. et al. (1981) Rep. CRRL, Cosmic-Ray Res. Lab. Nagoya Univ. No. 6.
(6). Takeuch, H. (1982) Sci. Papers IPCR, 75, 1.

N85-35080

ADDITIONAL FLUX OF PARTICLES AND ALBEDO-ELECTRONS IN UPPER ATMOSPHERE

Aitbaev F.B., Dyuisembaev B.M., Kolomeets E.V.
Kazakh State University, Timiryazeva St. 46,
Alma-Ata 480121,USSR

The paper presents the results of Monte Carlo simulation of albedo flux from the dense layers of the Earth"s atmosphere and the dependence of angular distribution on the rigidity of geomagnetic cut off and additional flux of particles at the depth in the atmosphere 15-20 g/sm^2.

Figure 1 shows the results of Monte Carlo simulation of albedo-electron fluxes from the dense layers of atmosphere. Influence of geomagnetic field on the propagation of charged particles was not taken into account. One can see that the albedo-electrons at energies more than 10 MeV show anisotropic angular distribution: fluxes of albedo-electrons at zenith angles close to horizon is $\sim$6 times greater than that directed vertically up. The ratio for the albedo-electrons at energies >100 MeV is $\sim$10. Integral energy spectrum within the range 10-100 MeV can not be described by power law function. It results from the fact that electrons produced by products of decay of pions directly contributes importantly to upward albedo. Averaged over zenith angle flux of albedo-electrons at geomagnetic equator at energies more than 10 MeV equals to 120 m^{-2} s^{-1} ster^{-1}, at energies more than 30 MeV - 80 m^{-2} s^{-1} ster^{-1} at energies > 100 MeV - 40 m^{-2} s^{-1} ster^{-1}.

Analysis of absorption curves of total ionising component obtained during balloon flights at latitude R_c =6,7 GV showed deformation of the depth dependence of cosmic ray intensity in the upper atmosphere (< 90 g/sm^2) after inversion of total solar magnetic field. Deformation of the form of the absorption curves (Table 1) one can explain by appearance additional flux of low energy particles.

Excluding variations produced by solar activity we reveal expected fluxes of abovementioned particles. Figure 2 shows dependence of additional flux on the depth for 1975. One can see that the curve of absorption has maximum at the depth 19-20 g/sm^2 and then drops sharply and at the depth 70 g/sm^2 its value is close to zero. Maximum of additional flux was observed in 1975-1976 at solar activity minimum. Effect was maximal at 15 g/sm^2 depth and was equal to 13%. Effect takes place in 1982-1983 that is after inversion of total solar magnetic field in 1979-1980 (Aitbaev et al., 1983) but its value is 2,3 times smaller than that in 1975.

Let's consider possible nature of the observed flux of low energy particles. First, it can be produced by meteorological effects. Analysis of the variations of barometrical pressure at the various depths in the atmosphere showed that the observed deformation of the form of the absorption curve was not produced by the variation of barometrical pressure.

Analysis of temperature variations at various depthes showed no anomalous change of temperature in the upper atmosphere and as a result no corresponding redistribution of air mass. Secondly, it can be produced by geomagnetic effects. Calculation of the variation of the rigidity cut off due to drift of balloon in the atmosphere over Alma-Ata revealed that maximal variation of counting rate produced by the factor did not exceed 0.3%. Analysis of the data on the variation of rigidity during magnetic storms in Alma-Ata region did not show possibility to attribute the observed flux of particles to the variation of cut off rigidity during magnetic storms. Third it can be produced by arrival to Alma-Ata of singly ionized atoms of < CNO > group. Calculations showed that the flux of the atoms allowed to explain additional flux of singly ionized atoms above 20 particles/ m^{-2} s^{-1} ster^{-1}. In order to discover the flux it is necessary to perform experiment,but experiment of the kind

ORIGINAL PAGE IS
OF POOR QUALITY

Figure 2. Absorption curve of additional flux of low energy particles (The data on of single counters obtained over Alma-Ata in 1975).

Figure 1. Dependence of electron albedo intensity at energies 10, 30, 100 MeV (histograms 1, 2, 3, correspondingly) at various geomagnetic latitudes on zenith angle.

N85-35080

has not been made at the bounúary of atmosphere.

Table 1. Annual means of counting rate of single counter calibrated to the maximum of absorption curve

Year	Depth in the atmosphere (g/sm^2)				
	10	15	21,5	30	50
1966	0,5487	0.6234	0.6890	0.7911	0.9309
1967	0.5586	0.6143	0.6920	0,7949	0.9282
1969	0.5420	0.6166	0.6799	0.7877	0.9271
1975	0.6200	0.6936	0.7730	0.8436	0.9497
1976	0.6182	0.6850	0.7655	0.837!	0.9465
1977	0.6191	0,6935	0,7725	0,8430	0.9442
1978	0.6098	0.6844	0.7593	0.8344	0.9460
1979	0.5831	0.6498	0.7324	0.8159	0.9355

R E F E R E N C E

Aitbaev F.B., Dyuisembaev B.M., Erkhov V.I., Likhoded V.A., Stekol'nikov N.V. Proc. 18th ICRC, 1983, v.10,p. 18-21.

SH-6.1-7

N85-35081

OBSERVATION OF ENERGY SPECTRUM OF ELECTRON ALBEDO IN LOW LATITUDE REGION AT HYDERABAD, INDIA.

Verma S.D. and Bhatnagar S.P.
Department of Physics, Gujarat University
Ahmedabad 380 009, INDIA

ABSTRACT

We present the preliminary results of the measurement of the energy spectrum of low energy (5-24 MeV) albedo electrons, moving upward as well as downwards, at about 37 km (~ 4 mb) altitude, over Hyderabad, India, in low latitude region. The flux and energy spectrum was observed by a bi-directional, multidetector charged particle telescope which was flown in a high altitude balloon on 8th December 1984. Results based on a quick look data acquisition and analysis system are presented here.

1. Introduction: The pioneer work of measurement of the flux and energy spectrum of electron and proton albedo was done at high altitude region over Palestine, Texas (Verma 1967) at high energies (20-1000 MeV). In low latitude region the flux of these albedo is expected to be somewhat less (Bhatnagar and Verma, 1983; Kothari and Verma, 1983) but larger at lower energies (5-40 MeV). In the present experiment measurements of low energy (5-24 MeV) Splash and Re-entrant albedo electron spectrum over Hyderabad at 4 mb altitude are reported. Details of the experimental set up and balloon flight are given by Verma et al (1985), for completeness a brief description is given in the next section.

2. Experimental Set-up: A multi detector charged particle telescope (Verma et al 1985) capable of observing simultaneously upward and downward moving singly charge particle (e,μ,p) was used. This telescope is shown in Fig.1. All particles incident on the telescope from above as well as below, and stopping in the central NaI (Tl) total energy detector C were selected for the present work. The arrival direction of the stopping particles was broadly known with the help of two sets of

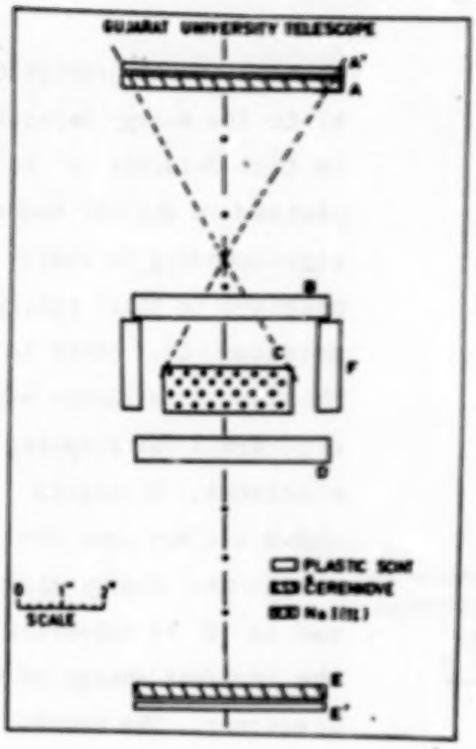


Fig.1

plastic scintillator detectors A B and D E in a combination such as AB C $\overline{DE}$ for downward and $\overline{AB}$ C DE for upward arriving particles. Cerenkov detectors A' and E' were used to identify relativistic electron among stopping singly charged particles. Pulses from total energy detector C and dE/dX detectors B and D were pulse height analysed event by event.

3. Energy Calibration: Various thin plastic detectors were tested using cosmic ray muons present at ground level. The total energy detector C was calibrated with γ-ray sources (e.g. Cs^{137} and Co^{60}) and mono-energetic electron beam of 8 MeV of Microtron of the Department of Physics, Poona University, Poona, India. Cosmic Ray muons and gamma ray sources were also used to test, calibrate and for constant monitoring and preflight check out of various detectors of charged particle telescope. A linear pulse generator was used to test linearity and stability of B, C, D detectors, its electronics and corresponding A/D convertors. Thus all the three P.H.A.'s were calibrated as well as checked for continuous operation for several weeks.

Whole system of CPT and flight electronics was taken through a temperature cycle in completely operating condition and it was found to have practically no drift of muon peak between 15°C and 25°C. Various data matrices were recorded and printed out time to time by quick look system. During these tests and long duration tests singles and coincidence rates, as well as peaks of muon P.H. distributions were monitored which were observed to be quite stable.

4. Data Analysis and Results: A typical two-dimensional pulse height distribution for downward incident is shown in Fig.2. In this the

ORIGINAL PAGE IS
OF POOR QUALITY

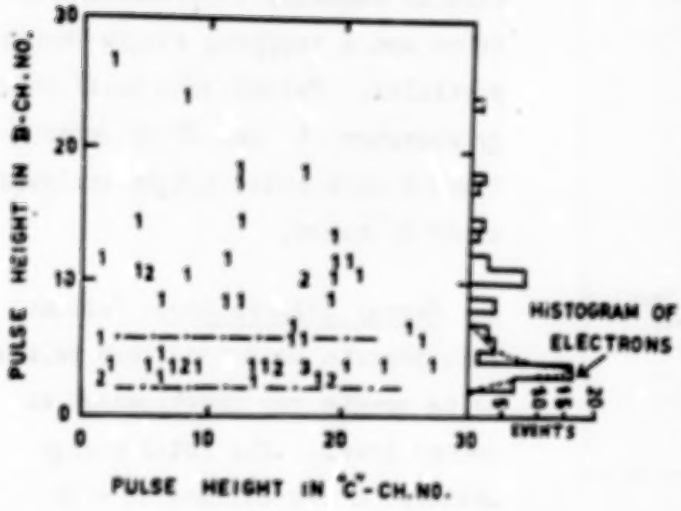


Fig. 2

channel number proportional to the energy deposited in thin detector B' is plotted vs channel number corresponding to energy observed in total energy detector C . Lines in the figure indicates expected track for stopping electrons. Histogram shows a clear peak for electrons. Energy observed in C is converted to the incident energy of the electrons. The events shown in the figure are part of sample of data recorded by quick look display and analysis system (Verma et al 1985). Using the event rate recorded, the geometrical factor (~ 13 cm^2 ster.) of the charged particle telescope and the two-dimensional matrix of stopping electrons shown in Fig.2 the flux and the energy spectrum of down moving low energy electrons were obtained. In the Fig.3 circles represent the flux and the spectrum of re-entrant albedo electronsat balloon altitude of ~ 4 mb in low latitude region, over Hyderabad, India, observed on 8th December 1984. Similarly squares represents the energy spectrum of splash albedo electrons.

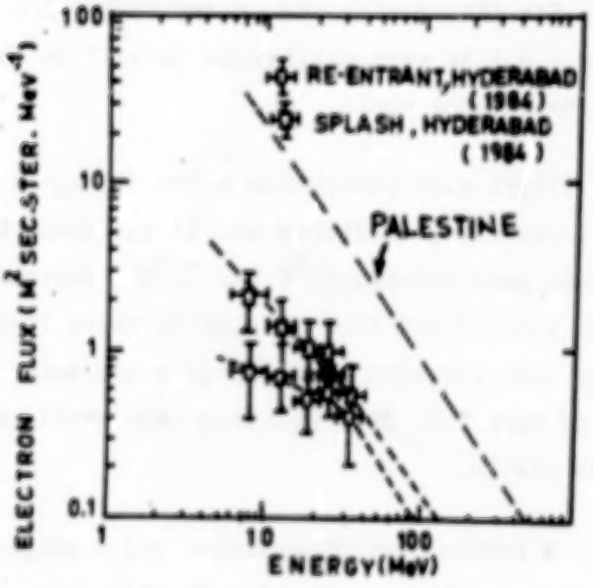


Fig.3

N85-35081

Lines shown in the figure are spectra observed over Palestine, Texas (Verma 1967).

5. Acknowledgement: Authors are thankful to ISRO for providing funds under Respond Program to fabricate Balloon payload and to carry out experiment in a high altitude balloon from Hyderabad. We are also thankful to UGC for providing funds for basic facilities and laboratory equipment to design, test and calibrate space science experiments. Thanks are also due to Dr. V.N. Bhoraskar and his senior and junior colleagues for providing mono energetic electron beam for energy calibration at Department of Physics, Poona University, Poona, India (1981). Thanks are due to Dr. P. Shea (Air Force Geophysical Lab., U.S.A.) for providing NaI(Tl) crystal, and Shri Vikram Shah for help (Metro, Kalol, India) in fabrication work. Thanks are also due to Dr. (Mrs.) Vijaya Sinha for discussions and reading the manuscript.

References

Bhatnagar S P & Verma S D, 17th ICRC, L, p. 266, (1981).

Bhatnagar S P & Verma S D , 18th ICRC, Bangalore, 3, p. 501, (1983).

Kothari S K & Verma S D, 18th ICRC, Bangalore, 3, p. 483, (1983).

Verma S D, Jr. Geop. Res. 72, 915, (1967).

Verma S D, Jr. Radio & Sp. Phys., 6, 171, (1977).

Verma S D, Bhatnagar S P & Kothari S K, 19th ICRC (HE-7), La Jolla, USA, (1985).

N85-35082

PROTON ALBEDO SPECTRUM OBSERVATION IN LOW LATITUDE REGION, AT HYDERABAD, INDIA

Verma S.D. and Kothari S.K.
Department of Physics, Gujarat University
Ahmedabad 380 009, INDIA

Abstract

The flux and the energy spectrum of low energy (30-100 MeV) proton albedos, have been observed for the first time in a low latitude region, over Hyderabad, India. The preliminary results, based on the quick look data acquisition and display system are presented. A charged particle telescope, capable of distinguishing singly charged particles such as electrons, muons, protons in low energy region, records the data of both upward as well as downward moving particles. Thus spectra of splash and re-entrant albedo protons have been recorded simultaneously in a high altitude Balloon Flight carried out on 8th December, 1985, over Hyderabad, India. Balloon floated at an altitude of ≈ 37 km (4 mb).

1. Introduction: The presence of low energy charged particles (albedo) among cosmic rays below the geomagnetic cut-off rigidity, have been predicted by Treiman (1953). However, systematic measurement of the flux and the energy spectrum of the albedos has been made by Verma (1967) at high altitudes, over Palestine, Texas. Large number of these are electrons, while protons are less in intensity. These measurements of proton albedos have been extended to high energies over same location upto thousands of MeV by Pennypacker et al (1973). It is expected that the spectrum of these albedo protons has a negative exponent. It is also expected, as shown by Kothari and Verma (1983) that the spectrum of albedos will be similar in low latitude regions such as Hyderabad, India. The flux however is higher at low energies. Next section describes briefly an experiment in which low energy proton albedo spectrum has been measured in low latitude region over Hyderabad, India.

2. Experiment: The flux and energy spectrum of upward moving splash albedo and downward moving re-entrant albedo protons have been first time

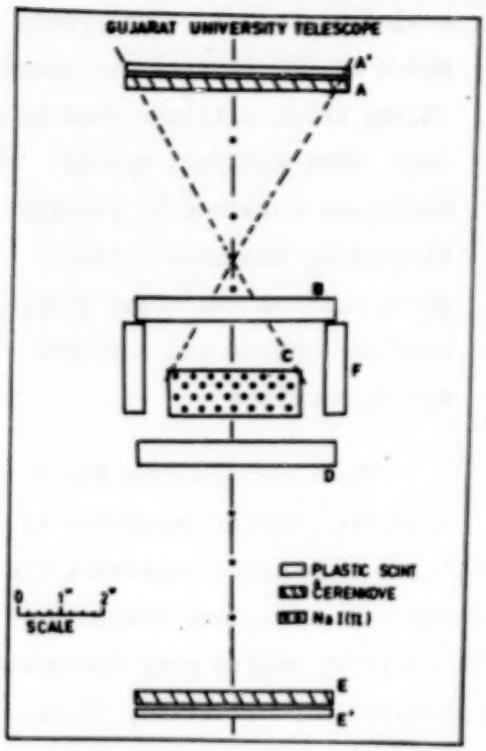


Fig.1

observed in 30-100 MeV energy interval in low latitude region at an altitude ≈ 37 km (≈ 4 mb), above Hyderabad, India. A bi-directional charged particle telescope, described in detail by Verma et.al. (1985), consisting of a total energy NaI(Tl) crystal detector, plastic scintillator and Lucite Cerenkov counters, was used for these observations. This telescope is shown in Fig.1. It has geometric factor ≈ 13 cm^2 Ster. It is capable of separating relativistic electrons from slow moving protons and muons, stopping in NaI(Tl) crystal detector 'C'. All charged particles, incident from upward and downward directions on the telescope and stopping in the NaI(Tl) total energy detector 'C', were selected for the present work. For the downward incident particles plastic scintillator 'B' was used as energy loss detector and D, F were used as anticoincidence counters. Similarly for upward moving particles scintillator 'D' was used as energy loss detector and B, F were used as anti-coincidence counters.

3. Calibration: Pulse amplitudes of B, C and D detectors are digitised by A/D convertors and recorded event by event (Verma et.al. 1985). The energy calibration of these detectors is done using ground level cosmic ray muons. These muons pass through the telescope and are registered as penetrating events. Their energy loss in B, C and D is well known from standard particle data book (Berger and Seltzer, 1966).

4. Data Analysis and Results: The proton flux measurement has been done for the energy range approximately 30 MeV to 105 MeV, both for upward and downward moving protons. A two-dimensional pulse height distribution for particles stopping in energy detector 'C' is shown in Fig.2, for upward

ORIGINAL PAGE IS
OF POOR QUALITY

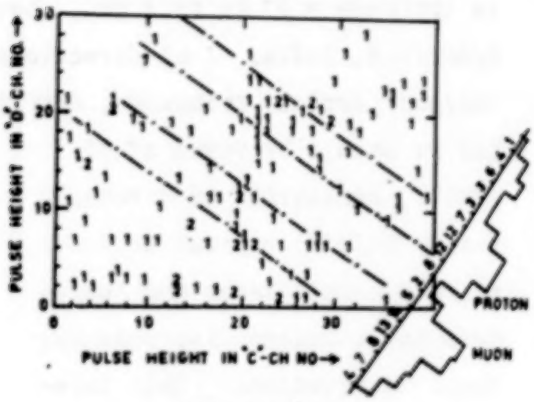
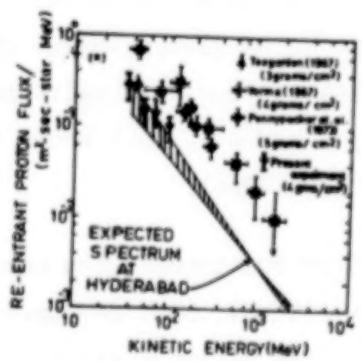


Fig.2

moving particles. The events shown in the Figures are taken during float altitude from quick look data analysis system. The histogram obtained by integrating along the track clearly gives protons and muons peaks both for upward and downward moving particles.

The flux observed for 4 different energy intervals is plotted in Fig.3 for upward moving particles. Triangles represent the flux for present observation of the re-entrant and splash albedo protons at balloon altitude of 4 mb in low latitude region over Hyderabad, India. The squares show the spectrum observed for Palestine, Texas, USA. The flux at Hyderabad, India, is lower for both re-entrant and splash albedo protons than at Palestine, Texas, as expected. The spectrum has a negative slope on a log-log graph, similar to that observed over Texas. The spectra of re-entrant albedo protons (Fig.3a) agree well with calculated spectrum. However, the flux and spectrum of splash albedo protons is somewhat higher than the calculated spectrum (Fig.3b). Data analysis with improved statistics to see if this trend persists, is under way.

Fig.3 a



Acknowledgement: Authors are thankful to I.S.R.O. for providing funds to fabricate balloon from Hyderabad. We are also thankful to U.G.C., India, for providing funds for basic facilities and laboratory equipment to design, test and calibrate space science experiments. Thanks are also due to Dr. V.N. Bhoraskar and his senior and junior colleagues for providing

N85-32085

mono-energetic electron beam for energy calibration at Department of Physics, Poona University, Poona, India (1981). Thanks are due to Dr. P. Shea (Air Force Geophysical Laboratory, U.S.A. for providing NaI(Tl) crystal, and Shri Vikram Shah (Metro, Kalol, India) for help in fabrication work. Thanks are also due to Dr. (Mrs.) Vijaya Sinha for discussing and reading the manuscript.

References:

Berger M.J. and Seltzer S.M. NASA Report, NASA SP-3036 (1966).

Bhatnagar S P and Verma S D, 17th ICRC SH.9, 1124, L, p.266 (1981).

Bhatnagar S P and Verma S D, 18th ICRC 3, p.501 (1983).

Kothari S K & Verma S D, 18th ICRC, Bangalore, India (1983)

Pennypacker C.R., Smoot G.F., Buffington A., Muller R.A., and Smith L.H., Jr. Geophys. Res.78, 1515 (1973).

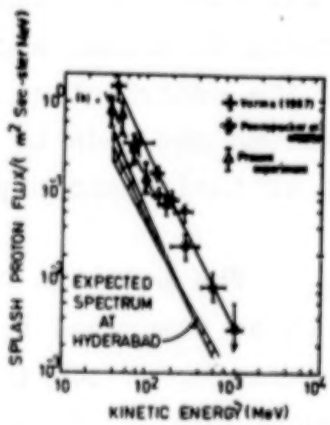
Treiman S.B., The Cosmic Ray Albedo, Phys.Rev., 91, 457 (1953).

Verma S D, Jr. Geophy. Res. 72, 915 (1967).

Verma S D, Jr. Radio & Sp. Phys., 6, 171 (1977).

Verma S D, Bhatnagar S P & Kothari S K, 19th ICRC HE-7, to be held in San Diego, California, USA, in August (1985).

Fig 3.b



N85-35083

SH 6.1-10

THE INFLUENS OF QUIET ASYMMETRIC MAGNETOSPHERE ON THE CUTOFF RIGIDITIES OF THE MAIN CONE

Tyasto M.I., O.A.Danilova
LOIZMIRAN, 2 line, Leningrad 199053
U S S R

1. Introduction. Some earlier studies (1-4) show that cutoff rigidities of cosmic-ray particles in the model magnetospheric fields of internal and external sources have daily variations caused by asymmetry of the magnetic field due to the currents induced at the magnetopause and tail currents.

The purpose of this paper is to examine cutoff rigidities of the charged particles coming down at the middle latitudes. The mathematical model that is used to specify the geomagnetic field for this investigation is due to Tsyganenko and Usmanov (5). This model of the magnetospheric field is based on the merged IMP-HEOS experimental data set and includes all known at the present time current systems of the magnetosphere: magnetopause, ring, magnetotail currents. Being based upon experimental data, this model implicitly takes into account the magnetic effect of field-aligned currents. Moreover this model includes the effects of changes in the tilt angle of the geodipole to the Sun-Earth line (Ψ) within the limits from -35° up to $+35^{\circ}$ according to annual and daily variations. A separate account of the contribution from different magnetospheric current systems has made it possible to track the Kp - dependence of their main physical parameters.

2. Methods. The suitable methods of trajectory calculations are to be described by Shea and Smart in (6). The trajectory-tracing of cosmic-ray particles is performed by the Gill modification (7) of the Runge-Kutta iteration method applied to the equation for charged particle motion

in a magnetic field:

$$\ddot{\bar{r}} = \frac{em}{c} \dot{\bar{r}} \times \bar{B}$$

The trajectory calculations has been performed for the particles with rigidities ranging from 750 Gv to the first forbidden trajectory with the step size of 0.01 Gv at the cosmic-ray stations Moscow, Irkutsk and Noricura in the superquiet conditions (Kp=0). A trajectory has been considered as forbidden if either 30 000 steps were not enough for a particle to pass beyond the sphere of the radius equal to 25 Earths radii or it returned to the Earth. The last allowed trajectory corresponding to main cone cutoff (1-2) was taken as the threshold rigidity.

3. Results and discussion. Cutoff rigidities were obtained for three Earths orbital positions (summer and winter solstice and equinox). Displaying the results of calculations one can see (Fig. 1) that the duirnal variation of the cutoff rigidities at the stations Irkutsk and Noricura have rather regular character with the maximum corresponding to the morning hours (9^h-12^h) and minimum in the evening (20^h-22^h). The time of the maxumum and minimum don't change appreciably throughout the year but the curve for the station Noricura has an additional maximum at the 18^h on the 22 of december. Diurnal variations for the station Moscow do not have such regular character. As the Fig. 1 shows the cutoff rigidity daily oscillation amplitude is greater for stations with lower cutoff rigidities. For example, the amplitude is 0.15 Gv and 0.02 Gv at the station Moscow and Noricura respectively. One can observe a certain variation of the differences between the maximum and minimum values of cutoff rigidities when the angle Ψ changes. These differences are maximal in summer and amount to 5%, 1.5%, 0.25% of the mean cutoff rigidity value for the stations Moscow, Irkutsk and Noricura respectively. The amplitude of the cutoff rigidity decreases by almost one half of that

quantity at the equinox. The latter result agrees with the Fig.4 of (8) showing that the cutoff rigidity daily variation (which is defind in (8) in the same manner as in the present study according to the last allowed trajectory) observed at the high-latitude station College (Alaska) is greater in summer than in winter or at the equinox.

4. Conclusions. Thus even in the superquiet periods (Kp= 0) the magnetosphere asymmetry causes the daily variations of cutoff rigidities at the middle-latitude stations which are expected to bring the greatest contribution to the observed daily variation of the cosmic- ray neutron intensity about 0.25% at the sea level station Irkutsk and 0.2% at the mount station Noricura.

References

1. Flückiger O.E. et al, (1981), On the effect of magnetospheric current systems on cosmic-ray cutoff rigidities., 17 Int. Cosmic Ray Confer., Paris, v.4, p.244-247

2. Flückiger O.E., (1982), Effects of asymmetric magnetosphere currents on cosmic radiation., AFGL - TR -82-0177

3. Smart D.F., et al, (1969), The daily variation of trajectory-derived high-latitude cutoff rigidities in a model magnetosphere., J. Geophis. Res., v.74,p.4731

4. Gall R., et al, (1971), The daily variation., Space Res., v.11

5. Tsyganenko N.A., A.V.Usmanov, (1982), Determination of the magnetospheric current system parameters and development of experimental geomagnetic field models based on data from IMP and HEOS satellites., Planet. Space Sci., v.30, p.985-998

6. Shea M.A., et al, (1976), Summary of cutoff rigidities calculated with the IGRF model for various epochs., ERP, NO 561, AFCRL-TR- 76-0115

7. Gill S., (1951), A process for the step-by-step integration of differential equations in automatic digital compu-

ting mashine., Proc. Cambridge Phil. Soc., v.47,p.47-96

8. Bravo S., (1981), The tilt effect on cutoff., Geophis. Internat., v.20-2, p.121-128

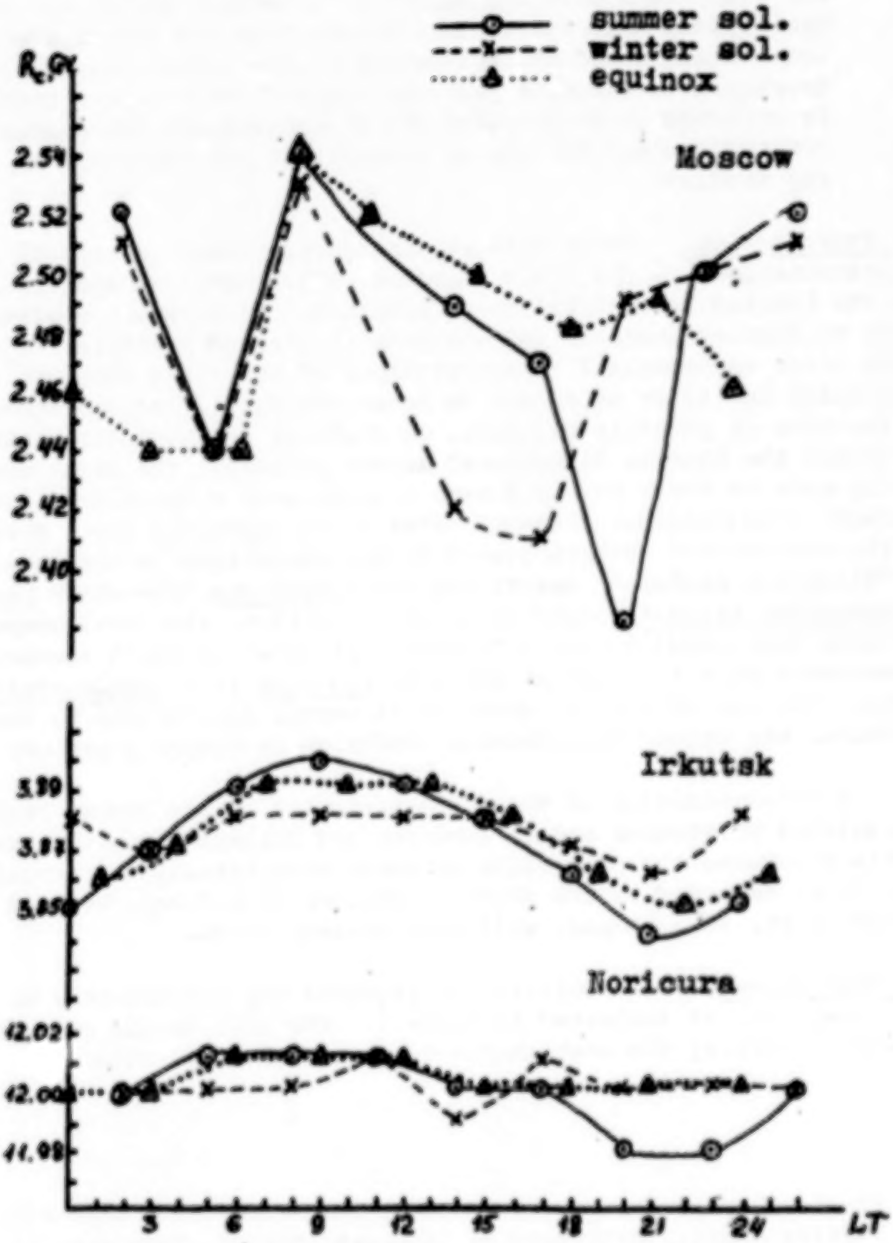


Fig.1. Daily variation of the vertical cutoff rigidities in the magnetospheric field according to the model of Tsyganenko-Usmanov (5).

N85-35084

RE-EVALUATION OF COSMIC RAY CUTOFF TERMINOLOGY

D. J. Cooke[1], J. E. Humble[2], M. A. Shea[3], D. F. Smart[3],
N. Lund[4], I. L. Rasmussen[4], B. Byrnak[4], P. Goret[5], N. Petrou[5]

ABSTRACT

The study of cosmic ray access to locations inside the geomagnetic field has evolved in a manner that has led to some misunderstanding and misapplication of the terminology originally developed to describe particle access. This paper presents what is believed to be a useful set of definitions for cosmic ray cutoff terminology for use in theoretical and experimental cosmic ray studies.

1. Introduction. Early work on cosmic ray motion in axially symmetric representations of the field (Stormer, 1930; Lemaitre and Vallarta (1936a, b) was limited to analytic considerations. More recent studies, which rely on digital computer calculations of charged particle trajectories in high order mathematical representations of the field (Shea et al., 1965) emphasize the study of access to locations within the geomagnetic field as a function of particle rigidity, in contrast to the earlier studies which examined the broader directional access picture. The terms used in the early work to refer to the access regions were carried over into the numerical computations, although often in an imprecise way. Whereas the early theoretical workers viewed access conditions in what may be called a "direction picture", describing the directions from which particles of a specified rigidity could or could not arrive, the later computer calculations have usually used a "rigidity picture" in which accessibility is considered as a function of particle rigidity in a single arrival direction. The use of the old geometrical terms, appropriate to the direction picture, has caused considerable confusion in rigidity picture studies.

A re-examination of the characteristics of the access regions distinguished by Stormer and by Lemaitre and Vallarta, together with a comparison between the properties of these analytically distinguished regions and those detected by the digital computer method has resulted in definitions which, it is hoped, will meet present needs.

2. Definitions. The definitions required may conveniently be subdivided by viewpoint, as indicated in Table 1. The list is not exhaustive, but seeks to portray the most useful quantities in each situation.

1. Physics Dept., University of Utah, Salt Lake City, Utah 84112, USA
2. Physics Dept., University of Tasmania, Hobart, Tasmania, Australia 7001
3. Air Force Geophysics Laboratory, Hanscom AFB, Bedford, MA 01731, USA
4. Danish Space Research Inst., Lundtoftevej 7, DK-2800, Lyngby, Denmark
5. Sect. d'Astrophys., Centre d'Etudes Nucl. de Saclay, Saclay, France

TABLE 1.

Summary of terms used in cutoff calculations. Quantities describing phenomena which are equivalent in both pictures are listed on the same line.

Direction Picture	Rigidity Picture
	Cutoff Rigidity
Allowed Cone	
Main Cone	Main Cutoff Rigidity
	First Discontinuity Rigidity
Shadow Cone	Shadow Cutoff Rigidity
Penumbra	Penumbra
Penumbral Band	Penumbral Band
	Primary Band
Stormer Cone	Stormer Cutoff Rigidity
Forbidden Cone	
	Upper Cutoff Rigidity
	Lower Cutoff Rigidity
	Horizon Limited Rigidity
	Effective Cutoff Rigidity
	Estimated Cutoff Rigidity

2.1. Directional Definitions. The following definitions appear to be appropriate for use with the directional picture. Each definition is for charged particles of a single specified rigidity value arriving at a particular point in the geomagnetic field.

Allowed Cone: The solid angle containing the directions of arrival of all trajectories which do not intersect the earth and which cannot possess sections asymptotic to bound periodic orbits (because the rigidity is too high to permit such sections to exist in the directions of arrival concerned).

Main Cone: The boundary of the allowed cone. The main cone is constituted in part by trajectories which are asymptotic to the simplest bound periodic orbits and in part by trajectories which graze the surface of the earth. (For this purpose the surface of the earth is generally taken to be at the top of the effective atmosphere.)

Forbidden Cone: The solid angle region within which all directions of arrival correspond to trajectories which, in the absence of the solid earth, would be permanently bound in the geomagnetic field. Access in these directions from outside the field is, therefore, impossible.

Stormer Cone: The boundary of the forbidden cone. In an axially symmetric field the surface forms a right circular cone.

Shadow Cone: The solid angle containing all directions of particle arrival which are excluded due to short range earth intersections of the approaching trajectories while loops within the local field line bundle are being traversed.

Penumbra: The solid angle region contained between the main cone and the Stormer cone. In general the penumbra contains a complex structure of allowed and forbidden bands of arrival directions.

Penumbral Band: A contiguous set of directions of arrival within the penumbra, the members of which are either all allowed or all forbidden.

2.2. Rigidity Picture Definitions. The following definitions are proposed as being applicable to the rigidity picture. Each definition refers to particles arriving at a particular site within the geomagnetic field from a specified direction.

Cutoff Rigidity: The location of a transition, in rigidity space, from allowed to forbidden trajectories, as rigidity is decreased. Unless otherwise defined, the value normally quoted in representing the results of computer calculations is, for practical reasons, the rigidity of the allowed member of the appropriate juxtaposed allowed/forbidden pair of trajectories computed as part of a spaced series of traces. Sometimes the term is employed to refer to the location of a notional transition from one region to another, for example at the Stormer cone, where an allowed trajectory may not perhaps exist at all.

Main Cutoff Rigidity, R_M: The rigidity value at which the direction concerned is a generator of the main cone as defined in the "direction picture". The associated trajectory is either one which is asymptotic to the simplest bound periodic orbit, or (owing to the presence of the solid Earth) is one which is tangential to the earth's surface.

First discontinuity rigidity, R_1: The rigidity associated with the first discontinuity in asymptotic longitude as the trajectory calculations are performed for successively lower rigidities, starting with some value within the allowed cone. The value of R_1 is approximately equal to the main cutoff as defined above.

Shadow Cutoff Rigidity, R_{SH}: The rigidity value at which the edge of the shadow cone lies in the direction concerned.

Penumbra: The rigidity range lying between the main and the Stormer cutoff rigidities.

Penumbral band: A continuous set of rigidity values within the penumbra, all members of which have the same general access characteristics, either all allowed or all forbidden.

Primary Band: The stable forbidden penumbral band which is associated with the earth intersection of a low point in the loop which lies at the last equatorial crossing before the trajectory (or its virtual extension in the assumed absence of the earth) takes on the characteristic guiding centre motion down the local field line bundle.

Stormer Cutoff Rigidity, R_S: The rigidity value for which the Stormer cone lies in the given direction. In a dipole field (and perhaps also in the real geomagnetic field) access for particles of all rigidity values lower than the Stormer cutoff rigidity is forbidden from outside the field. In a dipole approximation to the geomagnetic field, one form of the Stormer Equation gives the Stormer cutoff rigidity, in GV, as:

$$R_S = M \cos^4\lambda \,/\, \left\{ r^2\left[1 + \left(1 - \cos^3\lambda \cos A \sin Z\right)^{1/2}\right]^2\right\}$$

where M is the dipole moment and has a normalized value of 59.6 when r is expressed in units of earth radii, λ is the magnetic latitude, r is the distance from the dipole in earth radii, A is the azimuthal angle measured clockwise from the geomagnetic east direction (for positive particles), and Z is the angle from the local magnetic zenith direction.

Upper Cutoff Rigidity, R_U: The rigidity value of the highest detected allowed/forbidden transition among a set of computed trajectories. The upper cutoff rigidity can correspond to the main cutoff if and only if no trajectories asymptotic to bound periodic orbits lie at rigidities higher than this value. This can be identified from the nature of the trajectory associated with the main cutoff.

Lower Cutoff Rigidity, R_L: The lowest detected cutoff value (i.e., the rigidity value of the lowest allowed/forbidden transition observed in a set of computer calculations). If no penumbra exists, R_L will equal R_U.

Horizon Limited Rigidity, R_H: The rigidity value of the most rigid allowed trajectory found in a set of computer calculations performed for a below horizon direction at a location above the surface of the earth.

Effective Cutoff Rigidity, R_C: The total effect of the penumbral structure in a given direction may be represented usefully, for many purposes, by the "effective cutoff rigidity" - a single numeric value which specifies the equivalent total accessible cosmic radiation within the penumbra in a specific direction. "Effective cutoffs" may be either linear averages of the allowed rigidity intervals in the penumbra or functions weighted for the cosmic ray spectrum and/or detector response.

Estimated Cutoff Rigidity, R_{est}: A value obtained by using an empirically normalized equation to approximate the cosmic ray cutoff variation in the location of a particular point within a magnetic field in order to estimate a cutoff value pertaining to the point. This value can be found by use of a variety of interpolation techniques, one of which is application of the Stormer equation given above. Because the Stormer equation characterises the spatial variation of the cutoff rigidity, with appropriate normalization it may be used to obtain useful estimates of the various cosmic ray cutoff rigidities over intervals of latitude, longitude, zenith and azimuth, for example. In practice, estimates of the value of any cutoff can be obtained from adjacent calculated values to a reasonable accuracy by employing this method.

3. Discussion and Conclusion. Not all the cutoffs defined in the previous section exist for every location and direction. It should be borne in mind that, because the definitions have deliberately been kept usefully general, the application of the terms may require more detailed qualification in some individual circumstances. In addition, there is no doubt that other physically meaningful quantities exist. It is believed, however, that the cutoff concepts described in this paper presently have the greatest significance, and that the use of these definitions should alleviate most of the existing confusion and satisfy the current requirements of investigators involved in cosmic ray access studies.

4. Acknowledgements. DJC acknowledges support from the U.S. Air Force Geophysics Laboratory, under contract # F 19628-81-K0020.

References

Lemaitre, G., and M. S. Vallarta, "On the geomagnetic analysis of cosmic radiation", Phys. Rev., 49, 719-726, 1936a.

Lemaitre, G., and M. S. Vallarta, "On the allowed cone of cosmic radiation", Phys. Rev., 50, 493-504, 1936b.

Shea, M. A., D. F. Smart, and K. G. McCracken, "A study of vertical cutoff rigidities using sixth degree simulations of the geomagnetic field", J. Geophys. Res., 70, 4117-4130, 1965.

Stormer, C., "Periodische Elektronenbahnen im Felde Lines Elementarmagneton und ihre Anwendung auf Bruches Modellverauche und auf Eschenhagnes Elementarwellen des Erdmagnetismus", Astrophys., 1, 237-274, 1930.

332 N85-35085

THE USE OF THE McILWAIN L-PARAMETER TO ESTIMATE COSMIC RAY VERTICAL CUTOFF RIGIDITIES FOR DIFFERENT EPOCHS OF THE GEOMAGNETIC FIELD

M.A. Shea and D.F. Smart
Air Force Geophysics Laboratory
Hanscom AFB, Bedford, Massachusetts 01731, U.S.A.

L.C. Gentile
Physics Research Division, Emmanuel College
400 The Fenway, Boston, Massachusetts 02115, U.S.A.

ABSTRACT

A useful relationship employing the McIlwain L-parameter to estimate vertical cutoff rigidities has been derived for the twenty-five year period 1955-1980.

1. Introduction. It is intuitively pleasing to utilize the dipolar geometry inherent in the McIlwain L-parameter to order cosmic ray cutoff rigidities. However, in some areas of the world, secular changes in the geomagnetic field between 1955 and 1980 have been large enough to produce significant differences in both the vertical cutoff rigidities and in the L-value for a specified position. In this paper we show that these changes are complimentary, and it is possible to derive a relationship between the L-value and vertical cutoff rigidity that can be used for the twenty-five year period, 1955-1980.

2. Background. The trajectory-tracing process is generally recognized as the most accurate method for calculating cosmic ray cutoff rigidities. Since cutoff rigidities are a function of latitude, longitude, altitude, zenith angle, azimuthal angle, and field model, using the trajectory-tracing method for a large number of positions and directions is impractical. For this reason, cosmic radiation data from many experiments are often ordered by the cutoff rigidity values in the vertical direction.

One method of estimating vertical cutoff rigitities was suggested by Smart and Shea (1967) who derived three equations for the relationship between the McIlwain L-parameter (McIlwain, 1961) and (1) the upper calculated cutoff, (2) the lower calculated cutoff and (3) the effective cutoff rigidities.* These three equations were derived using cutoff rigidities calculated for the Finch and Leaton (1957) field for Epoch 1955.0 and the Jensen and Cain (1962) field for Epoch 1960. The equations thus derived for the upper calculated cutoff, the lower calculated cutoff and the effective cutoff rigidities were essentially the same for both field models.

At the time of this original work, cosmic ray physicists did not recognize that the secular changes in the geomagnetic field were sufficiently large over a relatively small time period (on the order of 25 years) to significantly affect the detection, at the surface of the earth, of galactic cosmic radiation above 1 GV. It was not until Shea (1971) suggested

* In the paper of Smart and Shea (1967), these rigidity values were called main cone cutoff, Stormer cone cutoff and effective cutoff, respectively. Since new terminology for cosmic ray cutoffs has been agreed upon by scientists working in this area (Cooke et al., 1985) we will use these newer terms throughout this paper.

that the decrease in vertical cutoff rigidity at Huancayo over a 20-year period might possibly be observed as an increase in the background radiation measured by a stable neutron monitor at this location (since verified by Cooper and Simpson, 1979), that it became apparent that the secular changes in the geomagnetic field might be sufficiently large in some areas of the world that changes in cutoff rigidities, and consequently measured changes in cosmic radiation, would occur.

In view of the changes in the main geomagnetic field and the related changes in the calculated cutoff rigidities, we feel it is necessary to re-examine the use of the McIlwain L-parameter to estimate cosmic ray vertical cutoff rigidities for the 25-year period 1955-1980.

3. Method. The world grid of vertical cutoff rigidities calculated each 5° in latitude and 15° in longitude for Epochs 1955, 1965 and 1980 (Shea et al., 1968; Shea and Smart, 1975, 1983) and the McIlwain L-values (McIlwain, 1961) calculated for these same locations comprised the basic data sets used for this analysis. All calculations were made for an altitude of 20 km above the surface of the earth as defined by the international reference ellipsoid. Both the vertical cutoff rigidities and the McIlwain L-values were calculated using the geomagnetic field coefficients for the appropriate Epoch (i.e., 1955, 1965 and 1980).

Expressing the cosmic ray cutoffs by an equation of the form $R=KL^{\gamma}$ where R is the cutoff rigidity, L is the McIlwain L-value, K is a constant and γ is an exponent, K and γ were evaluated by a least-squares fit of the (1) upper calculated cutoff rigidity, (2) effective cutoff rigidity and (3) lower calculated cutoff rigidity. Each of the equations derived for each Epoch, together with the RMS error for each set of calculations, is given in Table 1. It is important to note that vertical cutoff rigidities < 0.20 GV were omitted from these calculations. Since the cosmic ray equator and the equator defined by the minimum L-value do not coincide, all grid points within a band ±5 degrees of either equator (or between the two equators) were also omitted. Figure 1 illustrates the locations of each of these equators for Epoch 1980.

Table 1. Equations to estimate cutoff rigidities for various Epochs

Epoch	R_U =	R_C =	R_L =
1955	$16.727\ L^{-2.0054}$ RMS = 6.28 %	$16.192\ L^{-2.0177}$ RMS = 5.48 %	$14.992\ L^{-1.9986}$ RMS = 6.61 %
1965	$16.722\ L^{-2.0212}$ RMS = 6.70 %	$16.222\ L^{-2.0418}$ RMS = 5.52 %	$14.942\ L^{-2.0296}$ RMS = 6.98 %
1980	$16.717\ L^{-2.0206}$ RMS = 7.06 %	$16.222\ L^{-2.0441}$ RMS = 5.74 %	$14.823\ L^{-2.0311}$ RMS = 7.27 %
Composite 1955-1980	$16.762\ L^{-2.0174}$ RMS = 6.67 %	$16.237\ L^{-2.0353}$ RMS = 5.64 %	$14.912\ L^{-2.0185}$ RMS = 7.19 %

4. Discussion. From an inspection of the equations in Table 1 it is evident that the constants K and γ for each of the three vertical cutoff rigidities are essentially independent of Epoch. The root mean square values are also similar, with the slightly larger RMS values for 1980 attributed to the evolution of the magnetic field and an increasing divergence between the cosmic ray equator and the minimum L equator. The area between these two equators has increased approximately 10 percent between 1955 and 1980.

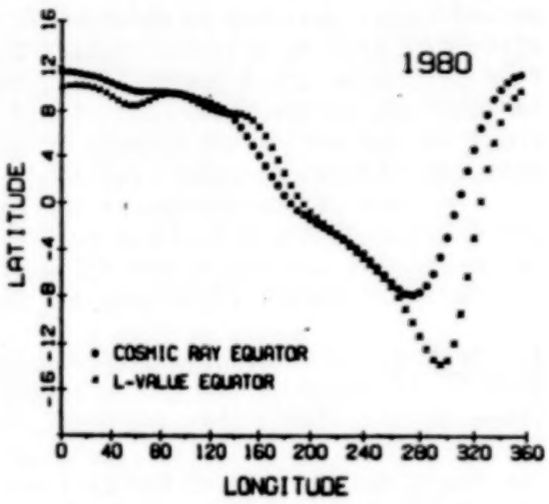


Figure 1. Geographic location of the cosmic ray equator and the minimum L equator for 1980.

Since these equations were almost identical we combined the data for all three Epochs in an effort to determine a suitable equation for the upper calculated cutoff, the effective cutoff and the lower calculated cutoff for the entire 25-year period from 1955 to 1980. Again all locations with cutoffs less than 0.20 GV were omitted from the analysis. Since the location of the cosmic ray equator changed between 1955 and 1980 (Shea et al., 1983), and different equatorial grid locations had been removed for each Epoch, we removed all locations within ±5° of any of the three equators (i.e., if a particular location had been removed for the analysis for one Epoch, it was removed from all three data sets for the composite analysis). Again the constants K and γ were determined by the method of least squares. The results for this composite set of over 1875 data

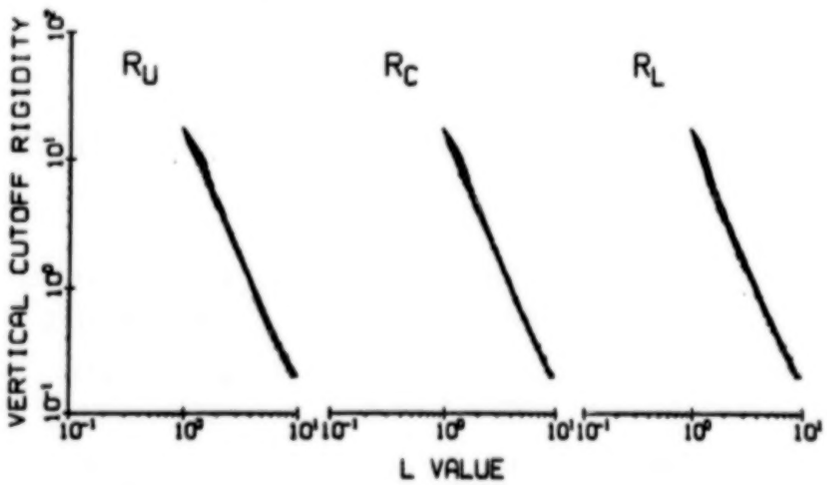


Figure 2. The upper calculated vertical cutoff rigidity (R_U), effective vertical cutoff rigidity (R_C), and lower calculated vertical cutoff rigidity (R_L), plotted as a function of the McIlwain L-value. The data set is a composite of the world grid locations for 1955, 1965 and 1980.

ORIGINAL PAGE IS
OF POOR QUALITY

points are graphically illustrated in Figure 2; the equations are given in the bottom line of Table 1. From these results we feel that it is possible to use these three equations to estimate the upper, effective and lower cutoff rigidities for the entire period 1955 to 1980 provided the L-values are calculated using the field model for the same time period that the cutoffs are needed.

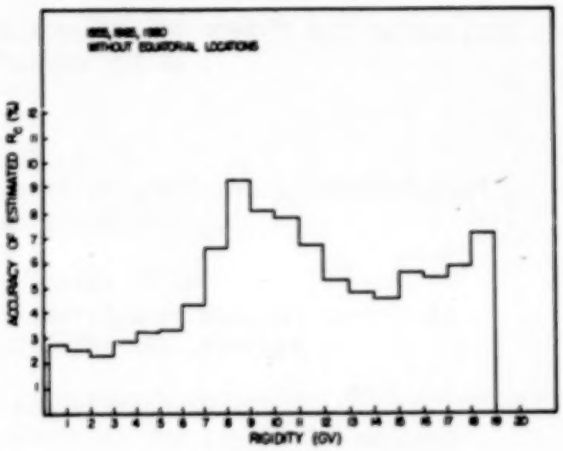


Figure 3: Accuracy of estimated vertical cutoff rigidity.

Figure 3 illustrates the accuracy that can be expected for an estimate of the effective vertical cutoff rigidity as a function of rigidity. These data were obtained by calculating for each location the percentage difference (in rigidity) between the cutoff rigidity value determined by the trajectory-tracing procedure and the value estimated by using the L-value approximation equation. These individual percentages were then averaged as a function of intervals of estimated cutoff rigidity.

5. Conclusion. From this analysis we conclude that the McIlwain L-parameter can be used to estimate upper calculated, effective, and lower calculated vertical cutoff rigidities for the period 1955 to 1980.

Acknowledgments. We gratefully acknowledge the computational assistance of A.A. Bathurst. LCG acknowledges support from the U.S. Air Force Geophysics Laboratory under contract No. F19628-82-K-0039.

References

Cooke, D.J., J.E. Humble, M.A. Shea, D.F. Smart, N. Lund, I.L. Rasmussen, B. Byrnak, P. Goret, and N. Petrou, Paper No. SH 6.1-11, 19th International Cosmic Ray Conference, these proceedings, 1985.

Cooper, J.F., and J.A. Simpson, 16th International Cosmic Ray Conference, Conference Papers, 12, 176, 1979.

Finch, H.P., and B.R. Leaton, Monthly Notices Roy. Astron. Soc., Geophys. Suppl., 7, 314, 1957.

Jensen, D.C., and J.C. Cain, J. Geophys. Res., 67, 3568, 1962.

McIlwain, C.E., J. Geophys. Res., 66, 3681, 1961.

Shea, M.A., 12th International Conference on Cosmic Rays, Hobart, Conference Papers (University of Tasmania), 3, 859, 1971.

Shea, M.A., and D.F. Smart, 14th International Cosmic Ray Conference, Conference Papers, 4, 1298, 1975.

Shea, M.A., and D.F. Smart, 18th International Cosmic Ray Conference, Conference Papers, 3, 415, 1983.

Shea, M.A., D.F. Smart, and John R. McCall, Can. J. Phys., 46, S1098, 1968.

Shea, M.A., D.F. Smart and L.C. Gentile, 18th International Cosmic Ray Conference, Conference Papers, 3, 423, 1983.

Smart, D.F., and M.A. Shea, J. Geophys. Res., 72, 3447, 1967.

N85-35086
SH 6.1-13

ESTIMATING THE CHANGE IN ASYMPTOTIC DIRECTION DUE TO SECULAR CHANGES IN THE GEOMAGNETIC FIELD

E. O. Fluckiger
Physikalisches Institut, Universitat Bern, Sidlerstrasse 5,
CH-3012 Bern, Switzerland

D. F. Smart and M. A. Shea
Air Force Geophysics Laboratory, Hanscom Air Force Base,
Bedford, Massachusetts 01731, U.S.A.

L. C. Gentile and A. A. Bathurst
Emmanuel College, 400 The Fenway, Boston, MA, 02115, U.S.A.

ABSTRACT

The concept of geomagnetic optics, as described by the asymptotic directions of approach, is extremely useful in the analysis of cosmic radiation data. However, when changes in cutoff occur as a result of evolution in the geomagnetic field, there are corresponding changes in the asymptotic cones of acceptance. We introduce here a method of estimating the change in the asymptotic direction of approach for vertically incident cosmic ray particles from a reference set of directions at a specific epoch by considering the change in the geomagnetic cutoff.

1. Introduction. Cosmic ray particles must travel along specific allowed trajectories through the geomagnetic field to reach a location on or near the earth. In order to relate cosmic ray intensity variations observed at different cosmic ray stations to the cosmic ray flux in space the concept of asymptotic directions of approach was developed (see McCracken et al., 1968, for a review). By application of the asymptotic directions of approach the user need not be concerned about the specific details of the allowed cosmic ray trajectories and can relate any specific cosmic ray particle with a unique direction in space. For a cosmic ray particle with rigidity R, arriving at a specific location (characterized by the geographic latitude Λ and the geographic longitude Φ) from a direction of incidence (described by the zenith angle θ and the azimuthal angle ϕ) the asymptotic direction of approach is given by the unit vector $\underline{A}(R,\Lambda,\Phi,\theta,\phi)$ pointing in the reverse direction to the particle's velocity vector prior to the particle's entry into the geomagnetic field. For the purposes of this paper and for a specific location the vector $\underline{A}$ is specified for vertical incidence in terms of the geocentric coordinate system as asymptotic latitude, $\lambda(R) = \lambda(R,R_1(\Lambda,\Phi), \theta = 0°)$ and asymptotic longitude, $\psi(R) = \psi(R,R_1(\Lambda,\Phi), \theta = 0°)$ where R_1 is the rigidity corresponding to the first discontinuity in asymptotic longitude as defined below.

The allowed rigidity spectrum of cosmic ray particles arriving from a specific direction at any location in the geomagnetic field contains distinct fiducial marks: R_1, the rigidity associated with the first discontinuity in asymptotic longitude occurring as the trajectory calculations are progressing down through the rigidity spectrum, and R_U, the rigidity at and above which the trajectory calculations yield allowed

orbits. The rigidity value R_1 is always greater than or equal to R_U if both are determined by employing the same uniform discrete (usually 0.01 GV) rigidity intervals in the trajectory calculations. R_1 is, in general, a value extremely close to the main cone cutoff rigidity as defined by Lemaitre and Vallarta (1936). A change in the geomagnetic field has an almost equivalent effect on both the rigidity corresponding to the first discontinuity and the vertical upper cutoff, and results in a similar effect on the vertical effective cutoff rigidity (Fluckiger et al., 1983a, 1983b).

Fluckiger et al., (1983b) have shown that geomagnetic disturbances reduce the cutoff rigidity in a predictable manner dependent on the strength and longitudinal structure of the magnetic perturbation and the longitudinal difference between the magnetic perturbation and the observing location. Furthermore, the change in asymptotic longitude (down to the first discontinuity) also behaves in a similarly predictable manner. Therefore the asymptotic directions of approach during perturbed geomagnetic conditions can be deduced with considerable accuracy from the asymptotic directions computed using the quiescent geomagnetic field if the associated change in cutoff rigidity is known. In this paper we extend these concepts to include the time evolution of the geomagnetic field on the asymptotic direction of approach for cosmic ray particles arriving at a particular location.

2. Method. We will define the terms $\delta\lambda^*(R)$ and $\delta\psi^*(R)$ as $\delta\lambda^*(R) = \lambda'(R) - \lambda(R-\delta R_1)$, and $\delta\psi^*(R) = \psi'(R) - \psi(R-\delta R_1)$, where $\delta R_1 = R_1' - R_1$, and the primed values indicate the evolved geomagnetic field and the unprimed values indicate the reference geomagnetic field. When these values are plotted as a function of rigidity, it has been found that there are practically no changes for $\delta\lambda^*$ down to the rigidity value of R_1'. Therefore, we may set $\delta\lambda^* = 0°$ (Fluckiger et al., 1983b). For $\delta\psi^*$ only small residual changes on the order of several degrees are found down to rigidities approaching the value of R_1. For any particular location and for rigidities up to several GV above the main cutoff the following expressions can be used to describe the correlation between the asymptotic directions in an evolved geomagnetic field and the asymptotic directions in a reference geomagnetic field:

$$\lambda'(R) = \lambda(R - \delta R_1), \text{ and } \psi'(R) = \psi(R - \delta R_1) + C \cdot \delta R_1,$$

where C is a measure of the residual change $\delta\psi^*$. This procedure is valid only for rigidities larger than R_1 or R_1', respectively.

At rigidities below R_1 no similar relation has been found, although coherent clusters of trajectories may be distorted uniformly by magnetic changes. It has been shown that the main features of allowed and forbidden regions in the penumbra are conserved to a certain extent in a perturbed geomagnetic field (Fluckiger et al., 1979, 1982). However, the asymptotic longitudes of the allowed trajectories of the fine detailed structure in the cosmic ray penumbra continue to be quasi-random.

3. Application. We have applied this procedure by comparing the asymptotic directions calculated for the International Geomagnetic Reference Field Epoch 1965.0 with those calculated for epoch 1980.0 for cosmic ray stations and world grid locations. To illustrate this application, we

the evolved values. We would expect a close comparison between the asymptotic directions above the first discontinuity (R_1) such that $\psi(R_1^*) + \Delta R = \psi'(R_1^{*'}) + \Delta R$ where ΔR represents an arbitrary rigidity value above R_1^* and $R_1^{*'}$. Here ψ denotes the asymptotic longitude in the reference field and ψ' the asymptotic longitude in the evolved field. R^* and $R^{*'}$ are approximations to the rigidity value of the first discontinuity obtained by examining the gradient in the change of the asymptotic direction with rigidity as the first discontinuity is approached from rigidity values above the main cutoff. The values selected to approximate the first discontinuity in asymptotic direction, R_1^* and $R_1^{*'}$ were the rigidity values where the gradient in asymptotic direction was greater than 1000° per GV and increased by more than 1.5 times in the next 0.01 GV increment. Examination of these results and comparison with other calculations have shown that this approximation is close to and slightly greater than the rigidity of the first discontinuity calculated using very small rigidity intervals.

For the examples given in the following tables, the increment of rigidity added to the approximation of the first discontinuity value was the change in rigidity of the first discontinuity between the reference field and the evolved field. This value was used because it was sure to be in the set of continuous asymptotic directions above the main cutoff in both data sets. In Table 1 we illustrate the results for cosmic ray stations at locations where the geomagnetic cutoff is decreasing with time. In Table 2 we show results for cosmic ray stations at locations where the cosmic ray cutoff is increasing with time. An inspection of the asymptotic longitudes given in the second and third columns from the right in these tables indicates that the asymptotic longitudes for the specified rigidity values are quite similar.

4. Conclusions. We have illustrated that the asymptotic directions for an evolved geomagnetic field for rigidity values above the R_1 value (the first discontinuity in asymptotic direction progressing down through the rigidity scale) can be obtained from a "known" reference set of asymptotic directions if the change in cutoff is known.

5. Acknowledgments. A. A. Bathurst and L. C. Gentile acknowledge support from the U. S. Air Force Geophysics Laboratory under Contract No. F19628-82-K-0039.

References.

Fluckiger, E., H. Debrunner, D.F. Smart, and M.A. Shea, 16th International Cosmic Ray Conference, Conference Papers, 4, 273, 1979.

Fluckiger, E., AFGL-TR-82-0177, 1982.

Fluckiger, E.O., D.F. Smart, and M.A. Shea, J. Geophys. Res., 88, 6961, 1983a.

Fluckiger, E.O., D.F. Smart, and M.A. Shea, 18th International Cosmic Ray Conference, Conference Papers, 3, 431, 1983b.

Lemaitre, G., and M.S. Vallarta, Phys. Rev., 50, 493, 1936.

McCracken, K.G., U.R. Rao, B.C. Fowler, M.A. Shea, and D.F. Smart, Cosmic Rays, Annals of the IQSY, Vol. 1, Edited by C.M. Minnis, Chapter 14, 198, The MIT Press, Cambridge, Massachusetts, 1968.

N85-35086

ORIGINAL PAGE IS
OF POOR QUALITY

TABLE 1.
Changes of Asymptotic Longitude for Cosmic Ray Stations Where the Cutoff is Decreasing.

ϕ for 1980 at $R_1^{*'} + |\Delta R|$ = ϕ for 1965 at $R_1^{*} + |\Delta R|$, where ΔR = ($R_1^{*'}$ for 1980) - (R_1^{*} for 1965)

STATION NAME	GEOGRAPHIC LAT	GEOGRAPHIC LONG	EPOCH 1965 R_U	EPOCH 1965 R_1^{*}	EPOCH 1965 ϕ	EPOCH 1980 R_U'	EPOCH 1980 $R_1^{*'}$	EPOCH 1980 ϕ'	ΔR_1^{*}	1965 RIG	1965 ϕ	1980 ϕ'	1980 RIG
Ahmedabad	23.01	72.61	15.90	15.92	46	15.77	15.79	51	-0.13	16.05	329	327	15.92
Alma Ata	43.20	76.94	6.92	6.93	36	6.87	6.90	30	-0.03	6.96	358	355	6.93
Brisbane	-27.50	153.01	7.39	7.42	121	7.22	7.26	116	-0.16	7.58	31	30	7.42
Buenos Aires	-34.58	301.50	10.59	10.61	266	10.12	10.15	246	-0.46	11.07	130	124	10.61
Chacaltaya	-16.31	291.85	12.85	12.87	257	12.53	12.54	263	-0.33	13.20	144	144	12.87
Climax	39.37	253.82	3.14	3.24	146	3.12	3.22	153	-0.02	3.26	124	128	3.24
Gulmarg	34.07	74.42	12.33	12.35	44	12.24	12.26	45	-0.09	12.44	336	337	12.35
Hermanus	-34.42	19.22	5.02	5.06	307	4.83	4.86	311	-0.20	5.26	215	214	5.06
Hobart	-42.90	147.33	2.10	2.12	44	2.06	2.08	43	-0.04	2.16	13	11	2.12
Huancayo	-12.05	284.67	13.24	13.25	266	12.91	12.93	253	-0.32	13.57	142	140	13.25
Mexico City	19.33	260.82	9.57	10.24	257	9.27	9.94	250	-0.30	10.54	121	123	10.24
Mildura	-34.23	142.22	4.56	4.59	97	4.43	4.46	87	-0.13	4.72	11	11	4.59
Mt. Wellington	-42.92	147.24	2.03	2.11	49	1.99	2.07	49	-0.04	2.15	14	12	2.11
Palestine	31.75	264.35	4.74	4.90	185	4.69	4.86	194	-0.04	4.94	145	147	4.90
Potchefstroom	-26.70	27.10	7.68	7.72	346	7.49	7.53	337	-0.19	7.91	247	245	7.72
Sydney	-33.60	151.10	5.16	5.19	86	5.06	5.09	84	-0.10	5.29	21	21	5.19
Tbilisi	41.72	44.80	6.96	7.00	357	6.95	6.97	14	-0.03	7.03	322	321	7.00

TABLE 2.
Changes of Asymptotic Longitude for Cosmic Ray Stations Where the Cutoff is Increasing.

ϕ for 1980 at $R_1^{*'} + |\Delta R|$ = ϕ for 1965 at $R_1^{*} + |\Delta R|$, where ΔR = ($R_1^{*'}$ for 1980) - (R_1^{*} for 1965)

STATION NAME	GEOGRAPHIC LAT	GEOGRAPHIC LONG	EPOCH 1965 R_U	EPOCH 1965 R_1^{*}	EPOCH 1965 ϕ	EPOCH 1980 R_U'	EPOCH 1980 $R_1^{*'}$	EPOCH 1980 ϕ'	ΔR_1^{*}	1965 RIG	1965 ϕ	1980 ϕ'	1980 RIG
Athens	37.97	23.72	8.98	8.99	355	9.06	9.08	340	0.09	9.08	280	275	9.17
Bologna	44.50	11.33	5.41	5.44	297	5.52	5.55	295	0.11	5.55	231	231	5.66
Budapest	47.50	18.90	4.74	4.77	309	4.82	4.83	309	0.06	4.83	254	253	4.89
Calgary	51.08	245.91	1.16	1.22	123	1.17	1.24	125	0.02	1.24	95	94	1.26
Deep River	46.10	282.50	1.13	1.19	170	1.25	1.32	150	0.13	1.32	80	85	1.45
Dourbes	50.10	4.60	3.42	3.44	298	3.57	3.60	294	0.16	3.60	208	215	3.76
Durham	43.10	289.16	1.67	1.69	197	1.84	1.86	179	0.17	1.86	93	103	2.03
Fukushima	37.75	140.48	11.36	11.38	104	11.45	11.47	100	0.09	11.47	40	38	11.56
Irkutsk	52.47	104.03	3.92	3.95	34	3.95	3.98	42	0.03	3.98	359	4	4.01
Jungfraujoch	46.55	7.98	4.81	4.82	300	4.91	4.94	289	0.12	4.94	222	220	5.06
Kerguelen Is.	-49.35	70.22	1.24	1.31	299	1.15	1.31	315	0.00	1.31	299	315	1.31
Kiel	54.33	10.13	2.39	2.50	298	2.59	2.61	307	0.11	2.61	224	226	2.72
Kiev	50.72	30.30	3.74	3.77	335	3.79	3.80	332	0.03	3.80	290	289	3.83
Leeds	53.82	358.45	2.26	2.35	265	2.41	2.48	267	0.13	2.48	191	204	2.61
Lomnicky Stit	49.20	20.22	4.21	4.24	314	4.28	4.31	329	0.07	4.31	256	257	4.38
Magadan	60.11	151.01	2.22	2.33	52	2.34	2.36	45	0.03	2.36	9	6	2.39
Morioka	39.70	141.13	10.47	10.51	122	10.61	10.63	109	0.12	10.63	35	32	10.75
Moscow	55.47	37.32	2.60	2.61	320	2.50	2.62	313	0.01	2.62	302	297	2.63
Mt. Norikura	36.12	137.56	12.02	12.04	09	12.09	12.11	107	0.07	12.11	45	46	12.18
Mt. Washington	44.30	288.70	1.41	1.50	165	1.55	1.66	214	0.16	1.66	89	96	1.82
Mussala	42.18	25.58	6.50	6.51	346	6.56	6.57	343	0.06	6.57	281	280	6.63
Pic du Midi	42.93	0.25	5.58	5.61	294	5.80	5.81	306	0.20	5.81	204	209	6.01
Predigtstuhl	47.70	12.88	4.59	4.60	309	4.68	4.70	299	0.10	4.70	235	232	4.80
Rome	41.90	12.52	6.35	6.37	318	6.50	6.54	324	0.17	6.54	235	236	6.71
Tokyo-Itabashi	35.75	139.72	12.12	12.13	115	12.19	12.21	99	0.08	12.21	45	41	12.29
Yakutsk	62.02	129.72	1.74	1.85	22	1.78	1.87	32	0.02	1.87	352	356	1.89
Zugspitze	47.42	10.98	4.62	4.64	314	4.72	4.75	298	0.11	4.75	230	227	4.86

340 N85-35087 SH 6.1-14

EMPIRICAL MODEL FOR THE EARTH'S COSMIC RAY SHADOW AT 400 KM: PROHIBITED COSMIC RAY ACCESS

J. E. Humble
Department of Physics, University of Tasmania
Hobart, Tasmania, 7001, Australia

D. F. Smart and M. A. Shea
Air Force Geophysics Laboratory
Hanscom AFB, Bedford, MA., 01731, U.S.A.

ABSTRACT

It is possible to construct a unit sphere of access that describes the cosmic radiation allowed to an earth-orbiting spacecraft. In the upper hemisphere of the allowed portion of the cosmic ray sphere of access, the cosmic ray cutoffs can be ordered by application of Stormer theory in offset dipole coordinates. In the downward hemisphere, in westerly directions, the cosmic radiation is allowed at large zenith angles well below the spacecraft-earth horizon, with particles being able to reach satellites at 400 km altitude from large zenith angles of ~140° at azimuthal directions equatorward of west in both the northern and southern hemispheres. We have found it is possible to model the occluded portion of the cosmic ray sphere of access as a circular projection having a diameter bounded by the satellite-earth horizon. Maintaining tangency at the eastern edge of the spacecraft-earth horizon, this optically occluded area is projected downward (toward the earth) by an angle β which is a function of the magnetic field inclination and cosmic ray arrival direction. This projected plane, corresponding to the forbidden area of cosmic ray access, is bounded by the spacecraft-earth horizon in easterly directions, and is rotated around the vertical axis by an angle α from the eastern direction, where the angle α is a function of the offset dipole latitude of the spacecraft.

1. Introduction. It is of considerable interest to evaluate the primary cosmic ray flux which is able to reach a satellite in earth orbit from any specified direction of arrival. The evaluation requires a knowledge of the geomagnetic cutoffs for all four pi steradins of possible arrival directions at all points along the spacecraft orbit. In practice, in order to keep the computational problem within manageable (and economic) bounds, cutoffs are generally calculated for a selected set of directions at each of a chosen set of representative directions along the orbit (Humble et al., 1979). It is then necessary to interpolate cutoffs for directions intermediate to those for which explicit calculations have been performed for a specific location, and for locations intermediate to those for which calculations have been undertaken for particular directions of particle arrival. For the upper hemisphere of arrival directions Smart and Shea (1977) showed that the cutoffs are reasonably

well ordered, for some locations, by Stormer theory. Humble et al. (1979) pointed out that at least some of the exceptions were due to the intervention of the 'shadow cone'.

Recent interest has focussed on particles arriving at the spacecraft from the lower, earthward facing, hemisphere. We have previously reported finding that primary cosmic rays are able to reach a satellite orbiting at quite low altitudes from zenith angles considerably larger than that of the local earth horizon. For a spacecraft at 400 km these angles are at least 140° at all latitudes we have investigated, and reach 150° at one location (Humble et al., 1983; Humble, 1983). We report here results from some further calculations of this type, and then describe a possible method for modelling the bounds of that portion of the unit sphere of access to which primary particles of any energy are unable to gain access because of the presence of the solid earth.

2. Method. A trajectory tracing technique has been devised to search rigidity/zenith-angle space for accessible arrival directions (Humble et al., 1983). The search proceeds, for a given location and azimuth, in the directions of increasing zenith angle and decreasing rigidity, until no further accessible directions of arrival can be found. A number of searches has been performed using this technique. Each was started at a zenith angle of 100° which is above the local satellite-earth horizon at all altitudes considered (Humble, 1984). It was found that, for zenith angles greater than that of the satellite-earth horizon, primary particles are only able to reach the satellite from generally westerly directions. Such particles experience a $\underline{V} \times \underline{B}$ force having a positive radial component in the final stages of their approach to the satellite. Their trajectories consequently have positive upwards curvature, and the local zenith angle of arrival can be greater than that of the satellite-earth horizon. The range of accessible azimuths increases with altitude, as would be expected.

3. Results at 400 km. A considerable number of trajectories have been calculated for the 400 km altitude. In analyzing these results we have found that it is possible to construct a unit sphere of access which describes the access of primary cosmic ray particles to any given detector. In the relatively simple case of a ground-level location the upper half of this sphere is totally allowed and the lower hemisphere is totally forbidden, due to the presence of the earth. For a satellite in earth orbit the situation is more complicated. All of the upper hemisphere is allowed to cosmic rays of some energy, as is part of the downward hemisphere. The latter may be divided into two parts. One is essentially a continuation of the allowed upper hemisphere - an annulus of allowed directions at zenith angles z_e such that $90° \leq z_e < z_h$, where z_h is the zenith angle of the horizon seen by the spacecraft. The second region lies at $z_e > z_h$, opens to the west, and is due to the $\underline{V} \times \underline{B}$ effect discussed in the previous section. The remainder of the sphere of access represents forbidden directions of arrival. We have found that it is possible to model the forbidden, or occluded, portion of the unit sphere of access, in an empirical manner and to varying degrees of accuracy, by the following technique.

Consider the equatorial plane of the unit sphere surrounding the spacecraft. Project the sphere onto a plane calibrated as a polar plot in zenith (as radius) and azimuth. Rotate the disc corresponding to the equatorial plane of the sphere through an angle β about a magnetic north south axis, until its projection, now an ellipse, on the polar plot has a minor axis which matches the distance between the largest and smallest values of zenith indicated. The rotated plane is then relocated, and subsequently rotated about a vertical axis, such that it is tangent to the satellite-earth horizon at the inner surface of the unit sphere at an angle α from the easterly direction. In our present model α is equal to the offset dipole latitude of the spacecraft. Figure 1 shows examples of the fit between the model curve and the points calculated for particular directions of arrival. The rms difference is about 3°; however, the greatest differences occur at positions where there is the largest deviation between the invariant latitude and the offset dipole latitude contours.

4. Results for Higher Altitudes. In general, it has been found that the largest accessible zenith angle for a given latitude, longitude, and azimuth, would also increase with increasing altitude. More detailed results are given by Humble et al. (1983) and Humble (1983). We have not yet applied the empirical model described in this paper to altitudes of 1000 km and above. Preliminary calculations have, however, been made. As the altitude increases above 1250 km a range of large zenith angles in generally easterly directions begins to become accessible, while smaller (but still below-horizon) zenith angles in the same azimuthal directions remain inaccessible. The higher altitude permits particles approaching the general region of the satellite at low altitudes from the west to pass above the top of the atmosphere more than one gyro-radius beneath the satellite. Such particles will arrive at the satellite from easterly directions at large zenith angles. The following table summarizes the results which have been obtained.

Altitude km	Maximum Zenith Angle
400	150°
600	156°
800	166°
1000	172°
1250	180°

Note that a zenith of 180° for an altitude of 1250 km means that primary cosmic ray nuclei are able to reach a satellite at that altitude from the nadir direction, directly underneath it, for at least one location somewhere on the orbit. This does not, however, mean that all possible directions of arrival are accessible at such a location. Easterly arrival directions at below-horizon zeniths are still forbidden.

References.

Humble, J.E: Proc. Astron.Soc.Australia, 5, 265-267, 1983.

Humble, J.E., D.F.Smart, and M.A.Shea: 16th ICRC, Kyoto, Conference Papers, 4, 303-308, 1979.

Humble, J.E., D.F.Smart, and M.A.Shea: 18th ICRC, Bangalore, Conference Papers, 442-445, 1983.

Humble, J.E., AFGL-TR-84-0258, 1984.

Smart, D.F., and M.A.Shea: 15th ICRC, Plovdiv, Conference Papers, 11, 256-261, 1977.

ORIGINAL PAGE IS
OF POOR QUALITY

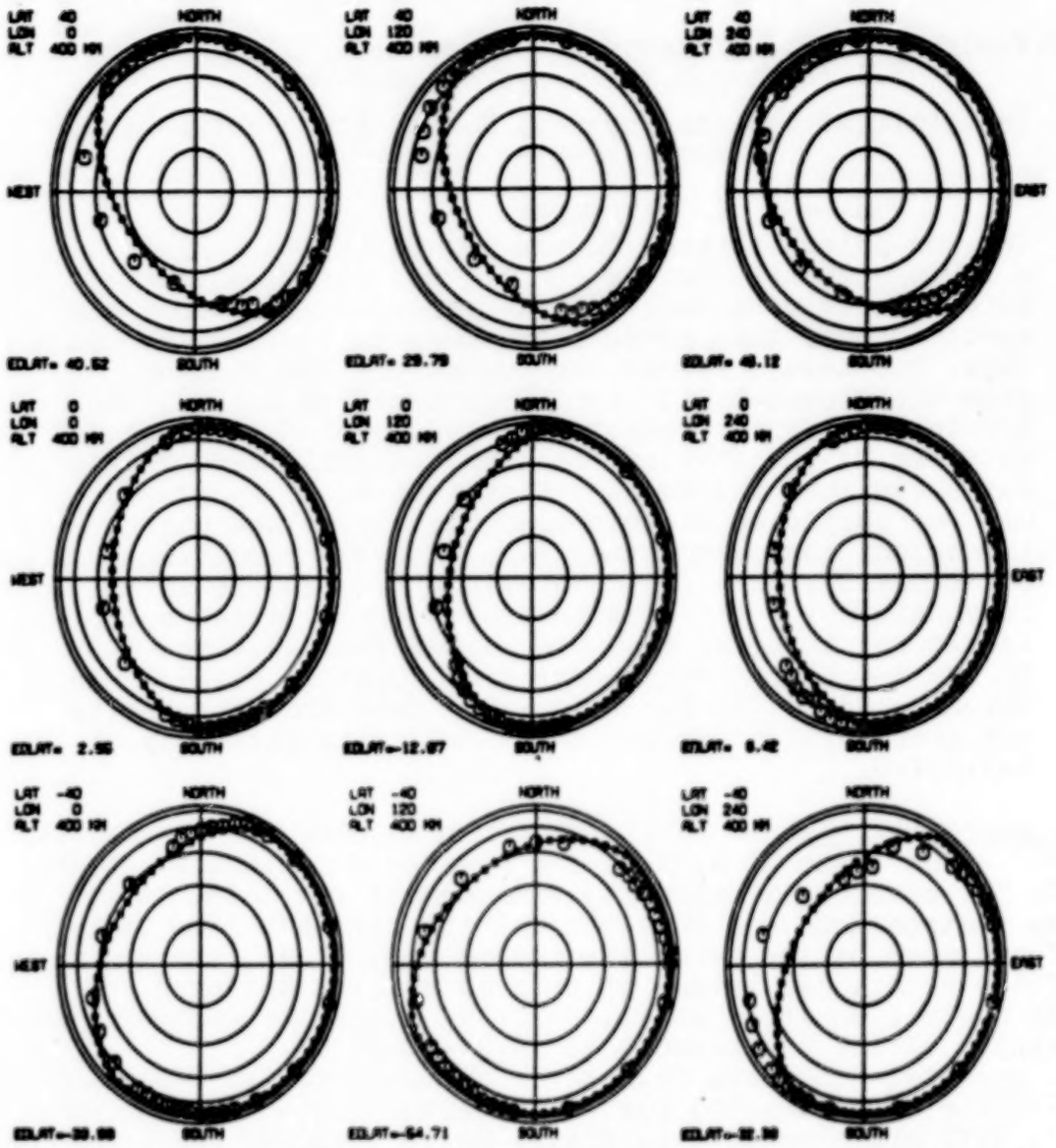


Figure 1. Polar projections of the downward hemisphere beneath an orbiting satellite. The occluded area beneath a satellite to which access is completely forbidden to galactic cosmic radiation of any energy is the area enclosed by the large dots in each projection. In this projection the observer is at the center of the spacecraft. This projection is looking downward from the center of the spacecraft; concentric rings represent 15 degree projections from the spacecraft equator to the nadir. Zero degrees is upward from the top of the spacecraft, 90 degrees is the spacecraft equator, and 180 degrees is in the nadir direction. At the 400 km altitude the local satellite-earth horizon is 109.8° from the zenith. The large open dots in each panel indicate where the maximum accessible zenith directions were determined by the cosmic ray trajectory-tracing method. The line connected with small solid squares indicates the result of applying the model described in this paper.

N85-35088

SH 6.1-15

PENETRATION OF SOLAR PROTONS INTO THE EARTH'S MAGNETOSPHERE ON NOVEMBER 22,1977

E.V.Gorchakov,V.G.Afanasyev,K.G.Afanasyev,P.P.Ignatyev, V.A.Iozenas,M.V.Ternovskaya,G.G.Zenchev

Institute of Nuclear Physics, Moscow State University, Moscow 119899, USSR

ABSTRACT

The low polar-orbiting Cosmos-900 satellite carried a large geometric factor (~0.9 m^2 sr) Cerenkov counter which may be used to study the particle anisotropy and spectrum near the proton increase peak in solar cosmic rays. The data obtained supplement the information from the ground-based cosmic ray stations and help understand different temporal behaviour of the increases detected at the stations because the whole set of data has shown that the angular distribution of solar cosmic ray particles in interplanetary space was narrow throughout the observation time, thereby resulting, particularly, in a rapid variation of particle intensity near the poles. The power-law index of the solar cosmic ray integral spectrum varied from -2.4 to -5.2 in the 1-4 GV rigidity range from 10.31 to 11.25 UT on November 22, 1977. The flare-time data from all orbits are indicative of an increased radiation intensity on L=3.5-4.0.

1. Introduction. The solar flare responsible for the Nov.22, 1977 event began at 9.45 UT and reached a maximum at 10.07 UT. The cosmic ray intensity enhancement was detected by the neutron monitors with the cut-off rigidity less than 5 GV and also by the satellite instruments /1-3/. The onset of the cosmic ray intensity enhancement was detected by the neutron monitors at 10.10-10.15 UT and the maximum intensity of the enhancement at 10.35-10.50 UT.

2. Results. The data from three channels of the Cerenkov detector on Cosmos-900 for the interval 8.45-11.50 UT, 22. 11, 1977 are presented in fig.1. Up to 10.30 UT the counting rate corresponds to the latitude behaviour of the cosmic-ray intensity during the quiet period. During the interval 10.30-11.50 UT, while Cosmoc-900 was outside the equatorial region, the intensity enhancement associated with the penetration of cosmic ray into the Earth's magnetosphere was observed. (The peak at 9.35 and 11.12 UT is detected during the passage of the satellite through the Brazil magnetic anomaly). The intensity enhancement was, mainly, due to protons of the solar cosmic rays since the electron contribution for our instrument according to ref. /4/, could not be > 4%. According to the 11th channel detected only particles with $Z \geq 2$, the intensity of these particles during the flare was smaller, at least, by a factor of 200 than the proton intensity. The maximum intensity

of >400 MeV protons was higher by 600 % then the pre-flare level, being equal to (2.3 ± 0.5) 10^4 $m^{-2}s^{-1}sr^{-1}$.

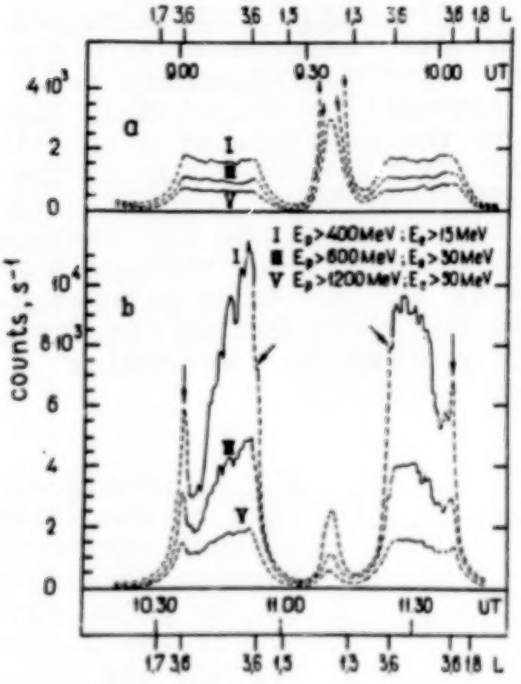


Fig.1. The cosmic ray count rates for three channels:
a) in the quiet time (prior to the flare),
b) during the flare.
The broken curves refer to the satellit passage through the region of action of geomagnetic cut-off.

ORIGINAL PAGE IS
OF POOR QUALITY

The intensity distributions are characterized by the peaks and irregularities in the count rates marked by arrows in fig.1b. Note that all these cases were detected on L = 3.6 which proves the spatial behaviour of these variations. Accord to the neutron monitors the latitude distribution is also characterised by irregularities /5/.

It must be noted that this phenomenon is observed on the magnetic shells where the energy of the geomagnetic cut-off is compared with the energy threshold of the instrument.

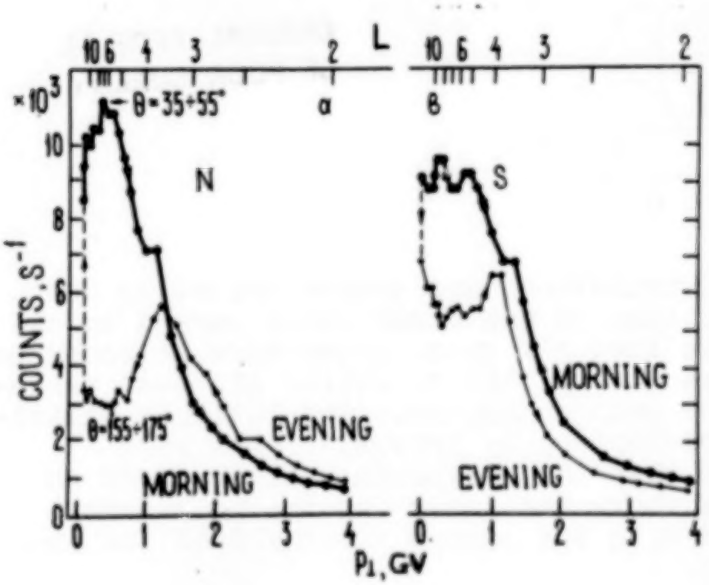
3. **Discussion.** The peaks and irregularities in the count rates cannot be attributed to the radiation belts and to the particle precipitation from them /2/. Hence, the peaks on L = 3.6 are connected with the propagation of cosmic rays into the magnetosphere and, possibly, with the albedo particles and, also the quasi-trapping effects.

In our case the flux anisotropy and the longitudinal distribution of the receipt cones are, seemingly, the simplest explanation of the count-rate peculiarities.

On L = 3.6 the receipt cones have a wide longitude distribution and the instrument detects an averaged intensity. In the region adjoining L = 3.6 from the side of high latitudes the longitude distribution of the cones is always narrow and in the case of peaks the sunward particles /6/ are, mainly detected whose intensity is known to be less then the mean intensity.

From our data it is possible to determine the flux ani-

sotropy during the flare. The angles θ between the axis of the solar proton flux in the interplanetary space and the axis of the asymptotic receipt cone for two points of the satellite trajectory (fig.2) in the high-latitude region of the Northen hemisphere, have been determined from the calculations /6/ including the outer magnetosphere currents. The difference in the intensities detected in these regions can be accounted for by the presence of a positive cosmic-ray flux anisotropy. If the time behaviour of the intensity in the interval 10.38-10.51 UT is neglected (according to the high-latitude neutron monitors the changes in intensity were small in the interval) the antisun-to-sunward ratio of particle fluxes for the above pitch-angles is estimated from our data to be ~6. During the interval 10.15-10.35 UT this ratio is close to 4 according to the neutron-monitor data /7/.



Pig.2a. Counting rate of the first channel versus the vertical rigidity of the geom. cut-off in the flight through the Northern hemisphere during the flare. The arrows mark the time flow. The thin and thick lines correspond to the satellite flight in the evening and morning sides of the Earth. Pig.2b. the same in the Southern hemisphere.

Assuming that in the South hemisphere in the high-latitude region the outer magnetosphere currents exert the same influence upon the asymptotic directions as they do in the Northern hemisphere, we may conclude that the solar cosmic-ray anisotropy decreases with time and maintains a positive sign (at least for high-latitude regions).

The spectra of observed particles within the rigidities 1-4 GV were obtained using the movement of the satellite in space. The calculations shown that in the interval 10.31-10.35 UT the index of the integral spectrum γ was 2.4 and in the intervals (10.54-10.58, 11.21-11.25, 11.40-11.44 UT) γ was on the average 4.1, 4.3 and 4.2, respectively. The slope of the spectra was not always the same, the index γ increased with rigidity, reaching the value 5.2. It follows that at 10.35 UT bulk of 400 MeV protons did

N85-35088

not reach the observing point, and during the next interval the spectrum was equilibrium.

In conclusion we note one more feature of the intensity distribution of the solar cosmic rays, namely the regular small peaks of intensity observed in the first channel every 2 minits throughout the flare observation period. We have failed to connect these variations with the peculiarities of the instrument operation and tentatively attribute them either to the solar or magnetospheric pulsations or to the propagation of particles in the interplanetary space. In the latter case these variations may be connected with the value of free path of particles.

References

1. Solar-Geophysical Data,1978, 405, Part II
2. E.V.Gorchakov et al.,Sov. journal Space Res.,1984, 22, 2, 312
3. M.Gro et al. The book of collected papers in Russian "Cosmic Rays", No. 21, 1980, 70
4. E.A.Devicheva et al.,Proc. of 16th ICRC, Kyoto, 1979,v.5, 170
5. A.G.Penton et al. Proc. of 16th ICRC, Kyoto, 1979, v. 4, 34
6. M.A.Shea et al. UAG-9, World Data Center A, 68, 1970
7. M. Debrynner et al. Proc. of 18th ICRC, Bangalore, 1983, v. 4, 144

N85-35089

SH 6.I-I6

DYNAMICS OF THE PENETRATION BOUNDARIES OF SOLAR PROTONS DURING A STRONG MAGNETIC STORM

G.A. Glukhov, Yu.P. Kratenko
The Tashkent State University, 700095, Tashkent, USSR

Yu.V. Mineev
Institute of Nuclear Physics, Moscow State University, Moscow II9899, USSR

Abstract. On the basis of the Intercosmos-I9 data, the variations in the equatorial penetration boundary of solar protons with E_p = 0.9-8.0 MeV during a strong magnetic storm of April 3-5, I979 are studied. The dynamics of this boundary is compared with the dynamics of the outer trapping boundary of electrons with E_e = 0.3-0.6 MeV. Alongside with the solar-proton penetration we study the structure of the real magnetic field. The uniqe data on the thin structure of development of a magnetospheric substorm have been obtained for the first time.

In our previous paper /I/ we have analyzed the features of the latitudinal profiles of the SCR protons with E_p = = 0.9-8.0 MeV in the polar regions during a strong magnetic storm of April 3-5, I979 on the basis of the Intercosmos-I9 data (a perigee of ~ 500 km, an apogee of ~ I000 km, a period of ~ I00 min, an inclination of ~ 74°). The present paper is a study of the dynamics of the equatorial penetration boundary (Λ_{pc4}) of the SCR protons for this magnetic storm (D_{st}-variation and the AE-index are presented in the lower part of fig.I). The variations in Λ_{pc4} are studied alongside with the dynamics of the outer trapping boundaries of electrons with E_e = 0.3-0.6 MeV and E_e = 0.9-I.2 MeV which enables us to investigate the thin structure of development of magnetospheric substorms. Observations of electrons and protons were made by a semiconductor telescope aboard Intercosmos-I9 (IC-I9)/2/.

The outer trapping boundary of electrons was ment to be the threshold sensitivity of the instrument to the particles with a given energy. This definition of the boundary is justified because near the trapping boundary there was a rapid decrease in the particle intensity. Λ_{pc4} was determined from the onset of a rapid decrease in intensity.

The dynamics of Λ_{pc4} during the event in question is shown in the upper half of fig.I. Data I refer to the day (open circles) and morning (solid circles) sectors MLT and data II, to the evening (open circles) and night (solid circles) sectors. Here is also given the averaged location of Λ_{pc4} for protons with $E_p \geq$ I MeV in the day (broken lines I), morning (solid lines I), evening (broken lines II) and night (solid lines II) sectors MLT according to the Cosmos-900 (C-900) and Cosmos-I067) data.

The comparison between the results of observations made on various satellites shows that at the day and night hours MLT the C-900 and C-I067 data, is available, are in good

agreement with the IC-I9 data. At the morning hours MLT on the main phase of the April, 3 magnetic storm at 20-23 UT the IC-I9 data are I-2° higher than the C-900 and C-I067 data, at the maximum D_{st} the IC-I9 data coincide with the C-900 and C-I067 data and at the end of the recovery phase the IC-I9 data coincide or are I° lower than the C-900 and C-I067 data at the pre-noon hours (9.5-II.5) MLT. A strong shift of the evening bouhdary to lower latitudes down to 55° was observed nearly an hour earlier on the IC-I9 as compared with C-900 and C-I067. According to the IC-I9 data, the evening boundary there shifted to larger latitudes, in conformity with the D_{st}-variation, and again to lower latitudes and the second minimum in the position of this boundary was observed at the maximum of the main phase of the storm. The complex analysis of the main parameters of the magnetosphere disturbance (D_{st}, AE) and the parameters of the interplanetary space (the magnitude and direction of the IMF, the solar wind velocity and density) shown that the strong shift of the evening boundary to lower latitudes is caused by the development of the magnetospheric substorm.

So, the IC-I9 data confirm the conclusion made in ref. /3/ about the prior and leading decrease in Λ_{pe} in the evening sector, that is connected with the asymmetric intrusion of particles of the storm ring current and the magnetic field decrease, yet, this effect is observed on the phase of development of an individual substorm and not of the storm as in ref./3/.

The evening boundary of penetration of solar protons coincides with the night boundary on the recovery phase of the storm.

The IC-data are obtained at later morning and later evening hours MLT which accounts for the differences in the location of the morning and evening boundaries determined from the IC-I9, C-900 and C-I067 data.

The dynamics of the outer trapping boundary of electrons is shown in the middle part of fig.I. A set of curves I is for electrons with E_e = 0.3-0.6 MeV and a set of curves II, for electrons with E_e = 0.9-I.2 MeV. The open circles correspond to the data obtained on the dayside and the solid circles, on the nightside. The position of the trapping boundaries of electrons is seen to be asymmetric in the midday-midnight plane and the asymmetry value depends on energy: the asymmetry decreases with increasing electron energy.

On the dayside the position of the trapping boundaries of electrons depends on rigidity. On the nightside this dependence is much weaker. As the magnetic field increases and decreases during the magnetic storms and substorms, the trapping boundaries shift to higher and lower in variant latitudes, respectively, in which case the trapping boundaries of electrons with different energies come close to each other as the magnetic field decreases and move away from each other as the field increases.

ORIGINAL PAGE IS
OF POOR QUALITY

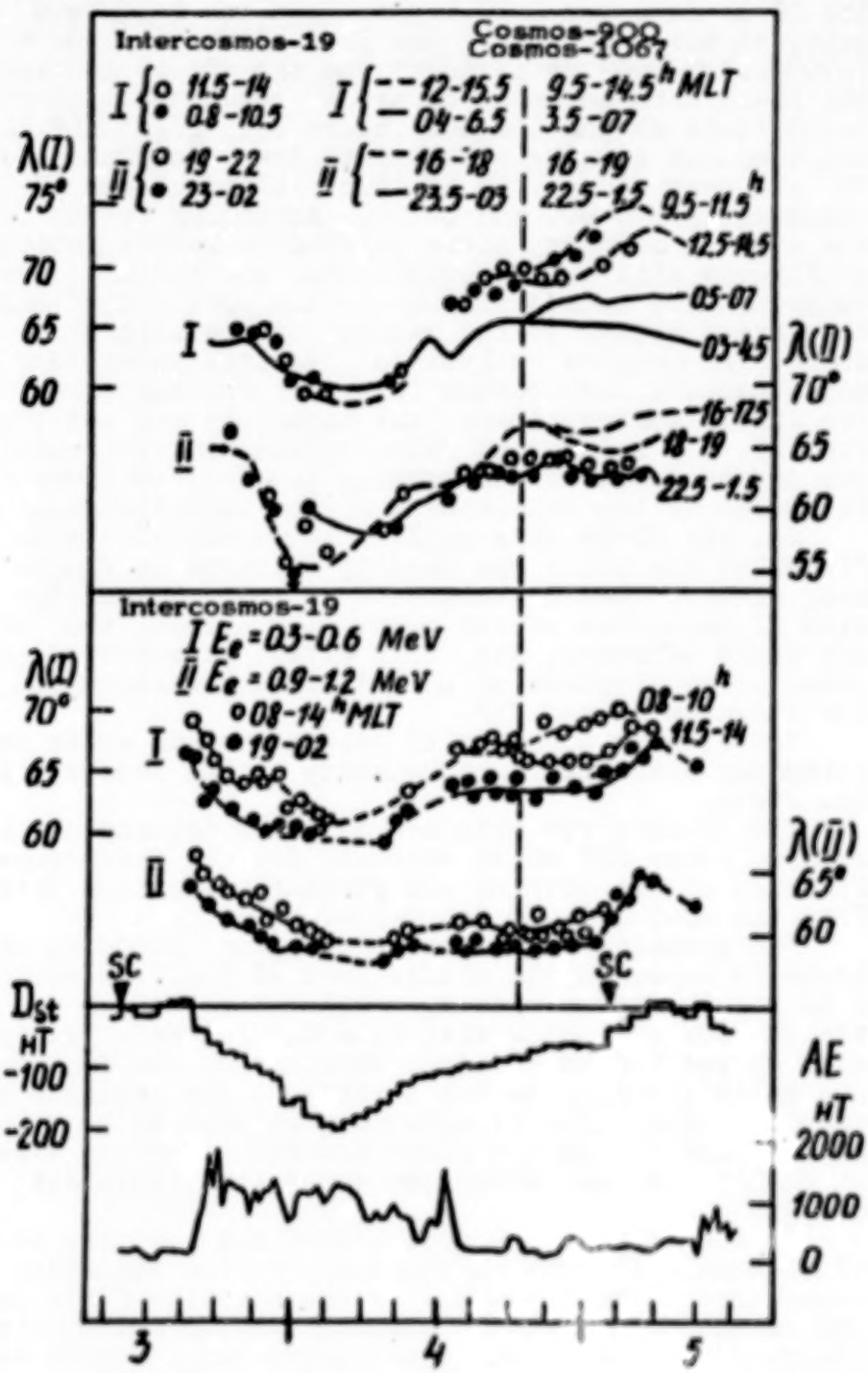


Fig.1

SH 6.I-I6

The comparison between the dynamics of the equatorial region of penetration of the SCR protons and the outer trapping boundaries of electrons with E_e = 0.3-0.6 MeV and E_e = 0.9-I.2 MeV shown that on the dayside these boundaries behave in a similar manner. On the nightside Λ_{pe} coincides to within I° with the trapping boundary of electrons with E_e = 0.3-0.6 MeV except for the time moments within several minutes before the onset of magnetospheric substorms when the SCR protons are injected into deep L-shells; in this case the proton intensity peaks near the injection boundary and then falls down abruptly towards low latitudes. The intensity maximum can, apparently, be explained by the proton acceleration under the action of the enhanced electric field. Following the injection the SCR protons with E_p = = 0.9-8.0 MeV penetrate deep into the trapping region of electrons with E_e = 0.3-0.6 MeV and during strong magnetospheric substorms, into the trapping region of prptons with E_p = 0.9-8.0 MeV.

Because of the violation of the adiabatic conditions of motion, a rapid precipitation of the SCR protons takes place following the injection in the trapping region of electrons with E_e = 0.3-0.6 MeV and also in the quasitrapping region on the dayside. The strong precipitation can also result from the parasitic scattering of the SCR protons on the electromagnetic radiation of the ring current protons.

References

I. Yu.V.Mineev et al. Proc. I8-th Int.Cos.Ray Conf., Bangalore, India, I983, 3, 262-265.
2. Yu.V.Mineev and E.S.Spirkova. Sov.Journal "Vestnik MGU", series 3, I98I, 22, I, 9I-95.
3. L.A.Darchieva et al. Sov. Journal "Geomagnetizm and Aeronomy", I983, 23, 59-64.

N85-35090

SHORT PERTURBATIONS OF COSMIC RAY INTENSITY AND ELECTRIC FIELD IN ATMOSPHERE

Alexeyenko V.V., Chudakov A.E., Sborshikov V.G. and Tizengauzen V.A.
Institute for Nuclear Research of the Academy of Sciences of the USSR, Moscow

Starting from 1975 an experiment was carried out using Baksan E.A.S. array (S = 200 m^2 of scintillators, h = = 1700 m, R = 6,5 GV) /1/ to look at short perturbations in cosmic ray intensity. More than 140 events were recorded up to now, nearly 100 % of them can not be explained by pressure or temperature variations (at the level of observation). The characteristic amplitude of the recorded intensity variations is about 1%, the specific time scale 10 ÷ 20 min and duration up to 5 h. The mentioned "time scale" can be affected by the 4 min read out period in this experiment.

The meteorological nature of observed intensity perturbations was found as most probable from strong association of the phenomenon with precipitations out of cumulonimbus clouds also out of nimbo-stratus clouds. Similar effects were observed by Attolini et all /2/, authors suggested temperature variations as most probable to explain the phenomenon.

In our experiment we installed an electric field meter (from 1982) and included in the read out system (1984) the counting rate of the 6 outside detectors. The latter have 6 x 9 m^2 total area, counting rate 4.10^6 counts/4 min. Though this is only 1/3 of the counting rate of the central part it is useful for speculation concerning energy spectrum of variations because of the difference in the thickness of the roofs, the muon energy threshold or central part being 90 MeV and outside detectors only 20 MeV. 43 events with complete information have been recorded in 1984. In all intensity perturbation cases, if electric field meter was in operation (80 total), a strong electric field ~20 kv/m was recorded. The fig.3 shows the correlation of durations of electric field (t_E) and intensity (t_I) disturbances. The typical examples of records (corrected for pressure) is shown on fig.1 and fig.2. There is no visible correlation between intensity perturbation and pressure or temperature. To explain fig.2 by temperature effect the increase of all the atmospheric temperature should exceed 15°C, which seems most unlikely. The difference of I_{20} and I_{90} responses (fig.1) is quite contrary to the temperature effect hypothesis (soft component contributes 40% to I_{20} and only 7% to I_{90} and temperature coefficient for soft component is smaller than for hard component /3/).

C-6

ORIGINAL PAGE IS
OF POOR QUALITY

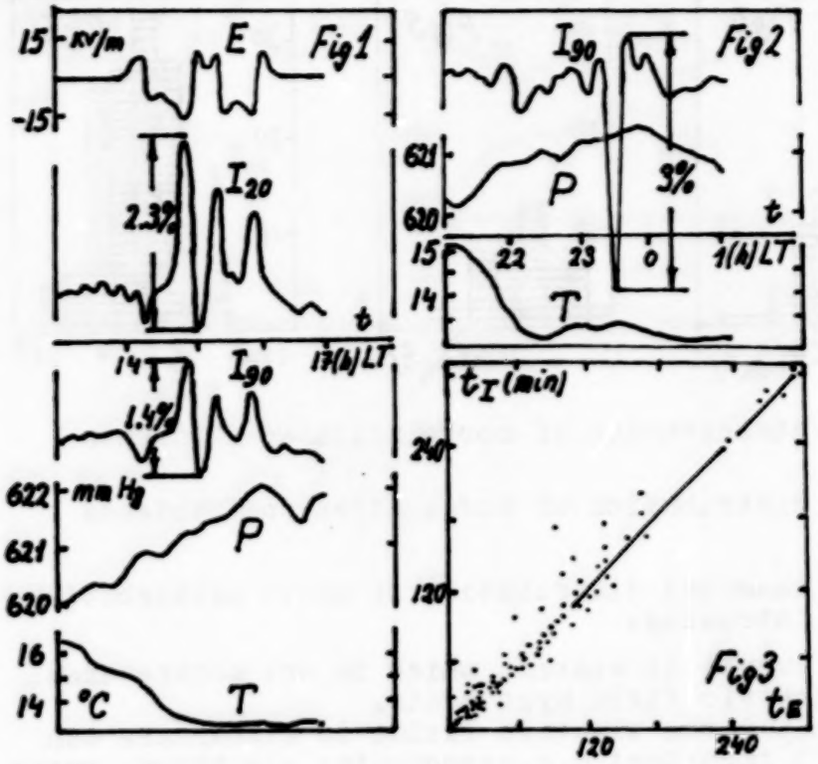


Fig.1. A typical event correlated with rain (13 July 1984) E - electric field. P - atmospheric pressure. T - temperature.

Fig.2. The biggest decrease during a thunderstorm (19--20 June 1983)

Fig.3. The correlation between t_I and t_E

The difficulties in explanation by temperature effect and the obvious connection of short intensity perturbations with electric phenomena (see fig.1,2,3,4,5) make us to examine hypothesis of the influence of electric field on intensity of cosmic rays. The question is not quite new. Many years ago C.T.R.Wilson /8/ suggested the acceleration of electrons by electric field in thunderstorm clouds. The atmospheric electricity effects have been investigated experimentally very long ago /4/, /5/ also /6/ but so far the evidence has been scarce and contradictory.

The main feature of electric field-intensity correlation consists in unambiguous strong connection between both phenomena and, on the other hand, in absence of a strong correlation between E(t) and I(t). More than that, fig.4 and fig.5 show, that there happened to exist events with correlation coefficients R of different sign. There is thought an obvious excess of events with negative R. As a positive direction of electric field was chosen down, so negative R corresponds to the negative charge excess of accelerated (decelarated) particles. Fig.6 shows the

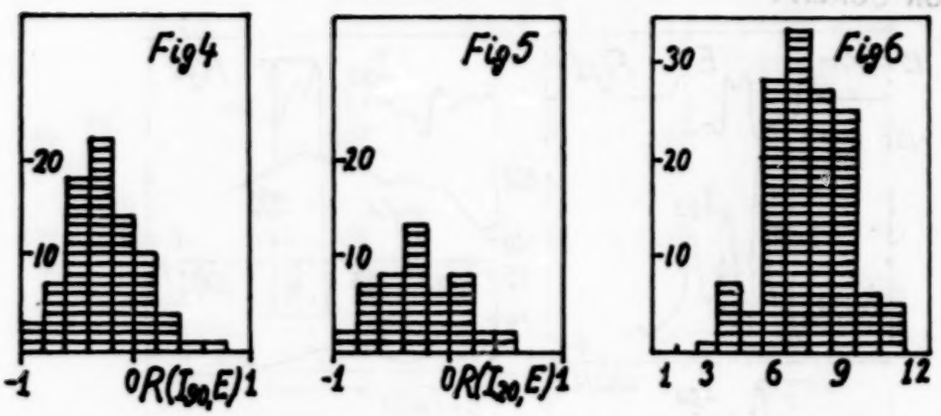


Fig.4. The distribution of correlation coefficients $R(I_{90},E)$

Fig.5. The distribution of correlation coefficients $R(I_{20},E)$

Fig.6. The seasonal distribution of short perturbations of cosmic ray intensity.

absence of events in winter, which is not controversal with the electric field hypothesis.

In principle the electric fields in atmosphere can affect all 3 important c.r.components: electrons, muons and primary protons.

1) e-mechanism due to the excess of negative electrons is presumably a local one because of the short range of electrons, therefore a strong E ↔ I correlation is expected, especially for I_{20}. But experimentally this is not the case - see fig.5 also fig.4. One can think of only small contribution of this mechanism to I_{20} and negligible to I_{90}.

2) μ - mechanism due to the positive excess of muons in the middle atmosphere. Because there is no $\pm$ excess for low energy muons at the level of observation /7/ this mechanism is not local, so the electric field of all atmospheric does affect the I_{20} and I_{90}. This can explain the small and of different signs correlation coefficients R.

3) p-mechanism is located especially high in the atmosphere where the interactions of primary protons with air nuclei give a contribution to the observed muon flux. The change of electric potential at these levels relative to the earth or ionosphere (we believe them to be zero) will change energy of interactions and accordingly the intensity of muon flux. To explain 1% variation in muon intensity the potential at 7 ÷ 15 km should reach 1 GeV or more.

Conclusions. Short perturbations of c.r. intensity were found to be quite common phenomenon. Its meteorological origin and correlation with electric field is established without doubt. The phenomenon probably can be expla-

N85-35096

ned by the electric field if the strength of this field at high altitudes is much bigger than the measured one at surface.

References

1. E.N.Alexeyev, P.Ya.Glemba, A.S.Lidvansky, V.Ya.Markov, N.I.Molchanova, B.B.Tatian, V.A.Tsengauzen and A.E.Chudakov. Proc. 14 ICRC, v.8, p.2996, München (1975)
2. M.R.Attolini, S.Cecchini, M.Galli and J.Guidi. Lettere al Nuov. Cim., 2, N7, p.329 (1971)
3. Dorman L.I. Cosmic ray variations (State Publishing House, Moscow), p.170
4. Shonland B.F.J. Proc.Roy. Soc.A, 130, 37-63 (1930)
5. Shonland B.F.J., Vilfoen J.P.T. Proc. Roy.Soc.A.140, 314 (1933)
6. Clay J., Jongen H.P. and Aart A.J.J. 1952, Physica, 18, 801
7. Singhal K.P.Proc. 18 ICRC, v.7, p.27, Bangalore (1983)
8. Wilson C.T.R. Proc. Camb. Phil. Soc. 22, 534 (1925)

N85-35091

SH 6.1-19

LONG-PERIOD COSMIC RAY VARIATIONS AND THEIR ALTITUDE DEPENDENCE

Belov A.V., Gushchina R.T., Dorman L.I., Sirotina I.V.
Institute of Terrestrial Magnetism, Ionosphere and Radio Wave Propagation, USSR Academy of Sciences, I42092 Troitsk, Moscow Region, USSR

I. The study of long-period variations from the data of ground-based cosmic ray (CR) observations encounters great difficulties. In spite of a large value of an II-year variation, it is more difficult to obtain its spectrum than, say, the spectrum of a solar diurnal variation. Serious obstacles are caused by changes in individual detectors and in the whole world-wide network of CR detectors, by the absence of continuity and uniformity of data series, by various apparatus variations, etc. Therefore, in discrimination and investigation of long-period variations an important and determining point is preparation and preliminary analysis of data.

We have used average monthly data from 28 neutron monitors for the period from IO to 26 years. All the data were preliminarily verified. We made some corrections connected with the change in the efficiency of CR detector and with an incompleteness of some data series. Corrections due to temperature effect were made. We have assumed that the long-period variation δ_i of an individual monitor is caused by an isotropic variation and by first two zonal components of primary CR anisotropy, i.e.

$$\delta_i = a_0 C_0^i(\gamma) + a_1 C_{10}^i(\beta_1) + a_2 C_{20}^i(\beta_2) \qquad (I)$$

where a_0, a_1, a_2 and γ, β_1, β_2 are amplitudes (for a rigidity R= IO GV) and indices of power-law spectrum of the isotropic part and of the zonal components of the primary variation. We have used the acceptance coefficients C_0, C_{IO}, C_{20} calculated in refs. /I,2/ and in the present paper. In average annual data processing the amplitudes a_1 and a_2 did not have a statistically significant difference from zero and variation in each station were determined only by the acceptance coefficient

$$C_0^i(\gamma) = 10^{\gamma} \int_g W(R,g,h) R^{-\gamma} dR, \qquad (2)$$

where g is a cutoff rigidity, h is hight, W(R.g,h) are the coupling coefficients of a given station.

In /3/ it is shown that if one uses the coupling coefficients of the neutron component calculated in /4/ and the approximation

$$W(R,g,h) = \alpha\varkappa \exp(-\alpha R^{-\varkappa}) R^{-\varkappa-1} / (1 - \exp(-\alpha g^{-\varkappa})),$$

the coefficients α and $\varkappa$ will be linearly connected with

the depth h in the atmosphere ($\alpha = \alpha_0 + \alpha_1 h$ and $\varkappa = \varkappa_0 + \varkappa_1 h$ for h > 300 mb. For the minimal solar activity $\alpha_0 = 6.25 \pm 0.03$, $\alpha_1 = 0.70 \pm 0.04$, $\varkappa_0 = 1.40 \pm 0.02$, $\varkappa_1 = -0.56 \pm 0.02$.

Figure I presents the behaviour of the isotropic component a_0 of the primary variation of CR (for a rigidity of 5, 10 and 20 GV) and the change in the intensity I_λ of the green coronal line during 1957-1982. Note that the rigidity spectrum of the long-period CR variation is apparently "softer" in the years closest to the maxima of solar activity and "harder" near the minima. The CR modulation depth in a 20-th cycle is much smaller than in a 19-th or a 21-st cycle. This difference is especially large for hard particles. The Table presents the indices γ averaged for years of high solar activity. In the CR spectrum variations a 22-year repeatability is observed. It can possibly be explained by the difference in the level of solar activity in the maxima of three last cycles.

cycle	years	γ
19	58-61	0.6 ± 0.1
20	68-71	1.2 ± 0.1
21	79-82	0.7 ± 0.1

2. The use of acceptance coefficients is not the only way for obtaining the energy spectrum of CR variations from the data of ground-based recorders. The other methods require the knowledge of the altitude dependence of the variation δ of the studied component of secondary CR. It is convenient to characterize the altitude dependence by the quantity $\beta_\delta = \frac{1}{\delta}\frac{\partial \delta}{\partial h}$; it is natural to call this quantity a variational barometric coefficient. The quantity β_δ for the neutron component can be calculated with the use made of the above-mentioned data on the altitude dependence of coupling coefficients and the expression

$$\beta_\delta(g,h) = \left(\int_g^\infty \beta_w(R,g,h) W(R,g,h) \Delta(R)\, dR\right) \Big/ \int_g^\infty W(R,g,h)\Delta(R)\, dR \quad (3)$$

where $\beta_w = \frac{1}{w}\frac{\partial w}{\partial h}$ and $\Delta(R) = \frac{\Delta D}{D}(R)$ is the variation of the primary spectrum of CR. The dependence of β_δ on the cutoff rigidity g and on the variational spectral index γ is shown in Fig.2. The value of the coefficient β_δ can be an indication of the slope of the rigidity spectrum of secondary CR variation. Besides, the calculation of β_δ can be used for reduction of the variations observed at different altitudes to one barometric level and for calculation of variations of the total barometric coefficient for different neutron monitors. With the help of the same data on one can calculate also the partial barometric coefficient $\beta_m = \frac{1}{m}\frac{\partial m}{\partial h}$ (m = m(R,h) is the integral multiplicity of neutron component generation) since $\beta_m = \beta_w + \beta$ where β is the total barometric coefficient. The dependence of β_m on rigidity for h = 600 mb and 1000 mb is shown in Fig.3.

ORIGINAL PAGE IS
OF POOR QUALITY

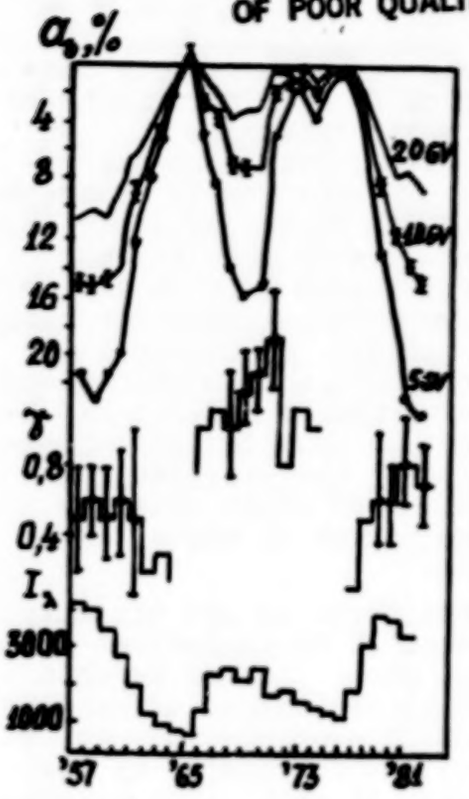


Fig. 1

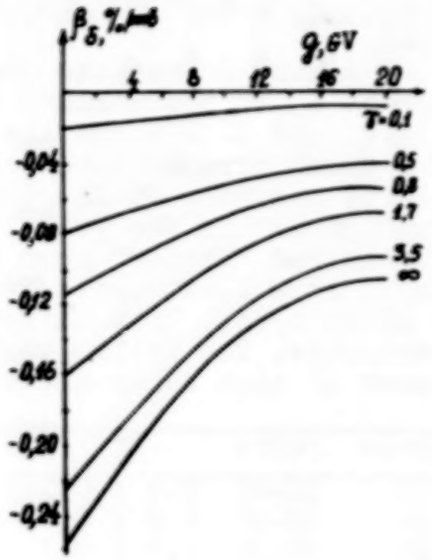


Fig. 2

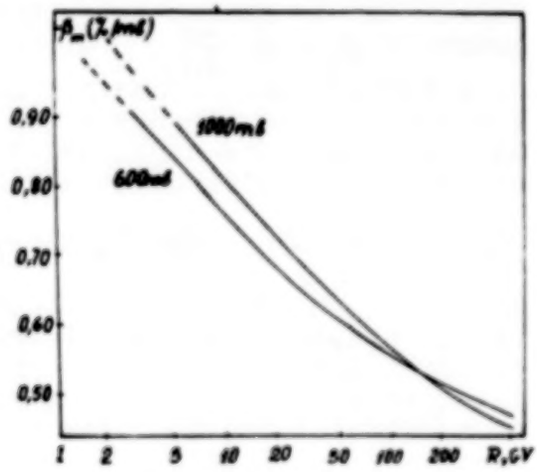


Fig. 3

REFERENCES

1. Yasue S., Mori S., Sakakibara S., Nagashima K. Report of Cos. Ray Res. Lab., 1982, 7, Nagoya, Japan.
2. Belov A.V., Kroshenko E.A. Proc. 17-th ICRC, Paris, v.4, 97, 1981.
3. Dorman L.I., Belov A.V., Yanke V.G. et al. Izv.AN SSSR, ser.fiz., 1982, v.46, 1689.
4. Dorman L.I., Yanke V.G., Proc. 17-the ICRC, Paris, v.4, 326, 1981.
5. Granitsky L.V., Rishe A. Acta Phys. Acad.Sci.Hung., 1970, v.29, Suppl. 2, p. 233.

SH 6.1-21

N85-35092

DIURNAL VARIATIONS OF COSMIC RAY GEOMAGNETIC CUT-OFF THRESHOLD RIGIDITIES

V.M.Dvornikov, V.E.Sdobnov, A.V.Sergeev (SibIZMIR, Irkutsk 33, P.O.Box 4, USSR)

O.A.Danilova, M.I.Tyasto (LO IZMIRAN, Leningrad,V-53)

Abstract. For the period 1 May-30 June 1972, using the method of spectrographic global survey we investigated the rigidity variations Rc of geomagnetic cut-off as a function of local time and the level of geomagnetic disturbance for a number of stations of the world-wide network.
It is shown that geomagnetic cut-off threshold rigidities undergo diurnal variations. The diurnal wave amplitude decreases with increasing threshold rigidity Rc, and the wave maximum occurs at 2-4 hr LT. The amplitude of diurnal variations increases with increasing geomagnetic activity.
The results obtained agree with those from trajectory calculations made for an asymmetric model of the magnetosphere during different geomagnetic fdisturbance conditions.

The study of cosmic ray (CR) intensity variations of magnetospheric origin observable on the ground is of interest for two reasons: first, we cannot study CR variations of interplanetary origin without making adequately allowing for the variations arising in the sphere of action of the magnetic field of the Earth and, second, the variations of magnetospheric origin themselves can be used as an additional source of information on processes occurring inside the magnetosphere at different distances from the Earth.

However, the study of the variations of this class becomes difficult because they are observed simultaneously with CR variations of a significantly larger amplitude which are associated with processes in interplanetary space. In order to separate these two types of variations, a method of spectrographic global survey (SGS) has been developed that makes it possible, using ground-based CR observations at the world-wide network of stations, to obtain information regarding the energy and pitch-angle distribution of primary CR in the interplanetary magnetic field (IMF), on the IMF orientation and on variations of the planetary system of geomagnetic cut-off rigidities (GCR). This method was used in /1/ to obtain information on GCR variations (Δ Rc) for a number of points of the world-wide network during the June 1972 geomagnetic storm; the latitude dependence of the amplitudes of these variations is studied and a quantitative estimation of parameters of current systems of disturbances made. The results obtained are consistent with current views of dynamical processes in the magnetosphere and agree with satellite measurements /2/.

This paper investigates GCR diurnal variations, their dependence on latitude and level of geomagnetic disturbance for the period 1 May - 30 June 1972.

The analysis employed data from 34 world network stations. In order to determine GCR variations at middle and lower-latitude stations it is necessary to have at least two detectors sensitive to these variations, with different coupling coef-

N85-35092

ficients at threshold rigidity. Since many middle and lower-latitude stations lack complexes of detectors required to determine Rc, near-by stations were combined into such complexes and were ascribed equal (averaged) threshold GCR (R c). The

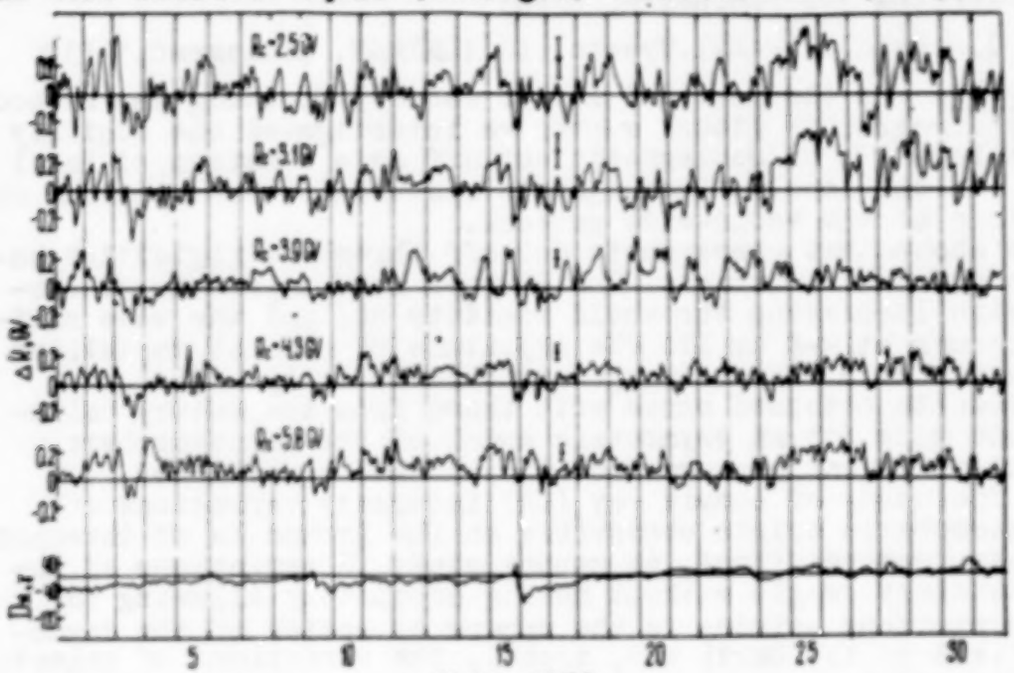
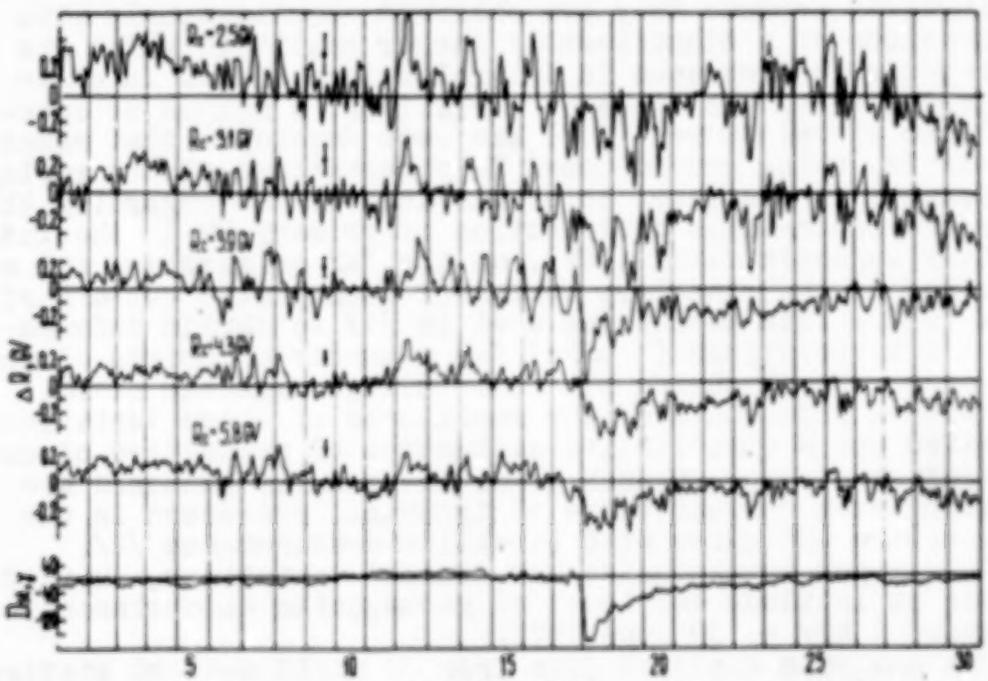


Fig. 1



ORIGINAL PAGE IS
OF POOR QUALITY

Fig. 2

analysis used observations from five such groups of stations: 1.Kiel and Utrecht (Rc=2.5GV);2.Dourbes and Lindau (Rc=3.1 GV);3.the Sayan spectrograph complex (Rc=3.9GV);4.Hafelekar, Zugspitze, Jungfraujoch (Rc=4.3GV);5.Rome and Pic-du-Midi (Rc=5.8GV). For each group of stations, we determined variations of threshold GCR using data averaged over a two-hour interval.

Figs 1 and 2 show the variations Rc as obtained by the SGS method, of threshold GCR for two months for each of the above groups of CR stations. The period of study includes intervals with both relatively weak geomagnetic activity (Kp ~ 1) and high geomagnetic activity (Kp > 3+). The mean Kp-index that defines the geomagnetic activity for the whole period considered is about 2+.

In order to separate the periodic part of the threshold GCR variation, we employed a numerical mathematical filter /3/ which was used to separate oscillations with a period $T \leq 24$ hr and the filtered-out data were then averaged by the superposed epoch method. The results of the analysis made are presented in Fig. 3 showing the variations of threshold GCR during 24 hr as a function of LT (solid curve). The upper panel of the plots represents the variations of threshold GCR during 24 hr for a period with Kp ~ 2 while the lower panel shows those for the period with Kp ~ 5.

As follows from the plots, the variations of threshold GCR involve a diurnal variation with its maximum occurring at 2-4 hr LT. For the group of stations with $\bar{R}c$=2.5GV, the amplitude of variations in threshold GCR during 24 hr is ~ 0.12GV for a period with Kp ~ 2 and ~ 0.3 GV for a period with Kp ~ 5; for the group of stations with $\bar{R}c$=3.1 GV, these variations are ~ 0.12GV and ~ 0.2GV, respectively, with $\bar{R}c$=3.9GV, ~ 0.1GV and ~ 0.16GV, with $\bar{R}c$=4.3GV - ~ 0.06GV and ~ 0.1GV, with $\bar{R}c$=5.8GV, ~ 0.05GV and ~ 0.08GV.

Thus, the amplitude of the diurnal variation in threshold GCR depends on threshold GCR, decreases with increasing

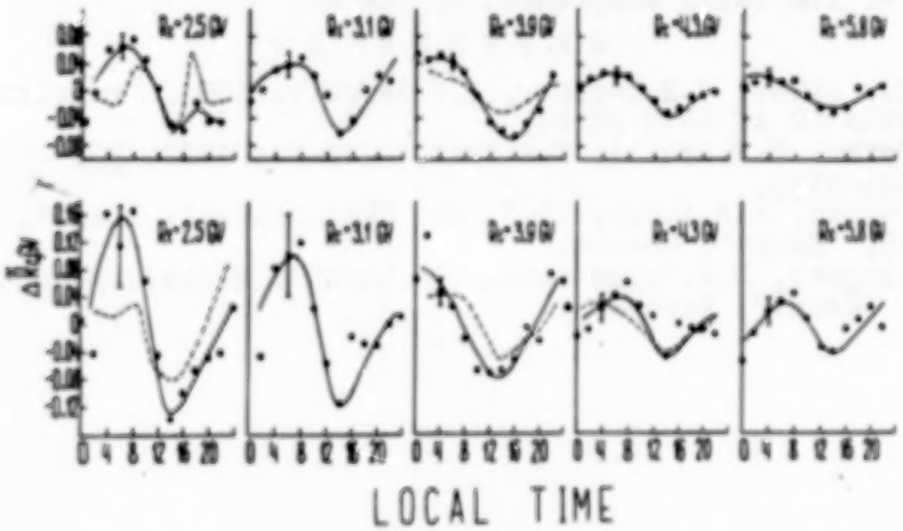


Fig. 3

Rc and increases with an enhancement of geomagnetic activity.

This diurnal variation in threshold GCR can be due to several reasons, in particular to an asymmetry of the magnetosphere as a consequence of its being compressed by the SW.

Since the diurnal wave in the threshold GCR variations was obtained from CR observations covering a rather long period, this indicates that the asymmetry source for threshold GCR in the magnetosphere is quasi-stationary.

In order to confirm this, we made numerical trajectory calculations of the motion of charged particles in a real geomagnetic field. The real geomagnetic field was specified in the calculations in terms of a model reported by Tsyganenko N.A. et al. /4/, in which a separate description is made of magnetic fields from each current system of the magnetosphere showing a substantially different spatial structure. The parameters of the model depend on the level of geomagnetic activity that is characterized by the Kp-index.

A dotted line in Fig. 3 shows the results from the numerical calculations of the dependence of threshold GCR on LT. The upper panel refers to a quiet period (Kp ~ 0) and the lower panel corresponds to the period with Kp > 3+. The numerical calculation results confirm the presence of a diurnal wave obtained from experimental data, the dependence of its amplitude on threshold GCR at the observation point and on the level of geomagnetic activity.

Conclusions. It is demonstrated both experimentally and theoretically that diurnal variations of CR threshold GCR do exist at middle and lower latitudes. The diurnal wave amplitude of threshold GCR decreases with increasing threshold GCR and increases with increasing geomagnetic activity. Diurnal wave maximum occurs at 2-4 hr LT. The trajectory calculations of the motion of charged particles in the geomagnetic field showed that the experimentally found diurnal wave in threshold GCR is due to the asymmetry of the magnetosphere because of its being compressed by the SW.

REFERENCES

1. V.M.Dvornikov, V.E.Sdobnov, A.V.Sergeev. 1984, Preprint SibIZMIR SO AN SSSR 25-84.
2. P.W.Berko, L.J.Cahill, T.A.Fritz, J.G.R., 1975, 80, p. 3549-3552.
3. L.I.Dorman, A.A.Luzov. 1967, In: "Kosmicheskie luchi", 8, 285, "Nauka", Moscow.
4. V.A.Sergeev, N.A.Tsyganenko. The Earth's Magnetosphere. 1980, "Nauka", Moscow.

N85-35093

SH-6.1-22

THE INFLUENCE OF THE EARTH'S MAGNETOSPHERE ON THE HIGH-ENERGY SOLAR PROTONS

G.A.Bazilevskaya
P.N.Lebedev Physical Institute of the Academy of Sciences of the USSR, 117924,Leninsky Prospect,53, Moscow, USSR

V.S.Makhmutov
Industrial Institute of Roudny, 459120,Roudny, USSR

T.N.Charakhchyan
Institute of Nuclear Physics, Moscow State University, 119899,Moscow, USSR

Abstract

The North-South asymmetry in the fluxes of solar protons with the energy ~70-200 MeV in stratosphere at the invariant latitudes 62°-76° is discussed.

1.Introduction. In the earth'S polar regions the intensity of the solar protons with the energy above the critical energy of geomagnetic cutoff is, according to the Liouville theorem, the same as in the interplanetary space. The penumbra in the polar regions is small and the East-West effect is also small /1/. However the geomagnetic cutoff rigidity R_c in polar regions is difficult to calculate because it is not sufficient to include only the internal sources of the geomagnetic field. According to /2/, during the magneto-quiescent periods the real value of R_c can be less by 0.1 GV than the calculated value because of the external sources. During the geomagnetic storms the real value of R_c is still lower.

2.Observations. The stratospheric exploration of the cosmic rays (CR) initiated in the USSR in IGY provides information on the energy spectrum and absolute flux of the solar protons intruding into the earth's atmosphere. The detector consists of two Geiger counters forming the telescope interlaid with the 7 mm thick aluminium filter /3/. The data on the stations of the stratospheric CR observations are listed in the Table. Although the calculated values of R_c are 0.5GV and 0.6 GV at Olenya and Apatity respectively, the lower

Table. Polar stratospheric stations

Station	Geograph.coordinates Latitude	Longitude	Invariant Latitude	R_c,GV /2/	E , MeV
Olenya, (Murm.reg.)	68.95 N	33.05 E	65.7	0.5	125
Apatity, (Murm.reg.)	67.55 N	33.33 E	62.5	0.6	175
Mirny	66.57 S	92.92 E	76.4	0.03	0.48

energy limit of the observed solar protons at these locations is nevertheless always determined by the ionization ab-

sorption in the residual atmosphere and is sometimes as low as 50 MeV. This means that even in the magneto-quiet periods the rigidity of geomagnetic cutoff at Olenya and Apatity is not higher than 0.3 GV.

Since the asymptotic directions of CR arrival in the Murmansk region (Olenya, Apatity) and at Mirny are different /2/, the N-S anisotropy in the stratospheric observations can be expected in case of the pitch-angular anisotropy of the solar cosmic ray (SCR) fluxes in the interplanetary space. This effect is usually observed only near the onset of a proton event. If the SCR intensity at the atmospheric boundary is not isotropic this leads to the discrepancy between the flux values of solar protons obtained with a single counter and a telescope. This effect sometimes happens /4/, but the present paper will deal with the N-S anisotropy which appears after the maximum of a proton event. In such cases the data of a single counter and a telescope coincide as a rule, so the pitch-angular isotropy at the atmospheric boundary takes place.

3.Comparison of the results for the Northern and the Southern hemispheres. During the period of combined measurements in the Southern and the Northern hemispheres, starting from 1963, about 60 solar proton measurements simultaneously within an hour have been performed. From these data we excluded the balloon flights during which the temporal dynamic of intensity was observed and also the data obtained at the onset of events when according to the neutron monitor data the SCR angular anisotropy was observed. In 31 of the remainder 43 flights the results agree within 10% accuracy. In 10 flights the SCR flux was higher in the Northern hemisphere, among them 6 flights manifested discrepancy more than 30%; 2 measurements showed the excess SCR flux at Mirny.

The most remarkable case of the N-S anisotropy is the SCR event of 12.10.81 reported in /5/. During this event 10 flights in the Southern hemisphere and 39 flights in the Murmansk region were carried out. Some energetic spectra measured during this event are presented in Fig.1 together with the Meteor /6/ and IMP-8 /7/ data. The IMP-8 differential spectrum is recalculated by us to the integral spectrum taking into account the intensity of protons with $E \geq 90$ MeV according to the Meteor data. The features of the event in question are: 1/ the anisotropy is not persistent; 2/ when the N-S anisotropy is observed the satellite data agree with the Mirny data, and thus in the Northern hemisphere there is an excess flux of particles. According to Meteor observations in the polar caps there was no any noticeable anisotropy at $E \geq 90$ MeV during this period /6/. We may infer that an excess flux of particles in the Murmansk region has a magnetospheric origin . The surplus flux causes the steepening of proton spectrum at $E < 200$ MeV which can be seen in Murmansk data even without any comparison with simultaneous Mirny data /5/. This excess cannot be accounted for by the bremsst-

ORIGINAL PAGE IS
OF POOR QUALITY

rahlung of the auroral electrons because these are not registered with a telescope. A certain contribution of the bremsstrahlung can be admitted only at 03-04 UT and 15-16 UT observations on 13.10.81.

The time behaviour of the anisotropy is shown in Fig.2 It is seen, that the value of the excess flux (if occurs) gradually decreases with time. The spectrum index of the excess flux, γ, is equal to 3-5 and it increases up to $\sim$ 14 during the last flight on 15.10.81. The anisotropy calculated as $\alpha = (I_N - I_S)/(I_N + I_S)$ also becomes stronger to the end of the event. In the bottom of Fig. 2 we give the values of K_p- index /8/. We failed to reveal any correlation between the N-S anisotropy and geomagnetic disturbances.

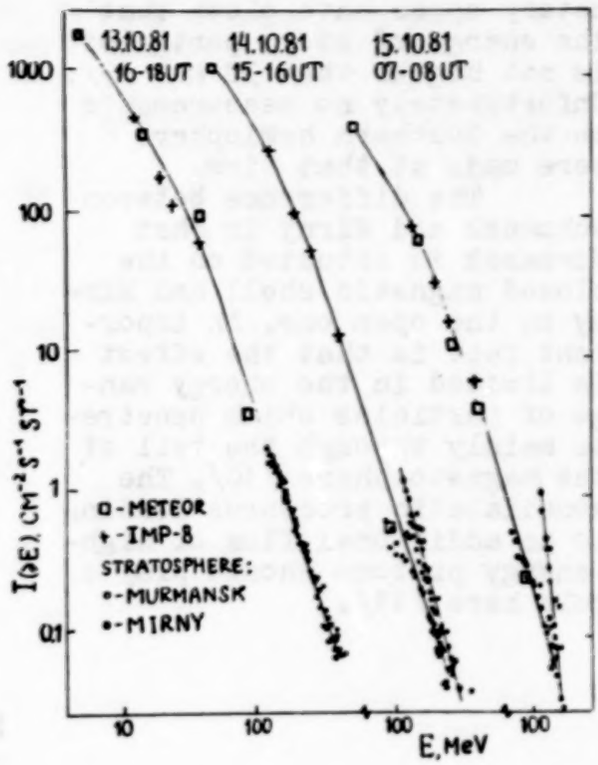


Fig. 1 Examples of energy spectra of solar protons according to stratospheric and satellite data

4.Discussion. The N-S asymmetry in the fluxes of solar protons with E=70-200 MeV is occasionally observed in the stratosphere. The 700-1000 km height satellite observations in the polar caps /6/ have not confirmed the presence of the anisotropy. The SCR fluxes in the polar caps agree with the Mirny data. The surplus flux of particles in the Murmansk region is not persistent, has a steep energetic spectrum and the maximal energy does not exceed $\sim$200 MeV. There is no correlation with the geomagnetic disturbances, but an especially strong anisotropy was observed during the latest phase of the event more than a day after the sudden commencement of the geomagnetic storm marked by a triangle in Fig. 2. Similar effects against a background of the geomagnetic storms were observed in the stratosphere during powerful proton events of the 19-th solar cycle /3/. The spectrum steepening was supposed to be associated with the particles accelerated or localized near the front of the interplanetary shock of flare origin. However the direct

SH-6.1-22

measurements in the interplanetary space have shown that the energy of storm particles is not higher than 30 MeV /9/. Unfortunately no measurements in the Southern hemisphere were made at that time.

The difference between Murmansk and Mirny is that Murmansk is situated on the closed magnetic shell and Mirny on the open one. An important fact is that the effect is limited in the energy range of particles which penetrate mainly through the tail of the magnetosphere /10/. The nonadiabatic processes leading to an additional flux of high-energy protons should play a role here /11/.

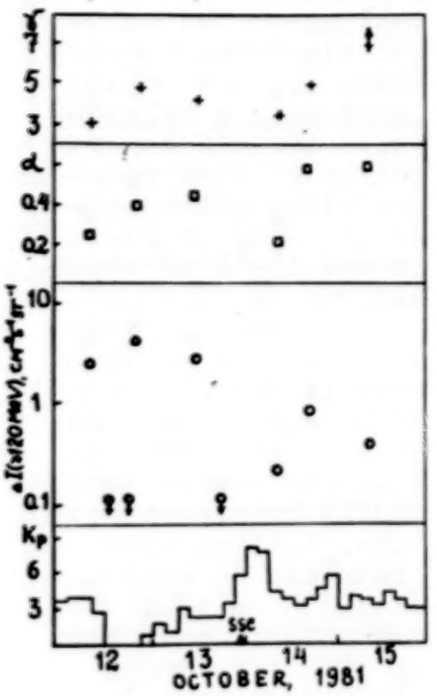


Fig. 2. Time behaviour of an excess flux of particles in Murmansk region.

References.

1. Dorman,L.I.,Smirnov,V.S.,Tyasto,M.I.,(1971),Cosmic Rays in the Earth's Magnetic Field.Moscow, Nauka.
2. Shea, M.A., Smart,D.F.,(1975), AFCRL-TR-0247.
3. Charakhchyan,A.N.,(1964),Uspekhi Fiz. Nauk, v.83,p.35.
4. Borovkov,L.P., et al.,(1982) Izv. Acad. Nauk SSSR, ser.fiz., v.46, p.1709.
5. Bazilevskaya,G.A., et al.,(1983),Proc.18-th ICRC, Bangalore, v.4, p.189.
6. Avdyushin,S.I.,Pereyaslova,N.K.,(1983),Izv. Akad. Nauk SSSR, ser.fiz., v.47, p.1805.
7. Solar-Geophysical Data,(1984),475(II), U.S.Dep.of Commerce, Boulder, USA.
8. Solar-Geophysical Data (1981),448(I), U.S.Dep.of Commerce, Boulder, USA.
9. McDonald, F.B.,(1981),Proc. 17-th ICRC., Paris,v.13, p.189.
10. Gall,R.,Bravo,S.,(1981),J.Geophys.Res.,v.86,p.2467.
11. Il'in,V.D., et al.,(1984),Izv. Acad. Nauk SSSR, ser. fiz., v.48, p.2200.

N85-35094
SH 7.1-1

COSMIC RAY ^{10}Be BIENNIAL DATA AND THEIR RELATIONSHIP TO AURORAE AND SUNSPOTS.

M.R.Attolini, S.Cecchini, Istituto TESRE del CNR, Bologna
G.Cini Castagnoli, Istituto di Fisica Generale, Università di Torino
M.Galli, Dipartimento di Fisica, Università di Bologna
T.Nanni, Istituto FISBAT del CNR, Bologna, Italy

1.Introduction. Studies of Galactic Cosmic Ray (C.R.) variations should give information on three dimensional aspects of the heliospheric magnetic fields and on the Solar wind, which modulate their influx into the Solar System. But in order to decode the information from the C.R. series it is necessary to know the mechanisms through which the modulation is produced; and this problem is not yet solved[1], although it is clear that a balance of effects with sources at different heliospheric latitudes results in the modulated C.R. intensity.

The investigation of the structure of various time series of data, characterized by the imprint of the Solar variability and its comparison with the structure of the C.R. time series may contribute to the phenomenological individuation of the different sources of modulation.

The C.R. data are of two types: a)the direct measurements of the C.R. intensity at ground since their discovery in the last four decades or b)the record of earlier C.R. flux that has been left as cosmogenic isotopes in different reservoirs. In this paper we examine the ^{10}Be series in polar ice from 1900 to 1976 A.D. measured by J.-Beer[2] et al.(1983) in core Dye3, Greenland.

The other time series that we take into consideration are those of the Sunspot[3] (S.S.) number (R_z)[4] of the global geomagnetic activity <aa>[5] and of the Aurorae[6].

The R_z time series is related to the contribution to the C.R. modulation resulting from the solar conditions in the equatorial region; its anticorrelation to the C.R. series is well known (see Figure 1). The Auroral activity is the result of energy transfer from the solar wind to the magnetosphere, when interplanetary shocks and recurrent wind streams with origin at different heliospheric latitudes pass by the Earth. The comparison of the <aa> index and of the aurorae series with the ^{10}Be series may lead us to the determination of a contribution to the ^{10}Be production due to effects with origin at the higher heliospheric latitudes: the effects of the stable polar high speed wind recurrent streams occuring much more frequently during the declining and minimum phases of solar activity and associated with coronal holes. The size of the polar coronal holes and the C.R. intensity from 1965 to 1976 were already found positively correlated by Hundhausen et al.[6] from 1965 to 1976. This correlation is an evidence for the importance of the drift effects or of the

large-scale structure of the magnetic field effects on the C.R. modulation[7]. Therefore we expect an increased C.R. flux associated to an auroral activity independent from R_z. The identification of two types of geomagnetic activity (the transient or Sunspot shaped activity and the stable wind stream activity) has been pointed out by Legrand and Simon[8].

2.The series of Aurorae, ⟨aa⟩ index and Sunspot number R_z. One of the most important historical series belonging to the study of the Solar-Terrestrial relationships is the millennial series of the Aurorae. It is therefore very important to compare the behaviour and structure of this series during recent times with that of the geomagnetic activity ⟨aa⟩ series available from 1868 and with the R_z series available from 1701. The annual average of ⟨aa⟩ is in fact a terrestrial parameter objectively measured, related[9] to the annual average solar wind parameter $|B_z| V^2$. In Figure 2 the time series are shown. The Aurorae from 1721 to 1780 are those collected by Rubenson and reported by Feynman and Silverman[10] (note that they may be not homogenous to those starting in 1780[5]). On the whole the Aurorae appear in phase with R_z except for the intervals before the most important maxima of R_z in which they appear to be also abundant a little before the R_z minima.

In Figure 3 the phase cyclograms of the three series are reported at τ =10y. We notice how similar the topology (i.e. loops, bendings and stretchings) of the three series looks like. Moreover a phase shift between the cyclograms of the Aurorae (or of ⟨aa⟩) and R_z can be observed. This phase shift is confirmed by the cross-cyclogram performed on the Aurorae and R_z series in the band around τ=11y (Figure 4), which is not stretched along the real axis. The two facts leed to the conclusion that there is a part of the Auroral activity which is not related to R_z and although with similar periodicity is substantially phase shifted. We have therefore computed the series of Aurorae linear-regression-corrected-for R_z, after the second order detrending. The phase cyclogram for τ=11,1y of these residual aurorae, obviously independent from R_z, is given in Figure 5, where we have also given how to find the time of maxima of the series. This cyclogram is very straight, showing that the periodicity is constant in time and equal to 11,1y. This is confirmed by the power spectral density (p.s.d.) analysis of the residual Aurorae, given in Figure 6 (lower graph) in which we give also for comparison the p.s.d. of the series of the total Aurorae (upper graph). Two interesting points must be noticed: a)the psd of total Aurorae shows two lines one at 10.0y and one at 11.1y; after correcting for the equatorial activity the residual Aurorae show only the second line; b)the psd of the residuals shows the peak at 21.6y with its third harmonic at 7y reinforced.The maxima starting from 1877 of the residual aurorae (see Figure 5) happen at about the same time of the recurrent geomagnetic

activity, which has been shown by Legrand and Simon (1981) in Fig.1 of their paper to be mostly due to the polar high speed wind streams.

3.The series of ^{10}Be. The biennial experimental ^{10}Be data were smoothed by the running mean of two data, giving a series of 39 data starting from 1900-1901. The global geomagnetic activity (or the Aurorae see Figure 7a) has been splitted into the two aforementioned series: the stable-wind-stream and the transient-R_z-related activity (Figure 7b) covering the same interval and with the same averaging time of ^{10}Be shifted by 3 years according to the cross cyclogram of ^{10}Be and R_z. The ^{10}Be series has been correlated in a threefold correlation, according to the statistical model: $^{10}Be = k\langle aa\rangle_{trans} + h\langle aa\rangle_{stab}$ The threefold correlation shows a negative coefficient k=-0,0047 ^{10}Be units/$\langle aa\rangle$ units, ave$[\langle aa\rangle_{trans}]$ =32.06 and a positive coefficient h=0,0057, ave$[\langle aa\rangle_{stab}]$ =14.79. With these coefficients the curve of the expected values of ^{10}Be was calculated and it is shown in Figure 7c together with the experimental data. The two curves agree rather well if one takes into account the measurement experimental errors. The errors account for about 20% of the total variance of the series so that only 80% of the variance should be explained from the correlation with $\langle aa\rangle_{trans}$ and $\langle aa\rangle_{stab}$. In our case the total correlation is 62%, covering almost the entire possibility.

4.Conclusions. We have found by statistical analysis that the modulation of ^{10}Be in polar ice may be due to at least two main contributions: one is negative and in phase with the Solar flare activity modulating the cosmic ray flux in Forbush-type decreases and one is positive in phase with the appearence of large wind streams situated at both polar coronal holes. Furthermore from the analysis of Aurorae we have found that the high heliolatitude activity is related to a stable periodicity of 11.1y whereas the low heliolatitude activity contributes to the wondering of the solar cycles.

References

1. Jokipii J.R., (1984), Proc.Int.Symp. on C.R., Morioka,Japan
2. Beer J., Andrée M., Oeschger H., Stauffer B., Balzer R., Bonani G., Stoller C., Suter M., Woelfli and Finkel R., (1983), Radiocarbon 25, 269
3. Waldemayer M., (1961), The Sunspost Activities in the years 1616-1960, Schulthess and CO, Zurich, Switzerland
4. Mayaud P.N., (1973), Iaga Bulletin 33
5. Legrand J.P., private communication (Aurorae 1780-1979)
6. Hundhausen A.J., Sims D.G., Hansen R.T., (1980), Science 207, 761
7. Fisk L.A., (1979), Proc.Conf. Ancient Sun (Pepin, Eddy, Merryl) Geochimica et Cosmochimica Acta suppl. 13 (1979),p.103
8. Legrand J.P. and Simon P.A., (1981), Solar Physics 70, 173,
9. Feynman J., (1983), Reviews of Geophysics and Space Phys. 21, 338
10. Feynman J., Silverman S., Nasa Conf. publication 2098

ORIGINAL PAGE IS
OF POOR QUALITY

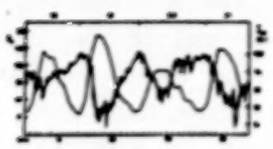


Fig.1

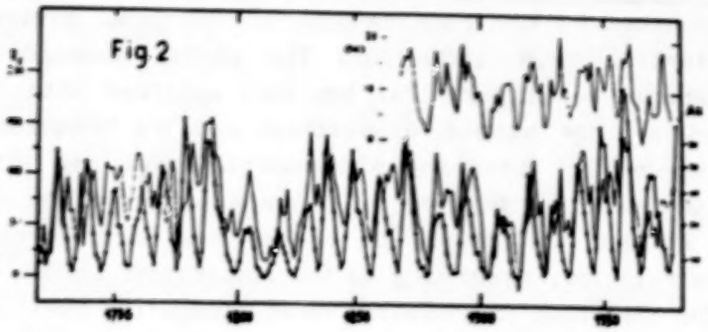


Fig.2

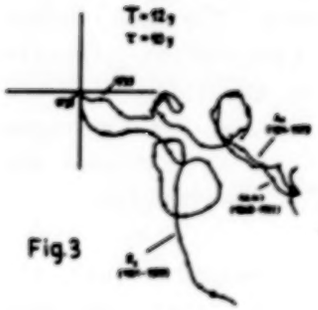


Fig.3

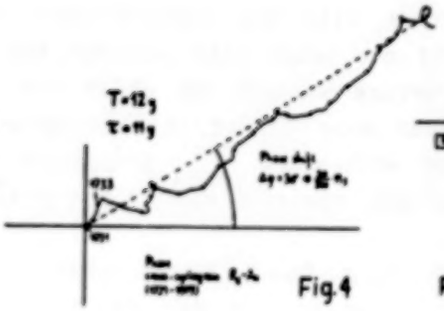


Fig.4

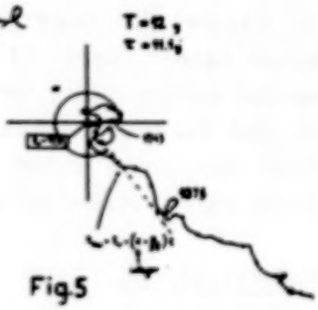


Fig.5

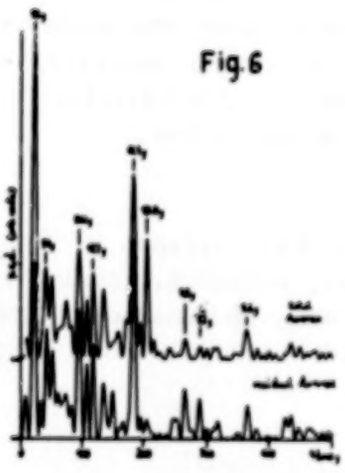


Fig.6

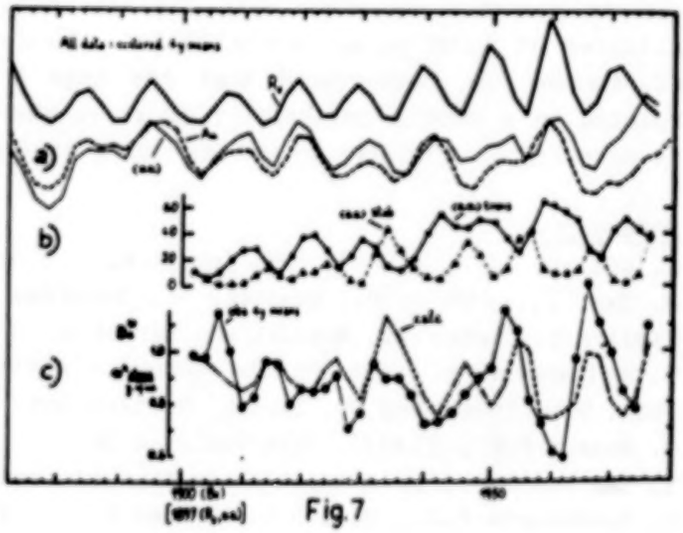


Fig.7

N85-35095

SOLAR MODULATION OF COSMIC RAY INTENSITY AND SOLAR FLARE EVENTS INFERRED FROM ^{14}C CONTENTS IN DATED TREE RINGS

C. Y. Fan
Department of Physics, University of Arizona, Tucson, AZ 85721, USA

T. M. Chen and S. X. Yun
Archaeological Section, History Department, Peking University
Beijing, China

K. M. Dai
Department of Physics, Nanjing University, Nanjing, China

We have measured the $\Delta^{14}C$ values in 42 rings (from 1824 to 1865 AD) of a white spruce grown in Mackenzie Delta (68°N, 130°W) as our continuing effort of tracing the history of solar modulation of cosmic ray intensity. We also measured the $\Delta^{14}C$ values in 6 rings (from 1940 to 1945 AD), searching for a ^{14}C increase due to two large solar flares that occurred in 1942 and were detected by Forbush. The results will be presented and discussed.

1. Introduction. Carbon-14 nuclei in the atmosphere are produced by cosmic-ray-generated neutrons in $^{14}N(n,p)^{14}C$ reaction. After the production, these nuclei react rapidly with ambient atmosphere to become $^{14}CO_2$ molecules. The concentration of the $^{14}C_2$ molecules is mainly determined by the rate of production and the rate of transfer, first to the troposphere from the stratosphere where most of them are produced, and then from the troposphere to the deep-sea sink reservoir. Since cosmic ray intensity is modulated by interplanetary magnetic fields whose strength depends on the solar activity, it is expected that the concentration is anti-correlated with sunspot numbers. While the long-term change in $\Delta^{14}C$ in tree rings samples, which reflects the variation of the atmospheric ^{14}C concentration, has been studied by many investigators and the correlation established beyond any doubt (e.g., Stuiver and Quay, 1980, and references therein), the question remains as to whether the amplitude of the expected 11-year variation is large enough to be measurable.

There was some indication that $\Delta^{14}C$ values in grains and trees grown at high lattitudes show 11-year periodicity (Baxter and Farmer, 1973). To study the possible latitudinal effect, we searched and, fortunately, obtained two sections of dated white spruce grown near Campbell River in Mackenzie Delta, Canada (68°N, 130°W) from Dr. M. L. Parker of the University of British Columbia; one of the sections contains rings from 1510 to 1972 AD. Initial measurements of 27 samples, covering the period from 1866 to 1925 AD, indicated that the $\Delta^{14}C$ values do exhibit a $10^{o}/_{oo}$ fluctuation, anticorrelated with sunspot numbers. The results were reported at the 18th International Cosmic Ray Conference (Fan et al., 1983a, 1983b). In this paper we shall report $\Delta^{14}C$ in the ring samples from 1824 to 1865 AD. We also measured the $\Delta^{14}C$ in 1940 to 1945 rings, looking for the signature of ^{14}C increase, due to two large solar flares that occurred in 1942 and were reported by Forbush (1946). The results will be discussed.

2. Experiment. The task of the measurements was divided between two institutions; the 1824 to 1865 rings were measured at the Department of History of Peking University, whereas the 1940 to 1945 rings were measured at the

Department of Physics of Nanjing University. The equipment used was similar; a liquid scintillator-photomultiplier tube device, which were carefully intercalibrated. Both systems used two photomultiplier tubes in coincidence to count ^{14}C decay electrons and a pulse height discrimination to reduce cross-talks between the two tubes. There was, however, a slight difference between the two systems. At Peking University, 5-10 cm of lead was used to reduce cosmic-ray-induced background, whereas at Nanjing University, in addition to a lead shield, a plastic scintillator-photomultiplier tube system was used as an anti-coincidence shield. The result of the addition was a reduction of the background from 6 cpm to 2 cpm. An overall precision of both systems was about 4‰, including a pure statistical uncertainty of ~3‰.

For each measurement, about 10 g of wood is needed. Because of the narrowness of the rings, except the 1928 ring, we had to combine two, and sometimes three, rings to obtain a sufficient specimen for one measurement. After being treated with the routine HCl-NaOH-HCl procedure to remove resin, the samples were converted to CO_2 and then to benzene. For one measurement, 5 cc of synthesized benzene was used. The net count rate for a modern sample was 39 cpm. For each sample, we measured $^{13}C/^{12}C$ for fractionation correction.

3. Results on Modulation of Cosmic Ray Intensity. The experimental results are expressed as $\Delta^{14}C$ values which are the relative deviations of the measured ^{14}C activities from the standard oxilic acid activity of the U.S. National Bureau of Standards, corrected for ages and isotope fractionations. For the sample prior to 1885, the correction for the Suess effect was not needed.

The data points, including 11 previously published values, are plotted in the bottom panel of Fig. 1, along with other published $\Delta^{14}C$ values for comparison. To show the correlation with solar activity, we plotted in the upper panel the sunspot numbers with ordinates inverted. It is seen that, except for the 1922 cycle, with a delay of about five years, the $\Delta^{14}C$ values are anti-correlated with sunspot numbers; the cross-correlation coefficient is ~0.6. At present, we are baffled by the reverse correlation in the 1822 cycle. Also, we feel uneasy about the five-year delay, which is longer than what we had expected. We do not rule out a possible error in the tree ring count.

4. Results on ^{14}C Produced by Solar Protons. Damon et a. (1973), in their study of the magnitude of the 11-year radiocarbon cycle, found that the ^{14}C content in the 1943 ring of their Arizona tree sample (32°N, 112°W) is exceptionally high. They attributed this high activity to the ^{14}C production by two large solar flares, on February 28 and March 7 of 1942, detected by Forbush (1946). A similar increase was also observed by Burchuladze et al. (1980). Since our tree section was from Mackenzie Delta, only about 10° from the geomagnetic pole, we expect to observe a larger ^{14}C activity in the tree rings than in the samples of Damon et al.

In Fig. 2 we plotted the six $\Delta^{14}C$ values, together with the measurements by Damon et al. (1973) and that by Stuver and Quay (1980), in the period from 1940 to 1954 AD. The high $\Delta^{14}C$ values in the Mackenzie wood, as compared with that in the Washington wood of Stuiver and Quay and that in the Arizona wood of Damon et al., can be explained by the fact that in the near arctic circle, the air is less contaminated by fossil fuel burning. Disregarding the difference in the

ORIGINAL PAGE IS
OF POOR QUALITY

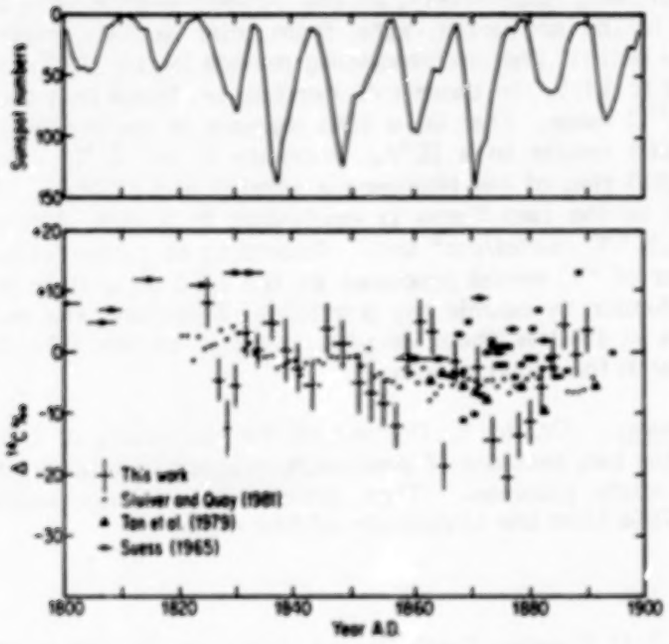


Fig. 1. Upper panel, sunspot numbers; lower panel, $\Delta^{14}C$.

general $\Delta^{14}C$ level, the increase in $\Delta^{14}C$ in the 1943 ring of the Mackenzie wood agrees remarkably well with that in the Arizona wood. The puzzling fact is that the Washington State sample does not show any sign of increase. If one assumes that the increase in $\Delta^{14}C$ in the Mackenzie wood was indeed due to the two flares in 1942, then the magnitude of the flares can be estimated as follows:

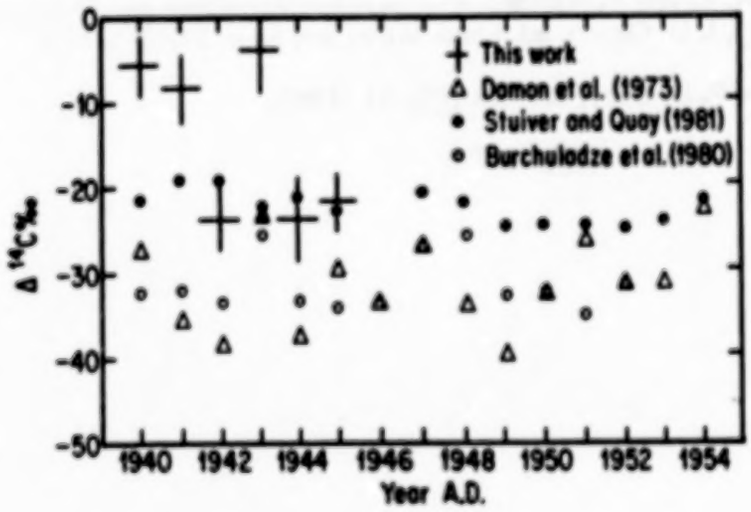


Fig. 2. $\Delta^{14}C$

Ligenfelter and Ramaty (1970) calculated the ^{14}C production rates during the 1953-1954 solar mnimum and the 1957-1958 solar maximum period as 5.0 and 3.5 ^{14}C nuclei/cm^2 sec, respectively, in the 70°-90° geomagnetic latitude range. A 42% increase in the production rate from solar activity maximum to solar activity minimum period. The corresponding periods in the 19th century are 1866 to 1867 and 1870 to 1871. In these two periods, we found that there is a 20°/$_{oo}$ increase in the $\Delta^{14}C$ value. That is, a 40% increase in the production rate in the high latitude region results in a 20°/$_{oo}$ increase in the $\Delta^{14}C$ value. The $\Delta^{14}C$ increase in the 1943 ring of the Mackenzie wood is about 20°/$_{oo}$. Therefore, the ^{14}C increase due to the two flares is equivalent to a 40% increase in the ^{14}C production, or, 1.5 ^{14}C nuclei/cm^2 sec. According to Lingenfelter and Ramaty (1970), the number of ^{14}C nuclei produced by the 1956 solar flare is equivalent to the one-year production by cosmic ray particles. Therefore, the combined effect of the two flares in 1942 is about one-half of that of the 1956 flare. We are continuing our search for larger events.

5. Acknowledgment. Dr. M. L. Parker of the University of British Columbia supplied us with the two sections of dendrochronolgocally calibrated white spruce that made this study possible. This project is partially supported by the subcontract R 277664 from the University of Maryland.

6. References

Baxter, M. S. and J. G. Farmer, Earth Planet. Sci. Lett. 20, 295 (1973).

Burchuladze, A. A. et al., Nature 287, 320 (1980).

Damon, P. E., A. Long and E. I. Wallick, Earth Planet. Sci. Lett. 20, 300 (1973).

Fan, C. Y., T. M. Chen, S. X. Yuu and K. M. Dai, Radiocarbon 25, No. 2, 205 (1983a); 18th ICRC, conference paper, vol. 3, 173 (1983b).

Forbush, S. E., Phys. Rev. 70, 771 (1946).

Lingenfelter, R. E. and R. Ramaty, Radiocarbon Variations and Absolute Chronology, I. U. Olsson, ed. (John Wiley and Sons, 1970), p. 513.

Stuiver, M. and P. D. Quay, Science 207, 11 (1980).

Tans, P. P., et al., Nature 280, (1979).

N85-35096
SH 7.1-3

COSMIC RAY SECULAR VARIATIONS IN TERRESTRIAL RECORDS AND AURORAE

M.R.Attolini, Istituto TESRE del CNR, Bologna
G.Cini Castagnoli and G.Bonino, Istituto di Fisica Generale, Università and Istituto di Cosmogeofisica,CNR,Torino, Italy
M.Galli, Dipartimento di Fisica, Università di Bologna
T.Nanni, Istituto FISBAT del CNR, Bologna

1.Introduction. The rediscovery that the Sun and the Solar wind can undergo important changes on historical time scales [1,2,3] has brought into question the stability of the cyclic behaviour of past time series of Solar and Solar-terrestrial origin. In preceding papers we have found [4,5,6] by Vector Fourier analysis that the solar eleven year cycle is present in the series of ^{10}Be, $\delta^{18}O$, in ice cores and of TL (thermoluminescence) in sea sediments during the last Millennia with a frequency modulation, that we could relate to the Sun behaviour, as tested by comparison with the Sunspot number R_z series [7], in recent times. In a companion paper of this Conference (SH 7.1-1) we have shown that the cyclogram of the series of yearly Aurorae from 1721 to 1979 linear-regression-corrected-for-R_z is straight for the periodicity τ=11,1y, indicating that such periodicity is constant in time corresponding to the only line present in the 11y band. The maxima of this component appear at the same time together with the high speed solar wind streams taking place in coronal holes situated at high heliolatitudes. This connection with a regular solar rithm induced us to search for the possibility that this frequency would be dominant also in the long running (2300 years) scanty record of historical Aurorae recorded at mid and low latitudes in European and oriental countries.

2.Historical Aurorae. The record of Aurorae [8,9] from 686BC to 1731AD is here analysed: unfortunately the Sunspot record is not available before 1700 so we cannot undertake the aforementioned procedure adopted for the yearly Aurorae. However similarities can be tested on the total series: the power spectral density (p.s.d.) of the Hystorical Aurorae has been computed for two subseries one from 687 BC to 1000 AD and the other from 1000 AD to 1731 AD; and compared to the p.s.d. of the Aurorae from 1721 to 1979 (see Figure 1). We may notice that all three p.s.d. show in the 11y band two peaks respectively around 11,1y and 10.0y: before 1000 AD at 10.8y and 9.5y whereas after 1000 AD at 11.4y and 10.5y, the recent p.s.d. at 11.1y and 10.0y. The phase cyclogram (see Figure 2) at τ=11y and T=100, infact shows frequency oscillations of duration of about 2 centuries around two main frequencies one of a little less than 11y (right bending) before 1000 AD and the other a little greater than 11y (left bending) after 1000 AD. The values of the periodicities (11.1y and 9.9y) in the recent Aurorae record could represent a transition similar to the one observable in Figure 2 around

the XI century (1016 AD) and perhaps to another one which could have occurred around the beginning of the Christian era.

3.Comparison of Solar-terrestrial records. The frequency modulation of the eleven year cycle on a 2 century time scale could be associated with the presence in the series of oscillations of the same period. Therefore we have performed the phase cyclogram of the historical Aurorae (Au) series at τ=200y together with those of three other series of data in which the Solar-Terrestrial relationships could be involved: D/H in a South Pole ice core[10], ^{14}C in tree rings[11], Thermoluminescence (TL) in a sea sediment[12], from 500 A.D. up to the present time. They are shown in Figure 3. All of these cyclograms are fairly stretched, indicating that this recurrency is present during this interval in all the four series. However the phases of the four cyclograms are different. The phase shift between Au and ^{14}C is about 180°. This can be interpreted as a consequence of the known fact that increasing Solar activity corresponds to decreasing C.R. intensity and therefore cosmogenic ^{14}C production.
The cyclograms of Au and TL are approximately in phase, this favours the hypotesis that the TL signal is in direct correlation with the Solar activity.
The cyclograms of Au and D/H are out of phase of about 90°. This corresponds to the fact that the global temperature index D/H has its maximum during the ascending phase of the 200y cycle of the Aurorae. These considerations however are not sufficient to assess that the origin of the 200y cycles is definitely of solar and not of terrestrial origin, in particular because the series which shows the strongest amplitude of 200y wave and its constancy in phase is indeed the series of D/H.
Moreover the phase-cyclogram for ^{14}C over the entire la Jolla series for 8400y (see Figure 4) shows that a regular bisecular wave is not always present: trains appear from time to time, the last one starting at about the third century B.C. For comparison the cyclogram at τ=178y is shown in the same Figure. The long periodicities "Suess wiggles" have been extensively discussed by Sonett[13] and the presence of common long periodicities in ^{14}C and TL were previously pointed out by us[14].

4.Conclusions. This analysis shows that a cyclicity of about 200y is present in terrestrial natural phenomena (^{14}C in tree rings, TL series in marine sediment, D/H global temperature index and Aurorae), which could have a common control processbased on Solar-Terrestrial relationships.
If one assumes that the Aurorae record can be used as proxy data of Solar activity then:
a) its anticorrelation with ^{14}C can be interpreted as a consequence of

ORIGINAL PAGE IS
OF POOR QUALITY

the well known fact that increasing Solar activity corresponds to decreasing C.R. intensity;
b) its direct correlation with TL favours the hypothesis that Solar activity is responsible for this effect;
c) the global temperature index D/H has its maximum during the ascending phase of the Solar activity.
The analysis of the eleven years cyclicity of the Solar activity through the structure of the Aurorae records seems to suggest that in modern time we are having a transition similar to the one observable in the XI century AD. Moreover there is strong evidence that the eleven year cycle has undergone frequency oscillations on a time scale of two centuries, although it is very difficult to determine the periodicities with high accuracy.

References

1.Eddy J., (1980), In Proc.Conf.Ancient Sun, Geochimica and Cosmochimica Acta suppl.13, p.119
2.Siscoe L., (1980), Rev.of Geophys. and Space Phys. 18, 647
3.Feynman J., (1983), Reviews of Geophys. and Space Phys., 21, 338
4.Cini Castagnoli G., Bonino G., Attolini M.R., Galli M. and Beer J., (1984), Il Nuovo Cimento 7C, 235
5.Attolini M.R., Beer J., Cecchini S., Cini Castagnoli G. and Galli M., (1984), Proc.of Int.Symp. on C.R. modulation in the heliosphere, Morioka, Japan
6.Beer J., Oeschger H., Finkel R.C., Cini Castagnoli G., Bonino G., Attolini M.R. and Galli M., (1984), Proc. 8th Conf. on the Application of Accelerators in Research and Industry, Denton,(Texas), 12-14 nov' 84 in Nuclear Instr.& Methods (In press)
7.Attolini M.R., Galli M., Cini Castagnoli G., (1985), Solar Physics, 95, 391
8.Aurorae records: Stothers, Link, Newton, Dall'Olmo, Keimatsu (kindly provided to us by Dr. F.R.Stephenson)
9.Shove D.J., (1980), Proc.of the SolarTerrestrial Predictions Workshop U.S. Dept.of Comm., Washington DC
10.Benoist J.P., Jouzel J., Lorius C., Merlivat L., Pourchet M., (1982), Annals of Glaciology 3, 17
11.Suess H.E., (1980), Radiocarbon 22, 200
12.Cini Castagnoli G., Bonino G. and Miono S., (1982), Il Nuovo Cimento 5C, 488
13.Sonett C.P., (1984), Reviews of Geophys. and Space Phys., 22, 239
14.Attolini M.R., Bonino G., Cini Castagnoli G. and Galli M., (1983), 18th ICRC, 9, 321

SH 7.1-3

ORIGINAL PAGE IS
OF POOR QUALITY

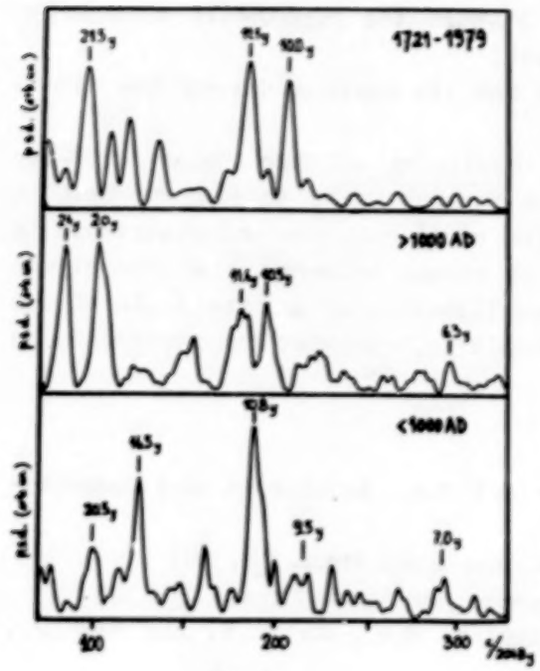


Fig.1

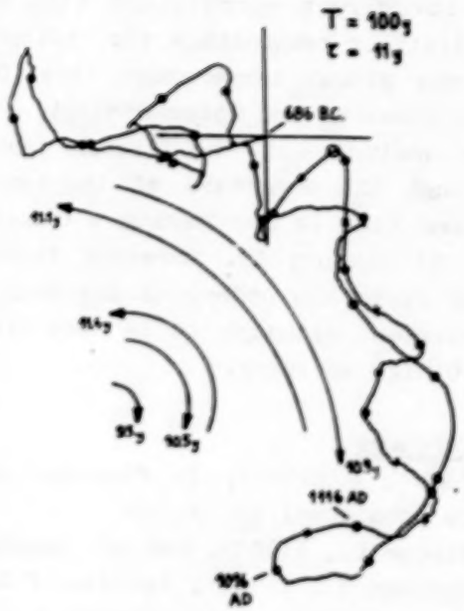


Fig.2

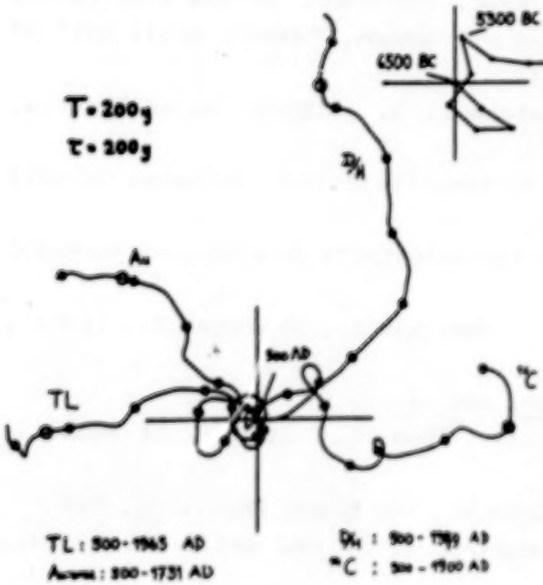


Fig.3

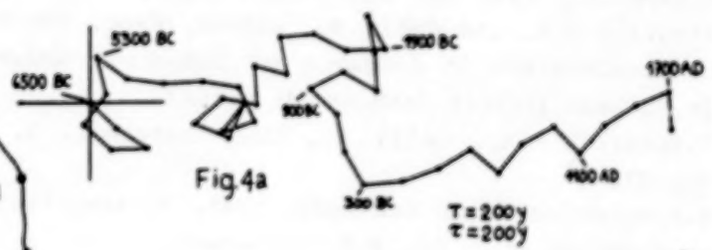


Fig.4a

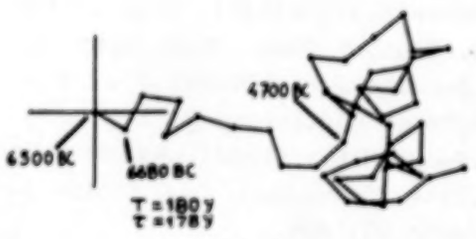


Fig.4b

WHEN DID THE AVERAGE COSMIC RAY FLUX INCREASE?

N85-35097

K. Nishiizumi, S. V. S. Murty, K. Marti and J. R. Arnold
Department of Chemistry, B-017
University of California, San Diego
La Jolla, CA 92093 (U. S. A.)

Abstract

We developed a new ^{129}I-^{129}Xe method to obtain cosmic ray exposure ages and to study the average cosmic ray flux on a 10^7-10^8 year time-scale. The method is based on secondary neutron reactions on Te in troilite and the subsequent decay of ^{129}I, the reaction product to stable ^{129}Xe. We report the first measurements of ^{129}I and ^{129}Xe in aliquot samples of a Cape York troilite sample.

Introduction

Several investigations were carried out regarding possible variations of cosmic ray intensity in the past. Cosmic ray produced ^{14}C in trees provides one of the most reliable records for the cosmic ray intensity in the past 10^4 years in spite of some uncertainties in the carbon cycle and/or past geomagnetic field variation [eg. 1]. For longer periods ^{10}Be ($t_{1/2}$ = 1.6x10^6 years) and/or ^{36}Cl (3.0x10^5 years) concentrations in ice cores or deep sea sediment cores may provide additional information on the cosmic ray flux in the past. However, there are many uncertainties in past climates, in precipitation and sedimentation rates, in geomagnetic fields, because the terrestrial environment is rather complex. On the other hand, the study of cosmogenic radionuclides in extraterrestrial matter provides key information for the history of cosmic rays. Kohl et al (1978) found that the average solar cosmic ray (SCR) flux changed relatively little over the last 1-10 million years, based on a study of cosmogenic ^{53}Mn ($t_{1/2}$ = 3.7x10^6 years) and ^{26}Al (7.05x10^5 years) in several lunar rocks [2]. The average SCR flux during the last few million years was similar to that measured during the last few decades by detectors on satellites. However, ^{14}C ($t_{1/2}$ = 5740 years) [3] and ^{81}Kr (2.1x10^5 years) [4] activities in lunar samples indicate that the average SCR flux during the last 10^4 - 10^5 years was somewhat higher than the recent average flux. Very useful records on the galactic cosmic ray (GCR) flux were observed in meteoritic detectors. Nishiizumi et al (1980) carried out systematic studies on cosmogenic nuclides of various half-lives such as ^{22}Na ($t_{1/2}$ = 2.6 years), ^{81}Kr, ^{26}Al, and ^{53}Mn in chondrites as a test for possible variation of the GCR flux during the last ~10 million years [5]. All sets of nuclides, with the possible exception of ^{26}Al indicate that the averaged GCR flux was constant within ~15%, at least during the last 5 million years. More recently, Moniot et al (1983) confirmed this result using ^{10}Be as the monitor [6]. On the other hand, the records of spallation K and Ar observed in iron meteorites reflect ~33% smaller average GCR fluxes on the 10^8-10^9 year timescale [7, 8]. This suggests a cosmic ray flux increase $\lesssim 2x10^8$ years ago.

^{129}I-^{129}Xe Method:

An investigation for possible intensity changes of GCR flux between 10^7 and 10^8 years is required. The half-life of ^{129}I (1.57×10^7 years) makes this an appropriate nuclide for such a study. The ^{129}I in extraterrestrial materials is produced by cosmic ray secondary neutron reactions on Te, ^{130}Te (n,2n,β) ^{129}I and ^{128}Te (n,γ β)^{129}I, and by high energy spallation reactions on Ba and the Rare Earth elements. Troilite inclusions in iron meteorites are ideal monitors among extraterrestrial materials because of their long cosmic ray exposure ages (10^8 to 10^9 years) their relatively high Te contents (~ ppm) and their low abundances of Ba and Rare Earth elements. The ^{129}I decays to stable ^{129}Xe. ^{129}Xe is not directly produced by cosmic ray secondary neutrons, yielding a fractional isobaric production ratio P (^{129}I)/P(^{129}I + ^{129}Xe) ~1 [9]. The simultaneous determination of cosmogenic ^{129}I and ^{129}Xe in the same troilite phase is the basic concept of the new method of determining ^{129}I-^{129}Xe exposure ages. This exposure age can be obtained without any shielding and target element corrections for a constant exposure geometry. The exposure age T can be calculated from the equation:

$$\frac{\lambda_{129}T - 1 + e^{-\lambda_{129}T}}{1 - e^{-\lambda_{129}T}} = \frac{^{129}Xe_{Te}}{^{129}I_{Te}}$$

where λ^{129} is decay constant of ^{129}I, $^{129}I_{Te}$ is ^{129}I content (atom/sample), and $^{129}Xe_{Te}$ is cosmogenic ^{129}Xe content (atom/sample) produced from Te after subtraction of other components. The comparison of ^{129}I-^{129}Xe exposure ages and with those obtained by methods such as ^{40}K-^{41}K [7], ^{26}Al-^{21}Ne, and ^{36}Cl-^{36}Ar could indicate either a complex exposure history of the meteorite or a change in cosmic ray flux intensity. We developed the experimental techniques and measured both ^{129}I and ^{129}Xe in the same troilite sample of the large Cape York iron meteorite. The ^{129}I measurement was carried out by accelerator mass spectrometry using the University of Rochester MP tandem van de Graaff accelerator [see 10], while the ^{129}Xe measurement was performed by static mass spectrometry.

Discussion:

The Cape York iron meteorite contains $(8.3 \pm 1.3) \times 10^6$ atoms ^{129}I/g troilite and $(2.6 \pm 0.3) \times 10^7$ atoms $^{129}Xe_{Te}$/g troilite. The ^{129}I-^{129}Xe exposure age of Cape York is calculated from the above equation as T = 93 $\pm$18 million years. This is the first determination of a cosmic ray exposure age of Cape York. The inferred Ar production rate P (^{38}Ar) ~ 200 atoms/g Fe x year [11] is one order of magnitude smaller than that corresponding to the most shielded location for which P(^{38}Ar) data are available. This result documents (a) the extremely heavily shielded location of our sample and (b) that secondary cosmic ray neutrons are very useful in unravelling exposure histories and geometries. The Cape York results, however, do not allow an evaluation of the average cosmic ray flux over the 93 million year exposure period, since no other

information on the exposure age is available. Therefore, we are now applying the ^{129}I-^{129}Xe dating method to meteorites for which independent exposure age information is either available, or can be obtained.

Acknowledgements: We thank D. Elmore for his collaboration on the ^{129}I accelerator mass spectrometry. This work was supported by NASA Grants NAG 9-33 and NAG 9-41.

References

1. Suess, H. E. (1980) Radiocarbon 22, 200-209.

2. Kohl, C. P. et al, (1978) Proc. 9th Lunar Planet. Sci. Conf., 2299-2310.

3. Boeckl, R. S., (1972) Earth Planet. Sci. Lett., 16, 269-272.

4. Yaniv, A., et al, (1980) (abstract) Lunar Planet. Sci., XI, 1291-1293.

5. Nishiizumi, K., et al, (1980) Earth Planet. Sci. Lett., 50, 156-170.

6. Moniot, R. K., et al (1983) Geochim. Cosmochim. Acta, 47, 1887-1895.

7. Voshage, H. (1962) Z. Naturforschg. 17a, 422-432.

8. Laviolle, B. et al, (1984) Proc. of Conf. on Isotopic Anomalies in the Solar System, Paris.

9. Marti, K., (1984) Proc. of Workshop on Cosmogenic Nuclides, (Los Alamos, New Mexico).

10. Nishiizumi, K., et al, (1983) Nature, 305, 611-612.

11. Murty, S. V. S. and Marti, K. (1984) Manuscript in preparation.

COSMOGENIC-NUCLIDE PRODUCTION BY PRIMARY COSMIC-RAY PROTONS

Robert C. Reedy
Nuclear Chemistry Group, Mail Stop J514
Los Alamos National Laboratory
Los Alamos, NM 87545, USA

N85-35098

ABSTRACT

The production rates of cosmogenic nuclides were calculated for the primary protons in the galactic and solar cosmic rays. At 1 AU, the long-term average fluxes of solar protons usually produce many more atoms of a cosmogenic nuclide than the primary protons in the GCR, the exceptions being nuclides made only by high-energy reactions (like Be-10). Because the particle fluxes inside meteorites and other large objects in space include many secondary neutrons, the production rates and ratios inside large objects are often very different from those by just the primary GCR protons. Thus it is possible to determine, by examining its cosmogenic nuclides, if a small object, such as found among deep-sea spherules, was small in space or broken from a meteorite. Because heliospherical modulation and other interactions change the GCR particle spectrum, the production of cosmogenic nuclides by the GCR particles outside the heliosphere will be different from that by modulated GCR primaries. Production rates and ratios for cosmogenic nuclides would be able to identify small particles, possibly interstellar in origin, that were exposed to an unmodulated spectrum of GCR particles and to characterize the spectrum of particles to which they were exposed.

1. Introduction. The energetic particles in the cosmic rays are about 90% protons and induce a wide variety of nuclear reactions in extraterrestrial matter (1). Relatively low energy (~10- to 100-MeV) particles are emitted occasionally from the sun--the so-called solar cosmic rays (SCR). The SCR particles are rapidly stopped in matter (within a few centimeters) and produce a high density of product nuclei very near the surface. The high-energy (~1-GeV) galactic cosmic-ray (GCR) particles produce a large cascade of secondary particles, especially neutrons, that penetrate meters into solid matter. The flux of GCR particles in the solar system varies with solar activity and is lowest at periods of maximum solar activity. Most studies of cosmogenic nuclides have been for large objects (the Earth, moon, and meteorites) and for long periods of time (averaged over many solar cycles). Recently, there has been more interest in cosmogenic nuclide production in very small objects (2) and also in the production variations over a solar cycle (3), outside the solar system (4), or for periods of unusual solar activity (5).

2. Primary Cosmic-Rays. The spectrum of solar protons is well approximated by an exponential function in rigidity (6); it has an average spectral shape over the last million years (1) of R_0 = 100 MV. Castagnoli and Lal (5) give an equation for the spectral shape of the GCR as a function of a solar modulation parameter (M). For the GCR protons, spectra like those for the last two solar minima (M = 375 MeV) and maxima

(M = 950 MeV) (1,5) were used, as well as one that is similar to the average over a solar cycle (M = 550 MeV). A fourth GCR spectrum was the expression of (5) for no modulation (M = 0), possibly like that of the GCR particles outside the solar system in the local interstellar space (IS). The shape for the expression with M = 0 is very similar to (E + 1050) to the -2.87 power, with E in MeV. Such an unmodulated spectrum could be approached in the solar system during the long periods of essentially no solar activity that occur about every few hundred years (1,5). One estimate of the proton spectrum at the source of GCR particles is a power law in rigidity. At high energies, this rigidity power law was assumed to have the same intensity and shape as that observed in the solar system. As any source GCR-particle spectrum is modified by passage through ~5 g/cm^2 of matter, this pure rigidity power-law spectrum overestimates the proton fluxes at lower energies, especially below ~100 MeV (6). Production rates for seven cosmogenic nuclides were calculated with these proton spectra and with cross sections for proton-induced reactions (see Table I). The production rates of these nuclides observed in meteorites (with typical radii of 10 to 30 cm) are also shown in Table I.

3. Cosmogenic-Nuclide Production Rates. Production by solar protons usually dominates that by primary GCR protons. Only nuclides made mainly by high-energy protons, such as Be-10 and Cl-36, have very low production rates by the low-energy solar protons. These high rates by solar protons only occur very near the surface, and solar-proton production rates become relatively unimportant below depths of a few centimeters (1,6). Only the GCR source spectrum exceeds the solar-proton production rates, mainly because of its high fluxes at lower energies. In most meteorites, production by solar protons is usually not observable because the surface layers are removed by ablation during the meteorite's passage through the Earth's atmosphere. The ratio of the amount of a nuclide readily made by solar protons (for example, Al-26) to that of a high-energy product (such as Be-10) is a good indicator of the object's size when it was irradiated in space. Activities of Al-26 and Be-10 were measured in several groups of small (0.3- to 0.5-mm) spherules collected from sediments on the ocean floor (2). The Al-26/Be-10 ratio and the Al-26 activity were quite high in several of them, which indicate that those spherules probably came from parent bodies less than a few centimeters in diameter. Studies of such small objects would be interesting because they may be different from the forms of solar system matter found in most meteorites.

The production rates of nuclides by GCR protons in interstellar space are high, similar to the rates produced by both primary and secondary GCR particles in meteorites. The relatively low-energy protons normally removed by solar modulation in the inner solar system have produced about the same number of nuclides as are made by secondary neutrons in meteorites. These high production rates, plus the relatively low loss of product nuclides by recoil in small grains (4), mean that one should be able to identify grains that were irradiated in interstellar space. Such grains may have been incorporated in meteorites or could enter the Earth's atmosphere as cosmic dust. The cross sections as a function of energy for making secondary neutrons are similar in shape to those for producing He-3. The He-3 production rate in interstellar space is 4 times that for the average over a solar cycle, and the flux of

protons above 1 GeV in interstellar space is 2.4 times that for the solar-cycle average. Thus, the production rates of cosmogenic nuclides by GCR particles that have not been modulated are higher (by factors up to 3 to 4) than those observed near the Earth during long periods of typical solar activity.

During periods of normal solar variations, the extremes in the activity of the sun and its subsequent modulation of the GCR particles are represented by the solar minimum and maximum used in Table I. The ratio of 2.4 for the He-3 production rates between these extremes is about the variation that would be expected for the production of secondary neutrons. When Evans et al. (3) measured the activities of short-lived radionuclides in a number of meteorites that fell from 1967 to 1978, the activities varied by about a factor of 3. Some of these variations probably were caused by differences in the meteorites' sizes or shapes or in the sample location. However, the calculations reported here show that most of these radioactivity variations are caused by the solar modulation of the GCR-particle flux. The observed radioactivity variations correlated well with other indicators of solar activity (3). Larger variations in nuclide production rates would be expected if the solar activity exceeded one or both of the average extremes used here.

In Table I, the ratio of the GCR production rates typically observed in meteorites to the solar-cycle-averaged rates for primary GCR protons ranged from 2.3 to 8.0. Because the flux of primary protons inside a meteorite is attenuated by nuclear interactions, the ratios of observed activities to those made only by the primary GCR protons should be even larger. These relatively low contributions by the primary particles illustrate the importance of secondary particles in nuclide production in large objects like meteorites. This big difference between nuclide production by primaries only and by the fully developed secondary cascade present in most meteorites indicates that small meteorites without a fully developed cascade could have some unusual production rates or ratios. Studies of such small meteorites also would help us understand the production and transport of secondary particles in meteorites.

4. Conclusions. The calculations and results in Table I show that the production of cosmogenic nuclides can vary considerably with both the size of the extraterrestrial object and the amount of the solar modulation of the primary GCR particles. Very small objects have high production rates by solar protons. Typical meteorites are large enough that the cascade of secondary particles dominates nuclide production. Intermediate-size objects could have some unusual production rates and ratios. Temporal and spatial variations in nuclide production can also result from differing GCR-particle modulation. Variations by factors of 2 to 3 can occur during a normal solar cycle, and even larger deviations can occur when solar modulation is much stronger or weaker than usual.

5. Acknowledgements. This research was supported by NASA work order W-14,084 and done under the auspices of the US DOE. Discussions with J. Evans, H. Völk, K. Jokipii, and M. Forman helped in planning this work.

N85-38039

References

1. Reedy, R. C., et al., (1983), Science 219, 127-135.
2. Raisbeck, G. M., et al., (1983), In Lunar and Planetary Science XIV (Lunar and Planetary Institute, Houston), pp. 622-623.
3. Evans, J. C., et al, (1982), J. Geophys. Res. 87, 5577-5591.
4. Ray, J., and H. J. Völk, (1983), Icarus 54, 406-416.
5. Castagnoli, G., and D. Lal, (1980), Radiocarbon 22, 133-158.
6. Reedy, R. C., and J. R. Arnold, (1972), J. Geophys. Res. 77, 537-555.

TABLE I. Nuclide Production Rates by Primary Cosmic-Ray Protons, Assuming C2-Chondritic Chemistry.

	10^6 years Av SCR	Solar Max. GCR	Solar Av GCR	Solar Min. GCR	Local IS GCR	GCR Source	Typical Meteorite
Parameter	R_o=100	M=950	M=550	M=375	M = 0	$R^{-2.65}$	
Integral Flux[a]	70	1.21	1.80	2.39	4.33	4.33	
Nuclide	(atoms/minute/kg)						
He-3	66.	190.	318.	459.	1258.	4095.	900.
Be-10	4.1	5.0	8.1	11.5	28.6	60.8	22.
Ne-21	395.	11.6	20.8	31.7	117.	1603.	150.
Al-26	344.	3.9	7.5	11.9	56.	1344.	60.
Cl-36	0.9	1.8	3.1	4.5	11.2	20.1	7.
Ar-38	72.	3.3	5.5	8.0	24.4	260.	20.
Mn-53	590.	7.6	13.6	20.8	90.	2177.	105.

[a] In protons/cm^2/s: solar protons for E > 10 MeV, GCR for E > 1 GeV.

N85-35099
SH 7.1-7

COSMIC-RAY EXPOSURE RECORDS AND ORIGINS OF METEORITES

Robert C. Reedy
Nuclear Chemistry Group, Mail Stop J514
Los Alamos National Laboratory
Los Alamos, NM 87545, USA

ABSTRACT

The cosmic-ray records of meteorites can be used to infer much about their origins and recent histories. Some meteorites had simple cosmic-ray exposure histories, while others had complex exposure histories with their cosmogenic products made both before and after a collision in space. The methods used to interpret meteorites' cosmic-ray records, especially identifying simple or complex exposure histories, often are inadequate. Besides spallogenic radionuclides and stable nuclides, measurements of products that have location-sensitive production rates, such as the tracks of heavy cosmic-ray nuclei or neutron-capture nuclides, are very useful in accurately determining a meteorite's history. Samples from different, known locations of a meteorite help in studying the cosmic-ray record. Such extensive sets of meteorite measurements, plus theoretical modeling of complex histories, will improve our ability to predict the production of cosmogenic nuclides in meteorites, to distinguish simple and complex exposure histories, and to better determine exposure ages.

1. Introduction. Meteorites are fragments from a variety of objects in the solar system and can provide important information about these bodies. Well-determined cosmic-ray exposure histories are needed to help to establish the origins of meteorites: where they came from and how they were produced (1,2). In principle, the exposure history of a meteorite should be well determined if sufficient measurements are made of its cosmic-ray record and if the production rates and profiles of the cosmogenic products used to interpret the measurements are known well enough. It is unlikely that many meteorites have had their cosmic-ray exposure histories properly determined. Wetherill (3) noted that complex histories should be common for most likely meteorite-origin scenarios. However, complex histories for meteorites are seldom reported, especially for stony meteorites. Is this discrepancy between the predicted and reported frequencies of meteorite complex histories a problem with the approaches presently used to study the exposure records of meteorites? Inadequacies in the interpretation of the cosmic-ray records of meteorites could mean that exposure ages and other results of meteorite studies, such as cosmic-ray variations, also might not be correct. Systematic experimental and theoretical studies are needed to study how well we have been determining the recent histories of meteorites and to develop better methods for unfolding the cosmic-ray records of meteorites.

2. Cosmic-Ray Exposure Records. Among the ages of a meteorite, the youngest are those determined from the activities or concentrations of cosmogenic products. Exposure ages, the lengths of time that meteorites

have been exposed to cosmic rays, are typically orders of magnitude shorter than their radiometric formation ages and, for some meteorites, their brecciation ages and collisional shock ages (4). The cosmogenic products used to study exposure records of meteorites include stable and radioactive nuclides and tracks of heavy cosmic-ray nuclei. If a meteorite had a simple exposure record, then the concentration of a cosmogenic product and its production rate can be used to determine an exposure age. However, the production rates vary considerably with meteoroid size and shape and with sample location (5), so corrections for the effects of the sample's shielding geometry must be applied. Most methods for estimating shielding corrections, such as the Ne-22/Ne-21 or He-3/Ne-21 ratios, do not yield unique production rates but only narrow the range of possible values (5).

Many meteorites had simple exposure ages. Detailed investigations of the cosmic-ray records of several meteorites, such as the tracks, radionuclides, and spallogenic noble gases in St. Severin (6), show that the cosmogenic products were made only during one exposure geometry. However, most meteorites have not had their exposure records shown to have been simple by such systematic studies. Another clue that a meteorite probably had a simple history is that its exposure age is the same as a number of other meteorites of the same type. However, there are only a few clusters for the exposure ages of meteorites; the exposure ages for most meteorites form a continuous distribution.

The clusters of exposure ages for a given class of meteorites, such as the ~675 Ma (675 million years) cluster for IIIAB irons (7) or the ~6 Ma peak for H-chondrites (8), suggest that these meteorites were all produced by single, major collisional events. If these two clusters really represent individual events, the widths of the peaks, about 15-20% of the age, indicate that the sums of the uncertainties in determining cosmic-ray exposure ages are fairly large. As the measurement uncertainties are much smaller than 15-20%, the spread in the exposure ages for these clusters probably results from interpreting the measurements (although pre-irradiation or gas losses could account for some of the spread). One likely source of this width in the exposure-age peaks is the significant correction for shielding.

Several meteorites clearly had their cosmogenic products made both before and after a major collisional event in space that changed the meteoroid's geometry. The Jilin chondrite was irradiated by a significant flux of cosmic-ray particles for ~10 Ma near the surface of a very large object prior to its ejection ~0.4 Ma ago as an 85-cm-radius sphere (9). Several other meteorites have had complex histories, such as several inferred from the disagreements among exposure ages determined with different radionuclides or stable cosmogenic products. In very large meteorites, such as the Canyon Diablo iron meteorite (10), one part could have been removed by a minor collision without seriously affecting the formation of cosmogenic products in other parts of the meteoroid.

The distinction between simple and complex exposure histories can be difficult in some cases. Some meteorites probably have small amounts of cosmogenic products made prior to the event that produced the object that eventually hit the Earth. In most cases, the amounts of cosmogenic

products made during the meteorite's final exposure geometry overwhelm any previous production. However, if this last exposure stage was short, then possibly the products made during the previous exposure could be detected. As suggested by (9), the high production rates inferred for Ne-21 from meteorites that have undersaturated Al-26 activities (that is, exposure ages of ~1 Ma) could be a consequence of pre-irradiation. A very special case of a complex history is when a foreign clast in a brecciated meteorite has had a previous exposure to the solar wind or cosmic rays prior to incorporation in the meteorite (11).

3. Systematic Experimental Studies. To properly calibrate the predicted production rates and profiles of cosmogenic products in meteorites, extensive sets of measurements are needed. The measurements should be made for samples from different, known locations and also of products with a wide range of production-rate-versus-depth profiles (tracks, high- and low-energy spallation, and neutron capture) and a variety of half-lives (including stable isotopes). For example, the Na-22 and Co-60 activities measured in Jilin (9) serve as a calibration points for cosmogenic nuclides in a meteoroid with a radius of 85 cm. The measurements of cosmogenic products in meteorite cores, such as those from St. Severin (6) and Keyes, also are valuable reference data.

However, few such well-characterized data sets for cosmogenic nuclides in meteorites exist (5). Most meteorites that have been investigated in detail have radii of ~10-40 cm, which are typical of most meteorites. There have not been many extensive studies of smaller meteorites. Laboratory irradiations of small spherical targets are helping to understand the production of cosmogenic nuclides in small meteoroids (12). While Jilin had a radius of 85 cm for its last 0.4 Ma, its initial exposure limits studies of cosmogenic nuclides in large spherical meteoroids mainly to short-lived radionuclides, such as Na-22 and Co-60. More detailed measurements are needed to calibrate the models used to predict the production rates and profiles of cosmogenic nuclides, especially for meteorites that had unusual preatmospheric sizes or shapes.

4. Theoretical Modeling. Calculated size- and depth-dependent production rates can be used to illustrate the use of a meteorite's cosmic-ray record to accurately unfold its exposure history. Most models do a fairly good job of reproducing the profiles of cosmogenic products in typical-sized meteorites, such as St. Severin (6). However, some models have trouble with very large meteoroids, like Jilin (9). Very small meteoroids are hard to model because the cascade of secondary particles, especially neutrons, is not fully developed (5,12) and solar-proton production is important. Improved models are needed for all sizes, shapes, and types (irons and stones) of meteorites.

Some of these model results have been used to study criteria for identifying complex histories. For example, the calculated track production rates and the Ne-22/Ne-21 ratios for meteorites with simple histories cover a small region of all possible values (13). Meteoritic samples with tracks and neon ratios that are outside this region have complex histories. The activities of cosmogenic radionuclides are often used in looking for complex histories, and often these activities versus track

production rates or Ne-22/Ne-21 ratios are used to search for unusual exposure histories. Artificial exposure records derived from calculated production rates and profiles can be used to test the methods used to infer the exposure histories of meteorites. These theoretically constructed records for complex histories will especially help to show which features of a meteorite's cosmic-ray record are best suited for distinguishing complex from simple histories and which types of complex histories are most easily detected. Such theoretical studies would help to find the areas where meteorite measurements or more laboratory simulations or cross sections would be most useful.

5. Conclusions. Many experimental and theoretical studies are needed to improve our ability to unfold the cosmic-ray exposure records of meteorites. More extensive measurements of cosmogenic products in meteorites, especially shielding-sensitive ones like tracks and neutron-capture-produced nuclides, will help to identify meteorites that had complex histories and to yield better exposure ages. Such improved recent histories could aid in identifying the parent bodies for certain meteorites, such as primitive carbonaceous chondrites (possibly from cometary surfaces) or the SNC meteorites (the Shergottites, Nakhlites, and Chassigny, which were possibly ejected from the martian surface). Detailed measurements of cosmogenic products in meteorites could be used to improve the models for predicting the production rates of these products. Theoretical studies of the production systematics of cosmogenic products in meteorites will help to identify areas where additional laboratory or meteorite measurements are needed.

6. Acknowledgements. This research was supported by NASA work order W-14,084 and done under the auspices of the U.S. Department of Energy. K. Marti and S. Regnier contributed to the ideas presented here.

References

1. Wetherill, G. W., (1985), Meteoritics 20, 1-22.
2. Greenberg, R., and C. R. Chapman, (1983), Icarus 55, 455-481.
3. Wetherill, G. W., (1980), Meteoritics 15, 386-387.
4. Bogard, D. D., (1979), In Asteroids, (T. Gehrels, ed.), pp. 558-578.
5. Reedy, R. C., (1985), J. Geophys. Res. 90, C722-C728.
6. Englert, P., and W. Herr, (1980), Earth Planet. Sci. Lett. 47, 361-369.
7. Voshage, H., and H. Feldmann, (1979), Earth Planet. Sci. Lett. 45, 293-308.
8. Crabb, J., and L. Schultz, (1981), Geochim. Cosmochim. Acta 45, 2151-2160.
9. Heusser, G., et al., (1985), Earth Planet. Sci. Lett. 72, 263-272.
10. Heymann, D., et al., (1966), J. Geophys. Res. 71, 619-641.
11. Schultz, L., (1979), Phys. Chem. Earth 11, 39-45.
12. Englert, P., et al., (1984), Nucl. Instrum. & Methods B5, 415-419.
13. Bhandari, N., and M. B. Potdar, (1982), Earth Planet. Sci. Lett. 58, 116-128.

N85-35100

SH 7.1-8

ACCELERATOR EXPERIMENTS ON THE CONTRIBUTION OF SECONDARY PARTICLES TO THE PRODUCTION OF COSMOGENIC NUCLIDES IN METEORITES

P.Dragovitsch and P.Englert
Department of Nuclear Chemistry, University of Köln,
D-5000 Köln 1, FRG

R.Michel
ZfS, University of Hannover, D-3000 Hannover 1, FRG

1. Introduction. Through the interaction of galactic cosmic particle radiation (GCR) a wide variety of cosmogenic nuclides is produced in meteorites. They provide valuable historical information about both the cosmic radiation and the bombarded meteorites. An important way to understand the production mechanisms of cosmogenic nuclides in meteorites is to gather information about the depth and size dependence of the build-up of GCR-secondary particles within meteorites of different sizes and chemical compositions. This can be obtained by analyzing cosmogenic nuclide depth profiles in meteorites [e.g. 1]. However, suitable meteorites are rare and the especially significant short-lived radioactive species have not been measured extensively. Simulation experiments with meteorite models offer an alternative to direct observation providing a data basis to describe the development and action of the secondary cascade induced by the GCR in meteorites.

2. Methods. A series of thick target irradiations of spherical meteorite models with radii (R) of 5, 15 and 25cm with 600 MeV protons, the maximum of the differential GCR proton fluxes, was performed at the CERN-synchrocyclotron [2]. The materials used to simulate the meteorite body were diorite (R=5cm) and gabbro (R=15,25cm), both having a density of $\sim$3g cm^{-3} and an extremely low water content of $\leq 10^{-3}$g/g. Pure elemental foils and simple chemical compounds were exposed to the particle fields along cores drilled perpendicular to each other through the center of the models. A homogeneous 4π isotropic irradiation was achieved combining four independent movements (two translational and two rotational) of the meteorite models in the fixed particle beam. The irradiation parameters for the three simulation experiments are given in table 1.

Table 1: Irradiation parameters of the 600 MeV proton simulation experiments

Model-radius [cm]	Irrad.time [min]	p-Dose [cm^{-2}]	"Exposure age" [10^6y]
5	489.5	4.82×10^{15}	76.0
15	750.0	2.17×10^{14}	3.4
25	763.0	5.99×10^{14}	9.3

3. Results and discussion. The depth-dependent production rates of radionuclides and stable isotopes from the target elements were determined by gamma spectroscopy, low-level counting techniques, accelerator- and conventional mass

spectrometry. The symbols in Figures 1a-e show the experimental production rates of five short-lived radioactive products in units of [10^{-4} atoms $s^{-1}g^{-1}$] as a function of depth within the meteorite models, assuming a primary proton flux of [$1cm^{-2}$ s^{-1}]. Product nuclides and targets are given in the Figures. The limits of uncertainty do not exceed the size of the symbols unless indicated by error bars. Figures 1a-e show only a small fraction of over 90 target-product-pairs obtained or in the process of reduction for each of the meteorite models. This selection especially emphasizes low energy secondary reactions. The extreme examples are the $^{27}Al(n,\alpha)^{24}Na$-reaction and the (n,p)-reaction on ^{54}Fe, mainly responsible for the ^{54}Mn production from iron. The other reactions occur at slightly higher threshold energies such as the $^{59}Co(n,2n)^{58}Co$ reaction, the mainly proton induced $^{27}Al(p,3p4n)^{22}Na$ reaction and the exclusively proton induced reaction $^{56}Fe(p,n)^{56}Co$.

Focussing on the measured data points in Figure 1, it is obvious that the depth profiles of all these low energy products increase from the surface to the center by 20%-30% independent of the radius of the meteorite model. This behavior was expected for the R=15cm and the R=25cm spherical model, but was striking for the R=5cm model, demonstrating that the contribution of GCR-secondaries cannot be neglected in small meteorites.

It is also remarkable that for all of the mainly neutron-produced species, the absolute production rates at the centers of the model meteorites increase with increasing model-radius, as predicted for low-energy secondary products in meteorites by various model calculations [3,4].For the exclusively proton produced $^{56}Co(Fe)$, the center activities for the two large meteorite models are indistinguishable within the limits of uncertainty. Moreover, for the ^{22}Na-production from Al, the highest center activity is found in the R=15cm model, whereas the center activity of the largest sphere is only slightly higher than that of the smallest. Taking into consideration that the production rates of the $^{56}Fe(p,n)^{56}Co$-reaction are more than an order of magnitude lower than those of the others the reversal of the sequence for ^{22}Na may then only be attributed to lower fluxes of charged secondaries above the threshold energy at the center of the largest model.

More precise information about the action of low energy secondary hadrons within the meteorite models can be obtained by calculating the contributions of primary protons to the production of the nuclides. The solid lines in Figure 1 show the calculated primary proton-induced contributions. The calculations consider stopping and absorption of the primaries, their fluxes for given energies and given positions [5] and excitation functions of the individual nuclear reactions[6]. The general tendency for cosmogenic nuclide production by primary protons is a decrease in production rate from the surface to the center. For the small R=5cm sphere the absolute contribution of secondary neutrons increases with increasing

threshold and charge (Z) of the target from the $^{27}Al(n,\alpha)$ over the $^{54}Fe(n,p)$ to the $^{58}Co(n,2n)$ reaction, i.e. the primary contribution becomes less important. For other nuclear reactions in all models a systematic description of the primary and secondary contribution as a simple function of Z of target, threshold energy and model radius cannot be observed. It is necessary to study the nuclear parameters of each individual target-product pair in detail. Nevertheless, the depth profiles presented provide an excellent basis for a quantitative description of primary and secondary particle fields in extended spherical targets under proton bombardment.

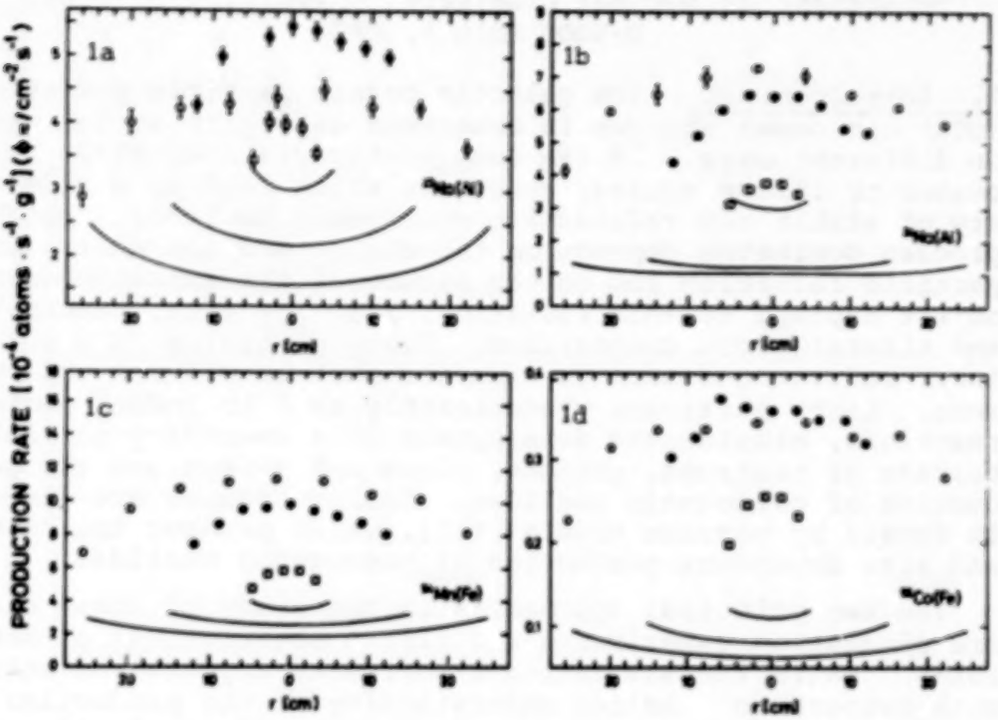
A more general point of interest is the question as to whether the 600 MeV simulation experiments performed are suitable to interpret observations in meteorites. There are several obstacles that prevent a direct comparison of the depth profiles in Figure 1 with meteorite data. Short-lived radionuclides have been measured only in a limited number of meteorite falls. Depth profiles of short-lived isotopes in meteorites have not been determined. Table 2 lists a number of meteorites of different preatmospheric sizes for which a few short-lived isotopes were measured [7]. Their production rates are given in the same units as in Figure 1. In view of these limitations the following conclusions can be made: ^{54}Mn and ^{22}Na-production rates follow directly the tendency given in Figure 1: they increase from the smallest to the largest meteorites. Assuming an average Fe-concentration of 25%, the respective production rates in table 2 will have to be multiplied by a factor of 4 to be directly comparable. In case of the ^{54}Mn-production in meteorites, Fe is the major target and the meteorite production rate thus exceeds the one found in the models by a factor of 3-4. The same is valid to a larger extent for the ^{22}Na-production, but here the largest contribution in a meteorite comes from Mg. The slight differences between actual meteorite data and the results of the simulation series presented may be caused by the use of diorite and gabbro to develop the secondary cascade, the density and average Z of which is somewhat lower than that of most meteorite classes; another reason may be found in using 600 MeV protons only.

Though the results of the 600 MeV proton irradiation series look very promising in modeling GCR primary and secondary fluxes in meteorites, further experiments using higher energies and different particles are necessary to more accurately simulate realistic conditions in space.

4. Acknowledgement. This work was partially funded by the DFG.

References: [1] P.Englert and W.Herr (1980), Earth Planet. Sci.Lett. 47 361-369. [2] R.Michel et al. (1984), Lun.Planet. Sci. XV, 542-543. [3] R.Reedy (1985), J.Geophys.Res. 90, C722-C728. [4] T.P.Kohmann and M.L.Bender (1967), in: B.S.P.Shen (ed.) High Energy Nuclear Reactions in Astrophysics, Benjamin, N.Y.. [5] R.Michel and R.Stück (1984),J.Geophys.Res. 89 B673-B684. [6] J.Tobailem, C.-H.de Lassus St. Genies (1975), CEA-N-1466 (1). [7] J.C. Evans et al. (1982), J.Geophys.Res. 87,

5577-5591. [8] N.Bhandari et al. (1980), Nucl.Tracks 4, 213-262. [9] P.Englert (1985), Lun.Planet.Sci. XVI, 215-216. [10] F.Marti et al. (1969), in: P.Millmann (ed.) Meteorite Research, Reidel, 248-266.



Figures 1a-e: Production rates of short-lived isotopes in meteorite models as a function of depth. A primary proton flux of [1cm^{-2}s^{-1}] is assumed.

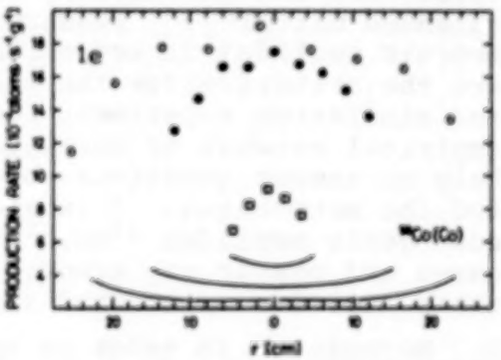


Table 2: Short-lived radionuclides in meteorites of different preatmospheric sizes [7]

Meteorite	Class	Preatm.[8] mass [kg]	Production rates [10^{-4}atoms s^{-1}g^{-1}] ^{22}Na	^{54}Mn
Denver	L6	1.35	5.74±0.16	6.50±1.70
Murchison	CM2	>15	6.75±0.25	6.40±0.33
Lost City	H5	<200[9]	5.67±0.16	5.33±0.25
St.Severin	LL6	372±14	8.41±0.66[10]	6.75±0.16[10]
Innisfree	L	350±100	7.92±0.41	6.92±0.33
Dhajala	H3	850±135	9.08±0.16	13.16±0.50
Jilin	H	>3000	9.50±0.41	11.30±1.50

N85-35101

SH 7.1-9

DEPTH AND SIZE EFFECTS ON COSMOGENIC NUCLIDE PRODUCTION IN METEORITES

P. Englert
Department of Nuclear Chemistry, University of Köln,
D-5000 Köln 1, FRG

1. Introduction. The galactic cosmic particle radiation (GCR) can cause changes in condensed extraterrestrial matter in different ways. It can lose energy via ionization processes or induce nuclear reactions which lead to a wide variety of stable and radioactive cosmogenic nuclides. Which process dominates depends on the charge and the energy of the particle radiation and on the nature of the extraterrestrial object exposed to this radiation, i.e. its size, chemical and mineralogical composition. Heavy particles ($Z \geq 20$) incur radiation damage in minerals such as olivine and pyroxene. Light particles predominantly tend to induce nuclear reactions, causing the development of a secondary particle cascade of neutrons, protons, pions and γ-rays and the production of cosmogenic nuclides. Such processes are described in detail by various models [1,2], which predict the depth and size dependent production of cosmogenic nuclides.

The two principal approaches to the study of these effects are simulation experiments and direct observations of meteorites. While the simulation experiments may have advantages with respect to a better understanding of the production processes and the development of secondary hadron cascades in extended matter [3], measurements of depth profiles of cosmogenic nuclides in meteorites fulfill two functions: They are the criterion for the validity of the model calculations and simulation experiment results and they establish an empirical network of cosmogenic nuclide relations, which may help to answer questions about the history of both the GCR and the meteorites. This study focusses on the long-lived cosmogenic nuclides ^{53}Mn, ^{26}Al and ^{10}Be, the light noble gases and cosmic ray tracks (CRT), keeping in mind that many other nuclides determined also bear valuable information.

2. Methods. In order to systematically study depth and size effects of cosmogenic nuclides in meteorites, one has to find objects of known preatmospheric size which survived entry into the earth's atmosphere with only a few cm of ablation losses. In addition, well-documented samples from a core drilled through the meteorite or from otherwise accessible parts must be available for a successful study. Table 1 lists a number of meteorites which fulfill these criteria and of which cosmogenic nuclides and CRT's have been measured extensively. In addition, several other meteorites are reported in the literature, for which a part of these measurements have been done [4,5]. The meteorites are listed in order of increasing preatmospheric radius ranging from 5 cm (77003) to approx. 1m (Jilin)[6]. The coverage of the full range of shielding depths is not always complete, as in

Table 1: Cosmogenic nuclide depth profiles in meteorites

Meteorite	Preatm. radius [cm]	^{53}Mn	^{26}Al	^{10}Be	light rare gases	cosmic ray tracks
ALHA77003	6	[T1]	[T2]	----	[T1]	P
ALHA78084	14	[T3,4]	[T3,4]	[T5]	[T4]	[T4]
Lost City	18	[T6]	[T7]	----	[T8]	[T9]
St. Severin	25	[T10,11]	----	[T12]	[T13]	[T14]
Keyes	25	[T15]	[T16]	P	[T17]	[T18]
Dhurmsala	>30	[T3,19]	[T3,19]	P	[T19]	[T19]
Jilin	85	[T20]	[T20]	[T20]	[T20]	[T20]

Footnotes: P - in preparation. [T1] P.Englert et al. (1982), Lun. Planet. Sci. XIII, 201. [T2] J.C. Evans et al. (1979), Proc. Lun. Planet. Sci. Conf. 10th, 1061. [T3] P.Englert et al. (1982), Fifth Int. Conf. Geochron., Nikko, Japan, 89. [T4] R.Sarafin et. al (1985), Earth Planet. Sci. Lett., to be published. [T5] R.K. Moniot et al. (1982), Nucl. Instr. Meth. 203, 495. [T6] P.Englert (1985), Lun. Planet. Sci. XVI, 215. [T7] P.J. Cressy (1971), J. Geophys. Res. 76, 4072. [T8] D.D. Bogard et al. (1971), J. Geophys. Res. 76, 4076. [T9] J.C. Lorin and P.Pellas (1975), Meteoritics 10, 445. [T10] P.Englert and W.Herr (1980) Earth Planet. Sci. Lett. 47, 361. [T11] S.K. Bhattacharya et al. (1980) Earth Planet. Sci. Lett. 51, 45. [T12] C.Tuniz et al. (1984), Geochim. Cosmochim. Acta 48, 1867. [T13] L.Schultz and P.Signer (1976), Earth Planet. Sci. Lett. 30, 191. [T14] Y.Cantelaube et al. (1969), In: Meteorite Research, (P.Millman, ed.), 705. [T15] P.Englert (1984), Lun. Planet. Sci. XV, 248. [T16] P.J. Cressy (1975), J.Geophys. Res. 80, 1551. [T17] R.J. Wright et al. (1973), J. Geophys. Res. 78, 1308. [T18] J.C. Lorin and G.Poupeau (1978), Meteoritics 13, 410. [T19] J.T. Padia et al. (1984), Meteoritics 19, 288. [T20] Jilin Consortium Study I (1985), Earth Planet. Sci. Lett. 72, 246.

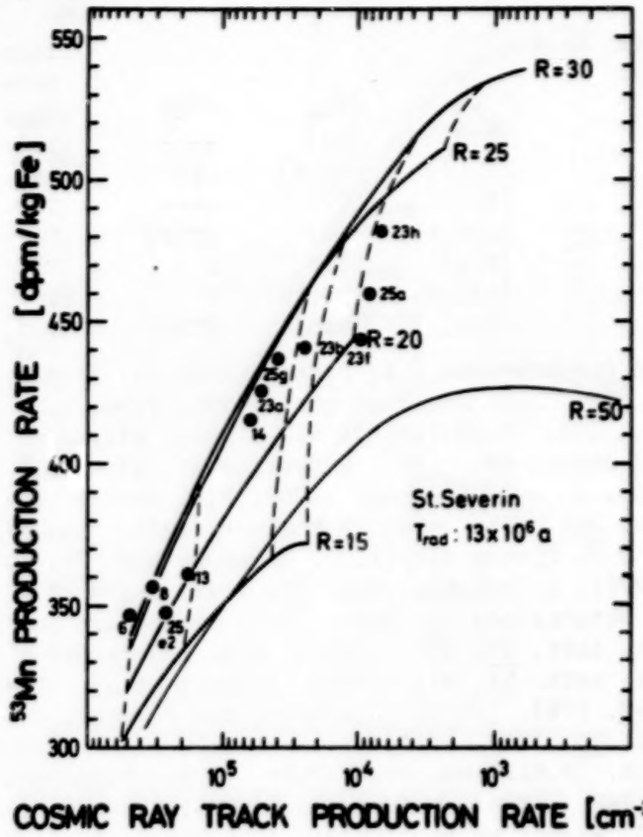
Dhurmsala and Lost City. In the case of 77003, possible contributions of the solar cosmic radiation to the ^{26}Al- and ^{53}Mn production are discussed [7]. Jilin, which underwent a two stage irradiation, provides a model for different irradiation geometries in space, depending on the half life of the cosmogenic nuclide considered [6].

Figure 1 is an example of the kind of multiple two dimensional relations which have been established for depth and size studies of the cosmogenic nuclide production in meteorites. The solid lines compare the semiempirical models for the ^{53}Mn production [1] and the CRT-production [8] in meteorites. The symbols represent same sample measurements of the ^{53}Mn and CRTs in core AIII of St. Severin [9,10]. If several cosmogenic nuclides are determined in one or two samples, this and other relations can be used to derive shielding depths in and preatmospheric sizes of meteorites.

3. Results and Discussion. Table 2 combines results of ^{53}Mn and other cosmogenic nuclides measured predominantly in meteorite falls with high exposure ages (exception: Leedy and

ORIGINAL PAGE IS
OF POOR QUALITY

FIGURE 1



New Concord). All of these meteorites are saturated with respect to the long-lived cosmogenic nuclides. Thus, only depth and size effects or complex irradiation histories can be responsible for the GCR-product signatures.

In general, $^{22}Ne/^{21}Ne$-ratios on the order of 1.1±0.3 indicate well-shielded locations within a meteorite. Thus the majority of the meteorite samples in Table 2 come from shielding depths as they can be found in Dhurmsala [11] and Jilin [10]. This conclusion is in agreement with most of the ^{53}Mn, ^{26}Al and ^{10}Be data.

Preatmospheric mass determinations via CRTs are given for Aztec (18kg) and Hainhotz (260 kg) and were tried for Rangala and Leedy without conclusive results [12]. In the case of Hainhotz, the ^{53}Mn activity of 352±21 dpm/kg Fe confirms the CRT result. Aztec, however, must have been a larger object in space than indicated by the CRT measurements, because of its low $^{22}Ne/^{21}Ne$ ratio and a ^{53}Mn production rate of 339±28 dpm/kg Fe, exceeding that of small bodies if compared with ALHA 77003 and ALHA 78084 [13,14]. Discrepancies between the ^{53}Mn production rates and $^{22}Ne/^{21}Ne$ ratios exist for some meteorites with very long exposure ages, such as H-Ausson, Charsonville, Breitscheid and Yocemento and are probably best explained by complex irradiation histories. [15].

Table 2:

Meteorite	Class	Recov.(a) mass [kg]	$(^{22}Ne/^{21}Ne)_c$	^{21}Ne(b) [$10^{-8}cm^3STPg^{-1}$]	T_{21}(c) [10^6y]	^{53}Mn(d) [dpm/kg Fe]	^{26}Al [dpm/kg]	^{10}Be(h) [dpm/kg]	(i)
Alfianello	L6	228S	1.103	8.40	26.2	490±25	55.5±3.5(f)	--	NNNN
Aztec	L6	2.83	1.103	11.20	35.0	339±28(e)	--	--	YYOO
Breitscheid	H5	1.0	1.075	9.25	27.0	297±18(e)	--	--	YYOO
Charsonville	H6	>27	1.066	22.00	61.2	333±23(e)	--	--	YYOO
Ergheo	L5	20	1.089	7.31	16.3	415±20	57.0±2.5(f)	--	YYNO
Kuyahinya	L5	500S	1.098	11.20	34.2	403±32	57.0±2.5(g)	--	NNNO
Merzö-Madras	L3	27.7S	1.085	9.77	28.0	447±23	55.0±2.3(g)	--	YYNO
Rangala	L6	3.2	1.078	9.14	25.2	485±25	54.2±2.2(d)	--	YYYO
Rose City	H5	>11	1.042	9.42	22.7	464±25	56.0±3.5(f)	--	YYNO
Khairpur	E6	>15	--	--	--	401±24	--	--	OOOO
Leedy	L6	50	1.085	2.34	6.1	410±34	--	--	NNOO
New Concord	L6	226	--	0.90	3.0	174±11	--	--	NNOO
H-Ausson	(H)	(50)	1.101	21.70	72.2	302±20(e)	--	--	YYOO
Ausson	L6	50	1.094	20.20	60.5	356±21	62±5(h)	--	NNNO
Menow	H4	10.5	1.16	4.90	17.5	382±32(k)	60±6(h)	19.6±2.0	YYYY
Selden	LL5	1.56	--	15.50(h)	≥50	359±28(k)	--	19.2±2.8	OYOY
Yocemento	L5	5.92	--	20.10(h)	≥65	256±26(k)	--	17.6±2.2	OYOY
Hainholz	MES	16.5	--	5.80	19.5	352±21	--	--	ONNO

Footnotes: (a) M.H.Hey (1966), Catalogue of Meteorites. (b) L.Schultz and H.Kruse (1978), Nucl.Track Det. 2, 65. (c) K.Nishiizumi et al. (1980), EarthPlanet.Sci.Lett. 50, 156. (d) this work. (e) W.Herr et al. (1981), Meteoritics 16, 324. (f) I.R.Cameron and Z.Top (1975), Geochim.Cosmochim.Acta 39, 1705. (g) D. Heymann and E.Anders (1967), Geochim.Cosmochim.Acta 33, 653. (h) R.K.Moniot et al. (1983), Geochim. Cosmochim.Acta 47, 1887. (i) Two Y confirm that aliquots of the same sample were analyzed for cosmogenic nuclides. (k) preliminary results.

References: [1] T.P.Kohmann and M.L.Bender (1969), in: B.S.P.Shen (ed.), High Energy Nuclear Reactions in Astrophysics, Benjamin, N.Y., 169. [2] R.C.Reedy (1985), J.Geophys.Res. 90, C722. [3] P.Dragovitsch et al. (1985), SH 7.1-8, this conference. [4] T11. [5] P.Englert and R.Sarafin (1984), Meteoritics 19, 223. [6] T20. [7] P.Dragovitsch et al. (1985), Proc.Nucl.Data.Conf. Santa Fe. [8] S.K.Bhattacharya et al. (1973), J.Geophys.Res. 78, 8356. [9] T10. [10] T14. [11] T3,T19. [12] N.Bhandari et al. (1980), Nucl. Tracks 4, 213. [13] T1. [14] T3, T4. [15] T15.

SPALLOGENIC ORIGIN OF NUCLEI IN METEORITES

N85-35102

B.ZANDA[1] AND J.AUDOUZE[1,2]

1 Institut d'Astrophysique du CNRS,
98 bis, boulevard Arago
75014 Paris, FRANCE

2 Laboratoire René Bernas,
91405 Orsay, FRANCE

1. Introduction

The study of the cosmic ray fluxes propagation inside meteorites is a way to improve our knowledge both on these objects (exposure ages, size of irradiated parent bodies, location of samples within these bodies...) and on these fluxes (spectral index, total intensity, time variation...).

In this communication, we present some preliminary results obtained from a model built to evaluate the different interactions between cosmic rays and meteorites. With this model, we are able to compute fluxes as a function of depth inside the meteorite, taking into account energy losses by ionization and spallation reactions which induce both particle destruction and production. This procedure, in which particle fluxes and cross sections are treated independently from each other, differs significantly from the thick target approach (see Kohman & Bender-1967, Trivedi & Goel-1973) based on the measurement of spallation products generated in accelerator experiments.

2. Cosmic rays propagation inside meteorites

The basic equation describing the independent of time variation with depth of the flux Φ_i (cm^{-2} s^{-1} MeV^{-1}) can be written as :

$$\Omega\nabla\ \Phi_i + \sigma\ n\ \Phi_i = Q_i + \frac{\partial(\omega_i\ \Phi_i)}{\partial E} \qquad (1)$$

where . σ is the total destruction cross section of nuclear species i
. n is the number of target nuclei per unit volume,
. Q_i is the production term of secondary particles,
. ω_i is the energy loss of nucleus i due to excitation and ionization of the target medium ($\omega_i = -dE/dx$)
. The streaming factor $\Omega\nabla$ depends on the geometry of the meteorite :
If θ is the propagation angle,

. $\Omega \nabla = \cos\theta \frac{\partial}{\partial x}$ in plane parallel geometry

x being the depth inside the meteorite

. $\Omega \nabla = \cos\theta \frac{\partial}{\partial r} + \frac{\sin^2\theta}{r} \frac{\partial}{\partial(\cos\theta)}$ in spherical geometry,

r being the distance from the center.

3. Asymptotical behaviour of the transport equation at high energy

Above 1 GeV N^{-1}, energy losses and secondary particles production become negligible. Therefore, equation (1) reduces to :

$$\Omega \nabla \Phi_i + \sigma n \Phi_i = 0 \qquad (2)$$

The boundary conditions are :

$\phi(0, \cos\theta) = \Phi_{i,o}$ $\quad (0<\theta<\frac{\pi}{2})$ in slab geometry

$\phi(R, \cos\theta) = \Phi_{i,o}$ $\quad (-\frac{\pi}{2}<\theta<\pi)$ in spherical geometry

(we assume here that the incoming cosmic ray flux $\Phi_{i,o}$ is isotropic).

With such conditions, the solutions of equations (2) are :

$$\Phi_{slab}(x,\cos\theta) = \Phi_o \exp(-\frac{\sigma n x}{\cos\theta})$$

$$\Phi_{spherical}(r,\cos\theta) = \Phi_o \exp[-\sigma n(r\cos\theta + \sqrt{R^2-r^2\sin^2\theta}]$$

In figure 1, we compare the integrated flux ϕ over all directions calculated as a function of depth inside a meteorite in the case (i) of a plane parallel shape and (ii) of a spherical shape with R= 40 cm. It can be seen that the flux is always lower if calculated in the plane parallel assumption than in spherical geometry. The error made in treating a spherical 40 cm radius meteorite as an infinite slab would only be of a factor 1.2 at the surface but it would become as high as a factor 8 in the center.

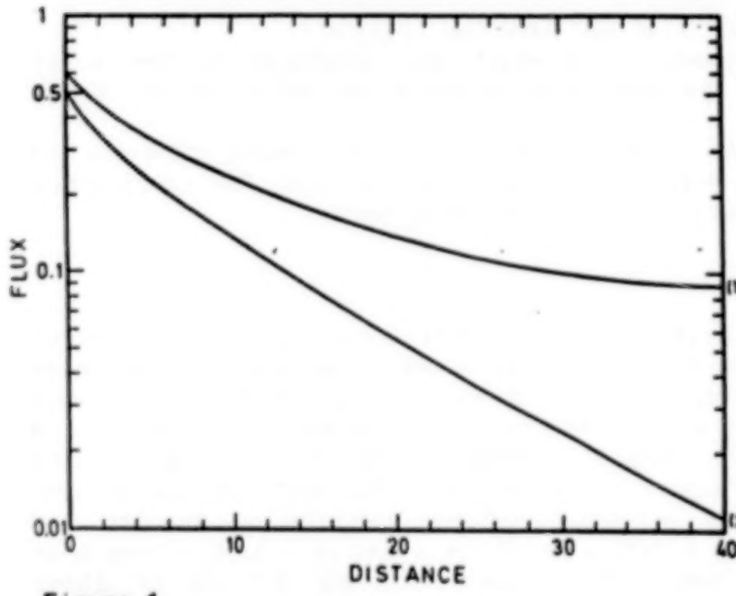


Figure 1

Comparison of depth dependent integrated fluxes (1) in spherical geometry and (2) in slab geometry. Note that the surface flux (1) is higher than (2) because of outgoing particles.

4. Solution of the complete equation including secondary particles production and energy losses

We have adopted the following procedure and assumptions:
(i) the ionization energy loss dE/dx was calculated from the Gloeckler formula (1970),
(ii) the secondary particles production can be written as :

$$Q(E,\cos\theta,r) = \int_E^\infty \sigma(E')\ P(E'\to E)\ \Phi(E',\cos\theta,r)dE'$$

where $P(E'\to E)$ is the probability to produce a secondary particle of energy E from a primary particle of energy E'.

In this preliminary approach, we used $P(E'\to E)= \frac{P}{E'}$,

where P, the average number of outgoing secondaries per spallation reaction is an ajustable parameter of our calculation, and the secondary spectrum is assumed to be flat.

The presence of an integral term in the second member of (1) requires the use of iterative computations.
This can be described as follows :

$$(\Omega\ \nabla + \sigma\ n - \frac{\partial \omega i}{\partial E})\ \phi^{(n)} = \int_E^\infty P\ \frac{\phi^{(n-1)}}{E'}\ dE'.$$

Details of the flux computations will be described in Zanda (1985).

The spallation cross-sections used to deduce nuclei production are derived from Silberberg and Tsao (1972a, 1972b, 1977, 1979).

The energetic particles may have two origins :
(i) the galactic cosmic rays which are modulated by the solar activity (we derived our modulated spectrum out of Proteroe, Ormes and Comstock -1981),
(ii) the solar cosmic ays. Since this solar source consists in particles with E<100 MeV, it only affects the first few centimeters of the meteorite and will not be considered here.

5. Preliminary results

Because of the existing experimental data, we chose to first test our model on the iron meteorite Grant. Computations were made for a meteorite having the same chemical composition and various radius (40 cm, 35 cm and 30 cm) admiting a secondary particle yield per interaction p=0.75. Figure 2 shows a comparison of our results with measurements by Signer and Nier (1960) for Ne21. It can be seen that there is a good agreement between calculation results and experimental datas for a radius of 35 cm which is a little less than the pre-atmospheric radius that these authors derived of their calculation.

ORIGINAL PAGE IS
OF POOR QUALITY

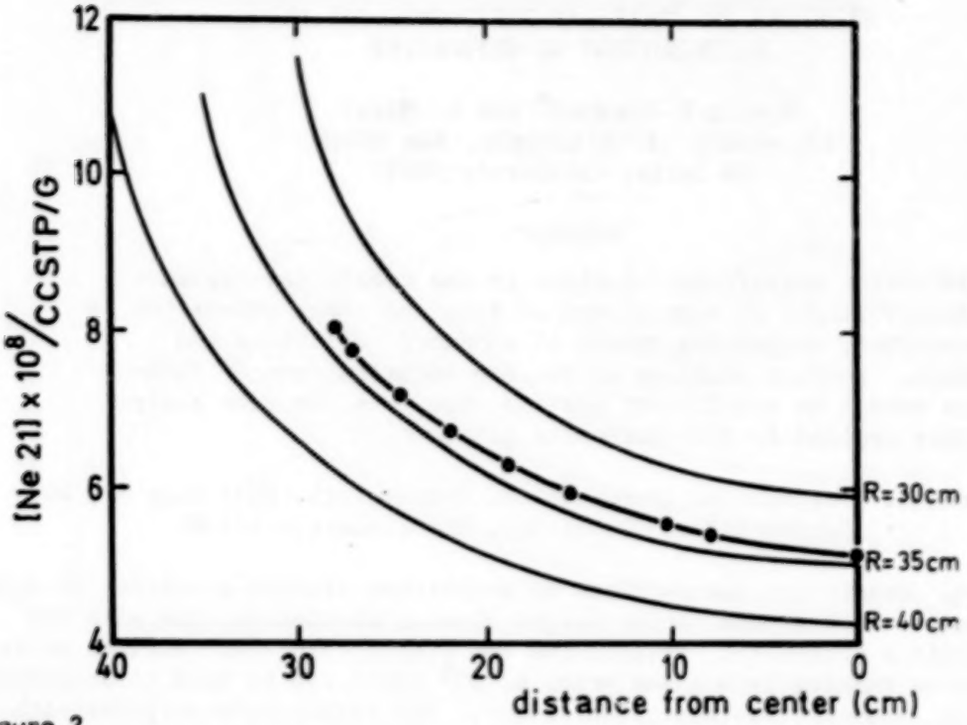


Figure 2
Comparison of computations results for various radius (single curves) and experimental datas from Signer and Nier (dotted curve).

6. Conclusion

The results obtained with the model presented here are sufficiently encouraging to pursue and improve that type of studies, in particular by finding a proper treatment for the outstanding problem of secondary particles production. Unfortunately, taking into account the actual geometry of a meteoritical sample at the time it suffers the bulk of the cosmic ray irradiation will still remind a difficulty.

We wish to thank G. Malinie for helpful discussions throughout the preparation of this paper.

7. References

1. Gloekler, G., (1970), in "Introduction to Experimental Techniques of High Energy Astrophysics" p.1, Ogelman H. and Wayland J.R. Ed. NASA SP-243
2. Kohman, J.P., and Bender, M.L., (1963) in "High Energy Nuclear Reactions in Astrophysics" p.169, B.S.P. Shen Ed. Benjamin, New York
3. Proteroe, R.J., Ormes, J.F. and Comstock, G.M., (1981) Ap.J., 247, p.362
4. Signer, P., and Nier, A.O., (1960), J.G.R., 65, p.2947
5. Silberberg, R., and Tsao, C.H., (1972a&b), Ap.J.Suppl. series, 220, p.315 & p.335
6. Silberberg, R., and Tsao, C.H., (1977), in 15th I.C.R.C., Plovdiv, 2, p.84
7. Trivedi, B.M.P., and Goel, P.S., (1973), J.G.R., 78, p.4845
8. Tsao, C.H., and Silberberg, R., (1979) in 16th I.C.R.C., Kyoto, 2, p.202.

N85-35103
SH 7.1-11

CLUSTERS AND CYCLES IN THE COSMIC RAY AGE DISTRIBUTIONS OF METEORITES

Martin F. Woodard* and K. Marti
University of California, San Diego
La Jolla, California 92093

ABSTRACT

Statistically significant clusters in the cosmic ray exposure age distributions of some groups of iron and stone meteorites are observed, suggesting epochs of enhanced collisions and breakups. Fourier analyses of the age distributions of chondrites reveal no significant periods, nor does the same analysis when applied to iron meteorite clusters.

*Present address: Smithsonian Astrophysical Observatory, Mail Stop 16, 60 Garden Street, Cambridge, Massachusetts 02138.

Introduction. Cosmic ray interactions in meteorites produce a variety of spallation products which depend on the target element abundances, the size and location within a meteorite. Radioactive and stable cosmogenic nuclide pairs with half-lives ranging from a few years to 10^9 years can be used to determine the cosmic ray exposure history of an object. The radioactive nuclides with half-lives short, compared with the time interval of exposure to cosmic rays, are in secular equilibrium and define the production rates. For a constant exposure geometry measured amounts of the stable integrating nuclides coupled with radionuclide measurements are used to obtain the integral time of exposure to cosmic rays. The advantage of this approach is that reliable exposure age information can be obtained in samples reflecting variable degrees of cosmic ray shielding as in large meteorites or in cases of incomplete development of the secondary cascade typically observed in small meteorites. A number of methods were developed for the calculation of production rates and of cosmic ray exposure ages (e.g. Voshage, 1962; Nishiizumi et al., 1980; Marti, 1984; Lavielle et al., 1984). Exposure ages for iron meteorites based on ^{40}K-^{41}K and ^{38}Ar data indicate some clustering of exposure ages for several groups of irons (e.g. Voshage and Feldmann, 1979; Lavielle et al., 1984). Exposure age distributions for chondrites were studied several times (e.g. Wänke, 1966; Crabb and Schultz, 1981). Noble gas data were recently compiled by Schultz and Kruse (1983).

Methods of Analysis. To test the significance of a cluster of M samples within a given group of N (>M) meteorites, we first assign an age span, T, to the group as a whole, based on the rough appearance of the age distribution of the group. We then select a value, W, much shorter than T, similar to the age spread of the candidate cluster. Under the assumption that the N group members are uniformly and randomly distributed over the age interval [0,T], we calculate the probability of finding at least M samples within some subinterval of duration W.

The cluster probabilities were computed by performing Monte Carlo simulations on a vax 11/780 computer. For each trial of the simulation, N pseudo-random numbers were generated on the interval [0,T]. A set of overlapping subintervals, each of duration W, were defined so that their starting

points form a uniform grid in which successive subintervals overlap by 90% so as to cover the interval [0,T]. If at least M of the N random numbers is found in one or more of the subintervals, a "success" is recorded. The estimated occurrence probability for a cluster of M meteorites is the number of successes divided by the total number of trials.

Various tests of the Pseudo-random number generator have been made, including a comparison with a direct calculation of the cluster probability in a limiting case where a simple analytic expression applies.

We have also searched for periodicity in the age distributions of both individual meteorite groups and in the age distributions of clusters. A discrete time series is formed by assigning to each of a set of uniformly-spaced time bins, the number of samples lying within the bin. A Fourier spectrum is then computed for these time series and is examined for outstanding peaks, the significance of a peak in the power spectrum is evaluated by computing the probability of finding a peak at least as high as the real one in the spectrum of a randomly generated age distribution (using a Monte Carlo procedure quite analogous to the above method of establishing cluster probabilities.

Results. A cluster is designated "probable" if its probability of occurrence, by the previously described test, is less than 10% and "very probable" if the probability is less than 1%. Groups of probable and very probable clusters are listed in the table below.

Table List of Significant Exposure Age Clusters and Calculated Probabilities.

Group	N	T (Myr)	Average Age of Cluster (Myr)	M	W	Probability
H Chondrites	95	20	7	45	3	$0/10^5$
Enstatite Achondrites	9	115	60	5	8	$94/10^4$
Irons IA	13	10^3	440	5	50	$20/10^3$
Irons IIA	7	10^3	25	4	50	$111/10^4$
Irons IID	3	10^3	360	3	50	$60/10^4$
Irons IIIA	19	10^3	650	7	50	$2/10^3$
Irons IIIE	6	10^3	475	3	50	$104/10^3$
Irons IVA	13	10^3	375	10	150	$1/10^4$
			400	6	75	$60/10^4$
			400	4	40	198/2000
Irons IVB	5	10^3	875	3	50	$50/10^3$

Column 1 gives the group containing the cluster, columns 2 and 3 give the size of the group, N, and its age span, T. Column 4 gives the estimated age and column 5 the number of samples in the cluster. Columns 6 and 7 give, respectively, the age span, W, of the cluster and the probability of random occurrence (the latter expression displays explicitly both the number of successes and the total number of trials from which the successes were derived). The table does not list all clusters found because some of these overlap in time.

A Fourier analysis of the H chondrite group, using only meteorites with exposure ages between 10 and 40 Myr (i.e., ignoring the big peak at 7 Myr) yielded no significant periods. Similarly, no significant peaks were found in the fourier spectrum of the L chondrites between 0 and 40 Myr. A power spectrum of the age distribution of the iron meteorites (see table) also yielded no significant periods.

Discussion. We regard the clustering as real since probable or very probable clusters occur in most of the major subgroups. The statistical significance assigned to the clusters depended on the assumed test model of a uniform distribution over the stated ranges, T. For instance, for each of the iron groups T = 1000 Myr is roughly the cutoff age for the irons as a whole. A more realistic hypotheses against which to test cluster significance might be to distribute the samples exponentially, to simulate the gradual decrease in the number samples of increasing age.

To obtain some idea of the sensitivity of the results to our assumptions, we have also computed the cluster probabilities by choosing a width W in excess of the apparent age range of the cluster, thereby overestimating the probability, for example, for the iron IIIE subgroup, changing W/T from 5% (corresponding to the result in the table) to 7% increases the probability from ~10% to ~20%, therefore, this cluster must be considered marginal. On the other hand, the probability of the cluster in the IA iron group increases from ~2% to ~9% when the assumed width of the cluster changes from 5% to 8%. The IA cluster and most of the clusters listed in the table are at least probable even when their age ranges are overestimated.

One interpretation of the clusters is that they represent epochs of increased meteorite formation resulting from individual collisions of asteroids or comets. In this case, one would expect to see a cluster of width corresponding to uncertainties in the age values. However, secondary breakups of the original collision products, complex exposure histories, and spatial variations in the cosmic ray flux, can all degrade the sharpness of the clusters. Thus it is important to know whether the actual spread in the ages of samples from a given cluster can be accounted for by any of the above factors.

Multiple collisions with asteroids might produce meteorites over an extended period. One possible example of such an enhancement is the iron IVA cluster at 400 Myr, extending over an age interval W = 150 Myr. The fact that this interval, containing 10 samples is exceptionally long leads us to suspect that two or more clusters are present. Belonging to the aforementioned 10 are 6 samples of average age 400 Myr, which themselves constitute a very probable cluster listed in the table. The remaining four samples do not constitute a cluster by our criterion, however a more sophisticated test might reveal a second cluster.

N83-33104

Conclusions. The record of cosmic ray effects in iron and stone meteorites was studied. Statistically significant clusters in the exposure age distributions of these objects were found, suggesting epochs of enhanced meteorite formation, possibly as the result of collisions and breakups. Significant exposure age clusters are found or confirmed for the following groups of meteorites: H-Chondrites at 7 Myr, enstatite achondrites at 60 Myr, iron group IA at 450 Myr, IIA < 50 Myr, IID at 350 Myr, IIIA at 650 Myr, IIIE at 475 Myr, IVA at 400 Myr and IVB at 875 Myr. A Fourier analysis of the age distributions of both H and L chondrites reveals no significant periods, nor does the same analysis when applied to the age distributions of iron meteorite clusters

Acknowledgements. This research was supported by NASA NAG 9-41.

References.

Crabb, J. and Schultz, L. (1981), Geochim. Cosmochim. Acta 45, 2151-60.

Lavielle, B., Marti, K. and Regnier, S. (1984), Proceedings of Conf. on Isotopic Anomalies in the Solar System, Paris.

Marti, Kurt (1984), Abstract, Workshop on Cosmogenic Nuclides, July, Los Alamos, New Mexico.

Nishiizumi, K., Regnier, S. and Marti, K. (1980), Earth Planet. Sci. Lett. 50, 156-70.

Schultz, L. and Kruse, H. (1983), Helium, Neon and Argon in Meteorites; A Data compilation. Special publication of the Max-Planck-Institute for Chemistry, Mainz.

Voshage, H. (1962), Z. Naturforsch. 17a, 422-32.

Voshage, H. and Feldmann, H. (1979), Earth Planet. Sci. Lett. 45, 293-308.

Wänke, H. (1966), Z. Naturforsch. 21a, 93-110.

N85-35104
SH 7.1-12

THE $^4He/^1H$ RATIOS IN THE CHEMICAL COMPOSITIONS OF SOLAR FLARE PARTICLES AND THE PRIMORDIAL SOLAR NEBULA

Kunitomo Sakurai

Institute of Physics, Kanagawa University
Rokkakubashi, Yokohama 221, Japan

ABSTRACT

Except for the proton component, it is well known that the chemical abundances of solar flare particles are similar to those of galactic cosmic rays at their sources. In order to infer the $^4He/^1H$ ratio in the solar atmosphere, this ratio as observed in the interstellar gases has been taken into account in addition to those which have been obtained of galactic cosmic rays and the stars classified as the early types. Since it is clear that the most of these ratios ever deduced for both of the sun and solar flare particles are lower than those for the interstellar gases, this ratio thus obtained seems to suggest that hydrogens are relatively overabundant in the chemical abundances of the sun and the primordial solar nebula as compared to those of the interstellar gases being currently observed.

1. Introduction

As well known, the relative abundance of the helium atoms in the sun has never been exactly determined spectroscopically because the temperature of the solar photosphere is too low for these atoms to be excited(1). Using the observed data on the chemical composition of solar flare particles and the solar chromosphere, the ratio of heliums to hydrogens in number, being denoted as $^4He/^1H$ in this paper, has thus been estimated so far. This ratio, however, gives a value about equal to 0.0625, which is not coincident with those which have been estimated as 0.091 - 0.11 from the spectroscopic observations of the early type stars. Even now, it can, therefore, be said that the ratio $^4He/^1H$ for the sun has not been determined as yet. For this reason, many people still use the values as estimated for these stars in investigating some problems on solar physics, though they do not seem to be confident of their usage of those values for this ratio.

Recently, the spectroscopic data on the ratio $^4He/^1H$ have been accumulated from the investigations on the chemical compositions of the interstellar gases and the planetary nebulae(2). In this paper, this ratio in the sun will be reexamined by taking into account these data.

2. The Relative Abundance of Helium Atoms in the Solar Atmosphere and Solar Flare Particles

It is thought that the chemical composition of solar flare particles may give us an important clue to understand the acceleration mechanism of these particles in solar flares. This composition has, therefore, been repeatedly observed by means of balloons, rockets and satellites since the late 1950's. At present, it is known that this composition tends to become systematically overabundant for the heavy nuclei with the increase of their charge numbers(3, 4). It has, however, been shown that the relative abundance of hydrogen atoms is somehow variable, but the ratio $^4He/^1H$ is given to be 0.063 ± 0.015 (1).

Since it is known that the ratio of helium to the medium nuclei (C,N,O) in number is almost constant from one observation to another, the variability on the ratio $^4He/^1H$ seems to have been caused by that of the hydrogen atoms in solar flare particle events. However, it should be noted that this ratio as given above is much less than that which is currently applied to the study of the solar interiour and atmosphere. Furthermore, this ratio is not coincident with those which have been determined from the spectroscopic observations on the interstellar gases and the planetary nebulae(2). Really speaking, the former is also much less than the latters.

In order to compare these ratios from each other, they are shown in Fig. 1 as a function of the logarythmic value

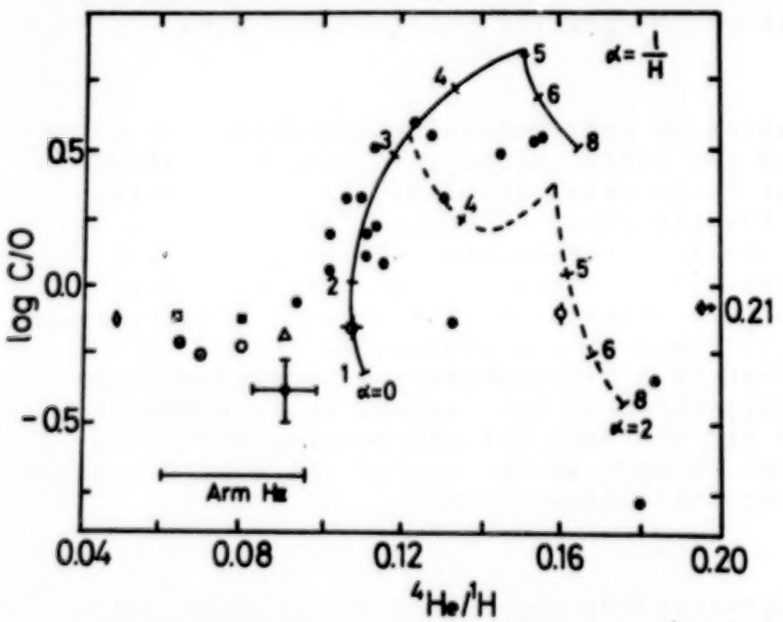


Fig. 1 Relation between the ratios C/O and $^4He/^1H$ for the interstellar gases, the solar atmosphere, solar flare particles and galactic cosmic rays(see text for the detail).

of the ratio C/O(2). In this figure, black circles(1) show the spectroscopic data on the interstellar gases and the planetary nebulae. White circles with and without dot inside (5, 6), black squares(7) and triangle(8) all indicate the data from the spectroscopic observations on the solar atmosphere by different authors. Two diamonds have been obtained from the chemical composition of galactic cosmic rays(9). The left-end one indicates the value for the high-energy galactic cosmic rays, which is still less than that for solar flare particles which is indicated by white square.

It is clear from Fig. 1 that the ratio C/O remains almost constant for all the values of the solar atmosphere and solar flare particles, whereas the ratio $^4He/^1H$ widely ranges from 0.06 to 0.095. In this figure, there are two curves for the relation between the ratios of C/O and $^4He/^1H$ which are given as a function of the stellar masses. Black and dashed curves, respectively, correspond to different values of the mixing length, l, in the convective layers of the stars of different masses, where H denotes the scale height of these layers. The numbers on these curves give the masses of the stars in the unit of the solar mass.

Since the ratio $^4He/^1H$ for the sun is highly deviated from these two curves, the relative abundance of hydrogen atoms may be overabundant to the sun as compared with other sunlike stars. If this is to be the case, the accretion of hydrogen gases may have happened very effectively during the early phase of the formation of the primordial solar nebula. Thus the excess of hydrogens seems to have resulted in the relative abundances of the present solar atmosphere.

3. Conclusion

The $^4He/^1H$ ratios in the chemical compositions of solar flare particles and the solar photosphere have been shown to be always less than those which are observed on the interstellar gases and the planetary nebulae. This tendency is also found on the chemical composition of the primordial solar nebula. These results suggest that the primordial solar nebula might have already been overabundant of hydrogen atoms in the initial stage of its evolution.

It is noted that this overabundance of hydrogen atoms in the chemical composition of the present solar atmosphere seems favorable to fix the case for the missing solar neutrinos, which is now thought as the one of the most difficult problems in astrophysical research(10).

References

(1) e.g., K. Sakurai (1974) Physics of Solar Cosmic Rays, Univ. of Tokyo Press, Tokyo.

(2) M. Peimbert, A. Serrano and S. Torres-Peimbert, (1984) Science 224, 345.

(3) A. Mogro-Campero and J.A. Simpson (1972) Ap. J. 171,L 5 and 173, L 35.
(4) J.-P. Meyer (1985) Ap. J. Suppl. Ser. 57, 151 and 173.
(5) E. Anders and M. Ebihara (1982) Geochim. Cosmochim. Acta 46, 2363.
(6) A.G.W. Cameron (1982) Essays in Nuclear Astrophysics, p. 22 (eds. C.A. Barnes et al.) Cambridge Univ. Press, Cambridge.
(7) J.E. Ross and L.H. Aller (1976) Science 191, 1223.
(8) L. Goldberg, E. Müller and L.H. Aller (1960) Ap. J. Suppl. 5, 1.
(9) J.A. Simpson (1983) Ann. Rev. Nuclear Part. Sci. 33, 323.
(10) K. Sakurai (1984) Space Sci. Rev. 38, 243.

N85-35105

SH 7.1-14

HIGH PRECISE MEASUREMENTS OF COSMOGENIC RADIOCARBON ABUNDANCE BY COMPLEX OF SCINTILLATION EQUIPMENTS

[1]G.E.Kocharov, [2]R.Ya.Metskvarishvili, [2]S.L.Tsereteli

1.Ioffe Physico-Technical Institute
Academy of Sciences of the USSR,Leningrad
194021, U S S R

2. Tbilisi State University,Tbilisi 380028
U S S R

The main characteristics of scintillation equipments which enable the measurements of radiocarbon content with high accuracy of 0.2-0.3% have been considered. The complex of scintillation devices has been operating very well for the last 15 years and has allowed to investigate the temporal variation of solar activity and intensity of cosmic rays for the last 300 years.

Studies of various astrophysical, geophysical and ecological phenomena by way of investigation of radiocarbon activity in dendrocronologically dated samples have been under way since 1965 [1].

Two types of detectors are used at present for the measurement of the ^{14}C concentration in dendrochronologically dated tree-rings: proportional and liquid scintillation counters. We prefer the liquid scintillation counter because it allows to use tens of gram of carbon in relatively small volume, which is important for high precise measurements of astrophysical samples. Firstly single-channel equipment with a stabilization of the photomultiplier and amplifiers was developed and used [2-3] . For stabilization the special light impulse generator with stable amplitude was developed. Counting rate of onefold standard was 48.33 imp.per min. at a background 6.5 imp.per min. Precision of radiocarbon measurements was of 0.3-0.4%.But use of an electron lamp 6G-14 B as a light impulse generator had several defects: a necessity of stabilization of light impulse amplitude, short life time

of the electron lamp,increased background of the scintillation equipments and so on.That is why light impulse generator using light diode KL 102B has been developed,which is smaller,more simple and has longer life in comparison with device with electron lamp.

Block-diagram of developed two-channel scintillation equipments is shown in Fig.1.

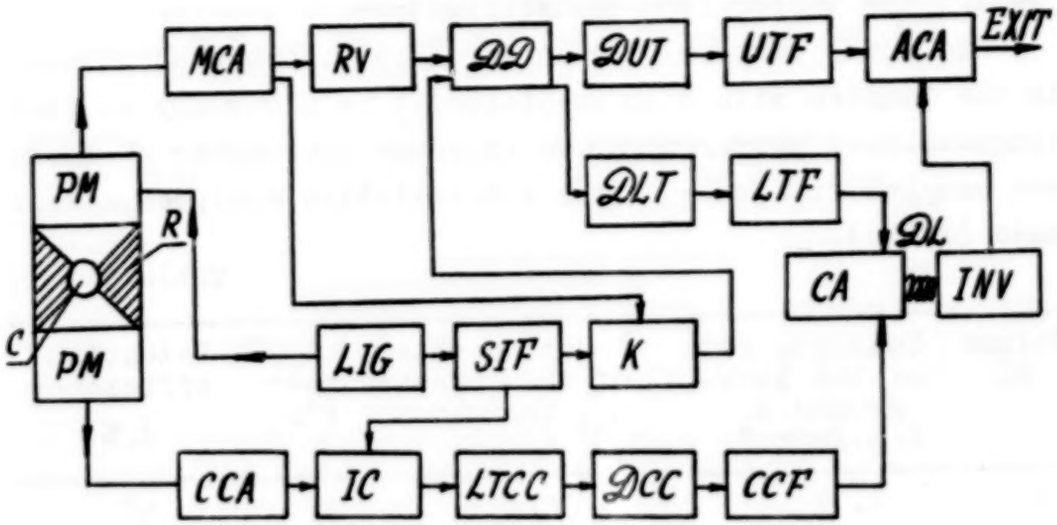


Fig.1. Block-diagram of two-channel scintillation equipment. C-cuvette with investigated sample,R-reflector,PM-photomultiplier,MCA-main channel amplifier,CCA-coincidence channel amplifier,LTG-light impulse generator,SIF-synchronous impulse former,RV-reference voltage,K-key,IC-intermediate cascade,DD-differential discriminator,LTCC-lower threshold of coincidence channel,DCC-discriminator of coincidence channel,DUT-discriminator of upper threshold,DLT-discriminator of lower threshold,UTF-upper threshold former,LTF--lower threshold former,CCF-coincidence channel former, CA-coincidence assembly, DL-delay line,INV-invertor, ACA-anticoincidence assembly.

Stabilization is made by light impulses of the diode KL 102B which is triggered by signals of electric impulses generator with a stable amplitide and definite frequency 1700 Hz.Generator operates the key which forbids a passing of the stabilization impulses.

Light impulses passing through photomultiplier and main amplifier form a voltage in the scheme of reference voltage which is proportional to the value of stabilization impulse and operate the thresholds of differential discriminators. With the variation of amplification coefficient of PM and amplifier the thresholds of discriminators are automatically changed into necessary direction and prevent the system from destabilization.

To study temporal variation of radiocarbon abundance in the samples with high precision it is necessary to make longcontinued measurements. To increase the number of measured samples five two-channel scintillation equipments were made (Table).

Table.

Volume ml	Counting rate of the background N_b imp./min	Counting rate of the standard N_{st} imp/min	$\frac{N_{st}}{\sqrt{N_b}}$	Detection efficiency ε, %
6	4.77	39.42	18	58
10	5.48	55.98	24	53
13	7.75	82.42	30	58
15	9.59	92.48	30	58
21	9.25	146.90	48	64

Different values of cuvettes allow to use the samples with different masses of carbon without dilution.

To investigate time variation of ^{14}C abundance in the Earth's atmosphere dendrochronologically dated annual rings of the trees of different species and from different regions of the Earth were used. Dated samples were transformed to a benzene in a chemical way.

Activity of investigated sample relative to the standard is calculated by the following formulae:

$$\delta^{14}C\,(‰) = \frac{N_s - N_{st}}{N_{st}} \cdot 1000.$$

N85-35106

where N_s and N_{st} - are counting rates of the sample and standard accordingly.

For fractionation correction we measured $^{13}C/^{12}C$ in the samples.

$$\delta^{13}C = \left[\frac{R_s - R_{st}}{R_{st}}\right] \cdot 1000‰$$

R_s and R_{st} are the ratios of $^{13}C/^{12}C$ in the sample and standard accordingly.

Radiocarbon activity with taking into account fractionation correction is calculated by the formulae:

$$\Delta^{14}C = \delta^{14}C - (2\delta^{13}C + 50)(1 + \frac{\delta^{14}C}{1000})‰.$$

Obtained results on time variation of cosmic rays are discussed in paper SH21-15 presented at this conference.

References.

1. Konstantinov B.P., Kocharov G.E., 1965. Dokl. AN SSSR, v.165, p.63.
2. Metskvarishvili R.Ya. et al. 1971, Radiocarbon, Vilnus, p.129.
3. Metskvarishvili R.Ya., Dergachev V.A., ibid., p.131.
4. Metskvarishvili R.Ya., 1974. Proc. All-Union Conference on the problem "Astrophysical phenomena and radiocarbon", Tbilisi University Press, p.27.

SH 7.1-15
N85-35106

RADIOCARBON CONTENT IN THE ANNUAL TREE RINGS DURING LAST 150 YEARS AND TIME VARIATION OF COSMIC RAYS

G.E.Kocharov[1], R.Ya.Metskvarishvili[2], S.L.Tsereteli[2].

1. Ioffe Physico-Technical Institute
Academy of Sciences of the USSR
Leningrad, 194021, USSR

2. Tbilisi State University, Tbilisi, 380028
U S S R

The results of high accuracy measurements of radiocarbon abundance in precisely dated tree rings in the interval 1800-1950 yrs have been discussed. Radiocarbon content caused by solar activity is established. Using obtained data the temporal dependence of cosmic rays is constructed.

Using the complex of scintillation equipments [1] temporal variations of radiocarbon content in the Earth's atmosphere have been obtained for the time interval 1800 to 1950 year. Accuracy of radiocarbon measurements in tree rings was 0,2-0,3%. For fractionation correction we measured $^{13}C/^{12}C$ by mass-spectrometer MI-1201 with the accuracy 0.03%.

To reveal the cyclic components in the radiocarbon abundance temporal dependence we used two possibilities: method of spectral analysis and Burg's method. Spectral analysis method can be used both for long and short temporal rows and allow to treat experimental data row with the gaps. Burg's method is used for short rows and allows to reveal a periodicity which is comparative with a length of the row.

Now we consider the concrete results for the period 1850-1940 years. Both using methods allow to establish in the radiocarbon row 11-years periodicity which can be connected with the well-known solar cycle. To reveal the nature of connection between the solar activity and the radiocarbon abundance we use correlative analysis: between $\Delta^{14}C$ and Wolf numbers W(t) not only for all the interval (1850-1940 yrs) but for single solar cycles too. Analysis shows negative correlation with a time shift about 4-5 yrs.

Negative correlation means that the main source of radiocarbon abundance variation is solar modulation of cosmic ray intensity. Based on this fact the time-variation of cosmic ray intensity in the past has been obtained.

The scheme is the following. One adopts a model for the carbon-exchange reservoir and establishes its dynamic parameters. Then one converts the radiocarbon content of tree-rings into the rate Q(t) of radiocarbon formation in the Earth's atmosphere in the time-interval of interest. And finally one transforms Q(t) into the galactic cosmic-ray flux.

We used the five-reservoir model, incorporating the atmosphere A, the biosphere B, humus H, the ocean surface layer S and the deep ocean O (for details see [2,3]).

Within the rigidity range $0.5 \leq R \leq 50$ GV, which contributes about 95% to Q(t), the variations of the primary spectrum D(R,t) caused by solar modulation are described by an exponential function of the type [3] :

$$\mathcal{D}(R,t) = \mathcal{D}(R,0)\, e^{-K(t)/R} \qquad (1)$$

where D(R,0) represents the interstellar cosmic-ray specrum and K(t) is a modulation parameter. Dorman [4] has obtained an expression relating the atmosphere ^{14}C formation rate to the variations in the primary cosmic-ray spectrum:

$$\frac{\delta Q(t)}{Q_0} = \frac{Q(t)-Q_0}{Q_0} = \int_0^\infty \frac{\delta \mathcal{D}(R,t)}{\mathcal{D}(R,0)} W(R)\, dR \qquad (2)$$

where W(R) serves as the planetary coupling factor for the rate of radiocarbon formation by cosmic rays.

In view of the normalization condition

$$\int_0^\infty W(R)\, dR = 1$$

and the relation

$$\frac{\delta \mathcal{D}(R,t)}{\mathcal{D}(R,0)} = \frac{\mathcal{D}(R,t)}{\mathcal{D}(R,0)} - 1 = e^{-K/R} - 1$$

one may put Eq (2) in the form

$$\frac{\delta Q(t)}{Q_0} = \int_0^\infty e^{-K/R} W(R)\, dR - 1 \qquad (3)$$

Using Dorman's values [4] of W(R) one readily obtains the expression [5]

$$\kappa(t) = 0.028 \left| \frac{\delta Q(t)}{Q_0} \right|^{1.29} \qquad (4)$$

Normalization is taken here at minimum solar activity (maximum radiocarbon formation rate).

If the primary cosmic-ray spectrum confirms to a power law with respect to total energy the intensity variation in the rigidity range (R_1, R_2) at the Earth's orbit will be:

$$\frac{\delta I}{I_0} = \frac{I - I_0}{I_0} = \int_{R_1}^{R_2} E^{-\gamma}(R) e^{-\kappa/R} dR \Big/ \int_{R_1}^{R_2} E^{-\gamma}(R)\, dR - 1 \qquad (5)$$

where $\gamma = 2.6$ is the spectral index, $E(R) = e\sqrt{R^2 + \frac{m_0 c^2}{e}}$ is the total energy of a proton (m_0, e are the proton mass and charge; c is the speed of light).

Figure 1 shows the cosmic-ray intensity variation we have obtained in this way within the rigidity interval

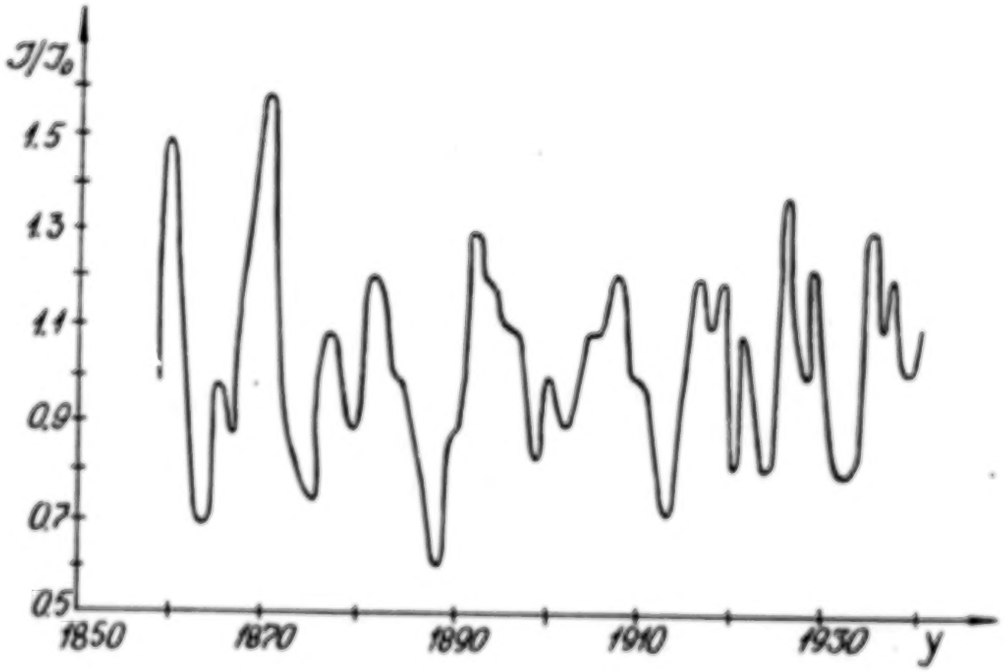


Fig.1. Intensity variations of galactic cosmic rays within the rigidity range $0.5 \leq R \leq 50$ GeV

N85-35107

$0.5 \leq R \leq 50$ GV. 11-year periodicity is clear seen in all considered time-interval. Amplitude of variation is in good agreement with the direct experimental data obtained during two last cycles of solar activity.

References.

1. Kocharov G.E. et al.,1985, paper SH 7.-14 presented at 19-th ICRC, San-Diego,USA.
2. Kocharov G.E. et al. 1983,Pis'ma Astronom.Zh. v.9,p.206.
3. Lockwood J.A.,Webber W.R.,1967, J.Geophys.Res.,v.72, p.5977.
4. Dorman L.I. in Proc.: 6-th All-Union Conf. on Astrophysical Phenomena and Radiocarbon, Tbilisi Univ.Press, USSR,1978,p.49.
5. Dergachev V.A.,Kocharov G.E.,Tleugaliev S.Kh.,1979, Proc. 16-th ICRC,Kyoto, p.142.

N85-35107
SH 7.1-17

COSMOGENIC Mn-53 IN METEORITES

Alexeev, V.A. and Lavrukhina, A.K.

V I.Vernadsky Institute of Geochemistry and Analytical Chemistry, USSR Academy of Sciences, Moscow, USSR

The distributions of the Mn-53 contents in 106 nonantarctic and 112 antarctic chondrites were analysed. A correlation analysis of these distributions showed that the correlation coefficient is a maximum (r_{max}=0.75±0.03) when the histogram for antarctic chondrites is displaced by 40±8 dpm kg^{-1}Fe towards lower Mn-53 contents.

The distribution of Mn-53 saturated contents in nonantarctic ordinary chondrites was investigated as a function of their radiation age (T). It is found that the Mn-53 average content is higher by (21±9)% in H-chondrites with radiation age T ≤ 12 Myr than in those with T > 12 Myr. This effect can be attributed to the fact that a considerable proportion of H-chondrites with T ≤ 12 Myr originates from a comet or from the objects of Chiron like, with the orbits more inclined to the ecliptic plane and/or more extended, which caused their irradiation by cosmic rays of higher intensity. The greater proportion of such chondrites in the antarctic meteorites might cause the aforementioned higher Mn-53 content in the meteorites from Antarctica.

Studies of long-lived cosmogenic radionuclide Mn-53 ($t_{1/2}$=3.7 Myr) in meteorites can supply evidence on both the cosmic-ray intensity variation and the radiation history of these cosmic bodies. The direct counting of Mn-53 presents difficulties because of the soft K-radiation; also rather large amounts of precious material would be needed. Millard /1/ pointed out the possibility of converting Mn-53 into the γ-emitting Mn-54 by a neutron capture. The large cross- section affords much greater sensitivity for the determination of Mn-53.

We studied the different procedures on the Mn isolation from the meteoritic metal, found the optimal conditions of the irradiation, and determined the Mn-53 content in the iron meteorites and in the metal of chondrites. About 1 g of meteoritic metal along with the Mn carrier (5 mg) were dissolved in HNO_3. Pre- and post-irradiation chemical procedures were mainly similar to those reported by Imamura et al. /2/. The manganese was isolated by ion exchange procedures and

then in the form MnO_2 was irradiated 1156 hours in the researh reactor. Results of our measurements were published in /3,4/. This paper presents an analysis of data reported in the literature and authorss data on the Mn-53 content in ordinary chondrites.

The distributions of the Mn-53 contents in 106 nonantarctic and 112 antarctic chondrites were analysed (see Fig.1). A correlation analysis of these distributions showed that the correlation coefficient is a maximum (r_{max}=0.75±0.03), when the histogram for antarctic chondrites is displaced by 40±8 dpm kg^{-1}Fe towards lower Mn-53 contents (Fig.2). That is, the Mn-53 content in antarctic chondrites is higher, on the average, than in nonantarctic chondrites, in spite of higher earth age of the antarctic meteorites.

This fact can be explaned by several reasons: (a) antarctic meteorites have higher radiation ages; (b) antarctic meteorites were irradiated in space by cosmic rays of higher intensity due to, possibly, a higher extent or a larger inclination to the ecliptic plane of the orbits of these meteorites /5/.

The distribution of Mn-53 saturated contents in nonantarctic ordinary chondrites was investigated as a function of their radiation age. The equation:

$$A_{sat}=A_{meas}/(1-e^{-T.\ln 2/t}),$$

was used to calculate the saturated content of Mn-53 (A_{sat}). Here A_{meas} is measured content of Mn-53, t is half-life of Mn-53, and T is radiation age of meteorite. The radiation age of chondrites was determined from the cosmogenic ^{21}Ne content and its production rate (P_{21}). The P_{21} values were calculated according to relation proposed by Nishiizumi et al. /6/. The noble gas data are from the compilation by Schultz and Kruse /7/. When more than one analysis was available for a given meteorite, the average of the exposure ages was used. Ne-21 and Ne-22 concentrations were corrected for a trapped component, using a solar isotopic composition for the solar-gas bearing meteorites and atmospheric ratios for the rest of the analyses /8,9/.

The results for 56 H-chondrite are shown in Fig.3. It is found that the Mn-53 average content is higher by (21±9)% in H-chondrites with radiation age $T \leq 12$ Myr years than in those with $T > 12$ Myr. A similar excess, though less pronounced, we observed for L- and LL-chondrites too. The analysis showed that this excess takes place both for the falls and for the finds, and is not due to the difference in meteorite mass distribution in different age groups. A similar, but less pronounced effect is noticed also for Al-26. The higher Mn-53 and Al-26 saturated contents in chondrites of low radiation age, especially in H-chondrites, can be attributed to the fact that a considerable proportion of

meteorites with $T \leq 12$ Myr originates from a comet or from the objects of Chiron like, with the orbits more inclined to the ecliptic plane and/or more extended /10,11/, which caused their irradiation by cosmic rays of higher intensity. The greater proportion of such chondrites in the antarctic meteorites might cause the aforementioned higher Mn-53 content in the meteorites from Antarctica.

These data can supply the additional information for study of variations of galactic cosmic-rays intensity during the last ~10 Myr.

References

1.Millard, H.T., Jr. Science, 1965, 147, 503.
2.Imamura, M., Matsuda, H., Horie, K., and Honda, M. Earth Planet. Sci. Lett., 1969, 6, 165.
3.Alexeev, V.A., Malishev, V.V., and Lavrukhina, A.K. Lunar Planet. Sci. XIII, 1982, 5.
4.Lavrukhina, A.K., Alexeev, V.A., and Malishev, V.V. Isotopenpraxis, 1980, 16,9, 301.
5.Ustinova, G.K. and Lavrukhina, A.K. Geochimia, 1983, 4, 483 (in Russian).
6.Nishiizumi, K., Regnier, S., and Marti, K. Earth Planet. Sci. Lett., 1980, 50, 1, 156.
7.Schultz, L. and Kruse, H. Helium, neon, and argon in meteorites. A data compilation. Max-Planck-Institut für Chemie, Mainz, 1983.
8.Crabb, J. and Schultz, L. Geochim. Cosmochim. Acta, 1981, 45, 11, 2151.
9.Wasson, J.T. Meteorites. Classification and properties. Springer, N.Y., 1974, 317 p.
10Lavrukhina, A.K. Acta Geophys. Polonica, 1973, XXI, 185.
11Wood, Ch.A. and Mendell, W.W. Lunar Planet. Sci. XIII, 1983, 877.

Figure captions

Fig.1. Distributions of Mn-53 content in 112 antarctic (dashed line, the histrogram is hatched) and 106 nonantarctic (solid line) ordinary chondrites.

Fig.2. Correlation coefficient (r) of the distributions of Mn-53 contents in antarctic and nonantarctic chondrites as function of the histogram displacement (δ). Displacement of the antarctic chondrites histogram towards lower Mn-53 contents corresponds to the positive values of δ. The equation of the parabola was derived by the least sguares method and is of the form:

$$r=(71\pm4).10^{-2}+(22\pm3).10^{-4}\delta-(27\pm3).10^{-6}\delta^2$$

Analysis of this eguation showed that the maximum of the r ($r_{max}=0.75$) corresponds to the δ = 40 ± 8dpm·kg^{-1} Fe.

ORIGINAL PAGE IS
OF POOR QUALITY

Fig.3. Distributions of Mn-53 saturated contents as a function of radiation age in 56 nonantarctic H-chondrites. Hatched areas correspond to the average Mn-53 contents ($N \pm \sigma_{\bar{N}}$) for $T \leq 12$ and $T > 12$ Myr. The open circles stand for the finds, and the full for the falls.

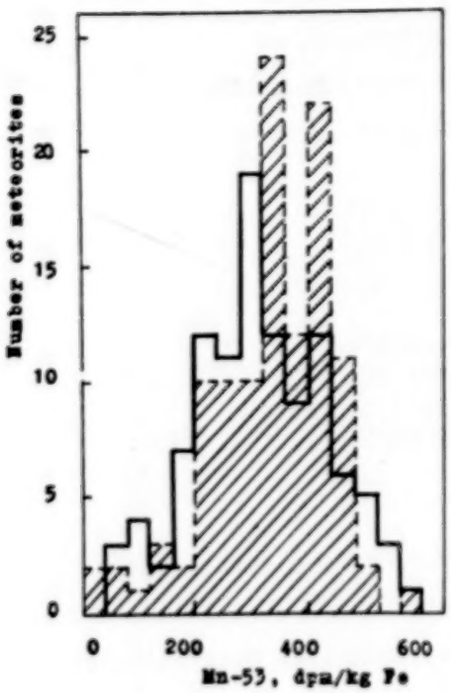


Fig. 1

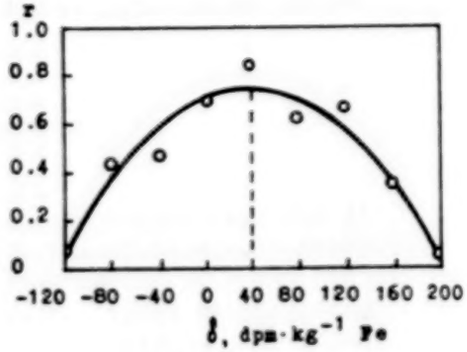


Fig. 2

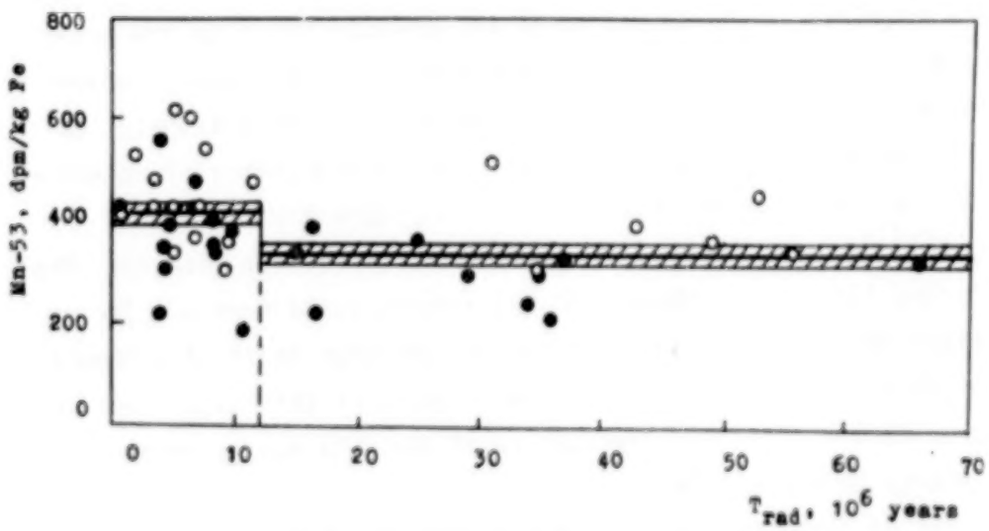


Fig 3

N85-35108

RESULTS OF ULTRA-LOW LEVEL ^{71}Ge COUNTING FOR APPLICATION IN THE "GALLEX"-SOLAR NEUTRINO EXPERIMENT AT THE GRAN SASSO UNDERGROUND PHYSICS LABORATORY

Hampel, W., Heusser, G., Hübner, M., Kiko, J.
Kirsten, T., Schneider, K. and Schlotz, R.
Max-Planck-Institut für Kernphysik, Postfach 103980
D-6900 Heidelberg, Federal Republic of Germany

ABSTRACT

It has been experimentally verified that the Ultra-Low-Level Counting System for the "Gallex"-solar neutrino experiment is capable to measure the expected solar ν-flux to $\pm$12% during two years of operation.

1. Introduction. More than a decade after Davis implemented his Chlorine detector, experimental solar neutrino spectroscopy is still in a state of infancy and lacks behind existing technical possibilities. The only available experimental result, a deficit of solar ^{8}B-neutrinos as measured with the Cl-detector, has caused serious doubts on the appropriateness of our understanding of stellar structure and evolution. Urgently required is the detection of the pp-neutrinos from the principal fusion reaction $p+p \rightarrow d+e^{+}+\nu_e$. Their flux is largely model independent and directly related to the solar luminosity. The extremely low energy of pp-neutrinos (maximum 420 keV) limits the choice of potential radiochemical detector materials. The Gallium detector, based on $^{71}Ga(\nu_e,e^{-})^{71}Ge$ is by far the most promising pp-neutrino detector. The newly formed "Gallex-collaboration" (1) intends to perform a solar neutrino experiment based on this reaction at the Gran Sasso Underground Physics Laboratory (Italy) (2). The major goals of this experiment are:

- to provide the first experimental proof that the sun is producing its energy by nuclear fusion.
- to limit or identify neutrino mass differences through eventual ν_e-disappearance between sun and detector via neutrino oscillations. The parameter range accessible in this way is many orders of magni-

tude below that for other ν-oscillation experiments.

- to identify the cause of the "solar neutrino puzzle" posed by the Chlorine solar neutrino experiment (3).

2. Outline of experiment components

(1) Underground laboratory

Cosmic ray-induced (p,n) reactions produce ^{71}Ge from ^{71}Ga just as solar neutrino capture. The overburden required to suppress the cosmic ray-induced ^{71}Ge production rate to $\leq$2% of the expected neutrino induced production rate is 3100 m.w.e. (corresponding to a muon flux of I_μ=21 $m^{-2}d^{-1}$). The generous space available in the Gran Sasso underground laboratory is shielded by 3200-3500 m.w.e., hence sufficient for the experiment. Background reactions will also be monitored by ^{69}Ga (p,n)^{69}Ge. This reaction has an even larger yield than $^{71}Ga(p,n)^{71}Ge$, whereas pp-neutrinos do not produce ^{69}Ge.

(2) Target

The high costs of Gallium force us to choose the smallest target size which is still sufficient to produce a $\pm$10% result within 4 years of measurements (this assumes the standard solar model neutrino flux). Given the achieved conditions (see below), this corresponds to 30 t of Ga (converted into 8m $GaCl_3$ solution). The required radiochemical purity of this solution has been demonstrated to be achievable even in the multiton scale. Ga acquisition is pending.

(3) Ge extraction system

The quantitative and reproducible extraction of Ge (as volatile $GeCl_4$) from $GaCl_3$ solution and its conversion into GeH_4 (Germane) to be used as counting gas has been developed and tested in the earlier BNL MPI 1.3 t Ga pilot experiment (4).

(4) Counting system

^{71}Ge ($T_{1/2}$=11.43 d) decays by K (88%) L (10.3%), and M(1.7%) electron capture. Auger-electrons and stopped X-rays are counted in GeH_4/Xe gas mixtures in miniaturized proportional counters made of ultrapure materials. Up to 8 counters can be accommodated in the well of a well type NaI pair spectrometer. Apart from its anticoincidence mode, it serves in the coincidence mode to

identify ^{69}Ge decays ($T_{1/2}$=1.6 d; EC; EC+γ; and $e^+ \overset{e^-}{\div} 2\gamma$). The NaI crystal is surrounded by plastic scintillator anticoincidence shields and passive Fe/Pb shields. The data from all active components (proportional counters, NaI halves, plastic scintillators)are fed into the PDP/LSI computer both for on line evaluation and for storage on magnetic tape ("Mulia" system) (4).

3. Results of Ultra-Low Level Background Reduction

In the proposed configuration of the Gallex experiment one expects per run an average of 7 ^{71}Ge decays during the first month after extraction according to the standard solar model. From this it follows that background rates of order $\lesssim$ 1 c/10 days must be achieved. Apart from the measures described above, this goal is in particular approached by a complete pulse shape analysis using a transient digitizer to reject background, mainly from Compton electrons and from electronic noise.

The energy deposition from Auger electrons and X-rays emitted in the ^{71}Ge electron capture decay results in a spectrum with 2 peaks: the L peak at $\sim$1.2 keV and the K peak at $\sim$10.4 keV. Counting efficiencies ε are determined using active ^{71}Ge in prototype counters. Thus, the acceptance fields of 95% are defined in an energy-pulse form parameter plot for K- and L peak (Fig.1). The pulse form is most efficiently parameterized as $G \cdot I = S(T)/S(t_{max}) \cdot \frac{1}{T} \int_0^T S(t)dt/S(t_{max})$ where S(t) is the pulse height at time t after pulse onset, t_{max} is the time at which S(t) is maximal, and T is an empirically selected parameter, here T=160 nanoseconds. In this way, background pulses simulated by Compton electrons from a ^{60}Co source are rejected with an efficiency of 96.3% (L peak) and 99.9% (K peak).

The values previously achieved with many counters (ε_L=25%, b=0.2 cpd; ε_K=38%, b=0.08 cpd) would allow to determine a solar neutrino rate of 90 SNU with a standard error of 14% in a two year experiment (50 extractions). 90 SNU is the rate compatible with the Cl detector result interpreted in terms of astrophysical causes ("consistent" model). Meanwhile, improvements have been made and background rates measured with some counters are about a factor of two lower than the values listed above. Fig.2 displays the results of a 51.5 day background measurement obtained with one of the best counters. Here b_K=0.04 cpd, b_L=0.08 cpd. This would allow to measure 90 SNU with a 30 t Ga detector during two years of operation

ORIGINAL PAGE IS
OF POOR QUALITY

to ± 12%, as compared to ±10% if the background were zero. Additional advances have been recently made with an improved counter design. Its dead volume is reduced to 5% by directly evaporating the Al-cathode onto the quartz tube and directly sealing the tungsten anode wire into the quartz ends. With this counter type we obtain an overall efficiency of 74% (ε_K=46%, ε_L=28%).

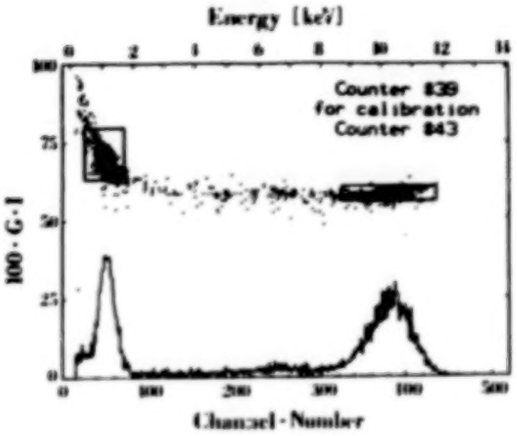


Fig.1: ^{71}Ge spectrum and 95% acceptance fields for genuine ^{71}Ge decays. The pulse shape parameter G·I is defined in the text.

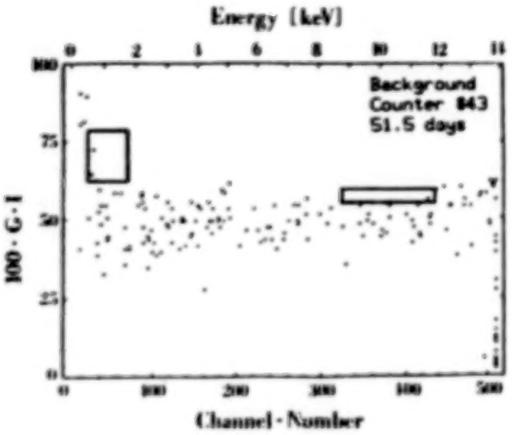


Fig.2: Result of 51.5 days of background counting of counter #43 applying pulse shape analysis with the MULIA system. Acceptance windows for K and L peak are indicated.

References

(1) Members of the collaboration: T. Kirsten (spokesman), W. Hampel, G. Eymann, G. Heusser, J. Kiko, E. Pernicka, B. Povh, M. Schneller, K. Schneider, H. Völk (HEIDELBERG) - K. Ebert, E. Henrich, R.Schlotz (KARLSRUHE) - R.L. Mößbauer (MÜNCHEN) - I. Dostrovsky (REHOVOT) - M. Cribier, G. Dupont, B. Pichard, J. Rich, M. Spiro, D. Vignaud (SACLAY) - G. Berthomieu, E. Schatzman (NICE) - E. Fiorini,E.Bellotti, O. Cremonesci, C. Liguori, S. Ragazzi, L. Zanotti (MILANO) - L. Paoluzzi, S. D'Angelo, R. Bernabei, R. Santonico (ROMA).

(2) A. Zichichi, AIP Conf.Proc. 96, 52 (1983).

(3) J. Rowley, B. Cleveland, R. Davis, AIP Conf.Proc. 126, 1 (1985).

(4) W. Hampel, AIP Conf.Proc. 126, 162 (1985).

CORRELATION BETWEEN SOLAR "NEUTRINO FLUX" AND OTHER SOLAR PHENOMENA

N85-35109

SIDDHESHWAR LAL,
DEPARTMENT OF PHYSICS,
UNIVERSITY OF INDORE,
INDORE - 452001.

A.SUBRAMANIAN,
TATA INSTITUTE OF FUNDAMENTAL RESEARCH,
BOMBAY-400005.

1.Introduction.

We have made a study of the solar neutrino data obtained by Davis et al (1) with a tank of CCl_4 located 4800 mwe underground and shown in Fig.1 for the period 1970-83.These observations are on the production rates of Ar^{37}atoms via the reaction $\nu_e + Cl^{37} \rightarrow Ar^{37} + e^-$ in the tank caused presumably by a flux of neutrino's from the Sun.

It is now well known that the combined average rate of production of Ar^{37}obtained as 0.47±.04 atoms/day and depicted in Fig.1 is too low by a factor ≈3 from that expected from thermonuclear chain reactions in the Sun (2).Added to this difficulty in understanding the source of discrepancy between the expected and observed reaction rates are the numerous suggestions that the obtained data exhibit temporal variations (3,4).Recently we have carried out a statistical analysis (5) of the data shown in Fig.1.While one cannot make a strong claim for time variations based on a simple χ^2 test,we have shown that the data represented by run numbers marked 27,71 and the sequence of low values following run no.60 and some others are significantly deviated.In fact there seems to be a correlation of adjacent data points exhibiting a pattern of variation shown in Fig.2 for which the χ^2 test of constancy hypothesis yields a probability of only 0.03% (χ^2=37.5/13d.f.)

In this paper we pursue the idea of possible time variations in the data shown in Fig.1 and attempt to correlate the variations to two other phenomena of solar origin-the sunspot number and the geomagnetic Ap index.

2. CORRELATION STUDIES WITH SUNSPOTS AND GEOMAGNETIC INDICES

Following the early suggestions(4), Basu (6) has found a positive correlation between the solar neutrino data of Davis of et al and monthly average of geomagnetic Ap indices.Sakurai (3) suggested the correlation with

biennial variations in the sunspots.

We have noted a correlation between the geomagnetic Ap index and $|\dot{R}_z|$, the derivative of smoothed sunspot number (7), which is shown in Fig.3. This correlation could merely suggest a common link of solar wind between $|\dot{R}_z|$ and monthly mean Ap index. We also find a fairly good correlation between the production rate of Ar^{37} atoms and $|\dot{R}_z|$ (Fig.4). The significance of this correlation is at a level of 4σ effect. $|\dot{R}_z|$ appears to be a better correlation parameter than the biennial periodicity of the sunspot number as orignially suggested by Sakurai (3). The correlation of Ar^{37} with Ap index is somewhat less significant (3.3σ effect) than with $|\dot{R}_z|$.

3. Conculsions.

A statistical analysis of the data obtained by Davis et al on the solar neutrino flux suggests fluctuations with time within a period of 12 years or so for which the data is currently available. These variations appear to have positive correlation with $|\dot{R}_z|$ (absolute rate of variation of smoothed sunspot number) which in turn has a positive correlation with the geomagnetic Ap index. Thus the solar neutrino flux recorded in the Davis et al experiment seems to have a connection with even a low energy phenomenon occurring on the such as the generation of solar wind. We admit the possibility of isolated large fluctuations like run nos.27 and 71 (Fig.1 and 2) being correlated to large solar flares occurring on the visible disc of the sun as has been suggested by Bazilevskaya et al (3).

We would like to thank Dr.S.P.Agrawal for discussions.

References.

1. R. Davis Jr., D.S.Harmer and K.C.Hoffman, Phys.Rev.Lett., 20, 1205, (1968).
   R.Davis Jr., B.Clevland and J.K.Rowley , in "Workshop on Science Underground," A.I.P.Conf.Proc.No.96, Los Alamos 1982, Published by A.I.P, New York, 1983. We thank Dr.R.Davis Jr. for sending a compilation of the data as of mid 1984 to one of the authors (A.S.).
2. See for e.g., J.N.Bahcall et al, Phys Rev.Letters, 45, 945 (1980).
3. W.R.Sheldon, Nature, 221, 650 (1969).
   P.Raychaudhuri, Ap SP.Sci. 13, 231, (1971).
   K.Sakurai, Nature, 279, 146 (1979); 18th Int.Cosmic Ray Conf., Conference Papers ed., Durgaprasad et al; Vol.4, Paper SP-1, Bangalore, 1983.
   G.A.Bazilevskaya et al, JETP Lett, 35, 341 (1982); 18th Int. Cosmic Ray Conf., Conference Papers ed., N.Durgaprasad et al, Vol.4, Paper SP-4, Bangalore, 1983.
   H.J.Haubold and E.Gerth, Astron.Nach. 304, 299 (1983)

4. A.Subramanian,Current Science,48,705(1979)
5. A.Subramanian,Current Science,52,342(1983)
A.Subramanian and Siddheshwar Lal,Preprint TIFR-BC-83-12, Submitted to Current Science.
6. D.Basu,Solar Physics,81,363(1982).
7. Solar-Geophysical Data,Reports Published by U.S.Dept.of Commerce,Boulder,Colarado,U.S.A..

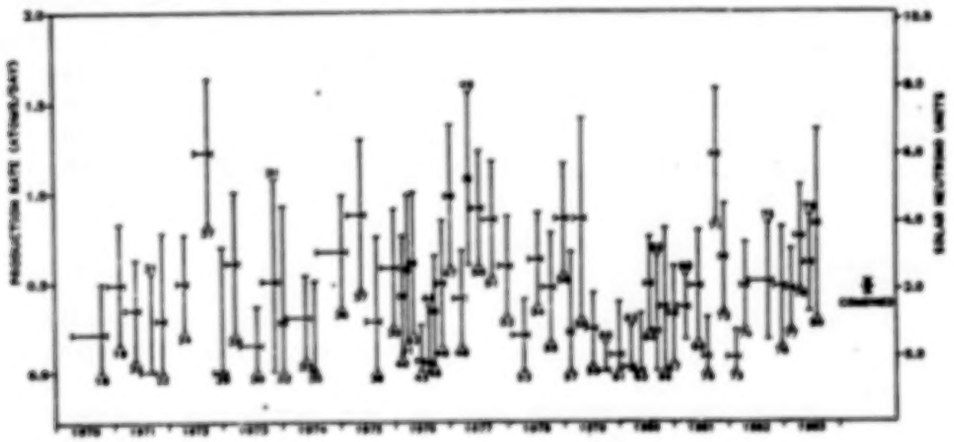


Fig.1 The data of R.Davis Jr. et al (1) on the solar neutrino flux during the period 1970-83.

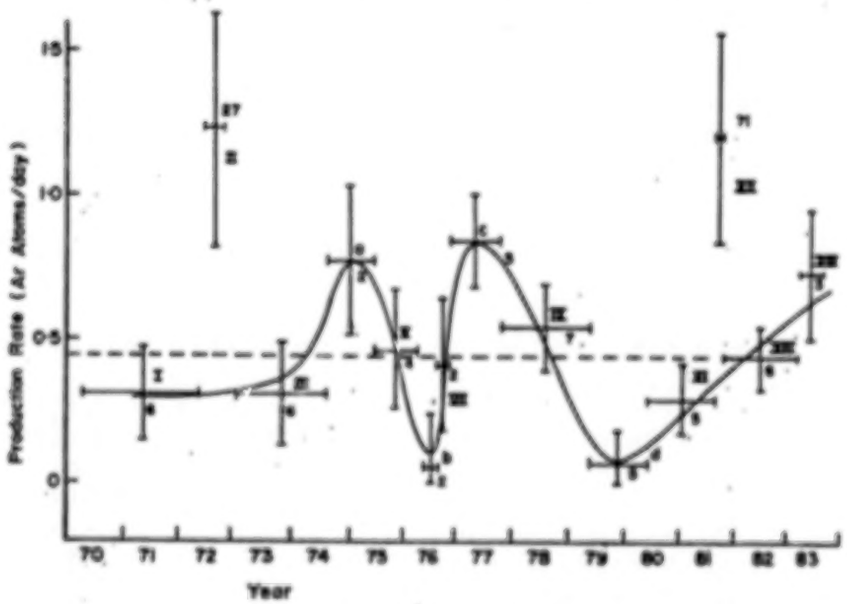


Fig.2 Grouped averages of the solar neutrino flux data given in Fig.1 which exhibit variations in time as suggested by the guiding continuous curve excluding run no.27 and 71. The grouped data points are labelled by Roman number or alphabets. The numbers attached to the groups except II and XII indicate the no.of independent measurements that have gone into the grouping.

ORIGINAL PAGE IS
OF POOR QUALITY

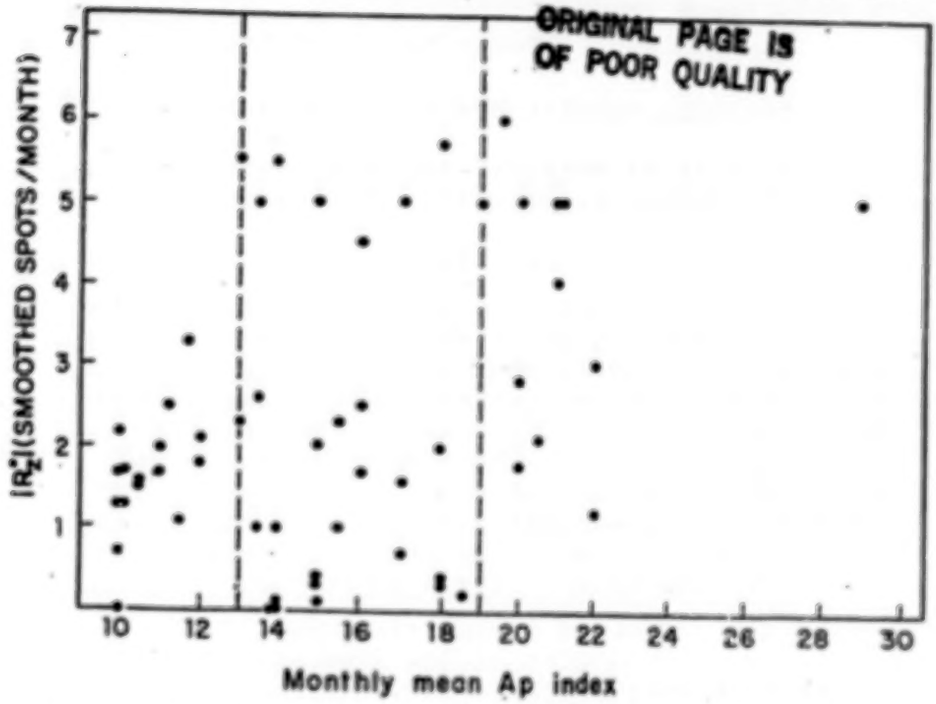


Fig.3 A plot showing the correlation between monthly average geomagnetic Ap index and the absolute derivative $|\dot{R}_z|$ of smoothed sunspots. Vertical dashed lines separate different regions of the mean Ap.

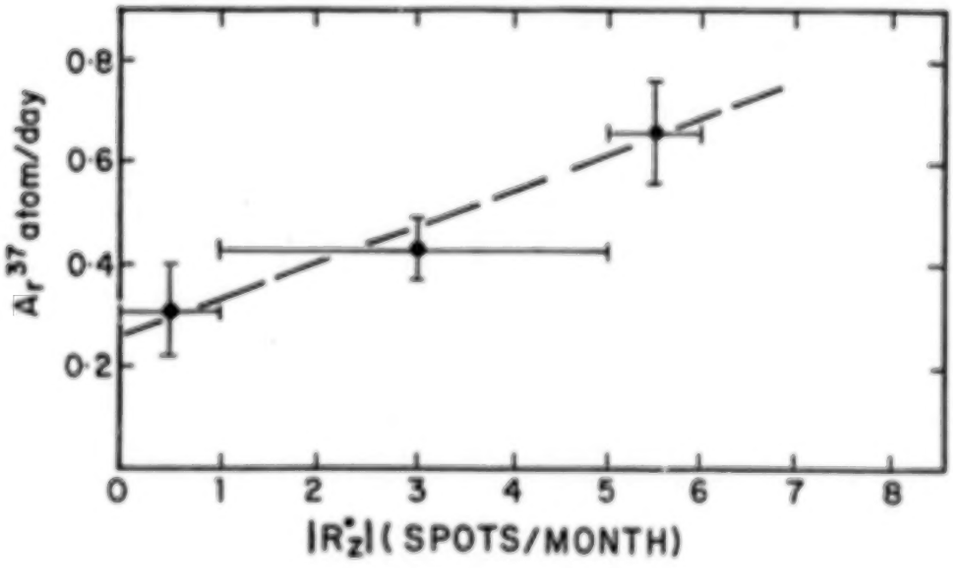


Fig.4 The correlation between Ar^{37} production rate in the Davis et al experiment and $|\dot{R}_z|$, the absolute derivative of smoothed sunspots.

N85-35110
SH 8.1-5

A POSSIBLE MECHANISM TO CAUSE THE QUASI-BIENNIAL VARIABILITY ON THE SOLAR NEUTRINO FLUX

Kunitomo Sakurai and Mitsuru Hasegawa

Institute of Physics, Kanagawa University
Rokkakubashi, Yokohama 221, Japan

ABSTRACT

It is suggested that the quasi-biennial change in the observed flux of the solar neutrinos is causally related to some non-linear process at the central core of the sun, being associated with the change in the central temperature. This process seems to be responsible for the physical adjustment of the internal structure of the sun. Numerical simulation on this process is able to reproduce the quasi-biennial change in the flux of these neutrinos.

1. Introduction In order to see the rate of the energy production at the central core of the sun, Davis and his associates have been measuring the flux of the solar neutrinos which are mainly produced from the PP III process(1). According to their results, the mean observed flux of these neutrinos for more than ten years is by a factor three or more less than the flux theoretcially expected from the standard model of the sun. At present, this discrepancy between observed and theoretical fluxes is thought as a serious problem in the research fields of astrophysics, being known as the "missing solar neutrinos,"because this has seemingly suggested that the proton-proton chain reactions have been prevented from working well effectively in a manner as predicted from the theoretical treatment for the internal structure of the sun on the basis of the standard model(2).

The observed results by Davis et al. certainly indicate that the proton-proton chain reactions are only ineffectively taking place in the interiour of the sun, but it has recently been suggested that these results further indicate that the rate of these reactions has been varying quasi-biennially with a period of about 26 months(3). Although the sun itself should be considered to be a self-regulating feedback system with respect to the energy generation, such periodic variation just mentioned may have been caused by some non-linear process taking place in association with the proton-proton chain reactions.

2. Quasi-Biennial Change in the Observed Flux of the Solar Neutrinos Davis and his associates have been making the measurement of the neutrino flux from the sun for more than ten years(1). Since the results obtained by them are now available to investigate the efficiency of the proton-proton chain reactions at the cnetral core of the sun and its long-term change if any. Using these results, an analysis has

been done to find out possible periodic change in the observed fluxes of these neutrinos during the last ten years or so(3,4,5).

Since the intervals between two successive measurements of these neutrinos are not equally distributed, but scattered at random, the observed fluxes have been averaged over for four monthly intervals without taking the number of the measurements in each interval into account(3). The analysed

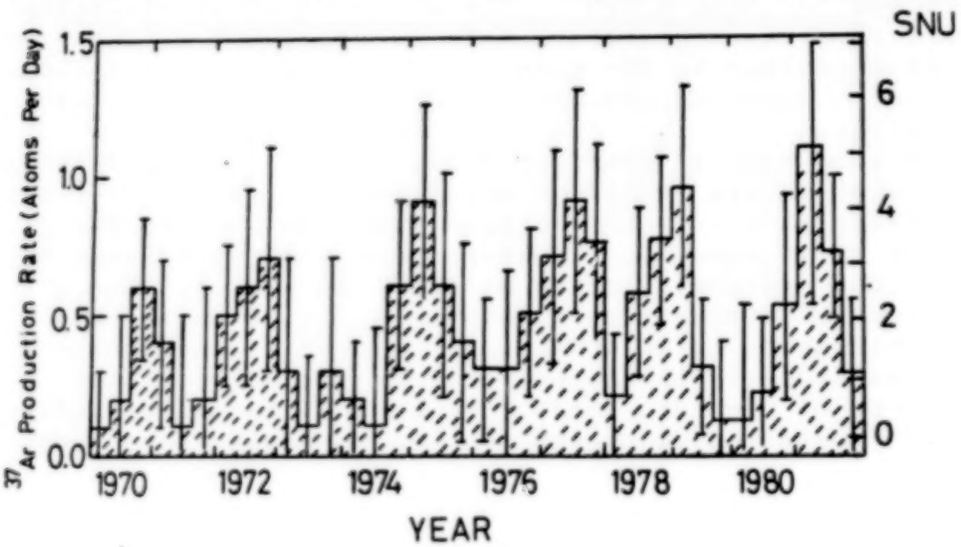


Fig. 1 A "periodic" variation of the four-monthly mean flux of the solar neutrinos produced mainly from the PP III reaction(3).

result is shown in Fig. 1, in which error ranges have been estimated using the error bars appeared in the original data given by Davis and his associates.

The result shown in Fig. 1 clearly indicates that the observed flux of the solar neutrinos had been varying quasi-biennially with a period of about 26 months during the years up to 1981. This seems to mean that the efficiency of the PP III process had been changing quasi-biennially because these neutrinos had been mostly released within three seconds into outer space after produced at the central core of the sun. According to Fig. 1, it seems that the observed background flux of the neutrinos has a tendency to vary throughout the solar activity cycle, since this flux seems to have been highest during the solar maximum. However, this tendency is not so clearly seen when compared with the quasi-biennial change as considered above.

3. Possible Mechanism of the Quasi-Biennial Change In order to explain the quasi-biennial periodicity on the time variation of the neutrino production at the central core of the sun, a non-linear process has been considered as a candidate to control the proton-proton chain reactions, in particular, PP III reaction. Since the efficiency of this reaction is shown to be strongly dependent on the temperature at the central core of the sun, this process seems to be controlled

by this temperature(6). Thus it seems appropriate to assume that this temperature, being denoted by T, is controlled by a non-linear process as following the equation described as

$$\frac{dT(t)}{dt} = [\,\underline{a} - \underline{b}T(t-\tau)\,]T(t),$$

where $\underline{a}$ and $\underline{b}$ are both constant. Time $T(t-\tau)$ is the one which is earlier than t by τ. The above equation, therefore, expresses that the temperature T(t) is regulated by the time $T(t-\tau)$ as dtermined by the time $(t-\tau)$. This has first been considered to apply to biological population and chemical reactions(7).

From the physical point of view, this process indicates that the temperature varies as being controlled by the time being earlier by τ. By taking some numerical values for $\underline{a}$ and $\underline{b}$, the above equation has been numerically simulated to reproduce the periodic change as shown in Fig. 1. One of these numerical simulations is shown in Fig. 2 as an example and this seems to be applicable to explain the quasi-biennial periodicity in the temperature variation at the central core of the sun. Thus, the quasi-biennial periodicity in the neutrino flux from the sun can be well reproduced

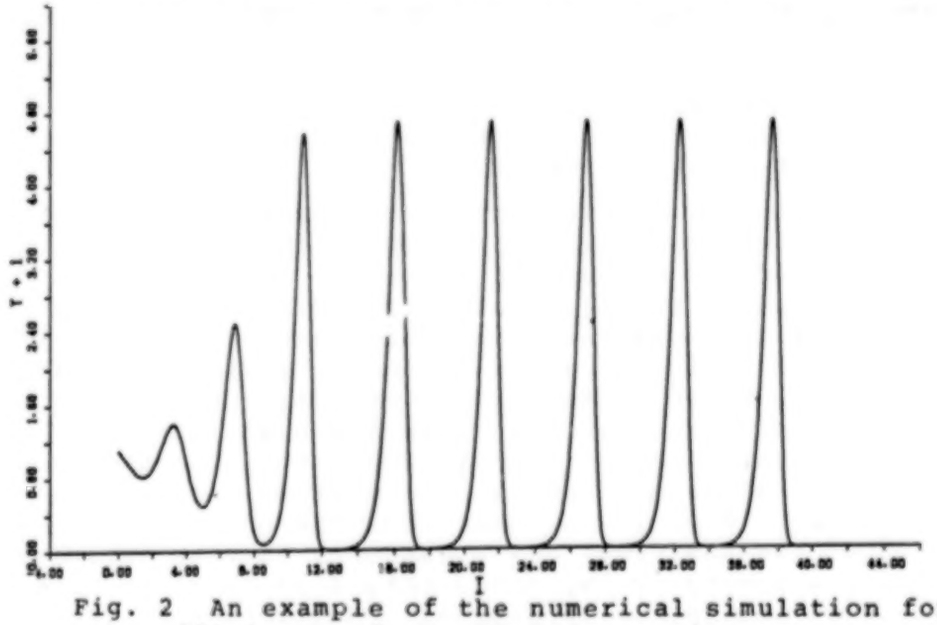


Fig. 2 An example of the numerical simulation for the efficiency of the PP III reaction.

from the non-linear process considered above.

As inferred from from Fig. 2, the occurrence of the periodicity as seen in this figure does not depend seriously on the initial condition which is related to the numerical values of τ, $\underline{a}$ and $\underline{b}$. For this reason, the quasi-biennial change in the efficiency of the PP III reaction as shown in Fig. 1 seems to be almost always excited easily whenever some instability is induced at the central core of the sun, which is associated with the change in the temperature there.

4. Concluding Remarks The quasi-biennial change as seen on the observed flux of the solar neutrinos has been numerically simulated by taking into account the non-linear process as described in this paper, which is associated with the change in the temperature at the central core of the sun. As theoretically deduced earlier, the sun is thought as a self-regulating feedback system with respect to the maintenance of the internal physical processes as related to the proton-proton chain reactions. It should be noted, furthermore, that the temperature and its radial gradient plays the most important role in adjusting the internal structure of the sun(2).

Thus it may be said that, as described in this paper, the non-linear process associated with the change in the central temperature is responsible for the quasi-biennial variation on the efficiency of the PP III reaction.

References

(1) R. Davis, Jr. et al. (1983) Science Underground, AIP Conf. Proc. No. 96, p. 2 (eds. M.M. Nieto et al.) Amer. Inst. Phys., New York.
(2) K. Sakurai (1984) Space Sci. Rev. 38, 243.
(3) K. Sakurai (1979) Nature 278, 146 and (1981) Pub. Astro. Soc. Japan 35, 547.
(4) D. Basu (1983) Solar Phys. 81, 363.
(5) H.J. Haubold (1983) Proc. 18th ICRC, Bangalore 10, 389.
(6) e.g., K. Sakurai (1981) Solar Phys. 74, 35.
(7) W.J. Cunnigham (1954) Proc. Nat. Acad. Sci., Math. 40, 708.

N85-35111

SH 8.1-6

THE CONJECTURE CONCERNING TIME VARIATIONS IN THE SOLAR NEUTRINO FLUX

H.J. Haubold and E. Gerth

Akademie der Wissenschaften der DDR
Zentralinstitut für Astrophysik
DDR - 1502 Potsdam-Babelsberg
German Democratic Republic

1. Introduction.

The most challenging problem in neutrino astronomy in the past two decades has been the solar neutrino problem, i.e., the discrepancy between the predicted rate of detection of neutrinos in the standard solar model of 6...8 SNU and the averaged value 2.1± 0.3 SNU actually observed (1SNU ≙ 10^{-36}captures/sec ^{37}Cl atom; cf. 1,2).

In this paper we shortly review the results of our Fourier transformation of the unequally-spaced time series of the recorded ^{37}Ar production rate of the solar neutrino experiment (runs 18-80, 1970-1983). We will determine significance criteria for every period discovered by the harmonic analysis (3,4). We will also perform a Fourier synthesis of certain discovered harmonics and it seems that the solar neutrino flux increases shock like with a period of approximately 8.3 years and after that breacks down. We point to possible connections between the periods found by the harmonic analysis and several observed phenomena on the solar surface.

2. Fourier Analysis of the ^{37}Ar Production Rate Measurements

For the harmonic analysis of the time series of 59 measurements of the ^{37}Ar production rate $f(t)$ (runs 18-80, cf. 1) we consider it as a stochastic process which we can split phenomenologically into two components : $f(t) = \mu(t) + \eta(t)$ where $\mu(t)$ denotes a non-stochastic function of time - the systematically varying component in $f(t)$ -, and $\eta(t)$ denotes the stationary stochastic process - the remainder in $f(t)$. The systematically varying component $\mu(t)$ can be split also into the trend β which we consider as time independent identified with the mean value over all n = 59 measurements ($\beta = 0.47$ ^{37}Ar atoms per day), and the non-stochastic periodic function $\nu_k(t) : \mu(t) = \beta + \sum \nu_k(t)$. Further we make the ansatz for $\nu_k(t)$ composed of sinusoidal and cosinusoidal terms : $\nu_k(t) = a_k \cos(2\pi\nu_k t) + b_k \sin(2\pi\nu_k t), k=1,\dots,n$. From the harmonic analysis of $f(t)$ by means of the finite Fourier transformation of unequally-spaced data described in (2,4) we obtain the power spectrum $N_1 = F(\nu)F^*(\nu)$ shown in Fig.1 by multiplying the Fourier transform $F(\nu)$ with its conjugate complex form $F^*(\nu)$. For a detailed discussion of the connection between the power spectrum $N_1(\nu)$ and the related spectral window see (4, 5). In Fig.1 are clearly recognizable the periods T_i = 8.33,

5.26, 2.13, 1.56, 0.83, 0.64, 0.54, and 0.50 (all T's in years, i = 1,...,8). We consider the complementary power quotient, $1-Q = (\sigma^2 - \sigma^2(\pi\nu_i))/\sigma^2$, shown in Fig.1 as a function of ν, as the significance criterion for every discovered harmonics of frequency ν_i (σ is the variance of the respective measurement). The higher the complementary power quotient the higher the significance of the considered harmonics. If we compare the power spectrum in Fig.1 obtained for runs 18-80 with earlier results of the Fourier analysis for runs 18-69 (2) and 18-74 (5) we find full consistency.

3. Fourier Synthesis of Certain Harmonics Discovered in the ^{37}Ar Production Rate

All variations in the power spectrum $N_1(\nu)$ shown in Fig.1 with power quotients $1-Q$ = 0.9500...1.0000 we consider as belonging to the stationary stochastic process $\eta(t)$ which has by definition no significant meaning for the search for periodics in $f(t)$. The periods $T_1 \dots T_6$ in Fig.1 are characterized by nearly equidistant frequencies and could be attributed to a series of harmonic waves. Taking every frequency of those six periods into consideration we can synthesize it to sinusoidal oscillations of the ^{37}Ar production rate belonging to a fundamental wave with T_1 = 8.33 years. For the purpose of smoothing the stochasticly caused function $\eta(t)$ in $f(t)$ we perform a folding of $f(t)$ with Gauss' normal distribution function. If we multiply the Fourier transform of $f(t)$ by the Gauss function the high frequencies will be smoothed out symmetrically to the frequency zero. In the process of the reconstruction (Fourier synthesis) of the time series $f(t)$ all harmonics with low frequencies will have the main contribution and determine the smoothed form of $f(t)$. This procedure applied to the ^{37}Ar production rate $f(t)$ with the fundamental wave T_1 = 8.33 years as shown in Fig.1, and a smoothing constant σ = 3 years^{-1} led to Fig.2. In Fig.2 we see that there occur three shock like rising waves within the fundamental period T_1 = 8.33 years up to a maximum ^{37}Ar production rate and after that a breack down of the ^{37}Ar production rate can be observed. To prove the influence of a curve shown in Fig.2 on the power spectrum given in Fig.1 we performed the Fourier analysis of $x(t)$ in Fig.2 and obtained the power spectrum $N_2(\nu)$ (see Fig.3). The power spectrum $N_2(\nu)$ in Fig.3 reproduces nearly completely all periods found in the harmonic analysis of the ^{37}Ar production rate measured in the solar neutrino experiment (1), T_2 = 4.5, T_3 = 2.34, T_4 = 2.17, T_5 = 1.73, T_6 = 1.49 (all T's in years), and fits into the fundamental period T_1 = 8.33 years the new period T_0 = 11.1 years. We believe that the value of the period T_0 = 11.1 years is connected with the total running period of the experiment of Davis and associates (1).

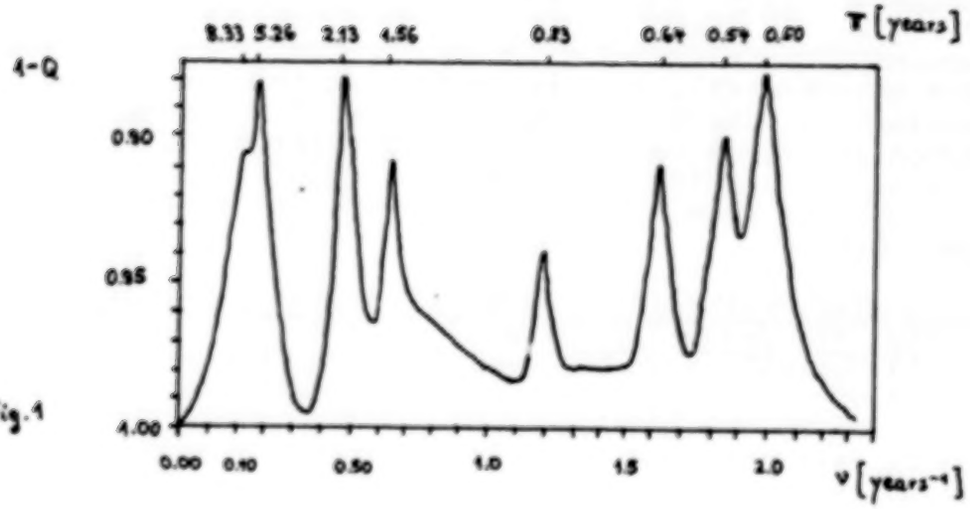


Fig. 1

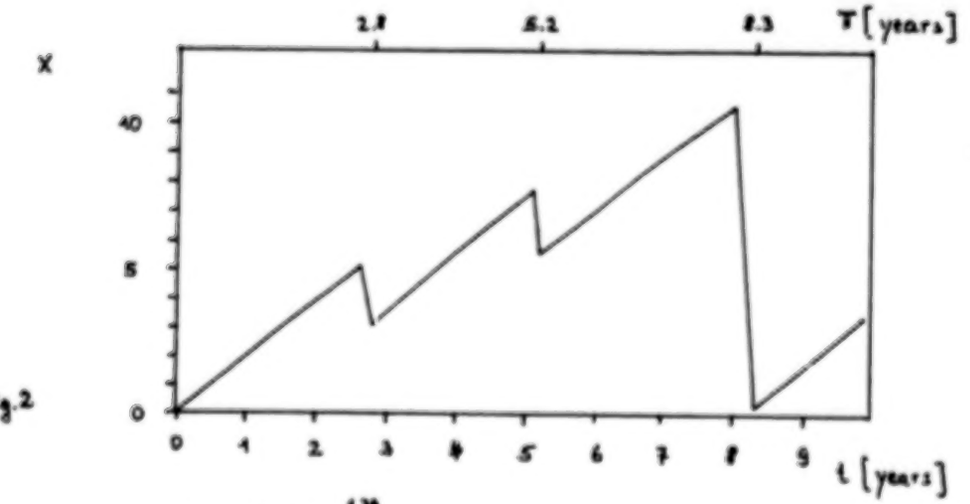


Fig. 2

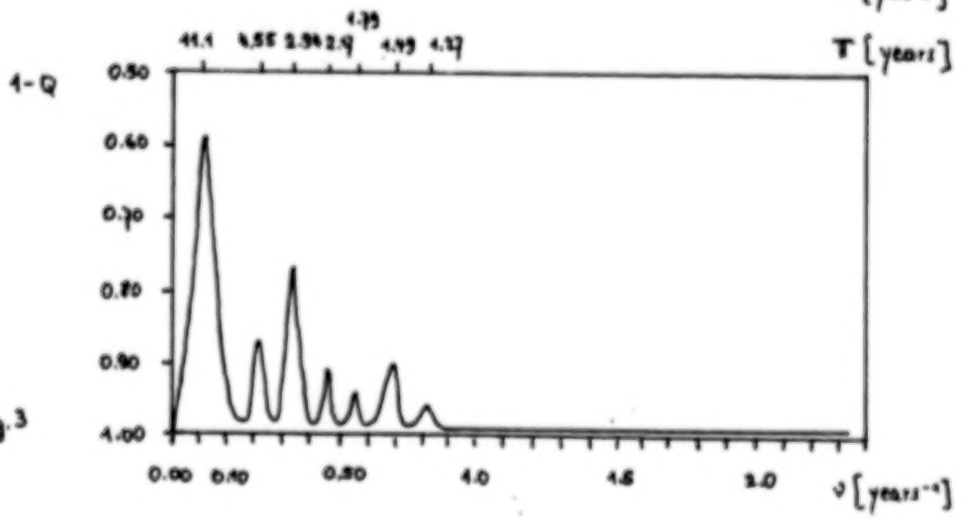


Fig. 3

4. Remarks

- One of the eight periods discovered by harmonic analysis, T_3 = 2.13 years, is identical with the quasi-biennial period obtained by Sakurai (6).

- It is interesting to note that Rieger et al. (7) recently published results concerning a 154 day periodicity in the occurence of hard x-ray flares of the Sun. Approximately the same periodicity observed Wolff (8) which he attributes to g-mode oscillations of the Sun. Both periods are rather close to our periods T_1 and T_2.

- In the present understanding of the solar interior only very few is known about physical processes which could lead to variations of the solar neutrino flux with periods in the order of years. However, non standard solar models are still under consideration where gravity mode oscillations are excited (9) and specific stratification of the solar interior exists (10). Such non standard solar models can explain, in principle, short time variations of the solar neutrino flux.

5. Acknowledgements

It is a pleasure for us to express our acknowledgement to Professor Dr. R. Davis, Jr. for his generosity of sending us the solar neutrino data and for many suggestions concerning our results.

References

1. Davis Jr.,R., Cleveland,B.T., and Rowley,J.K., (1984), Conference on the Intersections Between Particle and Nuclear Physics, Steamboat Springs, CO, May 23-30,1984.
2. Haubold,H.J., and Gerth,E., (1983), Astron. Nachr. 304, 299.
3. Haubold,H.J., and Gerth,E., (1983), Proc. 18th ICRC, Bangalore, 10, 389.
4. Haubold,H.J., and Gerth,E., (1985), AIP Conf. Proc., No. 126, 129.
5. Haubold,H.J., and Gerth,E., (1985), submitted for publication to Astron. Nachr., 306.
6. Sakurai,K., (1983), Proc. 18th ICRC, Bangalore, 4, 210.
7. Rieger,E., et al., (1984), Nature, 312, 623.
8. Wolff,C.L., (1983), Ap.J., 264, 667.
9. Kopysov,Yu.S., (1983), Preprint P-0317, Academy of Sciences of the USSR, Institute for Nuclear Research, Moscow.
10. Vandakurov,Yu.V., (1984), Pis'ma v Astron. Zhurnal, 10, 873.

ORIGINAL PAGE IS
OF POOR QUALITY

N85-35112
SH 8.1-7

SOLAR NEUTRINO:FLUX,COSMIC RAYS AND THE 11 YEAR SOLAR CYCLE

Probhas Raychaudhuri
Department of Applied Mathematics
Calcutta University,Calcutta-700009,INDIA

A B S T R A C T

It is shown that the results of maximum likelihood treatment of Monte Carlo simulation with constant production rate of 7·6 SNU and 1·8 SNU are consistent with the constant production rate when the tests of hypotheses(e.g. t-test,χ^2-test,Wilcoxon-Mann-Whitney test,run test etc.)has been applied to the two groups of data formed from sunspot minimum range and sunspot maximum range whereas the real data pulsates with the solar activity cycle.It is shown that SN flux-change is in opposite phase to the solar activity cycle and lags behind the latter by about one year.A correlation between SN flux and the cosmic rays has also been suggested.

Raychaudhuri(1,2,3,4,5,6)and Davrin et al(7)showed that the solar neutrino(SN)flux data is varying with the solar activity cycle.Raychaudhuri (3,4,5,6)showed that the fluxes will be higher in the sunspot minimum range than in the sunspot maximum range. This is supported by the data presented by Rowley et al(8)at the solar neutrino and neutrino astronomy conference held at Lead,South Dakota.Apart from the above variation Raychaudhuri(5,6)showed that there is also a quasi-decennial variation from 1970-1975 and 1979-1984. This type of variation is already observed by Chevyshev(9)and Filisetti(10)in the cosmic ray intensity(proton flare).

In this paper an estimate of the moving average(5 successive run number) data is considered to find the statistical significant variation of SN flux with the solar activity cycle of 11 years by t-test,χ^2-test,Wilcoxon -Mann-Whitney test and run test.To search variation in a convincing manner the above tests of hypotheses have been applied to the data that had been generated by Monte Carlo simulation and background parameters are typical of those in the actual experiment.

SOLAR ACTIVITY CYCLE AND(a)MOVING AVERAGE DATA,(b)MONTE CARLO SIMULATED DATA WITH CONSTANT PRODUCTION RATE(i)7·6 SNU AND(ii)1·8 SNU.

Here we apply the same proceedure as in Raychaudhuri(5,6).

1)Student t-test:-a(i)Moving average data

We form the two groups,the first group comprises sunspot minimum range (about 4·6 years)and the second group i.e.,the rest comprises sunspot maximum range.Let us now collect the data from the run number 36 to 58 from August 1974 to February 1979(about 4·6 years)for the first group.If we now set up the null hypothesis $H : m_1 = m_2$ against the alternatives $m_1 > m_2$ .The statistics t is given by(here the difference of variance is not significant).

$$t = \sqrt{\nu}\sqrt{\frac{N_1 N_2}{N_1+N_2}}\ \frac{\bar{x}-\bar{y}}{\sqrt{N_1 S_1^2 + N_2 S_2^2}}$$

where $\nu = N_1+N_2-2$.In the above case $N_1=23, N_2=27, \nu=48$ which gives t=4·54. Thus we can conclude that 99·9% of the data pulsates with the solar activity cycle.The standard error of the difference of means is 4·546.Hence the data are inconsistent with the assumption that the two means are equal.

(ii)Yearly average of the moving average data:-Here one group comprises the yearly average data from 1975 to 1978 and the other group comprises rest of the moving average data.We get for 9 d.f. t=2·76.The standard error of the difference of the means is 3·16 which suggests that the

ORIGINAL PAGE IS
OF POOR QUALITY

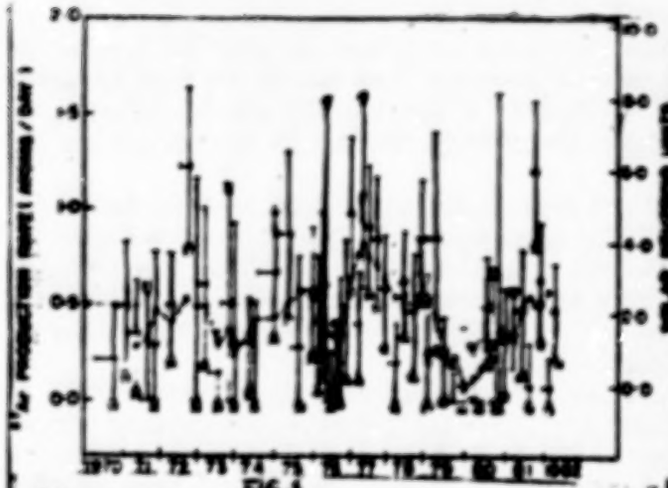


Fig.1

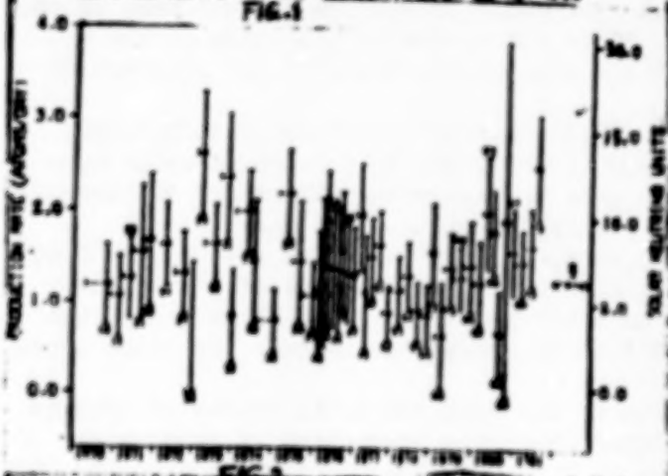


Fig.2

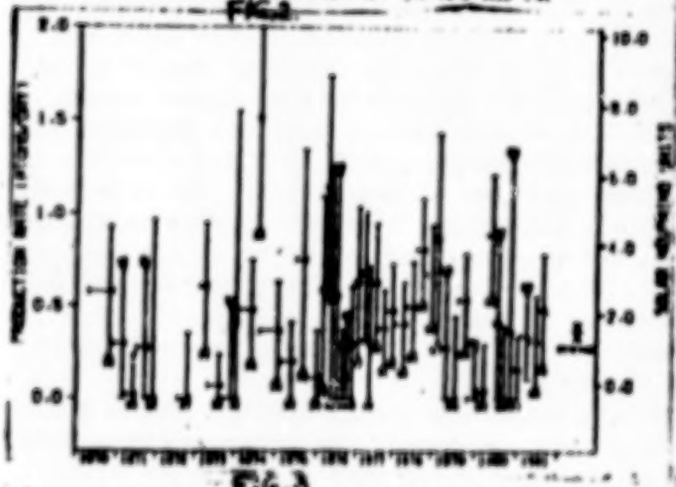


Fig.3

Fig·1 ^{37}Ar production rates observed in the Chlorine SH experiment 1970-1982 and the moving average data(dashed curve)·

Fig·2 and 3·Results of maximum likelihood treatment of Monte Carlo simulations with constant production rate of 7·6 SNU and 1·8 SNU respectively·

means of the two samples are not equal·

b)Monte Carlo simulated data :-i)7·6 SNU andii)1·8 SNU·We form the groups as in moving average data·In the case of 7·6 SNU the difference of variance is significant·We have to use the formula for fro the difference of two means·

$$t = \frac{\bar{x} - \bar{y}}{\left[s_1^2/n_1 + s_2^2/n_2\right]^{1/2}}$$

For d·f· 47,t=1·19·The standard error of the difference of two means is 1·1 ϵ ·Hence the two means are equal i·e·, the steady flux is acceptable·In the case of 1·8 SNU the difference of variance is not significant·Hence t=1·84,d·f· 45·The standard error is found to be 1·8 ϵ · Hence the data are consistent with the assumption that the steady flux is acceptable·Next we take the yearly average of the Monte Carlo simulated data from fig 2 & 3 and form the two groups as in t-test·Here in both cases difference of variance is not significant·In case 7·6 SNU,t=0·43 d·f· 9·In case 1·8 SNU,t=1·01 d·f· 9·Here the standard error is found to be (i)0·53 ϵ and(ii) 1 ϵ respectively·Hence the data are consistent with the assumption that the steady flux is acceptable·

II)χ^2-test:-(i)We form the group as in the t-test·For moving average data σ^2=0·02 and for d·f·49,χ^2=73·19·Thus the hypothesis of steady flux is not acceptable·For the case of 7·6 SNU, σ^2=0·291, χ^2=47·84 d·f·47· again for 1·8 SNU, σ^2=0·10, χ^2=46·83 d·f· 45·Hence the difference of two samples are not significant for the case of 7·6 SNU and 1·8 SNU·

ORIGINAL PAGE IS
OF POOR QUALITY

(ii)if we take the yearly average of the moving average data and Monte Carlo simulated data•We form the groups as in t-test•We get σ^2=01, χ^2= 18•55,d•f• 10 for moving average data•In this case steady SN flux is not acceptable•Again (i) σ^2=09, χ^2=9•39,d•f• 9 for 7•6 SNU and (ii) σ^2=05, χ^2=10•48,d•f• 9 for 1•8 SNU•Hence the steady SN flux is acceptable in Monte Carlo simulated data•

(III)Wilcoxon-Mann-Whitney test:-Here we take the yearly average data of moving average data and Monte Carlo simulated data 7•6 SNU and 1•8 SNU and form the two groups as in t-test and χ^2-test•If we set up the null hypothesis H_0 :the distribution of x and y are identical•If a two sided test at 5% is desired for m=4,n=7 we use $3 < U < 25$ as the accepted region•For this test $\alpha = P_{H_0}(U \leq 3 \text{ or } U \geq 25) = 042$•

a)Moving average data:- we write the two sets of data as y: 3552,•4740, •3546,•4007,•3089,•2469,•4707 and x:•5305,•4437,•7482,•5421•Putting these numbers in order and keep track of which numbers came from x and which from y:yyyyyxyyxxx•There are 12 inversions of the y's and the rank of y's is 1+2+3+4+5+7+8 =30 $= 2 + \frac{7 \times 8}{2}$ •Since the number of inversion of the y's is not within 3 and 25 ,we reject the null hypothesis,i•e• the constant SN flux is not acceptable•

b)(i)7•6 SNU :-y:1•408,0•993,1•430,1•286,1•277,1•928 and x:1600,1•396, 1•320,1•098•Putting these numbers in order and keep track of which numbers came from x and which came from y: yxyyxxyyxyy•There are 16 inversions of the y's and the rank of y's is 1+3+4+7+8+10+11 =44•

(ii)1•8 SNU:-y:1•545,•8001,•165,•805,•537,•307,•378 and x:•3755,•4900,•518,•581•There are 8 inversion of the y's and the rank of y's is 36• Since the number of inversion of the y is within 3 and 25,we accept the null hypothesis i•e•,steady SN flux is acceptable in both the Monte Carlo cases•

(IV)Run test:-In the case of run up and down the total number of runs is approximately normally distributed under the assumption of randomness with mean and variance is given by $E(r) = \frac{1}{3}(2n-1)$ and $V(r) = \frac{1}{90}(6n-29)$• For moving average data:- n=50,E(r)=33, V(r)=8•57•In this case there are 21 runs either positive or negative•If we take the critical region to be α =0•20 would yield a K of $33-0.84\sqrt{8.57} = 30.543$•Thus we cannot accept the randomness since $21 < 30.543$•Thus we can suggest that the constant SN flux is not acceptable•For case 7•6 SNU,n=49,E(r)=32•33 and V(r)=8•389•In this case there are 31 runs either positive or negative•For the case 1•8 SNU,n=47,E(r)=0•31 and V(r)=8•03•In this case there are 29 runs is either positive or negative•If ew take the critical region to be $r < K$,a choice of α =0•20 would yield a K of (i)$32.33-0.84\sqrt{8.389} = 29.9$;(ii)$31-0.84\sqrt{803} = 28.62$•Thus we accept the randomness in both the case since(i)$31 > 29.9$ and (ii)$29 > 28.62$•So we can conclude that the Monte Carlo simulated data do not pulsate with the solar activity cycle•

Sunspot cycle and SN flux:- We have taken the yearly average smooth sunspot from solar geophysical data,yearly average of the moving average data from fig•1•and yearly average of the cosmic ray data I with E =0•1-5•8 Gev(11)•We have displayed the data in Table I•

The correlation coefficient between sunspot cycle and ^{37}Ar production data are $r(S, Q_M) = -0.61$,when $\Delta T = -1$,$r(S, Q_M) = -0.49$ when $\Delta T = 0$,$r(S, Q_M) = -0.35$ when $\Delta T = -2$ where $\Delta T = T_S - T_{Q_M}$ (in years)•Thus the ^{37}Ar production rate anticorrelates with the sunspot cycle•The correlation coefficient between the galactic cosmic ray intensity and ^{37}Ar production data $r(I_0, Q_M) = 0.58$ when $\Delta T = 0$,$r(I_0, Q_M) = 0.31$ when $\Delta T = -1$,$r(I_0, Q_M) = 0.39$ when /

N85-35115

ORIGINAL PAGE IS
OF POOR QUALITY

SH 8.1-7

Table 1. Yearly averages of smooth sunspot number(S), Ar production data (Q_M), yearly average of cosmic ray data I_0 with E=0.1-5.8 Gev.

	1971	1972	1973	1974	1975	1976	1977	1978	1979	1980	1981
Yearly average Sunspot number (S)	66.6	68.9	38.5	34.4	15.5	12.6	27.5	92.7	155.3	155	140
Moving Average of the yearly Ar production data(Q_M)	.36	.44	.35	.40	.53	.44	.75	.54	.31	.25	.47
$I(10^3 m^{-2} s^{-1} st^{-1})$ Galactic cosmic ray intensity	2.01	2.86	2.80	2.71	3.11	3.20	3.29	2.79	1.89	1.24	1.13

$\Delta T=1$. Where $\Delta T = T_{I_0} - T_{Q_M}$ (in years). Thus there is an important correlation between the SN flux in Davis' data and galactic cosmic rays. This shows that the galactic cosmic rays and SN flux undergo the essential changes in the solar acivity cycle from 1970-1982.

From the SN flux data we see that SN flux is higher during the ascending phase(about 2-3 years)and descending phase(about 2-3 years)of the solar cycle avoiding the sunspot maximum time. We call the time 2-3 years before the sunspot maximum as the second minimum time. Thus SN flux is higher in both second minimum time and second maximum time and SN flux is lower in both first minimumand first sunspot maximum stage. In addition to two prominent maximum in the year 1957 and 1960 they(9,10)have found third maximum of smaller amplitude in the cosmic ray intensity but veru clear in 1963. From fig. 1 we see that run number 37 is connected with third maximum. This may have some connection with the quasibienniel variation of SN flux found from 1970-1975 and 1979-1984. From the moving average data in fig. 1 it appears that SN flux varies with a period of about 2.4 to 2.5 years from 1970-1975.

In conclusion it may be remarked that the present SN data exhibits a high level of statistically significant variation of SN flux with the solar activity cycle. The above results strongly suggests that the solar activity cycle is due to the pulsating character of the nuclear energy generation inside the core of the sun. We suggest that the chlorine SN experiment should be continued to get the data like the sunspot data etc. and this data could be of great impottance to our understanding of the sun and cosmic rays.

Acknowledgement:-The author would like to thank Professor R. Davis,Jr. for sending the SN data prior to publication.

References:-

1)P. Raychaudhuri(1976)JINR communications E2-10019, USSR, 2)P. Raychaudhuri (1976)Talk given at the International School of Cosmic physics,Erice,Italy 3)P. Raychaudhuri(1981)Spec. Sci. Tech. 4, 271. 4)P. Raychaudhuri(1983)Proc. 18th. ICRC, Bangalore 7, 108. 5)P. Raychaudhuri(1984)Solar Phys. 93,397. 6)P. Raychaudhuri(1984)Proc. 3rd. Asian Pacific regional meeting of IAU held at Kyoto(to be published)Ap. Sp. Science. 7)V. N. Gavrin et al.(1982)JETP lett 35 608, 8)J. K. Rowley et al.(1984)American Institute of Physics conference proceedings(to be published)held at South Dakota, USA., 9)M. N. Gnevyshev (1967)Solar Phys. 1, 67., 10)C. Fillisetti et al.(1974)Lett. Nuovo Cimento 11, 29, 11)G. A. Bazilevskaya et al.(1983)Proc. 18th. ICRC, Bangalore, 4, 218.

N85-35113

SH 8.1-8

SOLAR NEUTRINOS, SOLAR FLARES, SOLAR ACTIVITY CYCLE AND THE PROTON DECAY

Probhas Raychaudhuri
Department of Applied Mathematics
Calcutta University, Calcutta-700009, INDIA

A B S T R A C T

It is shown that there may be a correlation between the galactic cosmic rays and the solar neutrino data but it appears that the neutrino flux which may be generated during the large solar cosmic ray events cannot in any way effect the solar neutrino data in Davis experiment. Only initial stage of mixing between the solar core and solar outer layers after the sunspot maximum in the solar activity cycle can explain the higher(run number 27 and 71)of solar neutrino data in Davis experiment. But solar flare induced atmospheric neutrino flux may have effect in the nucleon decay detector on the underground. The neutrino flux from solar cosmic rays may be a useful guide to understand the background of nucleon decay, magnetic monopole search, and the detection of neutrino flux in sea water experiment.

Sheldon(1)indicated that the solar flares and solar active regions are energetic disturbances in the sun and may be associated with the production of neutrinos. The emission of particles from flares and active regions is well known phenomena. Thus any such relation between solar neutrino data and solar cosmic rays is important and may serve as an accurate long range predictor of solar cosmic ray activity properly. Recently Lanzerotti and Raghavan(2) and Raychaudhuri(3)suggested that the production of solar neutrinos by energetic particles involved in solar actvity is not a significant contributor to the solar neutrino flux recorded in the SN experiment(4). Again Raychaudhuri(5) pointed out that the neutrino flux which appears in the SN experiment can in no way connected with the solar surface nuclear reactions as the temperature and density are not suitable for such a rate of neutrino flux observed in the run numbers 27 and 71. We know that the energy release in solar particle flares where relativistic protons can be accelerated are seen typically in the energy range 10^{31}-10^{33} ergs or 10^{30} to 10^{32} Mev in about 5 minutes over an area of 10^{19} cm^2 projected on to the solar surface. Subramanian(6)and Bazilevskaya et al(7)suggested that the neutrino emission process underlying the flare mechanism may contribute to the higher SN flux as observed in Davis experiment. Recently Bazilevskaya et al(8) and Basu(9) have found that there is a significant relationship between SN data and solar particles. It is true that the geomagnetic index Ap is the index of solar particles but it may not have any connection with the SN flux. As mentioned earlier(3) that the surface nuclear reaction which may occur during large solar flare cannot account the flux observed in SN experiment. It is believed that the measurable fluxes of neutrinos could not be produced by solar flare particles interacting in the earth's atmosphere(10). The possible mechanism that may explain increased ^{37}Ar production from flares and cosmic ray intensity is that the particles with energy mostly less than 1 Gev, produced spallation products in the earth atmosphere(^{15}O, ^{13}N, ^{8}B etc.). The expected yield from ^{15}O, ^{13}N, ^{8}B (which decays into neutrino with energy greater than 1 Mev)are less than 10^{-2} cm^{-2} sec^{-1}. Although ^{8}B decays into high energy neutrino upto 14 Mev

but it cannot contribute an appreciable fraction in the SN data of Davis et al.(4). Thus the question remains whether the cosmic ray muons, pions and kaons at the time of large solar flare can produce detectable flux of neutrinos in the Davis experiment. We know that (11) in the biggest solar flare which occurs in August 1972 produced proton flux $5.5 \times 10^8 cm^{-2}$ above 100 Mev in about 5 minutes and thus we cannot expect to have neutrino flux as high as $5 \times 10^6 cm^{-2} sec^{-1}$ from pions, kaons and muons produced by relativistic protons through cascades in the earth's atmosphere. Thus from our present knowledge we cannot expect that the solar flare can effect the production of ^{37}Ar in the Davis experiment. We present below the solar cosmic ray event (12,13) which produces intense X-ray, γ-ray etc.) with the corresponding run in Davis experiment in Table I to see whether solar flare can contribute any detectable perturbation in the recorded SN flux.

Table I

No. of runs in SN experiment	Solar cosmic ray event connected with flare etc)	No of runs in SN experiment	Solar Cosmic ray event connected with flare etc.
19	24.1.71	67	25.11.80
21	1.9.71		24.12.80
27	4.8.72	68	1.4.81
	7.8.72		4.4.81
30	29.4.73		10.4.81
32	7.7.74		27.4.81
36	23.9.74		30.4.81
42	30.4.76	69	10.5.81
51	19.9.77		6.5.81
	24.9.77		7.10.81
52	22.11.77	71	12.10.81
53	29.4.78	75	12.7.82
55	23.9.78	76	26.11.82
60	20.8.79		7.12.82
	21.8.79		18.12.82
63	7.6.80		16.2.84
66	6.11.80		25.4.84

It is interesting to analyse the possible temporal fluctuation of SN flux with solar cosmic ray variation. If we see the data of fig. 1(14) we see that the run numbers 21,27,29,31,36,39,42,47,49,51,52,54,56,58, 64,71 gives the higher ^{37}Ar production than the average ^{37}Ar production rate. The run numbers 36-58 belong to the sunspot minimum range(5). According to Bazilevskaya et al (15) only solar cosmic ray events connected with the run numbers 21,27,51,71 can increase the production rate of ^{37}Ar in the SN experiment. But 2 solar cosmic ray events (connected with run numbers 21 and 51) took place on invisible side of the sun and therefore the increases of ^{37}Ar production will be absent. Raychaudhuri(16,17,5) showed that the SN data varies with 11 year solar cycle. He also explained why the SN flux is increased from 1975 to 1978. It is clear from the data(8,15) that there is a correlation between the galactic cosmic rays and the SN data and all of them vary with the 11 year solar cycle. Raychaudhuri(5,16) already explained the

ORIGINAL PAGE IS
OF POOR QUALITY

increase of SN data(in run numbers 27 and 71) due to large amount of ^{3}He is mixed periodically in the core after the sunspot maximum. Thus the largest solar flare and highest SN flux occurs synchronously and the solar flare has no direct connection with the SN flux. If the solar cosmic ray event has some effect on the SN flux we could have observed it from other solar flare events e.g. run number 55, since the proton fluence greater than 10 Mev and 30 Mev in run numbers 55,71 are almost the same(18), but it did not happen. The solar flare event cannot explain the higher counts in run numbers 27 and 71 in Davis experiment but it may have effect in the nucleon decay detector and also on the neutrino experiment in the accelerator etc. Thus the solar flare has no direct connection with the SN flux(5).

Proton decay:- Accurate calculation of low energy neutrino fluxes ($E_\nu \simeq$ 1 Gev)is necessary for the evaluation of the nucleon decay background. Gaisser et al(19)calculated the atmospheric neutrino flux by taking into account the effects of solar modulation that they did not consider the atmospheric neutrino flux from solar cosmic ray events. They consider only that the cosmic ray flux is higher at solar minimum and lower at solar maximum. But it was indicated by Kodama(20)that the unusual increases in cosmic rays and fast type PCA events occur only during the ascending(for about 2 years before sunspot maximum year) and descending phases(for about 2-4 years after sunspot maximum year)of the solar cycle avoiding the sunspot maximum year. The neutrinos are generated in the earth atmosphere by solar protons but because of the diffusion mechanism of protons moving between the sun and earth the whole process is very prolonged in time and difficult to identify against the background of an ordinary atmospheric flux. We have gathered from table I of King(11) that in August 1972 biggest solar flare events produces flux of protons above 200 Mev constitute 83% of the fluxes obtained by integrating over the entire solar cycle. The biggest solar flare which occured in October 1981 is almost the same as powerful as the August 1972 flare. The fluence of proton of 100 Mev—1 Gev constitute above $6{\cdot}6\times10^8$ cm^{-2}. We know fluxes of neutrinos around 1 Gev are $3{\cdot}93\times 10^{-2}$ cm^{-2} sec^{-1} $sterad^{-1}$ in vertical direction and $6{\cdot}20\times 10^{-2}$ cm^{-2} sec^{-1} $sterad^{-1}$ in horizontal direction at ground level from galactic cosmic rays. Again we know that the fluxes of protons around 1 Gev are 10^{-1} cm^{-2} sec^{-1} $sterad^{-1}$ from the best estimates of galactic cosmic rays as we have taken the fluxes of protons at the time of low solar activity. Thus we cannot expect the ratio between the neutrino flux and proton flux is within 2/5 and 3/5 around 1 Gev. From October 1981 to July 1982 the average fluence of proton greater than 100 Mev constitutes 5×10^7 cm^{-2} (roughly). Let us take that the solar flares lasted in such a way which produces significant fluxes of neutrinos. We get the neutrino flux is about $1{\cdot}8$ cm^{-2} sec^{-1} $sterad^{-1}$ and which is about 30 to 35 times higher than the cosmic ray neutrino flux around 300 Mev to 500 Mev. This supports also that the 100 Mev to 1 Gev solar proton flux is atleast an order of magnitude higher than the galactic proton fluxes. Here although neutrino energy is lower than 1 Gev but the fluences are higher so it is possible that the atmpspheric neutrinos from solar cosmic ray affect the underground experiment on nucleon decay. Similarly muon fluxes from solar cosmic rays will also be an order higher than the muon fluxes from galactic cosmic rays in the region from 100 Mev to 1 Gev. As the experiments of KGF, Mont Blanc, IMB, Kamiokande, Soudan I were operated within the range of bigger solar cosmic ray event we suspect that all the nucleon decay events observed by them are due to atmospheric neutrinos from solar cosmic ray

ORIGINAL PAGE IS
OF POOR QUALITY

in the large scale experiments conducted at great depths underground since 1965 KGF group(21)recorded several anomalous events some of which are suggestive of decay of new particles or some of nucleon decay. From the above preliminary analysis we suggest that previous events was also perhaps due to theatmospheric neutrinos produced from solar cosmic ray events. So to decide about the nucleon decay properly we need better estimate of neutrino flux from solar cosmic ray events. At present we do not have better estimate of solar cosmic ray proton flux from the 21st solar cycle. So it is necessary to know the better knowledge of solar proton fluxes around Gev. We hope to calculate the neutrino flux from solar cosmic ray event when the full data of solar proton fluxes will be available upto 1984 for the 21st solar cycle from space missions. The solar cosmic ray neutrino flux will be an important step and guide(i)to understand the background for nucleon decay research from atmospheric neutrinos and also (ii)to the neutrino experiment which is operated on the underground, sea water and accelerator.

References:-

1) M. R. Sheldon(1969)Nature 221,650
2) L. J. Lanzerotti and R. S. Raghavan(1981)Nature 293,122.
3) P. Raychaudhuri(1983)Ind. J. Theo. Phys. 31, (in press).
4) R. Davis,Jr., B. Cleveland and J. K. Rowley(1982)AIP conference proceedings 96,1.
5) P. Raychaudhuri(1984)Solar phys. 93,397.
6) A. Subramanian(1983)Current sci. 52,342.
7) G. A. Basilevskaya et al(1982)JETP lett 35,343.
8) G. A. Basilevskaya et al.(1983)Proc 18th. ICRC 4,218.
9) D. Basu(1982)Solar Phys. 81,363.
10) K. O'Brien and A. dela Zerda(1984)Am. Nucl. Soc. 46,64.
11) J. H. King(1974)J. Space Craft and Rockets 11,401.
12) M. Pomerantz and S. P. Duggal(1974)Rev. Geophys. &Space Phys. 12,343.
13) S. I. Avdyushin et al.(1982)Bull. Acad. Sci. USSR(phys. Ser)46,107.
14) P. Raychaudhuri(1985)Proc. 19th. ICRC SH 8.1-7., San Diego, USA.
15) G. A. Basilevskaya et al(1983)J. Nucl. Phys(submitted).
16) P. Raychaudhuri(1983)P_{r_0}c. 18th. ICRC,# 7, 108.
17) P. Raychaudhuri(1984)Proc. 3rd. Asian Pacific regional meeting held at Kyoto, Japan, 30th. Sept-6 Oct.(to be published in Astrophys. Sp. Science.
18) H. E. Moguire et al(1983)Proc. 18th. ICRC 2,66.
19) T. K. Gaisser et al(1983)Phys. Rev. Lett 51,223.
20) M. Kodama(1962)J. Phys. Soc. Japan 17, Suppl. II-A, 594.
21) M. R. Krishnaswami et al.(1981)Phys. lett 106B,339.

N85-35114

SH 8.1-9

NEUTRINO PRODUCTION FROM THE SOLAR ATMOSPHERE

Inazawa, H. and Kobayakawa, K.
The Graduate School of Science and Technology
and College of Liberal Arts, Kobe University
Nada, Kobe 657, JAPAN
Kitamura, T.
Institute for Cosmic Ray Research, University of Tokyo
Midori-cho, Tanashi, Tokyo 188, JAPAN

ABSTRACT

When the high energy primary cosmic rays enter near the solar surface, they pass through a thick matter but having a low density. If the density and path length satisfy an appropriate condition, the primaries collide with the constituents near the solar sphere (almost protons) and produce pions and kaons, most of which decay into $\mu+\nu_\mu$ without successive hadron collisions. Muons also decay into $\bar{\nu}_\mu$ and ν_e before reaching the earth. The neutrino flux of which the producer is matter near the solar surface is computed by solving cascade diffusion equations. The calculated differential flux of muon neutrino at 1 TeV is 1×10^{-13} $(GeV\cdot cm^2\cdot s\cdot ster)^{-1}$ which is rather difficult to be observed in the present apparatuses or DUMAND.

1. Introduction. Recently, the production mechanisms of cosmic ray neutrino with high energies are considered other than conventional ones which are decay products of pions and kaons in the primary - air nucleus collisions. One is the neutrino emission from the matter surrounding a source of very high energy cosmic ray protons (1, 2). The other is the neutrinos produced by the collisions of the primary and 3K background radiation (3) and so on. Besides these the following mechanism is treated here. As the high energy primary cosmic rays collide with nulei in terrestrial atmosphere and produce pions and kaons which decay into neutrinos (conventional neutrino), we expect that the primaries can produce high energy neutrinos from the solar atmosphere (we call this neutrino the solar neutrino, hereafter). Though the solar atmosphere takes a part of producer, the solar neutrinos at high energies (nearly equal to or more than 1 TeV) originate from the Sun. In this paper, the flux of the solar neutrino is estimated and its observation is discussed. The flux is so sensitive to the densities near the solar surface that the observation, if possible, gives informations the density which will be helpful for searching the solar models.

2. A Critical density and the density near the solar surface. Firstly, let us introduce a critical density with which produced pions (or kaons) decay into $\mu\nu$ or trigger a succesive collision with same probability. The critical density can be written by

$$\rho_{cr}(i) = m_i Br_i c/N_A E_i \tau_i \sigma_i \ , \qquad (1)$$

where N_A is Avogadro's number, the suffix i means π or K and m, Br, E, τ, σ are the mass, the branching ratio to $\mu\nu$, the energy, the mean life and the inelastic cross section, respectively. For σ_π = 30 mb and σ_K = 20 mb, we have

$$\rho_{cr}(\pi) = (2.11/E_\nu)\ 10^{-6}\ \ g/cm^3\ , \tag{2}$$

$$\rho_{cr}(K) = (2.23/E_\nu)\ 10^{-5}\ \ g/cm^3\ , \tag{3}$$

where the relation of E_i and the neutrino energy E_ν on the average is used and E_ν in the unit of TeV. When the target matter is the terrestial atmosphere, the relation of $z/\rho(z) = H$ (constant), where z is a hight in g/cm^2, holds in the upper part and decay constants defined by $m_i H/c\tau_i$ make the diffusion equations for pions and kaons simple. However the present problem is not the case.

Up to now, the density ρ near the solar surface is seemed not to be well confirmed. But referring to (4, 5), we express ρ for the quiet Sun as an approximate analytical form as follows:

$$\rho = 1.05\times10^{-11}\ (300-h)^{1.78}\ \ g/cm^3 \text{ for } h<100\ , \tag{4}$$

$$\rho = 3.29\times10^{-7}\ \exp\ (-h/107)\ \ g/cm^3 \text{ for } h>100\ , \tag{5}$$

where h in km is a height measured from the surface of the photosphere, which is $R = 6.96\times10^5$ km distant from the center of the Sun. For $h = 0$, $\rho = 2.7\times10^{-7}$ g/cm^3 which nearly corresponds to $\rho_{cr}(\pi)$ with $E_\nu = 10$ TeV. so the region of $h<0$, i.e. the inside of the photosphere, as well as $h>0$, i.e. the solar atmosphere, should be taken into account.

3. Derivation of the solar neutrino flux. We consider the production of the solar neutrinos at energies $1\sim100$ TeV. The contribution of produced charmed particles is neglisible. The source of muon neutrinos is π (or K) $\longrightarrow \mu\nu_\mu$ and $\mu \longrightarrow e\nu_\mu\nu_e$. On the other hand, electron neutrinos originate only from muon decays. After the diffusion equations for π, K, μ, ν_μ and ν_e are written down, fluxes of ν_μ and ν_e are solved and can be expressed by some multi-integral forms. These forms contain the variable represented by

$$dz = \rho(b,x)\ dx\ , \tag{6}$$

where z and x are path lengths in units of g/cm^2 and of cm, respectively and b means an impact parameter related to the center of the Sun. When b is fixed, the partial flux $f_\nu(E_\nu, z(b))$ can be obtained by multi-integration with respect to other variables including dx. In this procedure, the primary cosmic ray spectrum

$$I_0(E)dE = 1.8E^{-2.7}dE \tag{7}$$

(E in GeV, $I_0(E)$ in $(cm^2\cdot s\cdot sr\cdot GeV)^{-1}$) is used. The energy moments of π and k are taken as (6)

$$F_\pi = 0.0724\ ,\quad F_k = 0.00959\ , \tag{8}$$

and the average mass number is taken as 1.25 by considering the exsistence of He, C and O nuclei.

The partial flux $f_\nu(E_\nu, z(b))$ depends on the integrated path length given by

$$z(b) = \int_{-a}^{a} \rho(h)dx\ \ g/cm^2 \quad \text{with } h = (b^2+x^2)^{1/2}-R\ , \tag{9}$$

where as the origin of co-ordinate x is taken the closest point from the center of the Sun, namely $h = b-R$ at the origin. In eq.(9), since $\rho(h)$ is a steep decreasing function of h, $a \longrightarrow \infty$ may be allowed.

The observed differential flux of the solar neutrino on the earth can be expressed by

$$f_\nu(E_\nu) = \frac{1}{(S\Omega)_E}\int_{b_{min}}^{b_{max}} db\, \frac{d(S\Omega(b))}{db}\, f_\nu(E_\nu, z(b)) \quad , \tag{10}$$

where $(S\Omega)_E = 2\pi^2 R_E$, R_E is the radius of the earth and $S\Omega(b)$ is $S\Omega$ having a fixed b with respect to the center of the earth. In eq.(10), b_{max} and b_{min} are determined as follows: b_{min} is given by the condition

$$\rho(b_{min}-R) \approx 15\rho_{cr}(E) \quad . \tag{11}$$

when a primary cosmic ray passes with impact parameter less than b_{min} most produced π and K give rise to a successive collision before decay. As far b_{max}, inserting eq.(5) into eq.(9), one has

$$z(b) = \rho(b-R)(2\pi \times 1.07 \times 10^7 R)^{1/2} \quad g/cm^2 \quad . \tag{12}$$

Then $b_{max} = R+1000km$ where $z(b_{max})$ is about 0.1 g/cm^2. In case E = 10 TeV, h corresponding to ρ_{cr}(10 TeV) is about zero, i.e. just the surface of photosphere, z(R) = 810 g/cm^2 and $h_{min} = b_{min} - R$ is about -400km. These numerical values may give us some ideas.

4. Result and discussion. The derivation of the flux concerned with is necessary to carry out complex multi-integrations. In the present report, since the precision of numerical integrations is low, the following numerical values might more or less be modified. However our result say that $f_\nu(E_\nu)$ $(GeV \cdot cm^2 \cdot s \cdot sr)^{-1}$ of $(\nu_\mu + \bar{\nu}_\mu)$ are 1.1×10^{-14}, 3.8×10^{-14} and 2.7×10^{-15} for E_ν = 1, 10 and 100 TeV, respectively. These values are compared with the conventional fluxes through terrestial atmosphere: 2.3×10^{-11}, 7.2×10^{-13} and 1.6×10^{-15} at the vertical direction (7). On the flux of $\nu_e + \bar{\nu}_e$, we have 5.4×10^{-13}, 1.1×10^{-14} and 6.5×10^{-19}, corresponding to conventional ones at the vertical direction: 1.1×10^{-11}, 3.3×10^{-14} and 7.4×10^{-16} (7) for E = 1, 10 and 100 TeV, respectively.

In our case, because most of muons decay into $e\, \nu_\mu\, \nu_e$, the flux of ν_e is enhanced compared with the conventional one. Arbund E_ν = 10 TeV, our flux is enhanced. The reason is that at these energies the main contribution come from the pass near the solar surface which has an appropriate low density and long pass length. We have the ratio of the solar flux to the conventional ones is from several tens % to comparable order. But the angular resolution of apparatus should be taken into consideration in order to detect the solar neutrino flux. Since DUMAND's minimum detectable flux, as an example, is 10^{-10} $(cm^2 \cdot s)^{-1}$, the solar neutrino treated here is hard to be measured.

The flux of the solar neutrino is so sensitive to its density that the measurement of the flux in future may make clear the density or its change, say due to a violent solar flare, around the surface of the Sun.

References

1. Stenger, V.J., (1984), Astrophys. J. 284, 810.
2. Lee, H. and Bludman, S.A., (1984), preprint UPR-0259T.
3. Hill, C.T. and Schramm, D.N., (1983), Phys. Lett. 131B, 247.
4. Allen, C.W., (1962), 'Astrophysical Quantities' (2nd ed.) The Athlone Press
5. Gibson, E.G., (1978), 'The quiet Sun' translated into Japanese by Sakurai, K., Kodansha.
6. Thompson, M.G., and Whalley, M.R., (1977), J. Phys. G. 3, 97.
7. Mitsui, K. and Minorikawa, Y., (1985), the paper submitted to 19th ICRC.

N85-35115

SH-8.1-10

SOLAR COSMIC RAY BURSTS AND SOLAR NEUTRINO FLUXES

G.A.Bazilevskaya, S.I.Nikolsky, Yu.I.Stozhkov

P.N.Lebedev Physical Institute of the Academy of Sciences of the USSR, 117924, Leninsky Prospect,53, Moscow, USSR

T.N.Charakhchyan

Institute of Nuclear Physics, Moscow State University, 119899, Moscow, USSR

Abstract

The neutrino flux detected in the Cl-Ar experiment /1/ seems to respond to the powerful solar cosmic ray bursts. The ground-based detectors, the balloons and the satellites detect about 50% of the bursts of solar cosmic ray generated on the Sun's visible side. As a rule, such bursts originate from the Western side of the visible solar disk. Since the solar cosmic ray bursts are in opposite phase with the 11-year galactic cosmic ray cycle which also seems to be reflected by neutrino experiment, the neutrino generation in the bursts will flatten the possible 11-year behaviour of the ^{37}Ar production rate, Q, in the Cl-Ar experiment. The detection of solar-flare-generated gamma-quanta with energies above tens of Mev is indicative of the generation of high-energy particles which in turn may produce neutrinos. Thus, the increased Q during the runs, when the flare-generated high energy gamma-quanta have been registered, may be regarded as additional evidence for neutrino generation in the solar flare processes.

Definite evidence for neutrino generation in powerful solar cosmic ray bursts has been obtained by now /2-4/. During the period from 1970 up to the present the mean ^{37}Ar production rate in the Cl-Ar experiment /1/ was Q=0.47$\pm$0.04 ^{37}Ar atoms/day. The highest value of Q were observed during the periods when powerful solar cosmic ray bursts have been registered, namely, the run No 27, Q=1.23$\pm$0.41 ^{37}Ar atoms/day (the bursts of August 4 and 7, 1972) and the run No 71, Q=1.21$\pm$0.37 ^{37}Ar atoms/day (the burst of October 12, 1981) /5,6/. A powerful solar cosmic ray burst can hardly be ex-

pected in 1985-1987 because the solar activity will approach its minimum whereas the solar flare events are usually observed near solar maximum.

It should be noted that the solar-flare-generated neutrinos will flatten the 11-year cycle of Q which, according to /2-4/ is in the opposite phase with the solar activity.

The fluctuations of the Q-value from one run to another may be due to the cosmic ray bursts, which have not been detected at the Earth. Fig. 1 a, b shows the heliolongitudinal distribution of the parent flares of solar cosmic ray bursts detected at sea-level since 1942 (35 events) /7/, and in the stratosphere since 1958 (68 events). The strong heliolongitudinal dependence of detection probability of solar cosmic ray bursts gives a $\sim 50\%$ probability of the detection such events with the charged-particle detectors installed on the Earth'surface, on balloons and satellites.

It may be assumed that the detection of high-energy γ-quanta (E_γ is more than several tens of MeV) from π^0-meson decays in solar flares will significantly increase the detection probability of the events occurring on the Eastern side of the visible solar disk. Such events must generate π^+-mesons whose decays will produce ν_e. In their turn the fluxes of such neutrinos may raise the Cl-Ar detector counting rate.

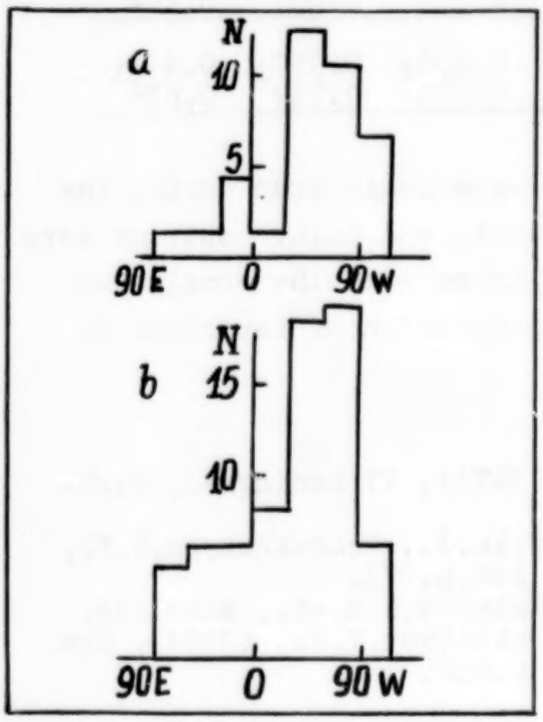


Fig.1. Heliolongitudinal distribution of the parent flares of solar cosmic ray bursts detected at sea-level (a), and in the stratosphere (b).

SH-8.1-10

The Table presents the solar flare events in which the γ-quanta with $E \gtrsim 50$ MeV were detected /8/. Solar neutrons were also detected in these events. It may be asserted quite safely that nuclear reactions, in which π-mesons are produced and then decay, occure in the solar flares presented. The rate of ^{37}Ar production in the Cl-Ar detector during the flare runs proved to be increased (Q_o) compared with the previous (Q_{-2}, Q_{-1}) and subsequent (Q_{+1}, Q_{+2}) runs. The run numbers which are indicated in the brackets and Q-values are taken from /5/. The bottom of the Table presents the mean values of Q for two events.

Table

No	Date of γ-burst	Q_{-2}	Q_{-1}	Q_o	Q_{+1}	Q_{+2}
1	21.06.80	(62)	(63)	(64)	(65)	(66)
		0.023±	0.000±	0.488±	0.224±	0.361±
		0.231	0.325	0.266	0.425	1.253
2	03.06.82	(73)	(74)	(75)	(76)	(77)
		0.077±	0.478±	0.503±	0.475±	0.461±
		0.151	0.242	0.327	0.231	0.224
the mean value		0.050±	0.239±	0.496±	0.350±	0.411±
		0.138	0.203	0.211	0.242	0.636

The increased values of Q were registered durihg the runs when the high-energy γ-quanta and solar neutrons were observed. The results obtained agree with the conclusion /2-4/ concerning the possible generation of neutrinos in solar cosmic ray bursts.

References

1. Davis,R.,Jr., Evance,J.C.,(1974), VI Leningrad. Mezhdunarodny Seminar, p.91.
2. Bazilevskaya,G.A., Stozhkov,Yu.I., Charakhchyan,T.N., (1982), Pisma ZhETF, v.35, No6,p.273.
3. Bazilevskaya,G.A., Mukhamedzhanov,A.M.-A., Nikolsky, S.I., Stozhkov, Yu.I., Charakhchyan,T.N., (1984), Sov. Nuclear Phys., v.39, No 4, p.856.

4. Bazilevskaya,G.A., Nikolskii,S.I., Stozhkov,Yu.I., Charakhchyan,T.N., Mukhamedzhanov,A.M.-A.,(1983), Proc. 18-th ICRC, Bangalore, v.4, p.218.
5. Cleveland,B.T., Davis,R., Rowely,J.K.,(1984), Proc. of the Second International Symposium on Resonance Ionization Spectroscopy and its Application, England, (in press).
6. Bahcall,J.N., (1985), Highlights in Astrophysics: Concepts and Controvercies, (in press).
7. Cliver,E.W., Kahler,S.W., Shea, M.A., Smart,D.F., (1982), Astrophys. J., v.260, p. 362.
8. Share,G.H., Chupp,E.L., Forrest,D.J., Riger,E.,(1983), Positron-Electron Pairs Astrophys. Workshop, Goddard Space Flight Center, p.15.

N85-35116

THREE DIMENSIONAL CALCULATION OF FLUX OF LOW ENERGY ATMOSPHERIC NEUTRINOS

H. Lee and S.A. Bludman

Department of Physics, University of Pennsylvania,
Philadelphia, PA 19104

Abstract; Results of three-dimensional Monte Carlo calculation of low energy flux of atmospheric neutrinos are presented and compared with earlier one-dimensional calculations [1,2] valid at higher neutrino energies. These low energy neutrinos are the atmospheric background in searching for neutrinos from astrophysical sources. Primary cosmic rays produce the neutrino flux peaking at near E_ν=40 MeV and neutrino intensity peaking near E_ν=100 MeV. Because such neutrinos typically deviate by $20^0 \sim 30^0$ from the primary cosmic ray direction, three-dimensional effects are important for the search of atmospheric neutrinos. Nevertheless, the background of these atmospheric neutrinos is negligible for the detection of solar and supernova neutrinos.

1. Introduction

Recently one-demensional Monte Carlo calculations of cosmic ray production of neutrinos in the Earth's atmosphere, including geomagnetic and solar modulation effects, were reported [1,2]. These calculations agree well with the flux and angular distribution of neutrinos of energy $E_\nu > 200$ MeV observed in underground detectors. But these earlier one-dimensional cascade calculations are inapplicable to neutrinos of lower energy $E_\nu < 50$ MeV important in neutrino astronomy. In fact, we shall see (Fig. 3) that the mean angular deviation between the primary cosmic rays and neutrinos is appreciable even for neutrinos of several hundred MeV. The flux of low-energy atmospheric neutrinos we obtain (Fig. 2) in the present three-dimensional calculation is negligible compared with the known flux of solar or supernova neutrinos, but maybe significant in the case of other sources of astrophysical neutrinos.

The three-dimensional atmospheric neutrino flux is

$$dN_\nu(E_\nu, \theta_\nu, \phi_\nu)/dE_\nu = \int \gamma_\nu \Omega\,(E_p, \theta_p, \phi_p, \lambda)(dN_p/dE_p)dE_p\,d\omega_p,$$

where $\gamma_\nu(E_\nu, \theta_\nu, \phi_\nu, E_p, \theta_p)$ is the yield of neutrinos of energy E_ν, zenith angle θ_ν and azimuth angle ϕ_ν by primary cosmic rays of energy E_p and zenith angle ϕ_p. dN_p/dE_p is the primary cosmic ray spectrum, and $\Omega\,(E_p, \theta_p, \phi_p)$ is the geomagnetic cut-off. This geomagnetic cut-off depends on geomagnetic latitude λ and magnetic rigidity $R = pc/e$ where p is the primary cosmic ray's momentum.

2. Calculational details

We modified the Gaisser-Protheroe-Stanev one-dimensional hadron interaction model [5] by assigning to secondary particles the transverse momentum distribution.

$$W(a,z_t)=(a+1)(a+2)z_t(1+z_t)^a.$$

Here $a=2p/<p_p>-3$ for $p>1.5<p_t>$, $a=0$ for $p<1.5<p_t>$, $z_t=p_t/p$ and p is the incident hadron's momentum. At high p, $W\sim p_t\exp(-ap_t)$. The angular deviation of secondary hadrons from the incident hadron direction produced by the above formula affects our results insignificantly.

In our computer program analytic formulae are used for the energy distribution of decay particles. For those energies, a microcanonical ensemble average is taken; total energy is conserved in each individual decay. The secondary directions are, however, assigned according to a canonical ensemble; the total momentum is conserved on average but not in individual decays. Interaction cases are treated similarly. We use energy-independent energy loss rates for charged particles by air ionization in a simple isothermal atmosphere to determine the decay height and energy, and energy-dependent formulae to determine the interaction height and energy. Our results are insensitive to these parameters.

For the comparison with the earlier one-dimensional calculation we calculated the yield function

$$Y_\nu(E_\nu,E^p,\theta_p)\equiv\int y_\nu(E_\nu,\theta_\nu,\phi_\nu,E_p,\theta_p)d\omega_\nu$$

integrated over appropriate neutrino directions.

3. Results and Conclusions

Fig.1 shows the yield Y_ν of vertically incident protons of several energies E_p, integrated over the downward 2π solid angle of neutrino's directions. Because low-energy neutrinos are made mainly from low-enrgy pions and muons at rest, for all primary cosmic ray energies the peak flux occurs near 40 MeV and the peak intensity near 100 MeV. Because most muons decay at rest and $<E_{\nu_e}>=0.3E_\mu$, $<E_{\nu_\mu}>=0.35E_\mu$, the atmospheric neutrino flux peaks near 40 MeV.

Fig.2 shows the downward neutrino flux produced by vertically incident primaries at high geomagnetic latitude, where

$$dN_\nu/dE_\nu\approx\int Y_\nu\Omega\,(dN_p/dE_p)dE_p.$$

While this expression is not exact for a three-dimensional cascade, it compares simply with the one-dimensional calculations. The near-vertical neutrino flux is also insensitive to zenith angle. Because, if not supressed by geomagnetic cut-off, the primary cosmic rays have a steep power-law spectrum, the main contribution to the low-energy neutrino flux is from primary cosmic rays just above the pion-production threshold energy. The total flux is therefore very sensitive to geomagnetic cut-off [6].

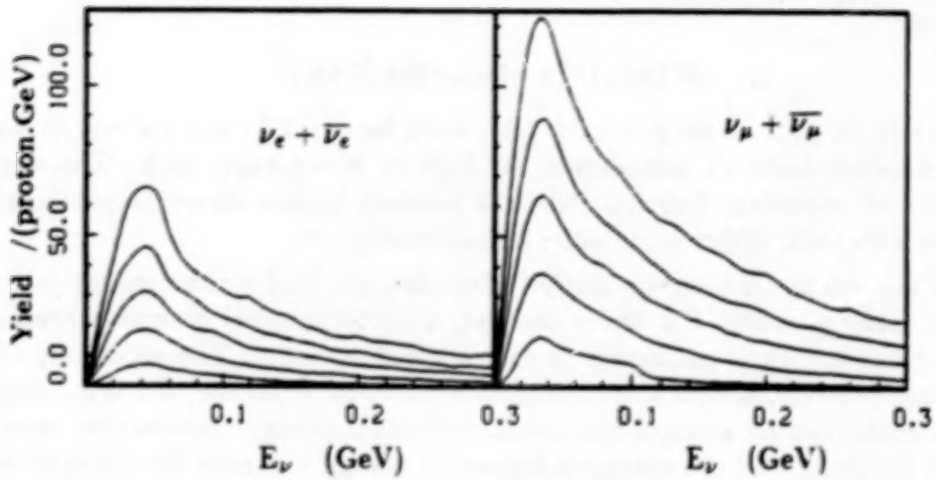


Fig. 1. Integrated neutrino yields from vertically incident protons. 2 5 10 20 50 GeV cases from bottom to top.

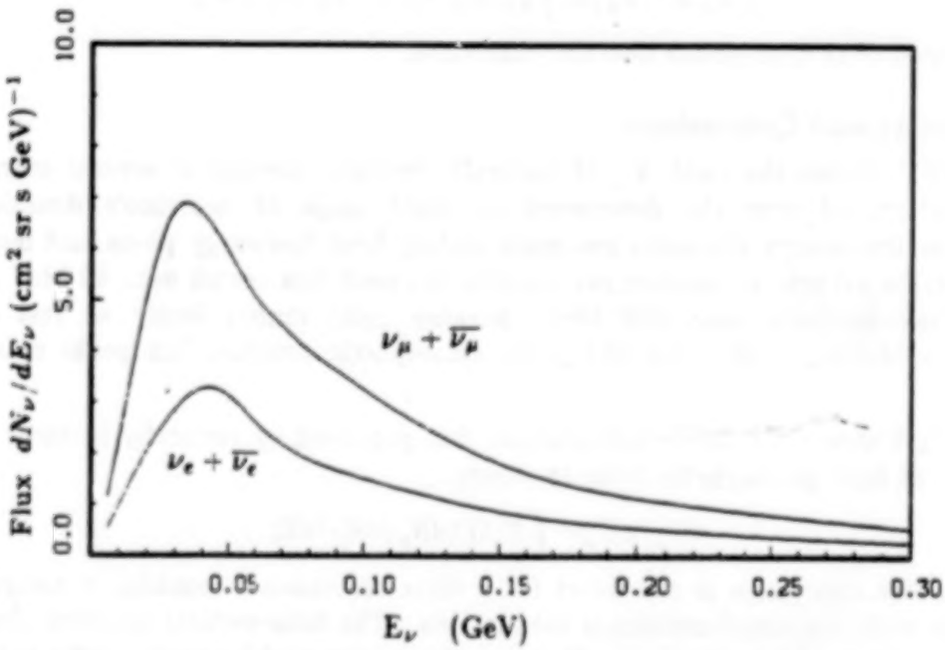


Fig. 2. Calculated downward neutrino flux at high geomagnetic latitude

For neutrinos above E_ν=200 MeV, this three-dimensional calculation agrees with earlier one-dimensional calculations [1,2]. At lower energies (E_ν< 50 MeV), however, we now obtain neutrino fluxes significantly lower than those one-dimensional calculations would give.

This atmospheric neutrino background is totally negligible compared to the solar neutrino flux and the flux of neutrinos expected from supernova at any reasonable distance (< 10^3 Mpc).

Fig.3 shows the average angular deviation of down-going ν_es of energy E_ν produced by vertically incident protons of energy E_p=2, 10, 50 GeV. Other neutrino types have similar spectra. While average angular deviation is $20^0 \sim 30^0$, neutrino direction at neutrino energy below 50 MeV is near isotropic and a long tail of more energetic neutrinos deviating by $5^0 \sim 10^0$ is produced at E_ν> 200 MeV.

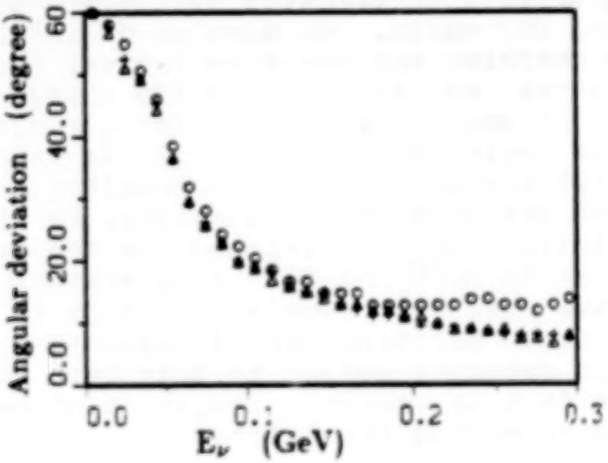


Fig. 3. ν_e angular deviation from primary proton.
2 GeV (○), 10 GeV (△), 50 GeV (+) cases.

Acknowledgements; We thank to T. K. Gaisser and Todor Stanev for useful discussions. This work was supported by U.S. Department of Energy.

References

[1] T. K. Gaisser, Todor Stanev, S. A. Bludman and H. Lee, Phys. Rev. Lett 51, 223(1983) and Fourth Workshop on Grand Unification (FWOGU), U. of Pennsylvania, (Birkhauser, Boston, ed. A. Weldon, P. Langacker, P. J. Steinhardt, p. 87 (1983)).

[2] T. K. Gaisser and Todor Stanev, to appear in Proc. ICOBAN

[3] Private communication with T. K. Gaisser and Todor Stanev, also *see*, T. K. Gaisser and Todor Stanev, to appear in Proc. Neutrino '84 conference, Dortmund, June 1984.

[4] D. J. Cooke, Phys. Rev. Lett. 51, 320 (1983).

[5] T. K. Gaisser, R. J. Protheroe and Todor Stanev, Proc. 18th ICRC (Bangalore) 5, 174 (1983)

[6] H. Lee and S. A. Bludman, exact 3-dimensional expression of neutrino flux and angular dependence is in preparation.

N85-35117

SH 9.1-2

DETECTOR CALIBRATION OF THE INDIAN COSMIC RAY EXPERIMENT (IONS) IN SPACE-SHUTTLE SPACELAB-3

J.S.Yadav, S.Biswas and N.Durgaprasad
Tata Institute of Fundamental Research
Bombay 400005, India.

ABSTRACT

In IONS experiment in Spacelab-3 we intend to study nuclei upto iron in low energy cosmic rays, using CR-39 (DOP) detectors. We have exposed CR-39 (DOP) to He^4, C^{12}, O^{16}, Ne^{20}, Si^{28}, Ar^{40}, Cr^{52} and Fe^{56} accelerated beams from various accelerator facilities available around the world. We have used different beam energies and exposure angles. From these exposures, we have studied the charge resolution and energy resolution for our detector in the region of our interest. We have also studied the effect of pre-annealing and depth on the response of our detector. For isotopic resolution, we have exposed the detector samples to Ne^{20} and Ne^{22} accelerated beams. We have also kept samples of CR-39 (DOP) exposed to different accelerated heavy ions in our detector module to take into account the effect of ambient conditions on detector response during the flight.

1. Introduction. The passive track detectors provide the advantage of high geometrical factor to study low intensity cosmic rays. CR-39 plastic detectors are the most sensitive among passive detectors.[1] However, CR-39 has following disadvantages: (1) Its surface becomes frosty after etching for long time, and (2) It shows track response variation along the depth of detector samples. The first problem makes the multisheet measurements difficult while second problem affects directly track identification and hence the resolution of the detector. Both these problems are very important for cosmic ray studies. These problems are overcome by using long curing cycle and adding 1% dioctyl phthalate in CR-39 monomer (CR-39 [DOP]).

We are using CR-39 (DOP) detectors in our cosmic ray experiment in Space Shuttle Spacelab-3.[2] This plastic (of thickness $\sim 250\mu m$) is prepared by Pershore Moulding Ltd., UK, using 32 hours of curing cycle. We have studied the response of this plastic detector using different heavy ion exposures. In this paper, the results of this study are presented.

2. Experimental Details and Results. Indian cosmic ray experiment in Space Shuttle Spacelab-3 has been designed to perform the measurements of the ionization states, flux and energy spectra of elements from alpha particles to iron ions in the low energy region below 100 MeV/N. We have exposed CR-39 (DOP) samples to different heavy ions in this charge region. The exposure details are given in Table 1.

Table 1 : Exposure Details

Ion Beams	Energies MeV/N	Angle of Exposure
He	1.0, 2.1, 7.5 and 10.5	90°
C	1.75, 3.5, 4.5, 7.0 & 8.8	30° and 60°
N	3.2 and 10.4	-do-
O	1.1, 4.2, 5.4 and 8.8	-do-
Ne^{20}	1.4, 7.3, 8.0 and 9.1	30°, 60° and 90°
Ne^{22}	2.65, 4.6 and 7.5	-do-
Si	6.5	30°
Cr	6.5	10°,20°,30°,45°, 60° and 90°
Ni	6.0	30°
Fe	$\leq$ 300	60°

The exposures to alphas are obtained from Variable Energy Cyclotron (VEC), Calcutta, India. The exposures to iron beam (all energies below 300 MeV/N) are obtained from Berkeley, USA. All other exposures are obtained from Joint Institute for Nuclear Research, Dubna, USSR.

All the exposed samples are etched in 6.25 N NaOH at 70°C simultaneously for different etching times. Different track parameters are measured to obtain the etch rate ratio for different particles of different energies. Different sets of four parameters are used to calculate the actual track length in order to cross check the values so obtained [3]. This method also gives the parameters with the least percentage errors in different etch rate ratio regions. The measured values of etch rate ratio are plotted as a function of dE/dX as well as $(Z_{effective}/\beta)^2$ calculated using different relations for energy loss and range [4]. Fig. 1 shows log-log plot between etch rate ratio and dE/dX (from Mukherjee and Nayak relations) [4]. The experimental data from other studies for relativistic ions are also included. It is clear from the figure that in low energy loss region, etch rate ratio is linear function of energy loss. However, in high energy loss

ORIGINAL PAGE IS
OF POOR QUALITY

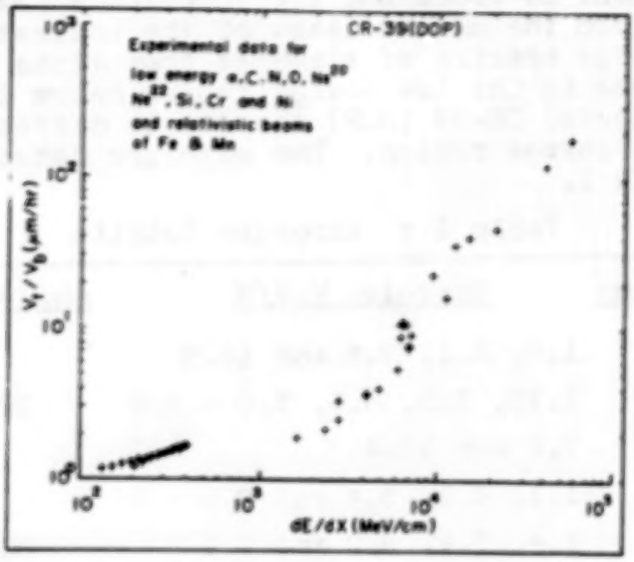


Fig. 1 Track response of CR-39 (DOP)

region, etch rate ratio is a power function of energy loss. A polynomial of the form

$$V_t/V_b = A + b\,(dE/dX) + c\,(dE/dX)^d$$

is fitted to data points (not shown in the figure). From response curve, we have generated curves between Vt/Vb versus residual range for different ions. From these curves, we have studied the charge resolution of CR-39 (DOP) in terms of standard deviation in measurements. The accuracy of the charge resolution turns out to be about 0.2 charge unit.

Isotopic resolution is studied from Ne^{20} and Ne^{22} exposures. The depth dependence of detector response of this plastic is studied from 6.5 MeV/N Cr exposures (range $\sim$95 μm). The track length measurements for different exposure angles, on both sides, do not show any difference beyond experimental error. We also do not find any significant effect of annealing on track response of this plastic.

N85-35119

References

1. Cartwright, B.G. et al. (1978), Nucl. Instrum. and Meth., 153, 457.
2. Biswas, S. et al., (1985), these proceedings.
3. Henke, R.P. and Benton, E.V., (1971), Nucl. Instrum. and Meth., 97, 483.
4. Mukherjee, S. and Nayak, A.K. (1979), Nucl. Instrum. and Meth., 159, 421.
5. Benton, E.V. and Henke, R.P. (1969), Nucl. Instrum. and Meth., 67, 343.
6. Thomas, W. et al., (1984), Nucl. Track, 9, 107.
7. Ahlen, S.P. et al., (1981), 17th ICRC, 8, 77.

N85-35118

SH9.1-3

A SILICON SURFACE BARRIER TELESCOPE FOR SOLAR PARTICLES IDENTIFICATION

J. Sequeiros+, J. Medina

Grupos Científicos CONIE
INTA. Torrejón de Ardoz. (MADRID). SPAIN.
+ and Physics Dpt. Universidad de Alcalá de Henares.

ABSTRACT

The calibration results of a laboratory model of a three silicon surface barrier detector telescope developed to identify energetic solar particles produced in solar flares and low energy cosmic rays in interplanetary space, by the ΔE-E method, are presented.

1. Introduction. During this last decade a number of experiment on board spacecrafts have been gathering information on the composition and energy of solar energetic particles and low energy cosmic rays. The most striking features to be extracted form the data are: a) Charge range $1 \lesssim Z \lesssim 28$ b) Energy range $\sim 1 \lesssim E \lesssim 50$ MeV/n c) Composition highly variable from event to event, with energy and even with time during a particular event. A detailed review has recently been published by J.P.Meyer (1985).

A International Solar-Terrestrial Physics programme is being studied by NASA, ESA and ISAS for the 90's, in which the European Space Agency is contributing with a multidisciplinary Solar-heliospheric observatory (e.g.SOHO) whose aims include the measurement of energetic particles in Interplanetary Space. The laboratory model of a detector telescope presented here is being realized as a first step towards our eventual participation in such programme.

2. Detector characteristics. The laboratory model of the heavy ion telescope has been designed to separate elements from $_2$He to $_{26}$Fe in the energy range of interest for solar energetic particles and C.R. anomalous component (Fig. 1). The telescope consists of three silicon solid state surface barrier detectors (D1, D2 and D3, Fig. 2) housed in a modular aluminium structure of cilindral symmetry which can easily be modified to hold different detector size and opening angles. The third detector (D3) is set in anticoincidence to reject particles which are not stopped in D2. TABLE I shows the main cha

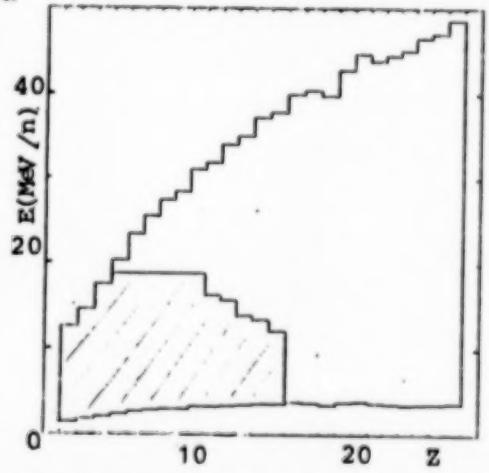


Fig. 1 Energy and charge ranges of the telescope.

ORIGINAL PAGE IS
OF POOR QUALITY

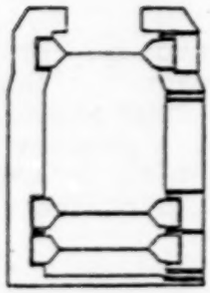


Fig. 2 Schematic cross section of the telescope.

TABLE I
Detector characteristics

	D1	D2	D3
Surface Area (cm^2)	3	4.5	4.5
Thickness (μm)	31 .	1014	470
Resistivity (KΩcm)	.408	12.5	6.7
Dead Layers ($\mu g/cm^2$)	40.0 Au 40.1 Al	40.1 Au 40.0 Al	40.3 Au 121.0 Al
Alpha Resolution (FWHM in KeV)	36.8	20.8	18.8



Fig. 3 D1 v.s. D2 matrix of raw data.

racteristics of the detector chosen. All detectors are ORTEC silicon surface barrier totally depleted. Alpha resolutions have been measured with an ^{241}Am source and include the contribution of noise from our electronic system. The geometrical factor of the model telescope has been G=0.4sr.cm^2.

3. Accelerator calibration. Absolute calibration of the telescope was performed in the VICKSI (Van-de-Graaff-Isochron-Cyclotron-Kombination fur Schwere Ionen) accelerator of the Hahn-Meitner-Institut (Berlin,F.R.G.). Two shifts, with beams of ^{20}Ne of 230 and 376 MeV, and ^{197}Au targets of 210 $\mu g.cm^{-2}$ and 6 mg.cm^{-2} and ^{12}C target of 50 $\mu g.cm^{-2}$, were used. The scattered and fragmented ions were detected by the telescope placed at 20 cm from the targets and at $\theta = 25°$ (gold targets) and $\theta = 15°$ (carbon target) with respect to the beam direction. The angular acceptance of the telescope was about 0.3°. The data were split by a data distributer and collected simultaneously by our ADC's interfaced to a HP 9825 minicomputer and the da

ta adquisition system of the Institute, in order to check the reliability of our system.

4. Results. The resolution of D1 and D2 detectors for ^{20}Ne of 230 MeV elastically scattered in a 210 $\mu g \cdot cm^{-2}$ ^{197}Au target were measured to be 1.7 MeV and 1.9 MeV FWHM which correspond to 7.6% and 0.9% respectivily. Fig. 3 shows a D1 v.s. D2 energy-loss matrix of raw data from ^{20}Ne (E=376MeV) + ^{197}Au (6mg$\cdot cm^{-2}$) which gives and idea of the charge resolution of the detector system in low gain mode.

The charge spectra, over the whole charge and energy ranges produced (shade area in Fig. 1), have been obtained using a particle identifier algorithm described by Seamster et al. (2). This algorithm is based on integrating Bragg curves using the Bethe-Bloch equation and assuming

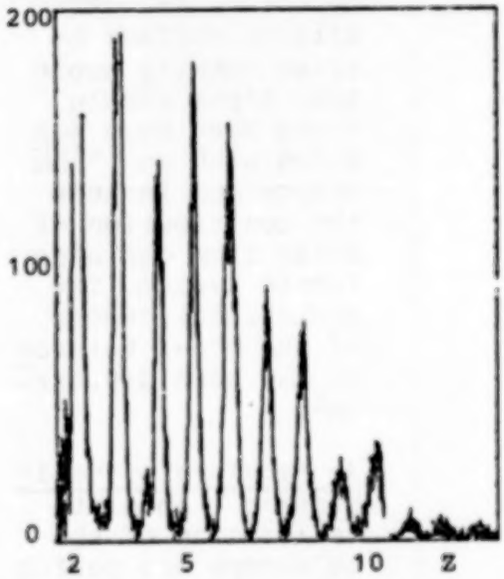


Fig. 4 Charge spectrum from de data of Fig. 3.

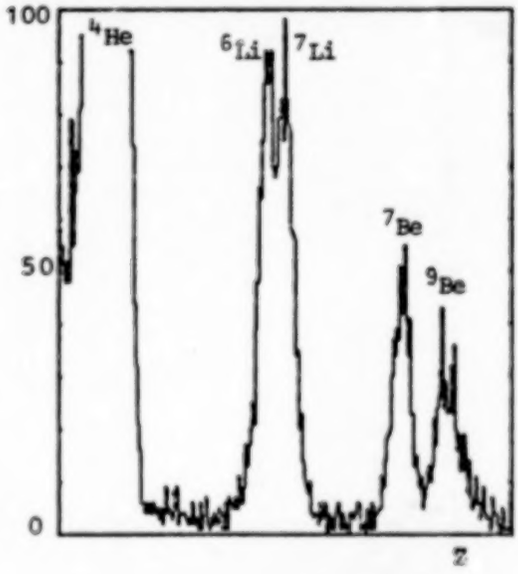


Fig. 5 Charge spectrum of ^{20}Ne (376MeV)+^{12}C(50μg cm^{-2}) in high gain mode.

M(amu)=2Z. For each event, by an iterative calculation, a particle identification parameter $PI=(1/2\,MZ^2)^{1/3}$ has been obtained. Fig. 4 shows the charge spectrum obtained from the data of Fig. 3. In Fig. 5 the low charge spectrum of the reaction products of ^{20}Ne (376 MeV) + ^{12}C(50 $\mu g \cdot cm^{-2}$) in high gain mode, is shown. No corrections have been performed on the data. The bias voltages were in creased 25% for detectors D1 and D3 and 50% for detector D2 above the depletion voltages, in order to reduce the contribution of plasma recombination to pulse hight defect.

5. Conclusions. From the results shown in Fig. 4 and 5 three conclusions can be made: a) The detector system described and tested is capable of good charge resolution from He to Al

N85-35119

although beyond Ne the statistic is very poor b) In the high gain mode, isotopic resolution has been acheived for $^{6}Li/^{7}Li$ and $^{7}Be/^{9}Be$ c) The much higher yield of ^{4}He over ^{3}He and of ^{9}Be over ^{10}Be in this type of nuclear reactions prevent from obtaining experimental evidence of those isotopes, although we believe that, at least $^{3}He/^{4}He$, can be resolved under other more favorable conditions (i.e. solar ^{3}He-rich events).

6. Acknowledgements. This work is being supported by the Comision Asesora de Investigación Científica y Técnica (CAICYT, grant 3433/79).

We are also grateful to Dr. V. Domingo and Mr. J. Henrion of the Space Science Dpt. of the European Space Agency, and Dr. H. Homeyer and Mr. J. Ucker of the Hahn-Meitner-Institut (Berlin, F.R.G.) for their advice and help.

References

1. Meyer, J.P. (1985) Ap.J.Suppl., 57,151
2. Seamster, A.G., et al. (1977) Nucl.Inst. and Meth., 145,583

N85-35119
SH-9.1-4

A BI-DIRECTIONAL CHARGED PARTICLE TELESCOPE TO OBSERVE FLUX, ENERGY SPECTRUM AND ANGULAR DISTRIBUTION OF RELATIVISTIC AND NON-RELATIVISTIC PARTICLES

S.D. Verma, S.P. Bhatnagar & S.K. Kothari
Department of Physics, Gujarat University
Ahmedabad 380 009, INDIA

1. INTRODUCTION

A Charged Particle Telescope[1] (CPT) was designed, fabricated and calibrated to make the following observations[2,3]:

(i) Discrimination between various singly charged particles e.g. electrons, muons and protons, in about 5-100 MeV energy range.
(ii) Measurement of the flux and the energy of the charged particles incident on telescope from two opposite directions and stopping in the Telescope, thus obtaining flux and energy spectrum of downward and upward moving charged particles.
(iii)Measurement of broad angular distribution of selected particles as a function of azimuthal angle.

This telescope can be used to study low energy electron, muon and proton energy spectra. The experiment was flown in a high altitude balloon from Hyderabad, India, in December 1984. This same equipment is also useful in ground level electron, muon spectrum study.

2. EXPERIMENT

The Charged Particle Telescope contains a stack of Plastic Scintillators, inorganic scintillator and Cerenkov detectors. The telescope is described below.

The total energy detector consisted of a 1" thick NaI(Tl) crystal of 3" diameter. The total energy of particles was observed for those stopping in the crystal. Pulse height analysis was done for stopping as well as for penetrating particles. To distinguish various singly charged particles, dE/dX vs E technique has been used, aided by a Lucite (plastic) Cerenkov detector. The capability of charged particle separation by

ORIGINAL PAGE IS
OF POOR QUALITY

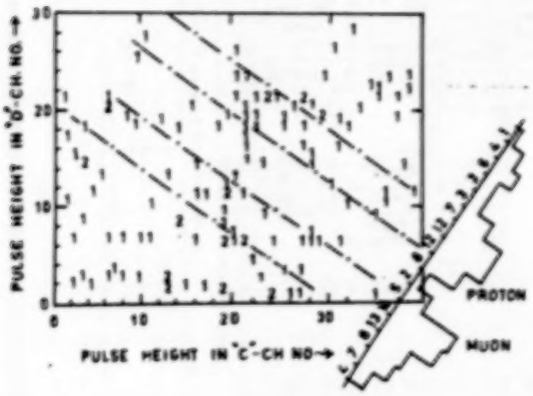


Fig.1

telescope is demonstrated by dE/dx vs. E graph with quick look data shown in Fig. 1. From Fig. 1, it is clear that various charged particles will produce different energy losses in a thin dE/dx detector for a given residual energy E, measured by Total energy detector. Those electrons which stop in total energy detector[4] are all relativistic while the stopping muons and protons are non-relativistic. Therefore, a velocity threshold Cerenkov detector will produce output for a stopping electrons only and other stopping particles will thus be separated. Combination of these two techniques results in an effective separation of electrons, muons and protons in selected energy interval of 5-30 MeV.

The up and down moving particles are distinguished using upper and lower dE/dx counters as anticoincidence detectors for upward and downward particles respectively.

3. ENERGY CALIBRATION

The energy calibration of various detectors of CPT was done using ground level Cosmic Ray Muons and radioactive Gamma Ray sources (Cs^{137}, Co^{60}). These sources were used for NaI(T1) detector energy calibration. Beta particle source Sr^{90} was used for dE/dx detector testing, energy calibration and monitoring. A 8 MeV monoenergetic electron beam from microtron was used for various detector calibrations and for determining efficiency of Cerenkov

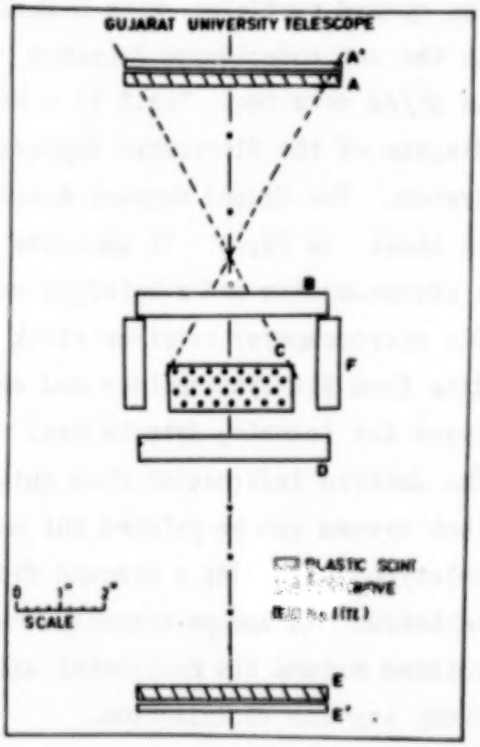
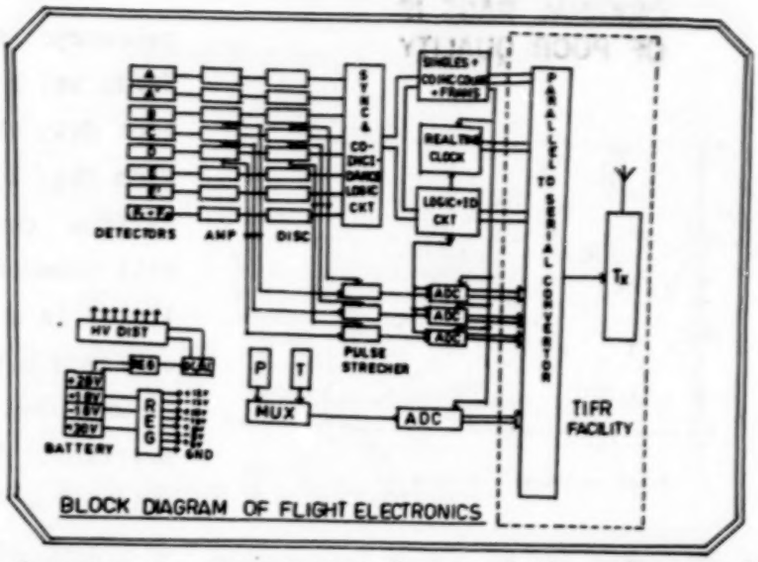


Fig. 2

detector.

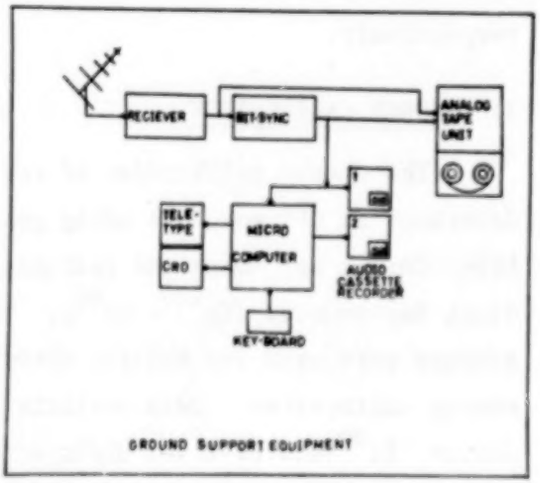
FIG3



BLOCK DIAGRAM OF FLIGHT ELECTRONICS

4. TELESCOPE HARDWARE

The Schematics of CPT is shown in Fig.2. The geometry of the telescope is defined by 1/8" thick plastic scintillator A' and 1" thick NaI(T1) detector C. Geometrical factor of the telescope is 13 cm^2 Ster. Detector A is a Lucite Cerenkov detector, used as velocity threshold discriminator for various stopping particles. The detector B is 1/2" thick plastic scintillator, working as energy loss (dE/dx) detector. Lower detector D is another 1/2" thick plastic scintillator working as anticoincidence detector for downward moving particles. Detectors E and E' are complementary to A and A', creating another telescope for upward particles, with B acting as the anticoincidence detector, D as dE/dx detector. Fig.3 is a block diagram of the Electronic Support subsystem. The Ground Support System is shown in Fig.4. It consists of a microcomputer and a teletype unit. The microcomputer receives clock and data from Bit-synchroniser and analyses the incoming data in real time. The desired information from quick look system can be printed out on teletype on getting a command from keyboard. Telescope assembly can be rotated around its horizontal axis to study angular distribution.



GROUND SUPPORT EQUIPMENT

FIG 4

The experiment was tested for several weeks before the flight for various detector characteristics, gain shifts, singles and coincidence count rates, high voltages, discriminator levels etc.

5. BALLOON FLIGHT

On 8th December 1984, this experiment was flown in a high altitude balloon in early morning hours (5.23 a.m. IST) from Hyderabad, India. Balloon ascended to an altitude of 37 km (4 mb) and floated for four hours. Experiment was cut down by telecommand at 12.00 noon and was picked up in a reasonably good shape. Post flight checkout runs indicate experimental condition to be good. Data analysis and results are presented in SH session[5,6].

6. ACKNOWLEDGEMENT

Authors are thankful to Mr. Vikram Shah of Metro Industries for support in fabrication of mechanical systems and to Dr. Peggy Shea of A F G L, Bedford, USA, for providing the NaI(Tl) crystal for this experiment.

Indian Space Research Organisation's financial support under RESPOND Programme is thankfully acknowledged, without which it would not have been possible to conduct this experiment. The important assistance of Dr. V.N. Bhoraskar and his colleagues in calibration of CPT using microtron at University of Poona, India, and the useful discussions with Dr. (Mrs.) V. Sinha are gratefully acknowledged.

References

1. Bhatnagar S.P. & Verma S.D., 17th ICRC, Paris, 1981, Vol. L, p.266.
2. Bhatnagar S.P. & Verma S.D., 18th ICRC, Bangalore, India, 1983, Vol.3, p.501.
3. Kothari S.K. & Verma S.D., 18th ICRC, Bangalore, India, 1983, Vol.3, p.483.
4. V.B. Asgekar et al, Technical Report on Microtron, University of Poona, 1979.
5. Verma S.D. & Bhatnagar S.P., 19th ICRC, La Jolla, USA, (1985) (SH-6).
6. Verma S.D. & Kothari S.K., 19th ICRC, La Jolla, USA, (1985) (SH-6).

PHOTOMETRIC AND SPECTROSCOPIC GAMMA-RAY OBSERVATIONS OF SOLAR TRANSIENT PHENOMENA USING LONG DURATION BALLOONS

N85-35120

Pelling, M.R. and Duttweiler, F.
UCSD/CASS, Code C-011
La Jolla, CA 92093

Lin, R.P., Levedahl, W.K., Primbsch, H., and Curtis, D.W.
UCB/SSL, Berkeley, CA USA

Burley, K.C.
CESR, Toulouse, FRANCE

ABSTRACT

We describe a program, currently in progress at UCB and collaborating institutions, UCSD and CESR Toulouse to conduct extended duration spectroscopic and photometric observations of solar X-ray phenomena from balloons. High photometric sensitivity to weak hard X-ray bursts is attained using a 600 cm^2 array of phoswich scintillators. High spectral resolution for stronger bursts is available from an array of planar germanium detectors. These instruments are carried in a novel balloon gondola designed for the 15 to 20 day float durations available through using conventional zero-pressure balloons in the radiation controlled (RACOON) mode.

1. Introduction Important new results concerning energetic flare processes have been obtained using a unique instrumental complement combining high spectral resolution and photometric sensitivity in a conventional balloon flight. The excellent spectral resolution available through the use of germanium solid state detectors permitted the discovery of a superhot (3.5×10^7 K) flare emission component (1) and the high photometric sensitivity of a large area phoswich scintillation counter permitted detection of ~25 "μ-flares" with fluxes 10^{-1}–10^{-2} lower than conventionally associated with major flare activity (2). The existance of superhot emission components has since been indirectly confirmed through Fe XXVI measurements (3) and continuum measurements below 30 keV (4). The optical counterpart of μ-flare events were subsequently discovered through analysis of co-ordinated H_α observations (5). The μ-flares have a non-thermal spectral distribution and show evidence for temporal structure faster than ~1 s.

2. Scientific Objectives The general significance of these phenomena is not clear since the superhot component has been directly observed in only one flare and the observed μ-flares were probably the product of a single active region. It is interesting to note; however, that the size/frequency distribution for the μ-flares suggests that their underlying particle population could be significant for heating of the active corona. Thus, it is of great interest to determine how general the acceleration of >20 keV

electrons is for transient processes on the sun. Other interesting questions include: How does the superhot component vary from flare to flare? Indeed, how hot do flare regions get? How are the heating and acceleration mechanisms related?

In order to clarify the role of these hard x-ray processes in overall solar energetic phenomena it is necessary to extend the observations to span a variety of solar activity conditions. The primary requirement for these follow-on studies is to attain a relatively long observing period (comparable to solar rotation period) using instrumentation having high photometric and spectroscopic sensitivity. For this purpose we have modified our original balloon instrument to provide additional sensitivity and to function within the constraints of a long duration balloon flight.

3. Flight Apparatus To attain the above objectives we have enlarged the collecting area of the original payload and adapted it to a unique balloon gondola designed to capitalize on the long float duration available using standard zero-pressure balloons in the radiation controlled (RACOON) mode. A block diagram for the detector system is shown in Figure 1.

Our detector complement consists of an array of four actively shielded high purity cooled planar germanium detectors totaling ~50 cm^2 active area plus three large area NaI(Tl)/CsI(Na) phoswich scintillation counters totaling ~600 cm^2. Cooling for the germanium detector array is provided by a 160 l dewar of liquid nitrogen. The aperture of the germanium array is oriented vertically with an acceptance angle of 40 degrees (full width, zero response). This permits sensitivity to solar transient events for roughly two hours of each day at >33% response. The phoswich scintillation counters have 3 mm thick primary detector elements and are optimized to respond in the 15 to 150 keV energy range. Each phoswich has a crossed slat collimator which defines a pyrimidal angular response with FWHM of 15 degrees.

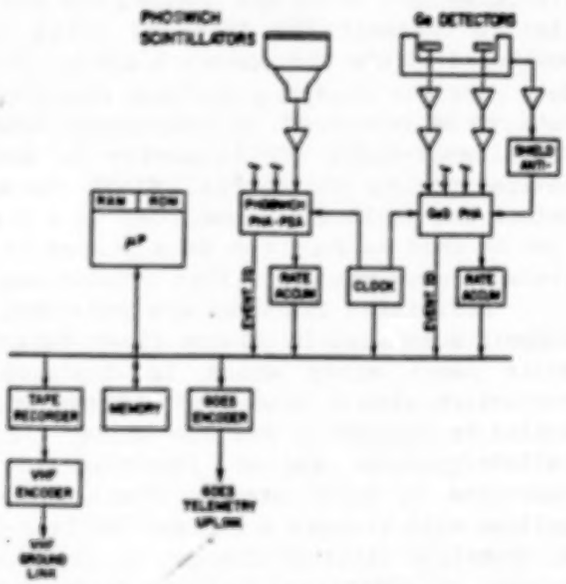


Figure 1 - The μ-processor based data system accommodates a wide dynamic range of detector event rates and prioritizes the data for storage or telemetered output (see text).

The phoswich array is carried in an alt-azimuth gimbal which is slaved to an external aspect sensor platform. The aspect sensor platform is programmed during the day to track the sun in azimuth and elevation with a precision of ± 1 degree. During night operation or periods when the sun is too low in the sky to permit useful x-ray observations the aspect sensor platform may be reprogrammed to track the local magnetic field. This

operating mode permits observation of non-solar sources via a pre-programmed tracking routine with an accuracy of ~2 degrees. The aspect sensor platform also incorporates a sunrise/sunset sensor to provide daily navigation updates to the tracking routines.

The data generated by these detector systems are processed by an on-board computor and prioritized for output via one or more of three channels as shown in Figure 1. Discrete x-ray event words in which pulse height and timing information are encoded are read directly into a large dynamic random access memory via direct memory access control. This memory is sized to hold the transient events totaling up to 10^6 discrete detected photons. The raw event rates are monitored in parallel with memory storage of the detector data streams by the on-board processor to detect the presence of solar burst events. Data segments which contain such burst events are then tagged for preferential storage and output. When ~50% of the main buffer RAM is filled (~2 hours under background rate conditions) the data are transferred to the on-board tape storage system. This system includes two 3M model HD-75 digital recorders having a total capacity of 136 Mbytes which is sufficient to hold all of the data generated during the nominal 20 day balloon flight. Burst event data from the previous day are read out of the burst memory section each night and transmitted via the Geostationary Orbiting Environmental Satellite (GOES) network at an effective rate of 60 bps. During the day this data channel is used in real time to transmit the integral rates in three broad energy windows as monitored by the the phoswich array. This channel provides a rudimentary data base for studying μ-flare characteristics should the tape recorder data not be recovered. An additional data transmission channel is provided via line-of-sight VHF telemetry to permit high rate monitoring of the payload during the initial float checkout phase of the balloon flight before the payload is committed to a circumnavigation. This channel will also be used to dump the data stored in the on-board tape recorders as a precautionary measure before cutdown and recovery of the payload.

Additional features are provided in the balloon gondola system to support a nominal 15-20 day float duration. Power is provided by an 8 m^2 solar panel array which is deployed after launch and operates in conjuction with a lead acid battery stogage system. The power system is scaled to support an average energy usage of 2500 watt-hours per day. The balloon/gondola system incorporates an auto-ballast system which functions in three stages. Nominal sunset cooling and settling of the balloon will trigger a minimal ballast drop of ~5% of the payload weight. An anomalous altitude change, as might occur over a cold cloud layer, will trigger an additional ballast drop of 10%. In the event of a very large altitude excursion (which might result in the payload descending below the tropopause) a ballast destruct occurs to provide some possibility of restoring the payload to a functional altitude. The primary payload is fully enclosed within an insulation blanket which includes additional thermal ballast to maintain tempertures above 0° C. Additional thermal isolation and heating is provided for the phoswich scintillator array which needs a 20-30 °C operating environment.

4. Long Duration Balloon Operation The RAdiation COtrolled balloON (RACOON) concept offers near ideal conditions for the study of solar phenomena (6, 7). Since essentially continuous exposure is possible for periods within ± 4 hours hours of local noon, one is not limited by the ~40 minutes of earth occulation which occur for a spacecraft instrument in

each 90 minute low earth orbit. The RACOON mode involves the use of a standard zero pressure polyethelyne balloon for multi- day flights without the use of extensive ballasting to maintain float altitude through sunset. The initial float altitude must be chosen such as to ensure that the sunset altitude change does not bring the balloon below the tropopause where the negative temperature gradient would result in loss of the flight. For the present system we require a daytime float altitude of ~3 gm/cm^2 residual depth to conduct x-ray observations. This is adequate to keep the balloon safely above the tropopause at night. Allowing 1 to 2 hours to reattain daytime float altitude we expect ~250 hours of total float duration at 3 gm/cm^2. This should be compared with the nominal maximum float durations of 25-40 hours which are occasionally attained under normal balloon flight conditions.

The balloon is to be launched in January, 1986 from Alice Springs, Australia, where the strong prevailing stratospheric winds will keep the system within ~2 degrees of a constant latitude for the 15-20 day duration of the global circumnavigation. Cutdown is planned for the Eastern coastal region of Australia.

5. Summary We have developed a sophisticated balloon gondola which will provide the first astronomical observations of solar and cosmic phenomena from long duration balloons. We will use the RACOON long duration mode which is ideally suited for observations of the sun. We expect one 20 day balloon flight to yield ~150 hours of solar and ~100 hours of cosmic source observations. We estimate that ~20 flare events strong enough for spectroscopic analysis should be observed in a January, 1986 flight.

6. Acknowledgements The authors wish to acknowledge the valuable asistance provided by the National Scientific Balloon Facility in the design and construction of the payload and planning for the long duration flight operation. We also wish to thank R. Sood and J. Thomas at the University of Melbourne for their assistance in preparations for the Australian lauch and recovery operation. We also wish to acknowledge the generous support of National Science Foundation Grant ATM-8402231, National Aeronautics and Space Administration Grant NAGW-516, and California Space Institute Grant CS30-82.

References

1. Lin, R.P., Schwartz, R.A., Pelling, R.M., and Hurley, K.C. (1981), *Ap.J. (Letters)*, 251, 109.
2. Lin, R.P., Schwartz, R.A., Kane, S.R., Pelling, R.M., and Hurley, K.C. (1984), *Ap.J.*, 283, 421.
3. Tanaka, K., Nitta, N., Akita, K., and Watanabe, T. (1983), *Solar Physics*, 86, 91.
4. Duijveman, A. (1983), *Solar Physics*, 84, 189.
5. Canfield, R.C. and Metcalf, T.R. (1984), *BAAS.*, 16, No. 4, 891.
6. Lally, V.E. (1981), *The Radiation Controlled Balloon*, Preprint, National Center for Atmospheric Research.
7. White, R.S. (1983), *A Plan for Long Duration Scientific Ballooning*, Report of the Long Duration Balloon Flight Study Committee, printed by the National Scientific Balloon Facility, Palestine, Texas.

474 N85-35121 SH 9.1-6

MONTE CARLO CALIBRATION OF THE SMM GAMMA RAY SPECTROMETER FOR HIGH ENERGY GAMMA RAYS AND NEUTRONS

J. F. Cooper and C. Reppin
Max Planck Institute for Extraterrestrial Physics
D-8046 Garching, F.R.G.

D. J. Forrest and E. L. Chupp
University of New Hampshire, Durham, N.H. 03824, U.S.A.

G. H. Share and R. L. Kinzer
Naval Research Laboratory, Washington, D.C. 20375, U.S.A.

1. Introduction. The Gamma Ray Spectrometer /1/ on the Solar Maximum Mission spacecraft was primarily designed and calibrated for nuclear gamma ray line measurements, but also has a high energy mode which allows the detection of gamma rays at energies above 10 MeV and solar neutrons above 20 MeV. The GRS response has been extrapolated until now for high energy gamma rays from an early design study /2/ employing Monte Carlo calculations. The response to 50-600 MeV solar neutrons was estimated from a simple model which did not consider secondary charged particles escaping into the veto shields /3/. In view of numerous detections by the GRS of solar flares emitting high energy gamma rays /4/, including at least two emitting directly detectable neutrons /3,5,6/, the calibration of the high energy mode in the flight model has been recalculated by the use of more sophisticated Monte Carlo computer codes described in Section 2. New results presented in Section 3 show that the GRS response to gamma rays above 20 MeV and to neutrons above 100 MeV is significantly lower than the earlier estimates.

2. Monte Carlo Simulation of the GRS. The simulation of GRS response in the high energy mode has required several stages of software development: (1) representation of the principal materials and structures, both active and passive, by combinatorial geometry routines, (2) propagation of primary photons, and their secondary interaction products, through the GRS with the Electron-Gamma Shower Code (EGS) /7/, (3) propagation of neutrons and their secondary products with the High Energy Transport Code (HETC) /8/ and with EGS, (4) calculation of charged particle scintillation efficiencies /9/, and (5) the final selection of events satisfying pulse height logic criteria.

The combinatorial geometry routines give an accurate representation of the GRS flight model /1/, consisting of seven (7.6-cm x 7.6-cm) NaI detectors in an upper array and a large (24.2-cm x 7.6-cm) CsI detector, located 18 cm below the upper array. These detectors are surrounded by an array of plastic and CsI veto shields to reject charged particle events.

In the calculations the flight model is represented by fifty active scintillator or passive structure elements. These volume elements are defined in terms of intersections or unions of solid cylinders, cylindrical shells, hemispherical shells, and planar boundaries, in order to represent the upper NaI and lower CsI detector crystals, photomultiplier tube assemblies between the upper and lower detectors, the plastic and CsI shields, and the principal supporting structures, including the metal housings for the active detectors and shields. A significant improvement over the previous study /2/ is in the treatment of empty interstitial spaces between the material volumes. Tracking of Monte Carlo particles through all of these volumes and boundaries is accomplished with common geometry routines in EGS and HETC.

The compatibility of the tracking routines is particularly useful for the simulation of neutron interactions, which produce secondary products requiring two-stage tracking, first by HETC for nucleons and pions, and then by EGS for secondary gamma rays from pion decay or the de-excitation of nuclei excited by collisions. Interactions of nucleons and pions with target nuclei, and the residual excitation energy emitted as gamma rays, are simulated with the two-stage intranuclear-cascade and nuclear evaporation routines in HETC. A low energy cutoff of 15 MeV is used for the propagation of nucleons and pions in HETC, although the intranuclear cascade model, decomposing interactions with nuclei into individual collisions with the constituent nucleons, is not valid for collision energies below 100 MeV. EGS uses cross sections derived from analytical formulae or experimental data to simulate the interactions of gamma rays above 100 KeV and electrons above 500 KeV. Cumulative errors due to Monte Carlo statistics and the accuracy of the interaction cross sections used in both HETC and EGS are about 10-20 percent.

The present calculations use only a rough approximation procedure for energy deposition in the detectors by secondary neutrons produced at energies below 15 MeV. The neutron response calculations have been run for two cases: (1) the low energy neutrons produced below 15 MeV deposit their full energy locally via nuclear recoil or inelastic interactions, or (2) these neutrons escape from the GRS without any further interaction. The final neutron responses are the average of the results from these two cases, significantly different for 50-100 MeV neutrons but much less so for higher energies.

The pulse height logic criteria for gamma ray or neutron events in the high energy mode are the following: (1) 10-100 MeV electron-equivalent energy deposited in either the upper NaI detector assembly or the lower CsI detector, or in both, (2) no deposits greater than about 3 MeV in the annular CsI side shields, and (3) no deposits greater than about 500 KeV in either the

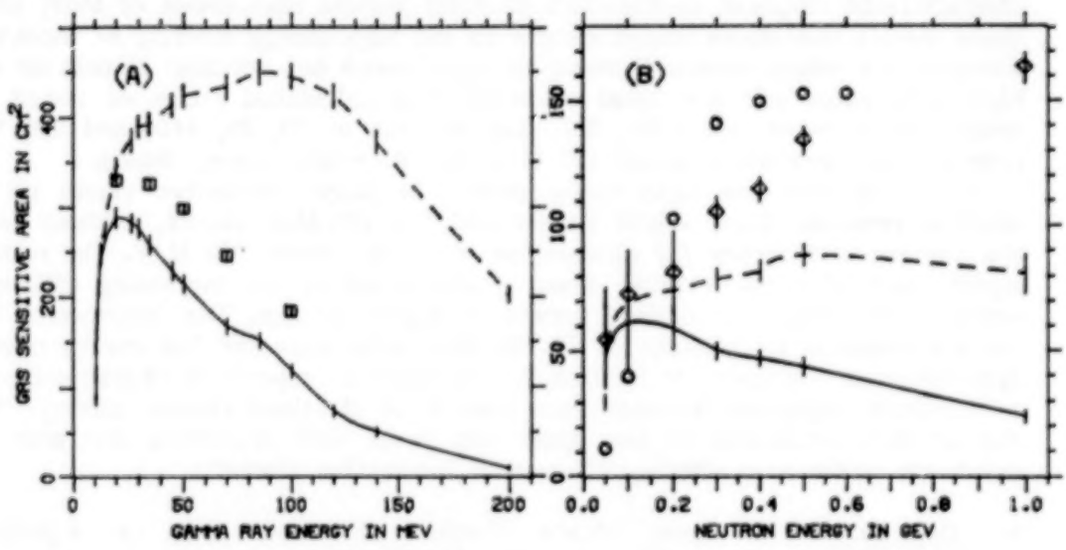


Figure 1: (A) 10-140 MeV gamma ray response. (B) 50-1000 MeV neutron response. Nominal high energy matrix response with (solid curves) and without (dashed curves) shield veto. Gamma ray response from /2/ with corrections for the GRS flight model (boxes). Neutron response without shield veto and 100-MeV cutoff from present work (diamonds) and /3/ (circles).

front or back plastic shields. Energy deposits in the upper and lower detector arrays are pulse-height analysed separately with four channels below 100 MeV, while deposits above 100 MeV in either array are not recorded due to preset electronics limitations. The four channels correspond to electron-equivalent energy deposits of 10-25, 25-40, 40-65, and 65-100 MeV. The GRS event logic also records a two-dimensional high energy matrix which includes "mixed" events triggering both the upper and lower detectors, as the result of secondary charged particle and photon showers, and depositing total energies up to 140 MeV. The total energy deposited in the matrix gives at least a minimum measure of the incident particle's energy, while the fraction of mixed events allows some discrimination between gamma rays and neutrons.

3. High Energy Gamma Ray and Neutron Response. Calculated results for the total GRS responses to gamma rays and neutrons as functions of incidence energy are shown respectively in Figures 1(A) and 1(B). The incident photons or neutrons are perpendicularly incident onto the front surface of the GRS, as would be the case for radiation of solar origin. The GRS response to high energy gamma rays from off-axis sources has also been calculated and used for in-orbit calibration and cosmic burst studies, the response being nearly constant up to 30 degrees off-axis at all energies and falling off by up to a factor of three at 90 degrees and 20 MeV.

The high energy matrix response for solar gamma rays, shown by the solid curve in Figure 1(A), is heavily attenuated above 15 MeV by the vetoing of events which produce shower electrons escaping through the active shields, where these electrons trigger the side and bottom shields at about the same rates. The new responses are ten percent below the earlier ones /2/ at 20 MeV, but the differences increase to thirty percent at higher energies. These differences arise from the use of different instrument models and shield veto criteria which produce increasingly divergent results above 20 MeV.

The strong forward showering of secondary photons and electrons produces a characteristic response in the GRS to solar gamma rays above 20 MeV, where these events contribute mixed events to the high energy matrix. At increasing energies the mixed events increase in significance but are also associated with high veto rates and low total response. The calculated ratios of mixed and total matrix events are 0.01, 0.2, 0.6, and 0.4 at 30, 70, 140, and 200 MeV respectively, decreasing above 140 MeV due to matrix energy limits.

In Figure 1(B) the solid curve shows the large cumulative effect on the neutron response from shield vetoes and the 100-MeV cutoff, without which the present and earlier /3/ calculations converge above 500 MeV. The relative significance of shield vetoing alone is illustrated by the increasing difference between the solid and dashed curves at higher energy. The large error bars for the response to neutrons at 50-100 MeV arise from the low energy neutron approximation discussed in Section 2. The neutron response is characterized by a relatively negligible fraction (less than 0.03) of mixed events, arising from the physical separation of the upper and lower GRS detectors, and from the relatively isotropic scattering of neutron interaction products.

4. Discussion. The new Monte Carlo calibration gives a significant improvement of the earlier results /2/ for higher energy gamma rays producing mixed events, the difference between the two calculations at 20 MeV being relatively negligible. Since average gamma ray energies in the high energy GRS flares /4/ were less than 25 MeV in the impulsive phase, the integral fluences for those flares do not require revision. Analyses of flares emitting higher energy gamma rays from pion decay /10/ are highly dependent

on the measured fraction of mixed matrix events and require the new calibration.

Aside from residual uncertainties regarding the newly calculated GRS response to solar neutrons below a few hundred MeV, the important effects of shield vetoing, the 100-MeV high energy mode cutoff, and details of the secondary interaction product distributions, have otherwise been accurately modeled for the first time. The earlier estimates /3/ of GRS response to neutrons, derived from simple cross section arguments without consideration of these effects, greatly exceed the new ones at neutron energies above 100 MeV. At 20-100 MeV the earlier estimates should be used, since neutron cross sections in the new HETC calculations have probably been overestimated at those energies. The total matrix responses of the GRS with shield vetoing to neutrons at 50, 100, 200, 300, 400, 500, and 1000 MeV are then 11, 40, 59, 50, 47, 44, and 24 cm^2 respectively, and the corresponding ratios of the new and old responses are 1.0, 1.0, 0.57, 0.36, 0.31, and 0.28 up to 500 MeV.

The in-flight GRS data provide some confirmation that the current calibration of the high energy mode is reasonably accurate. In-flight calibration data have confirmed the stability of energy deposit thresholds for the shields, although thresholds at 10 MeV and above for the high energy matrix are still uncertain by a few MeV. The gamma ray calibration has been checked at 30-200 MeV by measurements of atmospheric gamma rays, as the GRS points toward the earth's horizon during the night portion of its orbit, which agree within 20-30 percent with comparable SAS-2 data /11/. For a check of the neutron response, delayed neutrons from the June 21, 1980 solar flare /3/ provide a relatively "clean" neutron source, uncontaminated by high energy gamma rays emitted only in the initial impulsive phase. These neutrons produced a very small fraction of mixed events in the high energy matrix after background subtraction /6/, thereby confirming the predicted response from these calculations.

5. Acknowledgements. This work was supported partially by contracts 010K017-ZA/WS/WRK 0275:4 at the Max Planck Institute, NAS 5-23761 at the University of New Hampshire, and by NASA contract S.70926A at NRL.

References

1. Forrest, D. J., et al.: 1980, Solar Physics, 65, 15.
2. Kinzer, R. L., et al.: 1977, Monte Carlo Simulation of the SMM Gamma Ray Detector, unpublished report, Naval Research Laboratory, Washington, D.C.
3. Chupp, E. L., et al.: 1982, Ap. J. Lett., 265, L95.
4. Rieger, E., et al.: 1983, 18th Int. Cosmic Ray Conf. Papers, Bangalore, 10, 338.
5. Chupp, E. L., et al.: 1983, 18th Int. Cosmic Ray Conf. Papers, Bangalore, 10, 334.
6. Chupp, E. L., et al.: 1985, this conference, Paper SH 1.4-1.
7. Ford, R. L., and W. R. Nelson: 1978, The EGS Code System, Stanford Linear Accelerator Center Rep. 210, Stanford University, Palo Alto, Ca.
8. Chandler, K. C., and T. W. Armstrong: 1972, Operating Instructions for the High Energy Nucleon-Meson Transport Code HETC, Oak Ridge National Laboratory Rep. 4744, Oak Ridge, Tenn.
9. Birks, J. B.: 1964, The Theory and Practice of Scintillation Counting, Pergammon Press, Oxford.
10. Forrest, D. J., et al.: 1985, this conference, Paper SH 1.4-7.
11. Thompson, D. T., et al.: 1981, J. Geophys. Res., 86, 1265.

478 N85-35122 SH9.1-7

COMPARISONS OF MONTHLY MEAN COSMIC RAY COUNTING RATES OBSERVED FROM WORLDWIDE NETWORK OF NEUTRON MONITORS

Jai Young Ryu and Masami Wada*

Department of Physics, Kunsan National University,
Miryoung-Dong, Kunsan-city, Chullapuk-Do, 511 Korea

* Cosmic Ray Laboratory, Institute of Physical and Chemical Research,
7-13 Kaga-1, Itabashi-Ku, Yokyo 173, Japan

ABSTRACT

In order to examine the stability of neutron monitor observation, each of the monthly average counting rates of a neutron monitors is correlated to those of Kiel neutron monitor. The regression coefficients thus obtained are compared with the coupling coefficients of isotropic intensity variation. The results of the comparisons for five year periods during 1963 to 1982, and for whole period are given. The variation spectrum with a single power law with an exponent of -0.75 upto 50 GV is not so unsatisfactory one. More than one half of the stations show correlations with the coefficient greater than 0.9. Some stations have shifted the level of mean counting rates by changing the instrumental characteristics which can be adjusted.

INTRODUCTION

The relation between the long lived Forbush decreases and the 11 year variation has long been interested (see for example, Lockwood and Webber, 1984; Burlaga et al. 1984). In order to examine whether the neutron monitor counting rates are satisfactorily stable for periods of months to tens of months to be used to inspect the variations mentioned above, the present paper is given (Ryu and Wada, 1983). After some trials, Kiel has been selected as the main key station of neutron monitor data. Correlations of monthly averages between each of 65 stations and Kiel for 5 year periods during 1963 and 1982 are studied statistically. The years 1963-67 and 1973-77 are of the sunspot minimum periods, and those of 1968-72 and 1978-82 are nearly during the sunspot maximum years. All of the stations have more than five years continual data which are refered to WDC-C2.

ANALYSIS AND RESULTS

The correlation diagrams are prepared for any pairs of stations. Form inspections of these diagrams, we can classify them into three groups as a, b, and c. Group a shows close correlation of which the coefficients are greater than 0.9. There are 37 stations in the group a out of 65. For example, the diagrams between Thule and Kiel are given in Fig.1, and for Kerguellen and Kiel in Fig.2. The scales of both axes are of natural logarithms, so that the variational amounts are approximated in the values relative to the counting rates of each point. As seen in the figures, the standard deviation of the scatter about the regression line is extimated to be around 0.5 percent at the best condition.

Using the results of correlation, the regression coefficients are plotted in Fig.3 against the coupling coefficients of isotropic varistion normalized to that of Kiel. The coupling coefficients are derived from the variation spectrum of primary cosmic rays of a single power law with an exponent

-0.75 upto 50 GV (Yasue et al. 1982). From Fig.3, it can be seen the correlations are rather well, though there are some scatters in points. Most remarkable scatter is seen for the figure of 1968-72, the sunspot maximum period. There seems some tendency of downward shift of southern stations. The spread of decreases seen in plot of whole period in Fig.2 (left hand side) is also noticable aspect. We have examined whether this trend is statistically significant or not. After variaous test, we found no clear conclusion to prove the situation given above. That means the existence of limitation of the data stability.

Group b contains stations which have rather low correlation coefficients. Those stations are mostly situated in lower latitudes, and the amounts of variation are relatively small, which result lower coefficients. There are continuities from the stations whose coefficients are higher than 0.9. Some stations reveal hysteresis, but there is no systematic trend of hysteresis.

Group c diagrams in Fig.4 show significant level changes of the mean counting rates. They may mostly arise from artificial instrumental changes such as the number of counters. There are 15 stations in this group. We are trying to get the amounts of level changes for those stations by using reasonable method.

CONCLUSION

The monthly average counting rates of most of the existing neutron monitors are examined from a point of view of the stability of operation. More than a half of the stations treated show satisfactory operations. If the artificial level changes are adjusted, we can use practically all of the stations, except small number of stations whose data are significantly deviate with time. The standard deviation of the residual variation is around 0.5 percent in the best condition, which makes some limitation of the analysis. It can be improved if one uses multiple number of stations for such variations spanning months to tens of months period.

REFERENCES

Burlaga,L.F. et al. (1984), J. Geophys. Res. in press.

Lockwood,J.A. and W.R.Webber (1984), J. Geophys. Res. 89, 17.

Ryu,J.Y. and M.Wada (1983), Conf. Papers 18th ICCR,3,511.

Yasue,S. et al. (1982), Rep. CRRL. No. 7, Cosmic-Ray Res. Lab. Nagoya Univ. Nagoya, Japan.

FIGURE CAPTIONS

Fig.1. Correlation diagrams of monthly average neutron monitor counting rates between Thule and Kiel for 5 year periods and for all the period (left hand side).

Fig.2. The same as Fig.1, but for Kerguellen and Kiel.

Fig.3. The correlation diagrams of the regression coefficient against the coupling coefficient normalized to that of Kiel.

Fig.4. The same as Fig.1, but for the stations which show level changes due to artificial change in the operational condition.

ORIGINAL PAGE IS
OF POOR QUALITY

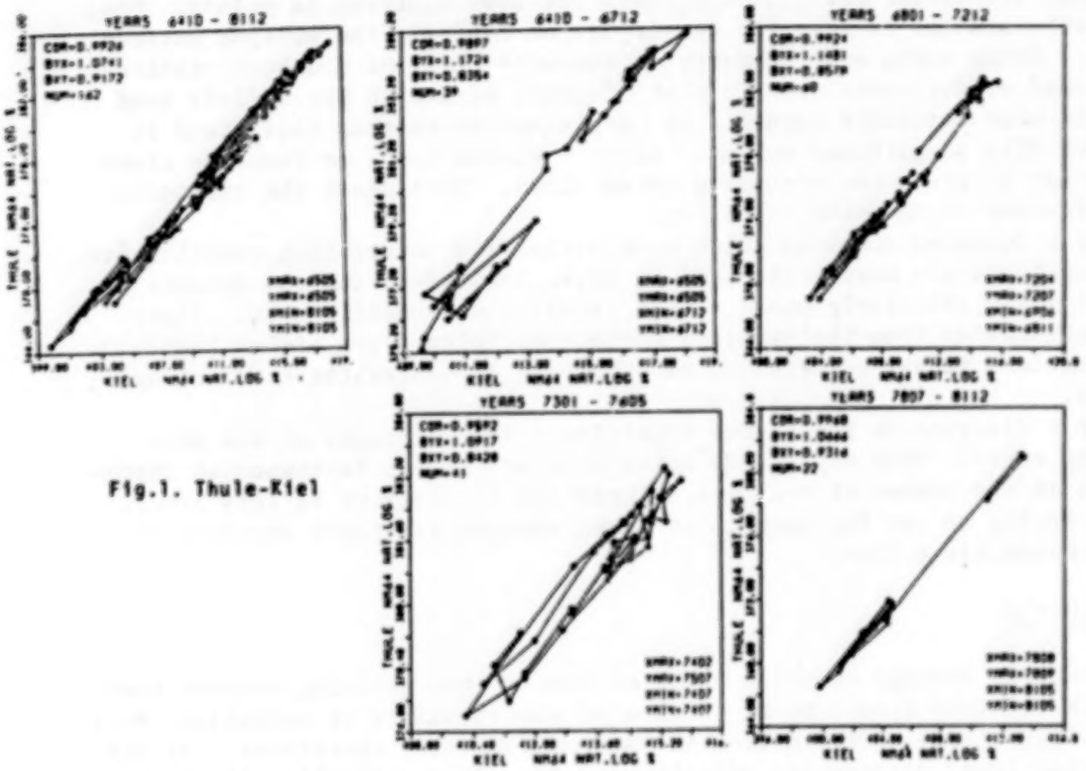


Fig.1. Thule-Kiel

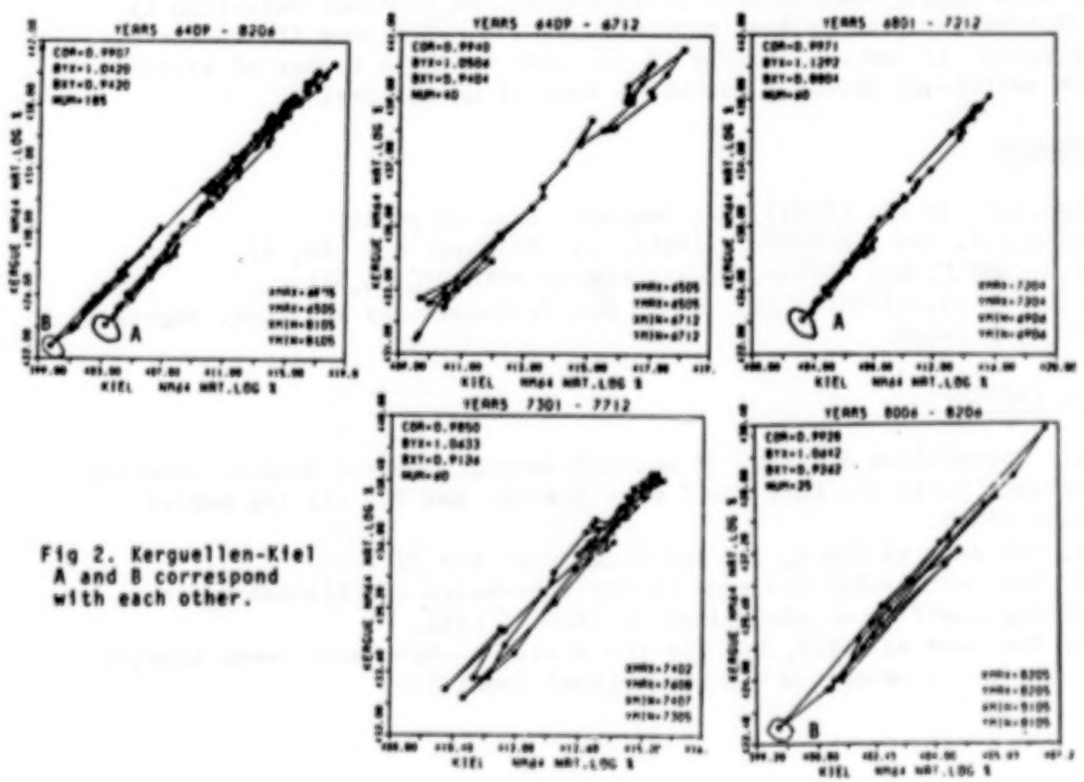


Fig 2. Kerguellen-Kiel
A and B correspond
with each other.

N85-35123

ORIGINAL PAGE IS
OF POOR QUALITY

SH 9.1-7

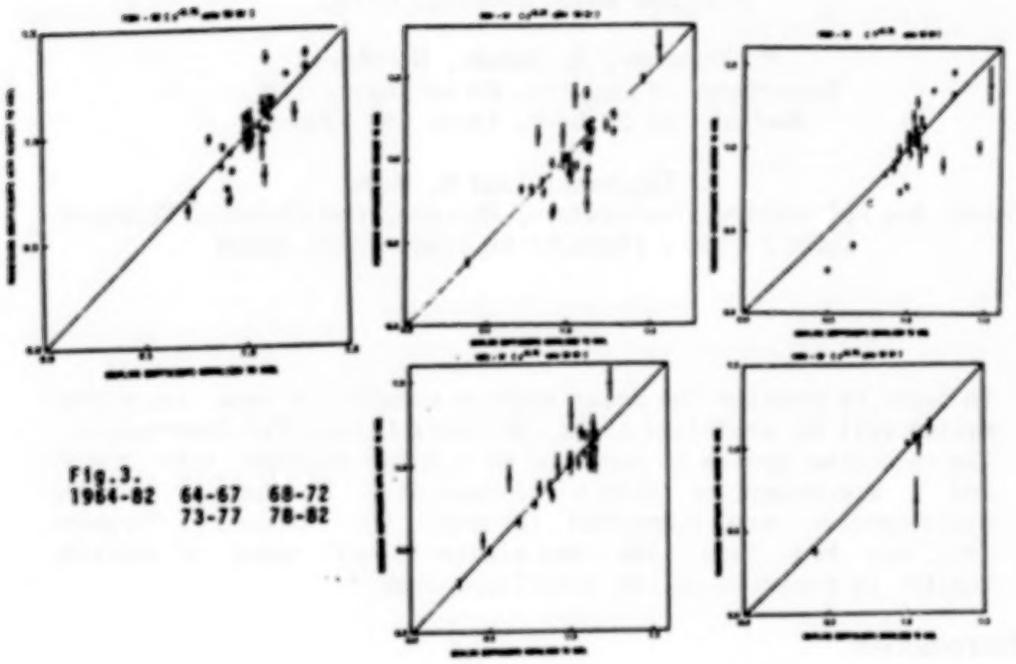


Fig.3.
1964-82 64-67 68-72
73-77 78-82

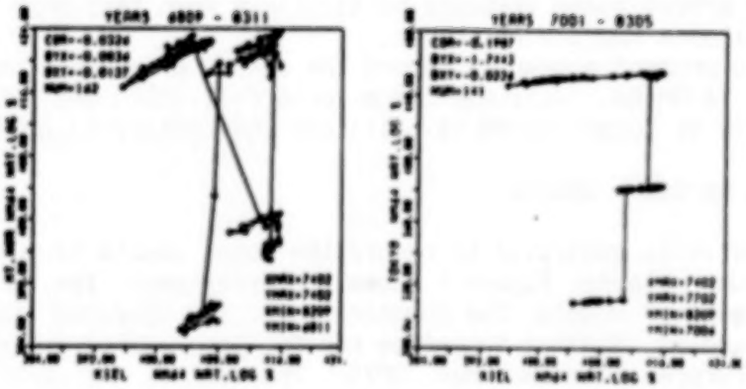


Fig.4.

N85-35123
SH 9.1-8

RECORDING SYSTEM FOR THE SOLAR NEUTRON MONITORING AT MT. NORIKURA

Yu Shao Hua
Institute of Space Physics, Academia Sinica,
P.O. Box 5112, Beijing, China

M. Kusunose, H. Sasaki, N. Ohmori
Department of Physics, Kochi University,
Akebono-cho 2-chome, Kochi 780, Japan

K. Takahashi, and M. Wada
Cosmic Ray Laboratory, Institute of Physical and Chemical Research,
Kaga 1-chome, Itabashi-ku, Tokyo 173, Japan

ABSTRACT

In order to monitor the solar neutron events, a new recording system will be installed at Mt. Norikura Cosmic Ray Observatory. The recording system is composed of a pulse counter with clock and a microcomputer with minifloppy disk. The counter and the microcomputer are connected through the General Purpose Interface Bus line. The one-minute total count of neutron monitor is recorded on the minifloppy disk.

1. Introduction

Direct observations of the solar neutrons associated with solar flares were made at the earth, on June 21, 1980 and June 3, 1982 by the Gamma-Ray Spectrometer (GRS) on board the Solar Maximum Mission satellite (SMM).[1,2] It was reported that, on June 3, 1982, the solar neutrons were also detected by the ground-based neutron monitors at Jungfraujoch,[2,3] Lomnicky Stit,[4] and Rome.[5,6] From the analysis of the Rome NM-64 data, Iucci *et al.*[6] analyzed that the solar energetic neutron events could be detected by ground-based stations particularly when they were located at mountain altitudes and low latitudes.

Here, we present a plan to record the output of neutron monitor at Mt.Norikura (4-NM-64, altitude=2770m, cutoff=11.36GV) and, if possible, simultaneously at Tokyo (36-NM-64, altitude=20m, cutoff=11.61GV).

2. Recording hardware system

This system is contrived to record the total counts from the neutron monitor in every minute. Figure 1 shows the arrangement for recordings of the neutron monitor counts. The counter/clock is operated through the IEEE-488 standard digital interface bus for programable instrumentation (or General Purpose Interface Bus, GPIB). The control of GPIB and the data acquisition is operated by an ordinary microcomputer.[7]

The interface between microcomputer and GPIB is made by using an LSI (TMS9914, Texas Instruments), and 4 MHz clock pulse is supplied from the microcomputer. The control of the counter/clock is operated through an interface LSI (SM8530B, Nippon Precision Circuits).

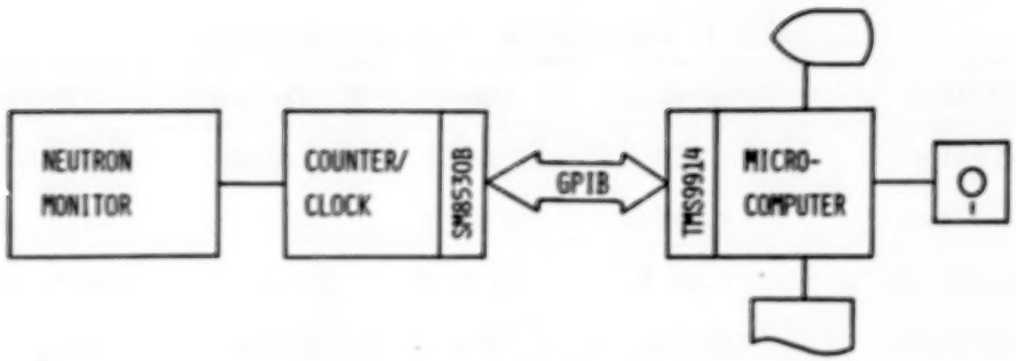


Fig.1. Blockdiagram of the recording system for the solar neutron monitoring.

3. Recording software system

The microcomputer is operated under the operating system of CP/M (Control Program for Microprocessors, Digital Research). The LSI TMS9914 that we used contains all of the logic necessary to interface TALK, LISTEN and CONTROL in accordance with GPIB. For the microcomputer, the control of GPIB means the read-and-write process to the various registers in the TMS9914. All programs which control the TMS9914, the floppy disk and the printer, are written in C language (C compiler by BD Software).

Figure 2 shows the flow chart of the operating program of the recording system. The counting rates of the neutron monitor in every one minute is transfered from the counter/clock to the memory of microcomputer, and written on the minifloppy disk in every ten minutes. Year, month, day, hour and minute are written at the beginning of the hour. The exchange of floppy disk can be operated between the ten minute recording. One block of data is composed of an hour data, which requires 128 bytes each. A sheet of floppy disk (in this case) can be operated for three months. The records on the floppy disk are transfered to a magnetic tape, and the data will be analyzed by using electronic computers.

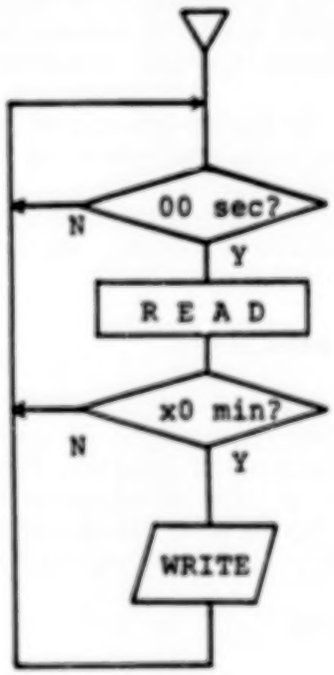


Fig.2. Flowchart of operating program.

Table 1. Distribution of neutron monitors.

Station	Jungfraujoch	Rome	Mt. Norikura	Tokyo
Monitor	IGY	12-NM-64	4-NM-64	36-NM-64
Latitude	46.55° N	41.91° N	36.11° N	35.75° N
Longitude	7.98° E	12.50° E	137.55° E	139.75° E
Altitude	3550 m	60 m	2770 m	20 m
Cutoff rigidity	4.48 GV	6.32 GV	11.36 GV	11.61 GV
Counting rates (Nov. 1977)	6.0×10^5 /hr	3.0×10^5 /hr	5.5×10^5 /hr	9.4×10^5 /hr

4. Discussion and Summary

As is seen in Table 1, Mt. Norikura station is located at an advantageous place, namely, mountain altitude, relatively low latitude, and different longitude from European stations. It is preferable that one minute record at Tokyo neutron monitor should be operated simultaneously to study the response and yield function for the solar neutron.

The features of the the recording system for the solar neutron monitoring are summarized as follows:

1) Using of the general purpose interface bus (GPIB) to facilitate the automatic data handling and also the alteration of the recording system.

2) By the adoptation of an ordinary microcomputer and the control and operation software in C language, it is easy to change operation system afterwards.

3) One minute count data from the neutron monitor are recorded on the minifloppy disk, which can endure for a long time record (in this case, three months).

5. Acknowledgments

One of the authors (YSH) had stayed for about three months at the Cosmic Ray Laboratory, Institute of Physical and Chemical Research and at the Department of Physics, Faculty of Science, Kochi University, and engaged in the development of the recording system of the solar neutron event. The authors are grateful to Mr. K. Kondo who is a student of Kochi University, for writing the control program mentioned in the text.

References

1) Chupp, E. L. *et al.*, (1982), Astrophys. J. (Letters), 263, L95.
2) Chupp, E. L. *et al.*, (1983), *Proc. 18th Int. Cosmic Ray Conf., Bangalore*, 10, 334.
3) Debrunner, H. *et al.*, (1983), *Proc. 18th Int. Cosmic Ray Conf., Bangalore*, 4, 75.

4) Kocharov, G. E., (1983), Invited talks, *8th E. C. R. Symp., Bologna*, Tecnoprint, 51.
5) Iucci, N. *et al.*, (1984), Detection of solar neutrons by ground-based neutron monitors, Preprint.
6) Iucci, N. *et al.*, (1984), *Proc. Int. Symp. on Moduration in the Heliosphere, Morioka*, 429.
7) Kusunose, M. *et al.*, (1984), Mem. Fac. Sci., Kochi Univ., Ser. B, 5, 19.

N85-35124

SH 9.1-9

BURST SIZE DISTRIBUTIONS IN THE DIGITIZED DATA OF THE ION CHAMBERS AT MT.NORIKURA AND SEA LEVEL STATIONS

M. Kusunose, M. Wada*, S. Kudo*, and L. S. Chuang**

Department of Physics, Kochi University,
Akebono-cho 2-chome, Kochi 780, Japan
* Cosmic Ray Laboratory, Institue of Physical and Chemical Research,
Kaga 1-chome, Itabashi-ku, Tokyo 173, Japan
** Department of Physics, The Chinese University of Hong Kong,
Shatin, New Territories, Hong Kong

ABSTRACT

A practical and simple method for burst rejection was applied to the digitized data of cosmic ray ion chambers at Mt. Norikura, Tokyo and Kochi. As a result of burst rejection, the burst size-frequency distributions in the digitized data at mountain altitude and sea-level ion chambers were obtained. The results show that there are no significant differences between the digital and analog data processing in the burst rejection.

1. Introduction

Cosmic ray ion chambers have been used for the continuous observation since the early days of cosmic ray studies. Five sets of Nishina-type ion chambers were built during the period from 1935 to 1941.[1,2] Continuous recording by those Nishina-type ion chambers had been started at Tokyo in 1948, Mt. Norikura in 1955, Hong Kong in 1970 and Kochi in 1979. At present, the digital recording systems for cosmic ray ion chambers[3,4] are in operation (see Table 1).

The burst distribution in ion chamber records is recognized from an abrupt change in charge up voltage. It is generated from a bremsstrahlung of muon or some nuclear interaction in lead absorber which covers the chamber to avoid undesirable radiation around the apparatus. Since the size of a burst sometimes exceeds total voltage variation in an hour, it should be rejected to reduce fluctuations. In this paper, we discuss on the burst rejection and the burst size distribution in the digitized data at Mt. Norikura, Tokyo and Kochi.

Table 1. List of Nishina type ion chambers in Japan

Station	Mt. Norikura	Tokyo	Kochi
Cutoff rigidity (GV)	11.36	11.50	12.88
Altitude (m)	2770	20	30
Atmospheric depth (g/cm^2)	740	1030	1030
Nishina type ion chamber	No.1	No.5	No.4
Argon gas pressure (kg/cm^2)	39	30	39
Electrometer output range (V)	30	10	10
Thickness of roof (g/cm^2)	20	10	120
Thickness of lead shield (cm)	10	10	10

2. Method of burst rejection

There is no *a priori* way of rejecting the burst data, since smaller bursts can not be distinguished from ordinary statistical fluctuations. As a method of burst rejection, Wada *et al.*[4] proposed to chose the threshold from the distribution, so that the average is not change.

Kusunose *et al.*[5] presented a practical method to separate bursts from the ordinary cosmic ray data on the assumption that the frequency of burst number per hour follows the Poisson distribution. We reduced the procedure of burst rejection, where the principle is the same as the previous method. The threshold of burst rejection is taken as $k_n\sigma_n$ (n=1,2,...), where σ_n are standard deviations and k_n are constants, which are determined so that the frequency of burst obeys the Poisson distribution. In the previous report, n was taken up to 10, now we reduce it to 3.

χ^2-test of the Poisson distribution was applied to the distribution of the burst frequency per hour. The results show fairly good fitness to the Poisson distribution except for a few cases. The distributions of one minute values as differences from averages of respective hours are shown in Fig.1. Curves A's are the distribution of one minute values due to ionization current of cosmic rays detected in the chamber, and B's are the distribution of the rejected burst values. As shown in the figures, both curves are separated each other reasonably.

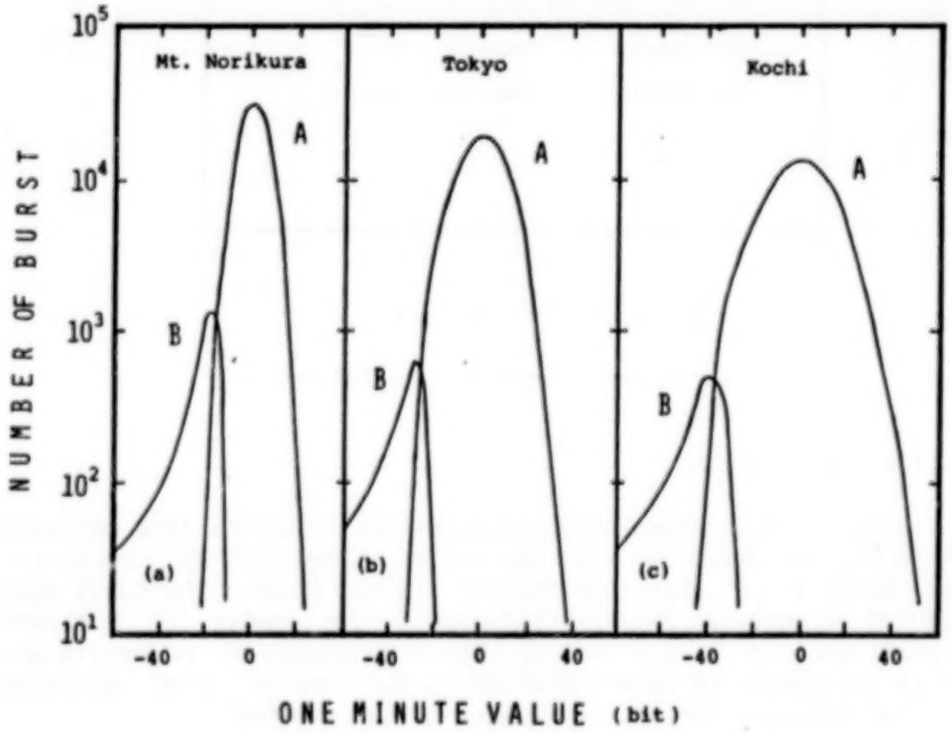


Fig. 1. Distribution of one minute values as deviation from the averages of respective hours at the period from May 24, 1980 to May 9, 1981.

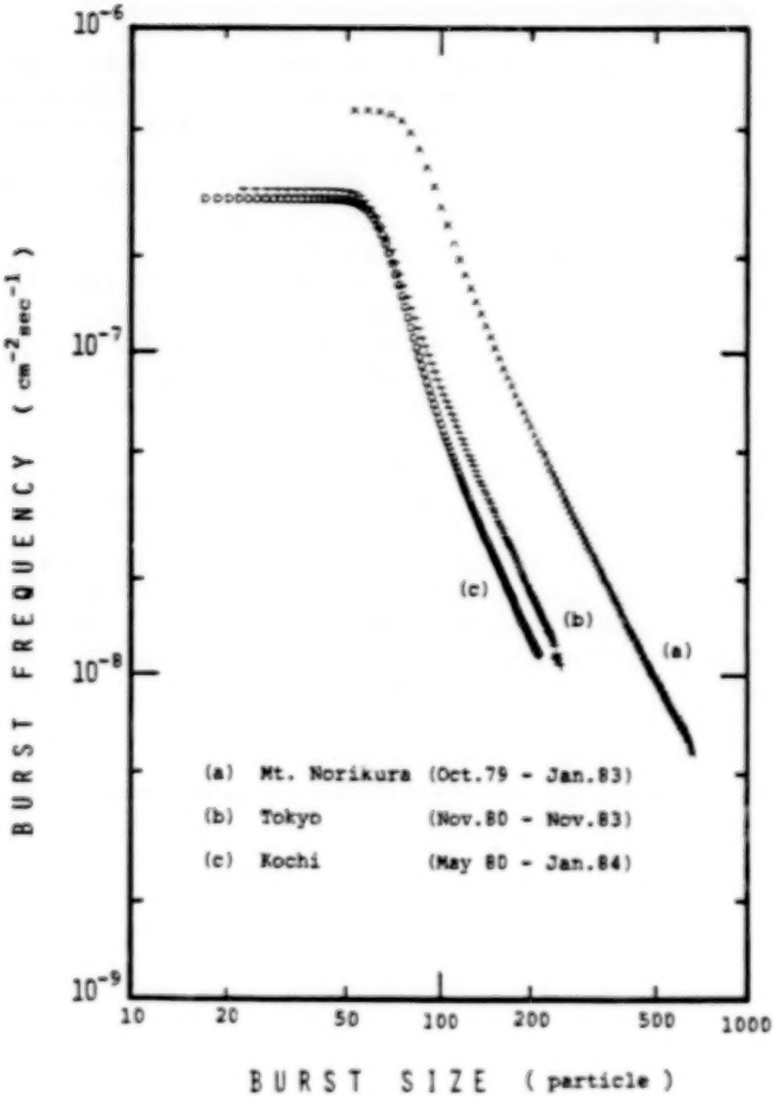


Fig. 2. Burst size-frequency distribution.

3. Burst size distribution

The integral size-frequency distributions of bursts thus obtained are shown in Fig. 2, where (a), (b) and (c) are those of Mt. Norikura, Tokyo and Kochi ion chamber respectively. In the figure, the burst size is represented in unit of particle that means the number of incident charged particles in a ion chamber. The frequencies of the bursts are indicated in the number of bursts divided by the time of total duration and by the horizontal cross-sectional area of the chamber.

The frequencies of the bursts at a point where the burst size is 200 particles, are shown as, 6.0×10^{-8} $cm^{-2}sec^{-1}$ at Mt. Norikura, 1.83×10^{-8} at Tokyo, and 1.35×10^{-8} at Kochi. The burst frequency at Mt. Norikura is 3.3 times that of Tokyo. According to Kameda and Wada[6], it means that considerable parts of the total bursts at sea level are those induced by N-components. The ratio of Tokyo to Kochi is found as 1.3. It will be

explained by the difference in the cutoff rigidities and the thickness of roof materials.

The burst frequency spectrum can be expressed partly by the form of power function as $S^{-\gamma}$, where S is the burst size in unit of particle. We calculated the power γ in the range of burst size from 150 to 220 particles by the least square method. The results are $\gamma=2.07\pm0.01$ at Mt. Norikura, $\gamma=2.09\pm0.01$ at Tokyo, and $\gamma=2.09\pm0.01$ at Kochi. There is no significant difference among them.

4. Summary

In summary, we separated one minute data of cosmic ray ion chamber into the ordinary cosmic ray data and the burst data by the statistical way under the assumption that the number of bursts in one hour follow the Poisson distribution. The merit of this method is capable of testing the appropriateness of burst rejection by application of χ^2-test on the Poisson distribution.

As a result of the burst rejection, the distributions of burst size-frequencies were obtained. The differences of burst size spectrum bwteen Mt. Norikura and sea level ion chambers are generally in coincidence with the results of Kameda and Wada.

5. Acknowledgments

The observations at Mt. Norikura were made in cooperation with the staffs of the Norikura Cosmic Ray Station (by Prof. I. Kondo) of the Institute for Cosmic Ray research, University of Tokyo. The compilation of the data of Tokyo-Itabashi was performed by Mrs. K. Imai. Computer works were performed by using M-380, M-140F, and F270-30.

References

1) Ishii,C, (1944), Bull. I. P. C. R. (in Japanese), **23**, 535.
2) Miyazaki, Y., (1954), J. Sci. Res. Inst., **48**, 80.
3) Chung, L. S. *et al.*, (1981), *Proc. 17th Int. Cosmic Ray Conf., Paris*, **8**, 154.
4) Wada, M. *et al.*, (1982), Nucl. Instr. Meth., **200**, 457.
5) Kusunose, M. *et al.*, (1984), Mem. Fac. Sci., Kochi Univ., Ser. B, **5**, 15.
6) Kameda, T. and M. Wada, (1952), Prog. Theor. Phys., **7**, 1.

SH 9.1-10

N85-35125

SENSITIVITY OF SINGLE AND MULTIPLE COSMIC RAY NEUTRONS TO THE SURROUNDING MEDIUM IN A LEAD-FREE MONITOR

Dorman I.V., Dorman L.I., Libin I.Ya.
Institute of Terrestrial Magnetism, Ionosphere and Radio Wave Propagation, USSR Academy of Sciences, I42092 Troitsk, Moscow Region, USSR

Korotkov V.K.
SVKNII, Magadan, USSR

In I98I-I985 the neutron component of cosmic rays was recorded, the effect of cosmic ray multiplication in lead being disregarded /I-2/. The recording device consisted of neutron counters placed in a polyethylene retarder (polyethylene tubes with wall thickness of 2 cm). The device registered neutrons formed directly on the surface or not deep underground; the intensity of neutrons depended on the chemical composition of the substance.

The neutron component was measured by a lead-free monitor in an expedition in the Moscow Canal, Belomor-Baltic Canal and in the Atlantic Ocean. Figure I presents the time variation of 5-minute data of the intensity obtained in the Belomor-Baltic Canal and in the Atlantic Ocean relative to the mean value in the open sea (in %, Fig.I b). The intensity is seen to increase considerably when cosmic rays pass through locks and ports. In different locks the amplitudes of the effect are different which is due to the difference in the depth, in the geometry of the locks, and in the chemical composition of the shore substance.

The observed intensity increases due to recording of additional neutrons formed in nuclear interactions in the shore substance. These neutrons leave the nucleus at the evaporation stage, and the larger the mass number of the nucleus, the more the amount of evaporating neutrons for a given energy of an incident particle. Thus, it seems possible to use the method of recording multiplicities for the determination of substance composition since these neutrons can be considered as multiple. The possibility of their recording is much smaller than in local-generation detectors because of a large distance from the place of their formation to the place of recording. For this reason the counting level for multiplicity $k = 2$ is not high relative to the total count and is negligibly small for higher multiplicities. Nonetheless, since the increase in the count is just due to multiple neutrons, it is reasonable to record multiplicities.

Besides the total intensity, the multiplicities were al-

ORIGINAL PAGE IS
OF POOR QUALITY

so recorded in the Belomor-Baltic Canal. Along with intensity variations δI, Fig.I demonstrates the $\delta I_{>2}$ time dependence of δI, which is the multiple neutron intensity variation for multiplicity $k = 2$ and the mean multiplicity k for the time of passing through the Canal (from 5-minute data). The results of these measurements show a synchronous variation in the level of count of I and $I_{>2}$. But if the increase of the intensity I in locks makes up on the average 20-30 %, for multiplicities $k \geq 2$ the increase reaches 2000-3000 %. This difference confirms the fact that the intensity increase in locks is due to recording of neutrons formed in interactions between cosmic rays and lock-wall or shore substance nuclei. (In the open see this effect is relatively small - the rate of counting of $I_{>2}$ is about 3 pulses per 5 minutes). Thus, the data on the multiplicities are many times more sensitive to the influence of the environment than the data on the total intensity, the rate of counting multiple neutrons formed in CR - air interactions being negligibly small. Standard deviations in locks for δI and $\delta I_{>2}$ make up 2 and 300 %, which in the relative units make up about 8 and II %, respectively. Therefore, in spite of the small rate of $I_{>2}$ count, the accuracy in determining the variation $\delta I_{>2}$ is comparable with the accuracy of determining the intensity variations. Thus, the information on the surrounding medium is more complete if neutrons are recorded by both methods. Because of its smallness, the mean multiplicity does not react to the surrounding medium since statistic fluctuations overlap possible variations.

The influence of the chemical composition of the surrounding medium on multiplicity distribution is of considerable interest. Within the statistical error of measurements the multiplicity distribution for a lead-free neutron monitor is exponential, $I_K \sim \exp(\alpha K)$ (Fig.2), the parameter α depending on the position of the neutron monitor; in locks with rocky shores (Fig.2, curve I) $\alpha = 3.70 \pm 0.08$; in locks with ordinary ground (curve 2) $\alpha = 4.00 \pm 0.10$; between locks with a distance to the shores of 4-8 m, $\alpha = 4.11 \pm 0.11$ (curve 3); in the open see $\alpha = 7.0 \pm 0.6$ (curve 4). In locks with rocky shores (Fig.I, locks N 6-9) α decreases, in locks with ordinary groung such a decrease is not observed. In the open see the intensity $I_{>2}$ makes up only 0.I % of the total intensity which is responsible for a corresponding maximum value of α. (It should be noted that the riverside effect on the intensity makes up I0-20 % if the distance to the banks is I0-I5 m. As the distance increases to I00 m, the riverside effect vanishes and the data on the intensity correspond to those obtained in the open see).

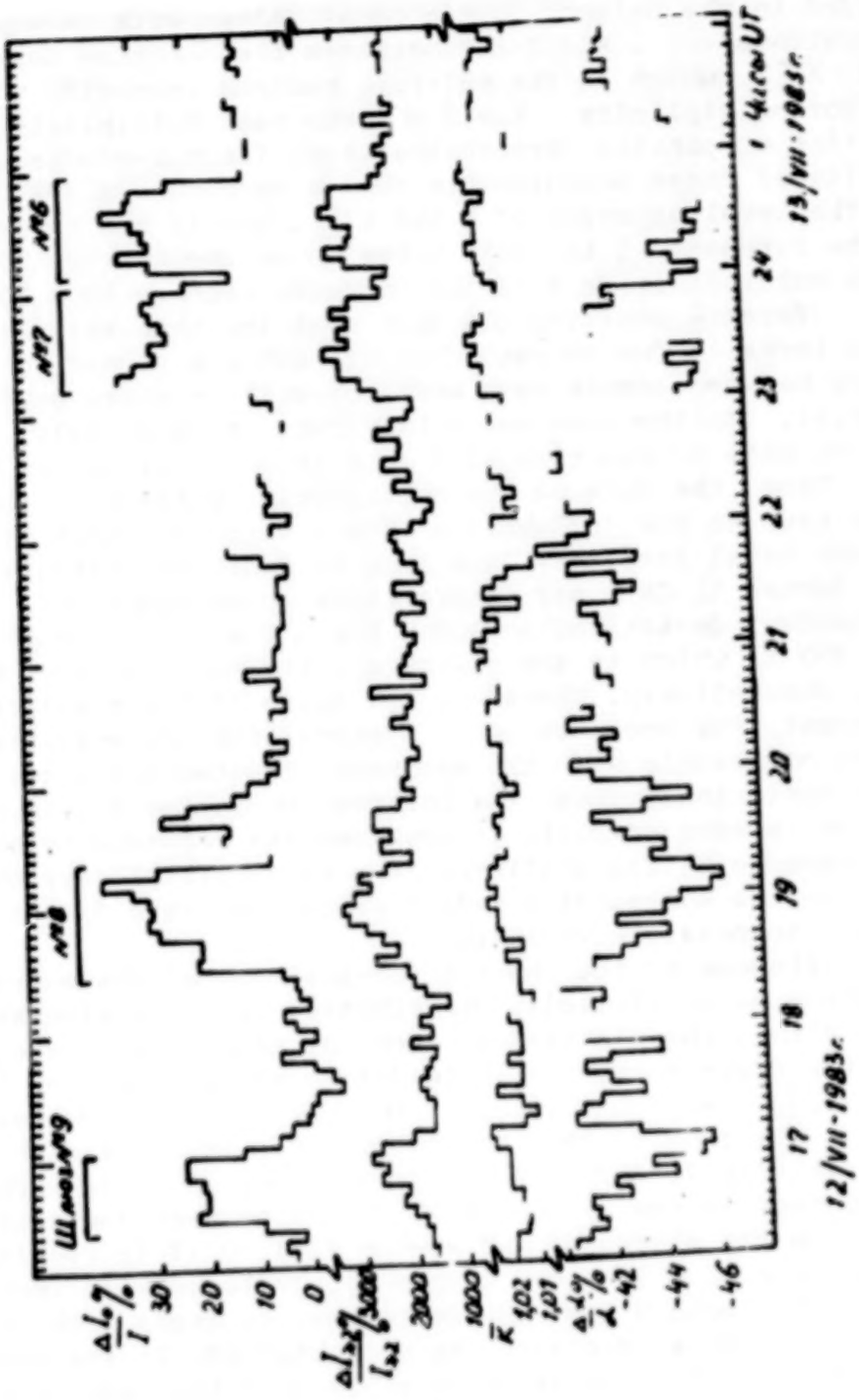


Fig.1

REFERENCES

1. Dorman L.I. Cosmic Ray Variations. M.: Gostekhteoretizdat, 1957, p.492.
2. Babayan V.Kh., Mashkov Yu.E., Ptuskin V.S. in: Cosmic Rays. M.: Nauka, 1983, p.66.

N83-33156

ORIGINAL PAGE IS
OF POOR QUALITY

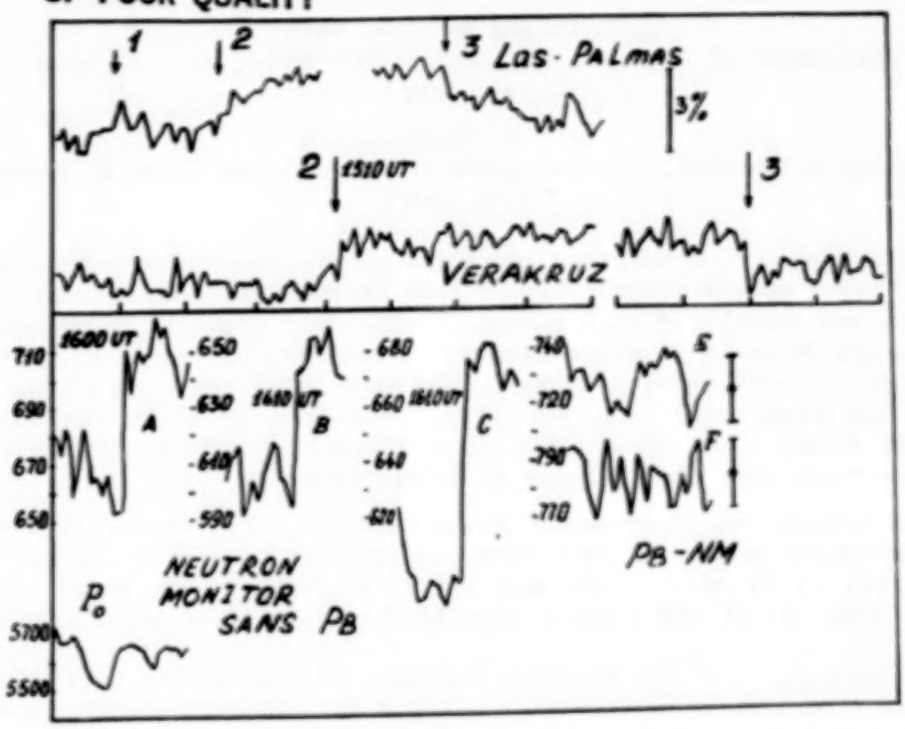


Fig. 2

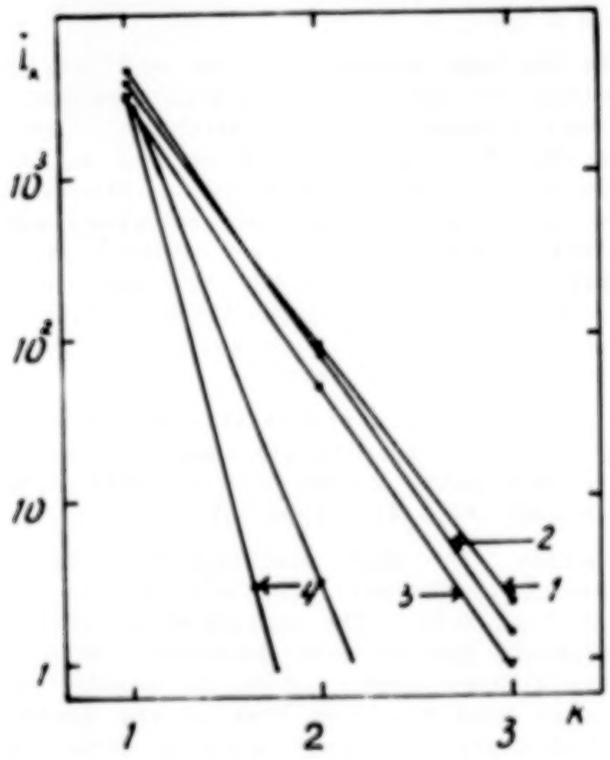


Fig. 3

N85-35126
SH 9.1-11

PLASTIC SCINTILLATORS IN COINCIDENCE FOR THE STUDY OF MULTI-PARTICLE PRODUCTION OF SEA LEVEL COSMIC RAYS IN DENSE MEDIUM

L.S. Chuang and K.W. Chan
Department of Physics, The Chinese University of Hong Kong
Hong Kong

M. Wada
Cosmic Ray Laboratory, The Institute of Physical and Chemical Research
Tokyo, Japan

1. Introduction. Cosmic-ray particles at sea level penetrate a thick layer of dense medium without appreciable interaction. These penetrating particles are identified with muons(1). The only appreciable interaction of muons are by knock-on processes(2). A muon may have single, double or any number of knock-on with atoms of the material so that one, two, three or more particles will come out from the medium in which the knock-on processes occur. The probability of multi-particle production is expected to decrease with the increase of multiplicity.

The present report presents measurements of the single, double, and triple particles generated in a dense medium (Fe and Al) by the sea level cosmic rays at 22.42 N. Lat. and 114.20 E. Long. (Hong Kong) using a detector composed of two plastic scintillators connected in coincidence.

2. Experimental. The detector consists of two units, each of which comprises a plastic scintillator, 1 m^2 x 5 cm, and an RCA-8055 (ϕ = 12.7 cm) photomultiplier tube installed in a light-tight iron case as shown in Fig. 1. A block diagram of the counting system is also shown in Fig. 1. The whole system is installed in a room where the room temperature is kept within 20 ± 1°C.

By adjusting the high voltages and the amplifier-gains, differential pulse height spectra for each of the detector systems, as shown by curve (A) in Fig. 2, were brought to nearly matching. Then, setting the high voltages and the amplifier-gains at the optimum values and the SCA discriminator of the upper detector fully open, coincidence measurements of the signals from the upper and the lower detectors were made by varying the SCA discriminator level of the lower detector with the channel width 0.1 V. A suitable resolving time of the coincidence unit was chosen to be 0.5 μs so that the accidental coincidence counts were always negligibly small (i.e. less than 0.01 cpm against a counting rate of about 1000 cpm in each of the two detectors.

Keeping the two detector surfaces 11.7 cm apart and having the dense medium, Fe or Al slabs, of varying thicknesses placed between the detectors, the coincidence pulse height spectra were measured for each of the varying conditions (Fig. 2; curves (B)).

With Fe-absorber, the peak positions for triple-particle spectra are clearly appearing in the multi-particle spectra, e.g. at discriminator level 2.48 in Fig. 3(B). The corresponding peak area, however, can hardly be determinable due to poor counting statistics. Existence of triple-particle is further confirmed by the nearly equidistances of the triple-particle peak position from that of the double-particle (ΔL = 0.76) and the double-particle peak position from that of the single-particle (ΔL = 0.72). (Fig. 2(B) and 3(B))

ORIGINAL PAGE IS
OF POOR QUALITY

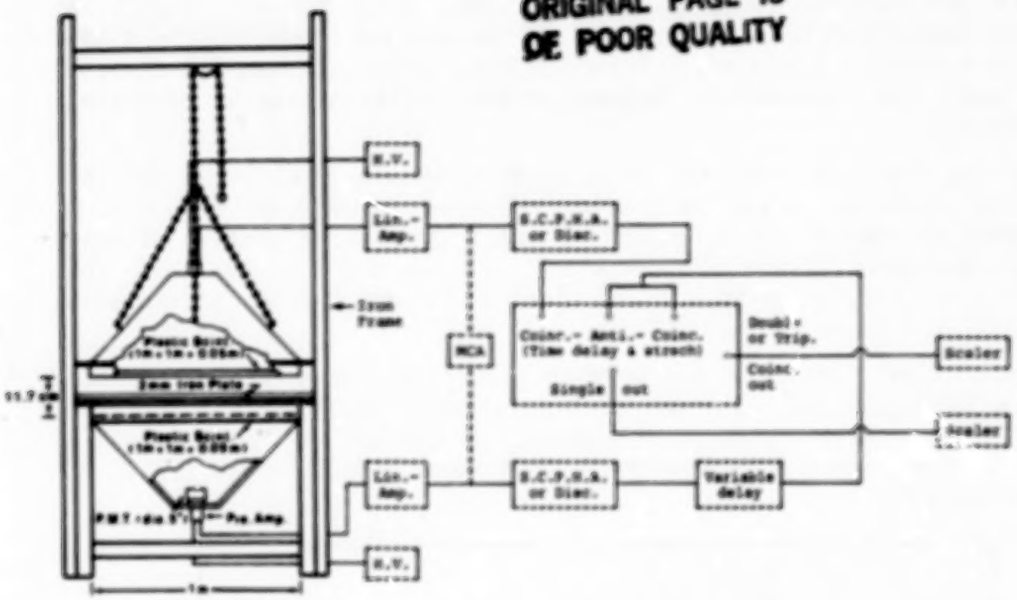


Fig. 1 The detector and the counting system.

The same procedures as above were applied in the measurements using Al-absorber of thicknesses 1.28 - 5.29 cm. None of the four absorption curves obtained gave good linearity to be able to obtain the absorption coefficient. Inspection by superpositions of the spectra for the four different absorber thicknesses with the single-particle spectrum reveals the poor absorption power of Al-absorber - little evidence of absorption or with irregularities, if any, in the multi-particle free portion and also in the portion where multi-particle contribute. This is thought to be due to very poor absorptivity and thus poor productivity for multi-particle of Al-absorber in the present experimental conditions.

3. Data analysis and Results. Each of the five pulse height spectra resulting from coincidence measurements, Fig. 2(B), is expected to be a result of superpositions of the multi-particle pulse height spectra over the single-particle spectrum.

To obtain the multi-particle spectra, the single particle spectrum (This spectrum too is superposed with multi-particle spectra due to the 0.4 cm thick Fe medium making up the surfaces of the detector housings) which has been corrected for absorption in the absorber is used for subtraction from the experimental spectrum which is placed with an absorber. An exponential form of absorption is adopted with reference to the nature of absorption of charged particles in passing through matter. In the lower pulse heights region, i.e. where the discriminator levels are smaller than that for the peak point of the spectrum, effect of multi-particle is absent. In this region, we have $\ln(I_0(L)/I(L)) = \mu(L - L_0)$ (where $I_0(L)$ and $I(L)$ are the coincidence counting rates of the single-particle, with pulse height L, before and after passing through the absorber, and μ is a linear absorption coefficient of the absorber for the sea level cosmic-ray particles. L_0 is a threshold discriminator level which is a constant of the system). From the plots of $\ln(I_0(L)/I(L))$ versus $(L - L_0)$ for the various absorber thicknesses, e.g. Fig. 3(A), the

slopes μs are obtained with an average value 0.15 ± 0.06. Once μ is known, the multi-particle spectra can be determined from $I(L) - I_o \exp(-\mu(L-L_o)) = I_2(L) + I_3(L) + \ldots$ (where $I_2(L)$, $I_3(L)$ ..., are the double-triple-, and the successive higher order multi-particle spectrum, respectively.)

Defining the peak area (K) as a product of the peak value and the FWHM of the peak, we obtain an average value of (K_d/K_s) as 0.07 ± 0.01 for Fe-absorber (where the subscripts d and s denote for double-particle and single-particle, respectively) which is identical to say that the probability of double-particle production in Fe-absorber of thicknesses ranging 0.65 - 4.97 cm is 0.07 ± 0.01.

To the single-particle spectrum, a Gaussian curve is fit to the single-particle portion. The difference between the experimental curve and this hypothetical curve is considered as due to the multi-particle spectra. A remarkable double-particle peak with a value 0.07 for K_d/K_s is also obtained.

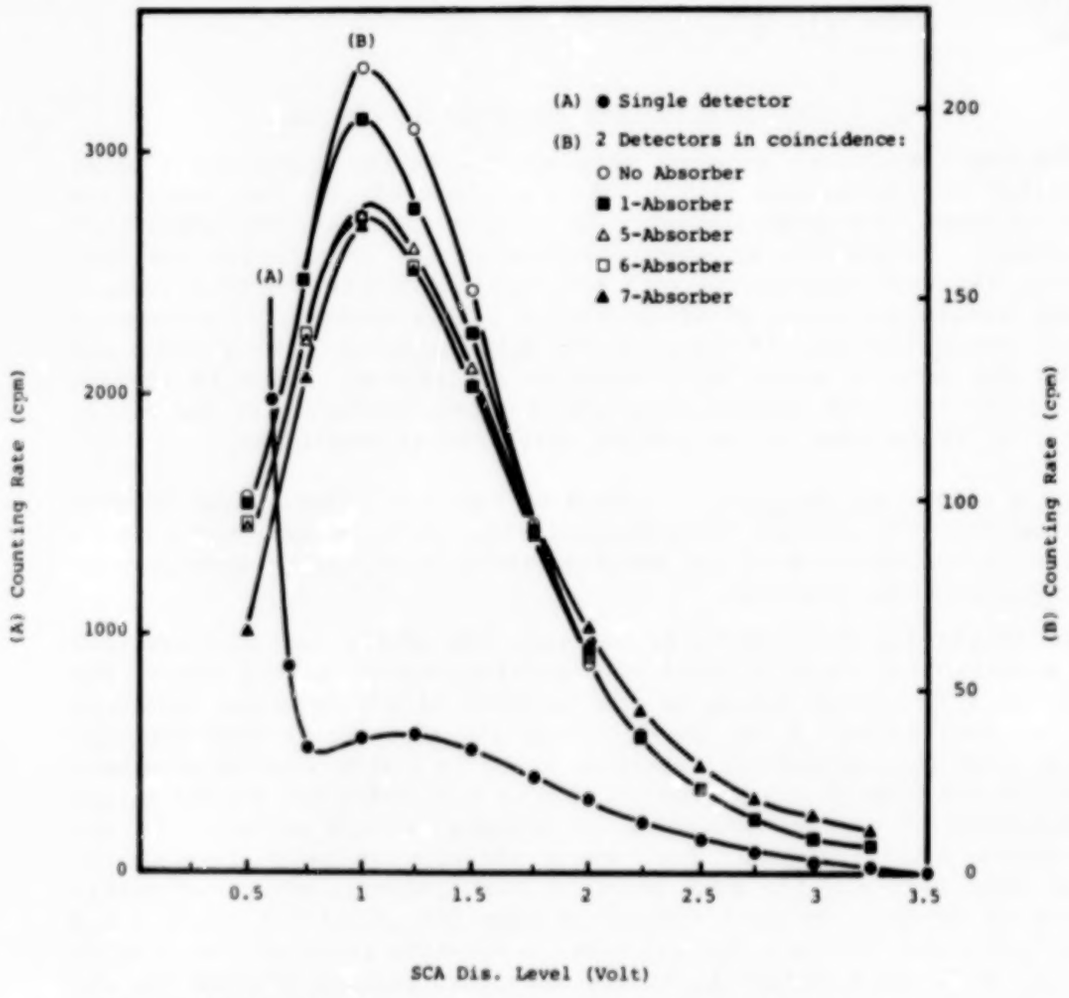


Fig. 2 Pulse height spectra: (A) taken with single detector (B) taken with upper and lower detector in coincidence (Dis. levels: upper fully open; lower varied from 0.5 to 3.25 with channel width 0.1 V).

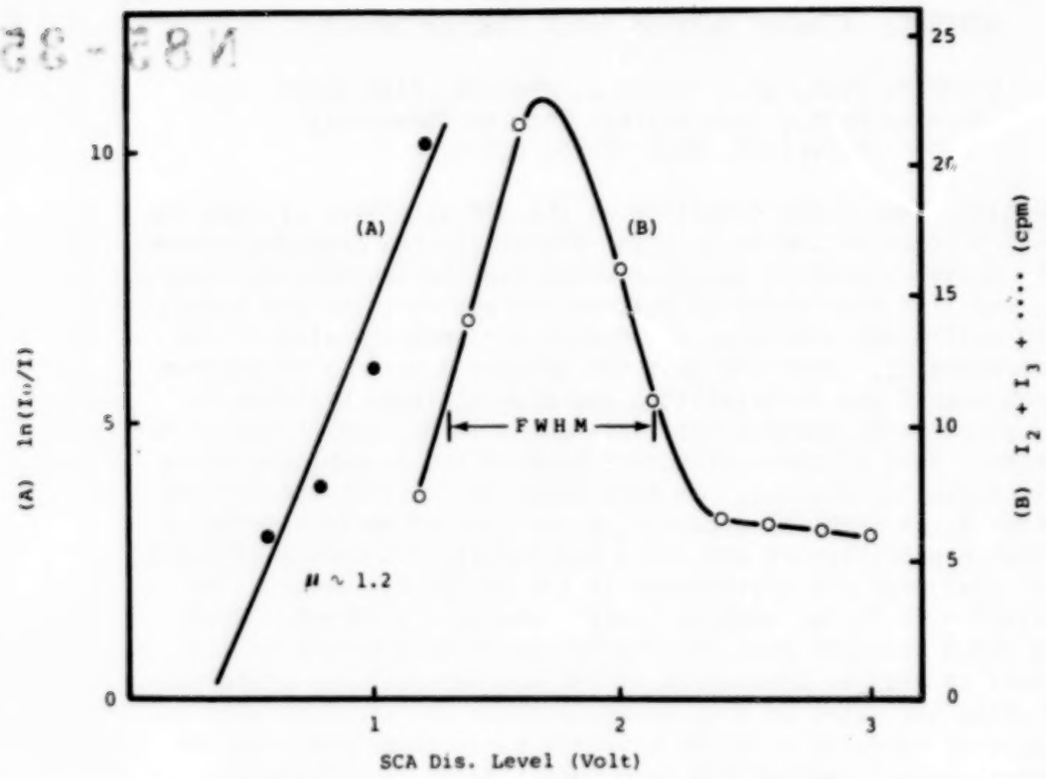


Fig. 3 (A) Absorption curve for single-particle in Fe.
(B) Double-particle peak and triple-particle component seen at Dis. level 2.3 - 3.0.

4. Discussion. The average value 0.07 ± 0.01 for the probability of double-particle production per muon (i.e. one knock-on process) in Fe-absorber of thicknesses 0.4 to 4.97 cm, which is negligibly small as compared to the range of sea level muons in Fe-absorber (e.g. 71 cm of Fe for muon with momentum 1000 MeV/c(3)) seems reasonable from the following comparisons with theoretical information: Taking the value 0.07 per g cm^{-2} to be the probability of double-particle production (one knock-on process) in Fe medium the agreement with the theoretical calculation of 0.14 per g cm^{-2} in Fe medium(4) for muons with the average momentum of sea level muons, 3500 MeV/c(5), is rather good. Present result for the average value of energy transfer per knock-on is estimated to be about 29 MeV with the rate of energy loss in Fe medium by 3500 MeV/c muons taken as 2 MeV per g cm^{-2}(3). While, the calculated maximum transferable energy per knock-on is 545 MeV.

References

1. Hayakawa, S., Cosmic Ray Physics, Interscience, John Wiley & Sons, New York, 318 (1969).
2. Bhabha, H.J., Proc. Roy. Soc. A154, 195(1936).
3. Rossi, B. and Greisen, K., Rev. Mod. Phys. 13, 240(1941).
4. Hayakawa, S., (1969), Cosmic Ray Physics, Interscience, John Wiley & Sons, New York, 412.
5. Kocharian, N.M., et al., J. Exp. Theor. Phys. USSR, 30, 243(1956). Janossy, L., Cosmic Rays, 2nd Ed., Oxford at the Clarendon Press, 172(1950).

SONTRAC: A Solar Neutron Track Chamber Detector

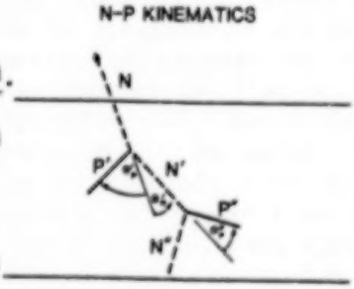
N85-35127

Glenn M. Frye, Jr., Thomas L. Jenkins, Alan Owens
Physics Dept., Case Western Reserve University
Cleveland, Ohio 44106, U.S.A.

1. Introduction. The recent detection on the SMM satellite of high energy neutrons emitted during large solar flares (1) has provided renewed incentive to design a neutron detector which has the sensitivity, energy resolution, and time resolution to measure the neutron time and energy spectra with sufficient precision to improve our understanding of the basic flare processes. Over the past two decades a variety of neutron detectors has been flown on satellites and high altitude balloons to measure the atmospheric neutron intensity above 10 MeV and to search for solar neutrons. Most of these detectors have relied on n-p scattering as the basic detection process. In this paper we describe the SONTRAC (Solar Neutron Track Chamber) detector, a new type of neutron detector which utilizes n-p scattering and has a sensitivity 1-3 orders of magnitude greater than previous instruments in the 20-200 MeV range. The energy resolution is 1% for neutron kinetic energy, $T_n > 50$ MeV. When used with a coded aperture mask at 50 m (as would be possible on the space station) an angular resolution of $\sim$4 arc sec could be achieved, thereby locating the sites of high energy nuclear interactions with an angular precision comparable to the existing x-ray experiments on SMM.

The scintillation chamber has been investigated as a track chamber for high energy physics, either by using arrays of scintillating optical fibers or by optical imaging of particle trajectories in a block of scintillator. Recently square plastic scintillation fibers 0.2 and 0.1 mm in size have been developed (2), which makes it possible to construct a block of plastic scintillator composed of alternate layers of x and y oriented fibers in which the range and direction of proton recoils from n-p scattering can be determined with a spatial resolution of approximately 0.1 mm. The 4π geometry and high spatial resolution make possible the enhanced detection efficiency and energy resolution over existing techniques.

2. Detection Efficiency and Energy Resolution. Neutrons interact in plastic scintillator either by elastically scattering from hydrogen or by interacting with carbon (n-C). The n-p events (Fig. 1) are the most useful. If the source is a point source and its direction is known, measurement of the energy and direction of the recoil proton in a single scattering is sufficient to determine the incident neutron energy. For a double scattering event where the energies and directions of both recoil protons are measured, the energy and direction of the incident neutron are uniquely determined. Thus double scattering events can be used to measure the neutron intensity from an extended source such as the secondary neutrons produced in the atmosphere



SINGLE SCATTER:

$$T_n = T_p' / \cos^2\theta_p' = T_p' / \sin^2\theta_n'$$
$$\theta_p' + \theta_n' = \pi/2$$

DOUBLE SCATTER:

$$T_n' = T_p'' / \cos^2\theta_p'$$
$$T_n = T_p' + T_n'$$
$$\vec{P}_n = \vec{P}_p' + \vec{P}_n'$$

Fig. 1. The kinematics for n-p scattering.

by the primary cosmic radiation. When a localized source such as the Sun is observed, the background is greatly reduced by restricting the accepted events to a cone about the solar direction. The interpretation of single and double tracks in plastic scintillator is complicated by (n,p) and (n,d) reactions in carbon. Fig. 2 shows the effective cross sections for $^{12}C(n,p)$ + $^{12}C(n,d)$ for proton kinetic energies T >10 and 15 MeV. Above 90 MeV the inelastic carbon cross section is an upper bound. The effective n-p scattering cross sections for the same threshold were calculated using the angular distribution parameterization of Rindi et al (3). Below 50 MeV n-p scattering predominates and single scattering can be used. Above 50 MeV, where the sum of the effective carbon cross section is larger than the effective n-p cross section, the kinematic criterion that $\Theta_p' + \Theta_n' = 90^o$ identifies the double scattering events in which the first proton is from an n-p scatter. Above about 200 MeV most of the interactions will result in the emission of several particles from carbon which can be used to infer the neutron energy. SONTRAC's performance therefore is characterized by three interaction modes. The energy ranges over which these modes are applicable overlap, thereby providing a check of internal consistency.

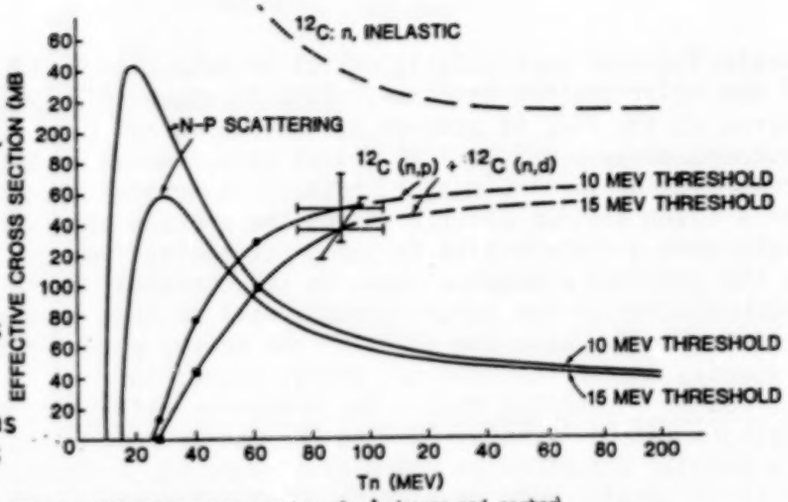


Fig. 2. Effective cross sections for hydrogen and carbon.

A. Single Scattering Mode. The detection efficiency in the single scattering mode is shown in Fig. 3 for an infinite slab of CH of various thicknesses where the neutron direction is normal to the slab and the proton track stops within the slab. The curves reflect the initial rise above the threshhold energy, the decrease in the n-p cross section with energy, and an increase in slope above 100 MeV as tracks are increasingly lost out the bottom. The corrections for loss of tracks out the sides of a finite size detector are small. For a cube 60 cm on a side, the efficiency is reduced by 2.7% at 100 MeV and 9.5% at 200 MeV. The high efficiency in the 15-40 MeV region where n-C contamination is low makes the single

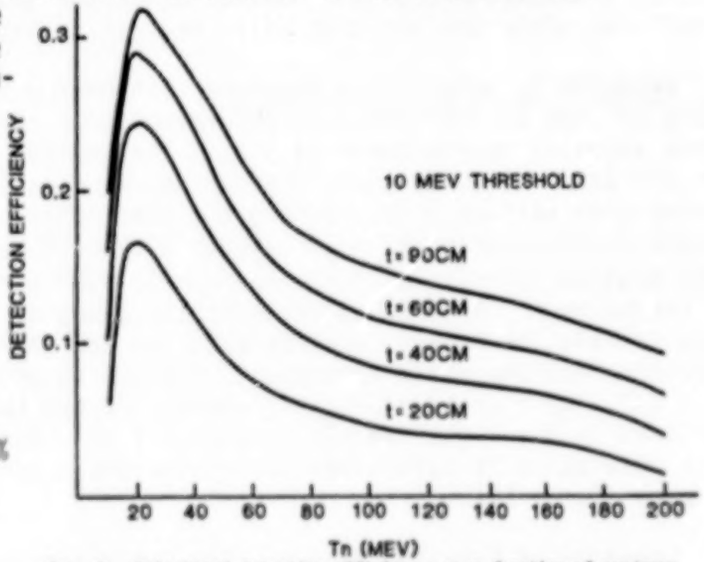


Fig. 3. Calculated detection efficiency as a function of neutron energy for an infinite slab of CH in the single scattering mode.

scattering mode particularly useful in determining the low energy portion of the solar neutron spectrum. This is especially important for small flares as the flux is reduced by neutron decay; e.g. 93% of the 20 MeV neutrons decay over the 1 AU flight path. Above 50 MeV the effective cross section for $^{12}C(n,p) + {}^{12}C(n,d)$ is greater than for n-p scattering. For a given neutron kinetic energy the protons observed at a particular angle have a distribution in energy extending from the maximum permitted by the reaction kinematics down to the threshold energy. In practice the deconvolution of the carbon protons will be less precise than that of the proton recoils where the width of the energy point spread function is due primarily to the instrumental energy resolution.

B. Double Scattering Mode. The detection efficiency for the double n-p scatters can be found by folding the single scattering results with the n-p angular distribution. The efficiency for a 60 cm thick infinite slab is 2% or greater over most of the 25-100 MeV range and > 1% for $T_n < 200$ MeV. This is two orders of magnitude greater than previous double scattering detectors where the energy and direction of both recoils were determined. Of comparable importance is the use of the 90° criterion to identify the first scattering as n-p. The neutron energy is given by $T_n = T_p/\sin^2\theta_n'$ and the uncertainty by $\Delta T_n/T_n = [(\Delta T_p'/T_p')^2 + (2\cot\theta_n'\Delta\theta_n')^2]^{\frac{1}{2}}$. The second term is small because $\Delta\theta \sim 10^{-3}$. For $T_n > 50$ MeV, the predominate contribution to ΔT_n comes from the straggling in the proton range; therefore $\Delta T_p/T_p < 1\%$. The second proton may result from n-C rather than n-p without affecting the above analysis for solar neutrons. However if the source direction is unknown, the contamination of n-C protons will introduce an additional contribution to ΔT_n. The energy and directional resolution can be determined by a Monte Carlo simulation or by an accelerator calibration of the instrument.

C. Calorimeter Mode. At 100 MeV the n-C inelastic cross section is a factor of three greater than the n-p cross section, increasing to a factor of six at 300 MeV. Although some of this energy escapes in secondary neutrons or γ's and the various possible reactions have different Q values, a measurement of the ionization of the secondaries and/or their ranges can yield the incident solar neutron spectrum.

3. Response to Solar Flare Neutrons. The energy spectrum of the solar flare of June 3, 1982 has been determined over the range 20-1000 MeV in three separate observations (4,5,6). The neutron fluence for 20-200 MeV was 500 cm^{-2}. A 60 cm cubic SONTRAC detector would detect 5×10^4 events spread over half an hour. During the same interval the atmospheric background could contribute $\sim 10^2$ events within 5° of the sun. Thus a flare with neutron emission 10^{-3} of the June 3, 1982 event would be detectable at the 5σ level. Also of interest in the study of solar flares is the time correlation between neutron emission and the time structure of flare emitted electromagnetic radiation. The timing uncertainty is given by $\Delta t = (\Delta T_n/T_n)\,\tau\,(\gamma+1)^{-1}(\gamma^2-1)^{-\frac{1}{2}}$, where γ is the Lorentz factor and $\tau = 500$s is the light transit time over 1 AU. For $T_n = 100$ MeV, $\Delta t = 3$s. This resolution is sufficient to resolve the 1 min time structure seen on some flares (4).

4. Location of Emission Region. The coded aperture mask technique has recently been applied to the imaging of high energy electromagnetic radiation. The complications introduced by a finite mask thickness and

only partial absorption in the mask have been considered in a similar context for high energy γ-ray astronomy (7), Because SONTRAC locates the neutron in the detector to an accuracy of 0.1 mm, the method is also applicable to the imaging of neutrons with an angular resolution determined by the pinhole geometry, as long as the mask cell size is large compared to the spatial resolution of the detector. For a cell size of 1 mm and a mask-detector separation of 50 m, the angular resolution is 4". At 50 MeV 10 cm of Fe gives 90% absorption. The mask vignetting angle of 0.6^{0} is greater than the angular width of the Sun; thus the entire solar disk can be imaged with comparable resolution.

5. Discussion. SONTRAC has the sensitivity and energy resolution to measure the temporal neutron energy spectrum from solar flares over a dynamic range of 10^3. This capability will make possible precision neutron measurements on a large number of flares during the next solar maximum. Determination of the neutron spectra for many flares will provide information on the statistics of ion acceleration, the acceleration time, the ion energy, the He content of the ions, the time dependence of the ion spectra, and possible beaming of the accelerated ions.

Observations of solar neutrons are best done from a satellite, since the long observing time makes it possible to detect a large number of flares in a low background environment. SONTRAC meets the criteria recommended for the neutron detector in the High Energy Cluster on the Advanced Solar Observatory (8). In the past it has not been practical to observe large flares from balloons because the flight times were at most of a few days duration and predictions of the flare time of occurrence were not reliable enough to give a reasonable probability of observation. Recently the RACOON technique has made it possible to obtain flights of several weeks duration (9). It has been found during the present solar cycle that large flares exhibit a 154 day periodicity (10) The combination of longer flight duration and cyclic flare occurrence make balloon observations of solar flare neutrons feasible. Flare observations from balloons have an advantage over satellites in that the 12 hr/day observation window is long compared to the flare duration. Therefore most flares will be observed in their entirety even though the neutrons are delayed in their arrival at the earth relative to the E-M radiation.

References

1. Chupp, E.L., et al, (1982), Ap. J. Ltts 263, L95.
2. Binns, W.R., et al, (1983), Nuc. Instr. Meth. 216, 475.
3. Rindi, A., et al, (1970), UCRL-20295.
4. Chupp, E.L., et al, (1983), 18th Int. Conf. CRP 4, 374, Bangalore.
5. Debrunner, H., et al, (1983), 18th Int. Conf. CRP 4, 75, Bangalore.
6. Evenson, P., et al, (1983), Ap. J. 274, 875.
7. Carter, J.N., et al, (1982), M.N.R.A.S. 198, 33.
8. Walker, A.B.C., et al, (1984), The Adv. Solar Obs. Exe. Sum. NASA GPO 1984-746-070/179.
9. Koga, R., et al, (1985) This Conference, Paper SH 1.4-6.
10. Reiger, E., et al, (1984), Nature 312, 623.

THE NEUTRON MODERATED DETECTOR AND GROUNDBASED COSMIC RAY MODULATION STUDIES

N85-35128

P.H. Stoker and B.C. Raubenheimer
PU-CSIR Cosmic Ray Research Unit
Department of Physics
Potchefstroom University for CHE
POTCHEFSTROOM 2520
South Africa

ABSTRACT

Over the past years several reports have appeared on modulation studies with the neutron monitor without lead. Some of these studies cast doubt on the reliability of this detector. We report here on the stability of the neutron moderated detector (NMD) at Sanae, Antarctic. The barometric coefficient of the 4NMD for epoch 1976 appears not to differ statistically from the 0.73%/mb of the 3NM64. The monthly averaged hourly counting rate of our 4NMD and 3NM64 correlates very well (correlation coefficient: 98%) over the years from 1974-1984, with the 4NMD showing a 8% larger longterm modulation effect than the 3NM64, indicating a difference in sensitivities of the two detectors. From this difference in sensitivities spectra of ground level solar proton events and modulation functions of Forbush decreases were deduced.

1. Introduction. A neutron counter surrounded by a low Z moderator records at ground level secondaries produced by primary cosmic rays with primary energies down to ~ 1 GeV. The counting rate may be increased significantly when high Z materials are also part of the neutron monitor geometry because of the much larger rate of neutron production by cosmic rays in the heavier materials (Simpson and Uretz, 1953).

It was shown by Mischke et al. (1973) that the neutron moderated detector (NMD), consisting of BP28 Chalk River neutron counters surrounded by paraffin wax but without lead, is more sensitive to low rigidity (~ 1 GV) primary cosmic rays than the NM64 super neutron monitor. They reported on differential response functions deduced from aircraft latitude surveys at 30 000 feet pressure altitude for both the NMD and NM64 and on the altitude dependence of the counting rates of these two detectors at different cutoff rigidities. They have also shown that the fractional variations in counting rates of these two detectors are different during ground level solar proton events and that the hardness of the relativistic solar protons as described by the spectral rigidity function may be deduced from the relative increases in counting rates above the cosmic ray background.

In this paper we report on the performance of the 4NMD in comparison with the 3NM64 at Sanae, Antarctica (72°S 02°W). Zhu and Kawasaki (1983) occasionally observed fluctuations in the counting rate of a neutron monitor without lead in comparison with the counting rate of the Tokyo super neutron monitor. When raining the counting rate of the neutron monitor without lead was decreased, while the cause of many other fluctuations in counting rate could not be traced. Similar problems were experienced by other investigators. We found on the contrary that changes in counting rates of the 4NMD and 3NM64 correlate well with each other and that the relative changes in counting rates of the two detectors may be related to temporal variations in the low rigidity portion (~ 1 GV) of the primary cosmic ray spectrum (Stoker et al., 1979). Simpson (1951) reported that local production in materials

of high atomic weight and slowing down of neutrons in hydrogenous materials were the principle sources of erroneous results with the neutron moderate detector. At Sanae the local environment is hydrogenous throughout the year and the snow fall amounting to 2 meters annually does not effect the counting rate. The station is situated on a ice shelf.

2. Experimental details. In Figure 1 curves a, b and c are representing the sensitivity of neutron counters surrounded by paraffin wax of thicknesses 1.25 cm, 7.5 cm and 12.5 cm respectively as a function of neutron energy (Hess et al., 1959). Also shown is the sensitivity as a function of neutron energy (curve d) for a NM64 neutron monitor (Hatton, 1971). It appears that the contribution to the counting rate by environmentally produced low energy neutrons may be reduced by surrounding a neutron counter with a relatively thick layer of paraffin wax.

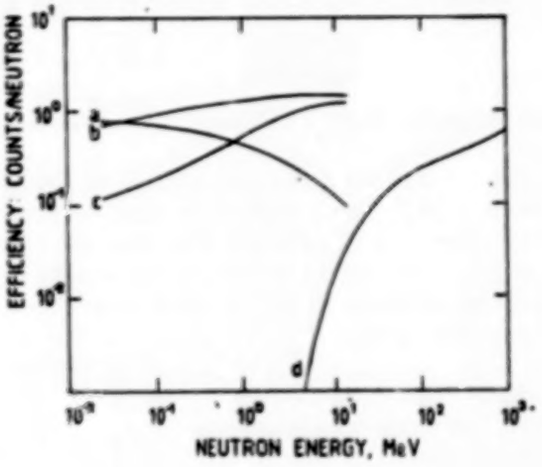


Figure 1

The 4NMD at Sanae consists of 4 BP28 Chalk River neutron counters, each of which is, together with its polyethylene cylinder, inside a paraffin wax cylinder with a wall thickness of 7.5 cm. These 4 paraffin wax cylinders with their neutron counters are enclosed in a rectangular aluminium container, having cavity walls filled up with paraffin wax of 5 cm thickness. This container is temperature controlled. The 3NM64 neutron monitor is enclosed in a similar temperature controlled container. Each container is inside a small wooden hut with heat insulated walls, about 3 meters above snow level and some 100 meters away from the station and its invironment.

3. Intercomparison of changes in counting rates. Since the fractional changes in pressure corrected counting rates of the two detectors differ during temporal variations of cosmic rays, 1976 was selected for intercomparing barometric pressure dependent changes in counting rates. During this period of minimum solar activity, temporal variations in counting rates due to cosmic rays may be neglected comparing to barometric pressure effects. Daily averaged hourly counting rates and barometric pressures were considered.

A linear regression fitting between the pressure uncorrected counting rates of the 4NMD and the 3NM64 yielded a gradient $m = (9.68 \pm 0.035) \times 10^{-2}$ with a correlation coefficient of 0.999. With the average ratio of the counting rates = 0.09670 it follows that the ratio of the barometric coefficients of the 4NMD to the 3NM64 is

$$\frac{\beta(4NMD)}{\beta(3NM64} = 1.0008 \pm 0.0035$$

This implies an identical pressure dependence for both detectors. In order to confirm this result, a linear regression analysis was also carried out on the ratio of the counting rates of the 4NMD and the 3NM64 as a function of the barometric pressure.

With

$$\ell n \frac{N(4NMD)}{N(3NM64)} = \ell n \left[\frac{N(4NMD)}{N(3NM64)}\right]_o + \Delta\beta(p-p_o)$$

we found $\Delta\beta = -(3 \pm 2).10^{-5}$/mb. with a correlation coefficient of $r = -0.33$. Since $\Delta\beta = \beta(4NMD) - \beta(3NM64)$, it means that the ratio of the barometric coefficients

$$\frac{\beta(4NMD)}{\beta(3NM64)} = 0.997 \pm 0.003$$

if one accepts that $\beta(3NM64) = 0.0073$/mb.

When the linear regression method for successive differences of Lapointe and Rose (1962) was used, the same value for the ratio of the barometric coefficients was obtained, but the correlation coefficient, r, was as small as - 0.05. The small correlation coefficients obtained by both linear regression methods confirm that the barometric coefficients of both detectors are the same.

In Figure 2 are shown the monthly averaged pressure corrected counting rates of the 4NMD and of the 3NM64 for the period from March 1974 through to December 1984. Different symbols have been used in the plot for different years. A linear regression analysis gives for the longterm variation of the 4NMD relative to the 3NM64 a ratio of 0.108 ± 0.002, with a correlation coefficent of 0.985.

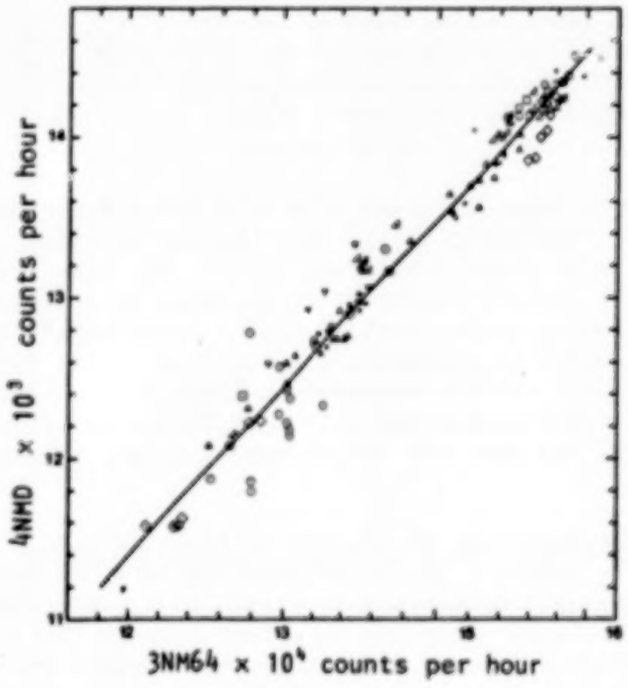


Figure 2

4. Discussion and conclusions. The results show a highly correlated variation of the counting rates of the 4NMD and the 3NM64, both due to pressure variations and to temporal variations in the primary cosmic ray intensity. No statistically significant difference in the pressure dependence of the two detectors could be established.

The 4NMD shows an 8% larger variation in counting rate than the 3NM64 on long term modulation. This relative larger variation in fractional counting rate of the 4NMD was expected from the larger latitude dependence of the 1NMD compared to the 1NM64 (Mischke et al., 1973). Also the larger variations of the counting rate of the 4NMD relative to the 3NM64 for Forbush decreases and ground level solar proton events (Stoker et al., 1979) show a larger sensitivity of the 4NMD relative to the 3NM64 for primary cosmic rays of rigidity $\leq$ 1 GV.

Mischke et al. (1973) reported a barometric coefficient of (0.76 ± 0.02)%/mb for the 1NMD, which was then in operation at Sanae, with the same nominal shielding by paraffin wax than the present 4NMD. This coefficient may be compared with the barometric coefficient of the 3NM64, which is 0.73%/mb. The pressure dependence of the 4NMD may be different from the 1NMD, because the inner tubes of the 4NMD are shielded from the environment by the outer tubes, since environmentally produced neutrons do contribute significantly to the counting rate of a neutron moderated detector (Simpson, 1951).

Zhu and Kawasaki (1983) reported a barometric coefficient of (0.593 ± 0.013)%/mb for their 6 BP28 neutron counters with only the 2 cm polyethylene cylinder, compared with 0.667%/mb for the Tokyo super neutron monitor. This difference in pressure dependence reported by Zhu and Kawasaki may also be due to environmental effects.

The scattering of the points in Figure 2 should be due to variations in the rigidity spectrum of primary cosmic rays. Variation in the rigidity dependence of the modulation function for galactic cosmic rays may be deduced from the relative variation in the counting rates of the two detectors, provided that the specific yield function of each detector at ground level is known.

References

Hatton, C.J., Progress in Elementary Particle and Cosmic Ray Physics 10, 5. Horth-Holland Publ. Co. 1971.

Hess, W.N., Paterson, H.W., Wallace, R. and Chupp, E.L., Phys. Rev. 116, 445, 1959.
Lapointe, S.M., and Rose, O.C., Canadian J. Phys. 40, 687, 1962.
Mischke, C.F.W., Stoker, P.H., and J. Duvenage, 13th I.C.R.C. Conf. Papers 2, 1570, 1973.
Simpson, J.A., Phys. Rev. 83, 1175, 1951.
Simpson, J.A., Fonger, W. and Treiman, S.B., Phys. Rev. 90, 934, 1953.
Simpson, J.A., and Uretz, R.B., Physical Rev. 90, 44, 1953.
Stoker, P.H., Potgieter, M.S. and Venter, A.J., 16th I.C.R.C. Conf. Papers, 4, 358, 1979.
Zhu, B.Y. and Kawasaki, S., 18th I.C.R.C. Conf. Papers 3, 507, 1983.

NEW MATSUSHIRO UNDERGROUND COSMIC RAY STATION (220 M.W.E. IN DEPTH)

N85-35129

Mori, S., S. Yasue, S. Sagisaka, K. Chino, S. Akahane, T. Higuchi, M. Ozaki and M. Ichinose*

Department of Physics, Faculty of Science and Faculty of Liberal Arts*, Shinshu University, Matsumoto 390, Japan

ABSTRACT

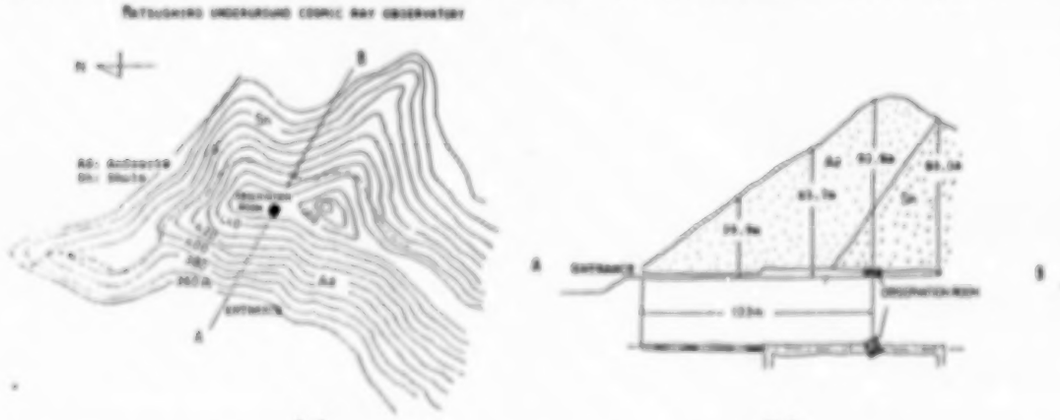
A new underground cosmic ray station has been opened at Matsushiro, Japan and multi-directional (17 directional channels) muon telescope has been installed at an effective vertical depth of 220 m.w.e. The counting-rates are; 8.7×10^5/hr for the wide-vertical component and 2.0×10^4/hr for the vertical component. The continuous observation has been performed since March 22, 1984. Some details of the telescope and preliminary analyzed results of the data are presented.

1. Introduction

More than a dozen of the underground cosmic ray stations have been actively operated, and invaluable data have been accumulated. Based on those data, a great deal of investigation has been performed on the cosmic ray modulation in the heliosphere, cooperated with small air shower measurements (e.g., Nagashima and Mori, 1976). Complete pictures of the modulation have not yet been established in the rigidity range of $10^{11}\sim10^{14}$ eV, therefore more accumulation of the data of high counting-rates with multi-directional channels would be mostly acknowledged.

2. Underground Site and Muon Telescope

Matsushiro is located in Nagano-city, Nagano Pref., Japan and ~40 km northeast of our Cosmic-Ray Lab. of Shinshu University in Matsumoto-city. A new station is very close to our elder one (~4 km in distance) (Yasue et al., 1981; also in this issue). Locality of the present station is; 36.53°N and 138.02°E in geographic coordinate and 360 m in altitude. Fig. 1(a) shows the contour map of the underground site and Fig. 1(b) illustrates one of the cross-sections along the line AB in Fig. 1(a).



(a) (b)

Fig. 1 (a) Contour map of tunnel area and (b) Cross-section along AB

ORIGINAL PAGE IS
OF POOR QUALITY

The vertical rock depth is 92.8 m, and the rocks overburden are mostly andesite (Ad) and shale (Sh), its average density ≅2.65 g/cm^3, therefore ≅240 m.w.e. The depth is somewhat different in each direction, and the effective vertical depth is estimated at ∿220 m.w.e.

The temperature inside the tunnel is 14∿15°C, almost constant throughout the year (precise temperature variations on the daily and seasonal bases have not yet been measured). Both observation room (10×10 m^2 in area) and recording room have been heated up to ∿19°C, and the humidity has been kept as $\lesssim$50%.

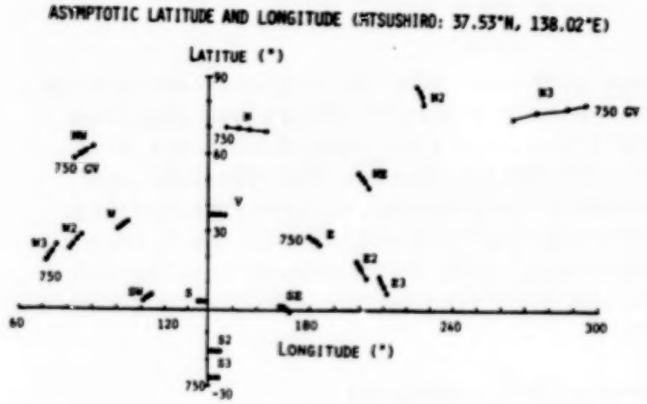


Fig. 2 Asymptotic orbit for 13 comp.'s.

Fig. 2 shows the asymptotic directions for 17 component telescopes calculated for the rigidities of 750, 450, 350 and 250 GV (Inoue, personal communication).

The median primary rigidity is estimated at ∿600 GV, using the response function given by Murakami et al. (1981). The corresponding Lamore radius for 6 nT of the IMF strength is ∿2 AU.

The muon telescope consists of 50 plastic scintillation detectors in all, as shown in Fig. 3, arranged in two layers spaced by 150 cm. The detectors are exactly the same as those of our elder Matsushiro station (Yazue et al., 1981); each having 1×1 m^2 in area, 4 plastic scintillators (50×50×10 cm^3), and viewed with double photomultipliers (5" in diameter), as shown in Fig. 4, to obtain good S/N ratio and high detection efficiency.

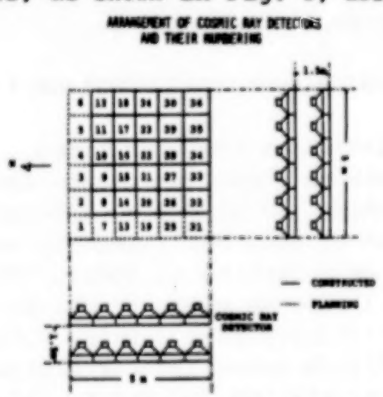


Fig. 3 Arrangement of detectors

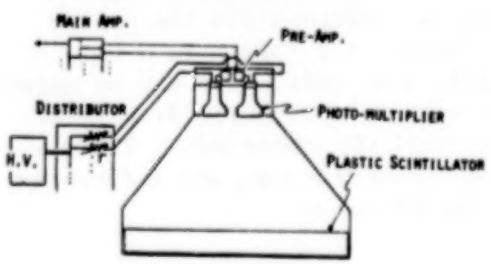


Fig. 4 Cosmic ray detector

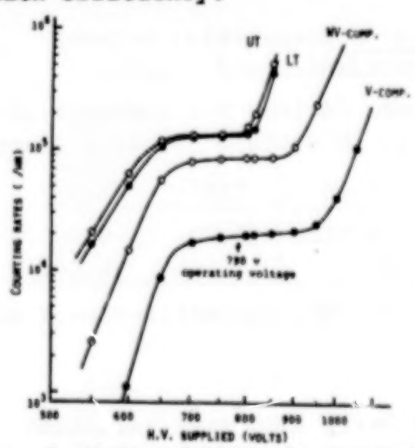


Fig. 5 High-voltage characteristic

Based on this arrangement, 17 component telescopes are constructed by taking an appropriate 2-fold coincidence between the detectors in upper and lower trays. In Fig. 5, high-voltage characteristics of some telescopes are plotted of real counts vs. high-voltage supplied for the upper (US) and the lower (LS) trays, the wide-vertical component (WT; 2-fold coincidence between US and LS) and the vertical component (V). The continuous observation has been performed since March 22, 1984 and the hourly counts have been recorded. In the followings, some preliminary analyzed results of the data are presented.

3. Data and Their Analysis

3.1 Atmospheric effect

Barometric pressure effect was examined; one for a short time-period of 6 days when transient large atmospheric pressure change was observed in a range of ∿30 mb and the other for a long time-period of abour 6 months (Mar.~Oct., 1984). Single correlation between the pressure and the counting-rate was taken. Barometric coefficients were obtained as; $\beta \simeq -0.01\%$/mb for the former short-period and $\alpha \simeq -0.04\%$/mb for the latter long-period. These are in good agreement with our previous results and can be well explained by taking accounts of the upper atmospheric temperature effect (Sagisaka et al., 1983).

3.2 Cosmic ray north-south asymmetry (N-S asymmetry)

Among 17 component telescopes, some telescopes (e.g., N, N2, ...) view rather northern latitude, while some (e.g., S, S2, ...) view rather southern latitude or equatorial plane, as shown in Fig. 2. Using the daily mean values of these directional intensities ($\sim 60\times10^{4}$/day), N-S asymmetry was evaluated daily as

$$\Delta = (N+N2+N3+NE+NW) - (S+S2S3+SE+SW)^{*}$$

where * indicates the normalized counts between these two groups (Mori and Nagashima, 1979). Also IMF-sense dependence of this N-S asymmetry was examined by referring to Toward (T)- and Away (A)-sense given by Stanford group (Solar-Geophysical Data, NOAA, 1985). Fig. 6 shows the correlation between derived N-S asymmetries of the present station and Misato (34 m.w.e. in depth). Table 1 gives the numerical values on T and A of these two stations for the period Mar.22~Oct. 31, 1984. From this result, some indication may be noted that even such high rigidity particles (∿600 GV) observed at 220 m.w.e. underground station, are influenced by the IMF-sense.

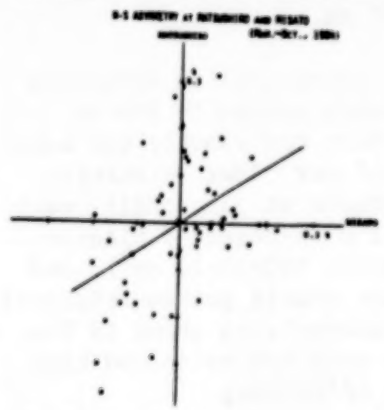


Fig. 6 Correlation between Matsushiro and Misato.

Station	T(%)	A(%)
Matsushiro	0.02	-0.05
Misato	0.066	-0.060

Table 1 N-S asymmetries on T and A

3.3 Daily intensity variation

The hourly data (without corrected for barometric effect) were harmonically analyzed in solar (SO), sidereal (SI) and anti-sidereal (AS)

ORIGINAL PAGE IS
OF POOR QUALITY

time for full one-year (Apr. 1984 Mar. 1985). Fig. 7 shows one of month-to-month variations of SO(1st) for V-comp. The monthly vectors move counterclockwise systematically, indicating the at deep undergrouns station SI(1st) may be more significant in the 1st harmonics. Fig. 8 illustrates some of the harmonics for 13 component telescopes (V, N, S, E, W, NE, NW, SE, SW, N2, S2, E2 and W2); Si(1st) in (a), AS(1st) in (b) and SO(2nd) in (c). In the figure, errors are derived from counting-rates. We may note that from their directional dependence, almost of them are significant.

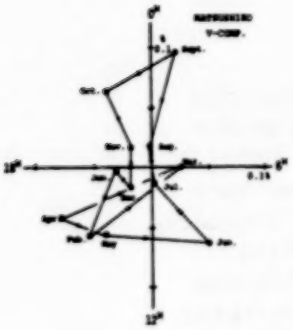


Fig. 7 Monthly movement of SO(1st) for V-comp.

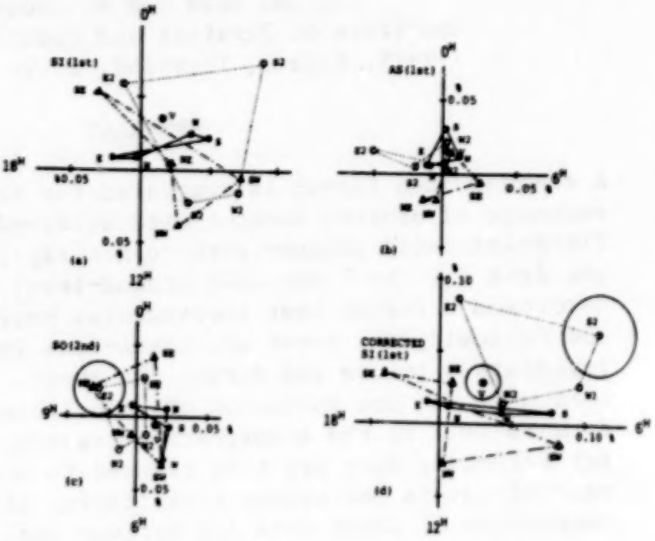


Fig. 8 Harmonics of; (a) SI(1st), (b) AS(1st), (c) SO(2nd) and (d) corrected SI(1st)

In a case, where SO(2nd) is observed significantly, as developed by Nagashima et al. (1983), space anisotropy of 2nd order responsible for the observed SO(2nd) produces the spurious SI(1st) and AS(1st) having equal amplitude and due phase. As in Fig. 8 (b), AS(1st) may be significant. Based on Nagashima correction (1983), the observed SI(1st) should be, at least, corrected for the above spurious SI(1st) by utilizing the observed AS(1st). Fig. 8 (d) shows the corrected SI(1st) thus derived. We may summarize that 1) these results are consistent with those so far reported; almost of them lie in the direction 3~5 hr LST. And 2) some of SI(1st)'s, e.g., S2-comp. is rather larger (~0.13% in ampltude) than others, which is consistent with that of Ueno et al. (1984) at Sakashita.

4. Acknowledgement

The authors express their aapreciation to Prof. K. Nagashima for his kind discussion.

References

Mori, S. and K. Nagashima, (1979), Plant. Space Sci., 27, 34.
Murakami, K. et al., (1981), Rep. CR-Lab., Nagoya Univ., No. 6.
Nagashima, K. and S. Mori, (1976), Int. CR-Symp. (Tokyo), p326.
Nagashima, K. et al., (1983), Nuovo Cimento, 6C, 550.
Sagisaka, S. et al, (1983), 18th ICRC (Bangalore), 10, 237.
Ueno, H. et al., (1984), Int. CR-Symp. (Morioka), p349.
Yasue, S. et al., (1981), 17th ICRC (Paris), 4, 304.
Yasue, S. et al., (1985) in this issue (SH 4.4-9).

510

N85-35130

A SUGGESTED STANDARDIZED FORMAT FOR COSMIC RAY GROUND-LEVEL EVENT DATA

M. A. Shea and D. F. Smart
Air Force Geophysics Laboratory
Hanscom AFB, Bedford, Massachusetts, 01731, U.S.A.

M. Wada and A. Inoue
Institute of Physical and Chemical Research
7-13, Kaga-1, Itabashi, Tokyo 173, Japan

ABSTRACT

A standardized format is suggested for the archival and exchange of neutron monitor data obtained during solar-flare-initiated ground-level cosmic ray events. Using the data for the 7 May 1978 ground-level event, we have developed a format that incorporates hourly data preceding and following the event and small-time interval data immediately before and during the event. Provision has been made for the inclusion of uncorrected and corrected data as well as the atmospheric pressure. The cosmic ray intensity data are then reduced to a standard counting rate of counts per second facilitating the graphing and comparison of these data for various analyses.

1. Introduction. Thirty-four relativistic solar proton events have been detected by ground-based neutron monitors since 1955. These events are intensely studied not only for the physics of the flare process, but also for information on relativistic solar particle propagation in the interplanetary medium and entry into the magnetosphere. The first ground-level cosmic ray event detected by neutron monitors on February 23, 1956, was so unexpected and unique that many scientific papers were written on the measurements at just one station. However, the events of May and November 1960 illustrated the necessity of utilizing data from the world-wide neutron monitor network to study interplanetary and magnetospheric propagation characteristics.

Unfortunately one of the most time-consuming tasks in the analysis of multi-station ground-level event data is the collection and assembly of these data into a common useable format since most cosmic ray stations use their own unique data collection system regarding time intervals, scaling factors, and normalization factors. Since the rapid and efficient exchange of data relating to solar-flare-initiated ground-level events would be practical and beneficial to the community, we have developed a format that includes the parameters that cosmic ray scientists use in the analysis of these relatively unusual events, and suggest that this format be adopted as a standard for the archival and exchange of these data.

2. Method. To develop a useful format we first identified the data we felt were essential for the analysis of any ground-level cosmic ray event that utilizes the data from the world-wide neutron monitor network. These included sufficient data to establish a pre-event level, small time increments during the rising and maximum portion of the event, and both uncorrected and corrected data to permit use of the two-attenuation

method of correcting the solar flare particle spectrum for atmospheric effects (McCracken, 1962). Using neutron monitor data from 32 stations for the ground-level cosmic ray event of 7 May 1978, we proceeded to identify the data we felt should be included as follows:

6 May 1978:	0000-2400 UT	Hourly data (uncorrected data)
7 May 1978:	0000-0200 UT	(corrected data)
		(barometric pressures)
7 May 1978:	0200-0700 UT	Small time interval data
		(uncorrected data)
		(corrected data)
		(barometric pressures)
7 May 1978:	0700-2400 UT	Hourly data (same as above)

The hourly data for the day preceding the event would permit consideration of any unusual daily variations that might be present for some stations. The small time interval data, which are station specific, would give information on the rate of rise and maximum intensity, as well as a portion of the decay of the event. The hourly data for the remainder of 7 May would cover the complete decay of the event for all stations. In order to be able to compare cosmic ray intensities both throughout the event and between stations, we adopted a standard counting rate in units of counts per second. This necessitated utilizing multiplication factors and/or normalization factors for each individual station. However, the advantange of this procedure is that odd time intervals, such as changes from hourly to five-minute or one-minute data, can be easily compared. The following format was adopted:

Columns 1 - 10:	Station identification (alphanumeric)
Columns 11 - 19:	Year, month and day (3I3)
Columns 20 - 23:	Number of minutes in this time interval (I4)
Columns 24 - 33:	Time interval included (I5, 1H-, I4)
Columns 34 - 50:	Uncorrected counting rate; counts per second (6X,F11.2)
Columns 51 - 57:	Barometric pressure (F7.1)
Columns 58 - 68:	Corrected counting rate; counts per second (F11.2)
Columns 69 - 75:	Percentage increase (F7.1) normalized to some pre-event level.

Table 1 illustrates a portion of the data for Leeds, UK. The intensity for the hour immediately preceding the increase (i.e., 0200-0300 UT) was selected as the pre-event level. Figure 1 illustrates the cosmic ray intensity increase for this same station. Notice that this method allows inclusion of "odd" time intervals such as the 3-minute value obtained prior to the activation of the flare alarm rapid time recorder.

3. Discussion. In compiling these data into a standard format it became evident that much of the data we wanted to include was not available from the data that had been exchanged among various investigators. The following data were most commonly found to be missing: all data for the day prior to the event, uncorrected data throughout the event, and data multiplication and/or normalization factors. Data given for different time intervals without any notation as to changes in multiplication and/or normalization factors were extremely difficult to include. In the case of Hermanus, hourly data were given for four sections of the

Table 1. An example of the ground-level event data, in the proposed standard format, for 0000-0500 UT for the event on 7 May 1978. Only a portion of the complete data set for the Leeds neutron monitor is shown. The time interval of 0200-0300 UT was selected as the pre-event level.

STATION	YY	MM	DD	MIN	TIME SPAN	UNCOR.	PRES.	COR.	% INC.
LEEDS	78	05	07	60	0000-0100	167.97	751.7	170.42	-.1
LEEDS	78	05	07	60	0100-0200	178.19	751.6	170.50	-.1
LEEDS	78	05	07	5	0200-0205	178.67	751.5	170.67	.0
LEEDS	78	05	07	5	0205-0210	175.67	751.5	168.00	-1.5
LEEDS	78	05	07	5	0210-0215	178.33	751.6	170.67	.0
LEEDS	78	05	07	5	0215-0220	178.00	751.6	170.33	-.2
LEEDS	78	05	07	5	0220-0225	178.67	751.6	171.00	.2
LEEDS	78	05	07	5	0225-0230	180.33	751.6	172.67	1.2
LEEDS	78	05	07	5	0230-0235	178.67	751.6	171.00	.2
LEEDS	78	05	07	5	0235-0240	177.67	751.5	170.00	-.4
LEEDS	78	05	07	5	0240-0245	180.00	751.5	172.00	.8
LEEDS	78	05	07	5	0245-0250	179.33	751.5	171.33	.4
LEEDS	78	05	07	5	0250-0255	177.33	751.5	169.67	-.6
LEEDS	78	05	07	5	0255-0300	178.00	751.5	170.33	-.2
LEEDS	78	05	07	5	0300-0305	178.67	751.5	170.67	.0
LEEDS	78	05	07	5	0305-0310	177.67	751.5	170.00	-.4
LEEDS	78	05	07	5	0310-0315	179.67	751.6	172.00	.8
LEEDS	78	05	07	5	0315-0320	176.00	751.6	168.33	-1.4
LEEDS	78	05	07	5	0320-0325	179.00	751.6	171.33	.4
LEEDS	78	05	07	5	0325-0330	179.67	751.6	172.00	.8
LEEDS	78	05	07	5	0330-0335	179.00	751.6	171.33	.4
LEEDS	78	05	07	3	0335-0338	217.22	751.6	207.78	21.8
LEEDS	78	05	07	1	0338-0339	301.67	751.6	288.33	69.0
LEEDS	78	05	07	1	0339-0340	316.67	751.6	303.33	77.8
LEEDS	78	05	07	1	0340-0341	331.67	751.6	316.67	85.6
LEEDS	78	05	07	1	0341-0342	328.33	751.6	315.00	84.6
LEEDS	78	05	07	1	0342-0343	315.00	751.6	301.67	76.8
LEEDS	78	05	07	1	0343-0344	308.33	751.6	295.00	72.9
LEEDS	78	05	07	1	0344-0345	300.00	751.6	286.67	68.0
LEEDS	78	05	07	1	0345-0346	293.33	751.6	280.00	64.1
LEEDS	78	05	07	1	0346-0347	288.33	751.6	276.67	62.1
LEEDS	78	05	07	1	0347-0348	280.00	751.6	268.33	57.2
LEEDS	78	05	07	1	0348-0349	266.67	751.6	255.00	49.4
LEEDS	78	05	07	1	0349-0350	271.67	751.5	260.00	52.4
LEEDS	78	05	07	1	0350-0351	260.00	751.5	248.33	45.5
LEEDS	78	05	07	1	0351-0352	258.33	751.5	246.67	44.6
LEEDS	78	05	07	1	0352-0353	240.00	751.5	230.00	34.8
LEEDS	78	05	07	1	0353-0354	245.00	751.5	235.00	37.7
LEEDS	78	05	07	1	0354-0355	240.00	751.5	230.00	34.8
LEEDS	78	05	07	1	0355-0356	238.33	751.5	228.33	33.8
LEEDS	78	05	07	1	0356-0357	235.00	751.5	225.00	31.9
LEEDS	78	05	07	1	0357-0358	228.33	751.5	218.33	27.9
LEEDS	78	05	07	1	0358-0359	220.00	751.5	210.00	23.1
LEEDS	78	05	07	1	0359-0400	226.67	751.5	216.67	27.0
LEEDS	78	05	07	1	0400-0401	220.00	751.5	210.00	23.1
LEEDS	78	05	07	1	0401-0402	211.67	751.5	201.67	18.2
LEEDS	78	05	07	1	0402-0403	211.67	751.5	201.67	18.2
LEEDS	78	05	07	1	0403-0404	215.00	751.5	205.00	20.1
LEEDS	78	05	07	1	0404-0405	213.33	751.5	203.33	19.2
LEEDS	78	05	07	5	0405-0410	205.67	751.5	196.67	15.3
LEEDS	78	05	07	5	0410-0415	199.00	751.5	190.33	11.5
LEEDS	78	05	07	5	0415-0420	194.33	751.5	186.00	9.0
LEEDS	78	05	07	5	0420-0425	192.67	751.6	184.33	8.0
LEEDS	78	05	07	5	0425-0430	189.00	751.6	181.00	6.1
LEEDS	78	05	07	5	0430-0435	186.33	751.6	178.33	4.5
LEEDS	78	05	07	5	0435-0440	184.00	751.6	176.00	3.1
LEEDS	78	05	07	5	0440-0445	186.00	751.6	178.00	4.3
LEEDS	78	05	07	5	0445-0450	184.33	751.6	176.33	3.3
LEEDS	78	05	07	5	0450-0455	185.33	751.6	177.33	3.9
LEEDS	78	05	07	5	0455-0500	183.00	751.6	175.00	2.6

monitor, but the flare data only included three sections. When the proper normalization factors are obtained, we will be able to include these data in the standard format. Another problem was encountered with small-time interval data corrected for small-time increments, which, when summed over the hour, were not in agreement with the listed hourly data. The use of local time instead of Universal Time without any notation as to the difference between these times also caused some difficulty. Some stations in the Soviet Union listed hourly data in Universal Time and small-time interval data in local time; some also listed hourly time for the hour ending with the indicated time, but small-time interval data were listed at the start of the interval. Consequently we utilized information available from the World Data Center records and from previously published tables to complete, as much as possible, a uniform set of tables for the 32 neutron monitors.

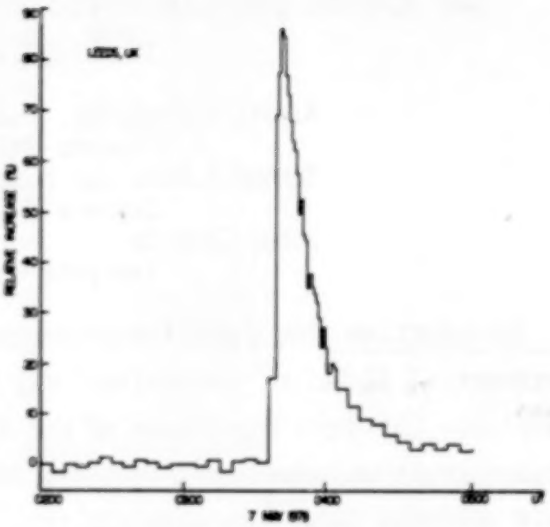


Figure 1. Relative increase recorded by the Leeds, UK neutron monitor for the 7 May 1978 ground-level event.

4. Future Plans. We plan to complete and publish the uniform set of tables for the 7 May 1978 ground-level event, at the same time work is progressing on similar tables for the following events: 21 August 1979, 12 October 1981, 8 December 1982, and 16 February 1984. To complete some of these tables it will be necessary to contact the principal investigator; we would appreciate cooperation in supplying the data requested. We also anticipate compiling similar records for as many of the 34 ground-level events as time (and patience) permits. We are afraid that many of the records for the earlier events, particularly those prior to this solar cycle, may be difficult to obtain. Therefore, we request all cosmic ray physicists who have ground-level event data for either their own or other cosmic ray stations to send the data to any of the authors of this paper and to the World Data Centers for archival in an effort to preserve this historical data set.

Acknowledgments. The computational assistance of M. Nichol and L.C. Gentile are gratefully acknowledged.

References

McCracken, K.G., "The Cosmic Ray Flare Effect; 1. Some New Methods of Analysis", J. Geophys. Res., 67, 423, 1985.

ORIGINAL PAGE IS
OF POOR QUALITY

N85-35131
SH 9.1-16

THE READ-OUT SYSTEM OF SPATIAL DISTRIBUTION OF THERMOLUMINESCENCE IN METEORITES

Kiyotaka Ninagawa, Isao Yamamoto and Yasumasa Takano
Okayama University of Science, Okayama Japan
Tomonori Wada and Yoshihiko Yamashita
Okayama University, Japan
Nobuo Takaoka
Yamagata University, Japan

1. Introduction The thermoluminescence [TL] technique used for dating the terrestrial age of the meteorites[1] was based on the TL fading of interior samples. The depth dependence of the TL for Antarctic meteorites with fusion crust was measured[2]. Usually, meteorites were powdered and their TL were measured under a photomultiplier. In this time, we have measured a TL spatial distribution of a cross section of antarctic meteorites by using a read-out system of spatial distribution of TL[3], because a meteorite is inhomogeneous material. Antarctic meteorites MET-78028[L6], ALH-77278[LL3] are used.

2. Methods The system is shown in Fig. 2 of this conference HE 7.1-7. TL data are recorded by video cassette tapes. TL data are able to be analysed repeatedly via image processor. For the case of taking emission spectra of TL, we have changed a camera lens with a filter for a spectroscope. One example of emission spectra is shown in Fig. 1. The sample is powdered

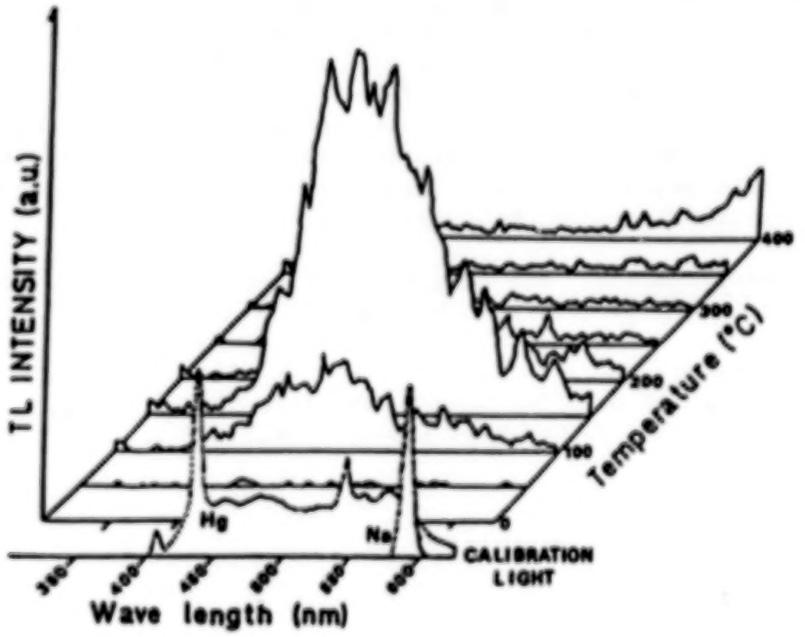


Fig. 1. Emission spectra of TL of MET-78028 at various temperature. For calibration, a Na-lamp and a fluorescent lamp are used.

meteorite MET-78028 irradiated with X-rays ($\sim 10^5$ R). The meteorite TL has a wide spectral band with a maximum at about 450 nm. So in the TL measurement of MET-78028, we have used the band pass filter, Corning 4-96 (blue-green).

3. The spatial distribution of TL for MET-78028 [L6].

Samples of slices of the meteorite are shown in Fig. 2. One slice of a pair was artificially exposed to ^{60}Co 1 kR γ-rays in addition to natural exposure. Using TV-camera system (Ref. 3), a pair of slices and an interior piece of the meteorite were heated (rising rate:2.3 °C/sec) and TL spatial distributions of these sample were recorded onto video cassette tape for about 160 sec ($\sim$5300 frames). Two examples of read out are shown in Fig. 3a, 3b. The Fig. 3a is TL spatial distribution

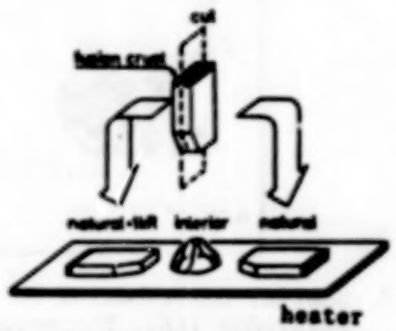


Fig. 2. Cutting and setting.

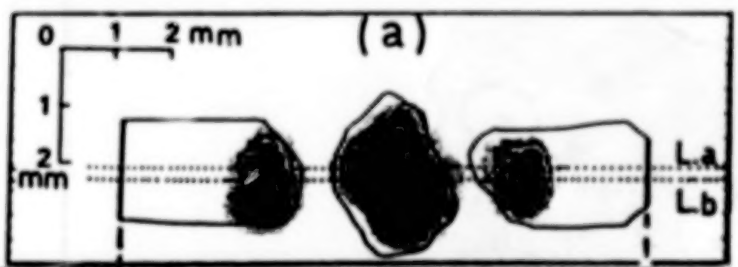


Fig. 3a. TL spatial distribution of slices in pair and of interior one. [MET-78028]

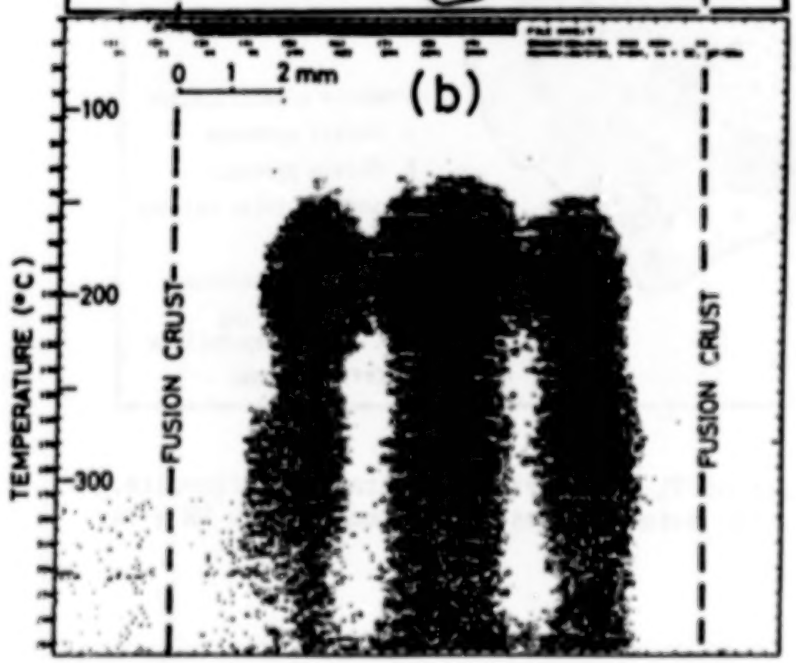


Fig. 3b. Time variation (corresponding to temperature) of TL for the area from line L.a to L.b in Fig. 3a. [MET-78028]

ORIGINAL PAGE IS
OF POOR QUALITY

SH 9.1-16

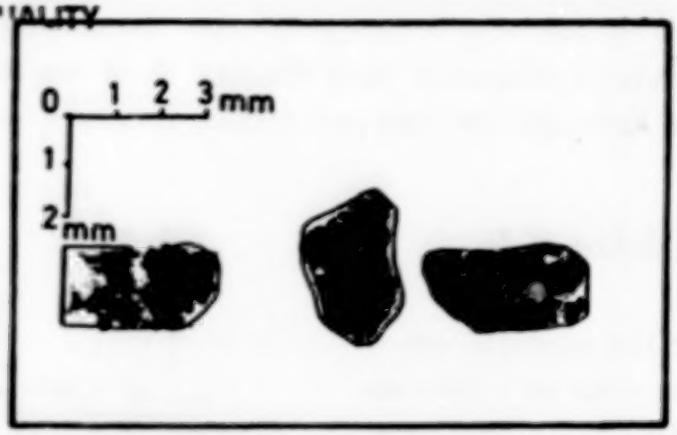


Fig. 4. Spatial distribution of TL sensitivity for antarctic meteorite, MET-78028 (L6). The meteorites were irradiated with 10^5 R X-rays.

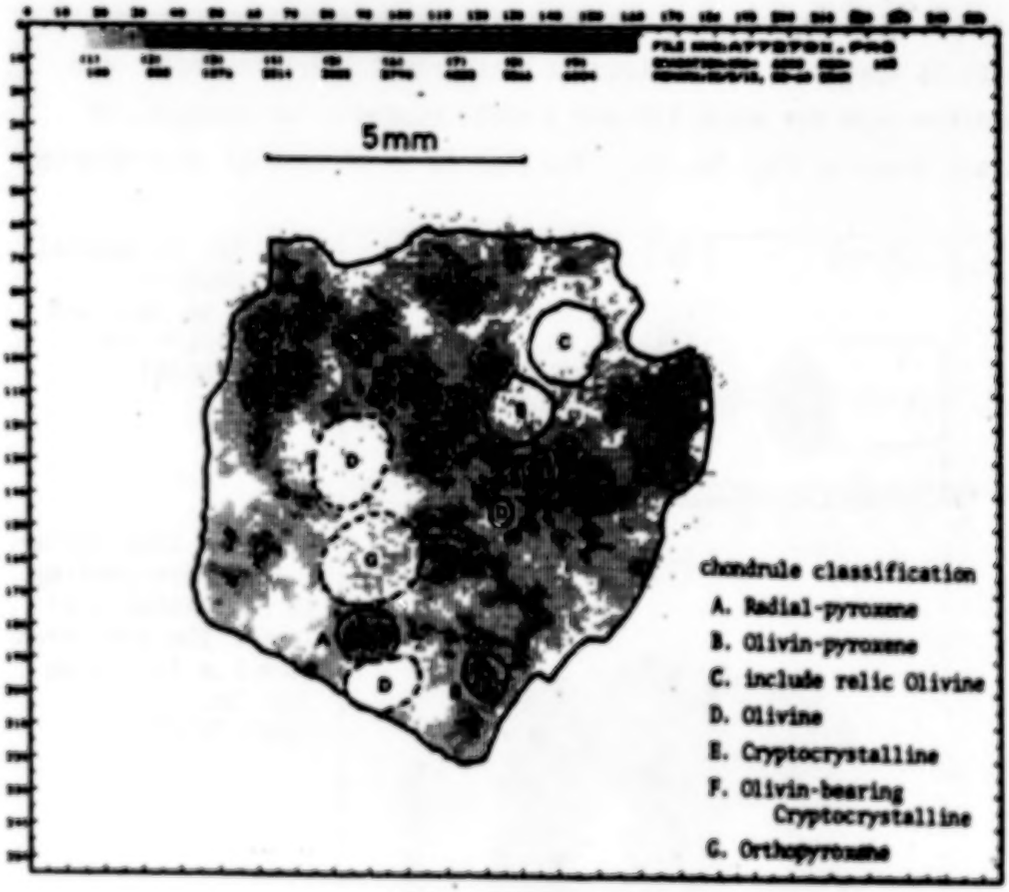


Fig. 5. Spatial distribution of TL sensitivity for antarctic meteorite, chondrite ALH-77278 (LL3). The meteorite was irradiated with 20 kR γ-ray.

of samples. The TL yeild of both slices was not detectable at near fusion crust. The fig. 3b shows the TL variation vs. heating temperature at the area from line L.a to L.b. The TL on the fusion crust side was obtained at higher temperature region.

4. Spatial distributions of TL sensitivity

(A) MET-78028 (L6): After reading out of natural TL, samples corresponding to Fig. 3a were irradiated with X-rays (10^5 R) and were heated. TL spatial distributions of these samples are shown in Fig. 4, which shows spatial distributions of TL sensitivity of these samples. Slices in pair of MET-78028 have low TL sensitivity near fusion crust. Here, the TL sensitivity is represented with logarithmic intensity.

(B) Chondrite, ALH-77278 (LL3): After reading out of natural TL, the sample was irradiated with ^{60}Co γ-rays (20 kR) and was heated. TL spatial distribution is shown in Fig. 5, which shows spatial distribution of TL sensitivity of the sample. Some chondrules have high TL sensitivity and other chondrules have low TL sensitivity or no sensitivity.

5.Conclusions. As shown in Fig. 4 and 5, the TL spatial sensitivity is not uniform, it may occur since meteorites are inhomogeneous material. So, when one searches the terrestrial age of antarctic meteorites or classifies the petrologic type of chondrites by using TL technique, one must investigate thoroughly TL spatial sensitivities. It is not only meteorites but also natural materials on the occation to measure natural TL.

6. Acknowledgements. The authors are greatly indebted to Prof. T.Nagata and Dr. K.Yanai, National Institute of Polar Research for the meteorite samples. They also thank Dr. Y.Ikeda, Ibaragi University for the chonrule classification.

References

1. Sears, D.W. and Durrani, S.A. (1980), Earth Planet. Sci. Lett., 46, 159.
2. Ninagawa, K. et. al., (1983), Lettere al Nuovo Cimento, Serie 2, 38, 33.
3. Yamamoto, I. et. al., (1985), This conference paper, HE 7.1-7.

N85-35132
SH 9.1-17

METHODS AND SOFTWARE FOR COSMIC RAY SCINTILLATION STUDIES

O.V.Gulinsky, L.I. Dorman, R.E.Prilutsky

Institute of Terrestrial Magnetism, Ionosphere and Radio Wave Propagation, USSR Academy of Sciences, 142092 Troitsk, Moscow Region, USSR

Methods and programs for statistical processing of cosmic ray intensity measured in the world-wide network are proposed.

The main instrument in scintillation studies is the cosmic ray spectrum constructed from the intensity onservation /I/. The problem of pectrum estimation from measured time series has a long-standing history, but the specificities of the phenomenon of interest do not permit the direct use of the classical methods. One of such specificities is that besides the appearance of regular trends, which can in principle be eliminated by different filtration methods, in the periods most interesting from the viewpoint of the physics of processes (for instance, Forbush decreases, solar flares) the statistical characteristics of the process undergo essential reconstruction, i.e. the process besomes nonstationary. In this case the concept of spectrum is not defined, and the methods based on Fourier transform, Blackman-Tusky method) give wrong results. The technique usual in this situation, i.e. discrimination of quasistationary regions, encounters the following difficulties. Such regions, if any, can be very short. When based on a small amount of data, the methods using Fourier transform are known to give inaccurate results, in particular, they do not allow us to separate close frequencies, whereas the second specific feature is just the necessity to separate close frequencies, some of which can be associated with a certain process in solar space. For a better separation of near frequencies in short regions, the so-called autoregressive methods have lately been used for spectrum estimation /2/. These methods suggest introduction of an additional possibility to describe the process by an autoregressive model

$$x_{t+1} = \sum_{i=0}^{p} a_i x_{t-i} + \xi_t , \quad t = 0, 1, \ldots \qquad (I)$$

where ξ_t is the sequence of independent random quantities of a certain unkhown order p. This assumption is based on the fact that a wide class of stationary processes can be described by such a model. The coefficients of regression are in this or that way estimated under this assumption for a certai chosen order p, and then the single-valued analytical estimate of the spectrum is found from these coeffi-

cients. Such an approach, using different algorithms for estimating the coefficients (of the type of Berg, Levinson-Durbin, Pisarenko, and other methods), is also realized in our methods. In some cases it gives satisfactory results. But it cannot be applied to essentially nonstationary processes either.

To eliminate these difficulties we have proposed the following two approaches. One of them suggests the description of a process by an autoregressive model in which the coefficients vary in time

$$x_{t+1}=\sum_{i=0}^{p} a_i(t)x_{t-i}+\xi_t, \quad t=0,1,\cdots \tag{2}$$

Each coefficient is represented as a series in a given complete set fo functions $\{\varphi_k(t)\}$

$$a_i(t)=\sum_{k=1}^{N} c_{ik}\varphi_k(t) \tag{3}$$

with the unknown coefficients $\{c_{ik}\}$. As a set of functions one can choose, in particuler, a power series $\{1,t,t^2,\dots\}$. Then, using the method of least squares, one can calculate the coefficients for the chosen order p of the model and for the number N in the expansion (3). The order p of the model and the number of terms N in the expansion ca be chosen, so to say, in the best possible way.

Such an approach makes it possible to introduce the concept of an instantaneous spectrum for a nonstationary process. At each time moment (estimated from the time series of lenght T) the parameters correspond to an autoregressive model with known constant coefficient $a_i^T=\sum_{k=1}^{N} c_{ik}\varphi_k(t)$

$$x_{t+1}=\sum_{i=0}^{p} a_i^T(t^*)x_{t-i}$$

Such a process will be thought of as stopped at a time moment t (starting at some initial point x_0, it passes through a stationary sequence). This process corresponds to a psectrum which can be calculated analytically from the moment t will be called a t -instantaneous spectrum of the nonstationary process (2).

Arranging the sequence of instantaneous spectra with respect to t, one obtains a dynamical picture of reconstruction of a nonstationary process.

The other approach to investigation of a nonstationary process is based on the on-line method for estimating the parameters of the model (2), i.e. on the stochastic approximation method. Let the coefficients $\{a_i^T(t^*)\}$ be time-independent (model (I)), then the algorithm of stochastic

approximation for estimating $\{a_i\}$ for a chosen order p of the model has the form ($\hat{a}$ is the vector of parameter estimation, $\varphi_t = (x_1, \ldots, x)$ is the measured time series):

$$\hat{a}_{t+1} = a_t - \gamma_t \varphi_t \left(x_{t+1} - \sum_{i=0}^{p} \hat{a}_i x_{t-i}\right) \qquad (4)$$

Under certain conditions, if the sequence γ_t tends to zero with an appropriate velocity, one can show (see, for instance, /3/) that as $t \to \infty$, the estimates of $\hat{a}_t$ converge to the vector of the coefficients a of model (I). It is a disadvantage of the method that it needs a large sample, which is hardly to be provided under the described conditions. At the same time, this difficulty can be eliminated if we reject the requirement concerning constancy of the coefficients and pass over to the model (2) without expanding a in the series (3).

In this case, to estimate the coefficients of the model (2), we use the algorithm /4/, in which the sequence γ_t is chosen differently. One can show that under certain conditions on the growth of the coefficients $a_i(t)$ and for a corresponding rate of convergency γ_t to a certain constant, the algorithm (4) will trace the trend of the parameter $a_i(t)$. Under these assumptions one can provide a large sample of data since the series need not necesserily be stationary, and the algorithm works well. The way of constructing an instantaneous spectrum is the same as described above.

The software considered includes all the approaches described above, namely, direct Fourier transform and its modifications, autoregressive and instantaneous spectrum methods. Being used in various combinations, they prove helpful in handling the time series. The methods have been verified in special tests. Some results of investigation of scintillations using these methods are presented in /4/.

REFERENCES

1. Libin I.Ya., Gulinsky O.V. In: Cosmic Rays N 22. M.Nauka, I979, 22.
2. S.M.Kay, S.L.Marple - Proc.of the IEEE - I98I, v.69, N II.
3. Y.Z.Tsypkin, E.D.Avedyan, O.V.Gulinsky, - IEEE TRANS on automatic control, I98I, v. AC-26, N 5.
4. O.V.Gulinsky, L.I.Dorman, I.Ya.Libin et al. - Proc.XIX-th ICRC, San-Diego, USA, I985.

N85-35133
SH 10.1-1

THE INFLUENCES OF THE GALACTIC COSMIC RAY ON THE ATMOSPHERIC OZONE

Ye Zonghai Xue Shunsheng
(Institute of Space Physics, Academia Sinica,
P.O.Box 5112, Beijing, China)
Wang Lianying
(Institute of Atmospheric Physics, Academia Sinica,
P.O.Box 2718, Beijing, China)

I. Introduction. Warneck [1] and Nicolet et al. [2] first put forward that cosmic ray is a source of NO production in the atmosphere. The Nicolet et al.[3,4,5] proved that each ion pair producted by cosmic ray forms about 1-1.5 NO molecules because of the ionization and the dissociation processes. Because of the reaction between NO and O in the atmosphere NO will dispapear in part, so the change of [NO] will directlly influence [O_3] in the atmosphere. The observational results proved that the solar cosmic ray events will cause the large decrease of[O_3] in the polar stratosphere [6] . Ruderman et al.[7] proved that[O_3] has the law of 11 years variation.

This paper has analysed the relationship between yearly variation of cosmic ray intensity and [O_3], and[O_3] disturbance initiated by Forbush decrease for 1965-1976. The data of cosmic ray intensity were selected from the records of the superneutron monitor at Deep River station and the ionization chamber at Beijing station;[O_3] data were selected from Resolute (74.4°N, 94.6°W), Canada, Bismarck (46.4°N, 100.5°W), America, Kagoshima (31.4°N, 130.4°E), Japan, Kodaikanal (10.1° N, 77.3°E), India. The statistical results show that [O_3] prominently is modulated and disturbed by 11 years variation and Forbush decrease of the galactic cosmic ray.

II. The modulation of 11 years variation of cosmic ray intensity on the ozone. Fig. 1c is the curves of yearly variation of cosmic ray intensity. The solid line is the data of the superneutron monitor at Deep River. The dashed line indicats μ meson component recorded by the ionization chamber at Beijing. It can be seen that there is the maximum of cosmic ray intensity during the solar activity minimum (1964-1965), there is the minimum of cosmic ray intensity during the solar activity maximum (1969-1970). Fig. 1 a,b are the corresponding content of O_3 at four variant latitudes. Used [O_3]data is selected from "Ozone data for the world" published by Canada[8] . The analysis results show that except Resolute Station at high latitude 11 years variation of [O_3] is very evident. The ozone content decreases when cosmic ray intensity increases. The ozone content increases whe cosmic ray intensity decreases. This means the relationship between the ozone variation and cosmic ray intensity variation is the nagetive correlation.

It is seen from fig. 1 that 11 years variation of [O_3]has evident latitude effect. From maximum year of cosmic ray in-

N85-35133

ORIGINAL PAGE IS
OF POOR QUALITY

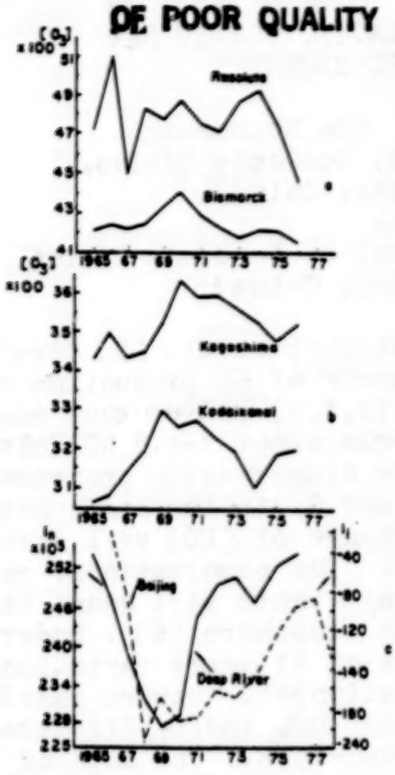


Fig.1 The modulation of 11 years variation of cosmic ray intensity on the ozone

tensity to minimum year $[O_3]$ increased by 7.8% and 5.8% at Kodaikanal and Kagoshima respectively. The increase of $[O_3]$ decreased with the increase of the latitudes, $[O_3]$ only increased by 4.8% at Bismarck. But 11 years variation of $[O_3]$ become indistinct at Resolute in the polar region.

III. The disturbance of Forbush decrease on $[O_3]$. 1. Data analysis. In order to study the disturbance stage of Forbush decrease for variant amplitudes on $[O_3]$, Forbush decrease events are divided >1%, >2%, >3% and >5% four importances based on their amplitudes. The disturbance analysis of the solar flare and Forbush decrease on vorticity arear index (VAI) showed that the disturbances of VAI have evident seasonal property [9]. So the time occurred Forbush decrease is also divided the winter (10-3 months) and the summer (4-9 months). According to the seasons and importances occurred Forbush decrease, their variant combination is analysed. There were 234 Forbush decrease events during 1965-1976. The distribution of various Forbush decrease events as table 1 shown.

Table 1 The distribution of Forbush decrease events

importance / season	>1%	>2%	>3%	>5%
winter	119	49	22	4
summer	115	48	28	4
total	234	97	50	8

The method of the statistical study has used the superposed epoch method. The day of the minimum of Forbush decrease is considered as the zero day. The abscissa denotes the time in days for all of the figures in this section. The ordinate represents the ozone content. The horizontal line refers to the average value of the total absembly of $[O_3]$. The dashed line represents confidence level with probability 0.05 or the degree of confidence 95%. n is the number of Forbush decrease events.

2. Analysis results. The statistical study for all Forbush decrease events shows that the disturbance of Forbush decrease on $[O_3]$ is of statistical significance, and the amplitude of $[O_3]$ disturbance increases with the increase of Forbush decrease amplitude. The disturbance of Forbush decrease on $[O_3]$ increases with the increase of the latitudes. But at

high latitudes, the effect of the solar cosmic ray and precipitating particles on [O_3] will be over Forbush decrease, so that the ozone disturbance produced by Forbush decrease all is covered.

The disturbance of Forbush decrease occurred in the winter on [O_3] is larger and more evident. Usually on the day started Forbush decrease, i.e. about at -1 day, [O_3] begins increase, and there is a larger increase after the fourth day. The amplitudes of [O_3] disturbance increase with the increase of the latitudes of the observational stations. Fig. 2 shows the disturbance of [O_3] for variant latitude regions in the winter. Because the data of [O_3] observed in the winter at Resolute is a few numbers, the change of [O_3] can not be given.

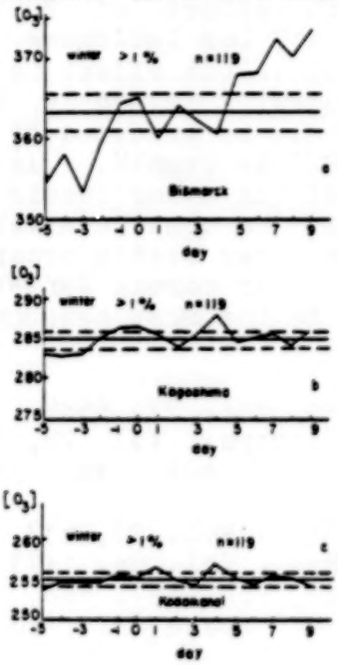


Fig.2 The disturbance of Forbush decrease in the winter on [O_3]

The disturbance Forbush decrease occurred in the witner on [O_3] at same latitude increases with the increase of Forbush decrease amplitudes. If the average value of [O_3] from the third day to the fifth day before the zero day is considered as the undisturbance value of [O_3], that the largest disturbance of >1% Forbush decrease on 0 was about 5.3%. The largest disturbance of >2%, >3% and >5% Forbush decrease events were 5.9%, 6.2% and 10.3% respectively.

The disturbance of Forbush decrease occurred in the summer on [O_3] in low latitudes can also be seen, but its disturbance is very less than in the winter. The disturbance of Forbush decrease on [O_3] all is covered at high latitudes. It always is the decrease tendency after the solar flare, and it lasts several days (see Fig.3).

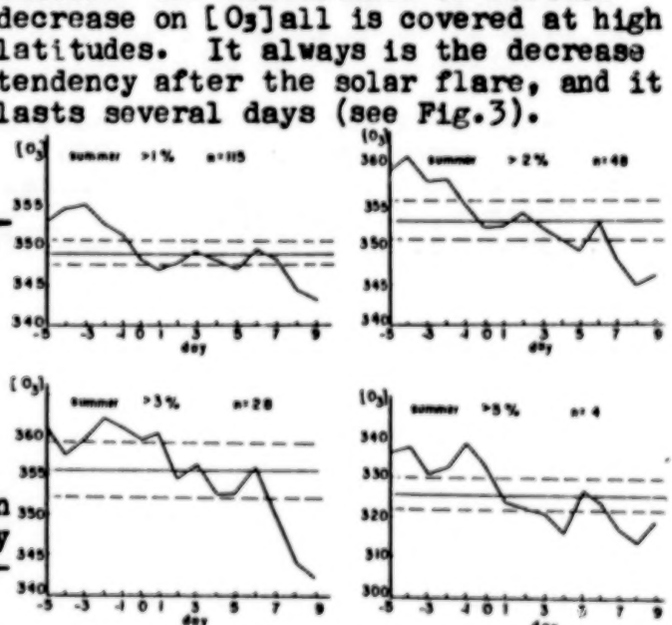


Fig.3 The change of [O_3] during Forbush decrease in the summer at Bismarck.

IV. Conclusions and discussion. According to the results discribed above, we obtain the following conclusions:

[O_3] is modulated by 11 years variation of cosmic ray intensity. The relationship between the ozone variation and cosmic ray intensity variation is the negative correlation. The 11 years vibration of [O_3] is most evident at the middle and the low la-

titudes. The law of this variation is more indistinct at the high latitudes. Because the influences of the solar cosmic ray and precipitating particles on [O_3] are so large that the effect caused by the long period variation of cosmic ray intensity is covered.

The disturbance of Forbush decrease occurred in the winter on [O_3] is very remarkable. The disturbance of [O_3] evidently increases with the rising of the latitudes. Usually [O_3] increases after Forbush decrease started, and lasts several days. The disturbance occurs the maximum after the fourth or the fifth day. The amplitude of [O_3] disturbance also increases with the increase of Forbush decrease amplitude.

The disturbance of Forbush decrease occurred in the summer on [O_3] is very interesting. The effect of Forbush decrease on [O_3] is also evident at the low latitudes, but the disturbance of [O_3] is just opposite to the effect caused by Forbush decrease at the high latitudes. Evidently, this is not produced by Forbush decrease. It is produced by the solar cosmic ray and precipitating particle events. As was shown by Shah [10] , the disturbance of the solar cosmic ray events occurred in the summer on VAI is the most remarkable. We discover that the larger solar cosmic ray events occur in the summer. So the disturbance of the solar cosmic ray events occurred in the summer on [O_3] can also be the most remarkable.

References.

1. Warneck, P. (1972), J. Geophys. Res., Vol. 77, 6589
2. Nicolet, M. et al. (1972), Annals Geophys., Vol. 28, 751
3. Brasseur, G. et al. (1973, Planet. Space sci., vol. 21 939
4. Nicolet, M. (1975), Planet, Space Sci,. Vol. 23, 637
5. Reagan, J. B. (1981), J. Geophys. Res., Vol. 86, 1473
6. Donald, P. H. et al. (1977), Science, Vol. 197, 866
7. Ruderman, M. A. et al. (1975), Planet. Space Sci., Vol. 23, 247
8. Ozone data for the world, environment Canada, atmospheric environment Service 1965-1976
9. Ye Zonghai et al. (1984), Chinese Journal of Space Science, Vol. 4, 198
10. Shah, G. N. (1981), J. Atmos. Terres. Phys, Vol. 43, 147

ORIGINAL PAGE IS
OF POOR QUALITY

Using the Information of Cosmic Rays to Predict Influenza Epidemic

Yu Zhen-dong

Hubei Research Institute of Environmental Protection, Wuhan, China

N85-35134

Abstract

Why does influenza become worldwide pandemic at times? This paper suggests some new observations. First, there is a remarkable relationship between influenza pandemics and cosmic ray environment. Second, there is an excellent correlation between influenza pandemics and bright novae and Nova ? Car. In addition, we propose four indexes to predict future influenza pandemics. Using one of these indexes we successfully predicted the influenza epidemic in 1984.

A. Introduction

Influenza has caused the greatest visitation and the severest natural calamity in this century. Unimaginably about twenty million people died in the influenza pandemic of 1918-1919. Why does influenza become worldwide pandemic at times? For exploring its basic cause, in 1970 R.Ing suggested that except for the pandemic of 1889, the beginning dates of historical influenza pandemic in the 18th and 19th centuries, as well as pandemics and viral antigenic shifts in this century, appear to have occurred in years of high sunspot number.[1] We have different views on this. At the time of suggesting his viewpoint, R.Ing cited seven influenza pandemics in the 18th and 19th centuries, based on the researches by J.R.Hote. But from complete data published by J.R.Hote, there were fifteen main influenza epidemics in the 18th and 19th centuries.[2] Although he employs different terms of "epidemic" and "pandemic", however, this distinction is purely for convenience as Hote indicated. Because different historical records had different criteria and different detailed extent, it is very difficult to compare epidemical scale one another exactly. The distribution of the beginning dates of fifteen main influenza epidemics in the sunspot cycle is shown in figure 1.

From figure 1 we can see that there are four times in years of high sunspot number(over 80) and five times in years of low sunspot number(below 25). In addition, from researches by W.I.B. Beveridge in 1977, there were seven considerable worldwide influenza pandemics in the 18th and 19th centuries.[3] The beginning dates of these pandemics are also shown in figure 1. We note that there are one time in year of high sunspot number and four times in years of low sunspot number. Therefore, according to the studies by J.R.Hote and researches by W.I.B.Beveridge, we can conclude that in sunspot cycle the phase that correlated to a certain extent with epidemics and pandemics of influenza should be the years of low sunspot number, it was more than the occurred number in high sunspot year.

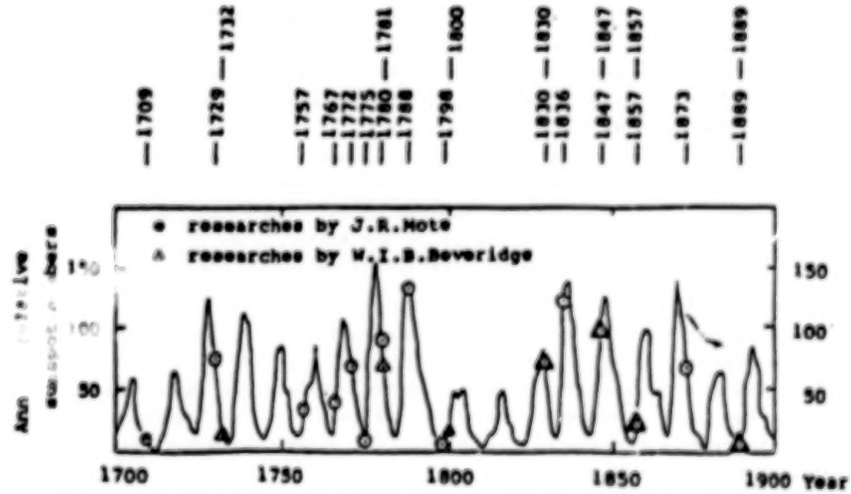


Fig.1 The distribution of the beginning dates of main influenza epidemics in the sunspot cycle in the 18th and 19th centuries

ORIGINAL PAGE IS
OF POOR QUALITY

For explaining the mechanism on how the high sunspot activity can affect influenza pandemics,Ing indicates that people conjecture that the amount of ultraviolet light(UV) incident on the surface of the earth is increased by enhanced solar activity, which might conceivably accelerate the mutation rate of the influenza virus. This speculation cannot, however, explain influenza pandemics occurred in years of low sunspot number. In this paper we try to offer an explanation for this based on cosmic ray researches.

But why have influenza pandemics occurred in some times and why have they not occurred in the others around the periods of low and high sunspot number? Actually, the periods of low and high sunspot number are merely a favorable conditions and a minor causing factor of influenza pandemic,and the dominant causing factor might be earth's cosmic ray environment.

B. Influenza and the cosmic ray environment

Since the start of systematic and continuous observations of cosmic ray in 1936,the number of ground level enhancement event had been rare in more than forty years. Among them large enhancement events happened only five times.[4] These large Ground Level Solar Cosmic Ray Events (GLEs) occurred on Feb.28,1942; Mar.7,1942; July 25,1946; Nov.19,1949 and Feb.23,1956.According to the researches by V.M.Zhdanov et al.[5]there were five influenza pandemics in the first half of this century. Among them the beginning dates of two pandemics were in 1943 and in 1947. They occurred just after the first three large GLEs respectively. After the large GLE on Nov.19,1949, in 1950-1951 there also occurred a severe influenza epidemic spreading to Europe,Africa, North America, Japan and other places. In Liverpool, the death rate even surpassed that of the pandemic of 1918.[5] So V.M.Zhdanov et al. held that the epidemic time of the fifth influenza pandemic in this century was 1947-Feb.1952. Even more, in 1957, the next year of large GLE on Feb.23, 1956, there occurred a worldwide influenza pandemic too. Among seven influenza pandemics occurred hitherto in this century, it was the second severest pandemic. We note that after five large GLEs occurred in the past forty years or so influenza pandemic invariably broke out in each case. Therefore, very remarkable is the corresponding relationship between influenza pandemic and the large variation in the cosmic ray environment.

These extraordinary events of cosmic ray environment all occurred before influenza pandemics one year or so. To start a new influenza pandemic this interval is reasonable, since it takes time for influenza viruses to mutate or to recombine genes and then for selection of human immunity to form new pandemic strains.

Among three pandemics the severest one was that of 1957. And the GLE on Feb.23,1956 was the largest GLE among all recorded GLEs. It seems as if the scale and harmfulness of influenza epidemic were related to the enhanced amplitude of ground level cosmic rays. But this relationship might not be simply understood as a direct proportion relationship.

The mechanisms on how the cosmic ray environment can affect influenza pandemics cannot be discussed here in detail. We presume it has these main aspects. First, the sudden enhancement of cosmic ray environment could deplete the atmospheric ozone layer and therefore bring the increase of the amount of ultraviolet light incident upon the surface of the earth. Second, the abrupt enhancement of ground level cosmic rays seems to give living things an X-ray. The ionizing radiation resulted from cosmic rays in human and animal body and the enhanced ultraviolet rays could lead to mutation of influenza viruses or gene recombination among different human and animal influenza viruses and therefore bring viral antigenic shifts and form new subtypes of influenza virus. Third, the large variation of cosmic ray environment could lead to corresponding variation of other natural environment elements and therefore bring a more favourable ecological environment for infection and transmission of new subtype of influenza virus.

From these mechanisms, we can understand the reasons that influenza pandemics sometimes occurred in the years of low sunspot number. Because the years of low sunspot number were just the years of high cosmic ray intensity on the earth[6], so the years of low sunspot number were just the years of high ultraviolet intensity incident on the surface of the earth.

C. Influenza and novae

The researches on the relationship between cosmic ray environment and influenza pandemic provide a new way for exploring causes of other influenza pandemics. We might envisage that influenza pandemic can also be aroused by other astronomical phenomena not just the sun, if these phenomena can cause large enhanced effect of cosmic ray environment of life on the earth.

Here we want to raise a new issue i.e. the relationship between the novae and influenza pandemics. From table 1 we notice that there is a very good corresponding relationship between bright novae and the front four influenza pandemics occurred in this century. In this century there have hitherto occurred only eight novae with maximum apparent magnitude(MAM) brighter

than 2.2. And table 1 listed as many as five bright novae. The three others are GK Per with MAM 0.2 in Feb.1901, V476 Cyg with MAM 2.0 in Aug.1920, and V1500 Cyg with MAM 2.2 in Aug.1975. After the occurrence of Nova V1500 Cyg, we have noted that swine influenza virus(H_{sw}1N1) reappeared in 1976 and the H1N1 subtype resurfaced in 1977 and spread to wide regions of the world. After the occurrence of Nova V476 Cyg, we have also noted that influenza epidemic occurred in many countries, such as UK, Ireland, Belgium, Norway etc., the influenza mortality reached a peak in 1922.[5] As regards the Nova GK Per, we have not had detailed epidemiological data of influenza in 1902, so we donot know whether an influenza epidemic occurred or not in that year. We note that after seven bright novae out of those eight all occurred epidemics or pandemics of influenza. Therefore, the corresponding relation between bright novae and influenza pandemics is also very remarkable.

About the great pandemic of 1918-1919 we think that its beginning was caused by other factor but the Nova V603 Aql took a decisive role for that why the second wave of this pandemic became very different than the first wave in harafulness and turned to the most spectacular outbreak of any disease for hundreds of years.

Table 1. The contrast between bright novae and the first four influenza pandemics in the 20th century

The beginning dates of influenza pandemics[5]	Bright novae[7]
1918	Nova V603 Aql, maximun apparent magnitude -1.1 on June 10,1918
1926	Nova RR Pic, maximun apparent magnitude 1.2 on June 8,1925
1936	Nova DQ Her, maximun apparent magnitude 1.4 on Dec.22,1934
	Nova CP Lac, maximun apparent magnitude 2.1 on June 20,1936
1943	Nova CP Pup, maximun apparent magnitude 0.2 on Nov.11,1942

Table 2. The contrast between the years of maximun of brightness of Nova η Car and the years of influenza pandemics in the 18th and 19th centuries

The years of epidemics and pandemics of influenza by J.R.Mote[2]	All the years of maximun of brightness of Nova η Car[7]	The years of influenza pandemics by W.I.B.Beveridge[3]
1709-1712		
1729-1733	1729	1732-1733
1757-1762	1752	
1767		
1772		
1775-1776		
1780-1782		1781-1782
1788-1790		
1798-1803	1801	1800-1802
1830-1833	1827	1830-1833
1836-1837		
1847-1850	1843	1847-1848
1857-1858	1856	1857-1858
1873-1875	1871	
1889	1889	1889-1890

ORIGINAL PAGE IS
OF POOR QUALITY

As regards the influenza pandemics of 18th and 19th centuries, we found that there existed an interesting relationship between them and Nova η Car. The brightness of η Car was variable. It was sometimes bright and sometimes dark. According to the researches by C.Payne-Gaposchkin,[7] in 18th and 19th centuries its maximum occurred only eight times. Table 2 shows that after every maximum of brightness of Nova η Car there was almost always the influenza pandemic. Especially in the 19th century, their relation was bordering on one to one corresponding relation. It is hardly conceivable for such good correlation. Is it possible that the Nova η Car could bring a very large amount of UV,X- and γ-rays incident on the earth when it turned up outburst?

Nova is a violent phenomenon of star explosion. People believe it is one of the sources of cosmic rays. If the nova can really bring the influenza pandemic, then the transmitter of nova information should be its high energy X-,γ-rays (nova's X-,γ-rays→ the depletion of the atmospheric ozone layer→ the strong increase in the solar UV incident on the surface of the earth → influenza pandemic). Nevertheless, bright nova is a rare astronomical phenomenon. In the past forty years or so there occurred only one bright nova with MAM 2.2. The modern data of cosmic ray intensity variation effect of nova are very few, so it is difficult now to make sound comments on affection extent of bright nova on earth's cosmic ray environment. However, the excellent correlation between influenza pandemics and novae implies strongly that the cosmic ray environment variation of earth should be seriously investigated after the occurrence of nova. Therefore, we suggest that the intensity variation of X-,γ-rays and UV will have to be investigated by various observation means from ground level to satellite altitude when turning up outburst for η Car or when occurring of bright nova in the future.

D. To predict influenza epidemic

According to the excellent correlation in the past, we propose four indexes to predict future influenza pandemics: first, the occurring of the large GLE; second, the occurring of the bright nova; third, the turning up outburst again for η Car; fourth, the large enhancement of life's cosmic ray environment caused by other astronomical phenomena.[8][9][10] When one of these indexes takes place, it would not at all be surprising if a new influenza pandemic should emerge soon after.

We are glad to report that according to the first index we successfully predicted the influenza epidemic in 1984. On Dec.8,1982 there occurred a middle GLE.[11] So the author wrote a report to the China Influenza Centre to predict that influenza epidemic would soon emerge in the world in 1984. As expected, the influenza epidemic has emerged. In the USSR in two months from the second half of January to the first half of March the number of cases of influenza illness reached several millions, about 3-5% of the population were affected during the week of highest activity,[12] in big cities and in the capitals of fifteen Soviet Socialist Republics the incidence reached about 10% of the population. In the same time, widespread influenza illness has been reported also in the USA, many european countries, Japan, Pakistan, Algeria, Morocco, Tonga etc..[13] Therefore, one of the viewpoints of this paper has got a successful verification.

References:

1. Ing R. Solar activity and influenza. Nature 1978; 276:556.
2. Note JR. Human and swine influenzas. In: Virus and Rickettsial Diseases. Harvard University Press, 1948: 429-516.
3. Beveridge WIB. Influenza,The Last Great Plague. New York: Prodist, 1977: 27-30.
4. Duggal SP. Relativistic solar cosmic rays. Rev Geophys Space Phys 1979; 17:1021-58.
5. Zhdanov VM,et al. Influenza. Moscow, 1958: 408-422. (in Russian)
6. Pomerantz MA, Duggal SP. The sun and cosmic rays. Rev Geophys Space Phys 1974; 12:347.
7. Payne-Gaposchkin C. The Galactic Novae. Amsterdam: North-Holland, 1957: 2-98.
8. Wdowczyk J, Wolfendale AW. Cosmic rays and ancient catastrophes. Nature 1977;268:510-12.
9. Clark DH, McCrea WH, Stephenson FR. Frequency of nearby supernovae and climatic and biological catastrophes. Nature 1977; 265:318-19.
10. Agraval SP, Ananth AG, Bemalkhedkar MN, Kargathra LV, Rao UR. High-energy cosmic ray intensity increase of nonsolar origin and the unusual Forbush decrease of August 1972. J Geophys Research 1974; 79:2269-80.
11. Fenton KB, Fenton AG, Humble JE. Cosmic ray flare increases. Proc 18th Int Cosmic Ray Conf 1983; 4:189.
12. WHO. Wkly Epidem Rec 1984; 59:115.
13. WHO. Wkly Epidem Rec 1984; 59:19-179.

ORIGINAL PAGE IS
OF POOR QUALITY

Strong Earthquakes, Novae and Cosmic Ray Environment

Yu Zhen-dong

Hubei Research Institute of Environmental Protection, Wuhan, China

N85-35135

Abstract

This paper suggests some new observations about the relationship between seismic activity and astronomical phenomena. First, after investigating the seismic data (magnitude 7.0 and over) with the method of superposed epochs we find that the world seismicity evidently increased after the occurring of novae with maximum apparent magnitude brighter than 2.2. Second, a great many earthquakes of magnitude 7.0 and over concentrated to occur in the 13th month after the occurring of two largest Ground Level Solar Cosmic Ray Events (GLEs). From these, we put forward explanations of the causes about three high level phenomena of global seismic activity in 1918-1965 and suggest that according to the information of large GLE or bright nova we shall be able to predict the occurring time of global intense seismic activity.

Is seismic activity affected by astronomical phenomena? This paper tries to offer some noticeable results.

A. Seismic data used in this paper

Gutenberg and Richter (1954)[1] edited the catalog of worldwide large earthquakes in 1904-1952. But the number of earthquakes is incomplete for magnitude below 7.9 in 1904-1917. Duda (1965)[2] and Rothe (1969)[3] continued Gutenberg-Richter's classical work. They extended the catalog to 1965. Therefore, this paper discusses world seismicity of magnitude 7.0 and over in 1918-1965.

B. The effect of bright novae on world seismicity of magnitude 7.0 and over

During this period of 1918-1965 there appeared six novae with maximum apparent magnitude brighter than 2.2.[4] For investigating the effect of novae on seismic activity, the method of superposed epochs requires to define the "zero day". This date ought to be the date when nova started explosion. But this date was often uncertain. Because brightness rose very fast for most novae, from starting explosion to maximum brightness the duration was only a few days, we unify to use the date of maximum brightness as the "zero day". It is available to those six except Nova RR Pic.The character for Nova RR Pic was that its risen period sustained for a long time (Payne-Gaposchkin,1957)[4]. Its maximum apparent magnitude was 1.2 on June 8,1925 and before two months, however, it had already reached apparent magnitude 3.0. It probably took a long time from starting explosion (apparent magnitude 12.7),to apparent magnitude 3.0. So for the present we move the date up 3 months from its maximum brightness date, namely March 8,1925, as the "zero day".

From the next day of the "zero day" on,we take every two months as one time-interval and investigate the numbers of worldwide earthquakes in every time-interval.For six novae we obtain the mean value of earthquake number in each time-interval.They are shown in figure 1.

From fig. 1 we note that after the occurrence of bright novae the curve of seismic activity was evidently higher than horizontal line. The increased effect showed successive two waves. In the forty months after the occurrence of bright novae the number of worldwide earthquakes of magnitude 7.0 and over increased eleven or so on average than the mean level before the occurrence of novae. Because there is no third party which can affect the nova and the seismic activity simultaneously, the obvious relationship of them has to be understood as the causation. Therefore, statistical analysis shows that there is an effect that bright novae caused enhanced seismic activity of magnitude 7.0 and over.

Although it is still unclear now about the variation of cosmic-ray environment around Earth after the occurrence of bright novae, yet we can presume that the enhanced seismic activity was caused by nova's x-, r-rays incident upon the earth.

C. The effect of large GLE on world seismicity of magnitude 7.0 and over

Since the start of systematic and continuous observation of cosmic rays,the number of GLE was rare in past forty years or more (Duggal,1979)[5]. Among them large GLE happened only five times and they are shown in table 1 (Dorman,1957)[6]. In table 1 in the years of the occurrence of front three GLEs there also occurred bright novae, their seismic effects were overlapped. The single seismic effect of large GLE cannot be shown. So we discuss the last two events, i.e.two largest GLEs.

From the next day of those two GLE's dates on, we investigate the numbers of worldwide earthquakes of magnitude 7.0 and over in every month and obtain fig.2. From fig.2 we note that in the

ORIGINAL PAGE IS
OF POOR QUALITY

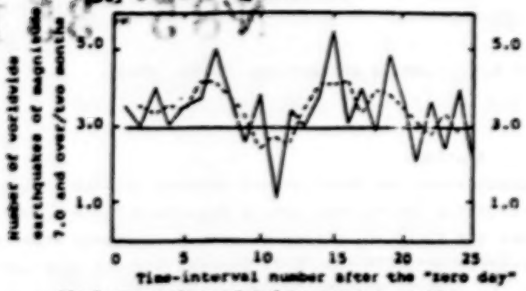


Fig.1 The effect of bright novae on world seismicity of magnitude 7.0 and over

six bright novae:V603Aql,V476Cyg,RRPic,DQHer,CPLac,CPPup.
solid line: curve of the average of earthquake numbers
dashed line:curve of three time-intervals running average

The horizontal line of 2.97 is two-monthly average of the number of worldwide earthquakes of magnitude 7.0 and over in six two-years before the "zero days" of six bright novae (before the "zero day" of each bright nova all take two years). It represents the mean level of seismic activity when the seismic effect of bright novae did not occur yet.

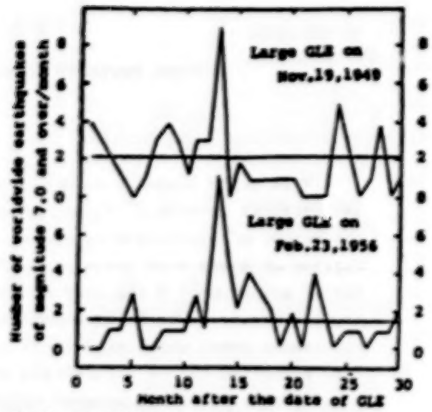


Fig.2 The effect of large GLE on world seismicity of magnitude 7.0 and over

The horizontal lines of 2.17 for upper part and 1.46 for under part represent respectively the monthly mean level of global seismic activity before the occurrence of two GLEs. They are the averages of the numbers of worldwide earthquakes of magnitude 7.0 and over in two years prior to the GLE date.

Table 1 The large GLE data

No.	Date	$\frac{I_{max}}{I}$ *, %	Remarks
1	Feb.28,1942	15.5	average on 15 minutes
2	Mar. 7,1942	15	"
3	Jul.25,1946	22	"
4	Nov.19,1949	57	"
5	[illegible]	200	

* The sea-level enhanced magnitude of cosmic ray hard component at high latitudes (Dorman,1957).



Fig.3 The annual number of worldwide earthquakes of magnitude 7.0 and over in 1918-1965

13th month after the occurrence of the GLE there occurred unusual groups of worldwide large earthquakes. Earthquake number increased extremely obviously. Both of two events were just the same. The risen amplitudes are so high and the peak times are so uniform, thereby fig.2 clearly shows the effect of large GLE on seismic activity of magnitude 7.0 and over. About large GLE in 1949, in increased period (7th-13th month after the GLE's date) the number of worldwide earthquakes of magnitude 7.0 and over increased eleven than that of mean level prior to the occurring of the GLE. About large GLE in 1956, in increased period (11th-18th month after the GLE's date) the number of worldwide earthquakes of magnitude 7.0 and over increased seventeen than that of mean level prior to the occurring of the GLE.

It can be questioned that whether the enhanced seismic activity would be able to cause by other emission component of those two solar flares on Nov.19,1949 and on Feb.23,1956.Among solar flare emissions, besides solar cosmic rays (SCR) there were also plasma cloud, visible light,UV, X-rays and radio emission. At the time of the occurring of other large solar flares, except for the large GLE the sudden big increase of these components had been observed many times. But after them the enhanced seismic activity has not been observed. The enhanced seismic activity was only after the large GLE. Therefore we could judge that the enhanced seismic activity was just caused by enhanced high-energy SCR.

D. About causes of three high level phenomena of global seismic activity of magnitude 7.0 and over

1. About the decade of the most earthquake number

From fig.3 we note that the forties were the decade of the most earthquake number. Why was this? It turned out to be that the Earth's cosmic ray environment occurred quite a few enhanced events. In the forties there occurred four times out of five large GLEs described above.At the same time, in 1942 there occurred the Nova CP Pup which is the brightest nova in the last sixty years. Besides, in 1946 there also occurred the recurrent Nova T CrB (Payne-Gaposchkin,1957)[4]. These astronomical phenomena all gave rise to enhanced effects of seismic activity. So the forties became the decade of the most earthquake number.

ORIGINAL PAGE IS
OF POOR QUALITY

2. About the year of the most earthquake number and about the years in which earthquake number strikingly increased

From fig.3 we note that in 1943 there occurred the most earthquake number and it unexpectedly was forty. Why was this? It turned out to be that in 1942 there simultaneously occurred two large GLEs and the bright Nova CP Pup. The enhanced periods of seismic activity caused by them were in 1943. So the number of large earthquakes was so high in that year. From fig.3 we note that in some years the earthquake number suddenly increased over ten than their last year. These years were1931, 1943 and 1957. Why was this? The reason for 1943 has explained above. For 1957 it was due to the occurrence of large GLE on Feb.23,1956 which was the largest GLE since the start of systematic and continuous observation of cosmic rays. The enhanced period of seismic activity caused by it was in 1957, so the number of large earthquakes unusually increased than 1956. As regards 1931,because at that time it had not the data of cosmic ray observation, we cannot explain it now.

3. About unusually concentrated periods of earthquakes of magnitude 7.0 and over

The yearly average of the number of worldwide earthquakes of magnitude 7.0 and over was 19.5 in 1918-1965. It corresponded to 3.25 per two months. Nevertheless, in the some periods the seismic activity was unusually high. The number of earthquakes reached over ten in two months and was three times or more of the average. Why was this? In table 2 we listed all of these data in 1918-1965 and put forward explanations of their causes.

The concentrated phenomenon of large earthquakes was more projecting for one month. The monthly average of the number of worldwide earthquakes of magnitude 7.0 and over was 1.6 in 1918-1965. Nevertheless, in the some periods the earthquake number reached unexpectedly 8 or 9 in a month and was five times of the average. In table 3 we listed all of these data in 1918-1965 and put forward explanations of their causes.

Above explanations could already illustrate that the occurring of high level phenomena of global seismic activity of magnitude 7.0 and over was neither accidental nor at random.

Table 2 The explanation of causes on all of the data which the earthquake number of magnitude 7.0 and over reached over ten in two months(61 days) in 1918-1965

No.	Date	Earthquake number M≥7.0	Explanation on causes
1	Jan.27,1931-Mar.28,1931	11	?
2	Oct.10,1938-Dec. 6,1938	11	The Nova CP Lac in 1936: Possible large GLE in Oct.1937?
3	Feb.16,1943-Apr. 9,1943	11	Large GLEs on Feb.28,1942 and on Mar.7,1942: Also existing the effect of the Nova CP Pup in 1942
4	Oct.21,1943-Dec. 1,1943	12	The Nova CP Pup in 1942: Also existing the effect of two large GLEs on Feb.28,1942 and on Mar.7,1942
5	Aug. 2,1946-Sept.30,1946	11	The Nova T CrB in 1946: Large GLE on July 25,1946
6	Jan. 4,1948-Mar. 3,1948	11	The Nova T CrB in 1946: Large GLE on July 25,1946
7	Oct.23,1950-Dec.14,1950	12	Large GLE on Nov.19,1949
8	Mar. 9,1957-Apr.25,1957	15	Large GLE on Feb.23,1956

Table 3 The explanation of causes on all of the data which the earthquake number of magnitude 7.0 and over reached eight in 31 days in 1918-1965

No.	Date	Earthquake number M≥7.0	Explanation on causes	Interval*
1	Nov. 5,1938-Nov.30,1938	8	Possible large GLE in Oct.1937?	
2	Mar. 9,1943-Apr. 9,1943**	8	Large GLEs on Feb.28,1942 and on Mar. 7,1942: Also existing the effect of the Nova CP Pup in 1942	12 months or more
3	Nov. 2,1943-Dec. 1,1943	9	The Nova CP Pup in Nov.1942: Also existing the effect of two large GLEs in 1942	12 months or so
4	Dec. 1,1950-Dec.14,1950	9	Large GLE on Nov.19,1949	12 months or more
5	Mar. 9,1957-Mar.23,1957	9	Large GLE on Feb.23,1956	12 months or more

* The interval between the beginning date of seismic activity increased period and the occurring date of its major cause.

** The interval was 30 days 23 hours between the large earthquakes on Mar.9 and on Apr.9.

E. Discussion

1. We discuss some tentative ideas on mechanisms that cosmic rays affect seismic activity. The cosmic ray particles incident in lithosphere were rare. It was still limited when occurring large GLE. So the effect of the direct action probably is very small for the mechanisms.

Cosmic rays gave rise to atmospheric ionization when they passed though the atmosphere. The ionicity had difference at different atmospheric altitude and at different geomagnetic latitude. From the atmospheric ionization there forms an atmospheric electric-field,we call it cosmic ray atmospheric electric-field. Its maximum intensity was at the top of troposphere or at the bottom of stratosphere. When occurring the large GLE the cosmic-ray atmospheric electric-field would intensify. The sudden intensifying of atmospheric electric-field probably was just the factor which led to the occurrence of enhanced seismic activity. Through affecting the telluric electric-field and atmospheric circulation which affected the rate variation of the Earth's rotation it finally led to the occurrence of large earthquakes. The possible mechanisms are as follows:

solar cosmic rays or nova's x-,r-rays ⟶ cosmic ray atmospheric electric-field ⟶ atmospheric circulation ⟶ Earth's rotation ⟶ earthquakes

cosmic ray atmospheric electric-field ⟶ telluric electric-field ⟶ earthquakes

2. About the groups of largeearthquakes in Mar.1943,Dec.1950 and Mar.1957(see table 3),we think they were caused by the corresponding large GLE one year ago.It seems to show that at least for some earthquakes of magnitude 7.0 and over their brewing time was not long,only one year or so.

3. Fig.1 shows the seismic effect of bright novae had successive two waves. We think that it probably was caused by two batches of nova's radiation which reached Earth in different time.The first batch reached Earth in the time which was soon after or simultaneous with the visible light. From fig.1 we estimate that the main current of the second batch reached Earth in the 17th month or so on average after nova started explosion. Aikin et al.(1980)[7] suggested that among supernova radiation caused Earth effects the first batch was prior to the second batch to reach Earth for several months. Maybe nova is similar to supernova.

4. The explosion scale of supernova is more violent than that of nova. If occurring the bright supernova visible to the naked eyes, we could infer that the global seismic activity will soon increase obviously.

5. Since aforesaid change of cosmic ray environment could lead to the increase of world seismicity, we could infer that the background and other variations of cosmic rays should also be able to affect the world seismicity.

6. The occurring of the groups of large earthquakes is not a mystery to us now.Moreover,as a means it could help us to research the changes of cosmic ray environment. That is,it is an "indicator", according to this indicator we can know the enhanced event of cosmic ray environment had already occurred before it. For example, about the groups of worldwide large earthquakes(M ≥ 7.0) in 1931 and in Nov.1938[1] we could infer that in 1930 there probably had occurred the enhanced event of cosmic ray environment and in Oct.1937 there probably had occurred a large GLE.

7. When occurring the large GLE or bright nova in future, according to fig.1,fig.2, and table 3 we shall be able to predict the occurring time of global intense seismic activity.

References

1. Gutenberg,B.,and C.F.Richter(1954). Seismicity of the earth and associated phenomena, Princeton University Press, Princeton, 133-160.
2. Duda,S.J.(1965). Secular seismic energy release in the Circum-Pacific Belt, Tectonophysics 2, 409-452.
3. Rothe,J.P.(1969). The seismicity of the earth 1953-1965, UNESCO, 29-307.
4. Payne-Gaposchkin,C.(1957). The galactic novae, North-Holland, Amsterdam, 2-146.
5. Duggal,S.P.(1979). Relativistic solar cosmic rays, Rev. Geophys. Space Phys. 17, 1021-1058.
6. ДОРМАН(Dorman),Я.Н.(1957). Вариации Космических Лучей, ГОСТЕХИЗДАТ, МОСКВА, 353-395.
7. Aikin,A.C.,S.Chandra,and T.P.Stecher(1980). Supernovae effects on the terrestrial atmosphere, Planet. Space Sci. 28, 639-644.

N85-35136
SH IO.I-5

OBSERVATION OF NUCLEI WITH ENERGIES 8-30 MeV PER NUCLEON IN THE EARTH's MAGNETOSPHERE AT THE ALTITUDES 350 KM

Bobrovskaya V.V., Grigorov N.L., Gordeev Yu.P., Zhuravlev D.A., Nymmik R.A., Podgurskaya A.V., Smolensky L.G., Tretyakova Ch.A., Gordeev I.V., Iyagushin V.I., and Soloviev A.V.

Institute of Nuclear Physics, Moscow State University
Moscow, USSR

ABSTRACT

Observations of the flux of nuclei with an energy of IO MeV per nucleon on the Salyut-7 Station in September I984 are presented. The observed flux is smaller by a factor of 50 than the flux detected in May, I98I.

I. Introduction. We continue investigations of the fluxes of nuclei with energies of 8-30 MeV per nucleon in the orbits of scientific stations (inclination $\sim 50^{\circ}$, height ~ 350 km). The noted nuclei cannot get into these orbits from the interplanetary space because of the insufficient magnetic rigidity. In ref. /I/ the nuclei observed in I973/74 year were interpreted as the particles of the anomalous cosmic ray component which, according to ref. /2/, are the singly-charged atoms. Our preceding experiment performed in May, I98I /3/ speake in favour of the magnetospheric origin of the observed particles, which was first suggested in ref. /4/.

This paper reports the preliminary results of a new experiment made with the improved technique enables one both to measure the flux of nuclei and to fix the registration point in the orbit.

2. Experiment. We used an instrument with 3 stacks of 3.7xI2.5 cm^2 dielectric track detectors. Each stack contained IO sheets CN-85 of I00 mkm thick and was protected against the ultraviolet solar radiation by two layers of aluminized lavsan film I.4 mg/cm^2 in total thickness. During the experiment the 3 mm thick Al screen was displaced above two stacks (No.I and No.2) to cover one of them depending on the value of proton flux incident upon the instrument. In the region of the Brasil magnetic anomaly when the proton flux ex-

ceeded 10^2 $cm^{-2}sec^{-1}$ the screen covered the stack No.I and the nuclei were detected with the stack No.2. Outside the Brasil magnetic anomaly the screen covered the stack No.2 and the nuclei were detected with No.I. The stack No.3 was open throughout the exposure time. The overall weight of the instrument with the self-contained power supply and detectors was ~ 2 kg.

The instrument was delivered into the orbit on August I5, I984, On September I9 the instrument was installed in the Salyut-7 lock-chamber and was exposed to space. The exposure time was I32 hours. On October 2, I984 the detectors were returned to the Earth.

3. Analysis. The detectors were etched and the developed tracks were analysed. In each stack we revealed about a hundred of nuclei most of which got into the stacks during the 43-day storage within the station. These so-called "background" tracks are produced by the nuclei with an energy of several hundreds of MeVs per nucleon in outer space. Being decelerated in the walls and matter of the station elements, some nuclei possessing an energy < 25 MeV per nucleon, arrived at the detectors and came to rest in the cellulose nitrate film. The density of background nuclei is the same throughout the depth of relatively thin stacks. Owing to this fact we succeeded in identifying the nuclei detected in outer space as excess tracks fixed in the upper sheets of the stacks.

4. Preliminary results. On the number of tracks detected with the stack No.3 the flux of nuclei with $Z \geq 6$ at an energy of I2 MeV per nucleon is estimated to be $2 \cdot 10^{-3}$ $(m^2 s.st\,MeV/nucleon)^{-1}$. In this case the energy was estimated from the range-energy dependence for oxygen nuclei and the detection time was associated with the exposure time, I32 hours. The data from the stack No.I and No.2 show that the significant part of nuclei were observed in the region of an increased proton flux, i.e. in the Brasil magnetic anomaly, but the statistical errors of these data are high.

5. Discussion. Comparing the present experimental data and the results /3/ we conclude that the flux of nuclei in September, I984

is by a factor of about 50 less than that of in May, I98I. This difference under identical experimental conditions indicates the large time fluctuations of the flux intensity observed in the orbit. These fluctuations can explain the result /5/ that the flux of oxygen nuclei with an energy ~IO MeV per nucleon in the same orbit in I978/79 years was IO^{-2} (m^2 s. st. MeV/nucleon)$^{-I}$ which is 20 times as small as the value we obtained in May, I98I at the same solar activity.

6. Acknowledgements. We are grateful to cosmonauts N.D.Kisim, V.A. Soloviev, and O.Yu.Atikov for the work done to expose the instrument and also to S.P.Tretyakova for the etching of the stacks.

References.

I. Biswas, S., Durgaprasad, N., (I980), Skylab Measurements of Low Energy Cosmic Rays, Space Science Reviews, v.25, No.3, pp.285-326

2. Fisk, L.A., Kozlovsky, B., Ramaty, R., (I974), An Interpretation of Observed Oxygen and Nitrogen Enhancement in Low-Energy Cosmic Rays, Ap. J., I90, I35.

3. Bobrovskaya, V.V., Gorchakov, E.V., Grigorov, N.L., Nymmik, R.A., Tretyakova, Ch.A., Marin, A., Haiduc, M., Hasegan, D., (I983), The Measurement of the Fluxes of Medium Nuclei (C,N,O) With an Energy of IO-25 MeV per Nucleon in the Near-Earth Space, (I983), I8th Int. Conf. Cosmic Rays, Bangalore, India, v.2, p.2

4. Chan, I.H., Price, P.B., (I975), Composition and Energy Spectra of Heavy Nuclei of Unknown Origin Detected on Skylab, Phys. Review Letters, v.35, No.8, p.538.

5. Gagarin, Yu.F., Gordeev, I.V., Ivanova, N.S., Lyagushin, V.I., Smirnov, A.B., Soloviev, A.V., Khilyuto, I.G., Yakubovskii, E.A., (I983), Anomalous Fluxes of Low-Energy Nuclei in the Salyut-6 Orbit, Izv. Akad. Nauk SSSR, ser. fiz., 47, №9, p.I844.

SH 10.1-6

MEASUREMENT OF LOW ENERGY COSMIC RAYS ABOARD SPACELAB-1

N85-35137

R.Beaujean, K.Oschlies, and W.Enge
Institut für Reine und Angewandte Kernphysik
der Universität Kiel, 23 Kiel, W.-Germany

Abstract

In December 1983 the first Spacelab mission was launched for a duration of 10 days. Aboard was the Kiel experiment "Isotopic Stack" designed for measurement of heavy cosmic ray nuclei with nuclear charge equal to or greater than 3 and energies up to some 100MeV/nuc. One part of the stack was rotated in well defined steps registered by an angle encoder to receive information on impact times of the nuclei. Using this time resolving system "geomagnetically forbidden" particles can be detected.
In this work the chemical composition and energy spectra of mainly CNO particles are examined using a rotated 300µm thick CR-39 foil beneath a fixed 100µm thick Kodak-Cellulose Nitrate foil. About 600cm^2 have been scanned yielding nearly 100 nuclear tracks within an energy range of approximately 8 to 30 MeV/nuc.
The calibration is done by means of a postflight irradiation with 410 MeV/nuc ^{56}Fe at Berkeley Laboratory, California, USA.
Relative abundances and energy spectra will be presented.

Keywords : Spacelab-1, heavy cosmic rays, plastic track detectors

N85-35138

N85-35138

SH 10.1-7

HEAVY COSMIC RAY MEASUREMENT ABOARD SPACELAB-1

R.Beaujean, J.Krause, E.Fischer, and W.Enge
Institut für Reine und Angewandte Kernphysik
der Universität Kiel, 23 Kiel, W.-Germany

Abstract

A stack of CR-39 plastic track detectors was exposed to the cosmic radiation during the 10 days mission aboard Spacelab-1. A part of the stack was rotated one revolution within 7 days. The impact time of most of the particles was correlated with the orbit position of the shuttle and thus with geomagnetic field parameters. In this work we report on the analysis of heavy particles with charge $Z \geq 6$ in the energy range 50-150 MeV per nucleon with special emphasis on "geomagnetically forbidden" particles.

Keywords: Spacelab 1, heavy cosmic rays, geomagnetic field effects, plastic track detectors

N85-35139

N85-35139

SPORADIC RADIO EMISSION CONNECTED WITH A DEFINITE MANIFESTATION OF SOLAR ACTIVITY IN THE NEAR EARTH SPACE

Dudnic A.V., Zaljubovsky I.I., Kartashev V.M., Shmatko E.S.

Kharkov State University, USSR.

Sporadic radio emission of near earth space at the frequency of 38 MHz is shown to appear in case of fast development of instabilities in ionospheric plasma. The instabilities are generated due to primary ionospheric disturbances occuring under the influence of solar chromospheric flares.

During the period close to 21st cycle maximum of solar activity the investigation of sporadic radio emission in the near earth space [1] was carried out at the frequency of 38 MHz using the experimental installation of Kharkov State University [2]. The results of the experiment confirmed the existance of sporadic radio emission in the meter radio wave range [3], in its long wave range in particular. All the types of noise radio emission mentioned in [1] were observed. Fig. 1 presents some examples of the short-time events (0,5 ÷ 7m) detected at the frequency of 38 MHz. Attention was focused on existance of short-time cosmic noise absorptions with sudden onset and end (5,6) . There phenomena are not observed at the dm and cm ranges and can't be identified as ionospheric disturbances of SCNA types [4]. Bursts andabsorptions with fine oscillatory structure can also be attributed to the type of events unobser-

vable in [1].

ORIGINAL PAGE IS
OF POOR QUALITY

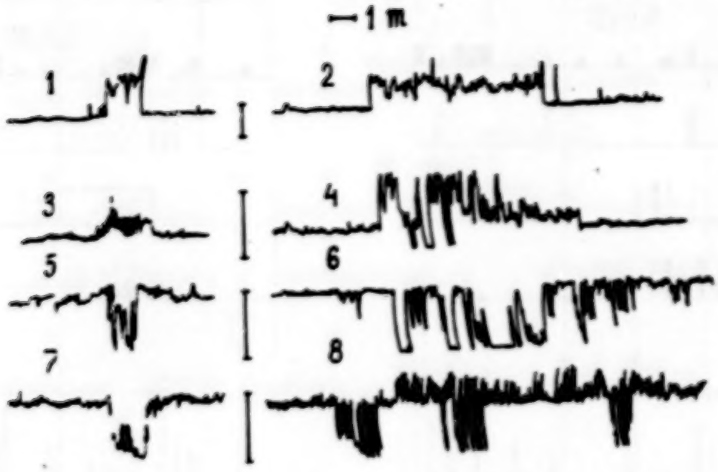
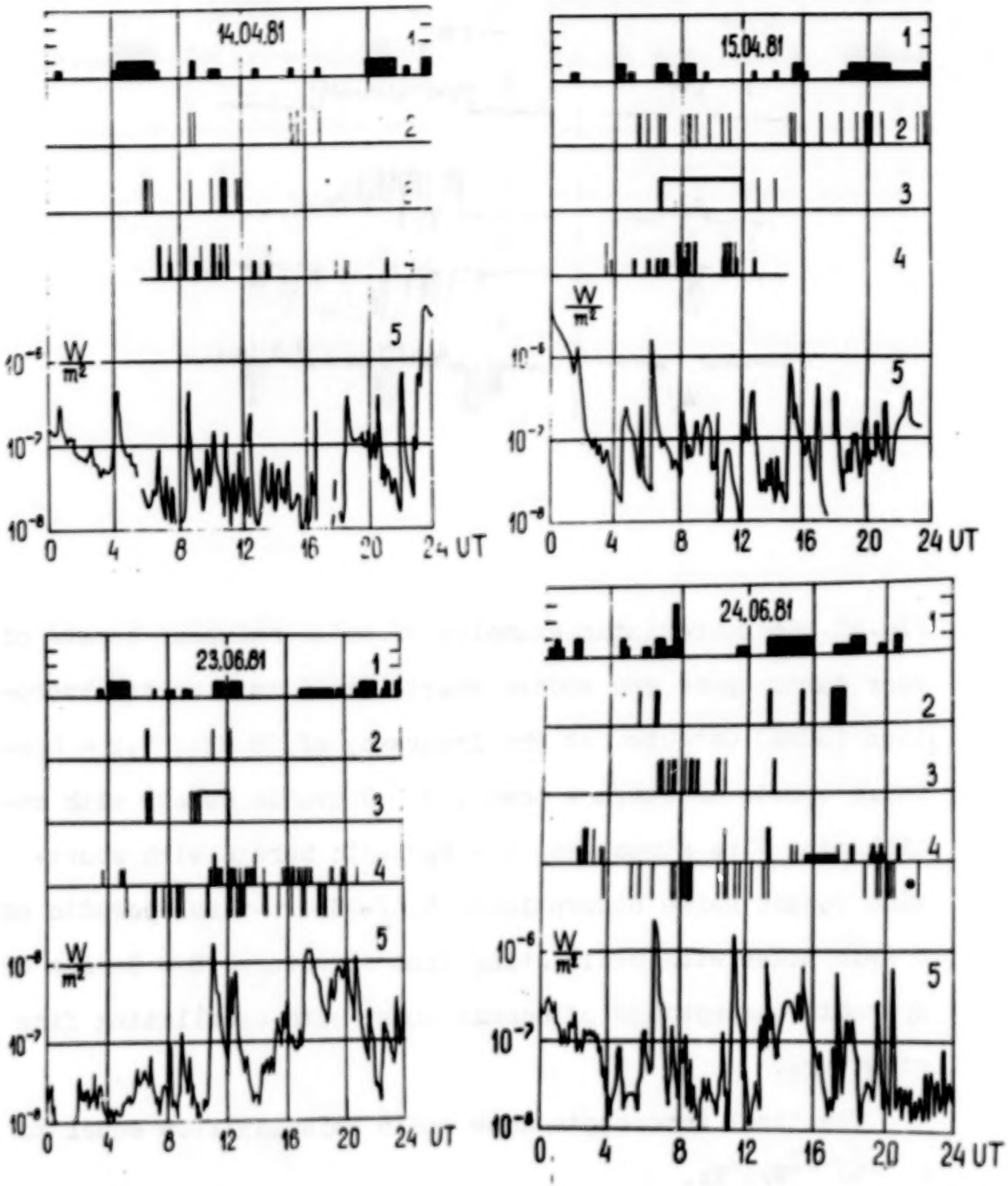


Fig. 1. Characteristic examples of radio emission bursts of near earth space and sudden short-time cosmic noise absorption (SCNA) detected at the frequency of 38 MHz. 1,2 - Sporadic bursts of overage power. 3 - Sporadic bursts with oscillating fine structure. 4 - Sporadic bursts with short-time cosmic noise absorptions. 5,67- Short-time sporadic of cosmic noise with oscillating fine structure. 8 - Series of sporadic absorptions of cosmic noise with oscillating fine structure.

Vertical intercepts show radio emission flow equal to $6 \cdot 10^{-22} W/m^2 Hz$.

The data about sporadic radio emission in near earth space at the frequency of 38 MHz obtained in spring and summer of 1981 were compared with solar data [5] in order to

find correlation with specific manifestations of solar activity. Figure 2 shows some examples of the comparison.



ORIGINAL PAGE IS
OF POOR QUALITY

Fig. 2. Time run of solar activity and near earth space spo-

radic bursts and sporadic absorptions during a sinle day and night period at the frequency of 38 MHz. UT - universal time. 1 - Chromosperic flares on the sun 1 + 3 balls. Small flares - 0.5 div. [5]. 2 - Solar radio emission bursts in cm wave range with intensity more than 1.10^{-20} W/m^{2}Hz [5]. 3 - Distinctive events on the sun in meter radio wave range [5]. 4 - Sporadic radio emission bursts (at the top) and absorptions (at the bottom) at the frequency of 38 MHz. Short vertical intercepts at the top part corresponds to radio emission bursts with signal/noise ratio less than 2. Long intercepts corresponds to radio emission bursts with signal/noise ratio $\geq$ 2. Horisontal black rectangle corresponds to noise storms. 5 - X-Ray solar emission intensity is in the spectral interval of 0.5 + 4.0 Å [5].

The main peculiarities of the events observed at the frequency of 38 MHz are the following:

1) the member of events in increased with the growth of solar activivity as is shown in [1]; 2) the rise of chromospheric flares and X-ray bursts at the Sun but there was no full coinsidence in all details; 3) there is no detailed coinsidence with distinctive solar events in radio frequency range; 4) probability of short-time sporadic absorption occurences in winter is lower than in summer; 5) series of quasiperiodic cosmic noise absorptions and quasiperiodic bursts with small signal/noise ratio are observed; 6) at day-time the probability of event occurences is higher than at night.

A detailed analysis of all peculiarities of the phenome-

N85-35140

NEAR EARTH SPACE SPORADIC RADIO EMISSION BUSTS OCCURING DURING SUNRISE

Dudnik A.V., Zaljubovs.. I.I., Kartashev V.M., Lasarev A.V., Shmatko E.S.

Kharkov State University, USSR

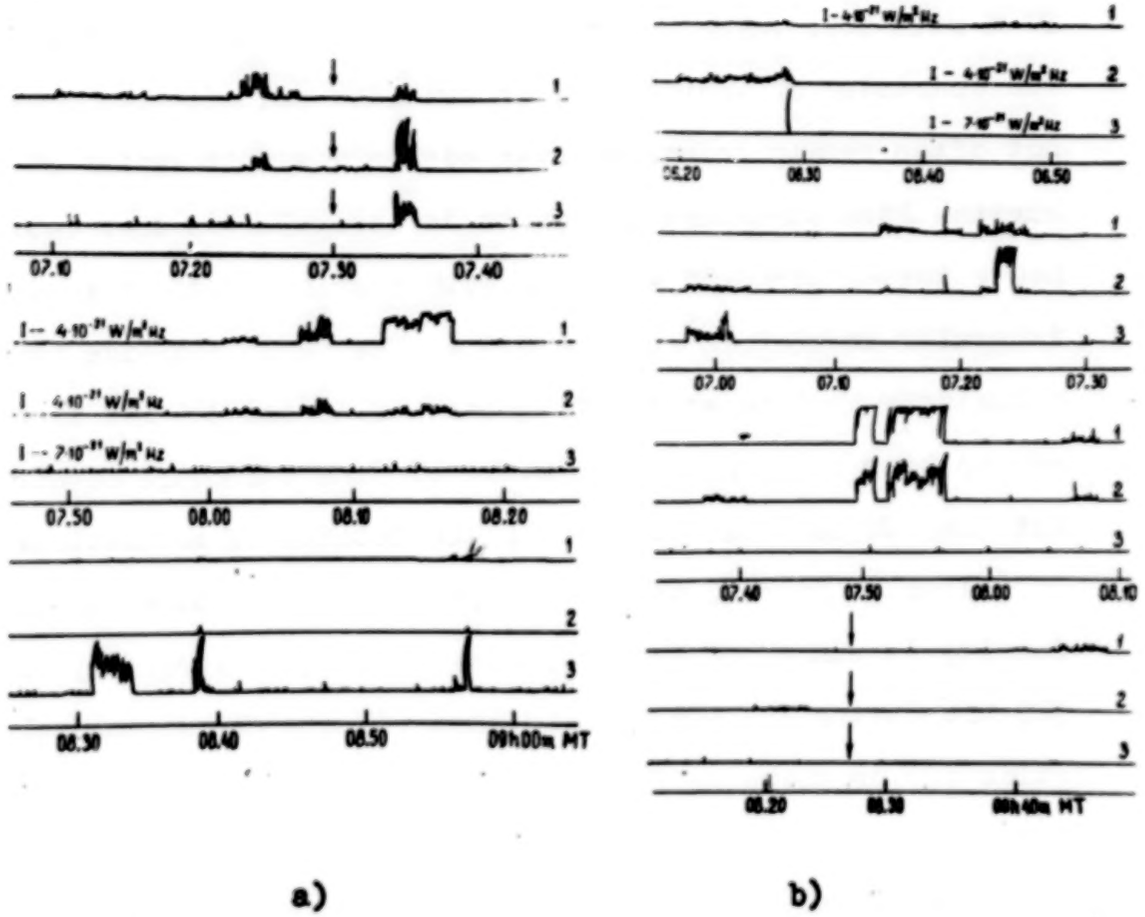
During the period of low solar activity sunrise effect of sporadic high frequency near earth space radio emission was experimentally discovered at middle lattitudes. The possible mechanism of its origin in discussed.

Since September 1984 during the period of low solar activity the study of sporadic near earth space radio emission at middle lattitudes [1] has been carried out at the experimental installation of Kharkov University [2]. The radio telescope with operating frequency of 38 MHz described in [2] was in addition provided with a mirror parabolic antenna having an effective area ~ 16 m^2 radiation pattern width $\sim 12°$ and receiving radio emission independently at the frequency of 325 MHz with East - West and North - South polarization; dual - channel radio frequency tract having the transmission band of ~ 4 MHz regulation sensitivity threshold being $2 \cdot 10^{-21}$ w/m^2 Hz for each channel. Tracing of signals was carried out with minimizing rate of 0.2 mm/s and integration time was not more than 1 s.

The analisis of experimental results proves that in

ORIGINAL PAGE IS
OF POOR QUALITY

the vicinity of the moment of morning shadow - light boundary passage through the local meridium series of radio high frequency emission burts arise diurnally at the frequecy of 325 MHz (fig. 1).



a) b)

Fig. 1. Characteristic examples of high frequency radio emission bursts series emerging during sunrise. MT - Moscow Time. Arrows show the moment of sunrise at a definite place of observation. 1 - Operating frequency of 325 MHz, East - West polarization. 2 - Operating frequency of 325 MHz, North - South polarization. 3 - Operating frequency of 38 MHz, East - West polarization. a) Morning recordig part September 28, 1984.

b) Morning recording part December 13, 1984.
The most probable duration of bursts is in the interval of 0.5 ÷ 4 m. The bursts growth and fall times are usually less than 5 s. Morning radio bursts tend to aries quasiperiodically. The quasiperiod of each bursts series is equal to 5 ÷ 20 m with mean value for full observation time being ~ 10 m. The character of sporadic radio emission polarization does not often remain unchanged even within a single series of bursts. Fine structure of bursts is irregular in most details has a period of ~0.01 ÷ 0.02 s with characteristic time of irregular modulation ~0.15 ÷ 0.5 s. The radio emission bursts coinsiding in time at the frequency of 38 and 325 MHz appeared to have similar minimal scale of fine structure details but they do not coinside in all the details of modulation.

Average diurnal course of sporadic radio emission bursts density (a number of bursts per an hour) at a frequency of 325 MHz during the autumnal equinox (1) and the winter solstice (2) is shown in fig. 2, where the sunrise and sunset are considered to take place at 6 and 18 o'clock of local time independently on the season respectively. The presence of strongly pronounced bursts density maximum during sunrise and its seasonal shift are worth emphasizing.

The observed morning effect is suggested to be connected with an excitation of internal gravity waves (IGW) by the solar terminator [3] moving in neutral atmosphere. Oscillations of IGW in neutral atmosphere draw in the ionospheric plasma and initiate its primary density disturbances. At some phase of primary disturbance in magnetized ionospheric plasma in-

ORIGINAL PAGE IS
OF POOR QUALITY

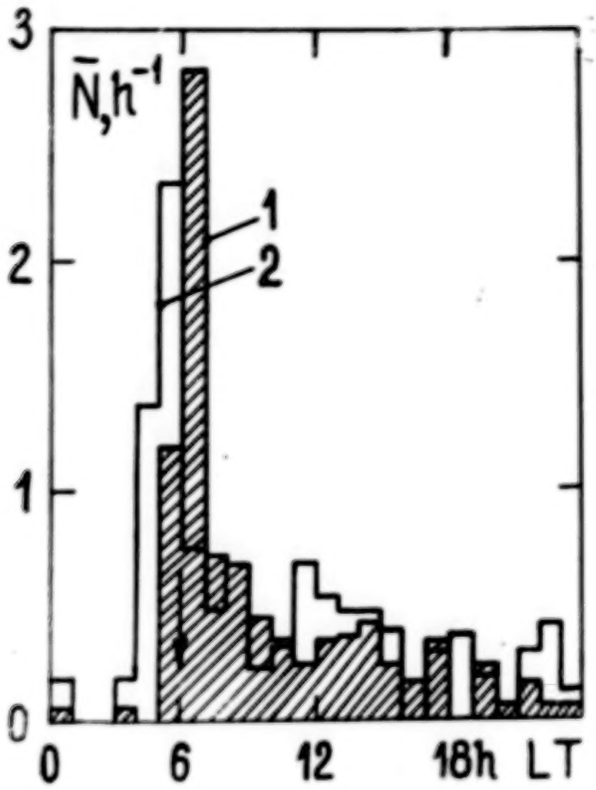


Fig. 2. Average diurnal run of near earth space sporadic radio emission reduced to equinox; $\bar{N}$ is a number of radio bursts per hour; the arrow shows the moment of sunrise; operating frequency is 325 MHz; LT is a local time. 1) September, October 1984; mean withrespect to 25 days period of observations. 2) December 1984, January 1985; mean with respect to 20 days of observations.

stabilities begin to swing quickly [4], for instance, gradient - cyclotron ion instabilities reach saturation and in this state remain unchanged during the time corres ponding to the sporadic radio emission burst duration. The instability can generate radio emission either of braking or dipole natu-

AUTHOR INDEX

AFANASYEV, KG
344
AFANASYEV, VG
344
AGRAWAL, SP
258,72,254
270,23,126
63
AHLUWALIA, HS
116,110
115
AITBAEV, FB
312
AKAHANE, S
506
ALANIA, MV
285
ALEXANYAN, TM
300
ALEXEEV, VA
418
ALEXEYENKO, VV
352
ANTONOVA, VP
278
ARNOLD, JR
379
ARVELA, H
274,242
ASATRYAN, GA
120
ATTOLINI, MR
367,375,67
71
AUDOUZE, J
398
AXFORD, I
189
BABAYAN, VKH
214,120
BADRUDDIN,
143
BADRUDDIN, RS
258
BAGDASARIAN, MB
214
BAKRADZE, TS
285
BATHURST, AA
336
BAZILEVSKAYA, GA
83,363,450
BEAUJEAN, R
537,536
BELOV, AV
356,296
BHATNAGAR, SP
316,466
BIEBER, JW
159
BISWAS, S
458,184
BLUDMAN, SA
454
BOBROVSKAYA, VV
533
BOCHIKASHVILI, DP
285
BOCHORISHVILI, TV
285
BONINO, G
375
BYRNAK, B
328
CASTAGNOLI, GC
375,71
CECCHINI, S
367,67,71
CHAN, KW
494
CHARAKHCHYAN, TN
75,90,363
79,450
CHEN, TM
371
CHIBA, T
19
CHINO, K
506
CHRISTON, SP
197
CHUANG, LS
134,494
486,486
CHUDAKOV, AE
352
CHUPP, EL
474
COOKE, DJ
328,328
COOPER, JF
474
CUMMINGS, AC
163,172
197
DAI, KM
371
DANILOVA, OA

PRECEDING PAGE BLANK NOT FILMED

AUTHOR INDEX

DANILOVA, OA
359,324
DATT, SC
126
DECKER, RB
202
DESPOTASHVILI, MA
285
DJAPIASHVILI, TV
87
DORMAN, IV
490,218
DORMAN, LI
214,293
300,518
356,296
490,281
DRAGOVITSCH, P
390
DUDNIK, AV
538,542
DULDIG, ML
5,44
DURGAPRASAD, N
458,184
DVORNIKOV, VM
359,151
DYUISEMBAEV, BM
312
ENGE, W
537,536
ENGLERT, P
394,394
390
ERDOS, G
111
EROSHENKO, EA
296
FAN, CY
371
FENTON, AG
308,39,60
60,42
FENTON, KB
308,39,60
FILLIUS, W
189
FISCHER, E
537
FISK, LA
180
FLUCKIGER, EO
336
FORREST, DJ
FORREST, DJ
474
FRYE, GM
498
FUJII, Z
35,147,106
FUJIMOTO, K
262
GALLI, M
367,375,67
71
GALVIN, AB
168
GENTILE, LC
332
GEORGIEV, L
139
GERTH, E
434
GLOECKLER, G
176
GLUKHOV, GA
348
GORCHAKOV, EV
344,90
GORDEEV, IV
533
GORDEEV, YUP
533
GORET, P
328
GRIGOROV, NL
533
GULINSKY, OV
518,281
GUSHCHINA, RT
356
HAKAMADA, K
13
HAMPEL, G
422
HASEGAWA, M
430
HAUBOLD, HJ
434
HEUSSER, G
422
HIGUCHI, T
506
HOVESTADT, D
168,176
HUA, YS
482
HUBNER, M

AUTHOR INDEX

HUBNER, M
422
HUMBLE, JE
328,308,39
60,42,340
HURLEY, KC
470
HYLAND, GB
308
ICHINOSE, M
506
IGNATYEV, PP
344
IMAI, T
130
INAZAWA, H
446
INOUE, A
309,510
IOZENAS, VA
344
IPAVICH, FM
168,176
IP, WH
1
ISHIDA, Y
31
ISHKOV, VN
296
ISKRA, K
138
IUCCI, N
226,230
234
IYAGUSHIN, VI
533
JACKLYN, RM
5,44
JAIN, AK
270,63
JENKINS, TL
498
KAMINER, NS
293
KARTASHEV, VM
538,542
KATO, M
266
KAVLAKOV, S
139
KAVLASHVILI, BG
87
KIKO, J
422
KINZER, RL
474
KITAMURA, T
446
KLECKER, B
168,176
KOBAYAKAWA, K
446
KOCHAROV, GE
414,414
410
KODAMA, M
246
KOJIMA, H
262
KOLOMEETS, EV
312
KOROTKOV, VK
300,490
KOTA, J
111
KOTHARI, SK
320,466
KRASOTKIN, AF
75
KRATENKO, YUP
348
KRAUSE, J
537
KRAVTSOV, NG
155
KRIMIGIS, SM
202
KRIVOSHAPKIN, PA
52,155,94
KUDO, S
246,486
KUMAR, S
124,125
126
KURGUZOVA, AI
75
KUSUNOSE, M
134,304
482,486
KUZ'MICHEVA, AE
293
KUZMIN, AI
250,52,155
LAL, N
193
LANZEROTTI, LJ
72
LALAREV, AV

LASAREV, AV
542
LAVRUKHINA, AK
418
LEE, HS
454
LEE, MA
180
LEVEDAHL, WK
470
LIBIN, IYA
490,281
LIN, RP
470
LOCKWOOD, JA
185
LUMME, M
274,242
LUND, N
328
MAKHMUTOV, VS
363
MARTI, K
379,402
MASON, GM
168
MCDONALD, FB
193
MCKIBBEN, RB
198,206
MEDINA, J
462
MERENYI, E
111
METSKVARISHVILI, RYA
414,410
MEWALDT, RA
167
MINEEV, YUV
348
MISHRA, BL
254
MOBIUS, E
176
MORAAL, H
222
MORI, S
506,31,35
147,56,106
MORISHITA, I
31,147,106
MULDER, MS
222
MUNAKATA, K
MUNAKATA, K
98,238
MUNAKATA, Y
13
MURAKAMI, K
262,309
MURTY, SVS
379
MYMRINA, NV
293
NACHKEBIA, NA
285,289
NAGASHIMA, K
48,9,31,35
98,102,147
238,106
NANNI, T
375
NASKIDASHVILI, BD
87,289
NIEMINEN, M
274,242
NIKOLSKY, SI
450
NINAGAWA, K
514
NISHIIZUMI, K
379
NISHI, K
309
NUMAKATA, K
9
NYMMIK, RA
533
OGITA, N
304
OHMORI, N
482
OKHLOPKOVA, LS
90
OKHLOPKOV, VP
90
OLENEVA, VA
296
OSCHLIES, K
536
OWENS, A
498
OZAKI, M
506
PANDEY, PK
270,63
PARISI, M
226,230

PARISI, M
234
PATHAK, SP
23,63
PEHL, RH
470
PELLING, MR
470
PELTONEN, J
274,242
PETROU, N
328
PINTER, S
234
PODGURSKAYA, AV
533
POMERANTZ, MA
5,159
POTGIETER, MS
180
PRIKHODKO, AN
94
PRILUTSKY, RE
518,281
PRIMBSCH, H
470
PYLE, KR
198,206
210
RASMUSSEN, IL
328
RAUBENHEIMER, BC
502
RAYCHAUDHURI, P
438,442
REEDY, RC
386,382
REPPIN, C
474
RIKER, JF
116,110
115
ROELOF, EC
1
ROGAVA, OG
87
RYU, JY
478
SAGISAKA, S
506,56
SAKAIBARA, S
238
SAKAI, T
266
SAKURAI, K
430,406
SAMSONOVA, ZN
250
SAMSONOV, IS
250
SASAKI, H
482
SBORSHIKOV, VG
352
SCHLOTZ, R
422
SCHOLER, M
176
SCHUSTER, P
193
SDOBNOV, VE
359,151
SEQUEIROS, J
462
SERGEEV, AV
359,151
SHAFER, GV
87,52,155
94
SHARE, GH
474
SHATASHVILI, LKH
87,289
SHEA, MA
328,340
332,336
510
SHIBATA, S
13
SHMATKO, ES
538,542
SHRIPIN, GV
52
SHRIVASTAVA, PK
23,63
SIDDHESHWAR, L
423
SIGNORINI, C
226,230
SIMPSON, JA
198,206
210
SINGH, RK
184
SIROTINA, IV
356
SKRIPIN, GV
155,94

SMART, DF
328,340
332,336
SMART, DR
510
SMITH, EJ
1
SMOLENSKY, LG
533
SOLOVIEV, AV
533
STOKER, PH
502
STONE, EC
163,172
197,167
STORINI, M
226,230
234
STOZHKOV, YUI
120,79,450
SUBRAMANIAN, A
426
SVIRZHEVSKAYA, AK
79
SVIRZHEVSKY, NS
75,79
SWINSON, DB
48
TAKAHASHI, H
15,15,19
TAKAHASHI, K
130,309
482
TAKANO, Y
514
TAKAOKA, N
514
TATSUOKA, R
9,102
TERNOVSKAYA, MV
344,90
TIZENGAUZEN, VA
352
TORSTI, JJ
274,242
TRAINOR, JH
193
TRANSKY, IA
155,94
TRETYAKOVA, CHA
533
TSERETELI, GL
289
TSERETELI, SL
414,410
TYASTO, MI
83,359,324
UENO, H
35,147,106
VAHIA, MN
184
VAINIKKA, E
274,242
VALTONEN, E
274,242
VAN HOLLEBEKE, MAI
193
VENKATESAN, D
72,202
VERMA, SD
316,320
466
VERNOVA, ES
83
VILLORESI, G
226,230
234
VON ROSENVINGE, TT
193
WADA, M
134,246
309,478
482,486
510
WADA, MM
494
WADA, T
514
WALKER, F
1
WEBBER, WR
163,172
197,185
WOODARD, MF
402
WOOD, D
189
XAO, S
27
XUE, S
27,521
YADAV, JS
458,184
YADAV, NR
258,143
YADAV, RS
258,143,23

AUTHOR INDEX

YADAV, RS
126
YAHAGI, N
15,19
YAMAMOTO, I
514
YAMASHITA, Y
514
YANKE, VG
300
YASUE, S
506,35,56
YE, Z
521
YOSHIDA, S
304
YUDAKHIN, KF
281
YUN, SX
371
ZALJUBOVSKI, II
542
ZALJUBOVSKY, II
538
ZANDA, B
398
ZENCHEV, GG
344
ZHANG, G
27
ZHEN-DONG, YU
529,525
ZHURAVLEV, DA
533
ZUSMANOVICH, AG
278

BIBLIOGRAPHIC DATA SHEET

1. Report No.	2. Government Accession No.	3. Recipient's Catalog No.
NASA CP-2376 Volume 5		

4. Title and Subtitle	5. Report Date
19th International Cosmic Ray Conference Conference Papers	August 1985
	6. Performing Organization Code 665

7. Author(s)	8. Performing Organization Report No.
Frank C. Jones, compiler	

9. Performing Organization Name and Address	10. Work Unit No.
Laboratory for High Energy Astrophysics Goddard Space Flight Center Greenbelt, MD 20771	11. Contract or Grant No.
	13. Type of Report and Period Covered Conference Publication
12. Sponsoring Agency Name and Address National Aeronautics and Space Administration Washington, D. C. 20546	14. Sponsoring Agency Code

15. Supplementary Notes

16. Abstract

These volumes contain papers submitted for presentation at the 19th International Cosmic Ray Conference, held on the campus of the University of California, San Diego in La Jolla, CA., August 11-23, 1985. The conference is held every other year. The present volume contains papers with Paper Codes SH 4.3 through SH 10.1 and deals with cosmic-ray gradients in the heliosphere, siderial, diurnal and long term modulation, geomagnetic and atmospheric effects, cosmogenic nuclides, solar neutrinos.

17. Key Words (Selected by Author(s))	18. Distribution Statement
gradients, colar neutrinos, geomagnetic effects, atmospheric effects, cosmogenic nuclides	Unclassified - Unlimited Subject Category - 93

19. Security Classif. (of this report)	20. Security Classif. (of this page)	21. No. of Pages	22. Price*
Unclassified	Unclassified		

*For sale by the National Technical Information Service, Springfield, Virginia

GSFC 25-44 (10/77)

STAR 23 SEP 20 1985 20933 NASA-CP-2376-Vol. 6

19TH INTERNATIONAL COSMIC RAY CONFERENCE

LA JOLLA, USA AUGUST 11-23, 1985

CONFERENCE PAPERS



HE SESSIONS VOL. 6

(NASA-CP-2376-Vol-6) NINETEENTH INTERNATIONAL COSMIC RAY CONFERENCE. HE SESSIONS, VOLUME 6 (NASA) 496 p HC as boxed set only $200/MF A01 per volum CSCL 03B

N85-35848 THRU N85-35967 Unclas G3/93 20933

19TH INTERNATIONAL COSMIC RAY CONFERENCE

LA JOLLA, USA AUGUST 11-23, 1985

CONFERENCE PAPERS



HE

SESSIONS
VOL. 6

PUBLICATION COMMITTEE

F.C. Jones, Chm.
J. Adams
G.M. Mason

NASA Conference Publication 2376

Published by
Scientific and Technical Information Branch
National Aeronautics and Space Administration
Washington, D.C. 20546

August 1985

For sale by the National Technical Information Service, Springfield, VA 22151

PREFACE

The 19th International Cosmic Ray Conference, under the auspices of the Cosmic Ray Commission of the International Union of Pure and Applied Physics, is being held on the campus of the University of California, San Diego, on 11 through 23 August 1985. In keeping with the tradition begun in 1971 by the Australian organizers of the 12th ICRC, the Proceedings of this conference are appearing in two sets of volumes. The first set, consisting of volumes 1 through 8, is being distributed to all participants at the beginning of the conference. This set contains the contributed papers. The second set, distributed after the conference, contains invited, rapporteur, and highlight papers. The papers are reproduced here exactly as they were received from the authors, without refereeing.

For the 19th ICRC, the scientific program was organized according to three major divisions-- OG (cosmic rays and gamma rays of Galactic Origin), SH (Solar and Heliosphere), and HE (High Energy). Technical papers are included in each of the three divisions.

This conference depended on funds from several agencies of the United States government, including major financial support from the National Aeronautics and Space Administration and support from the National Science Foundation, the Department of Energy, and the Air Force Geophysics Laboratory. Important financial support also came from the Center for Astrophysics and Space Sciences of the University of California, San Diego, from the California Space Institute of the University of California, from the Department of Physics and Astronomy of the University of Maryland, College park, from the International Union for Pure and Applied Physics, and from several corporate sponsors who will be acknowledged by name in the post-conference volumes.

We appreciate the confidence placed in the conference organizers by the Cosmic Ray Commission, and acknowledge with thanks the role of the Commission members in setting up the rules for the conference and in advising the organizers during its planning.

We are grateful to all of the members of the various organizing committees listed at the front of this volume. The three Program Committees went to great effort to organize a coherent scientific program and to schedule four parallel sessions with a minimum of conflicts. The Local Organizing Committee has worked long and hard to ensure efficient and hospitable accommodations for all the participants, both in the scientific sessions and outside them. The Publications Committee not only took great pains to assemble these volumes but also maintained an orderly data base of papers and authors which was extremely helpful to the program committees. The General Organizing Committee made important contributions of ideas and efforts to make the conference possible; this committee included international representation from all of North America, thus the departure from the traditional name of National Organizing Committee. And the entire effort was coordinated by the dedicated members of the Steering Committee.

Martin H. Israel, Chairman
General Organizing Committee

August, 1985

LETTER FROM THE EDITORS

This conference marks a departure from previous conferences in this series in that the publication of the Conference Papers was carried out an entire continent away from the activities of Local Organising Committee. This posed some problems but, to the considerable surprise of the Publications Committee members, the one that was expected to be the most trouble turned out not to be significant. The overwhelming majority of those submitting papers and abstracts sent them to the correct address, not to La Jolla as was feared. We wish to thank our many authors for their alertness and commend them for handling a complicated situation so well.

There are eight volumes to be distributed to the conference participants in addition to the Conference Program and Author Index: three volumes for OG, two for SH and three for HE. the detailed makeup of these volumes is described in the prefaces written by the Scientific Program chairmen for their respective volumes. Out of some 1100 abstracts that were accepted by the Scientific Program Committees for inclusion in the conference some 929 papers were finally received in time for inclusion in the Conference Papers. This represents a response of approximately 84 percent, a modest improvement. Even if one excludes the 42 one page papers that should be considered as 'confirming abstracts', even though there was no such formal category, the response was somewhat higher than that of recent years. We attribute this to the carrot of a later deadline than before coupled with the stick of there being no printing of post deadline contributed papers. We believe that this decision of the General Organising Committee was a wise one. Of course invited, rapporteur, and highlight talks will be printed in volumes to be distributed to the participants after the conference as usual.

The Publications Committee had much generous help in performing its duties: from Goddard Space Flight Center we had the help of B. Glasser, L. Harris, E. Schronce, N. Smith, J. Esposito and T. Smith. From the Naval Research Laboratory we were helped by T. Massotta, and at the University of Maryland M. L. Snidow and J. Mucha gave much needed assistance. Special thanks are due to Caryl Short, the lone staff member of the Publications Committee. She maintained the computer data base, organised the abstracts as they arrived, and kept track of the papers themselves to see that the finally arrived in the right place at the right time. Without her help the job would have been far more difficult than it was.

PUBLICATIONS COMMITTEE — August, 1985

Frank C. Jones, Chm.
Jim Adams
Glen M. Mason

HE SESSIONS
VOLUME VI

19th INTERNATIONAL COSMIC RAY CONFERENCE
LA JOLLA, USA
AUGUST 11-23, 1985

INTERNATIONAL UNION OF PURE AND APPLIED PHYSICS
MEMBERS OF THE COMMISSION ON COSMIC RAYS OF IUPAP

A.E. Chudakov, Chm.	P.H. Fowler	T.O. Montmerle	B.V. Sreekantan
F.B. McDonald	D. Hovestadt	H. Morsal	K. Suga
G.C. Castagnoli	J. Kota	J.R. Prescot	J. Wdowczyk

STEERING COMMITTEE

F. McDonald, Chm.	T. Gaisser	F. Jones	R. Mewaldt
G. Burbage	M. Israel	R. Lingenfelter	L. Peterson
M. Forman			

GENERAL ORGANIZING COMMITTEE

M. Israel, Chm.	V. Jones	B. Price	J. Simpson
M. Bercovitch	S. Krimigis	R. Ramaty	B. Stone
P. Freier	J. Kurfess	F. Reines	D. Venkatesan
R. Gall	J. Lockwood	M. Shapiro	J. Waddington
R. Jokipii	P. Meyer	M. Shea	S. White
L. Jones			

PROGRAM COMMITTEES

OG SESSIONS	SE SESSIONS	HE SESSIONS	PUBLICATIONS
R. Mewaldt, Chm.	M. Forman, Chm.	T. Gaisser, Chm.	F. Jones, Chm.
G. Cassiday	H. Hudson	K. Lande	J. Adams
C. Fichtel	G. Mason	J. Linsley	G. Mason
A. Harding	B. McKibben	E. Loh	
J. Matteson	M. Pomerantz	G. Yodh	
D. Muller			
W. Webber			

LOCAL ORGANIZING COMMITTEE

L. Peterson, Chm.	A. Buffington	J. Linsley	O. Piccioni
G. Burbidge	M. Burbidge	K. Marti	M. Thiemens
R. Lingenfelter	W. Fillius	G. Masek	W. Thompson
R. Rothschild	R. Gall	J. Matteson	H. Tycho
J. Arnold	R. Gould	C. McIlwain	R. White
W. Baity	H. Hudson	R. Mewaldt	

Sponsored by
National Aeronautics and Space Administration
National Science Foundation
Department of Energy
Center for Astrophysics and Space Science, University of California, San Diego
California Space Institute, University of California
Department of Physics and Astronomy, University of Maryland, College Park

Preface to HE Volumes

Papers contributed to the XIX International Cosmic Ray Conference were arranged into three major divisions: Origin and Galactic phenomena (OG), Solar and Heliospheric (SH), and High Energy (HE). The HE sessions at this conference comprise all the subjects formerly included in the muon and neutrino sessions (MN) and the extensive air shower sections (EA) as well as those on high energy interactions, new particle searches and emulsion chamber results, which were previously classified in HE. In addition, technical papers have not been classified separately, but have been inserted in appropriate subject sections. All the papers now classified as HE are contained in volumes 6, 7 and 8.

Volume 6 includes sessions HE1 (cross sections and interactions of particles and nuclei at high energy) and HE3 (emulsion chamber results). Extensive air shower papers (HE4) are in volume 7. Papers on muons and neutrinos (HE5), searches for new particles and processes (HE6) and some on new techniques (HE7) are in volume 8.

Altogether some 380 abstracts were received for the HE sections. These were divided into the 25 groups listed in the tables of contents of the HE volumes. (These groups correspond only approximately to the 26 contributed paper sessions at the conference.)

Four rapporteurs were selected to cover the subjects of the HE sessions:

L.W. Jones	High Energy Interactions and New Particle Searches (HE1 & HE6);
M. Shibata	Emulsion Chamber Observations and Interpretation (HE3);
R.W. Clay	Extensive Air Showers (HE4);
K. Sivaprasad	Muons and Neutrinos (HE5).

The written versions of the rapporteur talks are contained in the post-conference volume together with highlight and invited papers.

The work of arranging the HE program was shared by a committee consisting of

T.K. Gaisser (Bartol), Chairman
K. Lande (Pennsylvania)
E.C. Loh (Utah)
J. Linsley (New Mexico)
G.B. Yodh (Maryland)

This conference is the 19th in a series. Previous conferences in this series were held at:

Cracow, Poland	-	1947
Como, Italy	-	1949
Bagneres-de-Bigorre, France	-	1953
Guanjuato, Mexico	-	1955
Varenna, Italy	-	1957
Moscow, USSR	-	1959
Kyoto, Japan	-	1961
Jaipur, India	-	1963
London, UK	-	1965
Calgary, Canada	-	1967
Budapest, Hungary	-	1969
Hobart, Australia	-	1971
Denver, USA	-	1973
Munchen, FRG	-	1975
Plovdiv, Bulgaria	-	1977
Kyoto, Japan	-	1979
Paris, France	-	1981
Bangalore, India	-	1983

VOLUME 6

HE 1.1
CROSS SECTIONS

PAPER CODE		PAGE
HE 1.1-1	PROTON-AIR AND PROTON-PROTON CROSS SECTIONS FROM AIR SHOWER DATA J LINSLEY	1
HE 1.1-2	PROTON-AIR INELASTIC CROSS SECTION AT S**1/2 = 30 TEV RM BALTRUSAITIS,GL CASSIDAY,R COOPER JW ELBERT,PR GERHARDY,VD KOSLOV,EC LOH Y MIZUMOTO,P SOKOLSKY,D STECK	5
HE 1.1-3	HADRON CROSS SECTIONS AT ULTRA HIGH ENERGIES AND UNITARITY BOUNDS ON DIFFRACTION DISSOCIATION GB YODH,TK GAISSER,UP SUKHATME	9
HE 1.1-4	ON TOTAL CROSS SECTIONS AND SLOPES AT SUPERHIGH ENERGIES SHS YEREMIAN,VM ZHAMKOCHIAN	13
HE 1.1-5	DETERMINATION OF THE CROSS SECTION OF THE PROTON, PION AND NEUTRON INELASTIC INTERACTION WITH LEAD AND CARBON NUCLEI AT 0.5 - 5.0 TEV ENERGIES VV AVAKIAN,GV KARAGJOZIAN EA MAMIDJANIAN,MI KEROPIAN,RM MARTIROSOV GG OVSEPIAN,SO SOKHOYAN	17
HE 1.1-6	P(P)P ELASTIC SCATTERING AND COSMIC RAY DATA FE ALEEM,M SALEEM	21
HE 1.1-7	MEASUREMENT OF INTERACTION CROSS SECTION OF COSMIC RAY FE (E>4GEV/N) WITH AL TARGET GX REN,YZ ZHOU,RQ HUANG,MY CHEN	25

VOLUME 6

HE 1.1-8 HADRON THERMODYNAMICS IN RELATIVISTIC NUCLEAR COLLISIONS 28

P AMMIRAJU

HE 1.1-9 ESTIMATION OF THE TOTAL INELASTICITY COEFFICIENT IN INTERACTION OF > 20 TEV HADRONS WITH LEAD 31

BL KANEVSKY,IA MIKHAILOVA
IV RAKOBOLSKAYA,LG SVESHNIKOVA

HE 1.1-11 THE METHOD FOR THE STUDY OF THE INELASTIC CROSS - SECTION FOR HIGH ENERGY PROTONS BY MEANS OF SHOWER ARRAYS WITH THE LARGE CALORIMETER AREA 35

TV DANILOVA,AD ERLYKIN

HE 1.1-12 INELASTICITY PARTIAL COEFFICIENT K SUB GAMMA DETERMINATION IN PI C AND PI PB INTERACTIONS AT 10**14 EV 39

PAMIR COLLABORATION

HE 1.2
PARTICLE PRODUCTION - MODELS AND EXPERIMENTS

PAPER CODE		PAGE
HE 1.2-1	SINGLE PARTICLE MOMENTUM AND ANGULAR DISTRIBUTIONS IN HADRON-HADRON COLLISIONS AT ULTRAHIGH ENERGIES TT CHOU,CN YANG	43
HE 1.2-2	QCD-MOTIVATED DESCRIPTION OF VERY HIGH ENERGY PARTICLE INTERACTIONS TK GAISSER,F HALZEN	47
HE 1.2-4	EMPIRICAL DESCRIPTION OF THE HADRON-HADRON AND HADRON-NUCLEUS INTERACTION AT THE ACCELERATOR ENERGY RANGE G KUBIAK, SZABELSKI,J WDOWCZYK,J KEMPA A PIOTROWSKA	51
HE 1.2-5	MULTIPLICITY DISTRIBUTIONS IN INTERACTION MODELS USED FOR CASCADE SIMULATIONS RW ELLSWORTH,RK GAISSER,T STANEV	55
HE 1.2-6	SOME REMARKS ABOUT SIMULATION OF COSMIC RAY PHENOMENA WITH USE OF NUCLEAR INTERACTION MODELS BASED ON THE CURRENT SPS PROTON-ANTIPROTON DATA JA WROTNIAK,GB YODH	56
HE 1.2-7	LOW P**T HADRON-NUCLEUS INTERACTIONS R HOLYNSKI,K WOZNIAK	60
HE 1.2-8	ANGULAR DISTRIBUTION AND MULTIPLICITY OF BACKWARD HADRONS IN HFE INTERACTION AT 0.5-5.0 TEV ENERGIES (PION EXPERIMENT) VV AVAKIAN,MO AZARIAN,KSH EGIYAN EA MAMIDJANIAN,GZH OHANIAN SV TER-ANTONIAN	64

HE 1.2-9 A TEST OF THE FEYNMAN SCALING IN THE FRAGMENTATION REGION AT THE SQUARE ROOT OF S = 630 GEV — 68

T DOKE,V INNOCENTE,K KASAHARA,J KIKUCHI
T KASHIWAGI,S LANZANO,K MASUDA
H MURAKAMI,Y MURAKI,T NAKADA,A NAKAMOTO
T YUDA,M HAGUENAUER

HE 1.2-10 ANGULAR DISTRIBUTION OF SHOWER PARTICLES PRODUCED IN THE COLLISIONS OF 20-GEV/C AND 300-GEV NEGATIVE PIONS WITH EMULSION NUCLEI — 72

CO KIM,SN KIM,IG PARK,CS YOON

HE 1.2-11 NUCLEON-NUCLEUS INTERACTIONS FROM JACEE — 76

TH BURNETT,S DAKE,M FUKI,JC GREGORY
T HAYASHI,R HOLYNSKI,J IWAI,WV JONES
A JURAK,JJ LORD,O MIYAMURA,T OGATA
A OLSZEWSKI,TA PARNELL,T SAITO,S STRAUSZ
M SZARSKA,T TABUKI,Y TAKAHASHI
Y TOMINAGA,B WILCZYNSKA,JP WEFEL
RJ WILKES,W WOLTER,B WOSIEK

HE 1.2-13 AN UNIFICATION OF THE INTERACTIONS AND THE DIFFRACTIVE PROCESSES — 80

IA KUCHIN

HE 1.2-14 IS THE INELASTIC CHARGE-EXCHANGE CONTRIBUTION CONSTANT AT THE LARGE X AND SUPERHIGH ENERGIES? — 84

IA KUCHIN

HE 1.2-15 GENERAL CONSEQUENCES OF THE VIOLATED FEYNMAN SCALING — 88

G KAMBEROV,L POPOVA

HE 1.2-16 PROPAGATION OF COSMIC RAYS THROUGH THE ATMOSPHERE IN THE QUARK-GLUON STRINGS MODEL — 92

AD ERLYKIN,NP KRUTIKOVA,YM SHABELSKI

VOLUME 6

HE 1.2-17 SCALING VIOLATION IN THE FRAGMENTATION REGION OF INCLUSIVE NUCLEON SPECTRUM 96

SK MACHAVARIANI,SI NIKOLSKY,AP CHUBENKO

HE 1.3
NUCLEI AND NUCLEAR MATTER

PAPER CODE		PAGE
HE 1.3-1	DETERMINATION OF PRIMARY ENERGY IN NUCLEUS -NUCLEUS COLLISIONS AND THE HIGH P SUB T TAIL OG GAMMA-PARTICLES	100
	PS FREIER,TW ATWATER	
HE 1.3-4	STOPPING RELATIVISTIC XE, HO, AU AND U NUCLEI IN NUCLEAR EMULSIONS	104
	CJ WADDINGTON,DJ FIXSEN,PS FREIER	
HE 1.3-5	PHYSICAL MEANING OF THE MULTIPLICITIES OF EMITTED NUCLEONS IN HADRON-NUCLEUS COLLISIONS	108
	Z STRUGALSKI	
HE 1.3-6	HOW ARE PARTICLE PRODUCTION, NUCLEON EMISSION, AND TARGET FRAGMENT EVAPORATION PROCESSESS INTERRELATED IN HADRON-NUCLEUS COLLISIONS?	112
	Z STRUGALSKI	
HE 1.3-7	EXPERIMENTAL STUDY OF THE SPACE-TIME DEVELOPMENT OF THE PARTICLE PRODUCTION PROCESS IN HADRON-NUCLEON COLLISIONS, USING MASSIVE TARGET NUCLEUS AS A DETECTOR	115
	Z STRUGALSKI	
HE 1.3-8	EXPERIMENTAL EVIDENCE OF THE DECREASE OF KINETIC ENERGY OF HADRONS IN PASSING THROUGH ATOMIC NUCLEI	118
	Z STRUGALSKI	
HE 1.3-9	ENERGY-RANGE RELATIONS FOR HADRONS IN NUCLEAR MATTER	122
	Z STRUGALSKI	

VOLUME 6

HE 1.3-10 SCATTERING AND STOPPING OF HADRONS IN NULCEAR MATTER 125

Z STRUGALSKI

HE 1.3-11 MEASUREMENT OF HADRON MEAN FREE PATH FOR THE PARTICLE-PRODUCING COLLISIONS IN NUCLEAR MATTER 129

Z STRUGALSKI

HE 1.3-13 THE PHI-MESON AND "CHIRAL-MASS-MESON" PRODUCTION IN HEAVY-ION COLLISIONS AS A PROBE OF THE QUARK-GLUON-PLASMA AND THE CHIRAL SYMMETRY TRANSITIONS 133

Y TAKAHASHI,PB EBY

HE 1.3-15 SU(2) X U(1) VACUMM AND THE CENTAURO EVENTS 137

D KAZANAS,VK BALASUBRAHMANYAN
RE STREITMATTER

HE 1.3-16 HEAVY FLAVOURS PRODUCTION IN QUARK-GLUON PLASMA FORMED IN HIGH ENERGY NUCLEAR REACTIONS 141

J KLOSINSKI

HE 1.3-17 RINGLIKE INELASTIC EVENTS IN COSMIC RAYS AND ACCELERATORS 145

IM DREMIN,AM ORLOV,MI TRETYAKOVA

HE 1.3-18 PHASE SPACE FACTORS IN MULTIPARTICLE PROCESSES 149

RJ GOULD

HE 1.4
NUCLEUS-NUCLEUS COLLISIONS

PAPER CODE		PAGE
HE 1.4-1	THE RESPONSE OF A SCINTILLATION COUNTER BELOW AN EMULSION CHAMBER TO HEAVY NUCLEUS INTERACTIONS IN THE CHAMBER TH BURNETT,S DAKE,JH DERRICKSON,M FUKI JC GREGORY,R HAYASHI,T HAYASHI R HOLYNSKI,J IWAI,WV JONEW,A JURAK JJ LORD,CA MEEFAN,O MIYAMURA,H ODA T OGATA,TA PARNELL,E ROBERTS,T SAITO M SZARSKA,T TABUKI,Y TAKAHASHI,B WOSIEK JS WATTS,B WILCZYNSKA,RJ WILKES,W WOLTER	152
HE 1.4-2	HEAVY NUCLEUS COLLISIONS BETWEEN 20 AND 60 GEV/NUCLEON TH BURNETT,S DAKE,M FUKI,JC GREGORY T HAYASHI,R HOLYNSKI,J IWAI,WV JONES A JURAK,JJ LORD,O MIYAMURA,T OGATA TA PARNELL,T SAITO,T TABUKI,Y TAKAHASHI T TOMINAGA,B WILCZYNSKA,RJ WILKES W WOLTER,B WOSIEK	156
HE 1.4-3	CHARACTERISTICS OF CENTRAL COLLISION EVENTS IN FE-NUCLEUS INTERACTIONS FROM 20 TO 60 GEV/N TH BURNETT,S DAKE,JH DERRICKSON W FOUNTAINS,M FUKI,JC GREGORY,T HAYASHI TO HAYASHI,R HOLYNSKI,J IWAI,WV JONES A JURAK,JJ LORD,CA MEEGAN,O MIYAMURA H ODA,T OGATA,TA PARNELL,E ROBERTS T SAITO,S STRAUSZ,T TABUKI,Y TAKAHASHI T TOMINAGA,B WILCZYNSKA,RJ WILKES W WOLTER,B WOSIEK	160
HE 1.4-4	NUCLEUS-NUCLEUS INTERACTIONS ABOVE SEVERAL HUNDRED GEV/N TH BURNETT,S DAKE,M FUKI,JC GREGORY T HAYASHI,R HOLYNSKI,J IWAI,WV JONES A JURAK,JJ LORD,O MIYAMURA,H ODA,T OGATA TA PARNELL,T SAITO,S STRAUSZ,M SZARSKA T TABUKI,Y TAKAHASHI,T TOMINAGA,JW WATTS JP WEFEL,B WILCZYNSKA,RJ WILKES,W WOLTER B WOSIEK	164

HE 1.4-5 OBSERVATION OF DIRECT HADRONIC PAIRS IN NUCLEUS-NUCLEUS COLLISIONS IN JACEE EMULSION CHAMBERS 168

TH BURNETT,S DAKE,M FUKI,JC GREGORY
T HAYASHI,R HOLYNSKI,J IWAI,WV JONES
A JURAK,JJ LORD,O MIYAMURA,K ODA,T OGATA
TA PARNELL,T SAITO,T TABUKI,Y TAKAHASHI
T TOMINAGA,B WILCZYNSKA,RJ WILKES
W WOLTER,B WOSIEK

HE 1.4-6 EXCESSIVE PRODUCTION OF ELECTRON PAIRS BY SOFT PHOTONS IN LOW MULTIPLICITY ION INTERACTIONS 172

TH BURNETT,S DAKE,M FUKI,JC GREGORY
T HAYASHI,R HOLYNSKI,J IWAI,WV JONES
A JURAK,JJ LORD,O MIYAMURA,T OGATA
TA PARNELL,T SAITO,S STRAUSZ,T TABUKI
Y TAKAHASHI,T TOMINAGA,J WATTS
B WILCZYNSKA,RJ WILKES,W WOLTER,B WOSIEK

HE 1.4-7 FORWARD PARTICLE PRODUCTION IN INELASTIC **22NE INTERACTIONS IN EMULSION AT 4.1 A GEV/C 176

B WOSIEK

HE 1.4-8 ON THE MECHANISM OF ANOMALOUS NUCLEUS-NUCLEUS INTERACTIONS AT ENERGIES ABOVE 1 TEV/NUCLEON 180

SSH AMEEV,VL SHMONIN

HE 1.4-10 MESON MULTIPLICITY IN NUCLEUS-NUCLEUS COLLISIONS ABOVE 4 GEV/AMU 184

TN ATWATER,PS FREIER,MP KERTZMAN

HE 1.4-11 INCLUSIVE ANGULAR DISTRIBUTION OF SIGMA AND LI FRAGMENTS PRODUCED IN THE FE-C AND FE-PB COLLISIONS AT 1.88 GEV/U 188

CO KIM,SN KIM,IK CHAE,DH KIM

HE 1.4-12 EXPERIMENT "PAMIR"-III. COPLANAR EMISSION OF HIGH ENERGY GAMMA-QUANTA AT INTERACTION OF HADRONS WITH NUCLEI OF AIR ATOMS AT ENERGIES ABOVE (10**17) GEV 192

PAMIR COLLABORATION

VOLUME 6

HE 1.4-13 THE EFFECT OF THE RELATIVE NUCLEAR SIZE ON THE NUCLEUS-NUCLEUS INTERACTIONS 196

IN EROFEEVA,VS MURZIN,SYU SIVOKLOKOV
LN SMIRNOVA

VOLUME 6

HE 3.1
GAMMA-RAY AND HADRON SPECTRA

PAPER CODE		PAGE
HE 3.1-1	JAPAN-USSR JOINT EMULSION CHAMBER EXPERIMENT AT PAMIR AS BORISOV,KV CHERDYNTSEVA,ZM GUSEVA VG DENISOVA,AM DUNAEVSKY,EA KANEVSKAYA VM MAXIMENKO,RA NAM,SV PASHKOV VS PUCHKOV,SA SLAVATINSKY,MD SMIRNOVA YA SMORODIN,NG ZELEVINSKAYA,MV ZIMIN GB ZHDANOV,RA MUKHAMEDSHIN,OE NEDEL'KO LP NIKOLAEV,GT ZATSEPIN,TP AMINEVA LT BARADZEI,IP IVANENKO,NP ILIJINA TV LAZAREVA,AK MANAGADZE,IA MIKHAILOVA EA MURZINA,EI POMELOVA,EG POPOVA	200
HE 3.1-2	INTENSITIES OF HIGH-ENERGY COSMIC RAYS AT MT. KANBALA CHINA-JAPAN COLLABORATION,K MIZUTANI	204
HE 3.1-3	HIGH ENERGY GAMMA-RAYS AND HADRONS AT MT. FUJI M AMENOMORI,H NANJO,E KONISHI,N HOTTA K MIZUTANI,K KASAHARA,T KOBAYASHI E MIKUMO,K SATO,T YUDA,I MITO,M SHIBATA T SHIRAI,T TAIRA,N TATEYAMA,S TORII H SUGIMOTO,K TAIRA	208
HE 3.1-6	ON THE CHARACTERISTICS OF EMULSION CHAMBER FAMILY EVENTS PRODUCED IN LOW HEIGHTS G JING,C JING,Q ZHU,L DING	212
HE 3.1-7	HADRON INTENSITY SPECTRUM AT 4380 M ABOVE LEVEL SD CANANOV,EKH CHADRANYAN LA KHIZANISHVILI,DM KOTLYAREVSKI NN ROINISHVILI	216
HE 3.1-8	SOME CHARACTERISTIC COSMIC RAY EVENTS AND AN ATTEMPT AT THEIR EXPLANATION S BHATTACHARYYA	220

VOLUME 6

HE 3.1-9 THE NUCLEON INTENSITY IN THE ATMOSPHERE AND THE P**T DISTRIBUTION 224

A LILAND

HE 3.1-10 ENERGY SPECTRA OF PROTON AND NUCLEI OF PRIMARY COSMIC RAYS IN ENERGY REGION > 10 TEV/PARTICLE 228

KV MANDRITSKAYA,GP SAZHINA
NV SOKOLSKAYA,AYA VARKOVITSKAYA
EA ZAMCHALOVA,VI ZATSEPIN

HE 3.1-11 SCALING VIOLATION IN FRAGMENTATION REGION AT ENERGIES ABOVE 10**15 BASED ON THE DATA ON COSMIC RAY HADRON COMPONENT 232

PAMIR COLLABORATION

HE 3.1-12 CONNECTION BETWEEN VARIATIONS OF THE ATMOSPHERE TEMPERATURE PROFILE AND VARIATIONS OF THE MESON COMPONENT INTENSITY 236

YAL BLOKH,YL BLOCH

HE 3.1-13 HIGH SENSITIVE X-RAY FILMS TO DETECT ELECTRON SHOWERS IN 100 GEV REGION 239

T TAIRA,T SHIRAI,N TATEYAMA,S TORII
J NISHIMURA,M FUJII,A YOSHIDA,H AIZU
Y NOMURA,M KAZUNO,T KOBAYSHI,A NISHIO

HE 3.2
C-JETS

PAPER CODE		PAGE
HE 3.2-1	JETS IN AIR-JET FAMILY AC FAUTH,K SAWAYANAGI	243
HE 3.2-5	SEARCH FOR ANOMALOUS C-JETS IN CHACALTAYA EMULSION CHAMBER EXPERIMENT H KUMANO	246
HE 3.2-6	EXOTIC INTERACTIONS AMONG C-JETS AND PB-JETS BRAZIL-JAPAN	250
HE 3.2-7	X-RAY FILM CHAMBER WITH CARBON TARGET OF TIEN-SHAN COMPLEX ARRAY KV CHERDYNTSEVA,AP CHUBENKO,AG DUBOVY NP KRUTIKOVA,NM NESTEROVA,SI NIKOLSKY NM NIKOLSKAJA,EI TUKISH,NG VILDANOV TI YAKOVLEVA	254
HE 3.2-8	SCALING VIOLATION IN HADRON-NUCLEUS INTERACTION YG VERBETSKI,YG VERBETTSKI LP GARSEVANISHVILI,DM KOTLYAREVSKI MV MELKU,NG TATALASHVILI,NI SHERER YUM SHABEL'SKI,GZ STEMANETYAN	258
HE 3.2-9	FEW-PARTICLES GENERATION CHANNELS IN INELASTIC HADRON-NUCLEAR INTERACTIONS AT ENERGY ~ 400 GEV NG TATALASHVILI	262
HE 3.2-10	THE MODEL OF INDEPENDENT PARTICLES EMISSION IN THE MULTIPARTICLE PRODUCTION THEORY VV UCHAIKIN,VA LITVINOV	266

VOLUME 6

HE 3.2-11 THE MULTIPLICITY AND THE SPECTRA OF SECONDARIES CORRLEATED WITH THE LEADING PARTICLE ENERGY 270

NA KRUGLOV,AS PROSKURYAKOV,LI GARYCHEVA LN SMIRNOVA

VOLUME 6

HE 3.3
A-JETS

PAPER CODE		PAGE
HE 3.3-1	CHARACTERISTICS OF ANOMALOUSLY HIGH MULTIPLICITY COSMIC RAY INTERACTIONS	274
	IYA CHASNIKOV,YUA EREMENKO DT MADIGOZHIN,TKH SADYKOV,VG VOINOV	
HE 3.3-2	TRANSVERSE MOMENTUM DISTRIBUTION OF PI DEGREES IN THE FRAGMENTATION REGION OF SUPER HIGH ENERGY INTERACTIONS	278
	JR REN,HH KUANG,AX HUO,SL LU,S SU YX WANG,CR WANG,M HE,NJ ZHANG,PY CAO JY LI,SZ WANG,GZ BAI,ZH LIU,GJ LI QX GENG,WD ZHOU,RD HE	
HE 3.3-4	STUDY OF HADRON BUNDLES OBSERVED IN CHACALTAYA TWO-STORY EMULSION CHAMBER	280
	H AOKI	
HE 3.3-5	PENETRATIVE NATURE OF HIGH ENERGY SHOWERS OBSERVED IN CHACALTAYA EMULSION CHAMBER	284
	Y FUNAYAMA,M TAMADA	
HE 3.3-6	ANOMALOUS CORRELATION BETWEEN HADRON AND ELECTROMAGNETIC PARTICLES IN HADRON AND GAMMA RAY FAMILIES	288
	M TAMADA	
HE 3.3-7	ATMOSPHERIC INTERACTIONS DETECTED IN BOTH THE UPPER AND THE LOWER CHAMBERS AT CHACALTAYA	292
	NM AMATO,N ARATA,RHC MALDONADO	
HE 3.3-8	LATERAL DISTRIBUTION OF HIGH ENERGY HADRONS AND GAMMA RAYS IN AIR SHOWER CORES OBSERVED WITH EMULSION CHAMBERS	296
	T MATANO,M MACHIDA,N KAWASUMI I TSUSHIMA,K HONDA,K HASHIMOTO,CE NAVIA NJ MARTINIC,C AGUIRRE	

VOLUME 6

HE 3.3-9 SIZE DISTRIBUTIONS OF AIR SHOWERS ACCOMPANIED WITH HIGH ENERGY GAMMA-RAY BUNDLES OBSERVED AT MT. CHACALTAYA 300

T MATANO,M MACHIDA,I TSUSHIMA
N KAWASUMI,K HONDA,K HASHIMOTO
MJ MARTINIC,J ZAPATA,CE NAVIA,C AGUIRRE
L SILES,R MAGNANI

HE 3.3-10 EAS ACCOMPANIED BY GAMMA-FAMILIES AT MT. NORIKURA AND COMPARISON WITH MONTE CARLO SIMULATIONS 301

M SHIMA,T SAITO,M SAKATA,Y YAMAMOTO
K KASAHARA,T YUDA,S TORII,N HOTTA

HE 3.3-11 COMPARSION OF ABSOLUTE INTENSITY BETWEEN EAS WITH GAMMA-FAMILIES AND GENERAL EAS AT MT. NORIKURA 305

T MITSUMUNE,T NAKATSUKA,K NISHIKAWA
T SAITO,M SAKATA,M SHIMA,Y YAMAMOTO
S DAKE,M KAWAMOTO,M KUSUNOSE,N OHMORI
H SASAKI,N HOTTA

VOLUME 6

HE 3.4
SUPER FAMILIES I

PAPER CODE		PAGE
HE 3.4-1	A COSMIC RAY SUPER HIGH ENERGY MULTICORE FAMILY EVENT EXPERIMENT AND GENERAL FEATURES CHINA-JAPAN COLLABORATION	309
HE 3.4-2	A COSMIC RAY SUPER HIGH MULTICORE FAMILY EVENT (II) PRODUCTION AND FRAGMENTATION CHARACTERISTICS OF THE JETS CHINA-JAPAN COLLABORATION	313
HE 3.4-3	OBSERVATION OF SUPER HIGH ENERGY BIG FAMILY WITH LARGE SCALE EMULSION CHAMBERS CHINA-JAPAN COLLABORATION	317
HE 3.4-5	A HALO EVENT CREATED AT 200 M ABOVE THE CHACALTAYA EMULSION CHAMBER NM AMATO,N ARATA,RHC MALDONADO	320
HE 3.4-6	A BINOCULAR TYPE ATMOSPHERIC INTERACTION GENERATING SEQUENTIAL EXOTIC FEATURES NM AMATO,N ARATA,RHC MALDONADO	324
HE 3.4-7	GAMMA-HADRON FAMILIES AND SCALING VIOLATION TK GAISSER,T STANEV,JA WROTNIAK	328
HE 3.4-8	SUPER-FAMILY P2 C-96-125 OBSERVED BY JAPAN-USSR JOINT EMULSION CHAMBER EXPERIMENT EH SHIBUYA	332

HE 3.4-9 ON THE HALO EVENTS OBSERVED BY MT. FUJI AND MT. KANBALA EMULSION CHAMBER EXPERIMENTS 336

JR REN,HH KUANG,AX HUO,SL LU,S SU
YX WANG,YG XUE,CR WANG,M HE,NJ ZHANG
PY CAO,JY LI,SZ WANG,GZ BAI,ZH LIU,GJ LI
QX GENG,WD ZHOU,RD HE,M AMENOMORI
H NANJO,N HOTTA,I OHTA,K MIZUTANI
K KASAHARA,T YUDA,I MITO,M SHIBATA
T SHIRAI,N TATEYAMA

HE 3.4-10 EXPERIMENT "PAMIR"-II: "FIANIT"-A GIGANTIC SUPER-FAMILY WITH HALO (E SUB 0~10**17 EV) 340

PAMIR COLLABCRATION

HE 3.4-11 EXPERIMENT "PAMIR"-IV. ANALYSIS OF ELECTROMAGNETIC HALO SUPERFAMILY DETECTED IN DEEP XEC 344

PAMIR COLLABORATION

HE 3.5
SUPER FAMILIES II

PAPER CODE		PAGE
HE 3.5-1	PARTICLE INTERACTIONS AT ENERGIES OVER 1000 TEV INFERRED FROM GAMMA-FAMILIES OBSERVED AT MT FUJI M AMENOMORI,H NANJO,E KONISHI,N HOTTA K MIZUTANI,K KASAHARA,T KOBAYASHI E MIKUMO,K SATO,T YUDA,I MITO,M SHIBATA T SHIRAI,T TAIRA,N TATEYAMA,S TORII H SUGIMOTO,K TAIRA	348
HE 3.5-2	A SEARCH FOR MINI-CLUSTERS IN JAPAN-USSR JOINT CHAMBER AT PAMIR JAPAN-USSR	352
HE 3.5-3	MINI-CLUSTERS JA CHINELLATO,C DOBRIGKEIT,J BELLANDI CMG LATTES,MJ MENON,CE NAVIA,OA PAMILAJU K SAWAYANAGI,EH SHIBUYA,A TURTELLI NM AMATO,N ARATA,FM OLIVERIRA CASTRO RHC MALDONADO,H AOKI,Y FUJIMOTO Y FUNAYAMA,S HASEGAWA,H KUMANO,H SEMBA M TAMADA,S YAMASHITA,T SHIBATA,K YOKOI A OHSAWA	356
HE 3.5-4	GIANT MINI-CLUSTERS AS A POSSIBLE ORIGIN OF "HALO" PHENOMENA OBSERVED IN SUPER FAMILIES BRASIL-JAPAN	360
HE 3.5-7	STRUCTURE OF SUPER-FAMILIES S YAMASHITA,A OHSAWA,JA CHINELLATO	364
HE 3.5-8	EXTREMELY HIGH ENERGY HADRON AND GAMMA RAY FAMILIES (III) S YAMASHITA,A OHSAWA,JA CHINELLATO EH SHIBUYA	368

HE 3.5-9 NUMERICAL ANALYSIS OF ELECTROMAGNETIC CASCADES IN EMULSION CHAMBERS 372

AV PLYASHESHNIKOV,KV VOROBYEV

HE 3.5-10 AN EXPERIMENTAL STUDY OF CORRELATIONS IN THE DEVELOPMENT OF THE ELECTRON-PHOTON CASCADES 376

YUP KRATENKO,SA CHARISHNIKOV

HE 3.5-11 THE ELECTROMAGNETIC COMPONENT OF ALBEDO FROM SUPERHIGH ENERGY CASCADES IN DENSE MEDIA 380

RM GOLYNSKAYA,LA HEIN,AV PLYASHESHNIKOV
KV VOROBYEV

HE 3.5-12 INTEGRAL FUNCTIONS OF ELECTRON LATERAL DISTRIBUTION AND THEIR FLUCUATIONS IN ELECTRON-PHOTON CASCADES 384

IP IVANENKO,BL KANEVSKY,AA KIRILLOV
IA LINDE,YG LYUTOV

HE 3.5-13 ANALYTICO-NUMERICAL METHODS OF CALCULATIONS OF ENERGY AND THREE-DIMENSIONAL PARTICLE DISTRIBUTIONS IN ELECTROMAGNETIC CASCADES 388

IP IVANENKO,BL KANEVSKY,TM ROGANOVA
VV SIZOV,SV TRIPHONOVA

VOLUME 6

HE 3.6
EMULSION CHAMBER SIMULATIONS

PAPER CODE		PAGE
HE 3.6-2	MULTIDIMENSIONAL ANALYSIS OF DATA OBTAINED IN EXPERIMENTS WITH X-RAY, CHAMBERS AND EXTENSIVE AIR SHOWERS AA CHILINGARYAN,SK GALFAYAN,MZ ZAZYAN AM DUNAEVSKII	392
HE 3.6-3	A NEW METHOD OF DIFFERENTIAL STRUCTURAL ANALYSIS OF GAMMA-FAMILY BASIC PARAMETERS LG MELKUMIAN,SV TER-ANTONIAN YUA SMORODIN	396
HE 3.6-4	LPM EFFECT AND PRIMARY ENERGY ESTIMATIONS MF BOURDEAU,JN CAPDEVIELLE	400
HE 3.6-6	EXPERIMENTAL BASIS FOR THE MODELS OF CASCADE PROPAGATION IN ATMOSPHERE Z STRUGALSKI	404
HE 3.6-7	RELATION BETWEEN GAMMA-RAY FAMILY AND EAS CORE - MONTE-CARLO SIMULATION OF EAS CORE - T YANAGITA	407
HE 3.6-8	COMPARISION OF BIG EVENT WITH CALCULATIONS OF THE AIR SHOWER DEVELOPMENT M NIWA,A MISAKI,T MATANO,K HONDA I TSUSHIMA,N KAWASUMI,K HASHIMOTO	411
HE 3.6-10	THE LATERAL DISTRIBUTION OF CHARGED PARTICLES OF ENERGY GREATER THEN 0.3 E CRIT IN ELECTRON-PROTON CASCADES IN LEAD AND AIR A WASILEWSKI,E KRYS	412

VOLUME 6

HE 3.6-11 RESULTS OF MONTE-CARLO SIMULATIONS OF ELECTRON-PHOTON CASCADES IN LEAD AND LAYERS OF LEAD-SCINTILLATOR 416

A WASILEWSKI,E KRYS

HE 3.6-12 ON THE 'MINI-CLUSTER' OBSERVED BY THE CHACALTAYA EMULSION CHAMBER EXPERIMENT 420

T TATI

HE 3.7
EMULSION CHAMBER RESULTS

PAPER CODE		PAGE
HE 3.7-1	A COMPARATIVE ANALYSIS OF GAMMA AND HADRON FAMILIES AT THE SUPERHIGH ENERGIES RECORDED IN EXPERIMENT "PAMIR" SA AZIMOV,EJ MULLADJANOV,AN NOSOV H NURITDINOV,DA TALIPOV,DA HALILOV TS YULDASHBAEV	424
HE 3.7-2	STUDY OF GAMMA-FAMILIES GENERATED IN NUCLON-NUCLEUS (NA) AND PION-NUCLEUS (PI A) INTERACTIONS SA AZIMOV,EJ MULLAJANOV,H NURITDINOV TS YULDASHBAEV	428
HE 3.7-3	HADRONS REGISTRATION IN EMULSION CHAMBER WITH CARBON BLOCK A TOMASZEWSKI,Z WLODARCZYK	431
HE 3.7-4	NEW ANALYSIS OF NUCLEAR INTERACTION OBSERVED BY MT. KANBARA EMULSION CHAMBER EXPERIMENT H NANJO	435
HE 3.7-5	ON THE MEAN CHARACTERISTICS OF FAMILY EVENTS OBSERVED AT MT. KANBALA CHINA-JAPAN COLLABORATION	439
HE 3.7-7	STRUCTURED EVENTS IN "PAMIR" CARBON X-RAY CHAMBERS GG LEPTUKH	443
HE 3.7-9	ULTRA HIGH ENERGY EVENTS IN ECHOS SERIES AND PRIMARY ENERGY SPECTRUM JN CAPDEVIELLE,J IWAI,T OGATA	447

HE 3.7-10 PECULIARITIES OF GAMMA-RAY DISTRIBUTION AT 20 TEV ENERGY 451

PM ERMAKOV,AA LOKTIONOV,YUT LUKIN
TKH SADYKOV

N85-35849
HE1.1-1

PROTON-AIR AND PROTON-PROTON CROSS SECTIONS FROM AIR SHOWER DATA

John Linsley
Department of Physics and Astronomy
University of New Mexico, Albuquerque, NM 87131
USA

ABSTRACT

Data on the fluctuations in depth of maximum development of cosmic ray air showers, corrected for the effects of mixed primary composition and shower development fluctuations, yield values of the inelastic proton-air cross section for laboratory energies in the range 10^9-10^{10} GeV. From these values of σ_{pa}, corresponding values of the proton-proton total cross section are derived by means of Glauber theory and geometrical scaling. The resulting values of σ_{pp} are inconsistent with a well known $\ln^2 s$ extrapolation of ISR data which is consistent with SPS data; they indicate a less rapid rate of increase in the interval $540 < \sqrt{s} < 10^5$ GeV.

1. Introduction. The total inelastic proton-air cross section σ_{pa}, which is interesting in relation to the theory of hadron-hadron and hadron-nucleus interactions, can be derived from data on cosmic ray air showers. Cosmic ray evidence of an increase with increasing energy in σ_{pp}, the total proton-proton cross section, has been confirmed, first at ISR energies and more recently with the CERN SPS collider.[1-4] In the interval $10 < \sqrt{s} < 540$ GeV the increase, amounting to some 75%, agrees well with a $\ln^2 s$ dependence but is compatible with a slower rate.[3] A recent cosmic ray result for $2 \cdot 10^3 < \sqrt{s} < 2 \cdot 10^4$ GeV favors $\ln^2 s$,[5] while another result of this kind, for $\sqrt{s} = 3 \cdot 10^4$ GeV, favors a slower increase.[6] In case of the cosmic ray results, σ_{pp} is derived from σ_{pa} using Glauber theory.

My purpose here is to draw attention to another body of air shower evidence extending to even higher energies ($10^4 < \sqrt{s} < 1.6 \cdot 10^5$ GeV) which also bears on this question.[1,8] The evidence consists in part of data on the fluctuation of shower elongation x_m, and in part of data on the primary composition. These are combined using an expression for $\{x_m\}$ as a function of $\langle \ln A \rangle$, $\{\ln A\}$ and $\{x_{m,p}\}$, where A is the primary mass number, $\langle \ln A \rangle$, $\{\ln A\}$ are the mean value and dispersion about the mean of lnA for fixed primary energy, $\{x_{m,p}\}$ is the dispersion of x_m for proton-initiated showers of a fixed energy (allowing for fluctuations in shower origin and development), and $\{x_m\}$ is the observed dispersion of x_m, corrected for reception fluctuations (instrumental dispersion).[7] Using experimental evidence on $\langle \ln A \rangle$ and $\{\ln A\}$ from other air shower observations, the correction for contamination of the primary beam with heavy nuclei is shown to be small: $\{x_{m,p}\} \approx \{x_m\}$. Cascade simulations have shown that $\{x_{m,p}\}$ is proportional to λ_{pa}, the proton-air mean free path, with a proportionality constant equal to 1.4. From λ_{pa} one obtains σ_{pa}; σ_{pp} follows by application of Glauber theory.

2. Primary Composition Effect. I have shown elsewhere that if y is an observable such as x_m, whose mean value for proton showers can be graphed vs lnE as a straight line (over reasonably wide intervals, say 2 decades or more), and if the line width (fluctuation of y) for showers initiated

by various nuclei is approximated by $\{y(A)\} = \{y(1)\}(1 - k\ln A)$, where k is constant, then

$$\{y\}^2 = \{y(1)\}^2[1 - 2k\langle\ln A\rangle + k^2(\langle\ln A\rangle^2 + \{\ln A\}^2)] + b^2\{\ln A\}^2 , \quad (1)$$

where b is the slope of the straight-line graph.[7] This follows from elementary statistical theory and the superposition principle of Peters. For $y = x_m$, b is just $D_{e,p}$, the proton shower elongation rate. With these substitutions I solve (1) for $\{x_{m,p}\}$, obtaining

$$\{x_{m,p}\} = \{x_m\}\left[\frac{1 - (D_{e,p}\{\ln A\}/\{x_m\})^2}{1 - 2k\langle\ln A\rangle + k^2(\langle\ln A\rangle^2 + \{\ln A\}^2)}\right]^{\frac{1}{2}} . \quad (2)$$

The right hand side of (2) contains, besides the observed quantity requiring correction, 2 parameters which describe phenomenologically the relevant features of air showers ($D_{e,p}$ and k), and 2 parameters which describe the composition of the incoming cosmic ray beam ($\langle\ln A\rangle$ and $\{\ln A\}$).

The fluctuation of x_m has been studied experimentally for more than 10 years using the giant air shower array at Haverah Park,[8,9] and almost as long using a similar size array at Yakutsk.[10] It has been measured independently at Dugway using an array of atmospheric Cerenkov light detectors,[11] and at Akeno using data on the electron lateral distribution.[12] Results are given in Table 1.

I have shown elsewhere that under a wide range of assumptions about hadron-nucleus interactions $D_{e,p}$ cannot be appreciably greater than t_o, the radiation length. This insures that the numerator in (2) is approximately 1, so the exact value of $D_{e,p}$ is unimportant. For energy independent composition, $D_{e,p} = D_e$ (observed elongation rate). I adopt $D_{e,p} = 28$ g/cm^2, practically the experimental value of D_e at these energies.[14] As for the parameter k, Monte Carlo cascade simulations show that its value lies in the range $0.15 \pm .05$, depending on the choice of model.[11,15] The exact value is unimportant if $\langle\ln A\rangle$ is less than 1.

Data on $\langle\ln A\rangle$ and $\{\ln A\}$ at very high energies are summarized in Ref. 7 (see also conference paper OG5.4-4). They can be combined, as in Fig. 1, by plotting $\{\ln A\}$ vs $\langle\ln A\rangle$ in rectangular coordinates. Note that for any pure composition $\{\ln A\} = 0$. It is assumed that the possibilities range from $\langle\ln A\rangle = 0$ (pure protons) to $\langle\ln A\rangle = 4$ (pure Fe). The maximum dispersion for a given mean occurs for a mixture of protons and Fe nuclei. When the scales are chosen as I have done the locus of binary proton-Fe mixtures is a semicircle. The lower boundary of the diagram consists of smaller semicircles corresponding to other binary mixtures. The region inside the boundary represents all possible compositions. The observed equal-energy composition in the low energy region (10^2-10^5 GeV) is indicated by the heavy dashed line. The compositions experimentally allowed at very high energies ($E > 10^8$ GeV) are those within the shaded region. The heavy dotted line

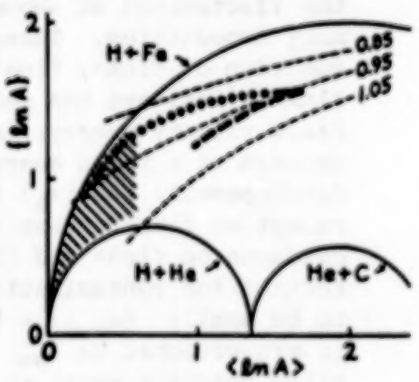


Fig. 1. Cosmic ray composition diagram: 2nd vs 1st moment of the lnA distribution, explained in the accompanying text.

Table 1. Summary of $\{x_m\}$ data

$\log E_{lab}$ (GeV)	$\{x_m\}$ g/cm^2	No. of events	Ref.
7.58	89 ± 15	?	12
7.82	90 ± 18	?	12
8.06	86 ± 19	?	12
8.24	80 ± 11	147	11
8.30	70 ± 13	?	12
8.30	69 ± 14	426	8
8.56	62 ± 9	1014	8
8.68	71 ± 6	519	9
8.78	73 ± 10	a	10
8.83	51 ± 7	652	8
8.88	79 ± 4	300	10
9.11	68 ± 10	334	8
9.15	69 ± 6	a	10
9.43	65 ± 11	a	10
9.45	74 ± 11	178	8
9.60	63 ± 5	201	10
10.00	54 ± 11	87	8
10.15	55 ± 13	a	10

[a] total of 464 events

represents a detailed model given in Ref. 7, which describes in a plausible manner the high energy region and the transition from lower energies. The correction factors $\{x_{m,p}\}/\{x_m\}$ for this model to be used with Table 1 according to (2) range in value from 0.91 to 0.95; thus they differ only slightly from 1 (no correction). These corrections have been applied in obtaining the present results, shown in Figures 2 and 3.

Also shown in Fig. 1 are contour lines corresponding to a typical value of $\{x_m\}$ (= 66 g/cm^2) and the indicated values of the correction factor. By examining these contours one sees that correction factors for any other allowed model will differ only slightly from those used here.

3. Development Fluctuations. The next step is to convert from $\{x_{m,p}\}$ to σ_{pa} allowing for shower development fluctuations. These arise primarily because of the leading particle effect. Thus one expects them to scale as λ_{pa}, so there will be a proportionality: $\{x_{m,p}\} = K\lambda_{pa}$ where K is a constant. On the basis of Monte Carlo cascade simulations by Walker and Watson[8] I adopt the value 1.40 for this constant. The resulting values for σ_{pa} are given in Figure 2.

There is of course some uncertainty in the value of K, due mainly to uncertainty about the elasticity of very high energy hadron-air collisions, denoted here by η. The result K = 1.4 rests on a conventional assumption that η is distributed uniformly between 0 and 1 with a mean value of 0.5. It has been pointed out by L.W. Jones that according to accelerator data the value of $\langle\eta\rangle$ for proton collisions with light nuclei is appreciably less, about 0.3.[16] The dependence of K on $\langle\eta\rangle$ can be estimated by assuming 1) that x_{av} of the partial electronic cascade originating from each collision of the leading nucleus is perfectly correlated with the depth of that collision, and 2) that $\{x_{m,p}\} = \{x_{av,p}\}$ (neglecting fluctuations in η). It is then easily shown that

$$K = [\Sigma_{j=1}^{\infty} j(1-\eta)\eta^{j-1}]^{\frac{1}{j}} = (1-\eta)^{-\frac{1}{1}}. \qquad (3)$$

For $\eta = 0.5$ one obtains K = 1.41; for $\eta = 0.3$ the result is K = 1.20. Thus the effect of assuming a smaller value of $\langle\eta\rangle$ is to reduce the apparent cross sections σ_{pa} and σ_{pp} at air shower energies.

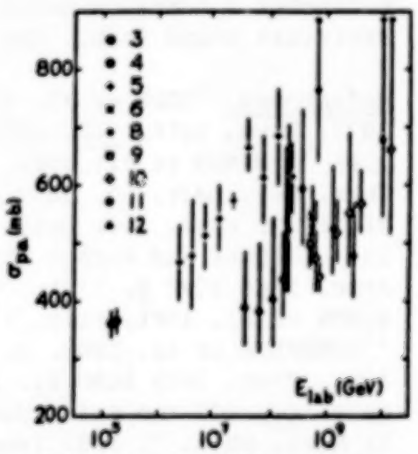


Fig. 2. Results on σ_{pa}. The numbers listed with the symbols are the corresponding references.

4. Results. Examining Fig. 2 one notes good agreement between the present results and one published recently by the Fly's Eye group.[6] The Fly's Eye result is derived from the decrement of the x_m distribution, rather than the dispersion, using a proportionality between Λ_{xm} and λ_{pa}. The value of the constant is taken as 1.6 ± 10% from simulations[15] similar to those of Walker and Watson. The present results disagree with those of Ref. 5, based on the zenith angle distribution of generally smaller air showers for fixed N_e and N_μ. Here also the relation between a measured attenuation length and λ_{pa} is found by means of simulations. There is an approximate proportionality, the value of the constant being 1.45-1.55. The value of $\langle\eta\rangle$ for the Akeno model is 0.44. A smaller value would result in a smaller value of the proportionality constant and a smaller apparent rise in cross sections. However it would not remove the discrepancy since a change in $\langle\eta\rangle$ will have a similar effect on results from Λ_{xm} and $\{x_m\}$.

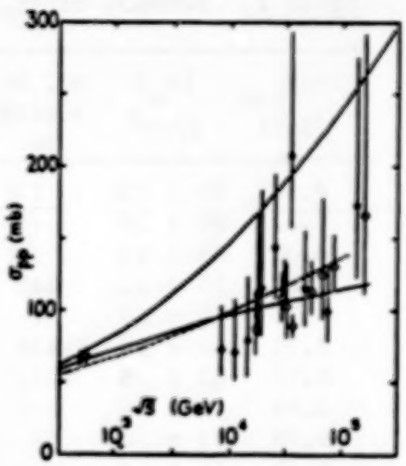


Fig. 3. Results on σ_{pp} (same symbols as Fig. 2). The lower solid curve, from Ref. 17, is a best fit to ISR data allowing deviation from the Froissart bound. The upper solid curve (same Ref.) is a best fit with Froissart bound form. The dashed curve is for the 'impact picture'.[18]

Fig. 3 shows the result of converting the new σ_{pa} values to σ_{pp}. This has been done the same way as in Ref. 6, using Glauber theory with an assumption that the nuclear slope parameter has the same energy dependence as σ_{pp} (geometrical scaling). In parametric form, the relation assumed is $\sigma_{pa} = 24.0\ \sigma_{pp}^{0.648}$ (cross sections in mb). Shown for comparison are the SPS results,[3,4] and well known extrapolations by Block and Cahn, based on ISR data, which successfully predicted those results.[17] Also shown is a recent prediction by Bourrely *et al.*, for the so-called impact picture.[18] The lower Block-Cahn curve is the best fit with a ≠ 0, where parameter a takes on small positive values to allow for deviations from Froissart bound form. The upper curve is for a = 0.

References. [1]YODH *et al.* 1972, Phys. Rev. Lett. 28, 1005; [2]AMALDI *et al.* 1977, Phys. Lett. 66B, 390; [3]BATTISTON *et al.* 1982, Phys. Lett. 117B, 126; [4]ARNISON *et al.* 1983, Phys. Lett. 128B, 336; [5]HARA *et al.* 1983, Phys. Rev. Lett. 50, 2058 and Proc. 18th ICRC 11, 354; [6]BALTRUSAITIS *et al.* 1984, Phys. Rev. Lett. 52, 1380; [7]LINSLEY 1983, Proc. 18th ICRC 12, 135; [8]WALKER and WATSON 1982, J. Phys. G: Nucl. Phys. 8, 1131 (also 1983, Proc. 18th ICRC 6, 114); [9]COY *et al.* 1981, Proc. 17th ICRC 6, 43; [10]DYAKONOV *et al.* 1981, Proc. 17th ICRC 6, 110 and Proc. 18th ICRC 6, 111; [11]CHANTLER *et al.* 1982, J. Phys. G: Nucl. Phys. 8, L51; [12]HARA *et al.* 1983, Proc. 18th ICRC 11, 272; [13]LINSLEY and WATSON 1981, Phys. Rev. Lett. 46, 459 and references therein; [14]WALKER and WATSON 1981, J. Phys. G: Nucl. Phys. 7, 1297 (see also Ref. 13); [15]ELLSWORTH *et al.* 1982, Phys. Rev. D 26, 336; [16]JONES 1983, Proc. 18th ICRC 5, 17; [17]BLOCK and CAHN 1983, Phys. Lett. 120B, 224 and in Proc. 18th *Rencontre de Moriond*, Vol. 3; [18]BOURRELY *et al.* 1985, Phys. Rev. Lett. 54, 757; [19]see also LINSLEY 1985, *Lett. Nuovo Cimento* 42, 403.

ORIGINAL PAGE IS
OF POOR QUALITY

N85-35850 HE 1.1-2

PROTON-AIR INELASTIC CROSS SECTION AT $S^{1/2}$ = 30 TeV

Baltrusaitis, R.M., Cassiday, G.L., Cooper, R., Elbert, J.W., Gerhardy, P.R., Ko, S., Loh, E.C., Mizumoto, Y., Sokolsky, P. & Steck, D.

Department of Physics, University of Utah, Salt Lake City, UT 84112

ABSTRACT

We have measured the distribution of the maxima of high energy cosmic ray induced extensive air showers in the atmosphere as a function of atmospheric depth. From the exponential tail of this distribution, we determined the p-air inelastic cross section at 30 TeV center-of-mass energy to be 540 ± 40mb.

1. Introduction. The technique of extracting the p-air cross section from the data obtained by the "Fly's Eye" detector has been described in detail in an earlier paper.(1) We report the results of a recent analysis from data accumulated through the month of April 1985.

2. Discussion. The "Fly's Eye" detector consists of 67 F/1 mirrors, each with 12 or 14 photomultiplier tubes mounted at the focus.(2) These mirrors are arranged so that they cover all but a small portion of the solid angle near the horizon. The detector records the passage of distant extensive air showers by means of the light produced by the shower particles which, depending on the relative geometry between the track and the detector, is usually an admixture of Cerenkov and fluorescent light. The shower direction is reconstructed from the timing information obtained by the photomultiplier tubes. Knowing the reconstructed geometry and the fluorescence efficiency and taking into account the Cerenkov intensity, we calculate the number of particles of each shower as it progresses through the atmosphere. Figure 1 shows the number of particles in a shower as a function of atmospheric depth.

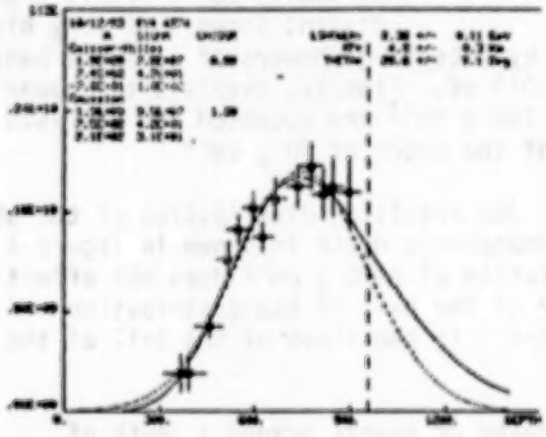


Figure 1. An Extensive Air Shower That Survives All Data Cuts. The solid curve is a GH. shower curve. The dotted curve is a Gaussian distribution.

The shower maximum is obtained by fitting a distribution to the shower profile. We ascertained that the shape of the shower profile can be fitted with either a Gaisser-Hillas (G-H)(3) distribution or a Gaussian distribution. Both distributions yield equally good fits, with the G-H fit consistently giving a slightly lower value (30 g cm^{-2}) to the depth of maxima. Such consistent difference does not affect the over-all shapes of the final data distributions obtained from the two fits.

The error in shower maximum, for showers whose

closest distance of approach of exceed one and one half kilometers, arises almost entirely from the uncertainty in the reconstructed polar angle. Showers with zenith angle larger than sixty degrees are excluded in this analysis to avoid bias toward large depths of maxima due to the exponential behavior of the atmospheric density.

Possible track reconstruction bias has been examined by using light beams generated by a roving light pulser, and a fixed position nitrogen pulse laser. Tracks reconstructed from such light pulses show that, regardless of the angle of the light beams, we can measure the polar angle to the order of one degree with a sigma of about 1.7 degrees. Figure 2 shows the result of one of the runs obtained with the roving flasher. Further checks are made with events that are visible from a partially built second detector located about 3.5 kilometers from the "Fly's Eye". In this case, the polar angle is determined from the intersection of the two planes which contain the track. Again, the zenith angles obtained with the coincidence events are in agreement within experimental uncertainties with the angles calculated with the timing information from one eye alone. Figure 3 shows the agreement between the two methods of calculating the zenith angle.

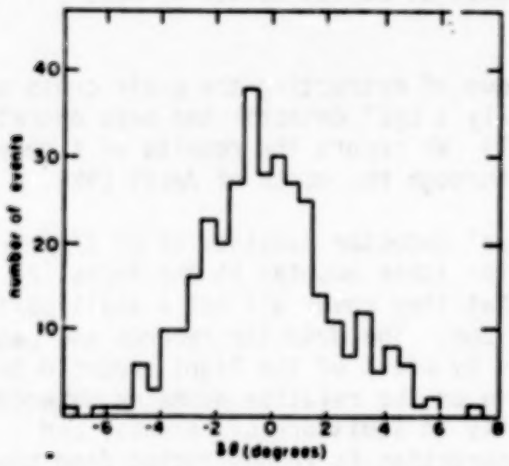


Figure 2. Distribution of differences between known and fitted zenith angles for "upward-going" showers of known geometry generated by a high intensity light flacher. The width of the distribution is σ=1.7°.

Bias toward large depths of maxima could result from distant showers of very high energy. Such bias is removed by accepting showers of a narrow band of energy between 10^{17} eV and 2×10^{18} eV. Finally, events with shower maximum uncertainty less than 100 g cm^{-2} are accepted for analysis with the average uncertainty of the order of 70 g cm^{-2}.

3. Results and Conclusions. The resulting distribution of the shower maxima as a function of the atmospheric depth is shown in Figure 4. The effect of the finite resolution of δ=70 g cm^{-2} does not effect the shape of the exponent behavior of the tail of the distribution beyond a distance of δ^2/λ where λ is the slope of the tail of the distribution.

A fit of the data based on events beyond a depth of ~ 760 g cm^{-2} is found to be =70±6 g cm^{-2}.

From a paper by Sokolsky et al(4) submitted to this conference, it seems likely that the primary particles consist of a considerable amount of light particles, i.e., protons. According to

ORIGINAL PAGE IS
OF POOR QUALITY

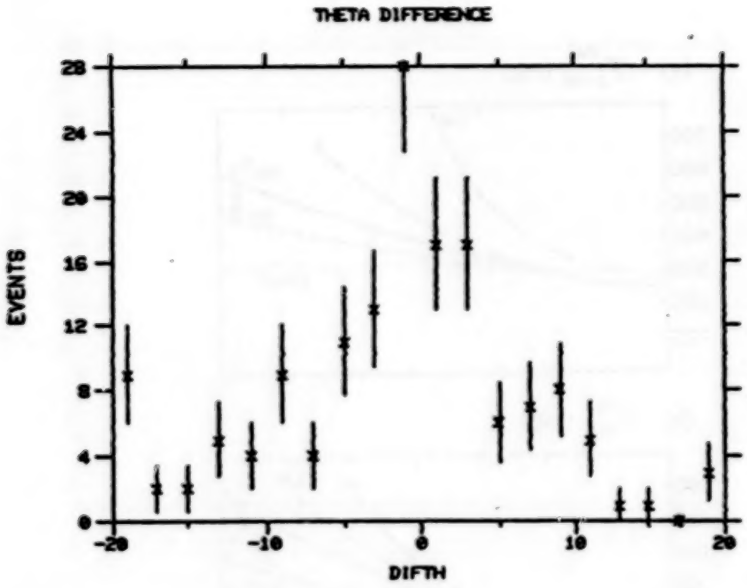


Figure 3. Difference in Zenith Angle for Events Observed by Both Detectors and With One Detector Alone. The average angular length for the track is about 40°.

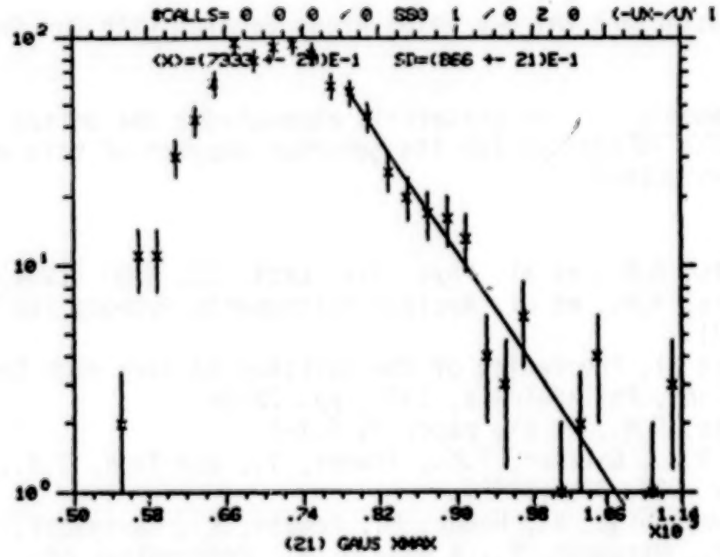


Figure 4. Distribution of Depth of Shower Maxima for Data Whose Fitting Errors Are Less Than 8,100 g cm^{-2}. The slope of the exponential tail is $\lambda = 70 \pm 6$ g cm^{-2}.

the paper by Ellsworth et al(5), those protons dominate the tail of the distribution. In this case, the proton-air inelastic cross-section is found to be 540±50 g cm^{-2}. This result is in agreement with the results published by Hara et al(6).

The extrapolation of proton-proton inelastic cross-section from p-air cross-section is model dependent. With the same assumptions made in our previous paper(1), the p-p inelastic cross-section is found to be 122±11 mb at $s^{1/2}$ of 30 TeV (Figure 5).

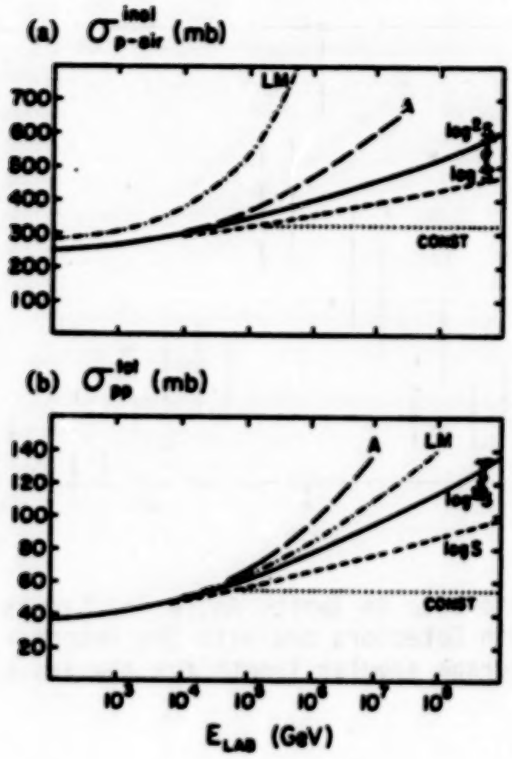


Figure 5.
(a) Pair Inelastic and (b) p-p Total Cross Section With Our Data.

4. Acknowledgements. We gratefully acknowledge the United States National Science Foundation for its generous support of this work under grant PHY8201089.

References.

1. Baltrusaitis, R.M., et al, Phys. Rev. Lett. 52, 1380 (1984).
2. Baltrusaitis, R.M., et al, Nuclear Instruments Methods (to be published).
3. Cassiday, et al, Proceeding of the Workshop on Very High Energy Interactions, Philadelphia, 1982, pp. 72-82.
4. Baltrusaitis, R.M., et al, paper OG 5.1-7
5. Ellsworth, R.W., Gaisser, T.K., Stanev, T., and Yodh, G.B., Phys. Rev. D26, 336 (1982).
6. Hara, T., Hayashida, N., Honda, M., Kamata, K., Kawaguchi, S., Kifune, T., Mizumoto, Y., & Nagano, M. Proceedings of International Symposium on Cosmic Rays and Particle Physics, March 19-23, 1984, Tokyo.

N85-35851

HADRON CROSS SECTIONS AT ULTRA HIGH ENERGIES AND UNITARITY BOUNDS ON DIFFRACTION DISSOCIATION

G. B. Yodh
Dept. of Physics and Astronomy, Univ. of Maryland
College Park, MD 20742

T. K. Gaisser
Bartol Research Foundation, Univ. of Delaware
Newark, Delaware 19711

U. P. Sukhatme
Dept. of Physics, Univ. of Illinois, Circle Campus
Chicago, Illinois 60680

1. Introduction: The behavior of total cross sections at ultra high energies, above $\sqrt{s}$ ~ 1 TeV has been derived from analysis of air shower observation.[1] The proton-air inelastic cross section must be related to the basic proton-proton interaction to determine which of the different models for the asymptotic behavior of the scattering amplitude are consistent with cosmic ray data which may be ruled out. The adjective inelastic for proton-air cross section ($\sigma_{p\text{-}air}^{inel}$) describes the fact that cosmic ray experiments do not measure all of the absorptive cross section because cascade development is not sensitive to processes that lead to quasi-elastic excitation of the air nucleus (σ_{qe}) or to diffractive excitation of one of the nucleons of the air nucleus (σ_{DD}). The method generally used to calculate p-air inelastic cross section from proton-proton parameters is the Glauber multiple scattering technique.[2] Application of this method leads to the relation

$$\sigma_{P\text{-}air}^{inel} = \sigma_{P\text{-}air}^{tot} - \sigma_{P\text{-}air}^{el} - \sigma_{qe} - \sigma_{D} - \Delta\sigma(\text{inelastic screening}) \qquad (1)$$

The term $\Delta\sigma$(inelastic screening) accounts for screening due to multiple scattering with excited nucleon intermediate states. To calculate terms on the right hand side of this relation it is necessary to know the values of σ_{tot}^{PP}, slope parameter $B^{PP}(t=0)$, single and double diffractive cross sections σ_{SD}^{PP}, σ_{DD}^{PP} the shape of $d^2\sigma/dtdM^2$ at t_{min} for the diffractive process P+P→P+X and the nuclear density profile.[3]

2. Discussion of Models of Elementary Interaction: Many different models for the high energy behavior of scattering amplitudes have been proposed, all of which agree with PP and $\bar{P}P$ data up to SPS-$\bar{P}P$ collider energies but give different extrapolations at higher energies. They may be classified into three types: (1) Geometric scaling models,[4] (2) Diffraction dominance models,[3] (3) Chou-Yang type models.[5]

The "Geometrical Scaling" models are those in which the interaction radius increases logarithmically with energy. The ratio σ_{el}/σ_{tot} is assumed to be energy independent. The rise in the total cross section comes from all three components, diffractive and inelastic processes.

The diffractive dominance models ascribe all the rise in total cross sections to σ_{el}, σ_{SD} and σ_{DD}, the "inelastic" cross section remaining constant. The ratio $\sigma_{inel}/\sigma_{tot}$ decreases with energy, σ_{el}/σ_{t} becomes energy independent, σ_{SD}/σ_{tot} slowly decreases with energy while σ_{DD}/σ_{tot} will be asymptotically constant.

In Chou-Yang type models the restriction of geometrical scaling that σ_{el}/σ_t = constant is released. However the detailed behavior of σ_{SD} or σ_{DD} is not generally prescribed.

This it may seem at first glance that with so much freedom it would be possible to fit the cosmic ray data with a large range of models. This is not [illegible], because the range of variation of the diffractive component cross sections are limited by unitarity bounds. There is only one proviso for this statement which is that Glauber techniques are valid at these energies.

3. Unitarity Bounds and Limits on Diffraction: The unitarity bound on elastic and diffractive cross section can be stated as[6]

$$\sigma_{el} + \sigma_{Diff} \leq \tfrac{1}{2}\sigma_{tot} \qquad (2)$$

One can write σ_{tot} in terms of its parts

$$\sigma_{tot} = \sigma_{el} + \sigma_{Diff} + \sigma_{ND} \qquad (3)$$

where σ_{ND} is the non-diffractive cross section. It follows from these relations that

$$\sigma_{ND} \geq \tfrac{1}{2}\sigma_{tot} \qquad (4)$$

which means that if $\sigma_{tot}(E)$ increases with energy then σ_{ND} cannot be energy independent.

Assuming the general validity of the bounds we apply it to the specific model of diffractive dominance proposed by Goulianos. The energy variation of σ_{el}, $2\sigma_{SD}$, σ_{DD} and σ_{tot} for this model is shown in figure 1. The value of $\frac{1}{2}\sigma_{total}$ is also graphed. The unitarity bound given by equation (2) is violated by this model at $\sqrt{s}$ - 200 GeV so is the inequality $\sigma_{ND} \geq \frac{1}{2}\sigma_{tot}$.

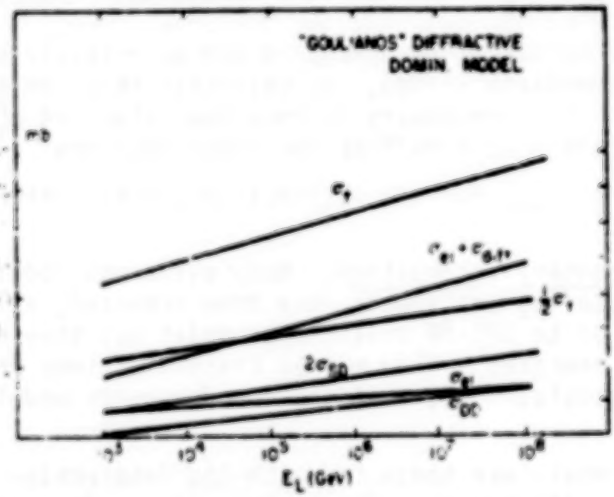


Figure 1: Predictions from a diffractive dominance model (Goulianos 1983) and its relation to unitarity bounds which require $(\sigma_{el} + \sigma_d)/\sigma_t$ to be less than or equal to 0.5

In fact any model which ascribes the increase in cross section entirely to diffractive processes will violate conventional unitarity requirements.

As representative of other models let us consider the model proposed by Block and Cahn. The model gives explicit fits for total and elastic cross sections as well as the slope parameter, (B), as a function of energy. To obtain $\sigma_{p\text{-air}}$ (inelastic) using equation (1) we must calculate the five terms on the right hand side using Glauber methods. The total, elastic and quasi-

ORIGINAL PAGE IS
OF POOR QUALITY

elastic proton-air cross sections can be calculated in straight forward manner using the model parameters: σ_{pp}^{tot}, σ_{pp}^{el}, B and ρ. To estimate σ_D and $\Delta\sigma$(inel-screening) a knowledge of the single diffractive cross section is needed, which is not given by the model. Of these two terms, $\Delta\sigma$(inel-screening) depends only on the value of $(d\sigma/dtdM^2)_{tmin}$ which varies as $1/M^2$.[2] Most of the contribution to this term comes from small values of M^2 and numerical evaluation gives a value for this correction which varies from about 8 mb at ISR energies to saturation at ~ 14 mb at ultra high energies.

The correction for diffractive dissociation of the target nucleon is given by

$$\sigma_D = (\sigma_{SD}^{PP}/\sigma_{inel}^{PP})\ \sigma_{p\text{-air}}^{1} \qquad (5)$$

Here $\sigma_{p\text{-air}}^{1}$ is the cross section for an absorptive -p-nucleus interaction involving exactly one elementary inelastic scattering encounter. It is easy to show that $\sigma_{p\text{-air}}^{1} \equiv 2/3\ \pi\ \langle r^2\rangle$ which corresponds to 142 mb for a root mean square radius of 2.6 fermis. The correction depends on the energy dependence of $\sigma_{SD}^{PP}/\sigma_{inel}^{PP}$ where $\sigma_{inel}^{PP} \equiv \sigma_{tot} - \sigma_{el} = \sigma_{ND} + 2\sigma_{SD} + \sigma_{DD}$.

What does the unitarity bound tell us about the size of this ratio? From the unitarity bound in equation (2) gives

$$2\sigma_{SD} + \sigma_{DD} \leq \tfrac{1}{2}\ \sigma_{tot} - \sigma_{el} \qquad (6)$$

The maximum value of σ_{SD} then is obtained by putting $\sigma_{DD} = 0$. The ratio $\sigma_{SD}/\sigma_{inel}$ is bounded by

$$\frac{\sigma_{SD}}{\sigma_{inel}} \leq \tfrac{1}{4}\ [1 - \frac{\sigma_{el}/\sigma_{tot}}{1 - \sigma_{el}/\sigma_{tot}}] \leq 0.25 \qquad (7)$$

The maximum value of σ_D is 36 mb if $\sigma_{el} = 0$! In the Block-Cahn model corresponding to a $\ell n^2 s$ energy dependence[5] the ratio of σ_{el} to σ_{tot} varies from 0.175 to 0.37 as energy is varied from $\sqrt{s}$ ~ 20 GeV to $\sqrt{s}$ ~ 10 TeV, corresponding upper limits to σ_D are 28 mb and 15 mb respectively. At ISR, however, there are direct measurements of σ_{SD} and σ_{inel} which give a 14 mb cross section for σ_D. A reasonable measure of the allowed range of σ_D can be obtained by assuming that the lower bound to $\sigma_{SD}/\sigma_{inel}$ is the ISR value and the upper bound is given by equation (8) with σ_{el}/σ_{tot} being taken from Block and Cahn's model. The result is shown in figure (2). Also shown in the figure is the sum of the last three terms in equation (1), i.e. $\sigma_{qe} + \sigma_D + \Delta\sigma$(inel. screening). The

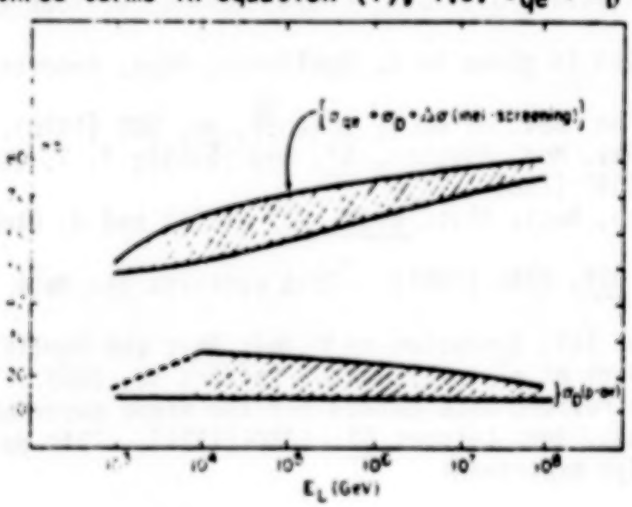


Figure 2: The allowed ranges for the correction for diffractive dissociation of the target nucleon. Also shown is the total correction as a function of energy.

ORIGINAL PAGE IS
OF POOR QUALITY

fractional uncertainty in the value of $\sigma_{p\text{-air}}$(inelastic) is less than three percent.

In figure (3) we compare the predictions of the $\ell n s$ and $\ell n^2 s$ models of Block and Cahn with air shower cosmic ray cross sections.[7,8,9] It is seen that the data clearly favor the faster energy dependence.

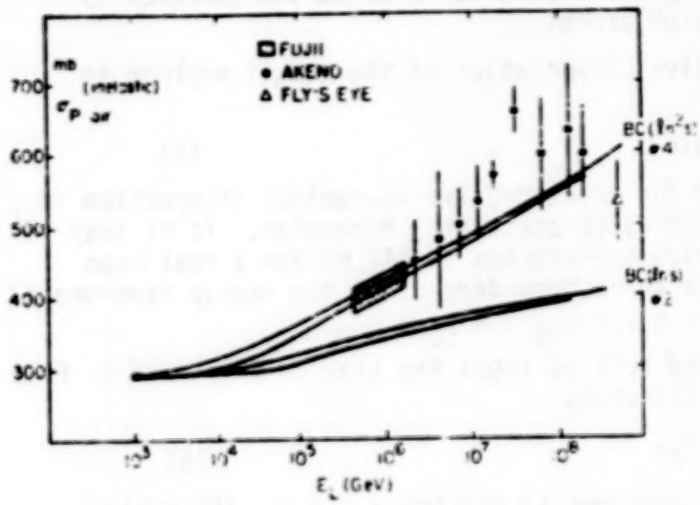


Figure 3: Comparison of predictions for $\sigma_{p\text{-air}}$ (inelastic) from two different models of Block and Cahn: No. 4 for which σ^t_{pp} increases as $\ell n^2 n$ and No. 2 which has a $\ell n s$ dependence

4. Conclusion: We have shown that if unitarity bounds on diffractive cross sections are valid at ultra high energies then (a) diffractive dominance models which ascribe the increase in total hadron-hadron cross sections to diffractive processes only are ruled out and (2) that cosmic ray cross sections derived from air shower experiments at ultra high energies clearly rule out models for hadron-hadron cross sections with $\ell n s$ energy dependence and favor those with $\ell n^2 s$ variation.

This work was supported in part by the National Science Foundation and the Department of Energy.

5. References:

1. G. B. Yodh, to be published in the Proceedings of the Aspen Winter Conference Series, Jan. 1985, Univ. of MD Physics Preprint PP No. 85-130.
2. V. Barger et al., Phys. Rev. Letters 33, 1051, (1974) and G. B. Yodh et al., Phys. Rev. D27, 1183 (1983).
3. A summary of data prior to 1983 is given in K. Goulianos, Phys. Reports 101, 170 (1983).
4. U. Amaldi, M. Jacob et al., Ann. Rev. of Nucl. Science, 26, 385 (1976).
5. M. M. Block and R. N. Cahn, Rev. Mod. Physics, 57, 563 (1985); T. T. Chou and C. N. Yang, Phys. Rev. 170, 1591 (1968).
6. U. P. Sukatme and F. S. Heyney, Nucl. Phys. B108, 317 (1976) and J. Pamplin, Phys. Rev. D8, 2899 (1973).
7. M. Akashi et al., Phys. Rev. D24, 2353 (1981). This contains the data from Mt. Fujii.
8. T. Hara et al., Proceedings of Int. Symposium on Cosmic Rays and Particles, Tokyo, Japan (1984), p. 756; T. Hara et al., Phys. Rev. Letters 50, 2058 (1983). The 1984 paper gives the revised data points for the Akeno experiment.
9. R. M. Baltrusaitus et al., Phys. Rev. Letters 52, 1380 (1984). This paper contains results from the Fly's Eye experiment.

N85-35852

ON TOTAL CROSS SECTIONS AND SLOPES AT SUPERHIGH ENERGIES

SH.S.YEREMIAN, V.M.ZHAMKOCHIAN

Yerevan Physics Institute, Markarian st.2
375036, Yerevan, Armenia, USSR

ABSTRACT

Hadron-hadron and hadron-nucleus interactions are investigated in the framework of the Reggeon field theory with critical and supercritical pomerons and multiple scattering theory. A good agreement is obtained with experimental data on cross sections of proton-proton and proton-nucleus interactions at high energies.

The theory with the renormgroup critical pomeron (RCP) ($\alpha_P(0) \equiv 1$) is compared with the supercritical one ($\alpha_P = 1+\Delta$) - froissarton. The theory with RCP is considered in detail in /1/, and with froissarton - in /2/, therefore, we will present here the basic results only.

In fig.1 total cross sections of pp-interaction at energies E_{LAB} from 10 to 10^{12} GeV are presented. Both models describe well the region of mean and high energies and practically coincide up to $\xi \leq 15$. The cross section given by RCP is presented in the figure by a coarse line. At mean values of energies it grows like ξ^2, at $\xi > 15$ the rate of growth gradually slows down and turns into asymptotic $\sim \xi^{0.277}$.

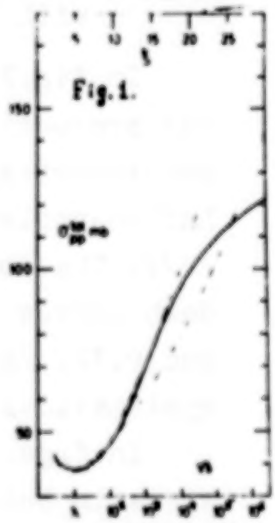


Fig.1. Total cross section of pp-interaction σ^{tot}_{p-air}.

The cross section given by the froissarton is presented by thin lines. The upper line corresponds to $\Delta = 0.12$, and the lower one to $\Delta = 0.07$. The cross section with $\Delta = 0.12$ rapidly

grows from the very beginning and at $\xi \geq 15$ begins to exceed the RCP and passes to its asymptotic regime $\sim \xi^2$. It is seen that σ_{pp}^{tot} cannot serve as a test for separating a correct model.

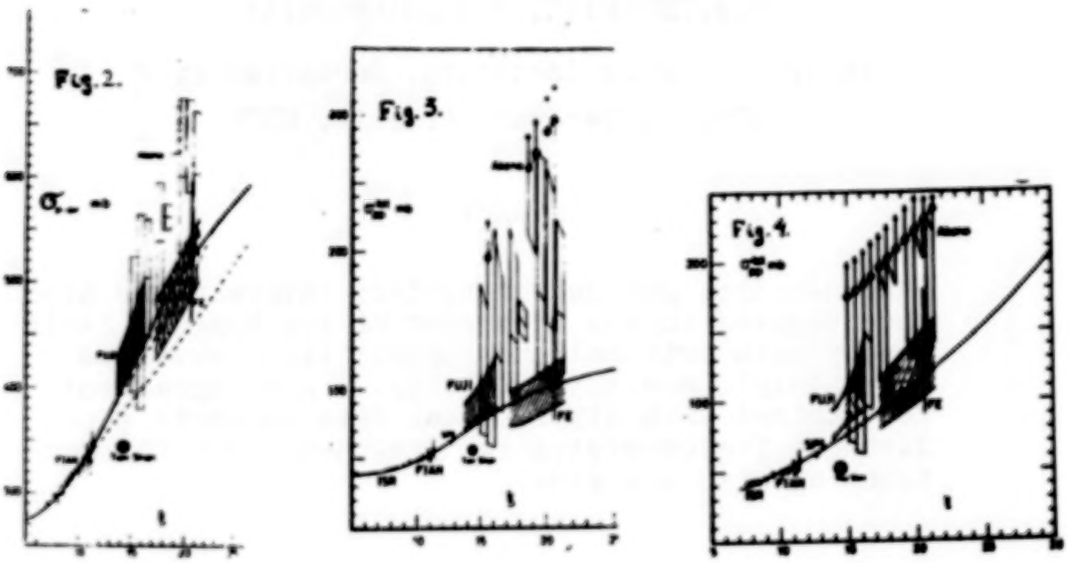


Fig.2. Production cross section on the nuclei of air atoms $\sigma_{p\text{-air}}^{prod}$ in theories with critical and supercritical pomerons (—— RCP, —·—·— froissarton).
Fig.3. Total cross section of pp-scattering in the theory with a critical pomeron.
Fig.4. Total cross section of pp-scattering in the theory with a supercritical pomeron.

In fig.2 theoretical curves are presented that describe the production cross section on nuclei of air atoms in the two theories considered (the calculation technique of the hadron-nucleus interaction characteristics is presented in /1/). The coarse curve corresponds to RCP, and the dot-and-dash curves to the supercritical pomeron with $\Delta = 0.07$ and 0.12. The curve corresponding to the froissarton lays systematically lower than RCP in the range $15 < \xi < 25$.

In figs. 3 and 4 total cross sections of pp-interactions in both theories as well as results of the pp cross sections extraction from experimental data on proton-nucleus interaction at cosmic energies are presented. The rings with arrows denote the values of separated points that lay above the unitarity limit for the given theory. It

ORIGINAL PAGE IS
OF POOR QUALITY

should be noted that according to /1/ the cross-section values $\sigma^{prod}_{p\text{-air}}$ depend essentially on the slopes of diffraction cone of the pp-interaction predicted by the given theory. It is clear that experiments with cosmic rays require a more rapid growth of slopes than the one which may be given by both theories. The theory with RCP seems preferable.

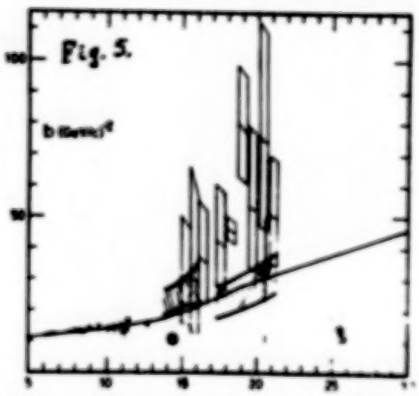


Fig.5. Slope of the diffraction cone of pp-scattering in the theory with a critical pomeron.

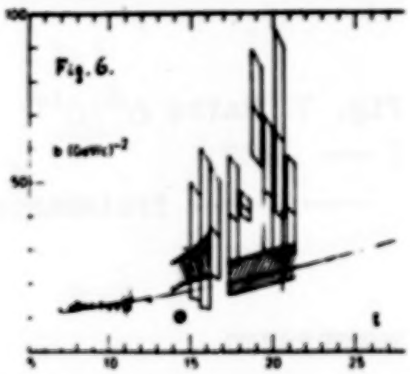
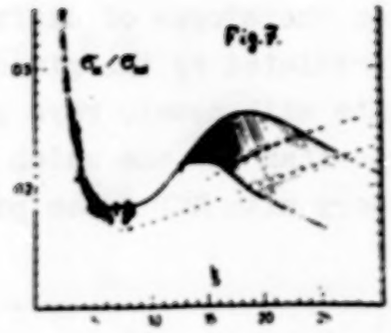


Fig.6. Slope of the diffraction cone of pp-scattering in the theory with a supercritical pomeron.

In figs. 5 and 6 diffraction cone slopes in RCP and froissarton theories are presented. The experimental data presented were extracted proceeding from the fixed cross sections of the elementary act in the given theory and are conventional, nevertheless, they indicate a necessity in a more rapid growth of slopes as compared with the theoretical one.

In fig.7 the ratio σ^{el}/σ^{tot} is presented. This value is crucial for the revelation of the question, which of these two theories is consistent at superhigh energies. In the RCP theory this ratio at $S \to \infty$ behaves like $\xi^{-0.862}$. In the froissarton theory we have $\sigma^{el}/\sigma^{tot} \to 1/2$. However, in the region of attainable energies we have an inverse picture: up to $\xi \leq 17$ σ^{el} and σ^{el}/σ^{tot} in RCP grow much more rapidly than in the froissarton, after which the RCP begins to slowly fall, and the froissarton continues to grow.



Pig. 7. Ratio σ^{el}/σ^{tot}
(—— RCP,
——·—— froissarton).

Summing up the abovementioned, one may state that even at ultracosmic energies it is apparently impossible to obtain an unambiguous answer to the question: which of these theories is consistent at superhigh energies?

REFERENCES

/1/ Yeremian Sh.S., Zhamkochian V.M., Yad.Fiz., 1984, 40, 1016.
/2/ Kaidalov A.B., Ter-Martirosian K.A., Yad.Fiz., 1984, 39, 1545.

N85-35853 HE 1.1-5

DETERMINATION OF THE CROSS SECTION OF THE PROTON, PION AND NEUTRON INELASTIC INTERACTION WITH LEAD AND CARBON NUCLEI AT 0.5 - 5.0 TEV ENERGIES (PION Experiment)

V.V.AVAKIAN, G.V.KARAGJOZIAN, E.A.MAMIDJANIAN, M.I.KEROPIAN, R.M.MARTIROSOV, G.G.OVSEPIAN, S.O.SOKHOYAN

Yerevan Physics Institute, Markarian st. 2
375036 Yerevan, Armenia, USSR

ABSTRACT

Experimental results on the cross section of the single pion, proton and neutron inelastic interaction with carbon and lead nuclei in the 0.5-5.0 TeV energy interval obtained on the PION installation (mount.Aragats, Armenia, 3250 m) are presented. For this purpose the N_{π} / N_p and $\sigma^{in}_{pPb} / \sigma^{in}_{\pi Pb}$ ratios measured directly on the installation as well as the calculated $\sigma^{in}_{pA} / \sigma^{in}_{\pi A}$ dependence on the target nucleus atomic number were used.

The PION installation combining an X-ray transition radiation multimodule detector (XTR detector) and an ionization calorimeter (IC) is shown in fig.1. The detailed description of the installation is given in /1/. 3 rows of multiwire proportional chambers (MWPC) identical to the chambers located in the XTR detector were used as detectors of the hadron interaction with the graphite nuclei. The thickness of the two graphite layers is 12 cm. The interactions in lead were registered by two rows of ionization chambers located under 3 cm (I layer) and 2 cm (II layer) of lead in the upper part of the IC.

To determine σ^{in} with the C and Pb nuclei, events were chosen that satisfied the following selection criteria: the energy release in the IC should be higher than 500 GeV;

N85-85853

ORIGINAL PAGE IS
OF POOR QUALITY

the axis of the nuclear-electromagnetic cascades (NEMC) should be within the solid angle of the installation (its geometric factor is $G = 1{,}28\ m^2 sr$); the ionization distribution in each row of the ionization chambers should have one maximum at a distance of 20 cm from the IC edge ($\sim$ two chamber diameters); the air accompaniment density should not exceed 1 part./m (the hadron "singleness" condition).

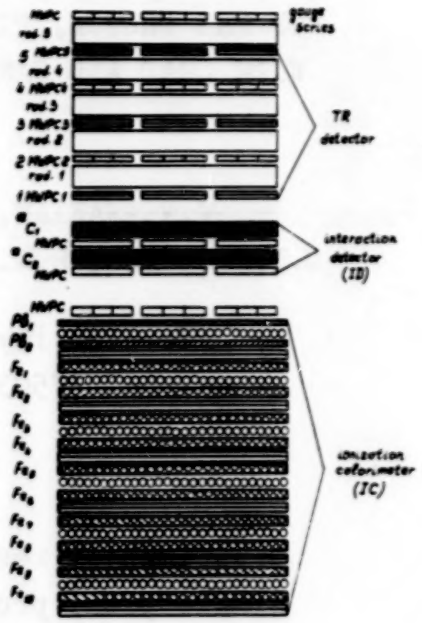


Fig. 1

In selecting the events identified as interactions in the graphite target the fulfillment of two additional criteria was required. The energy release in the interaction detector under the graphite target should correspond to the passage of $>$ 2 relativistic particles, and the summary energy release under the first layer should exceed 100 relativistic particles.

The additional condition for selecting the events identified as interactions in lead was the presence of energy release in the second row of ionization chambers in the absence of energy release in the first row.

According to these criteria 548 neutral and 876 charged hadrons having interacted in graphite as well as 1364 neutral and 1090 charged hadrons identified as having interacted in the second layer of lead were selected.

In determining the inelastic interaction cross sections corrections were introduced for "albedo" particles, the difference in the angular distribution of charged and neutral hadrons, the contribution of the cascades generated by muons, the transition effect Pb - ionization chamber wall. The measured cross sections of charged and neutral hadron

interactions with the C and Pb nuclei are plotted in Table 1.

Table 1

	500–1000 GeV	1000–2000 GeV	2000 GeV
σ^{in}_{nc}	254±21	263±28	261±34
σ^{in}_{chc}	214±19	228±21	247±36
σ^{in}_{pc}	236±23	236±30	255±39
$\sigma^{in}_{\pi c}$	179±18	179±23	193±30
σ^{in}_{npb}	1980±60	2100±81	2215±104
σ^{in}_{chpb}	1693±80	1762±94	1890±114
σ^{in}_{ppb}	1762±108	1809±101	1916±116
$\sigma_{\pi pb}$	1587±89	1630±83	1726±97

By means of these data the σ^{in} of pions and protons with the carbon and lead nuclei were determined. For this purpose we have used the calculated curve of the ratio $\sigma^{in}_{pA}/\sigma^{in}_{\pi A}$ dependence on the nucleus atomic number obtained in /2/ according to which $f(A)=\sigma^{in}_{pA}/\sigma^{in}_{\pi A}$ is practically independent of energy. The experiment shows a good agreement with the calculated curve, $\sigma^{in}_{pp}/\sigma^{in}_{\pi p}$ = 1.61 ± ± 0.03 at E = 345 GeV//3/, and $\sigma^{in}_{pFe}/\sigma^{in}_{\pi Fe}$ = 1.19 ± 0.05 for E = 1000 GeV /4/. On the PION installation the pion-to-proton ratio N_π/N_p for various intervals of hadron energy was directly measured /5/. The calculated values of $\sigma^{in}_{pA}/\sigma^{in}_{\pi A}$ for the C and Pb nuclei are equal to 1.32 ± 0.4 and 1.11 ± 0.03, respectively. The final revised data on the proton and pion cross sections are also plotted in Table.1.

Figure 2 presents the experimental results on σ^{in}_{pc} and σ^{in}_{ppb} obtained both on accelerator /5/ and in cosmic rays /6/. The curves denote the recalculation by the multiple scattering theory from the PP to PPb and PC interactions.

The authors are grateful to A.Ts.Amatuni and S.G.Matinyan for their interest in the work as well as to A.P.Garyaka, S.R.Gevorkian and V.M.Zhamkochian for stimulating discussions.

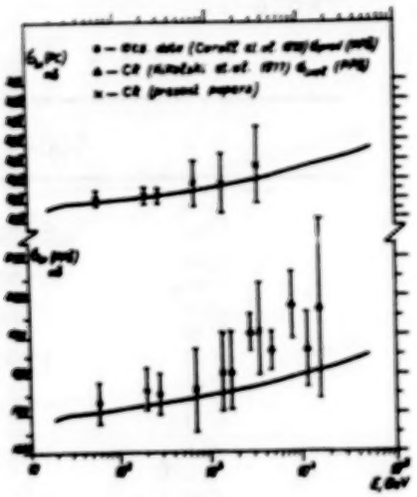


Fig. 2

REFERENCES

/1/ Avakian V.V. et al., XVI ICRC, Kyoto, 1980, 13, 61.
/2/ Badalian A.R., Gevorkian S.R., Mamidjanian E.A., XVIII ICRC, Bangalore, 1983, 5, 510.
/3/ Caroll A.S. et al., Fermilab-Pub., 78/85, 7110, 104, 1978.
/4/ Avakian V.V. et al., VANT, ser.tekh.fiz.eksp, 1983, 4(16), 56.
/5/ Avakian V.V. et al., XVIII ICRC, Bangalore, 1983, 5, 263.
/6/ Nam R.A., Nikol'sky S.I. et al., Preprint FIAN N.85, 1977.

N85-35854

HE 1.1-6

P($\bar{P}$)P ELASTIC SCATTERING AND COSMIC RAY DATA

Fazal-e-Aleem and Mohammad Saleem
Centre for High Energy Physics
University of the Punjab
Lahore-20, Pakistan.

ABSTRACT

It is shown that the total cross section σ_T for pp elastic scattering at cosmic ray energies, as well as the total cross section σ_T, the slope parameter b(s,t) and the differential cross section $d\sigma/dt$ for small momentum transfer at ISR and collider energies for p($\bar{p}$)p elastic scattering can be simultaneously fitted by using a simple Regge pole model.

1. Introduction. The total cross sections for proton-proton and proton-antiproton scattering for $20<\sqrt{s}<2\times10^5$ GeV have been measured at ISR and SPS collider and derived from the cosmic ray data[1,2]. The data show that the total cross section keeps on rising throughout the measured range. The results of these measurements are shown in Figs.1 and 2. The slope parameter b(s,t) for pp→pp at $\sqrt{s}$=53 GeV has been measured by various authors[3] and the results are shown in Fig.3. Accurate measurements of b(s,t) at collider energy $\sqrt{s}$=546 GeV were made by using luminosity independent technique[3] and are shown in Fig.4. It may be noted that the value of 15.3±0.3 $(GeV/c)^{-2}$ of slope parameter for $0.03<-t<0.1$ $(GeV/c)^2$ as measured by this group differs significantly from the earlier measurement of the slope parameter at $\sqrt{s}$=540 GeV which gives a value of 17.2±1.0 $(GeV/c)^{-2}$ in the range $0.05<-t<0.19$ $(GeV/c)^2$ [4].

Simultaneous measurements of differential cross sections for $\bar{p}p$ and pp elastic scatterings at $\sqrt{s}$=31, 53 and 62 GeV in the interval $0.05<-t<0.85$ $(GeV/c)^2$ have been made by Breakstone et al[5] at the CERN ISR. At 53 and 62 GeV, for $0.17<-t<0.85$ $(GeV/c)^2$ both pp and $\bar{p}p$ data show simple exponential fall. At $\sqrt{s}$=31 GeV, the data in the interval $0.05<-t<0.85$ $(GeV/c)^2$ are consistent with a change in slope near $-t=0.15$ $(GeV/c)^2$. Results of these ISR measurements are plotted in Fig.5. Very recently, UA4 collaboration[6] has measured the differential cross section of proton-antiproton elastic scattering at $\sqrt{s}$=546 GeV. The $d\sigma/dt$ distribution shows a steep exponential decrease, with a change of slope around the same value of -t as at ISR energies. The data for this reaction for $-t<0.8$ $(GeV/c)^2$ are shown in Fig.6.

2. Calculations and Discussion. Following Refs.7 8, we find that for both the reactions a very good fit with the total cross section, the slope parameter and the differential cross section for small momentum transfers is obtained by choosing

N85-35864

the residue function as a sum of two exponentials. Thus the scattering amplitude may be written as

$$T(s,t)=\beta(t)\xi(t)s^{\alpha(t)} = (Ae^{Bt}+Ce^{Dt})\xi(t)s^{\alpha(t)}$$

The differential cross section is then given by

$$d\sigma/dt = \frac{1}{s^2}|T|^2 = (Ae^{Bt}+Ce^{Dt})^2\ s^{2\alpha(t)-2}$$

The expression for the slope parameter b(s,t) can be obtained by using the formula

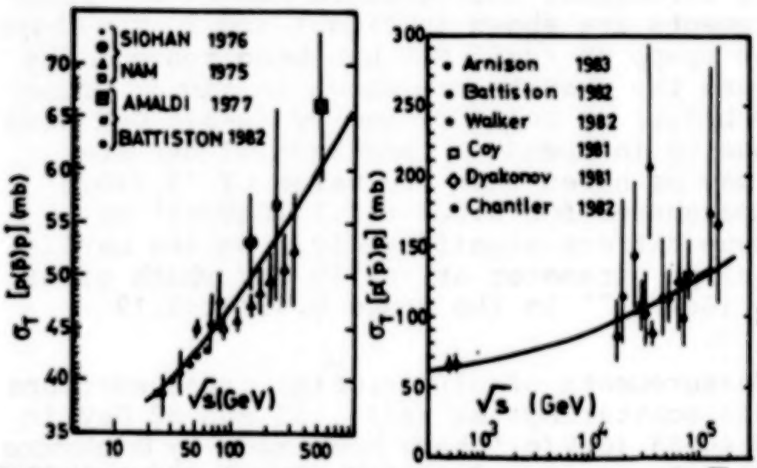
$$b(s,t)= d\ /dt\ (\ln d\sigma/dt)$$

It is found that a good fit with the experimental data, including the most recent results, is obtained by the following choice of residue function $\beta(t)$:

$$\beta(t)= 4.35e^{2.72t} + 1.45e^{10.93t}$$

The equation of the Pomeron has been chosen as [9,10]

$$\beta(t)= 1.069+0.3t$$

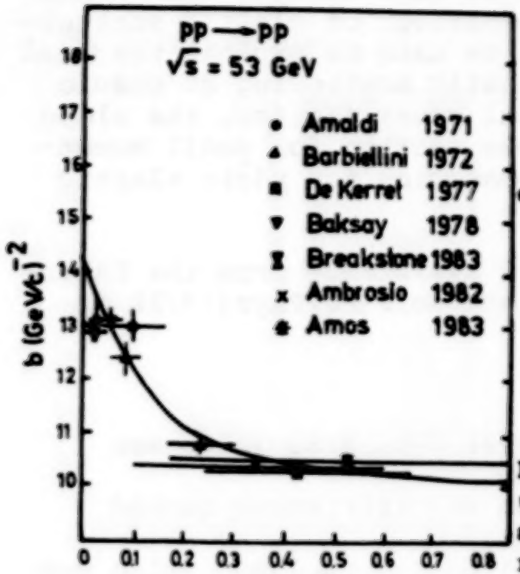


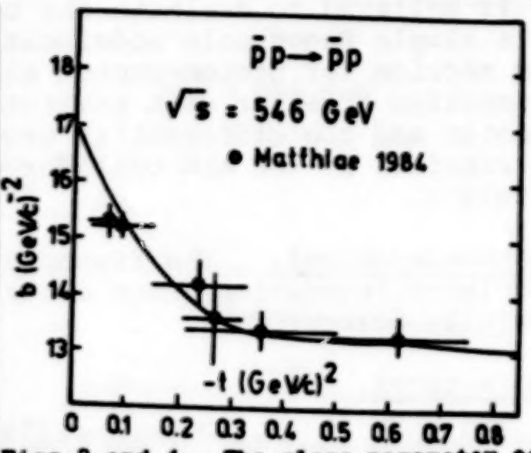
Figs.1 and 2. The total cross sections for $20<\sqrt{s}<2\times10^5$ GeV. Theoretical curves are the predictions of the model described in the text.

Figs.1 and 2 show the total cross sections for $20<\sqrt{s}<2\times10^5$ GeV. Theoretical curves are the predictions of simple Regge pole model. Figs.3 and 4 show the results of the slope parameter for $p(\bar{p})p$ elastic scattering at $\sqrt{s}$= 53 and 540 GeV respectively. The curves represent predictions of the model described in the text. In Figs.5 and 6 the measured differential cross sections for pp and $\bar{p}p$ elastic scatterings at ISR and collider energies have been plotted together with the predictions of the model described in the text.

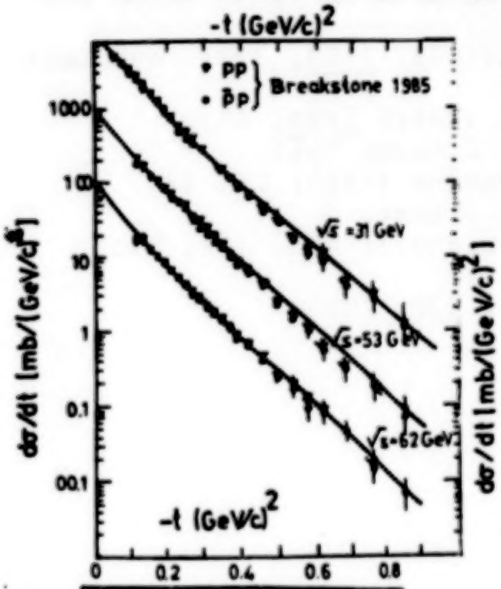
The CERN SPS proton-antiproton collider, after modifications which have enhanced the peak energy it can achieve, is back in action again. This time the collider is providing 630 GeV collision energy compared to the 546 GeV in previous runs. The results are expected to be available shortly. We predict the slope parameter at $\sqrt{s}$=630 GeV for $-t<1$ $(GeV/c)^2$. The curve in Fig.7 shows the predicted values.

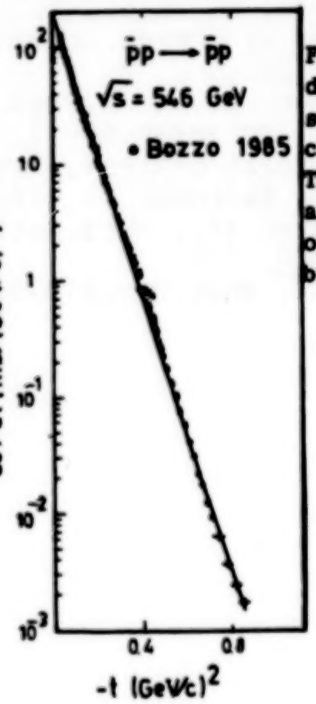
ORIGINAL PAGE IS
OF POOR QUALITY





Figs.3 and 4. The slope parameter at $\sqrt{s}$=53 and 540 GeV. Theoretical curves are the predictions of the model described in the text.





Figs.5 and 6. The differential cross sections at ISR and collider energies. Theoretical curves are the predictions of the model described in the text.

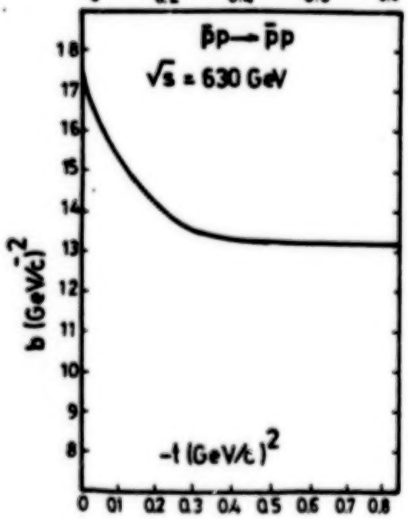


Fig.7. Predictions of the model described in the text for the slope parameter at $\sqrt{s}$=630 GeV.

3. Conclusions. We conclude that at high energies where pomeron is believed to dominate the behaviour of elastic scattering, a simple Regge pole model can be used to explain the total cross section for proton-proton elastic scattering at cosmic ray energies together with the total cross section, the slope parameter and the differential cross section for small momentum transfers at ISR and collider energies for p($\bar{p}$)p elastic scattering.

4. Acknowledgement. The financial assistance from the Pakistan Science Foundation under contract No.P-PU/Phys(11/2) is gratefully acknowledged.

References.

1. G.B.yodh et al., Phys.Rev.(1983) 27D, 1183 (Also see references quoted therein).
2. J.Linsley, UNML-5/4/84-2 (Also see references quoted therein).
3. G.Matthiae, CERN/EP 84-119, 11 September 1984 (Also see references quoted therein).
4. R.Battiston et al., Phys.Lett.(1982) 115B, 333; Phys.Lett. (1982) 117B, 126.
5. A.Breakstone et al., Nucl.Phys.(1984) 248B, 253.
6. M.Bozzo et al., CERN/EP 85-31, 7 March 1985.
7. M.Saleem and Fazal-e-Aleem, Pramana (1985) 24, 429.
8. Fazal-e-Aleem, Hadronic J. (In press).
9. P.D.B.Collins et al., Phys.Lett.(1973) 43B, 171; Nucl. Phys.(1974) B80, 135.
10. S.Y.Chu et al., Phys.Rev.(1975) 13D, 2985.

N85-35855

HE 1.1-7

MEASUREMENT OF INTERACTION CROSS SECTION OF COSMIC RAY Fe NUCLEI (E>4 GEV/N) WITH Al TARGET

G.X. Ren, Y.Z. Zhou, R.Q. Huang, M.Y. Chen
Institute of High Energy Physics
Academia Sinica
Beijing China

1. Introduction

Although the study of relativistic heavy ion interaction encumbered by the low intensities of the incident heavy nuclei in cosmic ray experiments, however, one can use a suitable structure of detector to attain a result with a reasonable accuracy.

In this paper we present a cross section value of Fe(E> 4 GeV/N) with Al. We use CR-39 as detector and Al as target. The cross section value is estimated using maximum likelihood method.

2. Detector

The detector which consists of a stack of CR-39 sheets sanwiched by Al plates is designed for measuring Fe-Al interaction cross section, the Al serving as target and CR-39 serving as detector. The thicknesses of a CR-39 sheet and an Al plate are 1.6 mm and 1.8 cm, respectively. There are 6 layers altogether.

3. Experiment procedure

The detector was launched by a balloon near Beijing in 1982 to a ceiling height of 37 km and lasted for 10 h. The effective cutoff rigidity is 9.4 GV, the recorded threshold for Fe E>4 GeV/N, a value slightly higher than the one reached by heavy ion accelerator so far.

The CR-39 sheets were etched in 6.8 normal NaOH

solution with temperature of 70°c for 40 h. The reduced etch rate of CR-39, V_T/V_B-1, and dip angle of impinge particle are obtained from the measurement of the major and minor axes of etch pit ellipses.

Among the recorded nuclei with charge $Z \geq 10$, 322 tracks are identified as Fe nuclei with resolution of 0.6 e.

According to the position and dip angle of impinge particle in a sheet of CR-39 and the thickness of target plate, one can calculate the expected position of the particle in the next sheet of CR-39 below target easily. If an etch pit at the expected position possesses a major and minor axes within the error 1.5 μm with the impinge particle at former sheet, namely possesses a charge within the error 1 e and a dip angle within 2° with the impinge one, then this particle is thought to pass through the target without interaction, otherwise a nucleus-nucleus interaction is assumed.

Every Fe track is followed downwards until an interaction takes place or it goes out the detector. 205 interactions satisfying this criterion mentioned above are observed and the total track length been followed $\sum_{i=1}^{N_0} L_i = 1854.3$ cm ($N_0=322$, the number of incident particles)

A maximum likelihood estimation of Fe-Al collision mean free path gives

$$\lambda = \sum_{i}^{N_0} L_i / N \qquad (1)$$

where N is the number of interactions.

The variance of λ is

$$\mathrm{Var}(\lambda) = \lambda^2 / N \qquad (2)$$

4. Result and discussion

According to eqs (1) and (2), the maximum likelihood estimation of Fe-Al collision mean free path is obtained as $\lambda = 9.04 \pm 0.63$ cm which corresponds to the cross section value $\sigma_{Fe\text{-}Al} = 1.83 \pm 0.13$ bar.

In our analysis the interaction point is assumed in the middle of plate when an interaction takes place inside it. The error of λ caused by the uncertainty of interaction points is estimated by

$$\Delta\lambda \cong H\sqrt{N_0}/N\sqrt{12} \qquad (3)$$

where H is the thickness of target plate.

In order to increase the measuring accuracy of λ, larger number of interactions is needed. It means H should be increased. However, increase of H is limited by the relation $\Delta\lambda < [\mathrm{Var}(\lambda)]^{1/2}$. In our case, $\Delta\lambda = 0.04$ cm is still much less than the statistical error. Even if the number of incident particles is not so large, we can obtain a comparable result with work performed on accelerator.

References

Li Tipei, " Treatment in experiments ", Science Press, Beijing, 1980.

F. Fumuro, R. Ihara, 16th ICRC., 6 (1979), 166.

HE 1.1-8

HADRON THERMODYNAMICS IN RELATIVISTIC NUCLEAR COLLISIONS

N85-35856

P.Ammiraju
Instituto de Física'Gleb Wataghin'
UNICAMP-CAMPINAS
BRASIL

1. Introduction. The current interest[1] in the study of nuclear collisions at very high energies - especially nucleus-nucleus collisions at several GeV/nucleon - stems from the expectation that one can investigate under laboratory conditions the early beginings of our present universe. Thereby, one hopes to observe qualitatively new states of matter-such as density isomers, pion condensates, quark-gluon plasma (QGP), etc. The question whether the anticipated phase transition from hadron gas to QGP is a sharp or continuous one can only be answered through experiments devoted to the subsequent decay modes of this phase transition since the various theoretical models suffer in one way or other in their ability to pin point clear cut signals of this phase transition.

The search for QGP is basically a search for collective phenomena in strong interactions. Among them are the Cronin effeet, the EMC effeet, the production of secondaries with a kinectic energy above the kinematic limit in collisions of nucleons with targets of varying mass number, strange hadrons such as K, Λ, Σ and the leptons. However, from the data obtained, it is difficult to separate the purely QGP signals from the predictions of non-equilibrium QG-dynamics which can equally well explain the observed phenomena.

2. Relativistic Hadron Thermodynamics. The application of thermodynamics formalism to the study of high energy hadron-hadron central collisions has been in vogue for over forty years. What is now new is the use[2] of transformation laws of temperature and quantity of heat in the special relativistic thermodynamic formalism which preserves all the laws of classical thermodynamics by giving specific prescriptions in the

application of Lorentz transformation to the various thermodynamic quantities.

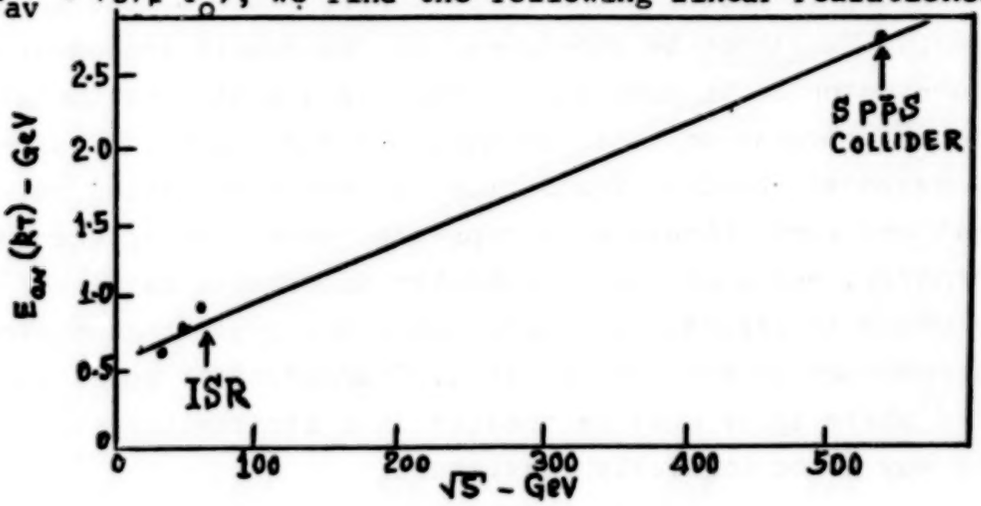
It is generally agreed that the entropy S is a Lorentz invariant and a unique answer is provided by statistical mechanics. In order to ensure the invariance of the entropy $dS = \delta Q/T$, the amount of (reversible) heat δQ and temperature T must transform in the same way. The problem comes in trying to preserve the first law $\delta Q = dU - \delta W$. The internal energy, U, cannot be considered as the fourth component of a four-vector as is done in the case of a mechanical point mass. The interpretation is to be modifild for hadrons considered as extended bodies. Statistically, the distinction between heat and work, though both represent some form of energy transfer, rests on the essentially disordered nature of energy which is regarded as heat. Also, the systems considered in thermodynamics are not isolated. Thermodynamic space and ordinary phase space must be treated in a similar Lorentz invariant way to be logically consistent.

3. "Derivation" of law of Lorentz transformation of temperature. In the literature there exist various "derivations" of the law of Lorentz transformation of temperature and other thermodynamic quantities. The transformation formulae for temperature accepted for over fifty years is the following

$$T = T_o(1 - v^2/c^2)^{1/2}$$

and consequently $\delta Q = \delta Q_o(1-v^2/c^2)^{1/2}$. Where the subscript o refers to the rest system and quantities in the lab system without subscript and $\vec{v}$ is the velocity of the rest system with respect to the lab system. In the rest system all the energy is of a disordered form but, in the lab system, a fixed amount equal to v^2/c^2 of the net increase goes over into the ordered form, leaving $(1 - v^2/c^2)$ of the net increase as disordered energy. However, the statistical measure of disorder (i.e. entropy) is an invariant and this requires a lower temperature, compatible with a lower quantity of heat observed in the lab system[3].

4. Experimental 'evidence' from large P_T phenomena. Chiu et al[4] and Chew et al[5] used the "two-temperature" concept for large P_T phenomena and fited reasonably well the single particle inclusive cross-sections as a functions of P_T in a thermodynamically based statistical distribution. If we identify their values of $\langle kT_1 \rangle$ and $\langle kT_2 \rangle$ with the E_{av} in formula of ref. [2] ($E_{av} \sim \sqrt{s}/\mu\ T_o$), we find the following linear realationship.



5. Conclusions: Various phenomenological models based on statistical thermodynamical considerations have been used to fit the experimental data at high P_T to a two-temperature distribution. Whether this implies that the two-temperatures belong to two different reaction mechanisms, or consequences of Lorentz-contraction factor, or related in a fundamental way to the intrinsic 'thermodynamics of Space-Time' can only be revealed by further theoretical and experimental investigations of high P_T phenomena in extremely energetic hadron-hadron collisions.

6. References.

1. P.Ammiraju, et al: Il Nuovo Cimento 78A, 172 (1983)
2. P.Ammiraju, Lett. Al Nuovo Cimento 39, 424 (1984)
3. R.K.Pathria, Proc.Ray.Soc.88, 791 (1966)
4. B.K.Chiu et al, Phys.Rev. D.12,2725 (1975)
5. C.K.Chew et al, Phys.Rev. D.29, 2127 (1984)

HE 1.1-9
N85-35857

ESTIMATION OF THE TOTAL INELASTICITY COEFFICIENT IN INTERACTION OF $\geq$ 20 TeV HADRONS WITH LEAD

Kanevsky B.L., Mikhailova I.A.,
Rakobolskaya I.V., Sveshnikova L.G.

Institute of Nuclear Physics, Moscow State University,
Moscow 119899, USSR

Experimental data on the interaction mean free path of hadrons with energy $E_o \geq 20$ TeV in lead obtained with multilayer X-ray emulsion chambers(XEC) are compared with results of simulation of nuclear-electromagnetic cascades in lead chamber. It is shown that, to explain experimental data, the value of the total inelasticity coefficient, $\langle K \rangle \sim .8$ should be assumed.

Multilayer XEC allow determination of gamma-ray and electron energy, E_γ, the energy $E_\lambda^{(\gamma)}$ released into the electron-photon cascade(EPC) in hadron-lead nuclear interaction, and the origin depth Δt of an electron-photon cascade induced in a chamber by gamma-rays, electrons, and hadrons. The experimental procedure and chamber design have been described in detail in /1/.

In paper /2/ of the "Pamir" Collaboration, the results have been presented of measurement of the hadron interaction mean free path, λ_{meas}, in lead chambers obtained by analyging the hadron flux(about 700 events) over an area of 140 m^2. After efficiency of hadron registration in chambers of different thickness has been allowed for more accurately, the authors of /2/ obtained the following results:

$\lambda_{meas} = 185 \pm 40$ g/cm^2 for energy $E_h^{(\gamma)} = 5$-10 TeV,
$\lambda_{meas} = 213 \pm 24$ g/cm^2 for energy $E_h^{(\gamma)} \geq 10$ TeV,
$\lambda_{meas} = 197 \pm 29$ g/cm^2 for energy $E_h^{(\gamma)} \geq 20$ TeV.

The measured value of λ_{meas} can be seen to be independent of $E_h^{(\gamma)}$ within errors and $\lambda_{meas} = 207 \pm 17$ g/cm^2.

The measured value of λ_{meas} concerns the summary flux of nucleons and charged pions with energies $E_o \geq 20$ TeV. The pion fraction in this flux can be estimated based on calculations in terms of quasiscaling models, e.g., from /3/. This magnitude is almost independent of a model and, on average, pions present ~30% and nucleons ~ 70% in the total hadron flux at the given depth(596 g/cm^2).

The value of λ_{meas} may differ from the proper interaction mean free path for hadrons in lead, λ_{prop}, due to the following causes:

A. The influence of an admixture of electron-photon component

N85-35857

When determining λ meas, cascades with $\Delta t > 8$ c.u. were taken into account. The number of EPC induced by gamma-rays and electrons at depth 8-10 c.u. from the chamber boundary was less than 2% of the hadron-induced cascades.

B. The influence of the boundary effects.

Using the angular distributions of $\cos\theta^{5.3}$ for hadrons and $\cos\theta^{5.8}$ for gamma-rays and the power law energy spectrum with the differential power index 3 , obtained in /4/, the procedure of hadron and gamma-ray registration in a 2mx5m chamber (a standard size of lead chambers in the "Pamir" Collaboration) was Monte-Carlo simulated. The cascades interacting in a chamber and leaving its volume and additional cascades arriving from air, when taken into account, change the value of λ meas by less than 3%.

C. Allowance for secondary interactions.

The impossibility to follow entirely the hadron cascades in a chamber due to a high registration threshold leads to appearing the hadron-induced cascades for which we measure Δt of the second and subsequent interactions instead of the first one. So, there exist cascades in which in first interaction the energy $E_n^{(1)}$ lower than threshold was released while the energy released in one of subsequent interactions exceeds the threshold. There are also the cascades with energy released in the first and second interactions being higher than the threshold and the second interaction occures at a point of 15-20 c.u. far from the first one. So, the second interaction was mistaken as the first one of another hadron.

The existence of these cascades leads to overestimation of λ meas compared with λ prop, Monte-Carlo simulations were performed to eliminate the distortions of λ meas. The scheme of simulations used is presented in /5/. Energy E_0 of the primary protons inducing in a chamber nuclear-electromagnetic cascades was simulated with respect to the spectrum with the differential power index 3 . The point of the first interaction in a chamber was computed with $\lambda_{prop} = 190$ g/cm^2. Random stars imitating nuclear interaction were simulated according to /6/.

In the first version of simulations, the difference in inelastic interaction of incident hadron with protons and nuclei was neglected, leading particles being simulated in the x-presentation with respect to the inclusive spectrum from /7/, and the mean value $\langle K \rangle$ being equal to .5. In the second version of simulations, use was made of the data on the inclusive spectrum of leading particles obtained in terms of an additive quark model regarding the atomic number of the target-nucleus in /8/, the mean value being $\langle K \rangle = .8$. The electromagnetic cascades resulting from the decay of π^0-meson for particles with energy $E_\gamma > E_{thr}^{em}$ ($E_{thr}^{em} = .5 \cdot 10^{12}$eV) were also Monte-Carlo simulated allowing for the processes of pair production, bremsstrahlung radiation, and Rutherford scattering. To obtain the electron number and

the optical density of X-ray film within a circle of given radius(R=140 um) caused at an observation level by the initial gamma-rays and electrons(with energies $E_{\gamma} < E_{thr.}$) use was made of the averaged cascade curves calculated to the core approximation. Optical densities in X-ray film produced by simulated cascades at various depths in lead were processed by the same program as experimental ones /1/.

For each version of calculations, ~1000 events with $E_0^{(x)} \geq 4$ TeV and 8 c.u. $\leq \Delta t \leq 64$ c.u. were simulated. The λ meas-values obtained for the two versions of calculations are listed in Table 1 together with the corresponding values of λ prop deduced from the experimental values of λ meas and from ratios of λ prop and λ meas obtained in different versions of calculations.

Table 1. Ratios of λ prop and λ meas obtained when analysing simulated cascades

	calculation		experiment	
	λ_{prop} g/cm^2	λ_{meas} g/cm^2	λ_{meas} g/cm^2	λ_{prop} g/cm^2
$\langle K \rangle$ =0.5	190	340^{+30}_{-30}	207 ± 17	115^{+22}_{-17}
$\langle K \rangle$ =0.8		230 ± 20		173^{+39}_{-29}

The contribution of the pion component allowed for do not practically change the obtained ratios of λ meas and λ prop. In the energy region ~ 200 GeV an inelastic cross section σ_{inel} in the π-Pb-interaction is by a factor of 1.1-1.3 less than in the pPb-interaction that may lead to an increase in λ prop for the total hadron flux by less than 5%. σ_{inel} of the pion and nucleon interactions on lead are expected to come closer with increasing energy/9/. $\langle K \rangle$ in the π Pb-interaction is larger than in the pPb-interaction, leading to a less diversity of λ meas from λ prop in the π Pb-interaction.

Experimental data obtained at accelerators and in cosmic rays for the hPb-interaction shows that up to energies of several TeV, an increase in σ_{inel}^{hPb} within errors is absent and σ_{inel}^{hPb}=1800 mb/10/. For higher interaction energies, in /9/, using the Glauber model, the following values have been obtained: σ_{inel}^{pPb}=1900 mb that corresponds to λ_{prop}^{pPb}=180 g/cm^2 and $\sigma_{inel}^{\pi Pb}$=1734 mb that corresponds to $\lambda_{prop}^{\pi Pb}$=199 g/cm^2 for E_0=20-100 TeV.

Thus, the experimental value λ meas=207±17 g/cm^2 for the summary hadron flux is consistent with the expected value λ_{prop}^{hPb}=180 g/cm^2 for $E_0 \geq 20$ TeV for the total inelasticity coefficient $\langle K \rangle \sim .8$ only.

References

1. Bayburina S.G. et al. Trudy FIAN, 1984, v.154.
2. Borisov A.S. et al. Proc. of Intern. Symp. on Cosmic Rays and Particle Physics, Tokyo, 1984, 426-430.
3. Erlikin A.D., Kuzuna N.P., Preprint N 95 FIAN, 1980.

4. Bayburina S.A. et al. Proc. 18th ICRC, 1983, 7, 420-423.
5. Belyaev A.A. et al. YPC in cosmic rays at superhigh energies, Moscow, "Nauka", 1981.
6. Astafiev V.A. et al. Proc. 14th ICRC, 1975, 7, 2593.
7. Eilten et al., Nucl. Phys., B44, 333, 1972.
8. Anisovich V.V., Braun Yu.M., Shabelsky Yu.M., Yadernaya Fizika, 1984, 39, vyp.4, 934-946.
9. Jofa M.Z., Pukhov A.E., Yadernaya Fizika, 1985, 40, vyp. 7.
10. Garyaka A.P. et al. Izv. AN Arm. SSR, 78, vyp.1, 1983, 66-78.

N85-35858

THE METHOD FOR THE STUDY OF THE INELASTIC CROSS-SECTION FOR HIGH ENERGY PROTONS BY MEANS OF SHOWER ARRAYS WITH THE LARGE CALORIMETRIC AREA.

Danilova T.V., Erlykin A.D.

P.N.Lebedev Physical Institute, Leninski pr. 53,

Moscow, 117924, USSR.

Proton initiated showers could be reliably separated from showers initiated by cosmic ray nuclei by means of arrays with large calorimetric area, using distributions of energy fractions for EAS electromagnetic muon and hadron components. Proton initiated showers penetrate deeper into the atmosphere and have relatively lower energy fraction in muons. Distribution of that energy fraction is sensitive to the value of the proton inelastic cross-section. It is shown that the analysis of this distribution let one distinguish between $\log^2 S$ -rise and $\log S$ -rise of the cross-section at energies above 10^{15} eV.

Methods of the direct study of interactions stop working at energies above 10^{15} eV since intensities of primary particles and particles in the atmosphere are small at such energies. In connection with this future arrays for the study of interactions must be based on arbitrary methods, that is mainly on the study of EAS cores.

The absolute value and the energy dependence of hadron cross-sections determine the distribution of interaction points of hadrons in the atmosphere. This distribution determines the speed of the cascade development, if all other factors are identical. For the analysis of EAS detected at arrays with large calorimeter areas like ANI or AKENO it was proposed to use new classification parameters: the total energy of the shower E_o or its energy at the observation level E_z /1/. Here $E_o = E_{e\&\gamma} + E_h + E_{\mu\nu} + E_Q$ (1) for EAS where one succeeded to measure the Cerenkov light and by this way - the energy E_Q, lost by the shower in the atmosphere and $E_z = E_{e\&\gamma} + E_h + E_{\mu\nu}$ (2) for EAS without measurements of the Cerenkov light. Calorimeters with large areas let one measure rather accurately the energy carried by electromanetic $E_{e\&\gamma}$ and hadron E_h components in every individual shower. The measure of the energy for the muon and neutrino component $E_{\mu\nu}$ is the total number of muons in the shower /1/.

In the paper / 1/ it was suggested to use the multidimensional analysis of tetrahedron and triangle diagrams - distributions of $E_{e\&\gamma}$, E_h, $E_{\mu\nu}$ and E_Q for the study of

primary mass composition. Such an analysis helps to analyse the cross-section behaviour too, since
a)providing the good energy resolution it let better determine the energy of primary particles;
b)among primary particles with the given energy it let reliably separate proton induced showers;
c)the analysis of the shape of distributions $W(\delta_e, \delta_\mu, \delta_h)$ or $W(\Delta_e, \Delta_\mu, \Delta_h, \Delta_Q)$, where $\delta_i = E_i/E_z$, $\Delta_i = E_i/E_o$ in "proton" part of these diagrams is equivalent to the analysis of distributions for the speed of the cascade development of proton induced showers and finally, let one find the value of the cross-section at chosen energies.

Accuracy estimates for the energy determination of different EAS components at ANI array show that the shower energy at the observation level E_z will be measured with ~11% accuracy. In the fig.1 the distribution of $E_o/\bar{E}_o$ ratio is shown for showers selected by E_{700} classification parameter from 100 up to 316 TeV at the mountain level 700 g/cm^2 (full line) compared with similar distributions for showers selected by the total electron number N_e in the interval $(1 - 1{,}58)\cdot 10^5$ (dotted line) and the muon number $N_\mu(>5$ GeV) in the interval $(1\text{-}1.58)\cdot 10^3$ (dashed line). All distributions are obtained by means of the simulation program /2/ for EAS with zenith angles $\theta \leq 30°$. Mass composition of primaries is similar to that at energies $\cdot 10^{11}$ eV /2/. It is seen that the total shower energy E_o may be determined by its energy at the observation level E_{700} with inaccuracy ~19%. It is better, than in the case, when the primary energy is determined by N_e or N_μ, where the error is ~(37-38)%. In the combination with the error of E_{700}determination this distribution gives on the average ~22% error in the determination of E_o at ANI array when energies of three EAS components are measured. Measurements of the fourth component E_Q let one reduce the error down to 8%.

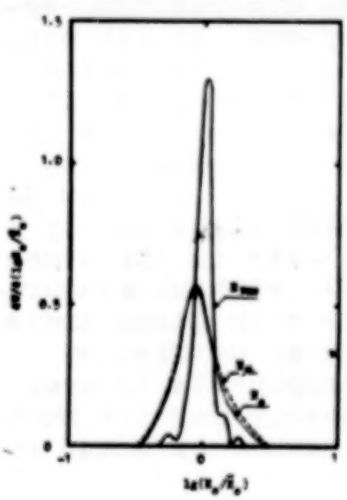


Fig. I.

The triangle diagram in the fig.2 demonstrates positions of gravity centres of δ_e, δ_μ, δ_h distributions for primary particles of different masses, which induce showers with E_{700} =31.6 - 100 TeV and 100-316 TeV. Here stars indicate positions of gravity centres for mixed primary composition. It is seen that all centres are located at one trajectory. Their position is determined by the energy

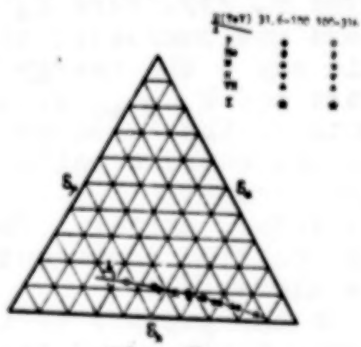


Fig. 2.

and the mass of the primary particle, i.e. depends in fact on the speed of the shower development. From this point of view the trajectory marked by the letter L may be called "the speed line".

Showers which develop faster are usually concentrated around points located at the right side of this line. In the left part on the average proton induced showers are concentrated which on the opposite, penetrate deeper into the atmosphere. The probability of such penetration and hence the $\delta_e, \delta_\mu, \delta_h$-distribution depends on the magnitude of the cross-section. The value of δ_μ varies most quickly along "the speed line", therefore δ_μ -distribution in the left part of the triangle diagram must be most sensitive to the proton cross-section σ_{pA}^{prod}. The ideology of this method is similar to that suggested by Ellsworth et al. /3/ for σ_{pA}^{prod} determination by the distribution of shower maximum depth in the region of large depths, i.e. again by showers with slowest development.

The analysis of diagrams $W(\delta_e, \delta_\mu, \delta_h)$ for primary particles of different masses demonstrates that proton induced showers may be effectively selected from the mixture corresponding to the normal mixed composition, if to restrict the region by values $\delta_\mu = \bar{\delta}_\mu - (0.1 \div 0.15)$. For example, for $E_{\gamma 00}$ =100-316 TeV $\bar{\delta}_\mu$ =0,514. The probability for the proton induced shower to hit the region $\delta_\mu <$ 0,35 is 0,492, the same probability for helium induced shower is 0,155. For other primary nuclei it is 0. For the region $\delta_\mu <$ 0,4 these probabilities are W_p =0,647; W_{He} =0,246, $W_{M,H,VH}$ =0. Taking into account that protons in the ordinary mixed primary composition are about twice as abundant compared with helium nuclei, one can say that in the region $\delta_\mu <$ 0,35 86% of showers are proton induced and only 14% of them are helium induced. For $\delta_\mu <$ 0,4 these values correspond to 83% and 17%.

Shower distributions for different values of σ_{pA}^{prod} and $\sigma_{\pi A}^{prod}$ differ most strongly just in the extreme left region of δ_μ. In the fig.3 distributions $W(\delta_e, \delta_\mu, \delta_h)$ are shown for proton induced showers with E_o =(1-3.16) $10^{}$ eV and for two versions: with logarithmic ($\sigma_{hA}^{prod} \sim \log S$) and maximum rising ($\sigma_{hA}^{prod} \sim \log^2 S$) cross-section. The quantitative analysis of these bilateral diagrams made by means of Kolmogorov criterium shows that in the region $\delta_\mu < 0.4$ these versions may be considered different with the probability to be wrong no more than 4%. At the same time the analysis of similar diagrams, calculated with constant or rising inelasticity does not reveal such a sensitivity.

In the fig.4 folded unilateral distributions $\Delta W / \Delta \delta_\mu$ are shown in the interval δ_μ =0-04. Essential difference in the shape of these distributions confirms above mentioned expectations and let one hope for the practical realizability of this method.

ORIGINAL PAGE IS
OF POOR QUALITY

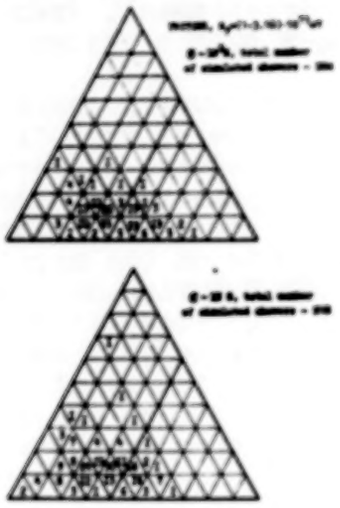


Fig.3

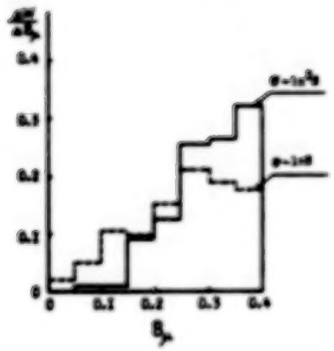


Fig.4

References.

1.Danilova T.V.,Erlykin A.D. 18 ICRC,1983,Bangalore,6, 262.
Preprint FIAN N°155,1982.

2.Danilova T.V. et al. 17 ICRC, 1981,Paris,6,146.
Preprint FIAN N°14,15,1984.

3.Ellsworth R.W. et.al. Phys.Rev. 1982,D26,336

ON A POSSIBILITY OF INELASTISITY PARTIAL COEFFICIENT K_γ DETERMINATION IN πC AND πPb INTERACTIONS AT 10^{14} EV (EXPERIMENT "PAMIR" I)

N85-35859

Pamir Collaboration:
Borisov A.S., Cherdyntseva K.V., Guseva Z.M., Denisova V.G., Dunaevsky A.M., Kanevskaya E.A., Maximenko V.M., Nam R.A., Pashkov S.V., Puchkov V.S., Slavatinsky S.A., Zimin M.V., Smirnova M.D., Smorodin Yu.A., Zelevinskaya N.G. and Zhdanov
-P.N.Lebedev Physical Institute, Academy of Sciences of USSR, Moscow
Mukhamedshin R.A., Nedel'ko O.E., Nikolaeva L.P.,
-Institute for Nuclear Research, Academy of Sciences of USSR, Moscow
Amineva T.P., Baradzei L.T., Ivanenko I.P., Iljina N.P., Lazareva T., Managadze A.K., Mikhailova I.A., Murzina E.A., Pomelova E.I., Popova E.G., Rakobolskaya I.V., Roganova T.M., Ryabova N.G., Sveshnikova L.G.
-Institute of Nuclear Physics, Moscow University, Moscow
Cananov S.D., Chadranyan E.Kh., Khisanishvili L.A., Ladaria N Leptukh G.G., Roinishvili N.N., Svanidze M.S.
-Institute of Physics, Georgian Academy of Sciences, Tbilisi
Asimov Z.A., Bobodjanov I.B., Gubar' N.E., Gulov Yu.A., Normuratov P., Shoboronov Kh.
-Institute of Physics and Engineering, Tajik Academy of Sciences, Dushanbe
Azimov S.A., Khalilov D.A., Mulladjanov E.G., Nuritdinov Kh., Talipov D.A., Yuldashbaev T.S.
-Institute of physics and Engineering, Uzbek. Academy of Sciences, Tashkent
Bakhtigireev S.E., Dobrotin N.A., Emeljanov Yu.A., Zaitseva E
-Institute of High Energy Physics, Kazakh.Academy of Sciences, Alma-Ata
Bielawska H., Linke M., Malinowski J., Novicka A., Podgorzak, Tomashewski A., Wlodarczyk Z., Wrotniak A.
-Institute of Physics, University of Lodz, Poland
and Sharvadze Z.SH.*, Institute of Physics, Georgian Academy of Sciences, Tbilisi

The investigation of hadron-nuclear interactions in "Pamir" experiment is carried out by means of X-ray emultion chambers of two types: carbon (C) and lead (Pb) ones [1].

While comparing the results from the chambers of both types [2] it was found a discrepancy in $\langle n_h \rangle$ and $\langle E^{\gamma}R \rangle$ values.

---

* This article only

Here $\langle n_h \rangle$ is an average hadron multiplicity normalized to one γ-h-family fitted the following selection criterion A: $\Sigma E_\gamma \geq 100$ Tev, $n_h \geq 0$, $E_h^{(1)} \geq 4$ Tev; $\langle E_h^{(1)} R \rangle$ is a space-energetic characteristics of hadrons in families fitted the criterion B: $\Sigma E_\gamma \geq 100$ Tev, $n_h > 3$, $E_h^{(1)} \geq 4$ Tev; $E_h^{(1)}$ is the energy registrated in hadron block. n_h values are corrected on interaction probability in each chamber.

Tables I and II represent our experimental results, where ν and χ parametres defined as

$$\nu = \frac{\langle n_h \rangle_{Pb}}{\langle n_h \rangle_C} \quad (1) \quad ; \quad \chi = \frac{\langle E_h^{(1)} R \rangle_{Pb}}{\langle E_h^{(1)} R \rangle_C} \quad (2)$$

Table I

	N_{fam}	$\langle n_h \rangle$	$\beta - 1$
C	169	3.0 ∓ 0.2	1.0 ∓ 0.1
Pb	41	4.2 ∓ 0.3	1.1 ∓ 0.1
ν	-	1.4 ∓ 0.2	

Table II

	N_{fam}	$\langle E_h^{(1)} R \rangle$ Tev mm
C	33	330 ∓ 30
Pb	22	455 ∓ 70
χ	-	$1,3 \mp 0,2$

N_{fam} is a number of families in C and Pb chambers fitted the above mentioned criteria, β-1 is a slope of integral energy spectrum of hadrons from families selected by A-criterion

In the present paper we connect the observed discrepancy between $\langle n_h \rangle$ and $\langle E_h^{(1)} R \rangle$ in C and Pb chambers with the difference in values of effective coefficients of energy transfer to the soft component K_{eff} for C and Pb chambers. The following considerations can be a ground of this suggestion:

1) It is known that a probability of hadron registration (in case of power like spectrum) is equal to $\langle K_\gamma^{\beta-1} \rangle$. Thus, the ratio of multiplicities

$$\nu = \frac{\langle n_h \rangle_{Pb}}{\langle n_h \rangle_C} = \frac{\langle K_\gamma^{\beta-1} \rangle_{Pb}}{\langle K_\gamma^{\beta-1} \rangle_C}$$

As $\beta - 1 \simeq 1$ (see Table I) we have:

$$\nu = \langle K_\gamma \rangle_{Pb} / \langle K_\gamma \rangle_C \quad (3)$$

2) $\langle E_h^{(1)} R \rangle$ value can be written down as $\langle K_\gamma \rangle \langle E_h R \rangle$ (in case of K_γ independent of E_h). Hence: $\chi = \langle K_\gamma \rangle_{Pb} / \langle K_\gamma \rangle_C$ (4).

To test this considerations some simulations on nuclear electromagnetic cascades in the atmosphere were made on the basis of fireball scaling model (S-model) [3]. Hadrons passage through the chamber was immitated in the simulations. For each hadron the value of K_γ coefficient was found by means of $f(K_\gamma)$ distribution function taken in the form of $f(K_\gamma) \sim K_\gamma^{\alpha} \cdot \exp(-K_\gamma / \beta)$ [4]. The parametres α and β define the momenta of this distribution. Two series of simulation with various $\langle K_\gamma \rangle$ values were carried out. One of them with $\langle K_\gamma \rangle = 0.17$ immitated the situation in C-chamber, the other-with $\langle K_\gamma \rangle = 0.30$ in Pb-chamber. The latter valueis greaterthan

the real one in Pb-chamber, was chosen especially to emphazise the effects connected with K_γ variations. The ratio of simulation values of $\langle K_\gamma \rangle$ is equal to

$$\langle K_\gamma \rangle_{Pb} / \langle K_\gamma \rangle_c = 1.76 \qquad (5)$$

A hadron was considered registrated one in case of $E_h^\gamma = K_\gamma E_h \geq 4$ Tev.

For $\langle E_h^\gamma R \rangle$ determination we selected the families with number of registrated hadrons $n_h > 3$. Table III represents the obtained results.

Table III

	N_{fam}	$E_h K$ Tev mm
C	126	285±20
Pb	275	510±15
χ		1,80±0.1

Table IV

	N_{fam}	$\langle n \rangle$	$\beta - 1$
C	505	2.3±0.1	0.9±0.05
Pb	505	3.9±0.1	1.0±0.05
ν		1.7±0.1	

As it is seen from Table III

$$\chi = \langle E_h^{(\gamma)} R \rangle_{Pb} / \langle E_h^{(\gamma)} R \rangle_c = 1.80 \pm 0.10 \qquad (6)$$

and that is in good agreement with value (5).

The incoming to the installation hadron families with $n_h > 3$ and $\sum E_h \geq 250$ Tev were selected to calculate ν parametre. The last condition provides registration of the same events in both sets of simmulation (in "both chambers").

Table IV represents the obtained values of mean multiplicities and energy spectra slope. ν value which is equal to 1.70 ± 0.10 is also in agreement with the given ratio of $\langle K_\gamma \rangle$(5). Thus, the experimental estimation of χ and ν values in the two types of chambers gives an opportunity to get a ratio of $\langle K_\gamma \rangle$ coefficients for lead and carbon nuclei.

Returning to preleminary experimental avaluations of χ and ν parametres (Table 1) one can see that the coefficients ratio turned to be roughly equal to 1.2 ÷ 1.5. This ratio corresponds to K_γ coefficients for pion-nuclear interactions as the majority of hadrons in families are π-mesons.

Experiments carried out in the low energy range yield that K_{π^0} partial inelastic coefficient dependence on atomic number of target nucleus is described as $K_{\pi^0} \sim A^\alpha$. Using this dependence and $\langle K_\gamma \rangle_{Pb} / \langle K_\gamma \rangle_C$ value we can estimate α-index at energy $\sim 10^{15}$ ev. Here we should bear in mind, that $K_\gamma^{Pb} \simeq K_{\pi^0}^{Pb}$, while K_γ^C can considerably differ from $K_{\pi^0}^C$. However, it was shown in simulations [5] K_γ value in carbon chamber in $E_h^{(\gamma)}$ energy range from 3 up to 30 Tev is similar to K_{π^0} value in pion-nucleon interactions. In such case $\frac{\langle K \rangle_{Pb}}{\langle K \rangle_C} \simeq A_{Pb}^\alpha$ and $\alpha \simeq 0.06 \pm 0.02$. This value is not in contradiction to α-measurings at lower energies

and confirms a possibility of the suggested method.

To determine α-value with 20% accurancy it is necessary to have approximately 100 families with $\Sigma E_\gamma \geq$ 100 Tev in each chamber as well as to make precise simulations of connection between partial K_π and effective K_γ inelasticity coefficients in chambers of both types.

References

1. Trudy FIAN, v.154, 1984, (in Russian)
2. Pamir Collaboration.Proc.of International Symposium of Cosmic Rays and Particle Physics, Tokyo, P292, 1984
3. Wrotniak I.A. Zess.Nauk.Univers.Lodz, vol.60, p.73, 1977
4. Malinowski A. et.al.Pamir Coll.Workshop, p.49, UL, Lodz, 1980
5. Wlodarczyk Z. et.al.Proc.of International Symp.of Cosmic Rays and Particle Physics, Tokyo, p 451, 1984

N85-35860

HE 1.2-1

SINGLE PARTICLE MOMENTUM AND ANGULAR DISTRIBUTIONS IN HADRON-HADRON COLLISIONS AT ULTRAHIGH ENERGIES

T. T. Chou
Department of Physics
University of Georgia
Athens, GA 30602, USA

Chen Ning Yang
Institute for Theoretical Physics
State University of New York
Stony Brook, NY 11794, USA

1. Introduction. The forward-backward charged multiplicity distribution $P(n_F, n_B)$ of events in the 540 GeV $\bar{p}p$ collider has been extensively studied by the UA5 Collaboration. It was pointed out that the distribution with respect to $n = n_F + n_B$ satisfies approximate KNO scaling and that with respect to $Z = n_F - n_B$ is binomial [1]. The geometrical model of hadron-hadron collision interprets [2] the large multiplicity fluctuation as due to the widely different nature of collisions at different impact parameters b. For a single impact parameter b, the collision in the geometrical model should exhibit stochastic behavior. This separation of the stochastic and non-stochastic (KNO) aspects of multiparticle production processes gives conceptually a lucid and attractive picture of such collisions [3], leading to the concept of partition temperature T_p and the single particle momentum spectrum to be discussed in detail below.

2. Description of Model. Assuming the separation of stochastic from non-stochastic aspects of collision to remain valid as $n \to \infty$, we expect [1] that the distribution in the two-dimensional $(n_F/\bar{n})$-$(n_B/\bar{n})$ plane would become more and more concentrated in a narrow region. For 540 GeV $\bar{p}p$ collisions this region is in the form of an ellipse as shown in Fig. 1(a). When $\bar{n}$ becomes large, it becomes thinner and eventually collapses into a line segment (Fig. 1(b)). This line segment is a collection of points, at each of which $n_F = n_B$ and both n_F and n_B fluctuate only to the extent of $\sqrt{n_F}$ (i.e., like a stochastic distribution). For example, if $n = 2\times10^6$, then n_F could easily be as small as 0.5×10^6 or as large as 2×10^6. But in either case, one can predict that $n_B = n_F$ with fractional

errors of the order $(\bar{n})^{-\frac{1}{2}} \sim 10^{-3}$.

Accepting this picture for very high energies, we see that for fixed n_F, the distribution of n_B is stochastic. How then is the energy partitioned in the backward hemisphere? We shall assume that the energy partition for each hemisphere for a fixed $z = (n_F + n_B)/\bar{n}$ is also stochastic but subject to a number of conditions: (a) that the total energy of all outgoing particles on each side is $E_0 h$, (b) Bloch-Nordsieck factor d^3p/E for each particle, and (c) transverse momentum (p_T) cutoff factor $g(p_T)$. In other words, the probability distribution for central particles on each side will be taken as

$$\delta(\sum_i E_i - E_0 h) \prod_i (d^3p_i/E_i) g(p_{Ti}) \tag{1}$$

where $E_0 = \sqrt{s}/2$, $E_0(1-h)$ = total energy of all leading particles, and $i = 1,2,\cdots$ ranges over all the particles (positive, negative, and neutral) on one side minus the leading particles. h is a parameter that describes the fraction of E_0 that fragments into <u>all</u> particles in the central region.

Now the mathematical problem (1) is well-known in statistical mechanics as describing a microcanonical ensemble. By the well-known Darwin-Fowler method the single particle distribution of such an ensemble is given by the canonical ensemble:

$$dn = K\ (d^3p/E)\ g(p_T)\ \exp(-E/T_p) \tag{2}$$

where T_p will be called the partition temperature and K is a normalization constant. Notice that all particles, positive, negative, and neutral, kaons, nucleons as well as pions, share the same T_p.

<u>3. Comparison with Experimental Angular Distribution at 540 GeV</u>. As Fig. 1(a) shows, at the 540 $\bar{p}p$ collider, the distribution is still an ellipse. We shall nevertheless test the validity of (2) at 540 GeV by evaluating the single particle angular distribution from it. We write

$$dn/d\eta = 2\pi K \sin^2\theta \int_0^{E_0 h} p^2 (dp/E) g(p\sin\theta) \exp(-E/T_p) \tag{3}$$

where η = pseudo-rapidity, $\cosh\eta = \csc\theta$, and

$$g(p\sin\theta) = \exp(-a p\sin\theta). \tag{4}$$

ORIGINAL PAGE IS
OF POOR QUALITY

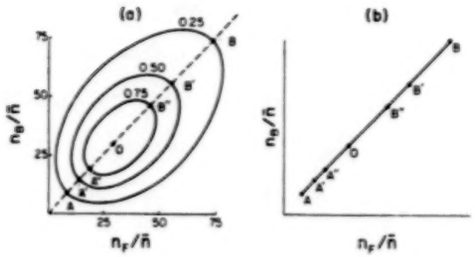


Fig. 1 Schematic diagram for forward-backward multiplicity distribution at very high energies. (a) The contour lines represent $P(n_F, n_B)$ at constant fractions of its maximum value at $\sqrt{s}$ = 540 GeV where $\bar{n} \approx 29$. (b) The same contour lines degenerate to straight lines for extremely large $\bar{n}$.

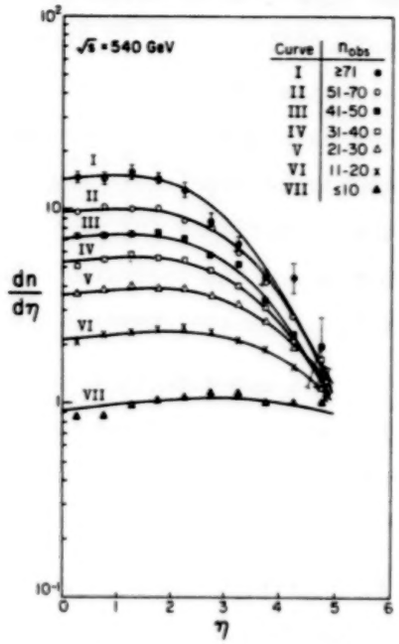


Fig. 2 Calculated and experimental dn/dη vs. η at $\sqrt{s}$ = 540 GeV.

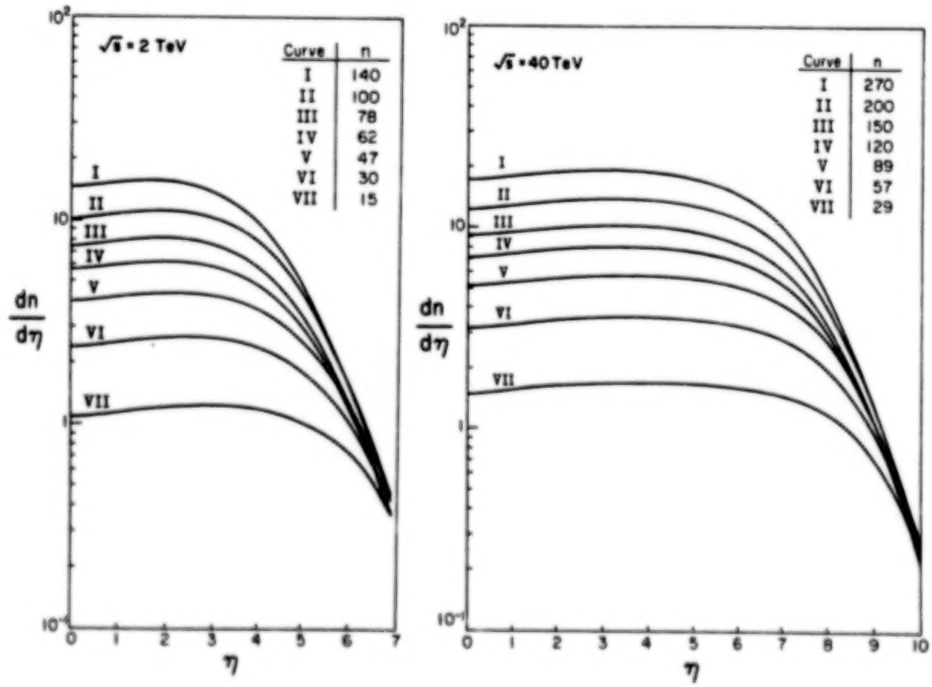


Fig. 3 Calculated dn/dη versus η at $\sqrt{s}$ = 2 TeV and 40 TeV.

We take α to be equal to $5.25(\text{GeV/c})^{-1}$. Only pions are included in this calculation. The angular distribution is evaluated from (3) and compared with the results [4] of UA5 in Fig. 2. It is found that the UA5 curve for each multiplicity n is well fitted by (3) for one value of T_p. We emphasize that there are no adjustable parameters in this computation, the cutoff α having been taken from experiments [5] concerning p_T distributions. The parameter h and normalization constant K are both determined from the curves themselves.

We conclude that the angular distribution (3) that results from (2) is in excellent agreement with experiment. Furthermore, we believe (2) would give a complete description of the single particle momentum distribution for central particles.

4. Extrapolation to Higher Energies. We made extrapolations of the angular distribution to $\sqrt{s}$ = 2 TeV (Tevatron) and 40 TeV (SSC). The assumptions made in these computations are as follows: (i) The values of α for these energies are taken to be 5.0 and 4.4 $(\text{GeV/c})^{-1}$, respectively [5]. (ii) The parameter h is taken to be a function of the KNO variable $z = n/\bar{n}$ only. (iii) The values of $\bar{n}_{ch}$ for these energies are taken to be 41 and 78, respectively, by extrapolation. The results are presented in Fig. 3.

5. Acknowledgments. This work is supported in part by the U.S. DOE Grant No. DE-FG09-84ER40160, and by the U.S. NSF Grant No. PHY 81-09110 A01.

References

1. T. T. Chou and C. N. Yang, Phys. Lett. 135B, 175 (1984).
2. T. T. Chou and C. N. Yang, Phys. Lett. 116B, 301 (1982).
3. T. T. Chou, C. N. Yang, and E. Yen, Phys. Rev. Lett. 54, 510 (1985).
4. J. G. Rushbrooke, in Proc. XIV Int. Symp. Multiparticle Dynamics, Lake Tahoe, 1983, edited by J. F. Gunion and P. M. Yager (World Scientific, 1984).
5. J. G. Rushbrooke, in Proc. DPF Workshop on $\bar{p}p$ Options for the Supercollider, Chicago, 1984.

QCD-MOTIVATED DESCRIPTION OF VERY HIGH ENERGY* PARTICLE INTERACTIONS

N85-35861

T. K. Gaisser
Bartol Research Foundation
University of Delaware
Newark, DE 19716

F. Halzen
Physics Department
University of Wisconsin
Madison, WI 53706

ABSTRACT

Cross sections for the production of secondaries with large transverse momentum can become comparable to the total cross section in the TeV energy range. We argue that the onset of this effect is observed at sub-TeV energies via (i) an increase of the rapidity distribution near $y = 0$, (ii) an increase of $\langle p_T \rangle$ with energy and, most directly, via (iii) a correlation between $\langle p_T \rangle$ and multiplicity. If indeed scaling violations are associated with the hard scattering of partons, then scaling violations are largely confined to the central region and have little effect on cosmic ray data which are sensitive to the forward fragmentation region.

Recent $p\bar{p}$-collider experiments confirmed the observation by the Brazil-Japan emulsion group that the average transverse momentum of secondaries is larger in events with high multiplicity,[1] see Fig. 1. QCD allows for a straightforward interpretation[1] of this observation: large p_T results from hard scattering of partons, and hard scattering is accompanied by abundant gluon radiation resulting in an increased multiplicity. This effect is most dramatically observed in hard quark + antiquark → weak boson events where the hadronic activity accompanying W,Z is larger[2] than that in average minimum bias events despite the fact that roughly 1/5 of the c.m. energy $\sqrt{s} = 0.54$ TeV is taken away by the W or Z mass. This interpretation of the $\langle p_T \rangle$-multiplicity correlation received further confirmation by the recent observation[3] that high multiplicity events indeed show jet-like final state structure. A large fraction of them contained at least one identified jet with $p_T \geq 5$ GeV. Although the QCD origin of large p_T jets has been quantatively verified we are here discussing events where the "large" p_T is not much larger than $\langle p_T \rangle$ and perturbative calculations are difficult. We discuss this next.

Perturbative calculations of jet cross sections are made possible by the fact that hadrons interact over a distance scale $0(1/p_T)$ which is small. The hadrons interact via a single quark or gluon in each hadron. When p_T becomes small many relative soft constituents are stacked in the interacting hadrons and therefore multiple parton-parton interactions become likely in a single hadron-hadron collision. Perturbation theory breaks down; e.g. for the SSC energy $\sqrt{s} = 40$ TeV we estimate following Ref. 4 that the cross section for double parton-parton interactions is 100 ~ 200 mb for $p_T \geq 6$ GeV. This is roughly

equal to the conventional single hard scattering cross section for $p_T \geq 6$ GeV as we will see further on. Conversely one might actually hope that naive perturbation theory yields reliable results for p_T-values as low as 5 → 10 GeV which corresponds to $x\ (= p_T/\sqrt{s}) \simeq 10^{-3}$ at $\sqrt{s} = 40$ TeV!

Using perturbative QCD jet calculations down to $x \simeq 10^{-3}$ we have made a toy model of hadronic interactions at all energies and all p_T. The basic idea is to integrate the perturbative QCD expressions for hard scattering of constituents down to an energy-dependent $p_{T\ min}$ defined by

$$\sigma_{tot} = \sigma_0 + \sigma_{jet}\ (p_{T\ min})\ , \tag{1}$$

where

$$\sigma_{jet}(p_{T\ min}) = \iiint_{p_{T\ min}} F(x_1)F(x_2)\sigma(\theta)\ . \tag{2}$$

$F(x_i)$ are the probabilities for finding constitutents with fractional momenta x_i in the incident hadrons and $\sigma(\theta)$ is the elementary cross section for scattering of constituents to angle θ defined in the parton-parton c.m. system. Unlike the calculation of Ding, et al.[5] we have no cutoff in θ except that required by $p_T > p_{T\ min}$. The factorization displayed in Eq. (2) is an approximate result suitable for practical calculations.[1] σ_0 represents the soft hadronic cross section and further results will depend on assumptions regarding its magnitude and energy dependence. For illustration we assume $\sigma_0 = 38$ mb at all energies. Table I shows values of σ_{jet}, $p_{T\ min}$ and mean values of Feynman x and rapidity of the scattered jet obtained from Eqs. (1, 2). For details of the calculation see Ref. 1. The values of $p_{T\ min}$ have been adjusted so that Eq. (1) reproduces the total cross section data shown in Fig. 2. Our calculation also reproduces the p_T-distribution measured at the $\bar{p}p$ collider, see Fig. 3.

Because of the large cross sections involved, such semihard processes can be expected to produce dramatic effects at high energy. Figure 4 illustrates the expected energy dependence of the rapidity distribution at various energies of interest. We have assumed that beam fragments in hard collisions produce rapidity distributions of secondary pions as in soft collisions, with two charged particles per unit of rapidity. The scattered jets are assumed to produce rapidity distributions of the same shape as beam fragments at the kinematic limits, and also with an asymptotic density of two charged particles per unit of rapidity. In the absence of significant scaling violation effects in the fragmentation functions, we would predict an asymptotic rapidity density of four charged particles.

By energy conservation one expects a violation of scaling in the fragmentation region as the central component grows with energy. The magnitude of this effect can be estimated from the values of $\langle x_{jet} \rangle$ tabulated above. At high energies, where semihard scattering events represent a significant fraction of the cross section, $\langle x_{jet} \rangle \simeq 0.05$ so we expect fragmentation region scaling violation only at the level of 5%. This is a smaller effect than suggested in Ref. 5.

We therefore conclude that if the association between hard scattering and increasing cross section described here is qualitatively correct, then scaling violations should have little effect on the behavior of the electromagnetic component of cosmic ray cascades because these depend primarily on the fragmentation region. In particular, use of scaling-type models to interpret the Fly's Eye experiment should be essentially correct. A non-trivial result of the calculation that increases our confidence in the correctness of the association between growing cross section and hard scattering is represented by the last column of Table I. The jet rapidities that come out of the QCD calculation are such that the excess rapidity density from the scattered jets joins smoothly onto the underlying rapidity plateau from beam fragments. The Gaussian-type rapidity distribution observed at $\sqrt{s}$ = 540 GeV is thus naturally reproduced.

REFERENCES

1. For a detailed discussion and further references see T. K. Gaisser and F. Halzen, Phys. Rev. Lett. 54, 1754 (1985) and Proceedings of the Aspen Winter Physics Conference (1985).
2. F. Halzen in Multiparticle Dynamics 1984, World Scientific, G. Gustafson and C. Peterson (editors).
3. G. Ciapetti, Proceedings of the $p\bar{p}$ Collider Workshop, Aosta, Italy (1985).
4. B. Humpert and R. Odorico, Phys. Lett. 154B, 211 (1985).
5. L. K. Ding, et al., ICR Report 107-83-1, Tokyo (1983).

ACKNOWLEDGEMENTS

We thank A. Mueller for discussions.

TABLE I. Properties of jet cross sections with $p_T > p_{T\,min}$ at different energies.

E (TeV)	$\sqrt{s}$ (GeV)	$p_{T\,min}$ (GeV)	σ_{jet} (mb)	$\langle x \rangle_{jet}$	$\langle y \rangle_{jet}$
2	43.	1.25	4	0.17	1.8
150	540.	2	26	0.07	2.9
10^4	4330.	3.2	63	0.05	4.2
10^5	43300.	6	127	0.03	5.9

ORIGINAL PAGE IS
OF POOR QUALITY

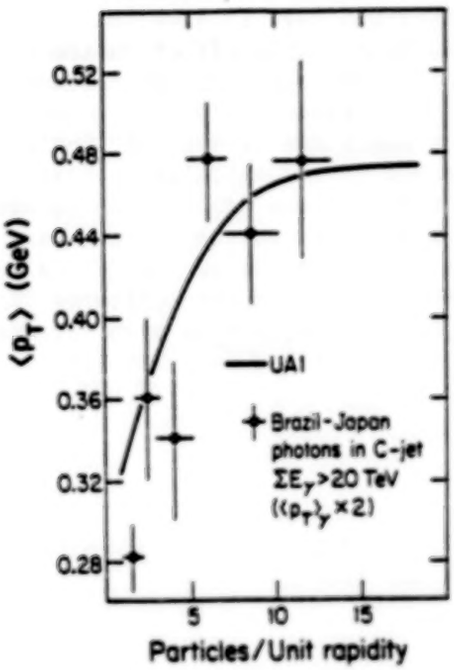


FIGURE 1. Increase of $\langle p_T \rangle$ associated with increasing multiplicity.

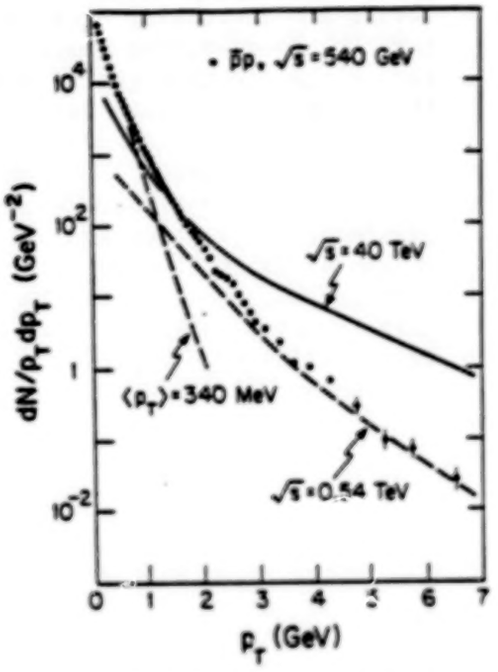


FIGURE 3. Two-component description of the charged particle transverse momentum distribution. The low-p_T component is described by an exponential fall-off with $\langle p_T \rangle$ = 340 MeV. The "high"-p_T component corresponds to hadrons which are the fragments of parton jets with $p_T > p_{T\,min}$ chosen as in Table I. Data from the UA1 experiment.

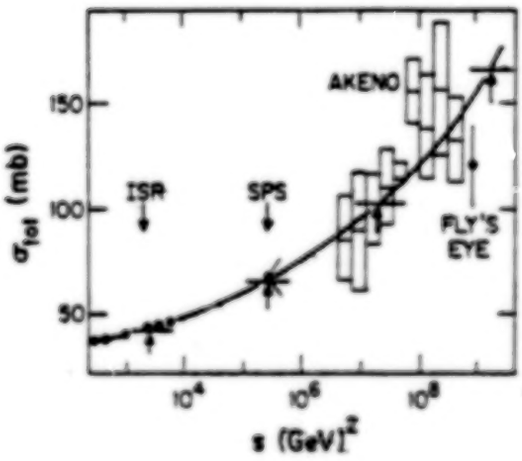
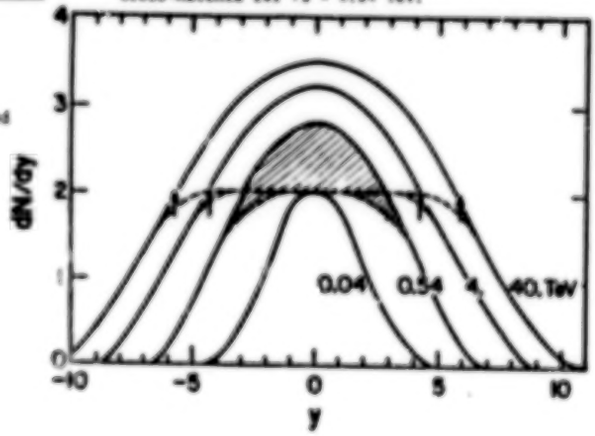


FIGURE 2. The increasing cross section associated with jets of moderate transverse momentum.

FIGURE 4. Sketch of the two-component rapidity distribution corresponding to the two-component total cross section shown in Fig. 2. At each energy the rapidity distribution consists of a plateau on which is superimposed the excess of hadrons near y = 0 due to fragmentation of the scattered jets. Rapidities of the scattered jets are indicated by arrows. The excess is cross-hatched for $\sqrt{s}$ = 0.54 TeV.



N85-35862
HE-1.2-4

EMPIRICAL DESCRIPTION OF THE HADRON - HADRON AND HADRON - NUCLEUS INTERACTION AT THE ACCELERATOR ENERGY RANGE

G.Kubiak,J.Szabelski,J.Wdowczyk

Institute of Nuclear Science and Technology,
90-950 Lodz,ul Uniwersytecka 5,Box 447,Poland

J.Kempa and A.Piotrowska

Department of Physics,University of Lodz,
90-236 Lodz,ul Nowotki 149-153,Poland

1. INTRODUCTION

It has been demonstrated by Wdowczyk and Wolfendale (1984) that the energy spectrum of the secondary pions produced in p - p interactions with energies up to a few times 10^{14} eV can be described well by a scaling violation formula of the form

$$P(E_\pi)=(E_o/205)^{\alpha} q((E_\pi/E_o)\ (E_o/205)^{\alpha})\ \frac{k(E_o,205)}{E_\pi}, \qquad (1)$$

where the parameter α, which is a measure of the scaling violation, is gradually increasing with energy. The coefficient $k(E_o,205)=K_\pi(E_o)/K(205)$ describes the variation of inelasticity coefficient for charged pion production.

The energy spectra of the others secondary particles can be obtained by similar transformations.

For purpose of numerical calculations the function q(x) is usually taken from Fermilab data at 205 GeV and approximated by the following formula (for $\pi^+ + \pi^-$)

$$q(x)=.692(1-x)^{7.4}\ \exp(2.185x) + .807(1-x)^{6.2}\ \exp(2.968x), \qquad (2)$$

which is obtained by integration over p_t of the more general expression fitting simultaneously the x and p_t variation for the same Fermilab data at 205 GeV (Kafka et al 1977). The expression has the form

$$q(x,p_t)=9.624(1-x)^{6.2}\ \exp(-5.963\ p_t^2\ \exp(-2.968x)) + 8.744(1-x)^{7.4}\ \exp(-6.318\ p_t^2\ \exp(-2.185x)) \qquad (3)$$

As a reasonable choice for α and k_π variation it is taken

$\alpha = .815((E_o/205)^{0.135} - 1)\ \ln(E_o/205)$, for $E_o \leq 7.7\ 10^4$ GeV

$\alpha = .072 + .0163\ \ln(E_o/205)$, for $E_o > 7.7\ 10^4$ GeV. (4)

82838-38A

$$k_{\pi tot}(E_o,205)=(E_o/205)^{-.042} \quad , \quad k_{\pi^\pm}(E_o,205)=(E_o/205)^{-.061} . \quad (5)$$

It is also assumed that formula (1) and (2) can be used for describing the energy spectra of kaons and baryons (antibaryons). All those are taken together but relative role of baryons and antibaryons increases with primary energy according to the expression

$$F = 1 - .77(E_o/205)^{-.043} . \quad (6)$$

It is assumed that the average energy of kaons and baryons (antibaryons) increases with energy faster than that of pions and the relative inelasticity coefficient for production of those also increases with energy. The expression giving the ratio of the particles average energy and their inelasticity coefficient to those of pions are respectively

$$b = .45 + .253 \ln\sqrt{E_o} \quad , \quad R = 1.81 - 1.5(E_o/205)^{-.042} . \quad (7)$$

The interactions of mesons with protons are also assumed to be described by the same expressions except that the total inelasticity coefficient is taken to be 0.6 instead of 0.5 with total multiplicity the same and average energy increased by factor of 1.2 .

Taking into account all these assumptions formula (1) is transformed into the following expressions for kaon and baryon plus antibaryon production in proton interaction and for pion production in pion interactions

$$P(E)=(E_o/205)^{\alpha} q((E/b/E_o)(E_o/205)^{\alpha}) \frac{R}{E} , \quad (8)$$

$$P(E)=(E_o/205)^{\alpha} q((\pi/1.2/E_o)(E_o/205)^{\alpha}) \frac{k(E_o,205)}{E} . \quad (9)$$

Combining both formulae we can obtain expression for the spectrum of kaons and baryons plus antibaryons produced in the meson interactions.

2. APROXIMATE FORMULAE FOR INTERACTIONS WITH AIR NUCLEI

For analysis of the cosmic ray propagation in the atmosphere in actual fact, instead of the formulae for interactions of protons and mesons with protons, we have to use formulae appropriate for interactions with air nuclei. Using the method outlined among others by Elias et al (1980) we have introduced simple corrections to the above given expressions to account for the fact that target is an air nucleus.

Similarly as Elias et al (1980) we have assumed that an interaction of hadron with nucleus is an superposition of subsequent interactions of leading nucleon. The nucleon interacting with nucleus is assumed to undergo with certain probabilities one , two or more interactions with nucleons in the nucl-

eus. The probabilities for the number of interactions used by us are given in the table I. The energy spectrum of the secondaries and the inelasticity coefficient distribution the case of one interaction are the same as for interactions with protons. When the number of interactions is higher those distributions are obtained by summing the contribution from subsequent interactions.

$$P_n(E,E_o)=P_{pp}(E,E_o) + \sum_{i}^{n} P_{pp}(E,E_o(1-K_1)(1-K_2)\cdots(1-K_i)) \quad , \quad (10)$$

where K_i is the inelasticity coefficient in the i - th subsequent interaction.

In similar way the inelasticity coefficient for p-nucleus interaction can be obtained. Overall spectra of secondary particles can be easily obtained adding the contributions from various number of interactions with probabilities given in table I. The distribution of the inelasticity coefficient for pA collision can be obtained by Monte Carlo allowing the subsequent inelasticities in p-nucleon interactions to fluctuate according to the assumed fluctuations of the inelasticity coefficient in pp interactions.

Table I

Probability of an incident proton having n collision within a carbon nucleus

n	1	2	3	4	5
P_n	.511	.301	.131	.044	.013

Detailed calculations showed that the obtained energy spectra of the secondaries can be well represented by very simple modification of the expression (1) and also the expressions (8) and (9). The modified formula (1) becomes

$$P(E_w)=(FC)^{1.5}(E_o/205)\; q((E_w/E_o)(E_o/205)\,FC^{.5})\,\frac{k(E_o,205)}{E_w} \quad , \quad FC = 1.32 \quad . \quad (11)$$

The inelasticity coefficient distribution calculated by the outlined above method is consistent with an expression which we have developed (Kempa and Wdowczyk 1985) on the basis of experimental data compiled by Jones (1983).

ORIGINAL PAGE IS
OF POOR QUALITY

The expression is

$$P(K)=1.9\exp(-2(1-K)), \text{ for } K \geq .1 \text{ and } P(K)=\sqrt{K}, \text{ for } K < .1 .$$

Kempa and Wdowczyk (1985) gives also additional expression for the quasielastic interactions but those practically can be neglected here. In spite of the fact that they give almost 20% of the total cross - section their contribution to the flux of secondaries is negligible. Their role practically amounts to an increase of the effective mean free path by a factor of 1.2

Predictions based on the formula (11) are compared with data of Elias et al (1980) in figure 1 where the distributions of pseudorapidities are given for various assumptions about relation of between p_{tpA} and p_{tpp}. It seems that the best value is obtained if we take

$$\langle p_{tpA} \rangle = 1.15 \langle p_{tpp} \rangle .$$

The above described picture of hadron-hadron interaction have been used in our calculations of cosmic ray propagation in the atmosphere presented elsewhere in this proceedings.

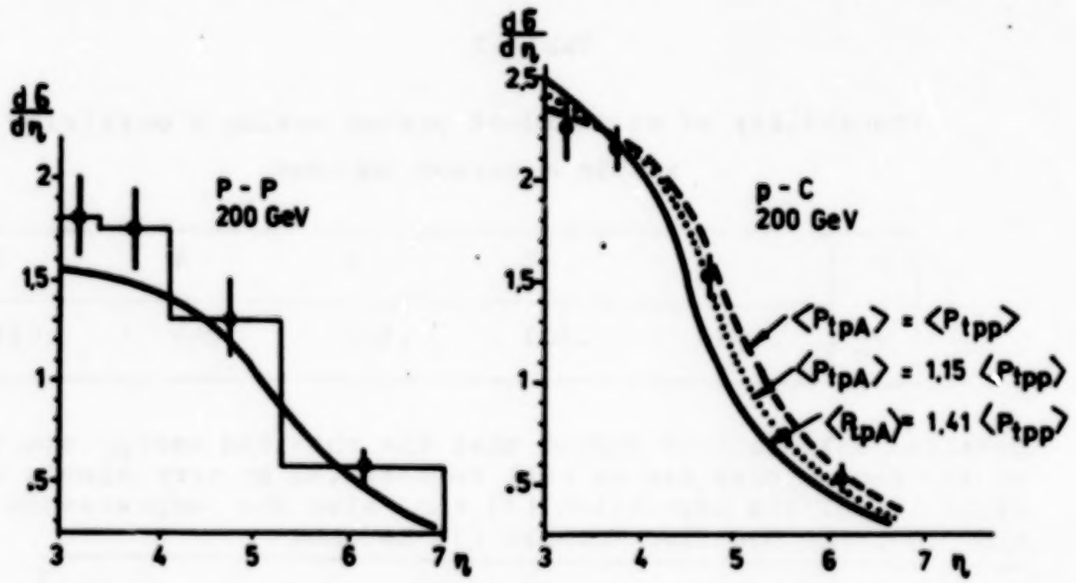


Figure 1

REFERENCES

Elias J E et al 1980 Phys.Rev.D,p.13
Jones L W 1983 18th ICRC,Bangalore,5,p.17
Kafka T et al 1977 Phys.Rev.D,16,p.1261
Kempa J and Wdowczyk J 1985 Presented to the 1st Symposium on Underground Physics,Italy,Saint-Vincent,25 - 28 April
Wdowczyk J and Wolfendale AW 1984 J.Phys.G:Nucl.Phys.10,p.257

N85-35863

55

N85-35863

MULTIPLICITY DISTRIBUTIONS IN INTERACTION MODELS USED FOR CASCADE SIMULATIONS

by

R. W. Ellsworth
Department of Physics
George Mason University
Fairfax, VA 22030

T. K. Gaisser and Todor Stanev
Bartol Research Foundation of the Franklin Institute
University of Delaware
Newark DE 19716

Abstract

In cascade simulations, conservation of energy is of paramount importance. We point out that it is possible to construct algorithms in which energies of secondaries are chosen from physically correct distributions in such a way as to conserve energy, and give physically correct multiplicity distributions without further adjustment. The resulting non-Poissonian nature of the distribution and the approximate KNO[1] scaling are related to the large fluctuations in the energy available for pion production and to the detailed shape of the inclusive momentum distribution.

We describe two multiparticle production algorithms which have these features. One is the algorithm used in the simulation of C-jets[2]; the other is for a hadron-nucleus interaction model used in the calculation of muon and neutrino fluxes[3,4].

References

1. Z.Koba, H.B.Nielsen and P.Olesen, Nucl Phys B40, 317 (1972)

2. R.W.Ellsworth, T.K.Gaisser and G.B.Yodh, Phys Rev D23, 764 (1981)

3. T.K.Gaisser and Todor Stanev, NIM A235, 183 (1985).

4. T.K.Gaisser et al., Phys Rev Lett 51, 223 (1983).

56 N85-35864 HE 1.2-6

SOME REMARKS ABOUT SIMULATION OF COSMIC RAY PHENOMENA WITH USE OF NUCLEAR INTERACTION MODELS BASED ON THE CURRENT SPS PROTON-ANTIPROTON DATA

J.A.Wrotniak(*) and G.B.Yodh

Department of Physics and Astronomy
University of Maryland
College Park, MD 20742, U.S.A.

We demonstrate, that claims about "models based on SPS collider particle distributions" do not unambigously predict properties of EAS generated by Monte Carlo simulation.

One of the main difficulties in interpreting extensive air shower data to derive the properties of particle production in the elementary act is that the data available at the highest accelerator energies (SPS proton-antiproton collider) do not include the features of interaction most essential in air shower propagation (e.g. x-distributions).

Therefore, one could think of different models of particle production, each of them adequately fitting the measured pseudo-rapidity distributions at SPS $p\bar{p}$ energies, but posessing different properties in other variable, for example the distributions in x.

In addition to this x-y ambiguity, there are some other degrees of freedom in utilizing the collider data in a phenomenological model of nuclear interaction:

* distribution in inelasticity,
* the fact that nucleon-air and (especially) meson-air interactions may differ from nucleon-nucleon interaction,
* the extrapolation of scaling violation at interaction energies above 155 TeV.

(*) On leave from Łódź University, Poland.

(**) Work supported in part by the U.S.National Science Foundation under Grant No. PHY 82-07425 .

However, in this study we will limit ourselves just to the x-y controversy, introducing models with as many features (except for x- and y-distributions) in common, as possible; to avoid the extrapolation problem, we consider only primary energies of 500 TeV (2*485 GeV in the CMS).

To prove our point, we have performed Monte Carlo simulations of EAS generated by 500 TeV vertical primary protons; four different nuclear interaction models were used. Two of them are described elsewhere in this volume [1] (also, a detailed writeup of models and the general simulation scheme in which they were immersed is available [3]); here we will only name them:

@ Model M-Y00 - with inclusive x- and y-distributions behaving in a "scaling" way (except for the rise in the total inelastic cross-sections, see below),

@ Model M-F00 - at and below ISR energies (1 TeV in Lab) exactly equivalent to the above, then gradually changing to provide the distributions in rapidity at 155 TeV as given by SPS $p\bar{p}$ [4]. This was achieved by gradual decrease in the "scale unit" in x-distributions of produced secondaries (see [1]), as interaction energy increases.

In addition to this pair, we modified the M-Y00 model by removing secondaries at x around and above 0.1 (this energy was used for production of low-x particles, to keep the inelasticity distribution unchanged). The probability of this removal was changed logarithmically between 0 at 1 TeV and 1 at 100 TeV.The resulting rapidity distribution at 150 TeV is much closer to that for M-F00 than for M-Y00. Thus, one could say that - at least as far as the rapidity distributions are considered - the modification resulted in

@ Model M-T00 (T standing for "truncated"), together with M-F00 reasonably well describing the rapidity distributions at ISR and SPS $p\bar{p}$ energies.

To check the effect of charge exchange (about which we know nothing from the collider data, either), a modification of M-T00 was introduced:

@ Model M-T01 - similar to M-T00, but 1/3 of interacting charged pions may emerge from the collision as pi-zeros.

Except for the differences mentioned above, all remaining simulation assumptions (including mean free paths and inelasticity) were the same for four models [1,3].

The x- and y-distributions for our four models at 1.5 TeV (ISR) and at 150 TeV (SPS $p\bar{p}$) are shown in Figs.1 and 2. At 1 TeV the distributions for all of them are exactly the same.

ORIGINAL PAGE IS
OF POOR QUALITY

(Rapidity for M-Y00 at 150 TeV, not shown, behaves just like it should).

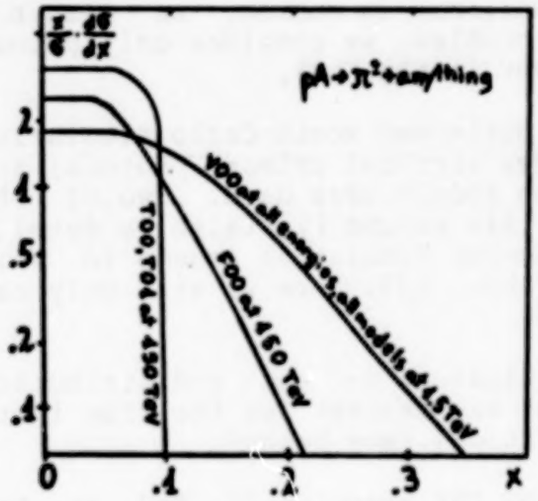


Fig.1 The distributions in x (in high energy approximation: E/E[inter]) for four models used in our study.

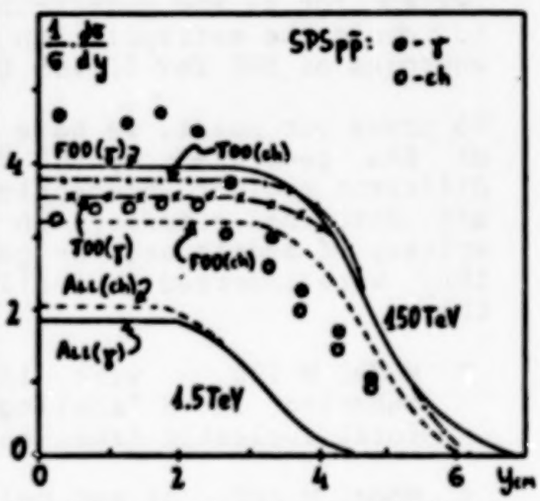


Fig.2 The distributions in rapidity for our models compared with the SPS pp̄ data [4] on pseudorapidity.

We are limiting the scope of this paper only to demonstration of the validity of the statement made in the abstract above; more detailed and systematic study of extensive air showers for a variety of models (including two of these) is presented by us in another contribution to this Conference [1,2].

The Table below presents a brief sample of Monte Carlo results for extensive air showers predicted by our four models (numbers in brackets denote mean square statistical errors in last decimal digit units).

Model:		M-Y00	M-T00	M-T01	M-F00
N_e at maximum		288(3)*10³	284(3)*10³	316(4)*10³	310(3)*10³
at 1000 g/cm²	N_e	80(3)*10³	61(3)*10³	75(4)*10³	64(3)*10³
	N_μ (> 2 GeV)	6.5(1)*10³	7.1(1)*10³	5.0(1)*10³	6.1(1)*10³
	N_μ (>.2 TeV)	30(1)	36(1)	31(1)	32(1)
	N_h (> 2 GeV)	237(11)	194(9)	109(9)	168(8)
	N_h (>.2 TeV)	12.3(4)	9.7(4)	6.4(3)	7.9(4)

N85-32805

One can notice, that the average shower size at maximum for M-T00 is basically the same as for M-Y00 (and not for M-F00, in spite of the similarity in rapidity distributions), the transfer of energy into the electromagnetic component had to be speeded up by charge exchange (M-T01) for maximum to reach the M-F00 level. The situation at 1000 g/cm^2 is just reversed. The increase in number of low-energy muons for M-T00 may be understood easily, though for high-energy ones it is not so obvious. For hadrons M-T00 gives results half way between M-Y00 and M-F00. Hadrons are affected to a greater degree then muons by introduction of charge exchange.

Therefore, statements about "models fitting the SPSpp data" may be often misleading; as the comparison of M-F00 and M-T00 shows, the shape of rapidity distribution (especially with the smallest angles excluded from the collider data) does not determine the interaction features most relevant to EAS development (and lack of information on inelasticity and on meson-nucleus interactions makes situation significantly worse).

Such statements may lead to a false belief, that one knows, what to expect from a nuclear interaction at a few hundred TeV, so (this factor fixed) the extensive air showers supply us with unequivocal information on other subjects: inelastic free path, primary composition. This is clearly not the case; air showers still remain one of basic information sources on the multiple production phenomenology in this energy region.

References

1. J.A.Wrotniak and G.B.Yodh; HE 4.1-7 in this volume

2. J.A.Wrotniak and G.B.Yodh; HE 4.1-2 in this volume

3. J.A.Wrotniak;SHOWERSIM/84, Univ.Md.Rep. PP 85-191 [1985]

4. N.Yamdagni; Workshop on Very High Energy Cosmic Ray Interactions, Univ.of Philadelphia, 36 [1982]

N85-35865
HE 1.2-7

LOW P_T HADRON-NUCLEUS INTERACTIONS

ORIGINAL PAGE IS
OF POOR QUALITY

R.Hołyński and K.Woźniak

Institute of Nuclear Physics,
Kawiory 26 A, 30-055 Kraków, Poland.

Introduction. We are discussing the possibility of describing hadron-nucleus (hA) interactions in terms of a number of independent collisions of the projectile inside the target nucleus. This multiple rescattering may occur on a particle or quark-parton level. To investigate the characteristics of hA interactions as a function of $\bar{\nu}$ we are taking advantage of the correlation between the average number $\bar{\nu}$ of collisions of the projectile inside the nucleus and the number Ng of fast protons ejected from the struck nucleus. We shall use the relation $\bar{\nu}$ vs Ng obtained in [1] (see Fig. 1). For a given target nucleus this allows us to select interactions occuring at different impact parameters.

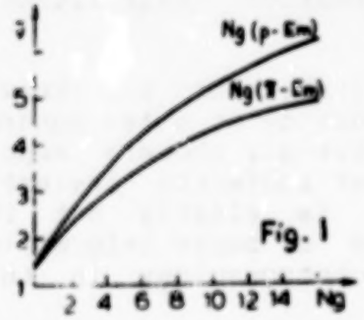


Fig. 1

Experimental material. Our data consist of more than eight thousand interactions of negative pions and protons with emulsion nuclei (see Table 1).

Table 1.

π^- - Emulsion		p-Emulsion	
E_0 (GeV)	# of events	E_0 (GeV)	# of events
60	789	67	1183
200	973	200	2595
300	2115	400	853

For a given energy the events were binned in five Ng-groups which correspond to the different $\bar{\nu}$. Details are given in Table 2.

Table 2.

Ng - interval	0	1	2-3	4-8	9-15
$\overline{Ng}$ (π^-Em)	0	1	2.40	5.40	10.6
$\bar{\nu}$ (π^-Em)	1.39	1.82	2.42	3.30	4.40
$\overline{Ng}$ (p-Em)	0	1	2.40	5.52	10.9
$\bar{\nu}$ (p-Em)	1.44	1.97	2.71	3.98	5.40

Thus for fixed target, by choosing events characterized by a given number of fast protons Ng, we have the possibility to investigate the characteristics of hA interactions in significantly greater interval of $\bar{\nu}$ than that, achieved by varying the atomic number of target nucleus. In the latter method by changing targets from hydrogen to uranium we get following $\bar{\nu}$ variation range: $1 \leq \bar{\nu} \leq 4$ and $1 \leq \bar{\nu} \leq 3$ for proton and pion induced reactions respectively.

ORIGINAL PAGE IS
OF POOR QUALITY

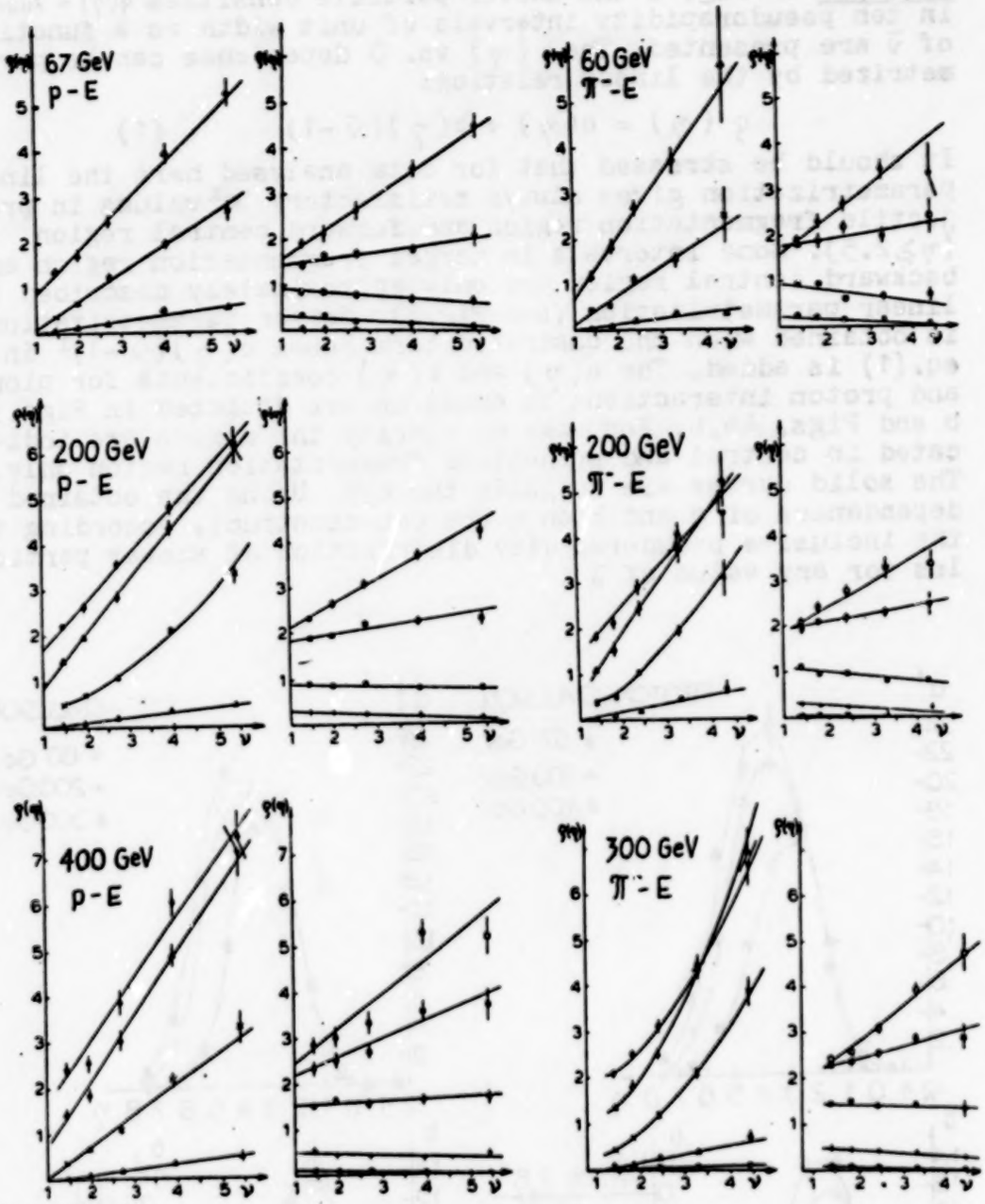


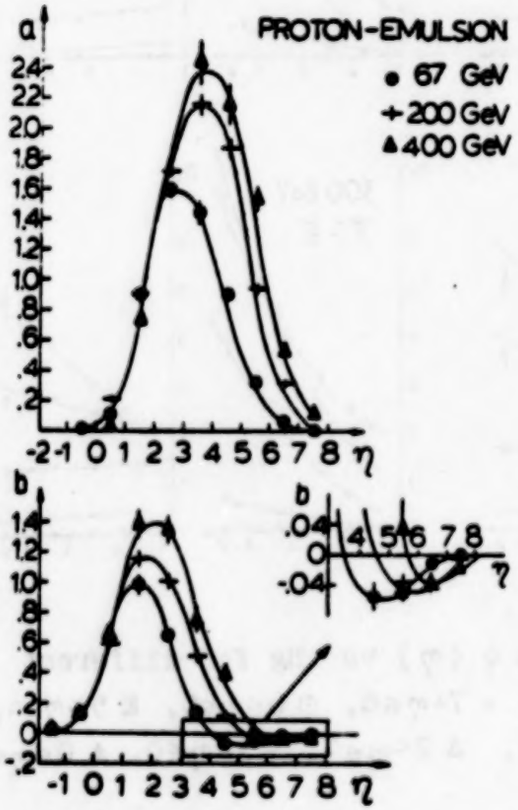
Fig. 2. Particle densities $\varrho(\eta)$ vs Ng for different η - bins: ◆ $8<\eta\leq7$, + $7<\eta\leq6$, ⊙ $6<\eta\leq5$, ■ $5<\eta\leq4$, □ $4<\eta\leq3$, ● $3<\eta\leq2$, Δ $2<\eta\leq1$, × $1<\eta\leq0$, ▲ $0<\eta\leq-1$, ○ $-1<\eta\leq-2$.

ORIGINAL PAGE IS
OF POOR QUALITY

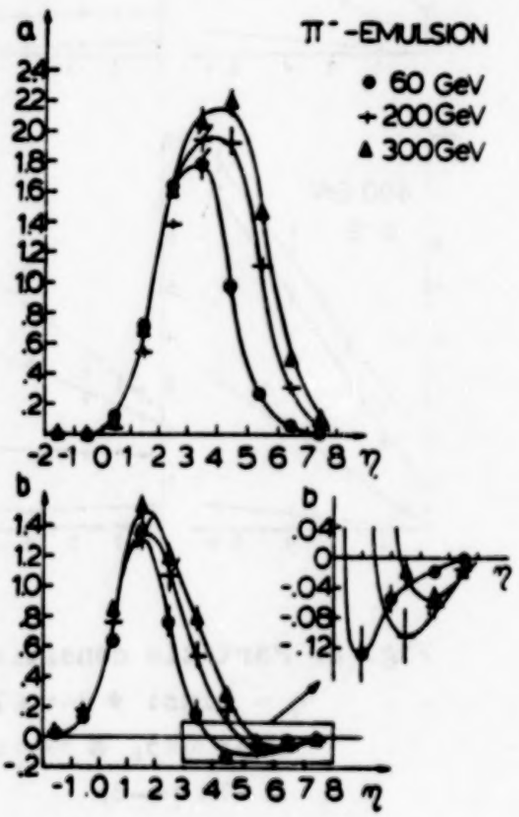
Results. In Fig. 2 the shower particle densities $\varrho(\eta) = {}^1/_{N_{ev}}\, dn_s/d\eta$ in ten pseudorapidity intervals of unit width as a function of $\bar{\nu}$ are presented. The $\varrho(\eta)$ vs. $\bar{\nu}$ dependence can be parametrized by the linear relation:

$$\varrho(\eta) = a(\eta) + b(\eta)(\bar{\nu} - 1) \qquad (1)$$

It should be stressed that for data analysed here the linear parametrization gives always satisfactory χ^2 values in projectile fragmentation region and forward central region ($\eta \gtrsim 2.5$). Some intervals in target fragmentation region and backward central region are only approximately described by linear parametrization (see Fig.2). Better parametrization is obtained when the quadratic term equal $c(\eta)(\nu - 1)^2$ in eq.(1) is added. The $a(\eta)$ and $b(\eta)$ coefficients for pion and proton interactions in emulsion are depicted in Figs.3a, b and Figs. 4a,b. For sake of clarity the errors are indicated in central and projectile fragmentation region only. The solid curves are to guide the eye. Using the obtained dependences of a and b on η one can construct, according to(1), the inclusive pseudorapidity distribution of shower particles for any value of $\bar{\nu}$.



Figs. 3a,b



Figs. 4a,b

Discussion and Conclusions. The dependence of particle densities $\varrho(\eta)$ as a function of $\bar{\nu}$ is not universal in the whole pseudorapidity range. For the highest pseudorapidity values the $\varrho(\eta)$ decreases with the increasing number of $\bar{\nu}$. In the forward region ($\eta \geq 2.5$) there is no evidence of intranuclear cascade because the ratio $b(\eta)/a(\eta)$ in this region is always less than unity. In backward region ($\eta \leq 2.5$) the increase of multiplicity is much faster than the multiplicity in elementary collision multiplied by $\bar{\nu}$. This should be interpreted as an evidence for the existence of cascade effect inside the target nucleus. This cascading is caused by interactions of pions produced in target fragmentation region. From the above, one can argue that in order to discriminate between different superposition models the experimental results in the forward region should be compared with the theoretical predictions. The agreement in the backward region can be obtained by excluding or including cascading of slow pions in the model. Having this in mind the attempt was made in [2] to describe the experimental results obtained in this work for forward region by the additive quark model (AQM). It was tested whether the particle production, in π^-- emulsion interactions can be described by the following relation resulting from AQM:

$$\varrho(\eta, Ng) = F_W(\eta)\bar{w}(Ng) + F_S(\eta)(2-\bar{w}(Ng)) \qquad (2)$$

where F_W and F_S are the fragmentation functions of wounded and spectator quark respectively and $\bar{w}(Ng)$ for a sample of events characterized by a given Ng is an average number of wounded quarks. To obtain $\bar{w}(Ng)$ the relation between $\bar{\nu}$ and Ng was used [1] and Glauber calculations were performed. It was found at η antylab $\simeq -3.0$, the values of F_W and F_S obtained from experimental data are equal. Thus, as follows from (2), the particle production at this η value should not depend on $\bar{w}(Ng)$ and $\varrho(\eta) = 2F_S$. Our π^--emulsion data are in good agreement with this prediction for all primary energies considered.

References: [1] E.Stenlund and I.Otterlund, Nucl. Phys. B198 (1982) 407.
[2] R.Hołyński, M.Jeżabek and K.Woźniak, to be published.

ANGULAR DISTRIBUTION AND MULTIPLICITY OF BACKWARD HADRONS IN hFe INTERACTIONS AT 0.5-5.0 TEV ENERGIES (PION Experiment)

N85-35866

V.V.AVAKIAN, M.O.AZARIAN, K.SH.EGIYAN,
E.A.MAMIDJANIAN, G.ZH.OHANIAN, S.V.TER-ANTONIAN

Yerevan Physics Institute, Markarian st.2
375036, Yerevan, Armenia, USSR

ABSTRACT

Basing on the analysis of $\sim 5 \cdot 10^3$ events registered on the PION installation, data are obtained on the angular distribution and multiplicity of particles, flying back into the laboratory coordinate system (LCS) that are identified mainly as hadrons produced in the reactions of $hFe \to h'X$ type. The inclusively produced hadron energy is > 200 MeV. The experimental data are compared to the results of the cumulative particle production in hA processes observed on accelerators at lower energies.

A large number of experimental studies (see e.g./1/) were devoted to the regularities and nature of backward particles. In generating the energetic charged and albedo particles the cumulative processes may also play a significant role /2/.

Basing on the analysis of $\sim$ 5000 events we report here the experimental data on multiplicity and angular distribution of albedo particles generated at $t > 100$ g/cm^2 depths of the PION installation calorimeter material. The detailed description of the installation is given in /3/. It consists of an ionization calorimeter (IC) and an X-ray transition radiation detector (XTR). The summary quantity of material in the IC is equal to $\sim$ 900 g/cm^2. A 5-module XTR detector is located above the calorimeter. The efficiency of the charged particle registration by one XTR proportional chamber is 96-98%, the accuracy of measuring the azimuthal angle of the charged hadron treak is $\pm 2^\circ$.

ORIGINAL PAGE IS
OF POOR QUALITY

The average number of backward particles is determined by the expression

$$\langle W_3 \rangle = \frac{\Sigma n_3}{N}$$

where Σn_3 is the number of backward charged particles tracks in events considered.

The efficiency of detection of particles, having escaped backward at various angles, versus the interaction depth and the zenith angle was defined by the Monte-Carlo calculations. ~ 78% of the 5346 events considered are the cases with albedo. The multiplicity of detected backward charged particles averaged over the whole effective depth of the calorimeter per one event equals $\langle W_3 \rangle = 0.55 \pm 0.06$ at the hadron energy $E > 500$ GeV.

The multiplicity of charged backward particles generated by hadrons with the same energy at the calorimeter material depths > 100 g/cm^{-2} equals $\langle W_3 \rangle = 0.37 \pm 0.04$.

Figure 1 shows the multiplicity distribution of backward charged particles produced at the depths > 100 g/cm^2. The data from /1/ are given ibidem. As is seen from the figure, the probability to observe backward particles with the large multiplicity grows with the increase in the primary hadron energy.

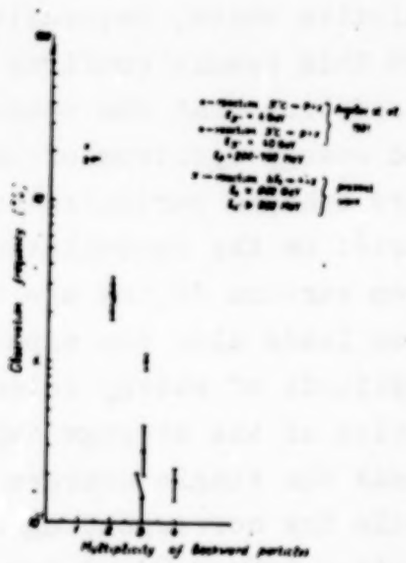


Fig.1. Probability of observing the cases with various multiplicities of backward charged particles produced at the IC material depths > 100 g/cm .

The dependence of the backward particle multiplicity on their generation depth in the interval > 100 g/cm^2 obeys the exponential law $\sim \exp(-t/\lambda)$, where λ equals 181 ± 32 g/cm^2. Such a large value of λ may testify the presence of hadrons with the energy > 400 MeV in the albedo flux.

ORIGINAL PAGE IS
OF POOR QUALITY

Figure 2 presents the distributions of amplitudes of signals from backward particles generated by hadrons with the energy > 500 GeV for the calorimeter two depths: small ($Pb_1 + Pb_2$) and middle ($Fe_2 \ldots Fe_5$), on the output of the multiwire proportional chambers (MWPC) of the XTR detector first row. The average values of the amplitude are equal to 84.67 ± 3.62 and 58.19 ± 2.10 relative units, respectively, and this result confirms our assumption that the nature and energy spectrum of backward charged particles detected on the installation from various depths are not identical. To a similar conclusion leads also the experimental fact that the average amplitude of energy release in the MWPC from charged particles of the average depths ($t > 100$ g/cm^2) 1.30 times exceeds the single charged hadron averaged energy release, while the corresponding ratio for the small depth of production ($Pb_1 + Pb_2$) equals ~ 1.9.

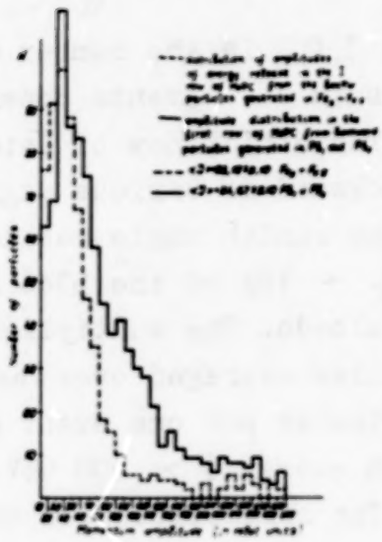


Fig.2. The backward particle energy release amplitude distribution in the first row of MWPC.

Figure 3 presents the backward angular distribution of 3 particles with the registration efficiency corrections. The 3 particles production cross section in the 120°-160° angle interval does not contradict the results obtained at the primary hadron low energies for cumulatively produced protons and pions /4/. In the $\gtrsim 160^\circ$ interval a peculiarity is observed at $\theta \approx 170^\circ$ as a minimum. For the first time a similar behaviour of the angular distribution has been observed for cumulative protons and π -mesons

N85-33807

ORIGINAL PAGE IS
OF POOR QUALITY

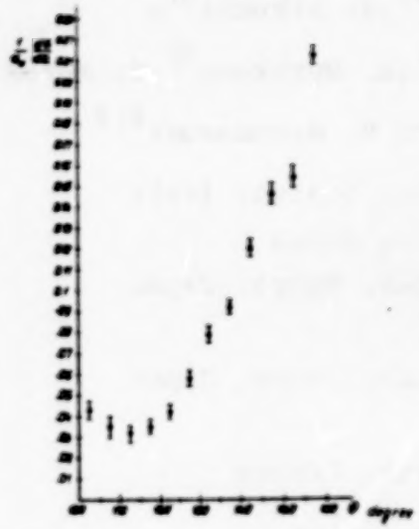


Fig.3. Angular distribution of backward charged particles generated at the calorimeter material depths > 100 g/cm^2.

produced in dA collisions at the primary energy ~ 4.5 GeV/nucleon /4/.

The authors are indebted to A.Ts.Amatuni, S.G.Matinyan, A.G.Oganessian for helpful discussions.

REFERENCES

/1/ Azarian M.O., Zazian M.Z., Mamidjanian E.A., Yad.Fiz., 1977, 26, N.1.

Avakian V.V. et al., Izv.AN SSSR, ser.fiz., 1981, 45, N.7, 1249-1254.

Ellsworth R.-W., Goodman J.A., Ito A.S. et al., NIM, 1982, 203, 167-177.

Angelov N., Litpulaev S.L., Nikitina V.F., Yad.Fiz., 1981, 33, N.1, 190-193.

/2/ Baldin A.M., E.Ch.A.Ya., 1977, 8, 429.

/3/ Avakian V.V. et al., 17th ICRC, Kyoto, 1980, 13, 61.

N85-35867
HE 1.2-9

A Test of the Feynman Scaling in the Fragmentation Region at $\sqrt{s}$ = 630 GeV

T. Doke[5], V. Innocente[1]#, K. Kasahara[2], J. Kikuchi[5], T. Kashiwagi[5], S. Lanzano[1], K. Masuda[5], H. Murakami[3], Y. Muraki[2], T. Nakada[4], A. Nakamoto[3], T. Yuda[2] and M. Haguenauer[6]#

1) Instituto di Fisica, Univ. of Naples, Naples, Italy
2) ICRR, Univ. of Tokyo, Tanashi, Tokyo, Japan
3) Dep. of Physics, Rikkyo Univ, Toshima, Tokyo, Japan
4) SIN, Villingen, Switzerland
5) Sci. Eng. Lab, Waseda Univ., Shinjuku, Tokyo, Japan
6) CERN UA-4 collaboration
#) Ecole Polytechnique, Palaiseau, Paris, France

(CERN UA-7 collaboration)

abstract

The result of the direct measurement of the fragmentation region will be presented. The result will be obtained at the CERN $p\bar{p}$ collider, being exposured the Silicon calorimeters inside beam pipe. This experiment clarifies a long riddle of cosmic ray physics, " whether the Feynman scaling does violate at the fragmentation region or the Iron component is increasing at 10^{15} eV".

1. Introduction

This experiment aims to measure the inclusive cross-section of neutral pions emitted into the very forward region in $p\bar{p}$ collision at $\sqrt{s}$ = 630 GeV. Fig. 1 represents an experimental result[1] which predicts the primary composition of cosmic rays is either proton dominat and Feynman scaling violates or iron dominant and scaling valid.

Until now, no direct measurement inside beam pipe of colliders was made due to a technical difficulty. We have developed a very compact silicon calorimeter with the tungsten target and they will be installed in the Roman pot of UA-4 at CERN

$p\bar{p}$ collider. The direct observation of the energy of the secondary particles with X_F= 0.05 - 0.5 gives rise to the final conclusion to a long riddle of cosmic ray physics and also gives a good data for the understanding of the forthcoming cosmic ray phenomena.

2. Geometry

The shower calorimeter consists of 20 layer of silicon wafers with diameter of 10 cm alternating with tungsten converters of thickness 3.5 mm and 7 mm. The total thickness of the calorimeter amounts to 21 radiation lengths.

All electrodes are segmented at the front and rear side of the silicon wafer into x and y electrodes with 5 mm pitch. The first layer of the silicon wafer is used to identify whether the incident particles are charged or photons. At the 8 radiation length from the front, 45° oriented u-chamber is installed to resolve the multi-hit events. Total number of electronics channel is 90 for one detector. The signal is recorded by Le Croy ADC 2281.

One chamber is located at 13 m from the interaction vertex and outside of beam pipe, while the other detector will be installed at 22 m away from the vertex inside the Roman pot (Fig. 2) . The tracking chamber is also located to obtain the interaction vertex,which covers η= 4.4 - 5.6,in front of the silicon detector at 13 m. The properties of the silicon calorimeter has been published elsewhere[2].

3. Trigger and Detector resolution

The trigger is made by UA-4 trigger logic[3]. The identification of the interaction vertex with use of tracking chamber is necessary for the single arm trigger (=single diffractive trigger) selects beam-beam collisions with 75 % probability. Even if the background rate becomes of the same order as the beam-beam collision for the triggered events, we could clearly find the pinote peak as in Fig. 3. For the double arm trigger

(double diffractive trigger)($3.0<|\eta|<5.6$), the beam-gas collision is selected with a rate of 2 %.

Under a typical low-β run with a luminosity of L = 1×10^{28} $cm^{-2}sec^{-1}$, and the exposure time of 2 minutes, 60,000 minimum bias events will be obtained which is already sufficient to measure the inclusive π° and η production spectra but in order to obtain K°_s and η' , we need further 20 minutes.

4. Energy calibration and Detection efficiency

The π°-mass distribution can be determined with the accuracy of $\Delta M = 8$ MeV. The double photon mapping technique provides a good energy calibration for the photon detector with an accuracy of ±3 % of its absolute value.

Fig. 4 represents the detectable region of photons by the present detector. Former UA-5 experiments observe the polar angle region greater than 30 m rad. Present experiment covers the polar angle between 0.5 and 17 m rad. Fig. 5 represents the detection efficiency of π° by each chamber located at 13 m and 22 m.

5. Schedule

The test exposure will be made on Jul. 10 - 16th with the use of 3" silicon calorimeter. The preliminary results will be presented at this conference. The experiments with the use of two 4" Si-calorimeters will start this September.

Acknowledgements

The authors would like to express their sincere thanks to Prof. G. Matthiae, sporksman of UA-4 collaboration, for his warm support and valuable suggestions.

We also thank to Prof. A. Staude for valuable discussions.

References

1) Mt. Fuji emulsion chamber collaboration: Phys. Rev.D24(81)2353.

2) A. Nakamoto et al.: N.I.M. (1985).

3) CERN UA-4 collaboration : N.I.M. (1985) and CERN EP 84-156.

ORIGINAL PAGE IS
OF POOR QUALITY

Fig. 1

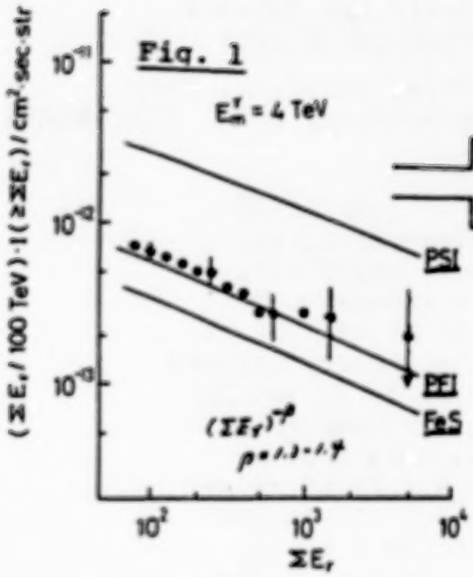


Fig. 2

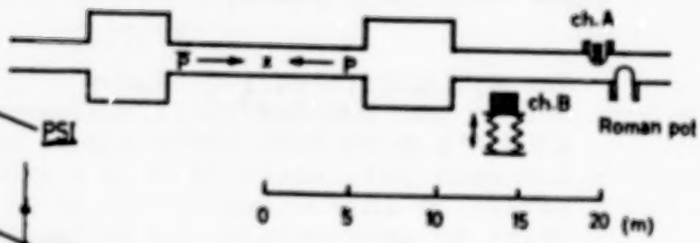
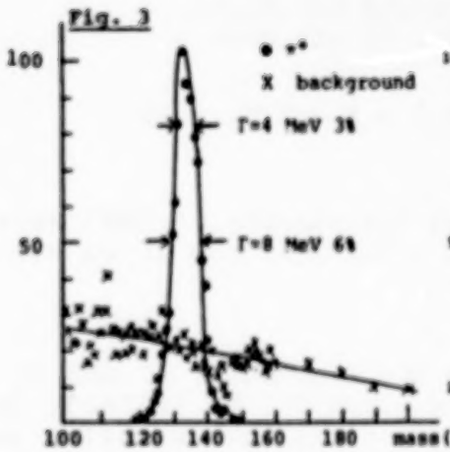


Fig. 3



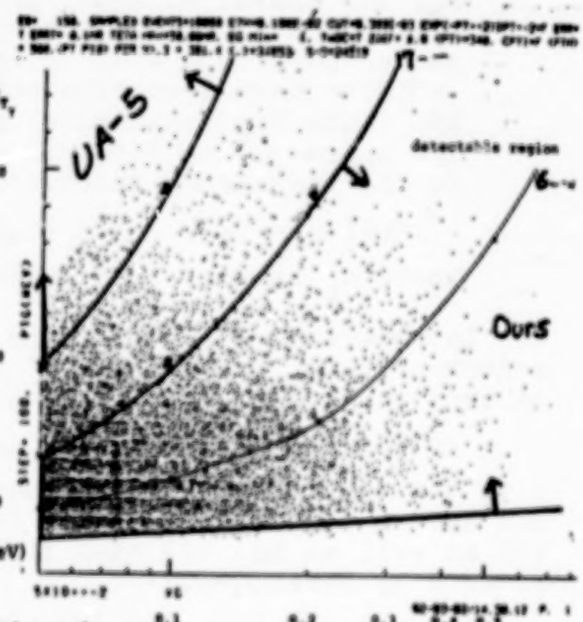
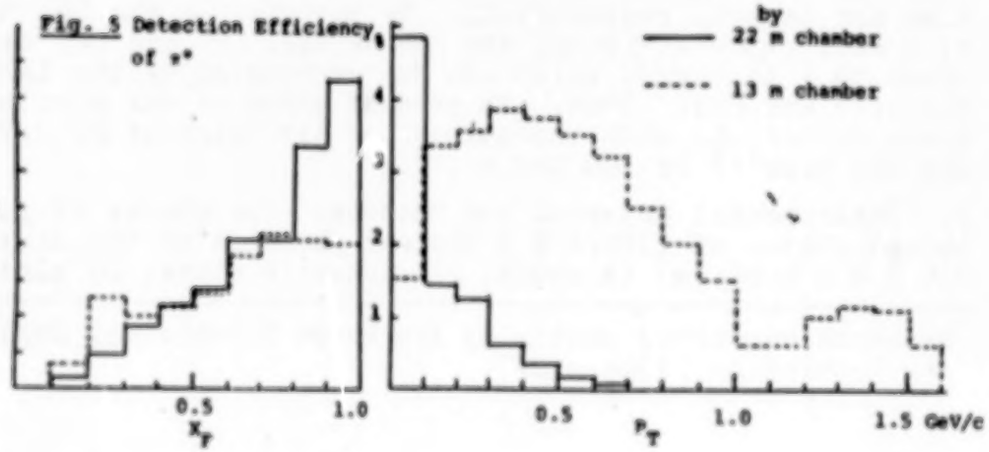


Fig. 4

Fig. 5 Detection Efficiency of π^0



N85-35868
HE 1.2-10

ANGULAR DISTRIBUTION OF SHOWER PARTICLES PRODUCED IN THE COLLISIONS OF 20-GeV/c AND 300-GeV NEGATIVE PIONS WITH EMULSION NUCLEI*

C. O. Kim, S. N. Kim, I. G. Park, and C. S. Yoon
Department of Physics, Korea University, Seoul 132, KOREA

ABSTRACT

For 435 accelerator-produced π^- jets of 20-GeV/c[1] and 300 GeV[2,3] in nuclear emulsion, $\langle\eta(\theta)\rangle$'s have been individually calculated for each jet, where $\eta(\theta)$ is a kinematic parameter introduced by one of us in 1967 in order to approximate the LS(laboratory system) rapidity, $\eta = \text{arctanh}\,(\beta\cos\theta)$.[4] By taking further averages by dividing the samples into groupings of the LS energy $E_\pi = m_\pi \cosh\eta_\pi$, N_h, the number of heavy prongs with LS velocity $\beta < 0.7$, and n_s, the number of charged shower particles with LS velocity $\beta \gtrsim 0.7$, $\ll\eta(\theta)\gg$ have been obtained. By use of the KNO (Koba-Nielsen-Olesen) scaling variable, $\xi = n_s/\langle n_s\rangle$,[5] we find good fit of our data to the regression function,

$$\ll\eta(\theta)\gg - \eta_\pi/2 - \tfrac{1}{2}\ln(m_\pi/m_p) = A + B/\xi, \quad (1)$$

where m_p is the proton mass.

1. Introduction. With the use of the samples of 3987 accelerator-produced proton jets of 30 - 400 GeV, one of us reported that the regression function,

$$\ll\eta(\theta)\gg - \eta_p/2 = A' + B'/\xi\,, \quad (2)$$

fits the angular data well, where the constants, A' and B' do not have any dependence on E_p ($= m_p \cosh\eta_p$).[6] In fact, Eq. (2) as well as Eq. (1) stem from the "scaling" asymmetry parameter R by Tavernier:[7,8]

$$R \equiv m_t \sinh(\langle\eta\rangle - \eta_t)/m_b \sinh(\eta_b - \langle\eta\rangle), \quad (3)$$

where m_b, m_t, η_b, η_t are masses and "initial" rapidities of beam and target, respectively. By putting, in the LS, $\eta_t = 0$, $m_t = \nu m_p$, $\langle\eta\rangle = \ll\eta(\theta)\gg$, the RHS of Eqs. (1) and (2) become equal to $\frac{1}{2}\ln(R/\nu)$, which can be represented by the LHS of Eqs. (1) and (2). Thus, the present paper is the similar analysis to Ref. 6, with the samples of 318 jets[1] of 20 GeV/c π^- and 117 jets[2,3] of 300 GeV π^-.

2. Experimental Material and Methods. Two stacks of glass-backed plates of Ilford K 5 nuclear emulsion of the size, 7.5 x 8 x 0.06 cm^3 (A stack, 21 plates; B stack, 20 plates)

*Research supported partly by the Korea Science and Engineering Foundation (1984 - 87).

were exposed "horizontally" to 300 GeV π^- beam at Fermilab in 1978 with a track density of about 3 x 10^4 particles/cm^2. The along-the-track scanning method was employed in order to find 207 inelastic events in tracing 100.374 m of the primary tracks; this gives the mean free path of 300 GeV π^- in Ilford K 5 nuclear emulsion, 48.5 $\pm$ 3.4 cm. Among these events, by following the procedure taken by Refs. 2 and 3, 126 interactions, whose origins were located more than 50 μm away either from the air surface or from the glass furface inside the processed emulsion plates, were subjected the analysis of counting the numbers of tracks to obtain $\langle N_h \rangle$ = 7.0 $\pm$ 0.4 and $\langle n_s \rangle$ = 13.2 $\pm$ 0.6. Further, we performed angular measurements to the charged shower particles of 117 interactions among the 126 interactions by applying the reference-track method of Ref. 6. The material and experimental procedure concerning the 20-GeV/c pion jets were reported in Ref. 1.

3. Dependence of $\ll\eta(\theta)\gg$. The LS emission angles of the charged shower particles were converted to $\eta(\theta)$ (Ref. 4) and for each jet $\langle\eta(\theta)\rangle$'s were calculated. Then, by grouping the 435 jets into subgroups, according to E_π, N_h = 0, 1, 2-4, 5-8, $\geq$9, n_s = 1, 2, 3, ..., 9, 10-14, 15-19, ..., $\ll\eta(\theta)\gg$ were calculated. As noticed in Refs. 1, 4, and 6, the trends shown in the values of $\ll\eta(\theta)\gg$, as a function of n_s and N_h, are:

(i) For $n_s \gg \langle n_s \rangle$ (i. e., $\xi \gg 1$), $\ll\eta(\theta)\gg$ becomes unreasonably larger. (Small $x_T = p_T/m$ effect.)
(ii) As N_h increases, $\ll\eta(\theta)\gg$ becomes smaller. (Nuclear target effect.)

As shown in Figs. 1 (a) - (e) and the values of A, B and χ^2/DF (and also A', B' and χ^2/DF for the 3987 proton jets of 30-400 GeV in parentheses) in Table I, our angular data of 435 π^- jets fit Eq. (1) rather well. The solid-line curves show

TABLE I. The values of A and B obtained by the least-squares fits for the 435 π^- jets (and those for the 3987 proton jets to Eq. (2)).

N_h	A (A')	B (B')	χ^2/DF
0	-0.18 $\pm$ 0.11 (-0.22 $\pm$ 0.03)	0.35 $\pm$ 0.09 (0.22 $\pm$ 0.02)	0.04 (1.63)
1	-0.08 $\pm$ 0.28 (-0.36 $\pm$ 0.05)	0.24 $\pm$ 0.20 (0.27 $\pm$ 0.04)	8.26 (1.35)
2-4	-0.38 $\pm$ 0.08 (-0.48 $\pm$ 0.03)	0.41 $\pm$ 0.06 (0.27 $\pm$ 0.03)	1.39 (1.87)
5-8	-0.53 $\pm$ 0.21 (-0.66 $\pm$ 0.05)	0.43 $\pm$ 0.25 (0.34 $\pm$ 0.06)	2.55 (1.46)
$\geq$ 9	-1.12 $\pm$ 0.005 (-1.03 $\pm$ 0.03)	0.75 $\pm$ 0.004 (0.48 $\pm$ 0.02)	4.12 (2.38)

ORIGINAL PAGE IS
OF POOR QUALITY

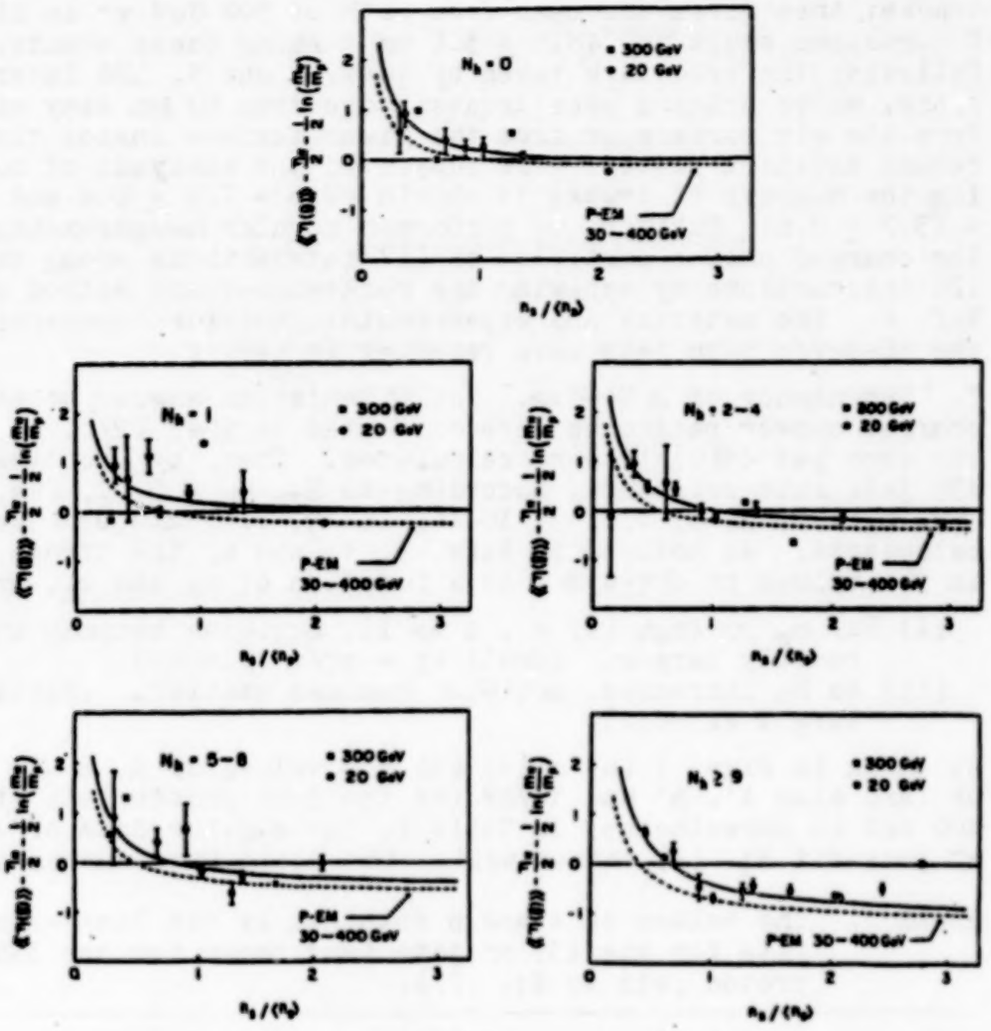


Fig. 1. Dependence of $\langle\langle\eta(\theta)\rangle\rangle$, according to Eq. (1) for the pion jets (solid-line curves) and to Eq. (2) for the proton jets (broken-line curves), for (a) $N_h = 0$, (b) for $N_h = 1$, (c) for $N_h = 2$-4, (d) for $N_h = 5$-8, and for $N_h \geq 9$.

the values of $\langle\langle\eta(\theta)\rangle\rangle - \gamma_\pi/2 - \frac{1}{2}\ln(m_\pi/m_p)$ versus ξ, and the broken-line curves show the values of $\langle\langle\eta(\theta)\rangle\rangle - \gamma_p/2$ versus ξ for proton jets of 30 - 400 GeV.

4. Discussion and Conclusion. As E. Gibbs et al.[9] first noted, the N_h dependence of A, listed in Table I, can be fitted by the regression function,

$$A = \alpha(1 + \gamma N_h)/(1 + \delta N_h), \qquad (4)$$

where the results are $\alpha = -0.152 \pm 0.001$, $\gamma = 0.520 \pm 0.004$,

and $\delta = 0.020 \pm 0.005$ with $\chi^2/DF = 0.4/2$.[6] And as in Ref. 6, N_h-dependence of B, listed in Table I, can be fitted well by the regression function,

$$B = \kappa + \zeta N_h, \tag{5}$$

where the results are $\kappa = 0.33 \pm 0.05$ and $\zeta = 0.025 \pm 0.03$ with $\chi^2/DF = 0.4/3$. Altogether, with the use of the data of angular measurements of 435 accelerator-produced jets of E_π = 20 and 300 GeV, we have obtained the empirical formula,

$$\langle\langle \eta(\theta) \rangle\rangle - \gamma_0/2 - \tfrac{1}{2} \ln (m_\pi/m_p) =$$

$$(-0.152 \pm 0.001) \frac{[1 + (0.520 \pm 0.004) N_h]}{[1 + (0.020 \pm 0.05) N_h]} +$$

$$[(0.33 + 0.05) + (0.025 \pm 0.03) N_h]/\xi.$$

We find the value of ν in Ref. 6 is almost in accord between the one obtained from the proton jets and the other obtained from the pion jets. But there exists some difference between the values of κ of Refs. 7 and 8, which is indeed scaling, for proton and pion jets, reflecting the fact that pion jets do not have two surviving baryons but one.[4,6]

REFERENCES.

[1] E. R. Goza, S. Krzywdzinski, C. O. Kim, and J. N. Park, Phys. Rev. 2, 1838 (1970).

[2] M. Jurić, Dj. Krmpotić, O. Adamović, V. Gerc, L. Rak, J. Lory, D. Schune, Tsai-Chü, B. Willot, K. P. Hong, C. O. Kim, S. N. Kim, K. A. Moon, R. Schmidt, I. Otterlund, G. Baumann, M. Lopez Agüera, R. Niembro, A. Ruiz, E. Villa, Z. Phys. C 22, 131 (1984).

[3] Lj. Simić, O. Adamović, M. Jurić, J. Lory, D. Schune, Tsai-Chü, B. Willot, K. P. Hong, C. O. Kim, and K. A. Moon, Nuovo Cimento 82A, 327 (1984).

[4] C. O. Kim, Phys. Rev. 158, 1261 (1967).

[5] Z. Koba, H. B. Nielsen, and P. Olesen, Nucl. Phys. B40, 317 (1972).

[6] C. O. Kim, Phys. Rev. D 31, 513 (1985).

[7] S. P. K. Tavernier, Nucl. Phys. B105, 241 (1976).

[8] S. P. K. Tavernier and M. Gijsen, Phys. Rev. D 16, 2818(1977).

[9] E. Gibbs et al., Phys. Rev. D 10, 783 (1974).

HE 1.2-11

N85-35869

NUCLEON-NUCLEUS INTERACTIONS FROM JACEE

The JACEE Collaboration:

T. H. Burnett[h], S. Dake[b], M. Fuki[c], J. C. Gregory[g], T. Hayashi[g], R. Holynski[c,i], J. Iwai[h], W. V. Jones[e], A. Jurak[c,i], J. J. Lord[h], O. Miyamura[d], T. Ogata[a], A. Olszewski[c,i], T. A. Parnell[f], T. Saito[a], S. Strausz[h], M. Szarska[c,i], T. Tabuki[a], Y. Takahashi[f], Y. Tominaga[d], B. Wilczynska[i], J. P. Wefel[e], R.J.Wilkes[h], W. Wolter[i], B. Wosiek[c,i]

a) Institute for Cosmic Ray Research, Tokyo; b) Kobe University; c) Okayama University of Science; d) Osaka University; e) Louisiana State University; f) NASA Marshall Space Flight Center; g) University of Alabama, Huntsville; h) University of Washington; i) Institute for Nuclear Physics, Krakow.

ABSTRACT

Results on hadron-nucleus interactions from the JACEE experiment are presented. Angular distributions for charged particles, and angular and transverse momentum spectra for photons have been measured for a sample of events with $\Sigma E_\gamma \geq 1$ TeV. Results on central rapidity density and transverse energy flow are discussed.

1. Introduction

JACEE (Japanese-American Cooperative Emulsion Experiment) was organized to study cosmic ray nucleus spectra and interactions at total energies approaching 100 TeV. The use of conventional emulsion chamber techniques permits the observation of secondary charged particles and individual high energy gamma rays. The results presented here were obtained from a series of balloon flights at 3.5-8 g/cm^2 altitudes[1].

The apparatus used in the experiment has been described in detail elsewhere[2]. All emulsion plates are made from 500~800 μm acrylic bases, coated on both sides with Fuji emulsion. Incident particles are identified in the primary charge detector section using grain, gap and delta-ray counts from thick (150~200 μm) emulsion layers, as well as pit measurements from CR39 etchable plastics. Charge resolution is typically 0.2~2.0 units. The target section contains thin (50-75 μm) emulsion plates interleaved with acrylic or Fe target sheets. Thick emulsions and CR39 sheets are inserted at intervals to permit identification of projectile fragments. Interactions occuring in the upper Pb layers of the calorimeter can also be fully analyzed. The spacer section permits gamma rays to diverge before reaching the calorimeter section, so that individual photon cascades can be observed.

The calorimeter contains ~5 vertical radiation lengths of Pb interleaved with 18-20 layers of emulsion plates and x-ray films. Cascades of energy $\geq$300 GeV make spots visible to the naked eye in the x-ray films, which serve both as threshold detectors and as templates for locating events in the emulsions. In addition, densitometric measurements in x-ray films provide an estimate of the shower energy.

Once an event has been located, a region of diameter 1-2 mm (depending upon vertex height) around the event axis is scanned for lower energy cascades.

Accurate energy determinations are made by performing track counts in the emulsion layers and comparing the results with calibration curves obtained from analytical shower theory calculations[3] and monte carlo simulations[4] which have been checked by accelerator calibration experiments[5]. The error in a single cascade energy measurement is ~20%. The directly measured event energy parameter is ΣE_γ, the total energy observed in the electromagnetic calorimeter. The primary energy E_0 can be estimated from ΣE_γ by using the gamma-ray inelasticity factor k_γ derived from measurements on protons at Fermilab[6], and independently from the charged particle angular distribution using the Castagnoli method.

2. Proton-Nucleus Interactions

Charged track angles are measured relative to the energy-weighted center of the event. Interactions occuring in acrylic base or target plates are assumed to be on carbon targets. Angular distributions are normally presented in terms of the pseudorapidity, $\eta = -\log_e \tan(\theta/2)$. In order to combine events of different energies, one can define a normalized pseudorapidity parameter, $\eta^* = -\log_{10}\tan(\Sigma E_\gamma * \theta)$. The normalized log tan θ distributions for nucleon interactions in C and Pb are shown in Fig. 1. For this sample, $\Sigma E_\gamma > 1$ TeV and $<\Sigma E_\gamma> = 4.9$ TeV (carbon) and 3.5 TeV (Pb).

The central pseudorapidity density ρ_c for each event has been estimated by excluding the forward 1.5 rapidity units (projectile fragmentation region) and calculating $dn/d\eta$ over the next 2 rapidity units. In Fig. 2 we plot $< \rho_c >$ versus the target mass A. The data are well represented by the relation $< \rho_c > = kA^{0.31}$.

For photons observed in the calorimeter, transverse energy flow as a function of rapidity y can be analyzed by defining an integral transverse energy flow parameter,

$$F(y) = \sum_{y_i > y} E_{ti}$$

where $E_{ti} = E_i sin(\theta_i)$. Plotting $F(y)$ vs η for individual events, and excluding the low-y region where detection bias may be present, one finds that $F(y)$ can be well represented by the form $F(y) \sim e^{-by}$. The fitted values for the slope parameter b have a bimodal distribution shown in Fig. 3, with about 15% of the events displaying a significantly steeper slope than the rest. In Fig. 4a we show several typical events displaying large b; the low-b events shown for comparison in fig 4b have been chosen to have a similar distribution of target mass and ΣE_γ. The data in Fig. 4 have been displaced vertically for clarity.

3. Acknowledgements

This work supported in part by DOE, NSF and NASA in the US, and JSPS in Japan.

78 ORIGINAL PAGE IS
OF POOR QUALITY

4. References

1. T. Burnett, *et al*, paper HE-1.4-4, this conference.

2. R.W. Huggett, *et al*, 17th Int. Cosmic Ray Conf. (Paris), **8**, 80 (1981).

3. J. Nishimura, *Handbuch der Physik* **46/2**, 1 (1967).

4. S. Dake, private communication.

5. N. Hotta, *et al*, Phys. Rev. **D22**, 1 (1980).

6. S. Dake, *et al*, 15th Int. Cosmic Ray Conf. (Plovdiv), **7**, 322 (1977).

5. Figure Captions

1. Normalized angular distributions for charged tracks observed in p-Pb interactions (solid line) and p-C interactions (dashed line). The normalized pseudorapidity parameter is defined as $\eta^* = -\log_{10}\tan(\Sigma E_\gamma * \theta)$.

2. Central pseudorapidity density ρ_c versus target mass A. Interactions in plastic and emulsion are taken to be on A=12 and 82 respectively. The solid line shows the results of a fit to $< \rho_c > \sim A^\delta$, with δ=0.31.

3. Distribution of fits to slope parameter b in the relation $F(y) \sim e^{-by}$. See text for definition of the integral transverse energy flow parameter F(y).

4. Plots of the integral photon transverse energy flow F(y) for individual events a) with slope parameter $b > 1.25$ and b) with $b < 1.25$. The events have been displaced vertically for clarity; the scales shown apply to the lowest data set.

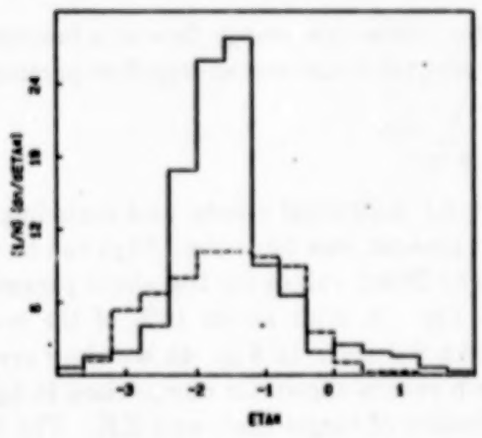


Figure 1

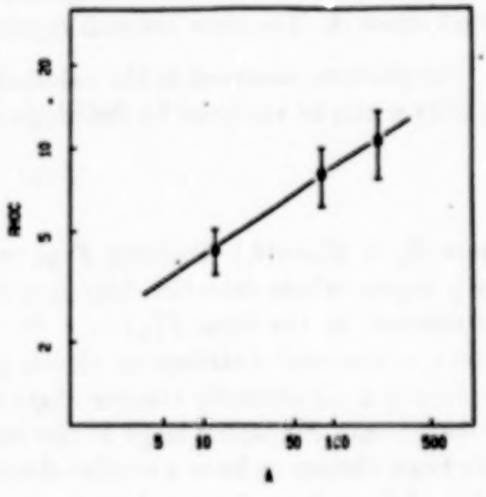


Figure 2

ORIGINAL PAGE IS
OF POOR QUALITY

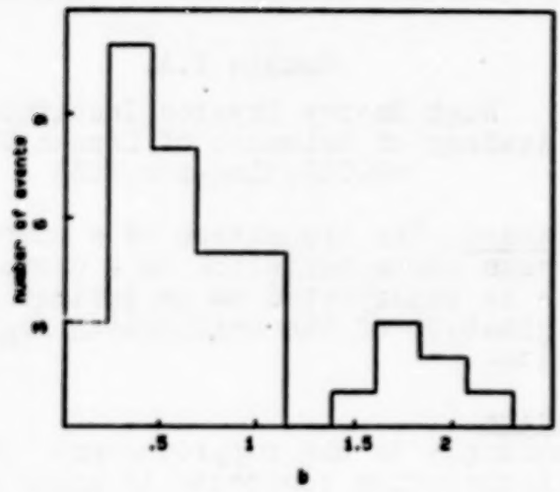


Figure 3

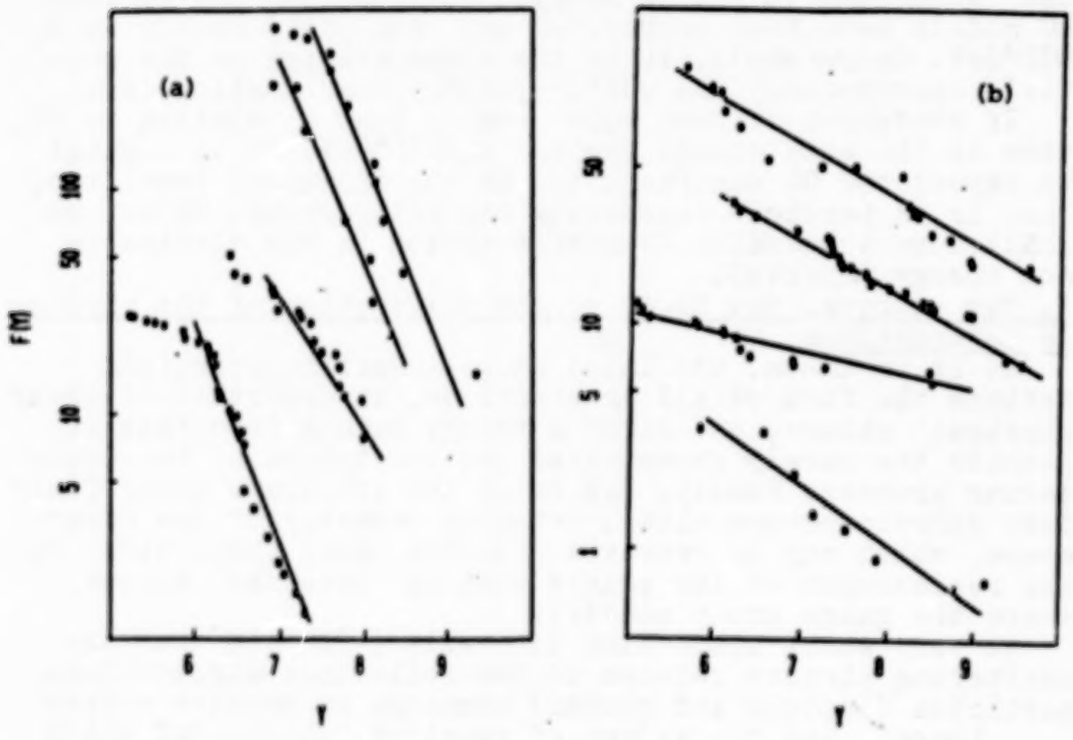


Figure 4

N85-35870

AN UNIFICATION OF THE INTERACTIONS AND THE DIFFRACTIVE PROCESSES

Kuchin I.A.

High Energy Physics Institute
Academy of Sciences of Kazakh SSR,
480082,Alma-Ata,USSR

Abstract. The transition of a number of hadronic process characteristics to a certain universal regime is interpreted as an indication to the early origination of the unification regime of the interactions.

I. Introduction.

Correspondingly to the rapprochement of the electroweak and strong interaction constants in grand unification (GU) models, one can expect a partial loss of the specific character of the mentioned interactions and the transition of their globbal characteristics to some general regime[I].

Though one expect GU coming at superhigh energies(10^{16} GeV according to proton decay), nevertheless the various GU models have been approbated and conformed really at $E_0 \simeq 10^5$GeV. On the whole, it is the argumentation on the particle spectroscopy and SU(5)-symmetry confirmation level.

If evidences of such sort really bear a relation to GU, then in the same energy region ($E_0 \geq 10^5$GeV) it is logical to expect the GU manifestation on the dynamical level too, that is in particle scattering characteristics. Below we shall show a possible GU-manifestation in the attainable now energy interval.

2. Two sources, two forms of the unification of the particle interactions.

As it is known, the local gauge-invariant principle defines the form of all interactions, irrespective of their physical nature, and gives a theory such a form that it permits the purely geometrical interpretation of the scattering process. Namely, one bring the arbitrary gauge field into correspondence with a definite geometry of the fiber space, which may be received from the usual space-time by the replacement of its points with an "internal" spaces, where the gauge group acts[2].

At very short space-time intervals ($\sim 10^{-4} \div 10^{-3}$fm) the scattering picture reduces to the following: structurless particles (leptons and quarks) exchange by massive vector bosons, and the values of coupling "constants," which depend on the transfer of the 4-momentum, come close (by magnitudes) as the energy increases, so that the strong interactions are weakened while a weak interaction and an electromagnetic one become stronger. If the universality of the interactions means the presence of one general coup-

ORIGINAL PAGE IS
OF POOR QUALITY

ling constant, then the unification of the interactions may take place, as it is expected, at the energies of the order of 10^{14}-10^{15}GeV, when it is necessary to take into account gravitation too.

On the other hand, right now (at FNAL- and ISR-energies) we are witnesses of the transition of a number of hadronic characteristics (the total cross-sections, the parameters of the diffractive cone for different pairs of the colliding particles) to a certain universal regime (Fig.I). This phenomenon is known to be caused by the diffraction predominance[4].

The contribution of the diffractive channel of the scattering does not depend on the nature of the colliding particles. To describe the diffraction the only quantum-mechanical(wave) properties of the scattering, some extent of the dynamical symmetry and the unitarity are essentially necessary. All these are discriminating features of some universal mechanism of the interaction.

Thus we may point out two sources (and two forms) of the unification of the interactions:the first comes from the processes at very short distances (for pointlike, structurless particles), the other- from a processes at comparatively large distances (~1÷2 fm), in soft interactions of the extensive objects.

3. The principle connection between the diffraction and gauge fields.

There is no satisfactory theory of diffractive high energy scattering of particles at present. In particular, it should be cleared up what "the internal spaces" are responsible for the gauge-invariance principle for the diffractive processes. Nevertheless, a principle connection between the diffraction and the Yang-Mills-type fields exists. It is traced e.g. in that line, which connects non-Abelian gauge theories and the Weyl's geometrical electrodynamics and a string-type solution of nonlinear equations[2]. After all, in the particle physics the string represents the neutral gluonic field - the carrier of the diffractive properties of the interactions on quark-parton level.

4. The predominance of the diffraction in hadronic interactions at high energies.

So one can think, that the more profound general understanding of the particle diffraction will lead to an essential expansion of the area of the diffractive phenomens, though even now their contribution to the total cross-section, by no means, is not small. According to special analysis[4] (the author makes use of the theoretical understanding of the diffraction in gauge theories (in RQT) and of the conception of the pomeron in QCD) in the FNAL -ISR energy interval, the contribution of the diffraction interactions is not less than 95 per cent from 6% up. The role

*) It is worth notice a tendency to growth of the total $\bar{p}p$-interaction cross-section in the region of $E_{\bar{p}} \geq 100$-200GeV (see ref. on the data in [3]).

of diffraction seems to be so large, that one may speak about true "regeneration" of the strong interactions in the $E_0 \geq$ I0 GeV region.

Since the universal properties of the scattering, which act in the diffraction, are important even for GU theory, then all these properties (and, together with them, the diffraction too) work up to complete strengthening of the GU regime. Therefore, there is no reason to expect the decrease of the diffractive contribution when passing to the region of higher energies. On the contrary, it should be expected the increase of its role, because the total unification of the interactions assumes the confluence of its two forms into one.

5. Conclusion. Taking into account that due to a large value of the coupling constant the strong interactions earlier than the others reach a large value of the cross-section and approach GU regime "from above" (whereas the electroweak interactions approach it "from below"), one may conclude, that the observed transition of a number of hadronic process characteristics to certain universal regimes (Fig.I) is the early evidence of the unification regime, in which strong interactions enter.

6. Proposal for cosmic ray investigators.

The interval from the energies of the electroweak unification (~10^3GeV) to the grand synthesis (~10^{16}GeV) is vast. Here one may expect for manifesting of quite new physics. We should remind that up to now any increase of the energy by several orders results in discovery of a new class of the phenomena. The possibility of the phenomenological generalization of the canonical commutation relations for processes at very high energies has been already discussed elsewhere.

For example, it is proved that such modification of the quantum mechanics becomes important at the energies which are typical for GU scheme (~10^{16}GeV)[5]. The other possibilities may appear in the course of more profound understanding both the phenomenon of the diffraction and the mechanism of the unification of the interactions.

A considerable part of the foregoing energy interval of the saturation of the GU regime is available for the cosmic ray particle experiments (up to $E_0 \geq 10^{11}$ GeV)[6]. Due to specific conditions of cosmic ray experiments (limited statistics, high registration thresholds of interaction products) practically only inelastic diffraction of incident hadrons and nuclei is observed in these experiments[7]. This allows to study the process of unification just in the experiments with cosmic ray particles.

References

[I] Freedman D.Z., van Nieuwenhuizen P.-Scien.Amer., 238, I978, I26.

[2] Konopleva N.P., Popov V.N. « Kalibrov. polya, Atomisdat

ORIGINAL PAGE IS
OF POOR QUALITY

I980.
[3] Roos M. et al. -Phys.Lett., BIII,I982,45.
[4] White A.R. - Prep. Fermilab-Conf-82/I6-THY,I982.
[5] Giffon M., Predazzi E. -Lett. Nuovo Cim., 37, I983,430.
[6] Gusev G.A. et al. - Pisma v ZHETF, 36, I982,2I6.
[7] Kuchin I.A. -Proc. of the XVIII ICRC,II,I983,I57.

Figure I.

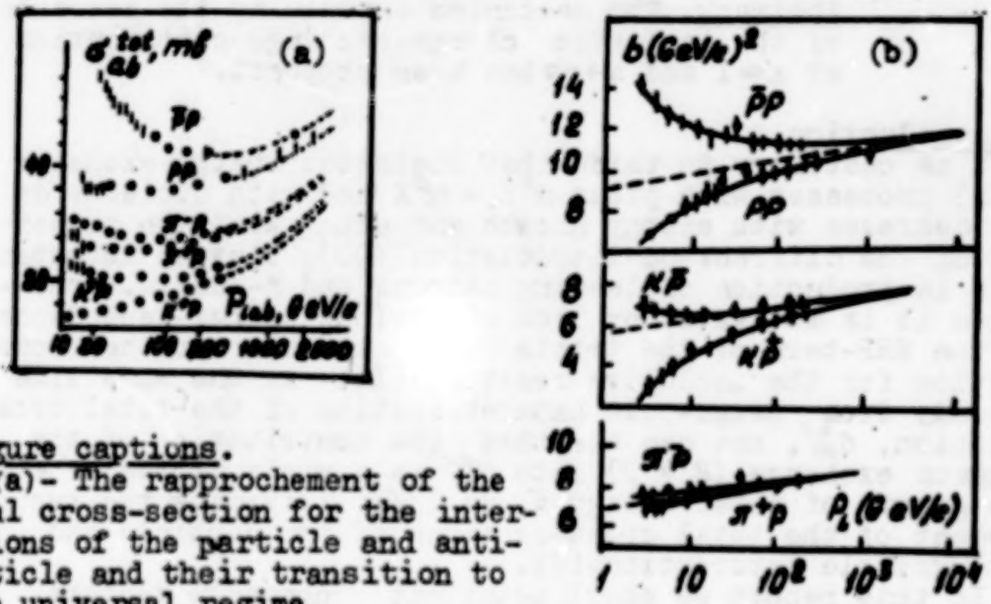


Figure captions.

(a)- The rapprochement of the total cross-section for the interactions of the particle and antiparticle and their transition to some universal regime.

(b)- The same for the slope parameters of the elastic scattering $b^{el}_{ab}(s)$.

IS THE INELASTIC CHARGE-EXCHANGE CONTRIBUTION CONSTANT AT THE LARGE x AND SUPERHIGH ENERGIES ?

N85-35871

Kuchin I.A.

High Energy Physics Institute
Academy of Sciences of Kazakh SSR,
480082, Alma-Ata, USSR

Abstract. The mechanism explaining the decrease of the inelastic charge-exchange contribution at $x \simeq 1$ and $s \to \infty$ has been proposed.

I. Introduction.

It is customary to think that inelastic charge-exchange (CEX) processes with pions $\pi^{\pm} h \to \pi^{0} X$ and with nucleons do not decrease with energy growth and along with the processes of the diffraction dissociation (DD), play an important role in production of leading hadrons and γ-quanta. Sometimes it is motivated by lack of obvious energy-dependence of the RRP-term of the triple Regge expansion of the cross-section for the inclusive reactions[1]. At the same time already from Regge-pole parametrisation of the total cross-section, σ_{ab}^{tot}, one can see that the contribution of the reggeon exchange ($R \neq P$) into σ_{ab}^{tot} as a whole decreases with the growth of total energy $\sqrt{s}$, as $1/\sqrt{s}$, providing the rapprochement of the total cross-sections of the particle and antiparticle interactions[2].

In this report we shall point out concrete factors, which are responsible for CEX-contribution decrease at $s \to \infty$ and work near the kinematical limit of the reaction $pp \to nX^{++}$.

2. Points of departure and formulas.

When discussing the relative contribution of the CEX and DD near the kinematics limit two factors should be taken into account: the limited value of the mass of the particle beam ($M_X^2 \neq$ const $\cdot s$ at $s \to \infty$) and the dual meaning of the M-dependence in the formula of the triple Regge expansion:

$$s\frac{d^2\sigma}{dt\,dM_X^2} = \sum_{ijk} G_{ijk}(t)\, s^{\alpha_i(t)+\alpha_j(t)-1} (M_X^2)^{\alpha_k(0)-\alpha_i(0)-\alpha_j(0)}$$

- the terms with $\alpha_k(0)=1$ give the background of the resonances in resonance mass region and the terms with $\alpha_k(0)=1/2$ give the resonances itself as a certain function of M.

Near the kinematical limit one may represent the ijk-term contribution as

$$\frac{d\sigma^{ijk}}{dM_X^2} = \int_{-\infty}^{t_{max}} dt \left(\frac{d^2\sigma}{dt\,dM_X^2}\right) = F_{ijk}(s, M_X^2)\cdot T(s, M_X^2),$$

-where $T(s,M_X^2)$- is the result of integration of the t-dependence of the process:

$$T(s, M_X^2) = \int_{-\infty}^{t_{max}} dt\, G_{ijk}(t) \left(\frac{s}{M_X^2}\right)^{(\alpha_i' + \alpha_j')t} \simeq \frac{\lambda_1}{B_{ij1}} + \frac{\lambda_2}{B_{ij2}}$$

ORIGINAL PAGE IS
OF POOR QUALITY

Here the two component form of the $G_{ijk}(t)$

$$G_{ijk}(t)=\sum_{i}^{2}\lambda_i e^{\mu_i t}, \qquad B_{ijl}=\mu_l+(\alpha_i'+\alpha_j')\ln\left(\frac{s}{M_i^2}\right)$$

and small value of $t_{min}\simeq\frac{m_p^2}{x}(1-x)^2$ in the region of $x\simeq 1$ ($1-x\simeq M_x^2/s$) are used. $T(s,M_x^2)$ is a weak (logarithmic) dependence of its arguments, and the behaviour of the triple Regge contributions is determined mainly by the F_{ijk}-function, the explicit form of which is given in the table for different sets of ijk. (Only two trajectories are considered: $\alpha_R(t)=1/2+t$ and $\alpha_P(t)=1+\varepsilon+\delta t$ $(\varepsilon=0.06,\ \delta=0.3)$).

To elucidate differences in CEX- and DD-behaviour near the kinematical limit we have considered the integral cross-section of the PPR- and RRR-contributions as a function of the upper limit for the integration over the mass.

Numerical estimations of the CEX- and DD- contributions have been carried out using the parametrisation of $G_{ijk}(t)$ from [3].

3. Results of the calculation and discussion.

If only the terms with k=P and i = j are taken into account, then the relative contribution of the CEX does not depend on the energy of the interaction and decreases with the growth of x:

$$R\equiv\sigma_{RRP}^{ex}/\sigma_{PPP}^{DD}\cong(1-x)^{1+2\varepsilon}$$

Then, the DD-contribution predominates over the CEX one, beginning with $x\simeq 0.85$ (fig.I).

However, it is impossible to extrapolate this dependence into the point x = I, without falling into contradiction with the experimental data. Near the kinematical limit of the inclusive reaction $hh\to hX$ the relation σ^{ex}/σ^{DD} is determined by cross-section of the relevant quasi-two-particle reactions:

$$\frac{\sigma^{ex}}{\sigma^{DD}}\xrightarrow[M_x^2\to M_{Res}^2]{}\frac{\sigma(pp\to n\Delta^{++})}{\sigma(pp\to pN^{*})}=Const(M^2)\frac{s^{2[\alpha_R(0)-1]}}{s^{2[\alpha_P(0)-1]}}\equiv c\cdot s^{-(1+2\varepsilon)}.$$

Such behaviour is described by the terms with k = R and i = j or, alternativelys, by the two-reggeon- approximation, which effectively takes into account the resonance and background contributions into the reggeon-hadron amplitude.

The ratio of the cross-section σ^{ex} to σ^{DD}, which is expressed via the contributions of the RRR- and PPR-terms, behaves as $\sim 1/s$ with the limited upper value of the mass M

$$r\equiv\sigma_{RRR}^{ex}(s,M)/\sigma_{PPR}^{DD}(s,M)\cong Const'(M^2)\cdot s^{-(1+2\varepsilon)}$$

However, on energy dependence, the relevant behaviour of the x-distributions (terms with k = R) does not join with the regime of the terms, which are dual to background (k = P) (fig.I.). To guarantee the smooth transition between them one should take into account the interference terms with $i\neq j$ and different k. The s- and M-dependences of the crossed terms at a given k obey the rule

$$\text{inter}=\sqrt{\text{diff}\cdot\text{nondif}}$$

The accounting of the interference leads to that, the energy-dependent form of the x-disrtibutions (the contribution of the terms with k=R) extends from the vicinity $x \simeq I$ to the broader region of $x < I$*). At large M_X, when only terms with k=P become essential, the cross-section will depend only on x, and the scaling regime is reconstructed (if $\varepsilon = 0$). The effect of the scaling reconstruction at large M is known[4].We accent our attention on the factors, which break it down at small M_X.

4. Conclusions.

When prognosing the x-distribution behaviour in superhigh energy region ($s \to \infty$) it is impossible to neglect non-scaling terms with k=R, extrapolating the scaling behaviour of the terms with k=P to the point x=I.

In the resonance and nearresonance mass region the diffractive and non-diffractive processes, $hh \to hX$, behave in essentially different way. The energy dependence of resonance diffractive production is approximately the same as for elastic scattering processes (one can expect even a weak growth ($\varepsilon \neq 0$!) of the contribution of the reaction $pp \to pN_i^*$), whereas the non-diffractive channel decreases as $\sim I/s$, involving the neighbour regions of the x-spectrum, owing to the action of the interference terms (with $i \neq j$), which decrease only as $\sim I/\sqrt{s}$ **).

All this taken together should lead to the gradual decrease of the CEX-contribution with energy growth at $s \to \infty$, which begins close to x=I and extends then to the region of the smaller x.

The study of the CEX processes in the experiments with cosmic ray particles is usually carried out at not too high energies ($E_0 \lesssim 10^{13}$-10^{14} eV) and in the limited region of moderately large x ($x \lesssim 0{,}7$ - $0{,}8$). Apparently, this is not enough to detect the considered effect. It is interesting to observe the CEX-behaviour directly in the region of the utmost large x.

References

1 Murzin V.S. et al.-Vzaimod.adr.vys.en.,M.,I983,p.20.
2 Mukhin S.V. et al.-Yad.Fiz.,30,I979,I680.
3 Chu S.-Y. et al.- Phys.Rev.,DI3,I976,2967.
4 Mukhin S.V. et al.-El.Part.Atomic Nuclei,8,I977,I030.
5 Breastone A. et al.- Prep.CERN/EX 84-I05.
6 Favier J.-In: Proc.XII Rencontre de Morion,I977,II,37.
7 Webb R. et al.- Phys.Lett.,B55,I975,33I.

*) It is even better to consider together the three - and one-reggeon formulas for one-particle distribution in the incident hadron fragmentation region.

**) By parameterisation of the $G_{ij}(t)$ the role of the interference terms is not always taken into account , as e. g. in[3].

ORIGINAL PAGE IS
OF POOR QUALITY

Table

		$d\sigma^{ijk}/dM^2$	
	ijk	$\varepsilon = 0$	$\varepsilon \neq 0$
diff	PPP	I/M^2	$s^{2\varepsilon} M^{-2(I+\varepsilon)}$
	PPR	I/M^3	$s^{2\varepsilon} M^{-(3+4\varepsilon)}$
quasi	RRP	I/s	$s^{-I} M^{2\varepsilon}$
	RRR	$I/(sM)$	$s^{-I} M^{-I}$
inter	PRP	$I/\sqrt{sM^2}$	$s^{\varepsilon}/\sqrt{sM^2}$
	PRR	$I/(M^2\sqrt{s})$	$s^{\varepsilon}/\sqrt{s}\cdot M^{-2(I+\varepsilon)}$



Fig. I.

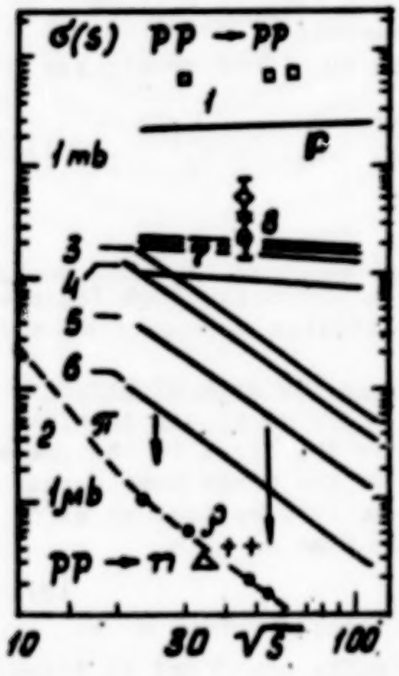


Fig.2.

Figure captions.

Fig.I. The behaviour of the x- distribution. I-the ratio R for $31 \leq \sqrt{s} \leq 100$ at $\varepsilon = 0.06$; 2- the same at $\varepsilon = 0$; 3,4- the ratio r for $\sqrt{s} = 31$ and 100, respectively.

Fig.2. The behaviour of the contributions with k = P and i = j near the kinematical limit ($M_x \to m_p$). I-the elastic scattering cross-section and the contribution of the P-pole (without accounting for the interference with f- and ω - poles); 2- the cross-section of the reaction $pp \to n\Delta^{++}$ (π- and ρ-regimes) from [6]; 3 - 6 — $\sigma^{RRR}(s, M_x^2)$ for M = 10; 7.1; 3.2; and 1.4, respectively; 7-$\sigma^{PPR}(s, M)$ for the same values of M ; 8 - the contribution of the reaction $pp \to pN_1^*$ from [7].

ORIGINAL PAGE IS
OF POOR QUALITY

GENERAL CONSEQUENCES OF THE VIOLATED FEYNMAN SCALING

N85-35872

G. Kamberov

Department of Mathematics and Mechanics, Sofia State University, Bld. A. Ivanov 5, Sofia, Bulgaria

L. Popova

Institute of Nuclear Research and Nuclear Energy, Bld. Lenin 72, Sofia, Bulgaria

1. Introduction The problem of scaling of the hadronic production cross sections represents an outstanding question in high energy physics especially for interpretation of cosmic ray data. A comprehensive analysis of the accelerator data[1] leads to the conclusion for existence of breaked Feynman scaling. It was proposed that the Lorentz invariant inclusive cross sections for secondaries of a given type approache constant in respect to a breaked scaling variable x_s . Thus, the differential cross sections measured in accelerator energy $\sqrt{s_0}$ can be extrapolated to higher cosmic ray energies

$$\frac{E\, d^3\sigma}{dp_1 dp_t^2} = g(x_s, p_t) = f(x(s/s_0)^{\alpha/2}, p_t)\,(s/s_0)^{\alpha/2}, \quad (1)$$

where $x = x(s/s_0)^{\alpha}$, $\alpha = 0.25$.

This assumption leads to some important consequences. In this paper we'll discuss the distribution of secondary multiplicity that follows from the violated Feynman scaling, using a similar method of Koba et al[2].

2. Derivation of multiplicity distribution in the case of breaked Feynman scaling. The distribution of secondary particles in high energy hadron interactions is an object from the first to the recent observations with accelerator facilities. On the other hand, assuming Feynman scaling it was theoretically derived by Koba et al[2] that asymptotically $\sigma_n(s)$ is only a function of $n/\bar{n}$

$$P_n(s) = \sigma_n(s)/\sigma_{tot}(s) = \frac{1}{\bar{n}}\Psi(n/\bar{n}), \quad (2)$$

where $\sigma_n(s)$ is the cross section for multiplicity being n at CMS energy $\sqrt{s}$, $\bar{n}$ is the average multiplicity and $\Psi(z)$ is independent function of $\sqrt{s}$ except through the variable $z = n/\bar{n}$. The shape of the multiplicity distribution has been obtained in a variety of models with rather different theoretical inputs (uncorrelated cluster model [3], geometrical models [4], quark parton model and dual parton models [6,7]. The theoretical predictions for multiplicity distribution have been found to be approximately true from $\sqrt{s} = 1.5$ Gev up to ISR energy $\sqrt{s} = 63$ Gev [8] where violation of Feynman scaling was observed. When studing the multiplicity distribution at the collider region at $\sqrt{s} = 540$ Gev the KNO scaling does not necessarily holds for part of the phase space corresponding to higher multiplicities [9]. There is a clear indication of an increa-

ORIGINAL PAGE IS
OF POOR QUALITY

sing high multiplicity tail. It causes that many of the original models have been amended to accomodate the observed scaling violation [10] by assuming that between the collider and ISR energies some new physical mechanism (rescattering [11], three gluon coupling [12] characterized by higher multiplicity started becoming important. We will examine what follows from breaking of Feynman scaling. Let us assume scaling on x_1 for the distribution functions integrated over the transverse momentum

$$\tilde{g}^{(q)}(x_{a1},\dots,x_{aq}) = \int g^{(q)}(x_{a1},p_{t1},\dots,x_{aq},p_{tq})\, dp_{t1}^2 \dots dp_{tq}^2 =$$

$$= \left(\frac{s}{s_0}\right)^{\alpha} \tilde{f}\left(x_1\left(\frac{s}{s_0}\right)^{\alpha},\dots,x_q\left(\frac{s}{s_0}\right)^{\alpha}\right) . \qquad (3)$$

There is needed only that the transverse momentum is limited as $\sqrt{s}$ goes to infinity. In eq.3 are used functions which incorporate a particular semi-inclusive cross sections. We can derive the moments of multiplicity distribution in an analogical way to that of Kobe et al [27]. Thus, for secondaries with rest mass m we set

$$\langle n(n-1)\dots(n-q+1)\rangle = \sum_n P_n(s)\, n(n-1)\dots(n-q+1) =$$

$$= \int g^{(q)}(x_{a1},p_{t1},\dots,x_{aq},p_{tq}) \frac{dx_{a1}\, dp_{t1}^2}{\sqrt{x_{a1}^2 + \frac{p_{t1}^2+m^2}{(s/4)^{1-\alpha}}}} \dots \frac{dx_{aq}\, dp_{tq}^2}{\sqrt{x_{aq}^2 + \frac{p_{tq}^2+m^2}{(s/4)^{1-\alpha}}}} =$$

$$= 2\int\left\{\left[g^{(q)}(x_{a1},p_{t1},\dots,x_{aq},p_{tq}) \cdot \ln\left(x_{a1} + \sqrt{x_{a1}^2 + \frac{p_{t1}^2+m^2}{(s/4)^{1-\alpha}}}\right)\right]_0^{\frac{\sqrt{s}}{2}}{}^{\alpha} -\right.$$

$$- \int dx_{a1}\, \frac{\partial}{\partial x_{a1}}\, g^{(q)}(x_{a1},p_{t1},\dots,x_{aq},p_{tq}) \cdot \ln\left(x_{a1} + \sqrt{x_{a1}^2 + \frac{p_{t1}^2+m^2}{(s/4)^{1-\alpha}}}\right) \times$$

$$\times\, d^2p_{t1} \frac{dx_{a2}\, dp_{t2}^2}{\sqrt{x_{a2}^2 + \frac{p_{t2}^2+m^2}{(s/4)^{1-\alpha}}}} \dots \frac{dx_{aq}\, dp_{tq}^2}{\sqrt{x_{aq}^2 + \frac{p_{tq}^2+m^2}{(s/4)^{1-\alpha}}}} =$$

$$= \int \ln\frac{(s/4)^{1-\alpha}}{(p_{t1}^2+m^2)} \left[g^{(q)}(0,p_{t1},x_{a2},p_{t2},\dots,x_{aq},p_{tq}) + \frac{W}{\ln\frac{(s/4)^{1-\alpha}}{(p_{t1}^2+m^2)}} \right] d^2p_{t1}$$

$$\times \frac{dx_{a2}\, d^2p_{t2}}{\sqrt{x_{a2}^2 + \frac{p_{t2}^2+m^2}{(s/4)^{1-\alpha}}}} \dots \frac{dx_{aq}\, d^2p_{tq}}{\sqrt{x_{aq}^2 + \frac{p_{tq}^2+m^2}{(s/4)^{1-\alpha}}}} \qquad (4)$$

where the integral $W = \int dx_{a1} \frac{\partial}{\partial x_{a1}} g^{(q)}(x_{a1},p_{t1},\dots,x_{aq},p_{tq}) \ln\left(x_{a1} + \sqrt{x_{a1}^2 + \frac{p_{t1}^2+m^2}{(s/4)^{1-\alpha}}}\right)$ converges. After integration of eq.4 we obtain

ORIGINAL PAGE IS
OF POOR QUALITY

$$\langle n(n-1)\dots(n-q+1)\rangle = \int \ln^{\frac{(s/4)^{1-\alpha}}{p_{t1}^2+m^2}} \dots \ln^{\frac{(s/4)^{1-\alpha}}{p_{tq}^2+m^2}} \left[g^{(q)}(0,p_{t1},\dots 0,p_{tq}) + O\left(\frac{1}{\ln s^{1-\alpha}}\right)\right] dp_{t1}^2 \dots dp_{tq}^2 = \tilde{g}^{(q)}(0,\dots,0)(\ln s^{1-\alpha})^q + O((\ln s^{1-\alpha})^{q-1}),$$

where $O((\ln s^{1-\alpha})^{q-1})$ means terms that at most go like $(\ln s^{1-\alpha})^{q-1}$. Consequently the same asymptotic behaviour has not only the mean value of any q-order polynomial of n but the mean value of n as well. Taking into account eq.3 we can set

$$\int_0^\infty n^q . P_n(s) . dn = \left(\sqrt{\frac{s}{s_0}}\right)^q \tilde{f}^{(q)}(0,\dots,0)\ (\ln s^{1-\alpha})^q + O(\ln s^{1-\alpha})^{q-1}) \ . \qquad (5)$$

Dividing eq.5 by $\left(\sqrt{\frac{s}{s_0}}\right)^\alpha (\ln s^{1-\alpha})^q \left[\tilde{f}^{(1)}(0)\right]^q$ we obtain

$$\int_0^\infty z^q . P_{z(n)}(s) . \left(\tilde{f}^{(1)}(0)\left(\sqrt{\frac{s}{s_0}}\right)^\alpha \ln s^{1-\alpha}\right)^q . dz = \frac{\tilde{f}^{(q)}(0,\dots,0)}{\left[\tilde{f}^{(1)}(0)\right]^q} + O\left(\frac{1}{\sqrt{s}^\alpha \ln s^{1-\alpha}}\right), \qquad (6)$$

where

$$z = \frac{n}{\tilde{f}^{(1)}(0)\left(\sqrt{\frac{s}{s_0}}\right)^\alpha \ln s^{1-\alpha}} \ . \qquad (7)$$

We assume that the function

$$\tilde{f}^{(1)}(0)\left(\sqrt{\frac{s}{s_0}}\right)^\alpha \ln s^{1-\alpha} P_{z(n)}(s) = \Psi(z) + O\left(\frac{1}{\sqrt{s}^\alpha \ln s^{1-\alpha}}\right)$$

is determined uniquely by the moments (5). Thus, to the highest order in $\sqrt{s}^\alpha \ln s^{1-\alpha}$ we have the following breaked scaling result

$$P_n(s) = \frac{1}{\langle n\rangle} \Psi(z) + O\left(\frac{1}{\langle n\rangle^2}\right) \ , \qquad (8)$$

where the mean multiplicity as function of $\sqrt{s}$ is

$$\langle n\rangle = \tilde{f}^{(1)}(0)\left(\sqrt{\frac{s}{s_0}}\right)^\alpha \ln s^{1-\alpha} \ . \qquad (9)$$

<u>3. Comparison of the breaked Feynman scaling results for the multiplicity distribution with experimental data in accelerator energy range.</u> In figure 1 we have compared the multiplicity distribution function specified by the semi-inclusive cross sections from FNAL which are published in the paper of Kafka et al[14] for multipartical production up to above two times larger than the mean value of multiplicity. It is seen that the distribution of relative multiplicity scales at least for the range of not very large multiplicities which are responsible for the typical events in cosmic ray experiments.

As far as the average multiplicity is concerned the assumption for breaking of Feynman scaling gives a good agreement with the acceleration observations in wide energy range up to 10^5Gev. The energy dependence of mean multiplicity according eq.9 is compared in figure 2 with accelerator data taken from Carlson[15].

N85-35815

ORIGINAL PAGE IS
OF POOR QUALITY

HE 1.2 - 15

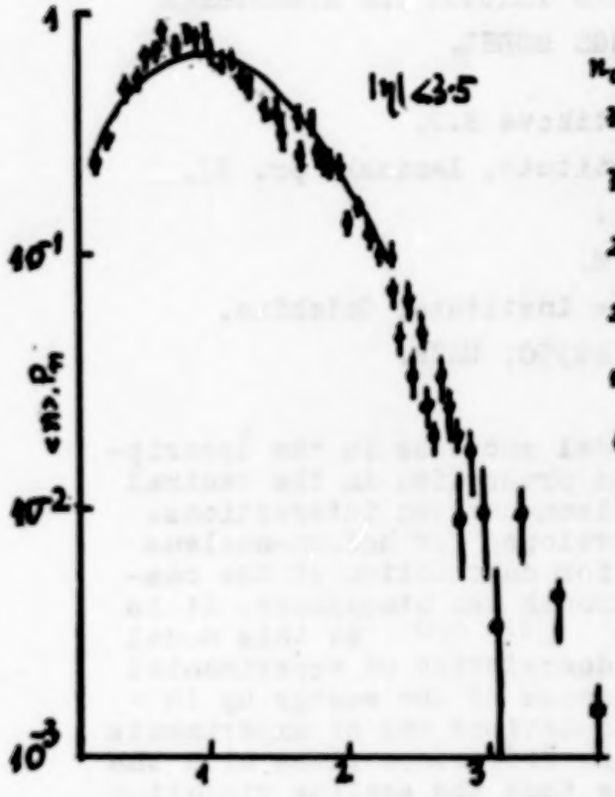


Fig.1 Comparison of our parametrisation of the multiplicity distribution (made on the basis of FNAL data) with SPS data for $|\eta| < 3.5$. The latter are representative of the shape of the full distribution.

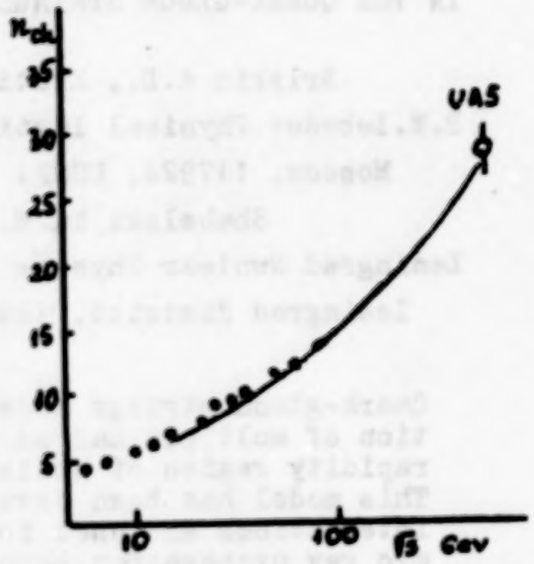


Fig.2 Energy dependence of the mean multiplicity of charged secondaries. Experimental data are taken from[16], the full line is after eq.9 .

We can conclude that for the purposes of cosmic ray investigation scaling of multiplicity distribution derived from breaked Feynman scaling can be assumed in order to prescribe the semi-inclusive cross sections at very high energies.

References

1. Wdowczyk J. and Wolfendale A. Nuovo Cimento 54,A,4,433,1979
2. Koba Z., Nielsen H.B. and Olesen P. Nucl.Phys. B40,317,1972
3. DeGroot E.H. Phys. Lett. 57B, 159,1975
4. Chou T.T. and Yang C.N. Phys. Lett. 116B,301,1982
5. Takagi F. Zeit.fur Phys. C13,301,1982
6. Kaidalov A.B. and Ter-Martirosyan K.A. Phys.Lett. 117B,247,1982
7. Capella A. and J.Tran Thanh Van,Phys.Lett.114B,450,1982
8. Thome W. et al. Nucl.Phys. B129,365,1977
9. Alner G.J. et al. Phys. Lett. 138B,305,1984
10. Pancheri G. Invited Talk XV Symp.Multipart.Dyn.Lund,1984
11. Capella A. and J.Tran Thanh Van,Orsay reprint LPTHE 83/39,1983
12. Pancheri G. and Srivastava Y.N. Frascati Preprint 1984
13. Cai Xu and Liu Lian-sou, Lettere al Nuovo Cimento 37,495,1983
14. Kafka T. et alPhys.Rev.D16,5,1261,1977
15. Per Carlson XI Intern.Winter Meet.on Fundamental Phys.,Toledo,83

N85-35873
HE 1.2-16

PROPAGATION OF COSMIC RAYS THROUGH THE ATMOSPHERE IN THE QUARK-GLUON STRINGS MODEL.

Erlykin A.D., Krutikova M.P.
P.N.Lebedev Physical Institute, Leninski pr. 53,
Moscow, 117924, USSR.
Shabelski Yu.M.
Leningrad Nuclear Physics Institute, Gatchina,
Leningrad district, 188350, USSR.

Quark-gluon strings model succeeds in the description of multiple hadron production in the central rapidity region of nucleon-nucleon interactions. This model has been developed for hadron-nucleus interactions and used for calculation of the cosmic ray propagation through the atmosphere. It is shown that at energies $10^{11} - 10^{12}$ eV this model gives a satisfactory description of experimental data. But with the increase of the energy up to ~ 10^{14} eV results of calculations and of experiments begin to differ and this difference rises with the energy. It may indicate that the scaling violation in the fragmentation region of inclusive spectra for hadron-nucleus interactions is stronger than in the quark-gluon strings model.

Quark-gluon strings model (QGSM) describes successfully rather wide set of experimental data on the multiple hadron production in nucleon-nucleon collisions /1,2/. One of us (Yu.M.Sh.) developed this model for hadron-nucleus interactions. The weak scaling violation typical for that model becomes stronger after the transition from hp to hA collisions. In the fig.1 inclusive spectra of charged pions are shown. They were calculated according to QGSM with a magnitude of pomeron intercept $\Delta = 0.14$ for pN^{14}-collisions at energies 10^{11} and 10^{16} eV. It is seen that spectra become considerably softer in this energy range. For instance pion spectra at x=0.5 fall down by the factor 2,17. This model was used to calculate the penetration of cosmic rays through the atmosphere. The calculation routine was worked

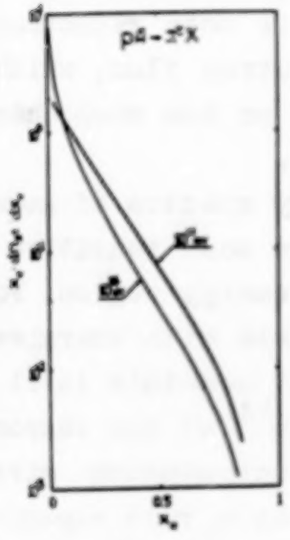


Fig.1.

out and used in papers /3,4/. Figures 2,3,4 demonstrate results of calculations compared with experimental data on energy spectra of muons at sea level, hadrons and gamma-quanta at different levels in the atmosphere. Energy spectrum and the mass composition of primaries were taken on the base of direct measurments at energies 10^{11}-10^{13} eV and small EAS data at energies 10^{13}-10^{15} eV /5/. These spectrum and the mass composition may be presented as

$$I(>E)=8.04\cdot10^{-4}(E/0.1)^{-1.70}\left[B_p\cdot(1+6\cdot10^{-4}\cdot E)^{-0.4} + \sum_A B_A(E/0.1)^{\Delta\gamma_A}(1+10^{-2}A^{-1}E)^{-0.4}\right] \text{ cm}^{-2}\text{sec}^{-1}\text{ster}^{-1} \quad (1)$$

where E - in TeV, B_p=0.41, B_4=0.22, B_{15}=0.13, B_{27}=0.14, B_{56}=0.10, $\Delta\gamma_4$ =0, $\Delta\gamma_{15} = \Delta\gamma_{27} = \Delta\gamma_{56}$ =0,04.

From the comparison of calculated and observed energy spectra of muons and hadrons at mountain level, which were measured by the most precise calorimetric method (fig.2,3), from similar comparison of mass and charge ratios of hadrons (data are not presented here due to the lack of space) one can conclude that QGSM gives a satisfactory agreement with experimental data at energies 10^{11}-10^{12} eV. Perhaps the only desirable improvement of this model at accelerator

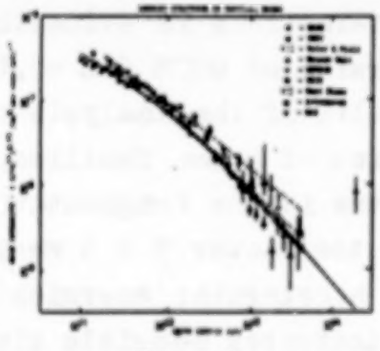


Fig. 2.

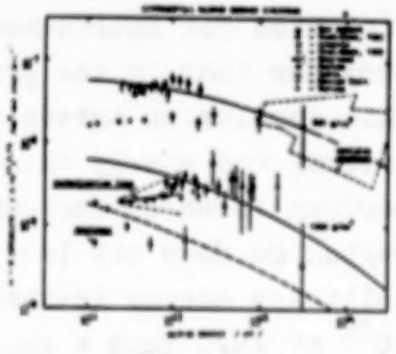


Fig. 3.

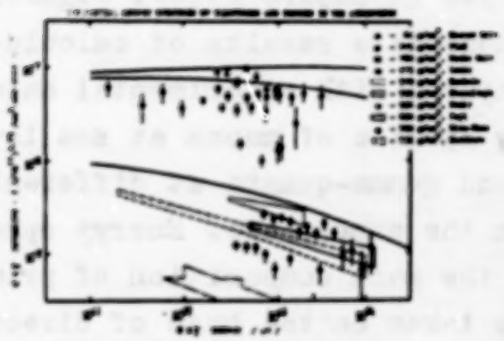


Fig.4. a)

energies is some reduction of the neutron flux, which influence on the muon charge ratio too.

Energy spectra of gamma-quanta are most sensitive to the high energy region. For gamma-quanta with energies 10^{13} eV at mountain level primary particles with energies above 10^{14} eV are responsible. It is seen in the figure 4 that calculation gives gamma-quanta intensities which exceed as a rule experimental values. This excess at mountain level is about the factor of 1.5. Uncertainties in the primary energy spectrum and mass composition could hardly explain the difference between calculations and experiments, since the spectrum (1) has the intensity at $\sim 10^{15}$ eV, which is at the lower end of the existing uncertainty. For example, spectra proposed by Nikolsky /6/ and by Maryland group /7/ give by $\sim$ 1.4 higher intensities at this energy. It is not possible to vary the mass composition too, not coming to a contradiction with experimental data /8/. It is known that energy spectra of muons and gamma-quanta are most sensitive to the scaling violation in the fragmentation region of pion and kaon inclusive spectra. The observed excess of calculated intensities above experimental ones, the latter being stable in the future, indicates that the scaling violation for hadron-nucleus interactions is evidently stronger than in the present version of QGSM ($\Delta = 0,14$). This conclusion agrees with results of the analysis of lateral and energy characteristics of gamma families, according to which inclusive spectra in the fragmentation region go down not less than by the factor $3 \div 5$ when the collision energy increases from accelerator energies to 10^{16} eV /9/. Such a conclusion indicates possible direc-

tions of further improvement of this model at high energies.

References.

1.Kaidalov A.B. Phys.Lett 116B,459,1982.
2.Kaidalov A.B., Ter-Martirosyan K.A. Phys.Lett.117B,247, 1982; Yad.Fiz.39,1545,1984;40,211,1984.
3.Erlykin A.D.,Kuzina N.P. 17 ICRC,Paris,1981,5,243.
4.Adamov D.S. et al. 18 ICRC, Bangalore,1983,5,275.
5.Danilova T.V. et al. VANT,3/20/,20,1984 (in Russian).
6.Nikolsky S.I. Workshops on cosmic ray interactions and high energy results, La-Paz-Rio de Janeiro,July 1982,336. JETP,87,18,1984 (in Russian).
7.Cowsik R. et al. 17 ICRC, Paris,1981,2,120.
8.Stamenov J.N. et al. 18 ICRC, Bangalore,1983,2,111.
9."Pamir" coll. 18 ICRC,Bangalore,1983,5,425.

*) Upper full curve in the Fig.4 corresponds to calculations for the depth 60 g/cm^2, middle one - for 260 g/cm^2 and the lower one - for 600 g/cm^2.

N85-35874

HE 1.2-17

SCALING VIOLATION IN THE FRAGMENTATION REGION OF INCLUSIVE NUCLEON SPEKTRUM

S.K. Machavariani, S.I. Nikolsky, A.P. Chubenko

P.N.Lebedev Physical Institute

Moscow, USSR

Spectra of EAS associated with hadrons of various energies from 5 to 80 Tev have been investigated. Results could be interpreted as scaling vaiolation in the fragmentation region of secondary particles generated in inelastic interactions of primary protons at the energy above 30 TeV.

Simultaneous observation of high energy hadron and EAS let us investigate inclusive spectra of hadrons in the fragmentation region.

Significant part of hadron flux in the atmosphere are nucleons. The connection between the nucleon flux at the depth and the spectrum of primary nucleons is

$$F(>E,t)=\sum_{n=0}^{\infty} F(>E_o)e^{-t}(t^n/n!)\, x^{\gamma-1}$$

where γ - the index of the primary spectrum, $x=E/E_o$, t- the observation depth in units of mean free path for inelastic collisions. It should be noted that events with $n \leq 3$ at the depth of 700g/cm^2 dominate. Qualitive experimental picture is not changed considerably if one takes into account the energy dependent cross-section of hadron interaction as well as the inclusive spectrum of secondary hadrons.

The table shows the percentage of the primary protons which had only one inelastic collision at 700g/cm^2. The calculation was made with the accelerator cross-sections and inclusive spectra.

x	0.9	0.82	0.67	0.54	0.44	0.36	0.3
n=1	100	70	60	55	50	40	35

If we add to mention above that at $x \geq 0.3$ all observed hadrons are produced by primary protons then it is clear that analysis of hadron data and EAS accampanying them give us good oppotunity to investigate hadron inclusive spectra in the fragmentation part.

In this paper the total EAS spectrum of accompanying hadrons of given energy is considered.

It appears that for scaling model and constant mass composition of primaries the investigated spectrum of EAS for various E_o must be similar or must have scaling behaviar.

The experimental data of Tien-Shan complex installation /1/ on the spectrum of EAS associated with hadrons for energy intervales (5-7.5), (10-20) and (40-80) TeV are presen-

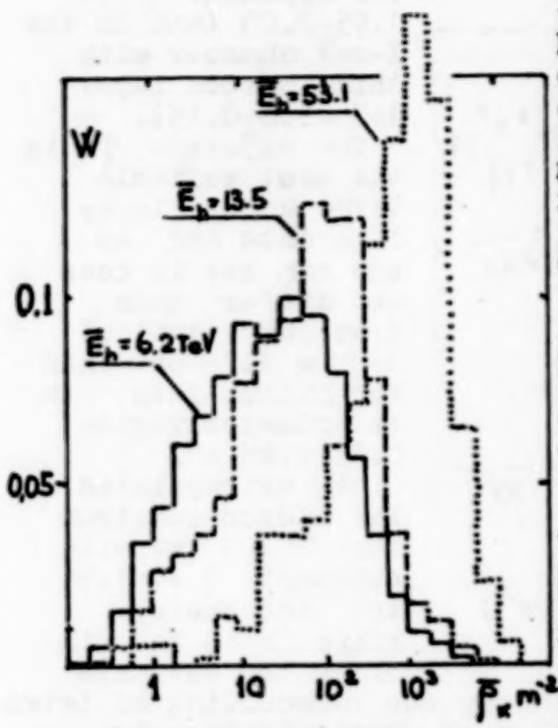


Fig.1 Spectra of EAS associated with hadrons of various energy (exper.) ρ_k-average density of particles in the centre $N_e = \rho_k \cdot 10^3$, $E_0 = 3 \cdot \rho_k$ TeV.

ted at fig.1. Separation of hadrons and measurement of its energy have been made by means of ionization calorimeter. The space resolution of the calorimeter is about 0.25x0.25m^2, that is why the hadron jet may consist of several hadrons. Our experimental data are related to the most energetic hadron jets in the calorimeter which occupy less than 0.75x0.75 m^2. We calculate the distribution of EAS for the average density of particles in the array which consists of 64 scintillator detectors and cover the area about 100 m^2 (ρ_k). The density of particles in the EAS centre has large fluctuations but it does not require knowledge of the lateral distribution of particles for E_0 estimation.

One can see that the experimental ρ_k distributions for various $\bar{E}_h$ presented in fig.1 have not the scaling character. The most probable value of ρ_k is not proportional to E_h ($\rho_k \sim E_h^{3/4}$) and the ρ_k distribution becoms narrower with increasing E_h. We can suggest three following reasons for this result:

1. Sistematic errors in the experiment.
2. Mass composition of primary cosmic rays is not constant.
3. The scaling violation in the fragmentation region of secondary hadrons.

The methodical effect can be evaluated by the following way. The fig.2 shows the fluxes of recorded hadron jets. In the first case the energy was obtained in the calorimeter over the square at 0.75xo.75 m^2 and in the second - the energy was determined over the square of 0.25x0.25 m^2 and multiplied by 1.5. The coefficient 1.5 was estimated from data on the lateral energy distribution for single hadron. The index of the hadron jet spectrum in the first case is $1+\gamma = 1.6$ for larger square and $1+\gamma = 1.75$ in the second case.

The results of our measurements of the total hadron jet flux in the energy range (200-2000) GeV /2/ are also shown in fig.2. The lack of calorimeter resolution doesn't effect intensities at these energies. It seems that our value for intensity is close to calculated one /2/ as well as to data /3/ obtained with spark chamber calorimeter. The power low fit for the data on hadron flux obtained with the help of X-ray film chamber /4/ in the energy range (20-500) TeV has

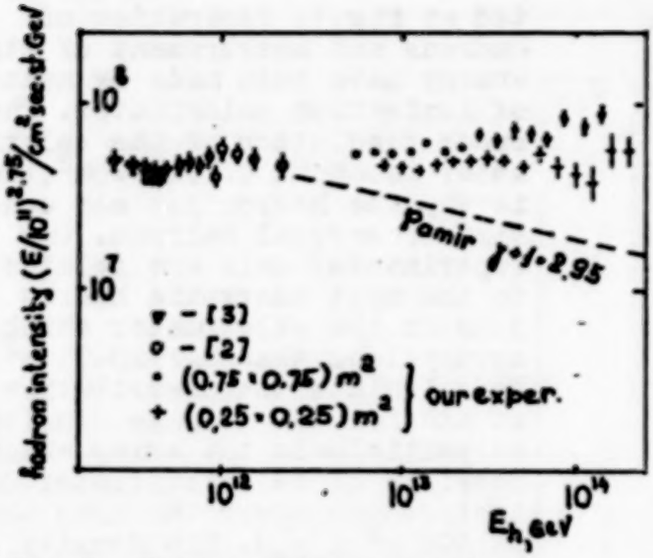


Fig.2 Hadron energy spectrum at mountains (H=700 g/cm^2)

the exponent $\gamma+1=1.95\pm0.05$ (and in the X-ray chamber with thick carbon layer $1+\gamma=1.8\pm0.15$).

The exponent γ is the most reliable value among X-ray film data and as one can see it does not differ much from our value of $1+\gamma = 1.75$ obtained for hadron jets in calorimeter region 0.25×0.25 m^2.

We extrapolated the hadron spectrum for $E \leq 1$ TeV with exponent $\gamma+1=1.95$ to the energy range $E>5$ TeV in order to estimate the error in determining the energy due to recording of jets. At the energy $E\sim5$ TeV the value of overestimation is about 1.25 and at E=100 TaV ~1.5. The spectrum of EAS associated with hadron may be distorted due to different overestimation of the hadron energy but the difference is not more than 20% for energy changing from 5 TeV to 100 TeV. Therefor we can neglect this methodical effect.

The distortion of experimental spectrum may be due to primary nuclei. In this case the leteral combination of nucleons into jets increases the number of observed events with the same energy per nucleon becaus the energy losses of the leading nucleon are compensated by another nucleons of the primary nucleus. This ability will be studied.

We have simulated only two possibilites. We assumed the model of hadron nucleus interection /5/ based on accelerator data. In the first vertion of calculation we proposed that the index of primary energy spectrum changes from $\gamma+1=2.6$ to $\gamma+1=3.6$ at the primary proton energy $E_0=10\cdot E_h$, were E_h is the energy of hadrons (histogram 2 in fig. 3). In the second version we suggested the reduction of the inclusive cross-section for the production of secondary nucleons with $X \geq 0.5$ by the factor 2 at the expense of increasing number of nucleons and pions with $x \leq 0.3$.

As one can see in fig.3 (histogram 3) the second version is in better agreement with the experiment than the first one which assumes the change of primary composition.

N85-35875

ORIGINAL PAGE IS
OF POOR QUALITY

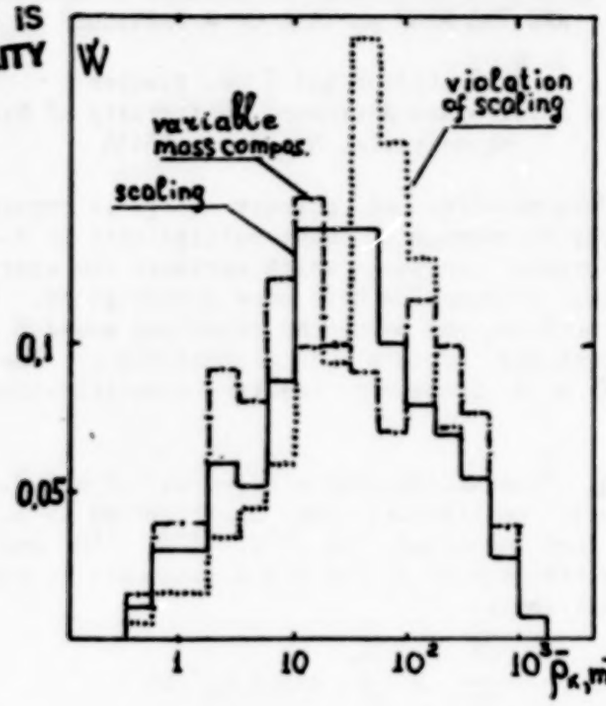


Fig.3 Spectra of EAS associated with hadrons (simulation).

Our conclusion about scaling violation in the fragmentation region of inclusive nucleon spectrum is not quite well-grounded. More detaled analises of experimental data, especially at $x \geq 0,3$ (pure proton region), and comparison with model simulation are necessary.

References

1. Amineva T.P., (1970), TRUDY FIAN, 46, 157
2. Adamov D.S.,et al, (1983), 18 ICRC,Bangalore, 5, 275.
3. Shmeleva A.P. et al (1983), 18 ICRC,Bangalore, 5,271.
4. "Pamir" coll., (1984), TRUDY FIAN, 154.

N85-35875
HE 1.3-1

DETERMINATION OF PRIMARY ENERGY IN NUCLEUS-NUCLEUS COLLISIONS AND THE HIGH p_T TAIL OF α-PARTICLES

P. S. Freier and T. W. Atwater
School of Physics and Astronomy, University of Minnesota
Minneapolis, Minnesota 55455

Abstract. A determination of primary energy is required in order to study the energy dependence of meson multiplicity in A-A collisions in cosmic rays. Various procedures which estimate the energy of a primary nucleus from its interaction have been investigated. We have used an average of two methods, one using the pions and wounded protons and the other using spectator protons and α-particles. The high p_T tail observed for Z = 2 fragments requires a modification of the latter method.

1. Introduction. From accelerator studies of 1.7 and 3.7 GeV/amu of A-emulsion inelastic collisions, the distribution in p_T for projectile fragments has been measured for ^{12}C, ^{14}N, ^{16}O and ^{56}Fe beams.[1-4] Although the distribution in p_T for Z = 1 fragments is consistent with a Gaussian-like distribution

$$\frac{dN}{dp_T} = \frac{p_T}{\sigma^2} \exp(-p_T^2/2\sigma^2) \qquad (1)$$

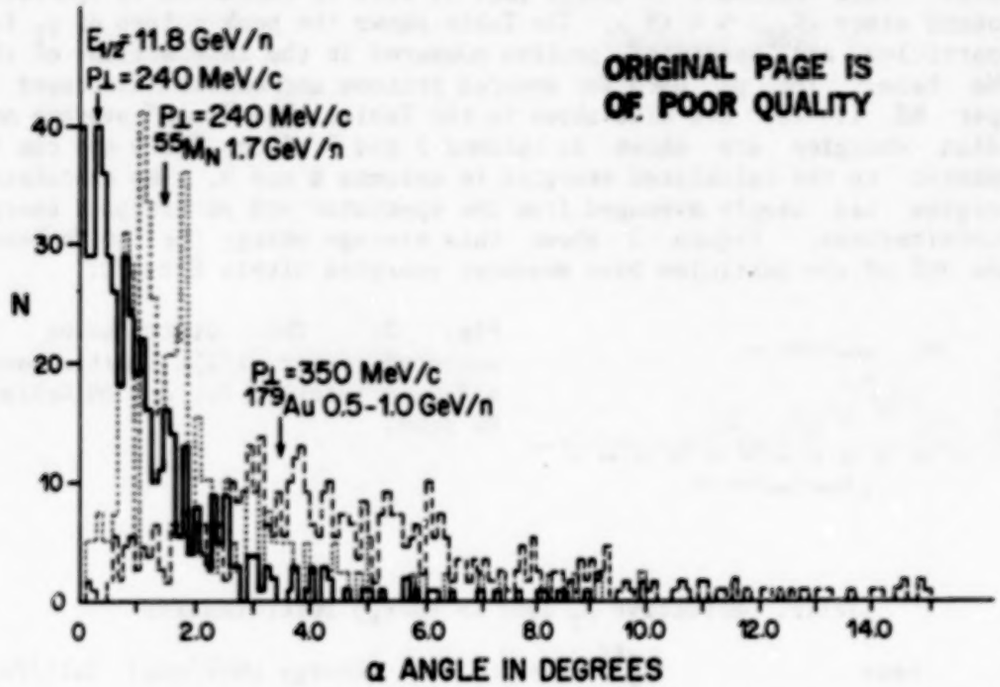
with σ = 100 MeV/c ($\langle p_T \rangle$ = 125 MeV/c),[3] for fragments of Z ≥ 2 there is a marked deviation from this shape due to the presence of a tail of large momentum transfers. This high p_T tail results in $\langle p_T \rangle$ being significantly larger than the $\langle p_T \rangle$ expected from eq. (1). For Z = 2 fragments from ^{12}C, $\langle p_T \rangle$ = 241±8 MeV/c,[1] and from ^{56}Fe, $\langle p_T \rangle$ = 370±10 MeV/c.[3] $\langle p_T \rangle$ seems to depend only weakly on target A, ($\sim A^{0.15}$) but the dependence on projectile A is more pronounced ($\sim A^{0.25}$).[3] This increase in $\langle p_T \rangle$ is mainly due to the enhancement of the high p_T tail with A_p of the projectile. We shall show that the high p_T tail is also enhanced as the energy of the projectile is increased.

2. Measurements on Beam Projectiles. We have analyzed 105 ^{55}Mn-emulsion interactions at $\langle E \rangle$ = 1.69±0.3 GeV/amu, measuring the emission angles of fragments, α-particles, protons, and mesons. The angular distribution of α-particles is shown in Fig. 1. The transverse momentum, p_T, is calculated from the angle assuming ^4He is emitted at the same momentum per nucleon, p_o, as the projectile had at the interaction:

$$p_T = 4\, p_o \sin\theta \qquad (2)$$

The peak in the angular distribution corresponds to p_T (peak) = 240 MeV/c, while $\langle p_T \rangle$ = 356±20 MeV/c. This $\langle p_T \rangle$ value agrees very well with the value 370±10 MeV/c measured by Chernov et al.[3] for α-particles from ^{56}Fe at 1.7 GeV/amu.

The emission angles of α-particles from ^{179}Au-emulsion interactions at 0.5 - 1.0 GeV/amu are also shown in Fig. 1. (The energy at each interaction was calculated by correcting for ionization loss of the



ORIGINAL PAGE IS
OF POOR QUALITY

Fig. 1. Angular distributions of α-particles from A-emulsion interactions. ····· Mn at 1.7 GeV/amu; --- Au at 0.5-1.0 GeV/amu; —— cosmic rays, $Z = 6$-26 at $E \geq 7.5$, $E_{1/2} = 11.8$ GeV/amu. The arrows show the angles corresponding to the measured p_T(peak) for Mn and Au and to p_T(peak) = 240 MeV/c at the median energy for cosmic rays.

projectile.) There is a marked shift of the angular distribution to larger angles due both to the lower primary energy but also to an increase in p_T(peak) and an enhanced tail of high momentum transfers. The peak corresponds to $p_T = 350$ MeV/c but $\langle p_T \rangle = 520$ MeV/c.

We have used the angles of emitted mesons, protons, and α-particles from ^{55}Mn-emulsion interactions to calculate the energy of the Mn projectile using two different methods: one uses the participant protons (WP) and produced mesons (M), and the second uses the spectator protons (SP) and α-particles. Paper HE 1.4-10 of these proceedings discusses the first method and the separation of spectator and participant protons.[5] This paper discusses the second method and what adjustments are required in applying it to higher energy cosmic ray projectiles.

Providing p_T is approximately independent of energy, we can estimate the primary energy from

$$P_{primary} = \frac{p_{T_{SP}}^{eff} \sum_i^{N_{SP}} \frac{1}{\sin \theta_i} + \frac{1}{4} p_{T_\alpha}^{eff} \sum_i^{N_\alpha} \frac{1}{\sin \theta_i}}{N_{SP} + N_\alpha} \qquad (3)$$

where $P_{primary}$ is the momentum per nucleon and the p_T are effective values of spectator and α-particle transverse momentum given in the

Table. This estimate of energy (eq. 3) will be dominated by spectator protons since $\langle N_{SP} \rangle \sim 4 \langle N_\beta \rangle$. The Table shows the peak values of p_T for α-particles and spectator protons measured in the interactions of the ^{55}Mn beam. The p_T used for wounded protons and mesons (discussed in Paper HE 1.4-10) are also shown in the Table. The "beam" average and median energies are shown in columns 2 and 3 of the Table and can be compared to the calculated energies in columns 8 and 9. The calculated energies are simply averaged from the spectator and participant energy determinations. Figure 2 shows this average energy for the Mn beam. Some 70% of the particles have measured energies within E ± E/2.

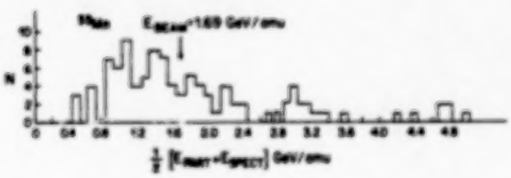


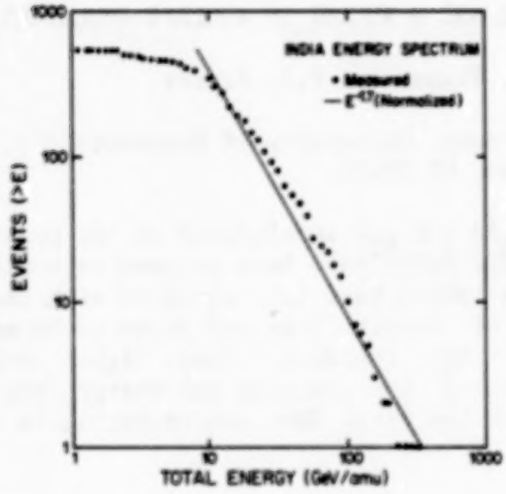
Fig. 2. The distribution in measured energy, 1/2[E (participant) + E (spectator)], for a 1.69 GeV/amu Mn beam.

Table. Effective p_T used in Energy Determination

Beam			p_T^{eff} (MeV/c)				Energy (GeV/amu)		Tail/Peak
$\bar{Z}$	$\langle E \rangle$	$E_{1/2}$	SP	α	WP	M	$\langle E \rangle$	$E_{1/2}$	
25.0	1.69	1.68	101	232	575	175	2.03	1.51	0.020
13.0	5.50	3.00	106	232	438	179	5.67	2.82	0.084
14.5	19.60	11.80	255	680	691	384	19.90	12.40	0.218

<u>3. Energy Measurements on Cosmic Ray Nuclei.</u> Using the same techiques as used for Mn, we determined the energy of each cosmic ray primary from its interaction. For the 1000 nuclei measured over Texas where E ≥ 1.7 GeV/amu, the p_T values determined from the Mn beam gave reasonable measurement of energy (see Table). However, for the 500 nuclei measured over India where E ≥ 7.5 GeV/amu, the energies determined from the spectators using the same values of p_T were far too low. A remeasurement of many of the angles showed they were correct to within ± 0.1°. The observed peak in the α-particle angular distribution is consistent with the beam value p_T(peak) = 240 MeV/c and the median cosmic ray energy, $E_{1/2}$ = 11.8 GeV/amu (see Fig. 1). However, the tail to peak ratio, where the cut is defined as six times the peak angle, is much larger in India (see Table). The result is too many low energy events. (For a higher angle cut there were no particles in the Mn tail; the tail to peak ratio for Au is 0.005.)

The effective p_T for the cosmic rays given in the Table were determined by the requirement that the calculated energies fit the cosmic ray energy spectrum as closely as possible. Figure 3 shows the resulting energy spectrum of the 500 particles measured in India compared to a power law in total energy of $E^{-1.7}$. The energy measured from 1000 particles at Texas (E > 1.7 GeV/amu) fits equally well.



ORIGINAL PAGE IS
OF POOR QUALITY

Fig. 3. The integral energy spectrum measured by $1/2\,[E_{part} + E_{spect}]$ compared to the accepted cosmic ray spectrum, $J > E = kE^{-1.7}$.

4. Conclusions. Calculation of energies of primary cosmic rays using a method assuming constant p_T of fragments fits the known energy spectrum for a low energy data set ($E > 1.7$ GeV/amu). The required effective p_T for cosmic rays > 7.5 GeV/amu are high. The high p_T^{eff} for α-particles can be attributed to the high p_T tail. Since p_T^{eff} for protons must be increased by about the same factor to fit the cosmic ray spectrum, it appears that a high p_T tail must also be present for spectator protons. The high p_T tail increases with energy.

5. Acknowledgements. This work was supported in part by NSF Grant PHY-8405852 and NASA Grant NGR 24-005-050.

References

[1]Bucharest-Warsaw-Dubna-Kosice-Leningrad-Moscow-Tashkent collaboration (1980), Sov. J. Nucl. Phys. 32(5), 716.
[2]Bjarle, C., et al. (1982), Nucl. Phys. A 381, 544.
[3]Chernov, G. M., et al. (1984), Nucl. Phys. A 412, 534.
[4]Bhalla, K. B., et al. (1981), Nucl. Phys. A 367, 446.
[5]Atwater, T. W., et al. (1985), this conf., Paper HE 1.4-10.

ORIGINAL PAGE IS
OF POOR QUALITY

N85-35876

HE 1.3-4

STOPPING RELATIVISTIC Xe, Ho, Au AND U NUCLEI IN NUCLEAR EMULSIONS

C.J. Waddington, D.J. Fixsen and P.S. Freier

School of Physics and Astronomy, University of Minnesota
Minneapolis, MN 55455

Abstract. Nuclei of $_{54}^{}Xe$, $_{67}^{}Ho$, $_{79}^{}Au$ and $_{92}^{}U$ accelerated at the Bevalac to energies between 1200 and 900 MeV/n have been stopped in nuclear emulsions. The observed residual ranges have been compared with those calculated from various models of energy loss and shown to be most consistent with a calculation that includes those higher order correction terms proposed previously to describe the energy loss of highly charged particles, for which the first Born approximation is not valid.

1. Introduction. We have previously reported, Waddington et al. (1983), on the stopping of 200 GeV gold nuclei in nuclear emulsions. Here we describe a new study of the residual ranges of energetic Xe, Ho, Au and U nuclei in nuclear emulsions.

2. Measurements. A single small stack of Ilford G5 nuclear emulsion pellicles, placed so that the pellicles were parallel to the beam, was exposed at the Lawrence Berkeley Laboratory Bevalac to beams of krypton ($^{84}_{36}Kr$), xenon ($^{132}_{54}Xe$), holmium ($^{165}_{67}Ho$), gold ($^{197}_{79}Au$) and uranium ($^{238}_{92}U$) nuclei. These exposures were made over a period of less than a week to nuclei accelerated at maximum rigidity of 5.6 GV and incident on the same edge of the pellicles. Those nuclei which did not interact in the emulsions were, apart from Kr-nuclei, brought to rest in the emulsions by energy loss, thus permitting their residual ranges to be measured. In order to determine the mean ranges of each nuclei species, individual tracks were not followed from the top edge of the emulsions,

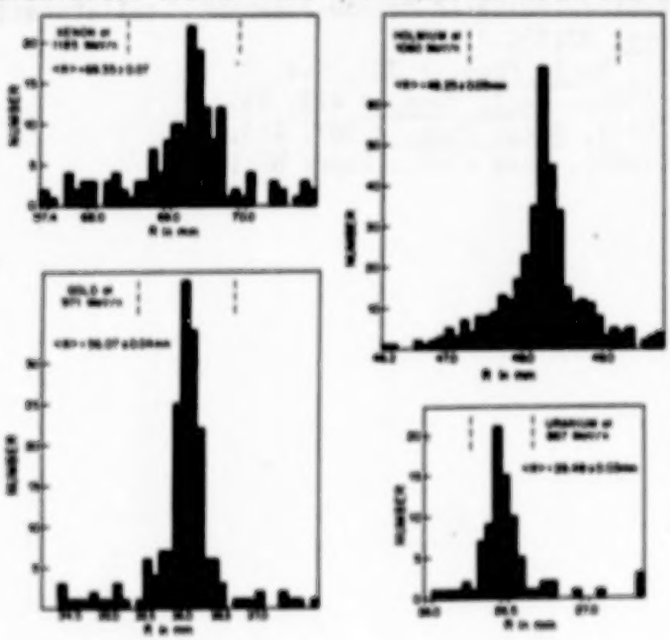


Fig. 1. The residual ranges, R, in mms of nuclear emulsions, measured for each beam. The mean values of range, <R>, are the arithmetic means taken between the values indicated by the dashed lines and the errors are the formal errors in the mean, not those in the width of the distribution.

but were detected by a line scan made a few mms above the estimated depth of stopping for each species. Each track recorded was then followed for a distance that at most would be a few mms beyond the expected stopping point for that species. Tracks of different primary nuclei than the one being studied could be readily eliminated by visual inspection. Hence each sample consisted of a group of primary nuclei with an admixture of fragments produced from interactions occurring above. The resulting range distributions, Fig. 1, show clearly defined peaks, superimposed on a background of secondary fragments. The peaks observed define the mean residual ranges of each species with adequate accuracy, given the uncertainties in the energies.

3. Discussion. Our previous study of Au-nuclei and that of Ahlen and Tarle (1983) on U-nuclei, both showed that there are large deviations in the residual ranges of highly charged nuclei from those calculated using the standard Bethe-Born formalism of energy loss. In order to fit the observations it is necessary to consider terms which are of higher order in Z than the Z^2 terms that result from assuming the validity of the first Born approximation. Instead, it is necessary to include additional terms that take account of the finite size of the projectile nucleus and the electron binding to the target nucleus. Ahlen (1980, 1982) has modified the energy loss expression by including the terms M, B and B_R as follows:

$$\frac{dE}{dx} = \frac{4\pi N Z_m e^4}{mc^2} \frac{Z_p^2}{\beta^2} . J \left[\ln \frac{2mc^2}{I_m} . \frac{\beta^2}{(1-\beta^2)} - \beta^2 - S - D + M - B + B_R \right]$$

Here the effective charge on the projectile, Z_p, is corrected for the effects of energy dependent electron pickup and D is a density correction that is $\simeq 0$ at these moderate energies. J is a correction for distant collision polarization effects. Energy losses calculated only using terms up to and including D we consider as the classical Bethe formalism, Fano (1963), denoted as Bethe + and will compare with the earlier calculation of Barkas (1963, 1973). Successive inclusion of the Mott correction for the finite size of the projectile, M; the Bloch correction for electron binding, B; and the relativistic Bloch corrections for relativistic terms of the electron binding, B_R, lead to a series of further estimates of dE/dx and hence to calculated residual ranges. Ahlen and Tarle (1983) showed that their observations on the range of U nuclei in a mostly copper medium were consistent with the calculated value using all the terms of the modified dE/dx expression. Our results on Au nuclei in nuclear emulsions were slightly more consistent with an expression that disregarded the relativistic Bloch term, unless the parameters assumed to be valid in that term were modified from those used to fit the U data. Whether there was a significant discrepancy between these two results was not clear, and as a consequence we decided to take advantage of the opportunity to study several different nuclei under as uniform conditions as possible.

The energy of each beam was measured by determining the magnetic field needed to guide the beam in a transport line. Similar measurements have been made many times before and checked by time of flight determinations. Provided that the beam is well focused these measurements should be reliable to ±3 MeV/n. In this case these

exposures were made during a calibration of the HEAO C3 UH-nuclei satellite detector, Binns et al. (1981), and an image of the beam spot was available in real time as output from a thin multi-wire proportional counter. Except for the U-beam a well-focused spot was obtained in every case and the energies should be reliable. For Uranium there were clearly multiple charge states present in the beam and the energy estimate is based on the assumption that the state with both K-shell electrons attached was dominant in the beam transport line. The Table shows the assigned energies for each beam.

Table of Energies and Ranges

Nuclei	$E_{measured}$	ΔE	E_{enter}	$R_{measured}$
	Mev per nucleon			mms
$^{132}_{54}Xe$	1239 ± 4	54	1185	69.35 ± 0.30
$^{165}_{67}Ho$	1128 ± 3	68	1060	48.25 ± 0.17
$^{197}_{79}Au$	999 ± 3	27.5	971.5	36.07 ± 0.17
$^{238}_{92}U$	899.4 ± 3	32.4	867	26.48 ± 0.08

The emulsions were exposed to particles after they had traversed the vacuum window, an air path and the light tight window in front of the emulsions. The MWPC counter used to examine the footprint of the beam was removed after defocusing to ensure a uniform exposure, but for the Xe and Ho exposures a scintillation counter was also present in the beam. The energy loss in these materials, ΔE, has been calculated from the full expressions for dE/dx, using all terms, for each Z and initial energy.

The charge or energy dependencies of these higher correction terms, M, B, and B_R are not obvious by inspection and indeed are not simple. We have calculated dE/dx and hence residual ranges, R, using the same assumptions as in our previous report. It is found that in every case the Bethe + terms lead to the lowest value of dE/dx, which would imply the largest range, and that the Mott correction alone leads to the highest dE/dx. Application of the Bloch and rel Bloch corrections gives intermediate values of dE/dx but reverse in magnitude as Z increases.

Integration of these dE/dx curves allow us to calculate the residual ranges. In practice these integrations have only been carried down to a residual energy of 10 MeV/n and a very small correction made for the additional range. These calculated ranges have been compared with those predicted from the proton ranges in nuclear emulsions determined by Barkas, scaled by A/Z^2. The ratios of $R_i/R(Barkas)$ are shown in Fig. 2 for each beam at the appropriate energy, Table. This figure shows that as Z increases the Bethe + expression deviates from the scaled proton range, being some 3% too high at U. All three of the higher order correction terms give ranges less than those predicted from Barkas, and, as suggested by the behavior of dE/dx, the Bloch and relativistic Bloch corrections interchange between Au and U. The experimental observations are in all four cases in good agreement with those predicted by including all terms, including the relativistic Bloch

ORIGINAL PAGE IS
OF POOR QUALITY

term. This result is not entirely consistent with our previous Au result, which was more consistent with the predictions that did not include the relativistic Bloch term. The magnitude of the correction

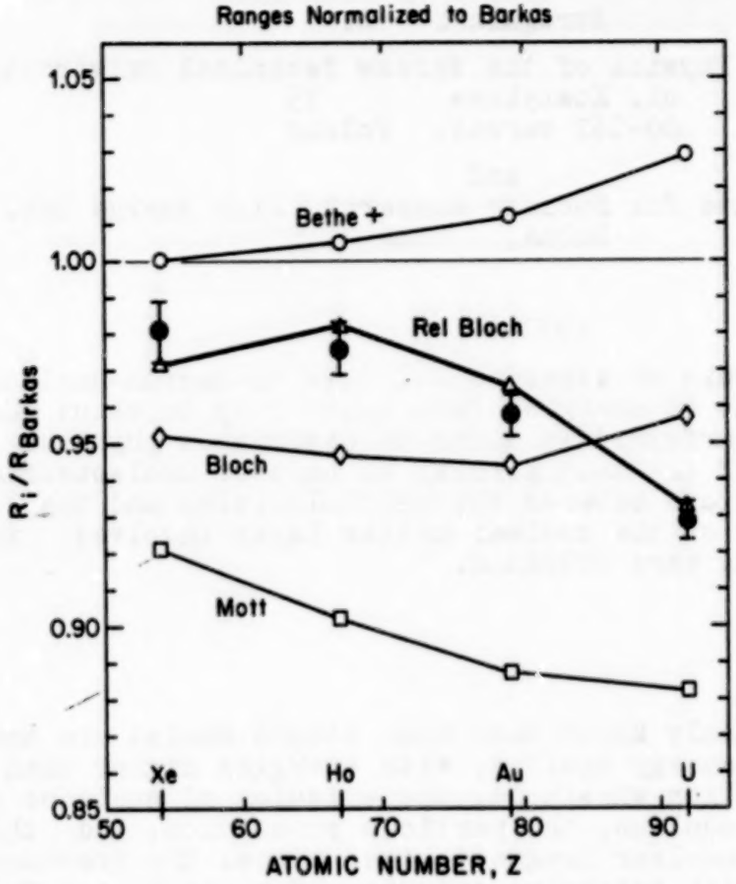


Fig. 2. Ranges normalized to those of Barkas (1973). Values calculated from the dE/dx equation are shown as open symbols, those from the measured ranges as solid with error bars.

that it is necessary to apply to the Barkas ranges steadily increases with increasing Z, reaching some 7% for U. However, it should be remembered that these four measurements are all at different energies and the corrections suggested by Fig. 2 do not truly represent solely the Z dependence of the corrections.

4. Acknowledgements. This work was partially supported by NASA Grants NGR 24-005-050 and NAG8-500 and by NSF Grant PHY-8405852.

References

Ahlen, S.P., and Tarle, G. (1983), Phys. Rev. Lett., **50**, 1110.
Ahlen, S.P. (1980), Rev. Mod. Phys., 52, 121.
Ahlen, S.P. (1982), Phys. Rev. A, 25, 1856.
Barkas, W.H. (1963, 1973), Nuclear Research Emulsions, **Vol. I and II**, Academic Press, N.Y.
Binns, W.R., Israel, M.H., Klarmann, J., Scarlett, W.R., Stone, E.C., and Waddington, C.J. (1981), Nucl. Inst. Meth., 185, 415.
Fano, U. (1963), Ann. Rev. Nucl. Sci., 13, 1.
Waddington, C.J., Freier, P.S., and Fixsen, D.J. (1983), Phys. Rev. A, 28, 464.

N85-35877

PHYSICAL MEANING OF THE MULTIPLICITIES OF EMITTED NUCLEONS IN HADRON-NUCLEUS COLLISIONS

Strugalski Z.

Institute of Physics of the Warsaw Technical University
ul. Koszykowa 75
00-662 Warsaw, Poland

and

Joint Institute for Nuclear Research, High Energy Lab.
Dubna, USSR

ABSTRACT

The analysis of experimental data on hadron-nucleus collisions at energies from about 2 up to about 400 GeV was performed in order to discover a physical meaning of the multiplicity of emitted nucleons. Simple relations between the multiplicities and the thickness of the nuclear matter layer involved in collisions were obtained.

1. Introduction

It is commonly known that when atomic nuclei are bombarded by high energy hadrons, with energies higher than the pion production threshold, the emission of nucleons from the target nucleus, the particle production, and the evaporation of nuclear fragments take place. The presence of events in which intensive emission of nucleons and fragment evaporation appear without particle production leads to the conclusion that the nucleon emission process can proceed independently of the particle production, Strugalski Z., Pluta J. (1974), Strugalski Z., Pawlak T., Pluta J. (1982); the emitted nuclei are with kinetic energies from about 20 up to about 400 MeV, in the emulsion technique the nuclei are known as the so called g-track leaving particles.

In considerations about the nucleon emission, the emission process can be treated separately, because the influence on it by the particle production process is negligible, Strugalski Z.(1984 a,b), and the fragment evaporation is due to the target nucleus destruction in the nucleon emission process, Strugalski Z. (1984 c).

But, the emitted nucleons are constituents of the target nucleus, and it is reasonable to expect that characteristics of these nucleons should be connected with the parameters of the target - with itssize and nucleon density distribution in it. When the connections will be found, simple physical meaning of the multiplicities of the emitted nucleons, of the protons in particular, may be achieved.

The subject matter in this paper is to present results of our investigations in question.

2. Method

The method of experimental investigations is based on two facts: a) It is possible now to realize experiments, using heavy liquid chambers as 4Pi geometry detecters, in which emitted protons and produced pions of any electric charge including zero are registered with the efficiency near to 100 %; additional suplementary information about the target nuclei fragmentation can be obtained from emulsion experiments. Characteristics of the outcomes in hadron-nucleus collisions, such as multiplicities of produced or emitted particles, and momentum and angular spectra can be obtained fully as well. This way, experimental data obtained now are of such a sort as data which one can expect to obtain in a total experiment. b) Now many aspects about the nuclear matter distribution in atomic nuclei are so firmly established that it has been possible to use them in order to investigate other physical quantities, Elton LRB (1961). It is possible, therefore, to estimate the number of nucleons, or protons only, contained within any cylindrical volume centered on the hadron course in an atomic nucleus.

The method of investigation of the physical meaning of the multiplicities of the emitted nucleons, or of the emitted protons in particular, consists in comparison of the data on nucleon multiplicity distribution, obtained in investigations of collisions of definite hadrons with definite target nucleus, with data on distributions of the nucleon numbers contained within some cylindrical volumes centered on various possible hadron courses in the target nucleus; the distributions are determined from the information about the target nucleus size and nucleon density distribution in it.

3. Experiment

In our investigations we have used the 26 and 180 litre xenon bubble chambers, Kanarek T.I. et al. (1959), Kuznetsov E.V. et al. (1970). The first one was exposed to 2.34 GeV/c, 5 GeV/c, 9 GeV/c momentum pions from the synchrophasotron of the Joint Institute for Nuclear Research at Dubna. The second one was exposed to 3.5 GeV/c negatively charged pions from the accelerator of the Institute of Experimental and Theoretical Physics in Moscow. About 20 000 pion-xenon nucleus collision events were analysed, Strugalski Z. et al. (1982, 1983). Additionally, compilations of corresponding data obtained in emulsion experiments were used, Andersson B. et al. (1978), Babecki J. and Nowak G. (1978), Busza W. (1977), Gurtu A. et al. (1974), Otterlund I. et al. (1978), Tsai-Chü et al. (1977).

4. Results

It was found that the thicknesses of nuclear matter layers involved in hadron-nucleus collisions should be naturally and conveniently expressed in number of nucleons per some area $S = \pi D_0^2 \approx 10$ fm^2, where D_0 is the diameter of the nucleon; they can be expressed as well in protons/S, or in neutrons/S. We use these units only later on.

The analysis of the experimental data, in the light of the data on the target nuclei, leads to conclusions that:
1. The number n_p of protons (or of the g-track leaving particles) emitted in a collision is a measure of the thickness λ in protons/S of the nuclear matter layer involved in the collision:

$$n_p = \lambda \cdot S \qquad (1)$$

2. The mean number $\langle n_p \rangle$ of protons emitted in a sample of the hadron-nucleus collisions equals the mean thickness $\langle \lambda \rangle$ in protons/S of the nuclear matter layer involved in the collisions:

$$\langle n_p \rangle = \langle \lambda \rangle S \qquad (2)$$

3. At the incident hadron energy larger than a few GeV, the mean number of protons $\langle n_p \rangle$ emitted in hadron-nucleus collisions is:

$$\langle n_p \rangle = \langle \lambda \rangle S \left(1 - \exp(- \langle \lambda \rangle / \langle \lambda_t \rangle) \right) \qquad (3)$$

where $\langle \lambda_t \rangle$ in protons/S is the mean free path for interaction of the incident hadron with a nucleon in nuclear matter, $\langle \lambda_t \rangle = 1 / \sigma_{tot}$, and σ_{tot} is the cross-section for the hadron-nucleus any-type collision.

More information can be found in my previous works , Strugalski Z. (1984 a - c).

5. Remarks

From formula (1) it follows that the nucleon emission proceeds monotonically. But, this formula is accurate when the multiplicity of the emitted protons n_p is not larger than DS, where D is in protons/s the diameter of the target nucleus. In some small number of collision events, in no more than about 10 %, $n_p > DS$. The appearance of such values of $n_p > DS$ is due to the perturbations in nucleon emission process, Strugalski Z. (1984 b).

Formulas (1) - (3) were tested experimentally within the incident hadron energy interval up to about 2000 GeV, where the nucleon emission intensities were under studies. Nevertheless, we hope that the formulas are valid through the total region of the projectile energies above the pion production threshold.

NE3-35878

We have investigated mainly the proton emission only, but additional analysis, Strugalski Z. (1984), provided results which incline us to think that formulas (1) - (3) are valid for both the nucleons together, and for the neutrons only, as well.

References

Andersson B. et al., 1978, Physics Letters, B73, 343.
Babecki J. And Nowak G., 1978, Acta Physica Polonica, B9, 401.
Busza W., 1977, Acta Physica Polonica, B8, 333.
Gurtu A.et al., 1974, Pramana, 3, 311.
Elton L.R.B., 1961, Nuclear Sizes, Oxford University Press, Oxford.
Kanarek T.I. et al., 1959, Proc. Intern. Conf. on High Energy Accelerators and Instrumentation, CERN, p. 508.
Kuznetsov E. V. et al., 1970, Sov. Journ. PTE, vol. 2, p. 56.
Otterlund I. et al., 1978, Nuclear Physics, B142, 445.
Strugalski Z., Pluta J., 1974, Sov. Journ for Nuclear Physics, 27, 504.
Strugalski Z., Pawlak T., Pluta J., 1982, Communications JINR, Dubna: E1-82-718, E1-82-719, E1-82-841.
Strugalski Z., 1984 a, Communications JINR, Dubna E1-84-268.
Strugalski Z., 1984 b, Communications JINR, Dubna E1-84-854.
Strugalski Z., 1984 c, Communications JINR, Dubna E1-84-195.

ORIGINAL PAGE IS
OF POOR QUALITY

HE 1.3:6
N85-35878

HOW ARE PARTICLE PRODUCTION, NUCLEON EMISSION, AND TARGET FRAGMENT EVAPORATION PROCESSES INTERRELATED IN HADRON-NUCLEUS COLLISIONS ?

Strugalski Z.

Institute of Physics of the Warsaw Technical University
ul. Koszykowa 75
00-662 Warsaw, Poland
and
Joint Institute for Nuclear Research, High Energy Lab.
Dubna, USSR

ABSTRACT

Relations between particle production, nucleon emission, and fragment evaporation processes were searched for in hadron-nucleus collisions. It has been stated that: 1. The nucleon emission and target fragment evaporation proceed independently of the particle production process. 2. Relation between multiplicities of the emitted protons and of the evaporated charged fragments is expressed by simple formula.

1. Introduction

When high energy hadrons - with energies larger than the pion production threshold - collide with atomic nuclei, nucleons are emitted always, target fragment evaporated, and particles may be generated, as it has been stated experimentally.

The emission of nucleons with kinetic energies of about 20 - 400 MeV, or of the so called g-track leaving particles, and the evaporation of the target nucleus fragments may occur without particle production. The question arises therefore: "How are the particle production, nucleon emission, and target fragment evaporation processes interrelated ?"

The answer to this question should be found experimentally. In this paper, results obtained in our searches for the relations in question are presented.

2. Method

In investigations we have used the 26 and 180 litre xenon bubble chambers, Kanarek T.I. et al. (1959), Kuznetsov E.V. et al. (1970), exposed to pion beams from the synchrophasotron of the Joint Institute for Nuclear Research at Dubna and from the accelerator of the Institute of Experimental and Theoretical Physics in Moscow.

General information about pion-xenon nucleus collisions is contained in a set of Communications of the Joint Institute for Nuclear Research at Dubna, Strugalski Z. et al. (1982, 1983); we applied for the analysis in this work the DST used in them. Additional appropriate information at higher energies we have found in various emulsion works : Andersson B. et al. (1978), Babecki J. and Nowak G. (1978), Bannik B. P. et al. (1980), Gurtu A. et al. (1974), Meyer H. et al. (1963), Otterlund I. et al. (1978), Tsai-Chü et al. (1977), Winzeler H. (1965); the accelerator data there are up to 400 GeV of the incident hadron energy in the laboratory system, some data from cosmic rays, Meyer H. et al. (1963) are up to about 3 500 GeV.

The method of investigation is based on the fact that at energies much larger than the pion production threshold hadron-nucleus collision events occur in which intensive emission of nucleons proceeds without particle production, without pion production in particular. It consists in preparation of various characteristics of the emitted nucleons - of the emitted protons in particular - in dependence on the multiplicity $n_\pi = 0, 1, 2, 3, \ldots$ of produced pions of any electric charge. Clearly : 1. We prepare firstly a set of various dependences of the characteristics of the emitted protons on the multiplicities n_π of produced pions , at 2 - 9 GeV/c momentum, and we discover general features of these dependences. It should be mentioned here that in the xenon chambers we register practically all the emitted protons and all the produced pions of any electric charge. 2. Secondly, we compare available characteristics of the proton emission process at higher energies, up to about 3 500 GeV, with corresponding characteristics in pion-xenon nucleus collisions at 2 - 9 GeV. Results of such a comparison allow to conclude about the behaviour of the nucleon emission process with the incident hadron energy increase, in other words - with increase of the multiplicity of produced particles. 3. Thirdly, we investigate the dependences of characteristics of the fragment evaporation process on the multiplicity n_p of the emitted protons at various hadron energy.

This way, the effects of the particle production process on the nucleon emission and fragment evaporation processes, and the relation between the nucleon emission process and fragment evaporation process may be discovered.

3. Results

In result of the analysis of various characteristics in question, Strugalski Z. (1984), it can be concluded that:

a) The particle production process in hadron-nucleus collisions does not effect on the nucleon emission process in them at any energy of the incident hadron.

b) The evaporation process of the fragments from the

target nuclei in hadron-nucleus collisions is not influenced by the particle production process at any projectile energy.

The analysis in details of the sequence of the three processes - particle production, nucleon emission, and target fragment evaporation allows to conclude that: Any hadron with energy higher than the pion production threshold causes emission of nucleons with kinetic energies from about 20 up to about 400 MeV from the target nucleus, in passing through it; the nucleon emission may, in many cases, go in advance of the particle-producing collision of the incident hadron inside the target nucleus; the fragment evaporation process appears in result of the target nucleus damage due to the nucleon emission; the multiplicity n_p of protons emitted and the multiplicity $\langle n_b \rangle$ of the charged fragments evaporated are connected by simple formula

$$\langle n_b \rangle = 1.25\left(n_p + \frac{A-Z}{Z} \right)$$

where A and Z are the mass and charge numbers of the target nucleus, Strugalski Z. (1984).

References

Andersson B. et al., 1978, Physics Letters, 73B,343.
Babecki J., Nowak G., 1978, Acta Physica Polonica, B142, 445.
Bannik B.P. et al., 1980, Communications JINR, Dubna, R1-13055.
Gurtu A. et al., 1974, Pramana, 3, 311.
Kanarek T.I. et al., 1959, Proc. Internat. Conf. on High Energy Accelerators and Instr., CERN,p.508.
Kuznetsov E.V. et al., 1970, Sov. Journ. PTE, 2,56.
Meyer H. et al., 1963, Nuovo Cim., 28,1399.
Otterlund I. et al., 1978, Nuclear Physics, B142,445.
Strugalski Z., Pawlak T., Pluta J., 1982, Communications JINR, Dubna, E1-82-718, E1-82-719, E1-82-841.
Strugalski Z. et al., 1983, Communications JINR, Dubna R1-83-68, R1-83-237, R1-83-564, R1-83-568.
Strugalski Z., 1984, Communications JINR, Dubna: E1-84-268, E1-84-853, E1-84-854, E1-84-195.
Winzeler H., 1965, Nuclear Physics, 69,661.

HE 1.3-7

N85-35879

EXPERIMENTAL STUDY OF THE SPACE-TIME DEVELOPMENT OF THE PARTICLE PRODUCTION PROCESS IN HADRON-NUCLEON COLLISIONS, USING MASSIVE TARGET NUCLEUS AS A DETECTOR

Strugalski Z.

Institute of Physics of the Warsaw Technical University
ul. Koszykowa 75
00-662 Warsaw, Poland

and

Joint Institute for Nuclear Research, High Energy Lab.
Dubna, USSR

ABSTRACT

Experimental study of the space-time development of the particle production process in hadronic collisions at its initial stage was performed. Massive target nuclei have been used as fine detectors of properties of the particle production process development within time intervals smaller than 10^{-22} s and spatial distances smaller than 10^{-12} cm. In hadron-nucleon collisions, in particular in nucleon-nucleon collisions, the particle production process goes through intermediate objects in $2 \longrightarrow 2$ type endoergic reactions. The objects decay into commonly observed resonances and particles.

1. Introduction

In searches for plausible mechanisms to explain the particle production in hadron-nucleon collisions, in nucleon-nucleon collisions in particular, characteristics of the collision reaction products appeared after relatively long time after the collision - not shorter than the life times of resonances - are usually analysed. It cannot be excluded a priori that the known particles and resonances are the decay products of some super-particle or super-particles created firstly as well.

Now experimental information is needed, adequate and of a new quality - relevant to the time intervals τ of the most short-living particles known up to now, and within the spacial distances z much smaller than $\tau c \gamma$, where γ accounts the Lorentz dilatation of the lifetime in the laboratory.

The shortenest decay times of the known resonances are $\tau \approx 10^{-23}$ s which corresponds to the smallest spacial distances z of some 10^{-13} cm in the laboratory, when $\gamma \approx 1$. So, the qualitatively new and adequate information which has to be used for elucidation of the process in question should be obtained at the times

$\tau \leq 10^{-22}$ s within the spacial distances $z \leq 10^{-12}$ cm. These space distances and time intervals we shall call "short". Experimental information about the particle production process obtained at larger time intervals and spacial distances only my yield false ideas of the collision reaction products and of the particle systematics in a whole as well.

The collision reaction products appeared in the initial stage - within the short time intervals and spacial distances - should interact with a surrounding medium and the interaction must produce observable effects, if one would study these products experimentally. The only tool available now to realize such experiments is to apply massive target nuclei as fine detectors, therefore, Strugalski Z. (1980, 1981, 1982 a);

The subject matter in this paper is to present results of our experimental study of the space-time development of the particle production process in hadronic collisions at its initial stage. In the study, our own experimental data on pion-xenon nucleus collisions obtained at 2 - 9 GeV/c momentum, Miller K. et al.(1976), Pluta J. et al. (1976), Okhrimenko L. et al. (1978), Strugalski Z. et al. (1974, 1981, 1982 a-c, 1983 a-g) and the wealth of experimental data on hadron-nucleus, Bannik B.P. et al. (1980), Busza W. (1975), Paessler M.A. et al. (1979), Gurtu A.et al. (1974 a and b), Otterlund I. et al. (1978), Tsai-Chü et al. (1977) and the data on hadron-nucleon collisions, Famino V. et al. (1979), Goldschmidt-Clermont Y. (1973), collected in the past by other physicists were used.

2. Method

The atomic nucleus used as the target in hadron-nucleus collisions serves as a fine detector. Its size r_A can be roughly up to about 10 fm, Elton L.R.B. (1961). The basic physical process underlying the operation principle of this fine detector is the emission of nucleons, Strugalski Z. (1983, 1984). Information in details about the method can be found in one of my papers, Strugalski Z. (1985).

3. Results

In result of the investigations performed, we can conclude that:

1. In hadron-nucleus collisions, particles are produced via some intermediate objects which decay after having left the parent nucleus into usually observed resonances and particles. We called these objects "generons".

2. It is reasonable to think that the particle production in elementary hadron-nucleon collisions, in nucleon-nucleon collisions in particular, goes through such intermediate objects as well, in endoergic $2 \longrightarrow 2$ type reaction; the objects decay into commonly known resonances and particles.

ORIGINAL PAGE IS
OF POOR QUALITY

It has been shown that the above presented mechanism of the particle production process allows to derive formulas which in a convincing manner can account for hadron-nucleus data in terms of our knowledge of hadron-nucleon data, Strugalski Z. (1982 b).

4. Remarks

The consequences of the picture of the particle production process, presented above, were proved experimentally, Strugalski Z. (1982 a), Sredniawa B. and Strugalska-Gola E. (1983, 1984), in hadron-nucleus collisions within incident hadron energy values from a few up to a few thousands GeV. Quantitative agreement of the predictions based on the picture presented with corresponding experimental data has been found.

References

Bannik B.P. et al., 1980, Communications JINR, Dubna, R1-13055.
Busza W., 1975, Proc. Intern. Conf. on High Energy Phys. and Nucl. Struct., Santa-Fe, p. 211.
Elton L.R.B., 1961, Nuclear Sizes, Oxford Univ. Press
Faessler M.A. et al., 1979, Nucl. Phys., B157, 1.
Famino V. et al., 1979, CERN-HERA, 79-01, 79-02, 79-03.
Goldschmidt-Clermont Y., 1973, Acta Physica Polonica, B4,805.
Gurtu A. et al., 1974, a) Phys. Lett., 50B, 391; b) Pramana, 3, 311.
Miller K. et al., 1976, Sov. Journ. of Nucl. Phys., 23, 754.
Otterlund I. et al., 1978, Nucl. Phys., B142, 445.
Pluta J. et al., 1976, Sov. Journ. Nucl. Phys., 24, 766.
Sredniawa B. and Strugalska-Gola E., 1983, Communications JINR, Dubna, E1-83-277.
Sredniawa B. and Strugalska-Gola E., 1984, Communications JINR, Dubna, E1-84-411.
Strugalski Z. et al., 1974, Sov. Journ. Nucl. Phys., 20, 204.
Strugalski Z. et al., 1981, Communications JINR, Dubna, E1-81-578.
Strugalski Z. et al., 1982, Communications JINR, Dubna, E1-82-718, E1-82-719, E1-82-841.
Strugalski Z. et al., 1983, Communications JINR, Dubna, a) R1-83-68, b) R1-83-155, c) R1-83-234, d) R1-83-237, e) R1-83-344, f) R1-83-564, g) R1-83-568.
Strugalski Z., 1980, Communications JINR, Dubna,E1-80-548
Strugalski Z., 1981, Comm. JINR, Dubna, E1-81-576, 81-577
Strugalski Z., 1982, Comm. JINR, Dubna, E1-82-401, 82-287
Tsai-Chü et al., 1977, Nuovo Cim. Lett., 20, 257.

N85-35880

EXPERIMENTAL EVIDENCE OF THE DECREASE OF KINETIC ENERGY OF HADRONS IN PASSING THROUGH ATOMIC NUCLEI

Strugalski Z.

Institute of Physics of the Warsaw Technical University
ul. Koszykowa 75
00-662 Warsaw, Poland

and

Joint Institute for Nuclear Research, High Energy Lab.
Dubna, USSR

ABSTRACT

Hadrons with kinetic energies higher than the pion production threshold lose their kinetic energies monotonically in traversing atomic nuclei, due to the strong interactions in nuc lear matter. This phenomenon is a crude analo gy to the energy loss of charged particles in their passage through materials. Experimental evidence is presented.

1. Introduction

We have observed, in the 26 and 180 litre xenon bubble chambers that GeV pions can be deflected or absorbed in nuc lei without causing particle production, without causing pi on production in particular, when are falling on layers of nuclear matter thick enough, Strugalski Z. and Pluta J. (1974), Strugalski Z., Pawlak T., and Pluta J. (1982); the deflection or absorption is always accompanied by intensive emission of nucleons with kinetic energies from about 20 to about 400 MeV.

The energy and angular distributions of the protons in such deflected and stopped events are the same, and they a- re identical with the distributions of protons in collisio- ns with particle production as well. It is remarkable and leads to the opinion that it is reasonable to think that ha drons lose their kinetic energies, in traversing nuclear matter, by causing nucleon emission.

The subject matter in this paper is to present short - ly our results of experimental investigations of degradati- on of hadron energy through nuclei.

2. Experimental Evidence

We found experimentally that the number n_ν of emit - ted nucleons which accompany the passage of a hadron thro - ugh a nucleus along a path λ fm equals the number of nuc-

leons contained within the volume $v = \pi D_o^2 \lambda$ fm^3 centered on λ in the target nucleus:

$$n_N = \pi D_o^2 \langle \varrho \rangle \lambda , \qquad (1)$$

where $\langle \varrho \rangle$ nucleons/fm^3 is mean density of nucleons in the target nucleus along λ, D_o is approximately as large as the nucleon diameter, Strugalski Z. (1978,1979), Pluta J. and Strugalski Z. (1985).

Relation (1) may be rewritten i a more convenient form:

$$n_N = \lambda S \qquad (2)$$

if the path length λ is expressed in nucleons per the area S, and $S = \pi D_o^2$; the number n_p of the emitted protons is:

$$n_p = \lambda S \frac{Z}{A} = \lambda' S \qquad (3)$$

where λ' is in protons per S, Z and A are the charge and mass numbers of the target nucleus.

The simplest observable effects which provide crucial evidence and support for formulas (1) - (3) are: a) At energies high enough, higher than a few GeV, the mean number $\langle n_p \rangle$ of emitted protons in the deflected events is constant and almost equals $\langle \lambda' \rangle S$, where $\langle \lambda' \rangle$ is the mean thickness of the target nucleus in protons/S. b) At some projectile energy, definite for a given incident hadron and a given target nucleus, the distribution of multiplicities of protons emitted in the stopped events is symmetrical and its maximum lies at the multiplicity n_p as large as D S, where D is the diameter of the target nucleus in protons/S. c) The probability of an appearance of the stopped events, in collisions of a given hadron with a given nucleus, decreases with the increase of the incident hadron energy; at energies high enough, the stopped events do not appear at all, only the deflected events present themselves in some portion of the collision events, Strugalski Z., Pawlak T., Pluta J. (1984).

An analysis in details of the experimental facts led to the conclusion that: A hadron of kinetic energy E_h larger than the pion production threshold loses its kinetic energy in passing through nuclear matter; the fraction ΔE_h of the energy lost on the path length λ nucleons/s is:

$$\Delta E_h = \epsilon_h \lambda \qquad (4)$$

where ϵ_h MeV/(nucleon/S) is the measurable coefficient which depends on the hadron identity - for pions $\epsilon_h = \epsilon_\pi \approx 180$ MeV/(nucleon/S), for protons $\epsilon_h = \epsilon_p \approx 360$ MeV/(nucleon/S), Strugalski Z. (1983).

ORIGINAL PAGE IS
OF POOR QUALITY

In support for this conclusion, some additional experimental facts of the crucial value may be adduced: a) The mean number $\langle n_p \rangle$ of emitted protons in the stopped events is quantitatively predictable by simple relation

$$n_p = (E_h / \epsilon_h) \cdot S \qquad (5)$$

which is valid for such values of E_h when $(E_h/\epsilon_h)\, S \leq DS$ where D in nucleons/S is the target nucleus diameter times Z/A, Strugalski Z. (1983). b) The mean multiplicity $\langle n_p \rangle$ of emitted protons is energy-dependent at the incident hadron energies $E_h \leq D\epsilon_h$, and the energy-dependence is predictable quantitatively if formulas (3) and (4) are used for a given target nucleus and for a given incident hadron, Strugalski Z. (1984). c) Indirectly, the degradation of the incident hadron energy manifests itself in observed degradation of the kinetic energy and of the momenta of produced pions with the increase of the nuclear matter layer thickness $n_p = \lambda S$ the incident hadron of a given kinetic energy interacted with, as it is shown in Fig..

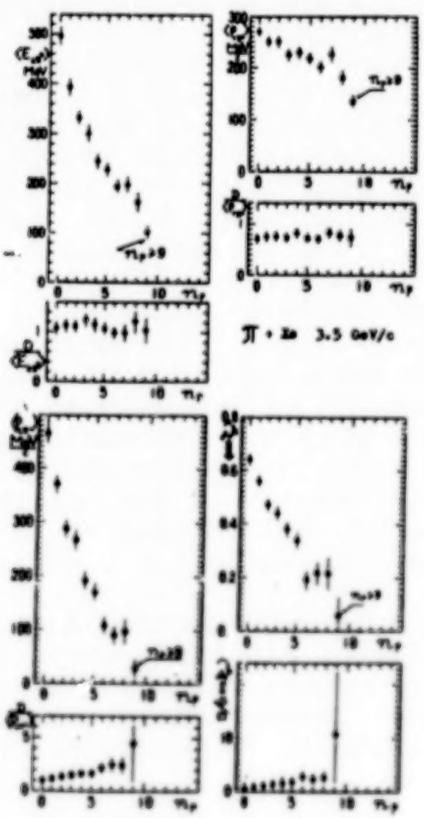


Fig. Mean kinetic energy $\langle E_{k,\pi^0} \rangle$, mean longitudinal momentum $\langle P_{L,\pi^0} \rangle$, mean transverse momentum $\langle P_{T,\pi^0} \rangle$ and mean cosine of the pion' emission angle $\langle \cos \Theta_{\pi^0} \rangle$ of neutral pions produced in pion-xenon nucleus collisions at 3.5 GeV/c momentum, in dependence on the multiplicity n_p of emitted protons; the multiplicity n_p is connected with the nuclear matter layer thickness λ the incident hadron interacted with as: $n_p = \lambda S$, where $S = \pi D_0^2 \approx 10$ fm^2 and D_0 is the diameter of the nucleon. $D/\langle\ \rangle$ are the normalized dispersions of corresponding quantities.

3. Conclusions

It should be concluded that, in sudying hadron-nucleus collisions, we have met a phenomenon which may be regarded as a crude analogy to the phenomenon consisting in the energy loss of a charged particle in materials; simi

N85-35881

larly, hadrons lose their energies in traversing nuclear matter. But, the newly observed energy loss of hadrons is due to the strong interactions of hadrons with nuclear mat ter.

In many cases, when particle-producing reactions oc - cur, the nucleon emission and therefore the incident had - ron energy loss, due to this emission, is going in advance of the particle-producing reaction; the incident hadron co vers firstly some path in the target nucleus without parti cle-producing reaction and then it causes this reaction in the nucleus; in many cases it may happen on the end of the hadron path in the target nucleus.

The effects caused by the hadron energy loss are ob - served clearly when the incident hadron energy is not lar- ger than $\epsilon_h D$, where ϵ_h is in GeV/(nucleons/S) and D in nucleons/S is the target nucleus diameter.

References

Pluta J. and Strugalski Z., 1985, to be published in Communications JINR, Dubna.

Strugalski Z. and Pluta J., 1974, Sov. Journ. of Nucl. Physics, 20, 504.

Strugalski Z., Pawlak T., Pluta J., 1982, Communicati- ons JINR, Dubna: E1-82-718, E1-82-719, E1-82-841.

Strugalski Z., Pawlak T., Pluta J., 1984, Communicati- ons JINR, Dubna, E1-84-855.

Strugalski Z., 1978, Communications JINR, Dubna, E1-11976.

Strugalski Z., 1979, Communications JINR, Dubna, E1-12086.

Strugalski Z., 1983, Communications JINR, Dubna, E1-83-850.

Strugalski Z., 1984, Communications JINR, Dubna, E1-84-268.

N85-35881

ENERGY-RANGE RELATIONS FOR HADRONS IN NUCLEAR MATTER

Strugalski Z.
Institute of Physics of the Warsaw Technical University
ul. Koszykowa 75
00-662 Warsaw, Poland
and
Joint Institute for Nuclear Research, High Energy Labor.
at Dubna, USSR

ABSTRACT

Range-energy relations for hadrons in nuclear matter exists, similarly to the range-energy relations for charged particles in materials.

1. Introduction

When hadrons of GeV kinetic energies collide with atomic nuclei massive enough, events occur in which incident hadron is stopped completely inside the target nucleus without causing particle production - without pion production in particular. The "stoppings" are always accompanied by intensive emission of nucleons with kinetic energy from about 20 up to about 400 MeV, Strugalski Z., Pluta J. (1974), Strugalski Z., Pawlak T., Pluta J. (1982). We showed experimentally that the mean number $\langle n_N \rangle$ of the emitted nucleons is a measure of the mean path $\langle \lambda \rangle$ in nuclear matter in nucleons/S on which the incident hadrons are stopped, where $S = \pi D_o^2 \approx 10$ fm^2 and D_o is the nucleon diameter, Strugalski Z. (1978,1979,1984):

$$\langle n_N \rangle \doteq \langle \lambda \rangle S \qquad (1)$$

Similar relation can be written for the mean multiplicity $\langle n_p \rangle$ of emitted protons only, usually observed in experiments:

$$\langle n_p \rangle \doteq \langle \lambda \rangle S \frac{Z}{A}, \qquad (2)$$

where Z and A are the charge and mass numbers of the target nucleus.

It is known as well, from our experiments, that the mean number $\langle n_p \rangle$ of protons emitted in the "stopped" events decreases with the incident hadron energy E_h decrease.

The question arises: Is the mean path $\langle \lambda \rangle$, in nucleons/S, of the incident hadron in nuclear matter related definitely to its kinetic energy E_h or not? The answer to the question should be find primarily in experiments, and we would like to find it.

2. Experimental Determination of the Range-Energy Relation

The method of determination of the relation between the hadron range R_h and the incident hadron energy E_h is simple - it consists in a determining of the mean multiplicities $< n_N >$ or $< n_p >$ in the "stopped" collision events of a definite hadron with a definite massive target nucleus at various energies E_h. Such measurements have been performed at two values of E_h: $E_h = E_\pi = 2.12$ GeV and $E_h = E_\pi = 3.2$ GeV, using pion-xenon nucleus collisions. For both the values of E_h the ratio

$$\epsilon_h = \frac{E_h}{\langle \lambda \rangle} = \frac{E_h}{R_h} \qquad (3)$$

is practically the same: $\epsilon_h = \epsilon_\pi = 180$ MeV/(nucleon/S).

It enables us to suppose that the relation exists

$$E_h = R_h \epsilon_h , \qquad (4)$$

where E_h is in MeV, R_h is in nucleons/S, and ϵ_h is in MeV/(nucleons/S).

Using data on the "stopped" events in proton-AgBr collisions, Sumbera M. and Vokal S. (1982), we determined the quantity $\epsilon_h = \epsilon_p = 360$ MeV/(nucleon/S), for incident protons.

The results obtained are based only on a few experimental points, at two values of E_h for the pion-xenon nucleus collisions and on one value of E_h for the proton-AgBr collisions. It would be not needless to test relation (4) in some other way. We have done it. Namely, we have made an expectation for the probability for the occurrence of the "stopped" events in dependence on the incident hadron energy E_h in pion-xenon nucleus collisions at values of E_h: 2.1, 3.2, 5, 9 GeV. Predictions are based on the relation (4), they are in agreement with corresponding experimental data, fig. ; more details concerning the calculations one can find in one of my works, Strugalski Z. (1983).

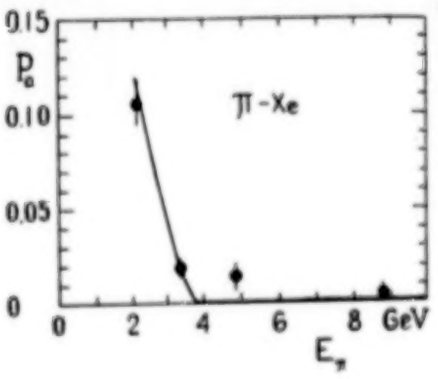


Fig. Probability P_a of the appearance of the pion-xenon nucleus collision events in which incident pion is stopped inside the target nucleus, in dependence on the incident pion momentum P_π. • - experimental data, —— - calculations, using formula (4) and data on the xenon nucleus, Strugalski (1983).

3. Conclusions

In result of the measurements, we obtained that defi - nite relation exists in nuclear matter between the hadron range R_h and the kinetic energy E_h of this hadron. This relation is an analog to similar range-energy relation in materials, for electrically charged particles.

Relation (4) , together with relations (1) and (2), allows to understand the energy-dependences of the mean multiplicity of the emitted nucleons in hadron-nucleus collisions at energies smaller than a few GeV, Strugalski Z. (1984), Abdurakhimov E.O. et al. (1978).

Relation (4) helps to determine the hadron energy loss in nuclear matter, from the energy-dependence of the mean multiplicity $\langle n_p \rangle$ of emitted protons in any-type hadron-nucleus collision reactions, as well, Strugalski Z. (1985).

References

Abdurakhimov E.O. et al., 1978, Sov. Journ. of Nuclear Physics, 27, 1020.

Strugalski Z., Pluta J., 1974, Sov. Journ. of Nuclear Physics, 20, 504.

Strugalski Z., Pawlak T., Pluta J. , 1982, Communications JINR, Dubna: E1-82-234, E1-82-718, E1-82-719, E1-82-841.

Strugalski Z., 1978, Communications JINR, Dubna, E1-11976.

Strugalski Z., 1979, Communications JINR, Dubna, E1-12086.

Strugalski Z., 1983, Communications JINR, Dubna, E1-83-850.

Strugalski Z., 1984, Communications JINR, Dubna: E1-84-268, E1-84-853, E1-84-194.

Strugalski Z., 1985, Communications JINR, Dubna, E1-85-231.

Sumbera M., Vokal S., 1982, Acta Physica Slov. 32, 265.

ME 13-10
N85-35882

SCATTERING AND STOPPING OF HADRONS IN NUCLEAR MATTER

Strugalski Z.

Institute of Physics of the Warsaw Technical University
ul. Koszykowa 75
00-662 Warsaw, Poland

and

Joint Institute for Nuclear Research, High Energy Lab.
Dubna, USSR

ABSTRACT

We have observed, in the 180 litre xenon bubble chamber, that when hadrons with kinetic energy higher than the pion production threshold fall on a layer of nuclear matter - on an atomic nucleus in other words - in many cases they can pass through it without causing particle production but they are deflected through some deflection angles; if the energy is lower than a few GeV and the nuclear matter layer is thick enough, the hadrons can be stopped in it. The amount of the deflection at a given incident hadron energy varies with the way the hadron strikes the atomic nucleus; the probability of the occurrence of stopping depends on the incident hadron identity and energy, and on the way the hadron passed through the nucleus, as well.

1. Introduction

Almost 75 years ago H. Geiger and E. Marsden, two of E. Rutherford students, directed a beam of alpha particles onto a thin foil of gold. With a screen of fluorescent material they then counted the number of particles scattered at various angles as a result of encounters with the gold atoms, Geiger H. and Marsden E. (1909). It was E. Rutherford who supplied the interpretation of findings obtained in the experiments; in the interpretation he had also introduced a method whose importance is indiminished today, Rutherford E. (1911).

I would like to communicate, in this paper, that now it is possible to perform similar experiments in which instead of the metallic foil the "foil" of nuclear matter of definite thickness will be used, and the projectiles employed will be the strongly interacting particles, pions or protons for example, raised to high energy by an accelerator.

In contrast to the Geiger-Marsden-Rutherford experiments, where the scattered alpha particles have been observed only, in the experiments with nuclear matter foils an

N85 - 33885

emission of nucleons from the "foil" is observed always and three general kinds of events occur against the background of this emission: a) Events in which the projectile is deflected only, without causing the particle production, Strugalski Z., Pluta J. (1974), Strugalski Z., Pawlak T., Pluta J. (1982). b) Events in which incident hadron is stopped completely without causing the particle production, Strugalski Z., Pluta J. (1974), Strugalski Z., Pawlak T., Pluta J. (1982). c) Events in which particles are produced.

The emitted nucleons are of kinetic energy from about 20 up to about 400 MeV, as it has been seen experimentally, Strugalski Z., Pawlak T., Pluta J. (1982).

2. A Massive Atomic Nucleus as the "Foil" of Nuclear Matter

Any of the atomic nuclei massive enough can be regarded as the lens-shaped "foil" or "slab" of nuclear matter, if the thickness $\lambda(b)$ of the nuclear matter layer at any distance b from the nucleus center is measured in units of number of nucleons per some area S fm^2, like the Earth atmosphere thickness is expressible usually in grams/cm^2, Strugalski Z. and Pawlak T. (1981).

Such a "slab" should be characterized generally by the maximum thickness of the nuclear matter layer - λ_{max}, the mean thickness $\langle\lambda\rangle$, and the thickness $\lambda(b)$ at any distance b from the nucleus center; the values of these quantities for many nuclei can be found in one of our works, Strugalski Z. and Pawlak T. (1981).

Results of experimental studies of the nucleon emission process in hadron-nucleus collisions, Strugalski Z., Pawlak T., Pluta J. (1982), prompt to us the procedure by which we can determine the quantity $\lambda(b)$; it was concluded that relation exists between the multiplicity of the emitted nucleons n_N and $\lambda(b)$ expressed in nucleons per $S \approx 10$ fm^2:

$$\lambda(b) \cdot S = n_N \qquad (1)$$

When the multiplicity n_p of the emitted protons is measured only, relation (1) should be rewritten:

$$\lambda(b) \cdot S \cdot \frac{Z}{A} = n_p \qquad (1')$$

where Z and A are the charge and mass numbers of the target nucleus, and $S = \pi D_0^2$ fm^2, and D_0 is the nucleon diameter, Strugalski Z. (1985).

3. Experiment

Experimental information about pion deflection in its passage through nuclear matter was obtained by means of the 26 and 180 litre xenon bubble chambers, Kanarek T.I. et al. (1959), Kusnetsov E.V. et al. (1970). The small chamber was exposed to the pion beam from the synchrophasotron of the Joint Institute for Nuclear Research at Dubna, 2.34 GeV/c,

the larger chamber was exposed to the beam of negatively charged pions of 3.5 GeV/c momentum from the accelerator of the Institute of Theoretical and Experimental Physics in Moscow. The massive nucleus of the xenon 131 atom was used as the nuclear matter slab, Strugalski Z., Pawlak T., Pluta J. (1982).

4. Results

It has been found experimentally that: a) A definite simple relation exists between the incident pion deflection angle Θ_π and the average multiplicity n_p of emitted protons; in other words - a definite simple relation exists between the pion deflection angle Θ_π and the thickness in protons/S of the nuclear matter layer traversed by this pion. b) The mean value of the cosine of the pion deflection angle, $<\cos\Theta_\pi>$, depends definitely and simply on the number n_p of emitted protons; in other words, the deflection angle of the incident pion increases in a definite manner with increasing the thickness λ of the nuclear matter layer traversed by the pion.

The analysis of experimental data, Strugalski Z.(1982), leads to the recognition: a) The observed deflection angle distribution is a result of two sorts of hadron deflections in nuclear matter - one is due to a multiple scattering from objects with the rest mass as large approximately as the pion rest mass is, the second one is due to a single scattering from massive objects with the rest mass as large as the rest mass of the nucleon. b) The multiple scattering may be described quantitatively by simple formula with a simple physical meaning, Strugalski Z. (1982):

$$<\Theta_\pi>^2 = <\vartheta_\pi>^2 \cdot \lambda \qquad (2)$$

where $<\Theta_\pi>$ is the mean deflection angle occurred on the thickness λ nucleons/S, $<\vartheta_\pi>$ is the mean deflection angle occurred on the thickness $\lambda = 1$ nucleon/S. Formula (2) is similar to the Rutherfords formula, Rutherford E. (1911).

When the incident hadron energy is smaller than a few GeV, events occur in which the hadron is stopped, Strugalski Z., Pluta J. (1974), Strugalski Z., Pawlak T., Pluta J. (1982). In pion-xenon nucleus collisions, the "stopped" events occur when the incident pion energy is smaller than about 4 GeV.

Simple relation exists between the range R_h of the hadron in nuclear matter and its kinetic energy E_h, Strugalski Z. (1983).

$$R_h = \frac{E_h}{\epsilon_h} \qquad (3)$$

where R_h is in nucleons/S, E_h in GeV, ϵ_h is experimentally determined coefficient in GeV/(nucleon/S) -for pions

$\epsilon_h = \epsilon_\pi \approx 0.18$ GeV/(nucleon/S) and for protons $\epsilon_h = \epsilon_p \approx$ 0.36 GeV/(nucleon/S).

5. Conclusions

Hadron deflections and hadron stoppings were observed experimentally. These phenomena are observed clearly at energies smaller than a few GeV. Many effects occur due to these phenomena - energy dependence of the mean multiplicity $\langle n_s \rangle$ of the emitted nucleons, for example. At energies high enough these phenomena do not influence on the observed outcomes in h-A collisions.

It should be noted that the energy spectra, the longitudinal and transverse momentum distributions of the emitted nucleons do not depend on the hadron deflection angle, at angles not larger than about 60 degrees; they are independent of the hadron range in nuclear matter as well.

References

Geiger H., Marsden E., 1909, Proc. Roy. Soc., A82,495.

Kanarek T. et al., 1959, Proc. Intern Conf. on Accelerators and Instrumentation, CERN, p. 508.

Kuznetsov E.V. et al., 1970, Sov. Journ. PTE, 2, 56.

Rutherford E., 1911, Phil. Mag., May, ser. 6, 21, 669.

Strugalski Z., Pluta J., 1974, Sov. Journ. of Nuclear Phys., 20, 504.

Strugalski Z., Pawlak T., 1981, Communications JINR, Dubna, E1-81-378.

Strugalski Z., Pawlak T., Pluta J., 1982, Communications JINR, Dubna, E1-82-718, E1-82-719, E1-82-841.

Strugalski Z., 1982, Communications JINR, Dubna, E1-82-455.

Strugalski Z., 1983, Communications JINR, Dubna, E1-83-850.

Strugalski Z., 1984, Communications JINR, Dubna, E1-84-853.

C - 3

N85-35883

MEASUREMENT OF HADRON MEAN FREE PATH FOR THE PARTICLE-PRODUCING COLLISIONS IN NUCLEAR MATTER

Strugalski Z.
Institute of Physics of the Warsaw Technical University
ul. Koszykowa 75
00-662 Warsaw, Poland

and

Joint Institute for Nuclear Research, High Energy Lab.
Dubna, USSR

ABSTRACT

It is not obvious a priori that the cross-section for a process in hadron collisions with free nucleons is the same as that for the process in hadron collisions with nucleons inside a target nucleus. The question arises: "What is the cross-section for a process in a hadron collision with nucleon inside the atomic nucleus ?". The answer to it must be found in experiments. The mean free path for particle-producing collisions of pions in nuclear matter is determined experimentally using pion-xenon nucleus collisions at 3.5 GeV/c momentum. Relation between the mean free path in question λ_i in nucleons/fm^2 and the cross-section σ_i in units of fm^2/nucleon for collisions of the hadron with free nucleon is: $\lambda_i = k / \sigma_i$, where $k = 3.00 \pm 0.26$.

1. Introduction

One of the main concepts which is useful in hadron-nucleus collision analysis is that of the mean free path λ; it always has a subscript denoting a particular process. Usually, the mean free path λ fm for a process is related to the cross-section σ fm^2/nucleon for such a process in collisions of the hadron with free nucleon as:

$$\lambda = \frac{1}{\rho\sigma} \qquad (1)$$

where ρ in nucleons/fm^3 is the mean nucleon density in the target nucleus along λ. Relation (1) can be expressed as

$$\lambda = \frac{1}{\sigma} \qquad (2)$$

when λ is in nucleons/fm^2. It is convenient to express λ

in units of nucleons/S where $S = \pi D_o^2 \approx 10$ fm^2 and D_o is the diameter of the nucleon.

The subject matter in this paper is to determine experimentally the mean free path λ, nucleons/S for the particle-producing hadron-nucleon collisions in nuclear matter.

2. Method

Two experimental findings provide the basis for experimental determination of the hadron mean free path for the particle-producing collisions in nuclear matter: a) The discovery of hadron-nucleus collisions in which incident hadron is stopped or deflected only in accompaniment by intensive nucleon emission from the target nucleus without causing the particle production; the emitted nucleons are with kinetic energies from about 20 up to about 400 MeV, Strugalski Z. and Pluta J. (1974), Strugalski Z., Pawlak T., Pluta J. (1982). b) The discovery of definite relation between the intensity of the emitted nucleons and the thickness of the nuclear matter layer involved in any-type collision events - when particles are produced or not, Strugalski Z. (1984 a).

We can consider a sample of hadron-nucleus collisions as a result of interaction of a beam of hadrons with a lense-shaped "slab" of nuclear matter, Strugalski Z. (1984 b). In fact, in any collision event the target nucleus is destroyed, but in any of the collisions a hadron collides with identical nucleus.

Let us consider a hadron flux I_o incident on a layer of nuclear matter of the thickness dt. The differential intensity loss dI due to interactions is given by the relation $dI = -I_o \sigma \varrho \, dt$, and so $I = I_o \exp(-\sigma \varrho t) = I_o \exp(-t/\lambda)$. The mean free path λ in fm can be replaced by λ in nucleons/S, where $S \approx 10$ fm^2; the thickness t in fm can be replaced by t in nucleons/S as well, and

$$I = I_o \exp(-t/\lambda) \qquad (3)$$

The thickness of the nuclear matter layer t in nucleons/S, involved in any type collision, is given from the relation between this thickness and the number n_p of the protons emitted in the event, Strugalski Z. (1984 a), as:

$$n_p = t \cdot S \cdot \frac{Z}{A} \qquad (4)$$

In measurements of the mean free path λ in nucleons/S the quantity I_o is simply the number of hadron-nucleus collisions analysed, the quantity I equals the number of events without causing an effect - the particle production, for example; all the quantities I_o, I, and t are measurable ones. Then, λ can be estimated simply from relation

(3).

For determination of the λ -s, the collision events observed in the 26 and 180 litre xenon bubble chambers , Kanarek T.I. et al. (1959), Kuznetsov E.V. et al. (1970), exposed to beams of pions were used.

3. Experiment

The smaller chamber was exposed to the positively charged pions with 2.34 GeV/c momentum from the synchrophasotron of the Joint Institute for Nuclear Research at Dubna. The bigger chamber was exposed to negatively charged pions with 3.5 GeV/c momentum from the accelerator of the Institute of Experimental and Theoretical Physics in Moscow.

In photograph scanning, any-type collision events were selected, a total information about the outcome in any of collisions was obtained, as it concerns the emitted nucleons and produced pions of any electric charge, including neutral pions, Strugalski Z., Pawlak T., Pluta J. (1982), Strugalski Z. et al. (1983).

4. Results

We measured the mean free path λ_i in nucleons/S for the particle-producing collisions, and the mean free path λ_d in nucleons/S for collisions without particle production when the incident hadronswere deflected through the deflection angles larger than $\theta_\pi \geq 30$ degrees, Strugalski Z. (1983). We obtained for the particle-producing mean free path $\lambda_i = 12.4 \pm 1.7$ nucleons/S and for the mean free path $\lambda_d = 12.8 \pm 1.5$ nucleons/S.

We found that the formula for dtermination of λ_i from σ_i taken from elementary hadron-nucleon collisions should be, instead of formula (2):

$$\lambda_i = \frac{k}{\sigma_i} \qquad (5)$$

where λ_i and σ_i are in nucleons/S and S/nucleon correspondingly. $k = 3.0 \pm 0.26$.

5. Conclusions

The mean free path λ_i for particle-producing hadron collisions in nuclear matter, determined by means of formula (2), does not correspond to the mean free path determined experimentally.

This path λ_i, for particle-producing collisions, and the path λ_d, for the deflections through angles larger than 30 degrees, are practically the same.

But, the deflections through large angles are from collisions of incident hadron with hard constituents of the nucleons, Strugalski Z. (1982). The observed equality between λ_i and λ_d may mean that particles are produced when collisions occur with the hard constituent of the nucleon.

The inequality of values of the quantity λ_i evaluated from formula (2) and determined experimentally using the method presented above may be regarded as an appearance of a nucleon structure in hadron-nucleus collisions, Strugalski Z. (1984 c).

References

Kanarek T.I. et al., 1959, Proc. Intern. Conference on Accelerators and Instrumentation, CERN, p.508.

Kuznetsov E.V. et al., 1970, Sov. Journ. PTE, 2, 56.

Strugalski Z. and Pluta J., 1974, Sov. Journ. for Nuclear Physics, 20, 504.

Strugalski Z., Pawlak T., Pluta J., 1982, Communications JINR, Dubna: E1-82-718, E1-82-719, E1-82-841.

Strugalski Z. et al., Communications JINR, Dubna, 1983 R1-83-68, R1-83-237, R1-83-564, R1-83-568.

Strugalski Z., 1982, Communications JINR, Dubna, E1-82-455.

Strugalski Z., 1983, Communications JINR, Dubna, E1-83-563.

Strugalski Z., 1984, Communications JINR, Dubna: a) E1-84-853, b) E1-84-268, c) E1-84-365.

THE ϕ MESON AND "CHIRAL-MASS-MESON" PRODUCTION IN HEAVY-ION COLLISIONS AS POTENTIAL PROBES OF QUARK-GLUON-PLASMA AND CHIRAL SYMMETRY TRANSITIONS

Y. Takahashi[+] and P. B. Eby

N85-35884

(NAS-NRC)[+], ES62 and ES63, Space Science Laboratory
NASA Marshall Space Flight Center, Huntsville, Alabama 35812, USA

ABSTRACT

Possibilities of observing abundances of ϕ mesons and narrow hadronic pairs, as results of QGP and Chiral transitions, are considered for nucleus-nucleus interactions. Kinematical requirements in forming close pairs are satisfied in K^+K^- decays of S(975) and δ(980) mesons with small P_T, and ϕ(1020) mesons with large P_T, and in $\pi\pi$ decays of familiar resonance mesons (ρ, ω, A_1, ...) only in a partially restored chiral symmetry. Gluon-gluon dominance in QGP can enhance ϕ meson production. High hadronization rates of primordial resonance mesons which form narrow hadronic pairs are not implausible. Past cosmic ray evidences of anomalous ϕ production and narrow pair abundances are considered.

1. Introduction. First (or second) order phase transitions have been demonstrated for Quark-Gluon-Plasma(QGP) and Chiral Symmetry Restoration in various lattice QCD calculations.[1] Phenomenological consequences of new states of matter have been discussed rigorously in the past few years. Some signatures which may discriminate new states from ordinary hadronic processes are considered for on-going and future experimental investigations: (i) direct photons and lepton-pairs;[2] (ii) large average P_T;[3] (iii) rapidity-azimuth fluctuations;[4] (iv) strangeness production;[5] (v) "fade-out" of resonance mass peaks.[6]

The first issue has been most quantitatively studied so far, but the results of calculations are found less prominent than initially expected.[7] The second item, large P_T, has been attracting some critical attentions, since there are some experimental indications in the JACEE cosmic ray data[8] and in $S\bar{p}pS$ data,[9] which can be discussed as influences of hydrodynamical expansion[10] and thermodynamical manifestation[11] of plasmas. The third issue has been only naively conjectured,[12] but some expectations are made on the basis of super-cooling and deflagration.[13] The fourth issue, strangeness, has been emphasized by several people,[14] however, negative arguments against its abundant production are also raised recently (based on large entropy consumption in pions).[15] The last issue, being least studied to date, seems to be of particular interest, because it has been the only predicted diagnosis of Chiral transitions.

We examine other potential probes of new states of matter, considering several anomalous symptoms uniquely shown for nucleus-nucleus interactions in the past cosmic ray experiments. First, the possibility of abundant ϕ meson production in QGP is considered. Then, we shall study the possibility of observing reduced-mass resonance mesons in partial chiral symmetry.

2. ϕ Meson Abundance. Koshiba et al.[16] and Kim[17] observed multiple Kaons in nucleus-nucleus collision events in Brawley Stack emulsion. The former, particularly, have shown that the observed Kaons are mostly due to ϕ mesons which are identified by an invariant-mass study of two Kaons. This is,

however, inconceivable at first glance, because strong suppression of ϕ mesons has been established in elementary particle interactions. This suppression is best understood by (1) its large mass (1,020 MeV/c^2), (2) small coupling constant of s-quark, and (3) Okubo-Zweig-Iizuka (OZI) rule for disconnected quark diagrams (small mixing of $s\bar{s}$ with $u\bar{u}$ and $d\bar{d}$).

These fundamental suppressions do not seem quite obvious in nucleus-nucleus collisions for the following reasons: (1) large mass suppression in the Boltzman factor may not be valid among different flavors; primordial $s\bar{s}$ can be as many as $u\bar{u}$ and $d\bar{d}$ in QGP, as often stressed by Rafelski.[5] (2) a small coupling constant is not unique for s-quark at high temperature as QCD reduces strengths of light quark couplings. Even if not, their intrinsic difference is small. (3) The OZI suppression is effective to $q\bar{q} \rightarrow q\bar{q}$ process, but it is absent for stronger (more rapid) $gg \rightarrow q\bar{q}$ process. In a gluon-rich environments(QGP) $s\bar{s}$ production is dominated by the latter.

The ϕ/π ratio should be enhanced in QGP at least to the 1 % level, apart from well-known low values (< 0.1 %). If we follow Rafelski's calculation of $s\bar{s}$ abundance in QGP, and separately apply the Boltzman factor to strange particles, we get ϕ/π ratio upto 23 %. (The P_T distribution of them may be different as well, if hydrodynamical flow of QGP is strong. A universal P_T formula, $dN/dP_T \propto \exp(-m_T/T_0)$; T_0 = 170 MeV, may not be valid in universal CM system, but only in the rest system of the hydrodynamical front plane.) Such a high ϕ/π ratio, though possible, is not guaranteed only from above considerations. Particularly, an alteration of the universal Boltzman factor for different flavors remains too arbitrary.

On the other hand, the Koshiba data implies ϕ/π ratio 32 ± 17 % in the target fragmentation region. It is also interesting to note that K/π ratios for nucleus-nucleus and proton-nucleus events in the same data turned out to be 0.41 ± 0.15 and 0.17 ± 0.11, respectively.[21] This value is consistent with the latest Rafelski estimate[22] and the upper bound given by McLerran.[15] If we accept Kaon data of Koshiba et al., we are inevitably compelled to reconsider the strangeness suppression.

The ϕ meson is an unique particle in the sense that it does not decay ($\tau \simeq 20$ fm/c) before leaving a "fireball", and its decay particles (K^+K^-) remain closely associated with each other. In this regard, it is interesting to note another cosmic ray data which showed pronounced narrow pairs in nucleus-nucleus collisions.[18,19] These data, if explained by ϕ mesons, require $P_T(\phi)$ more than 1.5 GeV/c (for pairs with $\Delta y < 0.2$ and $\Delta\phi < 30^0$).[23] S and δ mesons make "too narrow" K^+K^- pairs (Δy, $\Delta\phi \simeq 0$). The required high $\phi(P_T \geq 1.5$ GeV/c)/π(all P_T) ratio (~ several %) to account for all the pair abundances is unacceptable by any means, which eliminates the candidacy of high P_T ϕ mesons for the observed pairs. Nevertheless, as discussed later, ϕ mesons and other familiar resonance mesons can make very narrow hadronic pairs without high P_T in partial chiral phase.

3. Mesons in Partial Chiral Symmetry. Chiral Symmetry Restoration is shown by many calculations to take place at almost the identical critical temperature (T_{ch}) as the deconfinement (QGP) transition (T_c). The consequence of the chiral symmetry at high temperature is the reduction of resonance masses. Chiral transition above Tch may not alter the main scenario of dynamical processes of nucleus-nucleus interactions, at least, that of hydrodynamical expansion of QGP. Nonetheless, an influence on the hadronization process must be considered, because the hadronization process is at the same time a process of dynamical symmetry breaking of chirality.

At temperature just below the QGP phase transition ($T \leq T_c$) when early

hadronization starts, chiral symmetry breaking is incomplete. The mass of a resonance meson composed of u or d quarks is significantly light at high temperature, while those of π's and K's remain almost normal. Chiral counterparts, for example, $\rho((1^-)^-)$ and $A_1((1^+)^+)$, have different masses, 770 and 1,270 MeV/c^2, respectively in normal nuclear phase. Their mass difference vanishes above Tch. The mass formulae in the quark model gives a degree of symmetry breaking as a function of the temperature:[20]

$$m(T)/m_0|_{T\sim Tch} \rightarrow 2.03\{(T_{ch} - T)/T_{ch}\}^{1/2}, \quad (1)$$

where m_0 represents the constituent quark mass (~ 300 MeV). Using a formula given by Pisarski,[20] we get ρ meson mass at different T. When Tch = 215 MeV and Tc = 207 MeV, for example, m_ρ increases rapidly with decreasing T:

$$m_\rho \simeq 290 \text{ MeV } (T = 206 \text{ MeV}), 341 \text{ MeV } (T = 205 \text{ MeV}), \cdots . \quad (2)$$

The decay Pmax values for $\rho(T = 206, 205 \text{ MeV}) \rightarrow \pi\pi$ are only 63 MeV and 96 MeV, respectively, which can explain observed narrow pairs ($dN/d(\Delta\phi)$ for $\Delta y \leq 0.2$) satisfactorily without assuming high P_T.[23] Other resonance mesons are similarly lighter than their ordinary values in normal nuclear phase.

The number of primordial $q\bar{q}$ mesons can be evaluated by the combination rate at unit space-time,

$$A \equiv \frac{dN}{dt\,dx^3} = (1/2)\int_{4m^2}^{\infty} sds\cdot\delta(s - (k_1 + k_2)^2)\int\frac{d^3k_1}{(2\pi)^3|k_1|}\int\frac{d^3k_2}{(2\pi)^3|k_2|}$$
$$\times \{C_g f_g(k_1) f_g(k_2)\bar{\sigma}_{gg\rightarrow q\bar{q}}(s) + C_q f_q(k_1) f_q(k_2)\bar{\sigma}_{q\bar{q}\rightarrow q\bar{q}}(s)\}, \quad (3)$$

where C_g and C_q are determined by the number of degrees of freedom for gluons and quarks, and $\bar{\sigma}(s)$'s are cross sections for gluons and quarks to form a specific $q\bar{q}$ state. The ratio of $(q\bar{q})$ states frozen out in the temperature intervals Tc - T and Tc - Tf can be estimated by

$$R(T) \equiv \int_T^{Tc} dT\cdot A(T)\int_\Omega d^4x\ \delta(T - T(x))/\int_{Tf}^{Tc} dT\cdot A(T)\int_\Omega d^4x\ \delta(T - T(x))$$
$$\simeq \{(T_c/T)^6 - 1\}/\{(T_c/T_f)^6 - 1\}, \quad (4)$$

where $T_c > T > T_f$, with T_f being a final temperature ($T_f = T_0 \simeq 170$ MeV). When we consider R at T = 205 MeV, about 3 % of all final states are shared by primordial mesons in the earliest chiral breaking phase. Though the evaluation is crude (neglecting many dynamical factors), it is interesting to note that "chiral mesons" are not negligible in discussing the final state pair correlation. A question still remains how $\pi\pi$'s from chiral mesons can survive during meson-meson final state interactions. We tentatively neglect this, as the decay width Γ is proportional to $\{(T_c - T)/T_c\}^{3/4}$,[20] and the lifetime of "chiral ρ meson" is correspondingly long (several fm/c).

Chiral symmetry does not affect s-quark mesons very much. Nevertheless, a few times 10 MeV mass reduction is not unreasonable for ϕ mesons. This permits primordial ϕ mesons decay into narrow K^+K^- pairs even with small P_T.

The above discussions are highly speculative, as many assumptions are left unjustified. However, the hadronization mechanism from QGP, particularly from chiral symmetry, seems to have potential sources of narrow pairs.

4. Conclusions. The ϕ meson abundance in nucleus-nucleus interactions can be much higher ($\phi/\pi \geq 1$ %) than that in proton-proton collisions ($\phi/\pi < 0.1$ %). The highest possible value in QGP may be 23 %, though this is too optimistic. Some cosmic ray data suggest much higher values ($\phi/\pi \simeq 30$ %) in a narrow target fragmentation region. It is too high for a plausible

explanation without assuming some strangeness abundances in cosmic ray heavy-ion events. Though inspiring, the observed data are limited to only several events (E > 1 TeV/amu). Follow-up experiments are required to consider new states of matter for them.

The hadronic narrow pairs might involve decay products of "chirally symmetric primordial mesons" (bound state of $q\bar{q}$: cf. Cooper-pair, i.e. phonon). However, the existing pair correlation data might be mostly accounted by some unclarified experimental errors and by more conventional mechanism such as the HBT effect.[19] Further studies may be required for confirming non-trivial pair abundances in the existing data. We do not consider at present any direct relationship of the experimental data to the above described scenario, though tempting, because both studies are still very primitive. Experimentally, measurements of $\langle P_T \rangle$ and invariant mass of a pair (with identity of the particle species) are possible in the backward hemisphere within nuclear emulsion techniques. If these data become available, the study of pairs will be more interesting. However, pair observations have some difficulties to deal with very high multiplicity/high energy density events; too high a particle density obscures any meaningful narrow-pair correlations. (Rapidity densities for the study of pair abundances may be limited to, probably, dN/dy ~ 100.) In this sense, light nuclei collisions and/or intermediate impact parameter events at high energy would best suit for observations, but with a risk to fall short of energy densities for the phase change. Theoretical developments for early hadronization processes are important in confirming the suggested scenario of (chiral transition → primordial "chiral mesons" → narrow hadronic pairs).

No definitive judgements for existing data are possible at this stage, however, we conclude that these kinds of observations can be potential probes of QGP and Chiral Symmetry Restoration when new states of matter are actually realized in high energy nucleus-nucleus collisions with moderate rapidity densities.

5. Acknowledgements. The authors acknowledge discussions with Drs. O. Miyamura, T. A. Parnell, and T. Tabuki.

References. 1. H. Satz, Quark Matter '84, p.278(1984), Springer Verlag. 2. E.L. Feinberg, Nuovo Cimento 34A, 391(1976); G. Domokos and J.I. Goldman, Phys. Rev., D23, 203(1981). 3. E.V. Shuryak, Phys. Reports, 61, 71(1980). 4. M. Gyulassy et al., LBL preprint, 16277(1983). 5. J. Rafelski and B. Muller, Phys. Rev. Lett., 48, 1066(1982). 6. J. Kapusta, Phys. Rev., C15, 1580(1977). 7.L. McLerran, Quark Matter '84, p. 1 (1984), Springer Verlag. 8. O. Miyamura and JACEE, Quark Matter '84, p. 187 (1984), Springer Verlag. 9. K. Kajantie, H.I. Mittenen, Z. Phys., C9, 341(1981); C14, 356(1982). 10. M. Gyulassy, Nucl. Phys., A418, 59c(1984). 11. L.van Hove, Phys. Letters, 118B, 138(1982). 12. T.D. Lee, Columbia University preprint, CU-TP-170(1981). 13. L. van Hove, CERN preprint, TH3592 (1983). 14. J. Rafelski, Nucl. Phys., A418, 215c(1984). 15. L. McLerran and T. Matsui, private communication, 1985. 16. M. Koshiba et al., J. Phys. Soc. Japan, 22, 1321(1967). 17. C.O. Kim, Phys. Rev., 136, 515(1964). 18. P.S.Freier and C.J. Waddington, AIP 49, 87 (1979). 19. The JACEE Collaboration, this conference, HE 1.4-5, (1985). 20. R.D. Pisarski, Phys. Letters, 110B, 155(1982). 21. Y. Takahashi, talk presented at Quark Matter '84, Helsinki, (1984). 22. J. Rafelski, private communication at Quark Matter '84, Helsinki (1984). 23. P.B. Eby, T.A. Parnell and Y. Takahashi, preprint (unpublished) NASA/MSFC, (1985).

N85
35885

UNCLAS

HE 1.3-15

N85-35885

SU(2) x U(1) VACUUM AND THE CENTAURO EVENTS

D. Kazanas, V. K. Balasubrahmanyan and R. E. Streitmatter
NASA/Goddard Space Flight Center
Greenbelt, MD 20771
USA

ABSTRACT

We propose that the "fireballs" invoked to explain the Centauro events are bubbles of a metastable superdense state of nuclear matter, created in high energy ($E \sim 10^{15}$ eV) cosmic ray collisions at the top of the atmosphere. If these bubbles are created with a Lorentz factor $\gamma \approx 10$ at their CM frame, the objections against the origin of these events in cosmic ray interactions are overcome. A relationship then between their lifetime, τ, and the threshold energy for bubble formation, E_{th}, is derived. The minimum lifetime consistent with such an interpretation is $\tau \sim 10^{-8}$ sec, while the E_{th} appears to be insensitive to the value of τ and always close to $E_{th} \sim 10^{15}$ eV. Finally it is speculated that these bubbles might be manifestations of the SU(2) x U(1) false vacuum excited in these collisions. The absence of π^0's in the Centauro events is then explained by the decay modes of these excitations.

1. Introduction. The Centauro, events (Lattes et al. 1973) are high energy $\approx 10^{15\pm1}$ cosmic ray events detected in nuclear emulsion chambers at high altitudes ($\geq$ 4000 m) with characteristics which defy explanation in terms of "standard" high energy cosmic ray collisions and subsequent cascading of the produced particles. The characteristics which set these events apart from the typical events expected at these energies ($\approx 10^{15}$ eV) are the following:

a. They are observed deep in the atmosphere ($\approx$ 500 g cm^{-2}), only a few hundred meters above the emulsion chamber detector.
b. They have very high multiplicity.
c. They have very large mean transverse momentum, $\langle P_t \rangle$, 3-5 times larger than that of a typical nuclear fragmentation interaction.
d. There is a deficiency of neutral pion production.

Direct nuclear collisions fail to account for any of the above features, especially for the observed rate, $R \approx 10^{-2}$ m^{-2}sr^{-1}yr^{-1}, since the probability of penetration of strongly interacting particles to such depth is negligible. It was pointed out though, that most of the above features (multiplicity, $\langle P_t \rangle$), could be accounted for in terms of the explosive decay of an unknown state of matter. Bjorken and McLerran (1979) postulate a new metastable form of quark matter, introducing a new component in the cosmic ray spectrum, while Kinnunen and Rubbia (1981) argue that these events cannot be due to high energy cosmic ray interactions, thus in effect agreeing with the previous authors. In the present note we accept the interpretation of the Centauro events as the explosive decays of an unknown yet high energy particle deep in the atmosphere. However, contrary to the previous treatments, we relate the Centauro flux to the flux of high energy cosmic ray particles at the top of the atmosphere, thus avoiding the introduction of a new, unknown component in the primary cosmic ray spectrum. Then, the requirement that Centauros are

N85-35885

due to the explosive decay of a bubble of a metastable superdense nuclear matter, produced in a high energy collision on the top of the atmosphere, leads to a relation between the formation of such a metastable state and to its lifetime. This is done in the next section.

2. The Centauro Event Rate. In relating the Centauro rate to that of high energy cosmic ray interactions, we shall assume that a large fraction of high energy cosmic rays have interacted within 50 g cm^{-2} from the top of the atmosphere, which sets the interaction height to about 21 km. Given that the Mt. Chacaltaya detector is at a depth ~ 500 g cm^{-2} or a height of ~ 6 km, the bubbles of metastable matter will have to traverse a distance of about 15 km before they decay. We further assume that any decay at a distance dL > 100 m from the detector does not classify as a Centauro event, because the ensuing cascade will not have the characteristics of a Centauro (i.e. closeness to the detector, few π^0's). Then if τ_0 is the lifetime of the bubble and γ_L its Lorentz factor in the laboratory frame, the decay rate of bubbles as a function of time after the interaction will be

$$N(t) = N_T\, e^{-t/\gamma_L \tau_0} \tag{1}$$

or in terms of the distance d from the high energy interaction point,

$$N(d) = N_T\, e^{-d/c\gamma_L \tau_0} \tag{2}$$

Where N_T is the rate of bubble production at the top of the atmosphere. Then the differential rate with respect to the pathlength dl within which decays are identifiable as Centauro events is

$$\frac{dN(d)}{dl} = \frac{1}{c\gamma_L \tau_0} N(d)$$

and the Centauro event detection rate should be

$$R = \frac{dl}{c\gamma_L \tau_0} N_T\, e^{-d/c\gamma_L \tau_0} \tag{3}$$

Solving this relation for the rate of events at the top of the atmosphere, N_T, one obtains

$$N_T = R\, \frac{\gamma_L c\, \tau_0}{dl}\, e^{d/c\gamma_L \tau_0} \tag{4}$$

Since we expect the formation of bubbles to have a threshold energy E_i, N_T should be the integrated cosmic ray flux at the top of the atmosphere with $E > E_i$ or

$$N_T = \eta\, K\, E_i^{-1.7} = \eta\, 1.1\, 10^4\, E_i^{-1.7}\ \ m^{-2}\, Sr^{-2}\, s^{-1} \tag{5}$$

with E_i measured in GeV. The factor η denotes the fraction of these events that produce bubbles of metastable nuclear matter, which we will presently assume to be of the order of 1 ($\eta = 1$). If M_b is the mass (rest energy) of the bubble and E^*_b its CM energy then its Lorentz factor in the interaction CM frame will be

$$f = E^*_b / m_b$$

Hence the Lorentz factor of the CM will be $\gamma_{CM} = (\frac{E_1}{2m_p})^{1/2}$. Consequently the Lorentz factor of the bubble in the laboratory frame, γ_L, will be

$$\gamma_L = \frac{E_{b,lab}}{M_b} = \gamma_{CM} f + (\gamma_{CM}^2-1)^{1/2} \cdot (f^2-1)^{1/2} \cos\theta^* = f (\frac{E_1}{2m_p})^{1/2} \quad (6)$$

Substituting equations (5) and (6) into equation (4) and solving for E_1 we obtain the transcendental equation

$$E_1 = [\frac{1}{\eta\kappa} \frac{R}{dI} \cdot (\frac{E_1}{2})^{1/2} f \tau_0 \exp (d/c (\frac{E_1}{2})^{1/2} f \tau_0)]^{-0.59} \quad (7)$$

where $R = 10^{-2}$ m^{-2}sr^{-1}yr^{-1} is the Centauro event rate, $dI = 10^{5}$ cm, $d = 15$ km $= 1.5 \times 10^{6}$ cm, κ is defined by equation (5), and m_p has been taken as 1 GeV. Substituting the numerical values equation (7) reads

$$E_1 = [\frac{1}{\eta} 5.68 \times 10^{8} E_1^{1/2} f \tau_0 \exp (7.07\ 10^{5}/E_1^{1/2} f \tau_0)]^{-0.59} \equiv F(E_1, \tau_0)$$

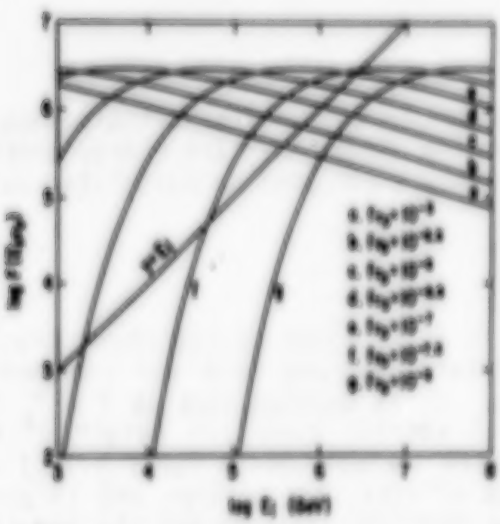


Figure 1

Equation (7a) can be solved graphically by plotting the curves $y = E_1$ and $y = F(E_1, \tau_0)$. The results are shown in Figure 1 where the families of curves $F(E_1, \tau_0)$ are shown as a function of E_1 with $f\tau_0$ as a parameter. One can distinguish two major features: (i) for sufficiently small values of the parameter $f\tau_0$ ($<10^{-6}$) no solution to equation (7a) exists. This means that for sufficiently small bubble lifetimes ($f\tau_0 < 10^{-6}$) not enough of them will survive deep enough in the atmosphere to account for the observed Centauro flux, (ii) For $f\tau_0 > 10^{-6}$ there are always two solutions to equation (7a) since the curve $y = E_1$ intersects the curve $y = F(E_1, \tau_0)$ at two points. It is interesting to note that of these two solutions the highest ones are always close to an energy $E_1 = 10^{3}$ GeV for a wide range of values of the paramter $f\tau_0$, (10^{-6}-10^{-8}), which corresponds to a CM energy of $\simeq 1$ TeV.

One can of course assume that the increased penetration is due to the smaller cross section of the"bubble". The difference is heights between 21 km (where presumably the metastable state forms) and 5 km where the fireball occurs and corresponds to ~ 500 g cm^{-2} or a cross section ≥ 10 times smaller than that of strong interactions. This corresponds to a linear dimension >3 times that of a proton and hence a $P_t \geq 3$ times that of strong interactions as indeed observed.

The assumption that the bubbles of the superdense metastable nuclear

state are produced with a certain kinetic energy at the CM of the collision can actually sidestep the arguments of Kinnen and Rubia (1981) against the origin of Centauros in high energy cosmic ray collisions. The latter authors have concluded so by noting that the kinematics of the Cenaturo event demand $\gamma \approx 10^4$ and $M_{fireball} \approx 200$ GeV. Assuming further (as they did) that all the primary energy goes into making the rest mass energy of the fireball (i.e. $\gamma_L = \gamma_{CM}$), they derived from the latter figures a primary energy $E_L = \gamma_{CM} M_{fireball} \approx 10^{17}$ eV. The flux of cosmic rays at these energies is much too low to account for the observed Centauro rate. Eq. (6) however shows that if the bubble is created in the CM frame with a Lorentz factor $f \approx 10$ then $\gamma_L \approx 10^4$ implies $\gamma_{CM} \approx 10^3$ and hence a primary energy $E_L \approx 10^{15}$ which provides sufficient flux to account for the observed rate.

3. Discussion - Conclusions. The next question one is called to answer is the nature of these "fireballs". (See Kazanas et al.1984). We consider the possibility of the SU(2)xU(1) vacuum as a means for producing these "fireballs". At the restoration of the symmetry there is a contribution to the energy density from the SU(2)xU(1) vacuum. The total energy density, ε, is then

$$\varepsilon = An^{4/3} + \rho$$

The first term is the energy density due to the quarks participating in the collision (assumed to be cold) and the second term the energy density of the vacuum. The pressure of the mixture can then be calculated using the thermodynamic relation

$$P = n \frac{d\varepsilon}{dn} - \varepsilon = \frac{1}{3} An^{4/3} - \rho \ .$$

One can now observe that for $An^{4/3} \approx \rho$ (i.e. close to the phase transition point) the pressure of the mixture goes to zero and the medium becomes unstable to bubble formation. It is assumed that at $T \approx T_c$ the two phases with $\langle\phi\rangle = 0$ and $\langle\phi\rangle \neq 0$ coexist since the height of the barrier between them is smaller than the thermal energy for $T \gtrsim T_c$ (Sher and Flores 1983). Neglecting surface effects, the bubbles are in pressure equilibrium between the positive particle pressure and the negative vacuum tension. The bubbles should therefore decay primarily into Higgs particles. It has been suggested (Willey 1984) that the particle $\xi(2.2)$ observed in the decay $J/\psi \to \gamma\xi(2.2)$ might be the Higgs boson. Such an identification would indeed fit the signatures of the Centauros. A ~ 100 GeV bubble would decay into ~ 50 Higgs and subsequently into ~ 100 $K\bar{K}$ ($\xi(2.2) \to K\bar{K}$ dominantly). These K's would have $P_t \sim 1$ GeV and would explain the absence of π^0's. Also only explosions close to the detector would classify as Cenaturos since for $dL > 300$ m the K's would have a chance to decay into π^0's, and then into photons.

4. References

1. Bjorken, J. D. and McLerran, L. D. Phys. Rev. D20 (1979), 2353.
2. Kazanas, D. et al. 1984, Phys. Let. 142 23.
3. Kinnunen, R. and Rubbia, C. 1981, Proc. 17th ICRC, Paris, 11, 112.
4. Lattes, C. et al. 1973, Proc. 13th ICRC, Denver, 3, 2227; 5, 2671.
5. Sher, M. and Flores, R., Anny. Phys. 148 (1983), 95.
6. Willey, R. S., Phys. Rev. Lett. 52 (1984), 585.

N85-35886

HE 1.3-16

HEAVY FLAVOURS PRODUCTION IN QUARK-GLUON PLASMA FORMED IN HIGH ENERGY NUCLEAR REACTIONS

J. KLOSINSKI *

RIVERS STATE UNIVERSITY OF SCIENCE AND TECHNOLOGY
Physics Department
P.M.B. 5080
Port Harcourt, Nigeria

ABSTRACT

Results on compression and temperatures of nuclear fireballs and on relative yield of strange and charmed hadrons are given in this paper. The results show that temperatures above 300 MeV and large compressions ($\gtrsim 10$) are unlikely achieved in average heavy ion collision. In consequence thermal production of charm is low. Strange particle production is, however, substantial and indicates clear temperature - threshold behaviour.

1. Introduction: Observation of QGP is one of the most desired arguments in favour of correctness of our understanding of strong interactions. Its formation needs a large deposition of energy in large enough volume. The interactions of cosmic ray particles, primarily nuclei, offer the unique opportunity of its detection.

One of the signatures of QGP formation is increased rate of heavy flavours as compared to the hadronic systems at the same temperature without QGP formation (1). The role of charm may be also peculiar; we forsee charmed quarks as a centers of hadronic buble formation in hot QGP and as a stabilizing factor in cold multicharmed globs (2). Both phenomena may lead to unusual events. Here we present only some of our results. The full paper will be published elsewhere.

2. The model: Several arguments, based on experimental observations (the transparency of nuclei being strongest one) and on results of relativistic of two fluid - hydrodynamics allows us to treat the bea nucleus (for definitness we will work in the lab frame) as a penetrating, shock-like discontinuity propagating with (almost) velocity of light through the nuclear matter. In equations of hydrodynamics its propagation is represented

as a source term of energy, momentum and colour (but not baryon number) transferred to the nuclear matter. These equations allow us to find (with assumed equation of state for nuclear matter) the heating curve i.e. temperature T and compression factor $f(= n_B/n_o, n_o = 0.17/fm^3)$ behind the front. Whenever T and f are in QGP sector of QGP-hadron phase diagram we assume that, within the slice 1-2 fm behind the traversing beam nuclei thermalized QGP is formed.

We tried several models of nuclear matter to get equation of state, but finally our results represented here are based on Walecka mean field model, Statistical bootstrap model of point particles, and Hybrid model of free N, Δ, π - gas with phenomenological repulsion potential fitted at low energies. The qualitatively the results for all models are the same.

QGP is described by standard model of four fermions (u,d,s, c - quarks) and eight bosons (massless gluons). The paritition function with several sets of parameters tried, has been calculated up to the lowest order of perturbative expansion. The masses and coupling constant are taken density and temperature dependend with the running momentum $q = ((2T)^2 + (\mu_B/3)^2)^{\frac{1}{2}}$.

The evolution of QGP (its expansion and flow) is governed by hydro-and thermodynamics. One of the strongest constraints is given by baryon number conservation and entropy production condition (1), (3): i.e. surface hadronic deflagration of QGP at thermal and chemical equilibrium is forbiden prior to the reversed phase transition QGP-Hadronic gas. In consequence all hadrons are produced at transition temperature, which (for $f \lesssim 10$) is roughly 160-180 MeV and, as entropy production in deflagration is low, they preserve degrees of freedom of QGP close to the transition.

3. Results: Our model gives a unique possibility to relate T and f when equation of state is given. According to the authors knowledge this result is unique and original (4). In the approximations used the result for T(f) do not depend on size of the neither beam not target nuclei. The result for assumed (ud), (uds), (udsc) QGP is presented on Fig. 1.

The second result of our model which we wish to present to the Conference is strangeness and charm relative yield when QGP is formed in nuclear collision. Due to high entropy per baryon and, in principle, unlimited temperature as well as due to peculiar properties of QGP evolution its presence offers more abundant production of heavy flavours than any hadronic process without QGP.

Due to the finite relaxation times the production of heavy flavours at lower temperatures is damped by finite life time of QGP. In consequence the production of strangeness and charm displays a pronounced temperature-threshold enhancements. For nuclear fireball created according to the our scenario the strange particles start to be copiously produced at T ≳ 240 MeV, (see Fig. 2) whereas charmed particles have threshold at T ≳ 500 MeV.

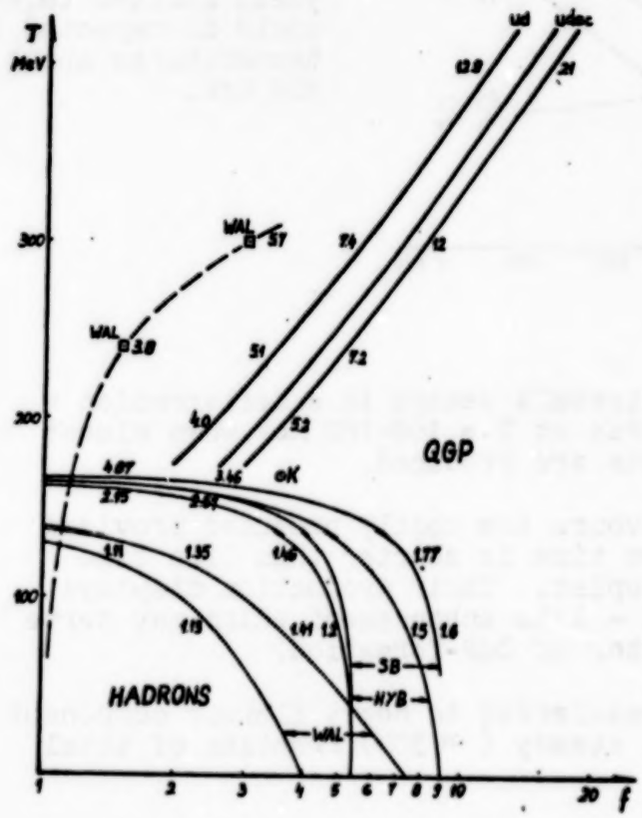


Fig. 1

Temperature T and compression factor (f) of nuclear fireball together with phase diagram for Walecka (WAL), Hybrid (HYB) and stat. Bootstrap (SB) models of hadronic gas.

T-f curve for hadronic fireball has been got for ud, uds and udsc flavours. WAL-curve has been got when compressed matter is assumed to be Walecka nuclear matter. K is "Kajantie point". All numbers refer to energy per baryon.

4. Conclusions: According to our model and within the approximations done our results indicates:

(i) High temperatures in nuclear fireballs are not likely to be common phenomenon at high energy interactions. It is relatively easy to heat nuclear fireball up to T = 200 - 240 MeV.

ORIGINAL PAGE IS
OF POOR QUALITY

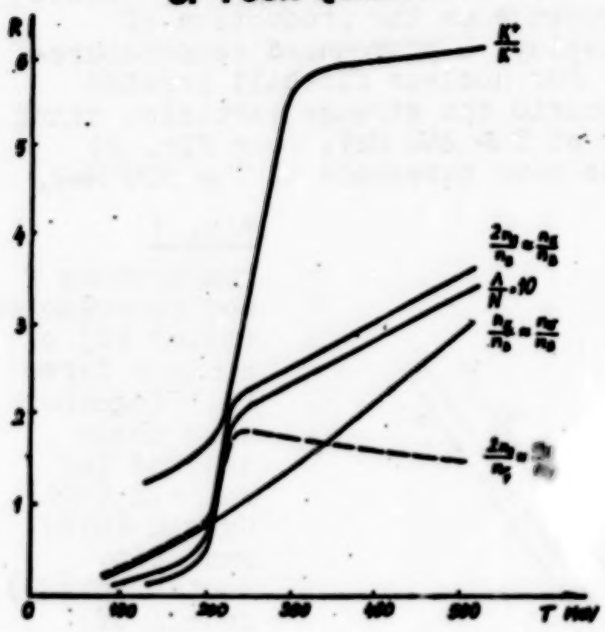


Fig. 2

Ratio R of strange quarks and hadrons yield v.s. initial temperature of nuclear fireball. The threshold behaviour is seen only for strange hadron yield but not for nonstrange component. For charmed particles yield similar threshold is expected for temperatures above 500 MeV.

(ii) Nuclear fireball decays in a deflagration - like process at T = 160-180 MeV when almost all hadrons are produced.

(iii) Heavy flavours are easily produced provided relaxation time is shorter than life time of QGP droplet. Their production displays threshold - like enhancement which may serve as indicator of QGP-formation.

(iv) Energy transferred to heavy flavour component is almost steady ($\approx$ 30%) fraction of total energy.

(v) Charmed quarks and consequently charmed particles are produced in very low amount (at T = 500 MeV n_c/n_B is $\approx 10^{-6}$).

---

*On leave of absence from University of Lodz, Poland.

References:

1. Quark matter Formation, Ed. M. Jacob, H. Satz: Singapore, 1982.
2. J. Klosinski, Proc. of 18th ICRC, Vol.II, p. 166.
3. L. Van Hove, Z, Phys. C, 21, (1983) 93-98.
4. R. Anishetty et al, Phys. Rev. 22 (1980) 2793.

N85-35887

RINGLIKE INELASTIC EVENTS IN COSMIC RAYS AND ACCELERATORS

I.M.Dremin, A.M.Orlov, M.I.Tretyakova
P.N.Lebedev Physical Institute,
Leninsky Prospect 53, Moscow, 117924, USSR

In cosmic rays [1-3] and in accelerators [4] there were observed single inelastic processes with densely produced (azimuthally isotropic) groups of particles exhibiting spikes in the pseudorapidity plot of an individual event (i.e. ringlike events).

Theoretically the existence of such processes was predicted [5] as a consequence of Cherenkov gluon radiation or, more generally, of deconfinement radiation [6].

Nowadays some tens of such events have been accumulated at 400 GeV [7] an at 150 TeV [8].

Analyzing ringlike events in proton-nucleon interactions at 400 GeV/c we show [7] that they exhibit striking irregularity in the positions of pseudorapidity spikes' centers which tend to lie mostly at 55,90 and 125° in cms. It implies rather small deconfinement lengths of the order of some fermi.

We have chosen high-multiplicity events with $n_{ch} \geq 12$ among all proton-nucleon interactions at 400 GeV in the photoemulsion experiment [9]. There were 284 events available. To select ringlike events we use some criteria (for more details see [7]) which single out those events with dense groups in the pseudorapidity plot containing more than 6 charged particles within the unit pseudorapidity interval.

In total 59 among 284 event have been chosen as ringlike events what corresponds to 1 mb of their production cross section.

The very important feature of ringlike events is the position of rings. The center of a ring should be in some way close to the direction of the gluon emission in the above treatment. We have determined the positions of the

ORIGINAL PAGE IS
OF POOR QUALITY

N85-15887

centers of rings in all 59 events. They are shown in Fig.1.

In Fig.2 we show the example of one ringlike event (among 59 available).

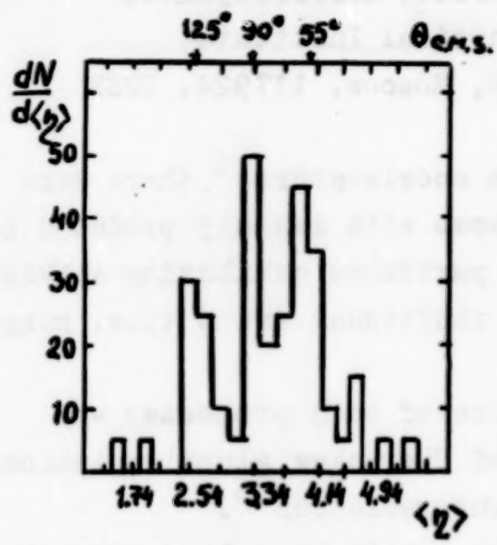


Fig.1 The pseudorapidity distribution of spikes' centers.

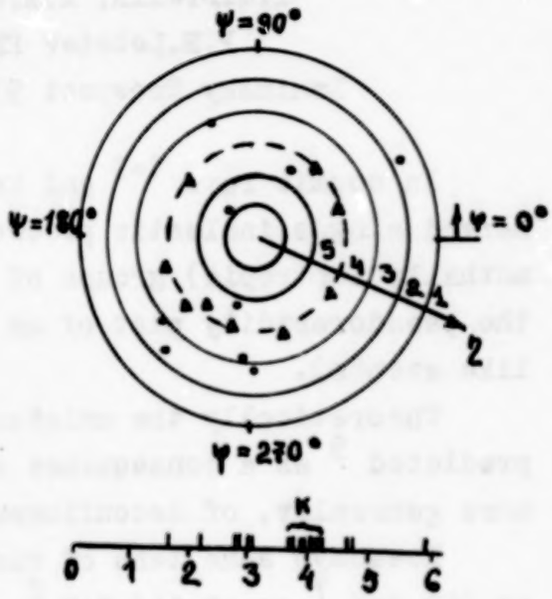


Fig.2 The pseudorapidity distribution (a) and the pseudorapidity azimuthal plot (b) of a pN-event (0+0+18p) with a ring of 9 charged particles ($\langle\eta\rangle$ = 4.02, $\langle\Delta\eta\rangle$ = 0.066). Triangles mark the particles, points correspond to other particles.

The most striking feature of Fig.1 is the irregularity in appearance of rings *) and their tendency to rather large cms angles (upper axis).

The only reliable explanation is that the particles within the rings are produced by some process the formation length of which is rather short. Actually, the large emission angles of Cherenkov gluon radiation were predicted [5] in 1979

*) The indirect confirmation to such irregularity can be drawn from ISR-data [10] about two-particle rapidity correlations (for more details see [7]).

as a consequence of a thinness of hadronic targets. Later it was shown [6] that the deconfinement of quarks within hadronic targets can provide stronger effect at the same angles. The maximum of forward (in cms) emission of gluon jets appears at the laboratory angle

$$\theta_{lab} \approx (2\pi/\omega l)^{1/2} . \qquad (1)$$

where ω is an energy of a gluon jet (i.e. of a group of particles) and l is a formation length which should be close to the deconfinement length. Let us remind that an analogous value for protons usually increases with primary energy E of an emitting particle as $\omega^{-1}\gamma^2 \equiv \omega^{-1}(E/m)^2$ i.e. it must be very large at 400 GeV and correspondingly the emission angle is small (of the order of m/E according to (1)).

The average number of emitted within the ring gluons in an individual event is estimated [6] as about 3 at 400 GeV and about 6 at 150 TeV. Therefore the rings could be totally isotropic at 150 TeV while some azimuthal substructure may be noticeable at 400 GeV. We have not investigated it in detail.

If the maxima at 55 and 125° shown in Fig.1 are interpreted as ones due to gluon emission by deconfined quarks then using (1) together with the obvious inequality $\omega < E$ one gets

$$l \gtrsim 2\,fm . \qquad (2)$$

The hadron momenta have not been measured [9] and therefore we can not estimate the value of ω in (1). However reasonable assumptions about transverse momenta show that the gluon radiation length l can not be much larger than, say, 10 fm.

This conclusion is strikingly different from above estimates for photon radiation length. It shows the fundamental difference between the electromagnetic and colour currents, the last one being strongly confined within small space regions. The formula (1) provides unique means to

determine the extension of that region.

In conclusion, the ringlike events (i.e. events with high density of secondary particles within a narrow pseudorapidity interval) provide an unique possibility to define the length of action of deconfined colour currents. The above investigation shows that this length appears to be quite short (of the order of the hadron size). They also could reveal such important facts as the vector nature of gluons and the macroscopic features of the quark-gluon medium (for example, its refractivity). Further experimental work with higher statistics is needed for detailed study of those problems.

References

1. Apanasenko A.V. et al. (1979), JETP Lett., 30, 157.
2. Dremin I.M., Tretyakova M.I., (1981), Proc. XVII ICRC, V5, p.149.
3. Arata N., (1978), Nuovo Cim., 43A, 455.
4. Marutyan N.A. et al., (1979), Sov. J. Nucl. Phys., 29, 1566.
5. Dremin I.M., (1979), JETP Lett., 30, 152; (1981), Sov. J. Nucl. Phys., 33, 1357.
6. Dremin I.M., (1981), JETP Lett., 34, 617; (1983), Sov. J. Nucl. Phys., 37, 649.
7. Dremin I.M., Orlov A.M., Tretyakova M.I., (1984), JETP Lett., 40, 320.
8. Rushbrooke J.G., (1983), Preprint CERN EP 84034.
9. AGMT-collaboration, (1979), Sov. J. Nucl. Phys., 29, 678.
10. Cavasinni V. et al., (1984), Z. Phys. C, 21, 299.

N85-35888
HE 1.3-18

PHASE SPACE FACTORS IN MULTIPARTICLE PROCESSES

Robert J. Gould
Physics Department B-019
Univ. of Calif., San Diego
La Jolla, CA 92093 USA

ABSTRACT

General phase space theorems are discussed for the cases (A) with only energy conservation applied and (B) with energy and momentum conservation applied. It is shown that in the non-relativistic limit for N particles there is a very close relationship between the multiparticle phase space integral in case B and that for case A and N-1 particles.

1. Introduction. There are in physics many phenomena that can be described as phase space effects. By this is meant effects that are determined essentially by the number of states available to the system. Examples may be found in equilibrium statistical mechanics and in the evaluation of dynamical processes. In particular, the cross sections and rates associated with processes initiated by binary collisions are determined by the interaction that causes the process and also by the number of final states associated with the various products or channels for the reaction. Applications or examples of this kind of effect occur in electronic and atomic processes, chemical kinetics, nuclear reactions, and elementary particle processes. All of these processes can be represented as a reaction of the type

$$a + b \longrightarrow \text{products } (c + d + e + \cdots) . \tag{1}$$

In the c.m. frame and for given energy (E) available to the outgoing particles, the total momentum-space volume available to these particles is, with momentum and energy conservation imposed,

$$\phi^{(N)} = \int \cdots \int \prod_{j=1}^{N} d^3p_j \, \delta^{(3)}\left(\sum_{j=1}^{N} p_j\right) \delta\left(\sum_{j=1}^{N} E_j - E\right). \tag{2}$$

This quantity, proportional to the number of available final states, is fundamental and simple expressions for $\phi^{(N)}$ can be derived for small N when the outgoing particles are non-relativistic (NR), extremely-relativistic (ER), or even of general energy. When all are NR or ER (or even a mixture), it is possible to derive expressions for $\phi^{(N)}$ for general N, using various mathematical methods or tricks. One such trick will be illustrated in this paper.

In the limit where one of the outgoing particles (say, particle N) has a large mass, its energy $(p_N^2/2m_N)$ is small and can be neglected. Then, the $\delta^{(3)}$ function can be eliminated by integrating over d^3p_N, and

$$\phi^{(N)} \underset{m_N \ell g}{\longrightarrow} \psi^{(N-1)} = \int \cdots \int \prod_{j=1}^{N-1} d^3p_j \, \delta\left(\sum_{j=1}^{N-1} E_j - E\right); \tag{3}$$

88826 - 38A

that is, the heavy particle just plays the role of satisfying the momentum-conservation restriction. The phase space integral (3), with only the energy-conservation restriction applied is the one appearing in statistical mechanics in the so-called microcanonical ensemble. It turns out, however, that, in the NR limit, $\phi^{(N)}$ is very closely related to $\phi^{(N-1)}$ for an arbitrary distribution of masses $m_1, m_2, \ldots, m_N$; we shall demonstrate this in a simple way.

Before proceeding to consider the very special problem mentioned just above, a few other introductory remarks should be made. In modern particle physics the use of the invariant phase space volume $\phi^{(n)}$ is more common; this quantity is the same as $\phi^{(N)}$ except each factor d^3p_j is divided by $2E_j$, yielding Lorentz-invariant factors; the two δ-functions are also combined to a single invariant $\delta^{(4)}$ factor. The factors ϕ are certainly more convenient than Φ in relativistic calculations, but it is not clear which is actually more fundamental. In a sense Φ is, since it is proportional to the number of states. For examples of the use of the invariant ϕ-factors the book by Feri [1] may be consulted; this work also gives references to earlier papers on the general subject. A general survey is also given in a monograph [2] in preparation by the author.

2. General Expressions; NR Limit. If we make the change of variable

$$\underline{P}_j = (2Em_j)^{1/2}\underline{p}_j \ , \tag{4}$$

thereby introducing dimensionless momentum variables $\underline{p}_j$, the integral can be written in more convenient form. It is also convenient to introduce dimensionless masses in terms of the total mass M:

$$m_j = v_j^2 M \ ; \ \sum_{j=1}^{N} v_j^2 = 1 \ . \tag{5}$$

Then, in the NR limit,

$$\phi^{(N)} = (2\pi)^{3(N-1)/2}\Big(\sum_{j=1}^{N} v_j\Big)^3 E^{3(N-1)/2-1} I_N \ , \tag{5}$$

where

$$I_N = \int\cdots\int \sum_{j=1}^{N} d^3\underline{p}_j \, \delta^{(3)}\Big(\sum_{j=1}^{N} v_j\underline{p}_j\Big)\, \delta\Big(\sum_{j=1}^{N} \underline{p}_j^{\,2} - 1\Big) \tag{7}$$

is a dimensionless integral. In terms of the variables $\underline{p}_j$ and parameters v_j, the phase space integral Φ [eq. (3)] is

$$\Phi^{(N)} = (2\pi)^{3N/2}\Big(\sum_{j=1}^{N} v_j\Big)^3 E^{3N/2-1} J_N \ , \tag{8}$$

where

$$J_N = \int\cdots\int \sum_{j=1}^{N} d^3\underline{p}_j \, \delta\Big(\sum_{j=1}^{N} \underline{p}_j^{\,2} - 1\Big) \ . \tag{9}$$

In the following section we shall outline the proof that

$$I_N = J_{N-1} \tag{10}$$

This is, at first sight, a remarkable result that means, for example, that I_N is independent of the mass spectrum $\nu_1,\nu_2,\cdots,\nu_N$. The integral (9) for J_N can be evaluated easily by a number of methods (see [2] or almost any book on statistical mechanics):

$$J_N = \pi^{3N/2}\Gamma(3N/2) \ . \tag{11}$$

3. Theorem [eq. (10)] on Phase Space Integrals. The theorem is easy to prove for N=2 and 3, but it is of interest to prove it for general N. This can be done by considering the indices j=1, 2, ..., N labelling the particles as designating an N-dimensional space. With $\hat{e}_j$ as a unit vector along the jth axis of this space, the axes are taken to be orthogonal: $\hat{e}_j\cdot\hat{e}_k = \delta_{jk}$. In this space $\hat{\nu} = (\nu_1,\nu_2,\ldots,\nu_N)$ is a vector of unit length: $\hat{\nu}\cdot\hat{\nu} = 1$, because of (5). Also, in terms of $\hat{x} = (x_1,x_2,\ldots,x_N)$, and

$$d^3\hat{x} = \prod_{j=1}^{N} d^3x_j = dx_1\cdots dx_N dy_1\cdots dy_N dz_1\cdots dz_N \ , \tag{12}$$

the integral (7) can be written

$$I_N = \int d^3\hat{x}\ \delta(\hat{x}^2 - 1)\delta^{(3)}(\hat{\nu}\cdot\hat{x}) \tag{13}$$

But $\hat{\nu}\cdot\hat{x}$ is invariant to a rotation of the axes in the N-dimensional space, as is $\hat{x}^2$. Essentially, such a rotation corresponds to a relabelling of the particles. With this invariance, it is convenient to choose an orientation such that the vector $\hat{\nu}$ is along one axis such that, say, $\hat{\nu} = (0,0,\ldots,1)$ corresponding, physically, to the case $m_N >> m_{i<N}$. The δ-function $\delta^{(3)}$ is then simply $\delta^{(3)}(x_N)$ which can be eliminated by integration over d^3x_N. The resulting integral is then just J_{N-1} and the identity (10) is obtained.

It is interesting how in this problem we make use of the mass spectrum $m_1,m_2,\ldots,m_N$ to prove a theorem and simplify a derivation. In the ER limit we have no such device to employ and the evaluation of the corresponding $\phi^{(N)}$ is more complicated. However, the same trick employed to prove the result (10) can be used to derive results when we have, say, N NR particles and N' ER particles. For more details, see [2].

4. Acknowledgements. This research is supported by NASA through Grant NGR 05 005 004.

References

[1] M. L. Perl, High Energy Hadron Physics (New York: John Wiley and Sons, 1974).

[2] R. J. Gould, High Energy Phenomena in Astrophysics (in preparation, Princeton Univ. Press).

N85-35889

THE RESPONSE OF A SCINTILLATION COUNTER BELOW AN EMULSION CHAMBER TO HEAVY NUCLEUS INTERACTIONS IN THE CHAMBER

THE JACEE[+] COLLABORATION

T.H. Burnett(h), S. Dake(b), J.H. Derrickson(f), W.F. Fountain(f), M. Fuki(c), J.C. Gregory(g), T. Hayashi(b), T. Hayashi(g,j), R. Holynski(e,i), J. Iwai(h), W.V. Jones(e), A. Jurak(e,i), J.J. Lord(h), C.A. Meegan(f), O. Miyamura(d), H. Oda(b), T. Ogata(a), T.A. Parnell(f), E. Roberts(f), T. Saito(a), T. Tabuki(a), Y. Takahashi(f), T. Tominaga(d), J.W. Watts(f), B. Wilczynska(i), R.J. Wilkes(h), W. Wolter(e.i), and B. Wosiek(e,i).

(a) Institute for Cosmic Ray Research, University of Tokyo, Tokyo, Japan; (b) Department of Physics, Kobe University, Kobe, Japan; (c) Department of Physics, Okayama University of Science, Okayama, Japan; (d) Department of Applied Mathematics, Osaka University, Osaka, Japan; (e) Department of Physics and Astronomy, Louisiana State University, USA; (f) Space Science Laboratory, NASA/Marshall Space Flight Center, USA; (g) Department of Chemistry, University of Alabama, Huntsville, USA; (h) Department of Physics, University of Washington, Seattle, USA; (i) Institute for Nuclear Physics, Krakow, Poland; (j) Science and Engineering Research Laboratory, Waseda University, Tokyo, Japan.

ABSTRACT

In 1982 a hybrid electronic counter-emulsion chamber experiment was flown on a balloon to study heavy nucleus interactions in the 20 to $\simeq$100 GeV/AMU energy range. A gas Cerenkov counter, two solid Cerenkov counters, and a proportional counter hodoscope gave the primary energy, the primary charge and the trajectory of the particles, respectively. Using the trajectory information cosmic ray nuclei of $Z \geq 10$ were found reliably and efficiently, and interaction characteristics of the Fe group nuclei were measured in the chamber. A plastic scintillator below the emulsion chamber responded to showers resulting from interactions in the chamber and to non-interacting nuclei. Data on the response of the counter have been compared with simulations of hadronic-electromagnetic cascades to derive the average neutral energy fraction released by the heavy interactions, and to predict the performance of this kind of counter at higher energies. For the interacting events of highest produced particle multiplicity comparison between various simulations and the shower counter signal have been made.

1. The Instrument. The hybrid electronic counter-emulsion chamber instrument has been described[1] and some results of the interactions studies are presented at this conference[2,3]. Information on the measurements of primary charge and energy with the electronic counters is also presented[4]. For the purpose of this paper the counters above the emulsion chamber give a sample of heavy nuclei, carbon and above, energy of 22 GeV/AMU and above with charge known within Z±1 and energy differentially to 65 GeV/AMU and integrally above 65 GeV/AMU. The data available in this energy range contain 2,408 total particles. The

relevant emulsion chamber features are: Dimensions 50 cm x 50 cm x 21.5 cm ; 65 gm/cm^2 thick; 7.0 total radiation lengths; 1.4 interaction lengths thick for oxygen and 2.5 for Fe.

The burst scintillator was a 0.635 cm thick sheet of Ne 102 plastic, 57 cm x 57 cm, enclosed in a diffusion box viewed by two sets of two 7.62 cm photomultiplier tubes. One set of two tubes covered the pulse height range to 200 equivalent minimum ionizing particles (MIP). The other set (using dynode pulses) covered the range to 6000 equivalent MIP. The usable range of overlap included the fraction (~20%) of C to Si nuclei which passed through the emulsion chamber and allowed in-flight calibration. Figure 1 shows the pulse height spectrum caused by oxygen nuclei with the prominant non-interacting peak. The use of only two photomultipliers resulted in nonuniformity (±15%) which was mapped with muons and checked with in-flight calibration for use in corrections. Because of the lateral spread of the showers in this energy range this correction has some residual error.

2. Simulations. A simulation program was developed to predict the shower signal in equivalent minimum ionizing particles [Σ(Z fragments)^2 + protons + charged pions + (electrons > 1 MeV)]. The simulation program is modular with options allowed for processes such as fragmentation, pion generation, and electromagnetic cascade. Most shower counter simulations used a wounded nucleon model (WNM) with the average number of wounded nucleons equal to 0.3, an average inelasticity of 0.5, number of pions from $\langle N \rangle = 2.3E^{1/4}$, pion energies from the CKP model, and pion angles from a distribution with average P_T = 300 MeV/C. The electromagnetic cascade was a linear shower development function at the correct angle based on Rossi-Greisen but adjusted to later experimental results[5].

3. Results. Figure 2 shows the data from the burst counter for individual events with Z = 24 to 28. Also shown are results of simulations at 20 GeV/AMU and 60 GeV/AMU. These simulations were done by choosing, according to interaction length, a random location in the chamber at an incident angle of 30°. The results of repeated event simulations match well in average values the data from Z = 6 through 26 over the narrow energy range available to this experiment. Table I shows the results of simulations up to 200 GeV/AMU and data from this experiment. The results agreed with the average value of heavy nucleus energy going into electromagnetic cascades (0.12 for Fe), which has been used for energy estimation in passive emulsion chamber experiments at higher energies.

TABLE I

Pulse height and standard deviation for burst counter and simulations. Burst signal is in range 21 to 25 and ≥55 GeV/AMU. Simulations are average of 40 events.

E(GeV/n)	20	60	200
O Burst	252 ± 190	604 ± 468	
O SIM	231 ± 132	640 ± 455	1554 ± 1200

Fe Burst	951 ± 333	2082 ± 856	
Fe SIM	851 ± 239	2130 ± 934	5861 ± 2716

It is noted from Figure 2 that the events of highest produced particle multiplicity (as determined from the emulsions, see paper HE1.4-3 this conference) do not give exceptional burst counter signatures. Some simulations of these events have been attempted, using as a starting point the first interaction characteristics from the emulsions. One method of simulation started with the primary angle, interaction position, and number of wounded nucleons. The remainder of this simulation was the same as the WNM simulation described above. Another used the produced particle angular distribution list (reduced by a number of leading particles equal to the primary charge); and assumed a pion transverse momentum distribution of average $P_{t\pi^0}$ = 340 MeV/c and conservation of isotopic spin. These simulation results for the five highest multiplicity events generally exceeded the burst counter pulse height by one to four standard deviations. An analysis of individual event simulation results to varying parameters in the models is in progress. For peripheral interactions. such simulations are more obscured by subsequent fragment interactions which are not usually measured in the chamber.

4. Discussion. The behavior of the burst counter described above and the results of the simulations using the WNM compare well in average values and variance in the energy range of this experiment. Several effects, including the loss of shower particles from the sides of the scintillator, effect of shower lateral spread on uniformity corrections, and knock-on electrons cascading in the calorimeter have been estimated but not modeled in detail.

References

1. Austin, R.W. et al., Papers of the 18th ICRC, T2-15 (1983).
2. Burnett, T.H. et al., presented by B. Wosiek, this conference.
3. Burnett, T.H. et al., presented by S. Dake, this conference.
4. Paper OG4.1-9, this conference.
5. Miller, D., Phys. Rev., 5:11, 2677-2683, 1972.

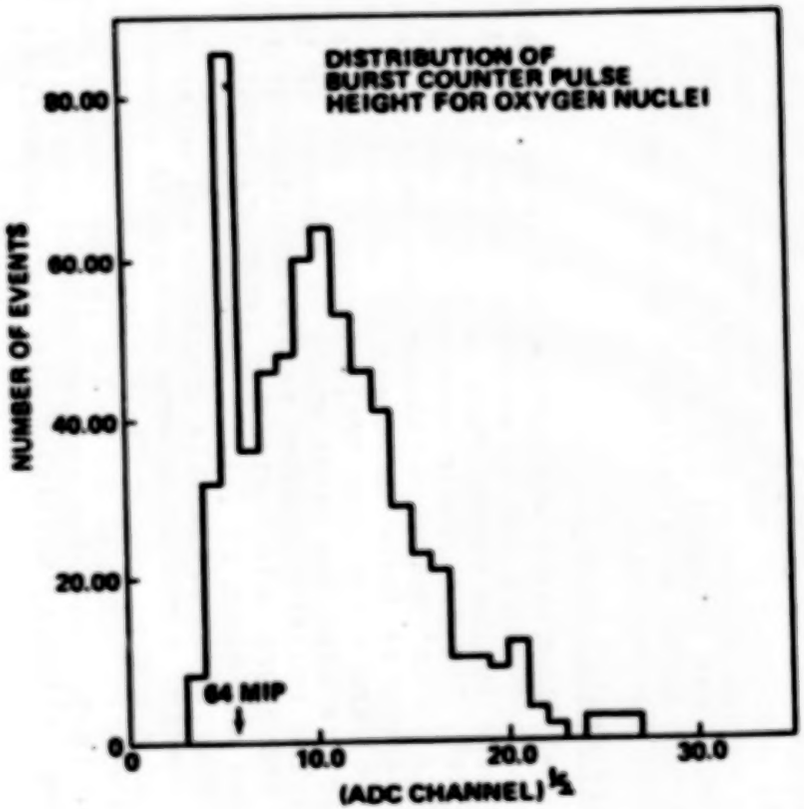


FIGURE 1

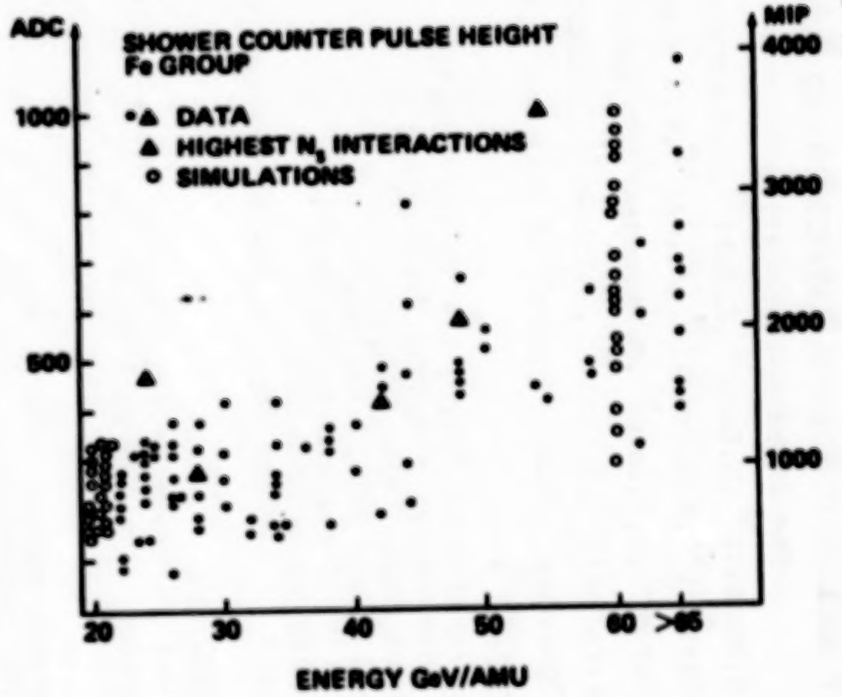


FIGURE 2

NASA - GSFC

HE1.4-2
N85-35890

HEAVY NUCLEUS COLLISIONS BETWEEN 20 AND 60 GeV/NUCLEON.

The JACEE Collaboration

T.H.Burnett[h], S.Dake[b], M.Fuki[b], J.C.Gregory[g], T.Hayashi[d], R.Holynski[i], J.Iwai[h], W.V.Jones[e], A.Jurak[i], J.J.Lord[h], O.Miyamura[c], T.Ogata[a], T.A.Parnell[f], T.Saito[a], T.Tabuki[a], Y.Takahashi[g], T.Tominaga[c], B.Wilczynska[i], R.J.Wilkes[h], W.Wolter[i], B.Wosiek[i].

a) ICR, University of Tokyo; b) Kobe University;
c) Osaka University; d) Waseda University;
e) Louisiana State University;
f) Marshall Space Flight Center;
g) University of Alabama in Huntsville;
h) University of Washington;
i) Institute of Nuclear Physics, 30-055 Kraków, Poland.

1. Introduction

Interest in studying ralativistic nucleus-nucleus interactions arises from the fact that they offer an opportunity to probe nuclear matter at high density and temperature. It is expected that under such extreme conditions a transition from hadronic matter into quark-gluon plasma occurs and that in the interactions of highly relativistic nuclei such conditions are created [1]. Before energetic nuclei beams will be available at new ion accelerators, cosmic rays remain a unique source of high energy heavy nuclei. JACEE-3 experiment was designed for study the collisions of heavy cosmic ray nuclei with different nuclear targets at energies beyond 20 GeV/nucleon.

2. Experimental method

JACCE-3 experiment was carried out using a combined electronic counters and an emulsion chamber detector, which was exposed to the cosmic rays on a balloon at an altitude of 5 g/cm^2. The electronic counters were placed on the top of a 50 x 50 cm^2 emulsion chamber. The counter system measures the energies (between 20 and 60 GeV/nucleon), charges (from Z=6) and determines trajectories of incident nuclei. It registers also the burst energies released in the interactions. The emulsion chamber serves simultaneously as both target and coordinate/ionization recorder. Details of the apparatus are given in [2].

The charges of projectile fragments and emission angles of all charged secondaries were measured in consecutive layers of emulsion and/or CR-39 plates downstream the interaction vertex. Charged particles in the forward cone were detected in the emulsion chamber without ambiguity. For each event the following multiplicities were determined:

N_F- number of multicharged projectile fragments ($Z \geq 2$);

N_p- number of released protons from incident nucleus, $N_p = Z_p - \sum_{i=1}^{N_F} Z_{F,i}$, where Z_p is the charge of primary nucleus;

N_{sf}- number of relativistic ($\beta \geq 0.7$) singly charged secondaries emitted in the forward hemisphere: $\theta \leq \theta_{1/2}$, where $\theta_{1/2}$ corresponds to $\pi/2$ in the center of mass of proton-proton collision;

$N_{mf} = N_{sf} - N_p$, number of produced charged particles (mesons);

N_{sp}-number of spectator protons (see explanation below);

$N_{part} = N_p - N_{sp}$, number of protons participating in the collision.

Spectator nucleons are not involved in the collision. The number of spectator protons, N_{sp}, can be determined for each event by selecting from singly charged particles those fulfiling a given emission angle criteria [3]. Among participated nucleons (N_{part}) are wounded nucleons which interact inelasticaly in the target and nucleons which do not contribute to the particle production but still participate in the collision as the secondaries scatter off them. It is not possible to distinguish experimentally between wounded protons and those originating from cascade processes, however it is natural to assume that N_{part} is related to the number of wounded protons.

3. Results

The analysis was performed on an unbiased sample of heavy primary ($Z_p \geq 22$) interactions with three different targets: light target=CHO, emulsion and lead. The detailed measurements have been completed for 70 interactions with $E_p \leq 60$ GeV/n out of 120 heavy nuclei recorded. Table 1 summarizes the inclusive data for interactions of "iron" group nuclei on different targets. Multiplicities and dispersions are calculated for the forward cone only. The values of the N_{mf}/D ratio are close to 1 independently of the target mass being consistent with the predictions of the superposition models for nucleus-nucleus interactions [4]. In Figs.1a,b,c the inclusive pseudorapidity distributions obtained on different targets are presented. The increased of the particle production on heavier targets in forward region is seen. In Table 2 we compare our results with the data for proton collisions with the same targets [5]. The p-nucleus data are taken in the same angular region and are extrapolated to the same primary energy $\langle E_p \rangle$. The ratio of the average multiplicity in nucleus-nucleus collisions to the mean multiplicity in p-nucleus interactions can be compared to the average number of wounded nucleons in projectile nucleus N_{wn}, calculated from the simple geometrical formula: $\bar{N}_{wn} = A_p \sigma_{pA} / \sigma_{pp}$. Within the limits

of statistical errors these two quantities agree with each other. Thus, we observe an extension of p-nucleus data to nucleus-nucleus ones on the base of simple superposition of independent collisions of nucleons from projectile nucleus.

If we select the events with different number of wounded nucleons than, we expect (basing on a superposition picture) that the multiplicity in nucleus-nucleus collisions will depend linearly on the number of wounded nucleons. Experimentally it is only possible to do a selection according to the number of participating nucleons, so the quantitative comparison with model predictions is not possible. Qualitatively we observe the increase of the multiplicity with increasing number of participating nucleons (Fig.2), but this dependence is much weaker than the one expected from superposition of p-nucleus collisions. This discrepancy may be explained by the fact that among N_{part} there are protons which do not contribute efficiently to the particle production. On the other hand we do not expect a dependence of $\bar{N}_{mf}$ on the number of spectator nucleons, unless the latter are not correlated with participating nucleons. Only for events with a total disintegration of primary nucleus into singly charged fragments such correlation exists. In Fig.3 the dependence of $\bar{N}_{mf}$ on the number of spectator nucleons is shown.

From the central rapidity densities we can estimate the energy density created in the collision. Using the formula given by Bjorken [1] and taking $\bar{P}_t$=0.4 GeV/c we obtain mean energy densities smaller than 0.5 GeV/fm^3. This is below the critical value required for the phase transition [1]. For the highest multiplicity events the energy density approaches 1 GeV/fm^3. The characteristics of these events will be presented separately at this conference.

4. Conclusions

The presented results from JACEE-3 experiment (multiplicities, $\bar{N}/D$ ratios, comparison with p-nucleus data) support the hypothesis that nucleus-nucleus interactions can be considered as a simple superposition of independent p-nucleus collisions. The similar conclusion was obtained from an analysis of ^{22}Ne-emulsion interactions at primary momentum 4.1 A GeV/c and with a high event statistics [6]. No evident signals of phase transition have been observed, suggesting that the detection of exotic phenomena requires a high statistics experiments with a possibility to look for specific signatures.

References

1. See for example: E.Shuryak, Phys.Rep. 61, 71 (1980), J.D.Bjorken Phys.Rev.D27, 140 (1983), J.Cleymans et al., Z.Phys.C17, 341 (83).
2. JACEE Collaboration, 18th ICRC Conf.Papers 9, 375, 379 (1983).
3. A.S.Goldhaber, Phys.Lett.B53, 306 (1974).
4. A.Bialas etal., Nucl.Phys.B111, 461 (1976), K.Kinoshita et al., Z.Phys.C8, 205 (1981), A.Capella et al., preprint TH.3700-CERN.
5. W.Busza et al., Phys.Rev.D22, 13 (1980).

N85-35891

ORIGINAL PAGE IS
OF POOR QUALITY

6.B.Wosiek et al.,this conference paper HE1.4-7.

Table 1.

A_T TARGET MASS	No. of events	$\langle z_p \rangle$	$\langle E_p \rangle_{cut}$	$\bar{N}_{mf}$	$\bar{N}_{mf}/D$
CHO	45	25.1	36	21.9± 3.0	1.09±.19
Emulsion	10	25.0	28	28.9±11.4	.80±.36
Pb	15	24.8	34	41.1±10.6	1.00±.32

Table 2.

A_T	$\bar{N}_m^{FeA_T}(\eta^{LAB}\geq 2)$	$\bar{N}_m^{pA_T}(\eta^{LAB}\geq 2)$	$\bar{N}_m^{FeA_T}/\bar{N}_m^{pA_T}$	$\bar{N}_m^{Fe}(A_T)^{calc.}$
CHO	22.8± 3.3	2.6±0.2	8.8±1.4	6.6
Em	29.8±11.6	3.0±0.3	9.9±4.0	10.3
Pb	45.5±12.3	3.0±0.45	15.2±4.7	18.3

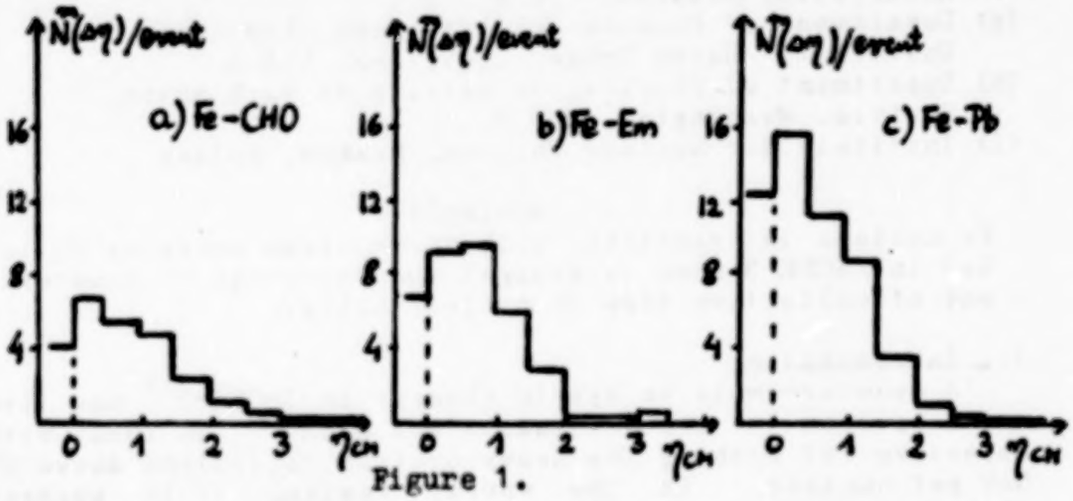


Figure 1.

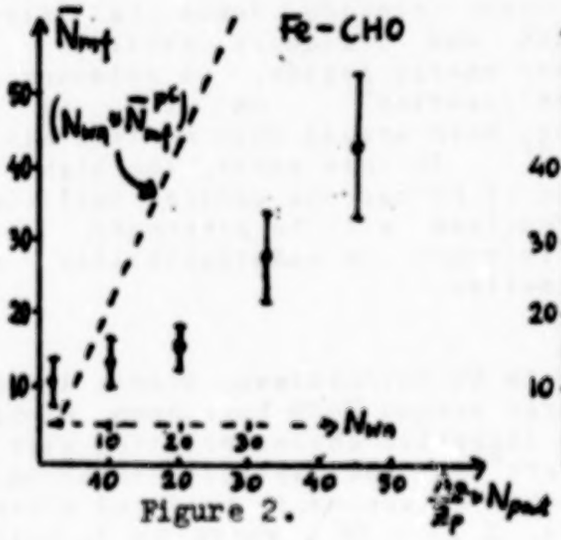


Figure 2.

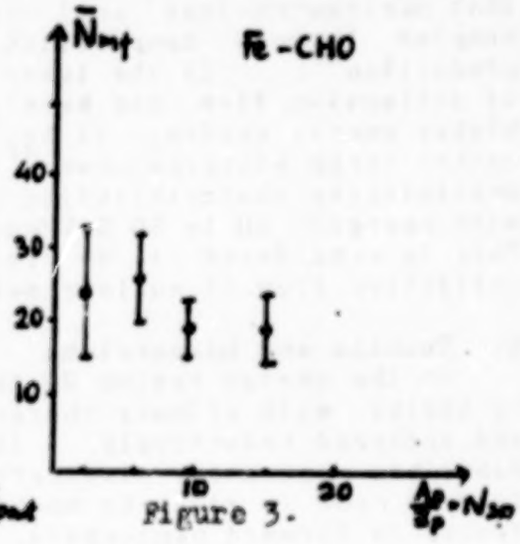


Figure 3.

N85-35891
HE 1.4-3

CHARACTERISTICS OF CENTRAL COLLISION EVENTS IN FE-NUCLEUS INTERACTIONS FROM 20 TO 60 GEV/NUCLEON

T.H. Burnett(h), S. Daka(a), J.H. Derrickson(f), W. Fountains(f), M. Fuki(c), J.C. Gregory(e), Ta. Hayashi(e), To. Hayashi(a), R. Holynski(i), J. Iwai(h), W.V. Jones(g), A. Jurak(i), J.J. Lord(h), C.A. Meegan(f), O. Miyamura(d), H. Oda(a), T. Ogata(b), T.A. Parnell(f), E. Roberts(e), T. Saito(b), S. Strausz(h), T. Tabuki(b), Y. Takahashi(e), T. Tominaga(d), B. Wilczynska(i), R.J. Wilkes(h), W. Wolter(f) and B. Wosiek(i)

(a) Kobe University, Nada-ku, Kobe 675, JAPAN
(b) ICR, University of Tokyo, Tanashi, Tokyo 188, JAPAN
(c) Okayama University of Science, Ridai-cho, Okayama 700, JAPAN
(d) Osaka University, Toyonaka, Osaka 560, JAPAN
(e) Department of Chemistry, University of Alabama in Huntsville, Huntsville, Alabama, U.S.A.
(f) Space Science Laboratory, Marchall Space Flight Center, National Aeronautics and Space Science Administration, Huntsville, Alabama, U.S.A.
(g) Department of Physics and Astronomy, Louisiana State University, Baton Rouge, Louisiana, U.S.A.
(h) Department of Physics, University of Washington, Seattle, Washington, U.S.A.
(i) Institute for Nuclear Physics, Krakow, Poland

ABSTRACT

Fe nucleus interactions with per-nucleon energies 20 to 60 GeV in JACEE-3 seem to suggest the existence of compression and of collective flow in nuclear matter.

1. Introduction

A counter-emulsion hybrid chamber in JACEE-3[1] was flown on a balloon at the altitude (5.4 g/cm^2) in 1982 with objective of probing the heavy nuclear collisions above 20 GeV per nucleon. In the energy region, it is suggested that nucleus-nucleus collisions provide dense collision complex through compression and secondary particle production[2]. In the lower energy region, an evidence of collective flow has been reported[3]. And also, at higher energy region, it has been argued that nucleus has rather large stopping power[4]. In this paper, the high multiplicity characteristics of Fe-nucleus central collisions with energies 20 to 60 GeV/nucleon will be presented. This is considered to be relevant to compressibility and collective flow of nuclear matter.

2. Results and Discussions

In the energy region 20 to 60 GeV/nucleon, events induced by nuclei with primary charge around Z=26 have been sampled and analyzed selectively. Inclusive characteristics will be described separately elsewhere[5]. Multiplicity (Nsh) in forward cone is given by number of secondary produced charged tracks in forward hemisphere, $\Sigma_{\theta i<\theta h} Zi - Zp$, where θh is half

angle defined by $\tan \theta h = 2m/(m(m+Ec))^{1/2}$.

The scattering plot between multiplicity and incident energy/nucleon is shown in Fig. 1. Average values of multiplicity in Fe-CHO collisions are represented by crosses. These values are consistent with factor, 0.8 times of average forward multiplicities in proton-proton collisions as presented by a dotted curve in the figure.

The high multiplicity events of Fe-nucleus collisions are summarized in Table 1.

Table 1
List of High Multiplicity Events

Event	Nsh	Ec	Zp	Mode	Non-sp	dN/dy	aF
< CHO Target >							
#6- 869	101	55.	Fe	128ch+3He	37	40.	0.9
#5- 393	60	45.	Cr	108ch+ He+Be	33	35.	1.3
#1-1214	57	28.	Fe	104ch+ He	41	40.	1.2
#5-1834	55	37.	Cr	87ch+2He	37	35.	1.8
#6-1596	51	51.	Fe	90ch+2He	41	25.	1.0
#7-1357	51	46.	Ti	73ch+2He	37	35.	1.1
#2- 191	46	40.	Fe	84ch+5He	24	30.	1.2
#5-1215	40	22.	Fe	75ch+ He	43	25.	1.2
#7-1689	36	55.	Fe	56ch+ He+N+Li	17	25.	1.3
#6-1114	36	30.	Cr	58ch+ He	30	25.	1.9
#6-1409	35	58.	Fe	59ch+2He+O	15	25.	1.3
#5- 607	34	22.	Fe	57ch+ He+B	26	25.	2.0
#6- 141	34	22.	Fe	62ch+3He	44	25.	1.5
#4- 876	34	35.	Fe	66ch+ Be	37	20.	1.0
#6- 733	35	30.	Cr	62ch+2He+Li	28	20.	
#2- 497	30	38.	Ti	53ch+3He	26	15.	1.0
< Pb Target >							
#7- 642	134	41.	Ti	267ch	48	125.	2.0
#8- 378	105	33.	Fe	160ch	54	100.	2.0
#1-1542	93	51.	Fe	123ch+ He	43	50.	1.3
#6-1927	82	24.	Fe	164ch	56	60.	1.8
#4-2006	52	25.	Cr	90ch+3He+Li	30	50.	2.0
#1- 308	41	34.	Fe	68ch+3He	28	25.	1.3
#4- 400	36	48.	Cr	56ch+5He	15	20.	1.3
< AgBr Target >							
#4- 749	150	26.	Ti	265ch	48	95.	1.8
#8-1063	38	23.	Fe	77ch+ He+Si	38	25.	1.8
#1-1004	39	27.	Fe	70ch+ He+C	24	25.	1.4

Notes : Ec:primary energy(GeV/nucleon), Zp:incident charge
Non-sp:number of non-spectator nucleons
dN/dy:max of rapidity density, aF:slope of F-plot;
$F/(1-F)=(\tan(\theta))^{aF}$

In Fig. 2, pseudo-rapidity distributions of Ti(41 GeV/nucleon)/Pb and Ti(26 GeV/nucleon)/Em are shown. In the figure, curves are calculations of multi-chain model(MCM)[7]. Both events have more tracks in the central region in comparison with the model calculation. The forward multiplicity (Nsh) of these events are 134 and 150.

ORIGINAL PAGE IS
OF POOR QUALITY

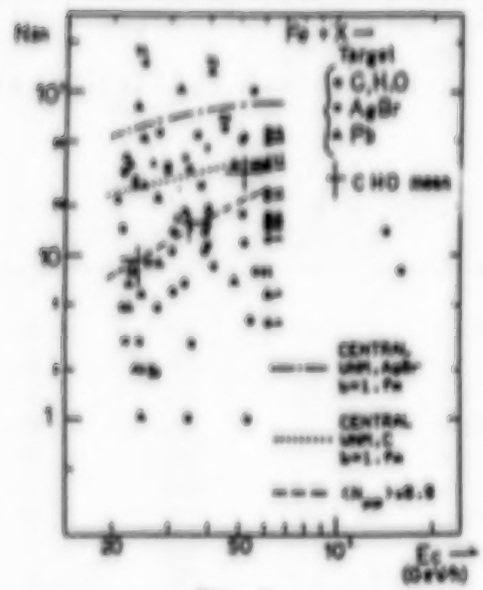


Fig. 1
Scatter Plots between Energy (Ec GeV/n) and Multiplicity (Nsh)

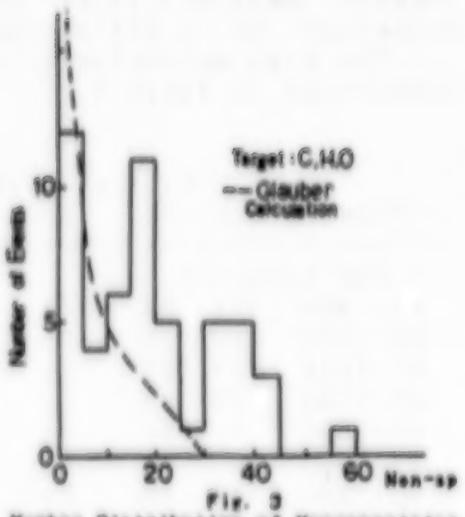


Fig. 3
Number Distribution of Non-spectator Nucleons

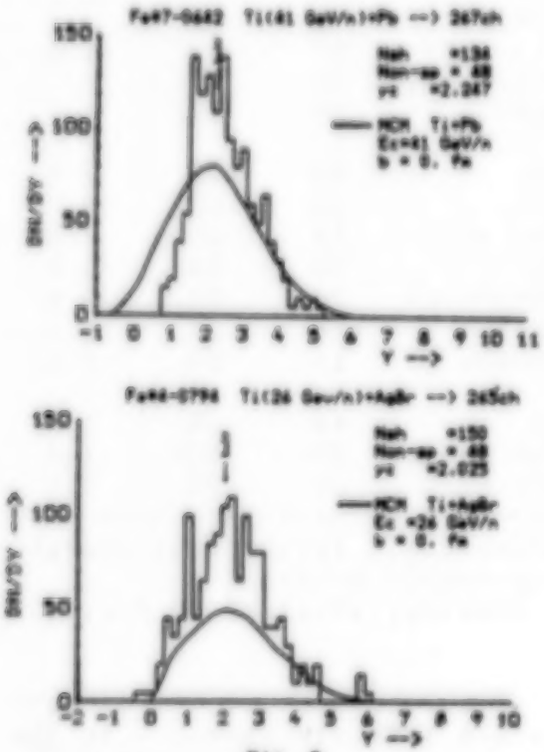


Fig. 2
Pseudo Rapidity Distributions of High Multiplicity Events

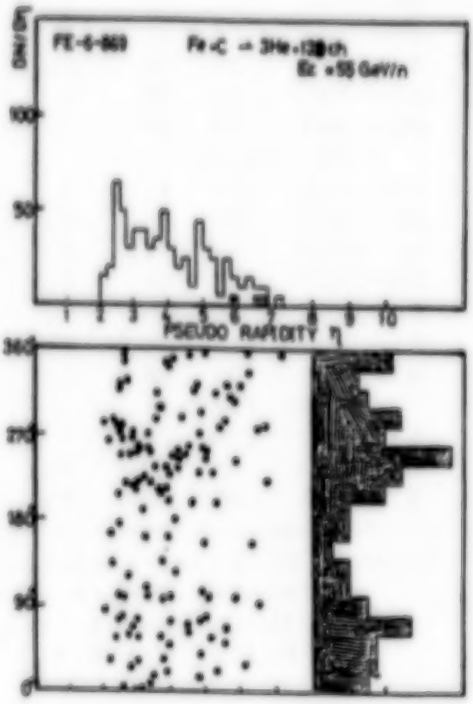


Fig. 4
Azimuth Angle and Pseudo Rapidity

N85-35839

ORIGINAL PAGE IS
OF POOR QUALITY

respectively, which are three standard deviation from average value. The maximum heights of pseudo-rapidity densities are 125 and 95, respectively. These values are comparable with the maximum height in high multiplicity events above TeV /nucleon region[7].

In the iron collisions with CHO-target, number of spectator protons was obtained by comsecutively adding all relativistic singly charged tracks starting with the most forward until mean value of tan θi coincides with that of evapolation formula of Goldhaber[8] boosted by projectile velocity (evapolation temperature was assumed as 10 MeV). Number of non-spectator projectile protons (which may or may not be 'wounded') are defined by Zp (projectile charge)-ΣZf(fragment)-Nsp(number of spectator protons). The number of non-spectator nucleon (Non-sp) is estimated by (Zp - ΣZf - Nsp) x Ap/Zp, where Ap is mass number of projectile. The distribution of the non-spectator nucleon number(Non-sp) is shown in Fig. 3. The curve in the figure is a calculation of Glauber's model[9]. Thus, we find a lump of events (12 events) in the region 25 < Non-sp < 56. We can define such events as central collisions. Six events of them have more tracks at the central region in comparison with multi-chain model assuming head on collision. This feature may be interesting in connection with the stopping power problem[4].

One of them, event Fe(55 GeV/nucleon)/CHO has very large multiplicity and dipole type azimuthal distribution as shown in Fig. 4. And also the slope of F-plot in this event is 0.9. The existence of such event is considered to be suggestive for collectiveness of nucleus-nucleus collision in the energy region. However, high multiplicity events Ti(41 GeV/nucleon)/Pb and Ti(26 GeV/nucleon)/Em show isotropical distributions of azimuthal angles and their slopes of F-plot are 2.0 and 1.8, respectively.

References

1) S. Dake et al. JACEE collaboration, Proceedings of the 18th International Cosmic Ray Conference, Bangalore (1983).
T. A. Parnell et al. JACEE collaboration, Quark Matter 84.
O. Miyamura et al. JACEE collaboration, Quark Matter 84.
2) T. Ludlum and H. Wegner(Ed. s), Proceedings of the Quark Matter 83, Nucl. Phys. A418 1(1984).
3) H. A. Gustafsson et al., Phys. Rev. Lett. 52 1950(1984).
4) W. Busza and A. S. Goldhaber, Nucl. Phys. A418 635c(1984).
5) T. H. Burnett et al. JACEE collaboration, Proceedings of this conference.
6) K. Kinoshita, A. Minaka and H. Sumiyoshi, Z. Phys. C8 205 (1981).
7) T. H. Burnett et al. JACEE collaboration, Phys. Rev. Letters 50 2062 (1983) and ibid 51 1010 (1983)
8) A. S. Goldhaber, Phys. Letters 53B 306(1974)
9) A. Bialas, M. Bleszynski and W. Czyz, Nucl. Phys. B111 461 (1976).

N85-35892

HE 1.4-4

Nucleus-Nucleus Interaction above Several Hundred GeV/n

The JACEE Collaboration

T.H.Burnett(h), S.Dake(b), M.Fuki(c), J.C.Gregory(g), T.Hayashi(g), R.Holynski(e,i), J.Iwai(h), W.V.Jones(e), A.Jurak(e,i), J.J.Lord(h), O.Miyamura(d), H.Oda(b), T.Ogata(a), T.A.Parnell(f), T.Saito(a), S.Strausz(h), M.Szarska(e,i), T.Tabuki(a), Y.Takahashi(f), T.Tominaga(d), J.W.Watts(f), J.P.Wefel(e), B.Wilczynska(i), R.J.Wilkes(h), W.Wolter(e,i), and B.Wosiek(e,i).

(a) Institute for Cosmic Ray Research, University of Tokyo, Tokyo, Japan
(b) Department of Physics, Kobe University, Kobe, Japan
(c) Department of Physics, Okayama University of Science, Okayama, Japan
(d) Department of Applied Mathematics, Osaka University, Osaka, Japan
(e) Department of Physics and Astronomy, Louisiana State University, Baton Rouge, Louisiana, USA
(f) Space Science Laboratory, NASA Marshall Space Flight Center, Huntsville, Alabama, USA
(g) Department of Chemistry, University of Alabama in Huntsville, Huntsville, Alabama, USA
(h) Department of Physics, University of Washington, Seattle, Washington, USA
(i) Institute of Nuclear Physics, Krakow, Poland

1. Introduction

At an extreme condition of high pressure, constituents of hadron, quark and qluon, are expected to be deconfined and then transit into a plasma phase(Quark-Gluon-Plasma). Such an extreme condition can be realized through high density hadronic matter and at present, we have no means other than to observe signals from such state through high energy heavy ion collision[7].

The Japanese-American Cooperative Emulsion Experiment(JACEE) have been investigating high energy nuclear interactions of cosmic ray nuclei by mean of balloon-borne emulsion chamber. Current exposure parameters are listed on Table 1. Analysis of last two experiments(JACEE4 and JACEE5) are still in progress. The quasi-inclusive characteristics of nucleus-nucleus collisions above TeV/n region obtained by first three experiments and some anomalous phenomena observed in our experiment had been already reported[1,2]. We present here, a result of semi-inclusive* analysis of sample set of central collision events, concerning to multiplicity, rapidity fluctuation for extremely high multiplicity events and correlation between transverse momentum and estimated energy density.

Flight	Altitude (g/cm^2)	Time (hrs)	Area (m^2)
JACEE0	8.0	29.0	0.20
JACEE1	3.7	26.5	0.80
JACEE2	4.0	29.6	0.80
(JACEE3	5.0	39.0	0.25)
JACEE4	4.5	56.0	0.80
JACEE5	5.0	15.0	0.80

Table 1. Exposure Parameter

2. Method

The emulsion chamber have primary, target, space and calorimeter

---

*) Address for correspondence: Institute for Cosmic Ray Research, University of Tokyo, 3-2-1, Midori-cho, Tanashi-shi, Tokyo 188, JAPAN

sections. The primary section contains emulsion layers of high and low sensitivity(Fugi ET7B and ET-6B), coated 0.150-0.200 mm thick on both side of 0.800 mm acrylic base, and CR-39, where primary charge is measured by grain counting, delta ray counting on emulsion and etched pitch rate in CR-39, errors contained in charge measurement being 0.2e, 0.5e and 1e, respectively. The target section contains sandwich of 2.0 mm thick acryl plate and thin (0.050 - 0.075 mm) doubly coated emulsion plates to follow secondary tracks from nuclear collision, thick emulsion plates are also placed in this section for measurement of heavy fragment charge, the spacer of honeycomb is located at the downstream thereof to separate secondary particle. The calorimeter contains 1.0 - 2.5 mm thick lead plates, X-ray films and thin emulsion plates, where gamma ray, most of all from π^0, makes electron cascade shower which is visible on X-ray films for high energy event. The shower energy is measured by electron counting method for the most of events which shower cores are separated enough for electron counting, error in energy measurement for shower core being 22%. Emission angle of charged particle is measured by track position on emulsion plates. Relative error in angle measurement is less than 0.1 in unit of pseudo-rapidity. Transverse momentum of shower core is obtained from the energy and an angle measured from energy weighted center of shower cores. The average transverse momentum of an event is estimated by fitting of the distribution assuming exponential function. The above procedure with energy measurement overestimates average Pt by 3-7% in average depending on observed gamma ray multiplicity. In addition to this, one should note that, in exclusive analysis, event to event fluctuation may be larger than the above error. As an estimation of Pt of π^0 from observed gamma ray Pt_γ, $\langle 2Pt_\gamma \rangle$ is used for conventionally, which procedure, from kinematic reason, overestimates 43%, 5% and 0.9 % for π^0 Pt 100, 300 and 700 MeV/c, respectively, and average Pt of pion in the concerning energy region is known to be over 340 MeV/c[4]. For the case that shower cores overlap with each other in the most forward region depending on vertex location in the calorimeter, the transverse momentum of secondary π^0 is estimated from shower transition in forward restricted angular region, since profile of such superposed shower is determined by both angular and energy/Pt distribution of the secondary. Some events in calorimeter permit measurement with each core separated at large angular region probably due to their very high transverse momenta. In such case, Pt of shower core should be regarded as that of π^0. For the primary energy estimation, the mean Castagnoli method as well as total radiated cascade energy ΣE_γ are used.

3. Results

Tables 2-a and 2-b shows seven high multiplicity events of Ns greater than 400 and of two events of light nucleus with Carbon target events. Three events in Table 2-a were already reported, where observed multiplicity can be interpreted within calculation of Multi-Chain-Model(MCM)[3]. And also, all

Event Type	E_0 (TeV/n)	Nch	$2Pt_\gamma$ (GeV/c)	Pt_{π^0}(cone) (GeV/c)	dn/dη|nc	#
Ca + Pb	1.5	1050^{+300}_{-50}	0.95±0.31	0.55±0.05	258±12	A88
Si + Ag/Br	4.1	1010±30		0.55±0.05	183±10	G03
Ca + C	100.	760±30	0.525±0.04		81±10	G00
Si + Pb	4.	780	not yet		not yet	B02
Ca + Pb	0.5	670±40	not yet		142±8.4	B60
Ca + Pb	1.8	457	2.1±0.1		100±16	D27
Ar + Pb	1.0	416	1.2±0.2		134±8	C27

Table 2-a. High multiplicity events(Nch > 400) in JACEE

observed multiplicity in Table 2-a are still within prediction at impact parameter b=0 fm,(maximum predictable multiplicity is not necessary realized at b=0 fm for heavy nuclei, A > 16, depending on nuclear density distribution), however events in Table 2-b are out of HCM calculation.

Event Type	E_0	Nch	ΣPtγ	dn/dη|nc	Nch(HCM)	D
Li + C	15.	217	0.76±0.08	37.5±4.3	154	37
Ne + C	20.	156	0.62±0.08	26.5±3.6	122	30

Table 2-b. Unit same as Table 2-a. 6 and 7-th column are model calculation by HCM at b=0 fm.

The averaged transverse momentum of listed events, which are considered to be central collision, exhibit extremely high Pt values comparing to interpolation value from CERN ISR and SPS collider experiments[4].

We now estimate energy density of event, for which we use that was proposed by Bjorken[5], as in the following.

$$\epsilon \equiv \sqrt{\langle Pt\rangle^2 + m^2}\ \cdot dn/d\eta|_{\eta_c} \cdot 1.5/V,$$

where $dn/d\eta|_{\eta_c}$ is a pseudo-rapidity density of charged particle at CMS system, V being an interaction volume for which we choose $V=C\ Amin^{2/3}$, $C=2\pi$. Amin is the minimum of Aproj and Atarget. In the case of heavy fragment(s) existing in the secondary, mass number reduction is applied for Aproj. Fig. 1 shows scatter diagram between estimated energy density and Pt for which we used $2\langle Pt\gamma\rangle$ for the most case, which procedure does not significant influence on the result as previously mentioned, for the events apparently giving π^0 Pt, measured values are used as themselves.

At present, pseudo-rapidity fluctuation analysis had been performed for two high multiplicity events(C0 and G3), wherein multiplicity and its dispersion in windows of width δ on pseudo-rapidity are estimated from Independent Emission Model(IEM) of pure statistical assumption and from HCM, respectively. Results is that both of event are favor for IEM but for HCM, due to the observed fluctuation is not so large comparing to HCM, events C0 and G3 deviating 3σ from HCM and within 1σ and 1.4σ from IEM, respectively.

Azimuthal angle distribution of four events from high multiplicity events(A88, C0, G3 and H66) are also analyzed by Fourier transformation method. Similar analysis had been already proposed by F.Takagi on pseudo-rapidity distribution[6]. According to this analysis, three events (A88, G3 and H60) exhibit dipole structure, which probability is expected to be one event among several ten to several hundred events assuming independent

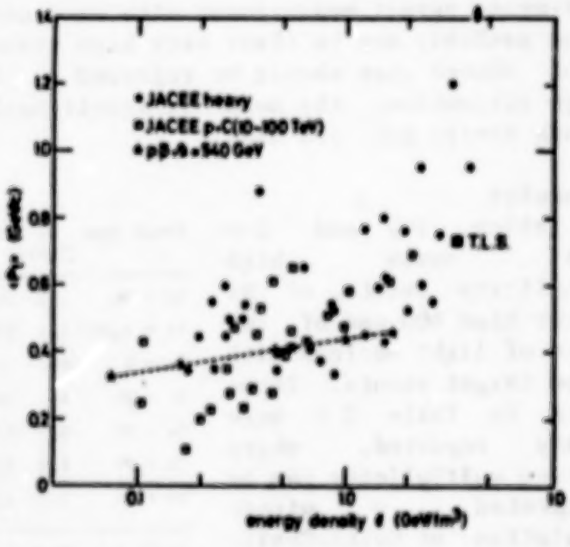


Fig.1 Correlation between energy density and Pt.

NSG-35393

emission of secondary, while event G3 is almost isotropic in azimuth.

4. Discussions and summary

As shown in Fig.1, the average transverse momentum seems to grow rapidly over the energy density around 2 GeV/fm . Multiple scattering effect for possible interpretation for this correlation does not describe qualitatively. If the observed correlation is attributed to phase transition of QGP, the observed characteristic energy density is consistent with the predicted critical value for deconfinement of quark and qluon at temperature around 200 MeV[7]. Though there still exists ambiguity in quantitative estimation for energy density such as volume estimation, the observed correlation characteristics might not change substantially.

From the view point of multiplicity, MCM gives fairly good estimation for high multiplicity events, however there still exist the events above maximum prediction of MCM. In the lower energy region of 20-60 GeV/n, there also observed extremely high multiplicity events from minimum bias sample of Fe group primary[8]. Because of a freedom of impact parameter, event to event analysis for multiplicity in nucleus-nucleus collision can not result in fruitful conclusion. However, this kind of analysis not only is a test for assumed conventional picture but also gives a key to reveal a mechanism which determines a final state of nuclear collision.

The present fluctuation analysis requires more statistics to get constructive conclusion. The current result indicates that angular distribution on pseudo-rapidity as well as on azimuth can not be interpreted by simple superposition of nucleus-nucleus collisions for some high multiplicity events.

While the present fluctuation analysis is related to many particles correlation in final state, few particles correlation analysis of charged particle is also possible from our data sample. Detail analysis and discussions on this regard from a short range pair correlation is presented in this conference[9].

Although there exists still theoretical ambiguity in final state estimation from QGP, it seems that we might come close to QGP signal.

Acknowledgements

This work is supported in part in Japan by ICR, JSPS and the Kashima fundation, and in part in the USA by DOE, NASA and NSF.

References

1. Proc. of 18-th ICRC, 5, 214, (1983); Recent review see AIP Conf. Proc., No.123, 723(1984), and Proc. of Quark Matter '84.
2. Proc. of 18-th ICRC, 5, 218, (1983); T. H. Burnett et al., Phys. Rev. Lett., 50, 2062(1983)
3. K. Kinoshita et al., Zeit. fur Phys., C8, 205(1981)
4. G.Giacomelli et al., Phys. Rep., 55, No. 1(1979); UAi Collaboration, Phys. Lett., 118b, 167(1982)
5. J. D. Bjorken, Phys. Rev., D27, 140(1983)
6. F. Takagi, Phys. Rev. Lett., 53, 427(1984)
7. E.V.Shuryak, Phys. Rep., 61C, 71(1980); M.Jacob et al., Phys. Rep., 88C,(1982); Proc. of Quark Matter '83, Nucl. Phys., A418(1984)
8. The JACEE Collab., presented by S. Dake and B.Wosiek in this conference
9. The JACEE Collab., presented by Y. Takahashi in this conference

N85-35893

HE 1.4-5

OBSERVATION OF DIRECT HADRONIC PAIRS IN NUCLEUS-NUCLEUS COLLISIONS IN JACEE EMULSION CHAMBERS

The JACEE Collaboration+

T.H. Burnett(h), S. Dake(b), M. Fuki(c), J.C. Gregory(g), T. Hayashi(g), T. Hayashi(b), R. Holynski(i), J. Iwai((h), W.V. Jones(e), A. Jurak(i), J.J. Lord(h), O. Miyamura(d), H. Oda(b), T. Ogata(a), T.A. Parnell(f), T. Saito(a), T. Tabuki(a), Y. Takahashi(f), T. Tominaga(d), B. Wilczynska(i), R.J. Wilkes(h), W. Wolter(i), and B. Wosiek(i)

+ Japanese-American-Cooperative-Emulsion-Experiment
(a) Institue for Cosmic Ray Research, University of Tokyo, Tokyo, Japan
(b) Department of Physics, Kobe University, Kobe, Japan
(c) Department of Physics, Okayama University of Science, Okayama, Japan
(d) Department of Applied Mathematics, Osaka University, Osaka, Japan
(e) Department of Physics & Astronomy, Louisiana State University, USA
(f) ES62, Space Science Laboratory, NASA Marshall Space Flight Center, Huntsville, Alabama 35812, USA
(g) Department of Chemistry & Res. Inst. Univ. of Alabama, Huntsville, USA
(h) Department of Physics, University of Washington, Seattle, USA
(i) Institute of Nuclear Physics, Krakow, Poland

ABSTRACT

In a number of high energy ($\geq$ 1 TeV/amu) nucleus-nucleus collisions observed in JACEE emulsion chambers, non-random spatial association of produced charged particles, mostly hadronic pairs, are observed. Similar narrow pairs are observed in about 100 events at much low energy (20 - 60 GeV/amu). Analysis shows that 30 - 50 % of Pair abundances are understood by the Hambury-Brown-Twiss effect, and the remainder seems to require other explanations.

1. Introduction. Frequent association of produced particles in pairs have been noticed in measurements of charged particle angular distributions in nucleus-nucleus collisions. Several high energy events manifested significant abundances in JACEE emulsion chambers. Statistical analyses of larger samples(106 events) at lower energy (20 - 60 GeV/amu) also indicate non-trivial pair abundances.

From the viewpoint of independent superposition models it is not unnatural to expect weaker particle correlations in nucleus-nucleus collisions than those in proton-proton collisions, as long as no space-time structures and no coherent mechanism are considered. Observed pair data does not seem to support an idea of statistical obscuration of correlations.

Recent development in QCD lattice calculations[1] and experimental studies of high multiplicity/high energy density phenomena[2] encourage searches for signatures of Quark-Gluon-Plasma, a new state of matter. Central or quasi-central collisions are most promising to realize the required high density for QGP transitions, while peripheral collisions are least likely to contain possible QGP signals. Inclusive studies of collisions are generally governed by a large fluctuation of impact parameter which only enhances peripheral phenomena, and are very insensitive to the interaction models.[3] Unlike these insensitive parameters ($\langle N \rangle$ and $\langle N \rangle / D$), an exclusive character of pair abundances may not be much obscured even in

ORIGINAL PAGE IS
OF POOR QUALITY

an inclusive analysis. We examine in this paper whether there are any non-trivial abundances of narrow hadronic pairs in both individual and inclusive nucleus-nucleus interactions.

2. Methods. The charged tracks emanating from the first collision vertices are measured for individual events. The psuedo-rapidity (η) and azimuth angle (ϕ) of a track are given by spatial coordinates measured at many emulsion layers downstream the vertex. Secondary interaction tracks and early $\gamma \rightarrow e^+e^-$ conversions are removed from the track data as much as possible. (Fine triangulation of tracks allows this elimination of contaminations whose origins are located at more than 50 - 150 μm downstream the first vertex, depending on η and vertex depth.) Obvious nuclear fragments (including spectator protons) are also excluded from the data.

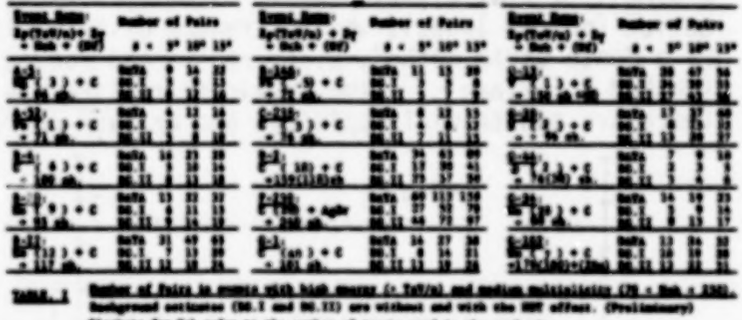
All charged tracks thus defined are used for obtaining the following three different measures of pair correlation.

$$\text{[Measure I]} \qquad P(\leq \alpha, \beta) \equiv \frac{\text{No. of pairs } (\Delta\eta \leq \alpha,\ \Delta\phi \leq \beta)}{\text{No. of all charged tracks (Nch)}} \tag{1}$$

$$\text{[Measure II]} \qquad W(\alpha_1 \leq \Delta\eta \leq \alpha_2) \equiv \int_{\alpha_1}^{\alpha_2} \frac{dN}{d(\Delta\eta)d(\Delta\phi)}\, d(\Delta\eta) \tag{2}$$

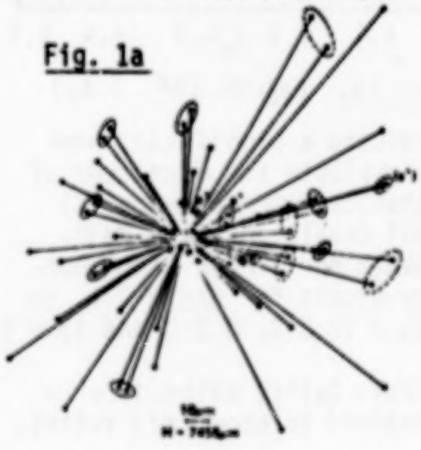
$$\text{[Measure III]} \qquad S(\text{all}) \equiv \frac{dN}{dR^2}, \text{ with } R^2 \equiv \begin{cases} \cosh(\Delta\eta)^2 - \cos(\Delta\phi)^2, \text{ or} \\ (\Delta\eta)^2 + (\Delta\phi) \end{cases} \tag{3}$$

Measure I is useful in the analysis of individual events, and Measure II enhances narrow pairs. Measure III convolves the correlation of the rapidity with that of azimuth angle over the entire available η - ϕ space.



3. Results. An example, event (G12), shows abundant pairs in its forward rapidity region: Figs. 1a and 1b show its linear target diagram and pseudo-rapidity distribution, respectively. It is interesting to note that these pairs in this event seem to form a "ring" structure in rapidities as well as a "jet" structure in the azimuth plane. (This event also contains two "direct e^+e^- pairs" [$m_{e^+e^-}$ being $\sim$ 100 and 300 MeV] in the same forward rapidity region.) Measure I is used for individual event analy-

Fig. 1a



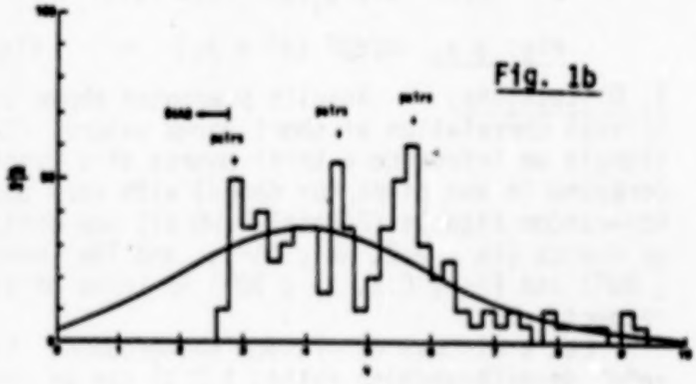
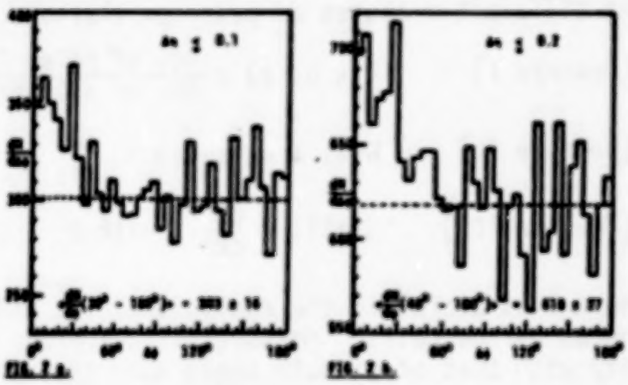


Fig. 1b

ORIGINAL PAGE IS
OF POOR QUALITY

ses at high energy ($\geq$ 1 TeV/amu). Table. I gives P($\leq$ 0.2, 15°)x Nch for 15 events (1532 tracks) with background expected from random coincidence of two particles(BG I) and that includes the HBT effect(BG II). The data show significant excess above background levels for several events. (Four events(B22, D2, F250, G20) show anomalous pair excess, while the other 11 events give P($\leq$ 0.2, 15°, - BG II) = 6.9 %.

For low energy events the statistics (106 events for $N_\pi \geq 2$; 3,695 tracks from 20 - 60 GeV/amu Fe + C, AgBr and Pb reactions) is sufficient that both Measure II and III are taken for all samples. $W(0 \leq \Delta\eta \leq 0.1)$ and $W(0.1 \leq \Delta\eta \leq 0.2)$ distributions as a function of $\Delta\phi$ are given in Figs. 2a and 2b, respectively. Since $W = dN/d(\Delta\phi)$ is constant for a random background (shown in Fig. 2 by dotted lines), a signal of pair correlation is apparent in the region $\Delta\phi < 30°$.



The same signals can be seen in the inclusive Measure III as well, though the S/N ratio is obviously reduced in dN/dR^2 as a result of inclusion of large population at $\Delta\phi > 0.2$. In Figs. 3a and 3b, the purely random (η, ϕ) background is a flat distribution (dotted lines), while a random distribution in ϕ only is evaluated by a Monte Carlo method; using real η and randomly reassigned ϕ values: (dashed-dot lines). The remainder in Figs. 3a and 3b indicates that there are non-trivial rapidity- and azimuth-correlations.

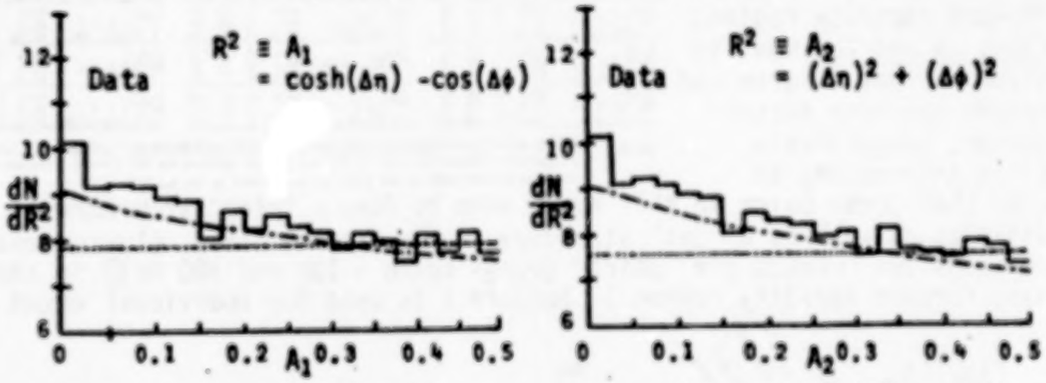


Fig. 3 a. dN/dR^2 ($R^2 \equiv A_1$)

Fig. 3b. dN/dR^2 ($R^2 \equiv A_2$)

4. Discussions. Results presented above indicate a significant non-trivial correlation of short range nature. To evaluate the magnitude of signals we introduce a trial source of a hypothetical parent meson (X) decaying in two pions (or Kaons) with very small Q-values ($\lesssim$ 100 MeV). Non-random signals (P(Data)-P(BG I)) are estimated for eleven high energy events ($\Delta\eta \leq 0.2$, $\Delta\phi \leq 15°$), and low energy events for ($\Delta\eta \leq 0.1$, $\Delta\phi \leq 30°$) and ($\Delta\eta \leq 0.2$, $\Delta\phi \leq 30°$) in terms of X/π = 10.2 %, 8.2 % and 13.9 %, respectively.

Let's discuss non-random backgrounds. First, Dalitz pairs in $\pi^0 \rightarrow \gamma e^+e^-$ decay(branching ratio: 1.2 %) can be contained in above X/π ratios.

N85-35804

However, this accounts for only 1.2 x ($\pi^0/(\pi^+ + \pi^-)$) = 0.6 %. Next, some early conversions of γ-rays can contaminate the data. As mentioned earlier, our track identification is not efficient for eliminating them within 150μm from the vertex, we expect this contamination upto (150/344,000) = 0.04 %. Even when we fully include proposed internal bremsstrahlung sources[4] in addition to $\pi^0 \rightarrow \gamma\gamma$ photons, they are not able to contribute more than 0.2 %. Thus, electron backgrounds from both internal and external conversions do not account for more than 0.8 %. Other experimental errors possibly inherent in measurements are not critically examined at present.

The Hambury-Brown and Twiss effect,[5] the fourth order quantum interference of Bose-Einstein particles, may possibly explain some of the observation, since this effect is of very short range nature for nucleus-nucleus collisions:

$$C \equiv \sigma_0 \frac{d^2\sigma}{d\vec{p}_1 d\vec{p}_2} / \left(\frac{d\sigma}{d\vec{p}_1} \frac{d\sigma}{d\vec{p}_2} \right) \approx 1 + \exp\left(- \frac{q^2 R^2}{2} \right). \qquad (4)$$

The hadron source in nucleus-nucleus collisions is considered to be expanded to the size larger than the colliding nuclear volume, and its known[6] radius 3 - 4 fm gives the effective momentum difference $|q| < 100$ MeV. This is sufficiently small that $\pi^+\pi^+$ and $\pi^-\pi^-$ form narrow pairs (mostly in $\Delta\eta < 0.1$ region). The HBT estimate by eq.(4) and flat η distributions gives $P(\text{HBT}) \approx 2 \times 0.5 \times n/2C_2 \times \alpha\beta/(2\pi\{\ln s - y_0\})/(n/2) \approx 3 \sim 7$ % at $\Delta\phi < 30^0$. (Note that this approximation depends on the event multiplicity and effective rapidity range.) An enhanced measure $W(0 \leq \Delta\eta \leq .1)$ would contain 0.5 x $\int W_{b.g.} d(\Delta\phi)$ HBT pairs, where the range of the integral must cover $\Delta\phi$ upto .5x $\tan^{-1}(100 \text{ MeV}/\langle P_T \rangle) \approx 30^0$. It is noticed that the observed pair correlation increased for $\Delta\eta \leq 0.2$ (see Fig. 2b), while the HBT particles should not. This, with the analysis in Fig. 3, favors consideration of some hypothetical parent particles (X).

Freier and Waddington[7] showed similar pair abundances in 2900 tracks obtained from much lower energy (≥ 7.5 GeV/amu) collisions. We estimated $P(0 \leq \Delta\eta \leq .1) = 255/2900 = 8.8$ %. For this result similar to our low energy data (20 - 60 GeV/amu), an HBT estimate explains about 67 pairs, which, with 20 Dalitz pairs, accounts for 35 % of all extracted abundances.

In conclusion, about 30 ~ 50 % of non-random signals can be attributed to the HBT effect from a large nuclear volume (3 ~ 4 fm). Nevertheless, there seem to remain some "unexplained signals" of narrow hadronic pairs. The net signals for "X" (not attributable to known backgrounds) in the present analysis become $X/\pi \rightarrow \sim 7$ %; 3.5 % and 6.3 %, for three groups defined previously. A particular group of events at high energies that had the enormous X/π ratio(~30 %) are by no means reconciled in the present analysis. All these results might require further examinations of systematic errors and background estimates before seriously considering (X) sources.

Further experimental and theoretical analyses of hadronic pairs seem to be interesting, not only because unexplained abundances still exist, but also because some exclusive characteristics of QGP, and particularly Chiral phase transitions, can be considered in the narrow pair phenomena.[8]

References: 1. J.Polonyi et al., Phys. Rev. Lett. 53, 644(1984). 2. T.H. Burnett et al.(JACEE), Phys. Rev. Lett. 50, 2062(1983). 3. T.H.Burnett et al.(JACEE), AIP 123, 723(1984). 4. J.D.Bjorken and L.McLerran, Phys. Rev. D31, 63(1985). 5. R.Hambury Brown and R.O.Twiss, Nature, 177, 27(1956). 6. W.A.Zajc et al., LBL-12652, 350(1981); D. Beavis et al., Phys. Rev. C27, 910(1983). 7. P.S.Freier and C.J.Waddington, AIP 49, 87(1979). 8. Y. Takahashi and P.B.Eby, this conference HE 1.3-13.

N85-35894

EXCESSIVE PRODUCTION OF ELECTRON PAIRS BY SOFT PHOTONS IN LOW MULTIPLICITY ION INTERACTIONS*

The JACEE Collaboration†

T. H. Burnett[b], S. Dake[b], M. Fuki[d], J. C. Gregory[g], T. Hayashi[d], R. Holynski[i], J. Iwai[h], W. V. Jones[e], A. Jurak[i], J. J. Lord[f], O. Miyamura[c], T. Ogata[c], T. A. Parnell[f], T. Saito[h], S. Strauss[h], T. Tabuki[d], Y. Takahashi[f], T. Tominaga[c], J. Watts[g], B. Wilczynska[i], R. J. Wilkes[e], W. Wolter[i], and B. Wosiek[i]

[a] Institute for Cosmic Ray Research, University of Tokyo;
[b] Department of Physics, Kobe University;
[c] Department of Applied Mathematics, Osaka University;
[d] Okayama University of Science;
[e] Department of Physics and Astronomy, Louisiana State University;
[f] Space Science Laboratory, NASA Marshall Space Flight Center;
[g] Department of Chemistry, University of Alabama, Huntsville;
[h] Visual Techniques Laboratory, University of Washington;
[i] Institute for Nuclear Physics, Krakov.

Abstract

We report here on three multiply charged primary cosmic ray interactions with carbon nuclei, in which the number of materialized electron pairs within a distance of about 0.3 conversion length is larger than predicted from isospin considerations. These are the most energetic ($\Sigma E_\gamma > 4$ TeV) of the low multiplicity (< 15 tracks) events observed in the JACEE-2 emulsion chamber.

1. Introduction.

The Japanese-American Cooperative Emulsion Experiment (JACEE) employs balloon-borne emulsion chambers to study the energy spectra, charge composition, and nuclear interactions of ultrahigh energy cosmic rays. Following exposure and processing, the emulsion plates are distributed to the participating laboratories for detailed scanning, tracing, and subsequent measurements using optical microscopes. Preliminary analysis is carried out on the data collected in the individual laboratories before it is combined with data from the other laboratories in the JACEE data bank. Comparisons among the datasets from the various laboratories are used to control the overall quality of the data.

The data presented herein were collected in the plates of the JACEE-2 (second in the JACEE series of annual balloon flights) emulsion chamber. The unusual nature of the events was discovered during a study of the techniques used for determining the transverse momenta of high energy gamma rays emanating from a primary vertex in the target section of the emulsion chamber.

The JACEE-2 chamber consisted of a target section upstream of a thin calorimeter, which was used to measure the energies of cascades initiated by energetic gamma rays. The target was comprised of approximately 50 layers of double-sided emulsion plates (50 micron emulsion films on both sides of an 800 micron acrylic base plate) interleaved with 2 mm thick acrylic sheets. The calorimeter, which was a multilayer sandwich of lead sheets, x-ray films, and emulsion plates, had a vertical thickness of about 7 c.l.

Except for high multiplicity events, individual tracks of hadrons and leptons can be resolved near the vertex and then followed plate-to-plate to the calorimeter section. Consequently, cascades developing in the calorimeter can be correlated with tracks from the vertex.

2. Results.

The cones defined by the tracks of energetic charged particles from low multiplicity (< 15 tracks) interactions were scanned for possible evidence that cascading had begun in the target section of the emulsion chamber, i.e., upstream of the calorimeter. In this report we discuss the observations on the three most energetic (ΣE_γ > 4 TeV) events in the sample. Using standard nomenclature the three events are of the types:

$He + C \rightarrow 2p + 9\pi^{\pm} + 2\gamma$	Event F0358
$N + C \rightarrow 3\alpha + p + 8\pi^{\pm} + 3\gamma$	Event F0312
$He + C \rightarrow 2p + 8\pi^{\pm} + 4\gamma$	Event F0214

where C represents the material of the acrylic target plates.

The detailed characteristics of the events are presented in Table 1. A total of 9 electron pairs were found near the interaction vertices. This is more than twice the number expected from photon conversions, assuming that the number of emitted photons in the volume scanned for pairs is equal to the number of charged pions emitted in that volume.

The pseudo-rapidity distributions of the produced hadrons in the forward cone are given in Fig. 1, which also shows the pseudo-rapidities of proton fragments, p, from the interactions and the photons, γ, producing the observed electron pairs. Proton fragments from the

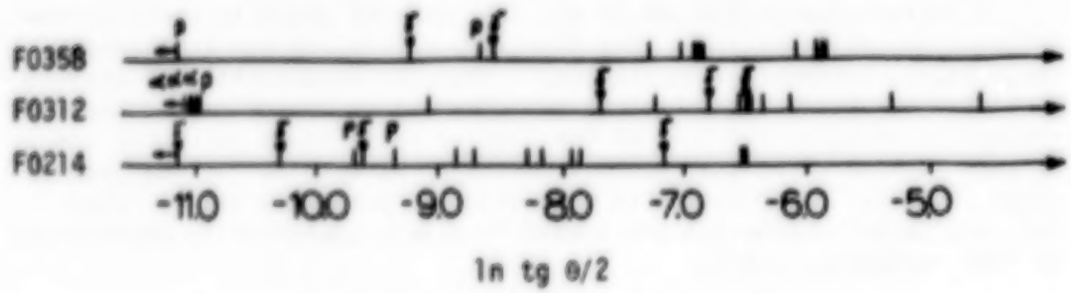


Fig. 1. Pseudo-rapidity distributions of produced particles, proton fragments, and gamma rays.

projectile were assumed to have the smallest emission angles among the charged particle tracks.

Figure 2 shows the dependence of the number of photons converted into electron pairs as a function of distance z from the interaction vertex. The solid line represents the number of materialized gamma rays, N_γ, producing electron pairs inside the scanned volume while the dashed line shows the number of pairs expected in that volume from isospin considerations.

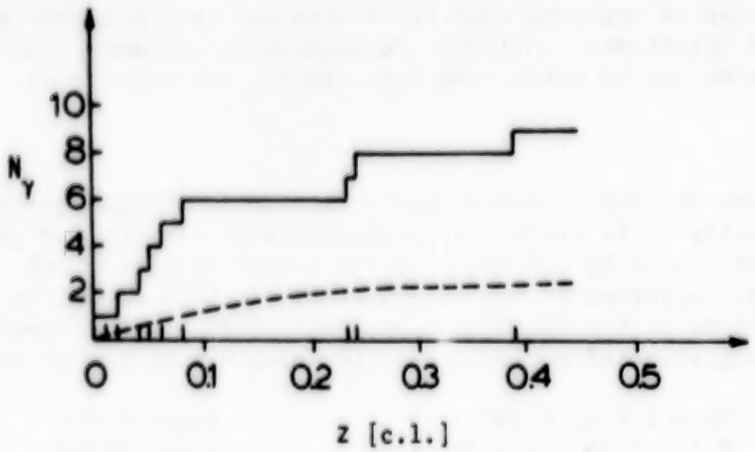


Fig. 2. Number of gamma rays producing electron pairs as a function of distance from the vertex.

3. Discussion.

The largest excess of pairs was observed in the most energetic event ($E_o \sim 60$ TeV), in which 4 photons materialized within a distance of 0.1 c.l. Three of the pairs were found in a very narrow cone of 0.0001 radians. The pairs evolved to 18 electrons in a distance of 0.4 c.l. and to 30 electrons in 0.5 c.l. A comparison with the results of cascade theory (Table 1, Col. 6) indicates that the materialization of one photon in the vicinity of the vertex is unlikely to produce the fast developing cascade. The observed pairs are most likely first generation and not fluctuations in the cascade development.

A characteristic feature of all the observed pairs is their narrow collimation, which suggests that they were emitted by the fragmenting projectile. Internal bremsstrahlung[2] from the deceleration of charged particles (or quarks) may explain the observed excess of pairs, since at projectile energies $E > 10^{12}$ eV the Doppler shift could raise the energy of soft photons above the ~0.5 GeV detection threshold. At the present stage, however, fluctuations in production of pairs can not be ruled out, and larger statistics are needed to give a quantitative description of these anomalous pairs.

N85-35895

Table 1. Characteristics of the interactions.

Event	E_o(TeV)	Pair	z(c.l.)	n_e	n_e^+	n_e^*
F0358	24.0	1	0.04			
		2	0.23	4	2.1	
F0312	24.6	1	0.05			
		2	0.24	4	1.2	
F0214	60.0	1	0.01	2		
		2	0.02	4		
		3	0.06	6		
		4	0.08	8	1.1	
			.....	.....		
			0.36	17		
			0.55	30		6
			0.73	30		9

Table Captions

E_o - primary energy estimated from the neutral component (ΣE_γ) and inelasticity coefficient k = 0.5.

z - distance to point of conversion (in conversion units).

n_e - number of electrons at given z.

n_e^+ - number of electrons predicted from the probability of pair conversion, based on isospin considerations.

n_e^* - number of cascade theory electrons with energies w > 0.5 GeV produced by an electron pair of energy W_o = 5 TeV[1]. The cascade energy W_o is estimated from the longitudinal development of the cascade downstream in the calorimeter.

References

* Research supported in part in the USA by DOE, NASA, and NSF and in part in Japan by JSPS and ICR.

† Mailing address for this paper: Institute for Nuclear Physics, ul. Kawiory 26A, 30-055, Krakow, Poland or Department of Physics and Astronomy, Louisiana State University, Baton Rouge, LA 70803, USA.

1) Janossy, L. and Messel, H., (1951) Proc. Royal Irish Acad. 54(A), 217.
2) Bjorken, J. D. and McLerran, L., (1983) Fermilab-Pub-84/35-T.

N85-35895

HE1.4-7

FORWARD PARTICLE PRODUCTION IN INELASTIC ^{22}Ne INTERACTIONS IN EMULSION AT 4.1 A GeV/c.

Alma-Ata, Bucharest, Dubna, Dushanbe, Erevan, Gatchina, Kosice, Kraków, Leningrad, Moscow, Tashkent, Tbilisi, Ulan-Bator Collaboration.

Presented by B.Wosiek,

Institute of Nuclear Physics, Kawiory 26 A, 30-055 Kraków, Poland.

1. Introduction

The collisions of high energy nuclei are likely to be the subject of intense experimental investigation in the near future. In this paper we present the results on multiple meson production in forward cone in inelastic interactions of ^{22}Ne nuclei in emulsion at a primary momentum 4.1 GeV/c per nucleon. The detailed characteristics of particle production and the fragmentation processes in collisions of ^{22}Ne nuclei in emulsion will be described in [1].

2. Experimental procedure

Stacks of BR-2 photographic emulsions were exposed to a 4.1 A GeV/c neon beam at the synchrophasotron of Joint Institute of Nuclear Research in Dubna. The intensity of the exposure was 10^4 particles/cm^2. In along the track scanning 10,000 neon interactions were found in emulsion. The detailed measurements (emission angles of all charged secondaries as well as charges of projectile fragments) for about 4000 inelastic interactions have been completed. The present paper is devoted to the study of fast ($\beta \geq 0.7$) particle production in the forward hemisphere. We define a forward hemisphere in the center of mass of proton-proton collision at the same primary momentum: $\theta_{forward} \leq 90^\circ_{cms,pp}$. We restrict ourselves to the analysis of forward particle production since in this hemisphere we can define experimentally the number of produced mesons. In a backward hemisphere it is not possible to separate produced mesons (both fast and slow) from a proton fragments of target nucleus. The presented investigation was carried out on a sample of 2031 inelastic interactions. For each event the following multiplicities were determined:

N_F - number of multicharged projectile fragments ($Z \geq 2$);

N_p - number of protons released from ^{22}Ne, can be evaluated from the charge balance between primary charge and sum of charges of heavier fragments: $N_p = 10 - \sum_{i=1}^{N_F} Z_{F,i}$;

N_{sf} - number of all relativistic ($\beta \geq 0.7$) singly charged tracks emitted in forward hemisphere;

$N_{mf} = N_{sf} - N_p$, number of produced mesons in forward cone;
N_{sp} - number of spectator protons (see explanation below) ;
$N_{part} = N_p - N_{sp}$, number of protons participating in the collision.

Not all nucleons released from incident nucleus $\left(\frac{A}{Z} \cdot N_p\right)$ participate in the collision. Part of them remains spectators. Spectator protons (N_{sp}) were identified by momentum measurements and from the angular distribution of singly charged secondary particles [2]. Thus, we can obtain the number of protons participating in the collision*.

The data presented in this paper are averaged over all emulsion components and over different impact parameters and are investigated in dependence of the number of participating nucleons from projectile nucleus only.

3. Results

The data on inclusive forward multiplicities are summarized in the Table. The errors quoted in the Table and in Figures include statistical uncertainties only.

In Figure 1 we present the inclusive distribution of produced mesons. Distribution is peaked at small multiplicities due to the low primary energy per nucleon with a very long tail of large multiplicities, which contribute to a large value of the dispersion. The ratio:

$$\overline{N}_{mf}/D = 1.06 \pm .03.$$

Multiplicity	Average
N_F, $Z \geq 3$	.42±.01
N_F, $Z = 2$	.84±.02
N_p	5.63±.08
N_{sp}	1.89±.03
N_{part}	3.74±.08
N_{mf}	3.76±.08

Different superpositions models [3] predict for this ratio a value close to 1 for inclusive nucleus-nucleus data (data averaged over all impact parameters and over all wounded nucleons). The measured value is consistent with these predictions.

It is interesting to study the characteristics of forward particle production in dependence of the number of participating protons from incident nucleus. In Fig.2 we show the distributions of N_{mf} for interactions with different values

---

*) Among participating nucleons there are wounded nucleons which interact inelastically in the target and produce secondaries as well as nucleons which undergo the elastic scatterings on wounded nucleons and other secondaries. It is not possible to separate experimentally wounded nucleons from those originated in second generation processes. It is natural to assume that participating nucleons are related to the wounded ones.

of N_{part}. With increasing N_{part} (more central collisions) the distributions shift towards the larger multiplicities and change the shape. The dependence of the moments of these distributions on N_{part} are shown in Figs.3a,b. One can observe that both average multiplicity and dispersion increase with increasing N_{part}. If we assume a simple superposition of independent elementary processes, we expect that the ratio $\bar{N}_{mf}/D^2$ will be independent of N_{part}. Qualitatively such an independence is observed for $N_{part} \geq 2$ and is illustrated in Figure 4.

We have separated from the released protons of ^{22}Ne projectile the spectator ones. Spectator protons are not affected by the collision and we do not expect the strong dependence of the average number of produced mesons on the number of spectator protons unless the N_{sp} is not correlated with the number of participating protons. A strong correlation between N_{sp} and N_{part} occurs only for events with a total desintegration of primary nucleus into singly charged fragments : $N_{part} = 10 - N_{sp}$. In other cases the spectator part of the incident nucleus may evaporate as protons as well as alpha particles and heavier fragments. The observed very weak dependence of $\bar{N}_{mf}$ on N_{sp} is shown in Figure 5.

4. Conclusions

The presented data on the multiplicities of mesons produced in forward cone and on the dependence of the production process on the number of participating nucleons from primary nucleus can be qualitatively explained by the hypothesis that a simple superposition of elementary collisions describes the interaction between nuclei. However it should be mentioned that some other characteristics of nucleus-nucleus collisions (collective behaviour, cascade processes in the target fragmentation region etc.) can not be described by such a simple model [1,4].

References

1. Alma-Ata,Bucharest,Dubna,Dushanbe,Erevan,Gatchina,Kosice, Kraków,Leningrad,Moscow,Tashkent,Tbilisi,Ulan-Bator Collaboration, papers to be published in Yad.Fiz. (1985).
2. A.S.Goldhaber, Phys.Lett. B53,306(1974).
3. A.Bialas et al.,Nucl.Phys. B111,461(1976), K.Kinoshita et al., Z.Phys. C8,205(1981), A.Capella et al., preprint TH.3700-CERN.
4. A.M.Baldin et al., Yad.Fiz. 20,1201(1974), L.S.Schroeder et al., Phys.Rev.Lett. 43,1787(1979).

N83-35839



ORIGINAL PAGE IS
OF POOR QUALITY

Figure 1.

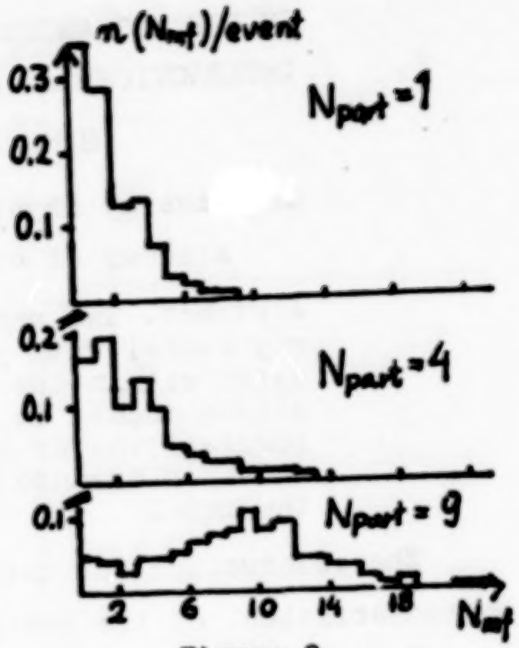


Figure 2.

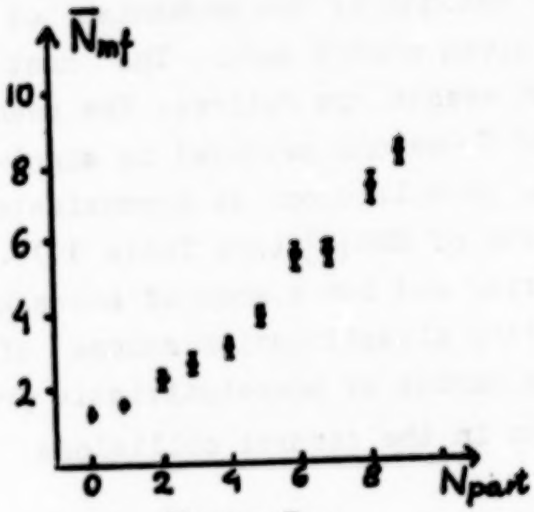


Figure 3a.

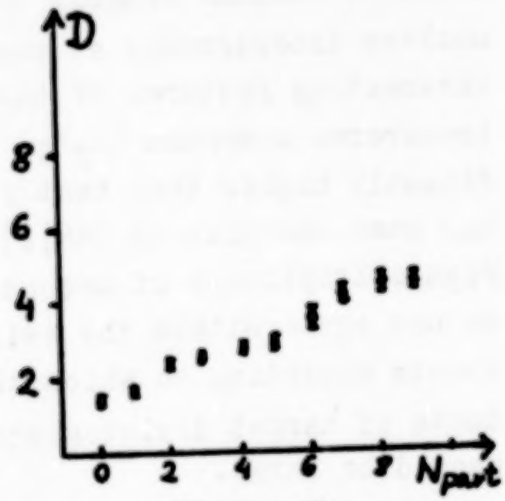


Figure 3b.

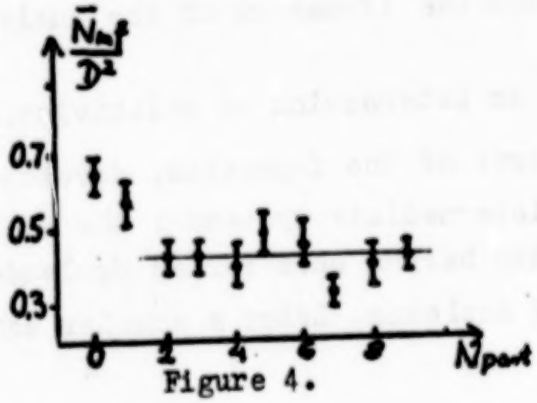


Figure 4.

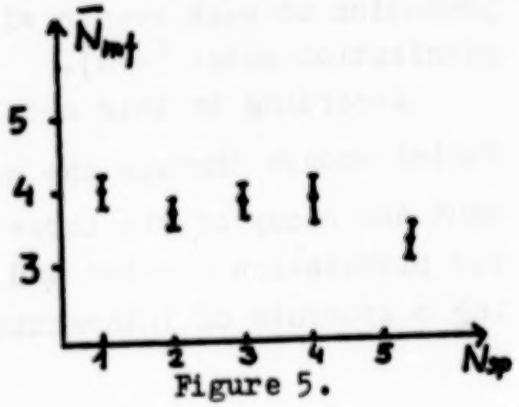


Figure 5.

N85-35896

HE I.4-8

ON THE MECHANISM OF ANOMALOUS NUCLEUS-NUCLEUS INTERACTIONS AT ENERGIES ABOVE 1 TEV/NUCLEON

S.Sh.Ameev, V.L.Shmonin

High Energy Physics Institute of the Kazakh SSR Academy of Sciences, Alma-Ata, 82, USSR

Abstract. Two anomalous interactions of cosmic ray nuclei with photoemulsion nuclei are considered within the framework of the nuclear pionization model. It is shown that the observed regularities of nuclear collisions at the given energy range are satisfactorily reproduced by the model.

The observation and determination of the number of the characteristics of the two heavy ion collisions at energies of 4 TeV/nucleon (Si+Ag) and of 100 TeV/ nucleon (Ca+C) [1] allow to examine roughly the notions of the mechanism of nuclear interactions at the given energy range. The most interesting features of these events are follows. The mean transverse momentum $\langle P_T \rangle_\pi$ of π -mesons produced is significantly higher than that for pp-collisions at approximately the same energies of ISR[2] and of SPS[3] (see Table 1) . High multiplicity of secondaries and low number of h-tracks do not agree within the existing classification scheme of events according to which the number of nonrelativistic products of target disintegration in the central collisions should be large.

In this report we analyse the possibility of an interpretation of such events within the framework of the nuclear pionization model [4-6].

According to this model an interaction of relativistic nuclei occurs through the stages of the formation, development and decay of the three intermediate systems : the central pionization cluster and two baryon ones formed by leading components of interacting nucleons. Later a similar sche-

me was used as the base of the model [7]. The numbers of interacting nucleons of the projectile, N_1, and target, N_2, are determined for a fixed impact parameter b from the formulae:

$$N_1=\int dx_1 dy_1 T_1(x_1,y_1,b)\left[1-\exp(-\alpha\sigma_{nn}^{in} T_2(x_2,y_2,b))\right]$$
$$N_2=\int dx_2 dy_2 T_2(x_2,y_2,b)\left[1-\exp(-\alpha\sigma_{nn}^{in} T_1(x_1,y_1,b))\right] \quad (1)$$

Here $\alpha=1$, $x_2=x_1-b$, $y_2=y_1$, $T_i=\int \rho(b,x_i,y_i,z)dz$, $(i=1,2)$, ρ is the Fermi distribution of the nucleon density in a nucleus. It was pointed out [8] that the existence of the channel of the total compound-system formation in nucleon-nucleon interactions [9,10] leads to the fact that the part of the interacting nucleons in A-A collisions turns out to be captured into the central pionization cluster. The numbers of such nucleons, N_1' and N_2', are also determined in terms of (1) with $\alpha=1/3\div1/4$. The numbers of nucleons entered the baryon clusters can be found from the equations:

$$N_1''=N_1-N_1' \qquad N_2''=N_2-N_2' \quad (2)$$

In the system where the nuclei collide with equal speeds the energies, masses and momenta of the baryon clusters are defined by the expressions:

$$E_i''=N_i''\left[(1-\langle\delta\rangle)^2 p^2+m_N^2\right]^{1/2},\quad M_i''=N_i''(m_N+\varepsilon_K),\quad P_i''=(E_i''^2-M_i''^2)^{1/2} \quad (i=1,2) \quad (3)$$

In (3) $\langle\delta\rangle=0.3$ is a part of a baryon cluster nucleon momentum spent on the central cluster production. $\varepsilon_K\approx0.2$ GeV is an average kinetic energy of the nucleon in a baryon cluster rest system.

Taking into account the conservation laws one can determine the energy, momentum and mass of the central cluster

$$E_c=E_1+E_2-E_1''-E_2'' \quad P_c=P_1+P_2-P_1''-P_2'' \quad M_c=(E_c^2-P_c^2)^{1/2}, \quad (4)$$

where E_1 and E_2 are the energies of the interacting parts of the nuclei before their collision.

The thermodynamical model [4÷6,8] is used to describe the decay of the clusters. The pionization cluster decay temperature is determined from the equation of the energetic balance with an account of π-, K-, ρ-, ω-mesons, nucleons and antinucleons among the secondaries. The decay

volume is defined by formula from [11]

$$V=\frac{4}{3}\pi(R_0+\varkappa\tau_h)^2(2R_0/\gamma+\varkappa\tau_h)$$

Here R_0 is the initial size of the central cluster Lorentz compressed in longitudinal direction (γ is the Lorentz-factor of the motion of a nucleus in the equal speed system). The parameter Ro is taken to be equal to the radius of the smaller colliding nucleus for the central collisions. τ_h =1.2 GeV·fm/c [12] is the hadronization time of the quark-gluon plasma forming the cluster matter. The value $\varkappa \geq 1$ takes into account the possible increase of τ_h in nuclear collisions in comparison with hadronic ones [13]. According to [14] the contribution of longitudinal collective motion in cluster is taken into account in the energetic balance. The results of the calculation of the multiplicity and average transverse momentum $\langle P_T \rangle_\pi$ for π -mesons from the considered events are given in the Table 1.

Table 1.

	E_0, TeV	Nch exper.	Nch theor.	$\langle P_T \rangle_\pi$, GeV/c exper.	$\langle P_T \rangle_\pi$, GeV/c theor.	ISR*	SPS**
Si+AgBr	4	1010 ±30	835	0.550 ±.100	0.541	0.340 ±.002	
Ca+C	100	760 ±30	597	0.700 ±.050	0.708		0.424 ±.001

* - data from Ref.[2]

** - data from Ref.[3]

For the second event the energy, transverse momentum and pseudorapidity restrictions for photons have been accounted in the same way as in the experiment[1]. All calculations were carried out for $\varkappa$ =3. The relativistic particle pseudorapidity distributions for these two events are shown in the Figs. 1. and 2. (histogram (experiment[1]), curves (this model)).

Taking into account that fact that the considerable fluctuations are possible in these unique events one can conclude that the nuclear pionization model satisfactorily

ORIGINAL PAGE IS
OF POOR QUALITY

reproduces the observed regularities of nuclear interactions at the given energy range.

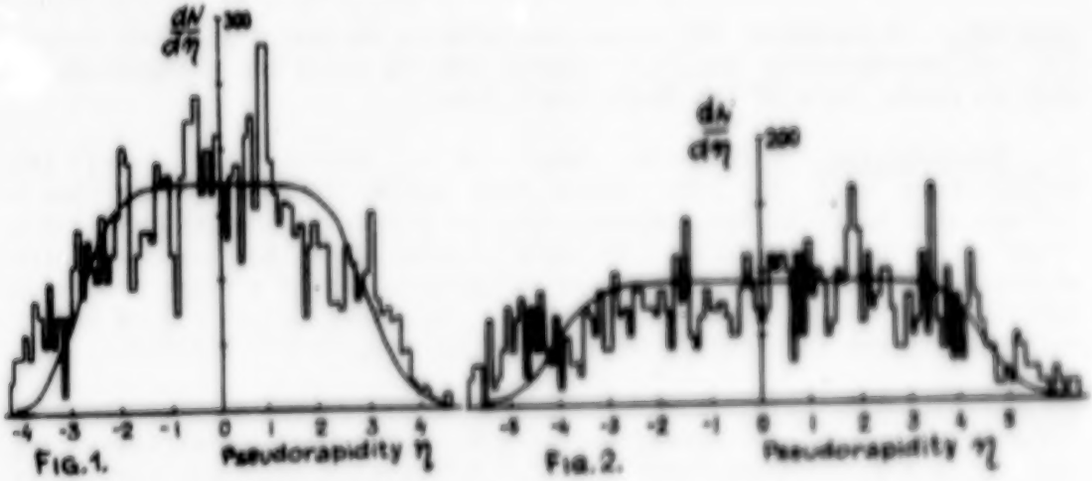


FIG.1. The CMS pseudorapidity distribution of charged particles in the Si+AgBr event.

FIG.2. The CMS pseudorapidity distribution of charged particles in the Ca+C event.

References

1. Burnett T.H. et al., 1983, Phys.Rev.Lett., v50,26,2062
2. Alper B. et al., 1975, Nucl.Phys., B100,237
3. Arnison G. et al., 1982, Phys. Lett., 118B, 167
4. Kalinkin B.N., Koltochnick S.N., Shmonin V.L., 1978 Preprint HEPI 61-78,Alma-Ata; 1980,Phys.Scr.,v21,792
5. Baranov D.G. et al., 1978, Pis'ma v JETP, v28, 7, 475 Varyukhin V.V. et al., 1979. Proc.16th ICRC, Kyoto, v6, 154-159
6. Ameev S.Sh. et al., 1982, Preprint HEPI 81-16,Alma-Ata
7. Bjorken J.D., 1983, Phys. Rev., D27, 140
8. Ameev S.Sh. et al., 1981, Proc.17th ICRC, Paris, 5, 80
9. Kalinkin B.N., Cherbu A.V., Shmonin V.L., 1980,Fortschr. Phys., 28, 35
10. Kalinkin B.N., Shmonin V.L., 1981, Phys.Scr.,v24, 3, 498
11. Ameev S.Sh., Shmonin V.L., 1984,J.Phys.G., v10,1311-1317
12. Kalinkin B.N., Cherbu A.V., Shmonin V.L., 1979,Acta Phys. Austr. v50, 165; 1980, Phys.Scr., v21, 797-801
13. Kalinkin B.N., Gagarin Yu.F., 1984, FTI im A.F.Ioffe Preprint, 848, Leningrad
14. Varyukhin V.V. et al., 1982, FTI im A.F.Ioffe Preprint, 756, Leningrad.

N85-35897

MESON MULTIPLICITY IN NUCLEUS-NUCLEUS COLLISIONS ABOVE 4 GeV/amu

T.W. Atwater, P.S. Freier and M.P. Kertzman
School of Physics and Astronomy, University of Minnesota
Minneapolis, Minnesota 55455

Abstract. Dependence of meson multiplicity on energy for 1486 cosmic ray nucleus-emulsion nucleus interactions is examined. Comparison is made to predictions of the Multi-Chain Model.

1. Introduction. In the near future, relativistic heavy ion accelerators will for the first time probe energies larger than 4 GeV/amu with heavy nuclei. Cosmic rays are currently the only available "beam" at such energies. To date little data has appeared which utilizes the cosmic rays in an unbiased manner to measure the meson multiplicity as a function of energy. This work presents data on the multiplicity per interacting projectile proton up to 100 GeV/amu.

2. Description of Data. Nuclear emulsions were exposed on three balloon flights: two each at cutoff energies $E > 1.7$ GeV/amu (over Texas) and one at $E > 7.5$ GeV/amu (over India). 1486 events have been completely analyzed, including angle measurements of mesons, protons, alphas and heavier projectile fragments. Projectile charge ranged from $Z_p = 6$ to 30, with average $Z_p = 13.5$. The number of charged mesons produced in one interaction is defined by charge conservation:

$$n_{\pi\pm} = n_s - (Z_p - \sum_i Z_i)$$

where n_s is the number of singly-charged particles with ionization $< 1.4\ I_{min}$, Z_p is projectile charge, and Z_i denotes projectile fragments with $Z_i \geq 2$. Identified lower energy mesons are also included. Error in determining $n_{\pi\pm}$ is less than one per event. Angle measurements, used to determine energy of the primary, have an estimated error of 0.1°. The number of wounded (inelastically interacting) projectile protons Q_p is estimated on an event-by-event basis, utilizing the fact that in many of the events projectile and central regions of the pseudorapidity histograms are well separated. Target diagrams, i.e., cross-sections of the secondary beam 1000 μ downstream from the interactions, are also used. While this method of determining Q_p is clearly approximate, it is justified by the fact that rough agreement is obtained with Glauber-type calculations of $\langle Q_p \rangle$.

Data taken from emulsions exposed to the 1.75 GeV/amu ^{55}Mn beam at the Bevalac were also used both to calibrate the energy determination and to supplement the $n_{\pi\pm}$ data.

It should be emphasized that all of the data was taken in an unbiased manner so as to detect all inelastic interactions. Defining the latter as those collisions in which the projectile charge is changed, it can be said that essentially all of the inelastic interactions in "along-the-track" scanning were found and measured. Due to time considerations many of the events with zero meson multiplicity were not completely analyzed for angles of nuclear fragments, most of which were in the lower energy (Texas) part of the data. A correction factor based on events that were completely measured has been applied to

correct for this. Thus the measured values should represent the true meson multiplicity for inelastic interactions.

The energy per nucleon of the primary cosmic ray nucleus is measured by utilizing the angular distribution of all charged secondaries. Several methods are employed, all of which depend on the relative constancy of the transverse momentum. One method uses wounded protons and mesons, as suggested by Varyukhin et al.[1] The primary momentum per nucleon is given by

$$P_{prim}(\text{GeV/amu}) = \frac{(\frac{3}{2} f_\pi \langle p_\perp \rangle_\pi + \frac{A}{z} f_Q \langle p_\perp \rangle_{Q_p}) \sum_i^{n_\pi + Q_p} \frac{1}{\sin \Theta_i}}{Q_p}$$

where $n_{\pi^\pm}(Q_p)$ is the number of charged mesons (wounded projectile protons) in an event, $f_\pi(f_Q)$ is the relative number fraction, and the factor $3/2(A/Z)$ accounts for π^os (neutrons).[2] The factor $1/Q_p$ is used because all of the momentum of the wounded protons and mesons after the interaction must arise form the Q_p wounded protons. For the first try at computing P_{prim}, values of $\langle p_\perp \rangle$ measured at accelerator energies were used, viz.: $\langle p_\perp \rangle_\pi$ = 235 (320) MeV/c for the Texas (India) data set;[3] $\langle p_\perp \rangle_{Q_p}$ = 575 MeV/c[4] for both data sets. The resultant energy distribution was then compared to the known cosmic ray energy spectrum, $N(>E) \sim E^{-1.7}$ (E = total energy/amu). The values of $\langle p_\perp \rangle$ are subsequently modified by a suitable factor so that agreement with the known spectrum is as close as possible. This factor is 0.76 for the Texas data set and 1.20 for the India data set. Primary energy is also measured using the spectator particles, i.e., protons and alphas. This is detailed in a separate paper.[5] The energies obtained by these two separate methods are simply averaged. The resultant energy distribution is considered to order the events in energy. For a comparison of the result to the cosmic ray energy spectrum, see Ref. 5. The fit to the high energy part of the spectrum is fairly good, but at the low end there are too many (~25%) events below the known cutoffs. A Monte Carlo simulation was performed assuming a Gaussian in energy with $\sigma \sim 0.5$ E, as seen in the Mn beam data. The result implies that many of the events below the cutoff may be due to the inherent spread in the measurement. However, when consolidating the data by binning the particles in energy, this does not matter, as long as the ordering in energy is correct. (For this reason also the precise values of $\langle p_\perp \rangle$ used are relatively unimportant.) The average energy of each bin is calculated using the number of events in the bin and the known energy spectrum.

3. Model. Comparison is made to the Multi-Chain Model (MCM) as formulated by Sumiyoshi,[6] which is essentially an independent particle picture utilizing Glauber theory concepts.[7] Input to MCM is the inelastic p-p cross-section σ_{pp}^{inel} and the p-p total charged multiplicity $\langle n_{ch} \rangle_{pp}$. Colliding nucleons are connected by chains which exchange energy. Equipartion of energy among chains is required. Cascade effects are roughly included by adding 1 to $\langle n_{ch} \rangle_{pp}$ for all collisions but the first for each wounded nucleon. Since the model predicts meson plus wounded proton multiplicity, in the model $\langle n_{ch} \rangle / \langle Q_p \rangle - 1$ should be compared to the data. The model is not claimed to be valid below 10 GeV/amu.[8]

ORIGINAL PAGE IS
OF POOR QUALITY

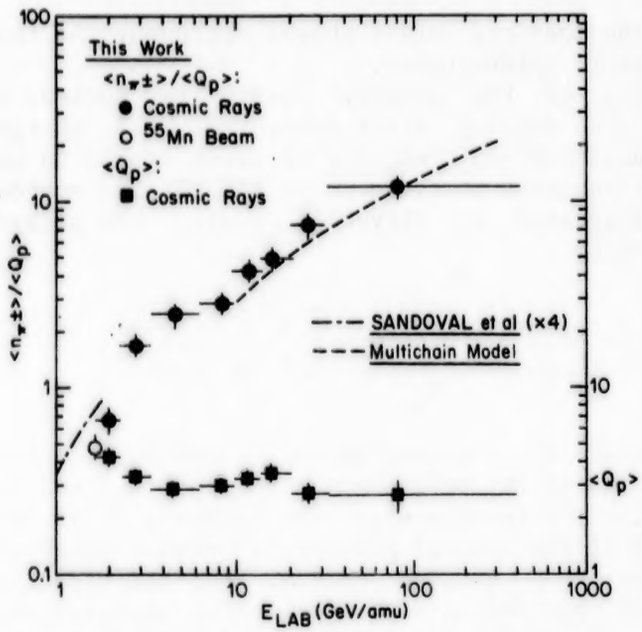
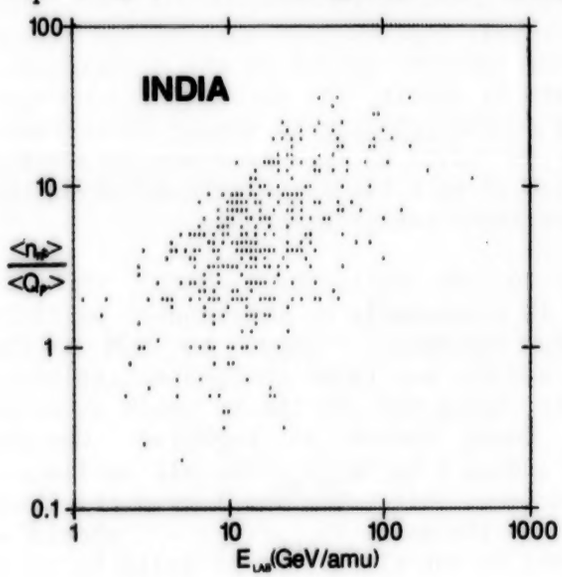


Fig. 1. Meson multiplicity per wounded projectile proton $\langle n_{\pi^\pm}\rangle/\langle Q_P\rangle$ vs. energy for cosmic rays in emulsion. Shown also are: ^{55}Mn-emulsion point; streamer chamber data of Sandoval et al.,[9] multiplied by 4 to account for target protons and π^+s; Multi Chain Model prediction,[7] valid for E > 10 GeV/amu; and average wounded projectile protons vs. energy. Note large uncertainty in assigning energy value to highest energy point.

4. Results. Meson multiplicity per interacting projectile proton $\langle n_{\pi^\pm}\rangle/\langle Q_P\rangle$ as a function of energy is shown in Fig. 1. Also shown is the ^{55}Mn-emulsion value at 1.69 GeV/amu. The experimental number of wounded projectile protons $\langle Q_P\rangle$ is also included on the plot. It is seen that $\langle n_{\pi^\pm}\rangle/\langle Q_P\rangle$ varies with energy approximately as $E^{0.7}$ above 4 GeV/amu. The data seem to follow the trend of the MCM prediction. Both the cosmic ray data and the Mn beam point fall below the Ar-KCl data of Sandoval et al.[9] For the cosmic ray data, this may partly be due to an overestimate of the number of wounded protons $\langle Q_P\rangle$ at this energy (see Fig. 1). However, for the Mn case, this is not true since $\langle Q_P\rangle$ (expt) = 5.2 while $\langle Q_P\rangle$(Glauber) = 5.0. According to Glauber theory $\langle Q_P\rangle$ is only a weak function of energy, viz. < 3% variation from 2-100 GeV/amu. $\langle Q_P\rangle$ (Glauber) = 3.1 for the average cosmic ray projectile on emulsion while $\langle Q_P\rangle$ (expt) = 3.3 integrated over energy.



To show the spread in the data, Fig. 2 gives a scatter plot of the 482 events from the India flight (E > 7.5, E = 19.6, median E = 11.8 GeV/amu).

Fig. 2. Scatter plot of meson multiplicity per wounded projectile proton vs. energy for India flight data.

N85-35808

Table 1 shows the projectile charge dependence of the multiplicity per wounded projectile proton integrated over energy. Higher Z_p appears to give lower $\langle n_{\pi^\pm}\rangle/\langle Q_p\rangle$. This can only partly be accounted for by the fluctuation in $\langle Q_p\rangle$ as shown in Table 1. As an aside, note that the value of $\langle n_{\pi^\pm}\rangle/\langle Q_p\rangle$ for high Z_p ($\geq$ 20, $\bar{Z}$ = 23.3) in the lowest energy cosmic ray bin is very close to the value for the Mn beam (Z = 25), both showing internal consistency of the results and lending credibility to the cosmic ray energy determination.

Table 1. $\langle n_{\pi^\pm}\rangle/\langle Q_p\rangle$ vs. Projectile Charge[a]

Flight	Projectile Z_p	Events	$\langle Q_p\rangle$ Expt	$\langle Q_p\rangle$ Glauber	$\langle n_{\pi^\pm}\rangle/\langle Q_p\rangle$
Texas	6-9	412	2.2 ± 0.1	2.22	2.9 ± 0.3
(E>1.7 GeV/amu)	10-19	508	3.7 ± 0.2	3.13	1.9 ± 0.2
	20-26	332	4.4 ± 0.3	4.53	1.5 ± 0.2
India	6-9	141	2.4 ± 0.2	2.24	5.5 ± 0.7
(E>7.5 GeV/amu)	10-19	236	2.8 ± 0.2	3.17	5.7 ± 0.7
	20-26	142	5.5 ± 0.5	4.58	3.8 ± 0.6

[a]Values are corrected for unmeasured zero meson events.

5. Conclusion. For the first time a systematic unbiased study has been made of the meson multiplicity in relativistic heavy ion collisons from 2 to 100 GeV/amu. Multiplicity per wounded proton rises roughly as $E^{0.7}$ at E > 4 GeV/amu. Heavier projectiles show a somewhat lower multiplicity per wounded projectile proton than lighter ones do. The data roughly follows the Multi-Chain Model prediction.

6. Acknowledgements. We thank Mary Olson and Hilde Rahlenbeck for the careful measurements of interactions. We acknowledge useful conversations with J. Kapusta and L. Csernai. We thank J. Mevissen for computing assistance. This work was supported in part by NSF Grant PHY-8405852, NASA Grant NGR 24-005-050, and the University of Minnesota Computer Science Center.

References

[1] Varyukhin, V. V., et al. (1984), Phys. Scr. **29**, 37.
[2] Note that Ref. 1 uses the same $\langle p_\perp\rangle$ for both mesons and wounded protons.
[3] The value 235 MeV/c is taken from an average over nucleus-nucleus data for $\langle p_\perp\rangle_{\pi^-}$ at 4.5 GeV/c/amu measured by Anikina et al. (1983), JETP Lett. **36**, 331; the value 320 MeV/c was extrapolated from the latter value using the energy dependence of $\langle p_\perp\rangle$ from proton-proton data.
[4] This value was derived from a distribution in Agakishiev et al. (1983), Sov. J. Nucl. Phys. **38**, 90.
[5] Paper HE 1.3-1, these proceedings.
[6] Sumiyoshi, H. (1983), Phys. Lett. **131B**, 241.
[7] Glauber, R.J. (1959), Lectures in Theoretical Physics, ed. W.E. Brittin, Vol. 1, Springer, Berlin, p. 315.
[8] Kinoshita et al. (1981), Z. Phys. **C8**, 205.
[9] Sandoval et al. (1980), Phys. Rev. Lett. **45**, 874.

N85-35898

HE 1.4-11

INCLUSIVE ANGULAR DISTRIBUTION OF α AND Li FRAGMENTS PRODUCED IN THE Fe-C AND Fe-Pb COLLISIONS AT 1.88 GeV/u*

C. O. Kim and S. N. Kim
Department of Physics, Korea University, Seoul 132, Korea
and
I. K. Chae and D. H. Kim
Department of Physics, Sookmyung Women's University
Seoul 140, Korea

ABSTRACT

The LS (laboratory system) emission angles θ for 2188 α and 298 Li fragments, produced inclusively in relativistic Fe-C and Fe-Pb collisions, have been measured in reference to incident Fe-ion beam tracks nearby in nuclear emulsion. An empirical differential frequency formula,

$$dN(\cot\theta) = \exp(a + b\cot\theta)d(\cot\theta) \quad (1)$$

is obtained with the constant $b \cong -0.026$ at 1.88 GeV/u, which seems to be independent on the kinds of target nucleus as well as on the kinds of projectile fragments. Equation (1) supports the conventional Kaplon's formula,[1] which has been a convenient tool for estimating the unknown primary energy of cosmic-ray primaries;

$$(\langle\theta^2\rangle)^{\frac{1}{2}} = \zeta/u\,\gamma_p, \quad (2)$$

with $\zeta \cong 0.056$, where $u\,\gamma_p$ is the primary energy in GeV/nucleon. Also, the significance of Eq. (1) is discussed.

1. Introduction. When nuclear interactions produced by high-energy singly-charged hadrons in nuclear emulsion ("stars") are observed in the LS, very slow fragments of the constituent nuclei (Ag, Br, C, N, O, H) of nuclear emulsion can be readily distinguished from relativistic shower particles. Nevertheless, it is usually difficult to identify these nonrelativistic fragments, mainly due to their high ionization and short track lengths. Now, owing to recent development in accelerating heavy ions, the "heavy evaporation fragments" in the projectile rest system (ALS; anti-laboratory system) can be observed as 'relativistic particles' in the LS. Particularly, the relativistic α and Li fragments are identified with ease in nuclear emulsion just by simple inspection through an optical microscope, since the former have about four times the grain density of minimum-ionizing tracks, and the latter about nine times. This very technique of identifying α fragments has been used by some recent angular measurements.[2]

*Research supported partly by Korea Science and Engineering Foundation (KOSEF) (1984-87).

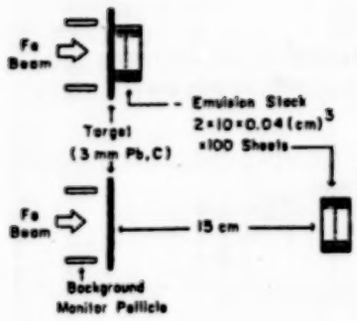


Fig. 1. Experimental Setup.

2. Experimental Setup and Method. The specific arrangements of the experiment to the Fe-ion beam of 1.88 GeV/u at the Lawrence Berkeley Bevalac are illustrated in Fig. 1. The 3 mm-thick target was made of either carbon or lead. The detector of fragments and incident Fe ions is an emulsion stack (made of 100 Fuji ET7B pellicles of sheet size, 2 x 10 x 0.04 cm^3) and is either placed just behind the target plate ("S-stacks") or 15 cm away from the back of the target plate ("L-stacks") in downstream. The shorter edges of pellicles were exposed 'horizontally' to the Fe-ion beam with a track density of about 5×10^3 ions/cm^2.

Because of large distortion present up to $\sim 500\ \mu m$ from the entrance edges of pellicles, α and Li fragments were picked usually at $\sim 500\ \mu m$ from the edges, and angular measurements were typically performed at ~ 1 mm downstream from the entrance edges. Special attention was given not to miss such α and Li fragments as were produced with large θ. In order to avoid the effect due to the distortion inherent in the processed emulsion plate, the LS emission angles θ were measured by use of the reference-track method,[3] i. e., always in reference to nearby Fe-ion beam tracks, which had the angular deviation of 2.3 ± 0.3 and 3.7 ± 0.3 mrad., respectively, for the pellicles behind the carbon and lead targets at the site of angular measurements.

3. Experimental Results. As shown in Fig. 2, the differential frequency $dN(\theta)$ versus θ (vacant circles for Fe-C collisions and filled circles for Fe-Pb collisions) resemble closely those of Ref. 2. The two plots in the above for each of S-stacks and L-stacks shown separately and the combined data are shown in the lowest in Fig. 2. There seem to be tendencies of more population of α fragments in the extreme angular regions of $\theta > 10^0$ and of $\theta \leq 1^0$ for Fe-C collisions than for Fe-Pb collisions. The results of fitting the angular data of $\theta \leq 3^0$ with the Gaussian regression function (χ^2/DF, 10 – 30) and those of θ 5^0 with the exponential regression function (χ^2/DF, 1 – 2) are also indicated as the curves and equations in the figure.

The root-mean-suare angles of fragments (Li fragments) $(\langle\theta^2\rangle)^{\frac{1}{2}}$, for $\theta < 5^0$, as advocated in Ref. 1, are 0.037 ± 0.02 and 0.038 ± 0.01 (0.032 ± 0.02 and 0.035 ± 0.01), respectively, for Fe-C and Fe-Pb collisions, which correspond to $\zeta = 0.057$ and 0.067 (0.056 and 0.062) in Eq. (2).

But, we find it most reasonable and revealing to plot the differential frequency $dN(\cot\theta)$ versus, as shown in Fig. 3 (a) for Fe-C collisions and (b) for the Fe-Pb collisions. In the figures the filled circles represent the angular data from 2188 α fragments, and the vacant circles those from 298 Li

ORIGINAL PAGE IS
OF POOR QUALITY

frgaments. Since no statistically significant differences between the angular data of S-stacks and those of L-stacks were detected, only the combined data are shown in the figure. For the least-square fit, we used the regression function,

$$dN(\cot\theta) = \exp(a + b\cot\theta)\,d(\cot\theta) \qquad (1)$$

with reasonable fits to most of the angular data, as seen from the best fitted values of a and b and χ^2/DF, separately, for Fe-C and Fe-Pb collisions in Table I. In Figs. 3, the straight lines in the figures and the dotted lines in the inserts show the best-fitted curves. For the interval of cot θ = 0-20, the amplified version of dN(cot θ) versus d(cotθ) with one-tenth the interval in the main figures are shown as the inserts, sharp fall-offs of dN(cot θ) for cot θ ≤ 4 can be seen. But those portions of α and Li fragments, with extremely small and large θ, which deviates apprecially from the general trends represented by Eq. (1) constitute only several percents.

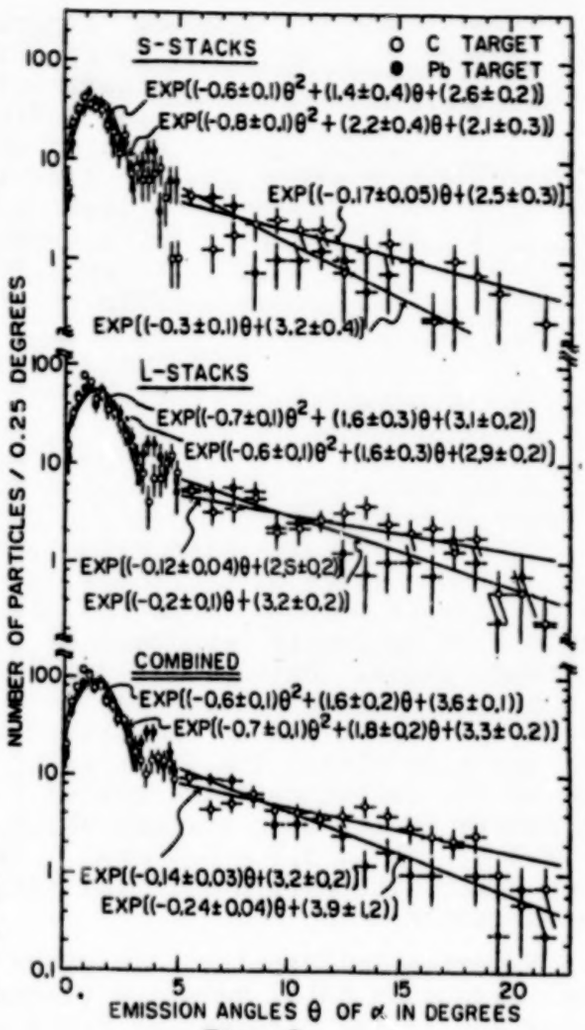


Fig. 2

Table I. The fitted values of a and b of Eq. (1) from the angular data of α fragments (and of Li fragments inside the brackets).

Target	# of α fragments = # from S-stacks + # from L-stacks	a	b	χ^2/DF
Carbon	1103 = 408 + 695	6.3 ± 0.05	0.0248 ± 0.0009	21/9
	(138 = 35 + 103)	(4.4 ± 0.1)	(0.029 ± 0.003)	(6/5)
	1085 = 408 + 677	6.3 ± 0.04	0.0265 ± 0.0009	27/10
	(160 = 62 + 98)	(4.4 ± 0.1)	(0.030 ± 0.003)	(11/5

4. Discussion and Conclusion. From the Lorentz transformation of cot Θ from the LS to the ALS,

$$\cot\Theta = \frac{M_F\,\gamma_p\,\bar{\bar{\gamma}}(\bar{\bar{\beta}}\cos\bar{\bar{\theta}} + \beta_p)}{M_F\,\bar{\bar{\gamma}}\,\bar{\bar{\beta}}\sin\bar{\bar{\theta}}} \cong \gamma_p\,\beta_p/(\bar{\bar{\beta}}\sin\bar{\bar{\theta}}), \quad (3)$$

where we used the fact that

$$\bar{\bar{\beta}}\cos\bar{\bar{\theta}} \ll \beta_p \quad (4)$$

from the observation of D. E. Greiner et al.[4] as well as our experience with the heavy evaporation prongs produced in high-energy jets in nuclear emulsion. Thus, we obtain the target-independent formula,

$$dN(1/\bar{\bar{\beta}}\sin\bar{\bar{\theta}}) \cong (\kappa/b)\times \exp(a + \kappa/\bar{\bar{\beta}}\sin\bar{\bar{\theta}})\times d(1/\bar{\bar{\beta}}\sin\bar{\bar{\theta}}), \quad (5)$$

with a Lorentz-invariant constant,

$$\kappa = \gamma_p\,\beta_p\,b. \quad (6)$$

In fact, Eq. (1) along with Eq. (6) is in accord with the Kaplon's formula, Eq. (2), by finding the median angle through integration of Eq. (1), as

$$\cot\Theta_{\frac{1}{2}} = \ln 2/|b| = (\ln 2)\,(\gamma_p\,\beta_p)/|\kappa|. \quad (7)$$

This method gives the value of $\zeta = 0.06 - 0.07$ in Eq. (2).

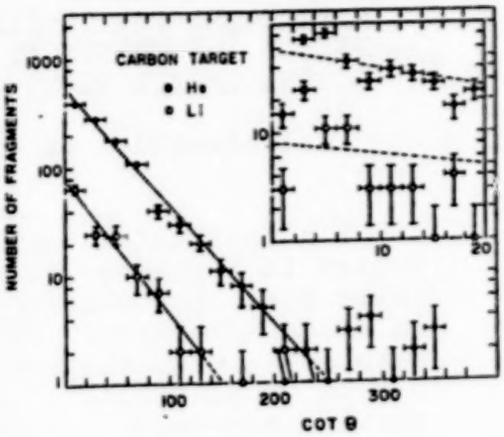


Fig. 3 (a)

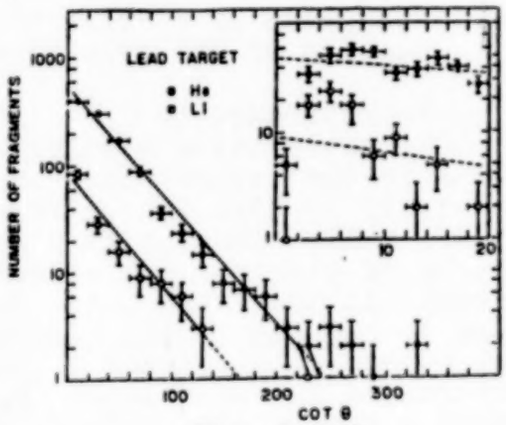


Fig. 3 (b)

REFERENCES

[1]M. F. Kaplon et al., Phys. Rev. 85, 295 (1952).

[2]H. H. Heckman et al., Phys. Rev. C 17, 1735 (1978); K. B. Balla et al., Nucl. Phys. A367, 446 (1981); M. M. Aggarwal et al., Phys. Rev. C 27, 640 (1983); G. M. Chernov et al., Nucl. Phys. A412, 534 (1984).

[3]C. O. Kim, Phys. Rev. D 31, 513 (1985).

[4]D. E. Greiner et al., Phys. Rev. Lett. 35, 152 (1975).

ORIGINAL PAGE IS
OF POOR QUALITY

N85-35899

EXPERIMENT "PAMIR"-III. COPLANAR EMISSION OF HIGH ENERGY γ-QUANTA AT INTERACTION OF HADRONS WITH NUCLEI OF AIR ATOMS AT ENERGIES ABOVE 10^7 GEV

Collaboration of the Experiment 'Pamir' *

ABSTRACT

At a systematic analysis of large γ-families, detected in X-ray-emulsion chambers, cases of multicore halos have been observed, and among them five events in which the halo is divided into three of four separate cores with their alignment observed in the target diagram (coplanarity of axes of corresponding electron-photon cascades). The halo alignment (tendency to the straight line) leads to the azimuthal asymmetry ("thrust"). The analysis of lateral and momentum distributions of particles in these families shows that they also have "thrust" that correlates with the direction of the halo core alignment.

1. Introduction

Recently halos - diffuse zones of darkening on X-ray films in the central part of large γ-families - are intensively studied in the framework of experiment "Pamir" /1,6/. While scanning on microdensitometers, five standard levels of electron number density (excess over the background) in the range $\Delta n = 0.015\text{-}0.16\ \mu m^{-2}$ are used. The area S_i bounded by the corresponding isodense, and the total number of electrons N_i confined at this area, have been determined for each level /2,3/. For quantitative evaluations a family with halo is defined as the family in which (1) the number of electrons N_3 on the third level of observation ($\Delta n = 0.04\ \mu m^{-2}$) satisfies the condition $N_3 \geq 2N_3^{(s)}$, where $N_3^{(s)}$ is the calculated number of electrons for the same level of observation in electron-photon cascades (EPC) from above-threshold γ-e particles of the family; (2) the area $S_3 \geq 1$ mm; (3) the number of above-threshold particles providing the first two conditions are fulfiled is > 1.

Analysis of the halo on the third level of observation has shown that its basic characteristics (spatial distribution of energy density, axial symmetry, values N_3, S_3 and their dependence on the depth in the chamber) allow to interpret most of them as a certain stage of the EPC development from the γ-e particle that has been formed with a large value of the Feynman variable ($x \geq 0.1$) /2/.

Thus, the presence of halo indicates the production of high energy γ-e particles in atmospheric cascades.

---

* Full list of authors see in HE 1.2-12. The authors of this paper are also T.L.Asatiani, L.E.Genina (Yerevan Physical Institute) and G.T.Zatsepin (Institute for Nuclear Researches, Moscow).

By the densitometric scanning of ~80 γ-families with $\Sigma E_\gamma \geq 250$ TeV 36 events with halo have been detected, and in 15 of them several halos (2-4) are observed (multicore or multiple halos). Each component or core was considered as a separate halo, if the above conditions were satisfied, the number of electrons in it was not less than 5% of N_3, and the distance between the cores exceeded that between the neighboring density level isodenses. In three- and four-core events a quasilinear alignment of halo cores is observed, i.e. coplanarity of axes of corresponding EPC /2,3/.

In the present report we continue investigating the nature of halo, structure of multicore halo, their alignment as well as correlations of the γ-family particles alignment with that of halo.

2. Structure of halo on upper density levels

The study of the halo structure on higher levels ($\Delta n = 0.08$ and 0.16 μm^{-2}) shows that the ratios N_5/N_3 and N_4/N_3 fluctuate not much which should be the case with EPC, and that large (1.5 order) fluctuations of the size of halo at the given energy of families ΣE_γ occur at all levels.

In Fig.1 the correlation field of points (N_i/s_i, s_i) for separate halo axes is shown. Crosses denote the results for high energy EPC according to calculations /4/. Small fluctuations ratios and proximity of the experimental mean value to the calculated one support the interpretation of halo as a definite stage of EPC development induced by a high energy quantum.

In the upper part of Fig.1 there are events with large halos which apparently begin to differ essentially from "electromagnetic" ones at the large depths of the chamber.

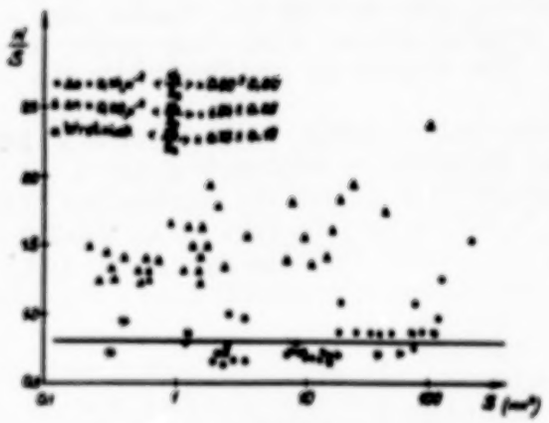


Fig.1

3. "Thrust" of halos and γ-quanta

Densitograms of events with multicore halos and their characteristics are presented in Fig.2a and Table 1, respectively. Each core of such halos may be considered as an event of generation of γ-e particle at a high altitude. Thus nuclear-electromagnetic cascades (NEC) are detected when several such particles are produced. Densitograms show an obvious tendency of halo components to be arranged

ORIGINAL PAGE IS
OF POOR QUALITY

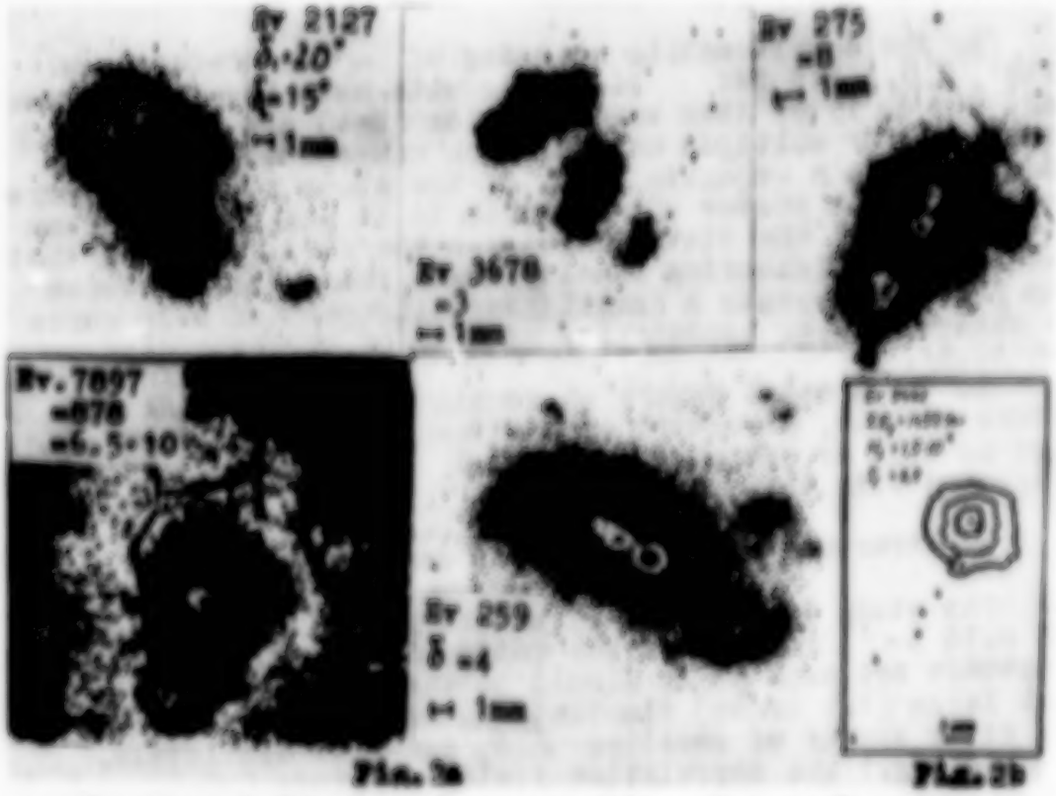


Fig. 2a

Fig. 2b

on the target diagram along one line, i.e. coplanarity of axes of corresponding EPC (alignment). As a quantitative measure of the alignment may serve the angle formed by lines that connect the second in number $N^{(2)}$ halo core with the first one and all the others. The estimate, based on experimental values of these angles, shows that the probability of a random imitation of the observed coplanarity in all five events makes $\sim 10^{-3}$.

The alignment of multicore halos leads to asymmetry in the distribution of transverse momenta - "thrust". As a quantitative dimension of "thrust" of halos or particles in families serves the value $T' = \sum_{i,k} |R_{ik}\, Q_{ik} \theta_{ik}| / \sum_{i,k} |R_{ik}\, \sin\theta_{ik}|$, where $R_{ik} = R_{ik} E_i E_k / (E_i + E_k)$; E_i, E_k are the energies of i-th and k-th core of the halo or particle, respectively; Q_{ik}, R_{ik} is the difference of azimuthal angles and distances in the plane of traget diagram between appropriate objects. (The value T' by its physical meaning is close to thrust used in analysis of collisions at high energies). Values of T' are plotted in table 2 for halo cores and above-threshold γ-particles of the family with $\gamma = E_\gamma / \sum E_\gamma \geq 0.04$. It is seen from table that the "thrust" of γ-quanta in families correlates with that of halos in events with multiple halos.

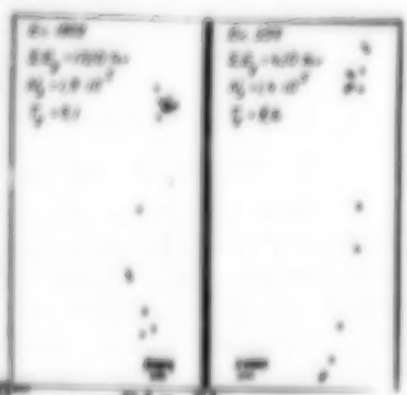


Fig. 2b

As far as most low energy γ-quanta come from low altitudes, this cor-

Table 1. Data on multicore halos

N event	ΣE_γ, TeV	$N_3/10^3$ S_3, mm	$x=N_3^{(1)}/N_3$, %	ΣE_γ, TeV in core	T'
275	2350	10.3 14.7	46, 25, 20	525, 678, 230	2.6
259	506	7.5 11.4	76, 12, 6	92, 80, 98	5.6
3678	1638	11.2 16.7	67, 17, 6	564, 248, 120	5.3
2127	1720	7.2 10.4	80, 6, 5,8	375,21,121,141	4.2

Table 2. Mean "thrust" of γ-quanta and halo axes

Number of axes	0	1	2	3	4
Number of events	38	10	10	4	1
Mean "thrust" of halo axes				4.4 ± 1.2	4.2
Mean "thrust" in γ-e particles with $f' \geq 0.04$	1.4 ± 0.2*)	1.15 ± 0.2*)	6.1 ± 2	2.8 ± 0.6	5.2
	2.8 ± 0.4	3.0 ± 0.4	6.4 ± 1.9	3.1 ± 0.6	5.2

*) for the arbitrarily chosen direction

relation shows that along with the generation of γ-e particles whose "thrust" is established by halo, at high altitudes other particles (hadrons?) are also generated with "thrust" that provide the conservation of the direction of "thrust" in the further development of NEC in atmosphere.

The "thrust" of quanta occurs not only in events with multicore halos but is observed also ($T' \geq 5$) in some families without or with one halo. Examples of target diagrams of such events are presented in Fig.2b for γ-e particles with $f' \geq 0.04$.

REFERENCES

/1/ Pamir Collaboration Proc.18th ICRC,HE 5-28,Bangalore.
/2/ Baradzei L.T. et al.Proc.Int.Symp.,Tokyo,1983,p.136.
/3/ Genina L.E.et al. Prepr.FIAN, N 54, 1981, Moscow.
/4/ Wrotniak I.A. 17th ICRC, Paris 11(1981)191.
/5/ Pamir Collab.Kratk.soobsh.fiz.FIAN,N 12,1984,39,Moscow.
/6/ Gulov Yu.A. et al. Preprint FIAN,N 143,1983,Moscow.

N85-35900
HE 1.4-13

THE EFFECT OF THE RELATIVE NUCLEAR SIZE ON THE NUCLEUS-NUCLEUS INTERACTIONS

I.N.Erofeeva, V.S.Murzin, S.Yu.Sivoklokov and L.N.Smirnova
Institute of Nuclear Physics, Moscow State University, Moscow II9899, USSR

Abstract. The experimental data on the interactions of light nuclei (d, He^4, C^{12}) at the momentum 4.2 GeV/c·A with the carbon nuclei were taken in the 2-m propane bubble chamber. The distributions in the number of interacting nucleons, the spectra of protons, the mean energies of secondary pions and protons, the mean fractions of energy transferred to the pion and nucleon components are presented. The results of investigation of the mechanism of nucleus-nucleus interactions can be used to calculate the nuclear cascades in the atmosphere.

Experimental Data

We analyze 2400 dC, II60 He^4C^{12} and I800 $C^{12}C^{12}$ events detected in the 2-m propane chamber at the momentum of projectile nuclei P_0 = 4.2 GeV/c·A. The momenta of all protons and nuclear fragments with P I50 MeV/c and charged $\pi^{\pm}$ mesons with $P_{\pi} > 70$ MeV/c have been measured. All negatively charged particles were regarded as π^- -mesons (the admixture of other species < I%). The event was identified as an interaction on carbon if one of the following conditions was satisfied /I/: a) $n_+ - n_- > (Z_{A_1}+I)$; b) $n_p > I$; c) $n_{\bar{p}} > 0$; d) $n_+ > 2$; e) $n_{\pm}$ is odd for the dC events. Z_{A_1} is the incident nucleus charge, n_p is the number of slow (with P< 750 MeV/c) protons, $n_{\bar{p}}$ is the number of backward emitted protons in the lab-system, $n_{\pm}$ is the number of charged particles in the event. Using these criteria we selected 70 to 80% of inelastic interactions on the carbon nucleus. The remainder events were statistically separated taking into account the known cross sections on a proton and carbon /2/ and the detection efficiency.

The spectra of protons are obtained by the subtraction of the π^--meson spectrum from the spectrum of all positive particles. The spectra of π^+ and π^--mesons were assumed to be identical because of the isotopic symmetry of colliding nuclei.

The Number of Interacting Nucleons

The distribution $P(\nu)$ in the number of interacting nucleons of the projectile nucleus in dC and He^4C^{12}-interactions was obtained on the basis of the data on the number of stripping particles and on the multiplicity of π^--mesons in the events with a different total charge of the stripping particles. The stripping particles are those ones with momentum P > 3 GeV/c and emission angle $\theta < 4^0$. The production in the interaction of a nucleon of the projectile nucleus is assumed to be independent of the other nucle-

on's interactions. The use of additional data on the multiplicity of π^--mesons in pC and dC-interactions /3/ enabled us to obtain six equations with unknown $P(\nu)$ ($\nu = 1...4$) for He^4C interactions /4/. The obtained probabilities $P(\nu)$ of the interaction of ν nucleons of the projectile nucleus for dC and He^4C interactions are given in Table I together. with the predictions of the multiscattering model (MSM) /5/. P(I) and P(4) in He^4C-interactions are in disagreement with the MSM results.

Table I

The interaction probabilities $P(\nu)$ of ν nucleons of the projectile nucleus A_i

$A_i A_t$ \ $P(\nu)$	P(I)	P(2)	P(3)	P(4)	
dC	0.68 ± 0.04	0.32 ± 0.04	-	-	1.32 ± 0.08
He^4C	0.24 ± 0.06	0.33 ± 0.15	0.20 ± 0.13	0.23 ± 0.05	2.42 ± 0.08
He^4C /5/	0.44	0.25	0.19	0.12	2.00

Table 2

The mean characteristics of dC, He^4C and CC-interactions

		dC	He^4C	CC
$\langle n_- \rangle$		0.61 ± 0.03	1.00 ± 0.04	1.51 ± 0.05
$\langle E_- \rangle$	GeV	0.62 ± 0.02	0.64 ± 0.02	0.64 ± 0.02
$\langle n_p \rangle$		2.7 ± 0.1	3.9 ± 0.1	5.2 ± 0.2
$\langle T_p \rangle$	GeV	0.67 ± 0.06	0.80 ± 0.06	1.11 ± 0.06
ε_{π^-}	GeV	0.38 ± 0.02	0.64 ± 0.03	0.97 ± 0.04
ε_p	GeV	1.6 ± 0.2	3.1 ± 0.2	5.7 ± 0.3
$\Sigma\varepsilon_i$		4.3 ± 0.2	8.1 ± 0.5	14.5 ± 0.5
T_0	GeV	4.4 ± 0.2	8.1 ± 0.2	12.9
α_π		0.26 ± 0.02	0.24 ± 0.02	0.23 ± 0.02
α_N		0.74 ± 0.07	0.76 ± 0.07	0.91 ± 0.09

The Partial Coefficients of Inelasticity of Pions and Nucleons

Table 2 lists the mean multiplicities and energies $\langle E_- \rangle$ of π^--mesons, the multiplicities and kinetic energies $\langle T_p \rangle$ of protons and also the mean energy of all π^--mesons ε_{π^-} and protons ε_p in an event.

Assuming that the mean multiplicities and energies of all species of π-mesons and nucleons are equal ($\langle n_{\pi^-} \rangle = \langle n_{\pi^0} \rangle = \langle n_{\pi^+} \rangle$, $\langle E_{\pi^-} \rangle = \langle E_{\pi^0} \rangle = \langle E_{\pi^+} \rangle$, $\langle n_p \rangle = \langle n_n \rangle$, $\langle T_p \rangle = \langle T_n \rangle$) we can determine the total energy of all secondaries: $\Sigma\varepsilon_i = 2\varepsilon_p + 3\varepsilon_{\pi^-}$. This value must coincide with the initial kinetic energy of interacting nucleons $T_0 = 3.37 \langle \nu \rangle_{AC}$ (GeV) to within the energy of particles below the detection threshold. For CC-interactions the magnitude $\langle \nu \rangle_{CC} = 3.83$ was taken from ref./3/. Table 2 presents also the partial coefficients of inelasticity for pions $\alpha_\pi = 3\varepsilon_{\pi^-}/T_0$ and protons $\alpha_N = 2\varepsilon_p/T_0$. The fraction of energy transferred to π-mesons is considered to be the same for all reactions in question. It is

much lower than the value of α_π for the nucleonic interactions at the energies > 20 GeV /6/.

The Momentum Spectra of Protons

The momentum spectra of protons in dC, He^4C and CC-interactions in the lab-system are presented in fig.I. The spectra are normalyzed to the mean number of protons in an event. Approximation of the spectra by the function $\exp(-bP)$ at P = I-3 GeV/c gives the following values of the parameter b : 0.62 ± 0.04 for dC, 0.49 ± 0.05 for He^4C and 0.29 ± 0.03 for CC-interactions. At the momenta > 3 GeV/c the spectra tend to steepen slightly, which is well seen in the case of CC interactions, yet, they are everywhere well outside the value P_0 = 4.2 GeV/c. If in dC-collisions the part of the plot $P > P_0$ is due to the errors in measuring of the particles momenta and to the cumulative particles contribution the increased yield of fragments with Z=I in this part in He^4C and CC-interactions requires an additional mechanism. The interacting many-nucleon fragments of the projectile nuclei with $P > P_0$ can contribute to the high-momentum part of the spectrum in these interactions.

The mean momenta of protons in dC, He^4C and CC-interactions are plotted in fig.2 versus the ratio of atomic weights of the colliding nuclei A_i/A_t. The mean value of $\langle P_p \rangle$ increases by a factor of I.5 in the transition of A_i from d to C, approaching the estimated value of the mean momentum of a proton in pp-collisions at 4.2 GeV/c. This implies that the cascade becomes less important inside the carbon nucleus for secondary nucleons in He^4C and CC-interactions. This effect is seemingly present in any collisions of the nuclei with comparable sizes.

Conclusions

The chief results are the following: I) the distribution in the number of interacting nucleons of the He^4 nucleus in the carbon nucleus is nearly uniform which is in contradiction to the MSM results /5/; 2) the partial coefficients of inelasticity for pions and nucleons are actually the same for dC, He^4C and CC-interactions; 3) the momentum spectra of protons and the mean values of their momenta are different for each type of interactions. The experimental results permit us to infer the presence of many-nucleon fragments in the spectrum of interacting particles and the minor role of cascade in the interactions of nuclei with identical atomic weights.

References

I. Agakishiev H.N. et al. JINR, I-83-662, Dubna, I983.
2. Angelov N. et al. JINR, PI-80-473, Dubna, I980; Yad.Fiz. I98I, 33, I046.
3. Agakishiev H.N. et al. JINR, EI-84-32I, Dubna, I984; Proc. XXII Int.Conf. on High Energy Physics, Leipzig, I98I.

ORIGINAL PAGE IS
OF POOR QUALITY

4. Gasparyan A.P. et al. Proc. I6th ICRC, Kyoto, I979, 6, HE 3-6, I76.
5. Gasparyan A.P. et al. JINR, I-80-853, Dubna, I980; Yad.Fiz., I98I, 34, I328.
6. Vlasov E.V. et al. Z.Phys.C, I982, I3, 95.

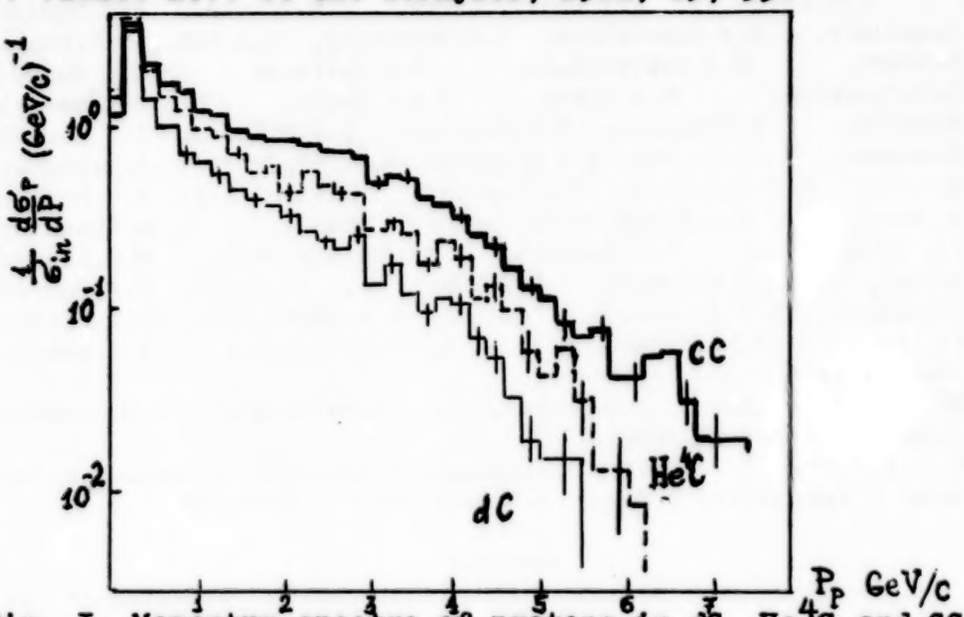


Fig. I. Momentum spectra of protons in dC, He^4C and CC-interactions

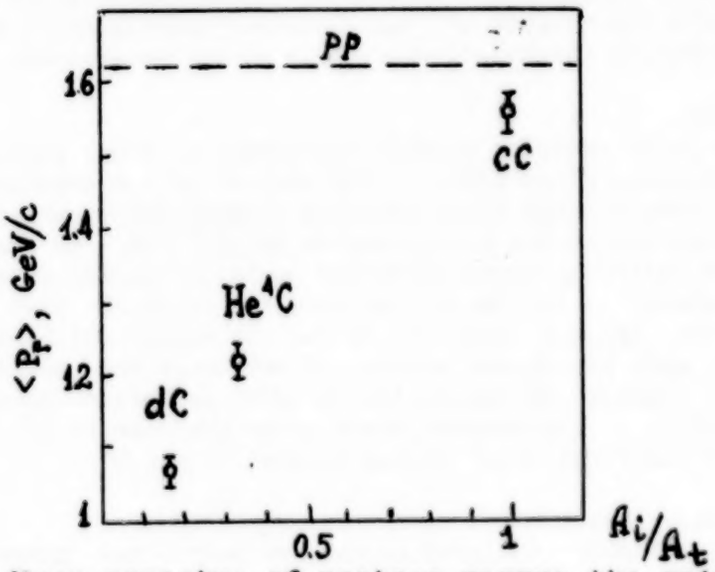


Fig. 2. Mean momentum of protons versus the ratio of atomic weights of colliding nuclei.

N85-35901

JAPAN-USSR JOINT EMULSION CHAMBER EXPERIMENT AT PAMIR

JAPAN-USSR JOINT EXPERIMENT (I)

USSR : A.S.Borisov, K.V.Cherdyntseva, Z.M.Guseva, V.G.Denisova, A.M.Dunaevsky, E.A.Kanevskaya, V.M.Maximenko, R.A.Nam, S.V.Pashkov, V.S.Puchkov, S.A.Slavatinsky, M.D.Smirnova, Yu.A.Smorodin, N.G.Zelevinskaya, M.V.Zimin, G.B.Zhdanov, R.A.Mukhamedshin, O.E.Nedel'ko, L.P.Nikolaev, G.T.Zatsepin, T.P.Amineva, L.T.Baradzei, I.P.Ivanenko, N.P.Ilijina, T.V.Lazareva, A.K.Managadze, I.A.Mikhailova, E.A.Murzina, E.I.Pomelova, E.G.Popova, I.V.Rakobolskaya, T.M.Roganova, N.G.Ryabova, L.G.Sveshnikova, S.G.Cananov, L.Kh.Chadranyan, L.A.Khisanishivili, G.G.Leptukh, N.N.Roinishivili, M.S.Svanidze, Z.A.Azimov, I.B.Bobodjanov, N.E.Gubar, Yu.,A.Gulov, F.Normuradov, Kh.Shoboronov, S.A.Azimov, D.A.Khalilov, E.G.Mullajanov, Kh.Nuritdinov, D.A.Talipov, T.S.Yuldashbayev, S.E.Bakhtigireev, N.A.Dobrotin, Yu.A.Emelyanov and E.G.Zaitseva
POLAND : H.Bielawska, B.Juskiewicz, J.Malinowski, A.Maciaszszyk, K.Milczarek and A.Tomaszewski
JAPAN : H.Aoki, Y.Fujimoto, Y.Funayama, S.Hasegawa, H.Kumano, H.Semba, M.Tamada, S.Yamashita, K.Yokoi, A.Ohsawa and E.H.Shibuya*

Abstract

The results are presented for the systematic measurement of showers in the first carbon chamber of Japan-USSR joint experiment at Pamir. The intensity and the energy distribution of electromagnetic particles, of hadrons and of families are in good agreement with the results of other mountain experiment if we take into consideration the relative error in energy estimation.

1. Introduction.

Japan-USSR joint emulsion chamber experiment at Pamir plateau (4370m) has been continuing since 1981. The purpose of the experiment is a test for the future large scale emulsion chamber experiment to observe nuclear interaction at the energy region of $10^{16} \sim 10^{17}$ eV and is also to work as a interface among different emulsion chamber experiment of mountain altitude. In Table 1 we show the exposure list of joint chambers. The chamber 'Pamir-1' is for the energy calibration and it is found that upto the shower energy $\sim$20 TeV there are no appreciable difference of energy determination between in Soviet group and in Japanese group[1]. The present paper gives the results of systematic measurement of the first joint carbon chamber 'Pamir-2'.

2. Carbon chamber 'Pamir-2'.

The carbon chamber designed to observe hadron and gamma families consists of three parts, that is, Γ-block of 6 cmPb, H-block of 5 cmPb and carbon layer of 60 cm thick between the two. The effective thickness of the chamber is about 1.5 λ geo.. Fig.1 shows the basic structure of the carbon chamber. Two types of Japanese (SAKURA N-type and FUJI #100-type) and Soviet (PTGM-type and PTCM-type) X-ray films are used as sensitive materials. About half, $\sim$33 m^2, of the chamber 'Pamir-2' has been systematically analysed[2].

---

*) On leave from UNICAMP,IFGW, Sao Paulo, Brasil

ORIGINAL PAGE IS
OF POOR QUALITY

Table 1. Exposure list of joint chamber at Pamir (4370m)

chamber	area(m^2)	period (days)	type	sensitive layers	remarks
Pamir-1 81/82	11.2	253 Oct.'81 ∿ June'82	flat 7 cmPb (calibration)	3, 3*	[1]
Pamir-2 82/83	72.0	415 June'82 ∿ Aug.'83	carbon chamber	2, 3* in Γ-block 2, 3* in H-block	present paper
	6.0	343 Aug.'82 ∿ July'83	flat 6 cmPb (calibration)	2, 3*	
Pamir-3 83/84	90.0	350 July'83 ∿ July'84	carbon chamber	2, 2* in Γ-block 2, 2* in H-block	under analysis
	4.0		flat 7 cmPb (calibration)	5, 5*	
Pamir-3' 83/85	∿ 100	Oct.'83 ∿	carbon chamber	2 in Γ-block 2 in H-block	under exposure
Pamir-4 84/85	∿ 17	Aug.'84 ∿	thick lead 50 cmPb		under exposure

*) number of sensitive layers of Soviet films.

3. Energy estimation.

Here we describe the procedure of Japanese group[2]. The detail procedure of Soviet group is described in Ref.[1,4]. The darkness of shower spot on X-ray films are measured by microphotometer with square slit of 200x200 μm^2. In this joint chamber, we have only two layers of Japanese X-ray films in each part of the chamber, Γ-block and H-block. Then we must estimate shower energy by using spot darkness on two layers of X-ray films except for the case that showers penetrate both Γ-block and H-block. The two different methods are applied. One (Method-I) is to use the following semi-empirical formula[2],

$$D_m^0 = Dmax(D_{10}^{\Gamma}/D_8^{\Gamma})^{-\beta}, \quad \beta=0.812-0.70\tan^2\theta$$

$$E = 10^{\cdot}(D_m^0\sqrt{1+\tan^2\theta}/0.54)1.234$$

where D_8^{Γ} and D_{10}^{Γ} are darkness of a shower spot at 4 cmPb and 5 cmPb in Γ-block and Dmax is larger one between the two. θ is zenith angle of shower direction. For the showers(hadrons) observed in H-block, D_8^{Γ} and D_{10}^{Γ} are replaced with D_6^H and D_8^H, where D_6^H and D_8^H are darkness of a shower at 3 cmPb and 4 cmPb in H-block. The other (Method-II,[3]) is to estimate the shower maximum by fitting experimental points, only two points except for penetrating showers, with calculated shower transition curve. Above two methods were applied to the individual simulated cascade showers of gamma-ray primaries[5] and it is found that the average value has expected one though the relative error, ΔE/E, is rather large (20 ∿30%). When the shower energy increases, ≳ 50 TeV, Method-I gives underestimation (by ∿20%) of the energy. The common shower spots are measured by Japanese group and by Soviet group. Fig.2 shows a correlation diagram on the energy of showers estimated by Soviet group and by Japanese group. As is seen in the figure there are no appreciable difference of energy estimation between the two.

4. Energy spectrum of (e,γ), of hadrons and of families.

Energy spectrum of (e,γ) Fig.4 shows integral energy spectrum of showers found in Γ-block. The spectra are expressed by the power function above energy 5 TeV. The Method-I gives steeper energy spectrum because of the underestimation of shower energy in high energy region. The straight line in the figure is a power function with index 2.0. Showers in Γ-block are mixture of electromagnetic showers and those from nuclear interaction of hadrons in Γ-block. About 20% of showers in Γ-block are considered as hadronic origin.

Energy spectrum of hadrons The visible energy spectrum of hadrons

constructed by showers observed in H-block is shown in Fig.3 by cross mark. The spectrum is also expressed by the power function with index 2.0 above energy 5TeV. The detection probability of hadrons in H-block is ∿33%. The spot darkness in H-block of hadronic showers becomes smaller because showers spread over during passage through the carbon layer, and then the visible energy is underestimated (by ∿20%). The flux of hadrons arriving at the chamber, indicated by broken line in the figure, is obtained by applying above two corrections. The relative ratio of intensity, $I_h/I_{e,\gamma}$, at the visible energy greater than 10 TeV, between hadrons and electromagnetic particles is about 2.

Energy specrrum of gamma-families Fig.5 shows integral energy spectrum of gamma-ray families. The spectrum is again well expressed by the power function with index 1.3, above total observed energy ∿ 20 TeV.

5. Comparison with the other experiment.

The relative error, $\Delta E/E$, in energy estimation affects the power index and the flux value of the energy spectrum. Suppose that the relative error in energy estimation has Gaussian type distribution with energy dependent dispersion $\sigma = \sigma_0(E/TeV)^{\delta}$ and spectrum is power type, then the ratio between the observed intensity, I, and the true one, I_0, is given by $I(>E)/I_0(>E) \simeq 1 + \varepsilon E^{2\delta}$. In the present experiment we have $\sigma_0 \sim 0.12$ and $\delta \sim 0.19$. Then we get $\varepsilon \sim 0.15$ under the assumption that power index of spectrum is 2.0. At the energy E=10TeV, observed intensity is considered ∿30% higher than the true one according to the above formula. The true intensity of (e,γ) is obtained by applying corrections for contamination of hadrons (20%) and for the effect of relative error in energy estimation (30%) to the observed intensity shown in Fig.3. Fig.6 shows the altitude dependence of the vertical flux of (e,γ) with energy greater than 10 TeV. As is seen in the figure, all experimental points are distributed around the expected exponential attenuation with $\Lambda_{att} \sim 120$ gr/cm^2. Thus we can conclude that there are no appreciable systematic difference of energy estimation between in the present experiment and in the other mountain experiments.

6. Discussions.

The relative error in energy estimation, by using two layers of X-ray films in the carbon chamber, is rather large, especially in high energy region. However, the vertical flux and the power index of spectra of electromagnetic particles, of hadrons and of families obtained in present measurement are not inconsistent with those of the other mountain experiment.

Aknowledgement. The collaboration experiment is financially supported in part by Grant-in-Aid from the Ministry of Education and Waseda University, in Japan.

References.

[1] H.Kumano, A.Ohsawa and V.Puchkov ; ICR-Report-115-84-4 (1984)
[2] M.Koike,T.Hibi,H.Tanaka,M.Tsuchiya and K.Teramura ; to be published
[3] A.Okamoto, A.Kashimura and K.Takewaka ; to be published
[4] Pamir Collaboration ; Trudi FIAN Vol.154(1984)
[5] M.Okamoto and T.Shibata ; Proc. 17th ICRC, Paris, 5(1981)p.214, 218
[6] Mt.Fuji Collaboration ; Proc. 18th ICRC, Bangalore, 11(1983) 57
[7] China-Japan Collaboration ; Proc. 18th ICRC, Bangalore, 5(1983) 285

N85-35905

ORIGINAL PAGE IS
OF POOR QUALITY

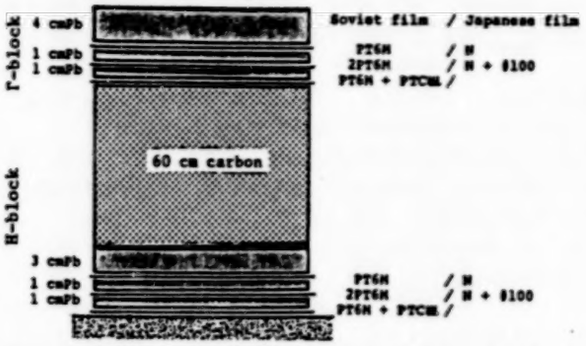


Fig.1 Basic structure of carbon chamber.

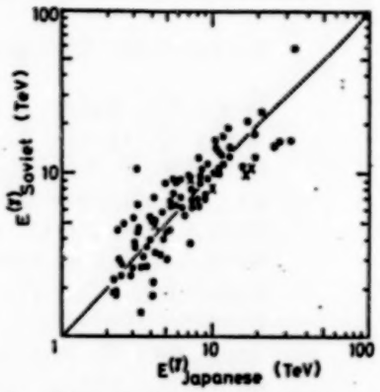


Fig.2 Correlation diagram on the shower energy estimated by Japanese group and by Soviet group. ● : (e,γ), X : hadrons

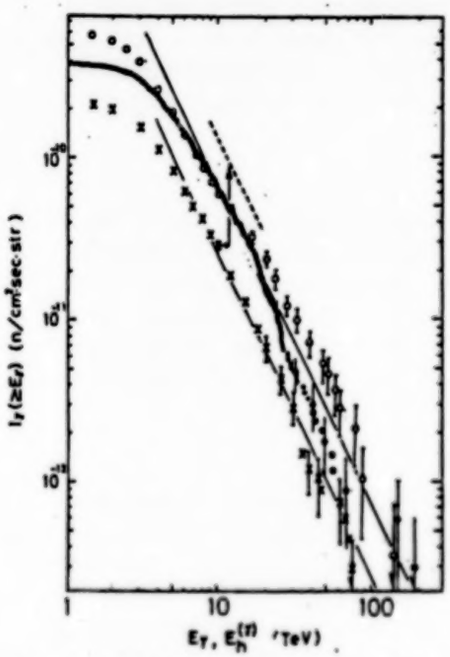


Fig.3 Integral energy spectra of (e,γ) and hadrons.
● : (e,γ) by Method-I
○ : (e,γ) by Method-II
X : hadrons by Method-I
Lines are power function with index 2.0. Broken line is corrected spectrum of hadrons.

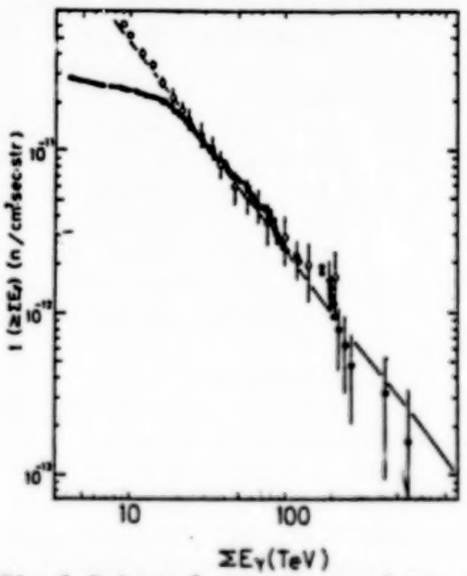


Fig.4 Integral energy spectrum of of gamma-ray families.
●: by Method-I
○: by Method-II

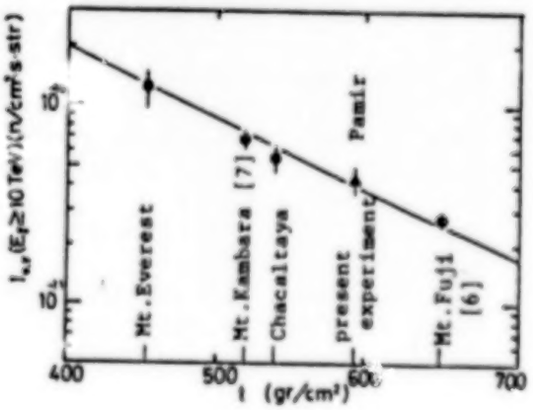


Fig.5 Vertical intensity of (e,γ) with energy greater than 10 TeV.

N85-35902

HE 3.1-2

INTENSITIES OF HIGH-ENERGY COSMIC RAYS AT MT. KANBALA

China-Japan Emulsion Chamber Collaboration

Ren.J.R., Kuang.H.H., Huo.A.X., Lu.S.L., Su.S., Wang.Y.X. and Xue.Y.G. (Inst. of High Energy Physics, Academia Sinica, Beijing, China), Wang.C.R., He.M., Zhang.N.J., Cao.P.Y. and Li.J.Y. (Shangdong Univ., Jinan, China), Wang.S.Z. (Zhengzhou Univ., Zhengzhou, China), Bai.G.Z., Liu. Z.H., Li.G.J. and Gang.G.X.(Chongqing Inst. of Architecture and Engineering, Chongqing, China), Zhou.W.D. and He.R.D. (Yunnan Univ., Kunming, China),
Amenomori.M. and Nanjo H. (Hirosaki Univ., Hirosaki, Japan), Hotta.N., Ohta.I. and Sakai.M. (Utsunomiya Univ., Utsunomiya, Japan), Mizutani.K. (Saitama Univ., Urawa, Japan), Kasahara.K. and Yuda.T. (Inst. for Cosmic Ray Research, Univ. of Tokyo, Tokyo, Japan), Shibata.M. (Yokohama National Univ., Yokohama, Japan), Shirai.T., Tateyama.N. and Torii.S. (Kanagawa Univ., Yokohama, Japan), Sugimoto.H. and Taira.K. (Sagami Inst. of Technology, Fujisawa, Japan).

Abstract

The energy spectra of atmospheric cosmic rays at Mt. Kanbala (520 g/cm^2) are measured with emulsion chambers. The power indeces of the spectra are values of about 2.0 for both gamma-rays and hadrons. Those fluxes are consistent with the ones expected from the model of primary cosmic rays with heavy nuclei of high content in the energy around 10^{15} eV.

1. Introduction

The China-Japan Cooperative Emulsion Chamber Experiment is continued with a large-area exposure at Mt. Kanbala, Tibet in China (5500 m above sea level, atmospheric depth 520 g/cm^2), in order to observe big families with energy over 1000 TeV. Details of characteristics of those families are discussed in another paper(1), by concerning with primary cosmic rays in the energy around 10^{15} eV or more. Also, uncorrelated particles of atmospheric cosmic rays, such as gamma-rays (hereafter, these mean high energy photons and electrons) and hadrons, are observed in a lower energy region with the same emulsion chambers. The intensities of those particles as well as the members of families are presented in this paper.

2. Experimental procedure

The emulsion chamber used in the Mt. Kanbala experiment consists of photosensitive materials and metal plates, piled up alternately. Several sorts of X-ray film with different sensitivity are generally used as the photosensitive materials, such as type-N (Sakura), type-III (Tianjin), type-100 (Fuji), Gongyuan (Shantou) and type-5F (Shanghai).

Two kinds of metal are used at Mt. Kanbala, as listed in Table 1. One is the lead emulsion chamber (Pb-EC), as generally

ORIGINAL PAGE IS
OF POOR QUALITY

used in mountain experiments. Another is the iron one (Fe-EC) which is exposed to observe efficiently hadron components. In this paper. the results are presented given from the Fe-ECs as well as the Pb-ECs whose preliminary data are shown in the previous paper(2).

Table 1. Exposure list at Mt. Kanbala.

Series	Date	Exposure (m^2 y)	Material	Thickness (c.u.)
K0	Sep.1980-Sep.1981	3.7	Pb	14
		11.0	Pb	30
K1	Sep.1981-Sep.1982	1.0	Pb	14
		49.0	Pb	28
K2	Oct.1982-May 1984	143.0	Pb	14
		39.1	Fe	29
K3	May 1983-May 1984	6.3	Pb	14
		31.1	Fe	29
K4	May 1984-May 1985	85.0	Pb	14
		58.0	Fe	29

The showers produced by high energy particles are observed as the series of shower spots on X-ray films over several layers and the energy of each shower is estimated by measuring optical density of those spots. Details of the method for the Pb-EC are found in the previuos paper(2). For the analysis of the Fe-EC. the similar manner is applied. For the purpose of energy determination of showers in the Fe-EC. massive simulations have been made on the cascade showers developing in iron.

3. Results

In order to get the intensities of atmospheric cosmic rays. a part of the emulsion chambers of thick type (28 - 30 c.u. thick) has been analysed with careful scanning, for the exposure of 7.0 m^2 y in the Pb-EC and 6.0 m^2 y in the Fe-EC.

The starting point of the observed showers is displayed in Fig. 1. The distribution of a deep region gives us the attenuation length of hadrons indicating 42.0 c.u. in lead and 13.5 c.u. in iron. Those values correspond to the collision length of 28.0 c.u. in lead and 9.0 c.u. in iron. both of which are consistent with the values expected from the respective interaction cross section. By taking the attenuation into account. the detection probabilities of hadrons are determined to be 39 % in the Pb-EC and 78 % in the Fe-EC. A statistical separation of gamma-rays and hadrons has been performed by using those detection probabilities(2),(3).

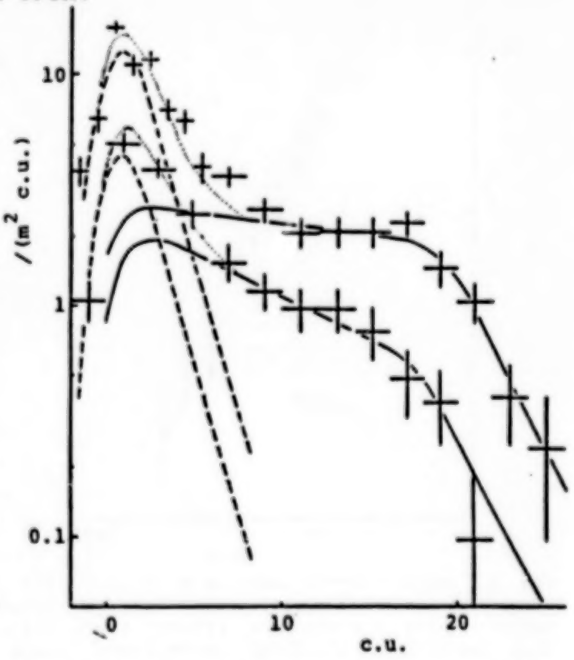


Fig. 1. Starting point distribution of showers in the emulsion chamber of thick type. The upper and lower crosses represent the number of detected showers with energy above 3 TeV for the Pb-EC and above 5 TeV for the Fe-EC. respectively. The dashed and solid curves are expected from gamma-rays and hadrons. respectively.

The resulting vertical energy spectra at Mt. Kanbala are shown

in Fig. 2 and Fig. 3 for the showers initiated by gamma-rays and hadrons. respectively. Both results given from the Pb-ECs and the Fe-ECs are consistent with each other. Those power indices and fluxes are listed in Table 2.

Table 2. Spectra of atmospheric cosmic rays at Mt. Kanbala.

	Spectral index	Intensity at 5 TeV (m^2 s sr)
gamma-rays	2.00±0.08	$(2.8\pm0.2)\times10^{-6}$
showers induced by hadrons	2.03±0.08	$(6.0\pm0.6)\times10^{-6}$

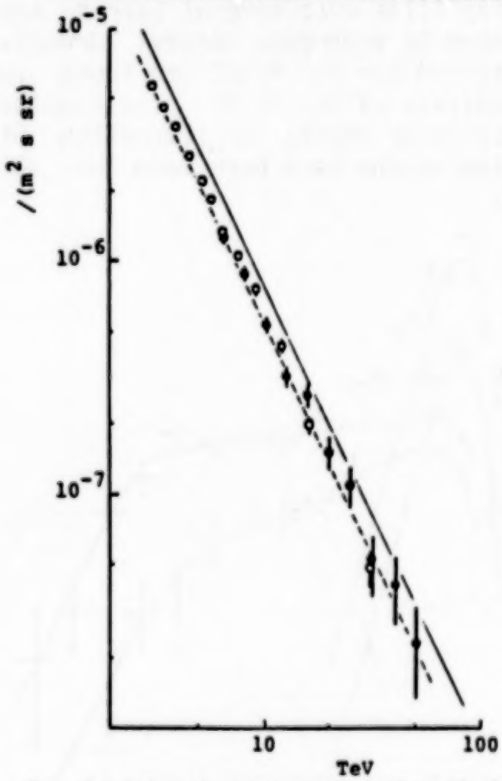


Fig. 2. Integral energy spectrum of vertical gamma-rays at Mt. Kanbala. The open and solid circles represent the results given from the Pb-EC and the Fe-EC. respectively. The dashed line is the best fit. The solid curve is expected by the assumptions mentioned in the text.

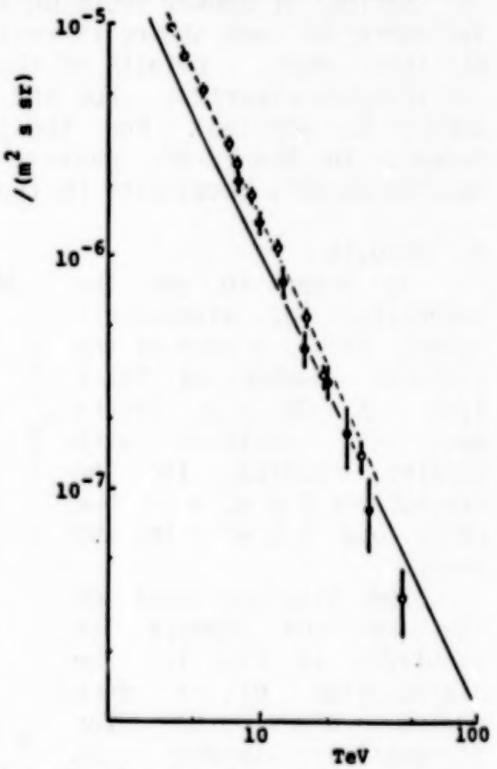


Fig. 3. Integral energy spectrum of showers induced by hadrons at Mt. Kanbala. The open and solid circles represent the results given from the Pb-EC and the Fe-EC. respectively. The dashed line is the best fit. The solid curve is expected by the assumptions mentioned in the text.

4. Discussions

There is no serious difference between both spectra derived from the Pb-EC and the Fe-EC. This indicates that on the experimental method and procedure. such as shower detection and energy determination. no systematic error is recognized for the Fe-EC. This gives a fundamental supporting factor for the reliability of the family data detected in the Fe-ECs(1).

According to the results of families. as described in another paper(1) and others(4).(5). the primary cosmic rays do not indicate

ORIGINAL PAGE IS
OF POOR QUALITY

proton dominant in the energy around 10^{16} eV. It seems that the portion of heavy nuclei gradually increases. Also, on the nature of high energy interaction, the Feynman scaling is not appreciably broken in the fragmentation region of particle production and the collision cross section of hadrons in air increases as $E^{0.06}$ corresponding to the $\ln^2 s$ dependence. In Fig. 2 and Fig. 3 are displayed the results calculated with almost the same assumption as the above mentioned. Those spectra of atmospheric cosmic rays are genetically related to the primary cosmic-ray spectrum of a proton equivalent in which the primary cosmic-ray nuclei are broken up into nucleons. Those spectra, therefore, do not much sensitive to the composition of primary cosmic rays. It is, however, interesting to indicate in these figures that the atmospheric cosmic ray spectra may be also interpreted by the same assumption in a slightly lower energy region.

On the atmospheric cosmic rays, the spectral measurements have been performed with emulsion chambers of a similar type at Mt. Fuji (3750 m. 650 g/cm^2)(3),(6) and other mountain altitudes (7),(8),(9). The present results are compared with those intensities in Fig. 4. The comparison shows the attenuation length also to be consistent with the assumption mentioned above.

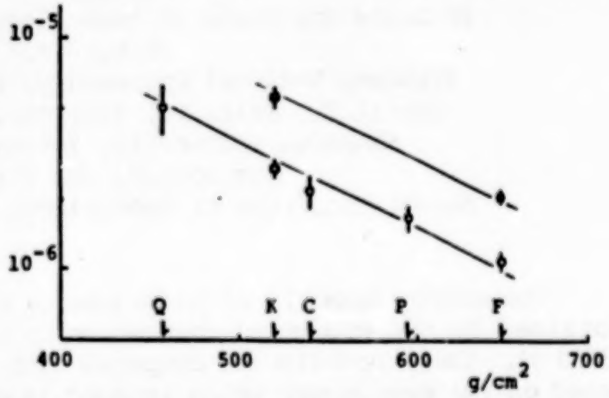


Fig. 4. Comparison of intensities of atmospheric cosmic rays at mountain altitudes. The open and solid circles represent the fluxes of gamma-ray and showers induced by hadrons, respectively, with the energy above 5 TeV; the present results (K) and the results at Mt. Fuji, (650 g/cm^2)(6) (F), at the Pamir plateau (594 g/cm^2)(7) (P), at Mt. Chacaltaya, (540 g/cm^2)(8) (C) and at the Qomolangma root (455 g/cm^2)(9) (Q). The curves represent the expected attenuation.

Acknowledgements

This work is supported by the grants from Academia Sinica in China and Japanese Ministry of Education including the Grant in Aid for Scientific Research. Data analysis was made with the computer FACOM M380R of Institute for Nuclear Study, University of Tokyo.

References

1. Ren.J.R. et al., the paper in this conference HE 3.7-5.
2. Ren.J.R. et al., 18th ICRC (Bangalore), 5, 285 (1983).
3. Akashi.M. et al., Nuovo Cimento, 65A, 355 (1981).
4. Akashi.M. et al., Phys. Rev. D, 24, 2353 (1981).
5. Amenomori.M. et al., Phys. Rev. D, 25.2807 (1982).
6. Amenomori.M. et al., 18th ICRC (Bangalore), 11, 57 (1983).
7. Pamir Collaboration, 17th ICRC (Paris), 5.297 (1981).
8. Brasil-Japan Emulsion Chamber Collaboration, Suppl. Prog. Theor. Phys., No. 47, 1 (1979).
9. Lu.S.L. et al., 17th ICRC (Paris), 5, 254 (1981).

N85-35903

HIGH ENERGY GAMMA-RAYS AND HADRONS AT Mt.FUJI

Mt. Fuji Collaboration

Amenomori,M., Nanjo,H. and Konishi,E.
Hirosaki University, Hirosaki, Aomori
Hotta,N.
Utsunomiya University, Utsunomiya, Tochigi
Mizutani,K.
Saitama University, Urawa, Saitama
Kasahara,K., Kobayashi,T., Mikumo,E., Sato,K. and Yuda,T.
ICR, University of Tokyo, Tanashi, Tokyo
Mito,I.
Shibaura Institute of Technology, Shibaura, Tokyo
Shibata,M.
Yokohama National University, Yokohama, Kanagawa
Shirai,T., Taira,T., Tateyama,N. and Torii,S.
Kanagawa University, Yokohama, Kanagawa
Sugimoto,H. and Taira,K.
Sagami Institute of Technology, Fujisawa, Kanagawa

The energy spectra of high energy gamma-rays and hadrons were obtained by the emulsion chamber with 40 c.u. thickness at Mt.Fuji (3750 m). These results are compared with the Monte Carlo calculation based on the same model which is used in a family analysis. Our data are compatible with the model of heavy-enriched primary and scaling in the fragmentation region.

1. Introduction.

The energy spectra of both gamma-rays and hadrons at high energies have been measured with the large-scale emulsion chambers at Mt. Fuji (3750 m, 650g/cm^2)[1),2)]. The present scale of Fuji experiment is possible to cover the energy range of 2-*100 TeV both for gamma-rays and hadrons with a sufficient statistics.

These spectra are known to be very sensitive to the proton component in the primary and also well reflect the particle production spectra in the fragmentation region, increasing cross sections. This problem has been frequently discussed by many authors, mainly based on the analytical calculation with some approximations.

In this report, we present new spectra of uncorrelated gamma-rays and hadrons observed with the emulsion chamber(FH) of 40 c.u. thickness and compare this with the Monte Carlo simulation made with the same model used in the family analysis.

2. Experiment

In the Mt.Fuji experiments, two types of emulsion chambers have been exposed, i.e., one is of thin-type, with the total thickness less than 10 c.u. and the other of thick-type. The total exposure amounts to about 1000 m^2.y. Among this, the chamber FH, exposed for two years

ORIGINAL PAGE IS
OF POOR QUALITY

from 1982 to 1984, has high quality for detecting both gamma-rays and hadrons. The detection efficiency of hadrons is estimated to be 60 %. The X-ray films were inserted at every 2 c.u. from 4 to 40 c.u.. In the depth shallower than 10 c.u., two kinds of films with a different sensitivity (Sakura-N and Fuji-#100) were used.

The energy of each shower is estimated by comparing the transition of shower spots in the x-ray films extending over several layers with the theoretical one (note that the energy of hadron is that released as the electro-magnetic component in the chamber). The separation of gamma-rays and hadrons is made statistically referring to the starting point of showers observed in the chamber. That is, if the showers start in the depth less than 6 c.u., except ones with successive interactions, then they are regarded as gamma-rays (including electrons and positrons) and others as hadrons.

As discussed already in the previous paper[2], the Landau-Pomeranchuk effect becomes dominant at high energies over several 10 TeV. Showers become more penetrative at higher energies so that some of gamma-rays are misidentified as hadrons in the usual statistical method mentioned above. In our data processing, this problem is adequately taken into account.

3. Monte Carlo simulation.

The Monte Carlo simulation has been done to get some conclusive results from our experimental data. The model adopted here is the same one as used in the family analysis[3]. That is, the scaling in the fragmentation region, increasing cross section as $E_o^{0.04}$ and the heavy enriched primary are assumed in the calculation. In the other papers, it has been shown that the scaling is not appreciably broken in the fragmentation region and the heavy enriched primary can well explain the family phenomena which are the products of nuclear interactions in air by primary particles at energies over 10^{15}eV. It is, therefore, of interest to examine whether the same model can also reproduce the energy spectra of uncorrelated gamma-rays and hadrons or not, since these are concerned in the wide energy range of primaries from several TeV to about 10^{16} eV. In Fig. 1 is shown the primary

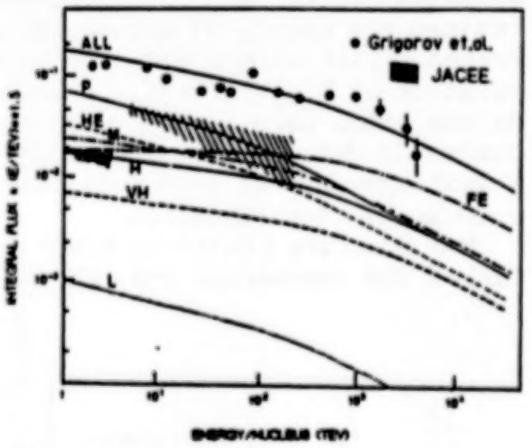


Fig. 1.

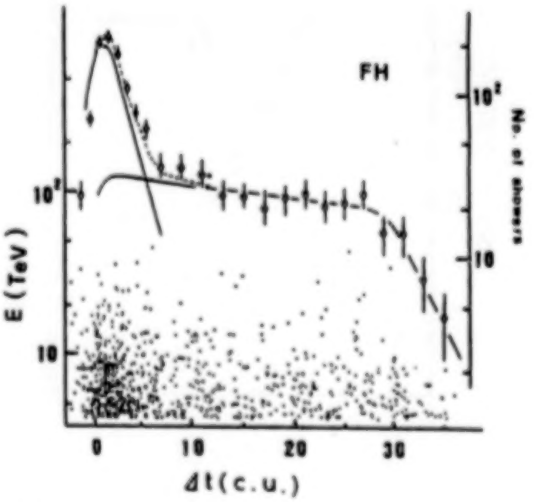


Fig. 2.

spectrum assumed in this calculation. A special feature of this spectrum is that the proton component becomes steeper (change of spectral index : 1.7->2.0) at around 10^{14} eV, lower than the knee (3×10^{15} eV) appeared in the total spectrum. This proton spectrum is not inconsistent with the JACEE data[4], though statistics is still insufficient.

4. Results.

In Fig. 2, we show the starting point (Δt) distribution of showers with energy higher than 4 TeV, observed in the FH-chamber. The curves are the expectation of attenuation of high energy showers in the chamber calculated by the Monte Carlo method. In this calculation, the collision mean free path of hadrons is assumed to be 28 c.u. in lead. This data is used for obtaining the absolute vertical fluxes of gamma-rays and hadrons.

The energy spectrum of gamma-rays and hadrons, obtained with the chamber FH, is shown in Fig. 3 and 4, with the one presented at Bangalore Conference[2]. As discussed in the previous paper[2], we revised the energy of showers by using a new energy-determination method. This change was made by a statistical way using a simple relation of $E_{new}=1.3 \times E_{old}$, i.e., old energy is increased by 30 %. On the other hand, the energy of each shower observed in the FH-chamber is determined individually by use of a new transition curve. A good agreement of both data means that the previous method is with considerable justification.

The absolute fluxes at 5 TeV and spectral indices are listed in Table 1 for gamma-rays and hadrons.

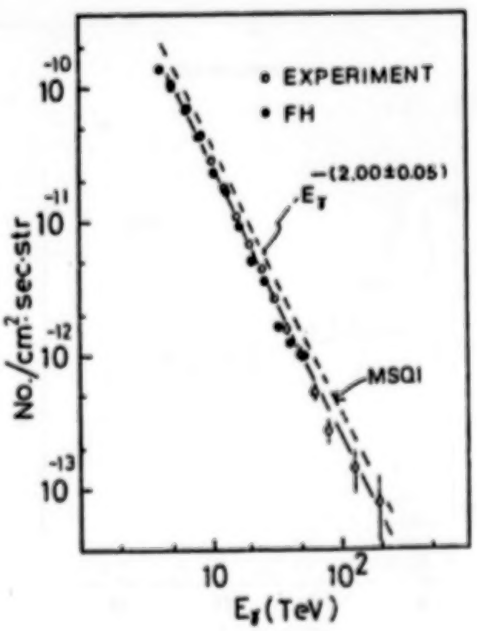


Fig. 3.

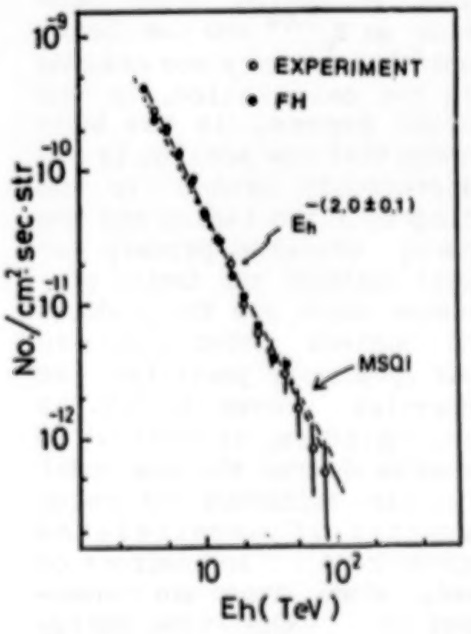


Fig. 4.

N85-35904

Table 1

	Spectral index	Flux value at 5 TeV ($cm^{-2}sec^{-1}sr^{-1}$)
gamma-rays	2.00 ± 0.05	(1.1 ± 0.1) x 10^{-10}
hadrons	2.0 ± 0.1	(2.1 ± 0.1) x 10^{-10}

5. Discussions.

We compare our data with the Monte Carlo result (dotted curve) in Fig. 3 and 4. As noticed from these figures, a slight difference may be found between the data and the calculation. But, this is not serious problem if we consider the uncertainty involving in the assumption of primary composition. Of course strong scaling break in the fragmentation region is compatible with proton dominant primary at least up to about 10^{15} eV. However, there is little hope for this possibility, because the primary energy responsible for generating these particles is not so high compared with the energy of CERN SPS collider where the strong scaling break has not been observed.

Our conclusion is that the model of scaling and heavy enriched primary can well explain both of uncorrelated particle spectra and family phenomena which are originated by the primary particles ranging from several TeV to about 10^{16} eV. The implication is that the fraction of primary proton decreases with increasing energy and reaches about 20 % at energies around 10^{15} eV. The proton spectrum should become steeper at least at around 10^{14} eV. This is very interesting result when we consider the problem of acceleration and confinement of high energy cosmic rays in our galaxy.

6. Acknowledgements

The authors would like to express their sincere thanks to Sengen Shrine, Kawaguchi-ko Office of the Ministry of environment Maintenance for extending every facilities necessary for carring out the experiment at Mt. Fuji to us.

References

1) Akashi, M. et al, Nuovo Cimento, 65A, 355 (1981).
2) Amenomori, M. et al, 18th ICRC(Bangalore), 11, 57 (1983).
3) Ding, L.K. et al, Proc. Int. Symp. of Cosmic Rays and Particle Physics (ICR, Univ. of Tokyo), 142 (1984, Tokyo).
4) JACEE Collaboration, ibid, 468 (1984, Tokyo).

N85-35904
HE 3.1-6

ON THE CHARACTERISTICS OF EMULSION CHAMBER FAMILY EVENTS PRODUCED IN LOW HEIGHTS

Jing Gu -ru, Jing Cai-liu, Zhu Qing-qi, Ding Lin-kai
Institute of High Energy Physics, Academia Sinica
P.O.Box 918, Beijing, China

1. Introduction.

The uncertainty of the primary cosmic ray composition at $10^{14}-10^{16}$ eV is well known to make the study of the nuclear interaction mechanism more difficult. Experimentally considering, if one can identify effectively the family events which are produced in low heights, then an event sample induced by primary protons might be able to be separated. It is undoubtedly very meaningful. In this paper we simulate the family events under the condition of mountain emulsion chamber experiments with a reasonable model. The aim is to search for the dependence of some experimentally observable quantities to the interaction height.

2. Method.

The model used is: proton incidence, total inelastic cross section rising with energies ($\sigma \propto E_0^{0.06}$), Feynman scaling in fragmentation region holding and mean transverse momentum increasing with energies ($\langle Pt\rangle \propto E_0^{0.05}$). The electromagnetic cascade and the multiple Coulomb scattering are also treated by Monte-Carlo method. Because the stress point is on the study of the qualitative charaters of the production height dependence on the transverse distribution of family events, the model used may be a suitable one.

The observation height is assumed at Mt. Kanbala (520 g/cm^2). The incident axis is taken uniformly on 40x50 cm^2 X-ray film, and the particle outside this area are ignored. Hadron showers are recorded by the same method as experiment with chamber thickness of 28 c.u. Pb. The criteria of a family are $\sum(E_\gamma+E_h^{(\gamma)})$ ($\equiv \sum E$) $\geqslant$ 30 TeV, $n_\gamma \geqslant 4$ and $n_h \geqslant 0$ (all symbols are in the common meaning). 546 family events with $\sum E \geqslant 100$ TeV are analysed.

The $\langle R\rangle$ and $\langle ER\rangle$ of a group of testing events with $\langle Pt\rangle$=330 MeV/c are shown in Table 1 to compare with M.Shibata's results (in parentheses) using model PRS[1]. The difference between them may be reasonable owing to the different observation levels. For families with $\sum E \geqslant 100$ Tev (E_{min} =4 TeV), we have $\langle \overline{R}\rangle$=2.75 cm which is close to the experimental value 2.5 cm[2].

Table 1 ⟨R⟩ and ⟨ER⟩ of family events

E (TeV)	30-50	50-100	100-200	200-500
⟨R⟩ (cm)	3.20 (3.3)	3.45 (3.1)	2.82 (2.5)	2.43 (2.3)
⟨ER⟩ (TeV.cm)	12.5 (13.6)	14.1 (13.7)	12.2 (11.7)	10.7 (10.6)

3. Average interaction times, mean interaction height and purity.

The average interaction times, N_{int} , for all observed particles of each family event is calculated. In Fig.1 is shown the N_{int} distribution with mean value 3.74. The

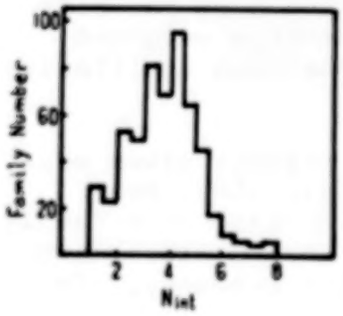


Fig.1

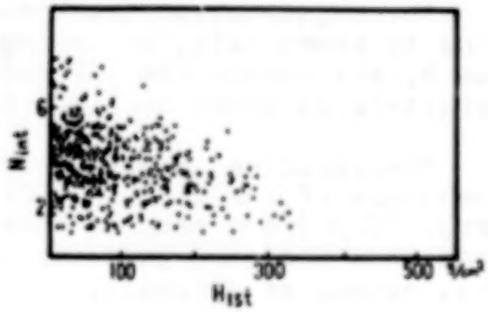


Fig.2

relation between N_{int} and the first interaction height, H_{1st} is seen in Fig.2. It is obvious that the events having both single interaction only and low interaction height are very rare.

For each event with multi-time interactions, imagine that there exists a main interaction. We devide the 520 g/cm² atmosphere into 21 layers with step 25 g/cm². Define the layer in which the produced particles contributes the most fraction of family energy ΣE as the main interaction layer and the corresponding height as main interaction height (H_{main}). The fraction mentioned above is defined as purity of the family (abbreviate as p hereafter).

The distribution of main interaction height is rather flat, slight favorable to lower height (or larger H_{main}) (see Fig.3). It is noticed that the events with larger H_{main} are not always very pure (Fig.4). The low-height event which we are interested in, of caurse, should those with lower main interaction heights and high purities.

R and ER.

The analysis shows that ⟨R⟩ and ⟨ER⟩ of family events are significantly dependent on H_{1st} (Fig.5): events with larger ⟨R⟩ and ⟨ER⟩ have smaller H_{1st} , events with larger H_{1st} have smaller ⟨R⟩ and ⟨ER⟩, but incorrect inversely. As to the dependence of ⟨R⟩ and ⟨ER⟩ on H_{main} , it is insensi-

ORIGINAL PAGE IS
OF POOR QUALITY

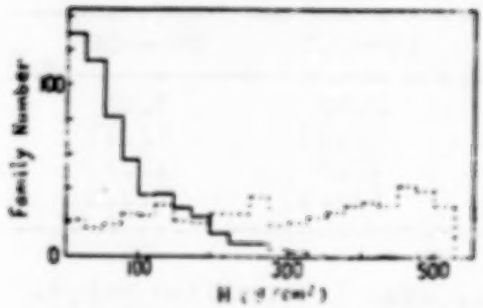


Fig.3 H_{1st} (real line) and H_{main} (dotted line) distribution

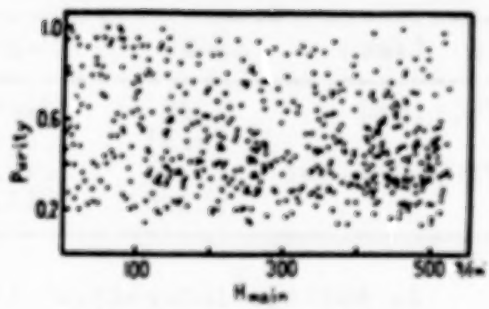


Fig.4 Purity vs. H_{main}

tive (Fig.6).

The rejuvenation treatment[3], or taking R as the distance to event axis, or taking ⟨R⟩ as the energy weighted mean R, all induce the ⟨R⟩ and ⟨ER⟩ with the same qualitative characters as shown in Fig.5 and 6.

"Decascading" treatment with full efficiency gives weak dependence of ⟨R⟩ on H_{main} (fig.7). Besides, ⟨ER⟩, mean energy ($\langle E_\gamma \rangle$) and maximum energy (E_γ^{max}) of γ-rays of a family event show the same tendency as ⟨R⟩. But at the other hand γ-ray number of a family, n_γ, shows opposite tendency. In

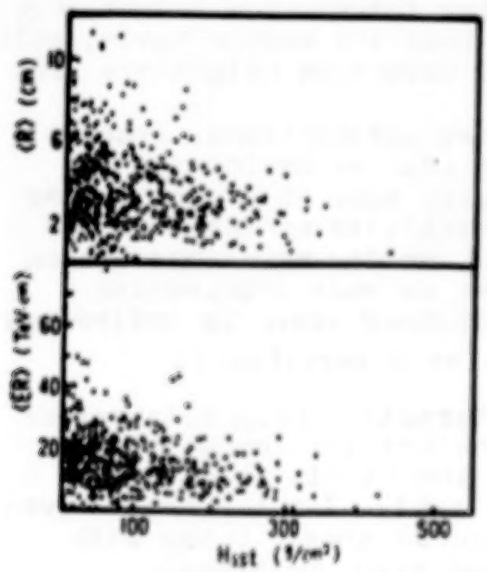


Fig.5

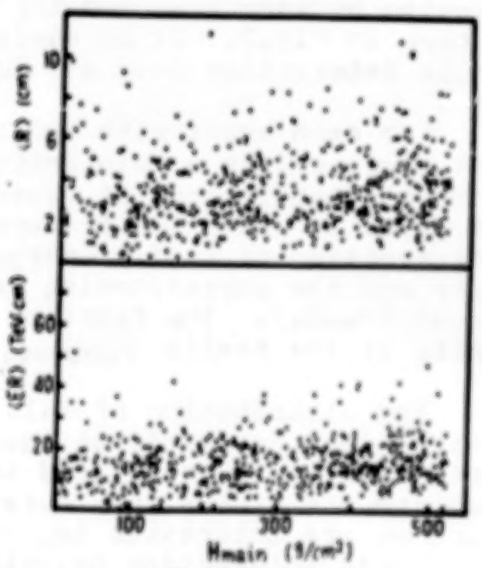


Fig.6

Fig.8 is shown the dependence of $\langle E_\gamma \rangle$ on H_{main}. When we analyse the relation between the composite quantity $C \equiv \langle R \rangle \cdot \langle E_\gamma \rangle E_\gamma^{max}/n_\gamma^2$ and H_{main} (Fig.9), it is seen that some low height events are condensed near C=0. Taking a C value cut (say C=5), the event sample selected will be dominant for low-height events.

ORIGINAL PAGE IS
OF POOR QUALITY

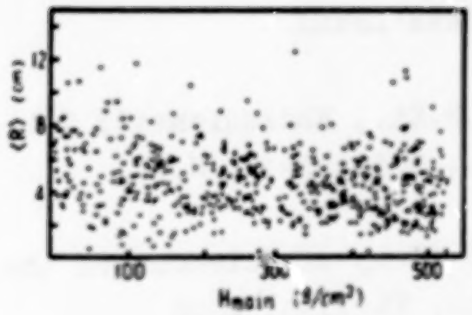


Fig.7

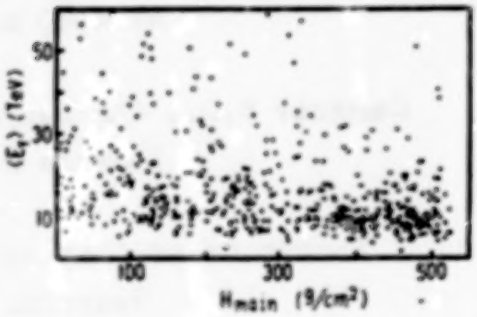


Fig.8

For the families not treated by decascading procedure, the composite quantity $A \equiv n_\gamma^3/(\langle R\rangle \cdot \langle ER\rangle \cdot \langle E_\gamma\rangle \cdot E_\gamma^{max})$ can also be used to separate the the concerned events. For example, there are 28 events satisfing the conditions $A<0.05$ and $\langle R\rangle <3$ cm, among which 12 have $H_{main} > 450$ g/cm , 7 events have both $H_{main} > 450$ g/cm and $p>0.7$. Considering the whole events satisfing these two conditions are not very rich (Fig. 4), this method may be useful.

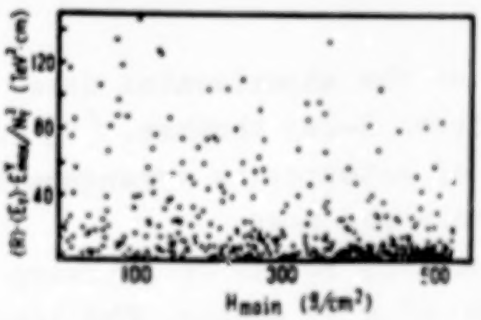


Fig.9

The condition $\langle ER\rangle <10$ TeV.cm and $\langle E_\gamma\rangle >12$ TeV can also separate about one half events having $H_{main} > 450$ g/cm and $p>0.8$.

Summary.

Due mainly to the multi-interactions in thick atmosphere target above the mountain emulsion chamber, the dependence of the observable quantities of family events on the main interaction height H_{main} is strongly smearing. However, weak dependence on H_{main} still exists in $\langle R\rangle$, $\langle ER\rangle$, $\langle E_\gamma\rangle$, n_γ and E_γ^{max} etc. A small sample with low-height and high purity is not impossible to be separated by suitable composing and cutting of these quantities.

References.

1. M.Shibata, Phys. Rev., D24(1981)1847.
2. T.Yuda, 18th ICRC, Rapporteur talk on HE 5.
3. Pamir Collaboration, 14th ICRC, 7(1975)2370.

N85-35905

HADRON INTENSITY AND ENERGY SPECTRUM AT 4380 m ABOVE LEVEL

Cananov S.D., Chadranyan E.Kh., Khizanishvili L.A.,
Ladaria N.K., Roinishvili N.N.

Institute of Physisc, Academy of Sciences of the
Georgian SSR, Tbilisi, USSR

The flux value of hadrons with $E_k^{(\gamma)} \geq 5$ TeV, where $E_k^{(\gamma)}$ is the energy transferred into electromagnetic component is presented. It is shown that the energy spectrum slope β of hadrons with $E_k \geq 20$ TeV is equal to 1.9.

The present work is based on the experimental data obtained by means of "Pamir" carbon X-ray chamber. [1] contains the detailed description of detectors's arrangement.

Two sets of experimental data are used.

The first of them represents the result of exposure of "Pamir 77-78" chamber ST = 60 m^2 x 11 months. The lead thickness t in hadron block is equal to 10 c.u. For each spot coordinates, zenith and azimuthal angles and darkness have been measured. Hadrons with zenith angle $\theta \leq 20°$ have been used only.

The second set of the experimental data is composed by selection of spots with darkness $D_{\infty} \geq 0.6$, measured by aperture of the radius $r = 140\mu m$, that approximately corresponds to $E_k^{(\gamma)} > 25$ TeV. On the total area S = 471 m^2 hadrons with zenith angles $\theta < 20°$ have been selected in the chambers with lead thickness in hadron t = 8

In all used chambers carbon layer was 60 cm thick.

Connection between $E^{\pm}$ and $E_k^{(\gamma)}$ spectra is given in the [2] (here $E^{\pm}$ is an energy estimated by means of the dependence E(D) for e^+e^--pair, the so-called "e^+e^--pair curves", and $E_k^{(\gamma)}$ is an energy in fact transferred into

electromagnetic component):

$$I(>E_i^{(\pi)}) = C\,10^{B\beta}(E^{\pm})^{\Delta}(E^{\pm})^{-\beta} \qquad (1)$$

According to [2], in the case of $r = 140\mu m$, if $E^{\pm}$ will be esimated by "e^+e^--pair curves" for $t_o + \Delta t$, where t_o is the lead thickness in chamber and Δt is equal to 2 c.u., the parameters will take the following values: $B = 0$, $\Delta = 0$.

Hence, to obtain the correct estimate of $E_i^{(\pi)}$ one can use curves for lead thickness $t = 12$ c.u. in the first set of experimental data and $t = 10$ c.u. in the second one.

Both sets of data are presented in Table 1.

Table 1

No of set	Area (m^2)	$N(E_i^{(\pi)} \geq 7$ TeV)	$N(E_i^{(\pi)} \geq 30$ TeV)	$N(E_i^{(\pi)} \geq 100$ TeV)
1	60	422	24	-
2	471	-	197	29

The value of vertical intensity of hadron flux is calculated by well-known formula:

$$I_o(>E_i^{(\pi)}) = \frac{N}{ST\omega}\,\frac{1}{\rho(\theta_o)}\,\frac{m+2}{2\pi} \qquad (2)$$

where N is number of hadrons with $E_i^{(\pi)}$ greater than the threshold; S is chamber area; $T = 2.7\cdot10^7$ s exposure time; $\omega = 0.55$ is the probability of hadron interaction in C-chamber; $\rho(\theta_o) = 1 - \cos^{m'+2}\theta_o$ is the angular factor, which converts hadrons intensity for $\theta < \theta_o$ to the global one with $\theta_o = 90^\circ$ (m' is the exponent of angular distribution of hadrons, registered in hadron block); $(m+2)/2\pi$ is converting factor from global intensity to the vertical one. Here m is the exponent of angular distribution for hadrons falling on the chamber. According to [1], $m = H/\lambda + 2 = 8 \pm 1$. Here $H = 600\,g/cm^2$ is atmospheric depth, $\lambda = 90 \div 100\,g/cm^2$ is the attenuation length for protons.

The experimental value of m', obtained by formula

$$(m'+2)/(m'+3) = \langle \cos\theta \rangle \qquad (3)$$

where $\langle \cos\theta \rangle = 0.92 \pm 0.01$ is the average cosinus of zenith angle is equal to $m = 9.5 \pm 1.5$, that is in a satisfactory agreement with results of Monte-Carlo simulations for $m = 8$.

Thus, vertical intesity values obtained from experimental sets turned out to be in a good agreement with each other

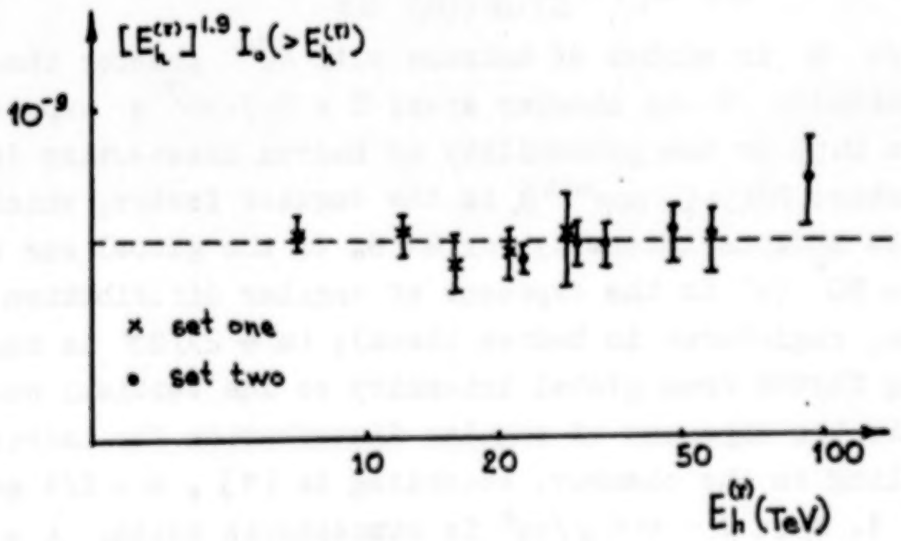
$$I_0(E_h^{(\gamma)} \geq 5\ \text{TeV}) = (2.7 \pm 0.1) \cdot 10^{-10}\ \text{cm}^{-2}\text{s}^{-1}\text{sr}^{-1} \qquad (4)$$

$$I_0(E_h^{(\gamma)} \geq 30\ \text{TeV}) = (0.7 \pm 0.1) \cdot 10^{-11}\ \text{cm}^{-2}\text{s}^{-1}\text{sr}^{-1} \qquad (5)$$

The slopes of energy spectra are in a good agreement also. In Fig.1 the concluding $E_h^{(\gamma)}$ spectrum with the slope 1.9 ± 0.1 is presented (here after the statistical errors are only given).

For chambers under investigation the value of effective coefficient $K_{eff} = E^{\pm}/E_h$ (here E_h is the energy of incident hadron) is given in [3]. At $E^{\pm} = 5$ TeV K_{eff} it is equal to 0.25. As energy $E^{\pm} = 5$ TeV turns into $E = 20$ TeV, and since the value $E^{\pm} = 5$ TeV corresponds to $E = 7$ TeV:

$$I_0(E_h^{(\gamma)} > 7\ \text{TeV}) = I_0(E_h > 20\ \text{TeV})$$



N85-32906

Thus, we can obtain energy spectrum of hadrons in the interval 20 ÷ 300 TeV:

$$I_0(>E_h) = (1.4 \pm 0.1) \cdot 10^{-10} \left(\frac{E_h}{20\ \text{TeV}}\right)^{-(1.9 \pm 0.1)} \quad \text{cm}^{-2}\text{s}^{-1}\text{sr}^{-1} \quad (6)$$

In Table 2 the comparison with data from different installations is given. Each value of hadron flux intensity is calculated for Pamir altitude ($H_0 = 600\ g/cm^2$) and energy $E_h^{(\gamma)} \geq 5$ TeV.

Table 2.

Experiment	$I_0(E_h^{(\gamma)} \geq 5\ \text{TeV})\ (\text{cm}^{-2}\text{s}^{-1}\text{sr}^{-1})$	The slope
Fudji [4]	$(3.2 \pm 0.2) \cdot 10^{-10}$	2.0 ± 0.1
Canbala [5]	$(2.9 \pm 0.1) \cdot 10^{-10}$	1.85 ± 0.1
"Pamir" Pb chamber [1]	$(1.9 \pm 0.4) \cdot 10^{-10}$	1.96 ± 0.1
This work	$(2.7 \pm 0.1) \cdot 10^{-10}$	1.9 ± 0.1

REFERENCES

1. Trudy FIAN, v.154, p.39 (in Russian)
2. Wlodarzcik et al. (in press)
3. Pamir collaboration, 18th ICRC v.11, p.122, 1983
4. Mt.Fuji collaboration, 18th ICRC v.11, p.57, 1983.
5. China–Japan collaboration, 18th ICRC v.5, p.411, 1983

N85-35906

HE 3.1-8

Some characteristic cosmic ray events and an attempt at their explanation

S. Bhattacharyya
Physical and Earth Science Division
Indian Statistical Institute
Calcutta-700035,
India

«ABSTRACT»

Some cosmic ray events with very large multiplicities and very high transverse momenta have recently been reported in balloon-borne emulsion chamber experiments. The explanation for these events by the standard approaches has become a bit problematical. We have attempted here to understand and interpret them in the light of a dynamical model of multihadron production phenomena with power-law nature of average multiplicity and automatic scale-breaking derived in the model.

1. Introduction

In the recent past some cosmic ray events with very high multiplicities and large average transverse momenta have been observed in a balloon-borne emulsion chamber experiment[1] in the collisions between Si-AgBr nuclei. The charged multiplicity range is 750 ~ 1000 and the range of the average transverse momentum lies between 550-700 Mev/c and the observed event number is two. The rising behaviour of the average transverse momentum with energy is also confirmed by the CERN $\bar{P}P$ collider experiments.[2] But the CERN $\bar{P}P$ collider results, it is believed, set an upper limit ($\langle n \rangle \sim \ln^2 S$) to the nature of growth of multiplicity which cannot accommodate such high multiplicity events. Herein lies the problem.

There has in recent times been a lot of theoretical studies[3] in understanding these events which are just not flukes. We would like to apply here a model for production of secondaries by BANDYOPADHYAY and BHATTACHARYYA[4] in order to see whether such events can be explained with the help of the expressions we arrive at from the viewpoint of this model.

2. The model and the method.

We will put our model for nucleon-nucleon reactions into use here for nucleus-nucleus collisions on the assumption that all nucleus-nucleus collisions can be treated with the basic dynamics of nucleon-nucleon interactions and taking into account an A-dependence term into final calculation in a somewhat hand-inserted manner, at least for the present.

ORIGINAL PAGE IS
OF POOR QUALITY

According to the present model, nucleons are thought to be composed of pions and spectators so far as strong interactions are concerned and all hadronic collisions thus boil down to pion-pion interactions. The interactions proceed in a sequential chain through some ρ-ω-π exchanges with emission of free secondary pions at each vertex on both sides of the horizontal ρ-ω chain giving rise to the spray-like nature of emission of the secondaries (and thus contributing to some form of 'jettiness'). The chain ends as soon as both the mediating and final ρ meson is absorbed by the pions in the target. Kaons are produced from the decay of the virtual ϕ^0 mesons which are generated through $\rho\pi\phi^0$ coupling and the secondary baryons-antibaryons (non-leading) are the products the decays of pions arising out of the sequential $\rho\omega\pi$ chains as prescribed in the pion production. This model gives a unified description for production of both low and large p_T secondaries, an explanation for the leading particle effect and accounts for the by-now established <<universality>> of all hadron-involved interactions as well as of e^+e^- annhilations.

3. Theoretical Results

By applying the Feynman diagram techniques and some standard high energy assumptions the following expressions, very crucial for our cosmic ray physics purpose, were derived

$$E\frac{d^3\sigma}{dp^3}\Big|_{pp\to\pi^- x} \simeq G_\pi \cdot \exp\left[-\frac{26.88}{\langle n_{\pi^-}\rangle}\frac{k_T^2+m_\pi^2}{1-x}\right] \exp\left[-2.38\langle n_{\pi^-}\rangle x\right] \quad -(1)$$

with

$$\langle n_{\pi^-}\rangle_{pp} \simeq \langle n_{\pi^+}\rangle_{pp} \simeq \langle n_{\pi^0}\rangle \simeq .33\, s^{\frac{1}{4}} \quad -(2)$$

and

$$E\frac{d^3\sigma}{dp^3}\Big|_{pp\to\pi^+ x} \simeq \left[1+2.7\,s^{-\frac{1}{2}}\right] E\frac{d^3\sigma}{dp^3}\Big|_{pp\to\pi^- x} \quad -(3)$$

and the inclusive crosssection for the π^0 production is just the mean of inclusive (secondary) π^+ and π^- crosssections.

The expression for the average transverse momentum of any type of particle C is defined by

$$\langle p_T\rangle_C = \frac{\int F(x,p_T)_C\, p_T\, dp_T^2}{\int F(x,p_T)_C\, dp_T^2} \quad -(4)$$

Using the above definition and making use of the expressions (1-2) deduced by our dynamical model we finally arrive at

$$\langle p_T \rangle_{\pi^-} \simeq 1{\cdot}1 \times 10^{-1} \, s^{\frac{1}{6}} \ \text{GeV/c} \qquad \text{—(5)}$$

The expression (2) with incorporation of a maximum $A^{\frac{1}{3}}$ (actually $\leq A^{\frac{1}{3}}$) dependence can account for the observed range of multiplicity events and the expression (5) gives their average transverse momenta in the expected limit. Why the number of such events is limited to two only could probably be explained in terms of phase transitional probability[3a] occurring in the structure of hadrons ; the pion clusters in the strong interaction domain might exhibit further structures leading to a change in the nature of interactions at such high energies. This aspect is now under study. Side by side, the explicit nature of A dependence is also being looked into.

4. Discussion and Conclusions

Our brief study shows that the problem might not be linked up with the validity or violation of the KNO scaling[3] or be connected with the unknown heavies as proposed by Sukuyama and Watanbe[3]. Some further comments are in order here : (i) it is seen and supported here that "$\langle p_T \rangle$ increases gradually with energy and this increase is associated events corresponding to average multiplicities - not with events higher than average multiplicity" as was argued by Halzen.[5] (ii) our multiplicity pattern follows power law (although the rate is a bit larger here) as advocated by Maraki.[6] This inevitably leads to the violation of both Feynman and KNO scaling as argued and/or observed by many authors.[7,8] But the fair agreement that we claim here might be proven wrong by the uncertainties in the correctness of the measurement of the average transverse momentum as pointed out by Hagedorn.[9]

We would like to emphasise here a few more points. Unless the experimental results from the Fermilab PP collider at higher energies than the CERN PP collider are to hand no one can and should put a queitus to the power law nature - whatever its magnitude far less than unity - of average multiplicity practically on the basis of quasi empirical type of QCD predictions. QCD has many intrinsic loopholes[10] even in its philosophy of confinement, the very kernel of the theory. Thus we hope our model might have had a modest prospect in future studies vis-a-vis this QCD state and the so far illusive[11] (experimental) behaviour of the quarks.

N85-35907

References

1. Burnett T.H. et al (1983) Phys. Rev. Letts. 50, 2062; Iwai J. et al (1982) Nuovo Cimento 69A, 295. Bhattacharyya, D.P. (1983) Canadian Journal of Phys. 61, 434.
2. UA(1) Collaboration (1982) Phys. Letts. 118B, 173
3. Stanev Todor (1985) Phys. Rev. D31, 1155 Pajares, C. and A.V. Romallo (1984) Phys. Rev. Letts. 52, 407; Sukuyama, H. and K. Watanbe, (1984) Lett. Nuovo Cimento 40, 243; Sukiyoshi, H. (1983) Phys. Letts. 131B, 343.
4. Bandyopadhyay, P. and S. Bhattacharyya (1978) Nuovo Cimento 43A, 305, 323, (1979), Nuovo Cimento 50A, 133 with D.P.B. and R.K.R.C. (1980) Phys. Rev. D21, 1861.
5. Halzen Francis (1984), Invited talk at the International Symposium on Cosmic Rays and Particle Physics, Tokyo, Japan (March 19-23) and Preprint; University of Wisconsin Madison (USA)
6. Muraki, Y. (1983) Proceedings of the 18th ICRC Vol.5 499 (Bangalore-India).
7(a). Kiang, D. et al. (1985) Phys. Rev. D31, 31 and the references therein UA(5) Collaboration (1984) Phys. Letts. 138B, 304 and the references therein
(b) Sreekantan, B.V., S.C. Tonwar and P.R. Biswanath (1983) Phys. Rev. D28 1050; Fakimuto, F. et al. (1983) Jour. of Phys. G9, 339; Tasaka, S. et al. (1982) Phys. Rev. D25, 1765; Amenomori, M. et al (1982) Phys. Rev. D25 2807; Akasi, M. et al (1981); Phys. Rev. D24, 2353; Shibata M (1981) Phys. Rev. D24, 1847.
8. Wdowczyk, J. and A.W. Wolfendale (1984) Jour. of Phys. G10, 257; (1979) Nuovo Cimento 54A, 433; (1973) Jour. of Phys. A6 L48.
9. Hagedorn, R. (1983) La Riv. Nuovo Cimento 6, p.37.
10. Altarelli, G. (1984) La Rivista Nuovo Cimento 7 (No.3); p5. Hagedorn, R. (1984) CERN Preprint TH3918/84
11. Trower, W.P. (1985) Nucl. Phys. B252, 285.

NOTE ADDED : In getting the order of magnitude of the multiplicity and the average transverse momentum we make use here of the relation $S = 2 i M_A E$ where i = number of nucleons involved in each collision and the other letters have their usual significances. It is seen that in order to have a good fit one has to take here $i \sim 30$.

N85-35907

The Nucleon Intensity in the Atmosphere and the p_t Distribution

A. Liland
N-3785 Veidnesklubben
Norway

ABSTRACT

The diffusion equation for cosmic ray nucleons in the atmosphere has been solved analytically, taking into account the transverse momentum distribution of nucleons produced in nucleon-air nucleus collisions. The effect of the transverse momentum distribution increases the nucleon intensity at large zenith angles and low energies.

1. Introduction

The intensity of cosmic ray nucleons in the atmosphere, due to cosmic ray primary protons, can be expressed by (1)

$$N(E,x) = C_p E^{-(\gamma+1)} e^{-x/\lambda} \qquad (1)$$

where $N(E,x=0) = C_p E^{-(\gamma+1)}$ is the primary proton spectrum, x the atmospheric depth and λ the diffusion length for nucleons in the atmosphere. This solution is obtained by the assumption that the secondary nucleons are moving in the same direction as their parent nucleons. It can be used for deriving the intensities of cosmic ray mesons in the atmosphere and muons at sea-level (1) because the energies of interest here are high such that the average transverse momentum of secondary nucleons $\langle p_t \rangle$ is very small compared to the energy E of the nucleon, $\langle p_t \rangle \ll E$. If $\langle p_t \rangle$ is no longer much smaller than E, as is the case, for instance, for low energy cosmic rays in the upper part of the atmosphere, equation (1) will give too low nucleon intensity at large zenith angles θ, as we shall see below.

2. The Atmospheric Depth

From the U.S. Standard Atmosphere (1976) (2) we obtain the atmospheric depth at sea-level and zenith angle 0°, $x_o = 1035.6$ g/cm^2. We approximate the Standard Atmosphere by an exponential atmosphere and obtain for the atmospheric depth at hight Z (km) above sea-level $x = x_o \exp(-Z/H)$, $H = 6.95$ km. The error is less than 12% for $x < 1$ g/cm^2 compared to the Standard Atmosphere. For an inclined direction, $0^\circ < \theta \leq 90^\circ$, we obtain for the atmospheric depth $x_{max}(\theta)$, at sea-level,

$$(2) \qquad X_{max}(\theta) = \frac{\rho_o \sqrt{\frac{\pi}{2} HR}}{\frac{1+\alpha}{2}\sqrt{\frac{\pi}{2}\frac{R}{H}}\cos\theta + \beta} \begin{cases} \theta \geq 67^\circ \begin{cases} \alpha = 0.398 \\ \beta = 0.96 \end{cases} \\ \theta < 67^\circ \begin{cases} \alpha = 0.96 \\ \beta = 0.398 \end{cases} \end{cases}$$

ρ_o is the density of air at sea-level
R is the radius of the earth, 6366 km.
The error, due to approximations, is less than 5%.

From the figure we obtain:
$\cos(\hat{\theta}) = \cos(\theta)\cos(\nu) + \sin(\theta)\sin(\nu)\cos(\varphi)$

ν will be given by $\frac{p_t}{E}$ later on and is small so that we can take

$\cos\hat{\theta} = \cos\theta + \sin\theta\,\nu\cos\varphi$

We introduce the reduced zenith angle $\bar{\theta}$,

$$\cos\bar{\theta} = \sqrt{\eta - \left(\frac{\sin\theta}{\eta + \frac{1}{2}\cos\theta}\right)^2}$$

which is the local zenith angle at approximately half the total atmospheric depth $x_{max}(\theta)$.

Let x be the atmospheric depth at hight Z above sea-level and zenith angle θ. Then the atmospheric depth $\hat{x}$ at hight Z and zenith angle $\hat{\theta}$ is given by $(\cos\hat{\theta} = \cos\bar{\theta} + \sin\bar{\theta}\,\nu\cos\varphi)$

$$\hat{x} = x\,\frac{x_{max}(\hat{\theta})}{x_{max}(\bar{\theta})} = \frac{x}{1 + \frac{\sin\bar{\theta}\,\nu\cos\varphi}{\cos\bar{\theta} + \eta}}$$

$$\eta = \frac{2p}{1+\alpha} = \begin{cases} 0.0362 & \theta \geq 87° \\ 0.0107 & \theta < 87° \end{cases}$$

3. The Diffusion Equation

Let the differential production cross section for nucleon production by nucleons have the following transverse momentum distribution

$$\frac{d^2\sigma}{dp_\parallel dp_\perp^2} \sim e^{-\alpha p_\perp^2} \qquad \alpha = \text{const.}$$

where $p_\parallel$ is the longitudinal momentum and $p_\perp$ is the transverse momentum of the produced nucleons. With $\nu = \frac{p_\perp}{E}$ we then obtain for cosmic ray nucleons

$$q(E,E',\nu,\varphi) = q(E,E')\,\frac{1}{2\pi}\,\frac{\pi}{4}\,\frac{1}{\langle p_\perp^2\rangle}\,e^{-\frac{\pi}{4}\left(\frac{E}{k\langle p_\perp\rangle}\right)^2\nu^2}$$

with $G_{NN} = \int_0^1 q(E,E/u)\,u^\gamma\,du$ (1)

We use the generation method and obtain the diffusion equation for the first generation nucleon

$$\frac{d\hat{N}_1}{dx} = -\frac{\hat{N}_1}{\lambda_N} + \int_E^\infty \frac{1}{\lambda_N} C_p E'^{-(\gamma+1)} \int_0^\pi \int_0^{2\pi} e^{-\frac{\hat{x}}{\lambda_N}} q(E';E,\nu,\varphi)\,d\varphi \cdot 2E^2\nu^2\,d\nu\,\frac{dE'}{E'}.$$

$\lambda_N = 84\ \text{g/cm}^2$ is the interaction length for nucleons.

ORIGINAL PAGE IS
OF POOR QUALITY

The analytic solution is

$$\hat{N}_1(E,X,\theta) = C_p E^{-(\gamma+1)} G_{NN} \frac{X}{\lambda_N} e^{-\frac{X}{\lambda_N}} \frac{1}{1-\left\{\varepsilon_1 \sqrt{\frac{\pi}{4}} \frac{X}{\lambda_N} \frac{\langle p_L \rangle}{E} \bar{T}(\bar{\theta},E)\right\}^2}$$

$\varepsilon_1 = 0.2845$

$$\bar{T}(\bar{\theta},E) = \frac{\sin\bar{\theta}/(\cos\bar{\theta}+\eta)}{1+(\sin\bar{\theta}\,\langle\frac{p_L}{E}\rangle\frac{\pi}{4})/(\cos\bar{\theta}+\eta)}$$

The solution for the m'th generation nucleon has the form

$$\hat{N}_m = C_p E^{-(\gamma+1)} \frac{1}{m!}\left(\frac{X}{\lambda_N} G_{NN}\right)^m e^{-\frac{X}{\lambda_N}} \prod_{m=1}^{m} q_{m,m}$$

$$q_{m,m} = \frac{t_m}{1-\left\{S_{m,m}\frac{X}{\lambda_N}\langle\frac{p_L}{E}\rangle\right\}^2}$$

If we define an average for $q_{m,n}$, for instance:

$$q(E,X,\theta) = \frac{\langle t_m\rangle}{1-\left\{\langle S_{m,m}\rangle \frac{X}{\lambda_N}\langle\frac{p_L}{E}\rangle\right\}^2}$$

we can sum over m and write an approximate solution for the nucleon intensity in the atmosphere

$$\hat{N}(E,X,\theta) = C_p E^{-(\gamma+1)} e^{-\frac{X}{\lambda_N}(1-G_{NN}q(E,X,\theta))}$$

$q(E,X,\theta) > 1$ and $\hat{N}(E,X,\theta)$ is increasing with increasing $\frac{X}{\lambda_N}\frac{\langle p_L\rangle}{E}$ and zenith angle θ.

If the differential production cross section is $\sim e^{-\alpha p_L}$ we obtain for the first generation nucleon

$$\hat{N}_1'(E,X,\theta) = C_p E^{-(\gamma+1)} G_{NN}\frac{X}{\lambda_N} e^{-\frac{X}{\lambda_N}} \frac{1}{1-\left\{\varepsilon_1'\frac{1}{2}\frac{X}{\lambda_N}\frac{\langle p_L\rangle}{E}\bar{T}(\bar{\theta},E)\right\}^2}$$

$\varepsilon_1' \approx 1.$

and we see that this flatter trans verse momentum

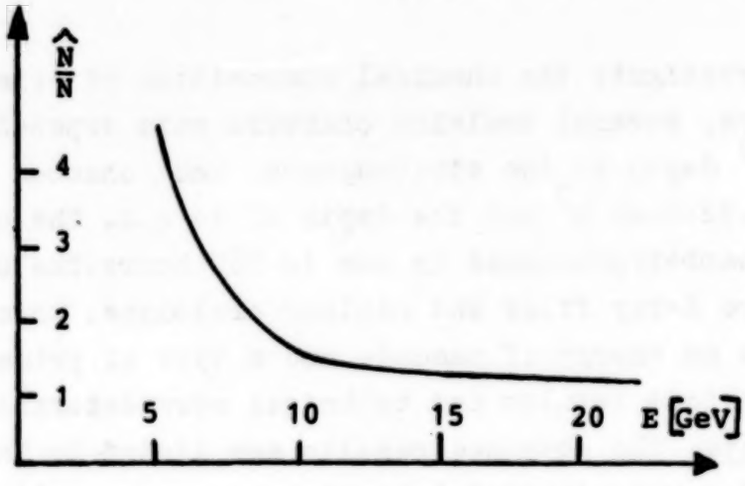
N85-35908

ORIGINAL PAGE IS
OF POOR QUALITY

distribution gives a greater effect.

4. Discussion and conclusion

$\hat{N}(E,x,\Theta)$ is the solution of the 3 - dimentional diffusion equation for nucleons in the atmosphere and $N(E,x)$ the 1-dimentional solution as given above. The figure shows, as an example, the ratio $\hat{N}(E,x,\Theta)/N(E,x)$ at 30 km above sea-level ($x(\Theta = 0^\circ) = 12.4$ g/cm^2) for $\Theta = 90^\circ$, $x = 350$ g/cm^2 as a function of energy E.



We see that below 10 GeV the ratio $\hat{N}/N$ is increasing rapidely with decreasing energy. This is because $\hat{N}/N$ is a function of E^{-2} as we see from the solution for $\hat{N}$ above.

In the case of $\frac{d^2\sigma}{dp_u dp_L^2} \sim e^{-a p_L}$, we obtain approximately the same curve, but with the energy a factor 2 higher and the rapide increase is between 20 GeV and 10 GeV. We see that the effect of the transverse momentum distribution is not only a function of the average transverse momentum $\langle p_t \rangle$, but depends also on the shape of the transverse momentum distribution.

References

1. A. Liland, Fortschritte der Physik 23, 571 (1975)

2. U. S. Standard Atmosphere (1976), Handbook of Chemistry and Physics. The Chemical Rubber Co., 1984.

N85-35908
HE 3.I - IO

ENERGY SPECTRA OF PROTON AND NUCLEI OF PRIMARY COSMIC RAYS IN ENERGY REGION > 10 TeV/PARTICLE

Mandritskaya K.V., Sazhina G.P., Sokolskaya N.V.,
Varkovitskaya A.Ya., Zamchalova E.A., Zatsepin V.I.
(Moscow University Balloon Emulsion Experiment - MUBEE)

Institute of Nuclear Physics, Moscow State University,
Moscow 119899, USSR.

To investigate the chemical composition of primary cosmic rays, several emulsion chambers were exposed at a 10.8 g/cm^2 depth in the stratosphere. Each chamber has the area of 0.92×0.46 m^2 and the depth of 14 c.u. The exposure time of chambers processed by now is 260 hours. The detecting layers were X-ray films and nuclear emulsions, which allowed to measure an energy of cascade and a type of primary particle. Previous results and technique were described in /1,2/

Results. The obtained results are listed in Table 1. All cascades were devided into six groups, according to the type of a primary. He and Z denote here the cascades produced in a chamber by He nuclei and nuclei with $Z \geqslant 3$. SH denotes the cascades produced in the chamber cover, these cascades were observed as a shower in the emulsion layer just below the cover. A fraction of cascades was induced by secondaries generated in the residual atmosphere (A-cascades). The cascades observed as groups of two or more members with the same zenith and azimuth angles are called A_p cascades. The events belonging to none of the above numerated types were attributed to p-cascades. This group consists of proton cascades with a small addition of single A-cascades. A small number of cascades were failure to identify due to technique causes (?-cascades). The third line in Table 1 lists the value of exposure factor $\langle S\Omega\varphi\eta\rangle \cdot T$, were S is the chamber area, Ω is the solid angle, φ is the efficiency of registration of given-type particles in

a chamber, η being the coefficient of intensity attenuation in the residual atmosphere, T - exposure time. The angular intervals for which the processing was made also presented here. Table 1.

primary	P		He		Z >3		SH		A_p		?	
$\theta°$	25-60	10-72	25-60	10-72	25-60	10-72	25-60	10-72	25-60	10-72	25-60	10-72
G·T. $m^2hr\,sr$	434	62.5	50	70.5	M 45 63 H 37 51 VH 31 43							
>1.6	292		39		58		68		60		39	
>2	170		35		41		44		49		23	
>2.5	115		23		30		30		40		13	
>3	80	99	18	23	27	30	25	34	36	40	10	17
>4	43	53	13	14	25	27	15	22	25	27	3	6
>5	26	31	10	11	17	19	11	12	18	18	1	4
>10	6	9	6	6	3	4	6	6	3	3		1
>20	1	2	1	1			2	2				
>40			1	1								

$\mathcal{E}$, TeV

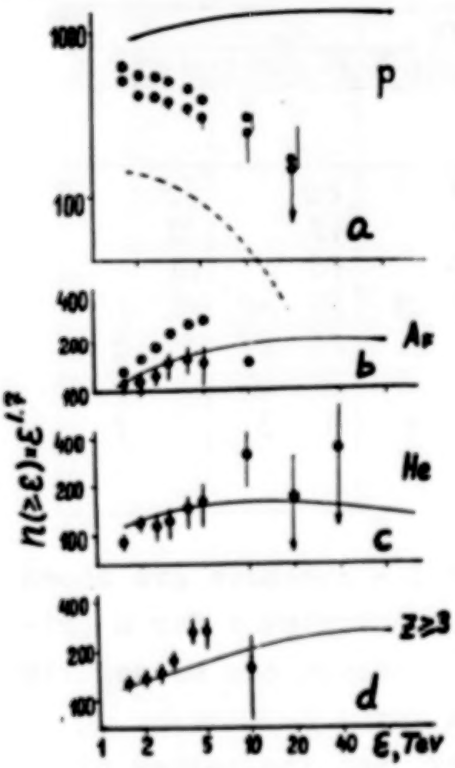
In Fig.1 the data for p, He and Z - cascades are shown along with the expected dependencies calculated for a primary composition model implying all spectra can be described by power-low dependences of the form $i_j = i_{oj} E^{-\beta_j}$, were E is the particle energy in TeV, and the values of parameters i_{oj} and β_j for various groups are given below:

Group	p	He	M	H	VH
i_{oj}, $m^{-2}hr^{-1}sr^{-1}$	240	90	75	107	67
β_j	1.7	1.8	1.7	1.7	1.7

These parameters were chosen when analysing experimental data obtained in /4-7/.

The expected number of cascades with energy $>\mathcal{E}$ was calculated by the formula: $n_j(>\mathcal{E}) = i_j(>E(\mathcal{E}))\langle S\Omega\varphi\eta\rangle T\zeta$, where ζ =1.25 is the factor allowing for overestimation of the measured intensity due to fluctuations. A relationship between the measured energy $\mathcal{E}$ and the total particle energy regarding fluctuations of the interacting nucleons number, fluctuations of K_γ and diversity of a nucleon cascade from an electromagnetic one has been considered in /1,3/.

Fig.1 shows a good agreement between the observed and expected spectra of He and Z-cascades and the difference between the observed and expected p-cascade spectrum being small at low energies and rapidly increasing with energy.



As note above, p-cascades include some fraction of single A-cascades. To estimate this fraction we performed simulations, which results are shown in Fig.1. The simulation was made by the program /8/, where interaction was assumed to quasi-scaling type, and a superposition model was used for nucleus-nucleus interaction. The expected number of single A-cascades is shown in Fig.1a by dashed line, the black circles denoting the corrected spectrum of proton cascades. Thus made correction is not quite reliable that follows from Fig. 1b, where the expected and observed numbers of A_p-cascades are shown (solid line and open circles). The observed number of A_p-cascades can be seen to somewhat exceed the calculated number. It must be note that the number of A_p-cascades is the strongly fluctuating magnitude. For instance, if one of 31 observed families is exclude from the A_p-cascades, the calculated and observed (black circles) spectra would coincide. However, it is desirable to have a reliable experimental identification procedure, that is our aim in the nearest future.

Discussion. Fig.2 summarizes the data available on the p and He-components. One can see that there is a discrepancy between our and JACEE proton data. Unfortunately, JACEE spectrum in various energy ranges was obtained over different exposures, that makes it difficult to analyse the

N85-35209

ORIGINAL PAGE IS
OF POOR QUALITY

origin of discrepancy.

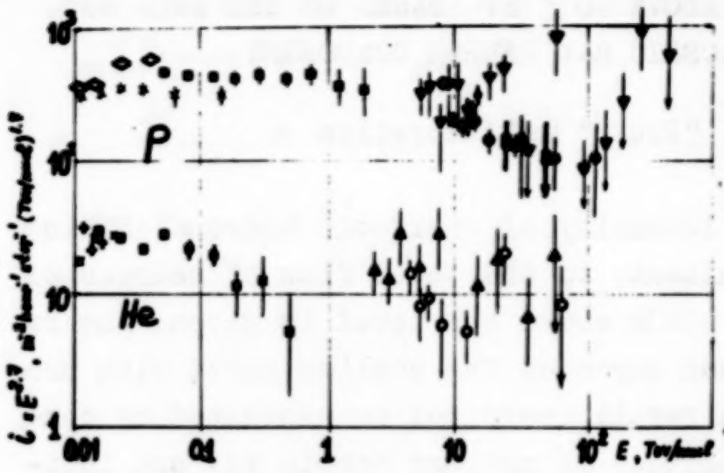


Fig.2. The differential energy spectra of protons and He at the atmospheric boundary.
□ - /4/
◇,+ - /6/
× - /7/
▽,△ - /9/
◇- /10/, □- /11/
●,○ -present work.

Furthermore the steepening of the proton spectrum measured in our experiment shows that the proton spectrum problem in the range 10^{12} - 10^{14} eV is still unsolved and requies further explorations. The proton spectrum being steep in the range 10^{12}- 10^{14} eV and the normal amount of protons being present at $E > 10^{15}$ eV may indicate the existence of two proton components of different origin /2/.

References.

1.Abulova V.G. et al, Proc. 18th ICRC, 1983, v9, p 179.
2. Abulova V.G. et al, Izv. AN SSSR, ser. fiz., v 48, p2083
3. Dezurko M.D. et al, Proc. 17th ICRC, 1981, v 9, p 324.
4. Ryan M.G. et al, Phys Rev Lett, 1972, v 28, n 5, p 985.
5. Simon M., Ap.J., 1980, v 239, p 712.
6. Ormes J.P. et al, Proc ICRC, 1965, London, v 1, p 349.
7. Smith L.H. et al, Ap.J., 1973, v 180, p 987.
8. Mukhamedshin R.A. Thesis, 1981, Inst. for Nucl. Reas., Moscow, USSR.
9. Burnett T.H. et al, Phys Rev Lett, 1983, v 51,11,p.1010.
10. Tasaka S. et al, Proc 17th ICRC, 1981, v 5, p 126.
11. Vakulenko E.S. et al, Vestnik MGU, ser.fis., 1985, v 26, n 4 (in Russian).

N85-35909

SCALING VIOLATION IN FRAGMENTATION REGION AT ENERGIES ABOVE 10^{15} EV BASED ON THE DATA ON COSMIC RAY HADRON COMPONENT

"Pamir" Collaboration 4

The ratio of intensity of energetic hadrons, having no visible accompaniment, to the total flux of hadrons of the same energy at 4380m above sea level is given. The ratio is much more than expected for scaling model with proton primaries. This result could not be explained by complex chemical composition of primary cosmic ray and indicates the scaling violation in fragmentation region.

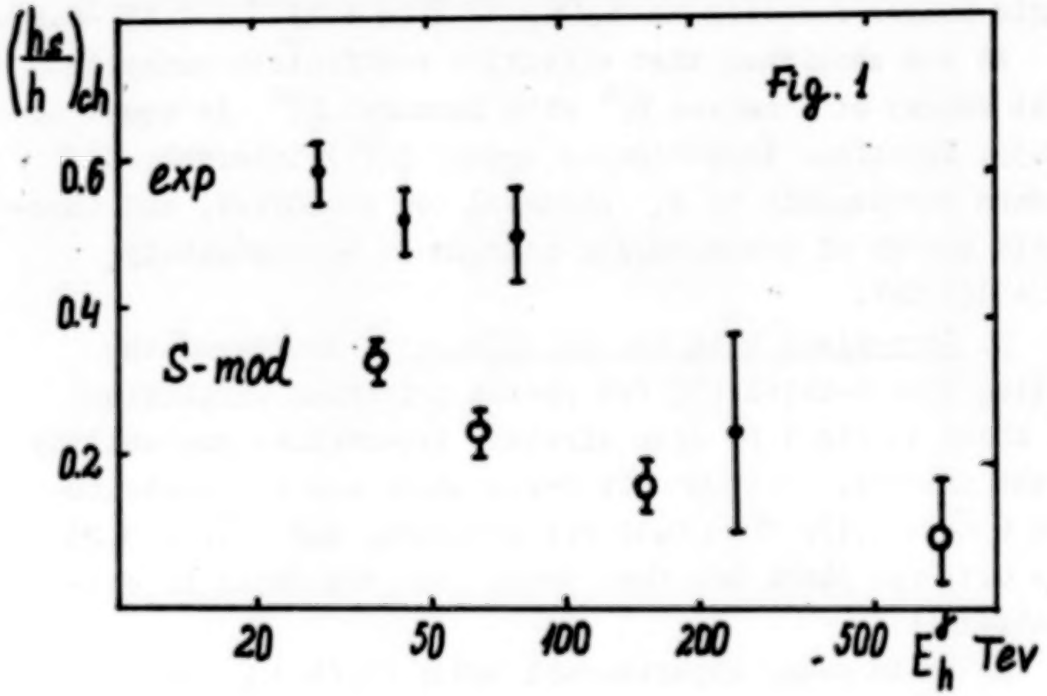
1. Experimental procedure. A special search of high energy hadrons in thick carbon type X-ray chambers [1] was made for investigation of hadron fraction having no accompaniment. 5 most energetic spots were selected in each X-ray sheet having 0.5 m^2 area. For them energy $E^{\pm}$ was determined by means of darkness dependence on E for e^+e^--pair. Then energy transferred by hadrons into electromagnetic component $E_{\gamma}^{(\pi)}$ was estimated using method described in [2]. For this procedure effective coefficient $K_{eff} = E_{\gamma}^{(\pi)}/E_{\gamma} \simeq 0.35$ [2]. Only hadrons having $E_{\gamma}^{(\pi)} \geq 25$ TeV (we call them leaders) are including in the following analysis. The scanning efficiency for such hadrons is very good, since their average number of them is approximately 1 per 1 m^2 and beforehand selected one was 10 times higher.

A search of hadron accompaniment for each leader was made on the same X-ray sheet in a circle with R = 30 cm. Energy threshold for accompaniying particles was $E_{\gamma}^{(\pi)} = 3$ TeV.

Total area treated by the described method was 615 m^2, 608 leaders were found and among them 332 were single one*.

*Note that here single hadron means that it has no visible accompaniment. Only part of them are primaries which did not interact in the atmosphere.

2. Results. Energy dependence of single hadron fraction $(h_s/h)_{ch}$ is shown in Fig.1. Up to $E_L^{(1)} \sim 100$ TeV it is



rather weak. The average value for $E_L^{(1)} \geq 25$ TeV $(h_s/h)_{ch} = 0.55 \pm 0.03$. Sign ch-marks the value h_s/h determined for the given type of chambers. To estimate the corresponding value for incident hadrons one needs to take into account interaction probability in the chamber and restore total energy of leaders and accompaniying particles.

Correction for interaction probability ($\omega \simeq 0.6$) was made in the following way. It was supposed that multiplicity distribution of accompaniying hadrons is $(n+1)^{-\alpha}$. Constant α was found from experimental value $(h_s/h)_{ch} = \frac{\sum_0^{\infty}(n+1)^{-\alpha} C_n (1-\omega)^n}{\sum_0^{\infty}(n+1)^{-\alpha}} = 0.55 \pm 0.03$. It turns out to be $\alpha = 1.6 \pm 0.1$.

To check hypothesis about n distribution experimental distribution N_m of accompanying particle multiplicity m was compared with expected at $\alpha = 1.6$:

$$N_m = \sum_m^{\infty}(n+1)^{-\alpha} C_n^m (1-\omega)^{n-m} \omega^m / \sum_0^{\infty}(n+1)^{-\alpha}$$

The experimental and expected distribution were in good agreement. This was the argument for estimation of incident single hadron fraction as $h_s/h = 1/\sum_0^{\infty}(n+1)^{-\alpha} = 0.45 \pm 0.05$.

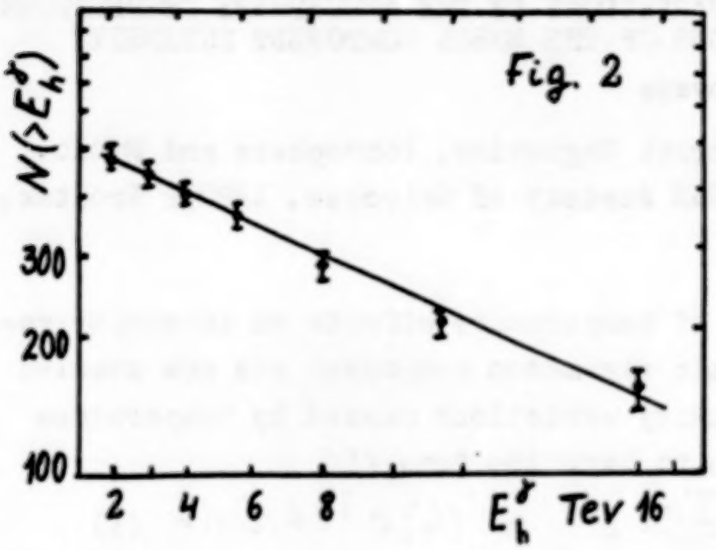
It was mentioned that effective coefficient connected total energy of a hadron $E_L^{(\gamma)}$ with measured $E_L^{(\gamma)}$ is equal to~ ~ 0.35. Therefore investigated energy ($E_L^{(\gamma)}$) interval of leaders corresponds to E_h interval (60 - 400)TeV, and threshold energy of accompanying hadrons is approximately (10 ÷ 15) TeV.

3. Comparison with the calculation. Results of the scaling type S-model [3] for proton primaries simulation are shown in Fig.1 by open circles. Interaction probability in the chamber, size of X-ray sheet and K_γ distribution ($\overline{K_\gamma} = 0.17$, $\sigma = 0.12$ for nucleons, and $\overline{K_\gamma} = 0.23$, $\sigma = 0.13$ fpr pions has been taken into accounted in calculations.)

As it is seen, experimental value $(h_s/h)_{ch}$ up to $E_L^{(\gamma)} = 100$ TeV is essentially larger than simulated one.

Two methodical effects have to be analysed before final conclusions. The first is possible systematical error in $E_L^{(\gamma)}$. No exact correspondence of $E_L^{(\gamma)}$ in the experiment and simulation could lead to false disagreement between them due to $(h_s/h)_{ch}$ dependence on $E_L^{(\gamma)}$. But Fig.1 shows that overstimation of $E_L^{(\gamma)}$ in the experiment has to be too large to explain observed discrepancy.

The second effect is the influence of bad correspondence between energy threashold of accompanying particles in the experiment and calculation. It turns out that change of $E_L^{(\gamma)}$ from 3 TeV to 7 TeV in the simulation increases $(h_s/h)_{ch}$ from 0.30 ± 0 02 to 0.36 ± 0.02 only. The experimental situation looks rather interesting. Integral spectrum of accompanying particles is shown in Fig.2, It has exponential form without any threshold effect up to 2 TeV. About 33% of particles has $E_L^{(\gamma)}$ less than 7 TeV. But they practically do not influence on $(h_s/h)_{ch}$ value. While one changes threshold energy from 3 to 7 TeV it increases only by 0.01. This is



because most of the low energy particles are in groups of accompanying hadrons with multiplicity more than 1 or even 2.

4. Conclisions.

a. The experimental data on single hadron fraction are in disagreement with S-model prediction.

b. This disagreement could not be explained by experimental inaccuracy.

c. As it is shown in [4] , an account for interaction cross-section increase leads to the decrease of $(h_s/h)_{ch}$, i.e. to the increase of contradiction between the experiment and the model.

d. An account for complex chemical composition of primary cosmic ray leads to the same effect. This was shown in a small set of simulation for Fe primaries.

Thus an agreement between experimental data and calculation can be found only in the frame of models with scaling violation in the fragmentation region, in which either number of secondaries with large X is essentially less or (and) inelasticity coefficient is significantly larger than in scaling type models.

REFERENCES

1. Pamir collaboration ZNUZ S 2 z 60, p.9-21, 1977.
2. S.D.Cananov et al. This procedings HE-5.
3. A.Krys et al. ZNUZ S 2 z 32, p.5-45, 1980.
4. Y.Malinovski et al. 18th ICRC v.5, p.429, 1983.

N85-35910 HE 3.1-12

CONNECTION BETWEEN VARIATIONS OF THE ATMOSPHERE TEMPERATURE PROFILE AND VARIATIONS OF THE MESON COMPONENT INTENSITY

Ya.L.Blokh, S.I.Rogovaya

Institute of Terrestrial Magnetism, Ionosphere and Radio Wave Propagation, USSR Academy of Sciences, I42092 Troitsk, Moscow Region, USSR

The influence of temperature effects on intensity variations of the cosmic ray meson component are now studied in detail. The intensity variations caused by temperature variations are known to have the form /I/

$$\frac{\Delta I^i(t)}{I} = \int_0 W^i(h)\,\Delta T(h,t)\,dh \qquad (I)$$

where $W^i(h)$ are densities of temperature coefficients. These coefficients were calculated by Dorman /I/ for a wide energy spectrum. Miyazaki and Wada /2/ were the first to consider the possibility to solve the problem inverse to (I) - to predict variations of the atmosphere temperature from intensity variations of the meson component measured on the Earth. With this purpose they proposed a model simple at first glance, in which the temperature variations for each isobaric level were determined linearly from the intensity variations of the meson component registered by several ground-base devices

$$\Delta T_j = \sum_i A_{ij}\,\Delta I_i \qquad (2)$$

Here ΔT is temperature variation of j-th isobaric level. ΔI is intensity variation of the i-th device. The coefficients A_{ij} were found by the method of least squares. The number of divices is as a rule limited to $i \leq 3$.

The present paper is aimed at establishing connection between the temperature variation ΔT and the intensity variation ΔI by using the temperature coefficient density technique developed by Dorman. To this end we divide the atmosphere into some number of isobaric levels n ; let inside each level the temperature variations be constant in magnitude, although vary in time. Then the relation (I) can

be reduced to the form

$$\Delta I^i(t) = \sum_{j=1}^{n} A_{ij} \Delta T_j , \qquad (3)$$

where

$$A_{ij} = \int_{h_i}^{h_{i+1}} W^i(h)\, dh \qquad (4)$$

Since the temperature coefficient densities are known for a large number of devices, the coefficients A_{ij} can be obtained in any set. And if we choose the number of devices equal to the number of isobaric levels, the system of equations (3)-(4) can be solved exactly relative to the temperature variations

$$\Delta T_j = \sum_i B_{ij} \Delta I^i \qquad (5)$$

The relation (5) resembles by its form the model (2) used by Japaneese authors, but the coefficients B_{ij} are easily expressed through the temperature coefficient densities

$$B_{ij} = A_{ij}^{-1} \qquad (6)$$

To realize how much devices are actually needed on the Earth for predicting the temperature variation of the atmosphere profile with a reasonable accuracy, we have carried out concrete calculations for IO isobaric levels and IO devices. As the components we have taken: I_1 - mesons registered by a cubical telescope with a IO-cm leed absorber. I_2 - mesons observed by ionization chamber at the see level. I_3 - mesons underground at a depth of 25 mwe. I_4 - slow mesons of energy 200-350 MeV. I_5-I_{IO} are mesons observed, respectively, underground at a depth of 55 mwe, at the see level with $\cos\theta = 0.2$, at the see level with $\cos\theta = 0.6$, underground at a depth of 55 mwe with $\cos\theta = 0.4$, at a depth of 25 mwe with $\cos\theta = 0.8$, at a depth of 55 mwe with $\cos\theta = 0.6$. Table I presents the values of the coefficients B_{ij} calculated for IO isobaric levels in atmosphere from 0 to IOOO mb.

ORIGINAL PAGE IS
OF POOR QUALITY

Table I

Values of the coefficients B_{ij}

0.872	0.577	-0.I63	0.789	0.058	-0.026	-0.345	0.596	-I.096
-4.742	-2.876	0.68	-2.I74	-9.I9I	0.075	0.834	0.295	4.33
-64.2I	-43.40	II.2I	-45.08	6.453	I.365	I8.60	I.207	72.59
60.I8	74.74	25.20	I53.3	2.2II	-3.665	-68.83	-3.998	-I69.3
-I2.2I	I5.37	-6.088	46.2I	-I.584	-0.599	-20.06	-0.435	3.55
I7.8I	4I.97	4.689	88.88	7.456	-2.I98	-42.69	-I.44	-37.69
-35.02	-85.67	I3.07	-254.9	-6.845	5.377	I28.I	3.809	II8.7
56.95	36.82	-8.23	40.74	-I.642	-I.237	-I8.02	-I.26I	-57.75
-0.553	-0.55I	0.I97	-I.767	-0.023	I.555	-0.399	I.026	I.I69
-24.86	-I3.I6	3.0I3	I3.56	I.298	-I.I05	-I5.28	0.353	20.44

We have varied the set of initial elements of the cosmic ray meson component. The calculation has shown that the matrix of the coefficients B_{ij} is rather sensitive to their choice. Moreover, the analysis of the results shows that if for the calculations of the atmospheric temperature variations the model (2) is used, the number of meson components, essentially exceeding 3, should be taken into account.

REFERENCES

I. Dorman L.I. Cosmic Ray Variations. M. Gostekhizdat, I957, 492 p.

2. Miyazaki Y., Wada M. Proc. II-th ICRC, Budapest, I969, v.2, p. 592.

239 N85-35911

High Sensitive X-Ray Films to Detect Electron Showers in 100 GeV Region

Taira,T., Shirai,T., Tateyama,N. and Torii,S.
(Kanagawa University, Kanagawa)
Nishimura,J., Fujii,M. and Yoshida,A.
(Institute of Space and Astronautical Science, Tokyo)
Aizu, H. and Nomura,Y.
(Kanagawa Prefectural J. College, Kanagawa)
Kazuno,M.
(Toho University, Chiba)
Kobayashi,T.
(Aoyama Gakuin University, Tokyo)
Nishio,A.
(Kyoto University, Kyoto)

ABSTRACT

Non-screen type X-ray films have been used in emulsion chamber experiments to detect high energy showers in cosmic rays. Ranges of the detection threshold is from about 1 to 2 TeV as depending on the exposure conditions. In order to improve this threshold, we have tested different types of X-ray films and sheets i.e. high sensitive screen type X-ray films (Fuji G8-RXO) and luminescence sheets (Fuji 'Imaging Plate'). For these, the threshold of the shower detection is found to be about 200 GeV, which is much lower than that of non-screen type X-ray films. These films are useful to detect showers in the medium energy range, a few hundred GeV, of the cosmic ray electrons[1].

1. Introduction.

In emulsion chamber experiments, the detection of high energy electron showers is usually carried out by naked eye scanning on X-ray films. This reduces a lot of labour for microscope scanning of high energy showers. The detection threshold, if we use non-screen type films such as the Sakura N-type, is about 1 to 2 TeV as depending on the exposure conditions. In order to improve this threshold, we tested other types of X-ray films and sheets i.e. the screen type X-ray films (Fuji G8-RXO), and the luminescence sheets (Fuji 'Imaging Plate').

These photographic materials have been irradiated to the INS electron synchrotron beams to obtain the characteristic curves for the particle densities[2]. The net optical density, D_n, of the RXO at the electron density of $10^6/cm^2$ has been confirmed to be about 10 times higher than that of the N-type. This result suggests that the detection threshold for G8-RXO is by a factor of 10 less than that of N-type. For 'Imaging Plate', the computer-aided laser beam scanning was performed for the measurements of D_n [3].

These films and sheets have been also tested to detect electron showers in the emulsion chamber exposed at balloon altitude. By track counting of the observed showers in nuclear emulsions, the detection threshold of G8-RXO has been found to be around 200 GeV, which is consistent with results of the accelerator experiment.

ORIGINAL PAGE IS
OF POOR QUALITY

N85-35011

2. Characteristic Curve of X-Ray Films and 'Imaging Plate'.

Several types of X-ray films (Sakura N type, Fuji #200 type and G8-RXO) and 'Imaging Plate' have been irradiated vertically to the 760 MeV electron beams. The setup of these materials is shown in Figure 1. The electron beam densities in this irradiation are covering from 6.7×10^4 to 2.7×10^6 /cm^2 at the center of the beams.

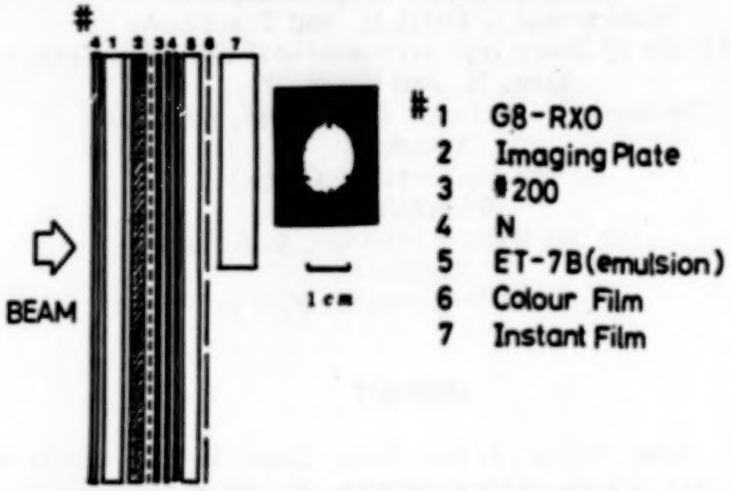


Fig.1 Setup of photographic materials.

The development times were 15 min., 20 min. and 25 min. for N-type and #200, and 10 min., 12 min., and 15 min. for RXO respectively, under the condition that Konidol developer was used at 20°C. After the development, the optical densities, D, on the films were measured with the microphotometer with the slit size of 200×200 μm^2. The electron densities were determined by the track counting in the emulsion plates. Figure 2 shows examples of the beam profiles on these films.

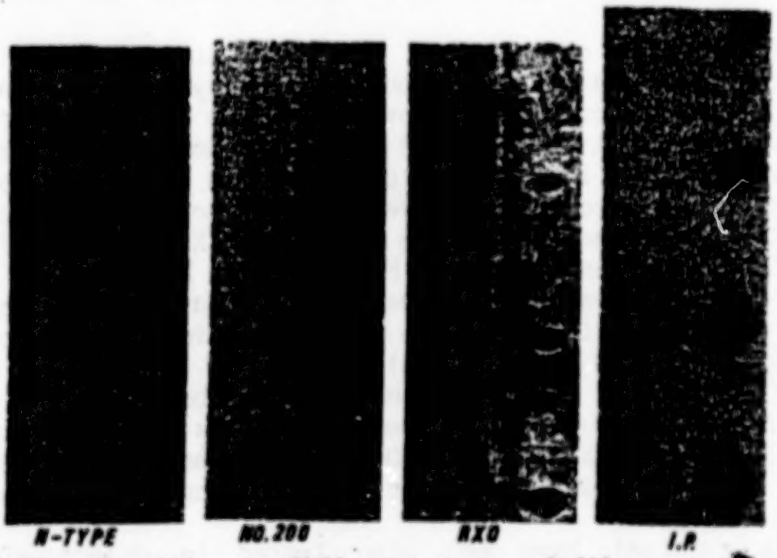


Fig.2 Beam profiles on different types of films are shown for comparison. Each black spot at the same relative position on a film corresponds to the same intensity of beam.

The characteristic curves for these films and sheets are shown in Figure 3. The data of N-type and #200 are those for the development time of 15 min. The D_n's of N-type and #200 increase with development times, but the ratio of sensitivities of #200 to N-type remains constant, keeping the value of ~2.5. The D_n of RXO, however, does not change with the development time. As shown in Figure 3, the characteristic curve for RXO shows a non-linear dependence on the electron density. This is due to the characteristics of the screen type X-ray films. As to 'Imaging Plate', the characteristic curve is derived after the computer processing. We can chose the most appropriate condition which is suitable for detecting the electron shower.

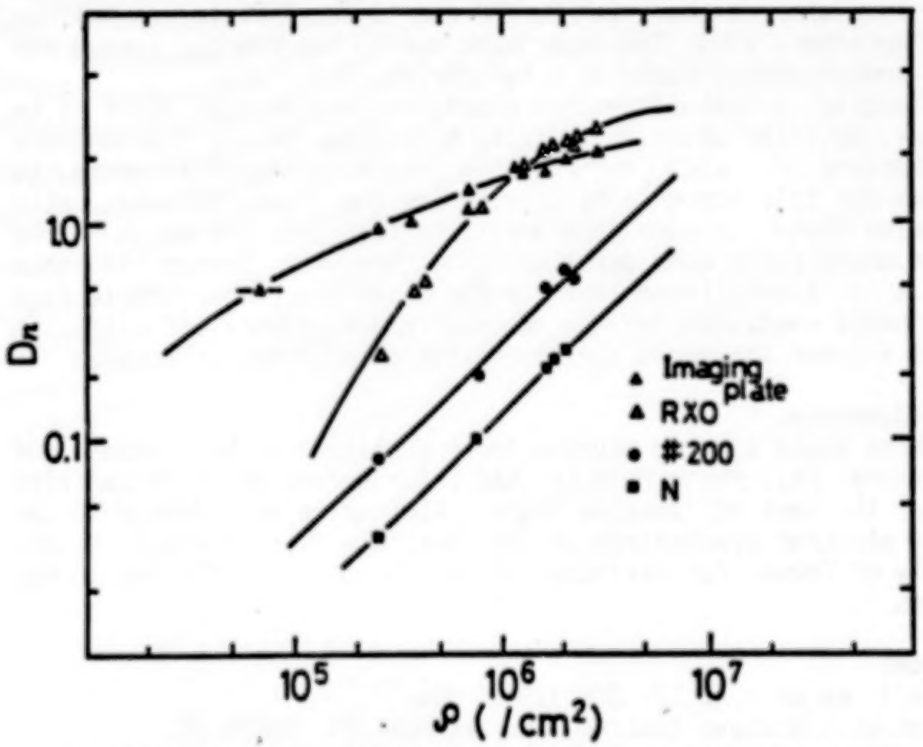


Fig.3 Characteristic curves of different types of films.

3. Discussion.

From the characteristic curves, we observe that the ratios of the sensitivities from N-type via, #200 and G8-RXO to 'Imaging Plate' are of *1:2.5:8:80* at the D_n of 0.1. This seems to indicate that the ratios of the detection threshold of electron showers are of *1:0.4:0.13:0.013* with respect to the foregoing ratios.

In actual case, however, the threshold is determined not only by sensitivity of the film, but also the signal to noise ratio of D, the noise in which is produced by the background tracks and chemical fogs. Fluctuations of the D due to background tracks depend on the number of grains developed by these tracks, and depend on the sensitivities and grain sizes of the films. Grain size in non-screen type X-ray films are larger than that in screen type X-ray films. The average area of grains in N-type and RXO are 16.5 μm^2 and 4.8 μm^2 respectively.

The sensitivity of each grain in N-type is high, and almost of all grains are developed when thin tracks penetrate through the grains. The sensitivity remains almost unchanged even for slow protons or electrons contained in the background tracks . This is the reason why non-screen type X-ray films have been used in the shower detection for long exposure experiment.

The screen type X-ray films have quite different characteristics. The sensitivity is almost proportional to the ionization loss of the penetrating particles. Thus screen type X-ray films and 'Imaging Plate' could be thought as the most effective in detecting showers for short exposure experiment such as the balloon's. Referring to these fact, we exposed the emulsion chamber with G8-RXO and 'Imaging Plate' at balloon altitude in September, 1984. The experiment was to observe the cosmic ray electrons at medium energy range of a few hundred GeV.

The detection threshold in this exposure has been made clear to be around 200 GeV. Detailed analysis has also been made for the fluctuations of the background D, and confirmed the detection threshold energy is around 200 GeV for this exposure by considering the signal to noise ratio of D. 'Imaging Plate' is much more sensitive than RXO, but as seen from the signal to noise ratio consideration, the threshold energy in this experiment is a little lower than the RXO's. We are now trying to find the most favorable condition for the computer-aided process of 'Imaging Plate' to get a lower threshold for the detection of electron showers.

Acknowledgements.

The authors would like to express their gratitude to Mr.Miyahara and his collaborators, Fuji Photo Film Co.,Ltd., for extending every facility necessary for the test of 'Imaging Plate'. They are also indebted to the staffs of the electron synchrotron of the Institute for Nuclear Study, the University of Tokyo, for carrying out the irradiation of films to the electron beams.

References

1. Nishimura,J. et al.: Ap. J. 238 (1980) 394.
2. Ohta,I. et al., Nuclear Instrum. and Methods 161 (1979) 35.
3. Miyahara,J. et al., Journal of Luminescence 31 & 32 (1984) 266; RADIOLOGY 148 (1983) 833.

ORIGINAL PAGE IS
OF POOR QUALITY

JETS IN AIR-JET FAMILY

N85-35912

NAVIA O., C.E. and SAWAYANAGI, K.
Depto.RC, IFGW, Univ. Estad. Campinas
Cx.Postal 6165, Campinas-13100-SP, BRAZIL

ABSTRACT

The A-jet families of the Brazil-Japan Collaboration on Chacaltaya Emulsion Chamber Experiments are analyzed by the study of jets which are reconstructed by a grouping procedure. It is demonstrated that large-$E_J R_J$ events are characterized not only by small number of jets and two-jet like asymmetric shape, i.e. the binocular events, but also by the other type. This type has a larger number of jets and more symmetrical shape in the p_t plane.

INTRODUCTION

Event shape is examined by using the following two quantities;

a) energy-weighted distance from the center of a family of reconstructed jet, $\overline{E_J R_J}$(TeVcm),

b) symmetry coefficient/1/ of jet, b_J, as defined

$$b_J=(\Sigma E_{Ji} Y_{Ji}^2)_{min.}/(\Sigma E_{Ji} X_{Ji}^2)_{max.}$$

The symmetry coefficient measures azimuthal symmetry, which will have a value of 0 for the case of in-line event and of 1 for the completely symmetrical azimuthal distribution. All the quantities with a letter of J are obtained after a grouping procedure to reconstruct jets. The energy weighted distance used is defined as $\chi_{ij}=R_{ij}E_iE_j/(E_i+E_j)$ and the cut-off value $\chi_c=25$ TeVcm as usual/2/. For this grouping procedure cascades with $E\geq 2$ TeV are used, γ-ray and hadronic components are treated equally and energies of hadronic cascades are used without correction of $K\gamma$.

RESULT

To grasp gross features of the A-jet families, are used all the 218 A-jet families including hadron-rich and exotic events. After the jet-grouping, 215 events have more than one jet. Then $\overline{E_J R_J}$ and the symmetry coefficient are calculated for each event.

We can see from Fig.1 that $\overline{E_J R_J}$ distribution has a peak at around 20 TeVcm and a very long tail over 300 TeVcm. On the other hand the b_J distribution is almost flat with a sharp peak at around $b_J=0$. This sharp peak should include the contributions of the binocular events/3/ and some excess

of the experimental data can be seen at b_J near to 1, comparing with the tendency of the Monte-Carlo simulation/1/. While we can see the correlation between b_J and $\overline{E_JR_J}$ exists, the dependence of b_J on $\overline{E_JR_J}$ is shown clearly in Fig.2, in which b_J distributions are given separately for three intervals of $\overline{E_JR_J}$. As increasing $\overline{E_JR_J}$ the fraction of $b_J=0$ is rising. It means that large $\overline{E_JR_J}$ is realized by two-jet like events, i.e. binocular-type events. We note that inspite of the very rapid decreasing of the fraction towards larger b_J's there exist non-zero experimental data at b_J near to 1 even at the highest-$\overline{E_JR_J}$ group.

The correlation between number of jet N_J and $\overline{E_JR_J}$ as given in Fig.3 shows that larger $\overline{E_JR_J}$'s are shared by less number of jets. That is large $\overline{E_JR_J}$ region is occupied by binocular-type events. And also some events are found to have very large N_J even at the highest-$\overline{E_JR_J}$ group.

It may be concluded that there exist those A-jet families which have large and comparable $\overline{E_JR_J}$ with the binocular events, but which contain many jets so as to give rise to very symmetrical azimuthal distribution. The reconstructed jets with the use of the cut-off value $\chi_c=25$ TeVcm seem to have a jet-size less than the actual size of the two clumps, because the N_J distribution of the group $\overline{E_JR_J}\geq 80$ TeVcm has a rather broad peak between 2 and 10.

ACKNOWLEDGMENTS

The author acknowledges financial supports by the local committee of the 19th ICRC and by the Conselho Nacional de Desenvolvimento Científico e Tecnológico—CNPq in BRAZIL.

REFERENCES

/1/ KRYS, A. et al., Proc. 17th ICRC(Paris, 1981), vol.11, p.187.
/2/ SEMBA, H., Proc. Intern. Symp. on Cosmic Rays and Particle Physics, edit. OHSAWA, A. and YUDA, T., 1984, Inst. for Cosmic Ray Research, Univ. of Tokyo, p.211.
/3/ LATTES, C.M.G. et al., Phys. Rep. 65(1980), p.151.

N83-38213

ORIGINAL PAGE IS
OF POOR QUALITY

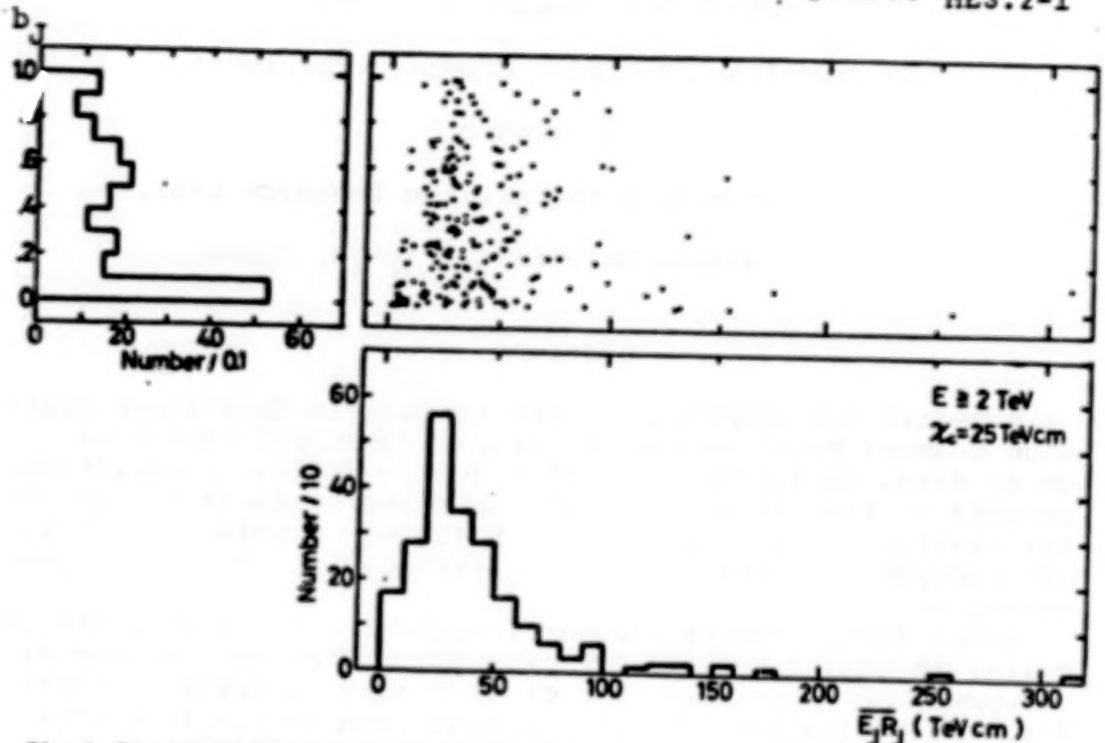


Fig. 1 The scatter plot of symmetry coefficient b_j(1/ of jet vs. $\overline{E_jR_j}$ of the A-jet families.

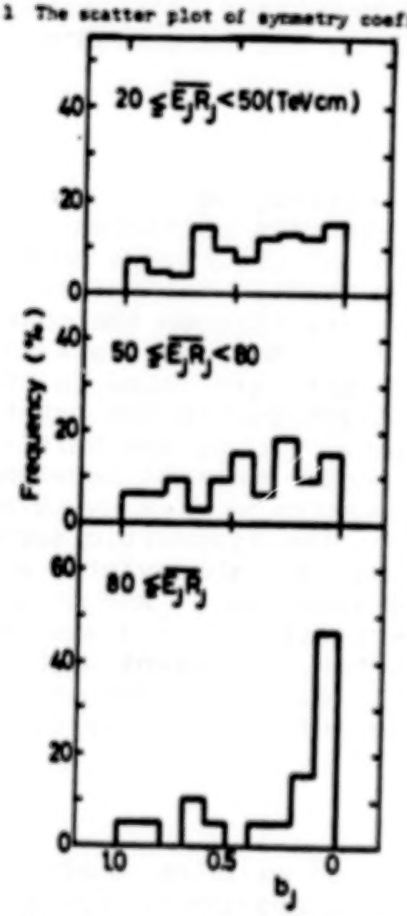


Fig. 2 The symmetry coefficient b_j distribution.

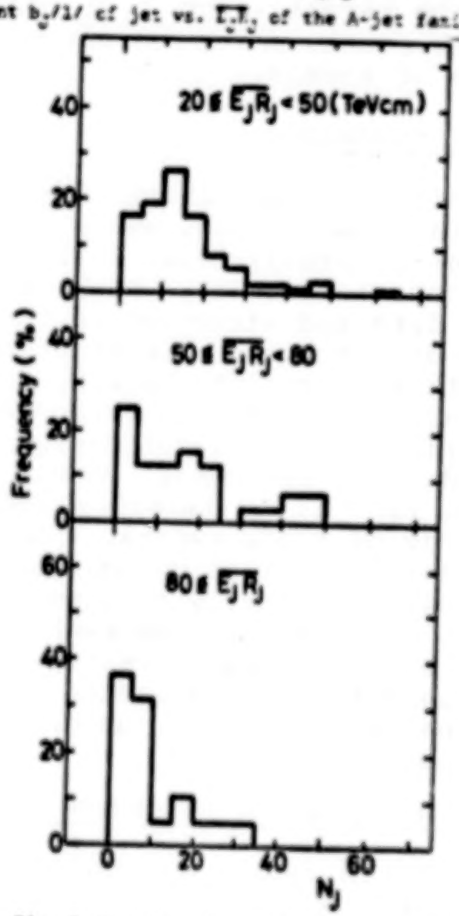


Fig. 3 The distribution of number of jet.

N85-35913

HE 3.2-5

Search for Anomalous C-jets in Chacaltaya Emulsion Chamber Experiment

H. Kumano

Science & Engineering Research Lab.,

Waseda University, Tokyo, Japan

Abstract

A search for anomalous C-jets is made in Chacaltaya emulsion chamber No.17 exposed by Brasil-Japan collaboration. Up to date, measurement of 150 C-jets (nuclear interactions occured in the target layer in the chamber itself) with total visible energy greater than 5 TeV was completed. They are recorded in area of 11 m^2, corresponding to 17.1 m^2·year exposure.

Among them, 7events has no pinaught and two events are peculiar in that 3 showers out of 4 show abnormal cascade development. Especially, two of them show remarkable characters indicating that they are coming from exotic interactions in the target layer. We present here some illustrations of these events and short discussions on the threshold of this type of events.

1. Introduction.

After the discovery of exotic interactions such as Chiron, Centauro and so on, among cosmic-ray induced nuclear interactions by Brasil-Japan collaboration of Chacaltaya emulsion chamber experiment, there has been studied extensively about the detailed structure of these events through the observation of atmospheric interactions. /1/ But there are no reports so far that these types of events are found in CERN SPS experiment at energy region around 200 TeV in lab. system nearly equal to C-jet energy region. As to the multi-pion production phenomena, we can see good agreement between the two. /2/ It is therefore urgent question what is the threshold energy of these events. Recently, the systematic survey of C-jets is carried out on chamber No.19 (abbreviated as CH19 hereafter) partly to answer this question. And it is found that there exist some exotic events with $\Sigma E^{(\gamma)}$ (sum of all visible energies) greater than 5 TeV. Present work is made to improve the statistics of exotic events in target interactions to give better understandings of the problem of exotic events.

2. Experimental Procedure.

C-jets recorded in the two-storeyed emulsion chamber No.17 exposed on the top of Mt.Chacaltaya are measured and partly reanalysed. Detailed description of the structure of the emulsion chamber and the method of observation is found elsewhere./2/,/3/

3 Result.

Up to date, 150 C-jets are accumlated from 55 blocks in CH17 corresponding 17.1 m^2·year of exposure. In Fig.1 we present ΣE_γ spectrum with the straight line power of which is -1.7. Fig.2 is the distribution of invariant masses of every possible pair of gamma rays from 78 newly measured events. The peak of pinaught is clearly seen which assures the accuracy of energy measurement. Fig.3 is the scattered diagram of observed showers of 120 events with multiplicity greater than 4. These figures show that the present measurement of C-jets is carried out without severe systematic errors.

Among 150 events, there are 7 pinaught-less events, i.e., there is no pair of showers whose invariant mass falls into pinaught region (100 - 170 MeV). In addition, two events show peculiar behavior indicating that constituent showers of these events are not simple gamma-ray originated showers. In table 1 these 9 events are summarized.

Among them, two-prong events with invariant mass about 4 or 5 hudreds of MeV can be interpreted as the result of fluctuation of normal multiple meson production. The remaining events are highly probable candidtes of non-pion interactions. Two events are illustrated here in detail. One is the event 17-151-3, which consists of 4 showers with energy 2.6, 1.3, 1.5 and 1.3 TeV, respectively. Careful search for another lower energy showers were in vain. Invariant masses are shown in Fig.4 with target map of the event. Numerical values in blackets are energies of showers. The constituent showers in this event have no partner to make up pinaught. Further, shower No.1 and 2 are not observed in 3 c.u. layer and shower No.2 shows abnormal development of track numbers in transition as well as shower No.4. Therefore, only No.3 can be considered as gamma-ray shower. In addition, transverse momenta of these showers are very large compared with the average ones ∿ 200 MeV. Sum of transverse momenta, $p_T^{(\gamma)}$, of the four is 2.0 GeV/c which gives 500 MeV/c as the average.

The other event 17-135-A is also shown in Fig.5, as in the same way in the former event. Shower No.1 has multi-core structure from 4 c.u. layer down to the last layer 12 c.u. peculiar to Pb-jet in the lower chamber (local nuclear interaction in the lower chamber). No.2 has two maxima in transition of track numbers. No.4 has only 12 tracks within the circle with radius 25 μm at 5c.u. and then develops and attenuate abruptly. No.3 has also double maxima in transistin, but rather smooth fitting to the calculated curve can be made. Consequently only No.3 can be interpreted as gamma ray originated shower as in the former event. As well as the event 17-151-3, transverse momentum of showers in this event as as large as 0.38 GeV/c on the average which value of transverse momentum is close to that of Mini-Centauro event observed by atmospheric interactions.

4. Discussions.

Preliminary comparison with Momte-Carlo simulation tells us that above two events can not be seen in the artificial events so far which reproduce well the over-all feature of multiple meson production phenomena observed in C-jets. It is highly probable that several events found by the present analysis are coming from the same origin as the exotic events found in the atmospheric interactions. Frequency of these anomalous events is the same as in the result of the analysis of CH19 as a first approximation, several percent of the whole events.

If we assume that gamma-ray inelasticity of these showers are usual one (average is about 1/4 ~ 1/3) and all showers are from the local nuclear interactions in the lower chamber itself, average energy of parent partiles producing these events is estimated as about 100 TeV which is within the limit of accelerator experiment. This seems to be a contradiction, which might be a fringe of the secrets of the nature.

Acknowledgement

The author expresses the sincere gratitude to all the members of Brasil-Japan collaboration of Chacaltaya emulsion chamber experiment for encouragement and offering him the data.

References

1. Brasil-Japan collaboration; Proc. of Workshop on Cosmic Ray Interactions High Energy Results, La Pas Rio de Janeiro (1982) 319.
2. Brasil-Japan collaboration; Supplement of Progress of Theoretical Physics, 1, and H. Kumano; ibid, 51.
3. Brasil-Japan collaboration; this issue, HE 3.2-6.

Table 1. List of Events

Event name	No. of showers	$\Sigma E^{(\gamma)}$ (TeV)	Remarks
17-89-2	5	8.00	Non pinaught
17-93-2	3	7.32	Non pinaught
17-116-3	2	6.90	Non pinaught, 560 MeV
17-122-14	2	5.55	Non pinaught, 519 MeV
17-140-C	2	5.60	Non pinaught, 559 MeV
17-144-24	2	> 6.9	Non pinaught, > 484 MeV One shower is gb-jet lower (Δt=8.3)
17-151-3	4	6.70	Non pinaught, See text
17-135-A	4	5.65	See text, at most one gamma ray
17-135-B	4	7.26	At most one gamma ray

N83-35914

ORIGINAL PAGE IS
OF POOR QUALITY

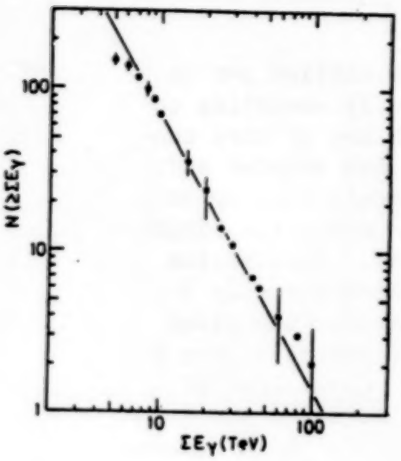


Fig.1 $\Sigma E(\gamma)$ Spectrum

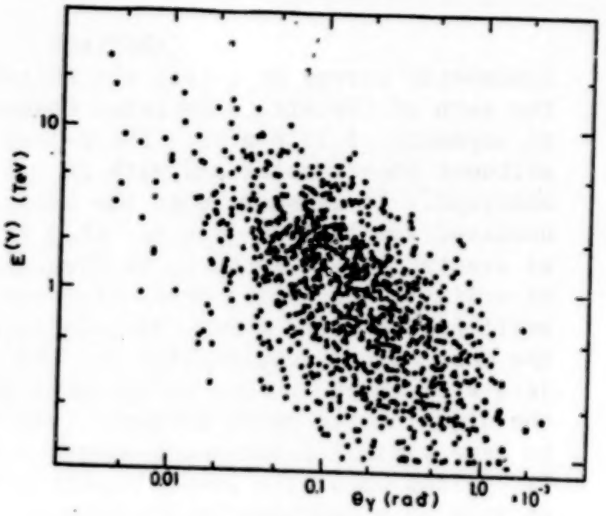


Fig.3 $\Sigma E(\gamma)$ $-\theta_\gamma$ correlatuion

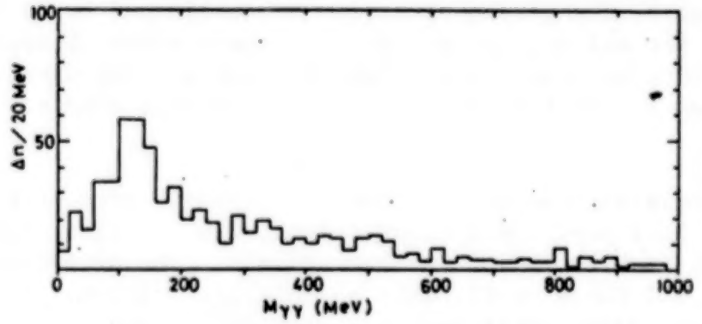
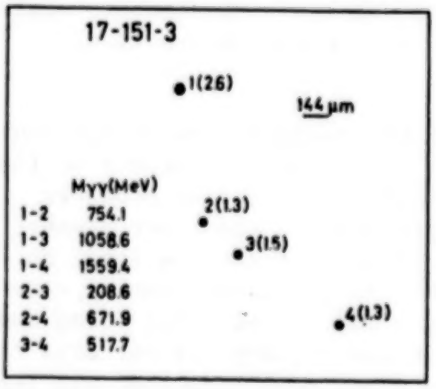


Fig.2 Invariant mass spectrum



Fi.4 Target map

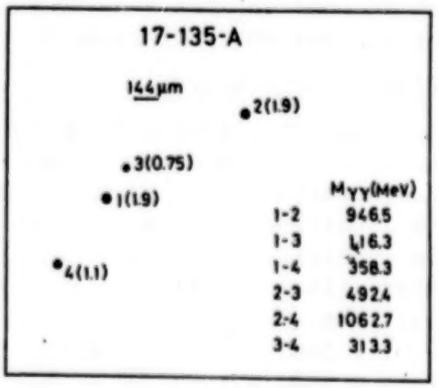


Fig.5 Target map

N85-35914

HE 3.2-6

Exotic Interactions among C-jets and Pb-jets

Brasil-Japan Emulsion Chamber Collaboration

ABSTRACT

Systematic survey of C-jets and Pb-jets is carried out on the part of Chacaltaya Emulsion Chamber No.19 amounting to an exposure of 28.8 m^2yr. 198 C-jets with two or more constituent shower cores and with $\Sigma E_\gamma \geq 5$ TeV are adopted and analysed. It is shown that the adopted events make up an unbiased sample of C-jets for $\Sigma E_\gamma \geq 7$ TeV. Among the adopted events, 16 are found to be pinaught-less. Fluctuation of ordinary multi-pion production can account for only a small fraction of them. Mini-Centauro interaction gives the most natural explanation for the eight pinaught-less C-jets with three or more constituent shower core. Out of the eight double-cored pinaught-less events, three are found to have visible invariant masses > 1.8 GeV/c , which strongly reminds us of the event "Castor-Pollux", the first clear example of a Geminion interaction.

In addition, three Pb-jets-lower are found to be composed of double cores whose respective visible transverse momenta are greater than 0.5 GeV/c, suggesting that they are of Geminion origin or chiron origin.

The energies of the parent particles are estimated to be 100 to 200 TeV for all the above-mentioned three kinds of events.

Discussions are made on the implications of this energy estimate and of the frequency of observed exotic events.

1. Introduction.

In mountain emulsion chamber experiments, several types of exotic nuclear interactions have been found among A-jets, i.e., nuclear interactions occurring in the atmosphere above the chamber/1/2/. The decisive characteristics common to all these exotic interactions are follows:

(i) they produce secondary particles with unusually large transverse momenta.

(ii) they are "pinaught-sterile", i.e., they produce pratically no pinaught.

Some of the above-mentioned exotic interactions were expected to occur at the CERN $\bar{p}$-p collider, but the search met with no success.

The present work is the report on a least biased systematic survey of the local nuclear interactions occuring within the emulsion chamber, aiming at making a guess on the threshold energy for the exotic interactions.

2. Experimental Procedure.

C-jets and Pb-jets-lower recorded in the two-storeyed Chacaltaya Emulsion Chamber No.19 are detected and analysed. The chamber consists of the upper chamber(area 44m^2, thickness 6cmPb), nuclear interaction producer (area 44m^2, thickness 23 cm asphalt), air gap(1.5m) and the lower chamber (area 33m^2, thickness 7cmPb). C-jets and Pb-jets-lower are the local nuclear interactions occuring in the producer and in the lower chamber, respectively. The chamber contains nuclear plates and N-type X-ray films under 1.5cm, 2cm, 2.5cm, 3cm, 4cm and 6cm of Pb. It was exposed for 667 days to cosmic rays at Chacaltaya(540 gr/cm^2). It is worth remarking that all the nuclear plates maintained excellent and uniform level of sensitivity even after this long exposure. 16m^2 of the lower chamber has been used in the

present work, which amounts to the exposure 28.8 m^2yr.

Scanning of C-jets and Pb-jets-lower are made in the same way as the previous works, and so is the energy measurement of their constituent showers/4/.

An electron shower satisfying one of the following criteria is identified as of a hadronic origin:

(i) It becomes observable only in greater depths, typically under at least 6 c.u.

(ii) The change with depth of electron number deviates significantly from that of a pure electron-photon cascade shower.

(iii) Clear multi-core structure is observed and traced at two or more successive layers.

3. Quality of Experimental Data

215 C-jets with $n \geq 2$ are found, where n denotes the number of constituent showers. Out of them 198 have visible energy $\Sigma E \geq 5$ TeV, of which 155 are isolated and 43 are accompanied by γ-hadron families (i.e., bundle of parallel γ-rays and hadrons). These 198 events are adopted and used for analysis.

The 145 C-jets with $n \geq 2$ and $\Sigma E_\gamma \geq 7$ TeV yield quite consistent and reasonable results for ΣE_γ-distribution, the zenith angle distribution and the vertical flux. This shows that the event detection has been made in the way free from any serious biases.

As for constituent showers, the detection efficiency turns out to be nearly uniform down to $E_\gamma \approx 0.2$ to 0.3 and up to $r = 1.5$ to 2.0 mm. Also the invariant mass distribution of all possible γ-ray pairs has quite a reasonable shape. This shows, firstly, that the present experimental method is free from any serious systematic errors and, secondly, that the overwhelming part of the C-jets in the present experiment are due to ordinary multi-hadron production.

4. Morphology of Pinaught-less C-jets

Eight events with n=2 and another eight with $n \geq 3$ are found to be "pinaught-less", i.e., every pair out of the constituent showers either has visible invariant mass $M(ij) > 200$ MeV/c , or contains at least one identified Pb-jet-lower.

As ΣE_γ of all the above 16 events are rather small(< 30 TeV), the question arises whether they are accounted for as the fluctuation tail of usual C-jets. In order to answer the question, simulation C-jets are constructed and compared with experiment. 200 Mirim-type C-jets (scaling multi-pion production via H-quanta) and 200 Acu-type C-jets (scale-breaking multi-hadron production via SH-quanta) are constructed. The rest masses of an H-quantum and an SH-quantum are assumed to be 2.3 GeV/c^2 and 18 GeV/c^2, respectively. For simplicity, SH-quanta are assumed to decay exclusively into pions in the present simulation.

Fig. 1 shows the E_1/E_2 vs. n plot of the observed and the simulated pinaught-less events, where E_1 and E_2 stand for the highest and the second highest, respectively, energies of the constituent showers.

Firstly one observes that the simulation produce only n=2 and n=3 events, while about one-third of the observed events have $n \geq 4$.

Secondly, only two Mirim-type C-jets (one double-cored and the other triple-cored), out of the 18 simulated pinaught-less events, are observed to reproduce the experiment. The remaining 16 yield E_1/E_2 far too large to be reconciled with experiment.

ORIGINAL PAGE IS
OF POOR QUALITY

The conclusion is that a minor part of pinaught-less C-jets might represent the fluctuation tail of Mirim-type ordinary C-jets, but that the main part is of genuinely different origin.

5. Nature of n≥3 Pinaught-less C-jets

Fig. 2 shows the superposed integral $p_T(\gamma)$-distribution of the constituent showers of the eight pinaught-less C-jets with n≥3, where $p_T(\gamma)$ denotes the observed part of the shower transverse momentum with respect to the respective energy-weighted center of each event. Also shown in the figure by a solid line is the same distribution of Event Centauro I. Both agree well with each other, giving

$$\langle p_T(\gamma) \rangle = 0.35 \pm 0.05 \text{ GeV/c},$$

which, at the same time, coincides with that of Mini-Centauro interactions.

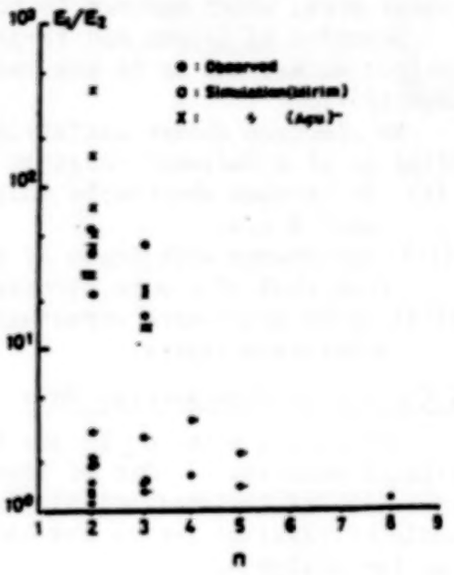


Fig. 1. E_1/E_2 vs. n plot

Fig. 3 shows the superposed fractional energy distribution of the constituent showers of the same eight events in an integral form. It fits well with an exponential form, and extrapolation down to zero energy gives

$$\langle m \rangle = 6 \pm 1 \text{ /event},$$

as the average observed multiplicity of cores.

Now let us assume that the events are due to bundle of non-rapid-gamma-decaying hadrons having the same nuclear mean free path as nucleons. Then the correction for escaping hadrons gives

$$\langle m_0 \rangle = 18 \pm 3$$

as the average multiplicity of hadrons produced in the parent interaction. Again this is in good agreement with

$$\langle m_0 \rangle = 15 \text{ to } 20$$

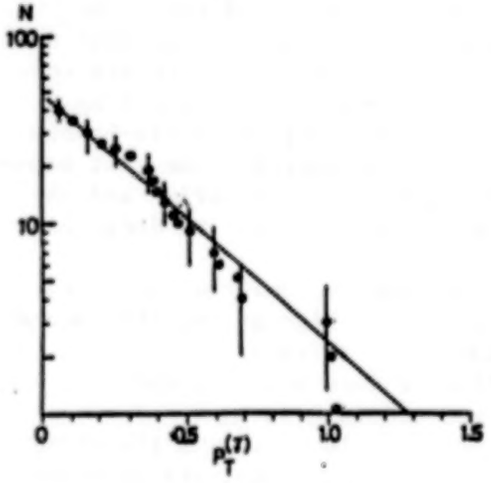


Fig. 2. Integral $p_T(\gamma)$-distribution.

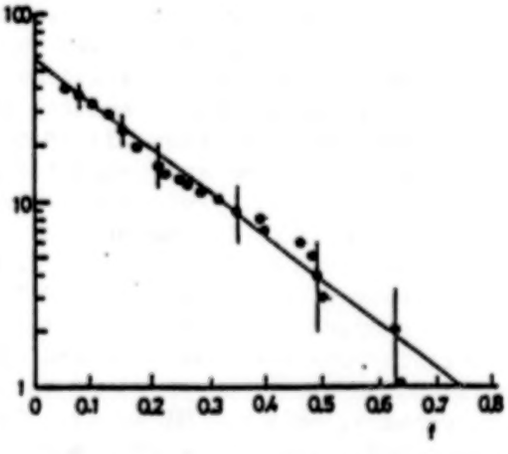


Fig. 3. Fractional energy distribution in the integral form.

of the Mini-Centauro interaction.

In view of the above results for $\langle p_T(\gamma) \rangle$ and $\langle m_0 \rangle$, the Mini-Centauro interaction seems to be the most natural explanation of the pinaught-less C-jets with $n \geq 3$.

Now the average energy of the parent particle responsible to these C-jets, $\langle E_0 \rangle$, is estimated by $\langle E_0 \rangle = \langle \Sigma E_h(\gamma) \rangle / (\langle K \rangle \langle f \rangle \langle k_\gamma \rangle)$, where $\langle E_h(\gamma) \rangle$ is the average observed energy sum of the hadron bundle, $\langle K \rangle$ the average inelasticity at a Mini-Centauro interaction, $\langle f \rangle$ the energy fraction of the released energy given to the detected hadrons, and $\langle k_\gamma \rangle$ the average fraction of the energy released to γ-rays at a successive interaction in Pb. Assumption $\langle K \rangle \sim 1/2$, $\langle f \rangle = 1/3$ to 1, $\langle k_\gamma \rangle = 1/5$ to $1/4$ yields

$\langle E_0 \rangle \approx 100$ to 400 TeV.

6. Double-cored Pinaught-less C-jets.

Out of the eight double-cored pinaught-less C-jets, three has striking features. The constituent shower-core pairs yield quite large visible invariant masses, M(1-2): 3.3 GeV/c^2, 1.85 GeV/c^2 and 2.9 GeV/c^2. They strongly remind us of the Geminions, whose first clear example is the "Castor-Pollux" with M(1-2)=5.8 GeV/c^2. The event with M(1-2)=3.3 GeV/c^2 has still another striking feature. Its constituent showers originate from a point in the air gap, indicating a decay of some unknown matter.

Now, the assumption that the constituent showers are due to ordinary hadrons gives an estimate $\langle E_0 \rangle \approx 100$ to 200 TeV. The remaining five events have M(1-2) falling between 0.2 GeV/c^2 and 1.0 GeV/c^2, and can be explained either as the fluctuation of Mini-Centauros or as that of Mirim-type C-jets.

7. Pb-jets-lower with High-p_T Double Cores.

Three Pb-jets-lower are found to be composed of two shower cores whose mutual opening angles are large enough to be measured. Their M(1-2) are 3.3 GeV/c^2, 2.77 GeV/c^2 and 1.1 GeV/c^2. They again strongly remind us of Geminions. Here also the "ordinary hadron assumption" gives an estimate $\langle E_0 \rangle \sim 100$ TeV.

8. Summary and Discussions.

1) A least-biased systematic study of C-jets is made in Chacaltaya Emulsion Chamber No.19. It is found out that 5-10 % of the C-jets with $\Sigma E_\gamma \geq 5$ TeV are genuine exotic events. This corresponds to an estimated incident frequency of $\sim$ 1 exotic-interactable particle per m^2yr at Chacaltaya.
2) Average energy of the parent particles responsible to the above exotic events are estimated to be 100 to 200 TeV, irrespective of types.
3) If a nuclear collision of ordinary hadrons can produce an exotic interaction directly, either the versioned-up CERN SPS Collider or the coming FNAL TEVATRON must produce one.
4) On the other hand, if we assume that only the secondary particles from a chiron interaction can produce exotic interactions/3/, the upper bound of the threshold energy for chiron production will be estimated, from flux consideration, as $E_0 \sim 10^{16}$ eV.

References

1. C.M.G.Lattes, Y.Fujimoto and S.Hasegawa: Phys. Rep. 65 No.3('80),p151.
2. S.Hasegawa: Proc. Intern. Symp. on Cosmic Rays and Particle Physics, 1984, Tokyo, p.319.
3. S.Hasegawa: ibid., p.718.
4. Brasil-Japan Emulsion Chamber Collaboration: ICR-Report-91-81-7, Institute for Cosmic Ray Research, Univ. of Tokyo, 1981.

N85-35915

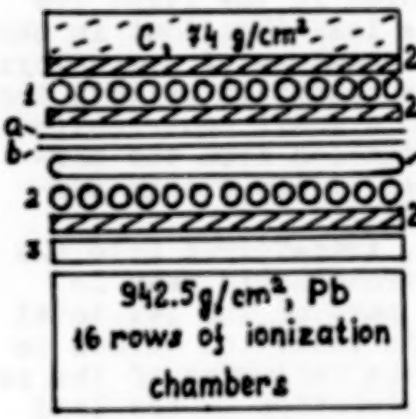
HE 3.2-7

X-RAY FILM CHAMBER WITH CARBON TARGET OF TIEN-SHAN COMPLEX ARRAY

K.V.Cherdyntseva, A.P.Chubenko, A.G.Dubovy,
N.P.Krutikova, N.M.Nesterova, S.I.Nikolsky,
N.M.Nikolskaja, E.I.Tukish, N.G.Vildanov,
T.I.Yakovleva
P.N.Lebedev Physical Institute
Moscow, USSR

The experiment was carried out at Tien-Shan highmountain station. X-ray films were exposed inside the ionization calorimeter under 74g/cm^2 of carbon and 5 cm of lead. The X-ray film chamber area is 36 m^2. To perform more reliable time selection of events in this experiment moving X-ray films have been used. 50% of events, in which we succeeded to determine incidence time, were identified with corresponding EAS. For such events the size spectrum of associated EAS was derived. Two methods of energy measurement using X-ray films (E_x^γ) and ionization calorimeter (E_{jet}^γ) have been compared. We obtained that $E_x^\gamma/E_{jet}^\gamma = 0.95$. In this work the plot is presented to illustrate energy transfer from selected hadron to electromagnetic component. We find cascades with high energy release into electromagnetic component and in which the hadron component is practically absent.

The experiment was carried out at Tien-Shan hihgmountain station /1/. The complex array included the big ionization calorimeter (BIC), the scintillation set for the size shower (N_e) determination with $N_e \geq 5 \cdot 10^4$, the central hodoscope for the size shower determination with $N_e < 5 \cdot 10^4$, the chronotron for the arrival angles detecting of EAS etc. The big ionisation calorimeter consists of the 19 rows of ionization chambers, its thickness is 1040 g/cm^2. The area of calorimeter is 36 m^2. The dead time of recording system of EAS data including calorimeter data was 17.5%. The BIC construction with the X-ray film chamber (X-chamber) is shown in Fig.1. Time selection of the events found in the X-chamber was performed. For this purpose the upper layer of the X-ray film was moved on several centimetres along the lower layer and a special time mark was put on the upper layer. When an electromagnetic cascade (EMC) crosses the both layers of the X-ray film, it marks them. Putting then together the two dark spots formed by the same EMC we can find the upper layer shift value along the lower layer. The inci-



1,2,3-the ionization chambers
a-upper moving layer of X-ray films
b-lower moveless layer of X-ray films

Fig.1. Construction of BIC with X-ray films (side view).

dence time was determined by the shift value. The accuracy of incidence time determination is several days in our experiment.

Every day the ionization calorimeter was stopped for several hours for the purpose of the maintenance and checks. To correlate the running time of X-chamber and ionization calorimeter EMC were not recorded on the X-ray films when calorimeter stopped running. That has been made as follows.

As one can see in Fig.1 the rubber cylinders were placed under the X-ray films. They had been pumped up to some surplus pressure, that caused the close contact between X-ray films and the lead plates. If the cylinders were not pumped up, air clearance was formed between the X-ray films and the lead. The EMC electrons are dispersed in the clearance and the marks did not arise.

The ionization calorimeter and the X-chamber run together for 2600 hours. The handled area of the X-ray films is 18.8 m^2. We have determined incidence time at 300 events which have been found in the X-chamber. 50% of these events have been combined with corresponding EAS. Some results of 150-event analysis are presented in this paper.

The X-ray films have been handled by the method used in the Pamir experiment /2/. The energy of EMC has been determined by means of theoretical curves calcucated for primary photon /3/.

The EAS size (N_e) was obtained by scintillation counter data for $N_e \geq 5 \cdot 10^4$. The size of small EAS was determined by hodoscope data according to the following expression

$$N_e \approx 10^3 \frac{K(\theta)}{\sigma_0} \ln\left(\frac{n}{n-m}\right),$$

where σ_0-the hodoscope channel area, $K(\theta)$-a coefficient depending on the arrival angle of EAS, n - the total number of channals, m -the number of fired channals.

The ionization calorimeter data have been handled as follows. The jet corresponding to the event found in the X-chamber have been separated in the ionization calorimeter. For these jets the energy E_{jet} and the energy E'_{jet} transferred into first electromagnetic peak have been calculated.

Two methods of the EMC energy measurement using the X-ray films (E^{γ}_{γ}) and using ionization calorimeter (E^{γ}_{jet}) have been compared. For this purpose the hadron jets satisfying the following criteria have been selected:

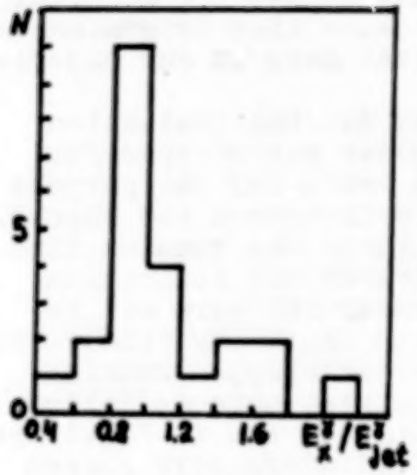
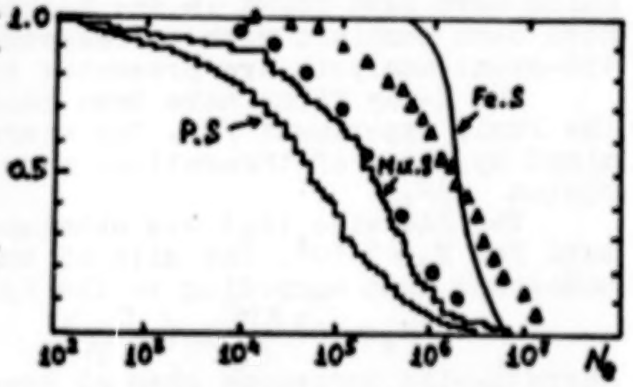


Fig.2.

1. The ionisation in the first row chambers is less than that in the second row chambers of the calorimeter. This condition selects the events with a small contribution to the ionisation from the cascades caused by low energy particles of EAS.
2. The energy, transferred into the first electromagnetic peak is about half part of the jet total energy. This condition allows us to escape the influence of the secondary interaction in the lead on the determination of the EM peak energy.
3. The shape of experimental electromagnetic peak is close to that of calculating curve for primary photon /4/. There are no obvious secondary interactions.

The 23 events satisfying these conditions have been selected. The ratio of the energy determined by X-chamber (E_x^{γ}) to the energy determined by the calorimeter (E_{jet}^{γ}) is presented in Fig.2. The mean value of this ratio is 0.95. According to these data one can say that there is quite good agreement of these two methods of the energy measurement.

The shower size spectrum of associated EAS was derived on the basis of the obtained data. Similar distribution has been obtained in the work performed at the Norikura mountain /5/. Comparision of the results is presented in Fig.3. The shower size of our experiment does agree with the simulation for Mixed primary mass composition and the scaling model /5/ and differs from the Norikura experimental result.



Δ - $\Sigma E_{\gamma,H} \geq 10$TeV, $n_{\gamma,H} \geq 1$, Norikura/5/ — - simulation, S implies a scaling model /5/
● - $\Sigma E_x^{\gamma} \geq 10$TeV, $n_x^{\gamma} \geq 1$, our experiment

Fig.3. Normalised integral size spectrum of showers combined with γ,H-families ($\Sigma E_x^{\gamma} \geq 10$TeV).

Fig.4 shows the $E_{jet}^{\gamma} - E_{jet}$ plot for our combined events. We find 16 cascades with high energy release into electromagnetic component and in which the hadron component is practically absent, that is $E_{jet}^{\gamma} \approx E_{jet}$. Out of them 8 events had equal EMC energies determined by means of both

ORIGINAL PAGE IS
OF POOR QUALITY

N85-33916

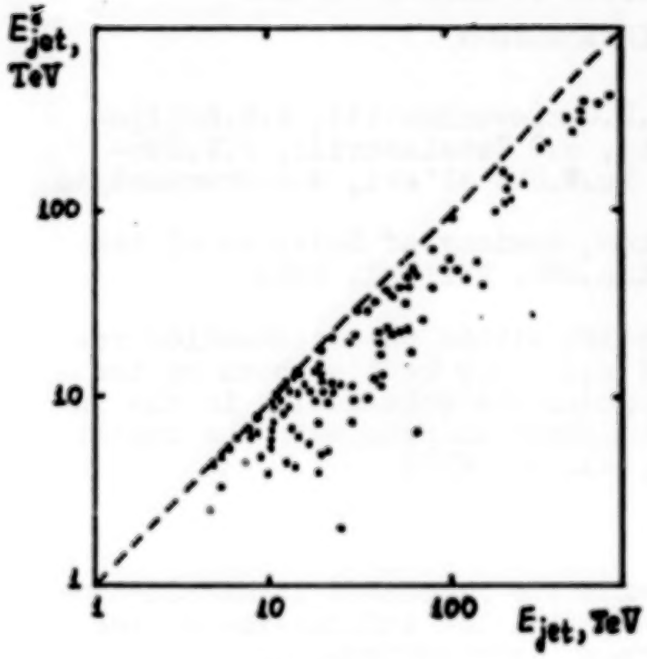


Fig.4.

HE 3.2-7
the X-ray film and the ionisation calorimeter (Table 1) that is in these events the hadron energy is transferred most likely into one or two electromagnetic particles mainly. To make the definite conclusion it is necessary to estimate the probability of such events in similar experiments.

Table 1.

No.	ΣE^{γ}_{x}, TeV	E^{γ}_{jet}, TeV	E_{jet}, TeV	n^{γ}_{x}	N_e
1	8.4	9.8	10.4	1	$1.6\ 10^4$
2	83.3	87.2	91.7	2	$6.3\ 10^4$
3	8.1	4.7	4.9	1	$2.9\ 10^3$
4	6.4	7.1	8.1	2	unknown
5	9.8	10.9	11.3	2	$4.4\ 10^4$
6	9.2	4.3	4.4	1	$1.8\ 10^5$
7	5.5	6.3	6.5	1	$3.7\ 10^4$
8	2.9	3.3	3.4	1	$1.8\ 10^4$

References

1. Erlykin A.D., Nesterova N.M. et al., (1965), Proc. 9th ICRC, London, 2, 731.
2. "Pamir" coll., (1984), Trudy FIAN, 154, p.14-27
3. Belyaev A.A., Ivanenko I.P. et al., (1980), Electron-photon cascads in cosmic rays at superhigh energies, Nauka, Moscow (in russian), p.197.
4. Ivanenko I.P., Samosudov B.B., (1967), Yad.phys., 5, 622.
5. Nakatsuka T., Nishikawa K., Saito T. et al., (1983), Proc. 18th ICRC, Bangalore, 11, 346.

N85-35916

SCALING VIOLATION IN HADRON-NUCLEUS INTERACTION

Yu.G.Verbetski, L.P.Garsevanishvili, D.M.Kotlyarevski, N.K.Ladaria, N.G.Tatalashvili, P.V.Tsomaya, N.I.Sherer, Yu.M.Shabel'ski, G.Z.Stemanetyan

Institute of Physics, Academy of Sciences of the Georgian SSR, Tbilisi, USSR

Summary. The scaling violation within the pionization region in the energy range of 0.2 - 2.0 TeV is shown on the basis of the analysis of angular characteristics in the interactions of the cosmic radiation hadrons with the nuclei of various substances (CH_2, Al, Cu, Pb).

The investigation of multiple processes in hadron-nucleus interactions allows to obtain the information on the space-time structure of strong interactions.

It is rather paradoxical, but at present, the so called soft processes of particle generation makind the overwhelming contribution to the inelastic interaction cross-section, remain the most obscure.

The most natural method to the understanding of the structure of such interactions is the investigation of hadron-nucleus interactions at high energies using nuclei of various atomic numbers A.

The experimental data presented in this work have been obtained at Chikovani Tskhra-Tskaro Station at the height of 2500 m above the sea level by means of the instalation consisting of the magnetic spark spectrometer and the ionization calorimeter /1/.

The targets of Al, CH_2, Cu, Pb with the thickness of 0.1 λ int. were exposed. Some interesting results have been obtained in the energy region of 0.1 ÷ 5.0 TeV using the data of several thousand of events.

Here the results of the investigation of interactions with the energy above 0.9 TeV are presented. The selected events have been generated, mainly, by primary protons which have had passed through the atmosphere without any interactions. That condition has been achieved by means of selection of showers without of other particles accompanying ($n_{acc} \leq 0.3/m^2$ /6/.

The aim of the present investigation is to reveal the dominating mechanism of the secondary particle generation. In the present paper the experimental data are analyzed with respect to the variable $\eta' = -\ln \operatorname{tg} \theta_{pr}/2$, where θ_{pr} is the projection of the secondary particle escape angle on the photography plane.

The experimental data have been corrected for the efficiency of secondary particle recording in wide-gap spark

chambers (depending on the track direction with respect to the electric field) and for the conversion of γ -quanta due to π^0 -meson decay /7,8/, The resolution of the appatus does not allow us to make some definite conclusions on the particles generated within the angle interval narrower than 0.1° (i.e. at $\eta' > 6.5$). The experimental distributions given in Fig.1 take into account the corrections over the whole rapidity region excluding (0° ÷ 0.1°) where the uncertainty in the estimations may be significant.

The experimental distributions have been compared with the predictions of additive quark model /9/. According to the latter, the component interact independently with the cross-section equal to 1/3 of nucleon-nucleon one, while the generated objects do not interact within the nucleus. In addition, the comparison has been made with the active leader model, according to which the leading object interacts with nucleons, while the newly-generated particles do not interact in the nucleus: as it follows from Fig.1, a considerable discrepancy with the experimental data takes place. To achieve the agreement of theoretical predictions with the experimental data, one may: assume 1) a significant violation of scaling laws within the fragmentation region or a significant decrease of the cross-section of secondary interactions of the leading object (quarks, diquarks) with the nucleons in the nucleus; and 2) take into account the cascade of particles generated in the nucleus, which is, apparently, growing with increasing E. Table and Fig.2 present the data on the extent of the scaling violation increasing with the growth of A within the pionization region in hadron--hadron and hadron-nucleus interactions.

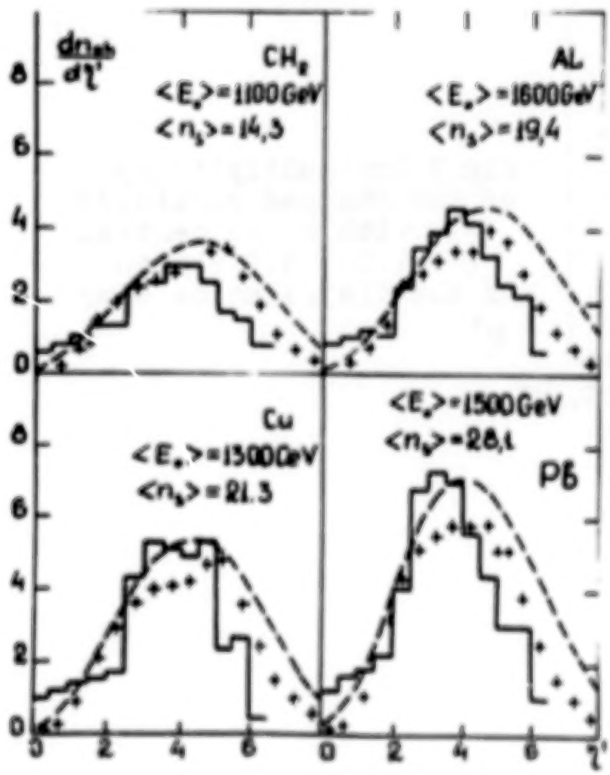


Fig.1 Inclusive distibutions over η' of secondary particles in hadron--hadron interactions. The histogram corresponds to the corrected data (see the text). Dotted line - the active leader model. Crosses-additive quark model with the shifts in distribution due to the errors in the determination of the primary particle direction, introduced by means of Monte-Carlo method.

Table

Reaction	Δn_s in the interval $\Delta\eta' = 2$ in the vicinity of $\eta' = 4$		$R = \frac{\Delta n_s(2.0)}{\Delta n_s(0.2)}$
	0.2 TeV	2.0 TeV	
pH	2.8 ± 0.1	4.0 ± 0.1	1.42 ± 0.08
pCH_2	3.9 ± 0.3	5.4 ± 0.6	1.38 ± 0.28
pH	4.2 ± 0.4	8.1 ± 1.0	1.93 ± 0.42
pC	4.0 ± 0.4	10.3 ± 1.1	2.58 ± 0.53
pPb	4.8 ± 0.5	12.1 ± 1.2	2.52 ± 0.51

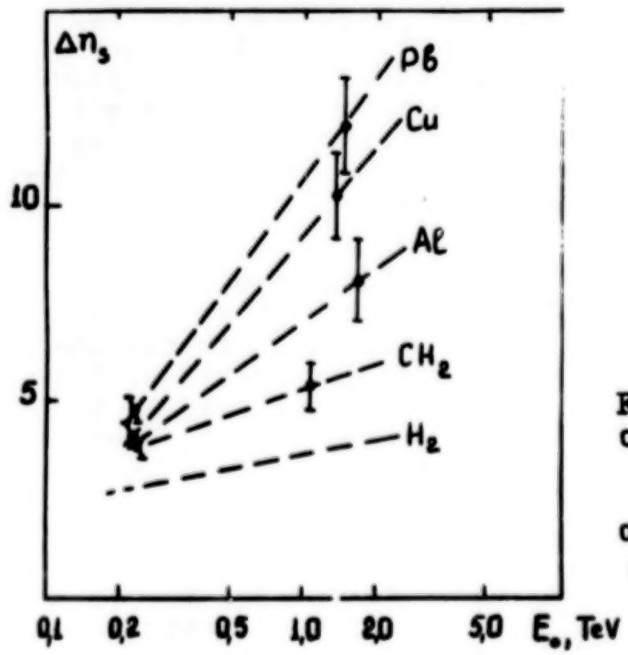


Fig.2 The multiplicity of the charged particles Δn_s within the central $\eta' = 4.0 - 1.0$ region of the distribution over η'

References

1. M.I.Atanelishvili et al., Izvestiya Akad.Nauk SSSR, 42, No.7, 1479 (1978)

2. M.I.Atanelishvili et al., Yadernaya Fizika, 24, 369 (1976)

3. O.L.Berdzenishvili et al., Bangalore, India XYIII YCRC HE 3-18 L.P., p.51 (1983)

4. M.I.Atanelishvili et al., Plovdiv XY ICRC, HE 7, p.66 (1977)

5. O.L.Berdzenishvili et al., Kioto XYI ICRC, HE 3-43, p.210 (1979)

6. O.L.Berdzenishvili et al., Kioto, XYI ICRC, HE 3-43, p.337 (1979)

7. D.M.Kotlyarevski. Pis'ma v JETF, 28, 4, 254 (1978)

8. K.G.Gulyamov et al. In: "Multiple Generation of Particles in pA-Interactions", ed. FTI of Izv.SSR, Tashkent, 78 (1976)

9. Yu.M.Shabel'ski, Proc XIII School of the LNPI, Leningrad, 90 (1978)

N85-35917

FEW-PARTICLES GENERATION CHANNELS IN INELASTIC HADRON-NUCLEAR INTERACTIONS AT ENERGY ≃ 400 GeV

Tsomaya P.V.

Institute of Physics, Academy of Sciences of the Georgian SSR, Tbilisi, USSR

Abstract. On the basis of experimental data obtained at "Tskhra-Tskaro" installation we investigate the behaviour of the few-particles generation channels in interaction of hadrons with nuclei of CH_2, Al, Cu and Pb at mean energy 400 GeV. The values of coherent prodiction cross-sections σ_{coh} at the investigated nuclei are given. A dependence of coherent and noncoherent events is investigated. The obtained results are compared with the simulations on additive quark model (AQM).

The presented data were found experimentally on G.Chikovani mountain cosmic rays station "Tskhra-Tskaro" (atmosphere depch ≃ 760 g/cm^2).

The installation consists of magnetic spark spectrometer and ionizational calorimeter /1/. We've got and analyseal about three thousands of hadron nuclear interactions in CH_2, Al, Cu and Pb targets.

The incoming hadrons flux consisted of 27% of pions and 73% of nucleons /1/. To estimate the multiplicity interval n_s where the contribution of coherent events was the most essential the angular distribution for various intervals were tested by means of dispersional analysis using F-criterion /2/. Such analysis is possible due to more narrow angular distribution of coherent generation particles events comparing with the rest ones. We found that multiplicity interval is equal to: $n_s = 3 \div 5$. On the other intervals n_s the coherent generation event contribution was less than

5%. We must note here that because of different methodical effects the events was $n_s < 3$ were not taken into consideration /1/.

The most simple and generally accepted criterian of coherent production on nuclei processes selection was the criterion /3/:

$$\sum_i \sin\theta_i \leq A^{-1/3}$$

where θ_i is the angle of produced particle.

This criterion is necessary because of the small impulse value transferred to the nucleus target in these processes. The most of multiplicity production events fit this condition as the secondary events distribution becomes more narrow with the increase of primary energy. That's why this background should be taken into account. It can be evaluated starting of com the fact that up to the mean multiplicity the hadron in nucleus interacts only with a nucleon. This can be seen from Fig.1 where we give a probability of fixed multiplicity production n_s on the nucleus as a function of the same probability in pp-interaction. We see that up to $\langle n_s \rangle$ this function doesn't depend on atomic number and is equal to ~ 1. That's why the events, concerning the investigations with only one nucleon which satisfies this criterion were subtracted.

For this we used the data on pp-interaction at energy of 400 GeV /4/.

The selection results are given in the Table where we also give a full statistics of the observed events.

Table

Nucleus	A full number of interactions	A number of coherent events	A number of ninco-herent events	σ_{coh}, mb (n_s=3÷5)
CH_2	589	26	95	9 ± 2
Al	680	27	77	16 ± 3
Cu	1173	50	110	33 ± 5
Pb	457	11	41	40 ± 12

ORIGINAL PAGE IS
OF POOR QUALITY

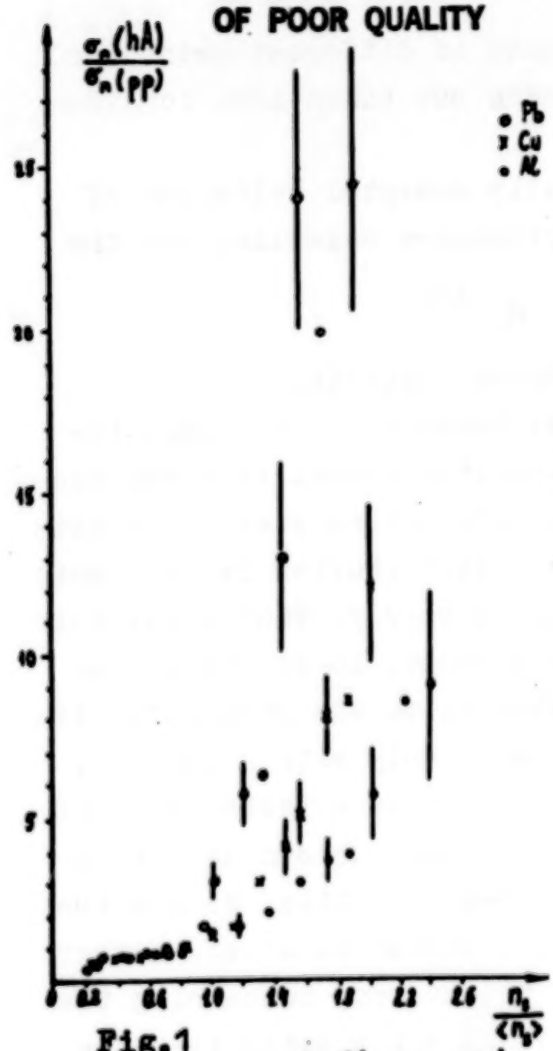


Fig.1

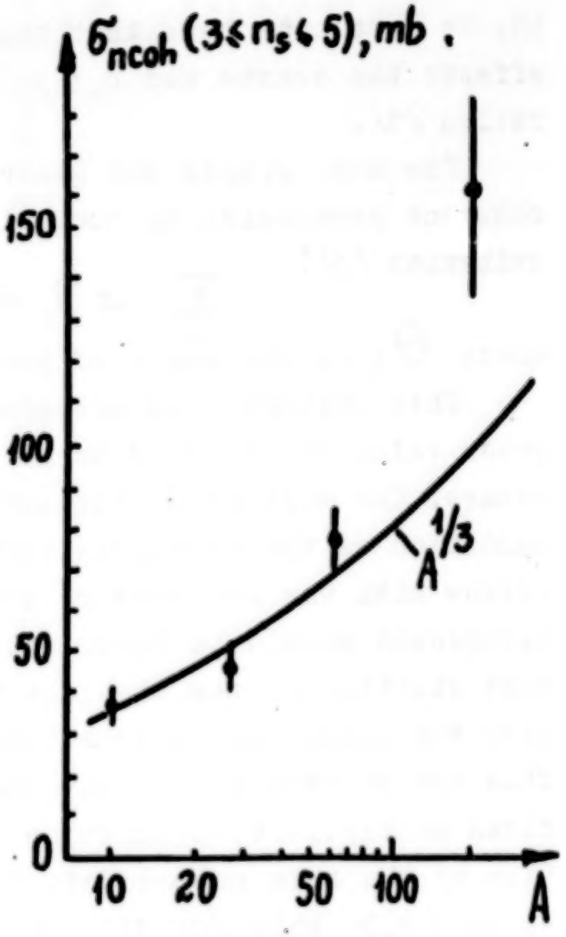


Fig.2

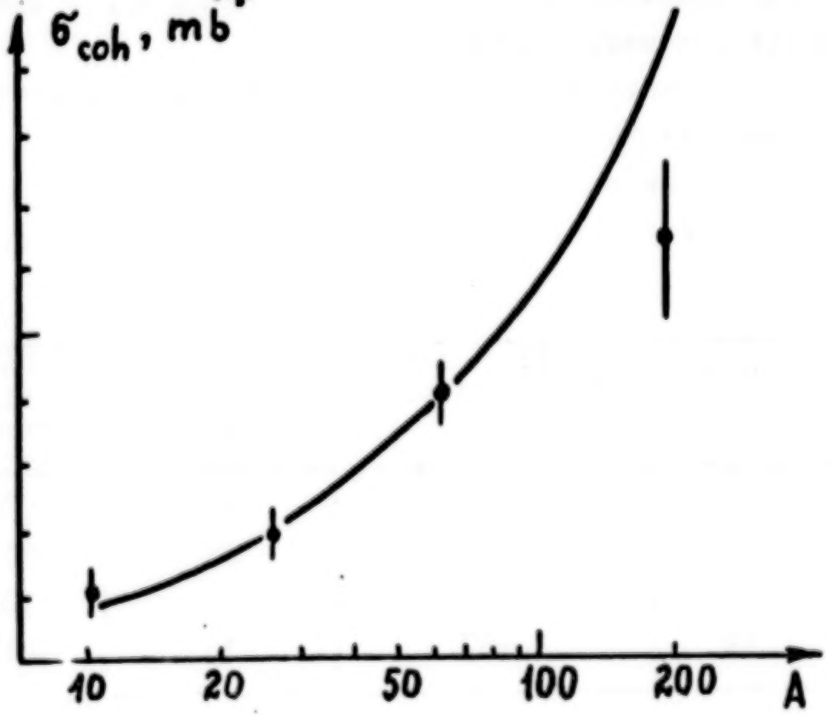


Fig.3

N85-32318

With the help of experimental data for $n_s < 3/5/$ the received values of $\sigma_{coh}(n_s = 3 \div 5)$ were restored to the full ones and compared with theoretical simulation on additive quark model results /6/ . This comparison is diven in Fig.2. We see that AQM describes light intermediat nuclei rather well and σ_{coh} isn't in accordence with simulation

On Fig.3 we've plotted the noncoherent events (witch $n_s = 3 \div 5$) depenedevce on atomic number. The curve corresponds to $A^{1/3}$ parametrisation. Such a dependence suggests a particle production at the nucleus edge. It can be seen from Fig. that this suggestion is true for light and intermediate nuclei.

The behaviour on Pb nucleus for coherent and noncoherent processes, evidently, is the consequence of the fact that "passive" quark states on heavy nuclei introduced into AQM manage to transform into active ones. This reduces coherent probability and respectively increases noncoherent events probabily.

References.

1. M.I.Atanelishvili et al. Izvestiya Akad.Nauk SSSR, 42, 1479, (1978)
2. S.A.Azimov et al. In: "Many Particles Processes at High Energies" ed. FTI of Izv.SSR (1976)
3. C.M.Fisher, W.H.Gibson et al. Nuov. Cim., 27, 761(1963)
4. Leningrad-Moscow-Gatchina-Tashkent Collaboration (Russian) Preprint IFHE 75-79, Akad.Nauk Kazakh.SSR, (1979)
5. W.Mollet, I.Biel, T.Ferbel. Phys.Rev.Lett., 39, 1646, (1977)
6. V.M.Brown, Yu.M.Shabelski. YaF, 37, 1011(1983)

N85-35918
HE 3.2-10

THE MODEL OF INDEPENDENT PARTICLES EMISSION IN THE MULTIPARTICLE PRODUCTION THEORY

V.V.Uchaikin, V.A.Litvinov
Altai State University, Barnaul, USSR

ABSTRACT

It is shown, that it is possible to obtain the degree dependence of average multiplicity from energy, KNO-scaling and the effect of leading , taking into account the law of energy preservation.

The following model of multiple process is offered for discussion. Particles are born independently of each other from some distribution $f(E)$, but a chance set of $E_1, \dots, E_n$ turns into realization of the multiple process only under the condition, that the sum

$$S_n = \sum_{i=1}^{n} E_i$$

will fall into the small interval ΔE_0 about E_0 (primary energy). The density of distribution $f(E)$ is assumed to be independent of E_0 .

The distribution of the thus obtained events on multiplicity n will be:

$$P_n = \mathrm{Prob}\{S_n \in \Delta E_0\} / \sum_n \mathrm{Prob}\{S_n \in \Delta E_0\} = f_n(E_0) / \sum_n f_n(E_0), \qquad (1)$$

where

$$f_n(E) = \underbrace{f(E) * f(E) * \dots * f(E)}_{n}$$

is fold single particle distributions. From the theory of probabilities it is known that if the second distribution $f(E)$ moment exists, then the sum S_n is distributed according to the normal law:

$$f_n(E) \sim \frac{1}{\sqrt{2\pi n}\,\sigma} \exp\left\{-\frac{(E-n\bar{E})^2}{2n\sigma^2}\right\}, \quad n \to \infty, \qquad (2)$$

where

$$\bar{E} = \int_0^\infty E f(E) dE, \quad \sigma^2 = \int_0^\infty E^2 f(E) dE - \bar{E}^2.$$

It is clear from here that the maximum of distribution falls on

$$\tilde{n} \sim E_0/\bar{E} \tag{3}$$

and the relative distribution width is

$$\Delta n/\tilde{n} \sim (\sigma/\bar{E})\tilde{n}^{-1/2}. \tag{4}$$

Thus, in this case we have the linear increase of the average multiplicity and the decrease of relative fluctuation according to the Poisson's law - both are inconsistent with the character of multiple processes.

Another case is discussed in the theory of probability too: when no second and even first moments of distribution $f(E)$ exist [1,2].

If that satisfies the condition

$$\int_E^\infty f(E')dE' \sim a E^{-\alpha}, \quad E \to \infty, \quad \alpha \in (0,2), \tag{5}$$

then instead of (2) there is a tendency to the stable law with the index α and parameter $\beta = 1$ (for positive random values)

$$\text{Prob}\left\{ \frac{S_n}{B_n} - A_n < x \right\} \Rightarrow G(x, \alpha, 1),$$

here

$$B_n = [\alpha a n]^{1/\alpha}$$

and A_n is determined by the index α. For $\alpha > 1$ the first moment exists and can be used for centering consequence $A_n = n\bar{E}/B_n$, for $\alpha = 1$ $A_n \sim \ln n$ and for $\alpha < 1$ $A_n = 0$ [3].
Using this result for each of these cases, we obtain:

$$\alpha > 1: \quad \tilde{n} \sim E_0, \quad \Delta n/\tilde{n} \sim \tilde{n}^{\frac{1}{\alpha}-1}; \tag{6}$$

$$\alpha = 1: \quad \tilde{n} \ln \tilde{n} \sim E_0, \quad \Delta n/\tilde{n} \sim [\ln \tilde{n}]^{-1}; \tag{7}$$

$$\alpha < 1: \quad \tilde{n} \sim E_0^\alpha, \quad \Delta n/\tilde{n} \to \text{const} \neq 0. \tag{8}$$

From here it is clear, that at $\alpha \in (1,2)$, when only the second moment doesn't exist $\tilde{n}$ is proportional E_0, although the relative fluctuations decrease at a slower rate; at $\alpha = 1$

when the first moment ceases to exist, the linear dependence $\bar{n}(\varepsilon_0)$ is violated and the decrease of fluctuations is slow, untill finally at $\alpha<1$ the dependence of multiplicity from ε acquires a degree character (with index α), and the distribution width of quantity ($n/\bar{n}$) stops to change with the increase of energy. Thus, at $\alpha<1$ we find the characteristic features of the multiple processes.

At $\alpha=1/2$, the analytical form of density of the stable law is

$$g(x,\alpha,1) = G'(x,\alpha,1) = \frac{1}{2\sqrt{\pi}}\, x^{-3/2} e^{-1/4x}$$

leading to one of the known approximation KNO-distribution

$$\psi(z) = \frac{\pi z}{2}\, e^{-\pi z^2/4}$$

and the average multiplicity $\bar{n} \sim \varepsilon_0^{1/2}$, which doesn't disagree the experiment (if ε_0 means the energy of the particles in the center-of-mass system).

For more detailed study of the given model, a Monte-Carlo simulation was carried out with the distribution function:

$$f(\varepsilon) = \begin{cases} \alpha \varepsilon^{-\alpha-1}, & \varepsilon \geq 1, \\ 0, & \varepsilon < 1, \end{cases}$$

$\alpha = 1/4, 1/2, 1, 2, 4.$

Results are shown in fig.1-3. Besides the confirmation of the above theoretical conclusions (3-8), it is clear from these calculation, that at $\alpha<1$ there exists a particle separated by energy, which carries away about a half all the energy of the born particles (effect of leading), and the distribution along the variable $z = n/\bar{n}$ has the typical form of KNO distribution and doesn't depend from primary energy (KNO-scaling). This circumstance, in particular, may be used for the working out of the simple algorithm for simulation the act of multipartical production by Monte-Carlo method in calculations of extensive air showers and perhaps, is of interest to the theory of multiparticle production.

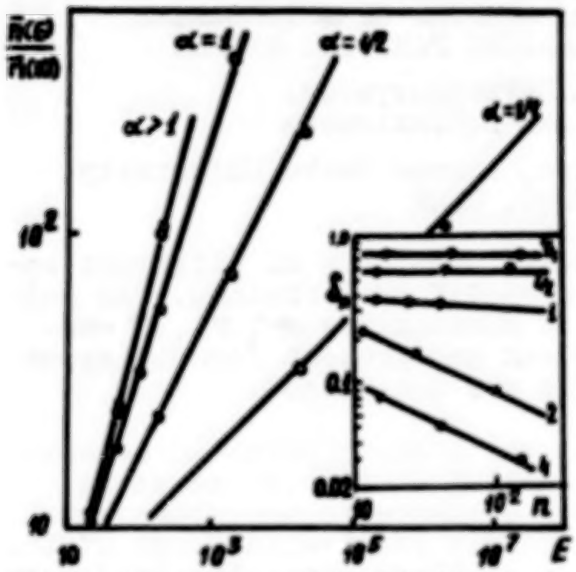


Fig.1.Average multiplicity and relative fluctuations.

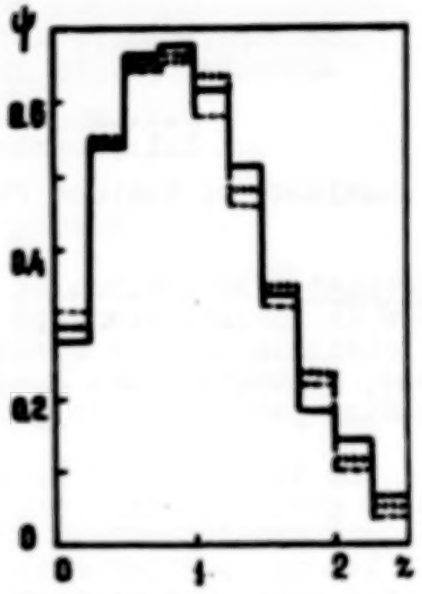


Fig.2.Distributions of multiplicity for E_{01}, $E_{02} = 10E_{01}$, $E_{03} = 100E_{01}$ ($\alpha = 1/2$)

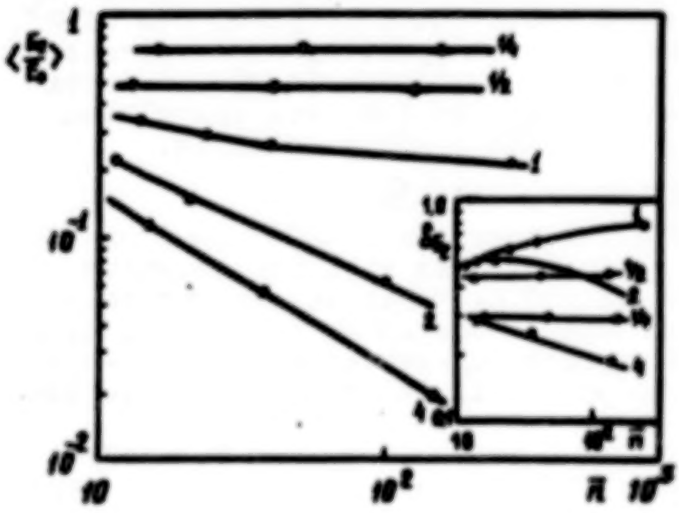


Fig.3.Average value and relative fluctuations of the leading particle energy.

References:

1.Gnedenko B.V., Kolmogorov A.N. Limit distributions for sums independence random values. Moscow, Gostehizdat, 1949, 264 p.

2.Zolotarev V.M. One dimensional stable distributions. Moscow, Nauka, 1983, 304 p.

3.Borovkov A.A. The theory probability lectures. Moskow, Nauka, 1972, 287 p.

N85-35919
HE 3.2-11

THE MULTIPLICITY AND THE SPECTRA OF SECONDARIES CORRELATED WITH THE LEADING PARTICLE ENERGY

N.A.Kruglov, A.S.Proskuryakov,
L.I.Sarycheva and L.N.Smirnova

Institute of Nuclear Physics, Moscow State University,
Moscow II9899, USSR

Abstract. The spectra of leading particles of different nature in pp-collisions at E_0 = 33 GeV are obtained. The multiplicities and the spectra of secondaries π^0, π^-, K^0-mesons, γ-quants, Λ and $\bar{\Lambda}$-hyperons and protons for different leading particle energy ranges are determined.

The interactions in which the leading particle conserves a great fraction of the initial energy are essential for the development of nuclear cascades in the atmosphere. The leading particles form a deeply propagating part of the cosmic rays. The accompaniment of these particles is determined by the peculiarities of the low-inelasticity interactions. Besides, the events with a leading particle are reliably identified in the cosmic-ray detectors.

The main information on the multiple production of particles obtained from accelerators, is averaged over all types of events. This paper reports the multiplicities of π^+, π^-, γ, K^0, Λ and $\bar{\Lambda}$-particles, the partial coefficients of inelasticity and the spectra of particles in $p\bar{p}$-interactions at E_0 = 33 GeV in the lab.system that are correlated with the origin and energy of the leading particle.

The experimental conditions

The experimental material consists of 200 thousands of inelastic interactions of antiprotons with the momentum 32 GeV/c observed in the liquid hydrogen Mirabelle bubble chamber. The large dimensions of the chamber provided high detection efficiency of photons, K^0_S-mesons and $\Lambda/\bar{\Lambda}$-hyperons. We use the events where all charged tracks are measured.

For the particles with the momentum $p_{lab} < 1.2$ GeV/c the protons were discriminated from the π^+-mesons by comparing track ionization. Neutrons and antineutrons are the only unobservable species in the chamber. Their mean characteristics are restored proceeding from the condition of energy balance /I/. In the present paper all inelastic interactions are analyzed in the system of an incident antiproton which will be mark in following as lab-system. This choice of system enabled us to establish the nature of a leading particle with the fraction of initial energy $x_{lead} = E/E_0 \geq 0.4$.

Classification of events

The particle carrying away the maximum, as compared with other particles, fraction of energy in the lab.system in an event is assumed to be the leading particle. When

ORIGINAL PAGE IS
OF POOR QUALITY

the total energy of unobservable neutral particles exceeds the energy of the leading particle, a neutral system X^0 is regarded to be the leader. Table I presents the cross sections of the events with the leading particle of different nature in different ranges of u_{lead}.

Table I

The cross sections of the picked out classes of interactions σ, mb

leader	leading energy ranges u_{lead}		
	0.4 - 0.6	0.6 - 0.8	0.8 - I.0
p	2.83 ± 0.03	3.43 ± 0.03	3.55 ± 0.I5
π^+	I.23 ± 0.02	0.23 ± 0.0I	0.0I5 ± 0.002
π^-	0.59 ± 0.0I	0.084 ± 0.005	0.007 ± 0.002
X^0	7.46 ± 0.04	6.78 ± 0.03	4.49 ± 0.03
Λ	0.35 ± 0.04	0.24 ± 0.03	0.07 ± 0.02
γ	0.I5 ± 0.09	0.0I7 ± 0.0I5	0.004 ± 0.004
K^0_s	0.09 ± 0.02	0.007 ± 0.005	-

$\sigma^{p\bar{p}}_{tot}(32^{Gev/c}) = 45.6 \pm 0.3$ mb, $\sigma^{p\bar{p}}_{in} = 37.2 \pm 0.5$ mb, $\sigma^{p\bar{p}}_{nonann} = 30.7 \pm 0.5$ mb /2/.

The events with the leader p, π^+, π^- and $u_{lead} \geq 0.4$ make up I2 mb, i.e. (32 ± 0.4)% of the inelastic $p\bar{p}$-cross section. The events with the leaders Λ, γ, K^0 (= $K^0 + \bar{K}^0$) at $u_{lead} \geq 0.4$ with the cross section I.04 ± 0.II mb are observed.

The total energy of the particles attending the charged and neutral leader is presented in units of $u = \Sigma E_i/E_0$ in fig.I. It is seen that the taking account of $\langle u_{lead} \rangle$ in the events with the charged leader permitted the complete recovery of the interaction energy. The measured fraction of energy of the attending particles in the events with the leader X^0 is higher as compared with the events with the p and $\pi^\pm$-leader. In this case according to the selection criteria a fraction of energy of the neutral leader X^0 is carried by photons and the mean value of this energy is measured in the chamber for each group of events. The unobservable energy is carried away by an outgoing neutron. The mean fraction of this energy is indicated in fig.I. Consequently, the class of events with the leader X^0 contains mainly the events with a leading neutron. The groups with u_{lead} (X^0) ≥ 0.6 correspond to the events with $u_{lead}(n) \geq 0.4$, since the mean value of α_γ in these events is ≤ 0.2. The events with the leader X^0 and $u_{lead} \geq 0.6$ are considered in what follows as two groups of events with a leading neutron: $\langle u_{lead} \rangle = 0.78 \pm 0.01$ and 0.50 ± 0.01. The cross sections of the events with a leading proton and neutron with $u_{lead} \geq 0.4$ are actually the same. This means that the leader in (68.8 ± 0.5)% of the nonannihilation $p\bar{p}$-interactions is a nucleon with $u_{lead} \geq 0.4$.

In fig.I there is no evidence for a fast neutron in the events with the $\pi^\pm$-leader and we therefore conclude that these events are mainly due to the $p\bar{p}$-annihilation. The cross sections of the events are in accord with this conclusion.

ORIGINAL PAGE IS
OF POOR QUALITY

Experimental Results

The spectrum of leading protons is uniform within $u_{lead} = 0.5 \div 0.9$ /2/. The spectra of leading $\pi^{\pm}$ and $K^{\pm}$-mesons with $u_{lead} \geq 0.5$ decrease with increasing u_{lead} and are described by the function $A_{exp}(-B u^2_{lead})$ with the parameters $B_{\pi^+} = 12.4 \pm 0.9$ and $B_{\pi^-} = 12.6 \pm 0.4$. To the spectrum of leading Λ with $u_{lead} \geq 0.5$ there corresponds the parameter $B_{\Lambda} = 8.1 \pm 0.3$.

The total multiplicity of the particles attending the leading p, n, π^+, π^-, Λ is shown in fig.2a. The right scale shows the ratio of the observed multiplicity to the estimated total multiplicity $\langle n_{tot} - 1 \rangle$ for pp-interactions at 32 GeV/c /3/. It is seen that at u_{lead} close to 0.5 the multiplicity reaches the mean value.

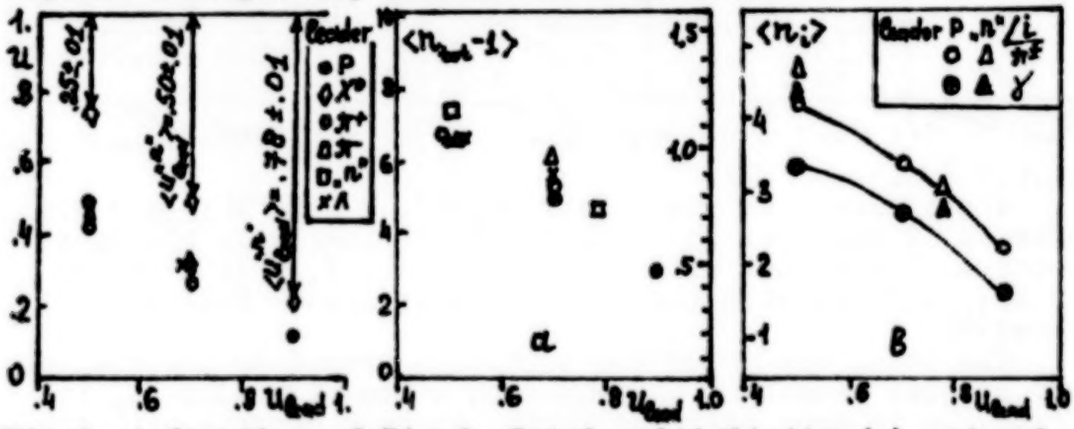


Fig.I. A fraction of the measured energy in the events with different leaders

Fig.2. Total multiplicity (a) and multiplicity of the attending particles of species i (b) for different leaders

The multiplicity of $\pi^{\pm}$ and $K^{\pm}$-mesons and photons attending the leading nucleon is shown in fig.2b. The total multiplicity of $\pi^{\pm}$-mesons is similar in the events with a leading proton and "neutron". The value of $\langle n_{\gamma} \rangle$ proves to be higher for a leading "neutron" which can be connected with the identification procedure used.

The mean fraction of energy carried away by the attending π^+, π^-, $K^{\pm}$, γ is shown in fig.3. The mean fraction of energy per π^+ and γ is the same whether the leader is a proton or a "neutron". The total fraction of energy carried away by these particles is plotted in fig.4 versus u_{lead} of a proton and "neutron".

The spectra of the attending particles are rather complex and concentrated in the region of low u for high u_{lead}. The parameters of the function describing these spectra are listed in table 2.

In the events with a leading proton a great fraction of the "invisible" energy carried away by the photons. In this case $\Sigma E_{\gamma} \approx E_0 - \Sigma E_{\pm} - \Sigma E_{K^{\pm}, \Lambda/\pi}$ and the spectrum of photons can be obtained from the variable $u_{\gamma} = E_{\gamma}/\Sigma E_{\gamma}$ used in the cosmic rays. The spectra $d\sigma/du_{\gamma}$ are presented in fig. 5

N85-35920

ORIGINAL PAGE IS
OF POOR QUALITY

for the events with a leading proton at $u_{lead} > 0.8$ and $u_{lead} = 0.4 \div 0.8$.

Table 2

Parametrization of the spectra of the particles attending the leading protons and "Neutrons" by the function $f = u^N \exp(-B1\,u - B2\,u^2)$

leader	u_{lead}	type of a secondary particles	N	B1	B2
p	0.4–0.6	π^+	-I.00±0.0I	-5.5 ±0.3	22.6±0.6
		π^-	-I.6I±0.0I	-7.5I±0.07	24.6±0.3
		γ	0.027±0.0I4	34.3 ±2.6	-9.0±I3.6
	0.6–0.8	π^+	-I.3I±0.06	-II.0±I.3	4I ± 2
		π^-	-I.85±0.0I	-7.9I±0.08	32.5±0.4
		γ	0.027±0.0I4	44.I ±2.3	-28 ±I0
	0.8–I.0	π^+	-0.2I±0.0I	3I.0 ±0.9	-I5.6±5.4
		π^-	-2.62±0.0I	I0.8 ±0.2	-6.7±I.4
		γ	-I.I5±0.05	32.5 ±I.8	58.3±6.3
Λ^0	0.6–0.8 $\langle u_{\Lambda^0}\rangle$=0.50 ±0.01	π^+	-I.25±0.02	-I4.9±0.4	54.8±0.7
		π^-	-I.20±0.05	-2.3 ±I.I	39.8±2.3
		γ	-2.4I±0.02	-20.2±I.3	83.4±8.4
("n")	0.8–I.0 $\langle u_{"n"}\rangle$=0.78 ±0.01	π^+	-2.66±0.0I	64.0±0.I	287.4±0.9
		π^-	-I.98±0.0I	-20.I±I.0	I79 ±7.8
		γ	-2.3 ±0.I	-I7.2±4.3	83.4±8.4

References:
1. Vinitskii A.A. et al., Sov.Journ.Nucl.Phys., I984, 40,474.
2. Hanumejah B. et al. Nuovo Cim., I982, 68A, I6I; I7 ICR, I98I, HE I-7, v.5, p.22.
3. Nikitaev D.N., Smirnova L.N. Sov.Journ.Nucl.Phys.,I985, 4I, No.3.

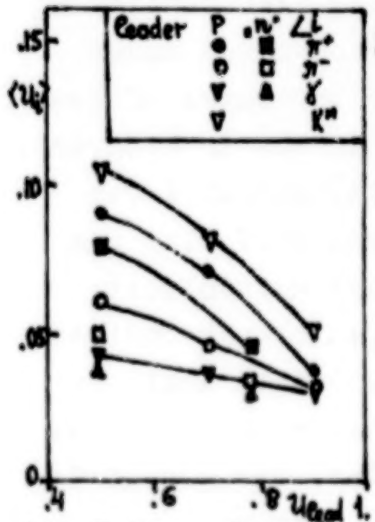


Fig.3.Mean fraction of energy per particle of species i for different leaders

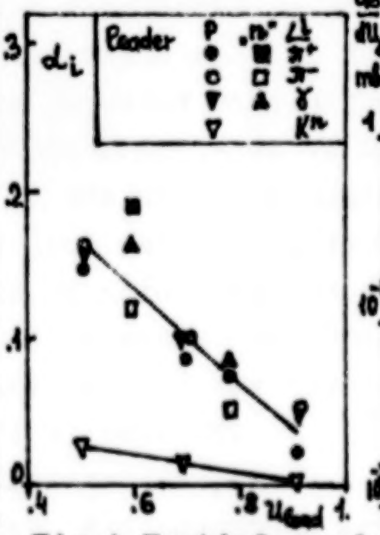


Fig.4.Partial coefficients of inelasticity of particles α_i for different leaders: $\alpha_i = \langle u_i \rangle \langle n_i \rangle$

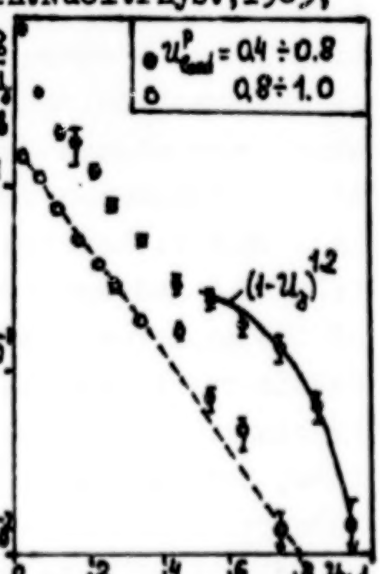


Fig.5.Spectra of γ in $u_\gamma = E_\gamma / \Sigma E_\gamma$ for the events with a leading proton

N85-35920
HE 3.3-I

CHARACTERISTICS OF ANOMALOUSLY HIGH MULTIPLICITY COSMIC RAY INTERACTIONS.

I.Ya.Chasnikov, Yu.A.Eremenko, D.T.Madigozhin,
T.Kh.Sadykov, V.G.Voinov
HEPI of Kazakh Academy of Sciences, Alma-Ata, USSR

Six events with the number of secondaries ranging from 250 to several thousands have been registered by means of the installation consisting of a thin graphite target above and under which were placed photolayers followed by the usual lead X-ray film and emulsion chambers. Data concerning the number of secondaries and their angular distribution are given. A comparison of the variance of the angular distribution with that obtained at accelerator energies is made.

It was planned to create the experimental installation described in paper [I] at cosmic ray station (3340 m above sea level) of HEPI of Kazakh Academy of Sciences. The altered version of such full-automatic installation has been created in 1984 [2] . It consists of a replaceable target, the X-ray film and emulsion chambers (XREC) and of the ionization calorimeter (total absorber spectrometer) with the area being equal to 44 m^2. While this installation was putting into the operation an experiment using XREC consisting of the graphite target of 5 cm thickness above and under which were placed photolayers followed by the layer of lead of 3 cm thickness and by other photopackets was in progress. Each photopacket contained two sheets of bilateral X-ray film RT-6 and one sheet of nuclear emulsion R-2T. The aim of the experiment was the searching of high multiplicity cosmic ray interactions the existence of which was indirectly confirmed by extensive air showers (EAS) data analysis (see, for instance, [3]). The idea of this experiment has been proposed in [4] , where, in particular, the ground for the choice of a target thickness has been made.

The total exposure time and the area of the installation are equal to 83.8 m^2 year. Under the target we have registered 6 dark spots which could not be explained by trivial

reasons: mechanical action on the X-ray films or electrization processes. The fact that the spots are formed by charged relativistic particles is confirmed by the examination of nuclear emulsion under a microscope. One does not able to find by the naked eye any dark spots on the X-ray film placed above the target. This means, that if there exists some microstructure of EAS, the particle density will be less than 200 particles per I mm^2. At present only the photomaterial placed under the target has been treated utterly.

The scanning of X-ray films was performed by means of laser beam of 20 microns in diameter on the special installation created at HEPI of Kazakh Academy of Sciences [5]. The calibration of readings (calculation of darkness density and charged particles density) was made by control X-ray film which were obtained by fixed flux of charged particles from a radioactive source, by dark spots from electromagnetic cascades with known darkness density, and also by direct comparison of readings with the number of particles registered in nuclear emulsion. Some characteristics of the events found are given in the table.

Table.

I	2	3	4	5	6
240	750	3800	I040	2500	950
0.4±.08	0.32±.08	0.48±.06	0.3I±.07	0.35±.06	0.33±.07

The number of particles in the spots was evaluated by the dependence of their number $N(\leqslant R)$ in a circle of radius R on the value of R (Fig.I). The variance of the angular distribution has been found as follows. If H is the height from the generation point to the observation level, R_i - is the distance of i-th particle from the centre of gravity of all secondaries, then $R_i/H \; tg\theta_i$, where θ_i is the emission angle of i-th particle in the laboratory system, and $\log R = \log \tan \theta_i + \log H$ distribution is actually the angular distribution of secondary particles in $\log \tan \theta_i$ coordinates displaced for the given event by the constant value

log H (Fig.2).

If the registered dark spots are actually the result of inelastic interactions, then one can evaluate the lowest limit for primary energy. Considering the secondaries as pions and assuming that the coefficient of inelasticity is equal to unit as well as that transverse and longitudinal momenta in CMS are equal, we get $E_{o\ min} \gtrsim 800$ Tev, if $P_{\perp}=0.4$ GeV/c.

Fig.3 shows the dependence of the variance δ of the angular distribution on primary energies according to the data of [6].

The value of the variance of the summarized angular distribution for all six events is also shown. Fig.4 gives the dependence of δ on the multiplicity of secondaries $n_{\pm}$ at 200 GeV and at more high energy. One can see, that δ -values do not depend within experimental errors on the multiplicity of secondaries, but they are systematically lower than those at our energies. We emphasize once again that if the observed dark spots in X-ray film are produced by inelastic interactions in the target, then these events not only confirm the existence of high multiplicity inelastic interactions, but also show that the variance of the angular distribution of secondaries can be essentially changed at superhigh primary energy.

The analysis of such events will of course be continued.

References

1. Buya S., Dobrotin N.A., Takibaev Zh.S. et al. Preprint of the institute of Nuclear Physics, N I00, Alma-Ata, I969.
2. Alibekov M.I., Baigubekov A.S., Eremenko Ju.A. et al. Preprint HEPI, N 84-09, Alma-Ata, I984.
3. Nickolsky S.I. "Proc. of Intern. Seminar on high energy Physics problems", Dubna, I978, P I60.
4. Eremenko Yu.A., Lukin Yu.T., Sadykov T.Kh., Preprint HEPI N 8I-I2, Alma-Ata, I98I.
5. Voinov V.G., Kuntukov E.Yu., Chasnikov I.Ya. et al. Preprint HEPI, N 84-26, Alma-Ata, I984.
6. Eremenko L.E., Chasnikov I.Ya., Shahova Z.I., Preprint HEPI, N 65-78, Alma-Ata, I978.

N85-35021

ORIGINAL PAGE IS
OF POOR QUALITY

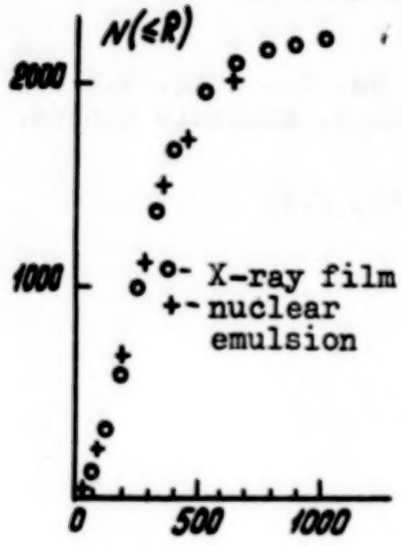


Fig .I

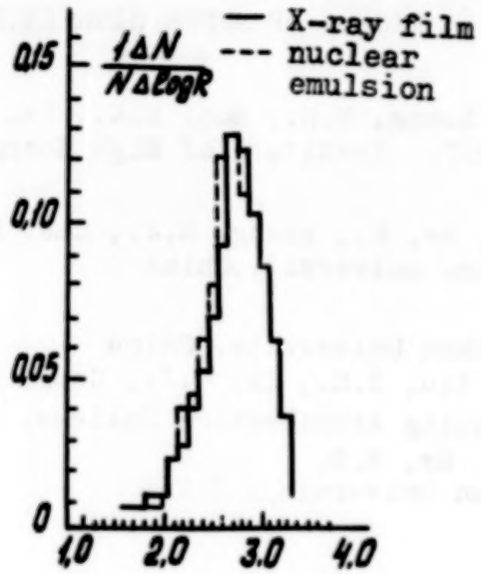


Fig.2

Fig.2. The angular distribution of charged particles for one of the events.

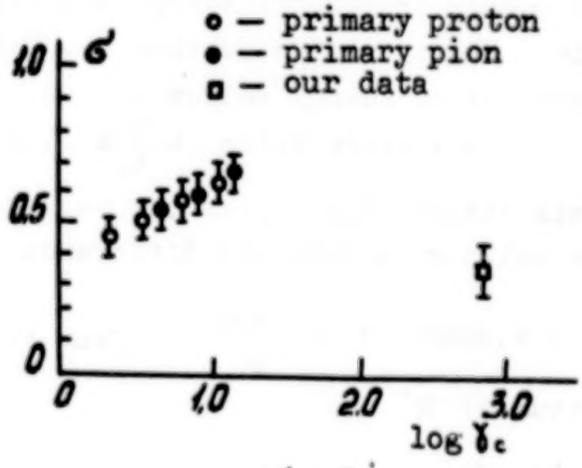


Fig.3

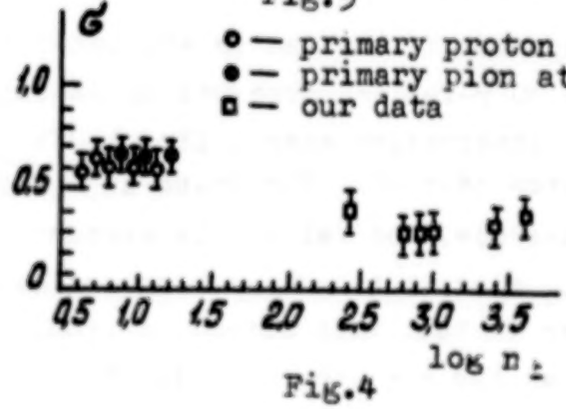


Fig.4

N85-35921

ORIGINAL PAGE IS
OF POOR QUALITY

TRANSVERSE MOMENTUM DISTRIBUTION OF π^0 IN THE FRAGMENTATION REGION OF SUPER HIGH ENERGY INTERACTIONS

Ren, J.R., Kuang, H.H., Huo, A.X., Lu, S.L., Su. S., Wang, Y.X., Xue, Y.G. Institute of High Energy Physics, Academia Sinica, China

Wang, C.R., He, M., zhang, N.J., Cao, P.Y., Li, J.Y.
Shandong university,China

Wang, S.Z.
Zhengzhou University, China

Bai, G.Z., Liu, Z.H., Li, G.J., Geng, Q.X.
Chongqing Architecture College, China

Zhou, W.D., He, R.D.
Yunnan University, China

The lateral distribution of γ-familige observed by emulsion chamber is sensitive to test transverse momentum of high energy interaction. But most part γ-families are succesive interation's resuts. so it is necessary to analyse the propagation of γ-ray in atmosphere. A γ-ray with energy Er and transverse momentum Pt is producted at the altitude h above the observation level (Fig.1). After cascade, the total observation energy reduce to Eob, the $P_{tr} = \frac{REr}{h} = R E_{ob} (\frac{1}{h} \frac{Er}{E_{ob}})$. The arerage valne $\langle h \frac{E_{ob}}{E_r} \rangle$ has been calculated by Monte-Carlo simulation, Fig 2 give the relation between $\langle h \frac{Eob}{Er} \rangle$ and h. From h=1.5km to 30km and difference Er, the $\langle h \frac{E_{ob}}{Er} \rangle$ approximately is a constant, $\langle h \frac{Eob}{Er} \rangle \sim 1.7$km. From here, the transeverse momentum of π^0

$$Pt\pi^0 \simeq 2Ptr \simeq 2R\ Eob/1.7km. \qquad \langle 1 \rangle$$

In the emulsion chamber experiment, Eob can be estimated by decascade method. There are 30 γ-familes observed by Ganbala emulsion Chamber with total observation energy $\Sigma Er \geq 100$Tev and lateral spread $\langle ER \rangle \geq 15$Tev·cm selected. The value $Xij = \sqrt{EiEj}\ Rij \leq 2.5$Tev·cm is used to decasecade. the value R is meamed from energy center, then the $P_{t\pi^0}$ distribution have been estimated by use relation<1>, In order to test this method, a group of Monte-Carlo simulation γ-families are used to compare with

ORIGINAL PAGE IS
OF POOR QUALITY

experimental data by same treatment. Fig 3 shows both distributions are consistent and consistent with a result of another analysis 2 ,but they have some difference with the Pt distribution of the model--- $\frac{dn}{dP_t^2} \propto e^{-4.5P_t}$. It means the relation<1>is a approximate average, but Fig 3 shows only few π^0 are with large Pt value, the mean value <Pt>=0.46±0.3 in the E≥10^{15}ev and $\eta > 2.5$ regeon.

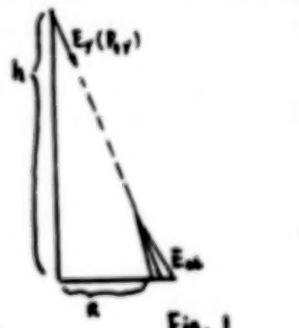


Fig. 1

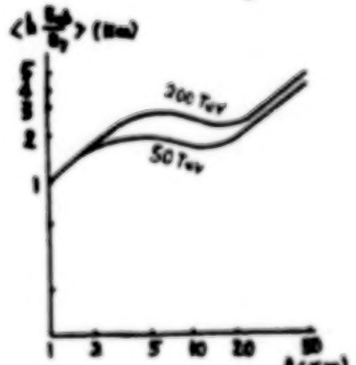


Fig. 2

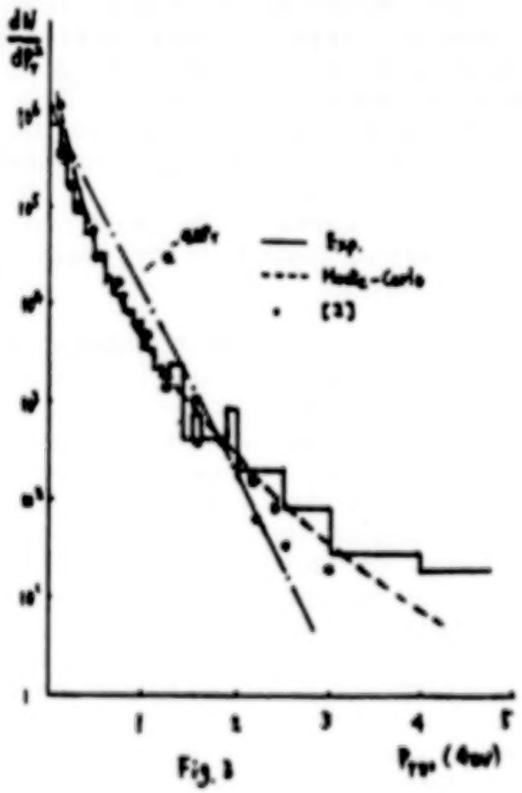


Fig. 3

Reference

[1] Jing et al.,This volume

[2] Huo et al.,Journal of Wuhan University,1983,p.45

N85-35922

HE 3.3-4

STUDY OF HADRON BUNDLES OBSERVED IN CHACALTAYA TWO-STORY EMULSION CHAMBER

AOKI,H.
SCIENCE AND ENGINEERING RESEARCH LAB.
WASEDA UNIV.
17, KIKUICHO, SHINJUKU-KU, TOKYO, JAPAN

1. INTRODUCTION

The existence of hadron-rich families associated with few gamma-ray emission named Centauro and Mini-Centauro phenomena was reported by Brasil-Japan collaboration.[1] Since,it is important to make clear whether these are produced by the special type of interaction different from the ordinary pion multiple production or not,a number of studies[2] have been made by various authors.

We have already presented the result of the systematic study of hadron bundles detected by Chacaltaya emulsion chamber No.15,17 and 18.[3]

In this paper the experimental results are compared with simulation calculation based on ordinary multiple pion production model.

2. EXPERIMENTAL PROCEDURE

We analyzed 172 blocks of the lower detector of each two-story emulsion chamber No.15,17 and 18.

Through the general scanning of X-ray films in the lower detector, we select parallel incident showers which pass through the upper chamber as hadron bundles, since such showers detected in lower chamber are originated by hadronic interactions in the chamber itself.

We studied core structure of showers in nuclear emulsion plates under microscope for all the detected X-ray film dark spots, and classify them into the following categories, (1) Pb-jet-upper with diffuse core structure, (2) C-jet with clean multi-core structure and (3) Pb-jet-lower with single collimated core structure.

We observed 90 hadron bundles in the present analysis. Among these hadron bundles, the following special events are included which were identified as Centauro I and IV, Mini-Centauro(7 events),and hadron-rich families(2 events).

Energies of showers are estimated by track-counting method for C-jets and by micro-photometry measurement for the others. The detection threshold energy was estimated around 2.0 TeV.

3. SIMULATION CALCULATION FOR HADRON BUNDLES.

In order to study hadron bundle phenomena originated from ordinary multiple pion production, a simulation calculation was carried out, based on the scaling model for nuclear interactions[4]

Two kinds of primary particles are assumed for the contrast, (a) proton primary and (b) iron nucleus, respectively. In both cases, the energy spectrum of primary particles is assumed to be $F(\geq E_0) \propto E_0^{-\beta}$ and the power index β is given

as 1.8 in integral form. The minimum energy of primary particle in the caluculation, E_{min}, is chosen as 500 TeV for proton primary and 1000 TeV for iron nucleus. The structure and geometry of Chacaltaya chamber is taken into account exactly. The unit of detection for hadron bundles is taken to be the size of one block of chamber 40cm×50cm. In order to adjust to the experimental conditions, the family center is randomely moved inside the size of one unit block. 76 hadron bundles ($N_h \geq 2$, $E_h \geq 1$ TeV) are obtained from 600 proton primaries and 36 from 600 iron primary.

4.COMPARISON

Fig.1 shows the differential distribution of observed multiplicity, N_h, for all hadron bundles (90 events). Simulation results (76 events) are shown by the dotted line in the same figure.

Fig.2 shows the differential distribution of $\langle E_h R \rangle$, and simulation results are shown by the dotted line in the same figure.

Fig.3 shows scattering plots of $\langle E_h R \rangle$ v.s. N_h, where • is simulation data based on proton primary, ✕ based on iron primary, ⊗ is Centauro events, ○ is Mini-Centauro events, ⊙ is hadron-rich families and ● is the other observed events.

5.CONCLUSION.

As is seen in Fig.1, both hadron multiplicity distribution, obtained from the present observation and the simulation calculation, show almost the same distribution in the range $0 \leq N_h \leq 8$. It means that hadron bundles of such smaller multiplicities are considered to be originated from successive interactions of surviving nucleon with the nature of multiple production during passing through the atmosphere. One cannot find, however, larger multiplicity hadron bundles, $N_h \geq 9$, in the simulation data.

Especially, Centauro I (N_h=27), Centauro IV (N_h=13) seems to be far beyond the fluctuation which is expected from the ordinary pion multiple production originated from proton primary.

Fig.2 shows similar tendency between the $\langle E_h R \rangle$ distribution obtained from the present observation and the simulation calculation in the range $0.80 < \langle E_h R \rangle < 6.7 \times 10$ TeV.cm . One cannot find, however, smaller $\langle E_h R \rangle$ hadron bundles, $\langle E_h R \rangle < 0.80$ Tev.cm, in the simulation data.

The comparison of scattering plots of $\langle E_h R \rangle$ v.s. N_h between the experimental results and the simulation data, based on proton and iron primary, shown in Fig.3 give the same conclusion. They are in the similar tendency, for the events with $N_h \leq 13$.

6.ACKNOWLEDGMENT.

The author would like to express his gratitude to all the members of Chacaltaya emulsion chamber collaboration, Prof.Y.Fujimoto and S.Hasegawa. In particular, to Prof.M. Sibata for his kind support.

ORIGINAL PAGE IS
OF POOR QUALITY

REFERENCES.

(1) C.M.G.Lattes et al, Phys. Report Vol.65, No.3 (1980)151
(2) A.S.Borisov et al, Proceeding of Workshops in La Paz Rio De Janeiro (1982)445
T.K.Gaisser and T.Stanev,Proceeding of Workshops in La Paz Rio De Janeiro (1982)281
B.S.Acharya et al, 16th Intern. Cosmic Ray Conf. Vol.6 (1979)289
(3) H.Aoki; Proc. of 18th ICRC 11(1983)96.
(4) M.Shibata, Private Communications.

Fig. 1 Differential Distribution of Multiplicity

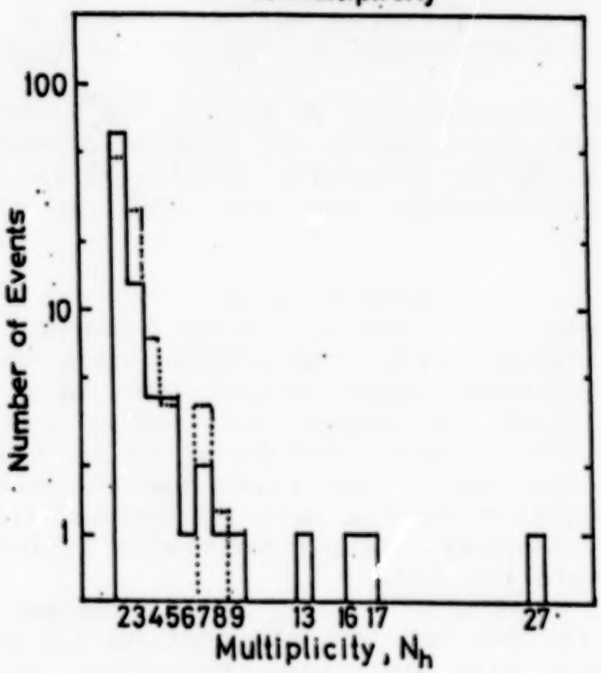


Figure shows the differential distribution of observed multiplicity, N_h.
——— is the experimental result for all hadron bundles (90 events).
..... is the simulation results (76 events from proton primary).

C-5

ORIGINAL PAGE IS
OF POOR QUALITY

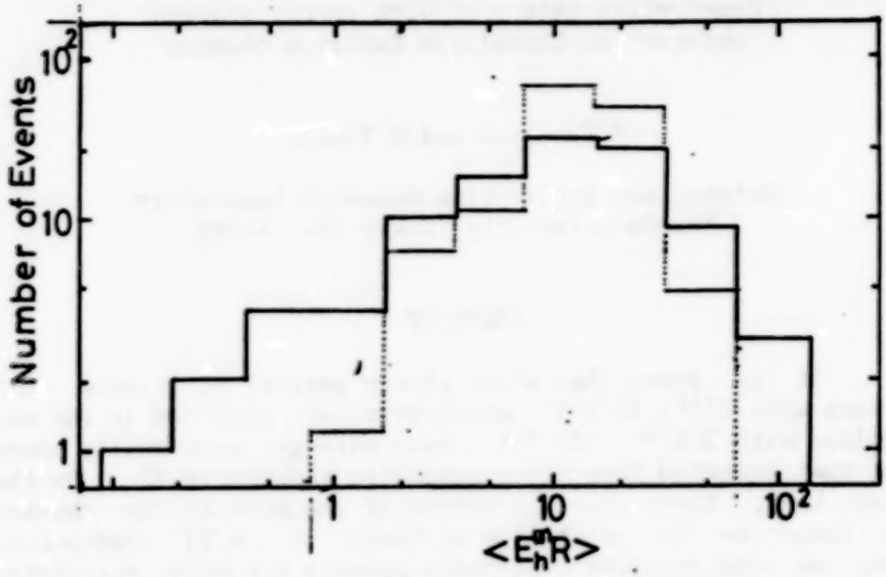


Figure 2; The differntial distribution of ‹ E_h R › is shown.
——— is the experimental result for all hadron bundles (90 events).
..... is the simulation results (76 events from proton primary).

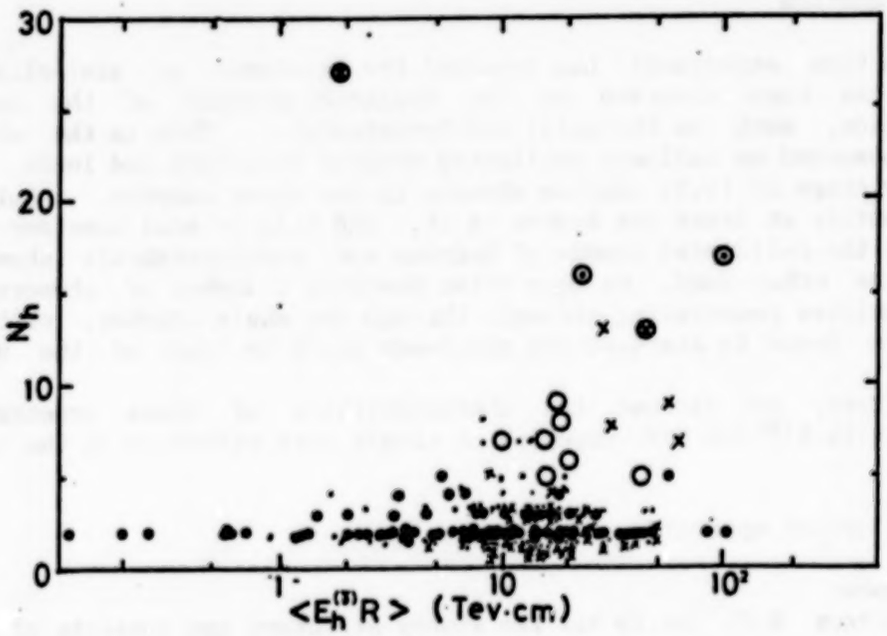


Figure 3; The scattering plots of ‹ E_h R › v.s. N_h is shown.
• is simulation data based on proton primary.
✕ based on iron primary.
⊗ is Centauro events.
○ is Mini-Centauro events.
⊙ is hadron-rich families.
● is the other observed events.

N85-35923

Penetrative nature of high energy showers observed in Chacaltaya Emulsion chamber

Y.Funayama and M.Tamada

Science and Engineering Research Laboratory,
Waseda University, Tokyo 162, JAPAN

ABSTRACT

It is shown that about thirty percent of single core showers with $E^{(\gamma)} > 10$ TeV , which have been observed in the air families with $\Sigma E^{(\gamma)} > 100$ TeV , have stronger penetrating power than that expected from electromagnetic showers (e,γ). On the other hand, their starting points of cascades in the chamber are found to be as shallow as those of (e,γ) components. Then, we can consider that those showers are very collimated bundles of hadron and (e,γ) component. Otherwise, we must accept that the collision mean free path of those showers in the chamber is shorter than that of hadron with geometrical value.

1. Introduction

Chacaltaya experiment has reported the existence of mini-cluster, which has been observed as the daughter product of the exotic interaction, such as Chiron[1] and Geminion[2]. This is the shower bundle observed as nallowly collimated cluster structure and looks like an early stage of (e,γ) cascade showers in the upper chamber. But, we can identify at least one hadron in it, and then we must consider that this is the collimated bundle of hadrons and electromagnetic showers.

On the other hand, we have often obeserved a number of showers in these families penetrating strongly through the whole chamber, although they are found to start at the shallower depth in lead of the upper chamber.

Here, we discuss the characteristics of those penetrating showers with $E^{(\gamma)} > 10$ TeV, obeserved as single core structure in the upper chamber.

2. Experimental apparatus and method

2.-1 chamber

Chacaltaya E.C. no.19 has two storey structure and consists of four parts, the upper chamber of 6 cm thick in lead, the target layer of 23 cm pitch, the air gap of 158 cm and the lower chamber of 8.4 cm thick in lead. Both the upper and the lower chamber are multi-layered sandwiches of lead plates and photo-sensitive materials (nuclear emulsion plates and X-ray films).

2.-2 selection of families

We here select 19 air families with $\Sigma E^{(\gamma)} > 100$ TeV, which have been

obtained by the systematic study of Chacaltaya E.C. no.19 (Japan part, ~30 m^2.yr). They have at least two showers which are detected both in the upper chamber and in the lower chamber.

2.-3 measurement of showers

In the present analysis, we pick up only single core showers with penetrative nature. Here, the penetrating shower means that it has at least two layers where its spot darkness on X-ray films is greater than 0.1 in the lower chamber. The spot darkness is measured by microphotometer with 200 μm x 200 μm square slit. The energy of shower with maximum darkness 0.1 is about 1 TeV, and it is the threshold energy obtained by X-ray film. We call showers as ' single core showers ' which accompany no showers within 1 mm around them. The energy measurement of each shower is also carried out by the track-counting method on nuclear emulsion plates.

3. Results

3.-1 (e,γ)-like behaviour of penetrating showers

Fig.1 is the integral energy distribution of observed single core showers (O) and those with penetration (●). That of simulated gamma-rays is also shown in the same figure. (—; all showers, -----; with penetration). Statistics of calculations is about 10 times larger than that of observed showers. Here, we consider the only showers with E_γ > 10 TeV, because the penetration probability of gamma-ray with E_γ < 10 TeV is found to be negligible small by the same calculations.

Fig.1 Integral energy distribution

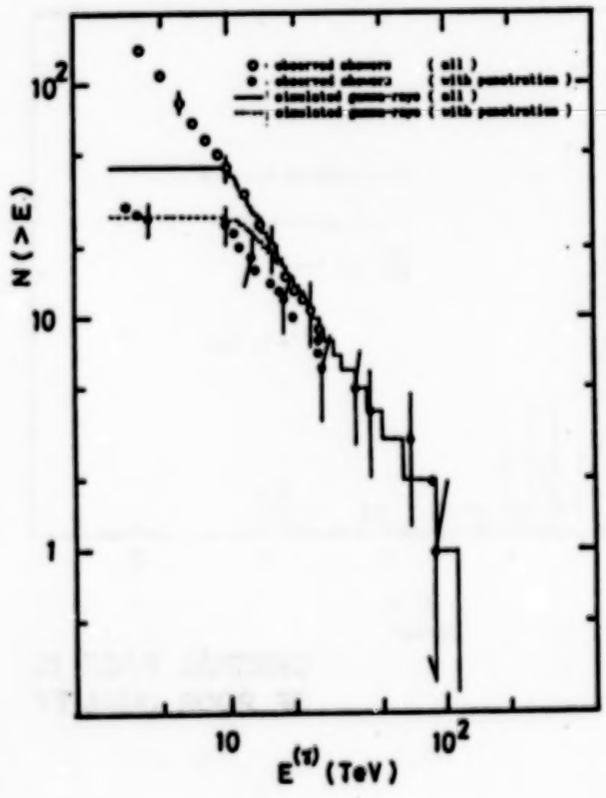
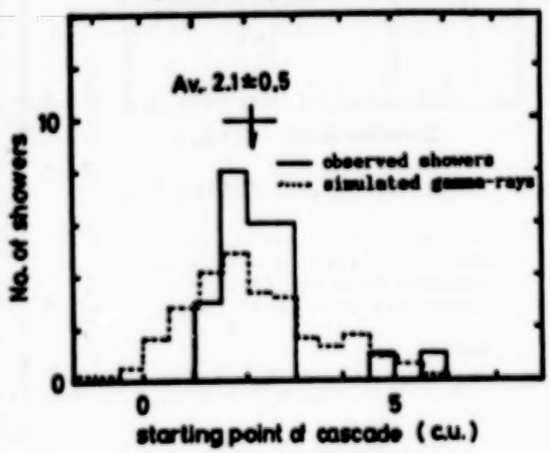


Fig.2 Starting point distribution of cascade in the chamber for penetrating showers $E^{(\gamma)}$>10 TeV



ORIGINAL PAGE IS
OF POOR QUALITY

Simulation calculation is constructed by T.Shibata et.al.[3] The exact structure of E.C. no.19, L.P.M. effect and spacing effect are taken into account. Fig 2. is the starting point distribution of cascades in the chamber only for penetrating showers with $E^{(\gamma)} > 10$ TeV (——; experiment, -----; simulated gamma-ray). We can see from these figures that the observed showers with $E^{(\gamma)} > 10$ TeV show the (e,γ)-like behaviour on the penetration probability and the starting point of cascades.

3.-2 hadron-like behaviour of penetrating showers

In order to investigate the penetrating power of showers, we define the quantity n_i at the i-th layer in the lower chamber, and introduce Σn_i as follows. (Fig.3)

$$\Sigma n_i = \Sigma (\log D_i - \log\langle D\rangle_i) / \log \sigma_i$$

D_i denotes the observed spot darkness on X-ray films at the i-th layer in the lower chamber. For each shower, we fit the observed spot darkness in the upper chamber to the transition curve, using the least square method. Here, the transition curve is constructed by the simulated (e,γ) cascade showers of electron pair origins in the chamber without air gap of 158 cm. $\langle D\rangle_i$ and σ_i is the average darkness and its one standard deviation at the i-th layer in the lower chamber, respectively, estimated from the above fitted curve. Σ means summing up of the quantity n_i only for the layers in the lower chamber where the spot darkness D_i is greater than 0.1. We assume $n_i = 0$ if $D_i < \langle D\rangle_i$. Then, it is considered that the showers with larger Σn_i have long tails with strongly penetrative nature.

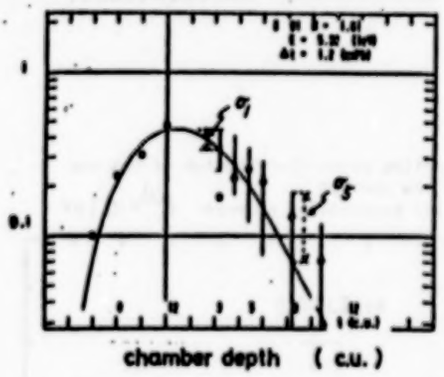


Fig.3 Procedure of calculating Σn_i

We get $\langle D \rangle_i$ and σ_i at the i-th layer in the lower chamber from the fitted curve and calculate $\sum_i n_i$.

where,

$n_i = 0$ (at $D_i < 0.1$ or $D_i \geq \langle D \rangle_i$)

$n_i = (\log D_i - \log \langle D \rangle_i) / \log \sigma_i$ (otherwise)

(see text.)

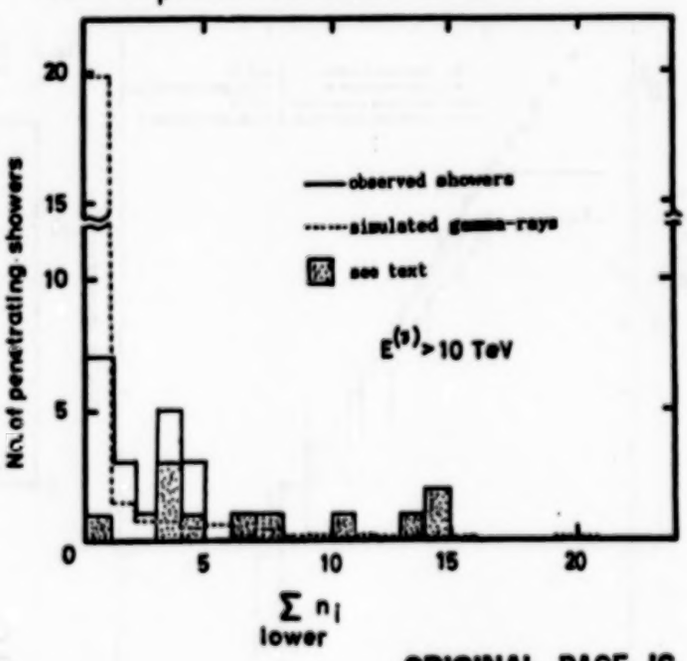
In this case,

$n_1 = n_2 = n_6 = n_7 = n_8 = 0$

$n_3 = 0.40$, $n_4 = 0.55$, $n_5 = 0.66$

then, $\sum_i n_i = 1.61$

Fig.4 Σn_i distribution of penetrating showers



ORIGINAL PAGE IS
OF POOR QUALITY

Σn_j distribution is shown in Fig.4 (—;experiment, ·····;simulated gamma-rays). That for simulated gamma-rays is obtained by applying the same method. We can expect that the showers with larger Σn_j have the new shower cores in the lower chamber, which make this quantity bigger. Thus, the showers, which were identified to have these new cores in the lower chamber under the microscopic observation, are shown by the ▨ marks.

As is seen from this figure, about one half of observed penetrating showers with $E^{(\gamma)} > 10$ TeV, that is, about thirty percent of observed single core showers with this energy region, have long tails of cascade developments in the lower chamber, which cannot be explained by the fluctuation of (e,γ) showers.

4. Conclusion and Discussion

About 30 % of single core showers with $E^{(\gamma)} > 10$ TeV, which have been observed in the families with $\Sigma E^{(\gamma)} > 100$ TeV detected by Chacaltaya E.C. no.19, start at the shallower depth in the upper chamber like (e,γ) components, but they penetrate strongly into the lower chamber like hadron components. This suggests that they consist of very collimated a gamma-ray and a hadron, the distance between the two is $< 100\mu m \sim 200\mu m$. That is, the gamma-ray starts cascade development in the upper chamber and the hadron interacts in the target layer, so that they look like just continuing single core shower, because there is an uncertainty of about $100\mu m \sim 200\mu m$ in the geometrical position when we identify the showers observed in the lower chamber with the continuation of the shower in the upper chamber. Then, when the hadron happen to interact in the upper chamber, we might recognize those showers as mini-clusters. Otherwise, from the argument on the detection probability of hadrons in the chamber, the collision mean free path of these showers is about one third of that of hadron with geometrical value [4].

Acknowledgement

The authors would like to express their gratitude to Prof.Y.Fujimoto and Prof.S.Hasegawa and to all the members of Chacaltaya emulsion chamber experiment for their valuable discussions and comments, especially to Dr.T.Shibata for simulation calculation.

References

[1] Brazil-Japan collaboration ; Proc. of Workshops on Cosmic-Ray Interactions High Energy Results, La Pas Rio de Janeiro (1982) 319
S.Hasegawa ; Proc. of Int. Sympo. on Cosic Rays and Particle Physics, Tokyo (1984) 319
[2] Brazil-Japan collaboration ; AIP Conf. Proc. no.49 (1979) 145
[3] M.Okamoto and T.Shibata ; Conf. Paper, 17th Cosmic Ray Conf.,Paris 5 (1981) 214,218
[4] Y.Funayama and M.Tamada ; to be published.

N85-35924

Anomalous correlation between hadron and electromagnetic particles in hadron and gamma-ray families

M.TAMADA
Science and Engineering Research Laboratory, Waseda University, Tokyo 162, JAPAN

Abstract

Correlations between hadrons and electromagnetic particles are studied in the hadron-gamma families observed in Chacaltaya emulsion chamber experiment. It is found that there exist a number of hadrons which associate electromagnetic showers in extraordinarily close vicinity. The probability to have such large number of hadrons associating electromagnetic showers, expected from background calculation, is found to be negligibly small, $\lesssim 10^{-5}$, and it means there exists anomalous correlation between hadrons and electromagnetic particles in the characteristic spread of atmospheric electromagnetic cascade.

1. Introduction.

Through the analysis on the structure of hadron and gamma-ray families, especially of the families with hadron-rich nature, we have noticed that there were a number of showers which penetrate through the hole chamber, the upper and the lower chamber. The core structure seen in the lower chamber tells us that considerable number of those penetrating showers are not simply pure electromagnetic cascades but are coming from nuclear interaction of hadrons in the chamber, that is, they are hadronic origin.[1][3] During studying on the core structure of those penetrating showers, we found some of showers which are considered as hadronic origin have separate multi-core structure in the upper chamber, not single core structure. That is, there exist hadron and electromagnetic showers which are located extraordinarily close each other, in the extreme case the relative distance between the two is $\sim 30\,\mu$m. Here we show how closely a hadron accompanies electromagnetic showers in its neighbourhood in the high energy hadron and gamma-ray families observed in Chacaltaya chamber no.19.

2. Experimental procedure.

Chacaltaya chamber no.19 The Chacaltaya chamber no.19 has two-storey structure with air-gap, that is, the upper chamber of 6 cmPb thick, target layer of 23 cm pitch, air-gap of 1.5 m and the lower chamber of 8.4 cmPb thick. The special character of the chamber no.19 different from the other chamber is that in all the area of the upper chamber nuclear emulsion plates together with X-ray films are inserted under 3, 4 and 6 cm lead plates. Then we can study very precisely on the core structure of showers, with accuracy of 10 μm, observed in the upper chamber as well as in the lower chamber.

The energy of each shower is estimated by track-counting method. Photometric measurement is also applied for high-energy showers.

Selection of the events Among the events observed in the chamber no.19 we pick up only the events which have at least one identified hadron and pass through the whole chamber, in order to get enough information on hadron component. In the Japanese part ($\sim 30\ m^2$year , a half of the total area) of the chamber no.19, we found 19 events

with total observed energy greater than 100 TeV, incident energy $E_0 \sim 10^{15}$ eV, which satisfy the above criteria. The detection threshold energy is put to 2 TeV.

Identification of hadrons The showers in the lower chamber are those from local nuclear interactions in the target layer (C-jet with clean multi-core structure), those from local nuclear interactions in the lower chamber (Pb-jet-lower with clean single-core structure) and tails of showers from the upper chamber (with diffuse core structure). Thus almost all showers observed in the lower chamber are hadronic origin. The showers observed in the upper chamber are mixture of electromagnetic showers from the atmosphere and those from local nuclear interactions in the upper chamber itself (Pb-jet-upper). Among showers observed in the upper chamber, we consider the showers as hadrons when the showers can be seen only after 8 cascade unit of emulsion plate, that is, no electron shower track can be seen at the expected place of emulsion plate at 6 cascade unit, and/or when the showers continue to the lower chamber and new core can be seen in the lower chamber. The above procedure for identification of hadrons in the upper chamber can not pick up all hadrons interacted in the upper chamber, 20 ~ 30% of them are left unidentified.

3. Results.

Here we study how closely hadrons accompany electromagnetic showers in their neighbourhood by comparing with background calculation where only azimuthal angle ϕ of observed hadrons are randomly chosen in the observed families. Fig.1a shows a distribution of relative distance, Rmin, between a hadron and its nearest neighbouring shower, and Fig.1b shows a distribution of energy-weighted relative distance, Xmin, between a hadron and a shower nearest neighbouring in X_{ij}-space for the events of Chacaltaya chamber no.19. X_{ij} is defined by $X_{ij} = \sqrt{E_i E_j} \times R_{ij}$ where E_i and E_j are visible energy of hadrons and of electromagnetic showers and R_{ij} is relative distance between the two. The distributions are compared with background calculation. As is seen in the figures, there exists a bump above the background distribution both in small Rmin region, Rmin < 400 μm and in small Xmin region, Xmin < 2 GeV.m. Figs.2a and 2b are the same distributions shown above in logR and in logX scale but here hadrons are divided into four parts depending on their distance Rh measured from energy-weighted center of a family. The background distribution in small Rmin and in small Xmin becomes negligibly small when distance Rh of hadrons becomes larger, in contrast to that in the experimental data there still exist hadrons which accompany a shower in very small Rmin and Xmin even when R_H is large. There exist two hadrons which accompany a shower in Rmin less than 160 μm and in Xmin less than 0.6 GeV.m for the case of Rh 5 cm where no hadrons are expected to accompany a shower in such small Rmin and Xmin region from the background calculation. The probability, p, that a hadron accompanies a shower at (energy-weighted) relative distance less than Rmin or Xmin is given by the background calculations. Then the probability Q_n that at least n hadrons accompany a shower at (energy-weighted) relative distance less than Rmin or Xmin is given by a binomial formula,

$$Q_n = \sum_{r=n}^{n_h} {}_{n_h}C_r \, p^r (1-p)^{n_h - r} \qquad (1)$$

here n_h is the total number of observed hadrons. The observed number

of hadrons which accompany a shower in small Rmin or Xmin is very large compared with background distributions and the probability that such large number of hadrons accompany a shower in such small Rmin or Xmin is negligibly small, for example, we have 21 hadrons which accompany a shower in Rmin less than 400 μm and 19 hadrons which accompany a shower in Xmin less than 2 GeV.m. The probability that these two cases are realized , expected from background calculation, is $\sim 8.3\times10^{-7}$ and $\sim 2.1\times10^{-5}$ respectively. Thus we can conclude that there exist hadrons which accompany electromagnetic showers extraordinarily close to them, and such closeness in relative distance Rmin and in energy-weighted relative distance X_{min} can not be reproduced simply by chance.

4. Discussions.

Those hadron and accompanied electromagnetic showers form isolated cluster of collimated showers, mini-cluster[2][3]. Then one may say that those cluster of showers are due to nuclear interaction at low altitude. However, if we interpret those clusters of showers as products of atmospheric nuclear interaction of normal type, $< p_t > \sim 350$ MeV/c, the interaction height of them always gives very small value, around several to several ten meters above the chamber. We can estimate the number of hadrons arriving at the chamber by the observed number of C-jet and Pb-jet-lower under the assumption of a collision mean free path of hadrons. Then we can estimate the number of atmospheric interactions at low altitude, H 50 m above the chamber for example. Table 2 shows a summary of the above argument for hadrons with visible energy, $E_h(\gamma)$,greater than 10 TeV. Almost all of shower clusters have their energy greater than 10 TeV. The estimated number of atmospheric interactions should be compared with the number of hadrons which accompany electromagnetic showers in the close vicinity of them. As one can see in the Table, the number of atmospheric interactions at such low altitude is very small compared with those hadrons unless we assume very short collision mean free path, $\sim 1/5\ \lambda_{geo.}$, of hadrons. The effect of the zinc roof of $\sim$1mm thick ($\lesssim 0.01\ \lambda_{geo}$) which is located 3m above the chamber is also negligible. Thus if we assume that those mini-clusters are due to nuclear interaction in the atmosphere, the interaction point should be much higher and the average transverse momentum of produced particles should be much smaller ($\sim$10 times smaller) than normal one. In many of mini-clusters, a hadron carries a large portion of energy of a cluster. This fact indicates that a hadron is a core of a cluster and electromagnetic showers are accompanied by unknown mechanism.

Acknowledgement

The author would like to express his gratitude to Professors Y.Fujimoto and S.Hasegawa and to all the members of Chacaltaya emulsion chamber experiment for their valuable discussions and comments.

References

[1] Y.Funayama and M.Tamada ;19th ICRC HE 3.3-6

[2] Brasil-Japan collaboration ; AIP Conf. Proceedings No.85(1981) p.500
S.Hasegawa ; Proceedings of Int. Sympo. on Cosmic Rays and Particle Physics, Tokyo(1984) 319

[3] H.Bielawska et al. ; Proceedings of Int. Sympo. on Cosmic Rays and Particle Physics, Tokyo(1984) 374

ORIGINAL PAGE IS
OF POOR QUALITY

N85-38925

no. of hadrons with $R_{min} \leq 400$ μm	number of "single hadrons"			arriving number of hadrons expected from C-jet and Pb-jet-lower			
	Pb-jet-upper identified	C-jet	Pb-jet-lower	λ geo.	$1/2\lambda$ geo.	$1/3\lambda$ geo.	$1/5\lambda$ geo.
21	12	8	1	23± 7 (1.8± 0.3)	21± 7 (1.8± 0.6)	24± 8 (3.2± 1.1)	41±14 (8.5± 3.2)

Figures in parenthesis are estimated number of atmospheric interactions at the heights less than 50 m above the chamber.

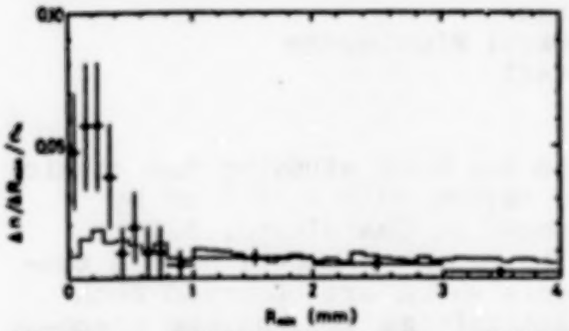


Fig.1a: Distribution of relative distance, Rmin, between a hadron and its nearest neighbouring shower. Histogram is a background distribution.

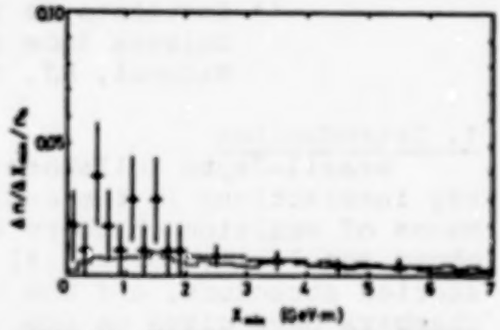


Fig.1b: Distribution of energy-weighted relative distance, Xmin, between a hadron and its nearest neighbouring shower in X_{ij}-space.

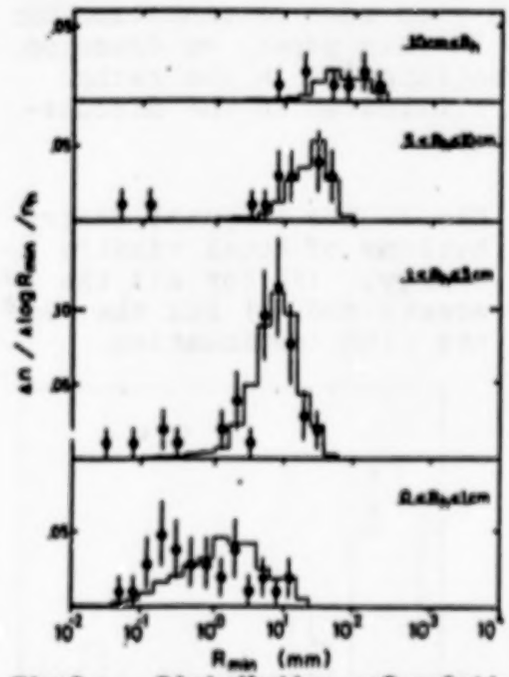


Fig.2a: Distribution of relative distance, Rmin, between a hadrons and its nearest neighbouring shower for four different intervals of distance R_h of hadrons measured from the energy-weighted center of the event. Histograms are bacnkgroumd distributions.

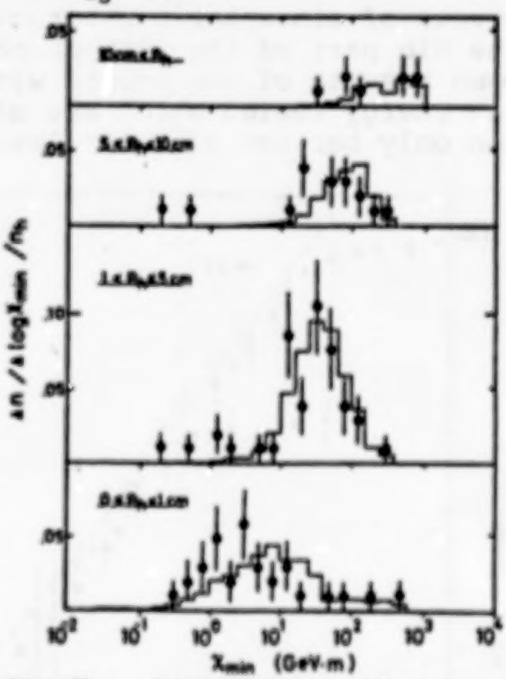


Fig.2b: Distribution of energy-weighted relative distance, Xmin, between a hadron and its nearest neighbouring shower in X_{ij}-space for four different intervals of distance R_h of hadrons.

ORIGINAL PAGE IS
OF POOR QUALITY

HE 3.3-7
N85-35925

Atmospheric Interactions detected in both the Upper and the Lower Chambers at Chacaltaya

N.M.Amato*, N.Arata* and R.H.C.Maldonado**

* Centro Brasileiro de Pesquisas Físicas
Rua Dr. Xavier Sigaud 150
22290 Rio de Janeiro, RJ, Brasil

** Instituto de Física
Universidade Federal Fluminense
Niteroi, RJ, Brasil

1. Introduction

Brasil-Japan Collaboration has been studying the cosmic ray interactions in the energy region 10^{13} - 10^{17} eV by means of emulsion chambers exposed at Chacaltaya, 5220 m above sea-level, Bolivia[1]. The recent chambers have a two-storied structure, and the events which are observed both chambers have given us important informations on the phenomena. For example, the first Centauro event was detected as a small shower at the bottom of the upper chamber and as a big fraction of energy deposit in the lower chamber, which indicated a high contribution of hadronic showers[1].

We are almost finishing the complete analysis of the events of atmospheric interactions with such continuation for the Rio part of the 19th chamber. In this paper, we describe some results of the events with continuation in the rather low energy region which are often eliminated in the discussion only because of their low energy.

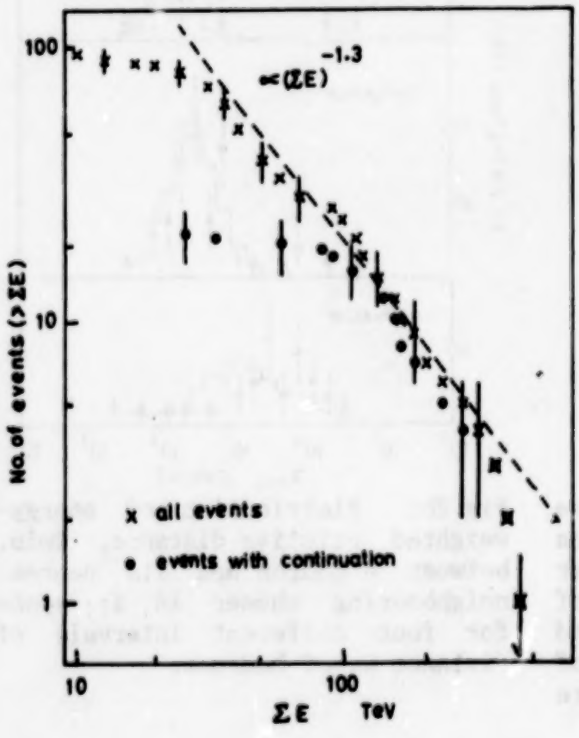


Fig.1 The integral distributions of total visible energy. (x) for all the events and (•) for the events with continuation.

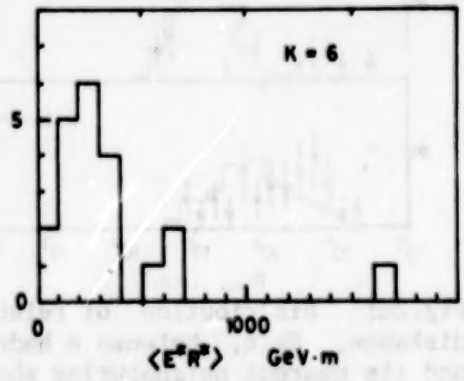


Fig.2 The histogram of $\langle E^* R^* \rangle$, where K=6 GeV·m is used for decascading.

ORIGINAL PAGE IS
OF POOR QUALITY

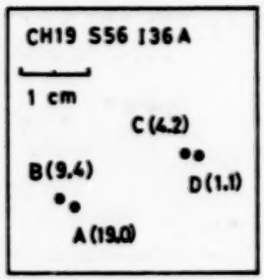


Fig.3 The target diagram of CH19 S56 I36 A. The name and energy of each core is shown.

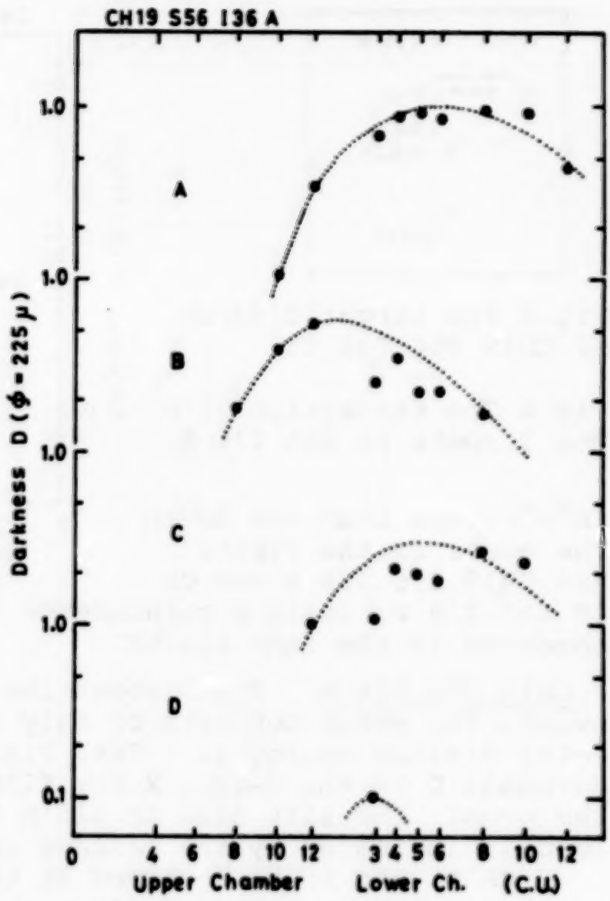


Fig.4 The transition of darkness D with slit diameter 225 μ for 4 cores in S56 I36 A. The fitting curves are also shown.

2. Experiment

The 19th chamber is two-storied, and for the whole upper and lower chambers, nuclear emulsion plates were inserted in sandwiches of lead plates together with X-ray films. The exposure time was 677 days. The upper chamber has total area of 44.2 m^2 and the lower chamber 32.4 m^2. They are formed by unit blocks of dimension 40 x 50 cm^2; in Rio de Janeiro have been analyzed 59 blocks of the upper chamber and 48 blocks of the lower chamber.

We must observe at least two penetrative shower cores in both the upper and the lower chambers, in order to determine the relative geometrical position of all the showers in both chambers. We have observed 21 events with such continuation. Fig.1 shows the integral distributions of the total energy visible in the form of electro-magnetic cascade showers for all the events and for the events with continuation. We notice that the distribution for all the events obeys $\propto (\Sigma E)^{-1.3}$, which is consistent with the previous measurements [1].

Fig.2 shows the distribution of average energy-weighted lateral spread, $\langle E^* R^* \rangle$, for the 21 events, where the so-called decascading constant K = 6 GeV·m was chosen [2]. We usually have a larger interest in the region of large ER, but in the following we describe three events in the small ER region.

3. Results

We have two events with continuation in the interval of

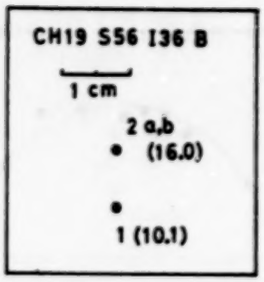


Fig.5 The target diagram of CH19 S56 I36 B.

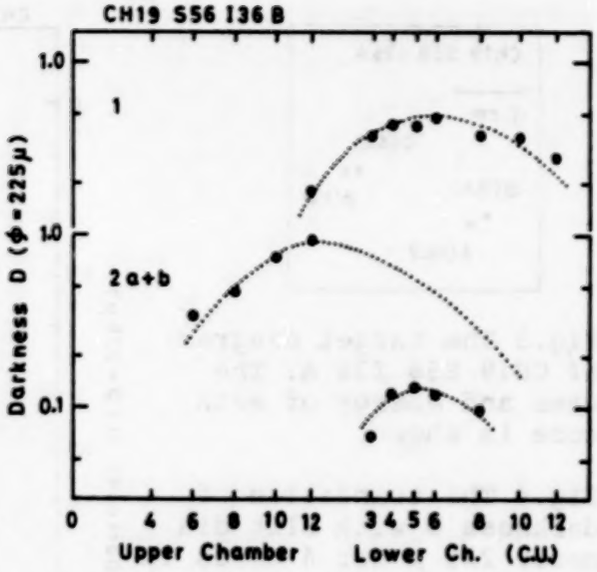


Fig.6 The transition of D for 2 spots in S56 I36 B.

$\langle E^* R^* \rangle$ less than 100 GeV·m. The names of the events are CH19 S56 I36 A and CH 19 S56 I36 B; it is a coincidence that these two events were observed in the same blocks.

CH19 S56 I36 A Fig.3 shows the target diagram of this event. The event consists of only four shower spots with the total visible energy 33.7 TeV. Fig.4 shows the transition of darkness D on the N-type X-ray films for the four spots of the event. The slit size is 225 μ in diameter. The depth of lead is indicated by the cascade unit of each chamber.

#A starts to be observed at the very deep layer, 8 cu on the emulsion plate and 10 cu on the X-ray film, as a sharply collimated shower core. #B starts to be observed at 8 cu and we can not find any track on the corresponding position at 6 cu. #C starts to be observed at 12 cu. #D is observed only in the lower chamber as a diffused small shower.

Down to 6 cu in the upper chamber, this event does not appear for detection, and the cores B, A, C and D start to appear, one by one, to form the event.

We can identify all the four cores as hadronic because of their deep penetration. This event is lacking in electromagnetic components at the entrance of the chamber within the limit of detection threshold (~1 TeV).

CH19 S56 I36 B Fig.5 shows the target diagram of this event. The event consists of two spots (#1 and #2) with the total visible energy 26.1 TeV. #2 consists of two constituent cores (a and b) with the very short mutual distance 33 μ. Both the two spots continue into the lower chamber.

Fig.6 shows the transition of spot darkness on the N-type X-ray films. #1 starts to appear at 12 cu in the upper chamber as a collimated core and in the lower chamber as multi-cores. #2 starts to be observed at 6 cu and the spacing effect of air-gap between the upper and the lower chambers is clearly seen in Fig.6.

We can identify #1 as a hadronic core, but we can not judge whether #2 contains hadronic nature.

CH19 S83 #200 This event is observed only in the upper chamber. Fig.7 shows the target diagram of this event. The event consists of two spots (#1 and #2) with the total visible energy ~30 TeV. #1 consists of two constituent cores (a and b) with the mutual distance 175 μ.

Fig.8 shows the transition of electron number counted on the nuclear emulsion plates in the area 78 x 78 μm². #1a appears as a normal shower, but #1b starts to appear at 8 cu and grows up remarkably down to 12 cu. #2 is observed only at 12 cu in the upper chamber.

We can identify #1a and #2 as hadronic cores. We can not judge #1b as a hadronic core.

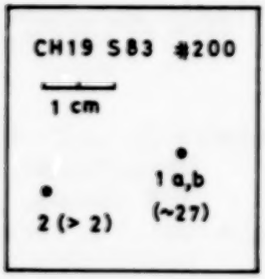


Fig.7 The target diagram of S83#200.

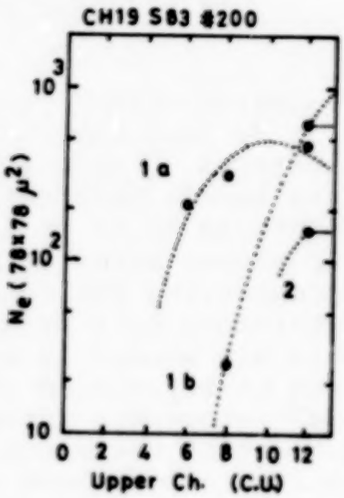


Fig.8 The transition of electron number inside the counting area 78 x 78 μm².

4. Discussions

We have encountered interesting (exotic) events in the high energy region, $\Sigma E > 80 - 100$ TeV [1,3]. But as shown in the previous section, we can pick up some events with an impressive character even in the lower energy region.

In the energy interval, 25 - 35 TeV, we have analyzed 18 events, among which 3 events showed a hadron-rich nature. If we use the power fit of $(\Sigma E)^{-1.3}$ in Fig.1, these 3 events are in the unbiased sample of ~40 events in that energy interval.

More details on the events with continuation will be presented at the Conference.

5. Acknowledgement

The authors wish to acknowledge all the members of the Brasil-Japan Collaboration for their kind support. They are grateful to Profs. F.M. Oliveira Castro and H.M. Portella for their continuous encouragement. They also thank T.T.Villar, N.Miranda and I.A.Lopez in CBPF for their help in scanning work. Thanks are also due to the CNPq, Brasil, for a financial support.

References

[1] C.M.G.Lattes, Y.Fujimoto and S.Hasegawa, Phys.Rep. 65 (1980) 151 and references therein.
[2] H.Semba, Supplement of Prog.Theor.Phys. 76 (1983) 111.
[3] Brasil-Japan Collaboration, AIP Conference Proceedings, 85 (1981) 500.

N85-35926

HE 3.3-8

LATERAL DISTRIBUTION OF HIGH ENERGY HADRONS AND GAMMA RAY IN AIR SHOWER CORES OBSERVED WITH EMULSION CHAMBERS

Matano,T. and Machida,M.
Department of Physics, Saitama University,
338 Urawa, Japan
Kawasumi,N., Tsushima,I., Honda,K. and Hashimoto,K.
Department of Physics, Yamanashi University,
400 Kofu, Japan
Navia,C., Martinic,N. and Aguirre,C.
Instituto de Investigaciones Fisicas
Universidad Mayor de San Andres, La Paz, Bolivia

1. Introduction

We have observed a high energy event of a bundle of electrons, γ rays and hadronic γ rays in an air shower core. This bundle were detected with an emulsion chamber with thickness of 15 cm lead installed in the central part of SYS air shower array at Mt. Chacaltaya. The size of air shower accompanying the bundle is 1.5×10^7 and the age parameter is determined 0.17 from the steepness of the lateral structure. This air shower is estimated to be initiated with a proton with energy around 10^{17} to 10^{18} eV at a altitude of around 100 gcm^{-2} above Mt. Chacaltaya. We have dtermined lateral distributions of the electromagnetic component (for simplicity, we call this component as gamma ray) with energy above 2 TeV and also the hadronic component of energy above 6 TeV of this air shower core respectively. These lateral distributions may also ones at the very early stage of air shower development.

We have also studied so-called $E_\gamma R_\gamma$, $E_H^\gamma R_H$ distribution. Here E_γ, E_H^γ are the energy of each gamma ray and hadronic γ ray respectively. R_γ, R_H are the radial distance from the center of the bundle of these particles. As well known, we can determine the transverse momentum from the product of energy and distance of a particle (ER) divided with a production height (H).

Since particles in the bundle are produced with process of the development of the nuclear cascade, we can not know the primary energy of each interaction in the cascade which produces these particles. In order to know the primary energy dependence of transverse momentum, we study the average products of energy and distance ($\langle ER \rangle$) for various average energies of secondary particle ($\langle E \rangle$).

2. Lateral distribution of gamma rays and hadrons

Centers of the bundle are determined from the energy weighted mean of positions of gamma rays and hadrons respectively. The deviation between two centers is only less than 1 mm and both are in agreement.

Lateral distributions of gamma rays and hadrons are shown in Fig.1 and Fig.2 for two different threshold energies. The slopes of these distributions are in agreement.

ORIGINAL PAGE IS
OF POOR QUALITY

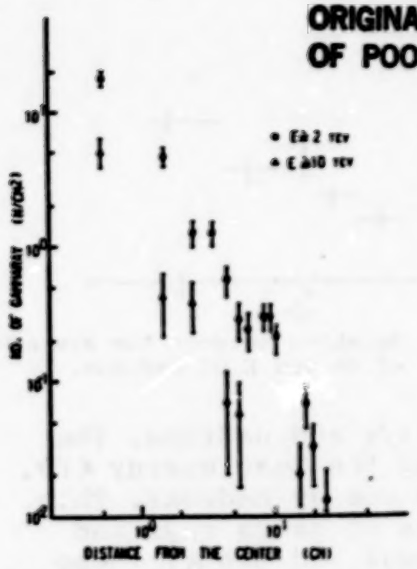


Fig.1. Lateral distribution of gammarays.

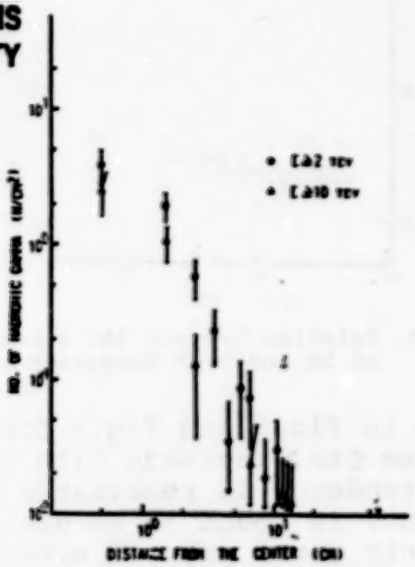


Fig.2. Lateral distribution of hadrons.

Distributions are represented by the power law of the form r^{-n}. The exponent (n) is about 1.8 for gamma rays and about 1.9 for hadrons.

3. ER distributions

ER is the parameter which reflect the transverse momentum of that particle. Fig.3 and Fig.4 show ER distribution for gamma rays and hadrons respectively. The distributions for hadrons with energy more than 10 TeV is flatter than others untill higher ER values.

The relation between the averages, $< ER >$ and $< E >$, are

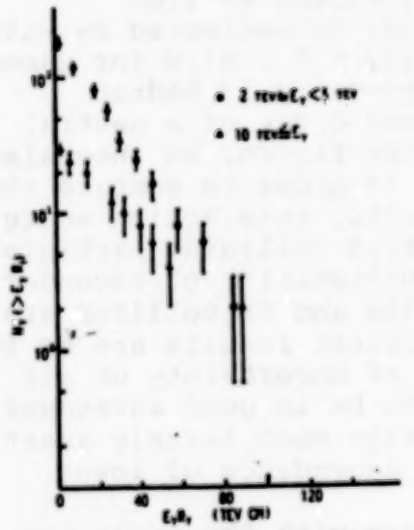


Fig.3. ER distribution of gammarays.

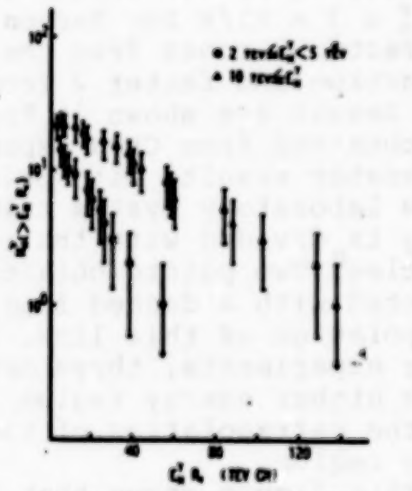


Fig.4. ER distribution of hadrons.

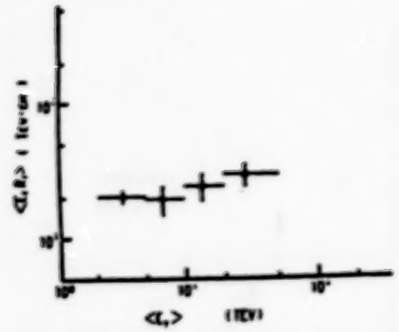


Fig.5. Relation between the average of ER and E of gammarays.

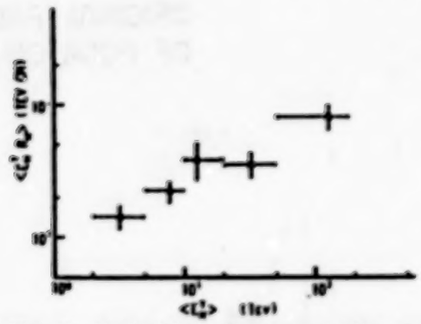


Fig.6. Relation between the average of ER and E of hadrons.

shown in Fig.5 and Fig.6 for gamma rays and hadrons. The average <ER> increase with increasing the mean energy <E>. This tendency is remarkable for high energy hadrons. This tendency is found in ER distributions of gamma rays and hadronic gamma rays of events Andromeda and M.A.[redacted]. These events are the most high energy events among five families of the highest energy range, $\Sigma E_\gamma > 1000$ TeV observed by Chacaltaya Emulsion Chamber Experiment of Brasil-Japan Collaboration.[1)]

4. Energy dependence of transverse momentum

Transverse momentum is determined from ER divided by production height. In the air shower, hadrons are not produced in a single interaction, but individual interactions at different stages in a nuclear cascade of air shower development. Radial distance R, however, corresponds to radial deviation caused by final interaction in which that particle is produced. Therefore, we can estimate P_T with these R and an estimated most probable production height above the observation level. In the present case, we use 80 gcm^{-2} which is consistent to a height estimated from calculations of air shower development. We estimated P_T with $P_T=(E_H^\gamma \times 3 \times R)/H$ for hadron and $P_T=(E_\gamma \times 2 \times R)/H$ for gamma ray. Facter 3 comes from the charge symmetry in hadron interaction and facter 2 from two gamma decay of a neutral pion. Result are shown in Fig.7. In the figure, we show also data obtained from CERN experiments.[2)] In order to compare the accelerator results with present results, interaction energy in the laboratory system transfered from colliding particle energy is divided with the average multiplicity of secondary particles.[2)] Two points obtained from ISR and $P\bar{P}$ collider are connected with a dashed line. The present results are on the extrapolation of this line. In spite of uncertainty of air shower experiments, these data seem to be in good agreement. In the higher energy region, P_T increase much largely apart from the extrapolation of the energy dependence of lower energy region.

This figure shows that P_T increase with the power law of the average energy of shower particle of the form E^n of the

N85-35927

ORIGINAL PAGE IS
OF POOR QUALITY

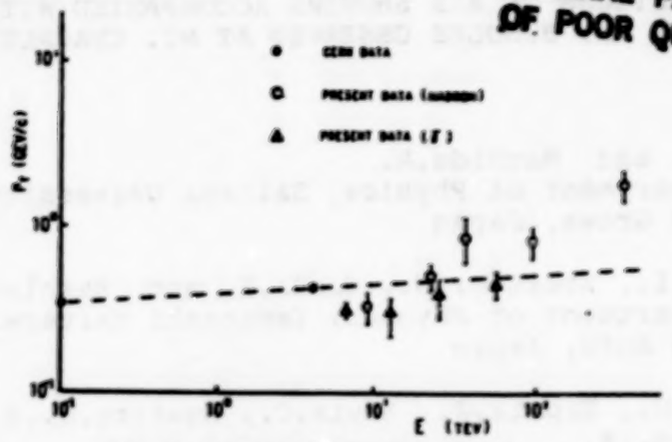


Fig.7. Relation between $\langle P_T \rangle$ and shower particle $\langle E \rangle$.

exponent n=0.06. However, in the extremely high energy region, the exponent increase to n=0.44.

In model calculations on the nuclear cascade of energy around 10^{17} eV, high energy hadrons can not be produced by secondary pion after passing through 80 gcm^{-2}. Consequently, hadrons with energy more than 100 TeV may be produced in fragmentation region of nucleon interaction.

We can conclude that this remarkable increase of P_T for hadrons above 100 TeV with increasing average hadron energy may be a noteworthy characteristics of the energy dependence of transverse momentum especially in the fragmentation region.

Acknowlegements

This work was supported by the Grant-in-Aid for Oversea Survey of the Ministry of Education, Science and Culture in Japan. The authors wish to thank prof. C. Grupen, Siegen University, for fruitful discussion during his stay in Japan.

References

1) Yamashita,S., et al, ICR-Report-112-83-6, 123(1983)
2) Arnison,G., et al, UA1 Collaboration,
Proc. Third Topical Workshop, CERN 83-04,75(1983)
3) Ward,D., et al, UA5 Collaboration,
Proc. Third Topical Workshop. CERN 83-04,75(1983)

300

N85-35927

SIZE DISTRIBUTIONS OF AIR SHOWERS ACCOMPANIED WITH HIGH ENERGY GAMMA RAY BUNDLES OBSERVED AT MT. CHACALTAYA

Matano,T. and Machida,M.
Department of Physics, Saitama University,
338 Urawa, Japan

Tsushima,I., Kawasumi,N., Honda,K. and Hashimoto,K.
Department of Physics, Yamanashi University,
400 Kofu, Japan

Martinic,N., Zapata,J., Navia,C., Aguirre,C.,Siles,L. and Magnani,R.
Instituto de Investigaciones Fisicas
Universidad Mayor de San Andres, La Paz, Bolivia

ABSTRACT

We reprot size distributions of air showers accompanied with bundle of high energy gamma rays and/or large size bursts under emulsion chambers, in order to study the composition of primary cosmic rays and also characteristics of high energy nuclear interaction.

Air showers initiated by particles with a large cross section of interaction may develop from narrow region of the atomosphere near the top. Consequently, fluctuations of sizes of air showers are not so large.

On the contrary, starting levels of air showers by particles with smaller cross section fluctuate in wider region of the atomosphere. Air showers of extremely small size accompanied with bundle of gamma rays may be ones initiated by protons at lower level after penetrating deep atomosphere without interaction. In such cases, the air shower size distribution may be flatter than privious case.

We have determined the relative size distribution according to the total energy of bundle of gamma rays and the total burst size observed under 15 cm lead absorber. These results are discussed on the point of view mentioned above.

N85-35928

HE-3.3-10

EAS ACCOMPANIED BY GAMMA-FAMILIES AT MT. NORIKURA AND COMPARISON WITH MONTE CARLO SIMULATION

Shima, M., Saito, To., Sakata, M. and Yamamoto, Y.
Konan University, Kobe, Japan
Kasahara, K. and Yuda, T.
Institute for Cosmic-Ray Research, University of Tokyo, Tanashi, Japan
Torii, S.
Kanagawa University, Yokohama, Japan
Hotta, N.
Utsunomiya University, Utsunomiya, Japan.

ABSTRACT

The experimental data of EAS accompanied by gamma-families, with total energy greater than 10 TeV, obtained at Mt. Norikura, were compared with a Monte Carlo simulation with a rising cross section proportional to $E^{0.04}$ for the p-air inelastic cross section. It is found that the absolute intensity of size spectrum of such EAS is strongly affected by the primary protons intensity at 10^{15}-10^{16} eV region and the experimental size spectrum agrees with the simulated spectra for the p-poor (<15%) primary composition better than the p-rich (≥30%) one.

1. Introduction

The longitudinal development of EAS cores, especially at its early stages, depends on the collision mean free path and/or mass number of primary cosmic-ray particle in the atmosphere. The penetrated protons through the upper atmosphere without collisions or with a few semi-elastic collisions, even though their primary energies are a little low, are more advantageous to yield gamma-families at high mountains than the survival nucleons with normal fraction of energy in the normal EAS development. The inverse power form of the primary energy spectrum hastens this tendency. On the other hand, primary heavy nuclei are quite disadvantageous to generate gamma-families at mountain altitudes, because their primary energies are rapidly splitted into a lot of particles in the upper atmosphere due to their short mean free path and the plenty of initial constituent nucleons. Then, the observation of EAS accompanied by gamma-families with total energy greater than a certain value in an appropriate size range at mountain altitudes is nearly equivalent to observe EAS initiated by primary protons preferentially.

The combined EAS with gamma-families, which were obtained by the cooperative experiment between the EX chamber and the EAS array at Mt. Norikura (738 gcm^{-2}), were compared with the simulation with respect to the shape of size spectrum once at Bangalore (Nakatsuka et al., 1983). After that, the experimental data were reanalysed and a few combined events were added. The summary of the new results is presented in this Conference (HE-3.3-11). On the other hand, the simulation calculation was thoroughly renewed by employing the rising cross section, zenith angle distribution of incident particles and by extending the Monte Carlo

N85-35928

calculation to lower energy than the former calculation by three orders. The results of new simulation are fairly different from the old one due to those changes, especially due to the last procedure described above. Then, we must abandon the former conclusions reported at Bangalore and the new results are presented here.

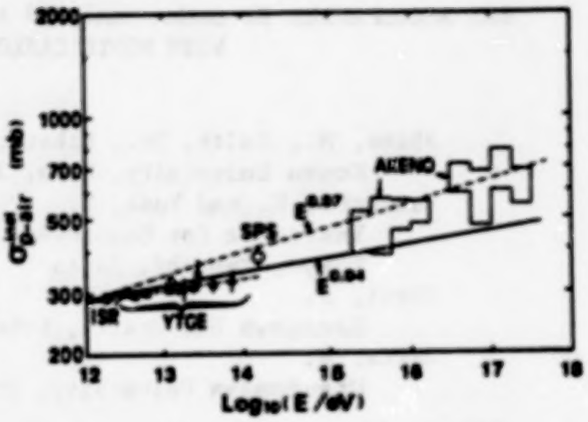


Fig. 1 Energy dependence of p-air inelastic cross section. $\bar{p}p$ accelerator data by ISR and SPS are transformed to p-air cross section. The solid curve with δ'=0.04 is assumed in the simulation. YTGE means the calculation by Yodh et al. (Yodh et al., 1983).

2. Assumptions and procedures in the simulation

First, the models about the hadronic interactions are summarized. The inelastic cross section of p-air collision has an energy dependence of a form E^{δ} instead of the constant cross section σ(p-air)=300 mb in the old model of simulation (Kasahara et al.,1979). When the energy dependence of $\bar{p}p$ cross section is expressed by E^{δ}, that of p-A cross section (A: mass number) is roughly given by $\propto(2E^{\delta}-1+A^{1/3})^2/(1+2A^{1/3}+A^{2/3})$ by a simple consideration that the increase of nuclear radius is due to swelling of only surface nucleons. This function is approximated by σ(p-air) $\propto E^{\delta'}$ again. For instance, the values δ=0.073 ~ 0.11 representing the $\bar{p}p$ cross section from ISR data up to SPS data (Matthiae et al., 1983) are converted to the values δ'=0.044 ~ 0.068 for p-air collisions. In this paper we use a moderate rising cross section δ'=0.04 as shown in Fig. 1. The multiplicity of secondary particles satisfies the KNO scaling in all energy region but the mean multiplicity depends on collision energy in the form a+blns+cln^{2}s with a=0.88, b=0.44 and c=0.118 as shown in Fig. 2, which is nearly equivalent to the old one. The inelasticity distribution is not changed from the old one. The rapidity distribution of secondary particles keeps nearly the form $(1-x)^4/x$ as in the scaling model although the cross section of QCD large p_T jets is added to the normal cross section in the new simulation. The calculation was done by the full Monte Carlo method until the energy of each shower particle becomes lower than 1 GeV. Hadronic jets in the iron EX chamber were simulated for the high energy hadrons arrived at the chamber and those which released electromagnetic energy greater than 3 TeV in the chamber were joined into gamma-families. We picked up only the simulated showers accompanied by a gamma-family with total cascade energy $\Sigma E_{\gamma,H} \geq 10$ TeV, $n_{\gamma,H} \geq 2$ for Emin=3 TeV, involving hadron initiated cascades, at the level of Mt. Norikura in accordance with the experimental conditions. And, the total number of shower particles (Ne) of them is calculated by connecting the one dimensional

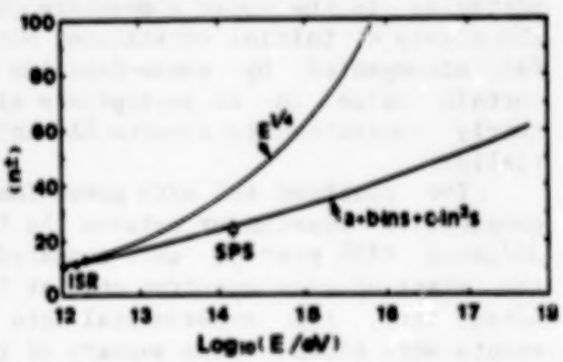


Fig. 2 Energy dependence of mean charged multiplicity. The solid curve is employed in the simulation.

ORIGINAL PAGE IS
OF POOR QUALITY

cascade function to each shower particles generated by the full Monte Carlo method. The contribution of hadrons with energies less than 1 GeV is neglected. The conversion factor, i.e., primary energy per maximum EAS size is about 1.5 ~ 1.7 GeV/particle for the normal EAS with sizes from 5×10^5-10^7 in this simulation.

Second, the models about the energy spectrum of primary cosmic rays are described. The experimental data are briefly summarized in Fig. 3 (a). The total energy spectrum is represented by the solid curve which is smoothly connecting the Grigorov's data (Grigorov et al., 1972) and the air shower data at Akeno (Nagano et al., 1983). In this simulation are assumed two extreme models about the primary composition, especially about the fraction of iron nuclei. One is the p-rich spectrum as shown in Fig. 3 (b), where the fraction of iron nuclei is very small. Another one is the p-poor spectrum as shown in Fig. 3 (c), where iron nuclei are extremely abundant. The fractions of proton, helium and iron are tabulated at several energies in Table 1. The flat distribution of zenith angle with which the primary particles rush into the atmosphere is adopted instead of the vertical incidence.

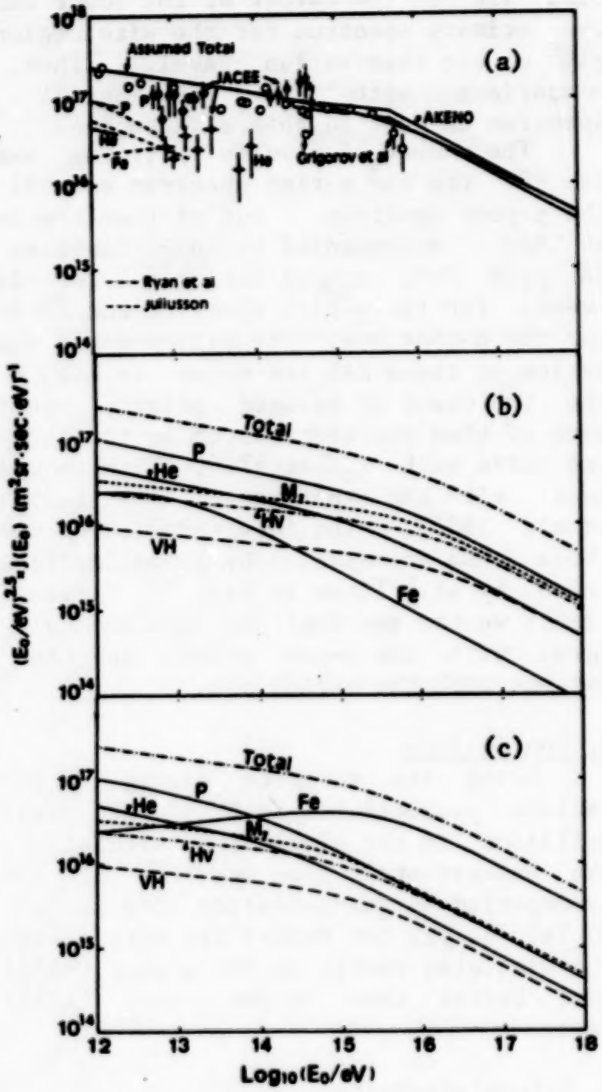


Fig. 3 Differential energy spectrum of primary cosmic rays.
(a); summary of experimental data. Some points are converted from integral form by Juliusson's way (Juliusson, 1975).
(b); p-rich primary spectrum assumed in the simulation.
(c); p-poor primary spectrum assumed in the simulation.

3. Results of calculation

The primary spectrum is cut at 10^{15} eV as its lower end in the calculation. This primary energy is corresponding to a mean shower size $\sim 6 \times 10^5$ at the shower maximum. Because EAS accompanied by such gamma-families we concern are generally at stages before the shower maximum and their sizes have a narrower correlation with primary energies than the general EAS, the size spectrum of them is surely free from the

Table 1

Energy	(eV)	10^{14}	10^{15}	10^{16}	10^{17}
p-rich	P	31.8 %	34.3 %	32.8 %	28.6 %
	He	17.3	15.7	12.2	10.7
	Fe	8.9	3.7	2.3	1.9
p-poor	P	25.4	14.8	10.0	8.1
	He	13.1	8.0	5.6	4.6
	Fe	30.0	45.5	58.5	61.4

bias due to the cutoff at the lower end of the primary spectrum for the size region Ne $\geq 10^6$ at the observation level. Then, the comparison with the experimental size spectrum is done in this size region.

The number of primary particles sampled is 480 for the p-rich spectrum and 561 for the p-poor spectrum. Out of them the number of EAS accompanied by gamma-families with $\Sigma E_{\gamma,H} \geq 10$ TeV, $n_{\gamma,H} \geq 2$ for Emin=3 TeV is 45 events for the p-rich spectrum and 25 events for the p-poor one. The zenith angle distribution of these EAS are shown in Fig. 4 for the two cases of assumed primary spectrum. Both of them are represented by the theoretical curve with $x_0/\lambda_{att}=7.0$, which is consistent with the experimental data (Mitsumune et al, 1985). The integral size spectra of those EAS accompanied by gamma-families are shown by step lines in Fig. 5. From this figure we can see that the experimental data agree with the p-poor primary spectrum but not with the p-rich one.

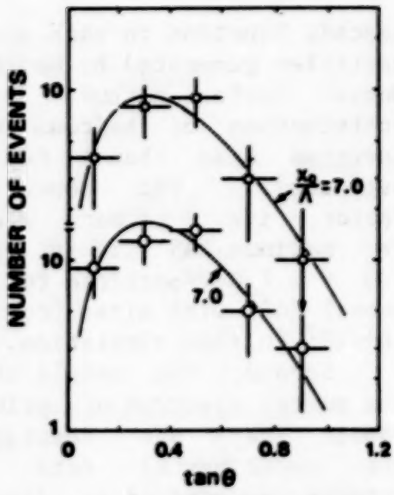


Fig. 4 Zenith angle distribution of simulated events with gamma-families. Open circles are for the p-rich spectrum and open squares for the p-poor one.

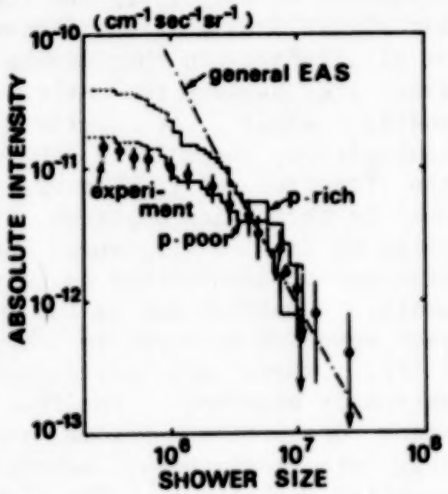


Fig. 5 Size spectra of EAS accompanied by gamma-families with $\Sigma E_{\gamma,H} \geq 10$ TeV, $n_{\gamma,H} \geq 2$ for Emin=3 TeV at the level of Mt. Norikura (738 gcm^{-2}).

4. Conclusions

Using the moderate rising cross section proportional to $E^{0.04}$ for p-air collision in the simulation calculation, the experimental size spectrum of EAS accompanied by gamma-famlies with $\Sigma E_{\gamma,H} \geq 10$ TeV, $n_{\gamma,H} \geq 2$ for Emin=3 TeV agrees with the simulated result in the p-poor (<15%) case better than in the p-rich ($\gtrsim$30%) case.

5. Acknowledgements

The calculation was carried by the computer FACOM 380R of the Institute for Nuclear Study, University of Tokyo.

6. References

Nakatsuka et al.,1983; Conf. Papers of 18th ICRC (Bangalore), 11, 346.
Kasahara et al., 1979; Conf. Papers of 16th ICRC (Kyoto), 13, 75.
Matthiae, 1983; Proceedings of Int. Europhys. Conf. on H. E. P., 714.
AKENO; Hara et al., Phys. Rev. Letters, 50 (1983), 2062.
Yodh et al., 1983; Phys. Rev. D, 27 (1983), 1183.
Grigorov et al., 1971; Conf. Papers of 12th ICRC (Hobart), 5, 1746.
Nagano et al, 1983; J. Phys. G, 10 (1984), 1295.
Juliusson, 1975; Conf. Papers of 14th ICRC (Munich), 8, 2689.
Ryan et al, 1972; Phys. Rev. Letters, 28 (1972),987.
JACEE; Burnett et al, Proceedings of Int. Symposium on Cosmic Rays and Particle Physics at Tokyo (1984), 468.
Mitsumune et al, 1985; this Conference, HE-3.3-11.

N85-35929
HE-3.3-11

COMPARISON OF ABSOLUTE INTENSITY BETWEEN EAS WITH GAMMA-FAMILIES AND GENERAL EAS AT MT. NORIKURA

Mitsumune, T., Nakatsuka, T., Nishikawa, K., Saito, To., Sakata, M., Shima, M. and Yamamoto, Y.
Konan University, Kobe, Japan.
Dake, S. and Kawamoto, M.
Kobe University, Kobe.
Kusunose, M., Ohmori, N. and Sasaki, H.
Kochi University, Kochi, Japan.
Hotta, N.
Utsunomiya University, Utsunomiya, Japan.

ABSTRACT

Gamma-families with total energy greater than 10 TeV, found in the EX chamber which was cooperated with the EAS array at Mt. Norikura, were combined with EAS triggered by big bursts. The absolute intensity of the size spectrum of these combined EAS was compared with that of general EAS obtained by AS trigger. EAS with sizes greater than 2×10^6 were always accompanied by gamma-families with $\Sigma E_{\gamma,H} \geq 10$ TeV, $n_{\gamma,H} \geq 2$ and Emin=3 TeV, although the rate of EAS accompaning such gamma-familyies decreases rapidly as their sizes decrease.

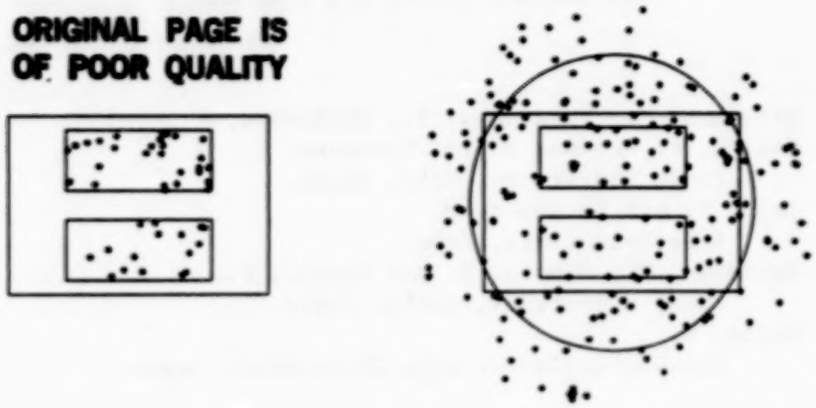
1. Introduction

The results of the cooperative experiment of the 20 m^2 iron EX (emulsion and/or X-ray film) chamber and the EAS array at Mt. Norikura (738 gcm^{-2}) were reported once at Bangalore (Nakatsuka et al., 1983). Thereafter, the reanalysis of combination between gamma-families and EAS was done and a few new combined events were obtained. And, some of the old data were revised, especially the EAS size Ne and age parameter s were renewed by taking account of the transition effect of the materials over the scintillation counters and of the plastic scintillator itself for EAS density measurement. The data of general EAS obtained by the AS trigger in the same period of this experiment were analysed. In this report the EAS combined with gamma-families of total energy greater than 10 TeV is compared with the general EAS thus obtained with respect to the absolute intensities of EAS size spectrum.

2. Experiment

The experimental apparatus was described before (Yamamoto et al., 1981). The EAS data were taken by two kind of triggers. One was a burst trigger under the 14 r.l. thick EX chamber when any one of 72 burst scintillation counters responded to bursts greater than about 2000 particles per detector of 0.25 m^2 unit area. These EAS events with big bursts were provided for the analysis of combination with gamma-families. Another one was an AS trigger by four sets of four-fold coincidence of the nearest four out of the central nine non-covered scintillation counters.

ORIGINAL PAGE IS
OF POOR QUALITY



(a) (b)

Fig. 1 Map of EAS axis locations.
(a): the EAS combined with gamma-families of $\Sigma E_{\gamma,H} \geq 10$ TeV. Two small rectangles indicate the EX chambers (10 m^2 each) and a big one is the spark area (9x6 m^2).
(b): the general EAS with $Ne \geq 2 \times 10^6$. Only the events hit the area within r=5 m were used for the analysis.

The period of the experiment was 302.5 days and the live time of recording system of EAS data was 292.2 days (95.7 %). The total number of EAS recorded by the burst trigger in this period was about 12000 events and the number of EAS obtained by the AS trigger was about 6000 events during about 240 days. The arrival angles of EAS, which are necessary for combining them with gamma-families and for deducing absolute intensity of EAS size spectrum, were detected by four sets of spark chambers. The live time of spark chamber system was a little higher than 80 %.

3. Selection of events

53 gamma-families with total energy $\Sigma E_{\gamma,H} \geq 10$ TeV and $n_{\gamma,H} \geq 2$ for Emin=3 TeV were found in our EX chamber and 44 events out of them were combined with EAS triggered by big bursts. The rate of combination was 83 %. Nine gamma-families were not combined with EAS. This is mainly due to the lack of arrival angle data of EAS because of dead time of the spark chamber system. The data of these 44 combined events were used for deducing the absolute intensity of EAS with big gamma-families assuming that the residual nine unknown EAS have the same size distribution as the combined events. The EAS size Ne and age parameter s were determined by fitting the experimental shower particle density to the NKG lateral function with the Moliere unit 110 m, where the shower axis was put on the location of the gamma-family whose map was given in Fig. 1 (a). On the other hand, about 4200 EAS recorded during the last 170 days by the AS trigger were served for the size spectrum of general EAS. The axis locations of the general EAS whose axes hit the area within radius r=7 m from the array center are shown in Fig. 1 (b) for $Ne \geq 2 \times 10^6$. But, only the EAS whose axes hit the area of $r \leq 5$ m were employed for the analysis here.

4. Results

Using the experimental result about the transition effect of EAS shower particle density by thin materials (Saito et al., 1983) the corrections were made on the raw values of Ne and s for the response excesses of 3 cm thick plastic scintillator and also for the transition effect due to the roof and ceiling materials for indoor counters and due to the counter box material for all counters. As a result, the age parameter s was increased by the amount of 0.18 - 0.16 and the shower size Ne was multiplied by a factor 0.65 - 1.16 depending on the raw values of s from 0.4 to 1.2. The Ne-s scatter plot of the combined events after the correction is shown in Fig. 2. In this figure are also shown the Ne-dependences of average age parameters for combined events (crosses) and for the general EAS (open diamonds).

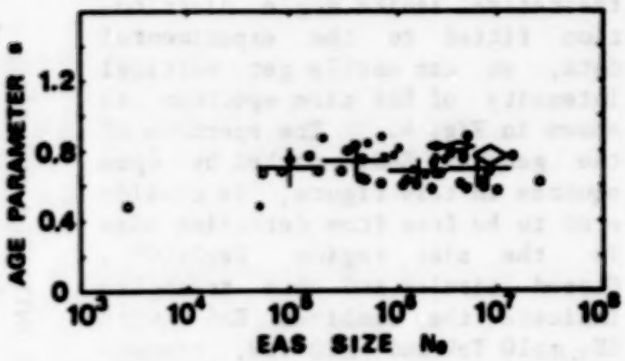


Fig. 2 Ne-s correlation for the combined EAS with gamma-families with $\Sigma E_{\gamma,H} \geq 10$ TeV (scatter plot and crosses) and for the general EAS with sizes $Ne \geq 2 \times 10^6$ (open diamonds).

In order to get the vertical intensity of size spectrum of EAS it is necessary to know the zenith angle distribution of them. In Fig. 3 (a) are shown the distributions for the combined EAS with gamma-families of $\Sigma E_{\gamma,H} \geq 10$ TeV (closed circles) and for the general EAS with $Ne \geq 2 \times 10^6$ (open circles). It is natural that the zenith angle distribution of the combined EAS is steeper than the general EAS but almost same as the gamma-families shown in Fig. 3 (b). Using the values of a factor $x_0/\lambda att$ in the

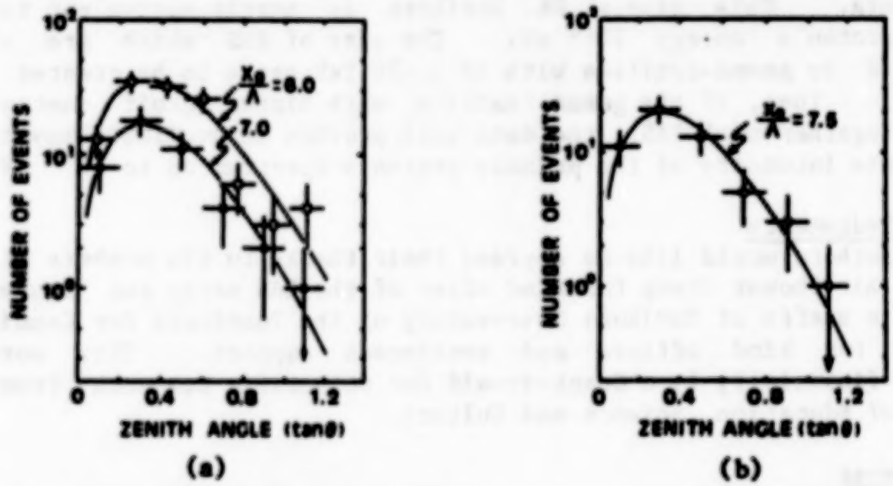


Fig. 3 Zenith angle distributions.
(a): the general EAS with $Ne \geq 2 \times 10^6$ (open squares) and the combined EAS with gamma-families with $\Sigma E_{\gamma,H} \geq 10$ TeV (closed circles).
(b): all gamma-families with $\Sigma E_{\gamma,H} \geq 10$ TeV, $n_{\gamma,H} \geq 2$ and Emin=3 TeV.

theoretical zenith angle distribution fitted to the experimental data, we can easily get vertical intensity of EAS size spectrum as shown in Fig. 4. The spectrum of the general EAS, marked by open squares in this figure, is considered to be free from detection bias in the size region $Ne \geq 2 \times 10^6$. Closed circles and open triangles indicate the combined EAS with $\Sigma E_{\gamma,H} \geq 10$ TeV and ≥ 20 TeV, respectively. It is concluded from this figure that the EAS with $Ne \geq 5 \times 10^6$ are always associated with gamma-families with $\Sigma E_{\gamma,H} \geq 10$ TeV at the altitude of Mt. Norikura (x_0=738 gcm^{-2}). This is consistent with the fact seen in Fig. 2 that both the average values of s agree each other for $Ne \geq 5 \times 10^6$ between the general EAS and the combined EAS with gamma-families with $\Sigma E_{\gamma,H} \geq 10$ TeV. Also, the figure 4 suggests that the EAS with $Ne \geq 10^7$ are always accompanied by gamma-families with $\Sigma E_{\gamma,H} \geq 20$ TeV at the same altitude. These results are important to study the absolute intensity of energy spectrum of the primary protons in the energy region $E_0 = 10^{15}$-10^{17} eV.

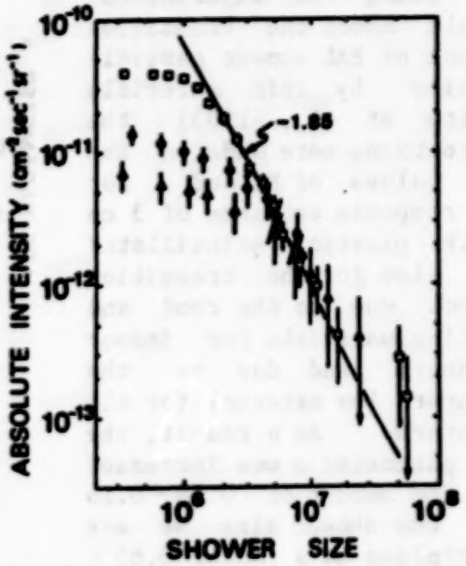


Fig. 4 Integral size spectra for the general EAS (open squares) and the combined EAS with gamma-families of $\Sigma E_{\gamma,H} \geq 10$ TeV (closed circles) and of $\Sigma E_{\gamma,H} \geq 20$ TeV (open triangles).

5. Conclusions

EAS with sizes greater than about 5×10^6 are always accompnied by gamma-families with $\Sigma E_{\gamma,H} \geq 10$ TeV, $n_{\gamma,H} \geq 2$ for Emin=3 TeV at the altitude of Mt. Norikura. This size at Mt. Norikura is nearly equivalent to the primary proton's energy 10^{16} eV. The size of EAS which are always accompanied by gamma-families with $\Sigma E_{\gamma,H} \geq 20$ TeV seems to be greater than about 10^7. Then, if the gamma-families with higher cutoff energy are observed together with EAS, the data will provide an available key to get the absolute intensity of the primary proton's spectrum up to 10^{17} eV.

6. Acknowledgements

The authors would like to express their thanks to the members of the Norikura Air Shower Group for kind offer of the EAS array and assistance and also to staffs of Norikura Observatory of the Institute for Cosmic Ray Research for kind offices and continuous support. This work is supported financially by a Grant-in-aid for Scientific Research from the Ministry of Education, Science and Culture.

7. References

Nakatsuka et al., 1983; Conference Papers of the 18th ICRC (Bangalore), Vol. 11, 346.

Saito et al., 1983; ibid Vol. 11, 217.

Yamamoto et al., 1981; Conference Papers of the 17th ICRC (Paris), Vol. 11, 130.

N85-35930

A COSMIC RAY SUPER HIGH ENERGY MULTICORE FAMILY EVENT (I) EXPERIMENT AND GENERAL FEATURES

CHINA-JAPAN EMULSION CHAMBER COLLABORATION
Ren,J.R., Kuang,H.H., Huo,A.X., Lu,S.L., Su,S., Wang,Y.X., Xue,Y.G.
Institute of High Energy Physics, Academia Sinica, China
Wang,C.R., He,M., Zhang,N.J., Cao,P.Y., Li,J.Y., Zou,B.T.
Shandong University, China
Wang,S.Z.
Zhengzhou University, China
Bai,G.Z., Liu,Z.H., LI,G.J., Geng,Q.X.
Chongqing Architecture College, China
Zhou,W.D., He,R.D.
Yunan University, China
Amenomori,M., Konishi,E., Nanjo,H.
Hirosaki University, Japan
Hotta,N., Ohta,I.
Utsunomiya University, Japan
Mizutani,K., Sato,T.
Saitama University, Japan
Kasahara,K., Yuda,T.
Institute for Cosmic Ray Research, University of Tokyo, Japan
Torii,S.
Kanagawa University, Japan

I. Introduction. Information on the fragmentation region in super high energy hadronic interactions can be obtained through the observations of γ-ray families produced by cosmic rays. γ-ray families with $\Sigma E_\gamma \geqslant 1000$ TeV are receiving increasing interests in emulsion chamber experiments. There exist some complications caused by the superposition of nuclear and electromagnetic cascades and the uncertainty in the nature of the primary particles. These complications usually make the conclusions drawn from various interesting phenomena observed in family events not so definite. Here we describe an interesting family event KO E19, which is likely to have suffered only very slight disturbances. It was found in Mt. Kambala emulsion chamber experiment. The production height of the event is determined to be $H=(70\pm30)$m and some conclusions are given.

II. Experiment. The event KO E19 was found in 14.8 m^2 of emulsion chamber (thickness 14 c.u.) exposed on Mt. Kambala during 1980.9-1981.9. The photosensitive materials of the emulsion chamber consist of x- ray films of Sakura N type and Fuji 100 type and nuclear emulsion plates of ET7C type. On the N type x-ray films, the central part of the event is completely blackened, forming a halo. The visible energies of the event are determined independently on the three kinds of photosensitive plates and crosschecked, yielding a consistent result.

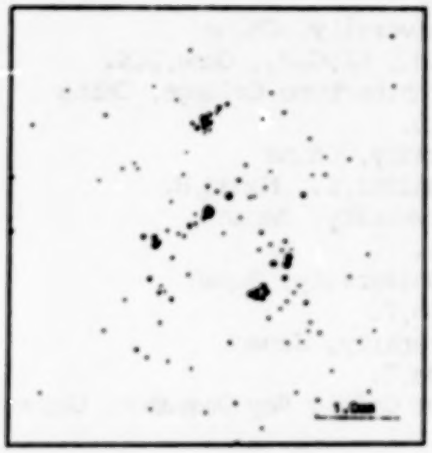
The optical density distributions in the halo part are determined on all layers of N type films. From the variation of the density distributions on consecutive layers, we can determine the electron number densities n_t and obtain the total number of electrons N and their total track length Z on the basis of the approximation B, thus giving the visible energy of the halo (1) $\Sigma E_\gamma = 1200$ TeV. Every shower in the central part of the event are clearly separated from each other on the 100 type x-ray films and the ET7C type nuclear emulsion plates (Fig.1). On the 100 type films, we can make accruate measurements of the positions and

N85-35930

ORIGINAL PAGE IS
OF POOR QUALITY

optical densities, shower by shower, using the Mitaka-Hamamatzu automatic microphotometer. From the darkness-energy relation with Landau effect correction, we can determine the total visible energy(2), yielding ΣE_γ= 1300 TeV (E_{min}=2 TeV). On the ET7C emulsion plates, the electron track counting method is used for the energy determination of the majority of showers except those of very high energies, for which the photometric method is applied. The resultant visible energy is ΣE_γ= 1537 TeV (E_{min}=1.5 TeV), which is somewhat higher due to the lower threshold in the energy determination.

Fig.1



With the photometer system used, x and y distances can be measured accurate to about 1 μm and shower centers (points of maximum optical density) can be determined with a small aperture.

III. General Features of KO E19. The general statistical characteristics of the event are listed in Table I, where N_γ is the number of γ-rays ($E_\gamma \geq 3$ TeV)and R the distance from the energy center of the event to the center of a shower. For families produced not too high above the detector, the electromagnetic cascades are usually not fully developed and thus $\langle ER \rangle$ will be small and $\langle E_\gamma \rangle$ large, while the energy spectrum will be exponential in form. This is the case for KO E19, as can be seen from Table I and Fig.2. Fig.3 shows the ER-R correlations of the showers in the event, points within the dashed circle representing those in the central part. It is this portion which is the least disturbed during the development and can provide interesting information about the super high energy hadronic interactions.

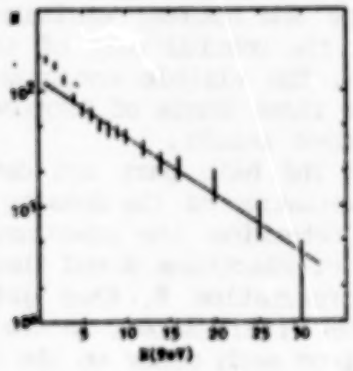


Fig.2

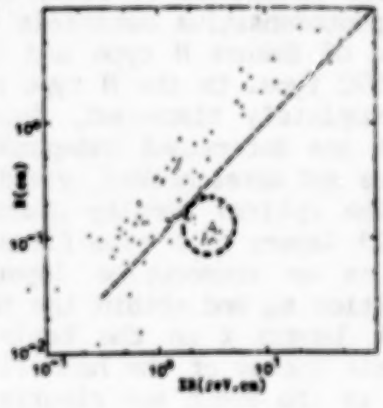


Fig.3

HE 3.4-1

Table I. Statistical characteristics of KO E19

$N_\gamma(E \geq 3TeV)$	ΣE_γ(TeV)	$\langle E_\gamma \rangle$(TeV)	$\langle R \rangle$(cm)	$\langle ER \rangle$(TeV.cm)
131	1083	8.3	0.39	3.23

IV.Production Height and Pseudorapidity Distribution. The exponential energy spectrum, the very low value of $\langle ER \rangle$ and the relatively high value of $\langle E_\gamma \rangle$ show some evidences of the small production height H of the main part of KO E19. For an accurate determination of H, a triangulation method is used. Among showers with $E_\gamma \geq$ 10 TeV and penetrating through the whole thickness, 14 c.u., of the chamber, choose those with favorable measuring conditions. Take a pair of such showers i,j and determine the separations between them, R^k_{ij} and R^{k+m}_{ij} , on the k-th and the (k+m)-th layers respectively. Repeat the same for every pair. Then the production height H can be calculated from

$$H = (m\Delta H \sum_{ij} R^k_{ij}) \; / \sum_{ij} (R^{k+m}_{ij} - R^k_{ij})$$

where ΔH is the distance between two consecutive x-ray film layers. In our actual measurements, k=1, m=5 and ΔH=1.3cm. The result is H=(70 ±30)m. As a rough check of this result, we make a mass distribution obtained from the coupling of the above showers pair by pair, where we take $m_{ij} = R_{ij}\sqrt{E_i E_j}/H$, with H=70m. This is compared with a simulation calculation shown in Fig.4. There are two peaks at m_{ij}=150 MeV and 500 MeV in the experimental distribution, corresponding to the masses of $\pi^0$and η^0 respectively. and thus confirming the result from triangulation.

With H=70 m, calculate the pseudorapidity $\eta = -\ln \tan(\theta/2)$ where θ is the emmision angle of a secondary particle. The distribution of η is shown in Fig.5. There is a hump near η=12, which may be attributed to the showers in the cores of the central part. The magnitude of the plateau is roughly $\Delta N/\Delta\eta$=40, a value about four times as large as that of the scaling extrapolation of accelerator results. The energy dependence of $\Delta N/\Delta\eta$ is shown in Fig.6, indicating a more rapid increase in $\Delta N/\Delta\eta$ above 10^{16} eV.

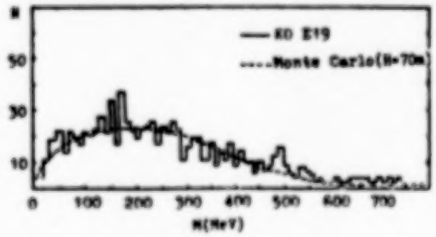


Fig.4

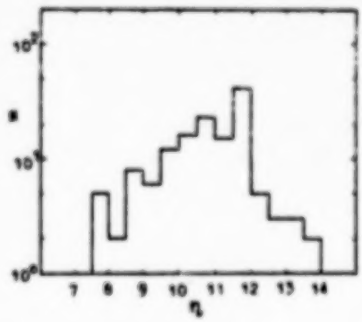


Fig.5

Taking H=70 m, the p_t distribution in the family is shown in Fig.7, where "o" represent data of KO E19 (E_{min}=4 TeV) and "+" come from C-jets (E_{min}=0.5 TeV) . In the p_t<800 MeV/c region, the p_t distribution of KO E19 is consistent with that of C-jets and both of them take the exponential form e^{-5P_t} . The central portion of the family will be treated in (5).

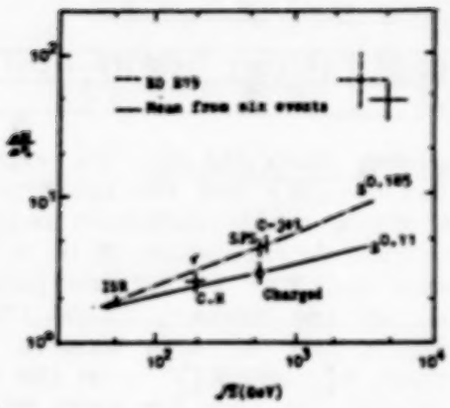


Fig.6

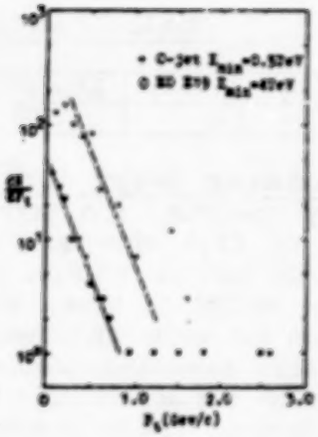


Fig.7

References.
(1) T.Yuda, Utsusen Kenkyu (in Japanese) 24(1981) 92.
(2) K. Kasahara, 18th ICRC, 5(1983) 303.
(3) T. Yuda, 18th ICRC, 12 (1983) 341.
(4) C.M.G. Lattes, Physics Reports, 65 (1980) 151.
(5) J.R. Ren et al., HE 3.4-2, this conference.

ORIGINAL PAGE IS
OF POOR QUALITY

N85-35931

HE 3.4-2

A COSMIC RAY SUPER HIGH ENERGY MULTICORE FAMILY EVENT (II) STRUCTURE AND FRAGMENTATION CHARACTERISTICS OF THE JETS

China-Japan Emulsion Chamber Collaboration*

I. Introduction. Quarks and gluons are not directly observable, but may be displayed through fragmentation in the form of hadronic jets, the evidence of which was first revealed in cosmic ray interactions before the advent of the modern theory of strong interactions. Experimental results from ISR(1) and SPPS collider rendered the jet phenomena more confident and definite. All the properties of jets observed up to now at ISR and SPPS collider are in agreement with the predictions of QCD(2-4). In order to make further test of QCD in still higher energy regions, detailed study of super high energy jet events in cosmic rays is very desirable. The event KO E19 observed in Mt. Kambala emulsion chamber is an interesting event for such study. The general features of KO E19 is described in (5). Its total visible energy is ΣE_γ=1537 TeV(E_{min}=1.5 TeV) and production height H=(70±30)m, with a hadron as its primary particle. Besides about forty small clusters, there are five super high energy cores or jets, one lying near the center of the event while the other four surrounding it, having incident directions making small angles (about 5°-6° in CMS) with that of the primary particle. Detailed analysis is done on the emulsion plates inserted in the chamber, making full use of their fine granularity, superior in detecting and analyzing jet events, especially their substructures.

II. Jets and jetty event. By jet we generally mean a bundle of fairly collimated hadrons in the final states of high energy interactions. It can also be considered as a cluster of particles in the pseudorapidity-azimuth (η-φ) space. We adopt a procedure for the jet clusterization similar to that in accelerator experiments as follows. Assign an energy vector to every shower (track), directed from the vertex of the event to the point of recording. Find out the largest of these vectors and compute the quantities d of other ones relative to the largest in η-φ space, where $d=\sqrt{(\Delta\eta)^2+(\Delta\varphi)^2}$. Add all energy vectors with d≤1.0 to the largest one vectorially, we then obtain a jet. Next find out the largest vector among the remaining ones and repeat the above procedure to get another jet, etc. A transverse energy threshold is taken, which may be 10-60 GeV. For the four outer jets in KO E19, the minimum E_t=10 GeV and the maximum d=0.82-1.0, corresponding to φ=38°—44° and θ=4.8°—6.1°. Adopt $\sum_K(\Sigma_{jet})_h/\Sigma E_\gamma \geq 70\%$ as a criterion for the so-called jetty events, conforming to the convention in accelerator experiments. In our case, the total energy of the four outer jets is 756 TeV and corresponds a fraction of 76% of the total visible energy 994 TeV(E_{min}=4TeV). If the energy of the central jet is also included, the fraction will increase to 79%. Therefore we may consider KO E19 as a jetty event. The characteristics of jetty events are closely related to the production and fragmentation behaviors of jets.

III. Structures and fragmentation characteristics of jets. The transverse momentum p_t of a jet can be obtained by vector addition of the p_t's of all its constituent particles. If the jet particles are assumed to be π's, then the p_t of the four outer jets are 12.77,11.42,6.81 and 8.63 GeV/c. Fig.1 gives the vector diagram of these jets. The sphericity of a jet is defined as $S_h = 3(\Sigma j_t^2)_h / 2(\Sigma j_t^2)$, where j_t is the momentum

* For full list of authors, see HE 3.4-1, this conference.

N85-35931

ORIGINAL PAGE IS
OF POOR QUALITY

of the i-th particle and $j_{t\ell}$ is its transvers component relative to the axis of the n-th jet. For an event with n jets, the total sphericity is the sum over all jets. The total sphericity of KO E19 is S=0.0074 and the total neutral transverse energy E°_{t} =148 GeV, which are compared with accelerator results qualitatively in Fig.2, showing no inconsistency

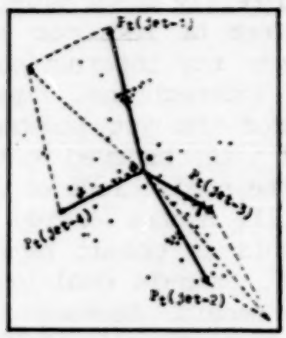


Fig. 1

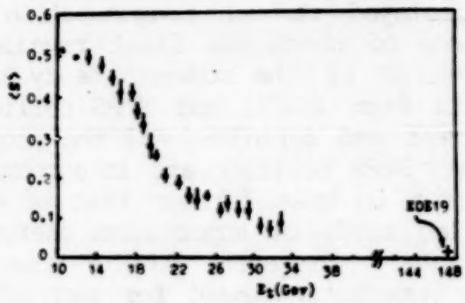


Fig. 2

in its trend. The distribution of θ^{*}_{j} , the angle between the particle momentum and the jet axis in CMS, is shown in Fig.3 for the four outer jets. The peak value of θ^{*}_{j} for KO E19 lies near 0.5°, consistent with the most probable values 7° and 2° in ISR and SPPS collider energy regions, respectively. Take H=70m, $\langle J_{t\gamma}\rangle$ =0.04 GeV/c, corresponding to $\langle j_{t}\rangle$=0.08 GeV/c, smaller than the average from $p\bar{p}$ collider.

The fragmentation variable is a useful quantity in jet analysis. It is defined as $z=2E_{j\gamma}/3(\Sigma E_{\gamma})_{j}$, representing the fraction of the component of shower energy along the jet axis in total visible jet energy. The factor 2/3 takes account of the fact that the secondary particles are mainly γ-rays, coming from the decay of π°'s. The distribution of z is called the fragmentation function of jet: $D(z)=(1/N_{j})dN_{ch}/dz$. Fig.4 gives the fragmentation function of the five jets in KO E19, Which

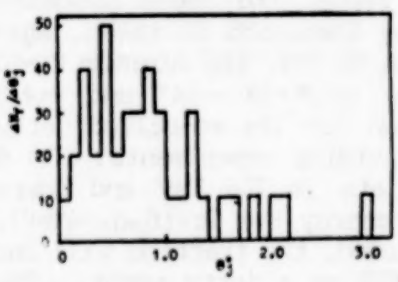


Fig. 3

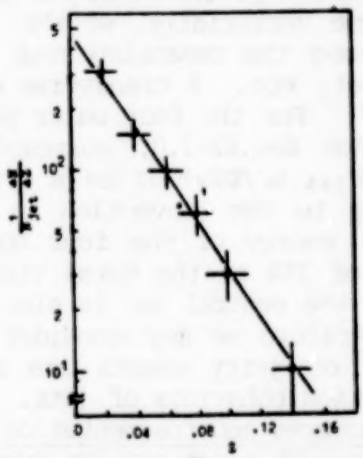


Fig. 4

is in the exponential form Exp(-Bz), with B=27.4. Data from ISR and FNAL are also included for comparison. In the ISR range, ABCS Collaboration gave an exponential D(z) for small z, with B≅7, while CCOR Collaboration obtained B≅5.3 at lower energies. FNAL(9) obtained B≅4.6,

ORIGINAL PAGE IS
OF POOR QUALITY

using jets with p_t lower than ABCS Collaboration. As noted in (7), when the energy of the scattered parton increases, the number of fragmentations increseases also, resulting in a decrease in z and an increase in the slope. KO E19 is a super high energy event and the value of B should be correspondingly larger. By integration of the jet fragmentation function, we can obtain the charged particle multiplicity in the jet. For the five jets of KO E19, $\langle N_{ch} \rangle \approx 18$, $\langle E_{jet} \rangle \approx 95$ GeV in CMS. A comparison between KO E19 and accelerator results(10) is shown in Fig.5. There is an evident increase in N_{ch} in KO E19.

IV. Comparison with QCD calculations at TeV energies. It is shown in the phenomenological QCD study of the properties of the jets produced in hadronic collisions in $\sqrt{s}$ = 10 TeV range(11), that hadronic jets are mixtures of quark jets and gluon jets and that 50% of the energy of quark jets is carried by particles with z=0.06 while the corresponding value for gluon jets is z=0.025. From KO E19 data, 50% of the jet energy is carried by particles with z=0.045, in reasonable agreement with the above estimation. The particle multiplicity of jets as a function of jet energy is shown in Fig.6(11). The value of $\langle N_{ch} \rangle$ is

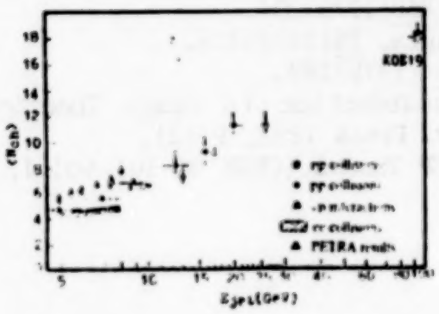


Fig. 5

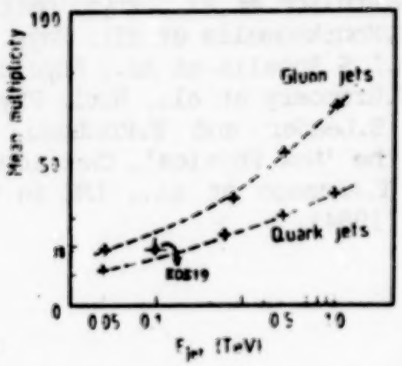


Fig. 6

about 18 and lies between the theoretical values for quark and gluon jets. The fractions of the numbers and energies of jet particles outside the jet cone in KO E19 are also close to the theoretical results. The high p_t Monte Carlo events generated by the ISAJET program are shown to have core structures. This is also the case for the four outer jets in KO E19. Fig.7 gives the jet number distribution reconstructed from

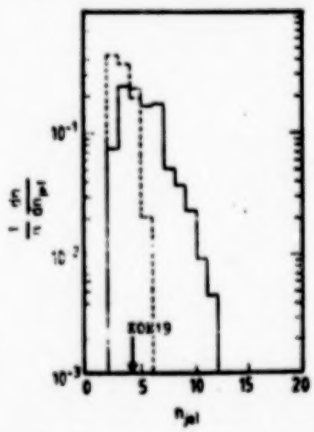


Fig.7

the TeV range Monte Carlo events by means of the clusterization techni-

que, where the solid line represents events with $E_t > 10$ GeV and the dotted line those with $E_t > 100$ GeV. For the four outer jets in KO E19, $E_t > 10$ GeV, $N_{jet} = 4$, lying within the theoreticlal prediction. From the above analysis, it can be seen that the characteristics of KO E19 are in agreement or not inconsistent with the predictions of the phenomenological QCD. Further analysis and confirmation require more events.

References

(1) M.Jacob et al., Phys. Rep. 48(1978) no.4.
(2) T.Akesson et al., 14th Inter. Symposium on Multiparticle Dyn. Lake Tahoe, CA(1983).
(3) M.Banner et al., PHys. Lett. 118B(1982)203; P.Bagnaia et al., Phys. Lett. 138B(1984)430; G.Arnison et al., Phys. Lett. 123B(1983)115.
(4) R.Horgan and M.Jacob, Nucl. Phys. B179(1981)441; R.Field, La Jolla Summer Institute,1978; AIP Conf.Proc., no.53(1979); R.Horgan and M.Jacob, CERN Rep. 81-04(1981).
(5) Ren Jingru et al., Physica Energiae Fortis et Physica Nuclearis (in Chinese); Ren Jingru et al., see HE 3.4-1, this conference.
(6) G.Arnison et al., Phys. Lett. 132B(1983)214.
(7) C.Kourkoumelis et al., Phys. Lett.86B(1979)391.
(8) A.L.S.Angelis et al., Physica Scripta, 19(1979)116.
(9) C.Brambery et al., Nucl. Phys. B134(1978)189.
(10) E.Leader and E.Predazzi, An Introduction to Gauge Theories and the 'New Physics', Cambridge Univ. Press 1982, P.421.
(11) T.Akesson et al., LHC in the LEP Tunnel,(CERN 84-10) Vol.I, P.165 (1984).

N85-35932

OBSERVATION OF SUPER HIGH ENERGY BIG FAMILY WITH LARGE SCALE Pb EMULSION CHAMBERS

China-Japan Emulsion Chamber Collaboration*

I. Introduction. In order to get higher efficiencies for detecting hadrons and to make technical improvements in the chamber structure, the Mt. Kambala Emulsion Chamber Collaboration constructed 57 m² of Pb chamber, with thickness 29 c.u.(1c.u.=17.5 mm Pb), using 300 tons of Pb plates and made the first exposure from Sept., 1982 to May, 1984. The photosensitive layers consist of x-ray films of Sakura N type, Fuji No. 100 type and Tianjin III type, some of them contain also emulsion plates of Fuji ET7B type. They are inserted between the Pb plates at every 2 c.u., beginning at 5 c.u. from the chamber top. In a number of blocks, 3 mm spacings are provided at every 2 c.u. of Pb plates to facilitate the replacement of photosensitive layers, without disassembling the chamber. On the bottom of the chamber Pb plates of thickness 9 mm are placed in order to shield the chamber from the radioactivities of the ground. An event, numbered K2 58 of visible energy ΣE_γ = 7345 TeV was found in this exposure. It is the event with the highest energy obtained in Mt. Kambala emulsion chambers up to now. No obvious halo is seen in the event and all the showers are clearly separated and easy to measure. A brief report of the preliminary results is given here.

II. General characteristics of the event. There are 566 showers with visible energies greater than 3 TeV, distributed as shown in Fig.1. It is evident that the event is a single core family. On the map of the event, 161 high energy showers of total visible energy ΣE_γ = 4228 Tev are concentrated within a circle of radius 8 mm, therefore it is not necessary to carry out clusterization of the showers. Fig.2 is the optical density distribution contours of K2 58, obtained by the automatic photometer NGD-17×17, with optical aperture 300×300 m².

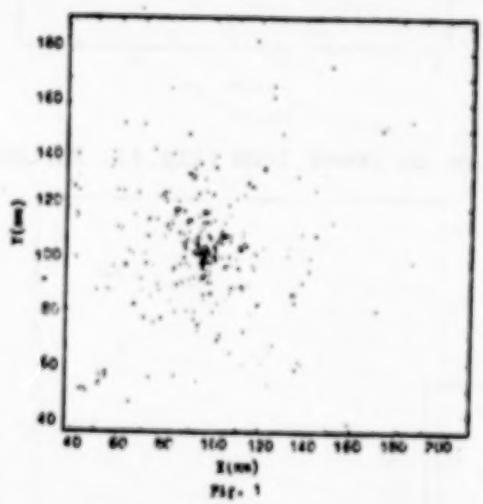


Fig. 1



Fig. 2

Various statistical averages are given in the table I, where Δt is the depth of the starting point of a shower. The various averages remain unchanged when Δt is taken either as $\leq$ 4 c.u. or as $\leq$ 6 c.u.. The data in the last row of the table I are the corresponding quantities

* For full list of authors, see HE 3.4-1, this conference.

N85-33932

for events with visible energies $\Sigma E_\gamma \geq 1000$ TeV obtained in earlier exposures at Mt. Kambala (2). Both results agree well.

Table I. Statistical Averages for Big Families (E_{min} = 4 TeV)

Event	t (c.u.)	N	R (cm)	ER (TeV.cm)	E (TeV)	E (TeV)
K2 58	4	417	2.02	19.9	15.1	6300
	6	455	2.04	19.9	14.9	6800
Mean for 5 Events	6	134	1.94	16.3	11.7	1530

III. Energy spectrum and ER distribution. Shower energy spectra and ER distributions taken with different values of Δt are shown in Fig.3. The shape of the energy spectrum remains almost unchanged as the value of Δt is varied. It is nearly of the form $N(>E) \propto E^{-\beta}$, where $\beta = 1.2$. All the energy spectra of showers in circles with different radii R and centered

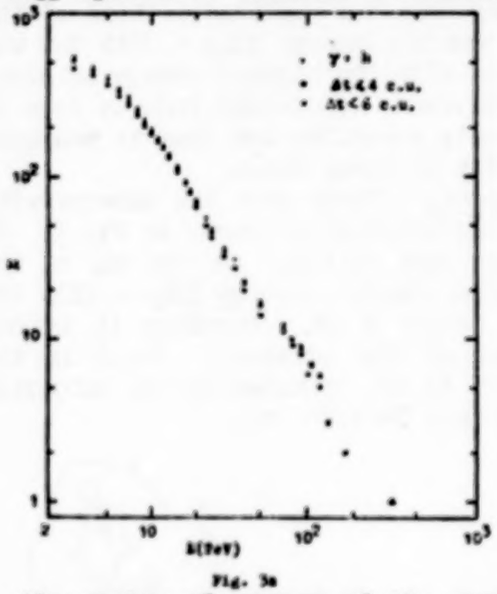


Fig. 3a



Fig. 3b

at the center of energy of the event are in power form (Fig.4). Furthe-

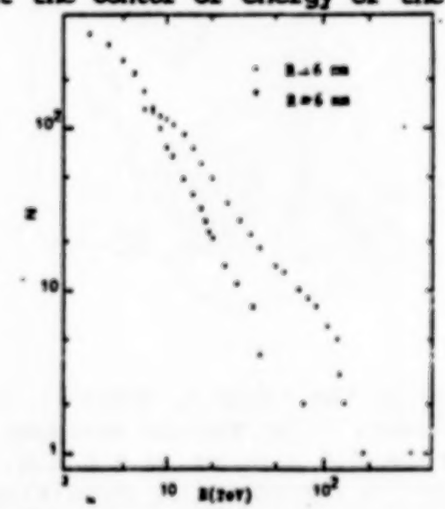


Fig. 4

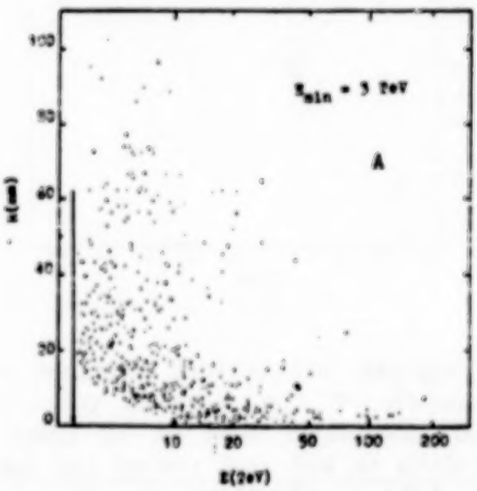


Fig. 5

ORIGINAL PAGE IS
OF POOR QUALITY

N85-33033

more, the energy spectrum of showers with $E_\gamma \geq 10$ TeV remains almost the same when R has increased to 8 mm. These indicate that the production height of the event is so high that both the central and the peripheral parts of the event have already undergone sufficient electromagnetic processes. In the R < 12 mm region, are concentrated a large number of showers of energies in the interval 3-10 TeV, making the optical densities in their neighborhood greatly exceeding those of the background and rendering the showers with lower energies obscure (see the triangular blank region A in Fig.5). From the energy spectrum $N(>E) \propto E^{-\beta}$ at $E_\gamma \geq 10$ TeV, it is estimated that there should be about 180 showers with $E_\gamma \geq 3$ TeV in the blank region A, with a corresponding total energy $\Sigma E_{\gamma A} = 808$ TeV.

Fig.6 gives the energy spectrum for showers with $\Delta t = 6$ c.u., corresponding to the energy spectrum of a part of the Pb-jets in Pb chambers. The result is the same as that in Fig.3.

Thick Fe chambers are more effective than Pb chambers in the detection of hadrons, but the method for disciminating Fe-jets and γ-rays (electrons) remains to be further explored. Criteria based on the difference in Δt are unfavorable but considerations about the consecutive interactions of hadrons in Fe may be more adequate. Fig.7 gives an example of the transition curve in Fe of a high energy shower, with $\Delta t \sim 0$. It is seen that the trend of the shower development distinctly deviates from the transition curve of the showers produced by γ-rays (electrons), corrected for the L-M effect (3). However, this is applicable only to high energy showers but is difficult for low energy ones.

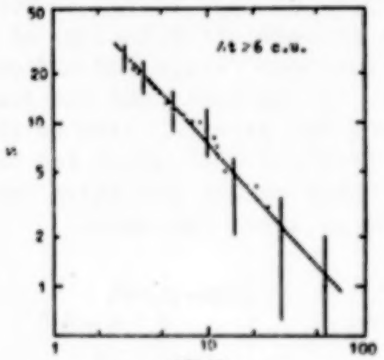


Fig. 6

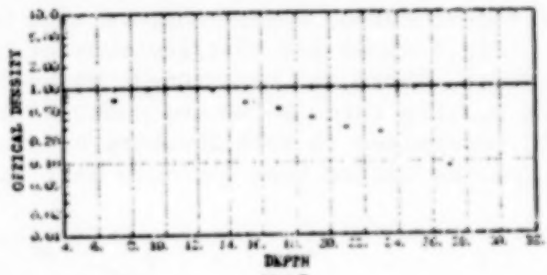


Fig.7

References
(1) I.Onta, Uchusen Kenkyu (in Japanese), 24(1980)147.
(2) J.R.Ren et al., Physica Energiae Fortis et Physica Nuclearis (in Chinese), to be published.
(3) K.Kasahara 1984, unpublished.

HE 3.4-5

N85-35933

A Halo Event Created at 200 m above the Chacaltaya Emulsion Chamber

N.M.Amato, N.Arata (CBPF, Rio de Janeiro, RJ, Brasil) and
R.H.C. Maldonado (UFF, Niteroi, RJ, Brasil)

1. Introduction

We present the results of analysis on a cosmic-ray induced nuclear event with the total visible energy ~1300 TeV which is characterized by the central (halo) part of a strong energy concentration and the outer part of a large lateral spread. The event (named as P06) was detected in the 18th two-storied emulsion chamber exposed at Chacaltaya by Brasil-Japan Collaboration. As the nuclear emulsion plates were inserted at every layer of the concerned blocks in the upper and the lower chambers together with RR- and N-type X-ray films, we can study the details of the event.

Some results on P06 have already been reported [1] based on the general measurement of opacity on N-type X-ray films: (1) the total energy of halo is ~1000 TeV; (2) the shower transition reaches its maximum at ~16 cu; and (3) the radius of halo is 6.5 mm (at the level of 10^6 electrons/cm^2). The results in more details will be described here.

2. Results

Fig.1 shows the target diagram of P06, where we notice a large lateral spread of the event and richness in hadrons in the outer region.*

Fig.2 shows the contour map of opacity (D=.2, .3, .4, .6, .8 and 1.) for the central part of halo on RR-type X-ray film at 14 cu in the upper chamber with slit diameter 113 μ, together with the high energy shower cores (E >10 TeV). A clear asymmetry is seen in both distributions of D and shower cores. Notice that it also holds for both γ-rays and hadrons.

Fig.3 shows the distributions of opacity in the upper and the lower chambers, where the measurement was made along the straight line on the film passing through the two hadronic cores (#40 and #58) which can be well recognized in both chambers because of their strong and sharp penetration. We notice that the halo part contains at least two peaks.

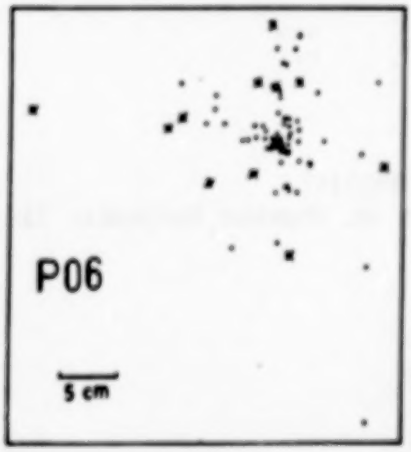


Fig.1 Target diagram of P06. γ-rays (•) and identified hadrons (×).

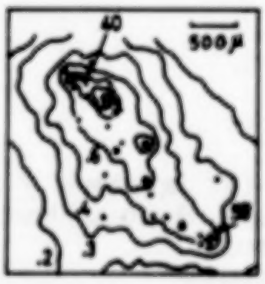


Fig.2 Contour map of opacity of RR-type X-ray film at 14 cu and shower cores: γ-rays (●: >20 TeV, • :10-20 TeV) and hadrons (+). The cores (#40 and # 58) are indicated.

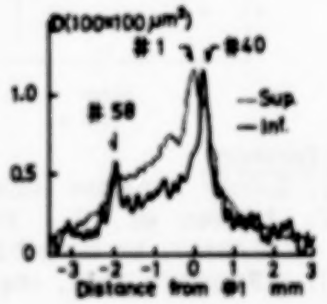


Fig.3 Distributions of opacity on RR-type X-ray film at 14 cu in the upper chamber(Sup) and on N-type X-ray film at 4 cu in the lower chamber (Inf).

ORIGINAL PAGE IS
OF POOR QUALITY

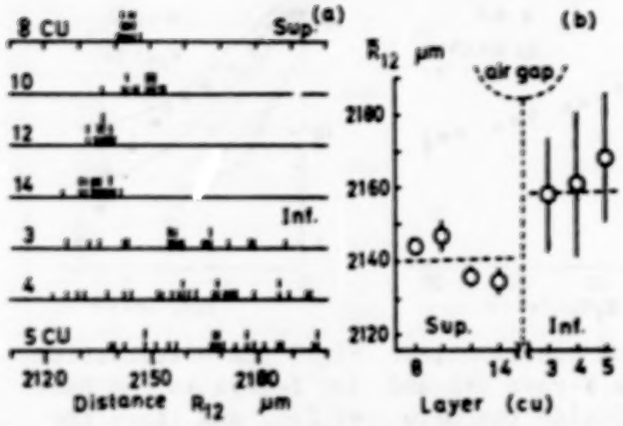


Fig.4(a) Measurement of the relative distances, R_{12}, between #40 and #58 in the upper (Sup) and the lower (Inf) chambers. 4(b) Variation of $\bar{R}_{12}$ at 8, 10, 12 and 14 cu in the upper chamber and at 3, 4 and 5 cu in the lower chamber. The best fitted straight line is also shown.

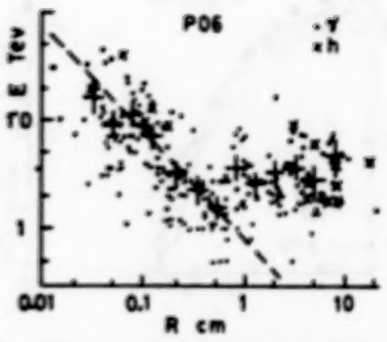


Fig.5 Correlation Diagram between energy and distance of P06. γ-rays(·) and hadrons(×). ± are for the average values.

Fig.4-a shows the results of measurement on the relative distance, R_{12}, between #40 and #58 on the nuclear emulsion plates which was done repeatedly after some blank days enough long to forget the previous measurement. Fig.4-b shows the average values of R_{12} at 7 layers together with the best fitted straight line given by the least-square method which corresponds to the interaction height $H = 208 \pm {}^{245}_{73}$ m. The value of χ^2 is rather large, 16.4 for the 7 points, of which 4 points in the upper chamber share 98% of the total; we could not resolve the fluctuation seen in the upper chamber. If we use the average value of 4 points, $H = 177 \pm {}^{165}_{58}$ m; if we take only the point at 10 cu, $H = 263 \pm {}^{784}_{112}$ m. In the following, we take 208 m as the vertical height above the chamber which corresponds to H_o - 250 m after the correction on zenith angle (35°).

Fig.5 shows the diagram of energy, E, and distance, R, for all the shower cores observed in P06, where R is measured from the energy-weighted center of shower cores which are located inside the halo radius, 6.5 mm. The dashed line stands for the fit to the averages in the central region,

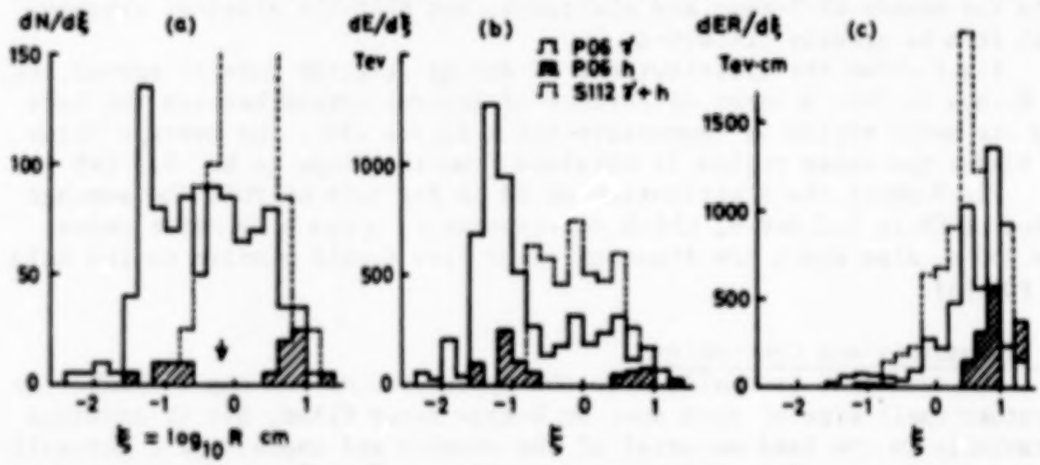


Fig.6 (a) Histogram of $\log_{10}R$, (b) energy-flow and (c) energy-weighted lateral distance ER-flow in $\log_{10}R$, for γ-rays and hadrons in P06, and for all the shower cores in the event S112.

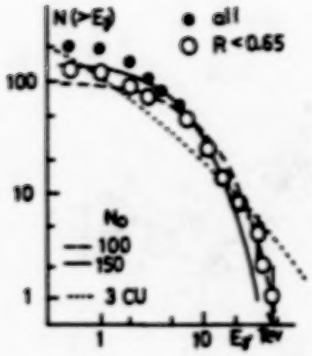


Fig.7 Energy distribution. All the γ-rays(•) and γ-rays in the halo radius (○) in P06.

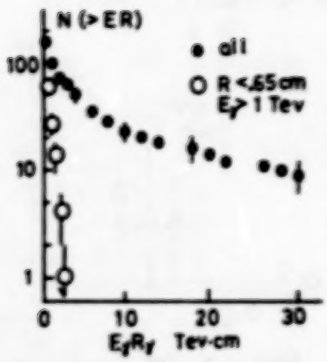


Fig.8 ER distribution. All the γ-rays (•) and γ-ray inside the halo radius (○) in P06.

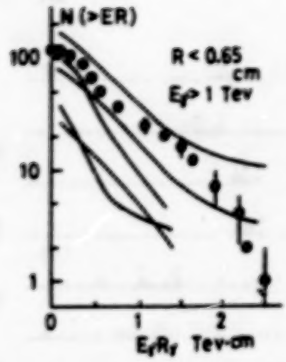


Fig.9 ER distribution for γ-rays in the halo of P06, and those for other 5 events [3].

$\langle ER \rangle$ = 8 GeV m which corresponds to p_T = 32 MeV/c under H_0 = 250 m. In the central region, the correlation between E and R shows some constancy of ER (or p_T) but the behavior in the outer region is quite different.

Fig.6 (a-c) show the flows of number, energy and energy-weighted lateral spread in the space of $\log_{10} R$, respectively. The γ-rays and the hadrons are shown separately. Also shown for the comparison are the results of the event S112 which is classified as Guaçu-type meson production characterized by the large p_T and the high multiplicity [2]. As the total energy (878 TeV) and the interaction height (~250 m) of S112 are nearly equal to those of halo part of P06, we can compare the two events with each other without any normalization. We notice that P06 contains a strong concentration of particles and energy in the small angular region as a clear peak of halo (75% of the total energy being inside the radius) but S112 not, and that the outer region of P06 is similar to S112.

Fig.7 shows the energy distribution of γ-rays in P06 in an integral form. The dashed and the solid lines stand for the exponential distributions of the form $N_0 \exp(-E_\gamma/\Sigma E_\gamma)$ with N_0 = 100 and 150, respectively. The dotted line is the result of analytic calculation with t=3 cu and N_0=6 where required are 1 TeV for the energy threshold and 1000 TeV for the total visible energy. We notice that a long passage in air does multiplicate the number of γ-rays and electrons, but that the original exponential form is greatly distorted.

Fig.8 shows the distributions of energy-weighted lateral spread, ER, of γ-rays in P06. A large difference of lateral spread between the halo and the outer region is impressive (of a factor ~30). The average value of ER for the outer region is obtained from the slope to be ~0.2 GeV km.

Fig.9 shows the distribution of ER in the halo of P06. The average value of ER is 7.2 GeV m, which corresponds to $\langle p_T \rangle$ = 29 MeV/c under H_0 = 250 m. Also shown are those of other five events similar to the halo of P06 [3].

3. Discussions and Conclusion

The event P06 is realized in the upper part of the upper chamber as a rather small size of dark spot on N-type X-ray films, but it develops remarkably in the lead material of the chamber and appears as a generally darkened wide area [1]. This area is called as "halo".

The total visible energy is 1275 TeV, 217 shower cores being observed

N85-35934

on the nuclear emulsion plates. Within the halo radius (0.65 cm), 965 TeV is emitted in 127 shower cores. To explain this large particle density in a small region, one might imagine a long passage in the atmosphere to include the cascade multiplication process. But the experimental results of P06 do not seem to support such a naive consideration:

(1) The halo energy estimated by the general measurement of opacity is nearly equivalent to the energy sum, ΣE_γ, of shower cores. The former should include the contribution of low energy showers which are not visible in the latter. In case of the event Andromeda, E(halo) ~ 3.5 ΣE_γ [4];

(2) The depth of shower maximum is very deep in P06 (~16 cu). In case of Andromeda, it is ~10 cu [4];

(3) The sharp alignment on azimuth is seen for both γ-rays and hadrons;

(4) The energy distribution is almost exponential.

The above results indicate that the halo of P06 does not suffer from a large cascade degradation during its passage in the atmosphere, and that the high energy shower cores observed on the nuclear emulsion plates play a decisive role in the halo.

The triangulation method gives us a direct check on that point. The interaction height is obtained to be ~250 m although some fluctuation is seen in four layers in the upper chamber. Taking 250 m, the halo part of P06 comes to be of abnormally small p_T (~30 MeV/c on the average) and of high γ-ray density in rapidity (~59 at the maximum). There is a possibility that a new phenomena happens to appear in the super high energy region which is characterized by a very small p_T (a few tens of MeV/c).

The large lateral spread with richness in hadrons is seen in the outer region of P06, which seems to be a common feature in the halo events [5]. It may be plausible to speculate that the mechanism of large p_T phenomena could produce some new character to create the halo.

The new characteristics seen in the halo of P06 could be compared with those of the so-called "mini-cluster" which is also characterized by the small p_T, 10-20 MeV/c [6].

4. Acknowledgement

The authors wish to express their thanks to all the members of the Brasil-Japan Collaboration for their kind and continuous support. They are grateful to Profs. C.M.G.Lattes, S.Hasegawa and S.A.Slavatinsky for their valuable comments. Thanks are also due to the CNPq, Brasil, for their financial support.

References

[1] N.M.Amato et al., Proc. of Internat. Symposium on Cosmic Rays and Particle Physics, Tokyo, 1984, p.123.
[2] H.Semba, Nuovo Cimento 49A (1979) 247.
[3] S.Hasegawa, Proc.of Internat.Symposium (see [1]), Tokyo,1984, p.62.
[4] A.Ohsawa, ICR-Report-112-83-6 (1983) 65.
[5] S.Yamashita, Journal of Phys.Soc.Japan 54 (1985) 529.
[6] Brasil-Japan Collaboration, AIP Conf.Proc., 85 (1981) p.500.

* We used the following criteria to identify hadrons: the starting point of cascade is estimated to be deeper than 4 cu and/or the transition curve indicates a successive interaction.

N85-35934
HE 3.4-6

A Binocular-type Atmospheric Interaction Generating Sequential Exotic Features

N.M.Amato*, N.Arata* and R.H.C.Maldonado**

* Centro Brasileiro de Pesquisas Físicas
Rua Dr. Xavier Sigaud 150
22290 Rio de Janeiro, RJ, BRASIL

** Instituto de Física
Universidade Federal Fleminense
Niteroi, RJ, BRASIL

Abstract A cosmic-ray induced nuclear event is presented, which is of clear binocular-type and contains several exotic features through its passage in the atmosphere and the emulsion chamber.

1. Introduction

Brasil-Japan Collaboration has observed some exotic events (Centauro family) in the high-energy cosmic-ray interactions, and they are classified into four categories as (original-) Centauro, Mini-Centauro, Geminion and Chiron according to their multiplicity and average p_T./1,2/ Their common feature is a lack of γ-ray emission in their interactions, and they are regarded as phenomena quite distinct from the normal pion production.

In this paper, we present a very special event which shows several exotic features in three generations of interactions.

2. Experiment

The event was observed in the 19th emulsion chamber at Chacaltaya. The chamber is two-storied, which consists of an upper chamber, a lower chamber and a target layer in-between. The chamber is multi-layered sandwiches of lead plates and photo-sensitive materials. In the unit block where the present event was detected, nuclear emulsion plates were inserted with N-type X-ray films at 6,8 and 12 cu in the upper chamber and 3,4,5,6,10 and 12 cu in the lower chamber. At 4 and 10 cu in the upper chamber and at 8 cu in the lower chamber, only X-ray films were inserted. Thanks to the high spatial resolution of nuclear emulsion, we can study a fine structure of shower cores in detail which is quite powerful to pick up and examine the exotic features.

3. Results

As the event was observed in the unit block 109 in the upper chamber and in the block 69 in the lower chamber, we name this event as CH19 S109 I69. In the following, the results corrected on the incident zenith angle (15 degrees) will be presented.

Fig.1 shows the target diagram of the event, which already visualizes the first impressive feature, i.e., a clear double-core structure. In the group A, 83.7 TeV is observed in the form of electro-magnetic cascade showers,and

ORIGINAL PAGE IS
OF POOR QUALITY

51.3 TeV in the group B. The relative distance between A and B is 22 cm, and the value $\chi(A,B) = R(A,B)/\sqrt{E(A)E(B)}$ is 1440 TeV·cm. We notice how large the spread of this event is, comparing the average value ~650 TeV·cm of the binocular-type events observed by the Brasil-Japan Collaboration./1,2/

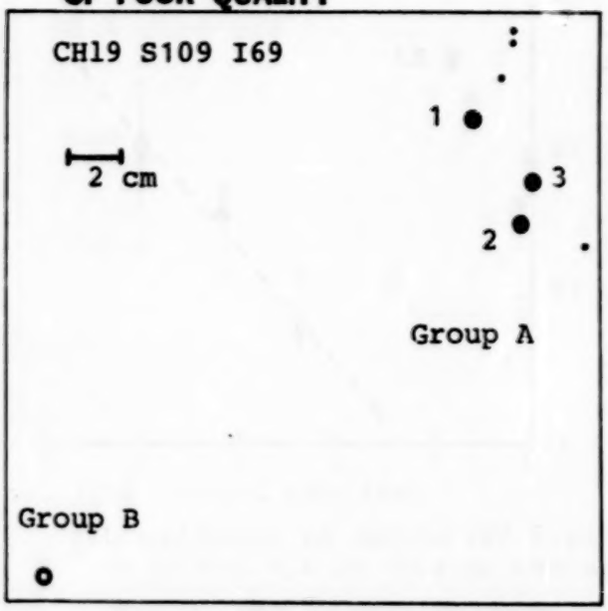


Fig.1 The target diagram of the event CH19 S109I69.

	Energy(TeV)	Comments
A1	16.3	A-jet
A2	31.5	Pb-jet-upper
A3	20.0	Pb-jet-lower
A4-7	15.9	A-jet
B	51.3	A-jet

Table 1 Groups A and B.

3-1. Group A The group A contains 3 high energy hadrons and 4 low energy showers as shown in Fig.1 and Table 1.

(#A1) #A1 has two cores in the upper chamber (10.5 TeV and 5.8 TeV with the relative distance 152 μ), and continues into the lower chamber where five weak and diffused showers and one very new core are observed inside the radius ~400 μ. Thus we can know that one of the two cores observed in the upper chamber or another hadron interacted to produce the showers observed in the lower chamber.

(#A2) #A2 starts to appear at 12 cu in the upper chamber as a very collimated core which can be realized only in the emulsion plate, and appears in the lower chamber as a multi-core event inside the radius 114 μ. The energy was determined for each of the 7 cores, and π^0-coupling confirms that they were born in a normal pion production at the lower part of the upper chamber. Outside the multi-cores, one new core of 8 TeV starts to appear at 10 cu in the lower chamber, its distance from the multi-cores being 187 μ. But we can not test whether it came from the emission point of the multi-cores or from the atmosphere. In case of the former, the electro-magnetic component of p_T of this hadron with respect to the emitted direction of the multi-cores is 0.80 MeV/c.

(#A3) #A3 starts to appear at 3 cu in the lower chamber as a single core, but at 4,5 and 6 cu as double cores, their energies being 17 TeV and 3 TeV. The relative distance between the two cores increases gradually at the deeper layers as shown in Fig.2. The convergence shows that #A3 is an interaction in lead plate in the lower chamber, and that the

ORIGINAL PAGE IS
OF POOR QUALITY

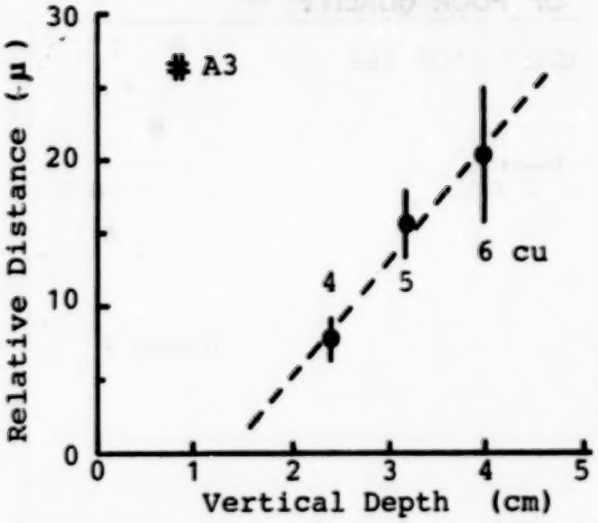


Fig.2 Variation of relative distances in #A3 at 4,5 and 6 cu.

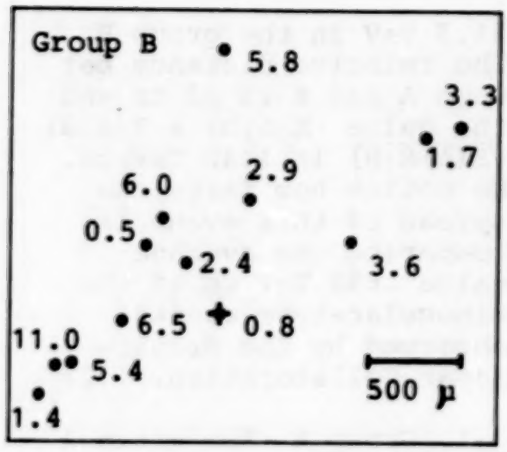


Fig.3 The target diagram of B. + stands for a hadron.

opening angle is $(7.6 \pm 1.8) \cdot 10^{-4}$ rad.. Their invariant mass is calculated only for the electro-magnetic component to be 5.4 GeV/c^2.

(#A4-7) #A4-7 are observed in the upper chamber as normal low energy showers.

The triangulation method was applied to determine the interaction height of the group A by measuring the relative distances between the higher energy core of #A3 and one of the multi-cores of #A2 at 3,4,5,6 and 10 cu in the lower chamber and between the higher energy core of #A3 and the new core of #A1 at 4 and 5 cu in the lower chamber. Within the error, the measurements on both pairs are consistent with parallelism, so we can say that the interaction height of the group A is higher than the limit of accuracy on the height determination, ~500 m above the chamber.

3-2. Group B The group B contains 13 shower cores with a quite small lateral spread; the average spread is 745 μ which is ~1 % of the average of atmospheric interactions. The target diagram of B is shown in Fig.3. One core indicated by the cross in Fig.3 appears at 6 cu as a very collimated shower core whose starting-point of cascade is estimated to be 2.2 cm·Pb, which is identified as a hadron.

4. Discussions and Conclusion

The event S109 I69 is of clear binocular-type consisting of two groups of particles well separated to each other. In the view-point of Centauro family, this event can be a Geminion-type. Using the average mass of Geminion ($k_\gamma M$ ~ 5 GeV/c^2), the production height is calculated to be ~3 km.

In the group A, the fraction of the energy sum of hadrons over the total visible energy is 81 %. This large fraction satisfies the criteria/3/ that the event can be of Mini-Centauro type. Using the average p_T of Mini-Centauro ($k_\gamma p_T$ -

0.35 GeV/c), the interaction height is calculated as ~1 km.

#A1 is an atmospheric interaction. If we assume that the two cores observed are decay-products of $\pi^0 \to 2\gamma$, the height is 8.8 m. If we assume that they are from mini-cluster/2,4/ with p_T = 20 MeV/c, the height is ~30 m above the chamber.

#A2 is an interaction in the upper chamber. If the hadronic core came from the same emission point of the multi-cores, #A2 can be a normal pion production in the chamber. If the hadronic core came from the atmosphere with another hadron producing the multi-cores, #A2 can be of mini-cluster. Using p_T = 20 MeV/c, the height is ~60 m.

#A3 is an interaction in the lower chamber, in which two cores are well separated with a very large transverse momentum ($k_\gamma p_T$ ~ 1.9 GeV/c). #A3 can be a Geminion.

#A4-7 may be products of normal pion production in the atmosphere.

The group B is an atmospheric interaction very near the chamber. If we assume that the interaction is of normal pion production with $\langle p_{T\gamma} \rangle$ = 200 MeV/c, the height is 15 m. If we assume a mini-cluster, the height is 150 m.

Summarizing the results and discussions on the event CH19 S109 I69 whose total visible energy is 135 TeV, our conclusion is as follows:

- S109 I69 (Geminion) ~3 km
  - Group A (Mini-Centauro) ~1 km
    - A1 (Mini-cluster, 30 m or Pion Production, 8.8 m)
    - A2 (Pion Production, 0 m or Mini-cluster, 60 m)
    - A3 (Geminion, 0 m)
    - A4-7 (Pion Production, ~500 m)
  - Group B (Mini-cluster, 150 m or Pion Production, 15 m)

Sequential appearance of exotic features in this event can be well understood by the hypothesis on genetic relation/4/ that an exotic interaction is generated by an exotic particle produced out of the exotic interactions.

5. Acknowledgement The authors wish to acknowledge all the members of the Brasil-Japan Collaboration for their kind and continuous support. Thanks are due to the CNPq, Brasil, for their financial support.

References (PIS=Proc.of Internat.Symposium on Cosmic Rays and Particle Physics, Tokyo, 1984; CFL=Contribution to a Festschrift for Prof.C.M.G.Lattes)

/1/ C.M.G.Lattes et al., Phys.Rep.65 (1980) 152.
/2/ Brasil-Japan Col., AIP Conf.Proceedings, 85 (1981) 500.
/3/ A.S.Borisov et al., PIS, 1984, p.248.
/4/ S.Hasegawa, PIS, 1984, p.718 and CFL, 1984,vol.1,p.71.
Brasil-Japan Col., CFL, 1984, vol.1, p.62.

N85-35935

GAMMA-HADRON FAMILIES AND SCALING VIOLATION

T.K.Gaisser(*), T.Stanev(**) and J.A.Wrotniak(***)

Bartol Research Foundation of the Franklin Institute,
University of Delaware,
Newark, DE 19816, U.S.A.

For three different interaction models we have simulated gamma-hadron families, including the detector (Pamir emulsion chamber) response. We compare with experiment rates of gamma families, of hadrons, and hadron-gamma ratios.

The Monte Carlo data on families in large emulsion chambers indicate, that simulations made for primary vertical protons are sufficient for the interpretation of observed gamma families (except of their intensity rates). However, for gamma-hadron families the increase in air thickness and the presence of heavier primaries may be important, as the hadron component has different penetrating power than the electromagnetic one.

Therefore we used our three different nuclear interaction models embedded in the same simulation framework, including heavy primaries and zenithal angles from 0 to 45 degrees.

Summary of models used in simulation

- @ FF-Y00 - scaling extrapolation of ISR data, constant AA and pA cross-sections.
- @ RR-F00 - energy dissipation increasing with energy; at 1.5 TeV as FF-Y00, at 150 TeV y-distributions reflect the SPS $p\bar{p}$ data (what by itself does not say much about the x-distributions, decisive for the family features), with fraction of neutral pions increasing with energy, rapidly rising AA and pA cross-sections.
- @ ST - based on a parametrization of hadron-nuclear collisions at accelerator energies, tuned to fit the balloon data in the TeV region. Scaling holds in the fragmentation region, while the central rapidity density increases as log E. Leading hadron energy is skewed towards smaller values and energy-dependent cross-sections correspond to $\log^2 E$ rise of the pp one.

(*) Work supported in part by the U.S.Department of Energy under contract No. DE-AC02-76 ER 05007.
(**) Work supported in part by the U.S.National Science Foundation under grant No. PHY 84-10989.
(***) On leave from the Łódź University, Poland.

First two models are described in detail by Wrotniak [4] (see also [7] in this volume), the third one - by Gaisser et al.[8]. Simulations were done in frames of the SHOWERSIM/84 standard [4], with Nikolskii [11] primary mass/energy spectrum; sampling threshold effects were avoided.

Simulation of the chamber response

The chamber [1,2] consisted of a 5 cm lead layer (gamma block), 60 cm (66 g/cm^2) of carbon and another 5 cm of lead (hadron block), with increase at non-zero zenithal angles.

Mean free path for nuclear interaction in carbon was 70, 91 and 102 g/cm^2 (nucleons, pions and kaons, respectively), and in lead - 168, 218 and 245 g/cm^2.

The effective gamma inelasticity of interacting hadrons was distributed as in [5] with mean value of .24 (nucleons) or .29 (mesons). Particles in the gamma block (including few interacting hadrons) were processed as in [9] (energy distortion, resolving power and a 15 cm cut-off).

Results

We compare our results with the Pamir Experiment data from Bangalore [1,2]. Both these papers refer to basically the same experimental results from a 250 m^{2}y exposure [1], expanded to 308 m^{2}y in [2].

Table 1 The ratio of gamma families with ΣE_γ> 100 TeV to primary flux above 1000 TeV/nucleus.

Primary	FF-Y00	RR-F00	ST	Exp [1]
p	.077(4)	.0153(11)	.039(5)	.
Alpha	.028(3)	.0051(9)	.016(5)	.
M	.007(2)	.0021(5)	.003(2)	..
LH	.011(3)	.0013(6)	.002(2)	.
VH	.0075(23)	.0011(2)	-	.
Total	.037(2)	.0073(5)	.018(2)	.0056(5)

Obviously, one can adjust the overall rate just by assuming different primary composition (cf Amenomori et al.[10]). However, at ΣE_γ>100 TeV there were 133 gamma families in experiment, versus 874 (FF-Y00), 173 (RR-F00) or 430 (ST) predicted by us for this exposure. Assuming the spectrum used by Gaisser (cf [3]) will reduce these numbers by about 6%; the spectra used by Kasahara et al. or M.Shibata (compared in [3]) - by 30-40%.

The experimental rates for hadron families (>100 TeV in total detected energy, at least 1 hadron) have not been published, but this should be not too difficult [6]:

Table 2 The ratio of hadron families with ΣE[detected] > 100 TeV to primary flux above 1000 TeV/nucleus.

Primary	FF-Y00	RR-F00	ST
p	.020(2)	.0017(4)	.0034(15)
Alpha	.013(2)	.0017(2)	.0012(7)
M	.004(1)	.0008(3)	.0022(16)
LH	.007(2)	.0005(4)	-
VH	.005(2)	.0006(1)	-
Total	.012(1)	.0013(2)	.0024(8)

The 308 m^2y exposure [2] gave 144 hadrons above 50 TeV (electromagnetic component energy in the chamber) and 41 hadrons above 100 TeV. We can compare these figures with ours:

Table 3 The ratio of hadrons with E > 50 TeV and E > 100 TeV to primary flux above 1000 TeV/nucleus.

Model:	FF-Y00	RR-F00	ST	Exp [2]
E > 50 TeV	.0164(11)	.0024(3)	.0051(11)	.0049(4)
E > 100 TeV	.0049(6)	.0006(1)	.0017(6)	.0014(2)

The hadron to gamma-family ratio is often quoted for the experimental data, being independent on the absolute primary flux: H = N[hadrons >100TeV]/N[gamma families >100TeV] .

Table 4 The hadron/gamma family ratio, H (as defined above)

Model:	FF-Y00	RR-F00	ST	Exp [1]
H	.13(2)	.08(2)	.09(4)	.27(5)!

The pattern emerging from Tables 1-3 is lost here! Also, simulations presented in [1] indicate, that H decreases with rising cross-section and increases with energy dissipation in nuclear interaction. This makes the experiment harder to explain with a quasi-scaling model with rising cross-section (needed to account for absolute rates); the rise assumed for non-scaling models should be much slower than ours.

Of course, higher effective gamma inelasticity and/or shorter interaction paths in the chamber would also bring

N85-35036

simulations closer to experiment. However, more than 2/3 of hadrons interact in the sensitive volume of our chamber, so the mean free paths will not give us even a 50% increase in H, and an approximate argument shows, that we need a much higher effective inelasticity to bring our results into agreement with experiment (the average of .4 for FF-Y00 or .5 for two other models).

Finally, let us compare the data on the accompaniment of high-energy hadrons:

S - the ratio of hadrons with neither gamma nor hadron accompaniment (above visible 2 TeV) to all hadrons above 50 or 100 TeV,
S' - the ratio as above, but no hadron accompaniment only,
S" - as above, but no gamma accompaniment only.

Table 5 The percentage of 50 and 100 TeV hadrons with no accompaniment at all, with no other hadrons and without gamma accompaniment.

	E > 50 TeV				E > 100 TeV			
	FF-Y00	RR-F00	ST	Exp[2]	FF-Y00	RR-F00	ST	Exp[2]
S	11(2)	25(5)	25(10)	45(4)	07(3)	10(7)	29(17)	41(8)
S'	23(3)	47(6)	40(11)	49(4)	14(5)	30(9)	43(19)	49(8)
S"	15(3)	26(5)	25(10)	71(4)	09(4)	10(7)	29(17)	61(8)

Once again, the discrepancy lies in the hadron/gamma ratio, as the S' values fit two of our models. One possible explanation is, that there are more hadrons produced than we assume (though there are no Centauros in Pamir), another - serious underestimation of gamma-ray energy or (perhaps more probable) overestimation of energy in the hadron block.

References

1. J.Malinowski et al.; 18th ICRC, Bangalore, 11, 179 [1983]
2. Pamir Collaboration; 18th ICRC, Bangalore, 5, 433 [1983]
3. T.K.Gaisser et al.; Bartol Report BA-81-21 [1981]
4. J.A.Wrotniak, SHOWERSIM/84; Univ.Md.Rep. PP 85-191 [1985]
5. J.Malinowski et al.; Pamir Coll.Workshop, Lodz, 49 [1980]
6. Pamir Collaboration; 17th ICRC, Paris, 11, 148 [1981]
7. J.A.Wrotniak and G.B.Yodh, HE 4.1-7 in this volume
8. T.K.Gaisser et al.; 18th ICRC, Bangalore, 5, 174 [1983]
9. H.Bielawska et al.; 18th ICRC, Bangalore, 11, 149 [1983]
10. M.Amenomori et.al.; Phys.Rev.D25, 2807, [1982]
11. S.I.Nikolskii; Izv.Akad.Nauk, Ser.Fiz., 39, 1160 [1975]

ORIGINAL PAGE IS
OF POOR QUALITY

N85-35936

HE 3.4-8

SUPER-FAMILY P2 C-96-125 OBSERVED BY JAPAN-URSS JOINT EMULSION CHAMBER EXPERIMENT

JAPAN-URSS JOINT EMULSION CHAMBER EXPERIMENT and
EDISON HIROYUKI SHIBUYA §
INSTITUTO DE FÍSICA 'GLEB WATAGHIN'
UNIVERSIDADE ESTADUAL DE CAMPINAS
CAMPINAS, SÃO PAULO BRASIL

1. INTRODUCTION: Since 1969, when it was observed the event 'Andromeda' by Brasil-Japan Emulsion Chamber Collaboration-BJECC, others events, looking like the pionner one, was detected and are turning to be one of the main themas of Cosmic Ray experiments. Nowadays, in 4 mountain stations(Kambala-China, Chacaltaya-Bolivia, Pamir-Soviet Union and Fuji-Japan), huge Cosmic Ray exposed Emulsion Chambers are constructed under name of International Collaborations, and constitute a world-wide effort to catch such type of events.
This paper aims to be a detailed description of the event detected in the second chamber of Japan-Urss Collaboration. A preliminary description was already published(1) and from that time a careful microscopic scanning was carried out.

2. METHODS: Fig.1 is the sketch of the chamber. As the Japanese sensitive X-ray films are inserted only in 4 layers, beeing 2 in the Γ-Block and the other 2 in the H-Block, the usual way of BJECC for energy determination is not applicable, a different method of energy determination was developped by T.Shibata(2), method that was used in the present paper. Japanese and Sovietic groups, using their respective materials and their own methods, made energy determination of this event. A check was recently made, obtaining consistent energy values.

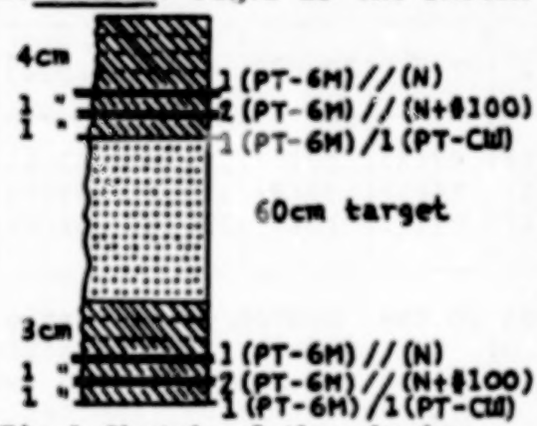


Fig.1 Sketch of the chamber

lead plates

rubber plates

3. RESULTS: Main characteristics of the event are summarized in Table I. From there we see that around half (56%) of the scanned individual showers are inside the central area of $(1.5 \times 1.5)\,cm^2$. They carries about 76% of the energy ($\Sigma E_\gamma + \Sigma E_h^\gamma$) of the individual showers and the energy inside the central square of $(1.5 \times 1.5)\,cm^2$ is equal to 2.5×10^3 TeV, approximately equal to the energy determined by halo measurement ($= 2.9 \times 10^3$ TeV). So, the remaining 400 TeV are distributed into many showers with energy less than 1 TeV and that causes the blacked region of the event.

TABLE I

Zenith angle: (18±2) degrees		
Detection: e,γ and hadrons (efficiency for hadrons = 80%)		
Halo	Radius R_{halo} = 1.2 cm	
	Energy = 2.9×10^{3} TeV	
$(E_\gamma^{e,\gamma}>1$ TeV)	Number	177 112 inside central square of $(1.5\times1.5)cm^2$
	Energy	2,000
	ΣE_γ/TeV	1,651 inside central sq. of $(1.5\times1.5)cm^2$
Hadrons $(E_h^{(\gamma)}>1$ TeV)	Number	35(44) 7(9) inside central sq. of $(1.5\times1.5)cm^2$
	Energy	1,254(1,567)
	$\Sigma E_h^{(\gamma)}$/TeV	822(1,028) inside sq. of $(1.5\times1.5)cm^2$

Notes: a) the efficiency was calculated as ref.4, i.e. efficiency = $\exp(-4/\lambda_h\cos\theta) - \exp\{-(T-T_o)/\lambda_h\cos\theta)\}$, where the nuclear collision mean free path λ_h was assumed as 30 c.u.Pb, T_o=vertical traverse in lead over which an electron shower develop above the detection threshold (assumed T_o=4 c.u.Pb) and T is the thickness of Pb layers + target.

b) radius of halo, R_{halo} is defined as the distance from the center to the point where the electron density is $10^6/cm^2$.

c) hadrons was identified as shower spots observed only in H-Block(22) + shower spots showing transition curve with 2 peaks(6) + shower spots showing transition curve adjustable to analytical γ transition curve(7).

d) figures in the parentheses gives the value after correction of detection efficiency.

Fig.2 shows the integral fractionary energy spectrum of electrons/gamma-rays. Others events are included and the marks are: Δ for the concerned event, O for Andromeda, X for Ursa Maior, ● for Mini-Andromeda III and the smooth curve is the average of five families with ΣE_γ=(1,000-3,000) TeV of Mt.Fuji experiment(3). Fig.3 shows the same kind of spectrum for hadrons. Marks are the same as Fig.2. From the coments of Table I, it is clear that the number of identified hadrons is the minimum, because it was used a very restrictive criterion. Also, looking for the figures (13 continuing showers from Γ-Block to H-Block and labeled as hadrons) and the 22 hadrons observed only in H-Block, we confirm the above affirmation. Fig.4 is the lateral distribution of energy flow, where R is the distance of shower from the energy weigthed center, center of γ's only. Hatched areas are for identified hadrons.

HE 3.4-8

ORIGINAL PAGE IS
OF POOR QUALITY

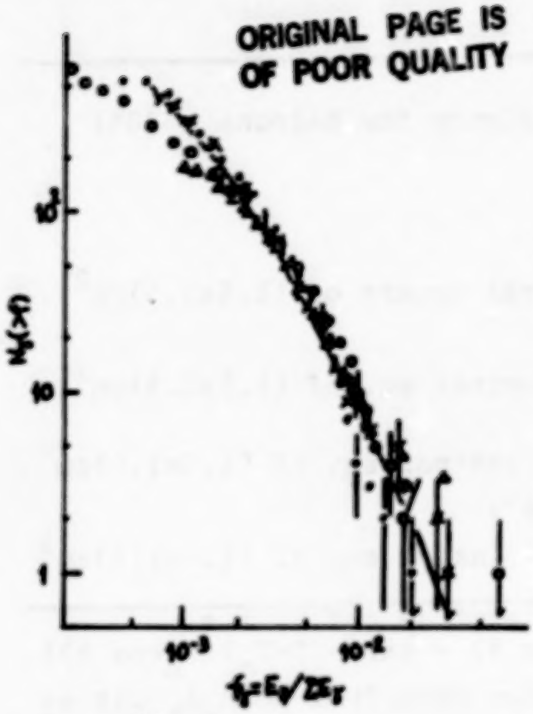


Fig.2

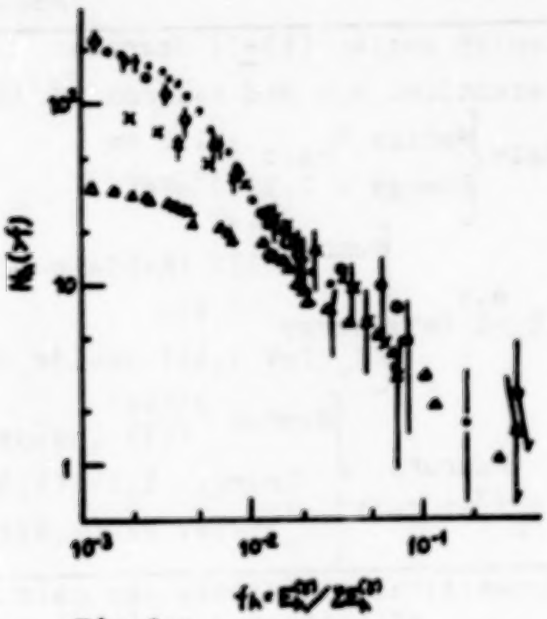


Fig.3

The individual showers was observed in the central (1.5x1.5) cm^2 area, by microscopic scanning in the #100 type Fuji X-ray films(fine grains) added to showers scanned by naked eyes in the N-type Sakura X-ray films(high sensitivity). From this scanning it is clear the existence of two clusters, formed by 76 spots, each one containing γ's and also hadrons. The showers of these two clusters are distributed in the distances smaller than R_c, that characterizes the pronounced pek of Fig.4.

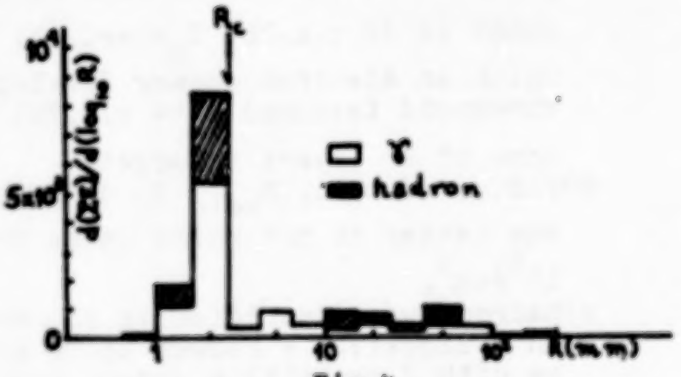


Fig.4

Table II*

event name	lateral spread R_c(mm)*	energy $\Sigma_{R<R_c} E_\gamma$(TeV)	energy-normalized lateral spread $R_c \times \Sigma_{R<R_c} E_\gamma$(GeV.Km)
P2 C-96-125	2.5	1,338(66.9%)**	3.3
Andromeda	1.0	323(7.2%)	0.32
Ursa Maior	4.0	700(52.1%)	2.8
M.A.I	6.3	734(55.0%)	4.6
M.A.II	1.6	390(43.9%)	0.62
M.A.III	2.5	796(31.5%)	2.0

N85-35037

ORIGINAL PAGE IS
OF POOR QUALITY

Notes:* For definition of R_c and data of other events see(4)

**Figures in the parentheses are the fraction of energy to the total energy of electromagnetic component

4.SUMMARY AND DISCUSSIONS: Comparison of this event shows similar features with other events. Remarkable difference is the existence of two central clusters carrying 67% of electromagnetic energy and 64% of hadronic energy. Under the same restrictive criterion for hadron identification, from where it was obtained the above figures, it was made a $E_\gamma R_\gamma$ integral distribution(fig.5). Marks are Δ for this event considering γ's with $R_\gamma < R_c$(=2.5mm) and ▲ for $R_\gamma < R_{halo}$(=12.0mm). The distribution for event P06 is from article:A Cosmic-Ray Nuclear...-Amato,Arata and Maldonado in this issue. Full lines are from ref.5. So, the distribution obtained for this event is similar to that one obtained for events containing the so-called Giant-Mini-Cluster phenomena (see article of BJ ECC in this issue).

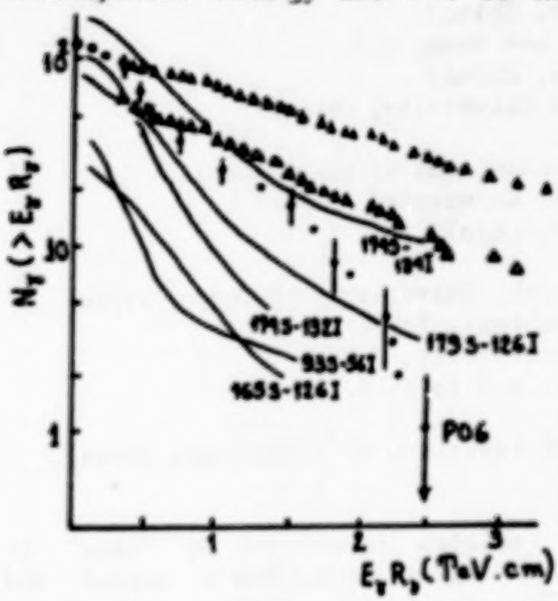


Fig.5

References:

1.Shibuya,E.H.-Proc.Int.Sympo. on Cosmic-Rays and Particle Physics, Tokyo,(1984),127
2.Shibata,T.-Internal Colloquium of Japanese Group of Japan-USSR Collaboration
3.Mt.Fuji Collaboration-Nuovo Cimento Ser.11,67A,(1982),221
4.Yamashita,S.-Jour.Phys.Soc.of Japan,vol.54,nº2,(1985),529
5.Hasegawa,S.-Proc.Int.Sympo. on Cosmic-Rays and Particle Physics, Tokyo,(1984),62

5 Permanent adress of E.H.S. is UNICAMP,Campinas-São Paulo, Brasil. He was visiting researcher during 1984 at the Institute for Cosmic Ray Research-University of Tokyo and Science and Engineering Research Laboratory-Waseda University, where the present work was developped.

Acknowledgments: The Japanese part of the JAPAN-USSR Collaboration is financially supported by Grant-in-Aid of Ministry of Education and Waseda University. One of the authors (EHS) was recipient of a Conselho Nacional de Desenvolvimento Científico e Tecnológico, Brasil during the year of 1984 - CNPq fellowship (Processo nº 200.881/83-FA), which is also gratefully acknowledged.

HE-3.4-9

N85-35937

On the halo events observed by Mt.Fuji and Mt.Kanbala Emulsion Chamber Experiments

--- Mt.Fuji Collaboration , Japan-China Collaboration ---

Ren J.R., Kuang H.H., Huo A.X., Lu S.L., Su S., Wang Y.X., and Xue Y.G.
(Institute of High Energy Physics, Academia Sinica, China)
Wang C.R., He, M., Zhang, N.J., Cao P.Y. and Li J.Y.
(Shandong University, China)
Wang S.Z. (Zhengzhou University, China)
Bai, G.Z., Liu, Z.H., Li, G.J. and Geng, Q.X.
(Chongqing Architecture College, China)
Zhou, W.D. and He, R.D. (Yunnan University, China)

Amenomori M. and Nanjo H. (Hirosaki University, Japan)
Hotta N. and Ohta I. (Utsunomiya University, Japan)
Mizutani K. (Saitama University,Japan)
Kasahara K. and Yuda T.
(Institute for Cosmic Ray Research, University, of Tokyo, Japan)
Mito I. (Shibaura Inst. of Technology, Tokyo),
Shibata M. (Yokohama National University, Japan)
Shirai T., Tateyama N., Taira T. and Torii S.
(Kanagawa University, Japan)
Sugimoto H. and Taira K. (Sagami Institute of Technology, Japan)

ABSTRACT

The intensity of big gamma-ray families associated by "halo" is obtained from Mt.Fuji experiment (650 g/cm^2 atmospheric depth) and Mt.Kanbala experiment (515 g/cm^2). The results are compared with Monte Carlo calculation based on several assumptions on interaction mechanisms and the primary cosmic ray composition. The results suggest more than 3 times lower proton abundance among primaries than that of 10^{12} - 10^{13} eV region within the framework of quasi-scaling model of multiple production.

1. Introduction Emulsion chamber experiments at high mountain altitudes are extending the concerned energy region over 10^{15}eV by the scale up of installations and accumulation of the exposure time. The integrated exposures have reached about 1000 m^{2}y and 300 m^{2}y at Mt.Fuji[1] and Mt.Kanbala[2], respectively, where the latter is already more than half of the former taking into account of the detection yield of the events. Some of the most energetic events ($\Sigma E\gamma$ >1000 TeV) observed by these experiments show a remarkable character of extremely high optical density on the X ray films at the gamma-ray family center, which we call halo. Some methodical problems connected to the energy estimation and the method of the analysis on the halo events are already reported in other papers[3),4)]. The responsible interaction energies for these events are estimated as 10^{16}-10^{17} eV. Since the extremely high energy density at the central part of the gamma-ray family is attributed to a number of energetic secondaries produced at the nuclear interactions in the atmosphere, the physical interest in the halo phenomena is connected to the feature of the multiple production mechanism in the fragmentation region at such a high energy

and also to the primary cosmic ray composition, especially to the portion of protons. As already reported in preliminary works[4),5)], the experimental data show less intensity of the halo type event than expected one based on simple extrapolation of lower energy data on multiple production and primary composition. Some possibilities resulting to the decrease of the halo intensity are considered in this paper. Namely, the fast incerease of interaction cross section, breakdown of scaling law as expected from the extrapolation of ISR-SPS[6),7)] results and possible change of the primary cosmic ray composition connected with the magnetic rigidity in the galaxy magnetic field are taken into account in the simulation.

2. Intensity of the halo events The number of big families with observed gamma ray energy more than 1000 TeV is 10 and 8 in Mt.Fuji and Mt.Kanbala experiment, respectively. The details of those events are described in ref. 2) and 5). The intensity of the halo events is examined in terms of the geometrical halo size defined as:

$$Smax = \int_{D>Dmin} dS \quad (cm^2) \quad , \quad Dmin=0.7 \quad (1) \quad ,$$

where Dmin is a given threshold for high optical density corresponding to the electron density of $3.24\times10^6/cm^2$ in case of double side coating N type X ray films. The integration is carried out over the area where the net optical density exceeds given threshold Dmin. We can obtain the transition curve of the halo size measuring on X ray films of every layers of the chamber, then the maximum value is adopted as Smax. Thus defined halo size well describes the feature of the energy flow at the gamma-ray family center. The integral spectrum of the halo size Smax is shown in Fig.1 (Mt.Fuji) and in Fig.2 (Mt.Kanbala) together with the results of Monte Carlo calculation made by one of the authors (M.Shibata). The main characters of models used in the simulation are as followings.

PS,αS,CNOS : Complete scaling model in entire energy range with constant interaction cross section, assuming primary cosmic ray particles as proton, helium and CNO group, respectively (pure composition).
PC : Proton primary with CKP model[8)].
PSq : Proton primary with quasi-scaling model, where increasing cross section ($\sigma \propto E_0^{0.06}$) and breakdown of scaling in pionization part is taken into account to be consistent with ISR-SPS results as shown in Fig.3. In this model, x-distribution in the fragmentation part shrinks very weekly with increasing energy as shown in Fig.4.
MSq : The same interaction model as PSq but assuming mixed primary composition of heavy nuclei dominance as shown in Table 1.

Table 1. The primary composition in mixed composition model (in %)

E_0 eV <A>	P 1	α 4	CNO 15	LH 25	MH 35	Fe 56
10^{15}	10.8	4.4	6.9	22.9	3.0	51.9
10^{16}	7.3	3.1	5.0	20.3	2.6	61.6
10^{17}	6.0	2.6	4.5	19.2	2.5	65.1

ORIGINAL PAGE IS
OF POOR QUALITY

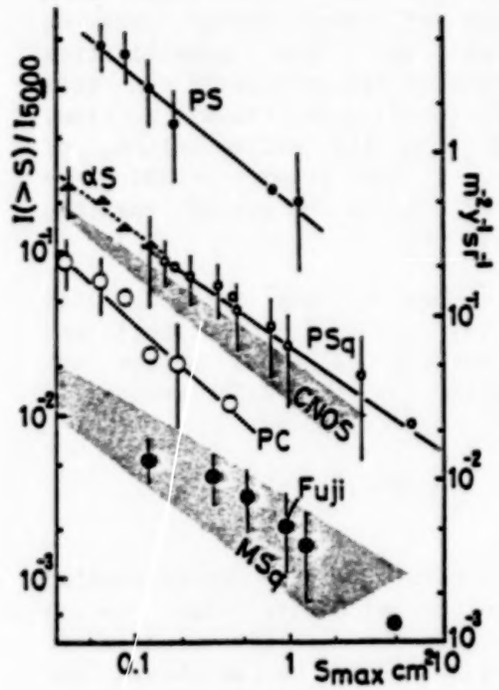


Fig.1 Intensity of the halo at Mt.Fuji. See eq.(1) for the definition of Smax.

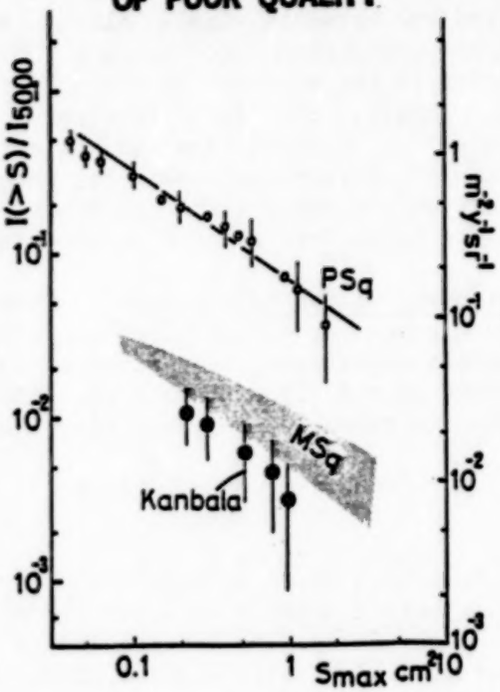


Fig.2 Intensity of the halo at Mt.Kanbala.

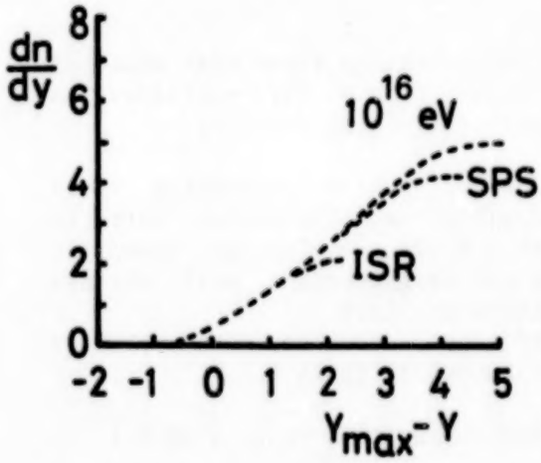


Fig.3 Rapidity distribution for quasi-scaling model.

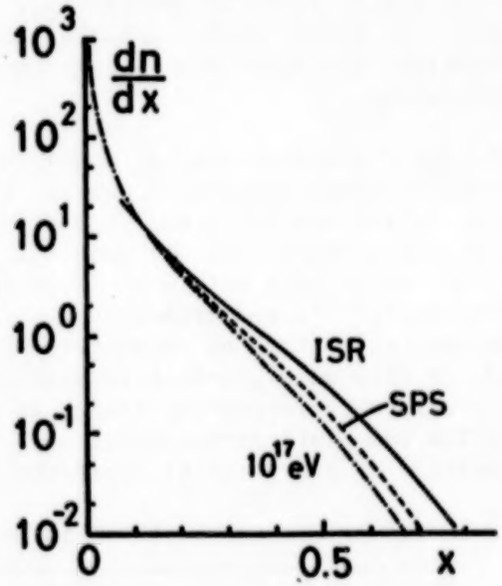


Fig.4 x-distribution for quasi-scaling model.

N85-35935

The intensities in Fig.1 and 2 are normalized to the number of primary cosmic rays at E_0>5000 TeV (left hand side scale) and to absolute intensity (right hand side scale) using I_{tot}(E_0>5000 TeV)=2.5/m^{2}y sr [9]. As is clearly seen from Fig.1, PS model is far from agreement with experimental data even if the portion of protons among total flux is considered. The quasi-scaling model with proton primary (PSq) still gives more than 10 times higher intensity. Therefore we can get agreement with experimental data within the framework of quasi-scaling model only when the portion of protons among total primary flux is less than 10 %, which is more than 3 times lower than the proton abundance known in 10^{12}-10^{13}eV region. The contribution of heavy nuclei for the creation of the halo events is expected to be very small from the results of αS and CNOS models (about 10 times lower efficiency compared with PS). In fact, the results of calculation with mixed composition described above (MSq:heavy nuclei dominance,quasi-scaling model) show most of the big events come from proton primary even its ratio is less than 10 % of total flux. (In present simulated statistics, only two events, one from helium nucleus and another from LH nucleus, contribute to the halo event among 25 observable events.)

Another possibility to interpret the low intensity of the halo events is to assume stronger breakdown of the scaling in fragmentation part than quasi-scaling model. But CKP type model is not suitable for this discussion because PC model in Fig.1 gives about 30 times less intensity than PS model. Therefore it cannot reproduce the halo intensity if the increase of cross section and primary composition is adequately incorporated.

Both results from Mt.Fuji and Mt.Kanbala experiments are in agreement with the discussion above within statistical error.

Refferences

1) M.Akashi et al., Phys. Rev. D, Vol.24, No.9 (1981) 2353
2) J.R.Ren et al., Proceedings of International Symposium on Cosmic Rays and Particle Physics, Tokyo, (1984) 87
3) M.Shibata, 18th International conference on Cosmic Rays, Bangalore, India, 1983, HE 5-16, Vol.11 (1983) 106
4) M.Amenomori et al., 18th International conference on Cosmic Rays, Bangalore, India, 1983, HE 5-15, Vol.11 (1983) 102
5) M.Amenomori et al., Proceedings of International Symposium on Cosmic Rays and Particle Physics, Tokyo, (1984) 76
6) W.Thome et al.,Nucl. Phys. B129(1977)365
7) K.Alpgard el al., Phys. Lett. Vol.107B, No.4 (1981) 310
8) G.Cocconi et al., Lawrence Radiation Laboratory, High Energy Physics Study Seminars, Report No. 28.2 (UCID-1444,1,1961) (unpublished)
9) N.L.Grigorov, Proc. of 12th ICRC, Hovart (1971) 1746

N85-35938

EXPERIMENT "PAMIR"-II. "PIANIT" - A GIANT SUPER-FAMILY WITH HALO ($E_o \sim 10^{17}$ eV)

Collaboration of experiment "Pamir" *)

1. Introduction. A supefamily with halo of extremely high energy named "Pianit" was recorded in X-ray emulsion chamber (XEC) at the Pamirs (atmospheric depth 600 g/cm^2). Here we present detailed description of the superfamily and results of its analysis.

2. Experimental set-up and description of the event. The "Pianit" was recorded in the XEC consisted of two registration blocks separated by the 1 m air gap which permit to evaluate (by a triangulation method) the height of the initial interaction in the atmosphere up to several kilometers. The method and the structure of the XEC were described elsewhere [1,2] . The superfamily was traced in all six layers of the XEC with selection of the cascades in the circle of R = 40 cm. Zenith angle of particle arrival was 18° the height of the initial interaction determined from the relative distances between the single γ-cascades at various depths in nuclear emulsions is equal to $3{,}5 \pm^{2}_{1.5}$ km. The γ-quanta of high enough energy used for the estimation of the height were located at distances from 4 to 12 cm from the family center.

In the center of the family there is a large dark diffused spot ("halo"), and on the background of it the separate cascades are visible in the upper layer of the XEC.

The energy determination for individual cascades was performed at the depth of 7.5 c.u., i.e. above the air gap. About 900 cascades are located out of the central circle with R = 2 cm, and they need no corrections taking into account the halo. On the background from halo, in the ring $0.5 < R < 2.0$ cm the energies of nearly 700 cascades were measured after the corrections connected with halo by the technique described in / 3/ . The results of the measurements of cascade energies are given in Table 1. In the region $R > 2$ cm integral spectrum of γ-quanta has the power index $\beta = 1.8 \pm 0.1$. As far as the total depth of XEC is equal (taking into account the inclination) to 13.3 c.u. the hadron registration efficiency is $\sim 15\%$ only. Selection of hadrons was made at the depth of 13.3 c.u. (the 6th layer) and as a criterion of a hadron-induced cascade served the absence of it at a depth 7.5 c.u. (it corresponds to depth of origin $\Delta t > 6$ c.u.). In the region with $2 < R \leq 40$ cm 46 of such the cascades were observed, 26 of them be-

---

*) Full list of authors see in HE 1.2-12. The author of this paper is also G.T.Zatsepin (Institute for Nuclear Researches, Moscow).

ing with energy $E_h^{(\gamma)} \geq 4$ TeV. The power index of this hadron spectrum occured to be $\beta_h = 1.5 \pm 0.2$. Some results of measurements for γ-quanta and hadrons are given in Table 1.

Table 1

	Particles with $2\text{cm} < R < 40\text{cm}$		All γ-quanta	
	N_γ or N_h	ΣE_γ or $\Sigma E_h^{(\gamma)}$, TeV	N_γ	ΣE_γ, TeV
γ-quanta, $E_\gamma \geq 4$ TeV	250	$2.7 \cdot 10^3$	720	$1.0 \cdot 10^4$
hadrons, $E_h^{(\gamma)} \geq 4$ TeV	26	192	-	-

2. Lateral distributions. The interesting feature of the superfamily "Pianit" consists in some structure of lateral distribution of γ-quanta. In the target diagram of the family (Fig.1) points the mean centers of the close groups of γ-quanta (clusters), obtained by the method of "nuclear decascading": to be included in the same cluster each pair of the cascades has to satisfy the condition $R_{ik} \cdot (E_i^{-1} + E_k^{-1})^{-1} \leq Z_0$, $Z_0 = 30$ TeV.cm (R_{ik} - the mutual distance, E_i, E_k - the energies of the cascades).

The number of clusters so obtained with energy $E_{cl} \geq 4$ TeV is equal to $N_{cl} = 55$, while 38 of them are located outside the circle of radius 2 cm. Differential distributions of R and ER for clusters are shown in Fig.1, the average values being $\langle R_{cl} \rangle = 10.5 \pm 1.4$ cm, $\langle E_{cl} \cdot R_{cl} \rangle = 5.8 \pm 0.6$ GeV.km. After the comparison with results of /4/ it can be stated that the high values of $\langle E_{cl} \cdot R_{cl} \rangle$ are connected with large ($\gg 1$ GeV/c) transverse momenta at least for the part of the initial hadrons or jets.

3. Properties of halo. To evaluate the energy of the halo the scanning of the area 4x4 mm^2 with a slit size 500x500 μm^2 was performed in the central part of "Pianit" for 5 depths: 3.8, 5.7, 7.5, 11.4 and 13.3 c.u. *) Analysis of the densitograms has shown, that the total number of particles reaches the maximum at 11.4 c.u. although the darkness density is still growing up to the last level, 13.3 c.u. The total numbers of particles at various depths is given in Table 2.

The energy of the halo can be calculated from the total number of particles at maximum of the transition curve and the typical average energy $\sim 10^8$ eV:

$$E_{halo} \cong 1.7 \cdot 10^8 \cdot 10^8 = 1.7 \cdot 10^{16} \text{ eV}$$

*) Scanning was done in P.N.Lebedev Physical Institute (Moscow) and in the Institute of Cosmic Ray Research (Tokyo).

ORIGINAL PAGE IS
OF POOR QUALITY

Table 2

t, c.u.	3.8	5.7	7.5	11.4	13.3
$H_{tot} \cdot 10^{-7}$	1.2	6.3	13.4	16.6	15.1

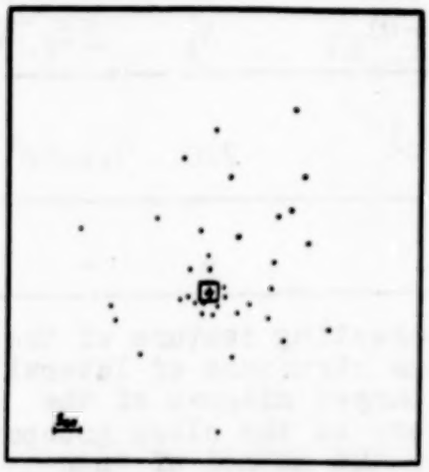


Fig.1. Target diagram of cluster lateral distribution (+ - central region of halo)

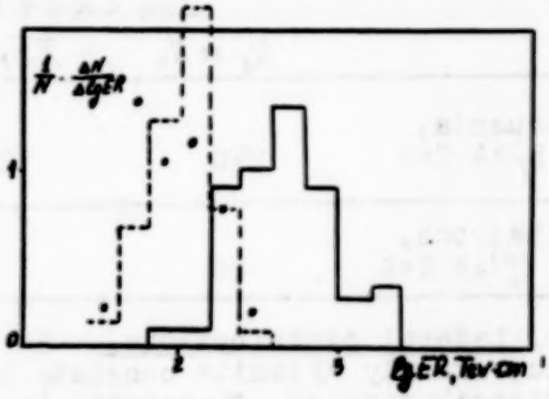


Fig.2. ER distributions of clusters: —."Pianit", O - big families of Fuji group, --- -calculations by model of high multiplicity

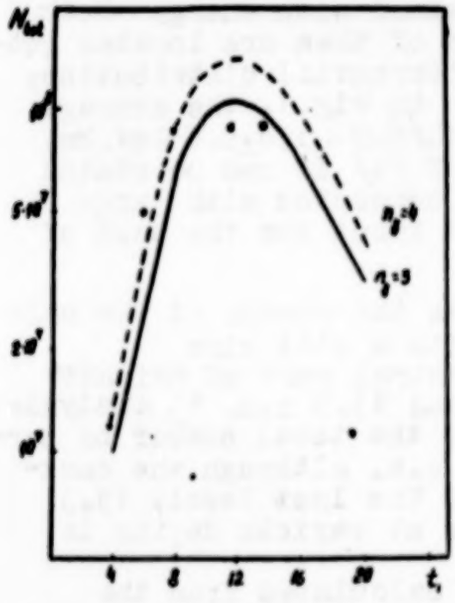


Fig.3. Transition curve of halo particles: • -experiment, — - and --- -calculations for various number of initial γ-quanta with energy 10^{16} eV

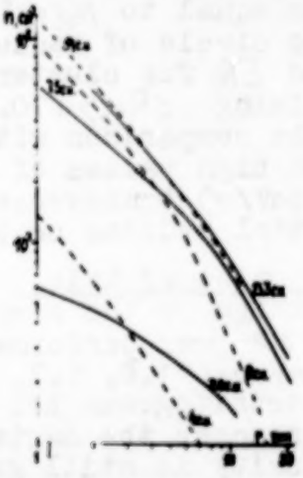


Fig.4. Lateral distributions of halo particles at various depths: — - experiment, --- -calculation /5/

N85-38933

Because of the possible influence of the large air gap this energy estimate is considered as a lower limit.

The comparison of the longitudinal and lateral development of the halo with calculations is given in the Figs.3 and and 4. The last 2 experimental points in Fig.3 are measured under the air gap, so they are underestimated. It can be seen that the longitudinal development can be explained /5/ by the production of 4 initial γ-quanta with energies of each of them $\sim 10^{16}$ eV at the height ~ 12 c.u. above the chamber. However for the lateral structure of halo the calculation differs from reality: it gives too high density in the center and ~ 2 times lower at the distance ~ 1 cm. This discrepancy cannot be explained by methodical reasons and it is necessary to admit the production of the considerable number of γ-quanta with initial lateral divergence.

4. Conclusions. The total energy of γ-component of superfamily "Pianit" occured to be $\sim 3.5 \cdot 10^{16}$ eV, the total multiplicity of γ-quanta ~ 1500 so it is now the most energetic event ever recorded by XEC. Its peculiar feature is the large number of clusters (55) anomally wide distributed over $R_{cl}R_{cl}$ values.

References

1. Puchkov V.S. Proc. 15th ICRC, V.9, p.190, 1977
2. S.G.Bayburina et al., Trudy FIAN, t.154, p.11, 1484 (In Russian)
3. Baradzei L.T. et al., preprint N 51, FIAN, 1976
4. Mt.Fuji collab., ICR-Report, 95-81-11
5. Ivanenko I.P., Managadze A.K., Proc. Inst. Symp. on Cosmic Rays and Particle Physics, Tokyo, March 1984, p.101

N85-35939

HE 3.4-11

EXPERIMENT "PAMIR"-IV. ANALYSIS OF SUPERFAMILY WITH HALO OF ELECTROMAGNETIC NATURE DETECTED IN DEEP XEC

Collaboration of Experiment "Pamir"*

1. Introduction. The family Pb2-11 was detected in the multilayer lead XEC with total thickness of 100 c.u. exposed at the Pamirs. Each lead layer was 1 cm thick, the first registering layer being located under 2 cm of Pb($\simeq$4 c.u.). The family comprised a narrow group of gamma-rays which near the maximum of cascade development($\simeq$14 c.u.) produced a dark spot of optical density $D \geq .4$ over area $S \simeq 25 mm^2$. The narrow group of gamma-rays was traced up to 14th layer corresponding to 30 c.u. Deeper in the chamber, for the space of 70 c.u. no hadron cascade was observed. Thus, the pure electromagnetic halo could be assumed.

Preliminary results of the analysis of the family Pb2-11 has been presented in /1/. We consider here in more detail the methods of estimation of energy of primary particle and height of nuclear interaction responsible for the observed halo.

2. Longitudinal and lateral characteristics of halo. To determine ΣE_γ released in the halo, the area of halo was scanned by two instruments at various depths in lead. From the measured optical densities we inferred the density of number of secondary electrons n(r) and subsequently the total number of particles N(4mm) within a circle of radius 4 mm. When determining ΣE_γ, restriction of the scanned area should be regarded. The ratio of the total number of secondary electrons in lead to the particle number within a circle of 4 mm, K(4 mm), was calculated for maximum of an electron-photon cascade(EPC) induced by primary gamma-ray and electron with various energies E_γ. The value of K(4mm) weakly depends on E_γ and is equal to 24. Thus, $\Sigma E_\gamma = K(4mm) \cdot \rho \cdot \int N(4mm) \cdot t dt$, where $\rho = 7.5$ MeV. After taking into account the scattering of shower particles within a gap, the total energy was found to be $\Sigma E_\gamma = 560$ and 610 TeV, respectively, for two scanning instruments.

In /2,3/, the EPC from one or few high-energy gamma-rays have been shown to dominate halo production. To evaluate the height ($t_{a/2}$) and the energy (E_0) of the primary interaction producing the halo, experimental characteristics of halo were compared with the characteristics calculated in /2,3/ for air-lead EPC induced by high-energy gamma-ray. The Table below lists the interaction parameters used in three calculational versions.

The choice of the best version of calculations was made by comparison of experimental and calculated lateral

---

* Full list of authors see in HE 1.2-12. The author of this paper is also Zatsepin G.T., Institute of Nuclear Research, Academy of Sciences of the USSR, Moscow

ORIGINAL PAGE IS
OF POOR QUALITY

distributions for 9 depths in the chamber, because the comparison on a single depth turned out to be insufficient. As an example the distribution n(r) for three depths are plotted in Fig.1. The best agreement of experimental and calculated distributions is obtained for version II.

If lateral distribution in the halo at various depths are available, the transition curve for the halo longitudinal development within circles of various radii in the chamber can be obtained. Fig.2 presents the experimental and calculated transition curves for a circle of radius 4 mm. The best agreement is also achieved for version II.

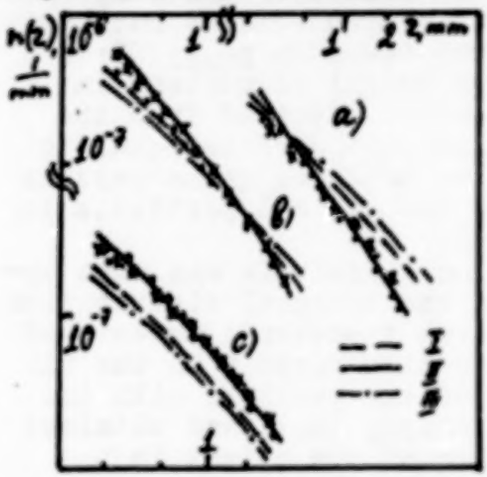


Fig.1. Lateral distributions n(r) for the depths in XBC equal to 8 c.u.(a), 14 c.u.(b) and 20 c.u.(c). Experimental data is observed with scanning systems of University of Tokyo (.) and P.N.Lebedev Physical Institute (x). Curves present results of three versions of calculations listed in Table

Table

Versions of calculations	I	II	III
E_o, TeV	100	700	1400
t_{ch}, c.u.	2	2	2
B_γ	1	1	1

Fig.3 presents the experimental energy spectrum of gamma-rays in the halo and calculated spectra for three versions of calculations and for version II with E_o=1000 TeV. The best description of experimental data gives version II with E_o= 1000 TeV.

Experimental lateral characteristics and multiplicities obtained for gamma-rays within halo area for two different threshold(4 TeV and 10 TeV) were compared with calculated ones/6/ and thus the values E_o=1000 TeV and $\tilde{t}_{all} \simeq$ 3-5 c.u.

3.Lateral and energy distributions of individual gamma-rays in the halo

To obtain the characteristics of individual particles in the halo, spots from them were photometered at a depth of 6 c.u. taking into account overlapping /4,5/.

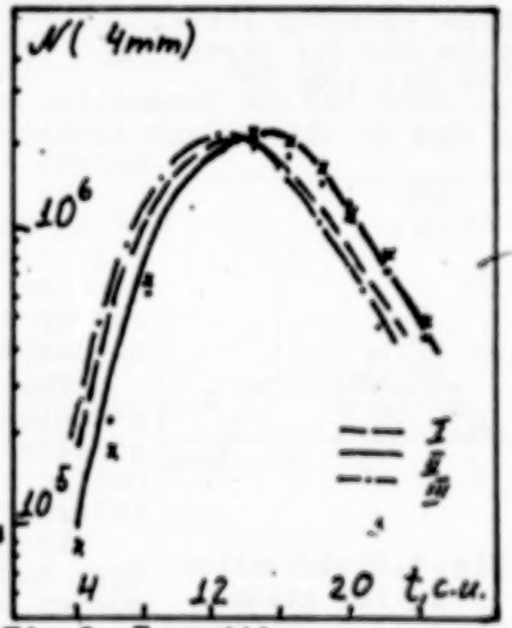


Fig.2. Transition curve N(4mm). Symbols are the same as in Fig.1.

were obtained.

Distribution of the relative transverse momentum z_{ik} for gamma-rays in the halo and for all gamma-rays in the family are shown in Fig.4. The distribution for all gamma-rays has two maxima. The first maximum corresponding to the component with momentum $p_{em} \sim 2 \cdot 10^7$ eV/c, i.e. typical value for Coulomb scattering of electrons in the EPC, is caused mainly by gamma-rays in halo. The second maximum is caused by the component with characteristic nuclear transverse momentum $p_{nucl} \sim 2 \cdot 10^8$ eV/c. The height of nuclear interaction (τ_{all}) derived from the dependence $z_{ik}(\tau_{all})$/7/ is equal to $\tau_{all} \simeq 5$ c.u. both for gamma-rays in the halo and for all particles in the family.

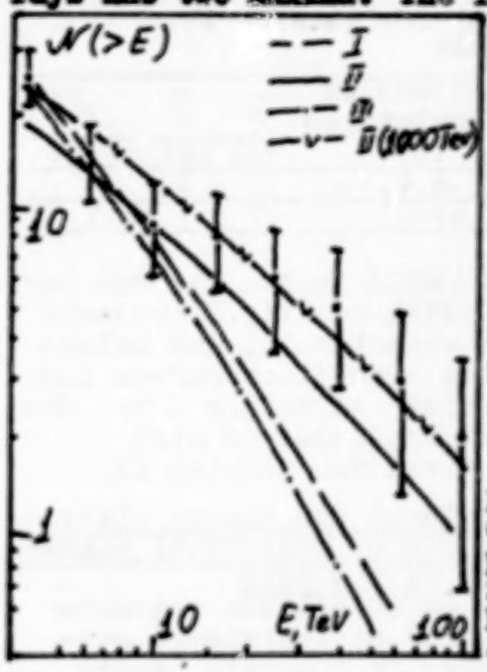


Fig.3. Experimental and calculated energy spectrum of gamma-rays in the halo. Calculations are made for three versions listed in Table and for version II with $E_o = 1000$ TeV

The same analysis was also applied to the integral distribution of relative transverse momenta of particles with respect to the direction of the particle with the highest energy (z_{io}), and obtained estimation of the height is $\tau_{all} \simeq$ 4 c.u. also both for gamma-rays in halo and for all particles.

4. Conclusion. Summarizing the results of the analysis, we can infer that the observed halo is caused by the EPC induced by a single gamma-ray with energy $E_o \sim 1000$ TeV and production height τ_{all} 3-5 c.u. The family is due to the nuclear interaction which has occurred at a height of 3-5 c.u. above the XEC.

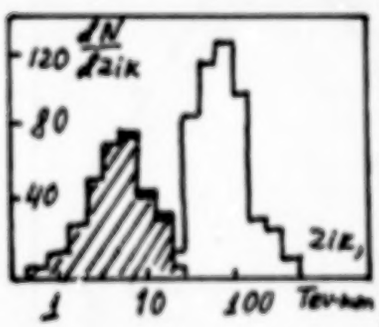


Fig.4. Distribution of z_{ik} for gamma-rays in halo (dashed) and for all gamma-rays in the family

It is important that the values of E_o and τ_{all} obtained by analysing the halo development in the chamber and by analysing the lateral and energy distributions of family particles are in a good agreement.

Thus, the information on the longitudinal and lateral characteristics of electromagnetic halo allows estimation of the parameters of primary interaction producing the halo.

Energy of the primary interaction E_{int} can be obtained as a sum of energy of gamma-rays and hadrons outside halo/1/ and above estimated energy of halo equal to 700-1000 TeV, and the result is E_{int} 1200-1500TeV.

The transfer of the large energy fraction into the electromagnetic component is an important feature of the family. The observed event can be treated as detection of the charge exchange process $\pi^{\pm} \to \pi^{0}$ with Feynman variable $x \simeq .6 \pm .1$.

References

1. Borisov A.S. et al. - Proc. of Int. Symp. on Cosmic Ray and Particle Physics, Tokyo, 1984, p.3-29.
2. Fedorova G.P., Managadze A.K.- Proc. 18th ICRC, 1983, v.5, p.466-469.
3. Ivanenko I.P., Managadze A.K., Roganova T.M., Osipova L.A. - Proc. 15th ICRC, 1977, v.7, p.267-280.
4. Aminava T.P., Lazareva T.V., Managadze A.K. - Acta Univ. Lodz. ZNUL, 1980, ser.II, v.32, p.199-216.
5. Ivanenko I.P., Managadze A.K., Roganova T.M. - Proc. 15th ICRC, 1977, v.7, p.280-284.
6. Adachy A. et al. - Prog. Theor. Phys., Suppl., 1964, v.32, p.154-191.
7. Baradzey L.T., Smorodin Yu.A., Solopov E.A. Preprint NN 103, 104, M.: FIAN, 1974.

N85-35940

PARTICLE INTERACTIONS AT ENERGIES OVER 1000 TeV INFERRED FROM GAMMA-FAMILIES OBSERVED AT Mt. FUJI

Mt. Fuji Collaboration

Amenomori,M., Nanjo,H. and Konishi,E.
Hirosaki University, Hirosaki, Aomori
Hotta,N.
Utsunomiya University, Utsunomiya, Tochigi
Mizutani,K.
Saitama University, Urawa, Saitama
Kasahara,K., Kobayashi,T., Mikumo,E., Sato,K. and Yuda,T.
ICR, University of Tokyo, Tanashi, Tokyo
Mito,I.
Shibaura Institute of Technology, Shibaura, Tokyo
Shibata,M.
Yokohama National University, Yokohama, Kanagawa
Shirai,T., Taira,T., Tateyama,N. and Torii,S.
Kanagawa University, Yokohama, Kanagawa
Sugimoto,H. and Taira,K.
Sagami Institute of Technology, Fujisawa, Kanagawa

Scaling, mean P_t, high P_t jets and others at energies over 1000 TeV are discussed on the basis of gamma-family data with $\Sigma E_\gamma > 100$ TeV, observed at Mt. Fuji (3750 m). These quantities are examined in connection with the primary composition.

1. Introduction.

At present, an observation of cosmic ray phenomena is a unique source to get a direct information about particle interactions at energies over 10^{15} eV. Among these, emulsion chamber experiments produce fruitful results for this purpose. Since 1970, the large-scale emulsion chamber experiments have been continued at Mt. Fuji (3750 m, 650 g/cm^2). Now, the total exposure of chambers reaches about 1000 m^2.y and about 200 family events with $\Sigma E > 100$ TeV have been observed. Also we have reliable data about particle interactions at energies up to 150 TeV and this energy will go higher at Felmilab in very near future. So, within one or two years, we may give a definite answer to the alternative of 1) scaling break in the fragmentation region and proton dominant primary or 2) scaling and heavy enriched primary, which have been repeatedly discussed for a long time.

In this report, we discuss general features of particle interactions expected from the Mt.Fuji experiment,comparing with the Monte Carlo results, and also describe some characters of

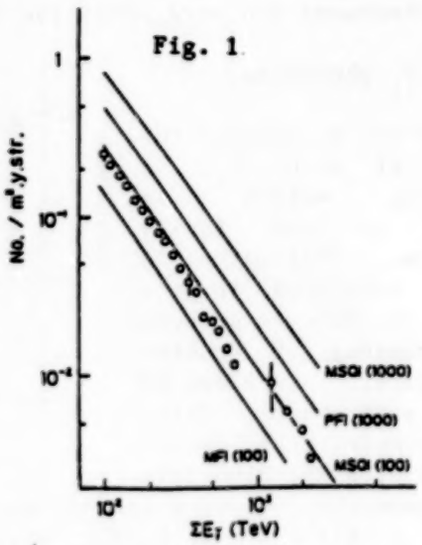
super-families.

2. Problem of the Feynman scaling in the fragmentation region.

It is well confirmed that the absolute flux of gamma-ray families at mountain altitude is the most sensitive to the energy spectra of particles in the fragmentation region, inelastic cross sections and also primary composition, 1).

In Fig.1 we compare our data with the Monte Carlo results which are simulated on the basis of the conventional model of the interaction and primary. The symbols used for classifying the model are : P means the proton primary , M the mixed composition (heavy dominant), S the scaling, F the fire-ball model (normalized to SPS data at 150 TeV), Q the QCD-jet, I the increasing cross section as $E^{0.04}$ and T the transverse momentum increasing with energy as $E^{0.04}$. The bending energy (Eb in TeV) of primary proton is denoted in the blacket (spectral index changes from 1.7 to 2.0) and other nuclei also become steeper at Z*Eb. The absolute intensity of assumed total spectrum is normalized to the Grigorov's one at energies around 10^{15} eV. Details of the simulation will be found in the other paper, 2).

Fig. 1

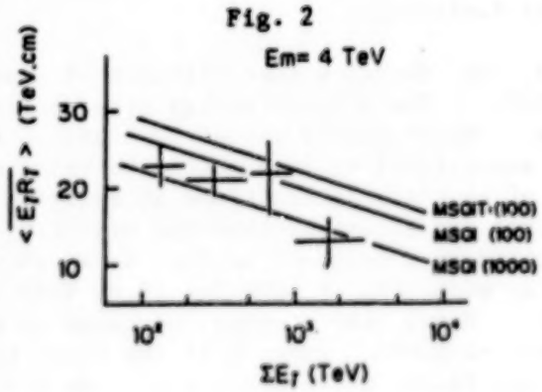


It can be understood that the scaling with heavy enriched primary is compatible with the experimental data. In this case, the proton component should become steeper at energies around 10^{14} eV. Of course, a strong scaling break and proton dominant primary (Eb~10^{3} TeV) can also explain our data, but the fraction of protons to the total would not exceed 50 % at around 10^{15} eV (bending energy of proton spectrum).

3. Mean P_t at high energies.

The lateral spreads of constituent gamma-rays in the families give a measure of the mean P_t of secondaries at collisions. In Fig. 2 is shown the lateral spread, $\langle \overline{ER} \rangle$, averaged in the respective energy range, with the Monte Carlo results. In the acccelerator energy region, the mean P_t near

Fig. 2

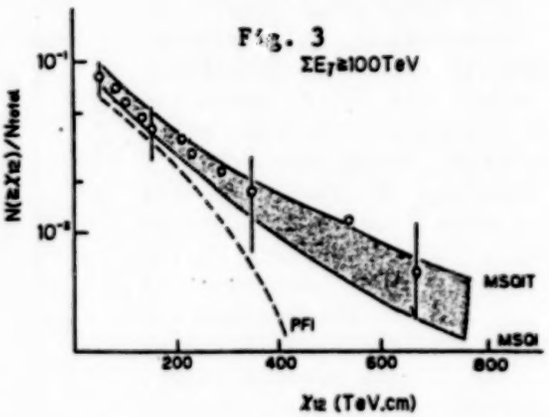


the central region seems to increase with energy as $E^{0.04}$. If this increasing rate is hold up to higher energies, it takes about 450 MeV/c at 1000 TeV. However, as learned from this comparison, our data do not favour to increasing P_t (Here we discuss the P_t in the small P_t region. Note that the QCD jets are speciously taken into account in the simulation.). This result may suggest that the mean P_t depends very weakly on the primary energy, if any, or remains almost constant, since the family phenomena are very sensitive to the fragmentation region.

4. High P_t phenomena.

In order to enhance the effect of high P_t, a clustering method is applied to the family phenomena. This method is already described in the paper, 3). Here we present the frequency of double-core events. In order to pick up such events, first we clusterize the gamma-families with ΣE_γ >100 TeV, then impose the following conditions : E1+E2 > 0.8 ΣE_γ and E1,E2> 10 TeV ; R12 > 5 max(r1,r2), where E1(E2) and r1(r2) is the energy and lateral spread of cluster 1(2) and R12 the distance between two clusters. In Fig.3 we show our data together with the Monte Carlo results. The frequency of double-core events with χ_{12}(=R12/$\sqrt{E1.E2}$) > 100 TeV.cm is about 7 %. This figure teaches us that such events are within the scope of expectation of the model based on the scaling with QCD-jets, and also a rapid energy dissipation model such as fire-ball is incompatible with the data.

Fig. 3



Concerning to high P_t jets, we should note here that the peculiar event "TITAN", observed in 1977 and composed of 6 very high energy showers with E > 100 TeV, 4), is by no means produced by the conventinal interaction models according to our Monte Carlo simulation.

5. Super-families.

Here, we describe some features of super-families with E 1000 TeV. The primary energy responsible for generating such families would mostly exceed 10^{16} eV. A general feature of these super-families is expected to bring us a new clue for the study of particle interactions at energies 10^{16} - 10^{17} eV. A remarkable structure is that the majority of super-families is accompanied by a halo. In Fig. 4, we show the flux of gamma-families with ΣE_γ > 1000 TeV (E_γ=4 TeV) and halo events at Mt.Fuji. Here, the energy of halos is estimated by using a relation of E=C*Z_* where Z_* is the total track length and C the conversion factor of 10 MeV/c.u.. As discussed in other paper, the flux of halo events can also be explained by the model mentioned above, 5).

ORIGINAL PAGE IS
OF POOR QUALITY

At present, we have 6 halo events with energy exceeding 1000 TeV. The biggest event is the FC-31 with energy of about 9000 TeV. Two patterns are found about halo structure, i.e., single and axial-symmetric core or multi-cores. Examples of the event, FH-89 (2500 TeV) and FC-104(4000 TeV) are shown in Fig. 5 and 6. Three among 6 events have a single-core structure. In particular, no high energy showers are found in the outskirts of the halo of the event FH-89 , strikingly different from other two, as noticed from Fig. 5. According to the Monte Carlo simulation, such type of events are possibly produced by protons deep in the atmosphere and the structure of the event FH-89 may suggest a look of very high multiplicity. We need more events to reach some conclusive results.

Fig. 4

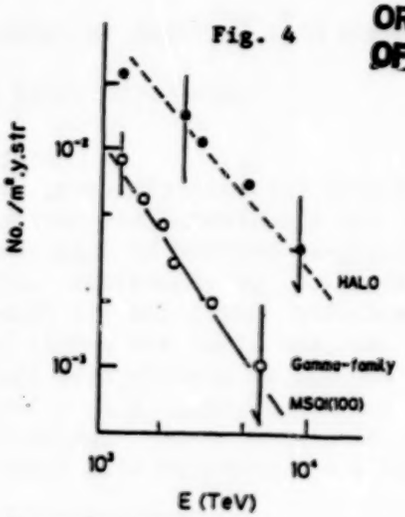


Fig. 5

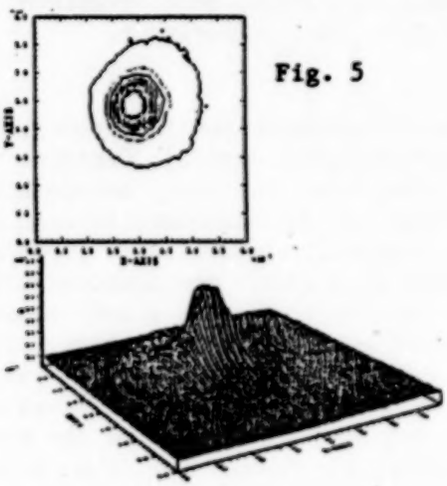


Fig. 6

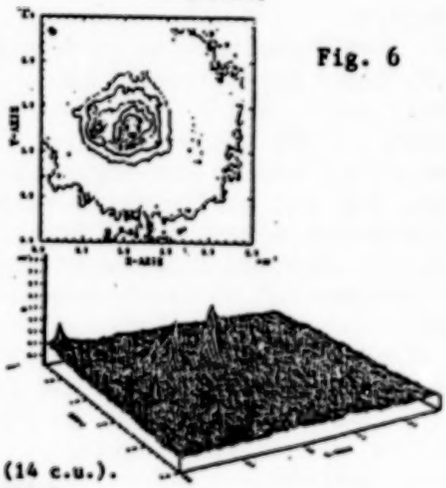


Fig. 5 : FH-89 (36 c.u.), Fig. 6 : FC-104 (14 c.u.). Density map of X-ray film measured by photometer. Area : 24x24 mm^2, Slit size : 300 microns, Z-axis : Density from 0-3.0.

1) Akashi, M. et al, Phys. Rev., D24, p2353 (1981).
2) Ding, L. K. et al, Prc. Int. Symp. on Cosmic Rays and Particle Physics, p142 (1984, ICR, Univ. of Tokyo).
3) Amenomori, M. et al, Phys. Rev., D25, p2807 (1982).
4) Akashi, M. et al, 15th ICRC, Vol.7, p184 (1977, Plovdiv) ; Amenomori, M. et al, Proc. Int. Symp. on Cosmic Rays and Particle Physics, p382 (1984).
5) Ren, J. R. et al, HE3.4- 9, in this volume.

HE 3.5-2

N85-35941

A SEARCH FOR MINI-CLUSTERS IN JAPAN-USSR JOINT EXPERIMENT AT PAMIR

JAPAN-USSR JOINT EXPERIMENT (II)

Abstract

A search for mini-clusters, very collimated shower clusters of hadrons and electromagnetic particles, is made for the hadron and gamma families observed by Japan-USSR joint carbon chamber at Pamir. The existence of anomalous correlation between hadrons and electromagnetic particles is found. The decascading method is applied to the families and it is found that 11 clusters which include hadrons as members have smaller spread, $\langle Er \rangle < 3.5$ GeV.m and larger lateral spread, $E^* R^* > 100$ GeV.m, from the family center. In the simulated events, we have found very rare such clusters. The results are compared with those of Chacaltaya experiment.

1. Introduction.

In the cosmic-ray nuclear interactions of incident particle energy $E_0 > 10^{15}$ eV, there exist several kinds of exotic phenomena[1], Centauro is a typical one, which are not yet observed in the accelerator experiments. The characteristics of those exotic phenomena is seen in the composition and in the magnitude of transverse momentum of produced particles, that is, particles unaccompanied with pions are produced with large transverse momentum. Recently, the existence of a new shower phenomenon is reported from Chacaltaya experiment ,that is, there exist hadrons accompanied by electromagnetic showers in very close vicinity and those hadrons and electromagnetic showers form very collimated shower cluster, the mini-cluster[2]. And now, it is one of the most important problems to make clear the physical nature of the mini-cluster. The carbon chamber is thick enough to detect hadrons and is suitable to detect mini-clusters. Here we show the results of systematic analysis on hadron and gamma families observed in USSR-Japan joint carbon chamber[3] exposed at Pamir plateau, paying special attention to the mini-clusters.

2. Experimental procedure.

The chamber, so-called carbon chamber, consists of three parts, i.e., Γ-block of 6 cmPb, H-block of 6 cmPb and carbon layer of 60 cm thick between the two. The detail structure of the chamber and the method of energy determination is described in the separate paper[3].

Identification of hadrons The showers observed in H-block are those from local nuclear interaction in the carbon layer(C-jet), those from local nuclear interactions in the H-block itself(Pb-jet-H) and tails of showers from Γ-block. Thus almost all showers in H-block are hadronic origin. The showers observed in Γ-block are mixture of electromagnetic showers from the atmosphere and those from local nuclear interactions in Γ-block itself(Pb-jet-Γ). Among showers observed in Γ-block, we consider the shower as hadronic-origin when the shower continues to H-block and the darkness of the shower in H-block is far above the expected darkness in case of electromagnetic shower. The detail argument on the identification is described in the Ref.[4]. The above procedure for identification of hadrons in Γ-block can not pick up all hadrons interacted in -block, and also the threshold energy for them becomes 5 ∿10 TeV although the detection threshold energy of showers is around 2 TeV. The detection probability of hadrons with

energy $E_h^{(\gamma)}$ greater than 2 TeV is estimated as $\sim$70 %.

Selection of the events The systematic measurement of gamma- and/or hadron- families is done in one section(24 m^2) of the joint chamber 'Pamir-2'[4], and we have about 110 unbiased events with total visible energy greater than 20 TeV. Among 52 families of total visible energy greater than 50 TeV, 21 events have hadrons in their member showers. Our main concern is to see correlations between hadrons and electromagnetic showers. Then we pick up only the events which have showers penetrating from Γ-block to H-block. Among 21 hadron and gamma families, 14 events have penetrating showers. In the following analysis, three high energy events(in the another section where systematic measurement is going on) together with 14 events above mentioned are used.

3. Results.

Correlation between hadrons and electromagnetic showers Fig.1a shows a distribution of relative distance, Rmin, between a hadron and its nearest neighbouring shower and Fig.1b shows a distribution of energy-weighted relative distance, Xmin, between a hadron and its nearest neighbouring shower in $X_{ij}(=\sqrt{E_i E_j} R_{ij})$-space, where E_i, E_j are energies of showers and R_{ij} is a relative distance between the two. Histogram in the figure shows a background distribution which is obtained by randomly changing azimuthal angle, ϕ , of hadrons in the observed events. As is seen in the figures, in contrast with that the background distribution is almost uniform, in the experiment there exists a peak, which is not seen in the background distribution, in small Rmin region, Rmin < 400 μm and in small Xmin region, Xmin < 2.2 GeV.m. We have 11 hadrons which accompany a shower in Rmin less than 400 μm and 9 hadrons which accompany a shower in Xmin less than 2.2 GeV.m. The number of those hadrons expected from the background distribution is $\sim$0.8 and $\sim$0.6 respectively. And the probability that the observed number of hadrons accompany showers in such small Rmin and Xmin is estimated $\sim 5\times10^{-10}$ and $\sim 8\times10^{-9}$. The result well agrees to that obtained in the Chacaltaya experiment[5], and the observed closeness in (energy-weighted) relative distance between hadrons and electromagnetic showers can not be simply accidental.

Mini-clusters Mini-cluster is a narrowly collimated shower cluster and it looks like pure young electromagnetic cascade in the atmosphere. The characteristic of mini-clusters different from pure electromagnetic cascade is its hadronic nature, that is, hadrons are included as members. Here we apply the decascading method[6] to the families in order to study cluster structure of hadrons and electromagnetic particles. Decascading method is a way to trace back to the original gamma-rays from the observed cluster of electromagnetic showers. The showers are amalgamated to one if $Z_{ij}=E_i E_j R_{ij}/(E_i+E_j)$ is less than a constant value k where E_i, E_j are energies of showers and R_{ij} is relative distance between the two. Here the decascading method is applied to all the members, including hadrons and electromagnetic particles, of the family, and we put parameter k=11 GeV.m($=k_s X_0$), characteristic spread of electromagnetic cascade at Pamir altitude. In this case, the decascading method loses its original meaning but simply means 'clustering'. Fig.2a shows a correlation diagram on the energy-weighted lateral spread E^*R^* of clusters with energy E^* greater than 10 TeV and the average lateral spread, $\langle Er \rangle$, of showers in the clusters, obtained by the above procedure. E^*, R^* are the energy and the

distance of the cluster from the family center. E and r are energy of shower in a cluster and distance of it from cluster center. In the figure, clusters which include hadrons as constituents are marked by triangles. For the comparison, the clusters with hadrons, obtained by the same procedure, in the Chacaltaya events are shown in the figures. Fig.2b shows the same diagram for the simulated events. Simulations are carried out under the assumption that the primary particles are protons with power energy spectrum. Two types of interaction model are assumed. One is fire-ball(H-quantum) model[7], Model-I, and the other is C-jet data model[8], Model-II, where C-jet events observed by Chacaltaya experiment are boosted to cosmic-ray energies. The above two interaction models can well reproduce results of accelerator experiment of ISR and SPS. As is seen in the figure, in the simulated events, too, there exist clusters which accidentally include hadrons as members. Those clusters which include hadrons, however, are distributed in the region of larger $\langle Er \rangle$ in the above diagram. The striking characteristics in the experiment is that there exist clusters including hadrons which have smaller $\langle Er \rangle$ and larger E^*R^*. For example, 11 among 16 clusters with hadrons in the events of joint chamber and 11 among 26 clusters in the Chacaltaya events are with $\langle Er \rangle < 3.5$ GeV.m and $E^*R^* > 100$ GeV.m, the region is indicated by broken lines in the figure, while in the simulated events almost all clusters with hadrons are distributed outside of the above region. Such smallness of $\langle Er \rangle$ of experimentally observed clusters with hadrons are coming from the anomalous closeness of hadrons and electromagnetic showers, discussed in the previous section. In Fig.2a we put special mark to the clusters which include hadrons with Rmin < 400 μm and/or $X_{min} < 2.2$ GeV.m.

4.Conclusion.

We have observed 11 clusters, mini-clusters, of anomalously collimated hadrons and electromagnetic particles through the systematic analysis on 17 hadron and gamma families, with total observed energy greater than 50 TeV, observed by joint carbon chambers at Pamir. Though the structure of the chamber and the accuracy of measurement are different from the Chacaltaya chambers, we have obtained good agreement on the characteristics of mini-clusters between the two experiments.

Aknowledgement. The collaboration experiment is financially suppotred in part by Grant-in-Aid from the Ministry of Education and Waseda University, in Japan.

References.

[1] C.M.G.Lattes et al.; Physics Report 65 no.3(1980) 151
L.T.Baradzei et al.; Proceedings of 18th ICRC, Bangalore(1983) p.441
A.S.Borisov et al. ; Proceedings of 18th ICRC, Bangalore(1983) p.491
[2] Brasil-Japan collaboration ; AIP Conference Proceedings (1981) p.500
H.Bialkowska et al. ; Proceedings of Int. Sympo. on Cosmic Rays and Particle Physics, Tokyo (1984) 374
[3] Japan-USSR Joint Experiment ; 19th ICRC (1985) HE 3.1-1
[4] M.Koike,T.Hibi,H.Tanaka,M.Tsuchiya and K.Terasawa ; to be published
[5] M.Tamada ; 19th ICRC (1985) HE 3.3-6
[6] H.Semba ; Supple. Prog. Theor. Phys. no.76(1983) 111
[7] T.Maeda ; to be published
[8] I.Takatsuka ; 'Uchusen Kenkyu' (in Japanese) vol.28 no.1(1984) 1

ORIGINAL PAGE IS
OF POOR QUALITY

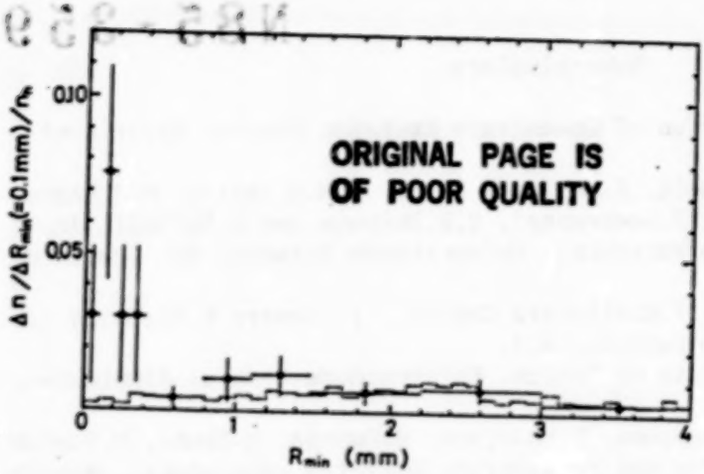


Fig.1a: Distribution of relative distance, Rmin, between a hadron and its nearest neighbouring shower. Histogram is a background distribution (see text).

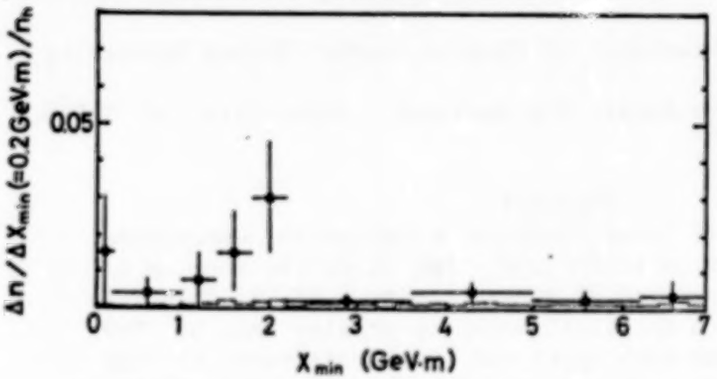


Fig.1b: Distribution of energy-weighted relative distance, Xmin, between a hadron and its nearest neighbouring shower in Xij-space.

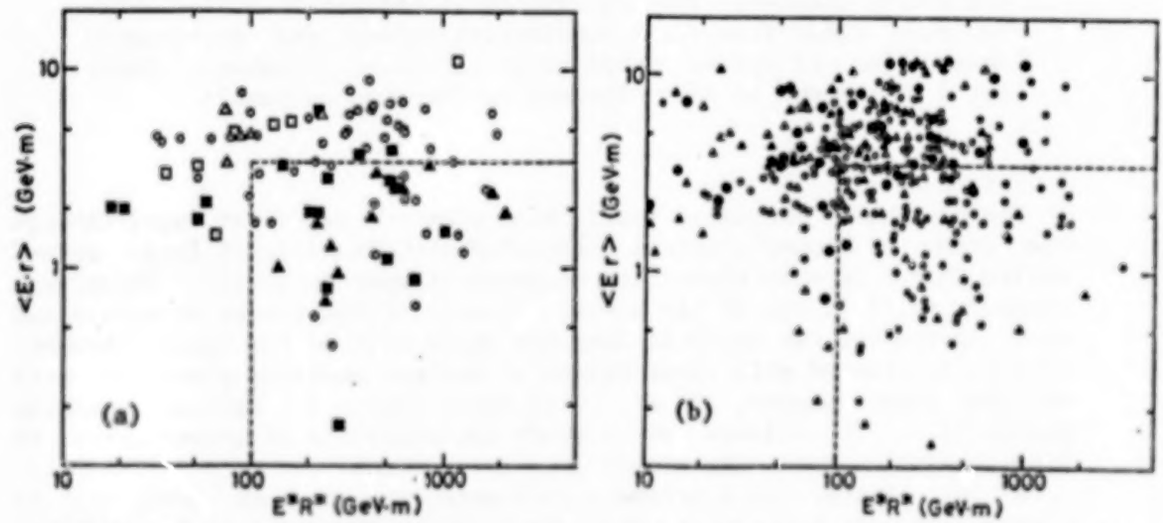


Fig.2a: Correlation diagram on energy-weighted lateral spread, E R of clusters and the average ⟨Er⟩ of showers in a cluster for the clusters with energy greater than 10 TeV.
○: clusters without hadrons, △: clusters which include hadrons,
▲: clusters which include hadrons with Rmin < 400 μm and/or Xmin < 2.2 GeV.m for the events of joint chamber.
□: clusters which include hadrons, ■: clusters which include hadrons with Rmin < 400 μm and/or Xmin < 2.2 GeV.m for the events of Chacaltaya chamber no.19.
Fig.2b: Same to Fig.2a for the simulated events. △, ▲: for Model-I and ○, ●: for Model-II. ▲, ● : clusters which include hadrons.

N85-35942

Mini-clusters

Brasil-Japan Collaboration of Chacaltaya Emulsion Chamber Experiment

J.A.Chinellato, C.Dobrigkeit, J.Bellandi Filho, C.M.G.Lattes, M.J.Menon, C.E.Navia O., A.Pamilaju, K.Sawayanagi, E.H.Shibuya and A.Turtelli Jr. ; Institute de Fisica Gleb Wataghin, Universidade Estadual de Campinas, Campinas, S.P.
N.M.Amato, N.Arata and F.M.Oliveira Castro. ; Centro Brasileiro de Pesquisas Fisicas, Rio de Janeiro, R.J.
R.H.C.Maldonado ; Instituto de Fisica, Universidade Federal Fluminense, Niteroi, R.J.
H.Aoki, Y.Fujimoto, Y.Funayama, S.Hasegawa, H.Kumano, H.Semba, M.Tamada and S.Yamashita ; Science and Engineering Research Laboratory, Waseda University, Tokyo
T.Shibata and K.Yokoi ; Department of Physics, Aoyama Gakuin University, Tokyo
A.Ohsawa ; Institute for Cosmic Ray Research, University of Tokyo, Tanashi, Tokyo

Abstract

Experimental result of 'mini-clusters' observed in Chacaltaya emulsion chamber no.19 is summarized. The study was made on 54 single core shower upper and 91 shower clusters of $E(\gamma)>10$ TeV from 30 families which are visible energy greater than 80 TeV and penetrate through both upper and lower detectors of the two-storey chamber. The association of hadrons in mini-cluster is made clear from their penetrative nature and microscopic observation of shower continuation in lower chamber. Small $p_t(\gamma)$ of hadrons in mini-clusters is remained in puzzle.

1. Introduction.

The new shower phenomena named "mini-cluster" was first found through the study of shower clusters associated with families of large spread called Chiron type in Chacaltaya emulsion chamber no.19[1]. Chacaltaya chamber no.19 is one of the series exposure of two-storey structure and what is special for no.19 is that the whole area of the upper chamber, 44 m^2, is covered with three layers of nuclear emulsion plates as well as the lower chamber, 33 m^2, with seven layers of nuclear emulsion plates[1]. It allowed us to study the behaviour of shower cores in fine resolution under the microscopic observation.

A mini-cluster is a narrowly collimated shower core bundle ; so narrow that, in many cases, it gives a single dark-spot in X-ray films, and it reveals itself a very closely distanced shower core cluster under the microscopic observation in nuclear emulsion plates. The characteristic dimension of lateral spread is of the order of a few GeV.m, the same as the spread of young atmospheric cascade showers. The difference is seen in the strong penetrative nature of mini-cluster, showing the shower cluster is not of simple electromagnetic nature but hadrons must be inside. The present paper describes the summary of study on mini-clusters in Chacaltaya chamber no.19 of 677 days exposure.

2. Statistics of families.

30 families with $\Sigma E(\gamma) > 80$ TeV are selected under the following

criteria.

i) A family penetrates through both upper and lower chambers.

ii) A family has wide spread ; ⟨ER⟩ > 180 GeV.m after the decascading procedure with constant Ec=6 GeV.m.

3. Shower core observation under microscope.

Every dark spots in X-ray films in the upper chamber are studied in nuclear emulsion plates under microscope, especially asking whether a dark spot in X-ray films is single core structure or closely distanced multiple cores. The track counting method is applied to all individual shower cores for their energy determination with radius r=25 and/or 50 μm.

4. High energy showers ($E(\gamma)$ > 10 TeV) in the upper chamber.

The high energy showers show the following characteristics.

(1) About one third of high energy showers are of single core structure. More than 60% of them penetrate into the lower chamber, indicating the majority are of hadron origin showers in the chamber materials.

(2) The rest are of multi-core clusters spreading over area 0.1 ∿ a few mm of radius. About one half of them are penetrative into lower chamber, indicating they all are not pure electromagnetic cascade in the atmosphere.

Table 1 gives the summary of observation of high energy shower-upper.

Table 1. Summary of high energy shower-upper

	no. of shower	no. of penetrative showers	%
single core	54	35	65 ± 12
mini-clusters	91	41	45 ± 8

Fig.1 shows the average transition curve of spot darkness in X-ray films (measured by slit size 200x200 μm^2) for 37 single core and 57 mini-clusters. The results of simulation calculations are drawn together for pure electromagnetic cascades of gamma-ray incidence with energies 10 and 20 TeV, respectively, since the average energies of single core shower-upper and the highest one in mini-clusters are 20 and 15 TeV, respectively. One sees qualitatively different behaviour between the two, especially in the deepest region in the lower chamber ; that is, experimental results have much larger and longer tail for both single and mini-cluster cases than the case of pure electromagnetic cascades in the chamber materials.

5. Mini-clusters.

5-1. Multiplicity Fig.2 gives the distribution of number of shower cores, n, for 91 mini-clusters(E > 10 TeV). We see most of mini-clusters are ranging n = a few ∿ 10. There are observed mini-clusters with extreme large multiplicity , say n ∿ 40, for which we put the name "Giant-mini-cluster" and we shall discuss specially the properties of those huge shower clusters in details in the separate paper[2].

5-2. Small pt of mini-clusters It is expected $p_t(\gamma)$ of shower cores at the mini-cluster formation must be small from their very small lateral spread. Fig.3 gives the scatter plots between the spread of 91 mini-clusters, ⟨Er⟩, versus that of parent Chiron family, ⟨ER⟩, measured by high energy showers (>10 TeV) by mark (O). The broken lines show the cases where the ratio of both spreads are 1/1000, 1/300 and 1/100,

respectively. Most of them are distributed in the region smaller than 1/100 and the average is given by ∿1/300. If we accept $\langle p_t(\gamma)\rangle$ of parent Chiron interaction is 2 ∿3 GeV/c, the $\langle p_t(\gamma)\rangle$ of mini-cluster formation is obtained 10∿20 MeV/c. In the same figure, we present the relation of spreads on binocular families by mark (●). We see the same small ratio in more than half of clusters from binocular families as in the case of Chiron families. The large pt nature at the geminion interaction, $\langle p_t(\gamma)\rangle$ = 2∿3 GeV/c, the same order of magnitude with the Chiron interaction, is suggesting that there might work the similar dynamics for secondary particle production.

5-3. Hadrons in mini-clusters Mini-clusters show strong penetraive nature than expected from pure electromag..etic cascades from X-ray film observation as shown in Table 1 and Fig.1. Table 2 gives the results of microscopic observation of shower continuation in the lower chamber for mini-clusters as well as single core shower-upper of E(γ) > 10 TeV.

Table 2 Microscopic observation of shower continuations in lower chamber.

	Pb-jet-upper	C-jets	Pb-jet-lower	any	not studied	sum
single-core	14	7	3	7	4	35
mini-clusters	22	8	5	6		41

Hadrons in mini-clusters are studied in much detail by observing the core configuration and by comparing transitions of electron number in individual shower cores with the expected behaviour of pure electromagnetic cascades of single gamma-ray incidence on the basis of a large number of simulation calculations by T.Shibata. The results show there are not small cases where mini-clusters include plural hadrons[3]. A study on hadron association in mini-clusters are made from the side of correlation analysis by M.Tamada[3]. Using 19 families of Japanese part of the chamber no.19, the distribution of the relative distance (and energy-weighted relative distance) between detected hadrons and the nearest shower in each family is constructed and compared with the one of random background (Fig.4). The anomalous correlation was found in the range R ≤ 1 mm which show the probability is nearly equal or less than 10^{-6} if the hadrons and electromagnetic particles are produced without any correlation.

6. Discussions.

A systematic search of mini-clusters was carried in the first carbon chamber at Pamir by USSR-Japan joint exposure[4]. There are found 11 penetrative mini-clusters among 17 families with energy greater than 50 TeV in ∿24 m^2year exposure. There was a report on study of penetrative cascade showers in Pamir carbon chamber, giving the consistent results[5]. Exotic behaviour of secondary particles of Chiron-type families is remarkable when one consid.. the small collision mean free path (1/2∿1/3 λ geo.) and small pt of hadrons and electron/gamma-rays seen in the mini-clusters.

Acknowledgement.

The collaboration experiment is financially supported in part by Conselho Nacional para o Desenvolvimento Cientifico e Tecnologico, Fundacao de Amparo a Pesquisa do Estado de San Paulo, in Brasil, and Institute for Cosmic-Ray Research, University of Tokyo and Grant-in-Aid from the Ministry of Education, in Japan.